Number 1 Volume 25 1961

PI

BULLETIN

of the

ACADEMY OF SCIENCES OF THE USSR

— PHYSICAL SERIES —

(Izvestiya Akademii Nauk SSSR)
(Seriya fizicheskaya)

Reproduction rights reserved
by
Columbia Technical Translations
5 Vermont Avenue
White Plains, New York

Single Issues
$20

Annual Subscription
$215

Lithographed in U.S.A. by
EDWARDS BROTHERS, INC.
Ann Arbor, Michigan

Transactions

of the

Ninth All-Union Conference on Luminescence (Crystal Phosphors)

(Kiev, 20-25 June 1960)

Digitized by the Internet Archive
in 2024

https://archive.org/details/russian-academy-of-sciences-physics-bulletin_1961_25_1

OPENING ADDRESS

- V.L.Levshin

Two years have passed since the last conference on crystal phosphors (the Seventh Conference on Luminescence), held in the summer of 1958 in Moscow. This is a relatively brief interval, yet, during this time there have been significant advances in luminescence research in the Soviet Union. The research centers already extant in Leningrad, Tartu and Moscow continued their purposeful work and obtained a number of interesting results. Significant investigations have been carried out in a number of other locations: there were formed new scientific collectives at the Academies of Sciences of several Soviet Republics and in a number of colleges and universities, where increasing emphasis has been placed on the creation of laboratories devoted to the problems of luminescence and spectroscopy.

I shall not speak here of individual investigations, many of which are of great interest, but will limit myself to a brief review of the significant advances realized during the past two years in different fields of the science of crystal phosphors.

I shall start with the chemistry of phosphors, the field that provides us with the subjects for our investigations. Research in the field of phosphor chemistry has undergone substantial changes in different directions. Numerous earlier studies provided the foundation on the basis of which one can now more intelligently choose the aims of chemical investigations. Consequently, we now have new possibilities of modifying the physical properties of phosphors in the desired direction by chemical means. For more precise determination of the useful means and the chemical-physical relationships involved there have been carried out many specific investigations: there have been studies of phosphors as distinctive physical-chemical systems, of the influence of structure on phosphor properties, and of the effects of dislocations and deformations of the crystal lattice.

A second direction in the evolution of chemical research in the field of crystal phosphors has been the development of methods of preparing crystal phosphors in new states or conditions. Here I have in view particularly the preparation of sublimated films, which are very convenient for investigating the absorption of phosphors as well as their electric properties. There have also been developed new methods of growing single crystals, the advantages of which over strongly scattering powdered phosphors are obvious.

In addition to improvement in the methods of preparing already known phosphors, there have been created a number of new luminescence materials that are of interest from the scientific standpoint and highly important for practical purposes.

In the field of physical investigations during the past two years there have been continued profound studies of luminescence centers and localization levels (traps) as well as of the energy storing ability of crystal phosphors.

The question of the composition of luminescence centers has a long history dating back to the important pioneering investigations of Verneuil and P.Lenard. While no one now holds to the obsolete concepts of Lenard, it must be admitted that no one knows exactly what constitutes a luminescence center. Various and greatly divergent views have been advanced on the question of the structure of luminescence centers and of the components entering into it, on the influence of auxiliary activators and co-activators, on the participation in the luminescence process of neighboring parts of the lattice and of the state of ionization of luminescence centers. These are all topics that still arouse heated arguments. In the past two years, however, there have been carried out a number of studies which, although they do not give a definitive answer to the question, still shed considerable light on the state of luminescence centers, at least in individual

cases. Particularly significant work in this respect has been done in investigating luminescence centers in alkali halide crystals. Of the new helpful methods of investigation developed in recent years one may note the method of paramagnetic resonance, which in a number of cases makes it possible to determine the state of the excited or unexcited activator ion.

Even more attention has been given to the investigation of the nature, location and filling of electron and hole trapping levels, which determine the kinetics of persistent luminescence of crystal phosphors and their ability to store energy. For solution of problems in this field extensive use is made of the method of thermostimulation (glow curves). Thanks to this procedure there have been obtained significant data on the trapping levels in alkali halide, zinc sulfide and other crystal phosphors.

However, the method of glow curves does not yield a complete picture of the location and filling of traps in phosphors, owing to the existence of complex processes of electron redistribution during thermostimulation and, particularly, owing to the onset of luminescence quenching at high temperatures. Hence other techniques are used for investigating the position of trapping levels, among which I want to note the new method based on recording exoelectronic emission curves; in using this method information on the location of trapping levels is obtained not on the basis of the luminescence intensity but on the basis of the intensity of emission of electrons from the surface of the excited phosphor during heating. This method has its own difficulties and shortcomings, but it often successfully supplements the method of glow curves.

On the basis of the information obtained on the location and nature of trapping levels it is much easier to construct more specific theories characterizing the different processes associated with the migration of electric charges in and the luminescence of crystal phosphors. Recently there have been a number of significant attempts at theoretical calculations and constructs. True, owing to the complexity of the problem these for the most part pertain to particular cases and are subject to various reservations and limitations. However, the value of such theoretical constructs lies in the fact that in them kinetic processes are related with quantities that have definite physical meaning and the numerical values of which can, at least in principle, be determined or checked by experiment. This represents a definite step forward as compared with setting down simple empirical formulas, which merely describe the course of the process, often without attaching any specific physical significance to the coefficients involved.

No less a significant achievement is the completion of numerous important experimental investigations of the kinetics and energetics of luminescence processes. These include investigation of the processes of stimulation and quenching under the influence of infrared light, investigation of transfer of electrons from one set of trapping levels to another during optical flashes, of natural decay and prolonged storage of excited phosphors, investigation of electron migration by resonance means and by movement of electrons and holes in the valence and conduction bands, study of the effect of exciton excitation and exciton energy transfer in crystals, and, finally, investigation of different forms of quenching that limit the luminescence yield and reduce the efficiency of transformation of energy from one form to another. All these interesting and practically important processes have been the subjects of attentive investigation in a number of Soviet laboratories.

Profound investigation of the kinetics and energetics of the luminescence of phosphors, which brings to light the simultaneous development and interaction of essentially different processes of luminescence, gives rise to certain difficulties in application of such fundamental concepts as the "luminescence yield", "mean luminescence persistence", and the like. In view of our new, more profound

understanding of the complex processes of luminescence in general and the luminescence of crystal phosphors in particular, these concepts require redefinition and redetermination of the conditions under which they are truly applicable.

Some particular classes of luminophors have attracted the special attention of investigators. These include alkali halide phosphors which are particularly attractive to experimenters in view of their regular lattice structure and the possibility of introducing into them diverse activators. There have been many studies of the luminescence of alkali halide phosphors by the members of the Tartu school and also in the laboratories in Irkutsk and Saratov. There have also been significant developments in the investigation of the properties of phosphors of the zinc sulfide, zinc selenide and zinc-cadmium sulfide types, which are particularly important from the technical standpoint.

One may also note the further extensive development of research in the field of electroluminescence. Aside from the practical results achieved in utilization of electroluminescence, one may point to significant advances in the theoretical treatment of the complex processes involved in electroluminescence.

Our conference is being held in Kiev; this is entirely natural. Kiev scientists have made great contributions in the field of luminescence. At today's meeting we shall hear two communications, one from Kiev University, the other from the Institute of Physics of the Ukrainian SSR Academy of Sciences.

The Optics Department of Kiev State University is headed by one of the outstanding students of the late S.I.Vavilov, Prof.A.A.Shishlovskii. The researches of Prof.Shishlovskii and his students have been devoted to luminescence and the absorption of electrolytes; they have elucidated the physical-chemical state of dissolved substances and the character of the complexes that form in solutions. The report which we shall hear today is devoted to the results obtained in Kiev State University in investigating the luminescence of semiconductors.

The second report, to be presented by M.T.Shpak, is concerned with the role of impurities in molecular crystals at low temperatures. In this report there are described some of the new results obtained at the Institute of Physics of the Ukrainian SSR Academy of Sciences in the laboratory of A.F.Prikhot'ko. We are all acquainted with the outstanding experimental work of the Institute of Physics of the Ukrainian Academy in the field of investigation of the structure of the luminescence spectra of organic crystals at low and superlow temperatures. Very important research on the luminescence and absorption of crystals is being carried out by S.I.Pekar and his co-workers.

We, the workers in the field of luminescence, gathered here from all ends of the Soviet Union, greet our dear hosts and wish our Kiev comrades success in their interesting and important research.

Before closing I would like to say a few words on further development in our scientific field in the future.

The development of the national economy in the coming five years poses problems, solution of which will be impossivle without extensive utilization of past and future achievements in the field of crystal phosphors. For example, it is proposed in the near future to convert most industrial enterprises to "fluorescent" illumination; fluorescent lighting will also be used increasingly in homes and offices. In fact, soon more than 60% of the light flux used for illumination will be provided by fluorescent lamps. Obviously, researchers must give great attention to the development of new and better phosphors for fluorescent lamps.

The imminent development of color television, the creation for various engineering purposes of efficient and specialized oscillographs, and improvements in radar equipment, all make it imperative to pay great attention to investigation of the phenomena involved in cathodoluminescence and to development of new cathodoluminophors.

No less important is the problem of electroluminescence. Cathodoluminophors and electroluminophors belong mainly to the class of zinc sulfide phosphors. Zinc sulfide from the practical standpoint is much more important than alkali halide crystals. In view of this I feel that it is essential to turn our attention to the investigation of the properties of zinc sulfide itself as well as cadmium sulfide and other similar substances with the same cations but different anions, to say nothing of the properties and behavior of phosphors with these sulfides as the base material. Although I fully understand the interest in alkali halide phosphors, I feel that in the immediate future we must concentrate our attention on zinc sulfide and other luminophors in its class.

For solution of the above mentioned technical problems there must be undertaken comprehensive theoretical investigations: we must investigate the composition of luminescence centers, their interaction with each other, the energy structure of phosphors, the different forms of energy transfer in phosphors, the kinetics of luminescence and transformation of absorbed energy, the nature of energy losses in phosphors and the phenomenon of quenching. We must also study the specific characteristics of the diverse processes involved in different forms of excitation: excitation by hard radiations, by electron beams and by electric fields.

Data obtained through such investigations will be important not only for the solution of practical and theoretical problems in the field of luminescence per se but will also influence progress in a number of allied branches of science, in particular the study of semiconductors.

The extensive development of scientific research institutes occupied with the problems of luminescence and the fact that work in this field is being undertaken in many Soviet institutions of higher learning gives reason to hope that we will see rapid progress in the investigation of luminescence and increase in our understanding of this phenomenon. I hope that physicists specializing in luminescence will apply all their energies to insure fulfillment of the Seven Year Plan both in the field of luminescence illumination and in the field of application of crystal phosphors in electron beam devices.

We shall next hear a number of extremely interesting communications as provided in the program of the conference.

I declare the Ninth Conference on the Luminescence of Crystal Phosphors open, and, in the name of the Organizing Committee, wish the Conference success in its work.

LUMINESCENCE OF SEMICONDUCTOR CRYSTALS WITH EXCITATION IN THE DISCRETE STRUCTURE REGION OF THE ABSORPTION SPECTRUM

- I.S.Gorvan', S.N.Rud'ko & A.A.Shishlovskii

At present many substances are known the crystals of which exhibit, near the long wavelength edge of the main absorption band, narrow bands associated with transitions to exciton states. Discrete structure in the long wavelength edge of the main absorption band is, as a rule, observed for crystals of semiconducting compounds that have a considerable internal photoelectric effect and, frequently, rather intense luminescence.[1,2]

Among such crystals is cuprous oxide. It was formerly believed[3] that when this crystal is excited in the intrinsic absorption region, its luminescence spectrum consists of one band in the near infrared. Comprehensive investigation[3,4] revealed, however, that this band is due to radiative exciton annihilation at Cu ion vacancies in the Cu_2O lattice. It was found later[5] that there are two more bands in the cuprous oxide luminescence spectrum, located on the short wavelength side of the first band. Our experiments show that the intensity of these new bands depends strongly on the conditions of synthesis and subsequent heat treatment of the samples.

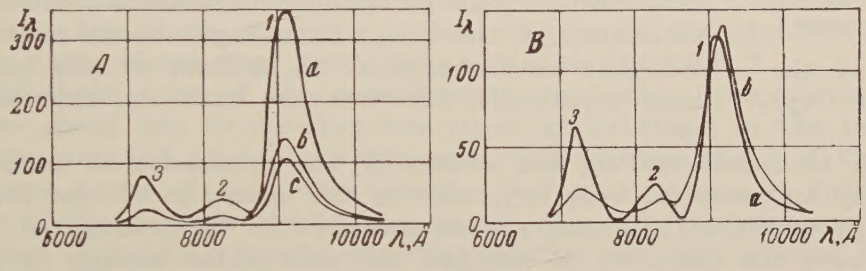

Fig.1. Luminescence spectra of Cu_2O recorded for specimens with different specific resistivities: A - T = 20°K: a) $\rho = 1.6 \cdot 10^3$ ohm cm, b) $1.68 \cdot 10^4$ ohm cm, c) $1.97 \cdot 10^6$ ohm cm; B - $\rho = 1.68 \cdot 10^4$ ohm cm: a) T = 20°K, b) T = 77°K.

Fig.1 shows the luminescence spectra at 20° and 77°K of crystals with different resistivities. The numerical values of the resistivity, peak wavelengths, peak separations and intensity ratios are given in the accompanying table.

Changes in the luminescence spectrum are accompanied by changes in the continuous absorption background near the luminescence band. The above mentioned properties indicate that impurity centers play a decisive role in the luminescence of Cu_2O crystals. The intensity ratio of bands 2 and 3 is the same for all crystals in which these bands are observed. Thus radiative transitions 2 and 3 belong to the same luminescence center, which is different and distinct from the center responsible for band 1.

	ρ, Ω cm	λ_1 max, Å	Δ_1, Å	λ_2 max, Å	Δ_2, Å	λ_3 max, Å	Δ_3, Å	$I_1:I_2:I_3$
At 20°	$1,6 \cdot 10^3$	9119	523	—	—	—	—	—
	$1,68 \cdot 10^4$	9098	510	8244	625	7200	435	3,5:1:2
	$1,97 \cdot 10^6$	9118	504	8270	505	7219	456	10,7:1:2
At 77°	$1,68 \cdot 10^4$	9159	585	8336	—	7276	~590	8,5:1:1,5

Bloem[5] showed that, according to the phase diagram, there exist in Cu_2O crystals at high temperatures two types of Schottky defects: copper vacancies and oxygen vacancies. These defects are frozen into the structure upon rapid cooling of the crystal. Band 1 is due to the copper vacancies, while bands 2 and 3 are due to the oxygen vacancies. The lattice defects may be either empty or occupied, depending on the temperature of the phosphor. This

explains the changes in the luminescence spectrum observed with increase of temperature. It will be evident from Fig.1,B that increase of the temperature results in a significant decrease in the intensity of the bands that are located in the short wavelength part of the spectrum (bands 2 and 3). In contrast, the intensity of band 1 exhibits a tendency to increase. This, in view of Tolstoi's[4] data on the kinetics of luminescence, gives reason to infer that in the range of low temperatures the decrease in the intensity of the short wavelength band with increasing temperature occurs not as a result of increase in the probability for nonradiative transitions, but mainly as a result of filling of defects with electrons. It must be recalled that Cu_2O is a hole type semiconductor, hence the normal states of the impurity centers in it must play the role of acceptors and be located near the valence band.

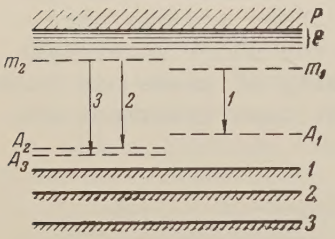

Fig.2. Diagram of the energy states in Cu_2O.

In the diagram of Fig.2 A_1 represents the ground state of the copper vacancies; A_2 and A_3 represent two levels belonging to the oxygen vacancies; m_1 and m_2 are the excited states of centers, the existence of which is indicated by the correlation between the luminescence intensity and the absorption near the luminescence bands. With increase of temperature the electrons first fill the lowest lying levels of the defects. Inasmuch as radiative transitions to occupied states are forbidden, the intensity of the short wavelength bands must obviously decrease as the crystal is heated; at the same time the long wavelength luminescence band can increase in intensity.

Fundamental to understanding the nature of the processes of luminescence and photoconductivity in semiconductor crystals is the question of the transfer of excitation energy to impurity centers when the crystal is irradiated in its intrinsic band, i.e., the question of whether the excitation energy is carried to the impurity centers by excitons or is transferred to them together with the carriers "falling" to the impurity levels m_1 and m_2 from the conduction band? At least a partial answer to this question can be found by analyzing the experimental data.

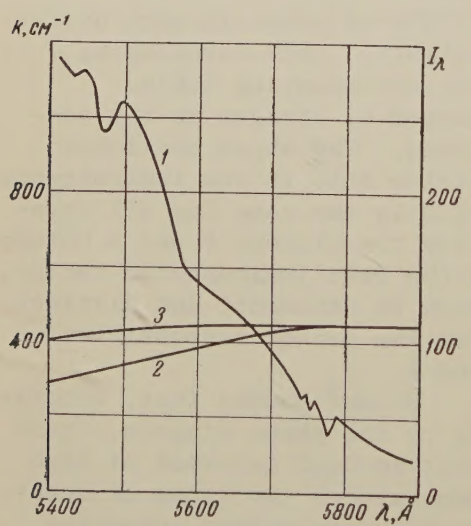

Fig.3. Cu_2O absorption spectrum (1) and luminescence excitation spectra for band 1 (2) and bands 2 and 3 (3).

The results of quantitative measurements of the absorption spectrum at liquid air temperature are shown in Fig.3 (curve 1). The presence of three exciton series in the spectrum of Cu_2O and of three continua accompanying these series has been discussed earlier[6]. Their origin is connected with the complex structure of the valence band, which consists of three subbands 1, 2 and 3 (Fig.2) that form as a result of splitting of the $3d$ shell of the Cu^+ ion owing to spin-orbit interaction.[7,8] We investigated the variation in the intensity of bands 1, 2 and 3 as a function of the wavelength with excitation in the region of the discrete structure of the absorption of the yellow and green exciton series at temperatures of liquid air, nitrogen and hydrogen. We used specimens of sufficient thickness to insure complete absorption of the incident light in the investigated spectral region. Curve 2 in Fig.3 gives the excitation function for band 1, curve 3 represents the excitation function for bands 2 and 3. It

will be evident that the excitation functions exhibit no structure corresponding to the exciton absorption structure, which indicates that the quantum luminescence efficiency is independent of the nature of excitation.[9]

This result can be understood if we assume either that the transfer of excitation energy to the impurity centers is accomplished with equal efficiency by current carriers and excitons or that the excitation of impurity centers is realized by excitons that are generated both directly in the process of light absorption and through the intermediary of the conduction band as a result of interaction between carriers of opposite polarity. We believe that the second mechanism is more likely. This follows from the fact that the exciton radius in Cu_2O is two or three orders of magnitude greater than the lattice constant[1], i.e., the electron-hole interaction begins at very large separations between the electron and hole. Assuming[10] that the exciton dimensions are commensurate with the cross section for capture of a free electron by a free hole, one can calculate the lifetime of a free electron-hole pair in Cu_2O; this for a dark hole concentration of 10^{14} cm^{-1} proves to be $< 10^{-9}$ sec. Hence in considering the kinetics of the excitation process one can replace band-band excitation by exciton excitation. The process of transformation of a free electron-hole pair into an exciton must be analogous to the process of attainment of thermodynamic equilibrium in the excited state of complex molecules. The interaction of excitons with luminescence centers may be regarded as ionization of excitons in the electric field of an empty defect, leading in the final analysis to the raising of the electrons to levels of the m_1 and m_2 type, where they must have a finite lifetime.[4]

Let us consider some of the consequences following from the above argument. To this end we shall try to develop the views of Tolstoi[4] on the temperature dependence of the excited state lifetime and luminescence yield of Cu_2O taking into account three types of impurity levels. For convenience we introduce the designations: n - the exciton concentration, N_1, N_2 and N_3 - the concentrations of the three types of defects in the crystal lattice per unit volume (in accord with the above said $N_2 = N_3 = N$), Np_1^-, N_2^- and N_3^- - the numbers of occupied levels, W_1, W_2 and W_3 - the probabilities of the excitons encountering an empty defect with resultant radiation, $W_{1\Phi}, W_{2\Phi}$ and $W_{3\Phi}$ - the probabilities of the excitons encountering an occupied acceptor with resultant photoionization, β - the probability for exciton decay or annihilation without encountering a defect, and kI - the volume density of excitation.

The number of electrons on the impurity levels depends on the temperature and is described by

$$N_1^- = C_1 e^{-\varepsilon_1/kT},\quad N_2^- = C_2 e^{-\varepsilon_2/kT},\quad N_3^- = C_3 e^{-\varepsilon_3/kT}.$$

If $W_{i\Phi} < W_i$, the temperature dependence of the exciton lifetime will be given by

$$\tau = \frac{1}{\beta + W_1 N_1 + (W_2 + W_3) N - (W_1 - W_{1\Phi}) C_1 e^{-\varepsilon_1/kT} - (W_2 - W_{2\Phi}) C_2 e^{-\varepsilon_2/kT} - (W_3 - W_{3\Phi}) C_3 e^{-\varepsilon_3/kT}}. \qquad (1)$$

This τ is not the afterglow duration, for calculation of which one must also take into account the finite lifetime of the electrons on the excited levels of the lattice defects. The electron lifetime must, however, in general affect the temperature dependence of τ. Experimental investigation of the temperature dependence of the afterglow time for band 1 at low temperatures shows three inflections or humps in the curve[4], which is in qualitative agreement with the presence of three exponentials in the denominator of (1).

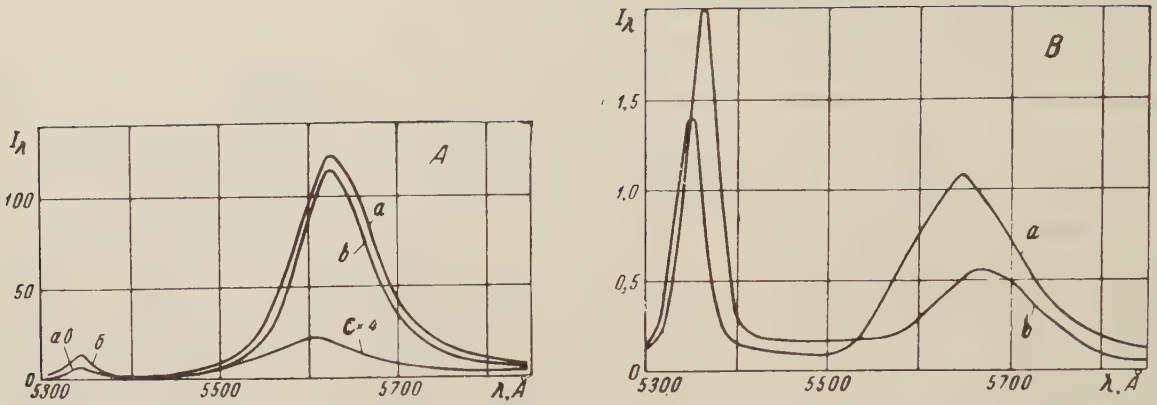

Fig.4. Luminescence spectra of HgI_2 at low temperatures obtained for specimens prepared in different ways. A - T = 20°K, B - T = 77°K: a) crystal prepared by sublimation (first batch), b) crystal prepared by sublimation (second batch), c) crystal grown from solution.

The exciton yield for the i-th band will be given by the formula

$$\eta_i = \frac{i_{\infty i}}{kI} = \frac{W_i (N_i - N_i^-) n_\infty}{kI} = \frac{W_i \left(N_i - C_i e^{-\varepsilon_i/kT}\right)}{\beta + W_1 N_1 + (W_2 + W_3) N - (W_1 - W_{1\Phi}) C_1 e^{-\varepsilon_1/kT} - (W_2 - W_{2\Phi}) C_2 e^{-\varepsilon_2/kT} - (W_3 - W_{3\Phi}) C_3 e^{-\varepsilon_3/kT}}, \quad (2)$$

where $i = 1,2,3$. Like Eq.(1), Eq.(2) does not pertain to the afterglow, but characterizes the efficiency of excitation by the excitons of the corresponding luminescence centers, which must naturally affect the luminescence efficiency. The temperature dependence of the luminescence efficiency for band 1 was investigated by Karkhanin & Lashkarev[3] who found an empirical formula fitting the experiment curve, the form of which is similar to Eq.(2).

Thus the deductions following from the above interpretation of the origin of the luminescence bands of Cu_2O not only agrees with experiment but also serves to explain a number of experimental results that were hitherto unclear.

We also investigated the luminescence and absorption characteristics of a number of other crystals. Fig.4 shows the energy distribution in the region of the two shortest wavelength luminescence bands of HgI_2, recorded for specimens prepared in different ways. The luminescence spectrum of HgI_2 was investigated earlier by Arkhangel'skaya & Feofilov[2]. Hence here we will give only the new data obtained in the present experiments. We note that for specimens prepared in different ways, in addition to variation in the wavelength of the peaks[2], there is observed noticeable variation in the widths and relative intensities of the bands. In contrast to the case of Cu_2O, in the case of HgI_2 there is observed increase in the intensity of the short wavelength band with increase of the temperature from 20 to 77°K, while the intensity of the long wavelength band decreases. The characteristics of the luminescence of such crystals as CsD, ZnS and PbI_2 are similar to those of HgI_2. In accord with many other authors[2,5,12,13], we assume that all the luminescence centers in these crystals are of the same type and that they are associated with Schottky or Frenkel defects. Numerous investigations[14,15] of the luminescence and photoconductivity of CdS and similar crystals show that in the region of exciton absorption the structure of the excitation spectrum is correlated with the absorption structure. The presence of this structure

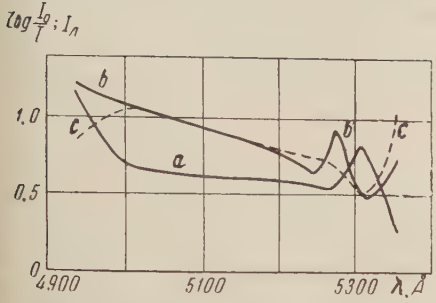

Fig.5. Absorption spectrum (a) and excitation spectrum of HgI_2 at T = 20°; experiment (b) and calculated (c).

in the spectra of crystals thick enough to insure complete absorption indicates that the luminescence efficiency and photoconductivity depend on the wavelength λ of the exciting light. Some authors[16] have been inclined to attribute this dependence to a variation in the nature of the absorption with change in λ.

We undertook a more thorough analysis of the origin of the structure in the excitation spectra of crystals of the CdS and HgI_2 type. A significant fact is that the luminescence intensity and photoconductivity of these crystals, in contrast to those of Cu_2O crystals, exhibit a linear dependence on the excitation intensity.[2,17]

Let i be the intensity of the given luminescence band, η - a constant, I_0 the intensity of the incident exciting beam, and γ the exponent. If γ is independent of I_0, the intensity of the luminescence emitted by a unit volume at depth x in the crystal plate will be given by the equation

$$\frac{di}{dx} = \eta\left(\frac{dI}{dx}\right)^{\gamma}. \tag{3}$$

Inasmuch as $\frac{dI}{dx} = kI_0e^{-kx}$, we have

$$\frac{di}{dx} = \eta k^{\gamma} I_0^{\gamma} e^{-\gamma kx}. \tag{4}$$

If the thickness of the crystal is d, the total radiation flux will be

$$i = \eta k^{\gamma} I_0^{\gamma} \int_0^d e^{-\gamma kx} dx = \eta \frac{k^{\gamma-1}}{\gamma} I_0^{\gamma}(1 - e^{-\gamma kd}). \tag{5}$$

In the limit as $d \to \infty$, we will have

$$i = \eta \frac{k^{\gamma-1}}{\gamma} I_0^{\gamma}. \tag{6}$$

For $\gamma = 1$, which, according to Eq.(6) corresponds to linear variation of the luminescence intensity with the degree of excitation, the luminescence intensity should not depend on the absorption coefficient. This case is realized in Cu_2O, all the luminescence bands of which exhibit a linear dependence on the degree of excitation.

For $\gamma > 1$ and with I_0 being independent of λ, the absorption peaks will correspond to the maxima of the excitation function, while for $\gamma < 1$ the absorption peaks will correspond to minima of the excitation function. The $\gamma > 1$ case is illustrated by HgI_2 crystals, the absorption and excitation spectra for which are given in Fig.5. It will be seen that in this case extrema in the absorption curve approximately correspond to extrema in the excitation curve. We carried out a comparison of the measured excitation function with the excitation function calculated on the basis of Eq.(6). The formula used for our calculations was of the form

$$\frac{i_1}{i_j} = \left(\frac{D_1}{D_j}\right)^{\gamma-1} \cdot \left(\frac{I_{01}}{I_{0j}}\right)^{\gamma}, \tag{7}$$

where $D = \log I_0/I$, and the subscript j pertains to the wavelength λ_j. Measurements of the dependence of the luminescence intensity on the excitation intensity for the investigated luminescence band yielded $\gamma = 1.62$. The results of calculations for $\lambda_1 = 5068$ A and $D_1 = 0.628$ are shown in Fig.5 by the dashed line (curve c).

Complete fit of the experimental to the calculated curve was not obtained. Possibly the discrepancy is due to the fact that the absorption and excitation spectra were measured for crystals prepared in different ways.

Thus the results obtained show that the structure of the excitation spectrum cannot be correlated fully with the nature of the absorption.

References

1. E.F.Gross, Usp.fiz.nauk, 63, 3 (1957).
2. V.A.Arkhangel'skaya & P.P.Feofilov, Optika i spektroskopiya, 2, 1 (1957).
3. Yu.I.Karkhanin & V.E.Lashkarev, Doklady AN SSSR, 97, 1007 (1954).
4. N.A.Tolstoi and others, Optika i spektroskopiya, 2, No.1 (1957); 2, No.2 (1957). (Trans.Optics & Spectroscopy.)
5. J.Bloom, Philips Research Reports, 13, 2 (1958).
6. I.S.Gorban', Ukr.fiz.zh. (Ukrainian Physics Journal), No.2 (1960); Optika i spektroskopiya, 9,6 (1960). (Trans.Optics & Spectroscopy.)
7. R.J.Elliott, Phys.Rev., 108, 1384 (1957).
8. S.A.Moskalenko, Dissertation, Kiev, 1960.
9. I.S.Gorban', S.N.Rud'ko & A.A.Shishlovskii, Ukr.fiz.zh. (Ukrainian Physics Journal), 5, 3 (1960).
10. A.Rose, in "Problemy fiziki poluprovodnikov" (Problems in the physics of semiconductors), 1957.
11. D.V.Chepur, Dissertation, Kiev State University, 1959.
12. G.Wendel, Fortschr.Phys., 1, 45 (1953).
13. R.J.Collins, J.Appl.Phys., 30, 8, 1135 (1959).
14. V.L.Broude and others, Transactions of the All-Union Conference on the Optical and Photoelectric Properties of Semiconductors, Kiev, 1957.
15. E.F.Gross, A.A.Kaplyanskii & B.V.Novikov, Doklady AN SSSR, 110, 5 (1956). (Trans.Doklady.)
16. V.L.Broude, V.V.Eremenko & V.S.Medvedev, Zhur.tekh.fiz., 28, 2261 (1958). (Trans.Soviet Physics - Technical Physics.)
17. A.A.Vuylsteke & Y.T.Sihvonen, 113, 40 (1959).

DISCUSSION

N.A.Tolstoi: Cuprous oxide, although it is one of the most thoroughly and extensively investigated materials, still has "surprises" for the investigator. Moreover in many earlier investigations one finds strange "details" that are ignored or glossed over. Actually they are treated as "details" simply because nothing definite could be said about them. Such facts, for example, are the temperature dependence of the brightness and persistence of luminescence of cuprous oxide. An important and interesting attempt to find an explanation for these obscure phenomena has been made in the work reported on by Gorban'. The results appear to be convincing, but in my opinion for definitive judgment one must carry out experiments in at least two directions.

1. One must investigate specimens annealed at high temperature (of the order of 1070°). Such specimens, as we discovered, yield a negative temperature quenching in the vicinity of 150°. The relaxation regularities here are also paradoxical. Survey of the published data shows that in "normal" specimens there are always observed to a greater or lesser extent the properties of "abnormal" specimens. It would be desirable to determine whether these anomalous features are the same as those reported on by Gorban'.

2. One should carry out a parallel investigation of the photoelectric and luminescence effects. Of great interest is the question of photoconductivity in cuprous oxide specimens in the state of negative temperature quenching. It would

seem that the absorbed energy that is not expended on luminescence should yield some sort of special "cold" photoconductivity. If this is not the case, then one must find some other explanation for the strange effect of "quenching by cold". It would be expedient to carry out the photoelectric measurements of "cold" photoconductivity by the capacitor procedure with single light pulse excitation.

* * * * * * *

ROLE OF IMPURITIES IN THE LUMINESCENCE OF MOLECULAR CRYSTALS AT LOW TEMPERATURES

(Review of work performed at the Institute of Physics of the Ukrainian SSR Academy of Sciences)

- M.T. Shpak

Introduction

The luminescence properties of molecular crystals are widely utilized in science and engineering. The question of the nature of their luminescence, however, still remains open. Numerous investigations (a review of recent studies in the field will be found in Ref.1) show that the luminescence of molecular crystals is, as a rule, connected with defects of the crystal lattice, which may be formed by minor extraneous additives or impurities, that are impossible to eliminate by the usual purification procedures, or other disturbances of the crystal lattice, for example, dislocations, which are always present in actual crystals. Thus it has been established that the long wavelength luminescence of phenanthrene is due to anthracene impurity[2], the luminescence of tolan and dibenzyl to stilbene impurity[3,4] the luminescence of naphthalene to β-methylnaphthalene and β-naphthol impurities[5-8]. Only in the case of crystalline naphthalene (see below) has there been observed luminescence that in view of its behavior and regularities may be termed true intrinsic luminescence of the crystal. Discovery of these facts stimulated a number of special investigations of the spectral properties of molecular crystals containing impurities.

For purposes of investigation at the Institute of Physics there were chosen a) simple polynuclear aromatic compounds (diphenyl, terphenyl, quaterphenyl, etc.), b) compounds with benzene groups linked by carbon atoms extraneous to the ring (dibenzyl, stilbene, etc.), c) compounds with condensed benzene groups (naphthalene, anthracene, phenanthrene, etc.), and d) derivatives and deuterated forms of some of the above substances. The introduced impurities were substances of the same classes.

Below we shall deal only with the spectra of substances dissolved in crystalline solvents.

The investigations were carried out, as a rule, on single crystals. In most cases the crystals were grown from the melt in special quartz cells ($d \approx 1\text{-}300\ \mu$). For obtaining the absorption spectra of the crystals in polarized light the experimenters used a microprojector consisting of a quartz lens, mounted near the sample, and two polarizers, mounted on the optical bench of the spectrograph. One of the polarizers was usually a large crystal of colorless calcite, which made it possible to project two light beams with mutually perpendicular electric vectors on the slit of the spectrograph. In investigating the luminescence spectra the analyzer was a Glan-Thomson prism, which was mounted in front of the spectrograph slit. In the case of measurements at liquid nitrogen temperature ($77^{\circ}K$) or at

liquid hydrogen temperature (20.4°K) the specimens were placed in a special metallic cryostat. Unless otherwise noted, the data given below pertain to the results obtained at liquid hydrogen temperature. The concentrations of the initial solutions were determined from the spectra of the solutions in ethyl alcohol; the concentrations in the crystals were evaluated qualitatively from the absorption spectra of single crystals of the same thickness.

1. General Characteristics of Molecular Crystal Spectra

The absorption bands of strongly absorbing compounds (stilbene, tolan, anthracene, etc.) are relatively wide (50-100 cm^{-1}) even at liquid hydrogen temperature. In contrast to this, the absorption spectra of these substances as impurities usually consist of very narrow weakly polarized[9] bands, which form series analogous to the series observed in the absorption spectra of vapors of the corresponding substances. This structure of the spectra makes it possible to carry out electrovibrational analyses thereof. Such analysis, in particular, shows that the vibrational frequencies of one and the same molecule in different solvents are nearly the same (for example, stilbene in dibenzyl and stilbene in tolan; naphthacene in dibenzyl, in diphenyl, in terpenyl and in tolane, etc.). The polarization of the impurity absorption bands shows that the impurity molecules incorporated into the host crystal lattice are generally regularly oriented relative to the crystallographic axes. In some cases the impurities form complex molecules or even oriented or nonoriented crystallites in the solvent crystal.

2. Nature of Impurity Centers

The spectra of impurity crystals are generally multiplet in character, i.e., they can be represented as the result of superposition of several series, the initial bands of which coincide in the absorption and luminescence spectra. The intensity of individual series in the luminescence spectra vary independently with variation of the impurity concentration, the temperature and the conditions of preparation of the crystals. Of particular interest are the spectra of monosubstituted derivatives of naphthalene in naphthalene.[8] Each of these spectra consists of two identical band series with corresponding members shifted a constant interval $\Delta\nu$ relative to each other: $\Delta\nu$ = 355 cm^{-1} for α-methylnaphthalene, 137 cm^{-1} for β-naphthol, and 376 cm^{-1} for α-naphthol. The vibrational frequencies of the series generally agree with the frequencies from the Raman spectra of the corresponding substances. In some cases increase of the temperature (α-methylnaphthalene in naphthalene) or increase of the concentration (β-naphtol in naphthalene) leads to the disappearance of one or more series. This behavior of the series indicates that upon introduction of impurity molecules into a solvent crystal there form spatially separated impurity centers of different types. In the case of solutions of mono- and disubstituted derivatives of naphthalene in naphthalene the nature of the impurity centers can be correlated with the structure of the solute and solvent substances. Inasmuch as the molecules of monosubstituted naphthalene derivatives do not have an inversion center, which is present in the naphthalene molecule, according to Kitaigorodskii[10,11], it may be assumed that the luminescence centers are complicated complexes consisting of at least two molecules, which in conjunction have an inversion center. A similar effect is not observed in the case of solution in naphthalene of molecules possessing an inversion center. The spectra of 2,6-dimethylnaphthalene in naphthalene[12], of anthracene in naphthalene[13], of naphthacene in naphthalene[14], of naphthalene in deuteronaphthalene[12] and of naphthalene in durene[15], all consist of single series.

The quantum mechanical theory of absorption and luminescence of molecular crystals in which the impurity molecules are arranged in pairs with the separation between pairs assumed to be much greater than the separation between the molecules of a pair, predicts a number of effects[16] (in particular, strong polarization of the bands in the absorption and luminescence spectra of the impurities) which still require experimental verification.

In the case of solutions of stilbene in tolane the differences in the structure of different centers are apparently connected with the fact that the stilbene molecules, which have a bend in the bridge linking the benzene rings, can readily deform in the host lattice, which leads to the formation of several different types of incorporated molecules. An interesting distinctive feature of the absorption of stilbene in tolane is that there are observed two types of absorption spectra differing markedly from each other as regards polarization of individual corresponding bands.

3. Role of Defects

In the spectra of a number of a number of crystals there are observed at the long wavelength edge of the intrinsic absorption - sometimes at a distance of several hundred cm^{-1} - very weak bands of variable intensity and frequency, which coincide in frequency with the shortest wavelength bands of the corresponding luminescence spectra. In the spectrum of anthracene there are observed six such bands[17], and in the spectrum of phenanthrene three bands[18]. In the spectrum of stilbene[19] at the edge of the intrinsic absorption there are evinced over 40 weak bands, most of which apparently belong to impurities. The shortest wavelength group of bands is analogous to the bands that are observed in the spectra of anthracene and phenanthrene. Noteworthy features of these bands are that they have the same polarization relationship in the absorption and luminescence spectra[20,21] and are the initial bands of independent series in which one can distinguish the characteristic frequencies of the intramolecular vibrations of these substances. The variability of the individual bands and series is enhanced by heat treatment of the stilbene crystals. The above-mentioned attributes of the spectra cannot be explained by transitions in an ideal crystal lattice and must therefore be connected with the presence of defects in actual molecular crystals.

4. Mirror Symmetry

The bands in the absorption and luminescence spectra of impurities, corresponding to both purely electronic transitions and to combinations thereof with molecular vibrations are almost always accompanied by groups of satellite bands of different intensity. Careful analysis of these bands in the region of the band of the purely electronic transition of anthracene impurity in 9,10-dihydroanthracene[22,23] showed that there obtains mirror symmetry in the arrangement of the satellite bands relative to the purely electronic transition band. This indicates that the satellite bands belong to discrete impurity centers of the same type and are the result of coupling between intramolecular transitions and vibrations of the solvent lattice. Such coupling may occur either with phonons or with local vibrations, arising as a result of introduction of impurity molecules into the host lattice.

Separation of the lattice modes is hampered by the fact that the bands corresponding to them are separated from the nonphonon transition bands by distances that do not correspond to the limiting frequencies of the crystal modes. Hence, utilization of the fact of mirror symmetry in the location of the satellite bands is at present the only spectral method for distinguishing lattice vibrations in the spectra of molecular crystals containing impurities.

5. Polarization of the Absorption Bands

Strongly polarized absorption bands that are similar in appearance to the exciton absorption bands of pure crystals were first observed by Davydov[9] in the absorption spectrum of stilbene in tolane[4]. It is significant that the most intense series in the complex luminescence spectrum of stilbene in tolane begins with a band that coincides in frequency with the strongly polarized band in the absorption spectrum. Later, sharply polarized bands were observed in the absorption spectra of other substances: anthracene in 9,10-dihydroanthracene[23], naphthacene in stilbene, tolane and para-ditolyl[24].

Increase of the impurity concentration usually leads to smearing out and broadening of the bands in the impurity absorption spectrum. In the case of solutions of naphthacene in tolane and stilbene in para-ditolyl increase of the impurity concentration leads to the appearance of sharply polarized bands in the spectra. Possibly this effect is connected with the formation of superstructure in these crystals at high impurity concentrations.

Of particular interest is the case of mutual solutions of ordinary hydrocarbons with their deuterated forms. In investigating the absorption spectra of mixed single crystals of isotopically substituted benzenes it was found[25] that the splitting of the pure electronic transition into two sharply polarized bands, peculiar to the spectra of pure crystals of benzene and hexadeuterobenzene, persist in the spectra of the mutual solutions with differently deuterated molecules. The magnitude of the splittings are proportional to the intensities of the corresponding transitions and are strongly dependent on the concentration of the responsible components. This behavior of the spectra indicates that in the investigated substances there form special states that might be called impurity exciton states.

The origin of the sharply polarized bands in the absorption spectra of impurities in organic crystals has not been fully clarified. Only the case when the impurity absorption bands are located near the intrinsic absorption edge has been considered theoretically.[26] According to this theory, one cannot speak of absorption of light by only impurity molecules in cases when the excited levels of these molecules are close to the exciton bands of the solvent crystal: light in this case is actually absorbed by a whole group of molecules which includes the impurity molecule and the neighboring host crystal molecules. This can lead to either increase or decrease in the intensity of absorption of light by the impurity molecule as compared with its absorption in the isolated state. Under certain conditions, i.e., with excitation of certain levels, the impurity absorption bands will be evinced only in one of the components of the spectra, that is, they will be sharply polarized.

6. Effect of Additional Impurities

When there is introduced into a molecular crystal already containing some impurity a new, second impurity, the spectrum of the first impurity usually undergoes significant changes. It has been shown, for example, in the case of naphthacene in dibenzyl[27-30] (the concentration of the components comprising the mixed crystal was varied from 0 to 100%; the naphthacene concentration was of the order of 0.01 to 0.05% by weight and remained constant) that the introduction into this system of stilbene or tolane impurity in increasing concentration leads to shift, splitting, and smearing out of the bands in the absorption and luminescence spectra of naphthacene and also to changes in the degree of their polarization. Similar behavior has been observed for other substances, as for example, naphthacene

in the stilbene-tolan system[30].

These changes are connected with the fact that increase in the concentration of the additional impurity leads to changes in the crystal field about the molecules of the first impurity owing to deformation of the solvent lattice. Essentially the additional impurity leads to the formation of a new, different solvent crystal. This fact must be taken into account in attempting to identify impurities in crystals from their absorption and luminescence spectra. The above arguments also pertain to some extent to the case when the concentration of one and the same impurity is increased, inasmuch as increase in the number of lattice disturbances about the impurity molecules as a result of introduction of additional molecules has the effect of altering the crystal lattice in the neighborhood of the earlier incorporated impurity molecules.

7. Nature of the Luminescence of Molecular Crystals

In order to understand the nature of the luminescence of molecular crystals one must first determine whether these crystals have an intrinsic luminescence. This problem proves to be rather difficult inasmuch as all known methods of purification are not 100% effective, and there need only be some hundredths or even thousandths of a percent of impurity in the host crystal for emission to occur at low temperatures from the low-lying excited levels of the impurity molecules. As noted above, the familiar luminescence spectrum of crystalline naphthalene is actually due to the presence in it of β-methylnaphthalene impurity. In the luminescence spectrum of crystalline naphthalene purified of β-methylnaphthalene by the method of zone melting, in addition to impurity luminescence there was detected[6] a weak band polarized in the *a* direction (A band) with $\nu = 31\ 480 \pm 3\ cm^{-1}$, which is virtually the frequency of the strongly polarized A_1 band in the absorption spectrum of the crystal[31]. The intensity of the A band increases with increasing purity of the samples. At 77°K there appears in the luminescence spectrum a new band with $\nu = 31\ 623 \pm 5\ cm^{-1}$ (B-band) which is polarized in the *b* direction and coincides in frequency with the sharply polarized B_1 band in the absorption spectrum at 77°K. Further increase of the temperature leads to smearing out and partial depolarization of the A and B bands and also to the appearance of two short wavelength bands, one of which is located in the region of the sharply polarized A_2 and B_2 absorption bands of naphthalene.

If we assume that the strongly polarized A_1 and B_1 bands are components of Davydov splitting of the 0—0 transition[32], these results can be explained as follows. The light energy absorbed by the crystal is transferred by electrons migrating through the crystal from the host lattice to the impurity molecules, where radiation occurs. With increasing purity of the crystal the probability of excitons encountering impurity molecules obviously decreases, which leads to the appearance of luminescence associated with transitions from exciton states to the ground state, i.e., to the appearance of a sharply polarized intrinsic or exciton luminescence of the crystal. The temperature dependence of this luminescence can be explained on the basis of the hypotheses advanced by Broude, Prikhot'ko & Rashba[1].

Conclusions

Interpretation of the above described experimental data is far from complete. So far there has been no theoretical investigation of the influence of the crystal lattice on the spectra of the molecules incorporated in it. At present, only a few of the observed effects can be reliably explained and at that, for the most

part, only qualitatively. In particular, it may be asserted that the role of excitons in molecular crystals at low temperature reduces mainly to transfer of the excitation energy from the host lattice to impurity centers and defects. On the other hand, so far it has proved impossible to establish any consistent dependence of the solute (impurity) spectra on the crystal lattice and properties of the solvent, although there have been accumulated extensive data on the spectra of impurity crystals, including data gained from special investigations of spectra of solutions of naphthacene and anthracene in crystals of organic compounds the properties of which are known to vary in a regular manner (polyphenol series).[33,34]

In conclusion, it may be noted that investigation of the absorption and luminescence spectra of molecular crystals incorporating extraneous molecules in their lattice yields valuable information on the energy structure of molecular impurities, on the character of incorporation of impurity molecules, on the properties of solvent crystals and, mainly, on the nature of the luminescence of an extensive class of organic crystals. Such data can be utilized for increasing the efficiency of organic luminophors and scintillation counters.

Institute of Physics,
Academy of Sciences of the Ukrainian SSR

References

1. V.L.Broude, A.F.Prikhot'ko & E.I.Rashba, Usp.fiz.nauk., 67, 99 (1959). (Trans.Soviet Physics - Uspekhi.)
2. A.F.Prikhot'ko, Izv.AN SSSR, 15, 608 (1951).
3. A.F.Prikhot'ko & M.T.Shpak, Optika i spektroskopiya, 4, 17 (1958).
4. A.F.Prikhot'ko & M.T.Shpak, Ibid., 4, 30 (1958).
5. A.F.Prikhot'ko & M.T.Shpak, Ibid., 6, 119 (1959). (Trans.Optics & Spectroscopy.)
6. M.T.Shpak & E.F.Sheka, Ibid., 8, 66 (1960). (Trans.Ibid.)
7. M.T.Shpak & E.F.Sheka, Izv.AN SSSR, Ser.fiz., 24, 553 (1960). (Trans. Bulletin, 24, 559.)
8. M.T.Shpak & E.F.Sheka, Optika i spektroskopiya, 9, 57 (1960). (Trans. Optics & Spectroscopy.)
9. A.S.Davydov, Teoriya pogloshcheniya sveta v molekulyarnykh kristallakh (Theory of absorption of light in molecular crystals), Kiev, 1951.
10. A.I.Kitaigorodskii, Kristallografiya, 2, 456 (1957). (Trans.Crystallography.)
11. R.M.Myasnikova & A.I.Kitaigorodskii, Ibid., 3, 160 (1958). (Trans.Ibid.)
12. M.T.Shpak & E.F.Sheka, Izv.AN SSSR, Ser.fiz. (In press). (Trans.Bulletin.)
13. J.W.Sidman, J.Chem.Phys., 25, 115 (1956).
14. J.W.Sidman, Ibid., 25, 122 (1956).
15. D.S.McClure, Ibid., 22, 1668 (1954).
16. A.F.Lubchenko, Optika i spektroskopiya (In press).
17. A.F.Prikhot'ko & I.Ya.Fugol', Ibid., 4, 335 (1958).
18. A.F.Prikhot'ko & I.Ya.Fugol', Ibid., 5, 582 (1958).
19. A.F.Prikhot'ko & I.Ya.Fugol', Ibid., 7, 35 (1958). (Trans.Optics & Spectroscopy.)
20. I.Ya.Fugol', Ukr.fiz.zh. (Ukrainian Physics Journal), 3, 40 (1958).
21. I.Ya.Fugol' & S.Z.Shul'ga, Optika i spektroskopiya, 5, 34 (1958).
22. V.N.Vatulev, Ibid., 8, 727 (1960). (Trans.Optics & Spectroscopy.)
23. V.N.Vatulev, Ukr.fiz.,zh. (Ukrainian Phys.Jour.), 5, 40 (1960).

24. A.F.Prikhot'ko & A.V.Solov'ev, Ibid., 4, 229 (1959).
25. V.L.Broude & M.I.Onoprienko, Optika i spektroskopiya (In press).
26. E.I.Rashba, Ibid., 2, 568 (1956).
27. A.F.Prikhot'ko & A.V.Solov'ev, Ukr.fiz.zh., 4, 92 (1959).
28. A.V.Solov'ev, Optika i spektroskopiya, 6, 258 (1959). (Trans.Optics & Spectroscopy.)
29. A.V.Solov'ev, Izv.AN SSSR, Ser.fiz., 24, 737 (1960). (Trans.Bulletin 24, 740.)
30. A.V.Solov'ev, Ukr.fiz.zh. (In press).
31. A.F.Prikhot'ko, Zhur.eksp.i teor.fiz., 19, 282 (1949).
32. D.S.McClure, J.Chem.Phys., 23, 1575 (1955).
33. A.V.Solov'ev, Ukr.fiz.zh. (Ukrainian Physics Journal), 4, 616 (1959).
34. A.V.Solov'ev, Ibid. (In press).

DISCUSSION

A.F.Prikhot'ko: The method of investigating the spectra of complex organic molecules in solution at low temperatures has gained general acceptance. Its further development - the use of crystals as the solvent - has led to a number of new discoveries and improved analytic procedures.

In experiments on crystals with impurities at very low temperatures there was discovered the effect of common resonance excitation of the impurity and the crystal and it was found that the emission of radiative energy at defects and impurities frequently masked the intrinsic luminescence of the crystal. Experiments have demonstrated that there occur substantial changes in the spectrum with increase in the number of impurities.

In detailed investigations of the spectra of crystals containing similar molecules as impurities (for example, deuteroderivatives of benzene in the benzene lattice or in the hexadeuterobenzene lattice) there has been demonstrated the existence of an "impurity" exciton - excitation of the impurity with the attributes characteristic of exciton excitation.

The method of investigating the luminescence of crystals with impurities at low temperatures is useful and important for studying processes in crystal phosphors and gaining an understanding of the mechanism of their luminescence.

PIEZOSPECTROSCOPIC EFFECT IN ANISOTROPIC CENTERS IN CUBIC CRYSTALS

- A. A. Kaplyanskii

Complex anisotropic centers constitute a common type of defect in cubic crystals. The anisotropy, which means that the center has a preferred direction, may be due either to anisotropy of the structure of the center encompassing several sites (multiple defects of the type of complex color centers in alkali halide crystals) or to anisotropy of position, when a "simple" center is located in the lattice at a point characterized by a lower degree of symmetry (for example, in an interstitial space or in a site with noncubic point symmetry). In such cases, owing to regularity of the lattice, the center axes N are oriented along several symmetry axes of the crystal ($3C_4$, $4C_3$ or $6C_2$). From the optical standpoint anisotropic centers behave like correspondingly oriented linear (π) or angular (σ) dipole oscillators, either electric (π_e, σ_e) or magnetic (π_m, σ_m). Anisotropic centers in cubic crystals are associated with a number of interesting optical effects, in particular, with polarized luminescence and anisotropic photochemical transformations (see review by Feofilov[1]).

The present report is devoted to consideration of a new effect peculiar to anisotropic centers in cubic crystals; we call this the "piezospectroscopic effect". In a sense this effect sharply limns the distinctive characteristic of such anisotropic centers, which means that investigation of the effect can yield valuable information on the centers. The piezospectroscopic effect may be briefly described as follows: when the crystal is subjected to appropriately directed uniaxial compression (or elongation), there appears in the spectrum of the centers a reversible splitting of the characteristic bands into several polarized components; the character of the splitting is essentially anisotropic and depends on the strain direction. The cause of this effect is to be sought in the different change in the energy level scheme of the given group of centers, which being oriented in the lattice in several ($12/n$) equivalent crystallographic directions C_n, are located in different ways relative to the deformation axis P. Thus each of the components of splitting in the spectrum of a unidirectionally stressed crystal is associated with a group (or number of groups) of centers oriented in a certain fashion relative to the compression axis.

Earlier[2,3] we carried out an analysis and calculation of the principal characteristics of the band splitting in the spectra of anisotropic centers: the multiplicity, the polarization of the components and the magnitude of the splittings for cases of elastic uniaxial compression of the crystals along different order symmetry axes: $P \parallel C_4$, $P \parallel C_3$ and $P \parallel C_2$ (the levels of the individual centers were assumed to be nondegenerate). The multiplicity of the splitting can readily be determined from purely geometric considerations, since it is equivalent to the number of different positions of the axes of the centers having a given orientation relative to the deformation axis. As our calculations showed, the multiplicity of the splitting for $P \parallel C_4$, $P \parallel C_3$ and $P \parallel C_2$ is wholly determined by the orientation of the centers in the lattice. Evaluation of the polarization was based on calculating for each of the splitting components of the electromagnetic field due to the group of centers corresponding to the given component, the centers being modeled by classical oscillators of different types. The state of polarization of the splitting components is determined in all cases exclusively by the multipolarity of the optical (radiative) transitions corresponding to the spectrum bands. Calculations of the magnitude of the splittings were carried out on the assumption that the shift of the levels (or change in the transition energy) in individual centers in an elastically strained lattice can be represented in the form of a linear function of the components of the lattice stress (or strain) tensor. It follows from considerations of symmetry that this dependence for $N \parallel C_4$

and $N \parallel C_3$ contains two and for $N \parallel C_2$ three independent coefficients characterizing the interaction of the centers with the lattice. Whence we were able to obtain the magnitude of the splittings of the bands for any given deformation of the crystal and in particular for uniaxial compression, expressing these splittings in terms of two ($N \parallel C_4, N \parallel C_3$) or three ($N \parallel C_2$) "piezospectroscopic" parameters. Thus investigation of the splittings of the spectrum bands of anisotropic centers under uniaxial compression of the crystals allows of unambiguous determination of the orientation of the centers, the multipolarity of the optical transitions in them and the "piezospectroscopic" parameters, i.e., allows of obtaining the data essential for understanding the structure of the center, the quantum scheme of its levels, and the character of the interaction of the center with the lattice.

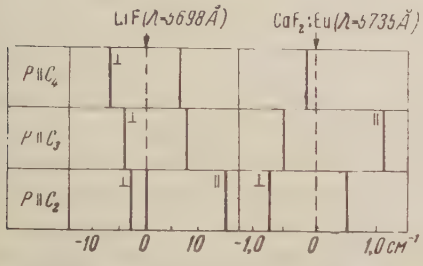

Diagram of polarized splitting of the spectrum bands of anisotropic centers in uniaxially stressed LiF and CaF_2:Eu crystals.

For purposes of experimental investigation[4,5], we used x-irradiated LiF crystals, which therefore contained luminescent color centers that have narrow absorption[6] and emission[7] lines in the visible part of the spectrum, and CaF_2 crystals activated with trivalent rare earth ions TR^{3+}, which have line spectra[8]. We studied the effect at 77°K of uniaxial compression along the symmetry axes C_4, C_3 and C_2 as regards the spectra of the crystals observed in the direction L perpendicular to the compression axis P. It was established that as a result of deformation a number of lines in the luminescent spectra of LiF, CaF_2:Eu and CaF_2:Sm undergo reversible splitting into a number of polarized components, and that the character of the splitting depends significantly on the direction of compression. The variation of the magnitude of the splitting with the uniaxial compressive stress is in all cases virtually linear. In the accompanying figure by way of example we show the splitting scheme for the lines of LiF (λ = 5698 Å) and CaF_2:Eu (λ = 5735 Å). In the diagram we have indicated the multiplicity of the splitting of the lines for $P \parallel C_4$, $P \parallel C_3$ and $P \parallel C_2$, the magnitude of the splittings under a compressive stress of 10 kg/mm^2, and the polarization of the splitting components in cases when these components are observed only in the states of polarization with $E \parallel P$ or $E \perp P$.

The experimentally observed splitting pattern is in good agreement with the results of calculation. From comparison of the experimental with the calculated data it was established that the centers responsible for the line luminescence of colored LiF and CaF_2:Eu and CaF_2:Sm crystals are anisotropic and oriented along the axes $6C_2$ (LiF) and $4C_3$ (CaF_2:TR^{3+}). We also determined the multipolarities of the transitions associated with all the investigated lines: for all the lines of LiF and the 5735 Å and 5282 Å lines of CaF_2:Eu - π_e, for the 5710 Å line of CaF_2:Sm - σ_e, for the 5808 Å line of CaF_2:Eu, and for 5720 Å line of CaF_2:Sm - σ_m. Where there were available the results of earlier determinations by other methods (for example, CaF_2:Eu crystals[1,9]) we found good agreement with our results. The magnitudes of the shifts of the split components for the three directions of compression (7 quantities for LiF and 5 for CaF_2:Eu) were also found to satisfy the deduced formulas for centers with $N \parallel C_2$ and $N \parallel C_3$, containing only three and two independent parameters, respectively. On the basis of the deduced values of the "piezospectroscopic" parameters we drew certain inferences regarding the interaction of the centers with the lattice and calculated the shifts of the bands under hydrostatic compression and their temperature displacements, all of which proved to be in good agreement with the experimental results.

Thus the experimental results obtained for crystals with two such different types of centers as color centers in LiF and TR^{3+} ions in CaF_2 substantiate the results of our calculations regarding the behavior of the spectra of anisotropic centers in a uniaxially stressed crystal. The calculations performed and the experimental data, which agree with the results of these calculations, clarify the principal regularities of the piezospectroscopic effect in anisotropic centers in cubic crystals. The fact that our experiments brought out important characteristics of the centers in LiF and CaF_2 crystals showed that investigation of the piezospectroscopic effects is a valid means for studying anisotropic centers in cubic crystals.

In conclusion, it should be noted that the above described influence of uniaxial compression on the spectra of local anisotropic centers in cubic crystals is only a particular case of piezospectroscopic effects in crystals. These effects, which consist of splitting in the spectra of crystals under elastic strain, have as their common cause removal of degeneracy of the energy states in crystals under elastic deformation tending to lower the degree of symmetry of the crystal. These effects in principle should be common and should be observed in the spectra of crystals various kinds, wherein they may be associated with intrinsic states of the crystals (bands, exciton levels) or with different types of local levels. Investigation of the piezospectroscopic effects, as is demonstrated by the above consideration of the case of anisotropic centers and by the results of investigation of the influence of deformation on the long wavelength absorption edge of Cu_2O (Ref.10), can yield valuable information on the energy structure of crystals.

References

1. P.P.Feofilov, Usp.fiz.nauk, 58, 69 (1956).
2. A.A.Kaplyanskii, Optika i spektroskopiya, 7, 677 (1959). (Trans.Optics & Spectroscopy.)
3. A.A.Kaplyanskii, Ibid., 10, No.1 (1961). (Trans.Ibid.)
4. A.A.Kaplyanskii, Ibid., 7, 683 (1959). (Trans.Ibid.)
5. A.A.Kaplyanskii, N.A.Moskvin & A.K.Przhevuskii, Ibid., 10, No.2 (1961). (Trans.Ibid.).
6. P.Pringsheim et al, J.Chem.Ph., 21, 794 (1953); Zs.Phys., 136, 573 (1954).
7. A.A.Kaplyanskii, Optika i spektroskopiya, 6,424 (1959). (Trans.Optics & Spectroscopy.)
8. I.V.Stepanov & P.P.Feofilov, Doklady AN SSSR, 108, 615 (1956). (Trans. Doklady.)
9. V.A.Arkhangel'skaya & P.P.Feofilov, Optika i spektroskopiya, 4, 602 (1958).
10. E.F.Gross & A.A.Kaplyanskii, Fiz.tverdogo tela, 2, 1676, 2968 (1960). (Trans.Soviet Physics - Solid State.)

MECHANISM OF ENERGY STORAGE BY CRYSTAL PHOSPHORS

- Ch.B.Lushchik, G.G.Liid'ya & I.V.Yaek

Energy storage by crystals is important where certain practical applications of phosphors are concerned. This phenomenon can be divided into three stages: 1) the process of creation of the long-lived excited state, 2) prolonged maintenance or preservation of the excited state, and 3) final de-excitation of the crystal.

Prolonged preservation of the excited state

Present day concepts regarding the second stage of energy storage by crystals are the most clear cut and are probably close to reality. Blokhintsev[1] showed that the electrons and holes appearing as a result of excitation are localized (trapped) at lattice defects that are located at appreciable distances from each other. Owing to this separation of the defects direct recombination is impossible and a necessary conditions for de-excitation of the crystal is release of the electrons or holes from the trapping centers. The necessary degree of separation for F and V centers in alkali halide crystals is approximately 10 lattice constants; with smaller separations tunnel recombination occurs. Earlier[2] we demonstrated that the second important condition for prolonged preservation of the excited state is low mobility of the defects serving as traps for the electrons and holes. This condition is not fulfilled in liquids; it is also not fulfilled in ionic crystals at temperatures exceeding half the melting temperature. Intense ionic diffusion mitigates against prolonged maintenance of the excited state. Experiments have not substantiated Seitz's hypothesis[3] that there may exist long-lived ($t \gg 1$ sec) metastable states of impurity ions[4-6].

Mechanism of creation of color centers in crystals

Most authors treat the first stage of the above mentioned phenomenon, namely, the creation of electron and hole color centers, in a simplified manner, i.e., view it as direct capture of the quasi-free electrons and holes appearing in the irradiated crystal by the lattice defects inevitably present in every crystal. Investigation of the processes of creation of even the simplest centers, such as F centers, shows that the mechanism is appreciably more complicated. As has been repeatedly noted[2,7] one must take into account not only electron-hole processes but also exciton, sensitization, ionic and other effects.

It is known that in the absorption spectra of activated alkali halide crystals there may be distinguished at least three distinct characteristic regions: 1) activator absorption bands (*ac* region), 2) exciton absorption bands (*ex* region), and 3) a region irradiation in which gives rise to electrons *e* and holes *p* (*ep* region). Using monochromatic radiation of different frequencies one can produce essentially different elementary excitations of the crystals and determine their role in producing color centers. Even the first semiquantitative experiments showed that different electron (F,M,N,O,Z_1 and different activator) and hole (V_1, V_2, etc.) color centers are produced with excitation of crystals in all the three above-mentioned spectral regions.[8-13] We hypothesized that there exist at least three different mechanisms of color center creation in crystals. To check this we measured the spectral characteristics which we call the "spectra of creation of color centers".[14] Specifically, we measured the number of color centers, for example, n_F, the number of F centers, produced in a previously unexcited crystal by equal numbers of photons of different frequency. The value of n_F could be evaluated either by measuring the absorption[15], since $\varkappa_F \sim n_F$, or it could be

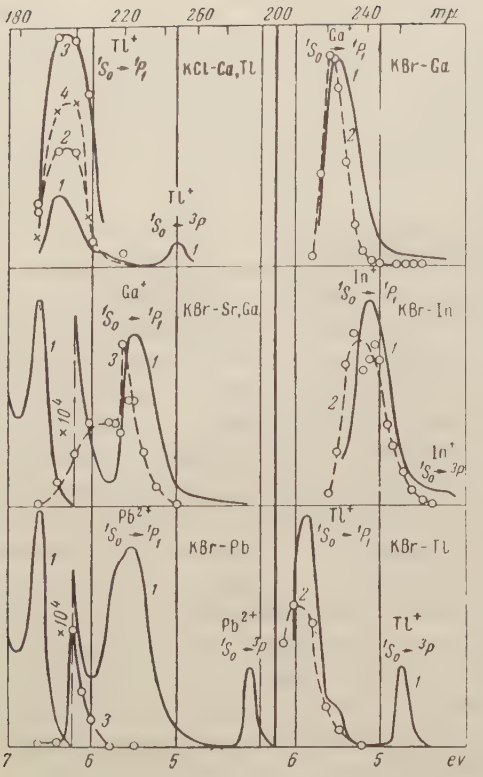

Fig.1. Absorption spectra (1), F center creation (2), creation of negative excited absorption (3) and creation of activator centers (4) spectra for alkali halide crystal phosphors.

determined by somewhat more sensitive methods, namely by measuring the intensity of luminescence photostimulated in the F region[16,17] or the photostimulated electron emission from the F centers[18].

By way of example, in Fig.1 we show the absorption spectra (1) and the spectra of creation of F centers (2) for KCl:Ca:Tl, KBr:Ga, KBr:In and KBr:Tl phosphors. For the first phosphor the center creation spectra were measured by the absorption method; for the other phosphors - by the luminescence method. Data obtained by the electric method will be found in Ref.18. The spectrum of F center creation encompasses the activator absorption region, corresponding, according to the data of Ref.19, to $^1S_0 \rightarrow {}^1P_1$ electron transitions in the Ga^+, In^+ and Tl^+ ions. Excitation of alkali halide phosphors with these ions in the region of the short wavelength activator absorption bands leads to decrease in the intensity of these bands (effect of negative excited absorption[20,21]). The spectra of creation of this effect in KCl::Ca:Tl and KBr:Sr:Ga phosphors are located in the region of the absorption band corresponding to $^1S_0 \rightarrow {}^1P_1$ electron transitions in the Tl^+ and Ga^+ ions. In KBr:Pb the effect appears only in case of irradiation in the *ex* region. This effect is at least partially connected with the appearance of atomic centers (for KCl:Ca:Tl λ_m^x = 285 mμ). Our data indicate that the $^1P_1$ states of monovalent impurity atoms can be "delocalized" with some probability, subsequently giving rise to F and V centers in the host crystal. This effect can be connected with mixing of the wave functions of the activator ions and the host ions.[22,23]

The spectrum of F center creation in KI:Tl phosphor, measured by the luminescence procedure, is shown in Fig.2. F centers are produced not only with illumination in the *ac* region but with even higher efficiency in the *ex* (~220 mμ) and *ep* (~190 mμ) regions. The difference between the spectra of excitation of optical flash and the spectra of excitation of recombination phosphorescence[24] for KI:Tl phosphor (Fig.2) indicates that different mechanisms are responsible for the production of F centers with illumination in the *ex* and *ep* regions. Thus our data indicate that there may exist two distinct mechanisms of F center creation: an exciton mechanism and an electron-hole mechanism. F centers may appear as a result of interaction of electrons and excitons with individual point defects in the lattice, with associations of such defects or with dislocations.[7] The cluster like distribution[25] of F, M, N and O centers in KCl:Tl crystals excited in the *ac* and *ex* regions, the fact that photostimulated luminescence is not connected with the block edges (according to micro-optical studies[28]), and the accelerated coloring of crystals by ultraviolet radiation after preliminary photoexcitation and photobleaching of the crystals, all indicate that a significant role in the process of creation of F centers is played by interaction of elementary excitations with associations of point defects. These defects are undoubtedly accompanied by ionic

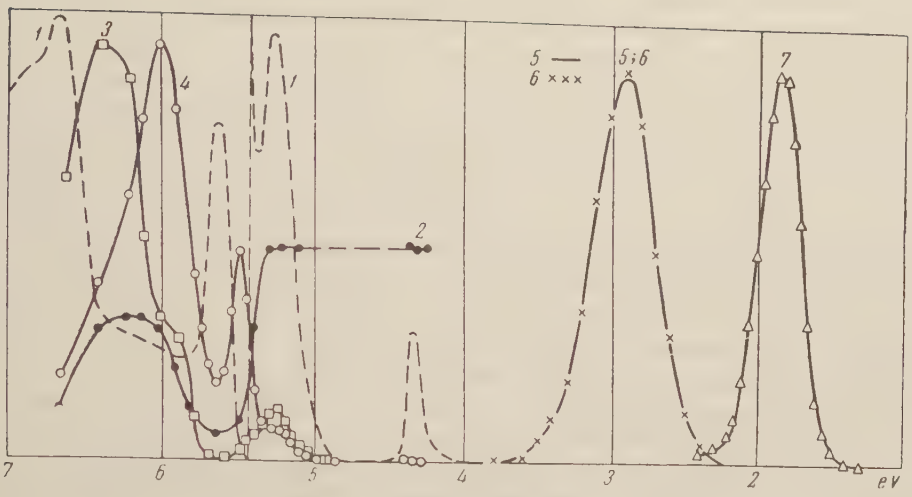

Fig.2. Spectra recorded for KI:Tl ($5 \cdot 10^{-2}$ mole percent Tl) phosphor: 1) absorption spectrum, 2) excitation of steady luminescence, 3) excitation of recombination phosphorescence, 4) excitation of optical flash, 5) steady luminescence emission spectrum, 6) optical flash spectrum, 7) optical flash stimulation spectrum.

processes. The dislocation mechanism of F center creation requires further investigation.

Mechanism of thermal and optical de-excitation of ionic crystals

The third stage of the effect under consideration (de-excitation) was studied in detail in our earlier experiments. By means of a combination of optical and electrical methods (see, for example, Refs.6, 27-30) we succeeded in showing that thermal break-up of F centers in alkali halide crystals does not amount simply to the process of direct thermal ionization. In the case of NaCl, KCl and KBr crystals in the 100 to 300°K temperature region thermal break-up of F centers is connected with hole processes, while in the 400 to 500°K region it is connected with electronic processes, accompanied by displacement of ionic vacancies (ionic-electronic processes).[31,32] Measurements of the spectra of optical bleaching of F centers indicate that these centers may be destroyed not only by direct photothermal ionization but also as a result of ionization of hole color centers incident to encounters of excitons with the F centers and also owing to the effect of sensitized emission[33,34] (in transfer of energy to the F centers from other electron color centers[10,2]). Ultraviolet radiation of the same frequencies (in the *ex* and *ep* regions) may either create or annihilate F centers (see Refs.33 & 34).

Alkali halide salts - typical crystal phosphors

An obvious question is to what extent are the results obtained for simple ionic crystals applicable to phosphors of other classes. Investigation[2,10,30] of the luminescence of alkali halide salts with excitation in the region of the fundamental absorption of the crystal (*ex* and *ep* regions) show that many effects in these crystals occur essentially in same way as in ZnS phosphors.

The prompt ($t \ll 1$ sec) build-up of luminescence characteristic of alkali halide phosphors is observed only with excitation in the *ac* region. With *ex* excitation of KI:Tl the fraction of lagging emission amounts to 10-20%. In this case the prompt component probably appears as the result of excitation of the lumines-

cence centers by exciton impact.[37] With excitation in the *ep* region the lagging component of the luminescence amounts to at least 80-90%, i.e., is almost as great as in ZnS phosphors. With increase of the temperature the prompt component of the emission of KI:Tl is quenched in the 500 to 600°K region. This is typical internal quenching of luminescence.[38] The lagging component of the luminescence is quenched at appreciably lower temperatures (260 to 370°K). Thus, in alkali halide phosphors there is observed external thermal quenching of luminescence. When a luminescing KI:Tl phosphor is acted on by light in the region of the F band, there are observed different effects depending on the region of excitation of the phosphor. With *ac* excitation irradiation in the F region does not affect the intensity of the steady luminescence. With *ep* excitation there is observed quenching of some of the steady luminescence. With *ex* excitation there is evinced a new effect, namely, intensification of the steady luminescence.

Many authors have emphasized the radical difference between the kinetics of relaxation processes in alkali halide as compared with ZnS phosphors. Our experiments showed that with *ex* excitation the kinetics of optical flash in KI:Tl is bimolecular. Only with excitation in the *ep* and *ac* regions does the optical flash mechanism become monomolecular. Thus with excitation in the fundamental absorption region alkali halide and ZnS phosphors do not differ greatly. A detailed description and discussion of the observed effects will be found in Ref.17. Here we only want to note that the results obtained substantiate the existence in alkali halide salts, which are typical crystal phosphors, of distinctive electron-hole, exciton and "delocalized" processes leading to energy storage by the crystals.

Institute of Physics and Astronomy
Academy of Sciences of the Estonian SSR

References

1. D.I.Blokhintsev, Doklady AN SSSR, 2, 76 (1934).
2. Ch.B.Lushchik & G.G.Liid'ya, Materialy VII Soveshchaniya po lyuminestaentsii (Transactions of the 7th Conference on Luminescence), p.101, Tartu, 1959.
3. F.Seitz, J.Chem.Phys., 1, 150 (1938).
4. V.V.Antonov-Romanovskii, Trudy FIAN SSSR (Proceedings, Inst. of Physics, USSR Academy of Sciences), 2, No.2-3 (1942).
5. I.A.Parfianovich, Izv.AN SSSR, Ser.fiz., 13, 161 (1949).
6. Ch.B.Lushchik, Trudy IFA AN ESSR (Proceedings, Inst.of Phys.& Astronomy, Estonian SSR Ac.of Sci.), No.3, 3 (1955).
7. F.Seitz, Revs.Mod.Phys., 26, 7 (1954).
8. A.Smakula, Z.Physik, 63, 767 (1930).
9. L.Apker & E.Taft, Phys.Rev., 82, 814 (1951).
10. Ch.B.Lushchik & G.G.Liid'ya, Trudy IFA AN ESSR, No.7, 193 (1958).
11. Ch.B.Lushchik, Kh.F.Kyaembre & I.V.Yaek, Transactions of the 7th Conf.on Luminescence, p.117, Tarty, 1959.
12. Ch.B.Lushchik & E.S.Tiisler, Trudy IFA AN ESSR, No.10, 135 (1959).
13. Ch.B.Lushchik & E.S.Tiisler, Ibid., No.11, 185 (1960).
14. Ch.B.Lushchik, Color Centers in Alkali Halides, International Symposium, p.29, Corvallis, Oregon, USA, 1959.
15. G.G.Liid'ya, Trudy IFA AN ESSR, No.12, 149 (1960).
16. I.V.Yaek, Ibid., No.10, 166 (1959).
17. G.G.Liid'ya & I.V.Yaek, Ibid., No.12, 281 (1960).
18. Kh.F.Kyaembre, Ibid., No.14 (1960).
19. N.E.Lushchik & Ch.B.Lushchik, Ibid., No.6, 5 (1957).

20. A.N.Arsen'eva, Z.Phys., 57, 163 (1929).
21. R.P.Shchukin, Zhur.eksp.i teor.fiz., 29, 834 (1955). (Trans.Soviet Physics - JETP.)
22. Ch.B.Lushchik & V.I.Volin, Trudy IFA AN ESSR, No.7, 311 (1958).
23. R.Knox, Phys.Rev., 115, 1095 (1959).
24. I.V.Yaek & G.G.Liid'ya, Optika i spektroskopiya, 8, 142 (1960). (Trans. Optics and Spectroscopy.)
25. P.A.Khellenurme, Ibid., 8, 729 (1960).
26. R.I.Gindina, Trudy IFA AN ESSR, No.12, 271 (1960).
27. Ch.B.Lushchik, Izv.AN ESSR (Bulletin, Ac.of Sci. of Estonian SSR), 5, No.1, 12 (1956).
28. Kh.F.Kyaembre & Ch.B.Lushchik, Trudy IFA AN ESSR, No.11, 150 (1960).
29. I.K.Vitol, Ch.B.Lushchik & I.V.Yaek, Ibid., No.12, 175 (1960).
30. I.V.Yaek & T.A.Eksina, Ibid., No.14 (1960).
31. F.N.Zaitov & V.Ya.Kark, Ibid., No.6, 82 (1957).
32. Ch.B.Lushchik, Ibid., No.8, 75 (1958).
33. F.N.Zaitov, Optika i spektroskopiya, 4, 102 (1957).
34. P.A.Khellenurme, Trudy IFA AN ESSR, No.7, 340 (1958).
35. V.V.Antonov-Romanovskii, Izv.AN SSSR, Ser.fiz., 13, 91 (1949).
36. N.A.Tolstoi, Radiotekhn.i elektronika (Radio Engineering & Electronics), 1, 1135 (1956).
37. Ch.B.Lushchik, F.N.Zaitov & G.G.Liid'ya, in Fotoelektricheskie i opticheskie yavleniya v poluprovodnikakh (Collected articles on photoelectric and optical effect in semiconductors) Kiev, 1959.
38. K.K.Shvarts, Trudy IFA AN ESSR, No.7, 153 (1958).

EFFECT OF ISOSTRUCTURE ON THE SPECTRA OF ACTIVATED MIXED CRYSTALS

- F.D.Klement & L.A.Teiss

It is known that in a unit cell of a mixed crystal the individual components may be present in different proportions, the proportion in any given case being determined by the law of statistical distribution and the relative concentrations of the components. Cells of the same composition form isostructures. Activator ions located in centers with different isostructures should have different "individual" spectra, and the corresponding band of the phosphor should be complex.

The present work was aimed at determining the effect of isostructure on the luminescence spectrum of KCl·KBr(Tl) phosphors. For every given ratio of KCl to KBr the luminescence band of the phosphor occupies a definite position between the locations of the bands in the spectra of the single-base material phosphors (306 mμ for KCl and 324 mμ for KBr). But even at low temperatures the mixed phosphor band does not exhibit structure. This may be explained by the close spacing of the elementary bands corresponding to different isostructures as compared with the intrinsic width of the entire band.

We excited this phosphor in different narrow regions within the activator excitation band. If the luminescence band is a superposition of bands from centers of different isostructures, there should be evinced a change in the shape of the band or some shift of its peak with change of the excitation wavelength. Fig.1 shows the short wavelength luminescence band of the phosphor 80 KCl·20 KBr (0.05 Tl) with variation of the excitation from 240 to 265 mμ.

There is evident a distinct shift of the luminescence peak to the side of longer wavelengths as the excitation region is swept in the same direction. The successive positions occupied by the luminescence peaks span almost the entire range between the positions of these peaks in the spectra of the single host material phosphors, i.e., there are represented in the luminescence spectrum of the mixed crystals centers with different isostructures, including the extreme isostructure with six Br^- ions surrounding a Tl^+ ion. In addition, although the mixed base material contains only 20 mole percent KBr, the luminescence spectrum of the phosphor is much closer to the spectrum of the isostructure with a predominance of bromine, while the band corresponding to pure KCl is absent. From this we concluded that the Tl^+ is located mainly in isostructures with the greatest number of heavy Br^- ions. This agrees with the deductions arrived at in other ways (see Ref.1, for example). Lastly, we note the absence from the spectrum of the mixed base phosphor of the second ultraviolet luminescence peak, which is characteristic of KBr(Tl) phosphor (even with only 50 mole percent KBr).

Similar experiments were carried out using other proportions of KCl and KBr and also with base mixtures of NH_4Cl + NH_4Br; essentially similar results were obtained. For a 50 mole percent KBr content, the location of the luminescence band no longer depends on the excitation region and completely coincides with its location in the spectrum of KBr. In this case the number of "pure bromide" isostructures is already so great that all of the Tl is located in them.

If the activator concentration is increased when the KBr content is small (i.e., when there are few isostructures with predominant Br^- content), after filling of the isostructures with 6 Br^-, the thallium should begin to fill the isostructures with 5 Br^-, etc.

This inference was confirmed by appropriate experiments. As will be evident from Fig.2, with increase of the activator concentration, the luminescence peak shifts to the short wavelength side, i.e., the amount of emission associated with centers with a higher Cl^- content increases. In these experiments the phosphors were excited with the same wavelength. We note that this activator concentration effect was not observed for the one host component systems.

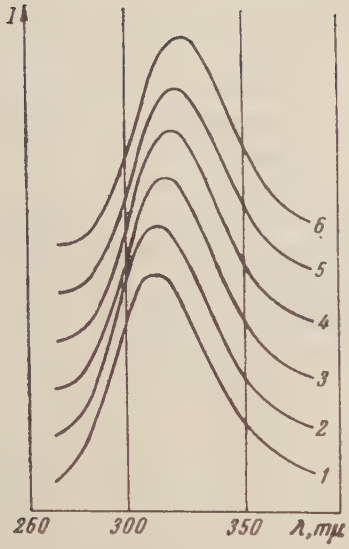

Fig.1

Fig.2

Fig.1. Luminescence spectra of 80 KCl·20 KBr(0.05 Tl) with excitation at different wavelengths: 1) 240 mμ, 2) 245 mμ, 3) 250 mμ, 4) 255 mμ, 5) 260 mμ, 6) 265 mμ.

Fig.2. Luminescence spectra of 87 KCl·13 KBr(Tl) with different Tl concentrations: 1) 0.0005, 2) 0.019, 3) 0.2 mole percent.

The position of the luminescence band of the KCl·KBr(Tl) phosphor corresponding to the 6 Br^- isostructure coincides with the position of the luminescence band of KBr(Tl) phosphor only when there is sufficiently high content of KBr in the mixed crystal. In the range of low KBr concentrations this band is shifted to the short wavelength side. This is explained not only by the influence of the nearest neighbors on the ion levels but also by the fact that for any given isostructure the cell dimensions depend on the average value of the lattice constant of the given mixed crystal.

The existence of isostructures of different composition in mixed crystals also serves to explain certain other phenomena, observed previously by other authors: the large width of the activator absorption and luminescence bands, as well as of the F-bands in mixed crystals, etc. Lushchik[2] demonstrated the effect of isostructures on the width and shape of thermostimulated luminescence peaks. Spectroscopic study of isostructures in mixed crystals, using rare earth activators, appears especially promising.[3]

References

1. N.I.Ivanova, Transactions of the Fifth Conference on Luminescence (Crystal Phosphors), p.93, Tartu, 1957.

2. Ch.B.Lushchik, Trudy (Proceedings), Inst. of Phys. & Astronomy, Estonian SSR Ac.of Sci., No.3, 173 (1955).

3. A.K.Trofimov, Thesis, 1959.

DISCUSSION

M.U.Belyi: In our laboratory we carried out preliminary investigations of the absorption and luminescence spectra of mixted Tl + KCl + KBr solutions. Our results have much in common with the reported data on the analogous crystal phos-

phors, although I also note certain differences. Thus, in the case of mixed solutions, during variation of the concentration of one of the components (KCl or KBr), there always appears an intermediate absorption spectrum which is characteristic of absorption centers of only one type. However, in the case of luminescence of such solutions, there are observed two overlapping luminescence bands, associated with two different types of centers. Thus, these data indicate (and this assertion apparently may be extended, with some reservations, to the analogous crystal phosphors) that here the absorption spectra are determined by transitions in the Tl^+ ion, the levels of which are deformed by the field of the neighboring Cl^- and Br^- ions, while the luminescence spectra are affected by the specific interaction of the Tl^+ ions with the Cl^- and Br^- anions, resulting in the formation of two distinct types of luminescence centers.

* * * * * *

INVESTIGATION OF LUMINESCENCE PROCESSES IN ALKALI HALIDE PHOSPHORS

- L.M.Shamovskii & P.A.Pipinis

It was established[1] from the results of thermal stimulation and bleaching of x-irradiated phosphors as well as from analysis of optical stimulation of phosphorescence that release of electrons from trapping levels is accompanied by luminescence characteristic of the activator impurities. These data served as justification for considering phosphorescence as the result of recombination of electrons with ionized luminescence centers. It was assumed that holes appearing in crystals in the process of excitation are trapped by activator ions, rob them of electrons and give rise to ionized centers.[2] It has been shown by experiments[3] that holes are not capable of bringing activator ions to the ionized state. In connection with this result, there was advanced a new hypothesis[4] that there may occur recombination of electrons with trapped holes and subsequent transfer of the released energy (by a resonance or exciton mechanism) to the activator. However, most hole trapping centers are either electrically neutral (V_1 or V_2 centers) or have an effective negative charge (V_3 or X_3^- centers). Hence this recombination mechanism appears unlikely, particularly if one recalls the high quantum efficiency of alkali halide phosphors.

There are in fact convincing indications of the opposite direction of the recombination processes resulting in luminescence. It was established that with all types of excitation of phosphorescence there form "atomic" centers. These centers form incident to localization (trapping) of electrons by the activator and are evinced in the absorption spectrum.[5] In the process they acquire a negative charge and therefore are more effective recombination centers for holes. It was shown that release of holes from V centers is sufficient for emission of the stored light sum, i.e., de-excitation of the phosphor.[6] In cases when the phosphorescence is stimulated by thermal dissociation of the donor levels (F centers), it is always accompanied by bleaching of the hole color centers (V_1 and V_2 centers).* It is entirely possible that release of electrons from trapping levels

---

*The thermal bleaching curves for electron and hole trapping levels coincide and their derivative with respect to temperature corresponds to the thermal luminescence band.[7]

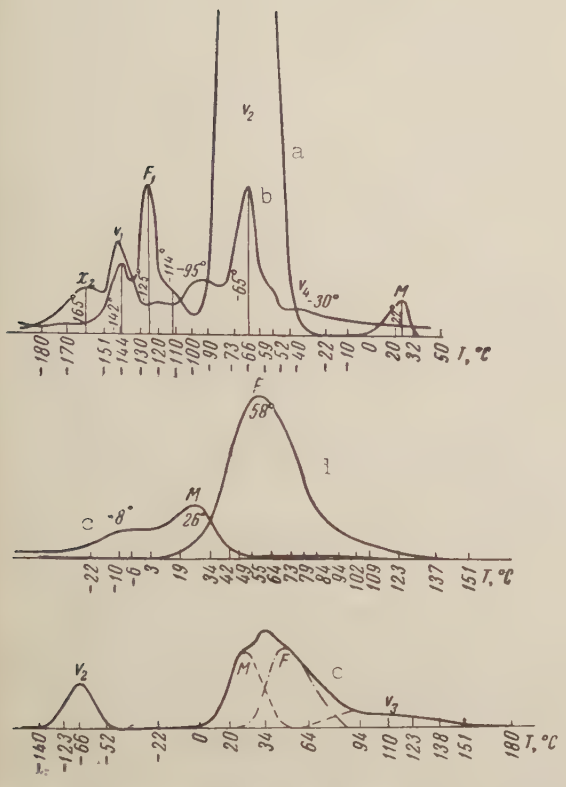

Fig.1. Glow curves for NaBr(In) phosphors excited by light in the activator absorption bands at different temperatures (PRK-2 mercury tube through a UFS-1 filter). $\beta = dT/dt =$ = 10 degree/min.

leads only to their redistribution in deeper traps and the observed emission is due to hole recombination.

For further investigation of the mechanism of recombination luminescence we used NaBr:In and KBr:In phosphors; these were activated with the bromides of mono- and trivalent indium in the process of growth from the melt. By way of illustration in Fig.1 we show the thermal stimulation curves for NaBr:In phosphors excited by light in the activator absorption bands at different temperatures. The classification of the glow peaks and their attribution to individual hole and electron trapping levels is based on the data of different authors[8]. Curve a corresponds to NaBr:In^{3+} phosphor (hereinafter I); curve b pertains to NaBr:In^{+} phosphor (II). Both the phosphors were excited at -196°. The dose of exciting light for II was 5 times greater than for I. It follows from the data of Fig.1 1) that in phosphors excited at low temperatures the thermal stimulation bands correspond primarily to release of holes from traps and recombination of the holes with atomic luminescence centers, 2) that the indium activator ions are incorporated in the NaBr lattice without change of valence; upon replacement of part of the Na^{+} ions by In^{3+} ions there form in the crystal additional cationic vacancies[9] - trapping centers for holes; hence with identical doses of exciting radiation the light sum stored in I is 10 times greater than in II and corresponds almost entirely to V_2 levels, and 3) that with increase in the density of trapped holes there is a corresponding increase in the concentration of donor levels; in I there is observed a thermal luminescence peak corresponding to M centers.

If I is excited at -28° (i.e., above the limit of stability of V_2 centers), there are observed two peaks in the thermal stimulation curve (curve c): at -8° and +26° (M levels). In the same phosphor excited at 36° (above the limit of stability of M centers) there is observed a thermal luminescence band peaking at 58°, which corresponds to the region of thermal ionization of F levels (curve d).*

Regardless of the conditions of photoexcitation the light sum is stored in the phosphor with trapping of the carriers at the same cationic and anionic vacancies, but in different proportions. This will be evident from curve e. Sample I was first excited for 4 min at 40° (above the level of stability of M centers) and then for the same length of time after cooling down to -196°. In this case, there are virtually no low temperature peaks evinced in the thermal stimulation curve. There are present only bands corresponding to the region of thermal breakup of the M and F centers and another wide but relatively weak band at 110°.

---

*For comparison of the stored light sums the ordinates of curves c,d and e must be multiplied by 10 to equal the scale of curves a and b.

Consequently, after filling of the deep traps there remain no free vacancies in the crystal and it loses its ability to store light energy on shallow levels.

After optical excitation of phosphors at low temperatures there are not observed in the glow curves peaks associated with ionization of F centers. It is usually assumed that localization of electrons in deep traps requires a certain activation energy and that consequently this process does not occur at low temperatures.[10] This restriction, apparently, does not apply to the investigated phosphors. Although F centers are not evinced in thermal luminescence, they do form in the process of excitation. In phosphor I after photoexcitation at -196° the entire stored light sum can be released by prolonged irradiation of the crystal with light in the F band (546 mμ) at low temperature. Simultaneously, with emptying of the shallow hole traps, the M centers are de-excited. It is significant that in the process there disappear not only the shallow acceptor levels but the deeper V_2 centers which are entirely stable at low temperatures. The process of emptying the V_2 centers is apparently connected with gradual redistribution of the holes from deeper to shallower traps, as the holes are released from the deeper traps in the process of de-excitation. Hence the process of emission of the light sum by photostimulation in the F band at low temperatures proceeds at a slow rate.

The stimulating action of light in the region of the F band is intimately connected with the character (depth) of the hole trapping centers. If phosphor I is excited at -196° and then in the process of slow heating is periodically illuminated with pulses in the F band, corresponding flashes of luminescence are observed up to -50°, i.e., as long as there exist V_2 centers. If the same phosphor is excited at 50° (above the limit of stability of V_2 and M centers) luminescences flashes are observed up to 120°, inasmuch as in addition to F levels there also exist V_3 centers in the crystal. Thus it would appear that release of electrons does not lead directly to emission of the stored light sum but only facilitates subsequent release of the holes from trapping levels and their recombination with atomic luminescence centers.

The question was investigated further by carrying out a series of experiments on KBr phosphors excited by a 4-5 kv cathode beam. Then there were recorded the thermal stimulation and exoelectronic emission curves. As will be evident from Fig.2, dissociation of the F centers corresponds to an appreciable exoelectronic emission (curve a). The luminescence in this temperature region is barely noticeable. The peak of the exoelectronic emission band corresponds to the beginning of the rise of the thermal luminescence curve. The highest luminescence intensity is observed after break-up of most of the F centers. The fact that the exoelectronic emission precedes the luminescence in time and temperature shows that ionized luminescence centers are not produced in process of excitation of the phosphor. Nor can the phosphorescence be identified with recombination of electrons with trapped holes. For any variant of the electron recombination scheme the thermal stimulation peaks should appear in ad-

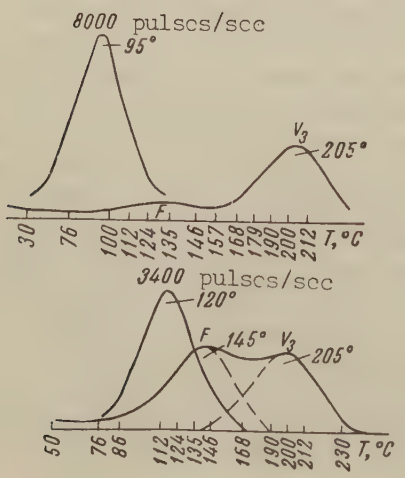

←Fig.2. Comparison of thermoluminescence and exoelectronic emission (from the F band) curves for KBr:In phosphor excited by cathode rays at -155°. The upper curves are for a freshly prepared specimen; the lower curves for a "sensitized" specimen. $\beta = dT/dt = 10$ degree/min.

vance of the exoelectronic emission band.[11] Obviously thermal break-up of the F centers leads only to redistribution of the electrons to deeper trapping levels. Such trapping centers are formed by activator impurities at defects.[12] Emission of luminescence occurs at a subsequent stage as the result of release of holes from trapping levels and their recombination with atomic centers. Advance of the exoelectronic emission relative to the thermal stimulated luminescence is observed in phosphors with a relatively high activator concentration* and with high densities and doses of excitation. Under these conditions there form the deepest hole color centers owing to reactions of the $V_2 + e = V_3$ type.[13] V_3 centers are characterized by deeper trapping levels for holes as compared with the trapping levels for electrons in F centers. Release of electrons leads only to their redistribution in deeper activator trapping centers. This process is nonradiative. The anionic vacancies forming can interact with V_3 centers with the formation of shallower hole trapping centers: $V_3 + v^- = V_4$. Following this there occurs radiative recombination of free holes with atomic luminescence centers. The process of formation of shallow hole trapping centers is entirely probable inasmuch as V_3 centers and anionic vacancies differ as regards the polarity of their respective charge. However, the rate of this transformation is limited by ionic conductivity. This explains the appreciable lag of the luminescence relative to the exoelectronic emission (by 25° or 2.5 min).

In the process of excitation of crystals with a relatively high activator concentration there forms a high density of atomic centers, but a low concentration of F levels.[14] But the number of holes on trapping levels is always equal to the number of trapped electrons. Hence after thermostimulated emission in the band corresponding to release of electrons from the F levels and their recombination with holes at luminescence centers there still remains in the phosphor part of the stored light sum, the part due to electrons trapped by the activator and holes localized on V_3 levels. This part of the stored energy is released upon thermal dissociation of the V_3 centers. The corresponding peak in the glow curve appears at 205°. No noticeable exoelectronic emission is observed in this temperature region. Consequently, the peak at 205° is connected with hole trapping centers and it cannot be attributed to thermal dissociation of atomic centers.

If the KBr:In phosphor is excited at 160°, it still retains its ability to store excitation energy, although F centers are no longer stable at this temperature. In this case there appear in the thermostimulation curve broad but relatively weak bands at 195 and 245°. These bands apparently correspond to luminescence owing to recombination of holes released from V_3 or X_3^- levels and their recombination with atomic luminescence centers.

Repeated excitation and de-excitation of phosphors leads to their "sensitization". With sensitization the concentration of F centers formed by the same dose of ionizing radiation increases.[15] Such sensitization is evinced in the thermal luminescence (Fig.2): the peak in the region of the F band is enhanced and the corresponding thermal luminescence and exoelectronic emission bands are shifted to the side of higher temperatures. It may be that the stability of the F centers is increased if they are located in the vicinity of V_3 levels which have an excess negative charge.

As will be evident from the accompanying table, most of the color centers in NaBr and KBr are characterized by deep trapping levels for carriers. Hence in crystals additively colored in alkali metal vapor or in a halide atmosphere, electron or hole centers exist up to a temperature of at least 450-500°.[16,17]

---

*We have in mind the activator concentration taking into account the coefficient of its dual distribution. The concentration must be appreciable in systems with good mutual solubility of the components.

Evaluation of the carrier trap depths in KBr:In and NaBr:In phosphors from the thermal stimulation data

Temp. of glow peak, °C	Character of trapping center in KBr:In	Trap depth E, ev	Temp. of glow peak, °C	Character of trapping center in NaBr:In	Trap depth E, ev
—186°	X_2^-	0,19	—165°	X_2^-	0,23
—155°	V_1	0,23	—140°	V_1	0,29
—130°	F'	0,29	—125°	F'	0,32
—100°	?	0,37	— 95°	?	0,39
20°	V_2	0,64*	— 65°	V_2	0,45
40°	M	0,68	25°	M	0,65
125÷135°	F	0,86—0,88	58°	F	0,71
205°	V_3	1,03	110°	V_3	0,83
245°	X_3^-	1,12			

*From data[16] on the temperature dependence of the hole conductivity in additively colored KBr calculated E = 0.74 ev for V_2.

Bleaching of such crystals is limited by ionic conductivity.[17]

The same color centers are formed under the influence of ionizing radiation. Their stability, however, is sharply reduced because at the same time electron-hole recombination becomes possible. Bleaching of such crystals usually occurs upon release of electrons from the M or F levels, although thermally they are more stable than V centers. The release of only holes is not sufficient for bleaching, inasmuch as the electronic traps (except F' centers) do not have excess charge and hence cannot serve as effective recombination centers for holes. Under these conditions the probability for retrapping of holes by cationic vacancies is substantially greater than the probability for their recombination with trapped electrons.

With the introduction of an activator crystals undergo qualitative changes. In the process of their excitation part of the electrons are trapped by the activator (on defects) and there form atomic luminescence centers with an effective negative charge. In these cases thermal dissociation of the V centers is sufficient for bleaching.[6] This process is accompanied by luminescence characteristic of the activator. The thermal stimulation bands are located at temperatures characteristic for dissociation of the holes trapping centers. Under these conditions there is emitted the part of the stored light sum corresponding to the number of electrons trapped by the activator. With liquidation of the atomic centers the stability of the V_2 centers increases and emission of the stored light sum ceases. Upon further heating of the phosphor there begins dissociation of the donor levels. The electrons are redistributed from M or F levels to deeper activator trapping centers. However, this stage of heating is not accompanied by emission (inasmuch as ionized centers are absent), but it stimulates release of holes from the V_2 levels and hole recombination.

In crystals with a low activator concentration and subjected to small doses of excitation there form a small number of atomic luminescence centers and a relatively high density of F centers[14], while V_3 centers do not form. In such phosphors an appreciable part of the light sum is emitted at temperatures corresponding to thermal break-up of the M and F levels.* Under these conditions the luminescence is determined by the number of electrons entering the conduction band of the crystal ($I \sim -\frac{dn}{dt} = pn$, where n is the number of donor levels and p is the

---

*The V_2 levels do not limit the process of emission of the light sum inasmuch as they are thermally less stable than M and F levels.

probability for their thermal release per unit time), and the exoelectronic emission $E(T) = pn \exp(-\alpha\varphi/kT) \cdot \exp\left(-\frac{xd}{kT}\right)$ is limited by the work function for raising the electrons from the bottom of the conduction band and the probability for the electrons diffusing from the depth of the crystal reaching the surface of the crystal.[11] Hence for such phosphors the thermal luminescence peaks appear before the exoelectronic emission peaks.[11]

In crystals with a relatively high activator concentration and subjected to large excitation doses there forms a large number of atomic centers but a low density of F levels.[14] Hence there are created favorable conditions for the formation of V_3 and X_3^- centers. In this case release of electrons from the F levels is not sufficient for emission of the stored light sum (luminescence), inasmuch as the holes are located at still deeper trapping levels. The thermal luminescence bands for such specimens are shifted into the region of higher temperatures and the peaks of exoelectronic emission from the F centers appear in advance of the corresponding thermal luminescence band.

On the basis of analysis of the data on thermal luminescence, exoelectronic emission and optical flashing we have come to the conclusion that with all methods of excitation of phosphorescence the observed emission of the investigated phosphors corresponds to the "hole recombination scheme". The luminescence centers are "atomic" centers.

All-Union Institute for Mineral Raw Materials &
Physics Faculty, Moscow State University

References

1. Ch.B.Lushchik, Trudy IFA AN ESSR (Proceedings, Inst.of Physics & Astronomy, Ac.of Sci. of the Estonian SSR), No.1, 57 (1955).

2. M.Schön, Z.Physik, 19, 361 (1938); H.A.Klassens, Nature, 158, 306 (1946).

3. L.M.Shamovskii & Yu.N.Zhvanko, Optika i spektroskopiya, 3, 267 (1957); M.L.Kats, Materialy VII Soveshchaniya po lyuminestsentsii (Transactions of the 7th Conference on Luminescence), p.131, Tartu, 1959.

4. Ch.B.Lushchik, N.E.Lushchik, G.G.Liid'ya & L.A.Teiss, Trudy IFA AN ESSR, No.6, 63 (1957).

5. M.L.Kats, Zhur.eksp.i teor.fiz., 23, 720 (1952).

6. L.M.Shamovskii & A.A.Dunina, Materialy II Soveshchaniya po stsintillyatoram (Transaction of the Second Conference on Scintillators), 1957; P.A.Khellenurme, Trudy IFA AN ESSR, No.7, 340 (1958).

7. F.N.Zaitov, Transactions of the 7th Conference on Luminescence, p.153, Tartu, 1959.

8. R.Casles, P.Pringsheim & P.Yuster, J.Chem.Phys., 18, 887, 1564 (1950); H.Dorendorf, Z.Physik, 129, 317 (1951); T.Castner & W.Känzig, Phys.Chem.Solids, 3, 178 (1957); D.Dutton & R.Maurer, Phys.Rev., 90, 126 (1953); G.Chiarotti & N. Inchauspé, Phys.Rev., 109, 345 (1958).

9. L.M.Shamovskii & A.A.Dunina, Transactions of the 7th Conf.on Luminescence, p.13, Tartu, 1959.

10. E.I.Adirovich, Nekotorye voprosy teorii lyuminestsentsii kristallov (Some questions in the theory of the luminescence of crystals), p.285, M., 1951.

11. A.Bohun & I.Dolejsi, Chekhosl.fiz.zhur. (Czech.Physics Journal), 9, No.5, 578 (1959).

12. L.M.Shamovskii & A.S.Shibanov, Izv.AN SSSR, Ser.fiz., 25, 3 (1961). (Trans.Bulletin, 25, No.3.)

13. F.Seitz, Revs.Mod.Phys., 26, I (1954).
14. M.L.Kats, Izv.AN SSSR, Ser.fiz., 21, 550 (1957). (Trans.Bulletin, 21, 546.)
15. H.N.Hersh, J.Chem.Phys., 30, No.3, 790 (1959).
16. E.Mollwo, Ann.Phys., 29, 394 (1937).
17. L.M.Shamovskii, A.A.Dunina & M.I.Gosteva, Fizika tverdogo tela, 2, 2526 (1960),(Trans.Soviet Physics - Solid State); L.M.Shamovskii, L.I.Rybakova & M.I. Gosteva, Doklady AN SSSR, 91, 67 (1953); L.M.Shamovskii, A.A.Dunina & M.I.Gosteva, Zhur.eksp.i teor.fiz., 30, No.4, 640 (1956), (Trans.Soviet Physics - JETP.).

DISCUSSION

Ch.B.Lushchik: The report presented by Shamovskii contains interesting experimental material; in my opinion, however, some of the inferences drawn are not convincing. I believe that Shamovskii underestimates the role of electron recombination luminescence in activated alkali halide crystals.

The appearance of optical flashes upon stimulation of an excited phosphor by radiation in the region of the F, M, N, 0 and other electron color center absorption bands is direct evidence of the existence of electron recombination luminescence. Flashing is observed even after cooling of the crystals excited at 300°K to 100°K. In this case all hole processes must be frozen and the ingenious variant proposed by Shamovskii cannot be realized. Evidence in favor of the possibility of electron recombination luminescence incident to thermal release of current carriers from trapping levels is furnished by the data obtained in Riga and Tartu on exoelectronic emission, on the sign of photopolarization of the crystal, on thermostimulated conductivity, etc.

This does not, of course, mean that hole recombination does not occur in alkali halide crystals. Our experiments convincingly show that luminescence of activator ions can occur upon release of holes from trapping levels with their subsequent recombination with localized electrons. A significant role in this effect may be played by sensitized energy transfer from recombination centers to luminescence centers. E.V.Yaek, in Tartu, experimentally detected "sensitized fluorescence" of an NaCl:Fe:Mn crystal.

One can propose for the results obtained by Shamovskii an alternative explanation from the standpoint of model schemes that do not require denying the existence of electron recombination luminescence. In comparing the data on thermal stimulation and exoelectronic emission it must be recalled that these processes may have different topography.

L.M.Shamovskii: In our report and in earlier communications (Second Conference on Scintillators, 1957, Pub.Moscow, 1960) we noted that stimulated luminescence of phosphors is usually accompanied by pair bleaching of electron and hole color centers. Thermal and thermal-optical bleaching of donor centers facilitates extinction of the light sums. In the process there is observed both exoelectronic emission and photo- and thermostimulated conductivity. However, all this is not sufficient for proof of the electronic scheme of recombination luminescence, inasmuch as the same facts equally support the hole recombination mechanism. Hence it became necessary to determine which of these two stages (releasing of electrons or of holes) leads to direct emission of the light sum, and which culminates only in redistribution of the carriers from trapping levels to luminescence centers. The hypothesis of electron recombination luminescence is disproved by the results of direct experiments: thermal dissociation of F centers does not stimulate phosphorescence if the holes are located on deeper trapping levels than the electrons. The results of our experiment cannot be explained on

the assumption of retrapping of electrons. We investigated the processes of thermal stimulation and exoelectronic emission in the region of thermal dissociation of F centers, and aside from these centers there do not form in crystals any deeper donor levels. In the course of thermal stimulation of phosphors there are not observed exoelectronic emission peaks after break-up of the F centers.

Differences between the topography of exoelectronic emission and thermal luminescence are taken into account by Bohun[11]. In the case of our specimens (characterized by a high activator concentration) this difference was of no significance inasmuch as the thermal dissociation of the F centers occurred in the entire volume of the excited phosphor layer, but this process was not accompanied by emission of the stored light sum.

If the crystals are excited at room temperatures but de-excited at a lower temperature, the phosphorescence is greatly slowed down even if it is stimulated by irradiation in the F band. In this case the emission is limited by release of trapped holes: $I \sim n_V P_0 e^{-\varepsilon/kT}$.

* * * * * * *

CONCERNING THE MECHANISM OF OPTICAL FLASH DECAY

- I.A.Parfianovich & E.I.Shuraleva

Detailed investigation of the decay of the optical flash, which is the result of recombination of free electrons with ionized luminescence centers, in alkali halide phosphors shows that for proper description of the kinetics of the process it is not sufficient to consider only the ratio of the cross sections of the recombination and electron trapping centers. This is particularly clearly evident in the case of NaCl:Ni phosphor excited with x-rays.

Fig.1 shows four decay curves for optical flash stimulated by light in the F band for NaCl:Ni phosphors with different activator concentrations. The initial F center concentration in all the specimens was the same. Comparison of the initial sections of the decay curves shows that the rate of decrease in brightness is greatest for crystals with the lowest nickel concentration (curve 4); the slowest initial decay is observed for phosphors with the highest activator concentration (curve 1). Investigation of the flash decay at different temperatures showed that the rate of decay diminishes with increase of temperature.

Another interesting and distinctive feature worthy of attention is the fact that there is no consistent correlation between the above dependences and the rate of emission of the stored light sums, as will be evident from Table 1. Column 1 in Table 1 gives the numbers of the crystals corresponding to the numbers of the curves in Fig.1; the second column gives the absorption coefficients at the peak of the activator band (λ_{max} = 246 mμ), which are proportional to the nickel concentration; the 3rd and 6th columns show the optical light sums obtained at room temperature and at 70°C, respectively, during the same interval. Inasmuch as the full light sum was not extracted by photostimulation, after exposure to light the crystals were heated. The remaining light sums extracted thermally are listed in columns 4 and 7, and the ratios $\Delta S_T / S_{opt}$ are listed in columns 5 and 8. The light sum is extracted most fully by photostimulation from crystals with the highest Ni concentration (crystal No.1). With decrease of the nickel concentration a greater fraction of the stored light sum remained unrecovered after stimulation by light.

Table 1

Degree of optical stimulation of NaCl:Ni phosphors with different activator concentrations

Crystal No.	k_{246} cm^{-1}	20°C			70°C		
		S_{opt}	ΔS_T	$\Delta S_T/S_{opt}$	S_{opt}	ΔS_T	$\Delta S_T/S_{opt}$
1	2	3	4	5	6	7	8
1	8,80	820	20	0,02	820	9,3	0,01
2	6,40	500	41	0,08	825	18,5	0,02
3	2,20	260	92	0,35	468	54,0	0,11
4	0,60	88	134	1,52	134	48,0	0,36

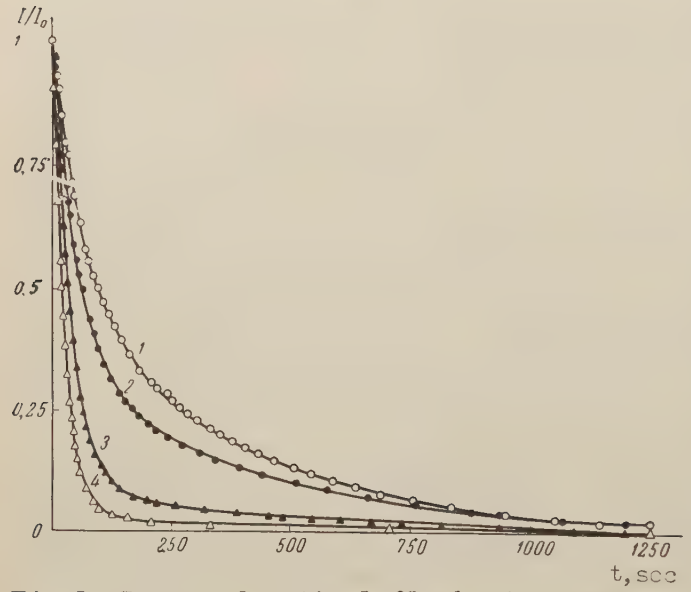

Fig.1. Decay of optical flash at room temperature for NaCl"Ni phosphors with different activator concentrations (curve 1 is for the phosphor with the highest Ni concentration; curve 4 is for the phosphor with the lowest Ni concentration).

At room temperature the optical flash is accompanied by localization of the electrons on shallower trapping levels (M and F' centers). At 70°C these centers are virtually unstable; hence photostimulated emission of the stored light sum at this temperature is more complete than at room temperature (see Table 1).

We were able to elucidate the reason for the above described regularities on the basis of the data obtained in investigating the influence of interrupted stimulating light. As was established earlier[1], under these conditions there is observed growth in the brightness of the flash after release of the electrons trapped on shallow levels.

Accumulation of electrons on shallow levels, on the contrary, is a hindrance to recombination of free electrons with ionized luminescence centers. This in turn is indicative of non-random distribution of ionized luminescence centers and electron trapping centers, which are less stable than F centers, in the phosphors. It is interesting to note that Compton & Klick[2], who investigated the changes in the absorption spectra of colored NaCl crystals, came to the analogous conclusion that "the R, M and N centers are not randomly distributed but are located near each other".

These concepts help understand the above described experimental results. Inasmuch as in phosphors with a lower activator concentration there form more light-stable M centers per F center destroyed than in crystals with a high activator concentration, naturally in low activator concentration crystals there is evinced a stronger influence of these centers on the process of recombination; hence in the phosphor with the lowest Ni concentration (crystal No.4) the flash brightness falls off most rapidly during the initial decay stage. For the same reason a smaller fraction of the light sum is extracted by optical stimulation in the case of phosphors with a lower activator concentration. Moreover, with decrease of the activator concentration the number of trapping centers per ionized luminescence center proves to be higher and the blocking action of the latter

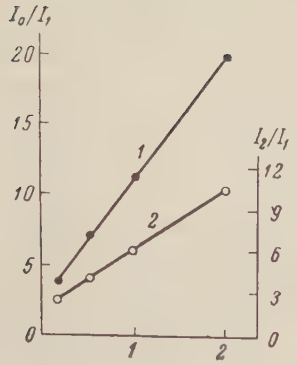

Fig.2

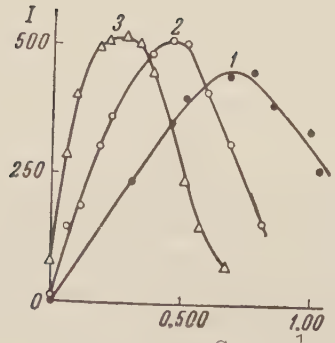

Fig.3

Fig.2. Variation of the rate of decay of the optical flash (1) and the effective growth in the brightness of the flash under intermittent stimulating light (2) with the time of irradiation of the NaCl:Ni phosphor with x-rays.

Fig.3. Variation of the initial flash brightness with the concentration of F centers for NaCl:Ni phosphors with different activator concentrations. The numbers at the curves correspond to the numbers of the curves in Fig.1 and the numbers of the crystals in Table 1.

becomes more appreciable. Upon accumulation of a certain number of electrons on shallow trapping levels recombination of electrons released from F centers with ionized luminescence centers virtually ceases and hence emission of the stored light sum stops. At the same time there are conserved in the phosphor electrons on flash levels and consequently the phosphor retains part of the stored light sum, which can be extracted only thermally.

At 70° the M centers in the phosphor with a high activator concentration are virtually unstable under the experimental conditions, but they may in part be conserved in specimens with a low activator concentration. This serves to explain why at 70° decay of the optical flash proceeds more slowly and a greater fraction of the stored light sum is released by stimulating light than at room temperature.

We obtained highly interesting data in investigating the influence of the dose of x-radiation received by the crystal on the rate of decay of the optical flash and the effect of growth in the flash brightness under intermittent stimulating light. Fig.2 shows how the ratio of the initial flash brightness to the final brightness (I_0/I_1) and the ratio of the flash brightness after release of the electron from the shallow levels to the brightness at the end of the preceding emission period (I_2/I_1) increase with increase of the x-ray dose. These

Table 2

Ratios of the optical and thermal light sums

x-irradiation time	Crystal No.2				Crystal No.4			
	S_{opt}	ΔS_T	S_T	S_{opt}/S_T	S_{opt}	ΔS_T	S_T	S_{opt}/S_T
1	2	3	4	5	6	7	8	9
20 min	386	21	143	2,7	135	29	116	1,2
2 hr	500	41	271	1,85	88	134	302	0,29
5 hr	165	206	327	0,5	34	197	306	0,10

effects cannot be explained solely by the blocking action of M centers. These effects can be interpreted only on the basis of the concept of the mechanism of recombination luminescence in NaCl:Ni phosphors. Data on this mechanism can be obtained in investigating the variation of the initial flash brightness and the optical light sum as a function of the x-irradiation time.

Fig.3 shows the variation of the initial flash brightness as a function of the F center concentration for crystals Nos.1, 2 and 3. Each of the curves has a maximum, the location of which is shifted towards the origin with decrease of the activator concentration in the crystal. Similar dependences are obtained for the variation of the optical light sum as a function of the time of x-irradiation of the phosphor (columns 2 and 6 in Table 2). Thus for example, the light sum extracted by optical stimulation from phosphors Nos.2 & 4 x-irradiated for 5 hours proves to be much smaller than the optical light sum obtained from the phosphors irradiated for only 20 min. On the other hand, the remaining light sums, i.e., the light sums subsequently extracted by thermal stimulation, are much greater for 5 hour x-irradiation (columns 3 & 7). Noteworthy is the fact that the total thermal light sums increase with the x-irradiation time (columns 4 & 8), which is consistent with increase in the number of electrons on trapping levels.

Observation of the variation in the brightness of the luminescence of NaCl: :Ni phosphors in the process of x-irradiation enabled us to bring out another distinctive feature of these phosphors. It is known that in general in the process of excitation of phosphors there occurs a gradual increase in the luminescence brightness with build-up in the number of electrons held on trapping levels. In the case of the NaCl:Ni phosphors, however, we observed a different picture: with the phosphor held in an x-ray beam its luminescence does not increase with time but on the contrary weakens.

Recombination luminescence may appear as a result of recombination of electrons with ionized luminescence centers or/and as a result of recombination of electrons with hole centers of the base material. Inasmuch as with increase of the x-irradiation time the number of electron and hole centers increases, the observed regularities cannot be reconciled with the mechanism of sensitized luminescence. Consequently, we come to the conclusion that recombination luminescence in NaCl:Ni phosphors is connected with the presence of ionized luminescence centers. It follows from a number of considerations and ample experimental data[3,4] that ionized luminescence centers are not produced by the exciting radiation. Hence it must be assumed that ionized luminescence centers are already present in NaCl:Ni phosphors prior to their excitation. Analysis of the above described experimental data on the variation of the initial flash brightness and the magnitude of the optical light sum as a function of the x-irradiation time as well as the results of observation of the variation in luminescence brightness in the process of x-ray excitation, leads us to the inference that as a result of x-irradiation there occurs a decrease in the number of ionized luminescence centers, recombination of free electrons with which leads to the appearance of different forms of emission (thermal luminescence, optical flash, and emission in the process of excitation with ionizing radiation).

Consequently, the greater the dose of x-rays received by the phosphor, the fewer the ionized luminescence centers remaining in it, which in turn leads to reduction of the initial flash brightness and decrease of the optical light sum. Since this regularity (decrease) is not observed when the stored light sum is extracted thermally, it follows that in the process of thermal stimulation part of the ionized luminescence centers destroyed or transformed by the x-rays are regenerated. In all probability this is realized by a hole mechanism.

Thus the observed dependence of the rate of decay of the optical flash as a function of the dose of x-rays received by the phosphor and the effect of growth in the flash brightness under the influence of interrupted stimulating light, can be explained by 1) decrease of the probability for recombination of free electrons with ionized luminescence centers owing to the blocking action of M centers, and 2) decrease in the number of ionized luminescence centers in the process of x-irradiation.

Before concluding, we must note the following regarding the ratio of the optical and thermal light sums. The dependence of the light sum on the method of its extraction has been investigated by one of the authors[5] and by Morgenshtern[6]. Morganshtern investigated this dependence in the case of a number of alkaline earth phosphors and established that the ratio between the optical and thermal light sums is constant. Our investigations, on the other hand, showed that the ratio between the optical and thermal light sums cannot be regarded as a constant quantity characteristic of the given phosphor. The ratio turns out to depend on the activator concentration and for a given specimen on the degree of excitation of the phosphor. This is clearly evident from the data of Table 2 (columns 5 & 9). In the case of 20 minute x-irradiation the optical light sums obtained from crystals Nos.2 and 4 are greater than the thermal light sums. Moreover, the difference for the first of the crystals is appreciably greater than for the second. In contrast, in the case of 5 hour x-irradiation the optical light sums are smaller than the thermal sums. A particularly great difference between the thermal and optical light sums is observed in the case of the phosphor with the minimum activator concentration (crystal No.4).

Thus it turns out that the dependence of the light sum on the method of its extraction is complex in character and is determined both by accumulation of electrons on shallow trapping levels in the process of optical stimulation and by the different variation of the state of the luminescence centers in extraction of the stored light sum by the optical and thermal methods.

"A.A.Zhdanov" Irkutsk State University

References

1. I.A.Parfianovich, Optika i spektroskopiya, 2, 392 (1957).
2. W.Compton & C.Klich, Phys.Rev., 112, 1620 (1958).
3. M.L.Kats & B.Z.Semenov, Doklady AN SSSR, 106, 415 (1956). (Trans.Doklady.)
4. M.L.Kats, Materialy VII Soveshchaniya po lyuminestsentsii (Transactions of the 7th Conf. on Luminescence), p.130, Tartu, 1959.
5. I.A.Parfianovich, Zhur.eksp.i teor.fiz., 21, 314, 1389 (1951).
6. Z.L.Morgenshtern, Doklady AN SSSR, 54, 791 (1946).

DISCUSSION

P.A.Pipinis: I think that the growth of the optical flash after a dark interval can be explained not by increase in the probability for recombination of optically released electrons from the F levels with luminescence centers, but by increase in the number of electrons released during the second illumination. We observed this in investigating the rise of the optical flash and photoelectron emission in the case of KBr:In crystal phosphors after excitation by cathode rays and illumination by light in the F band. After excitation at -25° there is observed an intense optical flash L (figure a) and photoelectron emission E. After the flash has almost completely decayed, the illumination is cut off and the phosphor is heated to 40°. This results in emission of part of the stored light sum

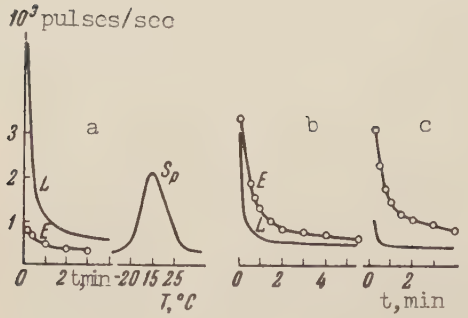

S_p. After cooling to the initial temperature (-25°) and second illumination there is observed a strong growth not only of the optical flash but also of the photoelectron emission (figure b). Both effects decay rapidly at almost the same rate. Similar results are obtained after a second heating (figure c). Such growth of the photoelectron emission and optical flash can be explained on the assumption that there exist two types of F centers: "soft" - photoactive - and "hard" - nonphotoactive centers. J.J.Oberly (Phys.Rev., 84, 1257 (1951)) postulated that existence of such "soft" and "hard" F centers to explain his results on the behavior of the photoconductivity of KBr under illumination in the F band. Apparently, during the dark interval and the subsequent heating the "hard" F centers transform into "soft" centers or perhaps the electrons from the "hard" centers go over to the "soft" centers. Whether a similar mechanism operates in NaCl:Ni phosphors is not known. It would be desirable to carry out similar experiments on these phosphors.

EXCITON EXCITATION OF LUMINESCENCE IN ACTIVATED ALKALI IODIDES AT LOW TEMPERATURE

- M.L.Kats, K.E.Gyunsburg & L.I.Golubentseva

The mechanism of energy transfer from the host lattice to the activator centers has scarcely been studied even in the case of crystal phosphors with the simplest structure such as activated alkali halide crystals.[1-7] More new experimental data are needed before one can elaborate a theory of energy transfer in crystal phosphors. In view of this we undertook an investigation of the excitation spectra of alkali iodides activated with divalent tin and lead ions.

Specifically, for the present investigation we chose KI and NaI phosphors, the exciton absorption bands of which lie at approximately 219 and 229 mμ, respectively. The excitation spectra were measured at +20° and -150° by means of a special cryostat incorporated into an SF-4 spectrophotometer which served as the monochromator. The phosphors were excited by the light from a VSFU-3 hydrogen tube or a condensed Cu spark, while the luminescence was detected by means of a FEU-19M photomultiplier.

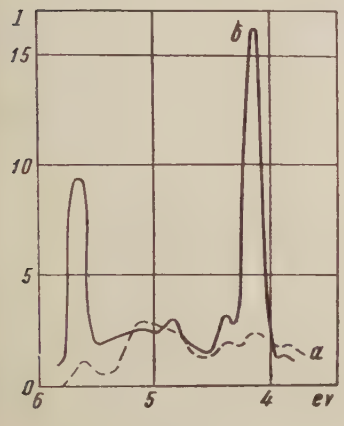

Fig.1

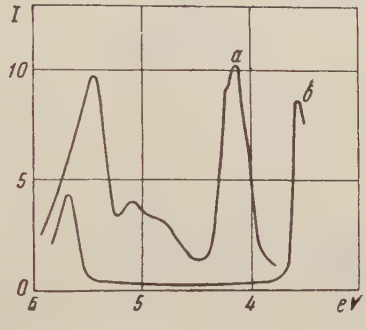

Fig.2

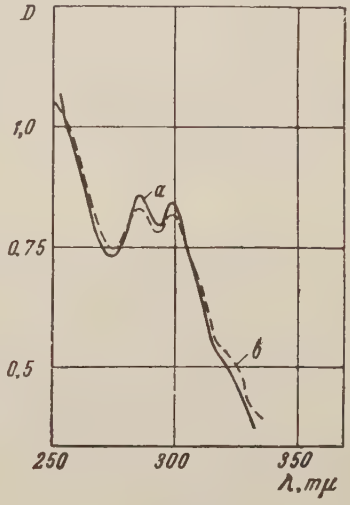

Fig.3

Fig.1. Excitation spectra of KI:SnI_2 (0.075 mole percent) at 20° (a) and -150° (b).
Fig.2. Excitation spectra of NaI:Sn (a) and KI:Pb (b) at -150°.
Fig.3. Absorption spectra of KI:Sn: a) before illumination in the exciton band and b) after illumination in the exciton band for 2 hours.

Investigation of the excitation spectra of the KI:Sn crystals showed the presence of an excitation band in the region of the exciton absorption, peaking at 219 mμ, and strong increase in the intensity of this band with decrease of temperature (Fig.1). The other bands evinced in the spectrum are due to the activating impurity. Similar bands in the region of the exciton absorption were observed in the spectra of KI:Pb and NaI:Sn crystals (Fig.2). Some distortion in the shape of the normal spectrum curve in the 240-250 mμ region is probably due to traces of thallium.

Measurements of the excitation spectra of these phosphors with different activator concentrations showed that with increase of the impurity content the intensity of the bands in the region of 219 mμ for KI and 229 mμ for NaI increases.

Earlier experiments showed that x-irradiation of Sn activated alkali halide crystals results in decrease of the activator absorption bands and reduction in the intensity of the luminescence, which is connected with formation of nonluminescing atomic tin centers.[8,9]

Additive coloring in potassium vapor of a KI:Sn crystal led to disappearance of the activator bands from the excitation spectrum owing to transformation of the ionic Sn centers into atomic ones. At the same time there was also observed complete disappearance of the exciton excitation band.

Visual observation of the luminescence of NaI:Sn with excitation in the range from 210 to 400 mμ showed that the color of the luminescence is the same with excitation in the activator and in the exciton bands.

One can judge of the interaction of the excitons with activator and thermal microdefects of the lattice from changes in the absorption spectrum of the phosphor. With a view to determining the changes in the absorption spectra of KI:Sn crystal phosphors under the influence of light in the region of intrinsic absorption, we measured the absorption of a sample before and after prolonged illumination in the exciton band. The phosphor was illuminated by the light of a condensed Cu spark through a KBr filter which completely absorbed the radiation corresponding to short wavelength intrinsic absorption and passes virtually all the light corresponding to the exciton band of KI. As a result of such irradiation in the exciton band, there occurs a noticeable decrease in the absorption in the region of the activator bands of KI:Sn (Fig.3).

Thus in alkali halide phosphors with divalent activators there apparently occurs interaction of the excitons with the activator centers, which leads both to excitation of luminescence centers and to the formation of singly charged ionic or atomic centers.

References

1. Z.L.Morgenshtern, Doklady AN SSSR, 105, 250 (1955).

2. Z.L.Morgenshtern, Zhur.eksp.i teor.fiz., 29, 903 (1955). (Trans.Soviet Physics - JETP.)

3. F.Seitz, Revs.Mod.Phys., 26, 7 (1954).

4. W.Van Sciver, Phys.Rev., 97, 1181 (1951).

5. Ch.B.Lushchik, N.E.Lushchik, G.G.Liid'ya & L.A.Teiss, Trudy IFA AN ESSR (Proceedings, Inst. of Phys. and Astronomy of the Estonian SSR Ac. of Sci.), No.6, 63 (1957).

6. G.G.Liid'ya, Ibid., No.10, 196 (1959).

7. K.J.Teegarden, Phys.Rev., 105, 1222 (1957).

8. A.S.Andrianov & M.L.Kats, Izv.AN SSSR, Ser.fiz., 21, 552 (1957). (Trans. Bulletin 21, 547).

9. Ch.B.Lushchik & G.G.Liid'ya, Trudy IFA AN ESSR, No.7, 193 (1958).

ATOMIC CENTERS IN NaCl:Ag AND KBr:Ag CRYSTAL PHOSPHORS

- V.K.Nikol'skii

It is commonly assumed that atomic centers appear in activated alkali halide crystals only after x-irradiation or additive coloring. Such centers have been investigated in detail by a number of authors[1-5], some of whom have proposed appropriate models.

We prepared polycrystalline NaCl(Ag) phosphors with an activator content of up to 20 mole percent. The phosphors were prepared by very slow cooling of the melt of the initial salts in evacuated quartz tubes. In the excitation spectra of such phosphors with activator concentrations from 1 to 20% there is evinced, in addition to the usual ionic bands, a broad band peaking at ~300 mμ; the shape of the spectrum and the frequency of this peak depend on the rate of cooling of the melt. The luminescence spectra of the NaCl:AgCl (20 mole percent) phosphor excited by monochromatic radiation and recorded photoelectrically are shown in Fig.1 (all appropraite corrections have been made in plotting the curves). Curves a and b characterize the luminescence of a very slowly cooled specimen with excitation by λ = 313 and 365 mμ, respectively. After additional heating to 250° (curve c) and 500° (curve d) followed by "quenching" to room temperature the luminescence spectrum is shifted to the short wavelength region and corresponds to the luminescence spectrum of atomic centers in an x-rayed NaCl:AgCl (0.01 mole percent) single crystal with excitation by λ = 280.3 mμ (curve e). It is obvious therefore that the luminescence of "quenched" NaCl(Ag) phosphors with a high activator concentration is due to atomic A centers.

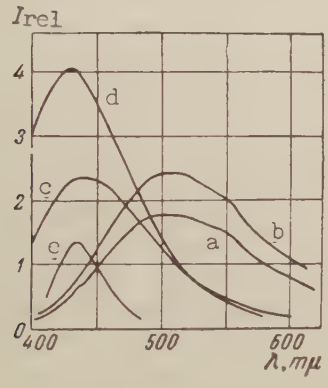

Fig.1

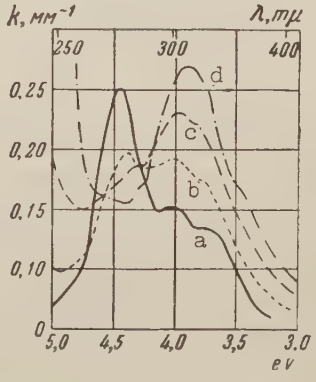

Fig.2

Fig.1. Luminescence spectra of NaCl:AgCl (20 mole percent) phosphor: a) λ_{ex} = 313 mμ, b) λ_{ex} = 365 mμ, c) after heating to 250° and rapid cooling, λ_{ex} = 313 mμ, d) after heating to 500° and rapid cooling, λ_{ex} = 313 mμ, e) luminescence spectrum of x-irradiated NaCl:AgCl (0.01 mole percent) single crystal, λ_{ex} = 280.3 mμ.

Fig.2. Absorption spectra of NaCl(Ag) single crystals x-irradiated and then bleached with visible light, prepared with different AgCl concentrations in the melt: a) 1.0, b) 2.5, c) 5.0, d) 10.0 mole percent.

Investigation of the absorption spectra of NaCl(Ag) single crystals colored with x-rays and then bleached by exposure to visible light shows that with increase of the activator concentration from 1 to 10 mole percent (in the melt) there is a tendency for the A and A^1 centers to associate into C centers, i.e., double atomic centers linked by the forces of dipole attraction.[2] The absorption peak of the C centers (Fig.2,d) approximately coincides with the peak in the excitation spectra of very slowly cooled NaCl:AgCl (20 mole percent) phosphors prior to irradiation. The peaks in the luminescence spectra of x-irradiated NaCl single crystals contain-

ing 1, 2.5 and 10 mole percent AgCl are located at 565, 550 and 545 mμ, respectively; the position of the 545 mμ peak is probably in closer agreement with the luminescence of C centers than is indicated by the data of Etzel & Schulman[1], inasmuch as at 10 mole percent AgCl these centers predominate in the absorption spectrum and the superposition of the long wavelength bands is less strongly evinced. Thus there is observed a definite similarity between the optical properties of atomic centers in x-irradiated NaCl(Ag) single crystals and the luminescence of polycrystalline NaCl(Ag) phosphors with a high activator concentration. Hence we consider that the luminescence of NaCl(Ag) phosphors with a high activator concentration both before and after "quenching" is due to atomic centers, the term being used here in the general sense of this concept.

In the spectra of nonirradiated KBr:AgBr single crystals with 2.5 mole percent activator there appears a hump on the side of the ionic band; at 5 mole percent AgBr this hump becomes a clearly pronounced absorption peak in the region of the A band (300 mμ). This peak was also obtained in the form of an individual band in the spectrum of a KBr:AgBr (1 mole percent) crystal in which the silver halide before growing the crystal was exposed to the integral light from a mercury discharge tube to the point of pronounced darkening, caused by segregation of atomic silver.

It may be inferred therefore that in silver activated alkali halide crystals there may under appropriate conditions form atomic centers, which are usually observed in x-ray or additively colored crystals.

I desire to express my gratitude to M.L.Kats for his guidance in the work and discussion of the report.

Saratov State University

References

1. H.W.Etzel & J.H.Schulman, J.Chem.Phys., 22, 1549 (1954).

2. Maenhout, W.Van der Vorst & W.Dekeyser, Physica, 23, 903 (1957).

3. M.L.Kats, Doklady AN SSSR, 85, 539 (1952); 85, 757 (1952); Optika i spektroskopiya, 3, 602 (1957).

4. L.M.Shamovskii & L.M.Rodionova, Doklady AN SSSR, 92, 939 (1953); L.M. Shamovskii & Yu.N.Zhvanko, Optika i spektroskopiya, 3, 267 (1957).

5. M.Ishiguro, T.Okuno & K.Kojima, Mem.Inst.Scient. and Industr.Res.Osaka Univ., 15, 1 (1958).

LUMINESCENCE OF NONACTIVATED ALKALI IODIDES

- N.N.Vasil'eva & Z.L.Morgenshtern

1. There have been relatively few investigations[1-7] of the luminescence of nonactivated alkali iodides. It is known that at low temperatures these crystals emit a luminescence that is not associated with an activator, but the nature of this emission is still unclear. Earlier one of us[6,7] carried out a number of studies on the general nature of the luminescence of CsI crystals. It was found that the emission spectrum of CsI comprises three bands: two of them not associated with an activator (ultraviolet and blue) and one associated with the presence of an activator. Investigation of the other characteristics of the luminescence led to the inference that these three bands are related to different luminescence centers.

2. The results obtained for CsI and the fragmentary data of other investigators led us to infer that a similar picture should be observed for other alkali iodides. Hence as the next subject for investigation we chose KI. Working with nonactivated KI crystals Teegarden[3] observed at low temperatures radiation close in frequency to that of Tl, but owing to the presence of traces of Tl in his crystals Teegarden was unable to isolate this luminescence of KI in pure form. In the present work we undertook to a) obtain crystals free of traces of Tl, and b) study the interaction of the bands, introducing In instead of Tl as the activator inasmuch as the intrinsic radiation of indium in KI is located at a lower frequency than that of Tl.[8] We obtained KI crystals free of traces of Tl from a water solution using raw materials purified of heavy metals (by means of rubinic acid) and subjected to repeated recrystallization. We also had available crystals* grown from the melt by the Stockbarger technique; some of these were free of activator, others contained different concentrations of Tl or In. We investigated the luminescence spectra of all the crystals at room temperature and at liquid nitrogen temperature with excitation by Co^{60} γ-radiation by the procedure described in Ref.7.

The following results were obtained (Fig.1):

1) In the spectra of KI crystals grown from solution there is observed one ultraviolet band peaking at ~370 mμ (Fig.1,a)[9];

2) In crystals containing high concentrations of Tl there is observed one activator band with $\lambda_{max} \approx 406$ mμ (Fig.1,c);

3) In the spectra of crystals containing low concentrations of Tl there is observed one band peaking at ~382 mμ (Fig.1,b); it may be assumed that this band actually consists of two bands - a thallium band and an ultraviolet band;

4) A clearer picture is obtained with In as the activator; at low indium concentrations there are observed two bands, an ultraviolet and a longer wavelength activator band; with increase of the In concentration the intensity of the ultraviolet band decreases while that of the activator band increases, and at high In concentrations the ultraviolet band disappears completely (Fig.1,d,e,f) just as in the case of Tl.

From these results it could be inferred that in the luminescence spectra of KI crystals there are only two bands: an ultraviolet band associated with the crystal lattice and an activator band. At first it appeared that no band analogous to the intermediate band of CsI was present in the KI spectra. More detailed investigation, however, led us to conclude that in some cases an intermediate luminescence band is present in the spectra of KI. We had available a number of nonactivated KI crystals of different origin. In the spectra of all these crystals there was observed one band in the ultraviolet region. Its peak, however, was

---

*We take this opportunity to thank L.M.Shamovskii for making available the crystals.

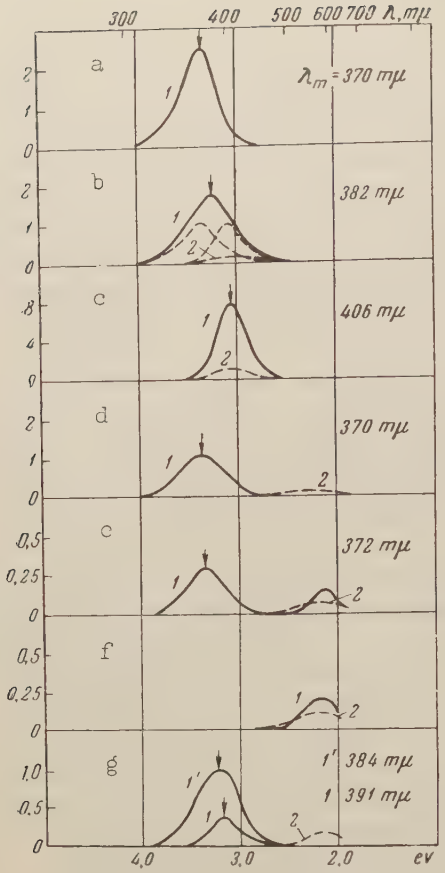

Fig.1. Spectral distribution of the emission from KI crystals excited by γ-radiation at liquid nitrogen temperature (solid lines) and at room temperature (dashed lines): a) KI crystal grown from solution, b) KI:Tl (low Tl concentration), c) KI: :Tl (high Tl concentration), d) KI:In (low concentration, e) KI:In (medium concentration), f) KI:In (high concentration), g) KI (without activator) grown from the melt (1') and KI:In (1 & 2).

not always located at the same wavelength. In crystals grown from solution this band had $\lambda_{max} \approx 370$ mμ, while in the spectra of the other crystals the band peaked at longer wavelengths. In the case of nonactivated KI the peak was located at $\lambda_{max} = 384$ mμ (Fig.1,g), i.e., virtually coincided with the emission band of KI:Tl with a low Tl concentration (Fig. 1,b). It might be assumed that this shift is due to traces of Tl; this is not the case, however, inasmuch as Tl would be evinced by its own luminescence spectrum at room temperature. In the luminescence spectrum of one of the KI:In crystals we also observed shift of the ultraviolet band to $\lambda_{max} \approx 391$ mμ (Fig.1,g). In this case again it is doubtful that the shift can be due to Tl inasmuch as the concentration of Tl to produce such a displacement of the band would have to be appreciable.

We assume, therefore, that in the luminescence spectra of these crystals, in addition to the ultraviolet band with $\lambda_{max} \approx 370$ mμ associated with the crystal lattice, there is a second, longer wavelength band analogous to the blue intermediate band of CsI. This band probably peaks somewhere in the neighborhood of 400 mμ; its precise position will be established in further investigations.

Thus it follows from our experiments that for KI crystals, just as for CsI crystals, there are observed three luminescence bands: an ultraviolet band associated with the pure lattice, and an intermediate and a long wavelength band, both of activator origin.

3. It is obviously of interest to elucidate the nature of the above-mentioned luminescence bands.

The long wavelength bands, which appear upon introduction of an activator, are undoubtedly connected with transitions inside the activator ions. Many investigations have been devoted to this luminescence, hence we will not discuss it further here. We must note, however, that as regards CsI this assertion is not trivial, inasmuch as some authors (Knoepfel et al[4]) advanced the hypothesis that the presence of Tl in CsI leads only to disturbances of the lattice, facilitating luminescence, but that the Tl itself does not yield intrinsic luminescence. In our opinion, however, the long wavelength luminescence band in the spectrum of CsI:Tl consists of radiation characteristic of the activator.*

---

*In addition to the long wavelength luminescence of Tl ($\lambda_{max} \approx 560$ mμ) in the spectra of CsI:Tl crystals at low temperatures there appears a shorter wave-

(continued on following page.....)

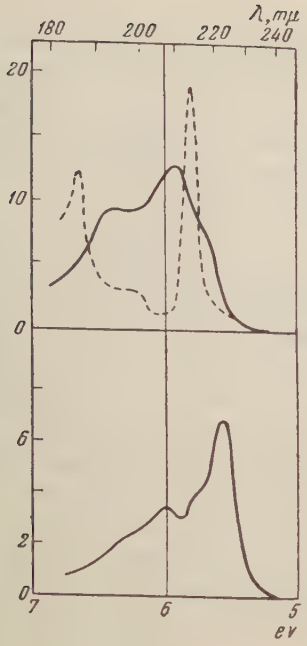

←Fig.2. Excitation spectra of the ultraviolet luminescence bands at liquid nitrogen temperature. Dashed line - spectral distribution of absorption according to Fesefeldt[11]. a) KI, luminescence band with λ_{max} = 370 mμ, b) CsI, luminescence band with λ_{max} = 340 mμ.

The intermediate band in CsI, according to Knoepfel et al[4], may be attributed to vacancy type defects. It is characterized by the highest intensity in the spectra of crystals grown from a superheated melt, and we never observed it in crystals grown from solution at room temperature, i.e., in crystals in which the equilibrium concentration of vacancies is minimal. The excitation spectrum of this band, as was shown earlier[6], is linked to the intrinsic absorption edge of the crystal. This band, in our opinion, is analogous to the blue band of zinc sulfide, which is also excited at the intrinsic absorption edge, and which some authors[10] also associate with vacancy type structural defects. It may be hypothesized that the intermediate band of KI is of the same nature, although admittedly at present there is a paucity of data on this band.

The short wavelength band in the luminescence of CsI and KI crystals, like the ultraviolet band in the luminescence of NaI observed by Van Sciver[2], may safely be attributed to the host lattice. Enz & Rossel[5], on the basis of the exponential character of the decay of scintillations corresponding to this band in CsI, infer that it is due to recombination of "degenerate" excitons. We feel that for definitive determination of the origin of this band it is essential to know the corresponding excitation spectrum.

Working with the crystals the luminescence of which comprised only this emission band we succeeded in measuring its excitation spectrum. For the measurements the crystal was placed in a cooled vacuum chamber between windows of crystalline quartz; the excitation was realized by a hydrogen tube through a vacuum monochromator with a fluorite prism and mirrors. The luminescence was recorded by means of an FEU-19 photomultiplier coupled to an amplifier. The results of these experiments are shown in Fig.2, in which we also reproduce the absorption spectrum of KI (sublimated layer) at liquid nitrogen temperature according to the data of Fesefeldt[11]. From a comparison of the curves it may be inferred that the excitation spectrum corresponds to the region of exciton absorption. It is interesting to note that in the short wavelength region ($\lambda < 185$ mμ), which corresponds to band-band transitions, the excitation curve falls off. A similar picture is observed for CsI crystals.

We also measured the decay of the ultraviolet band of KI at liquid nitrogen temperature. The decay proved to be exponential with τ = 0.9 microsec. In view of the character of the excitation spectrum and the exponential nature of the decay there is reason to assume that the ultraviolet band represents exciton radiation. This radiation is, apparently, not connected with constant structural defects, inasmuch as its intensity increases with increasing degree of perfection of the crystal lattice. This radiation appears to be quenched on structural de-

(footnote continued from preceding page)
length band of Tl, located in the blue region; this luminescence is excited in the long wavelength absorption band of the activator (~300 mμ) and at -60°K decays with $\tau = 1.8 \cdot 10^{-1}$ sec.[6]

fects and on centers of activator origin.

We felt it would be of interest to evaluate what activator concentration is necessary to quench this luminescence fully. We were able to do this on the basis of data for the KI:In crystals characterized by curves e and f in Fig.1. In the spectrum of one of them (e) the ultraviolet band is still present, while in the spectrum of the other (f) it is no longer apparent. The indium concentration in these crystals was determined from the values of the absorption coefficient in the first activator band (λ_{max} = 262 mμ), making use of the data of Shamovskii & Zhvanko[12] on the variation of the absorption coefficient at this wavelength as a function of the indium concentration in KI crystals. Knowing the activator concentration in the crystal one can readily calculate the number of unit cells per activator particle in the crystal, and, assuming a uniform activator distribution, the mean separation between activator particles. We found that in the first case the In concentration is $0.7 \cdot 10^{-5}$ mole In/mole KI (which corresponds to a mean separation between activator particles of 62 d or 218 Å); in the second case the concentration is $2.54 \cdot 10^{-5}$ mole In/mole KI and the mean separation is 43 d or 152 Å.

We desire to thank M.D.Galanin for his interest in the work and for measuring τ and N.V.Kostina for assistance in the experiments.

References

1. J.Bohanomi & J.Rossel, Helv.Phys.Acta, 25, 725 (1952); R.Hahn & J.Rossel, Ibid., 26, 803 (1953).

2. W.Van Sciver & R.Hofstadter, Phys.Rev., 97, 1181 (1955); W.Van Sciver, Nucleonics, 14, No.4, 50 (1956); IRE Trans.Nucl.Sci., NS-3, No.4, 39 (1956).

3. K.J.Teegarden, Phys.Rev., 105, 1222 (1957).

4. H.Knoepfel, F.Loepfe & P.Stoll, Helv.Phys.Acta, 29, 241 (1956); 30, 521 (1957); Z.Naturforsch., 12a, 348 (1957).

5. H.Enz & J.Rossel, Helv.Phys.Acta, 31, 25 (1958).

6. Z.L.Morgenshtern, Optika i spektroskopiya, 7, 231 (1959). (Trans.Optics and Spectroscopy.)

7. Z.L.Morgenshtern, Ibid., 8, 672 (1960). (Trans.Ibid.)

8. Yu.N.Zhvanko, Z.L.Morgenshtern & L.M.Shamovskii, Ibid., 2, 821 (1957); A.A.Dunina, Z.L.Morgenshtern & L.M.Shamovskii, Ibid., 4, 105 (1958).

9. N.N.Vasil'eva & Z.L.Morgenshtern, Ibid., 9, 676 (1960). (Trans.Optics and Spectroscopy.)

10. Z.A.Trapeznikova, Materialy V Soveshchaniya po lyuminestsentsii (Transactions of the 5th Conference on Luminescence), Tartu, 1957; F.A.Kröger & H.J. Vink, J.Chem.Phys., 22, 250 (1954).

11. H.Fesefeldt, Z.Phys., 64, 623 (1930).

12. L.M.Shamovskii & Yu.N.Zhvanko, Izv.AN SSSR, Ser.fiz., 21, 557 (1957). (Trans.Bulletin, 21, 551.)

Transactions

of the

Tenth All-Union Conference on Nuclear Spectroscopy

(Moscow, 19-27 January 1960)

(Concluded from Vol. 24, Nos.3,7,9 & 12)

ANALYSIS OF SECOND FORBIDDEN β-SPECTRA

- M.Vindushka & L.N.Zyryanova

The basic studies[1-6] devoted to analysis of the shape of second forbidden β-spectra are based on the assumption of combined S and T interaction. In the present work we give a treatment of nonunique second forbidden β-spectra ($\Delta I = 2$,no) on the basis of AV (axial vector) interaction. Our calculations show that one can find values of the nuclear parameters satisfactorily explaining the spectrum shape.

As is known, the shape of β-spectra of second forbidden transitions differs from the statistical shape. To date there have been experimental investigations of the shape of the β-spectra of the following nuclei: Cl^{36} (Ref.3), Sc^{46} (Ref.7), Fe^{59} (Ref.4), Tc^{99} (Ref.3), I^{129} (Ref.6), Cs^{135} (Ref.6) and Cs^{137} (Ref.8). The experimental correction factors for the β-spectra of Cl^{36}, Fe^{59}, Cs^{135} and Cs^{137} are shown in Figs.1-4.

The theoretical shape of second forbidden β-spectra ($\Delta I = 2$,no), according to Konopinski & Uhlenbeck[9], is defined by the following correction factor:

$$
\begin{aligned}
C_2 = {} & |g_V|^2 \Big\{ |R_{ij}|^2 \Big[\tfrac{1}{30} K^4 L_0 - \tfrac{2}{15} K^3 N_0 + \tfrac{1}{3} K^3 (2L_1 + M_0) - \\
& - 2KN_1 + \tfrac{9}{2} L_2 + 3M_1 \Big] + |A_{ij}|^2 \Big[\tfrac{1}{12} K^2 L_0 + \tfrac{3}{4} L_1 \Big] - \\
& - i (R_{ij} A_{ij}^* - \text{c.c.}) \Big[\tfrac{1}{30} K^3 L_0 - \tfrac{1}{6} K^2 N_0 + \tfrac{1}{2} K L_1 - \tfrac{3}{2} N_1 \Big] \Big\} + \\
& + |g_A|^2 \Big\{ |S_{ijk}|^2 \tfrac{1}{72} \cdot \Big[\tfrac{1}{15} K^4 L_0 + 2K^2 L_1 + 15 L_2 \Big] + \\
& + |T_{ij}|^2 \tfrac{1}{12} \Big[\tfrac{1}{15} K^4 L_0 + \tfrac{2}{5} K^3 N_0 + K^2 (L_1 + M_0) + 6KN_1 + 6L_2 + 9M_1 \Big] \Big\} + \\
& + g_A g_V \Big\{ i (R_{ij}^* T_{ij} - \text{c.c.}) \Big[\tfrac{1}{6} K^2 (L_1 - M_0) + \tfrac{3}{2} (L_2 - M_1) \Big] + \\
& + \tfrac{1}{4} (A_{ij}^* T_{ij} + \text{c.c.}) \Big[\tfrac{1}{15} K^3 L_0 + \tfrac{1}{3} K^2 N_0 + K L_1 + 3N_1 \Big] \Big\},
\end{aligned}
$$

where the R_{ij}, A_{ij}, T_{ij} and S_{ijk} are the nuclear matrix elements, the L_i, M_i and N_i are combinations of electron wave functions (these are tabulated in Ref.10), and K is the neutrino energy.

Assuming that T-invariance obtains, one can write the following ratios:[11]

$$
\frac{R_{ij}}{A_{ij}} = ix, \quad \frac{T_{ij}}{A_{ij}} = 2y, \quad \frac{S_{ijk}}{A_{ij}} = iz,
$$

where x, y and z are real numbers.

Table 1

Values of the nuclear parameters consistent with the experimental β-spectrum shape

Nucleus	x	y	z	Nucleus	x	y	z
Cl^{36}	−0,40	−0,80		I^{129}	−0,05	−0,2	10
Sc^{46}	0,5	0,5	10±5	Cs^{135}	−0,05	−0,2	10
Fe^{59}	−0,9	−0,3	0	Cs^{137}	−0,05	−0,04	0,5
Tc^{99}	−0,35	−0,45	5,5				

Using the value of 1.2 for g_A/g_V, one can obtain an equation for the theoretical correction factor C_2 in terms of the three unknown nuclear parameters x, y and z.

Comparing this equation with the experimental correction factor for the β-spectra one can determine the values of x, y and z giving the best fit.

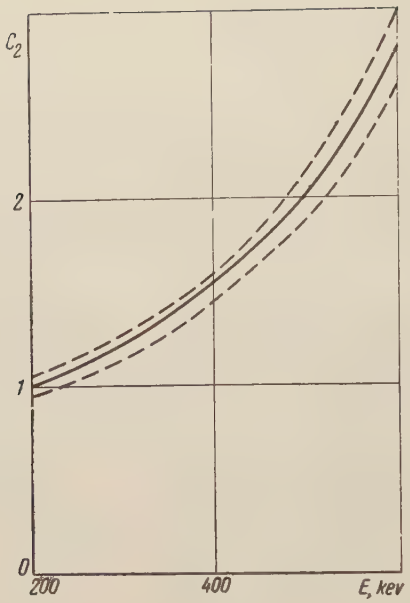

Fig.1

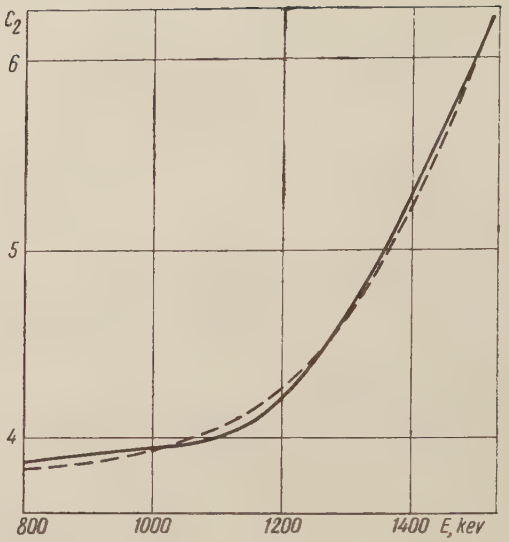

Fig.2

Fig.1. Correction factors for the β-spectrum of Cl^{36}: solid line - theoretical; dashed lines - experimental.

Fig.2. Correction factors for the β-spectrum of Fe^{59}: solid line - theoretical; dashed line - experimental.

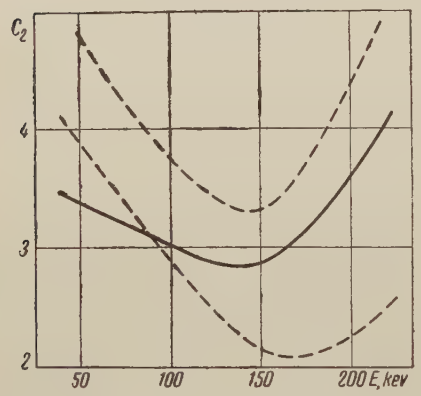

Fig.3. Correction factors for the β-spectrum of Cs^{135}: solid line - theoretical; dashed lines - experimental.

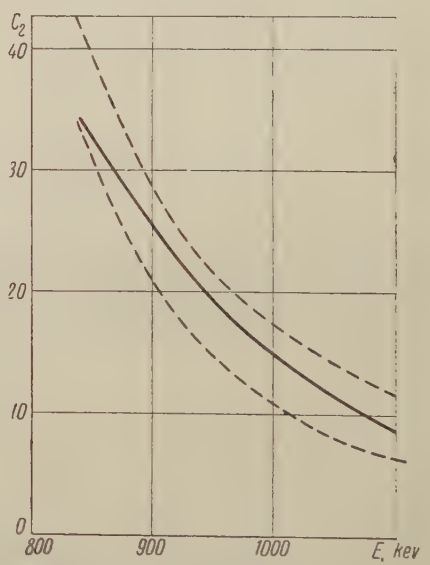

Fig.4. Correction factors for the β-spectrum of Cs^{137}: solid line - theoretical; dashed lines - experimental.

We solved the equations graphically and found the best values of x, y and z by varying the parameters to secure the best fit. Table 1 gives the values of the parameters x, y and z for the above mentioned β-spectra that yield the least root mean square deviation of the theoretical from the experimental correction factor curves. The theoretical and experimental C_2 curves for the β-spectra of Cl^{36}, Fe^{59}, Cs^{135} and Cs^{137} are shown in Figs.1-4. It can be seen that the AV form of the theory does make it possible to obtain agreement with experiment as regards the shape of the β-spectra of second forbidden transitions. In the case

of Tc^{99}, I^{129} and Cs^{135} there persist minor divergences between the experimental and theoretical factors in the low energy region (E < 100 kev) which cannot be eliminated by variation of the nuclear parameters.

The nuclear matrix element ratios x, y and z obtained from analysis of the β-spectrum shapes may be compared with the theoretical evaluations of these parameters. According to Yamada[12] there should obtain the following relationships:

$$\frac{A_{ij}}{R_{ij}} = i\frac{\Lambda\alpha Z}{2R}; \quad \frac{2A_{ij}}{T_{ij}} = \frac{\Lambda\alpha Z}{2R},$$

where

$$\Lambda = 1 + \frac{E_i - E_f}{m_0c^2}\frac{A^{1/3}}{Z}, \quad E_i - E_f = E_0 - 2{,}5,$$

and R is the nuclear radius.

Table 2

Comparison of the experimental and theoretical correction factors

Nuclei	$\left(\frac{A_{ij}}{R_{ij}}\right)_{theo} = \left(\frac{2A_{ij}}{T_{ij}}\right)_{theo}$	$\left(\frac{A_{ij}}{R_{ij}}\right)_{exp}$	$\left(\frac{2A_{ij}}{T_{ij}}\right)_{exp}$	Nuclei	$\left(\frac{A_{ij}}{R_{ij}}\right)_{theo} = \left(\frac{2A_{ij}}{T_{ij}}\right)_{theo}$	$\left(\frac{A_{ij}}{R_{ij}}\right)_{exp}$	$\left(\frac{2A_{ij}}{T_{ij}}\right)_{exp}$
Cl^{36}	4,05	2,5 ± 0,05	1,25 ± 0,03	I^{129}	10,3	20^{+10}_{-5}	5^{+4}_{-3}
Sc^{46}	6,27	⩾2	⩾2	Cs^{135}	10,7	20^{+10}_{-5}	5^{+4}_{-3}
Fe^{59}	7,38	3 ÷ 5	3 ÷ 5	Cs^{137}	12,5	20^{+10}_{-5}	25^{+12}_{-10}
Tc^{99}	8,07	2,9 ± 0,5	2,2 ± 0,4				

The values of the parameters deduced from analysis of the experimental β-spectra are compared with the values according to Yamada (theoretical values) in Table 2. It will be evident that the values of A_{ij}/R_{ij} deduced from experiment are in good qualitative agreement with the theoretical evaluations. It will be noted, however, that the equality

$$\frac{A_{ij}}{R_{ij}} \approx \frac{2A_{ij}}{T_{ij}}$$

is not fulfilled for I^{129} and Cs^{135}. Apparently, for proper evaluation of these matrix elements one must make certain more specific assumptions regarding the properties of the nuclei.

Making use of the correction factors found from analysis of the β-spectra and taking into account the corresponding log ft values for the β-transition, one can find the value of one matrix element. The values of $|A_{ij}|^2$ deduced in this manner are listed in Table 3.

In the $\langle C_2 \rangle$ column of Table 3 we list the values of the correction factor averaged over the β-spectrum. These values are necessary for calculating the reduced lifetimes of the nuclei, taking into account the nonstatistical shape of the β-spectrum. The values of log f_0t and log f_2t for second forbidden transitions are also listed in Table 3.

Table 3

Correction factor values that must be taken into account in calculating the reduced lifetime of β-transitions

Nuclei	$\lvert A_{ij}\rvert^2$	$\langle C_2 \rangle$	lg f_0t	lg f_2t	Nuclei	$\lvert A_{ij}\rvert^2$	$\langle C_2 \rangle$	lg f_0t	lg f_2t
Cl^{36}	6,5	2	13,5	13,8	I^{129}	0,4	0,13	13,5	12,6
Sc^{46}	2,5	2	13,1	13,4	Cs^{135}	0,25	0,16	13,2	12,4
Tc^{99}	1	5,6	12,3	13,0	Cs^{137}	0,006	0,06	12,0	10,8

References

1. C.S.Wu & L.Feldman, Phys.Rev., 76, 693 (1949).
2. H.W.Fulbright & J.C.D.Milton, Phys.Rev., 82, 274 (1951).
3. L.Feldman & C.S.Wu, Phys.Rev., 87, 1091 (1953).
4. F.R.Metzger, Phys.Rev., 88, 1360 (1952).
5. L.N.Zyryanova & L.A.Sliv, Izv.AN SSSR, Ser.fiz., 16, 310 (1952).
6. C.S.Wu, in "Beta- and Gamma-ray Spectroscopy", edited by Kai Siegbahn, Amsterdam, 1955.
7. G.L.Keister & F.H.Schmidt, Phys.Rev., 93, 140 (1954).
8. L.M.Langer & R.J.D.Moffat, Phys.Rev., 82, 333 & 635 (1951).
9. E.J.Konopinski & G.Uhlenbeck, Phys.Rev., 60, 308 (1941).
10. B.S.Dzhelepov & L.N.Zyryanova, Vliyanie elektricheskogo polya atoma na beta-raspad (Influence of the electric field of the atom on beta-decay), M.-L., 1956.
11. M.Yamada & M.Morita, Progr.Theoret.Phys., 8, 439 (1952).
12. M.Yamada, Progr.Theoret.Phys., 9, 268 (1953).

SYSTEMATICS OF REDUCED LIFETIMES FOR β-TRANSITIONS OF DIFFERENT DEGREES OF FORBIDDENNESS

- L.N.Zyryanova & V.M.Mikhailov

In constructing decay schemes and level diagrams the level spin assignments are frequently determined on the basis of the ft values for the β-transition. In addition, the reduced β-transition lifetime, which is directly related to the nuclear matrix element, is often helpful in elucidating the details of the nuclear structure. In view of this it is useful to consider the distribution of ft values for β-transitions of different degrees of forbiddenness.

In the present communication we give the results of calculation of the ft values for β-transitions of all types. By way of initial data we used the experimental results collected in the tables of Dzhelepov & Peker[1] and Strominger, Hollander & Seaborg[2], as well as more recent data published up to 1960 in the literature. At present about 2400 β-transitions are known. For purposes of the presented systematics we chose the 1100 most reliable cases; this group includes transitions for which there are available data on the end-point energy, the period, the branching ratio, and the spin and parity of the initial and final states.

For most of the β-transitions, except the unique group, the values of ft were calculated by means of formulas for allowed transitions. For the function

$$f = \int_1^{E_0} F(E, Z)\, Ep\,(E_0 - E)^2 dE$$

we used the tabulated values[3] calculated taking into account the Coulomb field, screening and finite nuclear size.

In the case of transitions by orbital electron capture for calculating ft we used the values of f_K and f_L, found in the work of Refs.4 & 5, also taking these effects into account.

For the unique transitions we took into account the divergence of the β-spectrum shape from the statistical one. The integral function for forbidden decay

$$f_n = \int_1^{E_0} C_n F(E, Z)\, Ep\,(E_0 - E)^2 dE$$

contains the correction factor C_n. In our calculations we used precise values of this function found by the method of numerical integration in the work of Ref. 6.

Work on the systematics of the lifetimes of β-transitions has been carried out by various authors[7-11] over a period of years and the principal characteristics of the distribution of log ft values are well known. The data presented below are based on more extensive statistical material and hence afford a more detailed picture of the distribution of log ft values.

Fig.1 tives a general histogram of log ft values for β-transitions classified according to the usual selection rules, i.e., into allowed, first and second forbidden transitions. It will be evident that in the 5 to 8 region there is considerable overlapping of the log ft values for allowed and first forbidden transitions. Hence in this log ft region spin assignments for nuclear levels on the basis of the log ft value can be made only if it is known from independent data whether parity changes in the given transition.

Fig.2 shows the log ft histogram for allowed transitions. There is clearly evinced a peak corresponding to the group of superallowed transitions (log $ft < 3.8$) including transitions between mirror nuclei and 0—0 transitions. Noteworthy is the rather slow descent of the curve on the side of high ft values. It will be seen that a large number of transitions are characterized by log ft values exceeding

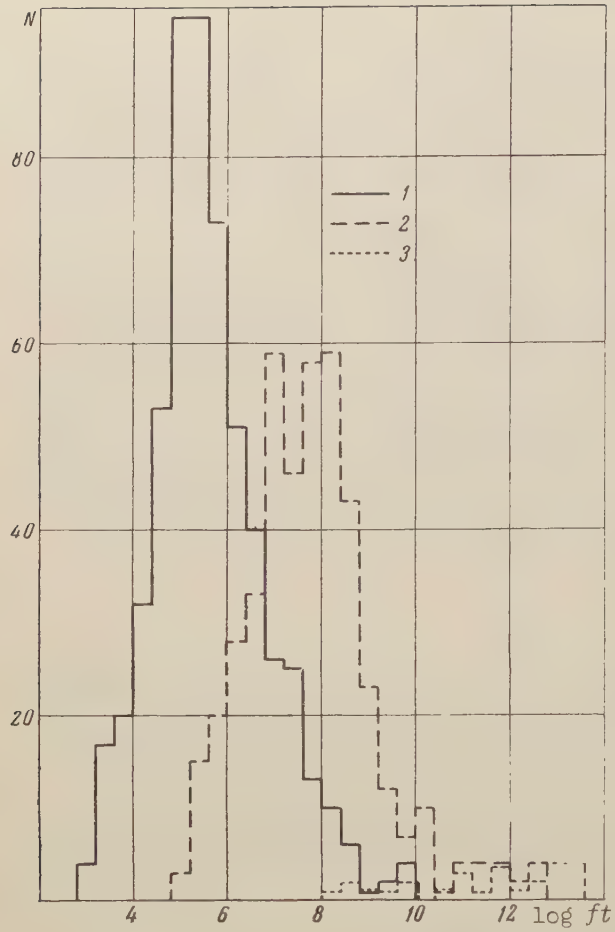

Fig.1. General log ft histogram for allowed (1), first forbidden (2) and second forbidden (3) β-transitions.

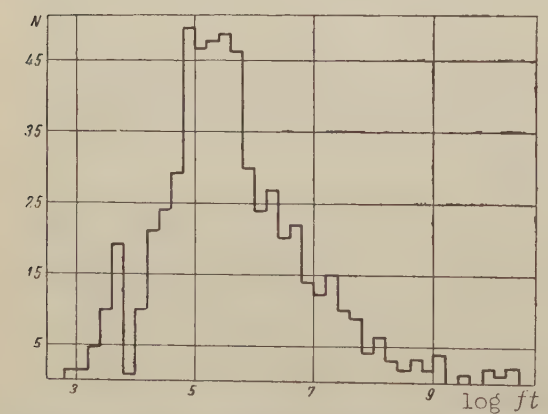

Fig.2. Log ft histogram for allowed β-transitions.

6, although it is often assumed that this is the upper bound for allowed transitions.

The histograms for first forbidden transitions with $\Delta I = 0$, 1 and 2 are shown in Fig.3. For unique transitions ($\Delta I = 2$) we give the values of log f_1t which are more representative of the influence of nuclear structure than the values of log ft.

The plot for $\Delta I = 0$ transitions shows the presence of a noticeable group of favored first forbidden transitions (log $ft < 6$). This group comprises mainly β-transitions in nuclei with values of Z and N close to twice the filled shell numbers: Z = 82 and N = 126. The low values of log ft for these transitions are explained by the maximal overlapping of the wave functions of the initial and final states in nuclei near twice the magic numbers.

In the case of $\Delta I = 1$ transitions the group of favored transitions is less clearly evinced.

Fig.4 shows the log ft distribution for second forbidden transitions. As a group (c) and separated according to ΔI. In the case of unique transitions ($\Delta I = 3$) we give the values of log f_2t.

The distributions for allowed and first forbidden transitions have central groups with a noticeable maximum, which makes it possible to calculate the mean value of log ft for each group. The calculated mean values are given in the accompanying table; the indicated uncertainties were found by comparing the given log ft values with the mean value and thus represent the arithmetic mean error.

It has been noted in the literature that the mean values of log ft for first forbidden transitions with $\Delta I = 0$ and $\Delta I = 1$ differ appreciably; thus Konopinski[12] gives 6.5 and 7.6, respectively. In the table we give the results of calculation of the average values of log ft for such transitions, excluding favored transitions. The mean values for first forbidden transitions with $\Delta I = 0$ and $\Delta I = 1$ are appreciably closer than indicated above: 7.3 and 7.8, respectively. Konopinski[12] explains the difference between the mean values of log ft for transitions with $\Delta I = 0$ and $\Delta I = 1$ by the contribution from pseudoscalar interaction. At present one cannot

Mean values of log ft

Degree of forbiddenness			Overall mean	Mean for nuclei with even A	Mean for nuclei with odd A
Allowed	Superallowed		3,5±0,2 (39)	3,5±0,2 (17)	3 5±0,2 (22)
	Unfavored		5,8±0,9 (522)	5,7±0,9 (240)	5,8±0,8 (282)
First forbidden	ΔI=0	Favored	5,4±0,3 (11)	5,4±0,2 (8)	5,3±0 1 (3)
		Unfavored	7,3±0,6 (117)	7,6±0,4 (62)	7,0±0,7 (55)
	ΔI=1	Favored	5,6±0,2 (6)	5,7±0,2 (5)	5,3 (1)
		Unfavored	7,8±1,0 (170)	8,2±1,2 (91)	7,4±0,7 (79)
	ΔI=2 (unique)		8,5±0,8 (123)	8,5±0,8 (75)	8,5±0,8 (48)
Second forbidden	ΔI=2		11,4±1,2 (22)	11,7±1,6 (8)	11,2±1,5 (14)
	ΔI=3 (unique)		11,7±1,1 (5)	11,7±1,1 (5)	—

The figures in parentheses give the number of cases on which the mean value is based.

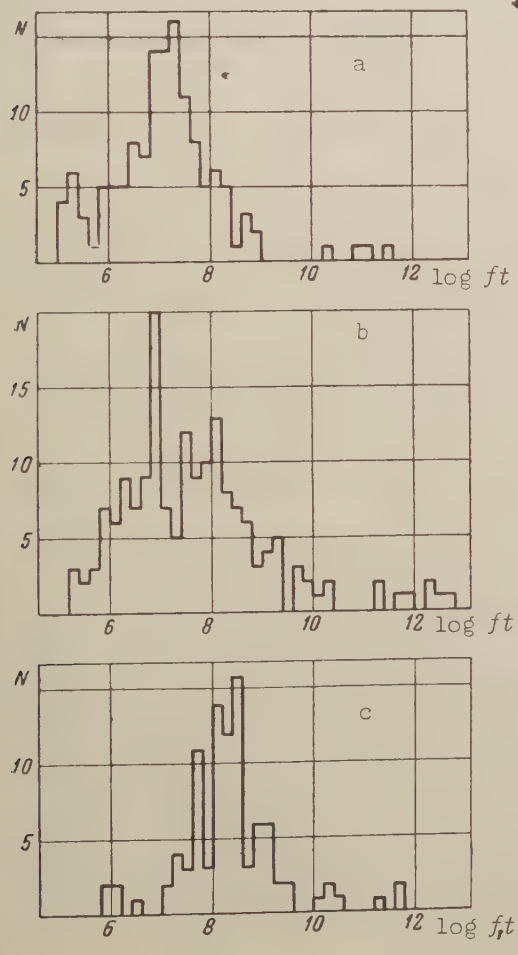

←Fig.3. Log ft histogram for first forbidden transitions with a) ΔI = 0, b) ΔI = 1, c) ΔI = 2.

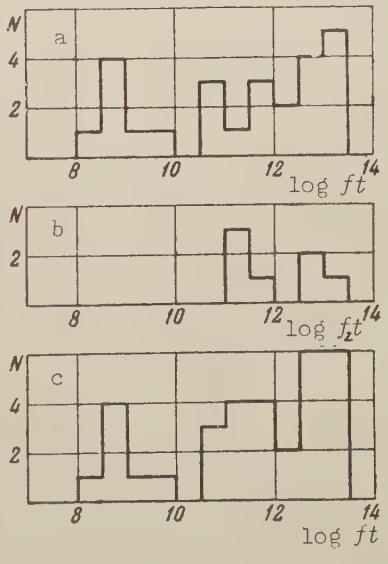

Fig.4. Log ft histogram for second forbidden transitions with a) ΔI = = 2 and b) ΔI = 3; c) common histogram for second forbidden transitions.

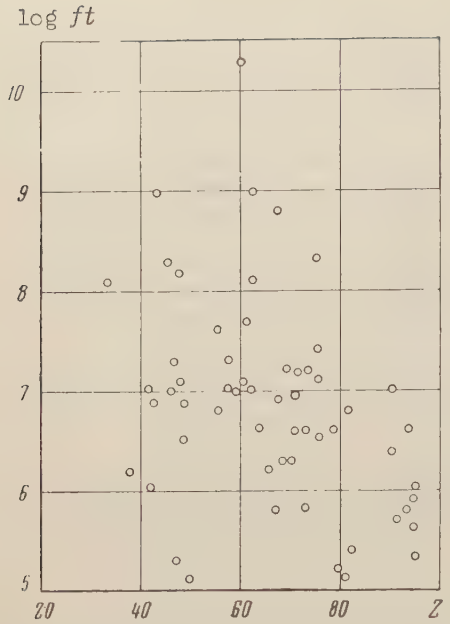

Fig.5. Variation of log ft with Z for ΔI = 0 (yes) transitions.

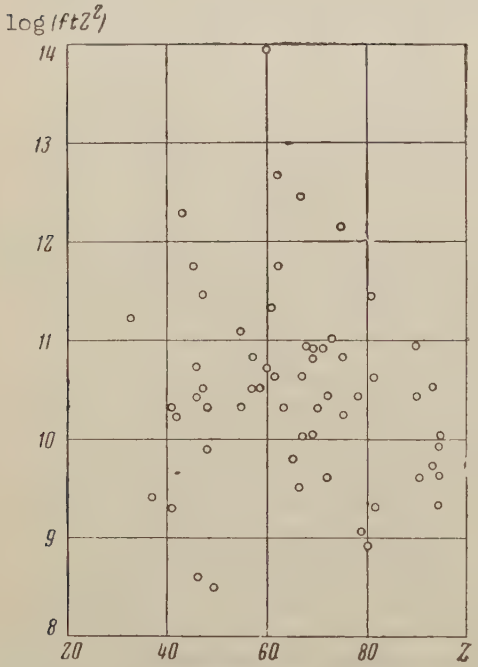

Fig.6. Variation of log (ftZ^2) with Z for ΔI = 0 (yes) transitions.

assert that the presence of this invariant form of interaction in β-decay is proved.

A number of authors[7] report that the value of log ft for allowed transitions in nuclei with odd A is on the average smaller than for nuclei with even A. As will be evident from the table, according to our calculations the values of log ft for nuclei with odd and even A are actually close: 5.8 and 5.7, respectively, so there does not appear to be any correlation between the mass number being odd or even and the log ft value.

In contrast to the above, in the case of first forbidden transitions (except unique) the mean values of log ft for nuclei with odd A are appreciably smaller than the values for nuclei with even A.

It is of interest to determine the variation of log ft with the number of nucleons in the nucleus. If one plots log ft vs N, Z and A for allowed transitions (excepting superallowed ones) it becomes apparent that there is no consistent dependence of the reduced probability on the number of particles in the nucleus. This is consistent with the theoretically inferred constant value of log ft, inasmuch as the nuclear matrix element operators for allowed transitions do not act on the radial part of the nuclear wave functions, wherein the dependence on the number of nucleons is contained.

In the case of first forbidden transitions, however, there is a noticeable decrease of log ft with increase in the number of nucleons in the nucleus. The Z dependence of log ft for ΔI = 0 (yes) transitions is shown in Fig.5.

This Z dependence can be explained on the basis of the ξ approximation.[3] The correction factor for first forbidden spectra leads to the appearance of the Coulomb factor $\left(\frac{\alpha Z}{2R}\right)^2$ in the expression for the total transition probability. If, in addition, for purposes of evaluation we assume that the matrix elements $|\int \mathbf{r}|^2$ and $|\int \vec{\sigma} \cdot \mathbf{r}|^2$ are proportional to the square of the nuclear radius, it becomes apparent that a more constant quantity with variation in the number of nucleons will be log (ftZ^2). The character of the distribution of this function for ΔI = 0 (yes) transitions is shown in Fig.6. As a result of introduction of the Z^2 factor the general tendency of log ft to decrease is reduced, but the scatter of log ft values for the same Z, which reflects the individual structure of the nuclei, remains equally significant.

We desire to express our deep gratitude to B.S.Dzhelepov for his interest in the work and F.I.Lanelen for assistance in carrying out the calculations.

References

1. B.S.Dzhelepov & L.K.Peker, Zkhemy raspada radioaktivnykh yader (Decay schemes of radioactive nuclei), M.-L., 1958.
2. D.Strominger, J.M.Hollander and G.T.Seaborg, Table of Isotopes, Revs. Mod.Phys, 30, 585 (1958).
3. B.S.Dzhelepov & L.N.Zyryanova, Vliyanie elektricheskogo polya atoma na beta-raspad (Influence of the electric field of the atom on beta-decay), p.103, M. 1956.
4. I.M.Band, L.N.Zyryanova & Ch'ing Ch'en Jui, Izv.AN SSSR, Ser.fiz., 20, 1387 (1956). (Trans.Bulletin, 20, 1269.)
5. I.M.Band, L.N.Zyryanova & Yu.P.Suslov, Ibid., 22, 952 (1958). (Trans. Bulletin, 22, 943.)
6. L.N.Zyryanova, Ibid., 23, 875 (1959). (Trans.Bulletin, 23, 867.)
7. E.Feenberg & G.Trigg, Revs.Mod.Phys., 22, 399 (1950).
8. B.S.Dzhelepov & A.V.Kudryavtseva, Zhur.eksp.i teor.fiz., 19, 791 (1949).
9. B.S.Dzhelepov, Ibid., 19, 784 (1949).
10. C.S.Wu, Revs.Mod.Phys., 20, 386 (1950).
11. L.A.Nordheim, Ibid., 23, 322 (1951).
12. R.W.King & D.C.Peaslee, Phys.Rev., 94, 1284 (1954).
13. E.J.Konopinski, "Theory of Forbidden β-Transitions" in Beta- and Gamma-Ray Spectroscopy, edited by Kai Siegbahn, Amsterdam, 1955.

INTERNAL CONVERSION WITH PAIR PRODUCTION IN THE DECAY OF Ta^{182}

- S.S.Vasilenko, M.G.Kaganskii, D.L.Kaminskii & S.F.Koksharova

The level diagram of W^{182} has a number of distinctive features. Up to an energy of 1 Mev there are present only excited states belonging to the ground state rotational band characteristic of all deformed even-even nuclei. Beginning with 1.2 Mev there appears an appreciable number of closely spaced levels, which at present are interpreted as rotational levels belonging to a number of different bands[1,2].

The diagram of Fig.1 shows the levels of W^{182} excited in β-decay of Ta^{182}. An appreciably greater number of levels is excited in decay of Re^{182} by electron capture; however, we shall not discuss these levels here.

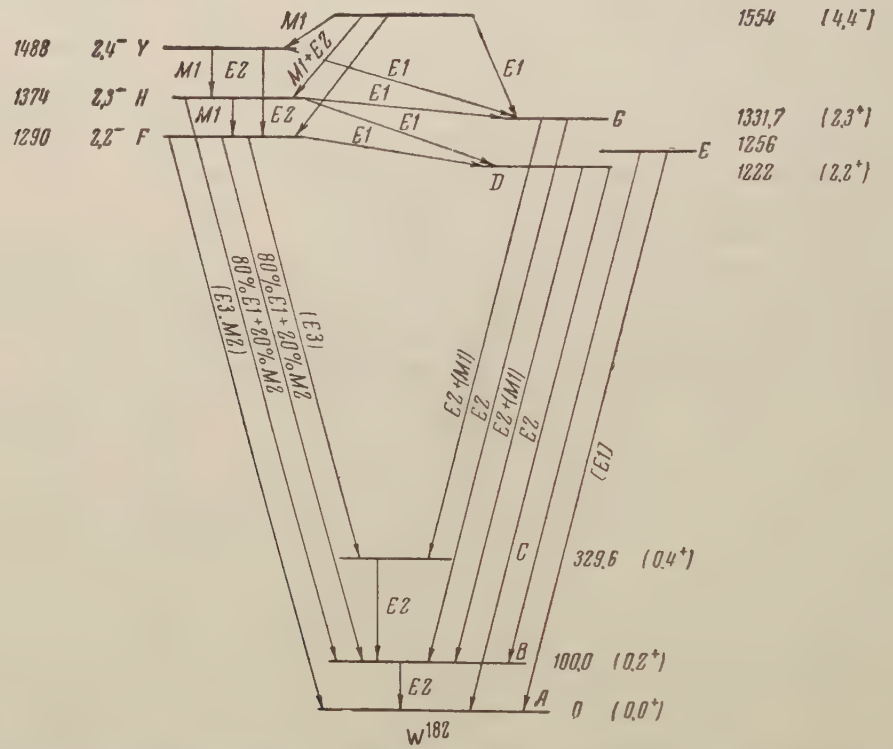

Fig.1. W^{182} level diagram. The multipole orders of the transitions with energies greater than $2mc^2$ are based on the data of the present investigation.

The purpose of the present work was to investigate the transitions with energies greater than $2mc^2$ by means of the data on internal conversion with pair production. As will be evident from Fig.1, the transitions of this energy may be regarded as transitions through an "energy slit". Hitherto, there have been few studies of these transitions. Of particular interest are the transitions between the levels of the rotational bands with K = 2- and K = 0+ (Fig.1). The nature of the negative parity levels consistently observed in the spectra of even-even nuclei is still unclear. Bohr & Mottelson[3] hypothesized that the excitation of these levels is due to collective octupole nuclear oscillations. In this case the E3 transition probability may be appreciably greater than the probability for the corresponding single-particle transition. Hence the data on the multipole orders of the FB, FC and HB transitions (see Fig.1), which may involve E3 radiation, are of particular interest. Little, however, is known regarding these

transitions; the multipolarity of even the strongest transition in this series - the FB transition - is unclear. According to the data of Murray, Boehm, Marmier & DuMond[4], this transition is characterized by a mixture of M2 and E3. Gallagher & Rasmussen[5] note, however, that the value of the K conversion coefficient for this transition obtained by Murray et al should be reduced by 20%. In view of this the FB transition may include a certain fraction of E1 radiation. Actually, the corrected value of α_K for this transition is $4.8 \cdot 10^{-3}$. The theoretical values given by Sliv & Band[6] are $1.1 \cdot 10^{-3}$ for E1, $5.2 \cdot 10^{-3}$ for E3 and $12.9 \cdot 10^{-3}$ for M2. It will be seen therefore that the experimental data are consistent with E3, E1 + M2 (with a major fraction of E1) and even E1 + M1 + E3.

The lifetime of the F level, according to the data of Sunyar[7], is $(1.0 \pm 0.05) \cdot 10^{-9}$ sec. This represents retardation by a factor of $\sim 10^8$ relative to the value for a single-particle transition, if it is assumed that the FB transition is mainly E1. If, on the other hand, it turns out that the multipole order of this transition is E3, its probability turns out to be 20 times greater than the probability for a single-particle E3 transition according to Weisskopf's formula.

In the present work for determining the multipolarities we used the procedure described in Ref.8. This procedure consists in comparing the intensities of the internal conversion positron peak with the K shell conversion electron peak for the same transition. In a number of cases this procedure is also convenient for analysis of mixed transitions. This pertains particularly to E1 + M2 and E1 + E3 transitions inasmuch as the Γ/α_K ratio for E1 transitions is approximately two orders of magnitude greater than the ratio for M1 and E3 transitions. Here Γ is the coefficient of internal conversion with pair production.

As will be evident from Fig.1, the FB and HB transitions may involve E1, M2 and E3 radiations (according to the spin and parity selection rules). In this case, as will be evident from the examples cited above, the availability of the data on the intensity of the γ-transitions and conversion electrons, i.e., knowledge of the value of α_K, is not sufficient for making an unambiguous multipole order assignment. If, however, one has data on internal pair production, one can determine the composition of the radiation. Thus, using x, y and z, respectively, to denote the fractions of E1, E3 and M2 radiations, we can write

$$x + y + z = 1; \tag{1}$$

$$\frac{x\Gamma_{E1} + y\Gamma_{E3} + z\Gamma_{M2}}{x\alpha_K^{E1} + y\alpha_K^{E3} + z\alpha_K^{M2}} = \left(\frac{\Gamma}{\alpha_K}\right)_{\text{exp}}; \tag{2}$$

$$x\alpha_K^{E1} + y\alpha_K^{E3} + z\alpha_K^{M2} = (\alpha_K)_{\text{exp}}. \tag{3}$$

Here $\left(\frac{\Gamma}{\alpha_K}\right)_{\text{exp}}$ is the ratio of the areas under the positron peak and the K conversion peak for the same transition, Γ_{E1}, Γ_{E3} and Γ_{M2} are the theoretical values of the pair conversion coefficients, and α_K^{E1}, α_K^{E3} and α_K^{M2} are the respective K shell conversion coefficients. Thus by solving the above set of equations we can find the composition of the radiation in the FB and HB transitions. Accordingly, in our work, we measured the pair conversion positron and conversion electron spectra. The data on the relative γ-ray intensities, necessary for determining the experimental K shell conversion coefficients, were taken from the work of Voinova, Dzhelepov & Zhukovskii[9].

The measurements were carried out on the β-spectrometer described in Ref.10. The sources were prepared of thermal neutron irradiated tantalum oxide. In obtaining the positron spectrum we used a relatively large source: 30 x 10 mm^2. The resolution of the spectrometer in the experiments was 1.8%.

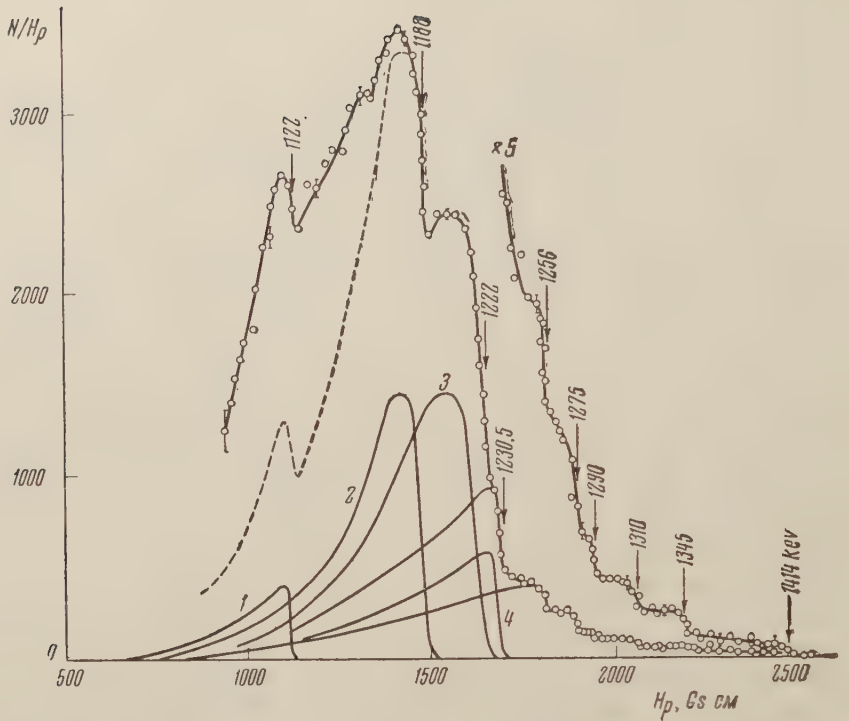

Fig.2. Spectrum of internal conversion positrons formed in the decay of Ta^{182}. Points - experimental results; dashed line - some of all the separated components; 1,2,3 & 4 - partial positron spectra associated with the 1122, 1189, 1222 and 1231 kev transitions, respectively. The figures at the jumps in the curve indicate the corresponding γ-transition energies.

Multipole order assignments for the γ-transitions in W^{182}

Transition energy, kev		K-line intensity S_K	Positron intensity S_+	$(\Gamma/\alpha_K)\cdot 10^3$				Multipole order
				calc.			exper.	
Our data	Backstrom[12]			*E1*	*E2*	*M1*		
1122	1121,6	140	16	2,90	0,38	0,11	0,32	*E2*
1188	1189,4	86	75	11,4	1,60	0,45	2,50	75%*E1*+25%*M2*
1222	1220	100	100	21,0	2,80	0,82	2,80	*E2*
1231	1231	35	36	23,0	3,10	0,94	2,90	*E2*
1256	1254	2,5	14	32,0	4,25	1,40	16,0	[*E1*]
1275	1273	3,3	13	41,0	6,2	2,15	11,0	80%*E1*+20%*M2*
1290	1289	20,0	5,5	49,5	7,9	2,40	1,0	*M2*
1310	—	—	4,0					?
340	—	—	3,6					?
410	—	—	2,3					?

Our measurements showed that internal conversion with pair production in the decay of Ta^{182} is very weak. The investigated effect is less than 20 times stronger than the background. For measuring the background we used the procedure described in Ref.11. The positron spectrum is shown in Fig.2. We determined the γ-ray energies from the midpoints of the rectilinear sections in the positron curves $E_\gamma = E_+ + 2mc^2$, where E_+ is the energy corresponding to the midpoint. The γ-transition energies determined in this manner are shown in the accompanying table together with the γ-transition energies obtained by Backstrom[12] in observing photoelectrons.

As will be evident from the table, there are evinced in the positron spectrum all the reliably known transitions in the decay of Ta^{182} except for the relatively weak transition with E_γ = 1155 kev. In addition, as will be evident from Fig. 2, there are manifested three new, hitherto unknown, transitions with energies of 1310, 1340 and 1410 kev. The intensities of these transitions are very low and we were unable to detect the corresponding conversion lines in the electron spectrum owing to the strong background. The location of the 1310, 1340 and 1410 kev transitions in the Ta^{182} decay scheme is unclear. Gallagher & Rasmussen[5] in investigating the decay of Re^{182} established that W^{182} has an excited level at 1406 kev. Possibly the observed 1310 and 1410 kev γ-rays correspond to transitions from this level to the first excited and ground states of W^{182}.

For determining the transition multipolarities one must know the intensities of the partial positron spectra associated with the individual γ-transitions. In order to resolve the partial spectra (Fig.2) in each case we determined the position and height of the hump corresponding to the end-point energy of the partial spectrum. For plotting the rest of the spectrum one must know the positron distribution in energy. This distribution was calculated in the Schrödinger approximation of the theory of internal conversion with pair production. The Schrödinger approximation, as was shown by Rose & Uhlenbeck[13], is valid for all Z in the range of transition energies $E_\gamma < 3\,mc^2$, i.e., can be used for all the transitions in W^{182}. The positron distribution for low energy transitions is the same for E1, E2 and M1 transitions. We assume that this distribution remains the same for all other multipole orders, although there are no theoretical calculations for these. By way of example, in Fig.2 we show the partial spectra of the positrons associated with the 1122, 1188, 1222 and 1231 kev transitions (solid curves 1, 2, 3 & 4). The spectrum representing the sum of all 10 components is given by the dashed line in Fig.2. It will be seen that in the low energy region this spectrum differs substantially from the experimental curve. This is due primarily to scattering of the positrons in the relatively thick source (2 mg/cm^2) used in our measurements.

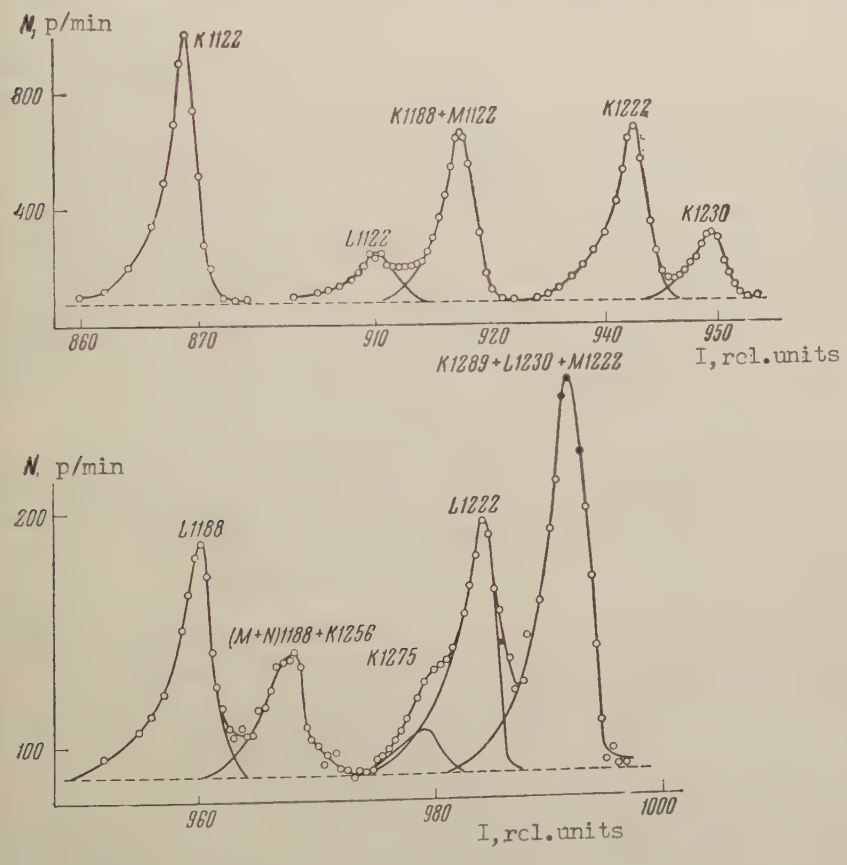

Fig.3. Ta^{182} conversion electron spectrum.

We note that investigation of the higher energy γ-rays accompanying the decay of Ta^{182} by observation of internal conversion with pair production is very convenient. Inasmuch as the energy of the γ-rays only slightly exceeds the threshold for pair production, the corresponding positron spectra are well

separated with a spectrometer resolution of 1.8%. Such resolution, however, is inadequate for analysis of the conversion electron spectrum. Hence in investigating the conversion electron spectrum we used narrow sources (1 mm width). The relative line half-width in this case was 0.30%. The recorded spectrum is reproduced in Fig.3.

The relative intensities of the K conversion lines and the corresponding partial positron spectra are given in the accompanying table. In both cases the intensity of the conversion electrons for the 1222 kev transition was taken as 100. The intensity of the K line of the 1256 kev transition was determined only approximately. As will be evident from Fig.3, the K1256 and (M + N)1189 conversion electron lines are not resolved. The intensity of the (M + N) line was evaluated from the intensity of the L line of this transition: it was assumed[14] that $S_{M+N} = 0.3\ S_L$. Clearly use of this approximation can lead to a great error in determining the intensity of the K line of the 1256 kev transition inasmuch as the intensity of this line proved to be about half the intensity of the (M + N) line of the 1189 kev transition.

In the table we list the values of the ratio Γ/α_K only for E1, E2 and M1 radiations, inasmuch as there are no calculations in the Schrödinger approximation for other types of radiation. However, when M2 or E3 radiation is present in mixture with E1, one can neglect the contributions from M2 or E3 to pair conversion. In calculating the Γ/α_K ratios the coefficient Γ was calculated by means of the formulas given by Rose & Uhlenbeck[13], while the conversion coefficient α_K was taken from the tables of Sliv & Band[6]. The experimental value of the Γ/α_K ratio was determined from the ratio of the areas under the positron and K conversion electron peaks:

$$\left(\frac{\Gamma}{\alpha_K}\right)_{exp} = f\frac{S^+}{S_K}. \qquad (4)$$

The normalizing factor f was taken so as to obtain agreement of the experimental Γ/α_K ratio for the 1222 kev transition with the calculated one, assuming it to be E2. Direct determination of $(\Gamma/\alpha_K)_{exp}$ by measurement of the positron and K conversion line using the same source, as was done in the work of Ref.8, was inconvenient in our case, for in using a wide source one could not resolve most of the conversion lines. The procedure employed has the further advantage that in normalizing the Γ/α_K ratio to the 1222 kev transition we indirectly take into account the scattering of the relatively soft positron radiation in the source, inasmuch as most of the investigated transitions lie in the same relatively narrow energy range, so that the corrections for positron scattering are approximately the same.

As a result of our measurements and calculations we arrived at the following multipole order assignments.

1122 kev. The experimental value of Γ/α_K agrees with the calculated value for E2. The admixture of M1, if any, must be small. This is in agreement with the available data on this transition.

1188 kev. As will be evident from the table this transition is mixed. Inasmuch as the parity of the F level (Fig.1) is undoubtedly odd and M1 and E2 radiation is forbidden by the parity selection rules, it is apparent that the FB transition must comprise E1 radiation. Calculations by means of Eqs.(1)-(3) yield 75% E1 + (25±8)% M2.

We note that the experimental value of the K conversion coefficient indicates 20% E1 + 80% E3; however, the experimental value of Γ/α_K in this case would be 3-4 times smaller than found in our work. Determination of the fraction of E3 in the 1188 kev transition is of great interest. Allowing for the measurement errors, we found that the admixture of E3 in this transition cannot exceed 20%.

1222 kev. In accord with the data in the literature, the multipolarity of this level was assumed to be E2.

1231 kev. This transition is predominantly E2; the admixture of M1, if any, is minor.

1256 kev. The E1 assignment give for this transition in the table is tentative, inasmuch as the experimental value of Γ/α_K differs appreciably from the calculated value for E1. As noted above, the error in determining the intensity of the K line for this transition may be appreciable.

1275 kev. The data for the experimental Γ/α_K ratio indicate that this transition is mixed. Our experimental results are in best agreement with the data of Voinova et al[9] on the intensity of this transition in the case of a mixture consisting of 80% E1 + 20% M2.

1290 kev. The experimental value of Γ/α_K indicates that the multipole order of this transition may be M2, E3 or higher. Comparison of the intensity data shows that this transition is probably M2. Thus, for example, according to the data of Voinova et al[9] the relative intensity of this transition is 5 ± 2; our data give an intensity of 3.3 for M2 and 10.2 for E3.

Using the data of Sunyar[7] for the lifetime of the F level and the data of Murray et al[4] and Voinova et al[9] for the relative intensities of the transitions departing from the F level, we calculated the partial lifetimes for these transitions. The calculations show that the probability for E1 transitions from the F level is appreciably lower than the probability for a single-particle transition according to Weisskopf. Thus the FD transition is retarded by a factor of $4 \cdot 10^3$, and the FB transition by a factor of $5 \cdot 10^7$. So great a hindrance for the FB transition can only be partially explained by K-forbiddenness. The probabilities for M2 type transitions from the F level to levels A and B are also lower than the probabilities for single-particle transitions. In this case the hindrance factor is 100.

According to our data, the fraction of E3 radiation in the FB transition does not exceed 20%. This means that the probability for an E3 transition can exceed the probability for a single-particle transition by not more than a factor of four.

Physical-Technical Institute,
Academy of Sciences of the USSR

References

1. G.Alaga, K.Alder, A.Bohr & B.Mottelson, Kgl.Danske Videnskab.Selskab, Mat.-fys.Medd., 29, 9 (1955).

2. L.K.Peker, Izv.AN SSSR, Ser.fiz., 24, 369 (1960). (Trans.Bulletin, 24, 354.)

3. K.Alder, A.Bohr, T.Huus, B.Mottelson & A.Winter, Revs.Mod.Phys., 28, 432 (1956).

4. J.Murray, F.Boehm, P.Marmier & J.DuMond, Phys.Rev., 97, 1007 (1955).

5. C.J.Gallagher & J.O.Rasmussen, Ibid., 112, 1730 (1958).

6. L.A.Sliv & I.M.Band, Tablitsy koeffitsientov konversii, Ch.I,K-obolochka (Tables of internal conversion coefficients. Part I - K-shell), M.-L., 1956.

7. A.Sunyar, Phys.Rev., 93, 1122 (1954).

8. S.F.Antonova, S.S.Vasilenko, M.G.Kaganskii & D.L.Kaminsii, Zhur.eksp.i teor.fiz., 38, 765 (1960). (Trans.Soviet Physics - JETP.)

9. M.Voinova, B.S.Dzhelepov & N.N.Zhukovskii, Izv.AN SSSR, Ser.fiz., 23, 828 (1959). (Trans.Bulletin, 23, 822.)

10. S.F.Antonova, S.S.Vasilenko, M.G.Kaganskii & D.L.Kaminskii, Zhur.eksp. i teor.fiz., 37, 667 (1959). (Trans.Soviet Physics - JETP.)
11. S.F.Antonova, S.S.Vasilensko, M.G.Kaganskii & D.L.Kaminskii, Ibid., 38, 379 (1960). (Trans.Ibid.)
12. G.Backstrom, Arkiv Fysik, 10, 387 (1956).
13. M.E.Rose & G.E.Uhlenbeck, Phys.Rev., 38, 211 (1935).
14. M.A.Listengarten, Izv.AN SSSR, Ser.fiz., 22, 759 (1958). (Trans.Bulletin, 22, 755.)

* * * * * * *

DETERMINATION OF THE K SHELL CONVERSION COEFFICIENT OF THE 143 kev TRANSITION IN Pr^{141} BY MEANS OF A 4π SCINTILLATION SPECTROMETER

- L. Nemet

The procedure employed in the present study for determining internal conversion coefficients is based on comparison, by means of a 4π scintillation spectrometer, of the number of K x-rays accompanying internal conversion with the number of γ-rays. We used a CsI(Tl) crystal with a channel for introducing the source. The advantage of this procedure as compared with the usual scintillation method (source located outside the crystal[1]) is that in this case no errors are introduced by back scattering and "escape" of fluorescence photons; moreover the efficienty of the crystal is close to 100%. Thus under favorable conditions ($E_\gamma <$ < 200 kev and simple decay scheme) one can determine the internal conversion coefficients with an error not exceeding ~2%. In contrast, in the best measurements (for example, Ref.1) based on the usual scintillation procedure the error attains 8%. A 4π scintillation spectrometer was originally used for determining internal conversion coefficients by Brosi et al[2,3]. These investigators worked with two NaI crystals (each viewed by a separate photomultiplier) and measured the internal conversion coefficients of K capture isotopes by comparing the x-ray-x-ray and x-ray-γ-ray coincidence peaks. In this case processing of the experimental results is somewhat more complicated and the resultant error more appreciable.

In the present work we determined the K conversion coefficient of the only γ-transition (143 kev) occurring in β-decay of Ce^{141} to Pr^{141}. This isotope has been thoroughly studied, and its decay scheme is known[4]. Different authors[5-8] have obtained values ranging from 0.22 to 0.48 for α_K.

The β-radiation was absorbed by plexiglas (80 mg/cm^2). The radiations were recorded by a 128-channel AMA-3 type analyzer. The experimental spectrum is shown in the accompanying figure.

The value of α_K was determined as

$$\alpha_K = \frac{N_X}{N_\gamma W_f},$$

where W_f is the fluorescence yield, and N_X and N_γ are the numbers of x- and γ-rays. In turn,

$$N_X = \frac{N'_X}{\Pi_X \varepsilon_X k_X} \quad \text{and} \quad N_\gamma = \frac{N'_\gamma}{\Pi_\gamma \varepsilon_\gamma k_\gamma},$$

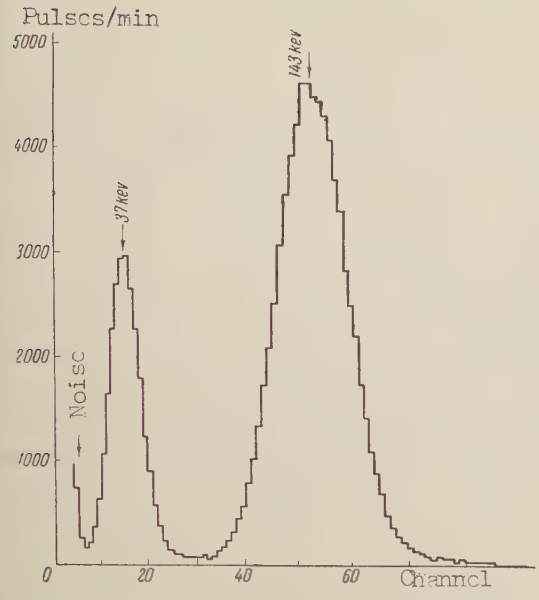

γ and K x-ray spectrum

where N'_X and N'_γ are the areas of the photopeaks (numbers of pulses) of the x- and γ-radiations, Π_X and Π_γ are the transmission coefficients of the plexiglas absorber, ε_X and ε_γ are the integral efficiencies of the crystal, and k_X and k_γ are the ratios of the photopeaks to the total count for the given radiation. The value of W_f according to Wapstra et al[9] is 0.90 ± 0.005. The average value of N'_X/N'_γ based on five measurements is 0.328 ± 0.003.

The values of the transmission coefficients were calculated on the basis of the absorption coefficients tabulated in the literature[10]; the calculations yielded $\Pi_X = 0.975 \pm 0.005$ and $\Pi_\gamma = 1.00$. Numerical integration over the volume of the CsI crystal (assuming μ equal 0.34 mm^{-1} for 143 kev and $\mu > 6.0$ mm^{-1} for 37 kev) yielded $\varepsilon_X = 0.997 \pm 0.001$ and $\varepsilon_\gamma = 0.992 \pm 0.002$.

In determining k one must take into account the escape peak and the Compton scattering. For the K x-radiation (37 kev) we found that the escape peak equals 20 ± 2% of the photopeak if the source is located outside the crystal. But in measurements with a 4π crystal most of the iodine fluorescence photons (29 kev) pass through the plexiglas container enclosing the activity and are finally absorbed by the CsI. Thus we obtained $k_X = 0.988 \pm 0.002$. For the γ-rays (143 kev) the influence of the Compton scattering and the effect of escape of the iodine fluorescence photons are negligibly small so that $k_\gamma = 1.00$. Johanson[6] and Zorzoli[8] in observing the spectrum of Ce^{141} detected in all their experiments a ~100 kev γ-line, the intensity of which amounted to ~10% the intensity of the 143 kev γ-line. It was inferred that this γ-line belongs either to Ce^{141} or to some impurity present in the source. In our measurements with the source outside the crystal there also appeared a peak with an energy of ~100 kev. It was reliably established, however, that this peak appears owing to scattering of the 143 kev γ-rays at an angle of 90-180% from the crystal container, lead shielding, etc. This peak was observed with all experimental geometries; it disappears only if the radiation is very carefully collimated and all possible scatterers above the source are eliminated.

Allowing for all the above mentioned sources of error, we obtained $\alpha_K = 0.376 \pm 0.006$. Repeat measurements with another similar Cs(Tl) crystal (20 x x 30 mm) yielded a value of $\alpha_K = 0.385 \pm 0.013$.

The weighted mean, accordingly, is

$$\bar{\alpha}_K = 0.379 \pm 0.005.$$

It follows from the tables of Sliv & Band[11] that for an M1 transition $\alpha_K = 0.403$, while for an E2 transition $\alpha_K = 0.412$.

I take this opportunity to thank V.N.Pokrovskii and E.P.Grigor'ev for valuable discussions and Yu.V.Narseev for assistance in preparing the Ce^{141} source.

References

1. F.K.McGowan & P.H.Stelson, Phys.Rev., 107, 1674 (1957).
2. B.H.Ketelle, H.Thomas & A.R.Brosi, Ibid., 103, 190 (1956).
3. A.R.Brosi, B.H.Ketelle, H.C.Thomas & R.J.Kerr, Ibid., 113, 239 (1959).
4. D.Strominger, J.M.Hollander & G.T.Seaborg, Table of Isotopes, Revs.Mod. Phys., 30, 585 (1958).
5. James T.Jones, Jr. & E.N.Jensen, Phys.Rev., 97, 1031 (1955).
6. S.Johanson, Arkiv Fysik, 3, 533 (1952).
7. M.S.Freedman & D.W.Engelkemeir, Phys.Rev., 79, 897 (1950).
8. G.B.Zorzoli, Nuovo cimento, 5, 289 (1957).
9. A.H.Wapstra, G.J.Nijgh & R.Van Lieshout, Nuclear Spectroscopy Tables, Amsterdam, 1959.
10. Beta- and Gamma-Ray Spectroscopy, edited by K.Siegbahn, Amsterdam, 1955.
11. L.A.Sliv & I.M.Band, Tablitsy KVK γ-izlucheniya Ch.I, K-obolochka (Tables of internal conversion coefficients, Part I - K-shell), M.-L., 1956.

* * * * * * *

COULOMB EXCITATION OF NUCLEAR LEVELS IN P^{31}, S^{33}, Mn^{55} AND Pr^{141} BY Ne^{20} IONS

- D.S.Andreev, A.P.Grinberg, K.I.Erokhina & I.Kh.Lemberg

The possibilities of investigating Coulomb excitation of nuclear levels are greatly enhanced if heavy ions are used as the bombarding particles. The reasons why it is advantageous to use heavy ions in Coulomb excitation experiments were examined in detail in Refs.1 and 2. Briefly, these are that when heavy ions are used as the projectiles the energy necessary to induce a significant number of transitions is relatively low compared to the Coulomb barrier, and the γ-background is less than when light particles are employed.

This circumstance enabled us to study the excitation of the following levels: 1.26 Mev in P^{31}, 0.84 in S^{33}, 0.98 Mev in Mn^{55} and 0.142 Mev in Pr^{141}. In other laboratories, where experiments were carried out with α-particles and protons, excitation of these levels could not be detected.

The measurements were carried out by means of a scintillation spectrometer with a NaI(Tl) crystal, 40 mm in diameter and 40 mm in diameter and 40 mm thick, coupled to an FEU-11 photomultiplier. The associated electronic equipment consisted of a preamplifier, a cathode follower, a nonjamming amplifier, and two pulse-height analyzers connected in parallel: a 63-channel analyzer (type AMA-2) and a 100-channel analyzer (type AI 100-1). The energy scale of the spectrometer was calibrated both before and after the experiment with reference to two γ-ray sources with γ-ray energies slightly higher and lower than the measured values.

The experimental procedure, equipment, and method of calculating the reduced transition probability B(E2) from the experimental data are described in detail in Refs.1, 2 and 3.

The greatest uncertainty in the determined values of B(E2) arises from errors in calculating the specific energy loss $dE/d(\rho x)$ of the heavy ions in the target and error due to the discrepancy between the calculated energy of the bombarding ions and the actual energy. The method of calculating $dE/d(\rho x)$ and the possible errors involved are described in Ref.4. The estimated error does not exceed 15% for nitrogen ions, but may attain 20-25% for neon ions.

Since the value of B(E2) calculated from the experimental data is proportional to $dE/d(\rho x)$, the computed values of B(E2) will comprise an error equal to that involved in determining $dE/d(\rho x)$. The error introduced into B(E2) as a result of using a value of the ion energy E differing from the actual value will increase with the parameter ξ, i.e., with the atomic number of the target nucleus and the energy ΔE of the excited level. For example, calculations show that in the excitation of the 1.26 Mev level in P^{31}, a 3% decrease in the energy of Ne^{20} ions (23.2 Mev) leads to decrease of the yield by a factor of 1.5.

It must also be noted that in the course of experiments on measuring the particle energy by deflecting the beam in a magnetic field we discovered that the deflected beam is split into several components, corresponding to different charges of the accelerated ions. This splitting into components occurs because the cyclotron accelerated quadruply charged ions undergo charge exchange along their trajectory through air at 10^{-4} mm Hg in the 3 meter ion channel; as a result there appear on the viewing screen, in addition to the intense main line corresponding to quadruply charged ions, fainter lines corresponding to ions carrying 5, 6 and 7 unit charges.

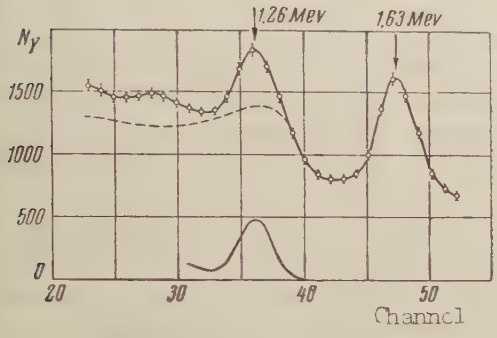

Fig.1. Experimental γ-ray spectrum obtained in Coulomb excitation of phosphorus by quadruply charged 27.8 Mev Ne^{20} ions.

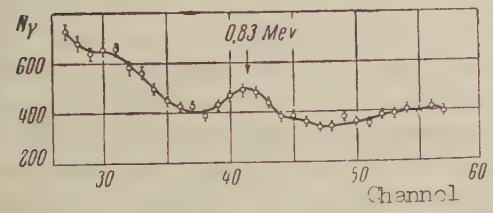

Fig.2. Experimental γ-ray spectrum obtained in Coulomb excitation of sulfur by quadruply charged 23.2 Mev Ne^{20} ions.

The change in the charge of the ions entering the Faraday cup changes the relation between the current and the number of particles caught. This leads to an error in determining particle energy and, consequently, impairs the accuracy of final calculation of the Coulomb excitation cross section. In order to reduce the error and thus obtain more accurate values of B(E2) we had recourse to a special procedure; this consisted of measuring, before and after determining the Coulomb excitation cross section for the studied level, the Coulomb excitation cross-section for a suitable "reference" level for which the value of B(E2) is known with good accuracy and which, therefore, could be used for normalization. In each case we chose for the reference level a level with an excitation energy close to that of the studied level, in a nucleus with Z as close as possible to the Z of the studied nucleus.

When the measurement of B(E2) for the reference level gave a value differing from the tabulated value, it was assumed that the discrepancy was due either to incorrect choice of $dE/d(\rho x)$ and/or the fact that part of the accelerated ions underwent charge exchange, or to incorrect determination of the bombarding ion energy. In the first case, since $dE/d(\rho x)$ and the number of bombarding particles enter into the expression for B(E2) the normalization amounted to multiplying the measured B(E2) for the studied level by the ratio of the known to the measured value of B(E2) for the reference level. In the second case the true ion energy was determined using the known dependence of the excitation yield on the ion energy for the case of the reference level. The reduced probability for the investigated level was then calculated using the corrected energy value. In general normalization was carried out by both methods, and the final result was taken

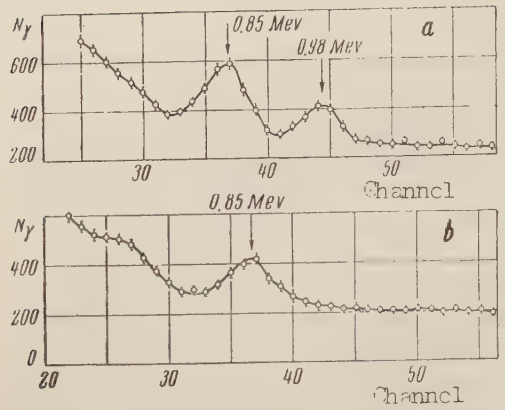

Fig.3. Experimental γ-ray spectra obtained in Coulomb excitation of manganese with quadruply charged 23.2 Mev Ne^{20} ions: a) without a lead absorber; b) with 1.25 mm lead absorber.

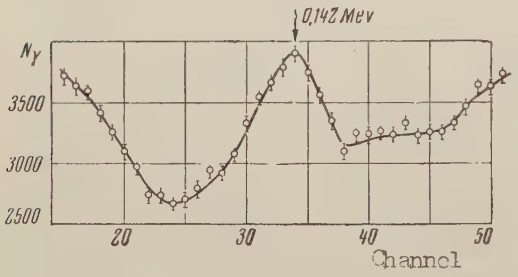

Fig.4. Experimental γ-ray spectrum obtained in Coulomb excitation of praseodymium with quadruply charged 27.8 Mev Ne^{20} ions.

as the average of the two resultant values of B(E2). As a rule, the difference between the two values did not exceed 10%.

Under conditions where cyclotron-accelerated heavy ions are used in Coulomb excitation experiments the above described method of normalizing the results with respect to the excitation of reference levels allows of reducing the experimental error. The error in determining reduced probability for the reference level itself is usually small (<15%) and the error in B(E2) for the studied levels usually does not exceed 20%. In the case of the level in P^{31}, however, the error was 30% for reasons which will be explained below.

The results of our experiments on Coulomb excitation of P^{31}, S^{33}, Mn^{55} and Pr^{141} are described below and summarized in the table. In these experiments the bombarding particles were quadruply charged 23.7 and 27.8 Mev Ne ions accelerated in the Physical-Technical Institute cyclotron. The beam current measured at the target was about 10^{-8} amp.

In the table ΔE is the level energy as measured in our experiments; ΔE^* is the energy as reported by other investigators; $B(E2)\uparrow$ is the reduced probability for electric quadrupole excitation of the level; $\tau(E2)$ is the partial lifetime of the level with respect to electrical quadrupole de-excitation to the ground state; τ is the total lifetime of the level (in order to calculate the total lifetime of the level from the measured $\tau(E2)$ it is necessary to know the intensity ratio of the E2 and M1 transitions from this level to the lower levels and to the ground state, as well as the intensity ratio for cross-over and cascade transitions, if the latter exist); τ^* is the lifetime of the level as reported by other investigators; F is the ratio of $B(E2)\uparrow$, obtained experimentally, to $B(E2)_{sp}$, calculated by means of the single-particle formula.

Reduced probabilities for Coulomb excitation of nuclear levels in P^{31}, S^{33}, Mn^{55} and Pr^{141}

Nucleus	ΔE, Mev	ΔE^*, Mev	$\frac{B(E2)\uparrow}{e^2} \times 10^{48}$, cm^4	$\tau(E2)$, sec	τ, sec	τ^*, sec	F
P^{31}	1,26 ± 0,02	1,264 [5]	0,011	$4,8 \cdot 10^{-12}$	$1,0 \cdot 10^{-13}$	—	9,1
S^{33}	0,83 ± 0,01	0,844± 0,006 [6] 0,839± 0,005 [7]	0,0019	$5,2 \cdot 10^{-11}$	$\leqslant 5,2 \cdot 10^{-11}$	—	3,0
Mn^{55}	0,98 ± 0,01	0,983 [8]	0,012	$(5 \div 13) \cdot 10^{-12}$	—	—	4,0÷5
Pr^{141}	0,142± 0,003	0,142 [9]	0,0036	$4,3 \cdot 10^{-7}$	—	$2 \cdot 10^{-9}$ [10,11]	4,3

Note: The numbers in brackets are references.

In our computations we took $R = 1.2 \cdot 10^{-13} A^{1/3}$ cm.

The experimental γ-ray spectra are reproduced in Figs.1 through 4.

Results and Discussion

P^{31}. The 1.26 Mev level in P^{31} is known from the data[12] on β-decay of S^{31}. The most accurate determination of the level energy was made by Van Patter et al who investigated inelastic proton scattering by P^{31}; these authors give ΔE = = 1.264 Mev.

Previous attempts[13] at Coulomb excitation of phosphorus were not successful owing to the interference of a strong background from the nuclear reactions induced by the bombarding α-particles. In our work Coulomb excitation of the 1.26 Mev level in P^{31} was investigated by means of 27.8 Mev Ne^{20} ions. The target was formed by compressing powdered red phosphorus. The γ-spectrum comprises a 1.63 Mev line (Fig.1), arising as a result of the Coulomb excitation of the 1.63 Mev level in Ne^{20}, and a 1.26 Mev γ-line corresponding to the excitation of P^{31}. In order to resolve the 1.26 Mev line, we had to subtract from the spectrum the shape of the 1.63 Mev line; this shape was determined in a separate experiment by bombarding a natural sulfur target with Ne^{20} ions of the same energy. The lower curve in Fig.1 shows the shape of the 1.26 Mev line obtained after subtraction.

The 1.37 Mev level in Mg^{24} was used as the reference level. The target was a magnesium plate. The value of $B(E2)\uparrow$ for the 1.37 Mev level was taken as $0.065 \cdot 10^{-48}$ e^2 cm^4 (Ref.1).

The reduced probability for the 1.26 Mev level in P^{31} was found to be $0.011 \cdot 10^{-48}$ e^2 cm^4. The spins of both the ground level and the 1.26 Mev level are known: $I_o = 1/2^+$ (Ref.14), and $I_f = 3/2^+$ (Ref.15). The latter assignment agrees with the results of earlier measurements of the angular correlation of γ-rays from P^{31}. Using these known values of I_o and I_f the partial lifetime of the 1.26 Mev state can be determined by means of the relations:

$$\tau(E2) = \frac{0.819 \cdot 10^{-13}}{(\Delta E)^5 B(E2)\downarrow}; \quad B(E2)\downarrow = B(E2)\uparrow \frac{(2I_o+1)}{(2I_f+1)}$$

wherein $\tau(E2)$ is measured in seconds, ΔE in Mev and $B(E2)$ in units of 10^{-48} e^2 cm^4. Calculations yielded $\tau(E2) = 4.8 \cdot 10^{-12}$ sec.

On the basis of experiments on the angular correlation of the cascade 1.26 Mev and 6.76 Mev γ-rays from P^{31}, Simons[16] found that the intensity ratio of E2 and M1 transitions is 0.02. Using this value and the above value of $\tau(E2)$, we calculated the total lifetime of the 1.26 Mev level and obtained $\tau = 1.0 \cdot 10^{-13}$ sec.

It must be noted that in view of the difficulties encountered in investigating the 1.26 Mev level in P^{31} (low yield, the necessity of resolving the 1.26 Mev and 1.63 Mev γ-lines, and the unavoidable use of a reference level for which the reduced probability is not known very precisely) above value of $\tau(E2)$ for the 1.26 Mev level may comprise an error of ~30%.

S^{33}. The existence of a level at 0.84 Mev in S^{33} is known from several studies of nuclear reactions. The most accurate measurements of the energy of this level were carried out by Endt et al[6,7] who studied the $Cl^{35}(d,\alpha)S^{33}$, and 7, $S^{32}(d,p)S^{33}$ reactions.

Coulomb excitation of sulfur has hitherto not been realized owing to use of α-particles for bombardment.[13] We used quadruply charged 23.2 Mev Ne^{20} ions. The target was compressed powdered sulfur enriched to 21.5% S^{33} (the abundance of S^{33} in natural sulfur is only 0.75%). The experimental γ-ray spectrum (Fig.2) shows a 0.83±0.01 Mev line arising from Coulomb excitation of S^{33} by Ne^{20} ions.

The reference level used was the 0.99 Mev level in Ti^{48}; in this case the target was a titanium plate. B(E2)↑ for the reference level was taken as 0.070 (Ref.1) which agrees with the value obtained by Knapp[17] from resonance scattering experiments.

The spin of the ground state of S^{33} is $3/2^+$ (Ref.14). The spin and parity of the 0.84 Mev level were determined by Holt & Marsham[18] and found to be $1/2^+$. The value of $\tau(E2)$ calculated using the above spins is $5.2 \cdot 10^{-11}$ sec.

The total lifetime of this state cannot be determined at present inasmuch as ΔI in this case is consistent with both E2 and M1 transitions, and the relative intensities of these are not known. It can only be said that $\tau \leqslant 5.2 \cdot 10^{-11}$ sec.

Mn^{55}. The 0.98 Mev level in Mn^{55} is known from several studies of inelastic neutron scattering (for example, the work of Nath et al,[8]) and from investigations of inelastic proton scattering[19].

In our experiments we used quadruply charged 23.2 Mev Ne^{20} ions. The target was a manganese film vacuum evaporated onto a nickel backing. As in the case of S^{33}, the 0.99 Mev level in Ti^{48} was chosen as the reference level.

In the spectrum obtained in bombarding manganese with Ne ions (Fig.3a) there appear two γ-lines with energies of 0.85 Mev and 0.98 Mev. The 0.85 Mev line arises in the cascade transition from the 0.98 Mev level via the 0.126 Mev level. The 0.98 Mev line results from simultaneous detection of the 0.85 Mev and 0.126 Mev γ-rays. This was established by means of the following experiment: a lead absorber 1.25 mm thick was placed between the target and the crystal; this absorber reduced the intensity of the 0.126 Mev γ-rays by a factor of 60 but virtually did not reduce the number of 0.85 Mev photons. With the absorber in place the 0.98 Mev line disappeared (Fig.3b), while the yield of 0.85 Mev γ-rays was almost euqal to the sum of the 0.85 Mev and 0.98 Mev γ-ray yields measured without the lead absorber. On the basis of the experimental data we evaluated the upper bound of the cross-over to cascade transaction abundance ratio as $I_{co}/I_{cas} < 0.1$.

According to Nath et al[8], this ratio is 1:13. The reduced probability for excitation of the 0.98 Mev level is $0.012 \cdot 10^{-48}$ e^2 cm^4. The spin and parity of the Mn^{55} ground state are $5/2^-$ (Ref.14). There are no data on the assignment for the 0.98 Mev level. Since Coulomb excitation induces an E2 transition, the possible assignments lie in the range from $1/2^-$ to $9/2^-$. The $1/2^-$ value can be discarded, since in this case the transition from the 0.98 Mev level to the ground state would be E2, while the transition to the 0.126 Mev level would be M3 (according to Bernstein & Lewis[20], the spin of the 0.126 Mev level is $7/2^-$); if the reduced transition probability from the 0.85 Mev level is taken as the value calculated by the single-particle formula, the intensity ratio of the cross-over to cascade transitions would be $2 \cdot 10^6$, which is in conflict with experiment. Similar reasoning does not, however, allow of giving preference to any one of the remaining possible assignments for the 0.98 Mev level. In view of this we could only calculate the possible range of partial lifetimes of the 0.98 Mev level with respect to E2 transitions to the ground state:

$$\tau(E2) = 5 \cdot 10^{-12} \text{ to } 13 \cdot 10^{-12} \text{ sec.}$$

Pr^{141}. Investigation[9] of β-decay of Ce^{141} has shown[9] that Pr^{141} has a level at 0.142 Mev. Coulomb excitation of this level was investigated by means of 6 Mev α-particles by Temmer and Heydenburg[21], who failed to detect the 142 kev γ-line. According to their data $B(E2) < 0.01 \cdot 10^{-48}$ e^2 cm^4.

Use of neon ions as the bombarding particles greatly reduced the γ-ray background associated with nuclear reactions on oxygen in the target; this enabled us

to investigate the excitation of praseodymium.

Fig.4 shows the γ-ray spectrum obtained in bombarding praseodymium oxide with quadruply charged 27.8 Mev Ne^{20} ions. The 130 kev level in Nd^{150} was chosen as the reference; the target was neodymium oxide enriched in Nd^{150} to 95.3%; the value of $B(E2) = 2.3 \cdot 10^{-48}$ e^2 cm^4 was taken from Adler et al.[22]

In the calculation of B(E2) for the 0.142 Mev level in Pr^{141} the conversion coefficient was interpolated from the tables of Sliv & Band[23]. Assuming that transition is M1, we have $\alpha = 0.427$.

The spin and parity of both the ground state and the 0.142 Mev state are known[9]: they are $5/2^+$ and $7/2^+$, respectively; thus from the measured value of B(E2) we could calculate the partial lifetime of the 0.142 Mev state; we obtained $\tau(E2) = 4.3 \cdot 10^{-7}$ sec.

The total lifetime of this state has been determined in several investigations. According to Berlovich[10] and Metzger[11], it is $2 \cdot 10^{-9}$ sec. Using this value of τ, and the above value of $\tau(E2)$, we calculated the intensity ratio for E2 and M1 transitions and obtained $I(E2)/I(M1) = 0.0045$. According to Cacho et al[24], this ratio is 0.007 ± 0.003.

Physical-Technical Institute,
Academy of Sciences of the USSR

References

1. D.S.Andreev, A.P.Grinberg, K.I.Erokhina & I.Kh.Lemberg, Nucl.Phys., 19, 400 (1960).
2. D.G.Alkhazov, A.P.Grinberg, G.M.Gusinskii, K.I.Erokhina & I.Kh.Lemberg, Zhur.eksp.i teor.fiz., 37, 1530 (1959). (Trans.Soviet Physics - JETP.)
3. D.G.Alkhazov, D.S.Andreev, K.I.Erokhina & I.Kh.Lemberg, Zhur.eksp. i teor.fiz., 33, 1347 (1957). (Trans.Soviet Physics - JETP.)
4. A.P.Grinberg, I.Kh.Lemberg, Izv.AN SSSR, Ser.fiz., 23, 887 (1959). (Trans. Bulletin, 23, 877.)
5. D.M.Van Patter, C.P.Swann, W.C.Porter & C.E.Mandeville, Phys.Rev., 103, 656 (1956).
6. C.H.Paris, W.W.Buechner & P.M.Endt, Phys.Rev., 100, 1317 (1955).
7. P.M.Endt & C.H.Paris, Phys.Rev., 110, 89 (1958).
8. N.Nath, M.A.Rothman, D.M.Van Patter & C.E.Mandeville, Nucl.Phys., 13, 74 (1959).
9. E.Ambler & R.P.Hudson, Phys.Rev., 97, 1212 (1955).
10. E.Berlovich, Izv.AN SSSR, Ser.Phys., 20, 1438 (1956). (Trans.Bulletin, 20, 1315.)
11. F.Metzger, J.Franklin Inst., 261, 219 (1956).
12. W.Lyon & J.Manning, Phys.Rev., 93, 501 (1954).
13. G.M.Temmer & N.P.Heydenburg, Phys.Rev., 93, 351 (1954).
14. I.E.Mack, Revs.Mod.Phys., 22, 64 (1950).
15. Yu.P.Antuf'ev, A.K.Val'ter, V.Yu.Gonchar, E.G.Kopanets, A.P.L'vov, P.M. Tutakin & S.P.Tsfytko, in "Yadrenye reaktsii pri malykh i srednikh energiykh" (Nuclear reactions at low and medium energies), M., 1958.
16. L.Simons, Nucl.Phys., 10, 215 (1959).
17. V.Knapp, Proc.Phys.Soc. A71, 194 (1958).
18. J.R.Holt & T.N.Marsham, Proc.Phys.Soc., A66, 467 (1953).
19. M.Mazari, A.Sperduto & W.W.Buechner, Phys.Rev., 108, 103 (1957).
20. E.M.Bernstein & H.W.Lewis, Phys.Rev., 100, 1367 (1955).
21. G.M.Temmer & N.P.Heydenburg, Phys.Rev., 100, 150 (1955).
22. K.Alder, A.Bohr, T.Huus, B.Mottelson & A.Winther, Revs.Mod.Phys., 28, 432 (1956).

23. L.A.Sliv & I.M.Band, Tablitsy koef.vnutrennei konversii γ-izlucheniya (Tables of Internal Conversion Coefficients), M.-L., 1956 and 1958.
24. C.Cacho, M.Grace, C.Johnson, A.Knipper, R.Kurlock & R.Taylor, Phil. Mag., 46, 1287 (1955).

* * * * * * *

PROBABILITIES FOR GAMMA-TRANSITIONS IN ODD-ODD DEFORMED NUCLEI

- D.A.Varshalovich

Introduction

The single-particle model with a deformed potential[1] (Nilsson's model) satisfactorily explains the level diagrams of odd-Z and odd-N nuclei in the $A \approx 25$-27, 150-190 and >225 regions.[2] This model can be applied not only to odd but also to odd-odd deformed nuclei, inasmuch as many characteristics of these nuclei are determined by the quantum states Ω_p^π and Ω_n^π of the last unpaired proton and neutron. According to the independent particle model the Ω_p^π and Ω_n^π states will be degenerate with respect to K. The residual interaction of the unpaired nucleons removes the degeneracy, splitting each such state into two, corresponding to the two possible projections of the total angular momentum I on the nuclear symmetry axis: $K_1 = \Omega_1 + \Omega_2$ and $K_2 = |\Omega_1 - \Omega_2|$ (the two-fold ±K degeneracy remains). Each state of the doublet will have its own rotational band. In the first approximation the wave functions of an odd-odd deformed nucleus may be presented in the form

$$\Phi(IM\pi;\ K = \Omega_1 \pm \Omega_2) = \sqrt{\frac{2I+1}{16\pi^2}}\{D^I_{MK}\chi_{\Omega_1}\chi_{\pm\Omega_2} + (-)^{I-J}D^I_{M-K}\chi_{-\Omega_1}\chi_{\mp\Omega_2}\}, \qquad (1)$$

where the χ_{Ω_1} and χ_{Ω_2} are Nilsson's functions characterizing the states of the unpaired proton and neutron, and D^I_{MK} is a function describing the rotation of the nucleus.

However, the residual nucleon interaction must somewhat mix the single particle configurations. Each state with quantum numbers $IM\pi$ and $K\Omega_1\Omega_2$ will have an admixture of states characterized by other values of Ω_1, Ω_2 and K, but with the same spin and parity:

$$\Psi(IM\pi) = \alpha_0\Phi_0(IM\pi;\ K\Omega_1\Omega_2) + \sum_i \alpha_i\Phi_i(IM\pi;\ K'\,\Omega_1'\,\Omega_2'). \qquad (2)$$

Here we shall consider only the cases when the residual nucleon interaction is weak, $\alpha_i^2 \ll \alpha_0^2$ and the levels of the odd-odd nucleus can be characterized by definite values of Ω_p^π, Ω_n^π and K. In such cases the γ-transitions in odd-odd nuclei can be divided into three groups:

1. Transitions between levels of the same rotational band:

$$\Omega_p^1 = \Omega_p^2, \quad \Omega_n^1 = \Omega_n^2, \quad K^1 = K^2.$$

2. Transitions between the levels of a doublet or their rotational bands:

$$\Omega_p^1 = \Omega_p^2, \quad \Omega_n^1 = \Omega_n^2, \quad K^1 \neq K^2.$$

3. Transitions between different doublets:

single-particle $\Omega_\alpha^1 \neq \Omega_\alpha^2, \quad \Omega_\beta^1 = \Omega_\beta^2, \quad K^1 \neq K^2;$

two-particle $\Omega_\alpha^1 \neq \Omega_\alpha^2, \quad \Omega_\beta^1 \neq \Omega_\beta^2, \quad K^1 \neq K^2.$

Below we shall consider all three types.

The characteristics of odd-odd nuclei (the spin and parities of the states, the γ-transition probabilities, and the electric and magnetic moments) can be inferred from the properties of neighboring odd nuclei if the residual nucleon interaction is weak and the odd-odd nuclei are deformed in the same way as the neighboring odd nuclei. The available experimental data on the spins of the ground and isomeric states of odd-odd nuclei indicate that for nuclei far from the edge of the deformation region these conditions are fulfilled.[3]

Mixing of states is observed in the case when two (or more) states with the same I and π have close energy values. Such mixing leads to some change in the excitation energies (levels with the same I and π are "repelled"), i.e., the order or sequence of such levels may change, but their spin and parity remain the same. The γ-transition probabilities, however, may undergo appreciable changes, particularly in the case of transitions that were forbidden or strongly retarded with respect to the main configurations. For allowed transitions the effect of an admixture is substantially less.

Electric and magnetic moments and probabilities for rotational transitions

As is known, the probability for γ-transitions between the levels of one rotational band can be related to the static moments of the nucleus.[4]

The electric quadrupole moment of a deformed nucleus and the probability for rotational E2 transitions are determined by the internal quadrupole moment Q_0:

$$Q(I) = Q_0 \frac{3K^2 - I(I+1)}{(I+1)(2I+3)}; \tag{3}$$

$$B(E2, I_1 \to I_2) = \frac{5}{16\pi} e^2 Q_0^2 (C_{I_1 K_1;\, 20}^{I_2 K_2})^2, \tag{4}$$

where I is the total angular momentum and K is its projection on the symmetry axis, and the $C_{I_1 K_1;\, \lambda\mu}^{I_2 K_2}$ are Clebsch-Gordon coefficients. According to the assumed model the value of Q_0 characterizes the degree of deformation of the nucleus and varies little in going from one nucleus to another, provided the given nucleus is not at the edge of the deformation region. Hence the quadrupole moment and the reduced probability $B(E2)$ for a rotational transition in an odd-odd nucleus can be evaluated using the values of Q_0 for neighboring nuclei.

It must be noted that in the case when K = 1 the quadrupole moment Q and the reduced probability $B(E2)$ are determined not only by the internal quadrupole moment $Q_0 \equiv \langle \chi_K | \hat{Q} | \chi_K \rangle$, but also by the cross matrix element $\langle \chi_{-K} | \hat{Q} | \chi_K \rangle$ ($\hat{Q}$ is the quadrupole moment operator, and χ_K is a function characterizing the internal state).

The magnetic moment μ of a deformed nucleus and the reduced probability $B(M1)$ for a rotational transition are determined by the gyromagnetic ratios g_K and g_R, characterizing the internal and collective nucleon motion:

$$\mu(I) = (g_K - g_R) \frac{K^2}{I+1} + g_R I, \tag{5}$$

$$B(M1, I_1 \to I_2) = \frac{3}{4\pi} (g_K - g_R)^2 K^2 (C_{I_1 K;\, 10}^{I_2 K})^2. \tag{6}$$

The value of the ratio g_K in an odd-odd nucleus can be expressed in terms of g_{Ω_1} and g_{Ω_2}, the internal gyromagnetic ratios of neighboring odd-proton and odd-neutron nuclei:

$$g_K = \frac{g_{\Omega_1}\Omega_1 \pm g_{\Omega_2}\Omega_2}{\Omega_1 \pm \Omega_2}, \qquad (7)$$

here the plus sign is taken for states with $K = \Omega_1 + \Omega_2$, and the minus sign for states with $K'' = \Omega_1 - \Omega_2$ $(\Omega_1 \geqslant \Omega_2)$. According to the collective nuclear model, $g_R = Z/A \approx 0.4$. Coupling between the internal and collective nucleon motions leads to some deviation of g_R from the indicated value, but this deviation is relatively small $(0.2 < g_R < 0.6)$.

Table 1

Magnetic moments of the "base" states of rotational bands $(I = K)$ and reduced probabilities for M1 type γ-transitions $(I_1 = K + 1 \rightarrow I_2 = K)$

Nucleus	Proton		Neutron		$\Omega_1+\Omega_2$			$\Omega_1-\Omega_2$		
	Ω^π	g_Ω	Ω^π	g_Ω	K_1^π	μ, n.m.	$B(M1)$ (n.m.)^2	K_2^π	μ, n.m.	$B(M1)$ (n.m.)^2
$_{11}Na^{22}_{11}$	$3/2^+$	+2,15	$3/2^+$	−0,89	3^+	+1,79	$0{,}7\cdot10^{-2}$	0^+	0	—
$_{11}Na^{24}_{13}$	$3/2^+$	+2,15	$5/2^+$	−0,67	4^+	+1,65	$3{,}0\cdot10^{-3}$	1^+	−2,20	2,06
$_{13}Al^{26}_{13}$	$5/2^+$	+1,89	$5/2^+$	−0,67	5^+	+2,96	$0{,}9\cdot10^{-2}$	0^+	0	—
$_{63}Eu^{152}_{89}$	$5/2^+$	+0,65	$3/2^-$	−0,60	4^- exp 3^-	+0,91	$3{,}4\cdot10^{-2}$	1^-	+1,47	0,32
$_{63}Eu^{154}_{91}$	$5/2^+$	+0,65	$3/2^-$	−0,62	4^- exp 3^-	+0,88	$3{,}3\cdot10^{-2}$	1^-	+1,48	0,32
$_{65}Tb^{156}_{91}$	$3/2^+$	+1,49	$3/2^-$	−0,60	3^-	+1,31	$3{,}4\cdot10^{-4}$	0^-	[+0,42]	—
$_{65}Tb^{158}_{93}$	$3/2^+$	+1,49	$3/2^-$	−0,62	3^-	+1,29	$2{,}5\cdot10^{-4}$	0^-	[+0,41]	—
$_{65}Tb^{160}_{95}$	$3/2^+$	+1,49	$5/2^-$	−0,38	4^-	+1,36	$4{,}6\cdot10^{-4}$	1^-	−1,39	0,93
$_{67}Ho^{160}_{93}$	$7/2^-$	+1,12	$3/2^-$	−0,62	5^+	+2,84	$2{,}5\cdot10^{-2}$	2^+	+3,50	0,92
$_{67}Ho^{162}_{95}$	$7/2^-$	+1,12	$5/2^-$	−0,38	6^+	+2,90	$7{,}2\cdot10^{-3}$	1^+	+2,64	1,43
$_{67}Ho^{164}_{97}$	$7/2^-$	+1,12	$5/2^+$	+0,18	6^-	+4,10	0,10	1^-	+1,94	0,67
$_{67}Ho^{166}_{99}$	$7/2^-$	+1,12	$7/2^+$	−0,25	7^-	+3,02	$1{,}2\cdot10^{-3}$	0^-	[+0,40]	—
$_{69}Tu^{168}_{99}$	$1/2^+$	−2,20	$7/2^+$	−0,25	4^+	−1,25	0,51	3^+	+0,48	$4{,}6\cdot10^{-2}$
$_{69}Tu^{170}_{101}$	$1/2^+$	−2,20	$1/2^-$	+1,38	1^-	−0,003	$4{,}8\cdot10^{-2}$	0^-	[+0,40]	—
$_{69}Tu^{172}_{103}$	$1/2^+$	−2,20	$5/2^-$	−0,55	3^-	−1,56	0,63	2^-	+0,08	$6{,}6\cdot10^{-2}$
$_{71}Lu^{172}_{101}$	$7/2^+$	+0,66	$1/2^-$	+1,38	4^-	+2,73	$7{,}1\cdot10^{-2}$	3^-	+1,53	$6{,}7\cdot10^{-3}$
$_{71}Lu^{174}_{103}$	$7/2^+$	+0,66	$5/2^-$	−0,55	6^-	+1,15	$6{,}7\cdot10^{-2}$	1^-	+2,05	0,78
$_{71}Lu^{176}_{105}$	$7/2^+$	+0,66	$7/2^-$	+0,16	7^-	+2,86	$4{,}2\cdot10^{-5}$	0^-	[+0,40]	—
$_{73}Ta^{178}_{105}$	$7/2^+$	+0,70	$7/2^-$	+0,16	7^-	+2,99	$5{,}2\cdot10^{-4}$	0^-	[+0,41]	—
$_{73}Ta^{180}_{107}$	$7/2^+$	+0,70	$9/2^+$	−0,18	8^+	+1,82	$6{,}1\cdot10^{-2}$	1^+	−1,43	0,96
$_{73}Ta^{182}_{109}$	$7/2^+$	+0,70	$1/2^-$	+0,16	4^-	+2,34	$3{,}4\cdot10^{-2}$	3^-	+2,08	$6{,}4\cdot10^{-2}$
$_{75}Re^{184}_{109}$	$5/2^+$	+1,63	$1/2^-$	+0,16	3^-	+3,43	0,40	2^-	+2,94	0,58
$_{75}Re^{188}_{113}$	$5/2^+$	+1,63	$3/2^-$	+0,46	4^-	+4,14	0,39	1^-	+1,89	0,64
$_{77}Ir^{190}_{113}$	$3/2^+$	−0,09	$3/2^-$	+0,46	3^-	+0,72	$2{,}1\cdot10^{-2}$	0^-	[+0,40]	—

Note: The magnetic moments μ given in brackets are for states with $K^\pi = 0^-$ and $I^\pi = 1^-$.

Thus one can evaluate the magnetic moments and reduced probabilities for M1 type transitions in odd-odd nuclei by using the values of g_K for neighboring

nuclei and assuming $g_R = Z/A$. It will be evident from Table 1, that in contrast to the case of nuclei with odd A, in odd-odd nuclei the values of μ and $B(M1)$ differ greatly from nucleus to nucleus. Hence rotational transitions in odd-odd nuclei can, in individual cases, be almost pure M1, or in other cases, almost pure E2.

Transitions between levels of a doublet

In $K_1 = \Omega_1 + \Omega_2 \rightleftarrows K_2 = |\Omega_1 - \Omega_2|$ γ-transitions the states of the individual nucleons do not change: there occurs only relative reorientation of the angular momenta of the unpaired proton and neutron. The reduced probability $B(\sigma\lambda)$ for such a transition can be written in the form

for $\Omega_1 > \Omega_2$
$$B(\sigma\lambda) = (C^{I_2K_2}_{I_1K_1;\,\lambda\mu})^2 |\langle \chi_{-\Omega_2} | \hat{\mathfrak{M}}_{\lambda\mu}(2) | \chi_{\Omega_2} \rangle|^2, \tag{8}$$

for $\Omega_1 = \Omega_2$
$$B(\sigma\lambda) = (C^{I_2K_2}_{I_1K_1;\,\lambda\mu})^2 |\langle \chi_{-\Omega_1} | \hat{\mathfrak{M}}_{\lambda\mu}(1) | \chi_{\Omega_1} \rangle + \langle \lambda_{-\Omega_2} | \hat{\mathfrak{M}}_{\lambda\mu}(2) | \chi_{\Omega_2} \rangle|^2. \tag{8'}$$

where $\hat{\mathfrak{M}}_{\lambda\mu}(i)$ is the operator of the multipole moment of the i-th nucleon.

The states of the doublet are characterized by the same parity. The spins of the state on which the rotational bands of the doublet are based differ by an odd number of units:

$$\Delta I = \Delta K = 2\Omega_2 \, (\Omega_1 \geqslant \Omega_2).$$

Hence between the "base" states of the doublet there must occur γ-transitions of the magnetic type with multipolarity $\lambda = 2\Omega_2$, to which there may be admixed electric transitions of multipolarity $\lambda = 2\Omega_2 + 1$, i.e., M1(E2), Ms(E4) and M5(E6) type transitions.

Between the rotational bands of doublets there may occur γ-transitions of multipolarity $\lambda < 2\Omega_2$. However such transitions will be forbidden by the K selection rules.

It is evident from Eqs.(8) and (8') that the transitions between the levels of a doublet will be of single-particle character. The transition probability is determined by the state of only the nucleon which is characterized by the minimum value of Ω. Only in the case when $\Omega_1 = \Omega_2$ will both unpaired nucleons make a contribution to the transition probability, and in this case there will enter into Eqs.(8) and (8') the same cross matrix elements that determine the static multipole moments of order λ.

For example, in the case when $\Omega_1 < \Omega_2$ and $\Omega_2 = 1/2$ the spins of the "base" states of the doublet will differ by one unit. The transition between these states will be of the M1 type. The probability for this transition will be determined by the same values of g_Ω, g_R and b_0 as the magnetic moment of a nucleus with $\Omega = 1/2$ (Ref.3). Knowing the magnetic moment and the probability for magnetic M1 transitions in an odd nucleus, one can determine the probability for an M1 type transition between the levels of a doublet in an odd-odd nucleus.

In general the probability for such transitions can be calculated using Nilsson's[1] single-particle functions, or it can be evaluated approximately by means of the selection rules[5] for the asymptotic quantum numbers N, n_z, Λ and Σ characterizing the nucleon states in deformed nuclei. For transitions between the levels of a doublet $\Delta N = 0$, $\Delta n_z = 0$, $\Delta\Lambda = 2\Omega \pm 1$, and $\Delta\Sigma = \pm 1$, so that magnetic transitions of multipolarity $\lambda = 2\Omega$ are allowed as regards the asymptotic quantum numbers, whereas all electric transitions are forbidden with respect to the quantum numbers Λ and Σ.

Transitions between different doublets

In odd-odd nuclei levels belonging to different doublets may differ as regards the state of one nucleon or as regards the states of both unpaired nucleons. Accordingly, the γ-transitions between such levels may be either single-particle or two-particle transitions. Two-particle transitions are strongly retarded as compared with single-particle ones. Hence in most cases the levels in question are de-excited by a cascade consisting of a number of single-particle transitions.

The reduced probability $B(\sigma\lambda)$ for a single-particle γ-transition

$$(\Omega_\alpha \Omega_\beta) K_1 I_1 \to (\Omega'_\alpha \Omega_\beta) K_2 I_2$$

in an odd-odd nucleus can be written as

$$B(\sigma\lambda, K_1 \to K_2) = (C^{I_2 K_2}_{I_1 K_1;\ \lambda\mu})^2 \left| \langle \chi_{\Omega'_\alpha} | \mathfrak{M}_{\lambda\mu}(\alpha) | \chi_{\Omega_\alpha} \rangle \right|^2. \tag{9}$$

Between the levels belonging to rotational bands of different doublets there may occur γ-transitions of multipolarity $\lambda < |\Omega'_\alpha - \Omega_\alpha|$. Such transitions will, however, be retarded owing to forbiddenness with respect to Ω, and their intensity will depend on the magnitude of the admixture of states with other Ω to the initial and final states of the nucleus. The probability for allowed transitions can be calculated using the Nilsson functions χ_Ω, and it can be evaluated approximately by means of the N, n_z, Λ and Σ selection rules. If the odd-odd nucleus is deformed in the same way as the neighboring odd nucleus, the γ-transition probability in the odd-odd nucleus can be expressed directly in terms of the probability for the corresponding γ-transition in the odd nucleus:

$$B(\sigma\lambda, K_1 \to K_2) = \left(\frac{C^{I_2 K_2}_{I_1 K_1;\ \lambda\mu}}{C^{j_2 \Omega_2}_{j_1 \Omega_1;\ \lambda\mu}} \right)^2 B(\sigma\lambda, \Omega_1 \to \Omega_2). \tag{10}$$

Experimental data

Odd-odd deformed nuclei constitute one of the least studied groups. Hence the experimental data now available are inadequate for a detailed check of the deduced relationships.

The experimental data of odd nuclei allow of predicting the spin and parity of the "base" and corresponding doublet states of odd-odd nuclei, calculating their electric and magnetic moments and the reduced probabilities for rotational M1 and E2 transitions. The calculated values of μ and $B(M1)$ are listed in Table 1. In cases where the spin and parity of the ground or isomeric state have been measured or can be deduced from the decay scheme, they agree with the predicted values (for $K^\pi = 0^-$ and $I^\pi_0 = 1^-$). The only exceptions are Eu^{152} and Eu^{154}. The deformation of these nuclei ($\Omega_p = 3/2$) differs from the deformation of neighboring odd nuclei ($\Omega_p = 5/2$), inasmuch as these two nuclei lie at the edge of the deformation region. The deformation of the other odd-odd nuclei apparently differs little from the deformation of neighboring odd nuclei. This assertion can be checked directly only for Lu^{176}, for which the quadrupole moment has been measured. The experimental value $\frac{Q(Lu^{176})}{Q(Lu^{175})} = 0.70$ (Ref.6) agrees with the theoretical value calculated on the assumption of equal deformation.

The magnetic moments of only six odd-odd deformed nuclei have been measured[7]; these are listed in Table 2.

Table 2
Magnetic moments of odd-odd deformed nuclei

Nucleus	I^π	$\mu_{exp.}$, n.m.	μ_{theo}, n.m.
Na^{22}	3^+	+1,75	+1,79
Na^{24}	4^+	+1,69	+1,65
Al^{26}	5^+	+2,8±0,3	+2,96
Eu^{152}	3^-	±2,0±0,5	+1,32
Eu^{154}	3^-	±2,1±0,5	+1,32
Lu^{176}	7^-	+2,8±0,3	+2,86

The experimental and theoretical values of the magnetic moments for Eu^{152} and Eu^{154} differ by 30%. For the other nuclei there is good agreement.

There are almost no data at present on the probabilities for γ-transitions in odd-odd deformed nuclei. The E2/M1 ratio has been measured only for the $2^- \rightarrow 1^-$ rotational transition in Lu^{174} ($K^\pi = 1^-$): Romanov et al[8] give (E2/M1) = $(5 \pm 3) \cdot 10^{-3}$. In the neighboring odd nucleus Lu^{175} ($K^\pi = 7/2^+$) the E2/M1 ratio for the $9/2^+ \rightarrow 7/2^+$ transition is reported[7] to be 0.30. If we assume that the internal quadrupole moment Q_0 is the same in Lu^{174} and Lu^{175} and that the parameter $b_0 = 0$, we obtain a value of 8.2 ± 2.0 for the $\frac{B(M1, Lu^{174})}{B(M1, Lu^{175})}$ ratio, which is in good agreement with the theoretical value of 9.3 calculated by means of Eqs.(5) and (7).

Physical-Technical Institute,
Academy of Sciences of the USSR

References

1. S.G.Nilsson, Kgl.Danske Videnskab.Selskab, Mat.-fys.Medd., 29, No.16 (1955).
2. B.R.Mottelson & S.G.Nilsson, Ibid., 1, 8 (1959).
3. L.K.Peker, Izv.AN SSSR, Ser.fiz., 21, 1029 (1957) (Trans.Bulletin, 21, 1030); L.K.Peker, Tezisy dokladov X Sovshchaniya (Program of the Tenth All-Union Conference on Nuclear Spectroscopy), M., 1959.
4. G.Alaga, K.Alder, A.Bohr & B.R.Mottelson, Kgl.Danske Videnskab.Selskab. Mat.-fys.Medd., 29, No.9 (1955).
5. M.E.Voikhanskii, Zhur.eksp.i teor.fiz., 33, 1004 (1957). (Trans.Soviet Physics - JETP.)
6. A.Steudel, Naturwissenschaften, 44, 371 (1957).
7. D.Strominger, J.M.Hollander & G.T.Seaborg, Revs.Mod.Phys., 30, 585 (1958).
8. V.A.Romanov, V.V.Tuchkevich, M.G.Iodko & O.M.Kresin, Trudy soveshchaniya po yadernoi spektroskopii (Transactions of the Conference on Nuclear Spectroscopy), Joint Inst. for Nuclear Research, Dubna, 1959.

ELECTROMAGNETIC TRANSITIONS IN DEFORMED NUCLEI

- Yu.N.Gnedin

1. In analyzing electromagnetic transitions in deformed nuclei one should distinguish between transitions taking place between levels due to collective excitation of nucleon motion and transitions associated with internal excitation of the nucleus. The transitions of the first type do not affect the internal structure of the nucleus, hence the transition matrix elements can be expressed in terms of the static multipole moments. Theoretical data on transitions of this type are in good agreement with experimental results. It is also of interest to compare the experimental data with the calculated probabilities for γ-transitions of the second type, inasmuch as this can serve to verify the validity of the assumed nuclear models. Thanks to the recent accumulation of extensive experimental data such comparison is now possible.

2. The theory of single-particle transitions in deformed nuclei was developed by Nilsson[1] on the basis of the earlier work of Bohr & Mottelson[2,3].

The probability for an electromagnetic transition from an initial state with energy E_i, angular momentum I_i, projection M_i of the angular momentum on an axis fixed in space, and parity π_i to a final state with E_f, I_f, M_f and π_f is given by[1]

$$W(\alpha\lambda) = \frac{8\pi(\lambda+1)}{\lambda[(2\lambda+1)!!]^2}\frac{1}{\hbar}\left(\frac{\omega}{c}\right)^{2\lambda+1} B(\alpha\lambda),$$

where $\hbar\omega = E_i - E_f$, λ is the multipolarity of the radiation, and

$$B(\alpha\lambda) = \sum_{M_f,\,\mu}\left|\int \Psi_f^* \mathfrak{M}(\alpha\lambda,\mu)\,\Psi_i\, d\tau\right|^2$$

is the reduced transition probability ($\mathfrak{M}(\alpha\lambda,\mu)$ is the multipole moment operator). The symbol α indicates the character of the transition: electric or magnetic. The single nucleon wave functions necessary for calculation of $B(\alpha\lambda)$ were obtained by Nilsson[1] in the adiabatic approximation for a deformed potential. In our calculations we used the internal conversion coefficients given by Sliv & Band[4]. The deformation parameters were taken from the data on Coulomb excitation[5]. In addition, we investigated the extent to which the asymptotic number selection rules proposed by Alaga[6] and Voikhanskii[7] are obeyed.

3. The results of our calculations are summarized in Tables 1 & 2, wherein we also give the asymptotic quantum number selection rules pertinent to each multipole order. The results of our calculations in the form of log (τ_{exp}/τ_{theo}) are also shown in Figs.1 and 2.

4. As will be evident from the tables, the best agreement with the experimental data is obtained for transitions of high multipole order. The divergence between the experimental and theoretical data is explained by the fact that the adiabatic approximation is not rigorous where description of actual nuclei is concerned and so that it is necessary to take into account collective effects. With increase of the multipolarity of the radiation the multipole moments associated with collective nuclear motion decrease and the transitions become almost single-particle in character.

In the case of electric transitions the calculated data for E3 transitions are in good agreement with the experimental data, inasmuch as at low energies the probability for excitation of octupole oscillations is low and the transitions are nearly single-particle transitions. In E2 transitions there do occur oscillations of the nuclear surface of the quadrupole type. In the region of energies under consideration oscillations of this type are most probable and make a substantial contribution to E2 transitions. In the case of one-phonon excitation the reduced transition probability is given by the formula

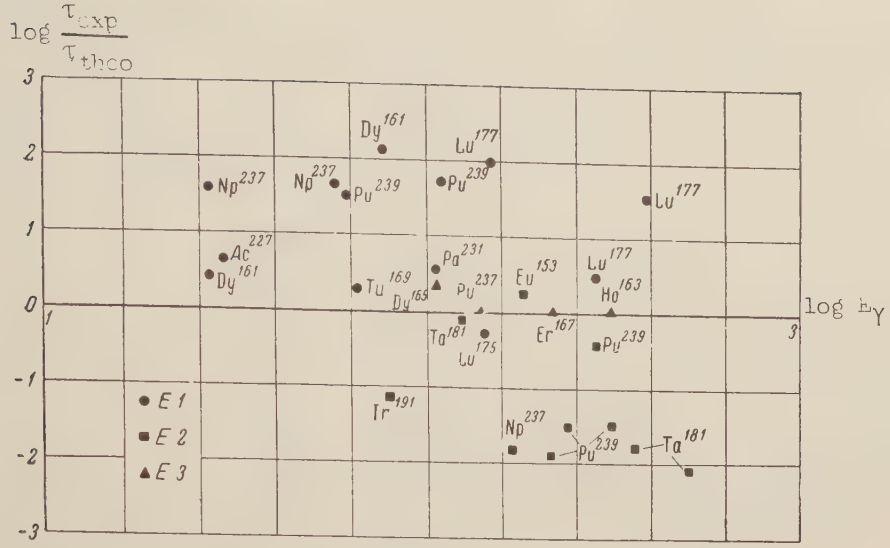

Fig.1. Comparison of the theoretical probabilities for radiative E1, E2 and E3 transitions calculated on the basis of the unified nuclear model with the corresponding experimental probabilities.

$$B(E\lambda) = \frac{3\lambda}{8\pi} Z^2 e^2 R_0^{2\lambda} \frac{\hbar^2}{AMR_0^2} \frac{1}{\hbar\omega_\lambda},$$

where AM is the nuclear mass, R_0 is the radius, Z is the charge, and $\hbar\omega_\lambda$ is the excitation energy. For $\lambda = 2$ this probability is approximately 100 times higher than the single-particle probability. Thus the contribution from collective oscillations of the nucleus leads to speeding up of the transitions relative to single-particle ones. It must be noted that E1 transitions are retarded by a factor of 10-100 as compared with what follows from the unified nuclear model. In this case collective effects do not play a significant role inasmuch as surface deformation with angular momentum equal to unity represents a simple displacement of the center of inertia, while the contribution from dipole oscillations at such energies is very small. Taking into account pair correlation leads to the appearance of an additional factor which reduces the transition probability by one order of magnitude. Near the Fermi surface this factor is of the order of $1/(\rho_0\Delta)^2$, where ρ_0 is the energy density of the levels at the Fermi surface and Δ is the width of the "energy slit". Taking this factor into account results in better agreement of the theoretical probabilities for E1 transitions with the experimental data.

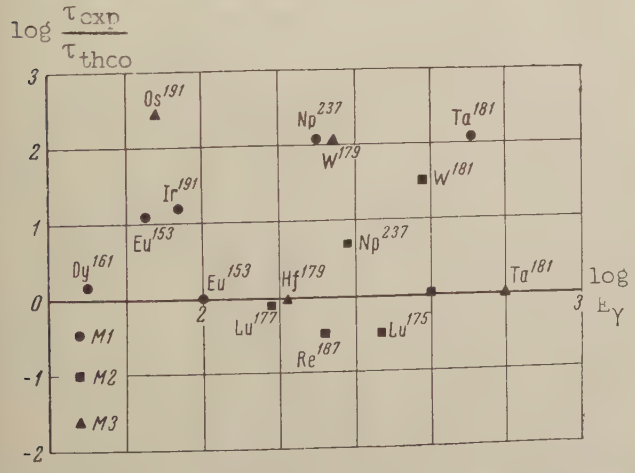

Fig.2. Same as Fig.1, but for M1, M2 and M3 transitions.

5. For magnetic transitions the agreement between the calculated and experimental data is on the whole good. The greatest deviation (~100) is observed for M1 transitions in Ta^{181}

Table 1

Comparison of the experimental probabilities for electric transitions with the theoretical values calculated according to the spherical and unified nuclear models

Nucleus	β	Ω_i, π_i; Ω_f, π_f	$N_i\, n_{zi}\Lambda_i\, \Sigma_i$; $N_f n_{zf}\Lambda_f\Sigma_f$	E_γ, kev	Char. of trans.	$\frac{W_{dcf}}{W_{exp}}$	$\frac{W_{sp}}{W_{dcf}}$
$E1$	$\Delta\Omega = 0$ $\Delta\Omega = \pm 1$	$\Delta N = \pm 1$	$\Delta n_z = \pm 1$ $\Delta n_z = 0$	$\Delta\Lambda = 0$ $\Delta\Lambda = \pm 1$		$\Delta\Sigma = 0$	
$_{66}Dy^{161}_{95}$	0,33	5/2⁻,5/2⁺	5 2 3⁻1/2 6 4 2⁺1/2	25,6	h	3,0	$1\cdot10^3$
		3/2⁻,5/2⁺	5 2 1⁺1/2 6 4 2⁺1/2	74,5	h	150	$4\cdot10^3$
$_{69}Tu^{169}_{100}$	0,32	9/2⁻,7/2⁺	5 1 4⁺1/2 4 0 4⁻1/2	63,1	h	1,7	$3\cdot10^4$
$_{71}Lu^{175}_{104}$	0,34	9/2⁻,7/2⁺	5 1 4⁺1/2 4 0 4⁻1/2	144,9	h	0,53	$4\cdot10^6$
		9/2⁻,7/2⁺	5 1 4⁺1/2 4 0 4⁻1/2	282,6	h	3,5	$6\cdot10^5$
		9/2⁻,7/2⁺	5 1 4⁺1/2 4 0 4⁻1/2	396	h	31	$1\cdot10^5$
$_{71}Lu^{177}_{106}$	0,29	9/2⁻,7/2⁺	5 1 4⁺1/2 4 0 4⁻1/2	147	h	94,5	$6\cdot10^4$
$_{89}Ac^{227}_{138}$	0,17	1/2⁻,3/2⁺	5 3 0⁺1/2 6 5 1⁺1/2	27,3	h	3,5	$1\cdot10^4$
$_{91}Pa^{231}_{140}$	0,25	3/2⁺,3/2⁻	6 5 1⁺1/2 5 2 1⁺1/2	107	h	4,3	$3\cdot10^5$
$_{93}Np^{237}_{144}$	0,233	5/2⁻,5/2⁺	5 2 3⁻1/2 6 4 2⁺1/2	26,4	h	29,4	$1\cdot10^4$
		5/2⁻,5/2⁺	5 2 3⁻1/2 6 4 2⁺1/2	59,6	h	50	$8\cdot10^2$
$_{94}Pu^{239}_{145}$	0,215	5/2⁻,5/2⁺	7 5 2⁺1/2 6 3 3⁻1/2	61,4	h	33	$1\cdot10^4$
		5/2⁻,5/2⁺	7 5 2⁺1/2 6 3 3⁻1/2	106,1	h	52	$4\cdot10^4$
$E2$	$\Delta\Omega = \pm 1$ $\Delta\Omega = \pm 2$	$\Delta N = 0$	$\Delta n_z = \pm 1$ $\Delta n_z = 0$	$\Delta\Lambda = \pm 1$ $\Delta\Lambda = \pm 2$		$\Delta\Sigma = 0$	
$_{63}Eu^{153}_{90}$	0,35	1/2⁺,5/2⁺	4 1 1⁻1/2 4 1 3⁻1/2	172	u	1,18	27
$_{73}Ta^{181}_{108}$	0,3	1/2⁺,5/2⁺	4 1 1⁻1/2 4 0 2⁺1/2	133	h	0,87	$2\cdot10^3$
		5/2⁺,7/2⁺	4 0 2⁺1/2 4 0 4⁻1/2	346	h	0,012	$6\cdot10^2$
		5/2⁺,7/2⁺	4 0 2⁺1/2 4 0 4⁻1/2	482	h	0,008	$8\cdot10^2$

Table 1 continued

Nucleus	β	Ω_i, π_i; Ω_f, π_f	$N_i\, n_{zi}\Lambda_i\, \Sigma_i$; $N_f n_{zf}\Lambda_f \Sigma_f$	E_γ, kcv	Char. of trans.	$\frac{W_{def}}{W_{exp}}$	$\frac{W_{sp}}{W_{def}}$
$_{77}Ir^{191}_{114}$	0,128	1/2+,3/2+	4 0 0+1/2 4 0 2−1/2	82,6	*h*	0,07	1,22
$_{93}Np^{237}_{144}$	0,233	3/2−,5/2−	5 2 1+1/2 5 2 3−1/2	164,6	*h*	0,012	$1{,}7\cdot10^3$
$_{94}Pu^{239}_{145}$	0,215	5/2+,1/2+	6 2 2+1/2 6 3 1−1/2	209,9	*h*	0,012	$1\cdot10^3$
		5/2+,1/2+	6 2 2+1/2 6 3 1−1/2	228,4	*h*	0,04	$1{,}10^2$
		5/2+,1/2+	6 2 2+1/2 6 3 1−1/2	277,7	*h*	0,31	60
		5/2+,1/2+	6 2 2+1/2 6 3 1−1/2	285,6	*h*	0,03	58
E3	$\Delta\Omega = \pm2$ $\Delta\Omega = \pm3$	$\Delta N = 1$	$\Delta n_z = \pm1$ $\Delta n_z = 0$	$\Delta\Lambda = \pm2$ $\Delta\Lambda = \pm3$	$\Delta\Sigma = 0$		
$_{67}Ho^{163}_{96}$	0,35	1/2+,7/2−	411−1/2 523+1/2	305	*h*	0,9	$1{,}4\cdot10^3$
$_{66}Dy^{165}_{99}$	0,33	1/2−,7/2+	5 2 1−1/2 6 3 3+1/2	108	*h*	2,3	$1\cdot10^3$
$_{68}Er^{167}_{99}$	0,318	1/2−,7/2+	5 2.1−1/2 6 3 3+1/2	207,5	*h*	1,01	$1{,}6\cdot10^3$
$_{94}Pu^{237}_{143}$	0,233	1,2+,7/2−	6 3 1−1/2 7 4 3+1/2	145	*h*	0,84	$2\cdot10^2$
E4	$\Delta\Omega = \pm3$	$\Delta N = \pm1$	$\Delta n_z = \pm1$	$\Delta\Lambda = \pm3$	$\Delta\Sigma = 0$		
$_{76}Os^{191}_{115}$	0,175	3/2−,9/2−	5 1 2−1/2 5 0 5−1/2	74,2	*u*	0,05	$1\cdot10^2$

and Np^{237}. In the first case (E2/M1) $\gg$ 1, which indicates that there is a considerable contribution from collective motion. In our calculations the gyromagnetic ratio for the collective motion was determined on the assumption of uniform charge distribution, i.e., we took $g_R = Z/A$, so that for Ta^{181} $g_R \approx 0.4$. In view of the fact that in the given case collective motion makes a large contribution, by increasing g_R one can obtain better agreement with experiment. Thus for g_R = = 0.6 the difference between the theoretical and experimental probabilities is reduced by a factor of about 10. In the second case, on the contrary, the 208 kev transition in Np^{237} is pure M1 and it can be regarded as a pure single-particle transition. In this case, if we take g_R = 0, the calculated probability agrees with the experimental one.

6. Analysis of the selection rules based on the asymptotic quantum numbers shows that these play a significant role in practice. If the transition is not forbidden, the ratio of the probabilities calculated on the basis of the shell model and the unified model is close to unity. If the transition is forbidden,

Table 2

Comparison of the experimental probabilities for magnetic transitions with the theoretical values calculated according to the spherical and unified nuclear models

Nucleus	β	Ω_i , π_i ; Ω_f , π_f	$N_i\ n_{zi}\Lambda_i\ \Sigma_i$; $N_f\ n_{zf}\Lambda_f\ \Sigma_f$	E_γ, kev	Char. of trans.	$\frac{W_{def}}{W_{exp}}$	$\frac{W_{sp}}{W_{def}}$
*M*1	$\Delta\Omega = \pm 1$	$\Delta N = 0$	$\Delta n_z = \pm 1$ $\Delta n_z = 0$	$\Delta\Lambda = \pm 1$ $\Delta\Lambda = 0$	$\Delta\Sigma = 0$ $\Delta\Sigma = \pm 1$		
$_{63}Eu^{153}_{90}$	0,35	1/2+,3/2+	4 1 1−1/2 4 1 1+1/2	69	*u*	11,6	12
		3/2+,5/2+	4 1 1+1/2 4 1 3−1/2	103	*h*	1,1	430
$_{66}Dy^{161}_{95}$	0,33	3/2−,5/2−	5 2 1+1/2 5 2 3−1/2	48,7	*h*	1,7	70
$_{73}Ta^{181}_{108}$	0,3	5/2+,7/2+	4 0 2+1/2 4 0 4−1/2	482	*h*	120	1.10^3
$_{77}Ir^{191}_{114}$	0,128	1/2+,3/2+	4 0 0+1/2 4 0 2−1/2	82,6	*h*	13	6.10^2
$_{93}Np^{237}_{144}$	0,233	3/2−,5/2−	5 2 1+1/2 5 2 3−1/2	208	*h*	120	120
*M*2	$\Delta\Omega = \pm 1$ $\Delta\Omega = \pm 2$	$\Delta N = \pm 1$	$\Delta n_z = \pm 1$	$\Delta\Lambda = 0$ $\Delta\Lambda = \pm 2$	$\Delta\Sigma = \pm 1$ $\Delta\Sigma = 0$		
$_{71}Lu^{175}_{104}$	0,34	9/2−,7/2+	5 1 4+1/2 4 0 4−1/2	282,6	*u*	0,25	8
		9/2−,7/2+	5 1 4+1/2 4 0 4−1/2	396	*u*	0,95	1,8
$_{71}Lu^{177}_{106}$	0,29	9/2−,7/2+	5 1 4+1/2 4 0 4−1/2	147	*u*	0,7	0,5
$_{74}W^{181}_{107}$	0,3	5/2−,9/2+	5 1 2+1/2 6 2 4+1/2	366	*u*	28,8	40
$_{75}Re^{187}_{112}$	0,19	9/2−,5/2+	5 1 4+1/2 4 0 2+1/2	206	*u*	0,26	30
*M*3	$\Delta\Omega = \pm 2$ $\Delta\Omega = \pm 3$ $\Delta\Omega = \pm 3$	$\Delta N = 0$ $\Delta N = 0$	$\Delta n_z = \pm 1$ $\Delta n_z = 0$ $\Delta n_z = \pm 1$	$\Delta\Lambda = \pm 1$ $\Delta\Lambda = \pm 2$ $\Delta\Lambda = \pm 2$	$\Delta\Sigma = \pm 1$ $\Delta\Sigma = 0$		
$_{72}Hf^{179}_{107}$	0,2	1/2−,7/2−	5 1 0+1/2 5 1 4−1/2	160	*h*	0,78	360

Table 2 continued

Nucleus	β	Ω_i, π_i; Ω_f, π_f	$N_i\, n_{zi} \lambda_i\, \Sigma_i$; $N_f\, n_{zf} \lambda_f\, \Sigma_f$	E_γ, kev	Char. of trans.	$\frac{W_{dcf}}{W_{exp}}$	$\frac{W_{sp}}{W_{dcf}}$
$_{74}W^{179}_{105}$	0,2	1/2⁻,7/2⁻	5 1 0⁺1/2 5 1 4⁻1/2	220	*h*	1,1·10²	280
$_{73}Ta^{181}_{108}$	0,3	1/2⁺,7/2⁺	4 1 1⁺1/2 4 0 4⁻1/2	615	*h*	1,1	80
$_{76}Os^{191}_{115}$	0,175	3/2⁻,9/2⁻	5 1 2⁻1/2 5 0 5⁻1/2	74,2	*u*	3,8·10²	300

the unified model leads to lower values of the transition probabilities. As will be evident from the table, the magnitude of this probability ratio depends appreciably on the degree of forbiddenness. Forbiddenness as regards each one of the asymptotic quantum numbers increases this ratio by a factor of 10-100.

Electric transitions prove to be more strongly forbidden than magnetic ones because in electric transitions the projection of the particle spin on the nuclear deformation axis does not change, whereas magnetic transitions can occur both with and without change of the projection of the spin on the deformation axis. Hence for electric transitions Σ is a more significant quantum number than for magnetic ones. Transitions of lower multipole order are more strongly forbidden than transitions of high multipolarity (for example, E1 and E3).

Inasmuch as coupling between the single-particle motion and the deformation leads to displacement of space with orbital momenta differing by two units (l and $l \pm 2$), in the case of high multipole order transitions the wave functions overlap to a greater extent because the number of states between which transitions of the given multipolarity may occur increases (>1). For example, M1 transitions occur between states with the same l, while transitions of higher multipole order may take place between states with different l as well.

I desire to express my deep gratitude to L.I.Rusinov for his constant interest in the work and valuable suggestions. I also desire to thank D.A.Varshalovich who participated in discussions of the results.

Physical-Technical Institute,
Academy of Sciences of the USSR

References

1. S.Nilsson, Kgl.Danske Videnskab.Selskab, Mat.-fys.Medd., 29, 1-68 (1955).
2. A.Bohr, Ibid., 26, 14 (1952).
3. A.Bohr & B.Mottelson, Ibid., 27, 16 (1953).
4. L.A.Sliv & I.M.Band, Tablitsy koeffitsientov vnytrennei konversii γ-izlucheniya, Ch.I (Tables of internal conversion coefficients, Part I), M.-L., 1956.
5. K.Alder, A.Bohr, T.Huus, B.Mottelson & A.Winter, Revs.Mod.Phys., 28, 432 (1956).
6. G.Alaga, K.Alder, K.Bohr & B.Mottelson, Kgl.Danske Videnskab.Selskab., Mat.-fys.Medd., 29, 9 (1955).
7. M.E.Voikhanskii, Zhur.eksp.i teor.fiz., 33, 1004 (1957). (Trans.Soviet Physics - JETP.)

INVESTIGATION OF THE DECAY SCHEMES OF Gd^{146}, Gd^{147} AND Gd^{149} BY MEANS OF A β-γ COINCIDENCE SPECTROMETER

- E.E.Berlovich, O.V.Larionov, E.N.Tunimanova & D.M.Khai

Introduction

The first investigation of neutron-deficient isotopes of gadolinium was that of Shirley et al[1] published in 1957. These authors investigated the conversion lines and the γ-spectra of Gd^{147} and Gd^{149}; in their report they also give unpublished data obtained by Strominger on γ-γ coincidences for these isotopes.

In 1958 at the Eighth All-Union Conference on Nuclear Spectroscopy, Anton'eva et al[2-4] reported on their detailed investigation of the conversion electron spectra of Gd^{146}, Gd^{147} and Gd^{149}. Then, in 1959, Dzhelepov et al[5,6] investigated coincidences between the conversion electrons from these isotopes. Despite these careful investigations, however, a number of features in the decay schemes of these isotopes remained unclear. Yet Eu^{146}, Eu^{147} and Eu^{149} are of undoubted interest inasmuch as these nuclei are located between the region of nuclei with a filled neutron shell (N = 82) and a region of abrupt change in the equilibrium shape of nuclei (N = 89).

The nuclei $_{63}Eu_{84}^{147}$ and $_{63}Eu_{86}^{149}$, which have less than 88 neutrons, may be classified among spherical nuclei and, accordingly, should be described by the Mayer single-particle model. As was noted by Anton'eva et al[4], however, interpretation of their decay schemes from the standpoint of the Mayer model encounters certain difficulties.

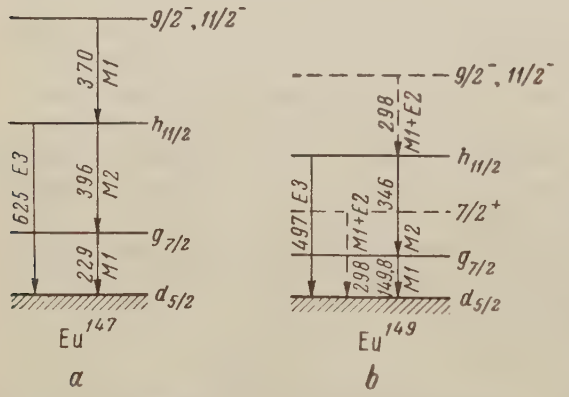

Fig.1. Schemes of principal transitions: a) in Eu^{147}, b) in Eu^{149}.

The most intense transitions, the 229 and 396 kev transitions in Eu^{147}, and the 150 and 346 kev transitions in Eu^{149}, fit readily into the decay schemes (Fig.1) in complete accord with the available experimental data on the multipole orders, transition intensities and coincidences. Location of the relatively intense 298 kev transition in Eu^{149}, however, encounters difficulties: as follows from the analysis carried out by Anton'eva et al[4], there are two alternatives for locating this level (see Fig.1,b), against both of which there may be raised serious objections, to say nothing of the fact that the spins in both cases cannot be explained in the framework of the Mayer model. A similar situation obtains in the case of the 370 kev transition in Eu^{149}, although the difficulty in this case is not as clearly evinced owing to the relatively lower intensity of this transition. With a view to clarifying some of the details of the decay schemes for these isotopes we undertook an investigation of the cascade transitions therein by means of the coincidence technique.

Equipment and procedure

The coincidence spectrometer used for the experiments is diagramed in Fig.2. It consists of two arms. One arm is comprised by a sector type magnetic spectrometer with improved focusing.[8] The luminosity of this spectrometer is about 1%; the resolution 1.9%. The electrons are detected by a stilbene crystal coupled to a photomultiplier. The second arm of the apparatus is a scintillation spec-

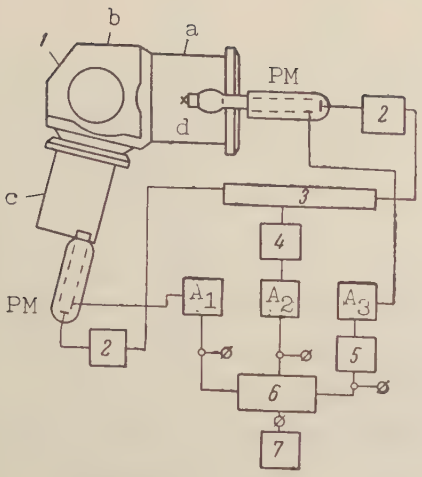

Fig.2. Diagram of coincidence spectrometer: 1) magnetic spectrometer (a - source chamber, b - deflection chamber, c - counter chamger, d - source); 2) limiter, 3) variable delay line, 4) fast coincidence unit, 5) differential pulse height analyzer, 6) triple coincidence circuit, 7) scaler; A_1, A_2 and A_3 - amplifiers; PM - photomultiplier.

trometer with an NaI(Tl) crystal. The luminosity of this spectrometer varies, depending on the geometry of the experiment, from 25 to 15%; the relative half-width of the Cs^{137} photopeak is 12-12.5%. The crystal is located in the vacuum of the source chamber and coupled by means of a light pipe to the photomultiplier which is mounted outside the source chamber. The photomultiplier is protected by a magnetic shield consisting of two coaxial cylinders of Armko iron. The resolution of the scintillation spectrometer was limited mainly by the quality of the crystal.

Both spectrometers were connected into a fast-slow coincidence circuit with a variable delay line.[8]

The detectors are two FEU-14 type photomultipliers designed by G.S.Vil'dgrube. The presence of a "slow" crystal in the scintillation arm limits the resolving time of the circuit; the apparatus time of the coincidence curve is $2\tau = 7 \cdot 10^{-9}$ sec (for β-γ coincidences obtained with a Co^{60} source, the energy of the continuum electrons being 150 kev and that of the Compton electrons 400-600 kev). The time resolution curve recorded under the same conditions but with a stilbene crystal in the scintillation arm is characterized by $2\tau = 5 \cdot 10^{-9}$ sec.

The described set-up is designed for measuring the lifetime of excited nuclear states in the range from $(2\text{-}3) \cdot 10^{-9}$ to $(6\text{-}8) \cdot 10^{-8}$ sec, for measuring partial spectra and also for investigating cascade transitions. The high ratio of the number of true coincidences to the number of chance coincidences makes it possible to measure coincidences between conversion electrons and γ-rays of low intensity.

Experimental results

Gd^{146}. The curve obtained in measuring the coincidences between the K conversion electrons of the (114.8 + 115.5) kev transitions with the γ-rays from the gadolinium fraction is shown in Fig.3. The measurements were carried out 100 days after separation of the fraction from the tantalum target bombarded with 660 Mev protons. The analogous curve for the K line of the 155 kev transition is shown in Fig.4.

In the first case there are two not fully resolved coincidence peaks: peak 1 represents K114.8-γ115.5 and K115.5-γ114.8 coincidences; peak 2 represents K(114.8+115.5)-γ155 coincidences.

The experimental results, although they substantiate the fact that all three transitions are in cascade, do not yield any new information to supplement the data obtained by Dzhelepov & Sergienko[5] on a twin magnetic lens spectrometer, inasmuch as no additional coincidences in the higher energy part of the spectrum were detected. Thus our experimental data merely substantiate the well-founded decay scheme for Gd^{146} proposed by Anton'eva et al[2].

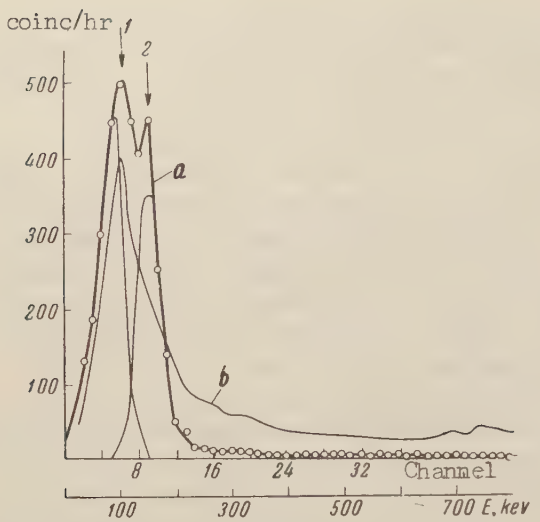

Fig.3

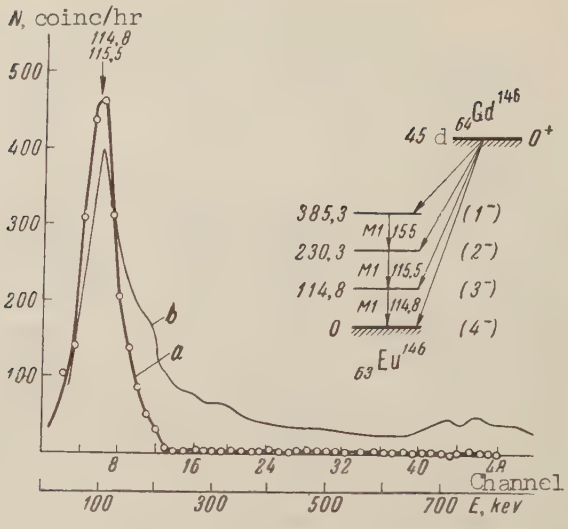

Fig.4

Fig.3. Coincidences between the K electrons of the (114.8 + 115.5) kev transitions and the γ-rays of Gd^{146} recorded by the scintillation arm of the spectrometer: a) coincidence curve, b) spectrum obtained by means of the γ-spectrometer.

Fig.4. Coincidences between the K electrons of the 155 kev transition and the γ-rays of Gd^{146}: a) coincidence curve, b) spectrum obtained by means of the γ-spectrometer. Insert - decay scheme for Gd^{146}.

Gd^{147}. For investigating the decay of 35-hour Gd^{147} the source with the gadolinium fraction was placed in the spectrometer a few hours after separation of the fraction from the proton bombarded tantalum target.

The experimental curves characterizing the coincidences of the K electrons of the 229 kev and 396 kev γ-transitions with the γ-rays of Gd^{147} are shown in Figs.5 & 6; in these figures we also give the singles γ-spectrum recorded by means of the γ-scintillation spectrometer.

As will be evident from Fig.5, the K-229 electrons yield coincidences with the 396 kev γ-rays. The coincidence peak, however, is noticeably broadened owing to an admixture of 370 kev γ-rays. The intensity of the 370 kev γ-transition, according to the data of Shirley et al[1], is about 1/2.5 the intensity of the 396 kev transition. However, the addition to the coincidence peak from the 370 kev photopeak is actually appreciably smaller; this is explained by the fact that the 370 kev γ-transition lies above the isomeric state, the lifetime of which is substantially greater than the resolving time of our coincidence circuit. In our experiments the apparatus time of the coincidence circuit was increased to $2 \cdot 10^{-8}$ sec, while the lifetime of the 625 kev state, according to our earlier measurements[7], is $\tau = 7.1 \cdot 10^{-7}$ sec.

The coincidence curve also has other maxima, although less pronounced, located at 560 ± 20 and 760 ± 25 kev and a weak rise in the vicinity of 900 kev. It must be noted, however, that owing to its small size the efficiency of the NaI(Tl) crystal used in our equipment is relatively low in this energy region.

The K-396 electrons yield coincidences with the 229 kev γ-rays (Fig.6). In addition there are evident low peaks at 480 ± 30 and 560 ± 30 kev. The number of coincidences with the K-396 electrons is an order of magnitude lower than the number of coincidences of the hard γ-rays with the K-229 kev electrons.

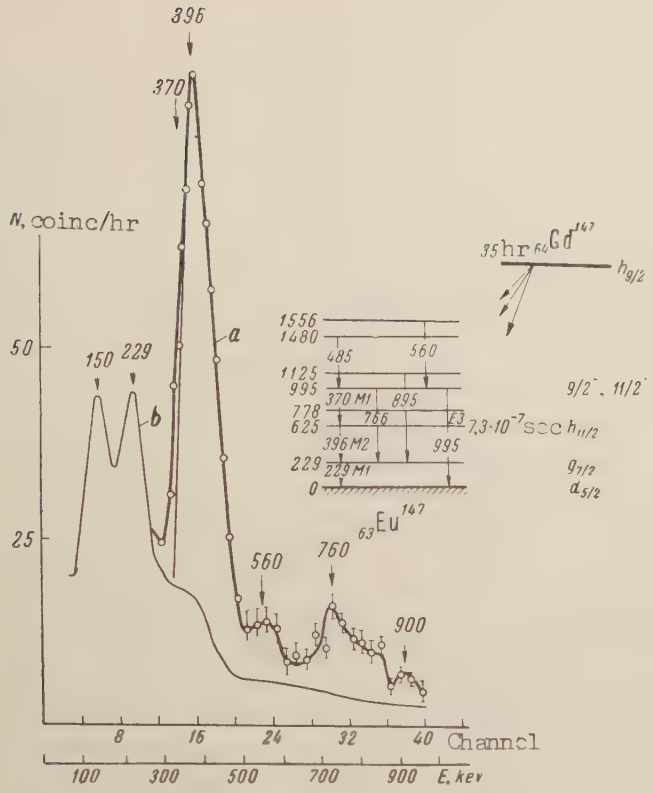

Fig.5

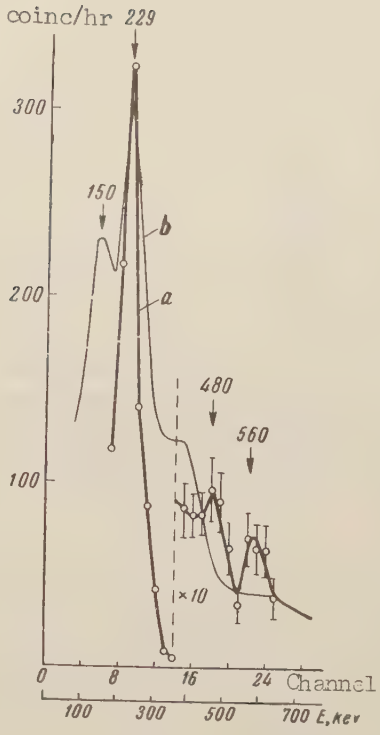

Fig.6

Fig.5. Coincidences between the K electrons of the 229 kev transition and the γ-rays of Gd^{147}: a) coincidence curve, b) spectrum obtained by means of the γ-spectrometer.

Fig.6. Coincidences between the K electrons of the 396 kev transition and the γ-rays of Gd^{147}: a) coincidence curve, b) spectrum obtained by means of the γ-spectrometer.

Gd^{149}. For investigating the decay of this 10-day gadolinium isotope we used a gadolinium fraction that was held for 10-15 days after separation from the tantalum target in order to allow the 35-hour Gd^{147} to die out. In one series of measurements we used gadolinium specially purified of the 24-day europium.

The curves for the K electrons of the 149.8 and 346 kev transitions in coincidence with the γ-rays of Gd^{149} are shown in Figs.7 & 8. As in the previous figures, we also give the singles γ-ray spectrum recorded by means of the γ-scintillation arm. As will be evident from Fig.7, the K-149.8 electrons yield coincidences with the 346 and 530 ± 20 kev γ-rays. There is also some indication of a rise in the region of 650 kev, but in view of the statistical uncertainty the existence of a peak at this energy is open to question.

The K-346 kev electrons yield coincidences with the 149.8 and 298 kev γ-rays.

In the work of Dzhelepov et al[6] there were observed no coincidences between the 149.8 & 298 and 346 & 298 kev transitions. According to our data, however, the existence of coincidences between these γ-rays is evident directly from the peak in the coincidence curve of Fig.8 and from the broadening of the coincidence curve in Fig.7, respectively. Moreover, as will be apparent from a careful examination of Figs.7 and 8, the heights of the 149.8 and 346 kev coincidence peaks differ from those of the lower peaks by at least an order of magnitude. Simple calculations taking into account the relative intensities of all the above transitions (taken from the work of Shirley et al[1]) show that the number of coincidences

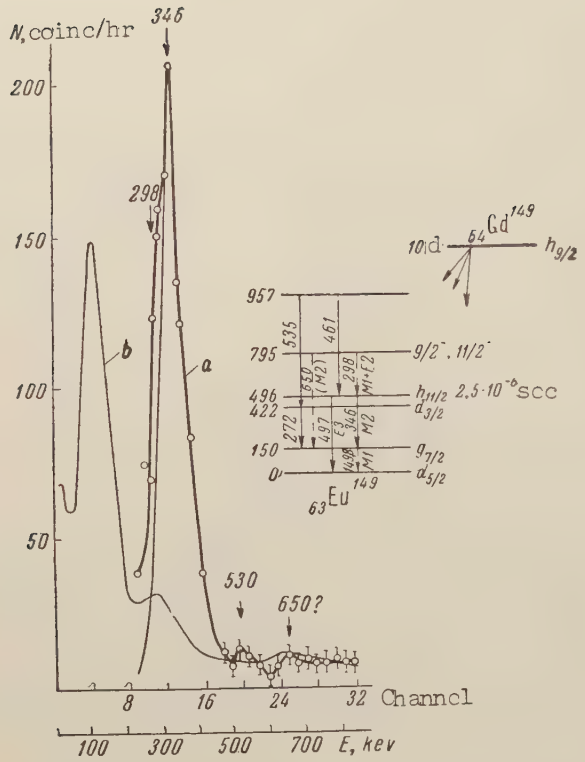

Fig.7. Coincidences of K electrons of the 149.8 kev transition with the γ-rays of Gd^{149}: a) coincidence curve, b) spectrum obtained by means of the γ-spectrometer. Insert - decay scheme for Gd^{149}.

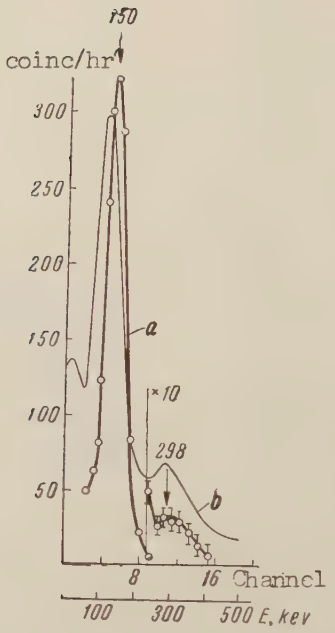

Fig.8. Coincidence of K electrons of the 346 kev transition with the γ-rays of Gd^{149}: a) coincidence curve, b) spectrum obtained by means of the γ-spectrometer.

of K-346 kev electrons with 298 kev γ-rays is less than the expected number by an order of magnitude. This becomes obvious from an examination of the data in the accompanying table in which we give the calculated and experimental ratios of the areas under the coincidence peaks for the transitions in Gd^{149}.

As will be evident from the table, in the first case the experimental and calculated ratios are close (6.6 and 10, respectively); in the second case, the experimental and calculated values differ by more than an order of magnitude. This divergence between the calculated and experimental values of the ratio is readily explained by the existence of an isomeric level at 497 kev ($h_{11/2}$). In the first case the 530 kev γ-rays, in cascade with the 149.8 kev transition K electrons, bypass the isomeric level and yield prompt coincidences. In the second case, the 298 kev γ-rays, yielding coincidences with the K-346 electrons, go through the isomeric level, the lifetime of which according to our earlier measurements[7], is $2.5 \cdot 10^{-6}$ sec, i.e., is two orders of magnitude greater than the appara-

Transition (K line on mag. spectr., kev	Energy to which analyzer gate is set, kev	Coincidence peaks	Calculated coinc. peak area ratio	Experimental peak area ratio
149,8	346 530	$\frac{149,8-346}{149,8-530}$	6,6	10
346	149,8 298	$\frac{346-149,8}{346-298}$	2,3	37

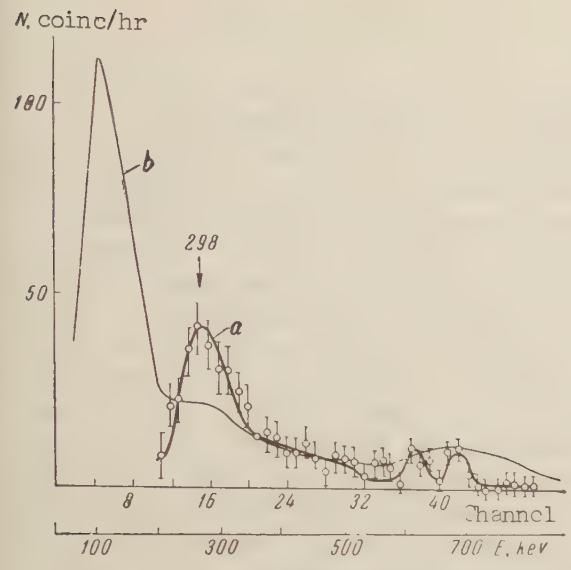

Fig.9

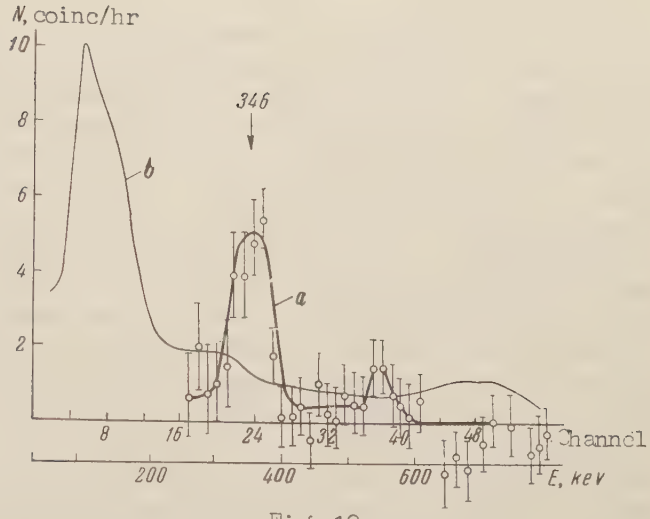

Fig.10

Fig.9. Delayed coincidences of the K electrons of the 149.8 kev transition with the γ-rays of Gd^{149}: a) delay coincidence curve, b) singles γ-spectrum.
Fig.10. Delayed coincidences of the K electrons of the 298 kev transition with the γ-rays of Gd^{149}: a) delay coincidence curve, b) singles γ-spectrum.

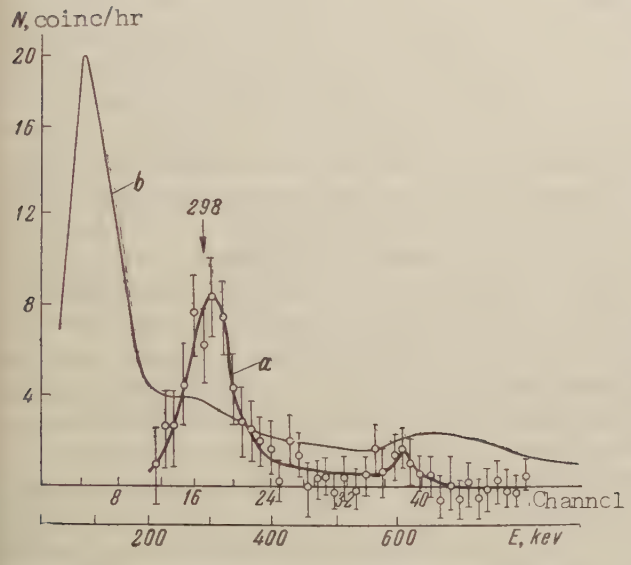

Fig.11. Delayed coincidences of the K electrons of the 346 kev transition with the γ-rays of Gd^{149}: a) delayed coincidence curve, b) singles γ-spectrum.

tus of our coincidence circuit. Hence the number of coincidences recorded is comparatively low.

To obtain direct evidence for the existence of the isomeric level we carried out a series of special measurements of the delayed coincidences of the K electrons of all three transitions with the γ-rays. These measurements were carried out by means of a 100-channel pulse height analyzer connected to the scintillation arm of the spectrometer. An additional delay of 2 microsec was introduced into the channel set on the 298 kev γ-line. The coincidence circuit was triggered by pulses from the magnetic spectrometer. These pulses, shaped and limited in height after amplification, were applied as synchronizing pulses to the 100-channel analyzer.

The delayed coincidence curves are reproduced in Figs.9, 10 & 11. As will be evident from the figures, delayed coincidence peaks were evinced in each case. In these experiments the ratio of the number of true coincidences to chance coincidences was greatly increased as compared with the previous experiments, inasmuch as the resolving time of the coincidence circuit in this case was $5 \cdot 10^{-7}$ sec.

Discussion

On the basis of the experimental data it may be asserted that the 298 kev transition in Eu^{149} is in cascade with the 346 and 149.8 kev transitions, that this transition occurs above the isomeric level and that it departs from a level at 795 kev (see Fig.7). This level, as was indicated by earlier authors[3], may be assigned a spin and parity of $9/2^-$ or $11/2^-$; inasmuch as in the given shell there are no other levels with so high a spin, this level cannot be regarded as a single-particle one. If we accept that the configuration of the ground state of Gd^{149} is $h_{9/2}$ (inasmuch as with $f_{7/2}$ electron capture from the metastable $h_{11/2}$ level is twice forbidden, which is in conflict with the experimental data), it follows that the 795 kev level may be excited with the same probability as the 496 kev level (the energy difference in both cases is approximately 30% and the transitions are allowed). However, the $9/2^-$ assignment implies the existence of a very intense E1 transition of 644 kev energy, which has not been observed. One could hypothesize the existence of some additional forbiddance for such a transition in view of the fact that the 795 kev level is not a single-particle one but has some other nature. It is more probable, however, that the assignment for the 795 kev level is $11/2^-$; in this case the transition from this level to the 149.8 kev level $(g_{7/2})$ can be of the M2 type. The lifetime of the level is determined by the appreciably more intense 298 kev transition (M1 + E2). The 644 kev transition, although it is admittedly weak, apparently does occur; this follows both from the data of Shirley et al[1] and from the results of our measurements.

The fact that the intensities of the 346 and 298 kev transitions are approximately equal can be explained by the fact that excitation of the 497 kev level by electron capture is more probable than excitation of the 795 kev level, which has a different internal structure.

In other respects our data on coincidences are consistent with the decay scheme for Gd^{149} proposed by Anton'eva et al[3].

The decay scheme for Gd^{147} (Ref.2) is, as far as the characteristics of the first three excited levels are concerned, analogous to the decay scheme for Gd^{149} (see Fig.5). However, in this case there obtains an intense transition from the 995 kev level to the first excited level at 229 kev, which is substantiated by our results. The intensity of this transition, according to the data of Shirley et al[1], exceeds the intensity of the 370 kev transition (M1) from the same level by a factor of two. In the insert in Fig.5 we give only the principal part of the decay scheme of Gd^{147} and indicate the cascade transitions observed in the present work. Anton'eva et al[2] observed a great number of conversion lines in the spectrum of Gd^{147}; as these authors note, many of the corresponding transitions can only be tentatively located in the decay scheme for this isotope.

Physical-Technical Institute,
Academy of Sciences of the USSR

References

1. V.S.Shirley, W.G.Smith & J.O.Rasmussen, Nucl.Phys., 4, 395 (1957).

2. N.M.Anton'eva, A.A.Bashilov, B.S.Dzhelepov & B.K.Preobrazhenskii, Zhur. eksp.i teor.fiz., 36, 28 (1959). (Trans.Soviet Physics - JETP.)

3. N.M.Anton'eva, A.A.Bashilov, B.S.Dzhelepov & B.K.Preobrazhenskii, Izv. AN SSSR, Ser.fiz., 22, 906 (1958). (Trans.Bulletin, 22, 899.)

4. N.M.Anton'eva, A.A.Bashilov, B.S.Dzhelepov & B.K.Preobrazhenskii, Ibid., 22, 895 (1958). (Bulletin, Ibid., 22, 889.)

5. B.S.Dzhelepov & V.A.Sergienko, Ibid., 23, 211 (1959). (Trans.Ibid., 23, 203.)

6. B.S.Dzhelepov, B.K.Preobrazhenskii & V.A.Sergienko, Ibid., 23, 219 (1959). (Trans.Bulletin, 23, 211.)

7. E.E.Berlovich, V.N.Klement'ev, L.V.Krasnov, M.K.Nikitin & I.Yursik, Doklady AN SSSR, 133, 789 (1960). (Trans.Soviet Physics - Doklady.)

8. E.E.Berlovich, Izv.AN SSSR, Ser.fiz., 18, 589 (1954). (Trans.Bulletin, 18, 274.)

9. E.E.Berlovich, Ibid., 19, 343 (1955). (Trans.Bulletin, 19, 305.)

* * * * * * *

THE PHOTORITRON
(A gamma-spectrometer for the low-energy region)

- B.S.Dzhelepov & Yu.V.Khol'nov

Introduction

The ritron[1], a magnetic γ-spectrometer utilizing recoil electrons, has been in use for a number of years in the Radium Institute for investigating the high energy sections of γ-ray spectra. This limitation of the ritron is connected with the fact that the spectral sensitivity of the instrument decreases with decrease of the γ-ray energy (see the S_γ curve in Fig.9). The decrease in efficiency becomes particularly noticeable at energies <600 kev, and at energies of 200-300 kev the ritron can no longer be used for studying γ-spectra.

Yet many isotopes emit γ-rays in the low energy region, and knowledge of their relative intensities is frequently essential for constructing the level diagrams.

Hence we undertook the task of extending the working region of the ritron to the side of lower energies.

In order to enhance the sensitivity of the ritron in the low energy region it was natural to attempt to use photoelectrons ejected by the γ-rays from a target located under the same conditions as the cellophane target employed in the ritron, but prepared of a substance with a substantially higher Z.

A large cross section for the photoeffect should lead to increase of the spectral sensitivity; a number of factors, however, act in the opposite direction: greater divergence of the photoelectron beam as compared with the Compton electron beam, greater scattering of electrons in high Z targets, etc. Hence utilization of the photoeffect can be advantageous only under certain conditions. Therefore, our first task was to determine these conditions.

Choice of conditions for measurement

We used our original instrument[1] a diagram of which is shown in Fig.1. In working with recoil electrons the target was usually a 50 μ thick cellophane film. For measuring the background the target was withdrawn from the beam, i.e., lowered to the bottom of the instrument by means of a slider in the lower part of the ritron. For the experiments with photoelectrons we prepared targets of lead and bismuth; these were mounted in frames attached to a second slider, which was in-

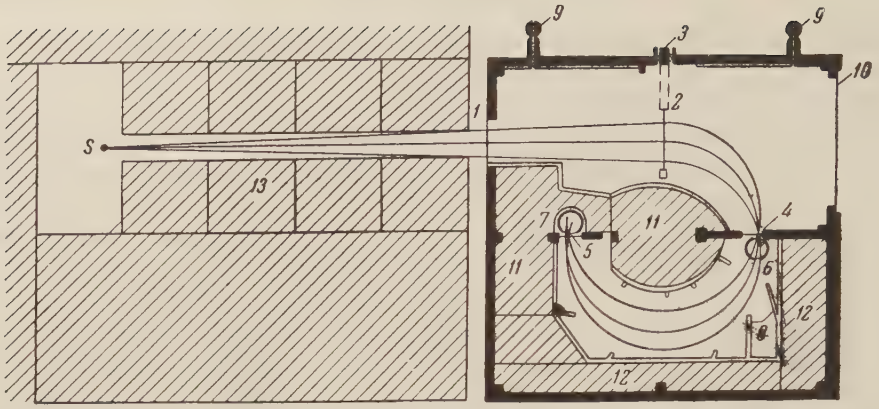

Fig.1. Horizontal section view of the ritron: S - source; 1 - window, 2 - target, 3 - slider for withdrawing target, 4 & 5 - principal slits, 6 & 7 - counters, 8 - auxiliary apertures, 9 - connections to vacuum pump, 10 - back wall of instrument, 11 & 12 - shielding blocks, 13 - collimator.

stalled in front of the first one, so that for measuring the background the photoelectron target could be pulled up out of the beam.

In order to determine the optimum target thickness we carried out experiments with $Eu^{152-154}$. This activity is convenient in that its spectrum comprises three intense lines with energies of 122, 244 and 345 kev, i.e., precisely in the low energy region of interest to us.

The $Eu^{152+154}$ activity also emits many hard γ-rays with energies up to 1400 kev. These γ-rays give rise to a recoil electron background (Compton "tails") in the region of the photoelectron lines corresponding to the 122, 244 and 345 kev γ-rays.

The spectrum of photoelectrons ejected by the 122, 244 and 345 kev γ-rays was investigated with three targets: 13.5 mg/cm^2 Pb, 7.5 mg/cm^2 Bi and 3.7 mg/cm^2 Bi. The results obtained are shown in Figs.2,3 & 4. In Fig.2 there are clearly discernible the three principal lines: L-122, K-244 and K-345.

Fig.3 gives the variation of the relative line half-widths and Fig.4 the variation of the height of the peaks (above the Compton tail) as a function of the target thickness. It will be evident that the resolution of the instrument increases with decrease of the converter thickness. The heights of the L-122 and K-244 peaks remain virtually constant, while the intensity of the K-345 line decreases with decrease of the target thickness. At the same time the height of the Compton tail from the high energy lines also decreases. We opted for the 3.7 mg/cm^2 bismuth converter. It was found that in this case the photoelectron counting rate at the peak of the K-345 line was approximately equal to the counting rate at the peak of the 345 kev Compton line with a 50 μ thick cellophane target.

Thus we chose a Bi target thickness for which the efficiency of the ritron in detecting photo- and Compton electrons in the 350 kev energy region is approximately the same, but as we shall show below the efficiency of the "photo-ritron" is appreciably higher than the efficiency of the "Compton-ritron" in the region of lower energies.

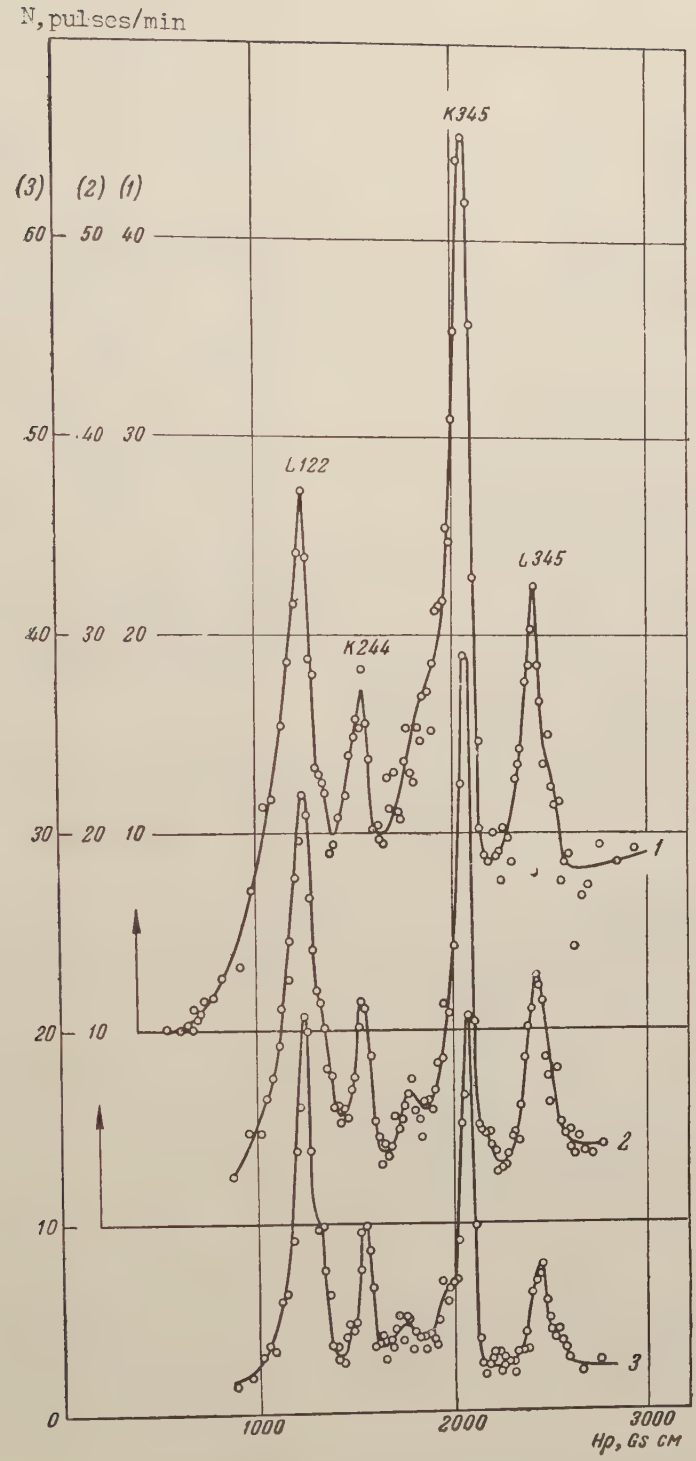

Fig.2. Low energy region of the photoelectron spectrum of $Eu^{152+154}$ recorded with converters of different thickness: 1 - 13.5 mg/cm^2 Pb, 2 - 7.5 mg/cm^2 Bi, 3 - 3.7 mg/cm^2 Bi.

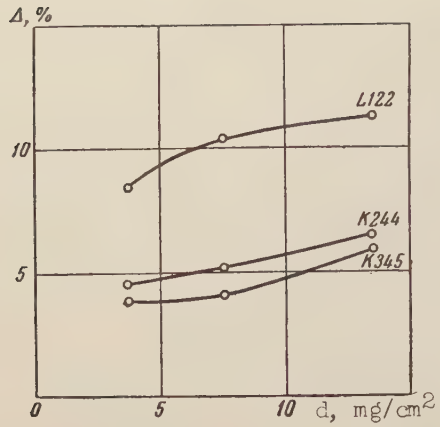

Fig.3. Variation of the relative photoelectron line half-width Δ with the converter thickness d.

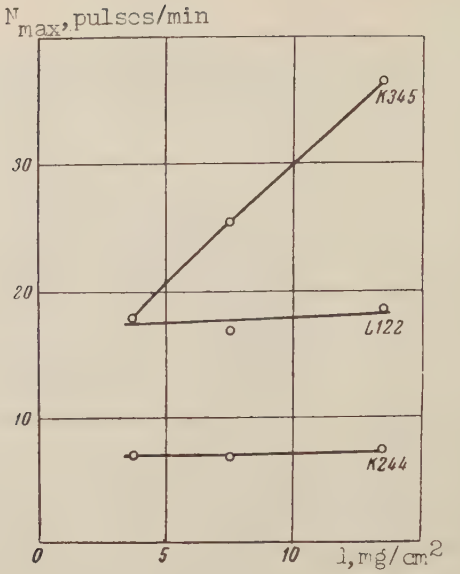

Fig.4. Variation of the counting rate at the peaks of the soft photoelectron lines of $Eu^{152+154}$ with the converter thickness d.

Spectrum line shape

In order to resolve experimental spectra into components, one must know the variation of the shape of the spectrum lines as a function of the γ-ray energy.

We investigated the spectra of electrons ejected from the 3.7 mg/cm^2 bismuth target by γ-rays with energies of 100 (Sm^{153}), 145 (Ce^{141}), 190 (In^{114}), 280 (Hg^{203}), 411 (Au^{198}) and 660 kev (Cs^{137}). The results of these measurements are shown in Fig.5.

The softest monochromatic γ-rays are evinced by one photoelectric line - the L line (with a small hump on the right side due to the unresolved M line). In the case of Sm^{153} the K electrons ejected from the Bi target have an energy of 10 kev and hence are not detected by the instrument (they are absorbed in the target and counter windows).

In the case of Ce^{141} (145 kev γ-rays) there already appears the K line. Then in the photoelectron spectrum of In^{114} the K line exceeds the L line in height. In the spectrum of Hg^{203} there appears the Compton electron line (5280) the Compton line becomes more intense in the spectrum of Au^{198}. In the case of Cs^{137} it becomes equal in height to the K-660 line.

Fig.6 shows the variation of the relative half-widths of the K and L lines as a function of the γ-ray energy. For comparison we also give the curve for the Compton electron lines (σ). The higher resolution of the photoritron is clearly evident. The variation of the K/L intensity ratio as a function of the γ-ray energy is shown in Fig.7. This ratio equals zero in the region of 100 kev and then rapidly increases to a "saturation value" at about 250 kev. We used this curve for plotting the spectral sensitivity function of the instrument.

Calibration in energy

The K and L lines shown in Figs.2 and 5 correspond to γ-rays the energies of which are known precisely. We determined $H\rho_{max}$ for the lines as the values on the $H\rho$ scale of the intersections of straight lines drawn through the steepest parts of the left and right hand sides of the line peaks.

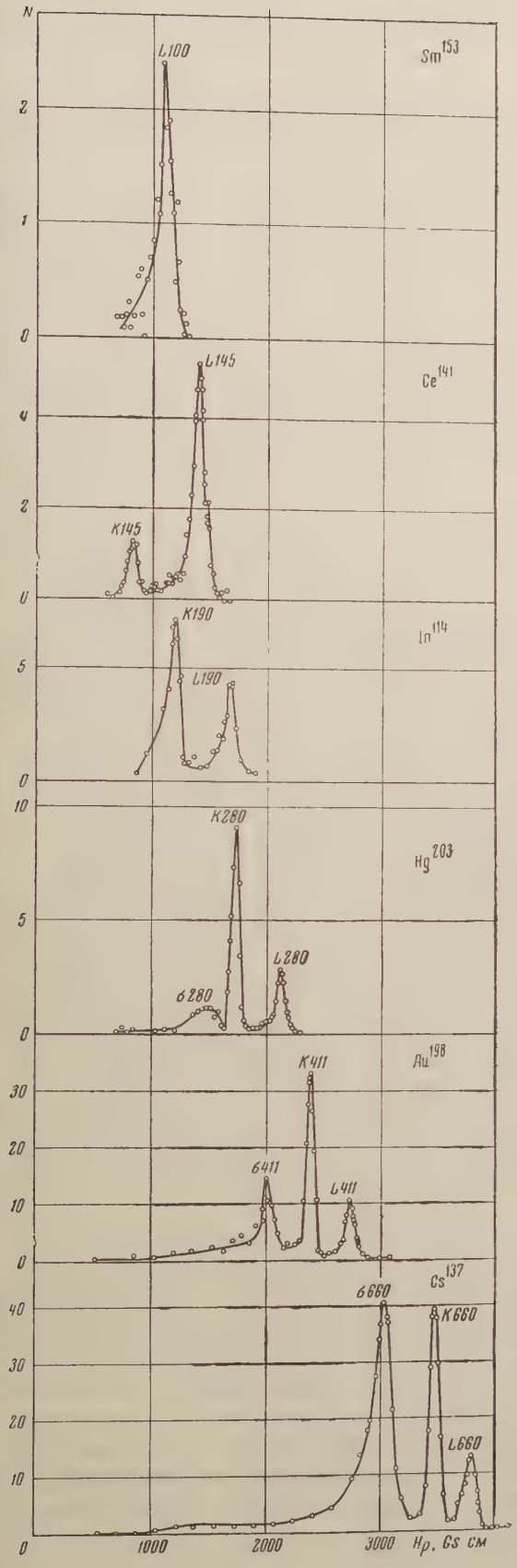

←Fig.5. Spectrum line shapes.

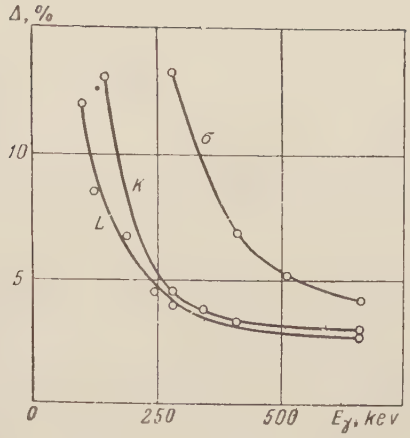

Fig.6. Variation in the relative half-width of the Compton (σ), K and L photoelectron lines as a function of the γ-ray energy.

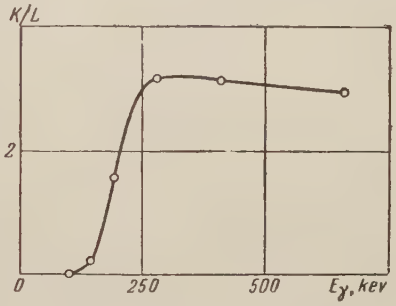

Fig.7. Variation of the intensity ratio of the K and L photoelectron lines with the γ-ray energy.

The relation between E_γ and $H\rho_{max}$ is shown in Fig.8 for the K and L lines. Using these curves one can readily determine the γ-ray energy to within 0.5%.

Calibration in intensity

The problem of calibrating the instrument in intensity is more complex. We define the spectral sensitivity function of the ritron as the variation in the counting rate at the line peak with the energy on the assumption that the γ-ray source emits equal numbers of γ-rays of different energies per unit time. This function S_γ was determined for the

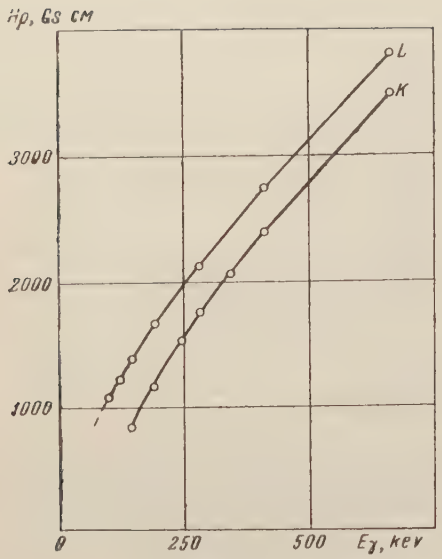

Fig.8. Calibration of the photoritron in energy.

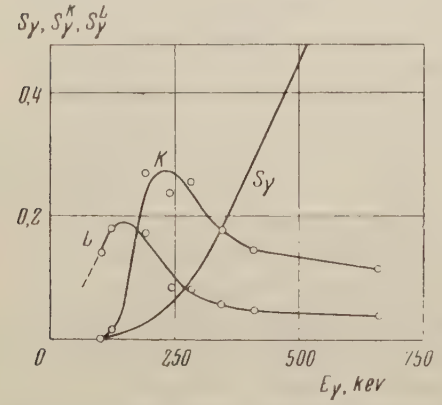

Fig.9. Spectral sensitivity functions of the ritron and photoritron in the low energy region.

ritron so that $S_\gamma = 1$ at $E_\gamma = 1$ Mev.

Let us determine the analogous function for the photoritron in terms of the heights of the K and L photoelectron lines (after subtraction of the background and the tails). In this case we obtain two curves for the efficiency of the instrument as regards the K and L lines, i.e., the functions S_γ^K and S_γ^L.

In the case of γ-rays having energies of 660, 411, 345, 280 and 190 kev one can readily obtain the corresponding points. Using the same sources we investigated the recoil electron spectrum (cellophane target) and the photoelectron spectrum (Bi target, K and L lines). Then from the ratio of the counting rates at the peak of the K or L line and the recoil electron line and the known value of S_γ for the given energy we could readily calculate $S_\gamma^K = \frac{N_K}{N_\sigma} S_\gamma$ and $S_\gamma^L = \frac{N_L}{N_\sigma} S_\gamma$. At energies under 190 kev, however, the Compton lines do not appear and hence the location of the calibration curve for the ritron is unknown. Therefore, for $h\nu$ = 100 kev (Sm^{153}) we determined the efficiency of the instrument by the following absolute procedure.

The absolute activity of the Sm^{153} source was determined by means of the β- and γ-calorimeters of the All-Union Scientific Research Institute for Metrology, and found to be 156 mC. Knowing the number of γ-rays per decay for the 100 kev line of Sm^{153} (0.33) and having determined experimentally the number of coincidences at the L peak, we calculated the coincidence counting rate at the peak of this line for an activity of 1 curie emitting γ-rays of the given energy in the amount of one photon per disintegration. Since we knew the absolute value of the division on the vertical scale in Fig.9 ($S_\gamma = 1$ corresponds to 654 coincidences per minute at the peak of the Compton line for 1 curie and $h\nu$ = 1 Mev), we could plot the point for L-100 in Fig.9.

We have also plotted in Fig.9 the points corresponding to the 122 and 244 kev γ-rays from $Eu^{152+154}$. The intensity ratios of the L-122 and K-244 lines relative to the K-345 line (S_γ^K for which is known) were determined experimentally. For determining $S_\gamma^L(122)$ and $S_\gamma^K(244)$ it was necessary to know the relative intensities of the 122, 244 and 345 kev γ-rays emitted by the $Eu^{152+154}$ source (the 122 and 244 kev lines belong to different isotopes). Zhukovskii[2] investigated the γ-spectrum of the same europium source and determined the relative activities of these two isotopes: $I_{152/154} = 0.21 \pm 0.03$. The relative probabilities of the transitions in question were also taken from the work of Zhukovskii, who analyzed the decay scheme for Eu^{152} and Eu^{154} on the basis of all the currently available experimental data.

Inasmuch as the L-345, L-244 and K-122 lines were not observed in the photoelectron spectrum, the corresponding points were plotted on the basis of the energy dependence of the K/L ratio (Fig.7).

Hence in investigating a radioactive isotope, for determining the relative γ-ray intensities, one must divide the experimental heights of the observed K and L peaks by the appropriate S_γ^K or S_γ^L.

Inasmuch as all three spectral sensitivity curves are uniquely related, they allow of determining relative intensities of γ-rays in the entire accessible energy range.

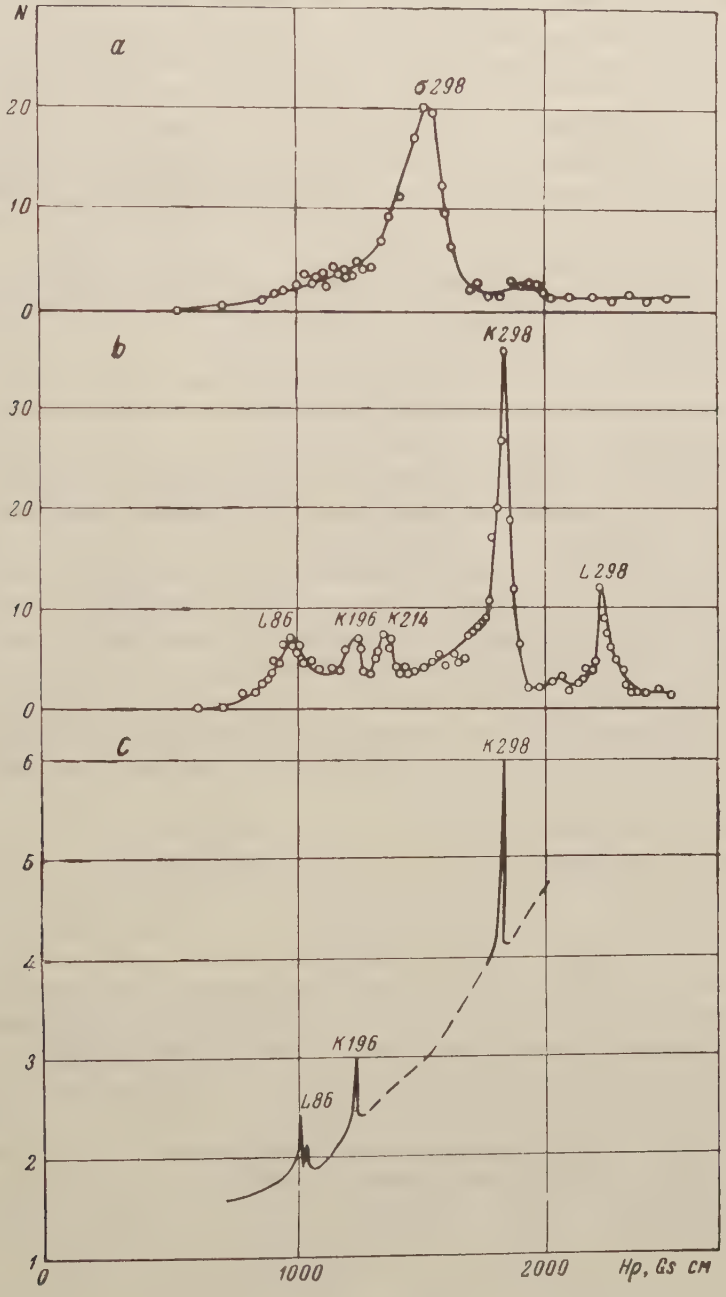

Fig.10. Tb^{160} Compton and photoelectron spectra: a - ritron, b - photoritron, c - $\pi\sqrt{2}\,\beta$-spectrometer[3].

Tb^{160} photoelectron spectrum

In order to illustrate use of the instrument under the new "photoritron" conditions we reproduced the spectrum of photoelectrons ejected from the Bi target by the γ-rays from Tb^{160}, which has a very complicated spectrum.

Fig.10,a shows the low energy part of the spectrum of Tb^{160} obtained by means of the ritron under the usual conditions, i.e., the recoil electron spectrum. One can clearly discern one line corresponding to 298 kev γ-rays.

In the photoelectron spectrum (Fig.10,b) there appear five lines: L-86, K-196, K-214, K-298 and L-298. Using the curves of Fig.9 we determined the relative intensities of the corresponding γ-rays; they proved to be, respectively, 34, 7.8 and 66 (in relative units, the intensity of the 965 kev line being taken as 100).

For purposes of comparison in Fig.10,c we reproduce the spectrum obtained by Kratsik[3] on a $\pi\sqrt{2}$ β-spectrometer. Although the lines in this spectrum are appreciably narrower than those obtained with our instrument, it will be evident that the ratio of the heights of the photopeaks to the Compton background is considerably higher in our spectrum.

Recently, operating the ritron under the new conditions, we succeeded in detecting the L line of the 65 kev γ-rays emitted by W^{187}.

Conclusions

Use of photoelectrons in the ritron enabled us:

1) to extend the useful range of this γ-spectrometer down to ~60 kev; thus one can now determine γ-ray energies and relative intensities in the entire range from 60 to 3000 kev by means of one instrument,

2) to enhance the resolution of the ritron in the region of low energies, and

3) to obtain a better photopeak height to Compton background ratio than is attainable with other spectrometers.

We take this opportunity to thank E.A.Khol'nov for the calorimetric measurements and students A.Ushakov, V.Rumyantsev and E.Vinogradov as well as E.Arutyunyan and G.Shchukin for assistance in carrying out the measurements on the ritron.

"V.G.Khlopin" Radium Institute,
Academy of Sciences of the USSR

References

1. B.S.Dzhelepov, N.N.Zhukovskii & Yu.V.Khol'nov, Izv.AN SSSR, Ser.fiz., 18, 599 (1954), (Trans.Bulletin, 18, 285); B.S.Dzhelepov, V.P.Prikhodtseva, A.I. Feoktistov & Yu.V.Khol'nov, Ibid., 20, 1361 (1956), (Trans.Bulletin, 20, 1245); N.B.Golovanov, B.S.Dzhelepov, V.P.Prikhodtseva & Yu.V.Khol'nov, Ibid., 21, 985 (1957), (Trans.Bulletin, 21, 987).

2. N.N.Zhukovskii, Thesis, Radium Institute, 1958.

3. B.Kratsik, Thesis, Leningrad State University, 1959.

DETERMINATION OF THE RELATIVE PROBABILITIES FOR ELECTRON CAPTURE FROM THE L AND K SHELLS IN THE DECAY OF Cr^{51}, Zn^{65} AND Ge^{71}

- A.A.Konstantinov & V.V.Perepelkin

The ratio of the probabilities for electron capture from the L and K shells has been determined experimentally only for a few electron capture isotopes. The results of theoretical calculations of this ratio[1,2] are in satisfactory agreement with the experimental data[3,4] only in a few cases. Yet knowledge of the L and K electron capture ratio λ_L/λ_K is necessary for determining the activities of electron capture sources and plotting the decay schemes.

For determining the values of the λ_L/λ_K ratio in the decay of Cr^{51}, Zn^{65} and Ge^{71} we used a 4π proportional counter to detect coincidences between the K x-rays and the L Auger electrons (L - MM and similar transitions). The small number of L x-rays (about 1%) emitted by sources of the above isotopes is virtually completely absorbed in the gas filling the counter; hence they are detected by the 4π counter just like L Auger electrons.

The radioactive isotope deposited on a thin (0.2-0.4 μ) celluloid film was mounted between the two halves of the 4π counter (see Fig.1 in Ref.5). The celluloid film was covered with a thin layer of bismuth (~0.01 μ) to insure greater reflection of the $V^{51}(Cr^{51})$, $Cu^{65}(Zn^{65})$, and $Ga^{71}(Ge^{71})$ Auger electrons.

The radioactive isotope was deposited by vacuum evaporation over an area of 2 to 7 cm^2. With a specific activity of 500 mC/g and a source activity of ~10^{-8} curie, the superficial density of the active layer is approximately 10^{-8} g/cm^2, so that the self-absorption of K Auger electrons was insignificant (smaller than 1%).

With the 4π counter filled with a mixture of methane (20 cm Hg) and xenon (15 cm Hg) the first half of the 4π counter (the 2π counter on the side of the source) detects (Fig.1) L Auger electrons (first peak) and K Auger electrons together with K x-rays absorbed in the xenon filling the 2π counter (second peak). Between these peaks there is evident a certain number of K Auger electrons that have lost part of their energy in being reflected from the backing.

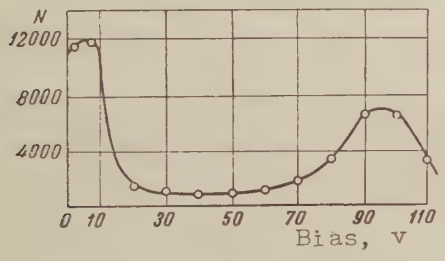

Fig.1. Spectrum of $Ga^{71}(Ge^{71})$ Auger electrons together with K x-rays detected in the first half of the 4π counter; filling - methane (20 cm Hg) and xenon (15 cm Hg).

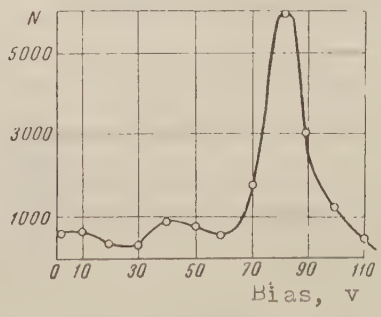

Fig.2. Spectrum of $Ga^{71}(Ge^{71})$ K x-rays detected in the second half of the 4π counter; filling - methane (20 cm Hg) and xenon (15 cm Hg).

The second half of the 4π counter detects only K x-rays (Fig.2), inasmuch as the Auger electrons are completely stopped by the celluloid support. The data of Figs.1 and 2 were obtained by means of a single channel differential pulse height analyzer.

The number N^{XL} of coincidences between the L Auger electrons in the first half of the 4π counter and K x-rays in the second half, and the number N^X of K x-rays and the number N^L of L Auger electrons are given by the following equations:

$$N^{XL} = \varepsilon^X \varepsilon^L k_1 N_0^X k_2; \quad (1)$$

$$N^X = \varepsilon^X N_0^X; \quad (2)$$

$$N^L = \varepsilon^L k_1 N_1^L, \quad (3)$$

where ε^X is a coefficient taking into account the efficiency in detecting the K x-rays in the second half of the counter and the corresponding solid angle, ε^L is a coefficient taking into account the efficiency in detecting L Auger electrons in the first half of the counter and the corresponding solid angle, k_1 is a coefficient depending on the width of the gate of the single channel amplitude analyzer by means of which the L Auger peak is discriminated from the general Auger electron spectrum, N_0^X is the total number of K x-rays emitted by the source in a 4π solid angle, k_2 is a coefficient taking into account the fact that not all the K x-rays yield coincidences with L Augers (k_2 is determined from the intensity ratio of the K_α and K_β lines of the isotopes), N_1^L is the total number of Auger electrons emitted by the source except for those that yield coincidences with the K Augers and the K x-rays detected in the first half of the 4π counter.

Combining Eqs.(1)-(3) one can write the following equation for N_1^L:

$$N_1^L = \frac{N^L N^X k_2}{N^{XL}}, \quad (4)$$

However, in counting L Augers by means of the single channel differential pulse height analyzer there is also detected a certain number of K Auger electrons scattered from the backing with loss of energy. In order to exclude them one must extrapolate over the spectrum (Fig.1); then Eq.(4) assumes the form

$$N_1^L = \frac{N^L k_3 N^X k_2}{N^{XL}} \quad (5)$$

where k_3 is a coefficient taking into account the fraction of K Auger electrons in the L Auger peak.

N_1^L can also be written as

$$N_1^L = n_0^L + k_2 N_1^X + k_4 N_1^K, \quad (6)$$

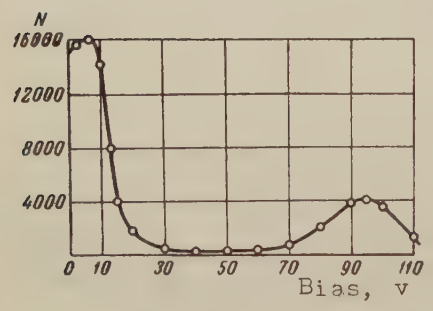

Fig.3. Spectrum of $Ga^{71}(Ge^{71})$ Auger electrons detected in the first half of a 4π counter; filling - methane (20 cm Hg).

where n_0^L is the total number of L Auger electrons emitted as the result of L capture in the given source, $k_2 N_1^X$ is the number of L Augers accompanying the K x-rays that are not detected in the first half of the 4π counter, $k_4 N_1^K$ is the number of L Augers accompanying the K Auger electrons that are not detected in the 4π counter, and k_4 is a coefficient that shows in what proportion L Augers accompany the K Auger electrons.

For higher accuracy in determining n_0^L it is desirable that N_1^X and N_1^K be as small as possible. This is realized for N_1^X by insuring the highest efficiency for detecting the K x-rays (filling the counter with 15 cm Hg xenon), and for N_1^K by depositing the radioactive isotope onto a celluloid film with a layer of bismuth (to insure the highest possible absorption of K Augers).

λ_L/λ_K probability ratio for Cr^{51}, Zn^{65} and Ge^{71}

Isotope	Our results	Other data	Calc. [1]	Calc. [2]
Cr^{51}	0,10±0,02	None	0,088	0,094
Zn^{65}	0,13±0.02	None	0,096 *	0,099 *
Ge^{71}	0,13±0,02	0,25 [7]; 0,128 [8]; 0,09 [9]	0,106	0,11

*The values of λ_L/λ_K for Zn^{65} were calculated as for an allowed transition[10].

For determining N_1^X and N_1^K it is necessary to know the total number N_0^K of K Auger electrons, the total number N_0^X of K x-rays emitted in a 4π solid angle and the number of K Auger electrons detected in the first half of the 4π counter. The last quality can be taken off the curve shown in Fig.3. The L Auger electron peak is excluded by extrapolation over the 40 to 60 v section.

The value of N_0^X was determined by means of a proportional 4π counter by the method of several fillings[6]. The value of N_0^K was determined from N_0^X and the K fluorescence coefficient.

The ratio of probabilities for electron capture from the L and K shells is related with n_0^L, N_0^X and N_0^K by the following simple equation:

$$\frac{\lambda_L}{\lambda_K} = \frac{n_0^L}{N_0^X + N_0^K}. \qquad (7)$$

Using the above described procedure we determined the values of λ_L/λ_K for Cr^{51}, Zn^{65} and Ge^{71}. The results are summarized in the accompanying table.

References

1. M.E.Rose & J.L.Jackson, Phys.Rev., 76, 1540 (1949).
2. I.M.Band, L.N.Zyryanova & Yu.P.Suslov, Izv.AN SSSR, Ser.fiz., 22, 952 (1958). (Trans.Bulletin, 22, 943.)
3. B.Pontecorvo, D.Kirkwood and G.Hanna, Phys.Rev., 75, 982 (1949).
4. P.Radvanyi, J.Phys.et radium, 16, 509 (1955).
5. A.A.Konstantinov, I.A.Sokolova & T.E.Sazonova, Izv.AN SSSR, Ser.fiz., 25, No.2 (1961). (Trans.Bulletin, 25, No.2.)
6. A.A.Konstantinov, PTE, No.1, 67 (1959). (Trans.Instruments & Experimental Techniques.)
7. J.Laberrique-Frolow, P.Radvanyi & M.Langevin, J.phys.et radium, 17, 530 (1956).
8. W.P.Drever & A.Molik, Phil.Mag., 2, 427 (1957).
9. D.E.Rehfuss & B.Crasemann, Phys.Rev., 114, 1609 (1959).
10. A.H.Wapstra, G.J.Nijgh & R.van Lieshout, Nuclear Spectroscopy Tables, Amsterdam, 1959.

DECAY OF Dy^{159}

- E.I.Biryukov, O.I.Grigor'ev, B.S.Kuznetsov & N.S.Shimanskaya

We investigated the electromagnetic radiation from 144-day Dy^{159}, obtained by spallation of a tantalum target with 660 Mev protons, by means of a spectrometer with a proportional counter and a scintillation γ-spectrometer.

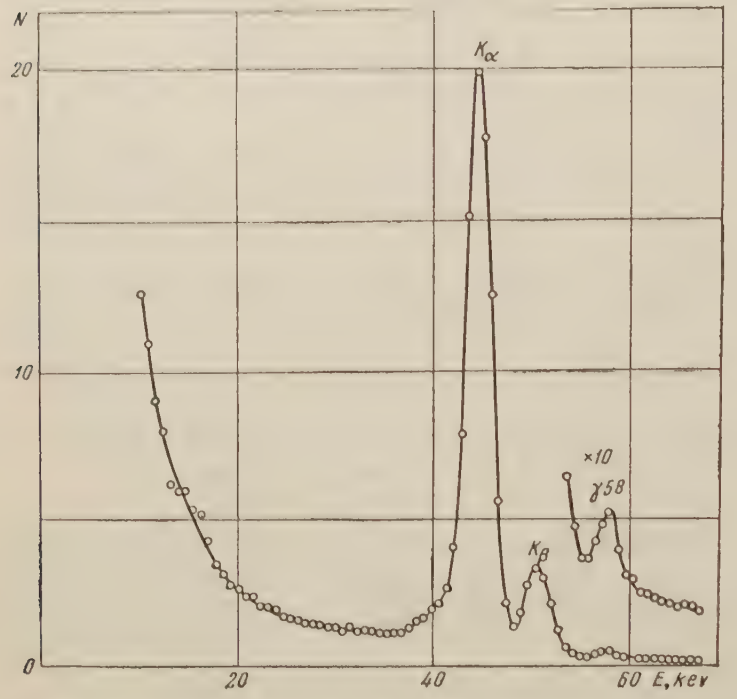

Dy^{159} spectrum in the 15 to 60 kev region recorded by means of a proportional counter with a 130 mg/cm^2 aluminum absorber (close geometry).

The spectrum of electromagnetic radiation from Dy^{159} in the 15 to 60 kev region obtained with a 130 mg/cm^2 aluminum absorber is reproduced in the accompanying figure. Evaluation of the relative intensities of the K x-rays (44.5 and 50.4 kev) and 58 kev γ-rays yielded $I_{KX}/I_{\gamma 58} = 53$. If one takes the probability for transition to the first excited level in Tb^{159} to be 0.32 (see below) the fraction of unconverted 58 kev γ-radiation amounts to 6.1%, which is in agreement with the data of Nielsen et al[1] on γ-decay of Gd^{159}.

In addition to the 58 kev γ-line, we observed a weak line with an energy of 350 kev, which was also detected in the recent work of Brosi & Ketelle[2]. According to our measurements, the intensity of this line is $2\cdot10^{-5}$ photons per disintegration. We failed to detect any higher energy lines in the range to 2 Mev with an intensity exceeding 10^{-4}–10^{-5} photons per disintegration.

Measurements using the same Dy^{159} source in a 4π scintillation counter and a 4π gas counter yielded the following relations between the intensities of the L and K x-radiation and the intensities of the corresponding L-L and K-K x-ray coincidences:

$$\frac{I_{KX}}{I_{KX-KX}} = 6.56 \pm 0.18, \quad \frac{I_{LX}}{I_{LX-LX}} = 48.1 \pm 4.1, \quad \frac{I_{KX-KX}}{I_{LX\ LX}} = 37.1 \pm 5.8, \quad \frac{I_{LX}}{I_{KX}} = 0.21 \pm 0.01$$

On the basis of these data we calculated the L_1/K_1 ratio for the transition to the first excited (58 kev) level in Tb^{159} and the branching ratio $\varkappa$ to this level. Using the value of the L fluorescence yield of Tb given by Robinson & Fink[3] (0.18 ± 0.02), we obtained $L_1/K_1 = 0.56$ and $\varkappa = 0.32 \pm 0.08$.

References

1. K.Nielsen, O.Nulsen & O.Skilbreid, Nucl.Phys., 7, 561 (1958).
2. A.Brosi & B.Ketelle, Phys.Rev., 116, 98 (1958).
3. B.Robinson & R.Fink, Revs.Mod.Phys., 32, 117 (1960).

NUCLEAR MOMENTS OF ODD GADOLINIUM ISOTOPES

- N.I.Kaliteevskii, M.P.Chaika, I.Kh.Pacheva & E.E.Fradkin

The present report is a more complete exposition of our investigation described earlier in Ref.1. Having carried out additional measurements and improved our methods of calculation, we succeeded in obtaining more accurate values for some of the data. The experimental procedure is described in Ref.2.

We used a photoelectric spectrometer with a Fabry-Perot interferometer[3] to investigate the hyperfine structure (hfs) of three lines of Gd I: 5015 Å ($z^{11}G_9 - a^{11}F_8$), 5103 Å ($z^{11}G_8 - a^{11}F_7$) and 4743 Å ($y^{11}F_3 - a^{11}F_4$). The measurements were carried out on separated gadolinium isotopes: Gd^{155} - 97.3% and Gd^{157} - 91.4%.

The hfs components of the gadolinium lines are so closely spaced (15-20 mK)* that complete resolution of the structure is impossible under the given experimental conditions. At the same time examination of all the spectrometer traces shows that the structure can be resolved only on the assumption that each of the atomic levels of Gd^{157} and Gd^{155} is comprised of four hfs sublevels. This unambiguously indicates[4-6] that the spin of both gadolinium isotopes is 3/2.

The positions of the hfs components were determined on the basis of the resolution of the line structure taking into account all the superimposed components belonging to other isotopes (see figure). The calculations were carried out for the four intense diagonal components of the investigated line, the separation between which depends on the hyperfine splitting of both the upper and lower levels:

$$\sigma(i-l) = \frac{1}{2}A(C_i - C_l) - \frac{1}{2}A'(C'_i - C'_l) + B[C_i(C_i+1) - C_l(C_l+1)] - B'[C'_i(C'_i+1) - C'_l(C'_l+1)] \quad (i,l = 1,2,3,4), \tag{1}$$

where

$$A = \frac{\mu}{I}\frac{\langle H(0)\rangle_{JJ}}{J}; \quad B = eQ\left\langle\frac{\partial^2 u}{\partial z^2}(0)\right\rangle_{JJ}\cdot\frac{3/8}{I(2I-1)J(2J-1)};$$

C_i is a combination of quantum numbers: $C_i = F_i(F_i+1) - J(J+1) - I(I+1)$; A and B are the interval factors of the magnetic dipole and electric quadrupole interaction of the nucleus with the electron shell of the atom for the lower level, and A' and B' are the corresponding interval factors for the upper level.

For each line we experimentally determined the three independent intervals: $\sigma(1-2)$, $\sigma(1-3)$ and $\sigma(1-4)$. Thus we obtained six equations for the following six unknowns:

$$A_{157},\ A'_{157},\ B_{157},\ B'_{157},\ \frac{A_{155}}{A_{157}},\quad \frac{B_{155}}{B_{157}}.$$

(For isotopes with the same spin the ratio of the interval factors A is equal to the ratio of the magnetic moments and the ratio of the interval factors B is equal to the ratio of the quadrupole moments of the corresponding nuclei.)

The ratio of the magnetic moments of Gd^{155} and Gd^{157} is obtained directly from the experimental data:

$$\frac{\mu_{155}}{\mu_{157}} = \frac{\sigma_{155}(1-2) - \sigma_{155}(1-3) + \sigma_{155}(1-4)}{\sigma_{157}(1-2) - \sigma_{157}(1-3) + \sigma_{157}(1-4)}. \tag{2}$$

On the basis of Eq.(1) without further theoretical assumptions one can with fair accuracy also calculate the ratio of the quadrupole moments of Gd^{155} and Gd^{157}. The calculations are based on the fact that for all three investigated

---

*K = kayser = cm^{-1}.

lines there is fulfilled with good accuracy the relation

$$A(C_1 - C_l) - A'(C_1' - C_l') = a_l A - b_l A' \approx a_l (A - CA');\ l = 2, 3, 4.$$

$$C \approx \frac{b_2}{a_2} \approx \frac{b_3}{a_3} = \frac{b_4}{a_4},$$

where a_l and C are numerical coefficients that are readily determined for each spectrum line. The error introduced in determining the hfs intervals $\sigma(1-l)$ by replacing the coefficients b_l/a_l by one value of C does not exceed 0.1 mK, i.e., is appreciably smaller than the experimental error in determining $\sigma(1-l)$.

The calculations were carried in two ways. In the first we used only the intervals $\sigma(1-2)$ and $\sigma(1-4)$ determined experimentally with the highest accuracy:

$$\frac{Q_{155}}{Q_{157}} = \frac{a_4\sigma_{155}(1-2) - a_2\sigma_{155}(1-4)}{a_4\sigma_{157}(1-2) - a_2\sigma_{157}(1-4)}; \qquad (3)$$

for $\lambda = 5015$Å: $a_4 = 51$, $a_2 = 19$;
for $\lambda = 5103$Å: $a_4 = 45$, $a_2 = 17$;
for $\lambda = 4743$Å: $a_4 = 21$, $a_2 = 9$.

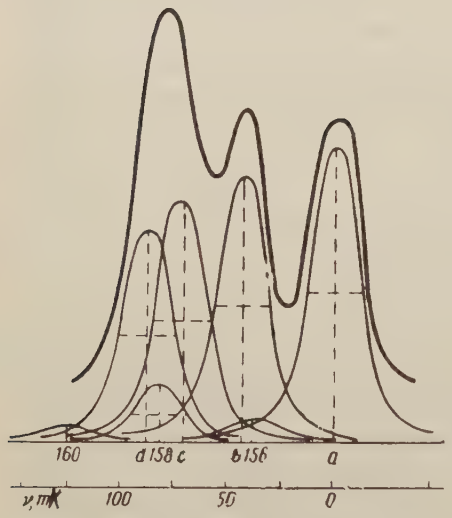

Resolution of the experimental trace of the hfs of the 5015 Å line of Gd^{157} into components a, b, c and d, the four diagonal hfs components. The contribution from the even isotopes, Gd^{156}, Gd^{158} and Gd^{160}, is taken into account, but the contribution from the nondiagonal hfs components (<1%) is neglected.

In the second method we used all three intervals and carried out the calculations by the method of least squares. The results representing averaged values for several measurements for each line are summarized in Table 1.

Our value for the magnetic moment ratio is in satisfactory agreement with the results of earlier determinations[5,6] and with the recent precise measurements of the magnetic moments by the method of paramagnetic resonance[7].

Our value of 0.8 ± 0.1 for Q_{155}/Q_{157} is in conflict with the results of Speck[4*] who obtained $Q_{155} > Q_{157}$. Hence it is of interest to compare our data with the results obtained by other methods. In measurements of the internal quadrupole moment Q_0 by the method of Coulomb excitation the ratio of the quadrupole moments of the two isotopes is not obtained directly. However, we calculated this ratio on the basis of the data of a number of authors[8-11] who measured the quadrupole moments of the odd isotopes of gadolinium. These data are summarized in Table 2. Apparently the most accurate procedure is that employed by Ramsak et al[10], who like ourselves, found that $Q_{155} < Q_{157}$, although their numerical value for the Q_{155}/Q_{157} ratio differs from ours by more than the estimated experimental error.

For calculation of the absolute values of the magnetic and quadrupole moments from the data of spectroscopic measurements one must evaluate the electron matrix elements $\langle H(0)\rangle_J$ and $\left\langle \frac{\partial^2 u}{\partial z^2}(0)\right\rangle_J$, which can be done only approxi-

---

*Speck used a less accurate method of recording the structure and the degree of enrichment of the samples was lower than in our investigation.

Table 1

Ratios of the magnetic and quadrupole moments of Gd^{155} and Gd^{157}

Ratio		λ=5015 A	λ = 5103 A	λ = 4743 A	Average value
$\frac{\mu_{155}}{\mu_{157}}$		0,80±0,02	0,77±0,01	0,79±0,02	0,78±0,03
$\frac{Q_{155}}{Q_{157}}$	1st method	0,76±0,04	0,82±0,02	0,88±0,05	0,8 ±0,1
	2nd method	0,76±0,03	0,82±0,05	0,86±0,07	0,8 ±0,1

Table 2

Values of the internal quadrupole moment Q_0 and the ratio $Q_{0_{155}}/Q_{0_{157}}$ obtained by the method of Coulomb excitation

$Q_{0_{155}}$	$Q_{0_{157}}$	$\frac{Q_{0_{155}}}{Q_{0_{157}}}$	Ref.	$Q_{0_{155}}$	$Q_{0_{157}}$	$\frac{Q_{0_{155}}}{Q_{0_{157}}}$	Ref.
6,8	6,2	1,1	[8]	6,7±2,4	8,8±1,8	0,76	[11]
7,6	8,1	0,94	[9]				
6,5	6,6	0,98	[10]	9,2±1,8		1,04	

mately. The error in evaluating $\langle H(0)\rangle_J$ is relatively small and for the magnetic moments we obtain $\mu_{157} = 0.34 \pm 0.04$ and $\mu_{155} = 0.26 \pm 0.03$ n.m.*, values which are in good agreement with the results of measurements by the method of paramagnetic resonance.[5,6] The accuracy in evaluating the quadrupole moments of the odd gadolinium isotopes is somewhat lower inasmuch as the uncertainty in calculating

$\left\langle \frac{\partial^2 u}{\partial z^2}(0) \right\rangle_J$ in this case is appreciable. As a result of averaging the results of different evaluations of the matrix element and our experimental results we obtained $Q_{155} = 1.45 \cdot 10^{-24}$ cm^2 and $Q_{157} = 1.8 \cdot 10^{-24}$ cm^2 (the corresponding values of Q_0 are $7 \cdot 10^{-24}$ cm^2 and $9 \cdot 10^{-24}$ cm^2), but precise evaluation of the uncertainty comprised in these values is difficult.

Using the formula[12]:

$$Q_0 = \frac{4}{5} Z R^2 \delta \left(1 + \frac{2}{3}\delta\right), \quad R = 1.2 \cdot 10^{-13} A^{1/3} \text{ cm} \qquad (4)$$

and the determined values for the internal quadrupole moments we calculated the deformation parameters and obtained $\delta_{155} = 0.27$ and $\delta_{157} = 0.33$. The ratio $\frac{\delta_{155}}{\delta_{157}} = 0.8 \pm 0.1$, naturally, directly follows from the above ratio for the quadrupole moments, which was obtained with good accuracy.

Using the extrapolated values of Nilsson's[12] wave functions for the ground state of the odd Gd isotopes (N = 5, I = 3/2 and $h_{9/2}$), we determined g_K, the gyromagnetic ratio for the internal motion of the unpaired nucleon. Using the value $\frac{\delta_{155}}{\delta_{157}} = 0.8$, we obtained $\frac{g_{K\,155}}{g_{K\,157}} = 0.9$, which is in good agrement with the experimental data[9,11].

We desire to thank V.S.Zolotarev for providing the separated isotopes and

---

*The absolute values of the magnetic moments given here are more accurate than those published earlier in Refs.1 & 2 because of additional investigation of the hyperfine structure of the 4743 Å $(y^{11}F_3 - a^{11}F_4)$ line.

L.K.Peker for discussion of the results.

Scientific Research Physical Institute,
Leningrad State University

References

1. N.I.Kaliteevskii, M.P.Chaika, I.Kh.Pacheva & E.E.Fradkin, Zhur.eksp.i teor.fiz., 37, 882 (1959). (Trans.Soviet Physics - JETP.)
2. N.I.Kaliteevskii, M.P.Chaika, I.Kh.Pacheva & E.E.Fradkin, Optika i spektroskopiya, 8, 13 (1960). (Trans.Optics & Spectroscopy.)
3. N.I.Kaliteevskii, G.M.Malyshev & M.P.Chaika, Ibid., 6, 820 (1959). (Trans.Ibid.)
4. D.R.Speck, Phys.Rev., 101, 1725 (1956).
5. A.A.Manenkov & A.M.Prokhorov, Zhur.eksp.i teor.fiz., 33, 1116 (1957). (Trans.Soviet Physics - JETP.)
6. W.Low, Phys.Rev., 103, 1309 (1956).
7. W.Low & D.Shaltiel, Phys.Rev., 115, 424 (1959).
8. N.P.Heydenburg & G.M.Temmer, Phys.Rev., 104, 981 (1956).
9. J.H.Bjerregard & U.Meyer-Berkhout, Z.Naturforsch., all, 273 (1956).
10. V.Ramsak, M.C.Olesen & B.Elbek, Nucl.Phys., 6, 541 (1958).
11. J.de Boer, M.Martin & P.Marmier, Helv.phys.acta, 32, 337 (1959).
12. S.G.Nilsson, Kgl.Danske Videnskab.Selskab, Mat.-fys.Medd., 29, 1 (1955).

THE (d,t) REACTION ON O^{16}, O^{18}, Mg^{24}, Mg^{25} AND Mg^{26}

- N.A.Vlasov, S.P.Kalinin, A.A.Ogloblin & V.I.Chuev

The present work was a continuation of our earlier investigations[1-3] of the (d,t) reaction, which is characterized by a high probability for excitation of hole neutron levels. Analysis of the angular distribution of the tritons on the basis of Butler's theory allows of determining with a fair degree of reliability the orbital angular momentum of the picked-up neutron and identifying the shell in which it was located. Hence investigation of the (d,t) reaction provides a means of determining to what extent single-particle states of the neutrons are retained in the inner filled shells of the nucleus, and if they are retained, makes it possible to determine the binding energy of the nucleus in these shells or the energy of intershell transitions. In pick-up of an outer neutron in the (d,t) reaction there may be evinced with high probability either rotational or vibrational levels of the residual nucleus, provided its collective motion makes a significant contribution to the ground state of the target nucleus.

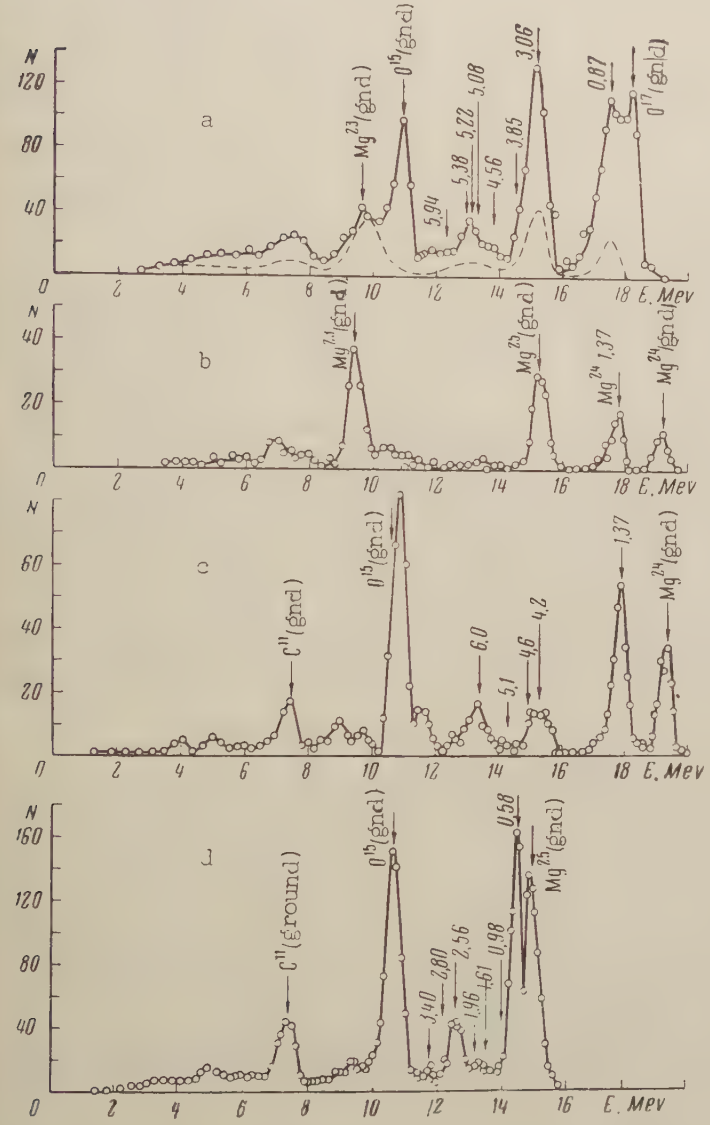

Fig.1. Triton spectra obtained with different targets: a) MgO^{18}, $\theta = 9^{o}$; b) natural Mg, $\theta = 13^{o}$; c) $Mg^{25}O$, $\theta = 11^{o}$; d) $Mg^{25}O$, $\theta = 7^{o}$.

The nuclei investigated in the present experiments have filled $1s$ and $1p$ shells and different numbers of neutrons in the outer shell. The configurations of the simplest nuclei in this region - O^{18} and F^{19} - were calculated by Elliott & Flowers[4] and Redlich[5]. The results of their calculations can be checked by comparison with the experimental data on the transition probabilities, in particular, in the O^{18}(d, t)O^{17} reaction. Magnesium isotopes are of interest in view of the indications of rotational structure and possible prolateness of the nuclei observed in this nuclear region.[6]

As in our earlier studies (Refs.1-3,7), the deuteron energy was about 20 Mev; the triton spectra were measured by observing the β-activity of the resultant tritium.

By way of targets we used MgO^{18} (60% O^{18}), $Mg^{25}O$ (86% Mg^{25}), $Mg^{26}O$ (90.5% Mg^{26}) and natural magnesium in the form of foil. The magnesium targets 2-3 mg/cm^2 thick were prepared by depositing the oxide from a suspension onto 0.4 mg/cm^2 magnesium supports.

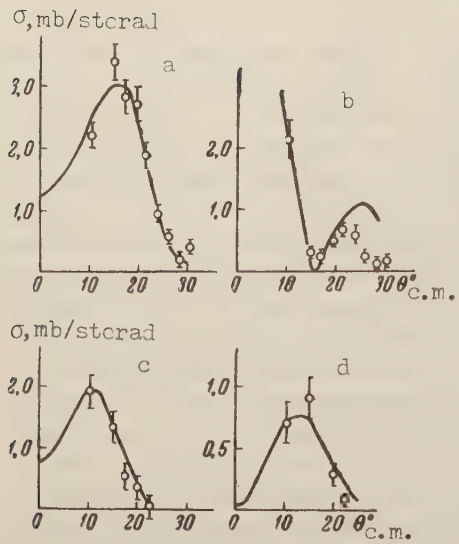

Fig.2. Angular distributions of proton groups from the $O^{18}(d,t)O^{17}$ reaction: a) ground state of O^{17}, $l = 2$, $r_0 = 6.5$; b) 0.87 Mev state, $l = 0$, $r_0 = 6.5$; c) 3.06 Mev state, $l = 1$, $r_0 = 7.0$; d) 5.38 Mev state, $l = 1$, $r_0 = 6.5$.

Typical triton spectra for each of the targets are shown in Fig.1. In addition to tritons from the (d,t) reaction on O^{18} and the magnesium isotopes, there was observed a strong triton group from the (d,t) reaction on O^{16} at $E_t = 10.5$ Mev. The $Mg^{25}O$ and $Mg^{26}O$ targets contained a minor admixture of carbon, as a result of which at $E_t \approx 7$ Mev there was observed a group of tritons from the $C^{12}(d,t)C^{11}$ reaction. The angular distribution of this group is in agreement with our earlier data[2]. The absolute cross sections were determined with an error of 20% for Mg^{24} and Mg^{26} and 25% for O^{18} and Mg^{25}.

In the case of the $O^{18}(d,t)O^{17}$ reaction there are observed four triton groups corresponding to the ground state and three excited states of O^{17} with energies 0.87, 3.06 and 5.3 Mev. The angular distributions of all four groups are shown in Fig.2. These distributions are consistent with angular momenta equal to 2, 0, 1 and 1, respectively. Fit to the Butler curve for other values of l can be obtained only by using highly unlikely values of the radius r_0.

The last neutron configurations corresponding to the low-lying states of the residual O^{17} nucleus with even parity (the ground state and the 0.87 and 5.08 Mev states) are $d_{5/2}$, $s_{1/2}$ and $d_{3/2}$, respectively. The probability for the formation of these states in the $O^{18}(d,t)O^{17}$ reaction characterizes the contribution of these configurations to the ground state of O^{18}. It will be evident from Figs.1 & 2 that there occur abundant transitions to the ground state ($l = 2$) and the first excited level ($l = 0$). The 5.08 Mev level is virtually not excited. It follows from this that there is strong mixing of the $(d_{5/2})^2$ and $(s_{1/2})^2$ configurations in the O^{18} nucleus, and that the admixture of $(d_{3/2})^2$ is small. Comparing the reduced width found for these three levels of O^{17} one can evaluate the probability ratios for the $(d_{5/2})^2$, $(s_{1/2})^2$ and $(d_{3/2})^2$ configurations in the ground state of O^{18}:

$$(d_{5/2})^2/(s_{1/2})^2 = 3.9 \pm 1.0 \text{ and } (d_{5/2})^2/(d_{3/2})^2 > 10.$$

According to the calculations of Elliott & Flowers[4], these ratios are

$$(d_{5/2})^2/(s_{1/2})^2 = 5.3 \text{ and } (d_{5/2})^2/(d_{3/2})^2 = 13.$$

Analogous results indicating strong mixing of the $d_{5/2}$ and $s_{1/2}$ states were obtained by us earlier[2] for F^{19}, with the difference that in the $F^{19}(d,t)F^{18}$ reaction the ground state of F^{18} was excited as a result of pick-up of an s rather than the d neutron, as in the case of the $O^{18}(d,t)O^{17}$ reaction. This means that the least strongly bound neutron in O^{18} is the d neutron, whereas in F^{19} it is the s neutron.

Excitation of the 3.06 and 5.3 Mev levels occurs by pick-up of a p neutron. Ajzenberg-Selove & Lauritsen[8] tentatively ascribed spin and parity $1/2^-$ to the 3.058 Mev level. Our results substantiate this if one assumes that the 3.06 Mev

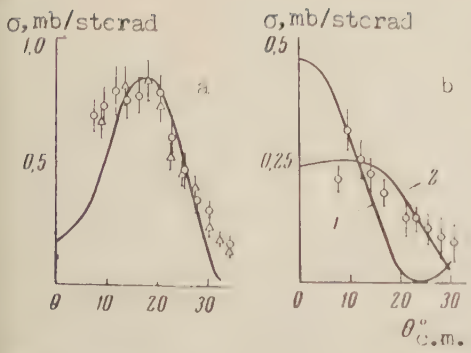

Fig.3. Angular distributions of triton groups from the $Mg^{24}(d,t)Mg^{23}$ reaction: a) ground state of Mg^{23}, $l = 2$, $r_0 = 7.0$; b) state with $E^* \approx 2.5$ Mev; 1 - $l = 1$, $r_0 = 7.0$, 2 - $l = 2$, $r_0 = 7.0$.

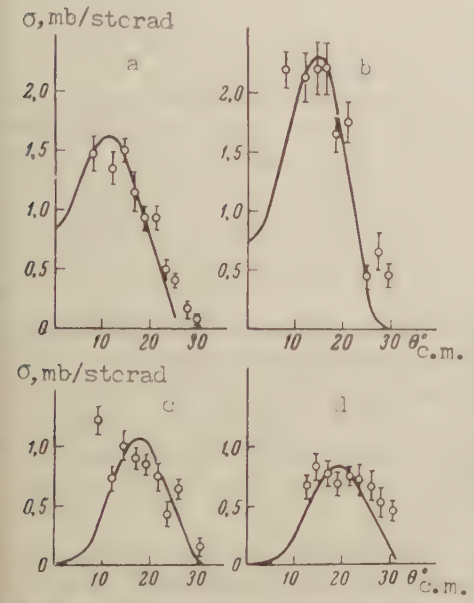

Fig.4. Angular distribution of triton groups from the $Mg^{25}(d,t)Mg^{24}$ reaction: a) ground state of Mg^{24}, b) 1.4 Mev state, c) 4.1 Mev state, d) 6.0 Mev state. In all cases $l = 2$, $r_0 = 7.0$.

level is a hole level and corresponds to pick-up of a neutron in the $p_{1/2}$ state. Two levels at ~5.3 Mev are known in O^{17}: 5.22 and 5.38 Mev. The resolution in our experiments was not sufficient to distinguish them, but it is highly probable that the observed transition corresponds to excitation of the 5.38 Mev state (3/2) and is a result of pick-up of a neutron in the $p_{3/2}$ state from the O^{18} nucleus. The fact that these levels at 3.06 and 5.38 Mev are hole levels is substantiated by the fact that excitation of these states was not observed[9] in the $O^{16}(d,t)O^{17}$ reaction. At the same time the 3.85 and 4.56 Mev levels excited in the (d,p) reaction are not evinced in the (d,t) reaction.

Thus we can determine the values of the neutron binding energy in O^{18} and F^{19}, pertaining to different states; the calculated values are listed in Table 1.

Table 1

Neutron binding energies in O^{18} and F^{19} (in Mev)

Nucleus	$d_{5/2}$	$s_{1/2}$	$p_{1/2}$	$p_{3/2}$
O^{18}	8.07	8.94	11.1	13.3
F^{19}	11.5	10.4	13.7	----

In the $Mg^{24}(d,t)Mg^{23}$ reaction there are excited with the highest probability the ground state of Mg^{23} (possibly with some admixture of the state at 0.45 Mev) and a group of states with an energy of about 2.5 Mev. The angular distribution of the first group is shown in Fig.3 and is in good agreement with $l = 2$. The spin of the ground state has never been directly determined hitherto; on the basis of the above data we infer $I = 3/2^+$ or $5/2^+$. In the angular distribution of the second group there may be present different components, including components corresponding to $l = 2$ and $l = 1$. It is noteworthy that there are no intense transitions with $l = 0$, which indicates appreciably less hybridizing of the s and d shells in Mg^{24} as compared with O^{18} and F^{19}.

In the $Mg^{25}(d,t)Mg^{24}$ reaction there are observed triton groups corresponding to formation of Mg^{24} in the ground state and in excited states with energies of 1.37, 4.12 + 4.23 (unresolved), 6.0 and 7.8 Mev. The angular distributions of the first four groups (the last group is difficult to observe owing to its proximity to an oxygen group) are shown in Fig.4. They all correspond to pick-up of a neutron with the same angular momentum: $l = 2$. In contrast to the case of (d,t) reactions on other light nuclei investigated by us[1,2] and other authors[10,11], in the $Mg^{25}(d,t)Mg^{24}$ reaction the probability for formation of the residual nucleus in the ground state is no greater than the probability for formation of excited

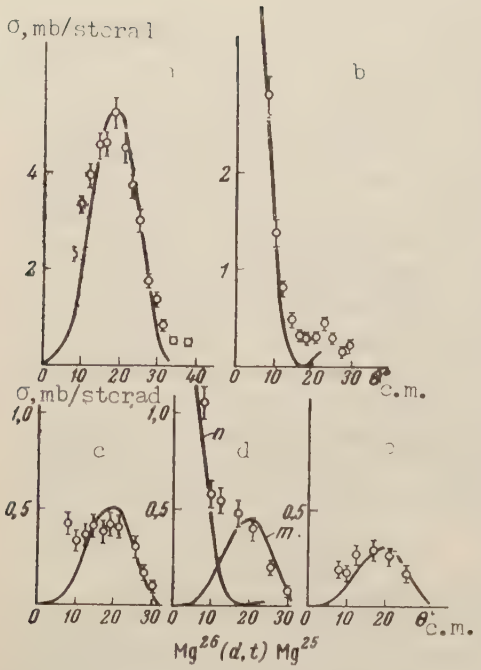

Fig.5. Angular distributions of triton groups from the Mg^{26}(d, t)Mg^{25} reaction: a) ground state of Mg^{25}, $l = 2$, $r_0 = 6.5$, b) 0.5 Mev state, $l = 0$, $r_0 = 7.0$; c) 1.61 + 1.96 Mev state, $l = 2$, $r_0 = 7.0$; d) 2.56 + 2.80 Mev state, $l = 0(n) + 2(m)$, $r_0 = 7.0$; e) 3.40 Mev state, $l = 2$, $r_0 = 7.0$.

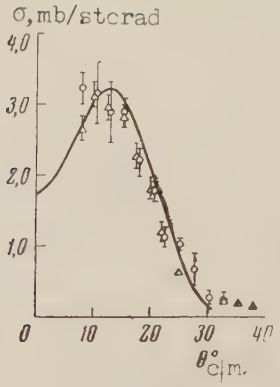

Fig.6. Angular distribution of proton group from the $O^{16}(d,t)O^{15}_{gs}$ reaction, $l = 1$, $r_0 = 5.5$.

Table 2

Comparison of relative widths of the rotational states in Mg^{24}

Method of determination	Ground state	1.4 Mev	4.1 Mev*
Theory	1	1.79	0.23
Experiment	1	1.7±0.2	1.0±0.2

states with energies up to 6 Mev. The most intense transition is observed to the level at 1.37 Mev. This result is difficult to explain from the standpoint of the shell model, according to which the reduced width of the ground state of the residual nucleus should be appreciably greater than the width of the other levels with the same configuration.

At the same time the observed distribution of reduced widths is consistent with the assumption that the evinced states of Mg^{24} are rotational states. V.M. Strutinskii (private communication) calculated the relative widths for rotational states; his theoretical data are compared with the experimental values in Table 2.

In investigating the Mg^{26}(d,t)Mg^{25} reaction we detected five triton groups, corresponding to known levels of Mg^{25}. The angular distributions are shown in Fig.5. The most intense is the proton group corresponding to formation of the ground state of Mg^{25} and characterized by $l = 2$. The probability for formation of the first excited state equals approximately 10% the probability for the ground state.

The results obtained in studying the Mg^{26}(d,t)Mg^{25} reaction can be explained on the basis of the shell model if it is assumed that in Mg^{25} the picked-up neutron is in the d state with a small admixture of s state. We obtained similar results earlier[2] for the neighboring nucleus, Al^{27}.

In addition to the above described reactions, we measured the differential cross section for the O^{16}(d,t)O^{15} reaction (Fig.6), inasmuch as oxygen entered

---

*The experimental width for this level pertains to two unresolved states, while the theoretical width was calculated only for one of them.

Table 3

Residual nucleus	States, Mev	σ_{max}, mb/sterad $\theta_{c.m.}$	l	r_0, 10^{-13} cm	θ^2, %
O^{15}	Grnd.	3,2 (10°)	1	5,5	1,4
	5,2	0,15	—	—	—
O^{17}	Grnd.	3,4 (15°)	2	6,5	1,75
	0,87	2,0 (10°)	0	6,5	1,3
	3,06	1,9 (10°)	1	7,0	0,55
	5,08	<0,3 (15°)	—	—	<0,15 l=2
	5,2	0,7 (10°)	1	6,5	0,3
Mg^{23}	Grnd.	0,85 (18,5°)	2	7,0	0,81
	2,5	0,25 (12°)	2 (1)	7,0	0,3 (l=2)
Mg^{24}	Grnd.	1,47 (8°)	2	7,0	0,74
	1,37	2,20 (14,5°)	2	7,0	1,27
	4,1+4,2	0,9 (17°)	2	7,0	0,71
	6,0	0,8 (14,5°)	2	7,0	0,51
	7,8	0,5 (17°)	—	—	—
Mg^{25}	Grnd.	5,0 (17,5°)	2	6,5	3,30
	0,58	1,38 (10°)	0	7,0	0,29
	0,98	0,12	(2)	(7)	0,09
	1,96 (1,61)	0,4 (18°)	2	7,0	0,34
	2,56	0,45 (10°)	0	7,0	0,09
	2,80	0,3 (20°)	2	7,0	0,30
	3,40	0,3 (20°)	2	7,0	0,22

into the composition of most of our targets. As might have been expected, the angular momentum transferred by the picked-up neutron in this case is $l = 1$. There is also observed a first excited state of O^{15} at 5.2 Mev, but the cross section for its formation is only 1/20 that for the ground state.

The principal results of the present investigation are summarized in Table 3.

We are grateful to the staff of the Cyclotron Laboratory for performing the irradiations, to V.S.Zolotarev and his colleagues for preparing the enriched Mg^{25} and Mg^{26} targets, and to V.M.Strutinskii and A.I.Bazyu for discussion of the results.

"I.V.Kurchatov" Institute of Atomic Energy

References

1. N.A.Vlasov & A.A.Ogloblin, Zhur.eksp.i teor.fiz., 37, 54 (1959). (Trans. Soviet Physics - JETP.)

2. N.A.Vlasov, S.P.Kalinin, A.A.Ogloblin & V.I.Chuev, Ibid., 37, 1187 (1959). (Trans.Ibid.)

3. N.A.Vlasoc, S.P.Kalinin, A.A.Ogloblin & V.I.Chuev, Ibid., 38, 280 (1960). (Trans.Ibid.)

4. J.P.Elliott & B.H.Flowers, Proc.Roy.Soc., A229, 536 (1955).

5. M.G.Redlich, Phys.Rev., 99, 1421 (1955).

6. A.E.Litherland, H.McManus, E.B.Paul, D.A.Bromley & H.E.Gove, Canad.J. Phys., 36, 378 (1958).

7. N.A.Vlasov & A.A.Ogloblin, Trudey konferentsii po yadrenym reaktsiyam pri malykh i srednikh energiyakh (Transactions of the conference on nuclear reactions at low and medium energies), M., 1958.

8. F.Ajzenberg-Selove & T.Lauritsen, Nucl.Phys., 10, 1 (1959).

9. T.S.Green & R.Middleton, Proc.Phys.Soc., A69, 28 (1959).

10. W.E.Moore, J.N.McGruer & A.I.Hamburger, Phys.Rev.Letters, 1, 29 (1958).

11. W.F.Vogelsang & J.N.McGruer, Phys.Rev., 109, 1663 (1958).

THE (n,α) REACTION IN Pu^{239} INDUCED BY THERMAL NEUTRONS

- V.N.Andreev

Hitherto the (n,α) reaction, accompanying thermal neutron capture, has been observed only for comparatively light elements[1,2] because the cross section for this reaction diminishes with increase of Z, owing to the decrease in penetrability of the Coulomb barrier. Evaluations show, however, that the barrier penetrability increases markedly for heavy nuclei, owing to the increase in the (n,α) reaction energy resulting from α-instability.

For long-lived nuclei that are heavier than lead the probability of alpha emission from an excited state is on the average 10^{-5} to 10^{-6} of the probability of gamma emission. However, in individual cases, for example, $Po^{210}(n,\alpha)Pb^{207}$, the probabilities of α and γ emission may be of the same order of magnitude.

This paper presents the results of an investigation of the thermal neutron induced $Pu^{239}(n,\alpha)U^{236}$ reaction. A diagram of the experimental set-up is shown in Fig.1. Pu^{239} was deposited in a 1 mg/cm^2 thick layer on an aluminum foil and was bombarded with a collimated neutron beam from the thermal column of the Academy of Sciences heavy water reactor. The α-particles resulting from thermal neutron capture were range analyzed. The ranges were determined with a T-25 BFL end-window proportional counter and an arrangement of aluminum absorbers equivalent to a range of 1.5 cm in air. The counter recorded only fully ionized α-particles stopped in the end of the sensitive volume. The α-particles were initially slowed by the aluminum absorbers. Precise measurements of the ranges were obtained by moving the counter and absorbers relative to the plutonium sample over a ~2 cm distance.

Fig.2 shows calibration curves obtained using a thin Po^{210} α-source. The different curves correspond to different thresholds of the pulse height discriminator. This figure shows that the resolution of the range measuring apparatus attained ~3 mm of air equivalent.

Background counts due to fission neutrons from Pu^{239} were the chief source of interference. Allen & Dewan[3] report that an average of one out of 450 fission events results in the emission of long range α-particle with a continuous spectrum extending to ~25 Mev. These α-particles were recorded by the counter and gave rise to a background which changes slowly with α-particle energy. Fast neutrons from Pu^{239} fission induced (n,α) reactions in the counter produced an additional background. To measure this portion of the background a 0.3 mm aluminum absorber, which stopped all α-particles but freely passed neutrons, was placed between the counter and the sample.

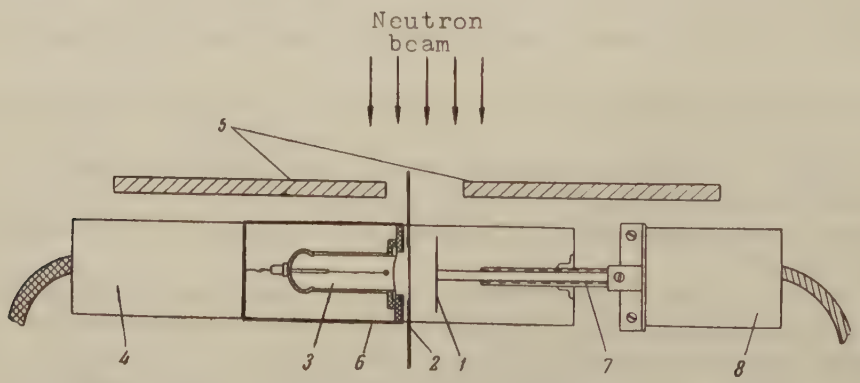

Fig.1. Experimental set-up: 1) plutonium sample, 2) disc with aluminum absorbers, 3) proportional counter, 4) preamplifier, 5) B_4C shields, 6) Cd shield, 7) feed screw, 8) drive selsyn.

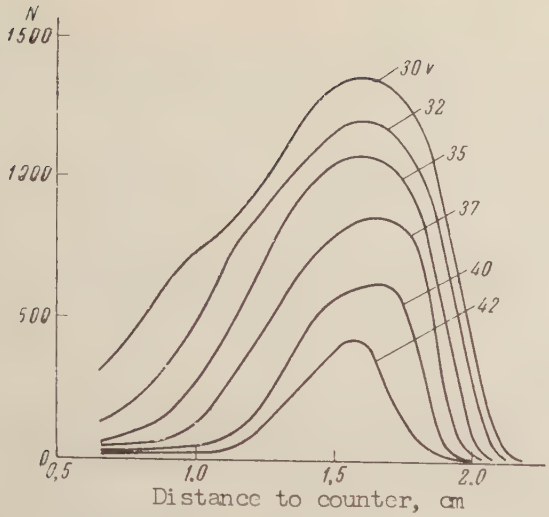

Fig. 2

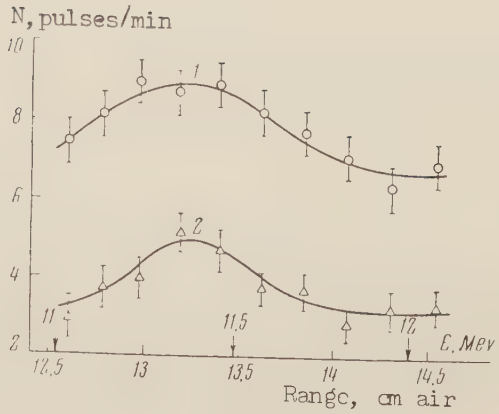

Fig. 3

Fig.2. Calibration curves obtained with a Po^{210} α-source. The figures at the curves indicate the discriminator thresholds (V_{bias}).

Fig.3. Spectrum of α-particles from Pu^{240*}. Curve 2 was obtained with higher resolution.

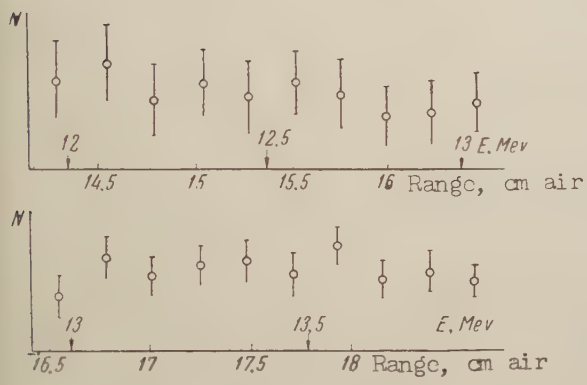

Fig.4. High-energy portion of the spectrum of α-particles from Pu^{240*}. N = 0 lies below the horizontal axis, which is drawn at the 0.4 level of the mean value for the spectrum.

The fast neutron background amounted to ~20% of the counts due to long range α-particles. Control experiments in which the beam was shuttered with cadmium showed that the interference due to radiation from the reactor was negligible.

The expected energy of the α-particles emitted in the decay of Pu^{240*} to the ground state of U^{236} is 11.46 Mev. Therefore, the α-spectrum was measured chiefly in this energy region. The results of measurements with two different resolutions are shown in Fig.3. There is a noticeable peak corresponding to $E_\alpha = 11.4 \pm 0.1$ Mev (range of 13.3 cm in air). This energy agrees well with the expected value for Pu^{240*}. For comparison in Fig.4 we show the high-energy α-spectrum. No deviations from the continuous spectrum were observed here. In the energy region below 11 Mev the α-spectrum is not monotonic; however, the different groups could not be clearly resolved. The spectrum of long range α-particles[1,3] and the cross section for production of α-particles by fission of Pu^{239} indicate that the cross section for the (n,α) reaction with emission of 11.4 Mev α-particles is ~20 mb. This result corresponds to $\Gamma_\alpha \approx 2 \cdot 10^{-6}$ ev (according to Ref.1, $\Gamma_\gamma \approx 4 \cdot 10^{-2}$ ev).

It is interesting to compare the above results with the predictions from the quasiclassical theory of α-decay. Inasmuch as the daughter nucleus U^{236} is in the ground state or a rotational state while the 11.4 Mev α-particle is passing through the Coulomb barrier, the potential barrier must have the same shape as the barrier penetrated by the α-particle in ordinary decay of Pu^{240}.

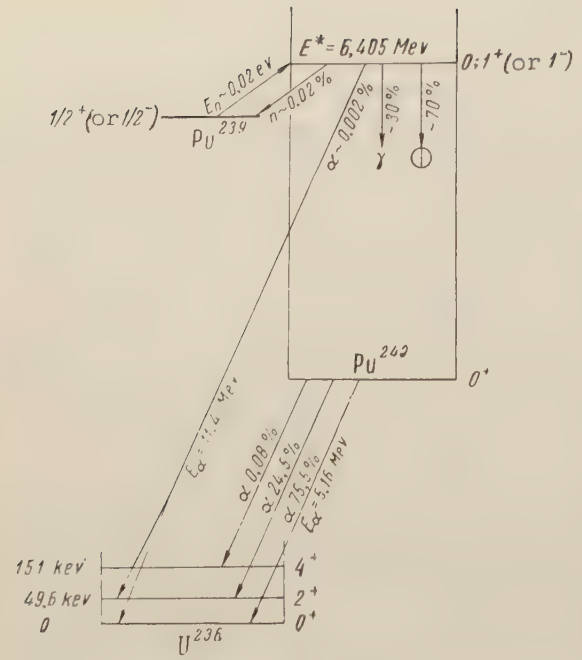

Fig.5. Diagram of α-transitions from Pu^{240} and Pu^{240*}.

Calculation for a barrier with R = $= 9.3 \cdot 10^{-13}$ cm (Perlman and Rasmussen[4]) gives the penetrability ratio:

$$(P^*/P)_{theo} = 3.3 \cdot 10^{20}.$$

The experimental ratio of the decay constants of Pu^{240*} and Pu^{240} is

$$(\lambda^*/\lambda)_{exp} = 10^{21}.$$

Fig.5 gives the level diagram for U^{236} showing the E_α = 11.4 Mev transition. On the basis of the selection rules applicable to s-neutron capture by Pu^{239} and α-decay of Pu^{240*} it may be asserted that a 0^+ or 1^+ state is formed when Pu^{239} captures a thermal neutron, if Pu^{239} has even parity[5,6], while if the parity is odd a 1^- state is formed. We note that transitions from a 1^+ state to the ground state of U^{236} are forbidden. If the state with 1^+ is formed, the E_α = = 11.4 Mev transition may feed the 49.6 kev level.

I desire to thank V.V.Vladimirskii for his interest in the work.

References

1. D.J.Hughes & R.B.Schwartz, Neutron Cross Sections, BNL-325. 1958.
2. E.Münnich, Z.Phys., 153, 106 (1958).
3. K.W.Allen & J.T.Dewan, Phys.Rev., 80, 181 (1950).
4. I.Perlman & J.O.Rasmussen, Alpha Radioactivity (Cited in Russian trans., M., 1959).
5. E.F.Tret'yakov, G.I.Grishuk & L.L.Gol'din, Zhur.eksp.i teor.fiz., 34, 811 (1958). (Trans.Soviet Physics - JETP.)
6. J.M.Hollander, J.O.Rasmussen, R.G.Albridge & W.G.Smith, Second Geneva Conference on the Peaceful Uses of Atomic Energy, Report No.650, 1958.

MASSES OF HEAVY ATOMS AND NUCLEAR BINDING ENERGIES IN THE 174 TO 239 A REGION

- R.A.Demirkhanov, T.I.Gutkin & V.V.Dorokhov

Isotopic masses and nucleon binding energies are important characteristics of nuclei. Mass data are useful in explaining many of the properties of nuclei. On the basis of the nucleon binding energies one can judge of the presence of proton and neutron shells in the nucleus, fine structure of the binding energy, regularities in the variation of nuclear shape, etc.

The scope of problems that can be solved with the aid of isotopic mass data is determined to some extent by the accuracy of the said data. For example, in order to detect with an accuracy of ~20% the discontinuity in binding energy, equal to ~3 Mev, in going from a filled shell to an unfilled one[1] (for instance, in the case of Pb^{208} and Bi^{209}), the masses of the respective isotopes must be measured with a relative accuracy $\Delta M/M \approx 3 \cdot 10^{-6}$. To establish the presence of fine structure in the binding energy curve for nuclei in the $A \approx 200$ region a measurement accuracy at least one order of magnitude higher is necessary.

Most of the data[2-5] available at present on isotopic masses and nuclear binding energies in this mass region have been obtained with an error of one part in $(1\text{-}1.5) \cdot 10^5$. In the present report we give the results of mass spectrographic measurements of nuclei in the 174 to 239 A range, which have been obtained for a large number of isotopes with a relative error of one in $(1\text{-}5) \cdot 10^7$.

For these measurements we used a double-focusing mass spectrograph with a resolution of 50 000-80 000. The measurements were carried out by the method of doublets. For obtaining the doublet pairs by way of standard masses we used organic compounds of the C_nH_m, $C_nN_mH_k$ and $C_nO_mN_kH_p$ types. The method of doublets has the advantage that it eliminates a number of steps in comparing the mass of the unknown isotope with the mass of O^{16}, thereby minimizing cumulative errors. Moreover, this method allows of direct comparison of the mass of the measured isotope with the mass of the corresponding secondary standard. Thus in using this method the accuracy in determining the mass of a heavy-element isotope depends primarily on the accuracy of measuring the masses of the isotopes of which the given organic compound is formed, i.e., of the masses of H, C, C^{13} and N. Measurements of the masses of the light atoms were carried out with great care under conditions excluding all possible systematic errors. The principal criterion for the absence of systematic errors was "internal consistence", i.e., good agreement between the values (within the limits of the experimental error) obtained for the mass of the given isotope by means of doublets in different compounds and combinations. Data on the doublets employed and the masses of the secondary standard isotopes are listed in Refs.6 & 7.

The masses of most of the isotopes in the 174 to 239 A region have not been measured mass-spectrographically hitherto. There are available at present the mass values for some isotopes determined mass spectrographically using multiply charged ions.[2-5] Some mass values have been determined by computation using nuclear reaction Q values and the mass values obtained for the initial nuclides by mass spectrographic measurements[8,9]. Obviously, these values were obtained with a relatively large uncertainty: 1500-3000 μMU.

Utilization of the developed procedure and the possibility of calculating the dispersion coefficient with great accuracy enabled us in the present measurements to enhance the accuracy of determination by a factor of 10-50.

In many cases the mass of a given isotope was determined from different doublets, thus providing an "internal consistence" check. The final values were calculated taking into account the relative "weight" of the measurements, inversely proportional to the estimated error. Specifically, we measured the masses of the isotopes of plutonium, uranium, thorium, bismuth, lead, thallium, mercury, gold,

Table 1

Masses of Re, W, Ta and Hf Isotopes

No.	Isotope	Doublet	ΔM, mMU	Isotope mass, MU	Mean mass, MU	Mass from data of Wapstra[3] (Quotient reactions)	Mass according to data of Duckworth et al.[4,5]
1	Hf^{174}	$C_{14}H_6 - Hf^{174}$	106,550 ± 0,105	173,995752 ± 110	173,995792 ± 110		
2	Hf^{176}	$C_{14}H_8 - Hf^{176}$	124,710 ± 0,094	175,996906 ± 100	175,996906 ± 100	175,996300 ± 2000	175,997700 ± 700 [4] 175,996300 ± 1100[5]
3	Hf^{177}	$Hf^{178} - Hf^{177}$ $Hf^{177} - Hf^{176}$	1000,613 ± 0,044 1002,328 ± 0,098	176,999613 ± 82 176,999234 ± 140	176,999516 ± 140		
4	Hf^{178}	$C_{14}H_{10} - Hf^{178}$	134,674 ± 0,050	178,000226 ± 70	178,000226 ± 70	177,999700 ± 2000	177,999800 ± 900 [4] 177,999300 ± 1300[5]
5	Hf^{179}	$C_{14}H_{11} - Hf^{179}$ $Hf^{180} - Hf^{179}$ $Hf^{179} - Hf^{178}$	130,975 ± 0,070 1001,419 ± 0,076 1002,571 ± 0,060	179,000307 ± 75 179,002924 ± 93 179,002797 ± 92	179,002768 ± 50		
6	Hf^{180}	$C_{14}H_{12} - Hf^{180}$	147,154 ± 0,069	180,004040 ± 75	180,004050 ± 75	179,999000 ± 2000	180,003400 ± 800 [4] 180,002000 ± 700 [5]
7	Ta^{181}	$C_{13}H_9O - Ta^{181}$ $C_{12}H_{11}N - Ta^{181}$	117,029 ± 0,040 141,060 ± 0,077	181,005000 ± 45 181,005080 ± 80	181,005054 ± 90	181,002000 ± 2000	181,003400 ± 1300[5]
8	W^{180}	$C_{13}H_8O - W^{180}$	111,093 ± 0,130	180,003693 ± 140	180,003698 ± 140	180,001450 ± 2000	
9	W^{182}	$C_{13}H_{10}O - W^{182}$ $C_{12}H_{12}N_2 - W^{182}$	124,915 ± 0,250 136,228 ± 0,077	182,000165 ± 250 182,000080 ± 80	182,000093 ± 75	182,003540 ± 2000	182,004100 ± 700 [4] 182,003300 ± 1400[5]
10	W^{183}	$C_{13}H_{11}N_2 - W^{183}$	142,021 ± 0,067	183,008429 ± 70	183,008429 ± 70	183,005300 ± 2000	183,006600 ± 700 [4] 183,005900 ± 1300[5]
11	W^{184}	$C_{13}H_{12}N_2 - W^{184}$	149,364 ± 0,102	184,009234 ± 110	184,009234 ± 110	184,006300 ± 2000	184,007400 ± 700 [4] 184,005200 ± 1100[5]
12	W^{186}	$C_{26}H_8 - W^{186}$	92,364 ± 0,068	186,013788 ± 80	186,013788 ± 80	186,010400 ± 2000	—
13	Re^{185}	$C_{15}H_5 - Re^{185}$	85,889 ± 0,094	185,012124 ± 100	185,012124 ± 100	—	
14	Re^{187}	$C_{15}H_7 - Re^{187}$	98,899 ± 0,030	187,015395 ± 50	187,015395 ± 50	187,011062 ± 2200	

platinum, iridium, osmium, rhenium, tungsten, tantalum and hafnium. The results obtained for the stable isotopes from Pu^{239} to Os^{186} have been published earlier (Refs.1,10-12). The values obtained for the isotopes of Re, W, Ta and Hf are listed in Table 1. For comparison we also give the mass values obtained by Duckworth et al[4,5] by the mass spectroscopic method and values calculated[8] using nuclear reaction Q values. The masses of Re^{185}, Hf^{179}, Hf^{177} and Hf^{174} were determined for the first time in the present study.

Analysis of the mass values shows that for most of the isotopes our values are higher by 1-1.5 mMU than the values of Wapstra[8] and Huizenga[9]. This can be explained by the incorrect value of the standard - the mass of Pb^{208} - used in the work of these authors.[13]

In Ref.10 we showed that the appreciable divergences between the mass values for Th^{232} and U^{238} obtained by mass spectrographic and nuclear measurements are due to the error in the early mass spectrographic measurements[14]. The mass values obtained for the isotopes of lead and mercury in subsequent measurements by the Minnesota University group[15] and Kerr & Duckworth[16] agree with the values found in our work.[1]

Table 2

Mass differences between Hf and W isotopes (in MU)

Isotope	Our data	Data of Johnson & Bhanot[17]*	Data deduced from nuclear reactions** [Ref.]
$Hf^{177}-Hf^{176}$	1,002610	1,002250	1,001815[18]
$Hf^{178}-Hf^{177}$	1,000710	1,000880	
$Hf^{179}-Hf^{178}$	1,002722	1,002360	1,002005[18]
$Hf^{180}-Hf^{179}$	1,001092	1,001130	
$W^{183}-W^{182}$	1,002336	1,002230	1,002305[19] 1,002365[20]
$W^{184}-W^{183}$	1,000805	1,000990	1,001035[20]

*Estimated error $\leqslant$ 0.0003 MU. **Error $\leqslant$ 0.0001 MU.

Of particular interest is comparison of our data with the values obtained by other methods. Unfortunately, there is a scarcity of mass data in the given A range; nevertheless some comparisons can be made. In Table 2 we list the mass differences measured in the work of Johnson & Bhanot[17] and the differences calculated on the basis of our data and using nuclear reaction Q values. It will be seen that the mass difference values for tungsten obtained by all three methods agree well. This cannot, however, be said regarding the Hf^{177} - Hf^{176} and Hf^{176} - Hf^{178} mass differences. The results of our work are in agreement with the data of Johnson & Bhanot within the limits of the experimental error, but differ from the data calculated using nuclear reaction Q values by about twice the measurement error. It will be noted that the data of Johnson & Bhanot for these mass differences differ from the nuclear reaction values less than do our data, but nevertheless the disagreements exceed the measurement error. In view of the above, it may be assumed that the Q values for the $Hf^{177}(\gamma,n)Hf^{176}$ and $Hf^{178}(\gamma,n)Hf^{178}$ reactions are erroneous or, in any case, that the estimated error involved in determining the Q values of these reactions must be increased by a factor of 2-3.

On the basis of the data obtained in the present work on the masses of 42 stable isotopes we plotted the variation of the binding energy per nucleon as a function of A in the 174 to 210 A region (see figure).

In addition to measuring the masses of the stable isotopes, we calculated the masses and binding energies of 66 radioactive nuclei. As the reference values

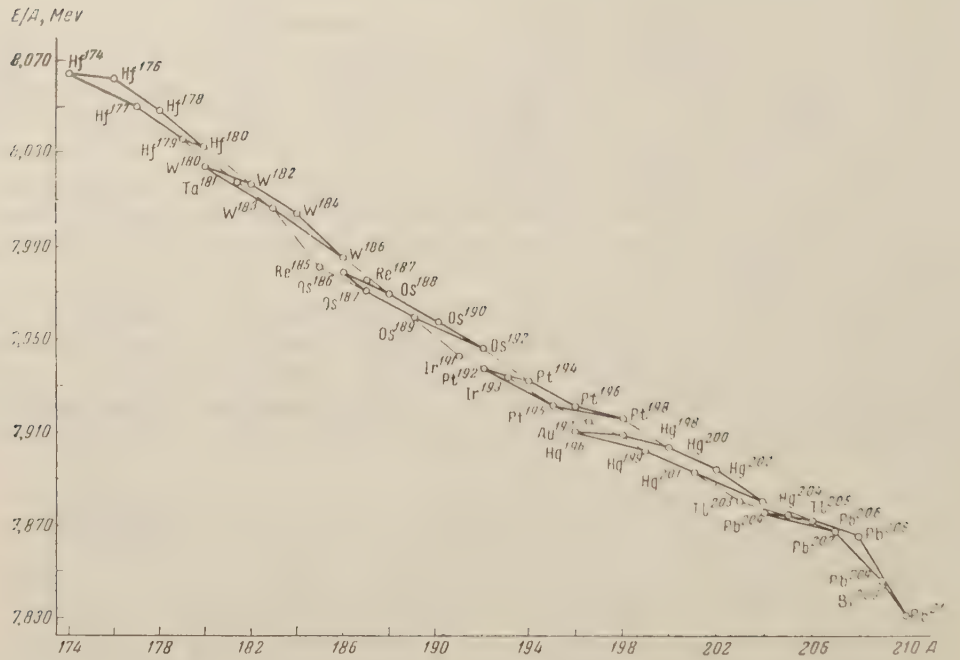

Binding energy per nucleon in the 174 to 210 A region.

Table 3

Neutron and proton binding and pairing energies in the isotopes of Hf, Ta, W and Re

No.	Isotope	Z	N	Nuclear binding energy E, Mev	Binding energy per nucleon E/A, Mev	B_n, Mev	B_p, Mev	P_n, Mev	P_p, Mev
1	Hf^{174}	72	102	1403,138	8,0640				
2	Hf^{176}		104	1418,834	8,0616				
3	Hf^{177}		105	1424,770	8,0495	5,936			
4	Hf^{178}		106	1432,475	8,0476	7,705		1,769	
5	Hf^{179}		107	1438,306	8,0352	5,831			
6	Hf^{180}		108	1445,650	8,0314	7,344		1,513	
7	Hf^{181}		109	1451,318	8,0183	5,668			
8	Ta^{180}	73	107	1444,175	8,0232		5,869		
9	Ta^{181}		108	1451,548	8,0196	7,373	5,898		
10	Ta^{182}		109	1457,712	8,0094	6,164	6,394		
11	Ta^{183}		110	1464,812	8,0044	7,100		0,936	
12	W^{180}	74	106	1444,404	8,0245				
13	W^{181}		107	1450,604	8,0144	6,200	6,429		0,550
14	W^{182}		108	1458,907	8,0160	8,303	7,359	2,103	1,461
15	W^{183}		109	1465,098	8,0060	6,191	7,386		0,992
16	W^{184}		110	1472,715	8,0039	7,617	7,903	1,426	
17	W^{185}		111	1477,968	7,9890	5,253			
18	W^{186}		112	1485,207	7,9850	7,239		1,986	
19	W^{187}		113	1490,774	7,9720	5,567			
20	Re^{185}	75	110	1477,608	7,9871	6,674	4,893		
21	Re^{186}		111	1483,945	7,9782	6,337	5,977		
22	Re^{187}		112	1491,292	7,9748	7,347	6,085	1,010	
23	Re^{188}		113	1497,215	7,9639	5,928	6,441		

Note: the estimated errors in the listed values are the following: 1) in the binding energies ~0.2 Mev, 2) in the values of E/A ~1 kev, 3) in B_n and B_p ~0.3 Mev, 4) in P_n and P_p ~0.4 Mev.

we used the masses of the stable isotopes as measured in the present work. These data were used for calculating the binding energy of the last neutron B_n, the binding energy of the last proton B_p, and the neutron and proton pairing energies P_n and P_p. The values of these parameters for rhenium, tungsten, tantalum and hafnium are listed in Table 3.

Analysis of the measurement results in the entire investigated mass range, i.e., from Bi to Hf, enabled us to draw certain inferences regarding the energy systematics obtaining in this range of nuclei.

The character of the binding energy per nucleon vs A curve (see figure) substantiates the presence of shell structure in nuclei with filling of the shell at Z = 82 and N & 126. The plot shows clear differences between the nucleon binding energies in nuclei with even- and odd-A.[21] The binding energy per nucleon in odd-A nucli is always lower than in even-A nuclei for the same Z (the E/A curve for odd-A nuclei nowhere intersects the curve for even-A nuclei).

The effect of shell structure can also be observed by following the variation of the attachment energies for the (Z + 1)-th proton and the (N + 1)-th neutron (Z = 82, N = 126). The increment in the values of these parameters after filling of the shell amounts to about 100%. It should be noted that in the entire investigated mass range the neutron binding energy as a whole is greater than the proton binding energy. The same thing may be said regarding the binding energy of two neutrons as compared with the binding energy of two protons. This is particularly clearly evident from comparison of the binding energies for the isobaric pair $_{82}Pb^{204}_{122}$ and $_{80}Hg^{204}_{124}$. In $_{82}Pb^{204}_{122}$ the proton shell is filled, hence for it one could expect a maximum value of the binding energy as compared with other isotopes with A = 204. Actually, however, the binding energy in $_{80}Hg^{204}_{124}$ proved to be greater owing to the greater binding energy of the two neutrons in this nuclide as compared with the two protons in $_{82}Pb^{204}_{122}$. An analogous situation is observed for the isobaric pairs

$$_{78}Pt^{198}_{120} - {}_{80}Hg^{198}_{118},\ {}_{78}Pt^{196}_{118} - {}_{80}Hg^{196}_{116},\ {}_{76}Os^{192}_{116} - {}_{78}Pt^{192}_{114},\ {}_{74}W^{186}_{112} - {}_{76}Os^{186}_{110},\ {}_{72}Hf^{180}_{108} - {}_{74}W^{180}_{106}$$

and for the isobaric pair with odd-A $_{75}Re^{187}_{112} - {}_{76}Os^{187}_{111}$. The mean energy difference for the listed isobaric pairs is 7.0 kev, while for $_{75}Re^{187}_{112} - {}_{76}Os^{187}_{111}$ the difference is 4.0 kev.

The binding energy of the last neutron or proton is consistent with the even-odd law, i.e., the attachment energy of each odd proton or neutron is less than the binding energy of the corresponding even nucleon. Analysis of the data on the values of B_n, B_p and P_n in the investigated mass range shows that both even and odd-Z nuclei having 116 neutrons are characterized by enhanced stability. In contrast to this, nuclei with N = 115 are distinguished by lower binding energies as compared with neighboring nuclei with odd-N. For even-even nuclei there are observed exceptionally high values of the proton pairing energy at N = 116 ($_{78}Pt^{194}_{116}$ and $_{80}Hg^{196}_{116}$). Analogous but less pronounced discontinuities in the values of B_n, B_p, P_n and P_p are evinced for nuclei with N = 122 and N = 121.

On the whole, for most of the isotopic masses measured in the present work and our earlier investigations[1,10-13] the nuclear binding energy is some 1500 kev lower than indicated by the data of Wapstra[8] and Huizenga[9]. This divergence can be explained by the difference between the mass values for Pb^{208} used as the basis in calculating the other masses by means of nuclear reactions Q values.[9] At the same time the divergences between the binding energies for the isotopes of osmium, tungsten, tantalum, and hafnium (Hf^{180}), which attain ~4 Mev, indicate that the masses of many isotopes utilized as references in calculating nuclear masses by means of nuclear reaction Q values[8] have been measured with inadequate accuracy.

We desire to express our deep gratitude to E.E.Baroni and his co-workers K.A.Kovyrzina and V.M.Soifer for preparing the metal-organic and chloride compounds of a number of elements and for making available the organic compounds; we also thank M.I.Dzkuya and G.A.Dorokhova for assistance in the work.

References

1. R.A.Demirkhanov, T.I.Gutkin & V.V.Dorokhov, Zhur.eksp.i teor.fiz., 35, 917 (1958). (Trans.Soviet Physics - JETP.)
2. B.G.Hogg & H.E.Duckworth, Canad.J.Phys., 30, 637 (1952).
3. B.G.Hogg & H.E.Duckworth, Canad.J.Phys., 30, 637 (1952).
4. B.G.Hogg & H.E.Duckworth, Canad.J.Phys., 32, 65 (1954).
5. H.E.Duckworth, C.L.Kegley, J.M.Olson & G.S.Stanford, Phys.Rev., 83, 1114 (1951).
6. R.A.Demirkhanov, T.I.Gutkin, V.V.Dorokhov & A.D.Rudenko, Atomnaya energiya, 2, 21 (1956). (Trans.Soviet Journal of Atomic Energy).
7. R.A.Demirkhanov, T.I.Gutkin & V.V.Dorokhov, Ibid., 6, 544 (1957). (Trans. Ibid.)
8. A.H.Wapstra, Physica, 21, 385 (1955).
9. J.R.Huizenga, Physica, 21, 410 (1955).
10. R.A.Demirkhanov, T.I.Gutkin & V.V.Dorokhov, Doklady AN SSSR, 124, 301 (1959). (Trans.Soviet Physics - Doklady.)
11. R.A.Demirkhanov, T.I.Gutkin & V.V.Dorokhov, Zhur.eksp.i teor.fiz., 36, 1595 (1959). (Trans.Soviet Physics - JETP.)
12. R.A.Demirkhanov, T.I.Gutkin & V.V.Dorokhov, Ibid., 37, 1217 (1959).
13. R.A.Demirkhanov, T.I.Gutkin & V.V.Dorokhov, Doklady AN SSSR, 118, 1103 (1958). (Trans.Soviet Physics - Doklady.)
14. G.S.Stanford & H.E.Duckworth, Bull.Amer.Phys.Soc., 26, No.3, 38 (1951).
15. J.L.Benson, R.A.Damerow & R.R.Ries, Phys.Rev., 113, 1105 (1959).
16. J.T.Kerr & H.E.Duckworth, Canad.J.Phys., 36, 986 (1958).
17. W.H.Johnson & V.B.Bhanot, Phys.Rev., 107, 1669 (1957).
18. R.Tobin & J.McElhinney, Bull.Amer.Phys., Soc.Ser., 11, 1, 340 (1956).
19. R.Sher, J.Halpern & A.K.Mann, Phys.Rev., 84, 387 (1951).
20. B.B.Kinsey & G.A.Bartholomew, Canad.J.Phys., 31, 1051 (1953).
21. V.A.Kravtsov, Uspekhi fiz.nauk, 47, 341 (1952).

COMPARISON AND SYSTEMATICS OF THE BINDING ENERGIES OF HEAVY NUCLEI FROM HAFNIUM TO FRANCIUM

- V.A.Kravtsov

Comparison of the experimental data on mass doublets, nuclear reaction Q values and radioactive decay energies provides a means for checking the values of isotopic masses and nuclear binding energies. For heavy nuclei from europium to lead such verification was until recently impossible inasmuch as there were not available sufficiently accurate mass-spectroscopic data, and α-decay energies had been measured for only a few nuclei[1]. In 1958-9, however, there were carried out a number of precise mass-spectroscopic measurements of nuclide masses from tungsten to bismuth[1-4]. This made it possible to compare and check all the experimental data on nuclear masses and energies from hafnium to francium. The comparisons were carried out over closed cycles, over chains of experimental data and by investigating the shape of the sections of energy surfaces (surfaces plotted in E, Z, A space) by the method used earlier by the writer[5,6].

In addition to the mass-spectroscopic data from Refs.1-4 there were utilized the reaction Q values taken mainly from the reviews of Van Patter & Whaling[7,8] and the β-decay energies taken from the reviews of King[9] and Lidofsky[10], as well as the data from some more recently published studies. Tables of the masses and binding energies of the nuclides from hafnium to francium are being prepared for publication.

All the Q values that are corrected or refined in the present work are listed in Table 1. The doubltful values were checked and corrected with reference to measured masses and also with reference to measured reaction and decay energies (the Refs. from which the latter were taken are not listed in Table 1). In most cases (except for Nos.2,3 & 5 in Table 1) cross checking was feasible with reference to several reaction and decay chains.

Table 1

Questionable Q values and corrected values obtained by comparison with the binding energies of nuclei from hafnium to francium

No.	Reaction	Questioned reaction Q (Ref 7), Mev	More reliable value, Mev	Refs.
1	$W^{186}(n,\gamma)W^{187}$	7,1±0,3	5,304±0,009	[11]
			5,33±0,03	[12]
2	$Ir^{191}(n,\gamma)Ir^{192}$	5,15±0,20	6,088±0,010	[12]
			6,085±0,015	[13]
3	$Pt^{194}(\gamma,n)Pt^{193}$	9,50±0,20	8,32±0,15	Our data
4	$Au^{197}(n,\gamma)Au^{198}$	7,3±0,4	6,494±0,008	[7]
			6,490±0,015	[12]
5	$Hg^{199}(n,\gamma)Hg^{200}$	7,1±0,4	8,03±0,03	[8]
6	$Tl^{203}(\gamma,n)Tl^{202}$	8,8±0,2	7,76±0,30	Our data
			7,45	[14]
			7,53	[15]
7	$Tl^{203}(n,\gamma)Tl^{204}$	6,54±0,03	⩽6,54⩾6,20	Our data
8	$Tl^{203}(d,p)Tl^{204}$	4,29±0,15	⩽4,29⩾3,93	Our data
9	$Tl^{205}(n,\gamma)Tl^{206}$	6,20±0,03	6,54±0,03	Our data
10	$Tl^{205}(d,p)Tl^{206}$	3,93±0,15	3,93±0,15	[15,16]
11	$Bi^{209}(n,\gamma)Bi^{210}$	4,170±0,015	4,56±0,03	[17]
12	$Bi^{209}(d,p)Bi^{210}$	1,94±0,03	2,34±0,03	[17]

According to Van Patter & Whaling[7], the Q value of the $Pt^{194}(\gamma,n)Pt^{193}$ reaction is 9.50 ± 0.20 Mev. From the calculated Pt^{194} - Pt^{193} mass difference, we found Q = 8.32 ± 0.15 Mev. This is not in conflict with the 9.50 Mev value inasmuch as the Q value for the (n,γ) reaction obtained in some cases when the daughter

nucleus is formed in the excited state is actually only the upper bound of the reaction energy. Cross checking of the mass values on the basis of which our Q value was calculated makes our value more reliable than that given in Ref.7.

For the $Tl^{203}(\gamma,n)Tl^{202}$ reaction, according to Van Patter & Whaling[7], Q = = 8.80 ± 0.20 Mev. Analysis of the energy surface section curves carried out by the writer[18] back in 1952 led to the inference that this Q value is an overestimate. This can now be verified by using the measured masses of Hg^{202} and Tl^{203} and the value of the electron capture energy $Q_{EC} = 1.1^{+0.40}_{-0.08}$ Mev calculated from the experimental value of the ratio of probabilities for L and K capture. Evaluated in this manner, the energy for the $Tl^{203}(\gamma,n)Tl^{202}$ reaction proves to be 7.76 ± 0.03 Mev, which is in good agreement with the value obtained by interpolation of the energy surface curves. Within the limits of the experimental error this value of Q corresponds to Q = 7.45 Mev obtained for the $Tl^{203}(n,2n)Tl^{202}$ reaction by Martin & Diven[14] and the value of 7.53 Mev calculated by Foreman & Seaborg[15] from the systematics of heavy nuclei.

The energies of the (n,γ) and (d,p) reactions on Tl^{203} and Tl^{205}, listed by Van Patter & Whaling[7] (see Table 1), in the opinion of Fritsch[16] and Foreman & Seaborg[15] should be attributed to the same isotope but reversed, i.e., the energy attributed to Tl^{203} should be assigned to Tl^{205}, and vice versa. Analysis of all the experimental data leads to the values listed in the fourth column of Table 1. These data can be verified and refined further only on the basis of new more accurate measurements of Q for these reactions on enriched isotopes or on the basis of more precise measurements of the masses of the Tl isotopes.

All the corrected reaction energies have been checked with reference to the appropriate energy surface section curves, and in all cases the values were found to be consistent.

The questionable decay energies in this region cannot be checked by comparison with the mass values obtained from other experimental data. Hence checking and correction of the questionable decay energies was carried out with reference to the energy surface section curves.

For convenience in investigating these curves we used energy surfaces with reduced slope. In the given nuclear region most convenient was consideration of the dependence of

$$E_0 - E_B = 400 + 6A - E_{bi}(Z, N) \text{ Mev} \qquad (1)$$

on the mass number A = N + Z or on N; here $E_{bi}(Z,N)$ is the binding energy of a nucleus with Z protons and N neutrons. The properties of these curves are described in more detail in Refs.5 & 6.

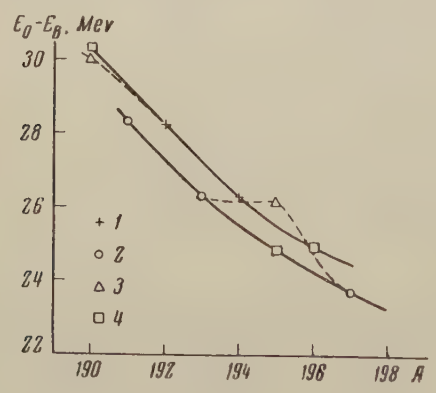

←Fig.1. Section of the energy surfaces with reduced slope (Eq.(1) cut by the Z = 77 plane. Upper curve - section of the odd-odd surface; lower curve - odd-even surface. The dashed line gives the variant of the curve passing through the doubtful points: 1 - points for odd-odd nuclei, 2 - points for odd-even nuclei, 3 - points for energies calculated on the basis of doubtful decay energies, 4 - points obtained by interpolation.

Table 2

Questionable β-decay energies and the corrected values taken from the corresponding energy surface section curves

No.	Nucleus	Period	Decay	Questioned decay energy, Mev	Corrected decay energy, Mev	Remarks
1	2	3	4	5	6	7
1	Ta^{184}	8,7 hours	β^-	$\geqslant$1,26 [10]	2,8±0,2	1.26 Mev β^--group to the 1.50 or 1.45 Mev level (Ref.22)
2	Re^{180}	20 hours 2,4 min	β^+ β^+	$\geqslant$2,9 [10] $\geqslant$2,1 [10]	2,2±0,3	1.1 Mev β^--group to the 0.102 Mev level (Ref.22)
3	Re^{182}	60 hours 13 hours	EC EC	2,3±0,2 [19] $\geqslant$1,96 [20]	2,2±0,3	For the transition to the ground state
4	Re^{184}	50 days	EC	1,32±0,30 [21]	1,6±0,3	
5	Re^{190}	2,8 min	β^-	>1,7; <3,2 [10,22]	2,8±0,4	1.7 Mev β^--group to the 1.13, 1.05 or 1.38 Mev level
6	Ir^{190}	11 days	EC	>1,33; <2,0 [10,22]	2,0±0,2	
7	Ir^{195}	2,3 hours	β^-	2,1±0,1 [23,24]	0,9±0,3	The 2.3-hr Ir is not the ground state of Ir^{195}
8	Ir^{196}	?	β^-	?[23,25]	2,7±0,2	
9	Hg^{195}	9,5 hours	EC	$\geqslant$1,25 [10,22] 1,7±0,1 [26]	1,25±0,20	
10	Pb^{203}	52 hours	EC	1,8 1,4 } [9,22] $0,95^{+0,30}_{-0,07}$ [27]	0,95±0,20	
11	Bi^{203}	11,5 hours	EC, β^+	3,20±0,05 [28] or 3,45±0,05	3,45±0,05	

The β-decay energies as corrected by means of the appropriate energy surface section curves are listed in Table 2. In most cases the energy values listed in column 6 were obtained by graphic interpolation of several sections.

It may be useful to consider the isotopes of iridium in some detail. As will be evident from Fig.1, the old binding energies for Ir^{190} and Ir^{195} are questionable. To obtain a "good" value of the binding energy for Ir^{190} one need only take the upper bound for the electron capture energy suggested by Lidofsky[10] (see Table 2). Particularly surprising is the deviation of the point for Ir^{195} from the general odd-even surface section curve. The point for Ir^{195} also occupies an anomalous position in the T = N - Z = 41 section (not shown). The decay scheme for 140-min Ir^{195} was established by Butement & Poe[23] on the basis of β-γ coincidence measurements and is, apparently, substantiated by the work of Baro & Rey[24]. The β^--decay energy is 2.1 Mev. The energy surface section cut by the A = const, plane for odd-A has only one branch: a parabola with an apex at $Z = Z_y$, corresponding to the β-stable isotope. For A = 195 the β-stable isotope is Pt^{195} (Z_y = 78); in this case, naturally, we should have

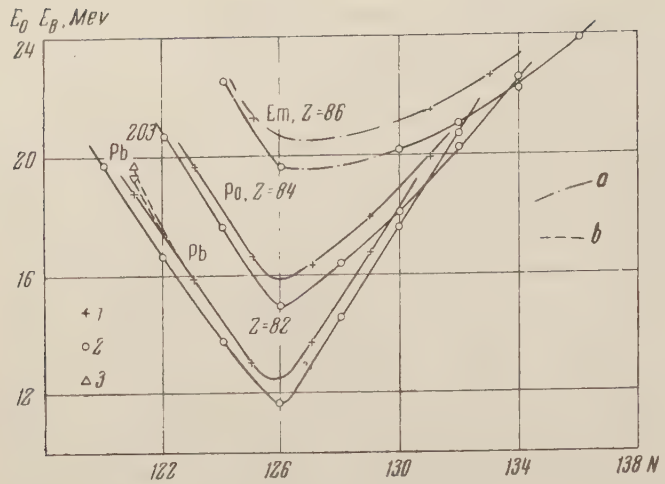

Fig.2

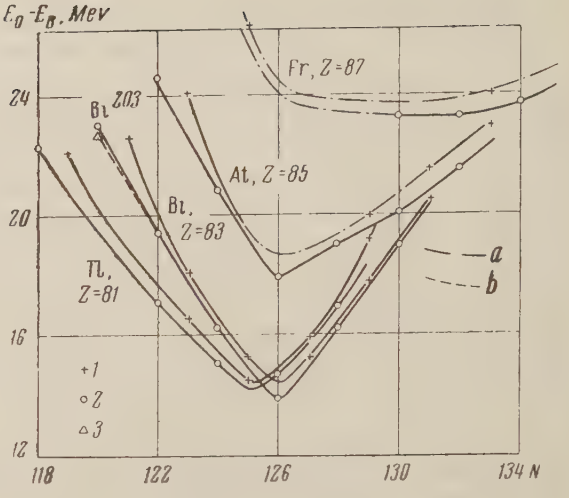

Fig.3

Fig.2. Sections of the energy surfaces with reduced slope cut by the Z = 82, Z = = 84 and Z = 86 planes. Upper curves - sections of even-odd surface; lower curves - sections of even-even surface; a - interpolated part of curve; b - variant of curve drawn through doubtful points; 1 - points for even-odd nuclei, 2 - points for even-even nuclei, 3 - points calculated on the basis of questionable decay energies.

Fig.3. Sections of energy surfaces with reduced slope cut by the Z = 81, Z = 83, Z = 85 and Z = 87 planes. Upper curves - sections of the odd-odd surface; lower curves - sections of the odd-even surface; a - interpolated part of curve, b - variant curve drawn through doubtful points; 1 - points for odd-odd nuclei, 2 - points for odd-even nuclei, 3 - points calculated on the basis of questionable decay energies.

$$Q_{\beta^-}(Z_y - 2) > Q_{\beta^-}(Z_y - 1);$$

actually Q_{β} for Os^{195}, according to Baro & Rey, is 2 Mev, i.e., is smaller than Q_{β} for Ir^{195} according to Butement & Poe[23]. Interpolation of the curves in Fig. 1, as well as other curves, leads to a value of $Q_{\beta} = 0.9 \pm 0.3$ Mev for Ir^{195} in agreement with all the inferences from the systematics. It may therefore be concluded that the mass number assignments made by the authors of Ref.23 for the 140-min and 9.7-day Ir isotopes are mistaken.

Gardner & Meinke[25], who bombarded enriched platinum isotopes, convincingly showed that the 9.7-day iridium is not Ir^{196}. Consequently, the isotopes Ir^{195} and Ir^{196} have not as yet been obtained and hence their decay energies can only be inferred from the systematics. These energies obtained by interpolation in the Z = 77, T = N - Z = 41, N = 119 and T = 42 sections are listed in Table 2.

The decay energy of electron capture Pb^{203} has been calculated repeatedly; according to Refs.9 and 22, it is 1.8 and 1.4 Mev, respectively, but according to the more recent work of Nijgh et al[27] $Q_{EC} = 0.95^{+0.30}_{-0.07}$ Mev. The Pb^{203} binding energy values calculated on the basis of the Q_{EC} values are indicated on the Z = = 82 section in Fig.2 by three points: triangles for the old values and a cross for the new one. It will be evident from Fig.2 that the "best" curve is the solid curve drawn through the cross, i.e., calculated on the basis of the new Q_{EC} value.

The positron decay energy of 11.5-hour Bi^{203}, according to Novakov et al[28], may have two values: $Q_I = 3.45 \pm 0.05$ or $Q_{II} = 3.20 \pm 0.05$ Mev. If we use Q_I to calculate the binding energy of Bi^{203}, we obtain the point indicated by a circle on the Z = 83 section in Fig.3, while using Q_{II} we obtain the point designated by a triangle. Inasmuch as odd-even sections usually lie at equal distances from the corresponding odd-odd sections it is logical to prefer the curve based on Q_I.

Binding Energy Systematics

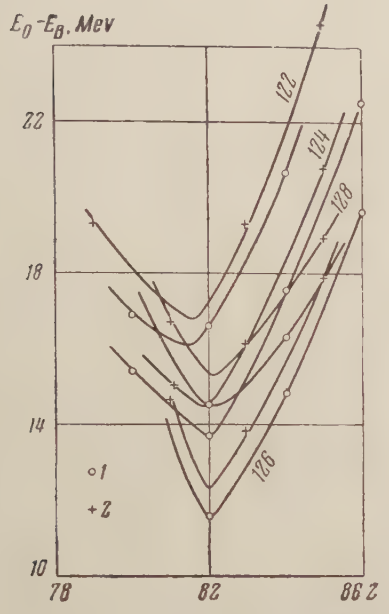

Fig.4. Sections of energy surfaces with reduced slope cut by the N = 122, N = = 124, N = 126 and N = 128 planes. Upper curves - sections of odd-even surface; lower curves - sections of even-even surface, 1 - points for even-even nuclei, 2 - points for odd-even nuclei.

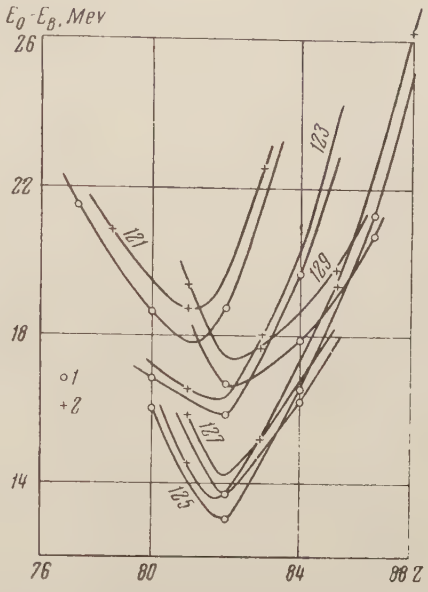

Fig.5. Sections of energy surfaces with reduced slope cut by the N = 121, N = = 123, N = 125, N = 127 and N = 129 planes. Upper curves - sections of the odd-odd surface; lower curves - sections of the even-odd surface; 1 - points for even-odd nuclei, 2 - points for odd-odd nuclei.

In earlier contributions[29-31] we spoke of the existence in the energy surfaces of grooves situated along the lines corresponding to the magic number of neutrons and the magic number of protons. The depth of these grooves is greatest in the center and decreases towards the edges of the energy surface. This assertion was based on investigation of sections of the energy surfaces for heavy nuclei. The values of the binding energy were taken from the tables compiled by the writer[18] in which only the energies for nuclei with an excess number of neutrons were taken from experimental data. The energies of nuclei with a deficiency of neutrons in most cases were obtained by extrapolation of curves. This, of course, reduced the reliability of the curves given in Ref.30. Now, however, after precise measurement of the mass of mercury and lead isotopes[1] and the energies of a number of decays[28] it has become possible to plot the same sections without extrapolation and with only a few interpolated intervals.

The curves of the isotope sections of the energy surfaces with reduced slope are given in Fig.2 for even-Z and in Fig.3 for odd-Z. We see that all the surfaces are intersected by grooves extending along the N = 126 line. In the even-

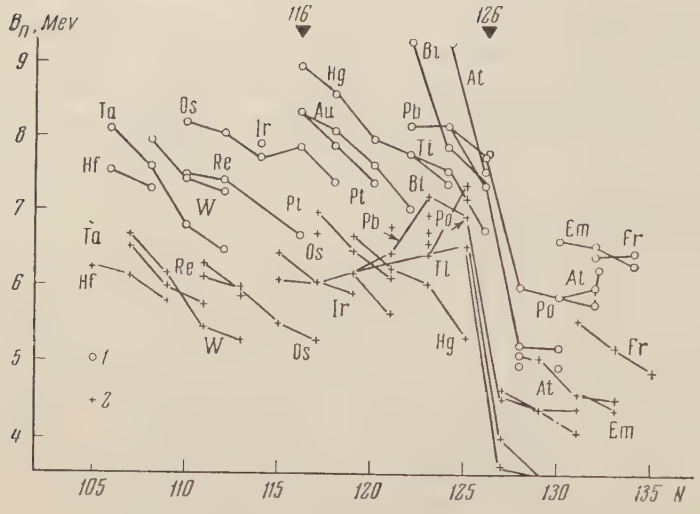

Fig.6. Variation of the neutron separation energy B_n as a function of the number of neutrons N: 1 - separation energy for even neutrons; 2 - separation energy for odd neutrons.

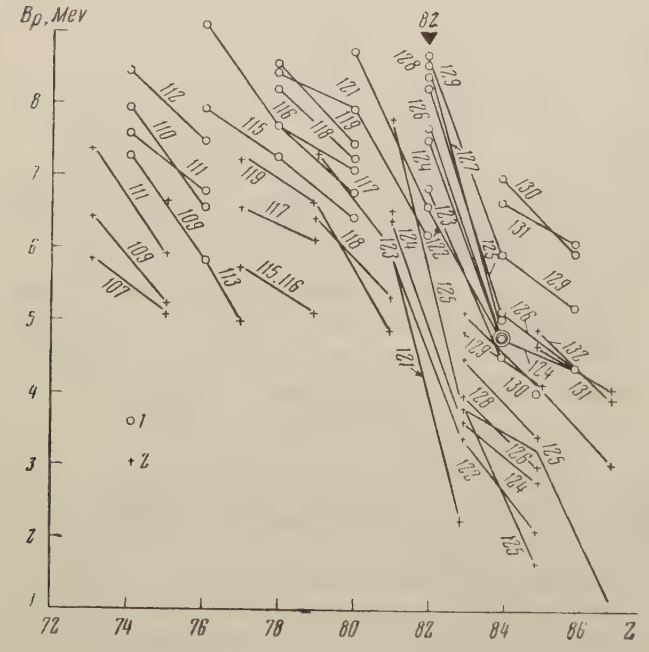

Fig.7. Variation of the proton separation energy B_p as a function of the number of protons Z: 1 - even protons, 2 - off protons.

even and even-odd surfaces (Fig. 2) the greatest depth of the groove, or, more accurately speaking, the greatest steepness of the sides of the groove is observed in the Z = 82 (Pb) section. In the Z = 84 (Po) section the sides are less steep, while in the Z = = 86 (Em) section the sides are almost flat and the groove is scarcely noticeable. In the odd-even and odd-odd surfaces (Fig.3) the steepest groove sides are evident in the Z = 83 (Bi) section; in the Z = 81 (Tl) and Z = 85 (At) sections the sides are considerably flatter and in the Z = 87 (Fr) section the sides are almost flat and the groove is barely distinguishable.

A similar situation obtains as regards the isoneutron sections intersecting the grooves extending along the Z = 82 line in the energy surfaces with reduced slope (Figs.4 & 5). In the even-even and even-odd surfaces (Fig.4) the greatest steepness of the groove sides is observed for N = 126. The steepness decreases in the N = = 124 and N = 128 sections and is minimal in the N = 122 section. In the odd-odd and even-odd surfaces (Fig.5) the steepest groove sides are observed at the N = 125 section; the steepness decreases in going to the sections with larger and smaller N.

Thus the new experimental data have fully substantiated our earlier views (see, for example, Ref.20) regarding the influence of nuclear shells on the shape of the energy surfaces of heavy nuclei. The energy section curve based on the new data are smoother and more consistent than the curves based on the earlier data.

Fig.6 shows the variation of the neutron separation energy B_n as a function of the number of neutrons N. The broken lines in Fig.6 connect the B_n of the same parity, for separation of the last neutron from nuclei of the same element, the symbol of which is indicated at the lines. Fig.7 shows the variation of the proton separation energy B_p as a

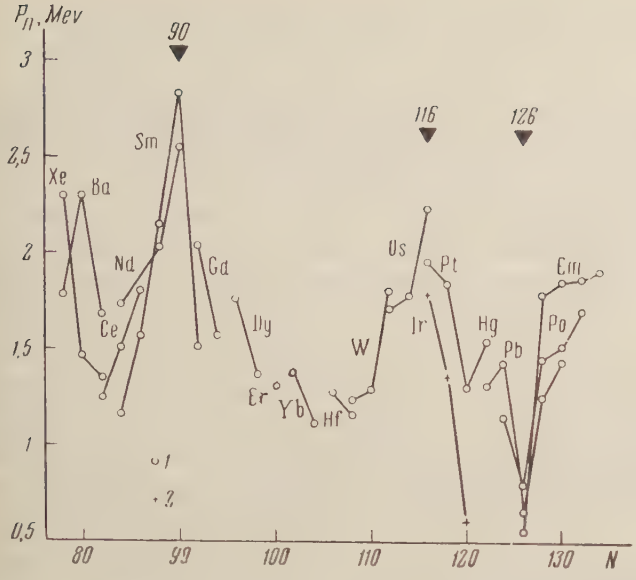

Fig.8. Variation of the neutron pairing energy P_n as a function of the number of neutrons N: 1 - points pertaining to nuclei with an even number of protons Z, 2 - points to nuclei with an odd number of protons Z.

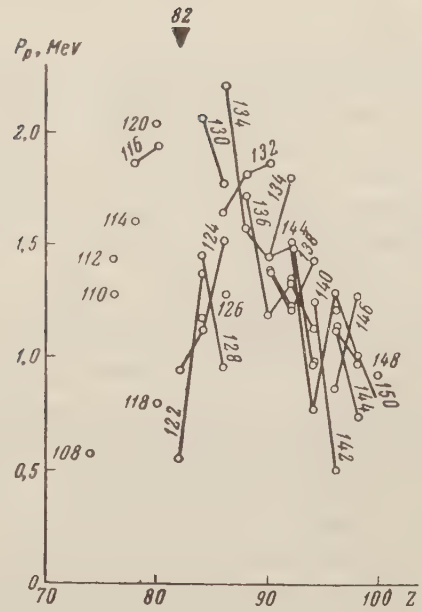

Fig.9. Variation of the proton pairing energy P_p with Z.

function of the number of protons Z. Here the broken lines connect the B_p of the same parity for separation of a proton from nuclei with different numbers of neutrons as indicated by the figures at the lines. The separation energies for even nucleons in Figs.6 & 7 are designated by circles; the separation energies for odd nucleons by crosses.

In Fig.6 we see a sharp decrease of B_n above the magic number N = 126, and in Fig.7 decrease of B_p above the magic number Z = 82. In Fig.6 we also see an increase in the fall off of B_n above N = 116 only for even neutrons, which is apparently connected with transition from the region of deformed nuclei to the region of spherical nuclei.

Fig.8 shows the variation of the neutron pairing energy with N, and Fig.9 shows the variation of the proton pairing energy with Z. The pairing energies were determined in the same way as in Ref.32. In Fig.8 the pairing energies of the nuclei of isotopes of the same elements are connected by broken lines with the element being identified by the appropriate symbol at the lines. In Fig.9 the pairing energies in nuclei with the same number of neutrons are connected by broken lines, the figures at the curves giving the number of neutrons. In addition to the pairing energies calculated on the basis of the new data, we also give for comparison the old pairing energies: in Fig.8 the values taken from the work of Johnson & Nier[33] and Johnson & Bhanot[34], and in Fig.9 the pairing energies calculated for $Z \geqslant 88$ from the values of B_p from the work of Foreman and Seaborg[15].

In Fig.8 we note a clearly evident maximum of P_n at N = 116, i.e., at the upper boundary of the rare earth element region of deformed nuclei. This maximum of P_n is somewhat lower than the maximum at N = 90, i.e., at the lower boundary of the region of deformed nuclei. The maximum at N = 116 in the old plots (for example, in Refs.32-34) is incorrect inasmuch as it was based on an error

in measuring the Q value of the $Ir^{191}(n,\gamma)Ir^{192}$ reaction (see No.2 in Table 1). Moreover, in Figs.8 & 9 there are evident minima at N = 126 and Z = 82; these are connected with the fact that close to the closed shell there occurs pairing of the 125th neutron and 81st proton with small angular momenta (j = 1/2). In Fig.9 there are also evident maxima of P_p at N = 116 and 120, connected apparently with the boundary of the rare earth region of deformed nuclei, and at Z = 88-90, i.e., at the beginning of the region of deformed heavy nuclei.

I take this opportunity to thank R.I.Demirkhanov, T.I.Gutkin and V.V.Dorokhov for communicating results of their nuclear mass measurements prior to publication and L.K.Peker and G.F.Dranitsyna for discussion of the doubtful decay energies.

Leningrad Polytechnic Institute

References

1. J.Benson, R.Damerow & R.Ries, Phys.Rev., 113, 1105 (1959).
2. R.Demirkhanov, T.Gutkin & V.Dorokhov, Zhur.eksp.i teor.fiz., 35, 917 (1958). (Trans.Soviet Physics - JETP.)
3. R.Demirkhanov, T.Gutkin & V.Dorokhov, Ibid.,37,1217 (1959). (Trans.Ibid.)
4. R.Demirkhanov, T.Gutkin & V.Dorokhov, Present issue of the Bulletin, p.119.
5. V.Kravtsov, Uspekhi fiz.nauk, 54, 3 (1954).
6. V.Kravtsov, Izv.AN SSSR, Ser.fiz., 19, 377 (1955). (Trans.Bulletin,19,338.)
7. D.Van Patter & W.Whaling, Revs.Mod.Phys., 26,402 (1954).
8. D.Van Patter & W.Whaling, Ibid., 29,757 (1957).
9. R.King, Ibid., 26,327 (1954).
10. L.Lidofsky, Ibid., 29,773 (1957).
11. B.Kinsey & G.Bertolomew, Canad.J.Phys., 31,1051 (1953).
12. L.Groshev, A.Demidov, V.Lutsenko & V.Pelekhov, Atlas spektrov γ-luchei radiatsionnogo zakhvata neitronov (Atlas of Gamma-ray Spectra from the Capture of Thermal Neutrons), M.,1958.
13. H.Knoepfel, P.Scherer & P.Stoll, Z.Phys.,156,293 (1959).
14. H.Martin & B.Diven, Phys.Rev., 86,565 (1952).
15. B.Foreman, Jr. & G.Seaborg, J.Inorg.Nucl.Chem., 7,305 (1958).
16. A.Fritsch, Thesis, University of California, 1956.
17. G.Holm, J.Burwell, D.Miller & F.Swanson, Bull.Amer.Phys.Soc.,Ser.11,No.4, 233 (1959).
18. V.Kravtsov, Uspekhi fiz.nauk, 47,341 (1952).
19. C.Gallagher,Jr. & J.Rasmussen, Phys.Rev.,112,1730 (1958).
20. C.Gallagher,Jr., J.Newton & V.Shirley, Phys.Rev., 113,1928 (1959).
21. C.Gallagher, D.Strominger & J.Unik, Phys.Rev., 110, 725 (1958).
22. B.Dzhelepov & L.Peker, Skhemy raspada radioaktivnykh yader (Decay schemes of radioactive nuclei), M.-L., 1958.
23. F.Butement & A.Poe, Phil.Mag., 45, 31 (1954).
24. G.Baro & P.Rey, Z.Naturforsch, a12,520 (1957).
25. D.Gardner & W.Meinke, Phys.Rev., 114,822 (1959).
26. J.Bruner, J.Halter, O.Huber, R.Joly & D.Maeder, New.Phys.Acta,27,572(1954).
27. G.Nijgh, A.Wapstra, L.Ornstein, N.Salamons-Grobben, J.Guizenga & O.Almen, Nucl.Phys., 9,528 (1958/59).
28. T.Novakov, R.Stockendal, M.Schmorak & B.Johansson, Arkiv fysik,14,85(1958).
29. V.Kravtsov, Zhur.eksp.i teor.fiz., 24, 242,244 (1953).
30. V.Kravtsov, Izv.AN SSSR, Ser.fiz., 18,5 (1954).
31. V.Kravtsov, Zhur.eksp.i teor.fiz.,30,408(1956).(Trans.Soviet Physics-JETP.)
32. V.Kravtsov, Ibid.,36,1224 (1959). (Trans.Soviet Physics - JETP.)
33. W.Johnson & A.Nier, Phys.Rev.,105,1014 (1957).
34. W.Johnson & V.Bhanot, Phys.Rev., 107,1669 (1957).

SCATTERING OF FAST NEUTRONS BY NONAXIAL NUCLEI

- V.I.Belyak

Small-angle scattering of neutrons by nonspherical nuclei can be treated in the diffraction approximation if $kR \gg 1$.[1,2] In this approximation[3] the wave function of the system satisfies the Schroedinger equation

$$(T_r + T_\omega)\,\Psi(\mathbf{r}, \omega) = 0, \tag{1}$$

for $z \geqslant 0$ (where $z = 0$ is the plane normal to the incident particle beam at the nucleus), where T_r is the kinetic energy operator of the scattered particles, and T_ω is the rotational energy operator of the nucleus. The interaction of the incident particles with the nucleus is accounted for by imposing a boundary condition on the wave function at $z = 0$. For particles with energies ~50 Mev, the nuclei may be considered black, and the wave function of the system consisting of an incident wave $\Psi_0(\mathbf{r}, \omega) = e^{ikz}\cdot\varphi_0(\omega)$ and a scattered wave $\Psi_s(\mathbf{r}, \omega)$ should satisfy the boundary condition

$$\Psi(\boldsymbol{\rho}, 0, \omega) = \begin{cases} 0, & \boldsymbol{\rho} \in S(\omega), \\ \Psi_0(\boldsymbol{\rho}, 0, \omega) = \varphi_0(\omega) & \boldsymbol{\rho} \notin S(\omega), \end{cases} \tag{2}$$

where $S(\omega)$ is the shadow of the nucleus in the $z = 0$ plane.

Similarly,

$$\Psi_s(\boldsymbol{\rho}, 0, \omega) = \begin{cases} -\varphi_0(\omega), & \boldsymbol{\rho} \in S(\omega), \\ 0, & \boldsymbol{\rho} \notin S(\omega). \end{cases} \tag{3}$$

Boundary conditions (2) and (3) imply that the motion of the nucleus is adiabatic relative to that of the incident neutron in the nucleus, which is the case if the neutron energy is much greater than the energy of the levels excited in the scattering process, i.e., if $\varepsilon_n / E \ll 1$.[4]

Making use of (1) and (3) and expanding $\Psi_s(\mathbf{r}, \omega)$ in nuclear wave functions $\varphi_n(\omega)$,

$$\Psi_s(\mathbf{r}, \omega) = \sum_n \Phi_n(\mathbf{r})\,\varphi_n(\omega),$$

one can set up a boundary-value problem for $\Phi_n(\mathbf{r})$, whose solution in the limit as $r \to \infty$ becomes

$$\Phi_n(\mathbf{r}) = \frac{e^{ik_n r}}{r}\cdot f_n(\Omega),$$

$$f_n(\Omega) = \frac{ik_n^z}{2\pi}\int d\omega \varphi_n^*(\omega)\,\varphi_0(\omega) \int\limits_{S(\omega)} d\boldsymbol{\rho} e^{-i\vec{\varkappa}_n\vec{\rho}}, \tag{4}$$

where $\mathrm{k}_n = (\boldsymbol{\varkappa}_n, k_n^z)$ is the wave vector of the neutron scattered in the excitation of the n-th rotational level. Equation (4) includes conservation of energy. Since, however, it is valid for $\varepsilon_n / E \ll 1$ and for small scattering angles, it can be rewritten in the usual form[1]

$$f_n(\Omega) = \int d\omega \varphi_n^*(\omega)\, f(\omega, \Omega)\, \varphi_0(\omega), \tag{5}$$

$$f(\omega, \Omega) = \frac{ik}{2\pi} \int\limits_{S(\omega)} d\boldsymbol{\rho} e^{-i\vec{\varkappa}\vec{\rho}}, \qquad \varkappa = k\theta. \tag{6}$$

Let us consider the differential cross section $d\sigma_n = |f_n(\Omega)|^2 d\Omega$ for excitation of rotational levels in even-even nonaxial nuclei.

According to the unified model, the equation for the nuclear surface is

$$R(\vartheta, \varphi, \omega) = R_0\left[1 + \sum_{\mu} a_{2\mu}(\omega)\, Y_{2\mu}(\vartheta, \varphi)\right],$$

where

$$a_{2\mu}(\omega) = \beta\left[D^{2*}_{\mu 0}(\omega)\cos\gamma + \frac{1}{\sqrt{2}}\left(D^{2*}_{\mu 2}(\omega) + D^{2*}_{\mu -2}(\omega)\right)\sin\gamma\right] \tag{7}$$

In the approximation linear in $a_{2\mu}$, the equation of the shadow coincides with that of the geometric cross section $R(\pi/2, \varphi, \omega)$ of the nucleus. The integral over the shadow $S(\omega)$, from which one obtains $f(\omega, \Omega)$, can be written as the sum of an integral over a circle S_0 of radius R_0 and the integral over $\Delta S(\omega) = S(\omega) - S_0$. The inelastic scattering is determined by the integral over $\Delta S(\omega)$ alone, and this is significantly nonvanishing for scattering angles $\lesssim 1/\beta kR$. Let us restrict our calculations of the inelastic scattering cross section to the case $\beta kR\theta \ll 1$. We can then neglect variations in the integrand of the integral over $\Delta S(\omega)$ for distances of the order of βR_0, and

$$f(\omega, \Omega) = ikR_0^2\left[\frac{J_1(kR_0\theta)}{kR_0\theta} - \sqrt{\frac{5}{16\pi}}\, a_{20} J_0(kR_0\theta) - \sqrt{\frac{15}{32\pi}}\left(a_{22}e^{2i\Phi} + a_{2,-2}e^{-2i\Phi}\right) J_2(kR_0\theta)\right]. \tag{8}$$

It follows from (8) that in this approximation small-angle scattering excites only states of angular momentum 2. The wave functions of such states are

$$\varphi_{001}(\omega) = (1/8\pi^2)^{1/2},$$

$$\varphi_{2m\tau}(\omega) = (5/8\pi^2)^{1/2}\left[a_\tau D^2_{m0}(\omega) + \frac{b_\tau}{\sqrt{2}}\left(D^2_{m2}(\omega) + D^2_{m-2}(\omega)\right)\right], \quad \tau = 1, 2. \tag{9}$$

Explicit expressions for a_τ and b_τ are given by Davydov and Fillipov.[5]

Using (5), (7), (8), and (9) and the properties of the D function, we obtain

$$f_{20\tau}(\Omega) = -i(1/16\pi)^{1/2} kR_0^2 \beta J_0(kR_0\theta)\,(a_\tau\cos\gamma + b_\tau\sin\gamma),$$

$$f_{2\pm 2,\tau}(\Omega) = -i\,(3/32\pi)^{1/2} kR_0^2\,\beta J_2(kR_0\theta)\, e^{\mp 2i\Phi}\,(a_\tau\cos\gamma + b_\tau\sin\gamma), \tag{10}$$

and then

$$d\sigma_{2m\tau}(\gamma) = d\sigma_{2m1}(\gamma = 0)\, b(E2, 2\tau \to 0), \tag{11}$$

where $b(E2, 2\tau \to 0) = (a_\tau\cos\gamma + b_\tau\sin\gamma)^2$ is the reduced probability for an E2 transition between the ground state and the corresponding spin 2 state. Explicitly,

$$b(E2, 21 \to 0) = \frac{1}{2}\left[1 + \frac{3 - 2\sin^2 3\gamma}{\sqrt{9 - 8\sin^2 3\gamma}}\right],$$

$$b(E2, 22 \to 0) = \frac{1}{2}\left[1 - \frac{3 - 2\sin^2 3\gamma}{\sqrt{9 - 8\sin^2 3\gamma}}\right]. \tag{12}$$

Thus the differential cross sections for small-angle inelastic scattering by nonaxial nuclei are equal to the corresponding differential cross sections for scattering by symmetric nuclei multiplied by the reduced probability for an electric quadrupole transition between the ground state and the appropriate state with spin 2. It will be evident from Eqs. (11) and (12) that $d\sigma_{2m2}$ vanishes for axial nuclei and for nuclei with $\gamma = 30^\circ$, and amounts to about 5-7% of $d\sigma_{2m1}$ for $\gamma = 15$-24°.

Inasmuch as $b(E2, 21 \to 0) + b(E2, 22 \to 0) = 1$, the angular distribution of neutrons scattered through small angles is independent of γ:

$$d\sigma_2(\gamma) = \sum_{m,\tau} d\sigma_{2m\tau}(\gamma) = d\sigma_2 \quad (\gamma = 0).$$

The existence of a second level with spin 2 in nonaxial nuclei can, however, be detected by measuring the energies of the scattered neutrons or of the emitted photons.

Let us consider the total cross section $\sigma_n = \int |f_n(\Omega)|^2 d\Omega$ for excitation of rotational levels. To do this one must take into account all the angles θ in the scattering amplitude. Then

$$f(\omega, \Omega) = \frac{iS(\omega)\cos\theta \cdot J_1\left(kR\left(\frac{\pi}{2}, \Phi, \omega\right)\sin\theta\right)}{\pi R\left(\frac{\pi}{2}, \Phi, \omega\right)\sin\theta}. \tag{13}$$

Assuming β and $1/kR$ small, and restricting our calculations to the first order in these quantities, we need consider the difference between $S(\omega)$ and a circle of radius R_0 only in the argument of the Bessel function, so that

$$\sigma_n = \frac{1}{8\pi^2}\int d\omega\, d\omega'\, d\Phi \varphi_n^*(\omega)\,\varphi_n(\omega')\,K(\omega, \omega', \Phi), \tag{14}$$

where

$$K(\omega, \omega', \Phi) = \int_0^{\pi/2} d\theta \cdot \frac{J_1\left(kR\left(\frac{\pi}{2}, \Phi, \omega\right)\sin\theta\right) J_1\left(kR\left(\frac{\pi}{2}, \Phi, \omega'\right)\sin\theta\right)\cos^2\theta}{\sin\theta}.$$

For $\beta kR \gg 1$, the small angle scattering is important; hence neglecting quantities of the order of $1/kR$, we can use the small-angle approximation and extend the integral to infinity. Then

$$K(\omega, \omega', \Phi) = \frac{1}{2} + \frac{1}{2}\left|R\left(\frac{\pi}{2}, \Phi, \omega\right) - R\left(\frac{\pi}{2}, \Phi, \omega'\right)\right|. \tag{15}$$

Inserting (15) into (14), for axial nuclei we obtain

$$\begin{gathered}\sigma_0 = \pi R^2\left(1 - (5/16\pi)^{1/2}\beta\right), \\ \sigma_{22} = \sigma_{2,-2} = (3/2)\,\sigma_{20}, \quad \sigma_2 = \sum_m \sigma_{2m} = (5/8)\,(5/16\pi)^{1/2}\pi R^2\beta.\end{gathered} \tag{16}$$

Since the cross section $\sigma = \sum_{e,m}\sigma_{em}$ does not contain a term linear in the deformation, in our approximation we have $\sum_{e>0,m}\sigma_{em} = -\Delta\sigma_{00} = (5\pi/16)^{1/2}R^2\beta$. For actual nuclei, the condition $\beta kR \gg 1$ is fulfilled only at energies for which the nucleus may not be considered black.

When $\beta kR \approx 1$, scattering through large angles is also significant. Since the diffraction approximation is no longer valid for large-angle scattering, the above deduced formulas for the total cross sections can be used only for purposes of rough approximation in this case.

When $\beta kR \approx 1$, it is convenient to write $K(\omega, \omega', \Phi)$ in the form

$$K(\omega, \omega', \Phi) = 1/2 - \left(\cos t + tSit + \frac{\sin t}{t}\cdot\alpha\right)\Big/\pi kR, \tag{17}$$

where

$$t = k\left[R\left(\frac{\pi}{2}\Phi, \omega\right) - R\left(\frac{\pi}{2}, \Phi, \omega'\right)\right], \quad 1/2 < \alpha < 1.$$

By using (17) one can write the total cross section in the form of an expansion in powers of $kR\beta$, which corresponds to expanding the scattering amplitude in powers of $kR\beta\theta$. Using only the first term of such an expansion (for $\alpha = 1$), we obtain the following expression for axially symmetric nuclei:

$$\sigma_2 = (1/3\pi)\,(kR\beta)\,R^2\beta. \qquad (18)$$

The second term of the expansion gives a correction equal to $-(1/98\pi^2)\,(kR\beta)^3\,R^2\beta$.

For nonaxial nuclei, if one keeps only the first term of the appropriate expansion, Eq.(11) remains valid for the total cross sections as well.

I desire to express my gratitude to A.S.Davydov and D.A.Zaikin for helpful advice and discussion.

"P.N.Lebedev" Physical Institute,
Academy of Sciences of the USSR

References

1. S.I.Drozdov, Zhur.eksp.i teor.fiz., 28, 734 (1955); 34, 1288 (1958); 36, 1875 (1959). (Trans.Soviet Physics - JETP.)

2. E.V.Inopin, Zhur.eksp.i teor.fiz., 31, 901 (1956). (Trans.Soviet Physics - JETP.)

3. A.J.W.Sommerfeld, Optics (English translation, Academic Press, N.Y.)

4. J.S.Blair, Phys.Rev., 115, 928 (1959).

5. A.S.Davydov & G.F.Filippov, Zhur.eksp.i teor.fiz., 35, 440 (1958). (Trans.Soviet Physics - JETP.)

DETERMINATION OF THE MEAN LIFETIME OF THE EXCITED STATES OF U^{235} FISSION FRAGMENTS

- B.M.Shiryaev

Determination of the lifetime of the excited states of fragments formed in fission of heavy nuclei is of interest from the standpoint of investigating the fission mechanism. Such lifetime measurements were carried out by Smith, Fields, & Friedman[1] who used a coincidence apparatus comprising a gas scintillator for detecting the fragments and a plastic scintillator for detecting the γ-rays and neutrons. These authors studied spontaneous fission of Cf^{252} and placed an upper limit on the intensity of neutrons and photons emitted in a time of the order of 10^{-9} sec after fission.

Sklyarevskii, Fomenko & Stepanov[2] compared the intensity of the γ-radiation emitted in thermal neutron induced fission of U^{235} for the case when the γ-rays are emitted only by the scattered fragments with the intensity of the γ-radiation emitted both from the target itself and from the outgoing fragments. They found that the main part of the γ-radiation corresponds to a fragment lifetime lying in the range from $0.5\cdot10^{-9}$ to $2.5\cdot10^{-9}$ sec. Both groups of authors come to the conclusion that the radiation is primarily dipole in character.

In the present work the mean lifetime of the excited states of fission fragments with regard to γ-ray emission was determined on the basis of measuring the solid angle of the γ-ray detector as viewed by the fragments.

An ionization chamber with a layer of the fissioning material[3] on its bottom and a scintillation counter[2], arranged as shown in the accompanying figure, were mounted in a neutron beam. The electronic circuit recorded the coincidences between the pulses from γ-rays and from the ionization chamber. The number of coincidences under these conditions should depend on the distance between the fissioning substance layer and the collecting electrode of the chamber, as long as this distance is shorter than the range of the fragments.

With increase of this distance the number of coincidences decreases owing to de-excitation of the fragments during the time of flight, i.e., owing to decrease of the solid angle from the fragments to the crystal. The mean lifetime is given by the formula

$$\tau = \frac{\frac{2N}{N_\gamma \xi} - \Omega}{v f(r)},$$

where $f(r)$ is a function that depends on the distance between the fissioning layer and the collecting electrode, N is the number of coincidence per fission event, N_γ is the number of γ-rays emitted per fission event, ξ is the efficiency of the gamma detector, v is the mean velocity of the fragments, and Ω is the solid angle comprised by the gamma counter as viewed from the fissioning layer.

In the given experiment for detecting the γ-rays we used a scintillation counter with an NaI(Tl) crystal. The fragments were detected by means of a single layer ionization chamber which was filled with a mixture of argon (95%) and carbon dioxide (5%). The uranium oxide layer on the bottom of the chamber contained 97.8% U^{235}, had a superficial density of 300 $\mu g/cm^2$ and was applied by electrolysis onto an aluminum backing. The distance between the uranium oxide layer and the collecting electrode could be varied from 5 to 22 mm by means of a sylphon bellows.

For calculating τ, we used the values of N_γ and ξ obtained in the work of Artem'ev et al[4], the solid angles were calculated using the data of Petrzhak & Bak[3]; the fragment velocities were taken from the work of Leachman[5].

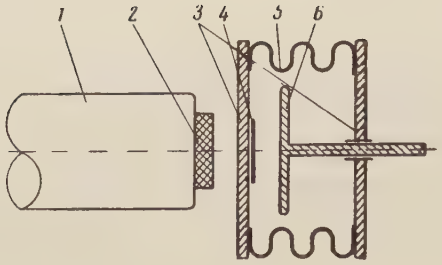

Counter arrangement: 1) photomultiplier, 2) NaI(Tl) crystal, 3) ionization chamber housing, 4) uranium oxide layer, 5) sylphon bellows, 6) collecting electrode.

It follows from the results of our measurements that the mean lifetime of the fission fragments as regards emission of γ-rays lies in the range from $0.5 \cdot 10^{-9}$ to $2.0 \cdot 10^{-9}$ sec. This is consistent with the values obtained by other methods.

The experimentally determined lifetime values indicate that the γ-rays are emitted mainly after evaporation of the neutrons from the excited fragments. However, a number of factors (angular anisotropy of the γ-rays, high value of the total energy of the γ-radiation emitted per fission event) are not consistent with the usual theory of neutron evaporation, hence it is of interest to search for shorter γ-ray emission times in the process of fission.

I am grateful to A.N.Protopopov and V.P.Eismont for valuable suggestions and for discussion of the results.

"B.H.Khlopin" Radium Institute,
Academy of Sciences of the USSR

References

1. A.B.Smith, P.R.Fields & A.M.Friedman, Phys.Rev., 104, 699 (1956).
2. V.V.Sklyarevskii, D.E.Fomenko & E.P.Stepanov, Zhur.eksp.i teor.fiz., 32, 256 (1957). (Trans.Soviet Physics - JETP.)
3. K.A.Petrzhak & M.A.Bak, Zhur.tekh.fiz., 25, 636 (1955).
4. Yu.M.Artem'ev, A.N.Protopopov & B.M.Shiryaev, Trudy (Proceedings), Radium Institute, 9, 78 (1959).
5. R.B.Leachman, Phys.Rev., 87, 444 (1952).

COLLECTIVE EXCITATIONS IN SUPERFLUID NUCLEAR MATTER

- B.B.Dotsenko

We use Bogolyubov's method[1] to find the excited and ground state energies of superfluid nuclear matter.

Consider a very large (infinite) collection of nucleons, the density of which is equal to the nucleon density inside heavy nuclei. Then the attractive nuclear potential can be divided into two parts, one of which (the basic part) is used to construct a self-consistent field (and causes a change in the effective nucleon mass)[2]. The remainder then appears in the form of a two-particle correlation, and leads to a superfluid condensate of pairs of particles (or holes) with momenta close to the Fermi surface.[3] * All the nucleons are also acted on by hard-core repulsive forces (repulsive forces due to the nucleon cores). We shall neglect the Coulomb repulsion between protons, taking account of the difference between neutrons and protons only through the isotopic spin. The repulsive forces do not contribute to the self-consistent field, and have to be included in the correlation part of the attraction.

Accordingly, we write the second-quantized Hamiltonian for nuclear matter in the form[1]

$$H = \sum_{f,f'} T(f,f')\, a_f^+ a_f + \frac{1}{2} \sum_{f_1, f_1'; f_2, f_2'} U(f_1, f_2; f_2', f_1')\, a_{f_1}^+ a_{f_2}^+ a_{f_1'} a_{f_2'}, \qquad (1)$$

where a_f^+ and a_f are fermion (nucleon) creation and annihilation amplitudes, f is a collective index denoting eigenstates of the momentum p, the spin σ, and the isotopic spin τ of a particle, T represents the one-particle Hamiltonian $T(f,f') = \{E(f) - \lambda\}\,\delta(f - f')$, wherein $E = (p^2/2m) + W$ is the basic part of the particle's energy (including the kinetic energy corresponding to effective mass m and the self-consistent field energy W, and λ is the chemical potential of the system, introduced to take into account number-of-particle conservation. We write

$$\lambda = \lambda_p \delta(\tau - 1/2) + \lambda_n \delta(\tau + 1/2),$$

where λ_p and λ_n are the potentials of the proton and neutron subsystems, respectively (in general $\lambda_p \neq \lambda_n$). (In the normal state, λ is equal to the Fermi energy.)

The remainder U of the potential is, in our case,**

$$U(f_1, f_2; f_2', f_1') = \frac{1}{V}\{J(p_1, p_2; p_2', p_1' | \sigma_1, \tau_1; \sigma_2, \tau_2; \sigma_1', \tau_1'; \sigma_2', \tau_2') + \\ + \varkappa(|p_1 - p_1'|)\}\,\delta(p_1 + p_2 - p_1' - p_2')\,\delta(\sigma_1 - \sigma_1')\,\delta(\sigma_2 - \sigma_2') \times \\ \times \delta(\tau_1 - \tau_1')\,\delta(\tau_2 - \tau_2'), \qquad (1')$$

where $J < 0$ is the effective attraction leading to the formation of the superfluid condensate, and $\varkappa(|p_1 - p_1'|)$ is the Fourier transform of the repulsive hard-core potential.

In the presence of an external perturbation, one must use Bogolyubov's generalized principle of compensation[1] to describe the superfluid state of a system of fermions. This principle forbids the appearance of two particles with very similar momenta p_1 and p_2; in the first approximation it may be written

---

*We do not consider four-particle correlations here.[4]

**All the p's are vectors.

$$\langle \alpha_{\nu_1} \alpha_{\nu_2} H \rangle_0 = 0, \tag{2}$$

where the α_ν are new fermion amplitudes obtained from the a_f by the canonical transformation

$$a_f = \sum_\nu (u_{f\nu} \alpha_\nu + v_{f\nu} \overset{+}{\alpha}_\nu) \tag{3}$$

and "orthonormalized" according to

$$\begin{gathered} \sum_\nu \{u_{f\nu} u^*_{f'\nu} + v_{f\nu} v^*_{f'\nu}\} = \delta(f - f'), \\ \sum \{u_{f\nu} v_{f'\nu} + u_{f'\nu} v_{f\nu}\} = 0, \end{gathered} \tag{4}$$

a condition which guarantees that the transformation be canonical. Here $\delta(f - f')$ is the Kronecker delta symbol, the asterisk denotes the complex conjugate, and the brackets $\langle \cdots \rangle_0$ represent the expectation value with respect to the vacuum state C_0 defined for the α_ν operators (i.e., $\alpha_\nu C_0 = C_0^{*+} \alpha_\nu = 0$). Bogolyubov has shown that Eq.(2) for the $u_{f\nu}$ and $v_{f\nu}$ is equivalent to the two relations

$$\mathfrak{A} \equiv \langle [a_{f_1} a_{f_2}; H] \rangle_0 = 0; \quad \mathfrak{B} \equiv \langle [a^+_{f_1} a_{f_2}; H] \rangle_0 = 0, \tag{5}$$

where $[\cdots]$ is the Poisson bracket.

The expressions for $\mathfrak{A}$ and $\mathfrak{B}$ contain C_0-expectation values of the form

$$\langle \overset{+}{a}_f a_{f'} \rangle_0 \equiv F(f, f') = \sum_\nu v^*_{f\nu} v_{f'\nu}; \quad \langle a_{f_1}, a_{f_2} \rangle_0 \equiv \Phi(f_1, f_2) = \sum_\nu u_{f_1\nu} v_{f_2\nu}, \tag{6}$$

which can be written out explicitly if we replace the a_f in (5) by the α_ν, according to (3). The functions $F(f, f')$ and $\Phi(f_1, f_2)$ can be interpreted as distribution functions for the system of particles and holes (F) or the system of pairs (Φ) They satisfy the conditions

$$\begin{gathered} F^*(f, f') = F(f', f); \quad \Phi(f_2, f_1) = -\Phi(f_1, f_2), \\ F(f_1, f_2) = \sum_f \{F(f_1, f) F(f, f_2) + \Phi^*(f, f_1) \Phi(f, f_2)\}; \end{gathered} \tag{7}$$

$$\sum_f \{F(f_1, f) \Phi^*(f, f_2) + F(f_2, f) \Phi(f, f_1)\} = 0. \tag{8}$$

It can be shown[1] that $\mathfrak{A}$ and $\mathfrak{B}$ are not independent, so that it is sufficient to consider just one of relations (5). Let us set $\mathfrak{A} = 0$, which corresponds to the superfluid ground state of the system, and let us write out $u_{ff'}$ and $v_{ff'}$ in a form that exhibits both their spin and isotopic spin dependence:*

$$\begin{gathered} u_{f_1 f'} = \frac{1}{2} u(p_1) \delta(p' - p_1) \{\delta(\sigma' + \sigma_1) + 2\sigma_1 \delta(\sigma' - \sigma_1)\} \times \{\delta(\tau' + \tau_1) + 2v_1 \delta(\tau' - \tau_1)\}; \\ v_{f_2 f'} = \frac{1}{2} v(p_2) \delta(p' + p_2) \{2\sigma_2 \delta(\sigma' - \sigma_2) - \delta(\sigma' + \sigma_2)\} \times \{2\tau_2 \delta(\tau' - \tau_2) + \delta(\tau' + \tau_2)\}. \end{gathered} \tag{9}$$

---

*We emphasize that this transformation is chosen only for the purposes of simplification. One could just as well have chosen the transformation proposed by Solov'ev et al[4]. It would then be possible to include not only correlation between particles with the same, but also with different isotopic spins. In heavy nuclei, however, the correlations are of the type obtained with our transformation (9).

Then for the distribution function of the system's ground state we obtain

$$F_0(f_1, f_2) = F(p_1)\,\delta(p_1 - p_2)\,\delta(\sigma_1 - \sigma_2)\,\delta(\tau_1 - \tau_2);\ F(p) = v^2(p); \tag{10}$$

$$\Phi_0(f_1, f_2) = \Phi(p_1)\,\delta(p_1 + p_2)\,\delta(\sigma_1 + \sigma_2)\,\delta(\tau_1 - \tau_2);\ \Phi(p) = u(p)\,v(p), \tag{11}$$

$$u^2(p) + v^2(p) = 1.$$

Taking U in the form given by (1'), using the relation $\mathfrak{A} = 0$ and Eq.(10), and recalling that the spin and isospin are uniquely specified by the correlation functions F and Φ, we obtain

$$2\xi(p)\Phi(p) + \frac{1}{V}[1 - 2F(p)]\sum_{p'} J(p, -p;\ -p', p') + \varkappa(|p - p'|)\}\Phi(p') = 0;$$

$$\xi(p) = E(p) - \lambda + \frac{1}{V}\sum_{p'}\{J(p, p'; p', p) - J(p, p'; p, p') + \varkappa\{|0|) - \varkappa(|p - p'|)\}F(p'), \tag{12}$$

$$F(p) = F^2(p) + \Phi^2(p).$$

Here we have assumed that the isotopic spin J is invariant.

Let us find the role of the repulsive potential $\varkappa(|p|)$ in (12). Mills et al[5] established the significant value of the nuclear repulsive forces, assuming the nucleon cores to be hard spheres. This assumption leads to a grossly overestimated value of the repulsive forces (see also Brueckner and Gammel[6]). We shall therefore use the more realistic assumption that the nuclear cores are not exactly hard spheres, but that their density decreases as $\exp(-r/a_c)$, where $a_c \approx \approx 2\cdot10^{-14}$ cm.[7] Accordingly, we shall assume that the short-range repulsive potential also drops off exponentially, and may be written

$$V_c(r) = A\{\exp(-r/a_c)\}/r, \quad A = \text{const.} \tag{13}$$

The Fourier transform of this potential is (cf. Chapter 6 of Bogolyubov, Tolmachev & Shirkov[3].)

$$\varkappa(|p|) = A\frac{A}{\frac{2\pi^2}{a_c}(p^2 + a_c^{-2})},$$

and a_c^{-2} is relatively large with the given value of a_c. Thus $\varkappa(|p|)$ is a decreasing function of p and hence is maximum at $p = 0$, where $\varkappa(|0|) = Aa_c^3/2\pi^2$. This means that even at $p = 0$ this function is not large. We may therefore assume that in a shell around the Fermi surface $\varkappa(|0|)$ is much less than $J(p, p'; p', p)$. This $\varkappa(|0|)$ enters only into $\xi(p)$. Since $\varkappa(|0|)$, which we are going to neglect compared to J, is the maximum value of $\varkappa(|p - p'|)$, we may neglect this function wherever it occurs in (12). But this will lead to an equation identical with Bogolyubov's[1] Eq.(32), which means that with the properties we have assumed for the repulsive forces, the repulsion has little effect on the superfluidity. If one wants to treat the effect of the repulsive force more accurately, one must consider the function

$$[J(p, p'; p', p) - J(p, p'; p, p') + \varkappa(|0|)]$$

in (12) (the other terms containing $\varkappa(|p - p'|)$ in (12) may be neglected). In other words, the repulsive forces in a sense "deform" the energy of the individual particle, but have virtually no effect on the form (or the solution) of the fundamental equation for the superfluidity of a system of fermions (Bogolyubov's Eq.(32)). Indeed, setting

$$-\frac{1}{V}\sum_{p'} J(p, -p; -p', p')\,\Phi(p') = C(p),$$

in (12) (again, we are neglecting $\varkappa(|p-p'|)$), we obtain

$$\begin{gathered}\Phi(p) = C(p)/2\Omega_1(p);\ F(p) = \{1-\xi_1(p)/\Omega_1(p)\}/2;\\ \xi_1(p) = E(p) - \lambda + \frac{1}{V}\sum\{J(p, p'; p', p) - J(p, p'; p, p') + \varkappa(|0|)\},\\ \Omega_1(p) = \sqrt{\xi_1^2(p) + C^2(p)},\quad \varkappa(|0|) = Aa_c^3/2\pi^2\end{gathered} \tag{14}$$

and the equation

$$C(p) + \frac{1}{V}\sum_{p'} J(p, -p; -p', p')\,C(p')/2\Omega_1(p') = 0, \tag{15}$$

whose solution gives the ground state of the superfluid condensate.[1]

Let us now turn to the problem of excitation from the ground state. It is shown by Bogolyubov[1] that such excitations correspond to variations of F and Φ from their ground-state values F_0 and Φ_0:

$$F = F_0 + \delta F,\ \Phi = \Phi_0 + \delta\Phi; \tag{16}$$

the variations satisfy the relations

$$i\frac{\partial\delta F(f_1, f_2)}{\partial t} = \delta\mathfrak{A}(f_1, f_2|F\Phi),\quad i\frac{\partial\delta\Phi(f_1, f_2)}{\partial t} = \delta\mathfrak{B}(f_1, f_2|F, \Phi) \tag{17}$$

and the subsidiary conditions

$$\begin{aligned}\delta F(f_1, f_2) &= \sum_{\nu_1\nu_2}\{v^*_{f_1\nu_1}u_{f_2\nu_2}\Lambda(\nu_1, \nu_2) + u^*_{f_1\nu_1}v_{f_2\nu_2}\Lambda^*(\nu_2, \nu_1)\},\\ \delta\Phi(f_1, f_2) &= \sum_{\nu_1\nu_2}\{u_{f_1\nu_1}u_{f_2\nu_2}\Lambda(\nu_1, \nu_2) + v_{f_1\nu_1}v_{f_2\nu_2}\Lambda^*(\nu_2, \nu_1)\},\end{aligned} \tag{18}$$

obtained from (7) and (8), where Λ is an antisymmetric parameter. According to Bogolyubov, Λ may be used to describe collective motion of a system of fermions, since ρ_q and p_q, the Fourier components of the particle density and momentum density, respectively, are related to Λ by[1]

$$\begin{aligned}\rho_q &= \frac{1}{V}\sum_{p_1+p_2=q}\{v(p_2)u(p_1) + v(p_1)u(p_2)\}\{\Lambda(p_1, p_2) + \Lambda^*(-p_2, p_1)\},\\ p_q &= \frac{1}{V}\sum_{p_1+p_2=q}\{v(p_2)u(p_1) - v(p_1)u(p_2)\}\{\Lambda(p_1, p_2) - \Lambda^*(-p_2, -p_1)\}.\end{aligned} \tag{19}$$

Equations (17) lead to complicated equations for Λ. (For all details of the derivation and solution of these equations, we refer the reader to Bogolyubov's work.[1]) The solutions may be written in the form[1]

$$\begin{gathered}\Lambda(\nu_1, \nu_2) = \sum_E e^{-iEt}\zeta_E(\nu_1, \nu_2);\quad \Lambda^*(\nu_1, \nu_2) = \sum_E e^{-iEt}\eta_E(\nu_1, \nu_2),\\ \zeta^*_{-E} = \eta_E.\end{gathered} \tag{20}$$

Inserting these expressions into the equation for Λ, one obtains general forms for the equations for the eigenvalues E and the functions ζ and η. If one then inserts (9), (10), and (1') into these general equations, it is found that the vibration spectrum given by (20) breaks up into four branches corresponding to correlation between particles for which 1) $\sigma_1 = \sigma_2;\ \tau_1 = \tau_2$, 2) $\sigma_1 = \sigma_2$,

$\tau_1 = \tau_2$, 3) $\sigma_1 = \sigma_2$; $\tau_1 = -\tau_2$, or 4) $\sigma_1 = -\sigma_2$; $\tau_1 = -\tau_2$. Taking case 2, we obtain equations for η and ζ, and it is found that p_1 and p_2 are related by the equation $p_1 + p_2 = q$, where q is fixed (the momentum of the excitation). Let us write $p_1 = p$ and $p_2 = -p + q$. Then the functions

$$\Delta_q(p) = \zeta(p_1, p_2) + \eta(-p_2, -p_1) \quad \text{and} \quad \theta_q(p) = \zeta(p_1, p_2) - \eta(-p_2, -p_1) \tag{21}$$

determine the contributions Δ_q and θ_q to the oscillations in particle and momentum densities, respectively, from such excitations.

From the equations for η and ζ we obtain equations for $\Delta_q(p)$ and $\theta_q(p)$:

$$\begin{gathered}
S(\Delta_q) = [\Omega_1(p) + \Omega_1(p-q)]\,\Delta_q(p) + \frac{1}{V}\sum_{p'}\{J'_q(p, p')\,L(p')\,L(p) + \\
+ G'_q(p, p')\,M(p')\,M(p)\}\,\Delta_q(p') = E\theta_q(p); \\
T(\theta_q) = [\Omega_1(p) + \Omega_1(p-q)]\,\theta_q(p) + \frac{1}{V}\sum_{p'}\{J'_q(p, p')\,P(p')\,P(p) + \\
+ I'_q(p, p')\,R(p')\,R(p)\}\,\theta_q(p') = E\Delta_q(p); \qquad (22) \\
L(p) = u(p)\,u(p-q) - v(p)\,v(p-q);\ M(p) = u(p)\,v(p-q) + v(p)\,u(p-q) \\
P(p) = u(p)\,u(p-q) + v(p)\,v(p-q);\ R(p) = u(p)\,v(p-q) - v(p)\,u(p-q) \\
J'_q(p, p') = J(p - p + q;\ -p' + q, p') + \varkappa(|p - p'|); \\
G'_q(p, p') = J(p, -p', -p' + q, p - q) + J(p, p' - q;\ p', p - q) - \\
- J(p' - q, p;\ p', p - q) + 2\varkappa(|q|) + \varkappa(|p - p'|); \\
I'_q(p, p') = J(p, p' - q;\ p', p - q) - J(p' - q, p;\ p', p - q) - \\
- J(p, -p';\ -p' + q, p - q) + \varkappa(|p - p'|).
\end{gathered}$$

As before, we can neglect the contribution of $\varkappa(|p - p'|)$ to the kernels J', G' and I', compared to the contribution from J for large p. The most dangerous case is $G'_q(p, p')$, which contains $\varkappa(|q|)$ (note that $q = p_1 + p_2$ is small). Considerations similar to those used in discussing the contribution of $\varkappa(|0|)$ in Eq.(12) lead to the conclusion that the contribution of the repulsive force to the "dangerous" kernel $G'_q(p, p')$ remains bounded as $q \to 0$, and leads to no divergence.

Let us now turn to the excitations described by (22). With Bogolyubov[1] we set

$$\theta(p) = s_1\delta(p - p_0);\ \Delta(p) = s_2\delta(p - p_0), \tag{23}$$

where s_1 and s_2 are constants, and p_0 is an arbitrary fixed momentum. Then dropping terms proportional to $1/V$, which vanish in the limit as $V \to \infty$ and thus cause only local changes in the wave function, we arrive at

$$s_1\{\Omega_1(p_0) + \Omega_1(p_0 - q)\} = s_2E;\ s_2\{\Omega_1(p_0) + \Omega_1(p_0 - q)\} = s_1E, \tag{24}$$

whence

$$E = \Omega_1(p_0) + \Omega_1(p_0 - q). \tag{25}$$

This means that for the given θ_q and Δ_q, the energy E of an elementary excitation depends continuously on p_0, and that for fixed q it is separated from the ground state by an energy gap ($C(p)$ in Ω_1).

Following Bogolyubov, one can show that $\Phi_0(p)\,\delta(\sigma_1 + \sigma_2)\,\delta(\tau_1 - \tau_2)$ corresponds to the bound state of a pair, and that $\delta\Phi$ breaks up into the product of two plane waves, which denotes the breaking up of the pair into two free particles.

Let us now go on to a consideration of collective excitations, whose energy values E form a discrete set for fixed q.

If we neglect all repulsive forces, all the J, G and I kernels become finite. Then for $q = 0$ Eqs.(22) have the solution[1]

$$\theta(p) = u(p)\,v(p), \quad \Delta = 0; \quad E = 0 \tag{26}$$

(i.e., the collective excitation spectrum starts at zero), and for small q the energy eigenvalue is

$$E = |q|\,c/\sqrt{3}, \tag{27}$$

where c is approximately equal to the particle velocity on the Fermi surface.

When repulsive forces exist at $q = 0$, the term with $I'_q(p, p')$ in the second of Eqs.(22) disappears, $J'_q(p, p')$ goes over into the expression for the effective attraction, (since $\varkappa(|p - p'|)$ may be neglected), and $G_q(p, p')$ is only slightly deformed by $\varkappa(|0|)$. Then for $q = 0$ the entire set of Eqs.(22) has a solution of the form of (26).

For $q \neq 0$ but nevertheless small, we may attempt a solution in the form of an expansion:[1]

$$\theta = u(p)\,v(p) + |q|\,\theta_1(p, e) + \ldots; \quad \Delta = |q|\,\Delta_1(p, e) + \ldots$$
$$E = |q|\,E_1 + \ldots; \quad \mathbf{e} = \mathbf{q}/|\mathbf{q}|. \tag{28}$$

Inserting these expressions into (22), one arrives at

$$T_0(\theta_1) = -\sum_{1 \leqslant \alpha \leqslant 3} e^{\alpha} \{\partial T_q(uv)/\partial q^{\alpha}\}_{q=0}; \tag{29}$$

$$S_0(\Delta_1) = E_1 uv; \tag{30}$$

$$T(\theta_2) = E_1\Delta_1 - \sum_{\alpha} e^{\alpha} \left\{\frac{\partial T_q(\theta_1)}{\partial q^{\alpha}}\right\}_{q=0} - \frac{1}{2}\sum_{\alpha,\beta} e^{\alpha} e^{\beta} \left\{\frac{\partial^2 T_q(uv)}{\partial q^{\alpha}\partial q^{\beta}}\right\}_{q=0}. \tag{31}$$

When this set of equations is solved[1], one finds that even when a hard-core repulsion is taken into account, the collective-excitation energy will be of the form

$$E_{\text{coll}} = |q|\,c_r/\sqrt{3}.$$

In this case, however, c_r is less than c of (27).

Thus, apparently, one can conclude that there are two types of collective excitations of nuclear matter. Those of the first type, which have been discussed by Glassgold et al[8], are excitations of an ordinary degenerate system of fermions (the "normal phase"). The energy of such excitations is relatively high[8] (~30 Mev). Excitations of the second type belong to the "superfluid phase" (or condensate), which is present mixed in with the "normal phase" in nuclear matter.* These excitations are of relatively low energy. (If one accepts the Bohr-Mottelson estimate of about 1 Mev for the energy "slit", the energy of this second type of excitation lies within the slit. Thus if one subjects nuclear matter to weak excitations, the energy should be absorbed by the "superfluid" phase, leading to a "second sound" wave, while the "normal" phase of the nuclear matter will remain unexcited.

---

*Since the superconducting condensate is formed entirely of nucleons lying close to the Fermi surface.

I desire to express my deep gratitude to N.N.Bogolyubov for suggesting the topic and his interest in the work, as well as to V.G.Solov'ev for discussions of a number of specific points involved in the work.

References

1. N.N.Bogolyubov, Uspekhi fiz.nauk, 67, 549 (1959). (Trans.Soviet Physics - Uspekhi.)

2. E.Clementel & C.Villi, Nuovo cimento, 9, 950 (1958); K.A.Brueckner, Phys. Rev., 97, 1353 (1955).

3. N.N.Bogolyubov, V.V.Tolmachev & D.V.Shirkov, Novyi metod teorii sverkhprovodimosti, M. 1958. (Trans. A New Method in the Theory of Superconductivity, Consultants Bureau, N.Y. 1958).

4. V.T.Belyaev, B.N.Zakhar'ev & V.G.Solov'ev, O sverkhtekuchesti legkikh yader (Superfluidity of light nuclei). OIYaI Preprint P-414, Dubna 1959.

5. R.L.Mills, A.M.Sessler, S.A.Moszkowski & D.S.Shankland, Phys.Rev.Letters, 3, 381 (1959).

6. K.A.Brueckner & J.L.Gammel, Phys.Rev., 109, 1023 (1958).

7. D.I.Blokhintsev, V.S.Barashenkov & B.M.Barbashov, Uspekhi fiz.nauk, 68, 417 (1959) (Trans.Sov.Phys.-Uspekhi); B.B.Dotsenko, Zhur.eksp.i teor.fiz., 37, 1478 (1958) (Trans.Soviet Physics - JETP).

8. A.E.Glassgold, W.Heckrotte & K.M.Watson, Ann.Phys., 6, No.1 (1959).

METHOD OF DISCRIMINATING PULSES DUE TO FAST NEUTRONS FROM PULSES DUE TO γ-RAYS BY MEANS OF PHOTOMULTIPLIER SPACE CHARGE

- G.G.Doroshenko and E.L.Stolyarova

The difficulty of detecting fast neutrons against a γ-ray background is well known. Until recently the problem was solved either by means of special electronic circuits (e.g., coincidence circuits, subtraction circuits) or by using complex phosphors (e.g., ZnS(Ag) grains in a hydrogenous medium such as plexiglas).

The chief drawback of these methods is their very low detection efficiency for fast neutrons; usually, the efficiency is of the order of 0.001%, and in the very best cases is only 0.1%.

High efficiency organic scintillators with a detection efficiency of 10% to 40% for fast neutrons could not be used because their light yield for the same particle energy is substantially less for protons, α-particles and heavy ions than for electrons.

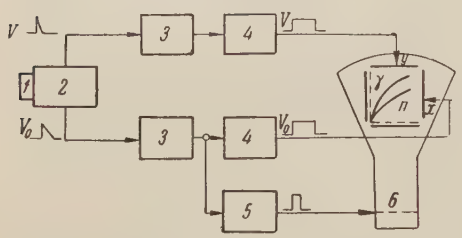

Fig.1. Diagram of the discrimination apparatus with an oscilloscope: 1) scintillator, 2) photomultiplier, 3) amplifier, 4) pulse stretcher, 5) trace intensifier, 6) cathode-ray tube.

It was recently observed that some organic scintillators exhibit an interesting property: their effective afterglow or decay time for fast neutrons is about twice as long as for γ-rays.[1,2]

Two methods have been suggested for making practical use of this property. Both methods employ ordinary photomultipliers operated under linear conditions and in both two pulses are taken off the photomultiplier: one from the anode, the other from the last dynode.

However, the methods differ as regards the detection circuits. In the first method[1] (Fig.1) the pulse from the anode is proportional to the amplitude of the scintillation, while the pulse from the dynode is proportional to the integral light yield. The pulses, after amplification and stretching, are displayed on an oscilloscope as two lines, one of which corresponds to neutrons and the other to γ-rays. Although the results of this method are very graphic, the electronic equipment involved is complicated and the method cannot readily be used to measure fast neutron fluxes and spectra.

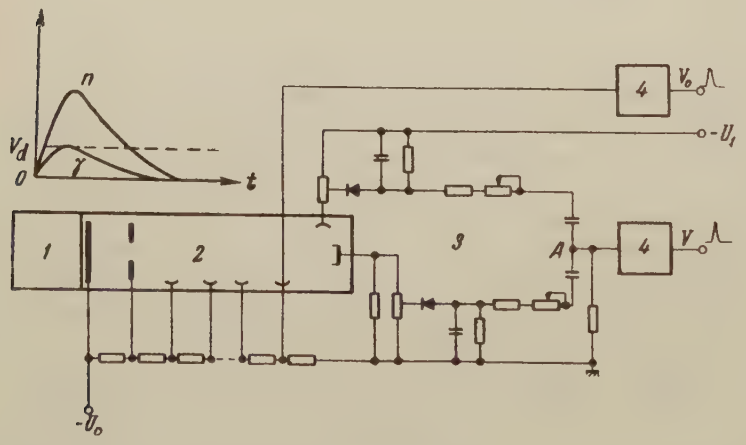

Fig.2. Brook's circuit: 1) scintillator, 2) photoplier, 3) discrimination apparatus, 4) amplifiers. Insert upper left - pulse shapes at point A, corresponding to neutrons and γ-rays.

The second method[2] employs a simpler circuit (Fig. 2). In practice, however, as Brooks[2] shows, the procedure demands scrupulous adjustment of all circuit elements, smoothing out the diode non-linearities, etc. Moreover, the output signal is very weak and hence considerable amplification is required.

The method proposed herein utilizes an artificially created space charge in

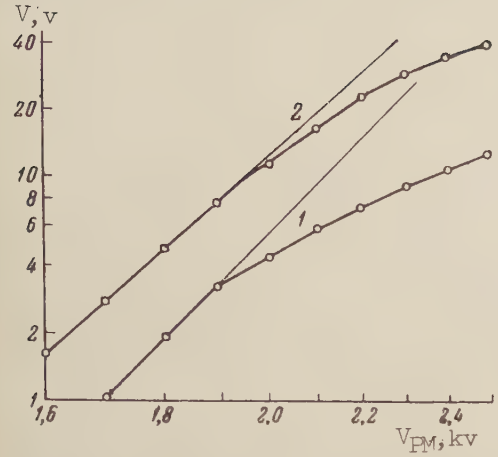

Fig.3. Effect of space charge as a function of the scintillation decay time: 1) stilbene crystal; 2) NaI(Tl) crystal. An FEU-33 photomultiplier and a Zn^{65} γ-source were used in the tests.

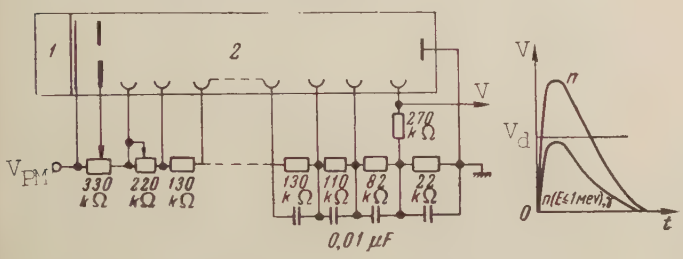

Fig.4. Discrimination apparatus: 1) scintillator, 2) FEU-33 photomultiplier. In the insert (right) for the sake of simplicity the negative output pulse is shown as positive.

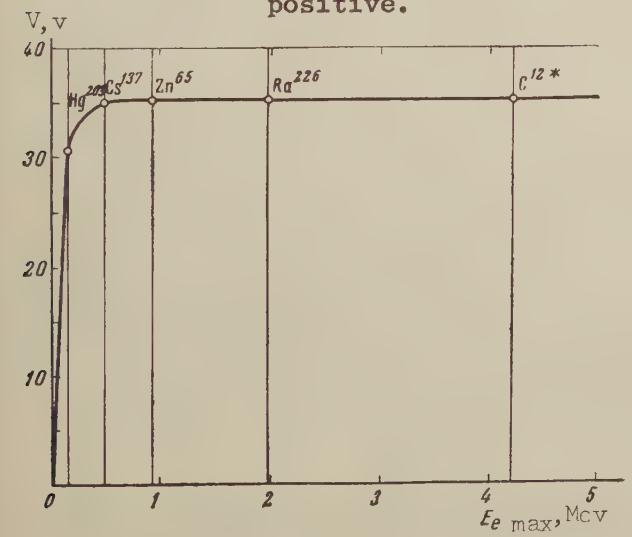

the last stages of the photomultiplier to separate pulses due to fast neutrons from those due to γ-rays. The action of the space charge in the last stage of the photomultiplier results in conversion of the difference in effective scintillation decay times to a difference in amplitudes. We know of no similar use of space charge, although Owen[1] notes that in using the first method improved discrimination is obtained if the "fast" component of the pulse is clipped by space charge. In a brief communication Litherland et al[3] mention limiting of the current leaving the last dynode during the "fast" part of the current pulse by the space charge between the dynode and the anode; they assert that as a result the amplitude of the positive pulse from the "slow" component depends on the relative intensities of the "slow" and "fast" components.

Fig.3 shows the results of an experiment to test the possibility of using space charge to distinguish between two scintillation components with different decay times. It will be evident that for the short decay time of stilbene space charge has a substantially stronger effect despite the lower light yield. The scintillations from fast neutrons have a decay time approximately twice that of the scintillations from γ-rays, leading us to expect that space charge can be used to convert the time difference to an amplitude difference.

To produce a high current density and an adequate space charge we need a large amplification factor and a reduced voltage on the last stages of the photomultiplier. The "slow" component decay time is of the order of 0.3 μsec,[1] and consequently the time constant of the output RC circuit must be fairly large.

←Fig.5. Gamma-calibration. Overall photomultiplier voltage 2.4 kv. All the points for the γ-sources were determined from the Compton edges of the amplitude distributions. The C^{12*} point was obtained from the amplitude distribution for a Po-Be source with the fast neutrons stopped by 406 mm of paraffin.

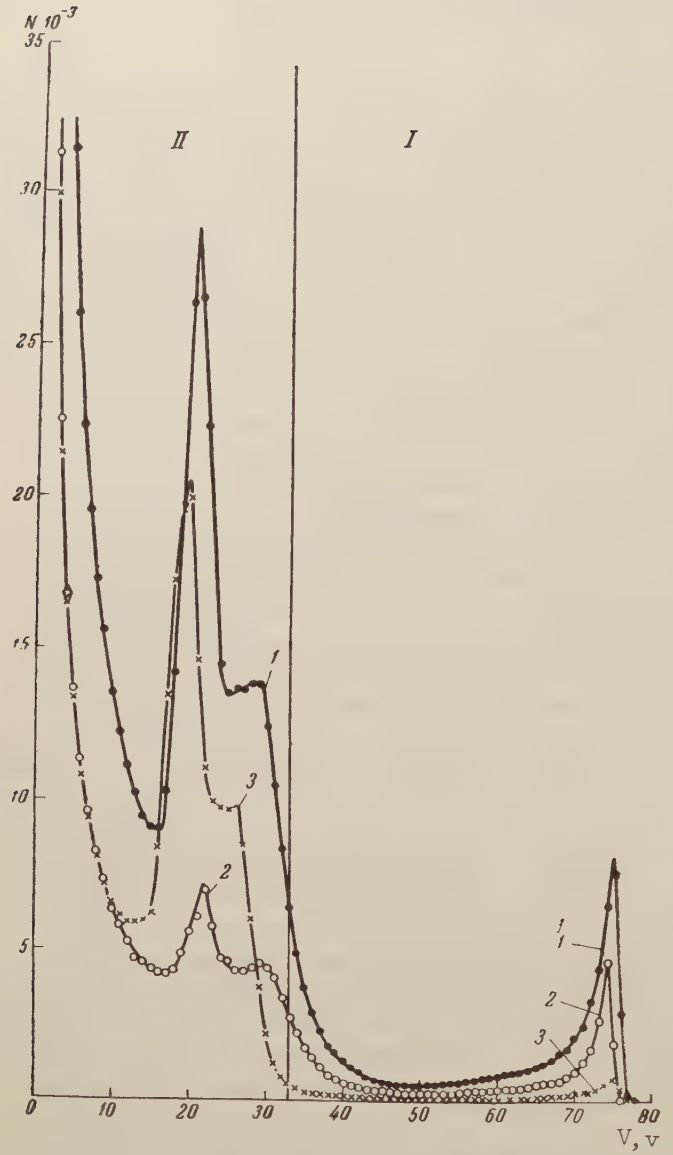

Fig.6. Curve 1 is the amplitude distribution of pulses from a Po-Be source; curves 2 & 3 are the same but with a 12.8 cm layer of lead and 25.8 cm layer of paraffin, respectively. Region I corresponds to pulses solely from fast neutrons with energies of $\geq$ 1 Mev; region II corresponds to γ-rays and recoil protons of lower energy.

To block out the γ-background, the output pulse amplitude must be independent of the recoil electron energy in a wide energy range. This independence can also be assured by space charge in the last stages of the photomultiplier.

The proposed discriminator circuit is extremely simple (Fig. 4), and gives good results. We carefully selected the circuit parameters by studying their influence on the amplitude distributions from a Po-Be source and various γ-sources. The final characteristics are shown in Figs.5 & 6.

Fig.5 gives the γ-calibration. Clearly, to reduce the threshold for detection of fast neutrons one must adjust the circuit so as to bring the pulse amplitudes corresponding to the lowest-energy gammas out onto the plateau; this can be realized by providing sufficiently high potentials on the photomultiplier.

Fig.6 shows the amplitude distribution of pulses from a Po-Be source. The pulses in region I correspond solely to fast neutrons with energies of $\geq$ 1 Mev. The pulses in region II correspond to γ-rays and low-energy ($<$1 Mev*) protons. Thus, simple amplitude discrimination in region II is enough to record exclusively pulses due to fast neutrons. Experiments on attenuation in lead and paraffin of the fast neutrons and γ-rays from the Po-Be source (Fig.6) qualitatively confirm the discrimination effect. The ratio of the peak amplitudes due to fast neutrons and γ-rays is of the order of 2.

We tested 25 stilbene crystals and 12 FEU-33 photomultiplier tubes. All the crystals gave the same results, while the six photomultipliers with the greatest multiplication factor gave results similar to those shown in Fig.6. Tests with a diphenyl acetylene crystal showed no discrimination effect, which is in agreement with the data of Brooks[2] and others.

---

*The lower bound of 1 Mev is inferred here from the known relation of the light yields from electrons and recoil protons.[4]

The proposed discriminator should find extensive practical application because the output pulse amplitude is approximately 100 volts, which makes it feasible to design simple equipment for measuring fast neutron and heavy ion spectra in the presence of a considerable γ-ray background.

References

1. R.B.Owen, IRE Trans. on Nucl.Sci., NS-5, 198 (1958).
2. F.D.Brooks, Nuclear Instruments and Methods, 4, 151 (1959).
3. A.E.Litherland, E.Almqvist, R.Batchelor & H.E.Gove, Phys.Rev.Letters, 2, 104 (1959).
4. C.J.Taylor, W.K.Jentschke, M.E.Remley, F.S.Eby & P.G.Kruger, Phys.Rev., 84, 1034 (1951).

LONGITUDINAL POLARIZATION OF PARTICLES IN WEAK FOUR-FERMION INTERACTION

- B.K.Kerimov

1. It was shown in previous contributions[1-4] that by means of the theory[5,1] of Dirac particles with oriented spin one can relate parity nonconservation in weak interactions with the spin of the elementary particles. In these previous contributions there were calculated, on the basis of the theory of longitudinally polarized Dirac particles, the angular symmetry and the degree of longitudinal polarization of the particles emitted in β-decay of nuclei, in the decay of a polarized free neutron and in $\pi^{\pm}\to\mu^{\pm}$ decays. In Ref.4 there was proposed a different explanation of the theorem "ICT = const. in weak interactions" on the basis of the theory of the neutrino with oriented spin[6].

In the present work we calculate the angular distribution and longitudinal polarization of particles emitted in the decay in flight of a fully polarized free fermion b into three fermions:

$$b\to a+c+d, \tag{1}$$

and, accordingly, for the reaction $b+d\to a+c$.

In our treatment the wave functions of the free fermions $\psi_i\,(i=a,b,c$ and $d)$, entering into the four-fermion interaction (V,A):

$$H_{\text{int}}=\sum_{j=V,A} C_j\,(\psi_a^{+}O_j\psi_b)\,(\psi_c^{+}O_j\psi_d), \tag{2}$$

$$O_V\equiv\alpha_\mu=(i\vec{\alpha},\,I),\quad O_A\equiv\sigma_\mu=(\vec{\sigma},\,i\rho_1),$$

are determined by simultaneous solution of the Dirac equation for a free particle and the equation

$$(\vec{\sigma}_i\,\mathbf{p}_i-p_i s_i)\,\psi_i=0, \tag{3}$$

where $\mathbf{p}_i=\frac{\hbar}{i}\nabla_i$ is the particle momentum operator, $\vec{\alpha}=\rho_1\vec{\sigma}$, ρ_1 are Dirac matrices, $s_i=\pm1$ is the eigenvalue of the projection operator $\vec{\sigma}_i\mathbf{p}_i/p_i$, which characterizes the helicity of the fermion and is an integral of motion (see Refs.1-5).

For s_i = 1 the fermion has positive helicity (the fermion is polarized in its direction of motion), while for s_i = -1 it has negative helicity (the fermion is polarized opposite to the direction of motion).

Such states with full longitudinal polarization of the spin may be realized in the limit at relativistic velocities of the fermions. In this treatment the matrix elements of the decay process (1), pertaining to longitudinally polarized fermions with different masses $k_{0i}\neq k_{0j}$, can readily be calculated by means of the formula[1,5]

$$b_i^{+}(\mathbf{k}_i,\,s_i,\,\varepsilon_i)\,\gamma_{\mu'\nu'}b_j(\mathbf{k}_j,\,s_j,\,\varepsilon_j)\,b_j^{+}(\mathbf{k}_j,\,s_j,\,\varepsilon_j)\,\gamma_{\mu\nu}b_i(\mathbf{k}_i,\,s_i,\,\varepsilon_i)=\frac{1}{4}\rho_{\mu'\mu}\sigma_{\nu'\nu}, \tag{4}$$

where

$$\rho_{\mu'\mu}=\frac{1}{4}\,\text{Spur}\,\rho_{\mu'}\left(1+\rho_1\varepsilon_j s_j\frac{k_j}{K_j}+\rho_3\varepsilon_j\frac{k_{0j}}{K_j}\right)\rho_\mu\left(1+\rho_1\varepsilon_i s_i\frac{k_i}{K_i}+\rho_3\varepsilon_i\frac{k_{0i}}{K_i}\right),$$

$$\sigma_{\nu'\nu}=\frac{1}{4}\,\text{Spur}\,\sigma_{\nu'}\left(1+s_j\frac{\vec{\sigma}\mathbf{k}_j}{k_j}\right)\sigma_\nu\left(1+s_i\frac{\vec{\sigma}\mathbf{k}_i}{k_i}\right), \tag{5}$$

$$\mu,\mu'\ \text{ and }\ \nu,\nu'=1,2,3,4;$$

here $i = b$ or d; $j = a$ or c; $\gamma_{\mu\nu} = \rho_\mu \sigma_\nu = \sigma_\nu \rho_\mu$ are matrices defining the type of interaction, ρ_μ and σ_ν are Dirac matrices ($\rho_4 = \sigma_4 = I$); the $b_{i,j}(\mathbf{k}, s, \varepsilon)$ are the spinor amplitudes of the free fermions; $\varepsilon_{i,j} = \pm 1$ determines the sign of the energy $\varepsilon_{i,j} c\hbar K_{i,j} = \varepsilon_{i,j} c\hbar \sqrt{k_{i,j}^2 + k_{0i,0j}^2}$ and the momentum $\mathbf{p}_{i,j} = \varepsilon_{i,j} \hbar \mathbf{k}_{i,j}$, and $k_{0i,0j} = \frac{m_{0i,0j}}{\hbar}$ is the fermion rest mass.

2. The differential probability of the decay process (1) is determined by the following formula

$$dW = \frac{(d\mathbf{k}_c)\,(d\mathbf{k}_d)}{c\hbar^2 (2\pi)^5} |M_{ba}|^2 \delta(K_b - K_a - K_c - K_d), \tag{6}$$

where $\mathbf{k}_b = \mathbf{k}_a + \mathbf{k}_c + \mathbf{k}_d$, and

$$|M_{ba}|^2 = \sum_{j,j'=V,A} C_j C_{j'}^+ (b_b^+ O_{j'}^+ b_a b_a^+ O_j b_b)(b_d^+ O_{j'}^+ b_c b_c^+ O_j b_d). \tag{7}$$

Calculating the matrix elements of the (V,A) form of interaction by means of Eqs.(4) and (5), from Eqs.(7) and (2) we obtain the following general expression for the square of the matrix element of the decay process (1) for fixed longitudinal polarizations s_i of all the decay fermions:

$$\begin{aligned}
|M_{ba}|^2 = {} & \frac{1}{16} \rho_{44}^{ba} \rho_{44}^{cd} (\sigma_{44}^{ba} \sigma_{44}^{cd} |C_V|^2 + \sigma_{jj'}^{ba} \sigma_{jj'}^{cd} |C_A|^2) + \\
& + \frac{1}{16} \rho_{11}^{ba} \rho_{11}^{cd} (\sigma_{jj'}^{ba} \sigma_{jj'}^{cd} |C_V|^2 + \sigma_{44}^{ba} \sigma_{44}^{cd} |C_A|^2) - \\
& - \frac{1}{16} \rho_{14}^{ba} \rho_{14}^{cd} \{2 (|C_V|^2 + |C_A|^2) \Phi_1 + (C_V^+ C_A + C_A^+ C_V)(\sigma_{44}^{ba} \sigma_{44}^{cd} + \sigma_{jj'}^{ba} \sigma_{jj'}^{cd})\} + \\
& + \frac{1}{16} (C_V^+ C_A + C_A^+ C_V)(\rho_{44}^{ba} \rho_{44}^{cd} + \rho_{11}^{ba} \rho_{11}^{cd}) \Phi_1 + \\
& + \frac{1}{16} i (C_V^+ C_A - C_A^+ C_V)(\rho_{44}^{ba} \rho_{44}^{cd} - \rho_{11}^{ba} \rho_{11}^{cd}) \Phi_2;
\end{aligned} \tag{8}$$

here

$$\begin{aligned}
\rho_{44}^{ba} \rho_{44}^{cd} &= (1 + \varepsilon_a \varepsilon_b s_a s_b \beta_a \beta_b + \varepsilon_a \varepsilon_b \beta_{0a} \beta_{0b})(1 + \varepsilon_c \varepsilon_d s_c s_d \beta_c \beta_d + \varepsilon_c \varepsilon_d \beta_{0c} \beta_{0d}), \\
\rho_{11}^{ba} \rho_{11}^{cd} &= (1 + \varepsilon_a \varepsilon_b s_a s_b \beta_a \beta_b - \varepsilon_a \varepsilon_b \beta_{0a} \beta_{0b})(1 + \varepsilon_c \varepsilon_d s_c s_d \beta_c \beta_d - \varepsilon_c \varepsilon_d \beta_{0c} \beta_{0d}), \\
\rho_{14}^{ba} \rho_{14}^{cd} &= (\varepsilon\, s_b \beta_b + \varepsilon_a s_a \beta_a)(\varepsilon_d s_d \beta_d + \varepsilon_c s_c \beta_c), \\
\sigma_{44}^{ba} \sigma_{44}^{cd} &= (1 + \varepsilon_a \varepsilon_b (\mathbf{s}_a \mathbf{s}_b))(1 + \varepsilon_c \varepsilon_d (\mathbf{s}_c \mathbf{s}_d)), \\
\sigma_{jj'}^{ba} \sigma_{jj'}^{cd} &= 3 - \varepsilon_c \varepsilon_d (\mathbf{s}_c \mathbf{s}_d) - \varepsilon_a \varepsilon_b (\mathbf{s}_a \mathbf{s}_b) - 2\varepsilon_b \varepsilon_d (\mathbf{s}_b \mathbf{s}_d) + 2\varepsilon_a \varepsilon_d (\mathbf{s}_a \mathbf{s}_d) + \\
&\quad + 2\varepsilon_b \varepsilon_c (\mathbf{s}_b \mathbf{s}_c) - 2\varepsilon_a \varepsilon_c (\mathbf{s}_a \mathbf{s}_c) - \varepsilon_a \varepsilon_b \varepsilon_c \varepsilon_d (\mathbf{s}_a \mathbf{s}_b)(\mathbf{s}_c \mathbf{s}_d) + \\
&\quad + 2\varepsilon_a \varepsilon_b \varepsilon_c \varepsilon_d ((\mathbf{s}_b \mathbf{s}_d)(\mathbf{s}_a \mathbf{s}_c) + (\mathbf{s}_a \mathbf{s}_d)(\mathbf{s}_b \mathbf{s}_c)), \\
\Phi_1 &= \varepsilon_b \varepsilon_d (\mathbf{s}_b \mathbf{s}_d) + \varepsilon_a \varepsilon_d (\mathbf{s}_a \mathbf{s}_d) + \varepsilon_b \varepsilon_c (\mathbf{s}_b \mathbf{s}_c) + \varepsilon_a \varepsilon_c (\mathbf{s}_a \mathbf{s}_c) - \\
&\quad - \varepsilon_a \varepsilon_b \varepsilon_d ((\mathbf{s}_b \mathbf{s}_d)(\mathbf{s}_a \mathbf{s}_c) - (\mathbf{s}_b \mathbf{s}_c)(\mathbf{s}_a \mathbf{s}_d)), \\
\Phi_2 &= \varepsilon_a \varepsilon_b \varepsilon_d (\mathbf{s}_d [\mathbf{s}_d \mathbf{s}_a]) + \varepsilon_a \varepsilon_d \varepsilon_c (\mathbf{s}_c [\mathbf{s}_b \mathbf{s}_a]) + \varepsilon_c \varepsilon_d \varepsilon_b (\mathbf{s}_d \mathbf{s}_c]) + \\
&\quad + \varepsilon_c \varepsilon_d \varepsilon_a (\mathbf{s}_a [\mathbf{s}_d \mathbf{s}_c]),
\end{aligned} \tag{9}$$

where

$$\mathbf{s}_q = s_q \mathbf{k}_q^0, \quad \mathbf{k}_q^0 = \frac{\mathbf{k}_q}{k_q}, \quad s_q = \pm 1, \quad \varepsilon_q = \pm 1,$$

$$\beta_{0q} = \frac{k_{0q}}{K_q} = \sqrt{1 - \beta_q^2}, \quad \beta_q = \frac{k_q}{K_q} = \frac{v_q}{c}, \quad k_{0q} = \frac{m_{0q} c}{\hbar}, \quad q = a,\ b,\ c,\ d.$$

For neutrino ($q = \nu$) and antineutrino ($q = \bar{\nu}$) decay $\beta_{0q} = 0$ and $\beta_q = 1$. The momentum of one of the fermions can readily be eliminated from (8) and (9) by means of conservation laws. Equations (8), (9) and (6) describe the spin and angular correlations of the particles in decay in flight of a fully polarized fermion b.

In particular, the deduced formulas allow of investigating the angular distribution and longitudinal polarization of particles forming in decay in flight of a polarized neutron or a polarized muon.

If the decaying polarized fermion is at rest ($\mathbf{k}_b \to 0$, $\mathbf{s}_b = s_b \mathbf{k}_b^0$ is the spin vector of the fermion b), from the deduced formula for $|M_{ba}|^2$ as a particular case we obtain the expressions for the angular distributions in the decay of a polarized neutron and muon at rest taking into account the longitudinal polarization of the forming fermions.

In case of decay in flight of a fully polarized neutron $n \to p + e^- + \bar{\nu}$, in (6)-(9) we should set

$$b = n,\ c = e^-,\quad \varepsilon_a = \varepsilon_b = 1,$$
$$a = p,\ d = \bar{\nu},\ \varepsilon_c = -\varepsilon_d = 1. \tag{10}$$

For decay of an antineutron $\tilde{n} \to \tilde{p} + e^+ + \nu$, we should write

$$b = \tilde{n},\ c = e^+,\ \varepsilon_a = \varepsilon_b = -1,$$
$$a = \tilde{p},\ d = \nu,\ \varepsilon_c = -\varepsilon_d = -1. \tag{11}$$

In the case of decay in flight of a fully polarized $\mp$ muon $\mu^\mp \to e^\mp + \nu' + \nu$, we must set

$$b = \mu^-,\ c = e^-,\ \varepsilon_a = \varepsilon_b = 1,$$
$$a = \nu',\ d = \nu,\ \varepsilon_c = -\varepsilon_d = 1 \tag{12}$$

(ν' is a neutrino, ν is an antineutrino) and, accordingly

$$b = \mu^+,\ c = e^+,\ \varepsilon_a = \varepsilon_b = -1,$$
$$a = \nu',\ d = \nu,\ \varepsilon_d = -\varepsilon_c = 1 \tag{13}$$

(ν' is an antineutrino, ν - a neutrino). For "ordinary" particles (n, p, μ^-, e^-,...) we have $\varepsilon_q = 1$, while for antiparticles ($\tilde{n}$, $\tilde{p}$, μ^+, e^+,...), we have the negative value $\varepsilon_q = -1$.

3. First let us consider β-decay of a polarized neutron at rest ($\mathbf{k}_n \to 0$) taking into account proton recoil ($k_p \neq 0$). According to (10) and (9), from Eq.(8) we have for the square of the matrix element after summing over the longitudinal spin states of the recoil proton

$$\begin{aligned}
\sum_{s_p=\pm 1} |M_{np}|^2 = {} & \frac{1}{8}\xi(1+\beta_{0p}\eta_1)\{1+\beta_e(\mathbf{k}_e^0\mathbf{k}_\nu^0) - s_e(\beta_e s_\nu^- + s_\nu^-(\mathbf{k}_e^0\mathbf{k}_\nu^0))\} + \\
& + \frac{1}{8}\xi(1-\beta_{0p}\eta_1)\{3-\beta_e(\mathbf{k}_e^0\mathbf{k}_\nu^0) + 2s_\nu^-(\mathbf{s}_n\mathbf{k}_\nu^0) - 2\beta_e s_\nu^-(s_n\mathbf{k}_e^0) + \\
& + s_e(s_\nu^-(\mathbf{k}_e^0\mathbf{k}_\nu^0) + 2(\mathbf{s}_n\mathbf{k}_e^0) - 2\beta_e(\mathbf{s}_n\mathbf{k}_\nu^0) - 3\beta_e s_\nu^-)\} + \\
& + \frac{1}{4}\beta_p\xi\{(1+\eta)(\beta_e s_\nu^-(\mathbf{s}_n\mathbf{k}_e^0) - 1 + s_e(\beta_e s_\nu^- - (\mathbf{s}_n\mathbf{k}_e^0)))(\mathbf{k}_p^0\mathbf{k}_\nu^0) - \\
& - (1-\eta)(\beta_e - s_e s_\nu^-)(1+s_\nu^-(\mathbf{s}_n\mathbf{k}_\nu^0))(\mathbf{k}_p^0\mathbf{k}_e^0)\} + \\
& + \frac{1}{4}\xi\eta\{s_e((\mathbf{s}_n\mathbf{k}_e^0) + \beta_e(\mathbf{s}_n\mathbf{k}_\nu^0)) - s_\nu^-((\mathbf{s}_n\mathbf{k}_\nu^0) + \beta_e(\mathbf{s}_n\mathbf{k}_e^0))\} - \\
& - \frac{1}{4}\xi\eta_2\beta_{0p}\{\mathbf{s}_e s_\nu^-(\mathbf{s}_n[\mathbf{k}_\nu^0\mathbf{k}_e^0]) - \beta_e(\mathbf{s}_n[\mathbf{k}_\nu^0\mathbf{k}_e^0])\},
\end{aligned} \tag{14}$$

where $\mathbf{s}_n = s_n\mathbf{k}_n^0$ is the neutron spin vector, and

$$\xi = |C_V|^2 + |C_A|^2, \quad \eta\xi = C_V^+ C_A + C_A^+ C_V,$$
$$\eta_1\xi = |C_V|^2 - |C_A|^2, \quad \eta_2\xi = i(C_V^+ C_A - C_A^+ C_V)$$
$$\beta_p = \frac{k_p}{K_p} = \frac{v_p}{c}, \quad \beta_{0p} = \frac{k_{0p}}{K_p} = \sqrt{1-\beta_p^2}, \quad \beta_e = \frac{v_e}{c}, \quad K_p = \sqrt{k_p^2 + k_{0p}^2}; \tag{15}$$

$\mathbf{k}_p = -\mathbf{k}_e - \mathbf{k}_{\bar{\nu}}$ is the recoil momentum.

On the assumption that the recoil momentum is small ($k_p \ll k_{0p}$, $\beta_{0p} \approx 1$), from (14) after integration over the solid angle $d\Omega_{\bar{\nu}} = \sin\theta_{\bar{\nu}} d\theta_{\nu} d\varphi_{\nu}$ of emission of the antineutrino, we obtain the following expression for the angular distribution of the decay electrons from a polarized neutron at rest, taking into account the longitudinal polarization of the electron, antineutrino and recoil proton:

$$W(\theta, s_e, s_{\bar{\nu}}) = \pi\eta_{VA}\{1 - \eta_2^{VA} s_{\bar{\nu}}\beta_e \cos\theta + s_e[\eta_2^{VA}\cos\theta - s_{\bar{\nu}}\beta_e +$$
$$+ \eta_3\left(\frac{\hbar}{m_{0p}c}\right)\left((1+\eta)(\cos\theta - \beta_e s_{\bar{\nu}})k_{\bar{\nu}} - s_{\bar{\nu}}(1-\eta)\left(k_e + \frac{1}{3}k_{\bar{\nu}}s_{\bar{\nu}}\cos\theta\right)\right)] -$$
$$-\eta_3\left(\frac{\hbar}{m_{0p}c}\right)\left[(1+\eta)(\beta_e s_{\bar{\nu}}\cos\theta - 1)k_{\bar{\nu}} - (1-\eta)\left(k_e + \frac{1}{3}k_{\bar{\nu}}s_{\bar{\nu}}\cos\theta\right)\beta_e\right]\}; \tag{16}$$

here

$$\cos\theta = (\mathbf{s}_n \mathbf{k}_e^0), \quad \eta_{VA} = |C_V|^2 + 3|C_A|^2,$$
$$\eta_2^{VA} = \frac{1}{\eta_{VA}}(2|C_A|^2 + C_V^+ C_A + C_A^+ C_V), \quad \eta_3 = \frac{1}{\eta_{VA}}(|C_V|^2 + |C_A|^2),$$

$p_e = \hbar k_e$ and $p_{\bar{\nu}} = \hbar k_{\bar{\nu}}$ are the momenta of the electron and antineutrino, and m_{0p} is the proton rest mass. In Eq.(16) the terms s_e and $s_{\bar{\nu}}$ characterize parity nonconservation in β-decay of a polarized neutron. Summing (16) over longitudinal polarizations of the electron (s_e), we obtain the following expression for the angular distribution of electrons taking into account recoil:

$$W(\theta) = \sum_{s_e = \pm 1} W(\theta, s_e, s_{\bar{\nu}}) = 2\pi\eta_{VA}\left\{1 - \eta_2^{VA} s_{\bar{\nu}}\beta_e\cos\theta -\right.$$
$$\left. -\eta_3\left(\frac{\hbar}{m_{0p}c}\right)\left[(1+\eta)(\beta_e s_{\bar{\nu}}\cos\theta - 1)k_{\bar{\nu}} - (1-\eta)\left(k_e + \frac{1}{3}k_{\bar{\nu}}s_{\bar{\nu}}\cos\theta\right)\beta_e\right]\right\}. \tag{17}$$

Eqs.(14)-(17) enable us to investigate the influence of proton recoil on the angular distribution and degree of longitudinal polarization of the decay electrons from a polarized neutron at rest. The degree of polarization $P(\theta)$ of electrons emitted at angle θ to the direction of the neutron spin can readily be determined from (16) by means of Eq.(13) in Refs.2 & 3.

If in Eqs.(16) and (17) we neglect proton recoil ($m_{0p} \to \infty$), we obtain Eqs. (11) and (14) of Ref.2 & 3 for the angular electron distribution. In this case the V - A form of interaction with $C_A/C_V \approx -1.2$ and a right-handed antineutrino ($s_{\bar{\nu}} = 1$) is in good agreement with the results of measurements associated with the decay of a polarized neutron[2,3,7,8].

4. Now let us consider muon decay. Invoking (12) and (13), from Eqs.(8) and (9) we obtain the following expression for the square of the matrix element of decay in flight of a fully polarized muon, taking into account the longitudinal polarization of the particles formed:

$$|M_{\mu e}|^2 = \frac{1}{8}\xi(1 - \beta_e s_e s_\nu)(1 + s_{\nu'}s_\mu\beta_\mu)(1 + s_\nu s_{\nu'}\eta)\{2 + s_\nu(1 - s_\nu s_{\nu'})(\mathbf{s}_\mu \mathbf{k}_\nu^0) -$$
$$-(1 + s_\nu s_{\nu'})(\mathbf{k}_{\nu'}^0 \mathbf{k}_\nu^0) + s_e[(1 + s_\nu s_{\nu'})(1 - (\mathbf{k}_{\nu'}^0 \mathbf{k}_\nu^0))(\mathbf{s}_\mu \mathbf{k}_e^0) +$$
$$+ s_{\nu'}(1 - s_\nu s_{\nu'})(s_{\nu'}(\mathbf{s}_\mu \mathbf{k}_\nu^0) - 1)(\mathbf{k}_e^0 \mathbf{k}_{\nu'}^0)]\}; \tag{18}$$

here $\beta_\mu = \frac{v_\mu}{c}$ and $s_\mu = s_\mu \mathbf{k}_\mu^0$ are the velocity and spin vector of the μ-meson; if the μ-meson is polarized in the direction of motion $s_\mu = 1$, while if it is polarized in the opposite direction $s_\mu = -1$. Recent experimental results[9] apparently indicate that μ^--mesons appearing in the decay of π^--mesons are polarized in the direction of their motion ($s_{\mu^-} = 1$). If in agreement with the theory of β-decay[1-4,10-12], the neutrino and antineutrino emitted in decay of $\mu^\mp$-mesons are, respectively, left-hand and right-hand polarized, then in (18) for $\mu^- \to e^-$ decay we must take $s_\nu = 1$ and $s_{\nu'} = -1$ (ν = antineutrino, ν' = neutrino), while in $\mu^+ \to e^+$ decay we must set $s_\nu = -1$ and $s_{\nu'} = 1$ (ν = neutrino, ν' = antineutrino).

Then from (18) we obtain

$$|M_{\mu e}|^2 = \frac{1}{4}\xi(1-\eta)(1 \mp \beta_\mu s_\mu)(1 \mp \beta_e s_e)(1 \pm (\mathbf{s}_\mu \mathbf{k}_\nu^0))(1 \pm s_e(\mathbf{k}_e^0 \mathbf{k}_{\nu'}^0)); \qquad (19)$$

here and below the upper sign pertains to decay of a μ^--meson, while the lower sign to decay of a μ^+-meson; the momentum of one neutrino is readily eliminated by means of conservation laws:

$$K_\mu = K_e + k_{\nu'} + k_\nu,$$
$$\mathbf{k}_\mu = \mathbf{k}_e + \mathbf{k}_{\nu'} + \mathbf{k}_\nu.$$

For a polarized $\mu^\mp$-meson at rest ($\beta_\mu = 0$) and for high energy electrons ($\beta_e = 1$) Eq.(19) becomes

$$|M_{\mu e}|^2 = \frac{1}{4}\xi(1-\eta)(1 \mp s_e)(1 \pm s_e(\mathbf{k}_e^0 \mathbf{k}_{\nu'}^0))\left[1 \mp \frac{k_e(\mathbf{s}_\mu \mathbf{k}_e^0) + k_{\nu'}(\mathbf{s}_\mu \mathbf{k}_{\nu'}^0)}{k_{0\mu} - k_e - k_{\nu'}}\right]. \qquad (20)$$

Let us determine the helicity of $\mu^\mp \to e^\mp$ decay electrons and positrons. As will be evident from (20), for values of the parameter $\eta = -1$ for which $C_V = -C_A = G_\mu$, the square of the matrix element $|M_{\mu e}|^2$ is nonzero only with $s_e = -1$ (μ^--decay) and with $s_e = 1$ (μ^+-decay). Consequently, high energy electrons in μ^--decay must be polarized opposite to the direction of their motion ($s_{e^-} = -1$), while the high energy positrons emitted in μ^+-decay must be polarized in their direction of motion ($s_{e^+} = 1$). The presence of the factor $(1 \mp s_e)$ in (20) shows that the high energy electrons and positrons appearing in the decay of unpolarized $\mu^\mp$-mesons will also be fully longitudinally polarized ($s_{e^-} = -1$ and $s_{e^+} = 1$).

Such polarization of the electrons and positrons in $\mu^\mp$-decay is in agreement with the results of measurements. Recently the polarization of electrons and neutrons from muon decay was measured by determining the circular polarization of their bremsstrahlung by the method of absorption in magnetized iron[13,14]; it was found that the electron has negative helicity ($s_{e^-} = -1$), while the positron has positive helicity ($s_{e^+} = 1$).

From Eqs.(20) and (6) we obtain the following formula for the distribution of the longitudinally polarized electrons forming in the decay of a longitudinally polarized $\mu^\mp$-meson at rest:

$$dW(\theta, s_e) = \frac{k_{0\mu}^5 x^2 dx d\Omega}{384(2\pi)^4 c\hbar^3}\xi(1-\eta)\{(3-2x) \mp$$
$$\mp (2x-1)\cos\theta + s_e[(2x-1)\cos\theta \mp (3-2x)]\}, \qquad (21)$$

here θ is the angle between the muon spin and the electron momentum:

$$\cos\theta = s_\mu(\mathbf{k}_\mu^0 \mathbf{k}_e^0) = (\mathbf{s}_\mu \mathbf{k}_e^0),$$
$$x = \frac{k_e}{k_{e\,\max}} = \frac{2k_e}{k_{0\mu}}, \quad k_{0\mu} = \frac{m_{0\mu} \cdot c}{\hbar}.$$

Equation (8) deduced above can also be used for investigating the spin and angular correlations in lepton decay in flight of a fully longitudinally polarized strange particle ($\Lambda^0 \to p + e^- + \bar{\nu}$, etc.).

I am grateful to A.A.Sokolov for valuable discussions.

Physics Faculty,
Moscow State University

References

1. A.Sokolov & B.Kerimov, Ann.Phys. (DDR), 7, 46 (1958).
2. B.Kerimov, Izv.AN SSSR, Ser.fiz., 23, 924 (1959). (Trans.Bulletin, 23, 911).
3. B.Kerimov, Izv.vyssh.uchebn.zaved. Fizika (Bulletin of Higher Schools - Physics), No.4, 111 (1959); Nauchn doklvyssh shkoly, Fiz.-mat.nauki (Transactions of Higher Schools, Phys.-Math.Sciences), No.5, 151 (1958).
4. A.Sokolov, Nucl.Phys., 9, 420 (1959).
5. A.Sokolov, Vvedenie v kvantovuyu elektrodinamiku (Introduction to quantum electrodynamics), M., 1958.
6. A.Sokolov, Nuovo cimento, 7, 240 (1958); Zhur.eksp.i teor.fiz., 33, 794 (1957). (Trans.Soviet Physics - JETP.)
7. A.Sosnovskii, P.Spivak and others, Zhur.eksp.i teor.fiz., 35, 1059 (1958). (Trans.Soviet Physics - JETP.)
8. M.Burgy, V.Krohn, T.Novey, G.Ringo & V.Telegdi, Phys.Rev., 110, 1214 (1958); Phys.Rev.Letters, 1, 324 (1958).
9. W.A.Love, S.Marder, I.Nadelhaft, R.T.Siegel & A.E.Taylor, Phys.Rev.Letters, 2, 107 (1959).
10. J.Marklund & L.A.Page, Nucl.Phys., 9, 88 (1958).
11. M.Goldhaber, L.Grodzins & A.W.Sunyar, Phys.Rev., 109, 1015 (1958).
12. R.Feynman & M.Gell-Mann, Phys.Rev., 109, 193 (1958).
13. P.C.Macq, K.M.Crowe & R.P.Haddock, Phys.Rev., 112, 2061 (1958).
14. G.Culligan, S.G.F.Frank & J.R.Holt, Proc.Phys., Soc.A73, 169 (1959).

ELECTRON-POSITRON CORRELATION IN PAIR PRODUCTION BY A POLARIZED PHOTON

- B.K.Kerimov & I.M.Nadzhafov

1. In recent years there has been increased interest in investigation of the polarization properties of particles evinced in processes due to electromagnetic interactions. A number of authors[1-5] have calculated the differential cross sections for bremsstrahlung and electron-positron pair production by photons, taking into account the polarization of the particles involved. Of greatest interest, however, from the standpoint of comparison with experimental results are the integral cross sections for these effects.

In the present work we deduce the integrated (over all angles) cross sections for pair formation by photons and bremsstrahlung by electrons in the field of the nucleus for fixed longitudinal polarizations of all the particles participating in the process.

2. In the Born approximation the cross section for pair formation taking into account the longitudinal polarization of the electron, positron and incident photon, integrated over the solid angles of emission of the electron ($d\Omega_- = \sin\theta_- d\theta_- d\varphi_-$) and the positron ($d\Omega_+ = \sin\theta_+ d\theta_+ d\varphi_+$) is of the form

$$d\sigma_{ls_+s_-}(E_+, E_-) = \int d\Omega_+ \int d\sigma_{ls_+s_-}(\theta_+, \theta_-)\, d\Omega_- = \frac{1}{4} d\sigma_{B-H}(E_+, E_-) +$$
$$+ Z^2\alpha^3 \frac{c^2 p_+ p_- dE_+}{\varepsilon_\gamma^3} \{s_+s_- q_1(E_+, E_-) - ls_+ q_2(E_+, E_-) - ls_- q_3(E_+, E_-)\}; \qquad (1)$$

here $s_+ = \pm 1$ and $s_- = \pm 1$ are the eigenvalues of the projection operator $\vec{\sigma}_\pm \mathbf{p}_\pm / p_\pm$ characterizing the longitudinal polarization of the electron and positron spins[6]; for $s_+ = 1$ ($s_- = 1$) the spin of the positron (electron) is aligned with its momentum, while for $s_+ = -1$ ($s_- = -1$) the spin is directed opposite to the momentum. The quantity $l = \pm 1$ defines the circular polarization of the incident photon; $l = 1$ corresponds to a photon with right-handed polarization, while $l = -1$ corresponds to left-handed polarization. $E_\pm$ and $p_\pm$ are the total energies and momenta of the positron and electron, respectively; $\varepsilon_\gamma = E_+ + E_-$ is the energy of the incident photon. The functions $q_i(E_+, E_-)$ entering into (1), are very complicated and hence we shall not write them out here.

The deduced pair production cross section (1) is a generalization of the familiar Bethe-Heitler cross section $d\sigma_{B-H}(E_+, E_-)$ taking into account the $e^-\gamma$, $e^+\gamma$ and e^-e^+ spin correlations (terms ls_-, ls_+ and s_+s_-) due to longitudinal polarization of the electron and positron of the produced pair and the incident photon.

In the case of extreme relativistic energies, when $\varepsilon_\gamma, E_+, E_- \gg m_0c^2$, Eq.(1) is simplified and for the energy distribution of longitudinally polarized positron-electron pairs we obtain the simpler formula

$$d\sigma_{ls_+s_-}(E_+, E_-) = \bar{\varphi} \frac{dE_+}{\varepsilon_\gamma^3} \left(\ln \frac{2E_+E_-}{\varepsilon_\gamma m_0c^2} - \frac{1}{2}\right) \left\{\left(E_+^2 + E_-^2 + \frac{2}{3}E_+E_-\right) -\right.$$
$$\left. - s_+s_- \frac{1}{3}(E_- - E_+)^2 + ls_+ \varepsilon_\gamma \left(E_+ - \frac{1}{3}E_-\right) + ls_- \varepsilon_\gamma \left(E_- - \frac{1}{3}E_+\right)\right\}, \qquad (2)$$

where

$$\bar{\varphi} = Z^2 r_0^2 \alpha, \quad r_0 = \frac{e^2}{m_0c^2},$$
$$\alpha = \frac{e^2}{\hbar c} = \frac{1}{137}.$$

Upon averaging over the polarizations of the incident photon and summing over the longitudinal polarizations of the electron and positron Eq.(2) becomes the familiar Bethe-Heitler formula for the extreme relativistic case when all energies are large compared with the rest energy of the electron (Eq.(26.9) in Ref.7).

The integral cross section for production of longitudinally polarized pairs averaged over two polarizations of the photon is

$$d\sigma_{s_+s_-}(E_+, E_-) = \bar{\varphi}\frac{dE_+}{\varepsilon_\gamma^3}\left(\ln\frac{2E_+E_-}{\varepsilon_\gamma m_0c^2} - \frac{1}{2}\right)\left\{\left(E_+^2 + E_-^2 + \frac{2}{3}E_+E_-\right) - s_+s_-\frac{1}{3}(E_- - E_+)^2\right\}. \quad (3)$$

From Eq.(3) for the relative probabilities of production of pairs in states with spin correlations $s_+s_- = 1$ and $s_+s_- = -1$, we have

$$dW_1 = \frac{\{d\sigma\}_{s_+s_-=1}}{\{d\sigma\}_{s_+s_-=1} + \{d\sigma\}_{s_+s_-=-1}} = \frac{\varepsilon_\gamma^2}{3E_+^2 + 3E_-^2 + 2E_+E_-},$$

$$dW_2 = \frac{\{d\sigma\}_{s_+s_-=-1}}{\{d\sigma\}_{s_+s_-=1} + \{d\sigma\}_{s_+s_-=-1}} = \frac{2\left(E_+^2 + E_-^2\right)}{3E_+^2 + 3E_-^2 + 2E_+E_-}. \quad (4)$$

It follows from Eq.(4) that at ultrarelativistic energies the relative probability for pair formation in the state with $s_+s_- = -1$ (dW_2), corresponding to a positron and electron with antiparallel longitudinal polarizations ($s_+ = -s_-$) is greater than the relative probability for pair formation in the state with $s_+s_- = 1$ (dW_1), corresponding to a positron and electron with polarizations in the same direction ($s_+ = s_-$). If the energy of the incident photon is symmetrically distributed between the electron and positron

$$E_+ = E_- = \frac{1}{2}\varepsilon_\gamma,$$

then

$$dW_1 = dW_2.$$

By means of the substitutions $E_+ \to -E$, $E_- \to E'$, $\varepsilon_\gamma \to -\varepsilon_\gamma$, $s_+ \to s$, $s_- \to s'$ and $l \to -l$ from (2) we obtain the following expression for the integral cross section for circularly polarized bremsstrahlung ($l = \pm 1$) from a longitudinally polarized ($s = \pm 1$) ultrarelativistic electron taking into account the longitudinal polarization of the last in the final state ($s' = \pm 1$):

$$d\sigma_{lss'}(E, E') = \bar{\varphi}\frac{E'd\varepsilon_\gamma}{E\varepsilon_\gamma}\left(\ln\frac{2EE'}{\varepsilon_\gamma m_0c^2} - \frac{1}{2}\right)\times$$

$$\times\left\{\left(\frac{E^2 + E'^2}{EE'} - \frac{2}{3}\right) + ss'\frac{(E + E')^2}{3EE'} + ls\frac{\varepsilon_\gamma(3E + E')}{3EE'} + ls'\frac{\varepsilon_\gamma(3E' + E)}{3EE'}\right\}; \quad (5)$$

here $E = cp$ and $E' = cp'$ are the kinetic energies of the electron before and after emission of the bremsstrahlung, and ε_γ is the energy of the emitted photon. If we average Eq.(5) over the longitudinal polarizations of the initial electron and sum over the longitudinal polarizations of the emitted photon and the final electron, the terms proportional to ss', ls' and ls vanish and we obtain the Bethe-Heitler cross section for bremsstrahlung emitted by a nonpolarized ultrarelativistic electron (see Eq.(25.21) in Ref.7).

The authors are grateful to A.A.Sokolov for his constant interest in the work and discussion of the results.

Physics Faculty,
Moscow State University

References

1. B.K.Berimov & I.M.Nadzhafov, Izv.AN SSSR, Ser.fiz., 22,886 (1958). (Trans. Bulletin, 22, 879.)
2. K.W.McVoy, Phys.Rev., 111, 1333 (1958).
3. H.Banerjee, Phys.Rev., 111, 532 (1958).
4. H.Olsen & L.C.Maximon, Phys.Rev., 110,589 (1958); 114,887 (1959).
5. C.Fronsdal & H.Uberall, Phys.Rev., 111,580 (1958).
6. A.A.Sokolov, Vvedenie v kvantovuyu elektrodinamiku (Introduction to quantum electrodynamics), M., 1958.
7. W.Heitler, The Quantum Theory of Radiation, Oxford, 1954.

POLARIZATION ELECTRON-POSITRON CORRELATION IN PAIR PRODUCTION TAKING INTO ACCOUNT FINITE NUCLEAR SIZE

- B.K.Kerimov & F.S.Sadvkhov

1. The polarization properties of particles involved in bremsstrahlung emission by an electron and electron-positron pair production by photons in the Coulomb field of a point nucleus have been considered in Refs.1-6. At present it is of particular interest to investigate the influence of finite nuclear size on the polarization and angular correlations in pair production by high-energy photons. Experimental and theoretical investigation of the polarization correlation of the particles, in addition to the angular correlation, in the process of pair production in the region of high energies and large angles may yield significant information on the form factor and the root mean square radius of nuclear charge distribution.

In the present work we have found the dependence of the production cross section for longitudinally polarized electron-positron pairs on the positron emission angle, taking into account the finite size of the nucleus. The deduced cross section formula makes it possible to investigate the influence of the extent of the nucleus on the angular and longitudinal spin electron-positron correlations in the process of pair production.

2. At not very high energies the form factor $F(q)$ of the nuclear charge distribution $\rho(r)$ may be written in the form[7]

$$F(q) = \int_0^\infty \rho(r) \frac{\sin(qr)}{qr} 4\pi r^2 dr \approx 1 - \frac{1}{6} q^2 \langle r^2 \rangle, \tag{1}$$

here $\langle r^2 \rangle$ is the root mean square radius of charge distribution in the nucleus, and $\hbar\mathbf{q} = \hbar\boldsymbol{\varkappa} - \hbar\mathbf{k}_+ - \hbar\mathbf{k}_-$ is the momentum transferred to the nucleus in the process of pair production.

In the Born approximation, we obtain the following expression for the longitudinally polarized pair production cross section averaged over the polarizations of the incident photon and integrated over the electron emission angle ($d\Omega_- = \sin\theta_- d\theta_- d\varphi_-$), taking into account the finite size of the nucleus:

$$\begin{aligned} d\sigma_{s_+s_-}(\theta_+, \langle r^2 \rangle)\, d\Omega_+ &= d\Omega_+ \int |F(q)|^2 d\sigma^T_{s_+s_-}(\theta_+, \theta_-)\, d\Omega_- = \\ &= d\sigma^T_{s_+s_-}(\theta_+)\, d\Omega_+ - \eta_p \{\langle r^2 \rangle F_0(\theta_+) + s_+ s_- \langle r^2 \rangle F_2(\theta_+)\}\, d\Omega_+, \end{aligned} \tag{2}$$

wherein the functions $F_0(\theta_+)$ and $F_2(\theta_+)$ in the case of high particle energies (ε_γ, E_+, $E_- \gg m_0c^2$) are equal to

$$\begin{aligned} F_0(\theta_+) = \frac{1}{3}\Bigg\{ &-\frac{3}{2} + \frac{2}{1-\cos\theta_+} - \frac{\varkappa^2}{2T_p^2} - \frac{\varkappa^2 k_-}{2T_p^2 k_+ (1-\cos\theta_+)} - \\ &- \frac{\varkappa^2}{4k_+k_-} L_p + \frac{\varkappa^2 k_+ \varepsilon^T}{2k_- T_p^3}(k_+ - \varkappa\cos\theta_+) + \frac{\varepsilon_-}{2k_+k_-}\left[\frac{k_+^2 + k_-^2}{1-\cos\theta_+} + k_+k_-\right]\Bigg\}, \end{aligned}$$

$$\begin{aligned} F_2(\theta_+) = \frac{1}{6k_+k_-}\Bigg\{ &-(k_+^2 + k_-^2 - 3k_+k_-) + 2(\varkappa^2 + 2k_-^2 - k_+k_-)\frac{1}{1-\cos\theta_+} + \\ &+ \frac{\varkappa^2 k_+k_-}{T_p^2} + \frac{\varkappa^2 k_-^2}{T_p^2(1-\cos\theta_+)} + \frac{\varkappa^2}{2} L_p - \frac{\varkappa^2 \varepsilon^T k_+^2}{T_p^3}(k_+ - \varkappa\cos\theta_+) - \\ &- \varepsilon_-\left[k_+(k_- - k_+) + (k_-^2 + k_+^2)\frac{1}{1-\cos\theta_+}\right]\Bigg\}, \end{aligned} \tag{3}$$

and

$$\varepsilon_- = 2\ln\frac{2k_-}{k_0}, \quad \varepsilon^T = \ln\frac{T_p + k_-}{T_p - k_-}, \quad L_p = 2\ln\frac{2k_+k_-}{\varkappa k_0},$$

$$T_p = |\vec{\varkappa} - \mathbf{k}_+|, \quad \eta_p = \frac{Z^2\alpha^3}{2\pi}\cdot\frac{k_+k_-dk_+}{\varkappa^3}, \quad \varkappa = k_+ + k_-. \tag{4}$$

Here $E_+ = c\hbar k_+$ is the kinetic energy of the positron and $E_- = c\hbar k_-$ is the kinetic energy of the electron in the extreme relativistic case, $\varepsilon_\gamma = c\hbar\varkappa = E_+ + E_-$ is the energy of the incident photon, $k_0 = \frac{m_0c}{\hbar}$ is the electron rest mass, and $d\Omega_+ = \sin\theta_+ d\theta_+ d\varphi_+$ is the solid angle positron emission; the quantities $s_- = \pm 1$ and $s_+ = \pm 1$ determine the projection of the electron and positron spins in the direction (+1) and opposite to the direction (-1) of their momenta (see Refs.2 & 8). For $s_- = 1$ ($s_+ = 1$) we have a right-hand polarized (spin parallel to the momentum), while for $s_- = -1$ ($s_+ = -1$) a left-hand polarized (spin antiparallel to the momentum) electron (positron). $d\sigma^T_{s_+s_-}(\theta_+)$ is the average over polarizations of the incident photon cross section for pair production on a point nucleus taking into account the longitudinal polarization of the produced electron and positron. The terms $\langle r^2\rangle$ describe the effect of finite size of the nucleus on the spin ($s_+s_-F_2$) and angular (F_0) electron-positron correlations. The presence in Eq.(2) of the spin correlation term s_+s_- indicates that even a nonpolarized photon of high energy may produce a pair consisting of a longitudinally polarized electron and positron. The electron and positron may have longitudinal polarizations in the same direction ($s_+ = s_-$, $s_+s_- = 1$) or in opposite ($s_+ = -s_-$, $s_+s_- = -1$) directions. Eq.(2) enables us in the general case to investigate the influence of the root mean square radius $\langle r^2\rangle$ of the nucleus on the angular distribution of the longitudinally polarized electron-positron pairs formed by nonpolarized high energy photons.

Thus, Eq.(2) is a generalization of the familiar Bethe-Heitler equation for pair production taking into account longitudinal spin correlation ($s_+ s_- = \pm 1$) between the electron and positron and finite nuclear size.

Suming Eq.(2) over the longitudinal polarizations of the electron and positron of the produced pair we obtain

$$d\sigma(\theta_+, \langle r^2\rangle)\, d\Omega_+ = d\sigma_{B-H}(\theta_+)\, d\Omega_+ - 4\eta_p\langle r^2\rangle F_0(\theta_+)\, d\Omega_+, \tag{5}$$

here $d\sigma_{B-H}(\theta_+)$ is the Bethe-Heitler production cross section for a nonpolarized pair on a point nucleus (see Ref.9), while the second term is the correction to the nonpolarized pair production cross section connected with taking into account the finite size of the nucleus.

We desire to thank A.A.Sokolov for his constant interest in the work.

Physics Faculty,
Moscow State University

References

1. B.K.Kerimov & I.M.Nadzhafov, Izv.AN SSSR, Ser.fiz., 22, 886 (1958), (Trans. Bulletin, 22, 879.); Nauchn.dokl.Vyssh.shkoly.Fiz.-mat.nauki (Transactions of Higher Schools, Phys.-Math.Sciences), No.1, 95 (1958).
2. B.K.Kerimov & I.M.Nadzhafov, Present issue of the Bulletin, p.156.
3. K.W.McVoy, Phys.Rev., 106, 828 (1957) & 110, 1484 (1958); 111, 1333 (1958).
4. H.Banerjee, Phys.Rev., 111, 532 (1958).
5. C.Fronsdal & H.Eberall, Phys.Rev., 111, 580 (1958).
6. H.Olsen & L.C.Maximon, Phys.Rev., 114, 887 (1959); 110, 589 (1958).

7. R.Hofstadter, Revs.Mod.Phys., 28, 214 (1956); Ann.Rev.Nucl.Sci., 7, 231 (1957).

8. A.A.Sokolov, Vvedenie v kvantovuyu elektrodinamiku (Introduction to quantum electrodynamics), M., 1958.

9. V.Heitler, The Quantum Theory of Radiation, Oxford, 1954.

Bulletin of the Academy of Sciences of the USSR - Physical Series
Vol. 25, No. 1 - January 1961

TABLE OF CONTENTS

Transactions of the Ninth All-Union Conference on Luminescence (Crystal Phosphors)
(To be continued in Vol.25, Nos.3 and 4)

	Page Orig.	Trans.
Opening address - V.L.Levshin	2	3
Luminescence of semiconductor crystals with excitation in the discrete structure region of the absorption spectrum - I.S. Gorban', S.N.Rud'ko & A.A.Shishlovskii	6	7
Role of impurities in the luminescence of molecular crystals at low temperatures - M.T.Shpak	13	13
Piezospectroscopic effect in anisotropic centers in cubic crystals - A.A.Kaplyanskii	20	20
Mechanism of energy storage by crystal phosphors - Ch.B.Lushchik, G.G.Liid'ya & I.V.Yaek	23	23
Effect of isostructure on the spectra of activated mixed crystals - F.D.Klement & L.A.Teiss	28	28
Investigation of luminescence processes in alkali halide phosphors - L.M.Shamovskii & P.A.Pipinis	31	30
Concerning the mechanism of optical flash decay - I.A.Parfianovich & E.I.Shuraleva	38	37
Exciton excitation of luminescence in activated alkali iodides at low temperature - M.L.Kats, K.E.Gyunsburg & L.I.Golubentseva	43	43
Atomic centers in NaCl:Ag and KBr:Ag crystal phosphors - V.K. Nikol'skii	45	45
Luminescence of nonactivated alkali iodides - N.N.Vasil'eva & Z.L.Morgenshtern	47	47

Transactions of the Tenth All-Union Conference on Nuclear Spectroscopy
(Concluded from Vol.24, Nos.3,7,9 & 12)

Analysis of second forbidden β-spectra - M.Vindushka & L.N.Zyryanova	52	53
Systematics of reduced lifetimes for β-transitions of different degrees of forbiddenness - L.N.Zyryanova & V.M.Mikhailov	56	57
Internal conversion with pair production in the decay of Ta^{182} - S.S.Vasilenko, M.G.Kaganskii, D.L.Kaminskii & S.F.Koksharova	61	62
Determination of the K-shell conversion coefficient of the 143 Kev transition in Pr^{141} by means of a 4π scintillation spectrometer - L.Nemet	68	68
Coulomb excitation of nuclear levels in P^{31}, S^{33}, Mn^{55} and Pr^{141} by Ne^{20} ions - D.S.Andreev, A.P.Grinberg, K.I.Erokhina & I.Kh.Lemberg	70	70
Probabilities for gamma-transitions in odd-odd deformed nuclei - D.A.Varshalovich	77	76
Electromagnetic transitions in deformed nuclei - Yu.N.Gnedin	83	82
Investigation of the decay schemes of Gd^{146}, Gd^{147} and Gd^{149} by means of a β-γ coincidence spectrometer - E.E.Berlovich, O.V. Larionov, E.N.Tunimanova & D.M.Khai	90	88
The Photoritron (A gamma-spectrometer for the low-energy region) - B.S.Dzhelepov & Yu.V.Khol'nov	98	95

Determination of the relative probabilities for electron capture from the L and K shells in the decay of Cr^{51}, Zn^{65} and Ge^{71} - A.A.Konstantinov & V.V.Perepelkin 106 103
Decay of Dy^{159} - E.I.Biryukov, O.I.Grigor'ev, B.S.Kuznetsov & N.S.Shimanskaya 109 106
Nuclear moments of odd gadolinium isotopes - N.I.Kaliteevskii, M.P.Chaika, I.Kh.Pacheva & E.E.Fradkin 111 107
The (d,t) reaction on O^{16}, O^{18}, Mg^{24}, Mg^{25} and Mg^{26} - N.A.Vlasov, S.P.Kalinin, A.A.Ogloblin & V.I.Chuev 115 111
The (n,α) reaction in Pu^{239} induced by thermal neutrons - V.N.Andreev 121 116
Masses of heavy atoms and nuclear binding energies in the 174 to 239 A region - R.A.Demirkhanov, T.I.Gutkin & V.V.Dorokhov 124 119
Comparison and systematics of the binding energies of heavy nuclei from hafnium to francium - V.A.Kravtsov 130 125
Scattering of fast neutrons by nonaxial nuclei - V.I.Belyak 139 133
Determination of the mean lifetime of the excited states of U^{235} fission fragments - B.M.Shiryaev 143 137
Collective excitations in superfluid nuclear matter - B.B.Dotsenko 145 139
Method of discriminating pulses due to fast neutrons from pulses due to γ-rays by means of photomultiplier space charge - G.G.Doroshenko & E.L.Stolyarova 152 146
Longitudinal polarization of particles in weak four-fermion interaction - B.K.Kerimov 157 150
Electron-positron correlation in pair production by a polarized photon - B.K.Kerimov & I.M.Nadzhafov 163 156
Polarization electron-positron correlation in pair production taking into account finite nuclear size - B.K.Kerimov & F.S.Sadykhov 166 158

Translated in 1962 by
Columbia Technical Translations
5 Vermont Ave., White Plains, N.Y.

Transactions

of the

Eleventh Annual Conference on Nuclear Spectroscopy

(Riga, 25 January - 3 February, 1961)

STRUCTURE OF LIGHT NUCLEI*

- V.V.Balashov, V.G.Neudachin & Yu.F.Smirnov

In the present report we shall discuss only two aspects of describing the properties of light nuclei, aspects which, in our opinion, are the most important and interesting: we shall consider use of the modern shell model for calculating the characteristics of the ground and low-lying states in nuclei and the question of correspondence of different models of light nuclei, the understanding of which has greatly advanced in recent years.

1. Many-particle Aspects of the Shell Theory

At present the shell model is extensively and successfully employed for calculating energy spectra, momenta, transitions probabilities and other properties of nuclei. Proposed initially for interpretation of the magic numbers and intended only for explanation of the "single-particle" spectrum, this model has undergone substantial modifications in recent years. In its modern form the shell model has increasingly become a model taking into account the distinctively many-particle properties of nuclear structure. As for the specific concepts of its first, simple version (independent particle model), such as the Weisskopf units for electromagnetic transitions and the Wigner single-particle limit for reduced nucleon widths, the range of their application is extremely limited; these concepts, in the main, have retained only the role of a physical scale for measuring the corresponding quantities.

According to the shell model, the main part of the nucleon-nucleon interaction in the nucleus is taken into account by introduction of a mean single-particle potential. However, this mean potential, the form of which determines the sequence of filling of the shells, does not comprise the entire interaction. The rest is the so-called "effective interaction", which removes the degeneracy of the levels with respect to the total momentum J of all the nucleons and the isotopic spin T, peculiar to the independent particle model. On the basis of the same considerations, it may be assumed[1] that the effective interaction is apparently less singular than the true interaction of the nucleons inasmuch as all fluctuations are averaged out. From this it can, apparently, be concluded that the shell model must correctly give the probability of finding two nucleons at a great distance (of the order of $2 \cdot 10^{-13}$ cm). As for the correlation of nucleons at small distances, it is usually assumed that inasmuch as the nucleon energies in the nucleus are small, these correlations only weakly affect the shape of the spectra and in individual cases can be taken into account in the form of corrections to the model.

In the present review we shall leave aside the questions of theoretical justification of the shell model, in particular, questions on the correspondence of the effective and true interactions, self-consistence and the like. We consider the shell model as a semi-empirical method, as a working tool with the aid of which one can successfully explain many experimental data and make certain predictions regarding low-lying nuclear levels. This viewpoint is consistent with the actual situation of this model among other nuclear models and correctly reflects its evaluation by the authors of numerous investigations in which the shell model is used for specific calculations. This view is also supported by the fact that all the principal inferences drawn on the basis of this model are found to be in excellent agreement with experiment.

---

*This review was presented at the Tenth All-Union Conference on Nuclear Spectroscopy, Moscow, 1960.

There are commonly distinguished two types of configuration mixing due to effective nucleon interaction.

The first type of mixing is connected with excitation of individual nucleons to higher shell states, differing from the ground state as regards the principal quantum number. Configurations corresponding to such excitations are usually called "higher configurations". Calculations carried out with a specific potential show that the admixture of higher configurations in the first approximation of perturbation theory is very small; it must be noted, however, that nothing is known regarding the convergence of the method of perturbation theory in the given case. Thus, neglect of the admixture of higher configurations is essentially a postulate of the shell model, which again is directly related with the semiempirical character of this model

The second type of configuration mixing is connected with addition of individual nucleon momenta and spins within shells with a given value of the orbital quantum number l. Under this second type one must also include mixing with respect to l within the range of the same principal quantum number n, characteristic of oscillator states (for example, $2s - 1d$ mixing). In general the character of the coupling proves to be very complex and the wave functions of states with a definite integral of motion represent linear combinations of functions determined in the limiting cases by LS or jj coupling.

Construction of wave functions in the shell theory

In this section we shall touch on some of the elementary questions of the formalism of the shell model, in order to introduce the basic concepts and designations necessary for further discussion; these concepts and designations are extensively used in the original investigations but, unfortunately, have not yet been adequately described in the Russian review literature.

In the shell model theory the state of the nucleons in the nucleus, in addition to the usual quantum numbers L (total orbital momentum), S (spin), J (total angular momentum), etc., are characterized by specific shell quantum numbers connected with the properties of the states relative to exchange of the particle coordinates. Related to these quantum numbers are the peculiarities of the energy spectra, the selection rules for reactions and electromagnetic transitions, etc. Thus, the simple matter of taking into account the Pauli principle is the primary and one of the most important aspects of the shell model.

LS coupling.[2] The LS coupling approximation is realized when one neglects the spin-orbit interaction of the outer nucleons with the nucleons in the filled shells

$$V_{sl} = -a \sum_i \mathbf{l}_i \mathbf{s}_i \tag{1.1}$$

as compared with the central pair interaction between nucleons

$$V = \sum_{i<j} V(r_{ij}). \tag{1.2}$$

In this case the total orbital momentum $\mathbf{L} = \sum_i l_i$ and the total spin $\mathbf{S}_i = \sum_i \mathbf{s}_i$ are integrals of motion. Additively, they form the total momentum of the nucleon system.

The total wave function of n nucleons must be antisymmetrical with respect to exchange of any pair of particle coordinates. It is equal to the product of the orbital function, which depends on the spatial coordinates of each nucleon,

by the spin-isotopic function, which depends on the generalized spin-isotopic variables $\gamma_i = \{\sigma_i, \tau_i\}$, which characterize the projection of the ordinary spin σ_i and the isotopic spin τ_i of the nucleon and can obviously assume four different values: $\{1/2, 1/2\}$, $\{1/2, -1/2\}$, $\{-1/2, 1/2\}$ and $\{-1/2, -1/2\}$. The property of symmetry of the orbital function can be represented by a Young diagram $[\lambda] = [\lambda_1, \lambda_2, \ldots]$, containing λ_i cells in the i-th row, for example

$[521] \equiv$

The function of n particles is symmetrical with respect to the variables in one row and antisymmetrical with respect to variables in a column. The symmetry properties of the charge-spin function are the opposite; in other words, it can be represented by a diagram similar to that above but rotated about the principal diagonal. Inasmuch as γ_i can assume only four different values, $[\lambda]$ cannot have more than four columns.

The greater the length of the row in Young's diagram, the more complete the symmetry of the orbital function; hence functions with the greatest symmetry correspond to a Young diagram with a maximum number of filled rows, i.e., with the maximum number of "fours".

Thus the functions characterizing the state of n nucleons in the l shell will be written in for form

$$\Psi = \Psi(l^n [\lambda]: {}^{2T+1,2S+1}L_J). \tag{1.3}$$

The introduction of Young's diagram $[\lambda]$ for classification of states in the LS coupling approximation is a generalization of the Russel-Saunders coupling scheme for the atom. There are, however, substantial differences between these two cases.

First, whereas in the atom $[\lambda]$ is uniquely determined by the spin S, in the nucleus there may correspond to the same values of the spin S and isotopic spin T different $[\lambda]$, and vice versa.

The second difference is connected with the attributes of interaction. The interaction of electrons in an atom is repulsion. Hence in an atom the ground state has the lowest orbital symmetry, i.e., has the greatest spin and the greatest L (Hund's rule). In a nucleus, the major part of the effective interaction is attraction. Hence here the ground state has the maximum orbital symmetry and the lowest value of L. Thus the ground state function in the nucleus in the LS coupling scheme is characterized by Young's diagram with a maximum number of "fours".

In the general case of central interaction containing different exchange terms, Young's diagram is not a good quantum number. However, if we restrict the consideration to only Wigner and Majorana forces that are independent of the spins and isotopic spins, $[\lambda]$ will be a good quantum number owing to orthogonality of the charge-spin functions corresponding to different $[\lambda]$.

In this particular case of LS coupling one can speak of the supermultiplet structure of the levels (the set of T and S corresponding to the given $[\lambda]$ is called the Wigner supermultiplet). The levels with different $[\lambda]$ prove to be greatly split in energy. Under actual conditions disturbance of the supermultiplet structure of the levels is produced both by noncentral, in particular, spin-orbit forces, and by central forces that depend on the spins and isotopic spins of the nucleons (Bartlett-Heisenberg forces).

Table 1

Classification of the ground states of p-shell nuclei in the LS and jj coupling limits

Nucleus	J, T	Classification LS-coupling	Classification jj-coupling	Nucleus	J, T	Classification LS-coupling	Classification jj-coupling
He^5	$^3/_2$, $^1/_2$	$p[1]:^{22}P_{3/2}$	$p_{3/2}:^3/_2\ ^1/_2$	B^{11}	$^3/_2$, $^1/_2$	$p^7[43]:^{22}P_{3/2}$	$p^7_{3/2}:^3/_2\ ^1/_2$
He^6	0,1	$p^2[2]:^{31}S_0$	$p^2_{3/2}:01$	C^{12}	0,0	$p^8[44]:^{11}S_0$	$p^8_{3/2}:00$
Li^6	1,0	$p^2[2]:^{13}S_1$	$p^2_{3/2}:10$	C^{13}	$^1/_2$, $^1/_2$	$p^9[441]:^{22}P_{1/2}$	$p_{1/2}:^1/_2\ ^1/_2$
Li^7	$^3/_2$, $^1/_2$	$p^3[3]:^{22}P_{3/2}$	$p^3_{3/2}:^3/_2\ ^1/_2$	N^{14}	1,0	$p^{10}[442]:^{13}S_1$	$p^2_{1/2}:10$
Be^8	0,0	$p^4[4]:^{11}S_0$	$p^4_{3/2}:00$	N^{15}	$^1/_2$, $^1/_2$	$p^{11}[443]:^{22}P_{1/2}$	$p^3_{1/2}:^1/_2\ ^1/_2$
Be^9	$^3/_2$, $^1/_2$	$p^5[41]:^{22}P_{3/2}$	$p^5_{3/2}:^3/_2\ ^1/_2$	O^{16}	0,0	$p^{12}[444]:^{11}S_0$	$p^8_{3/2}p^4_{1/2}:00$
Be^{10}	3,0	$p^6[42]:^{13}D_3$	$p^6_{3/2}:30$				

The well known classification of the ground states of p shell nuclei in the LS coupling scheme is given in Table 1.

By way of illustration of the selection rules associated with Young's diagram let us consider the nucleus C^{12} (configuration p^8). The possible Young diagrams for it are [44], [431], [422] and [332]. In the case of resonance capture of a p nucleon by B^{11} (configuration p^7, Young diagram [43]) or absorption of a γ-ray by C^{12} there can be excited only states with diagrams [44] and [431], and in capture of a deuteron by B^{10}, in addition, [422]. States with diagrams [422] and [332] cannot disintegrate with ejection of a nucleon to the lowest lying states of B^{11} or C^{11} with [43], i.e., they will disintegrate only by emission of nucleon associations (for example, $1s^4 \cdot 1p^8[332] \to 1s^4 \cdot 1p^3[3] + d + t$). Actually all these Young diagram selection rules are not rigorous.

jj Coupling.[3] jj Coupling is realized in the case when the interaction of the nucleons with each other is negligibly small as compared with the spin-orbit interaction. In this case the individual momentum j of the nucleon is an integral of motion. Combining with each other, the momenta of the outer nucleons form the total nuclear spin.

According to the theoretical group classification of nuclear states in the jj coupling model, the property of symmetry of the states of n particles with respect to exchange of the particle coordinates is characterized by the diagram $[\lambda] = [\lambda_1, \lambda_2, ..]$ for the spin-orbital part of the function and, accordingly, the conjugate (rotated about the principal diagonal) diagram $[\lambda^+]$ for the isotopic part. Thus, in the given case $[\lambda^+]$ may have not more than two rows and the Young diagram $[\lambda]$ is uniquely determined by the isotopic spin T of the state: $\lambda^+_1 = \frac{n}{2} + T$ and $\lambda^+_2 = \frac{n}{2} - T$. For example, for $n = 4$:

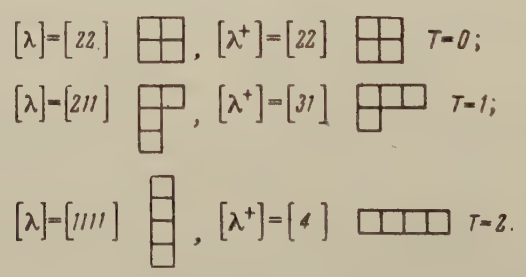

Among the j^n states with a given Young diagram $[\lambda]$ (isotopic spin T) there may be states in which part of the nucleons is combined in pairs ("paired") in a

state with $J = 0$. For classification of such states in a framework of the jj coupling model there is introduced an additional quantum number, the seniority s, equal to the number of unpaired nucleons. If one takes into account the interaction between nucleons, the state with the maximum number of paired nucleons (i.e., with the lowest seniority) proves to be energetically the most advantageous. Thus in the ground states of odd nuclei, characterized by the configuration j^n, there are paired all the nucleons except the last odd one: thus the seniority of such a state is 1, and the total nuclear momentum J equals the momentum of one nucleon j.

In the general case the total momentum J of the j^n state with a given T and s may assume different values.

Thus the state of n nucleons having the same individual momentum j is determined by the specified values of J and T, their projection on the Z axis and the seniority s. The wave function of such a state is written in the form

$$\psi = \psi(j^n(1, 2, \ldots, n) : sJT) \qquad (1.4)$$

(the classification of the ground states of p shell nuclei in the jj coupling scheme is given in Table 1).

The question of the precision of the seniority quantum number has been considered in the work of Flowers[4]. This question is intimately connected with the question of the accuracy of the jj coupling model, but does not reduce to it alone. It has been shown that seniority is a good quantum number in the limit of infinitely short range forces (δ interaction). If it is assumed that the seniority s is a good quantum number, there appear specific selection rules with regard to s, which are evinced in nuclear reactions and radiative transitions in nuclei. These rules are essentially the following[5]:

1) In reactions involving pick-up or emission of a j nucleon (initial configuration j^n, final configuration j^{n-1}, or vice versa) $\Delta s = \pm 1$.

2) In M3 transitions in cases when in the unfilled shells there is only a neutron or only a proton characterized by the configuration j: $\Delta s = 0$. The strong retardation, as compared with the single-particle transition probability of the M1 transition in V^{51}, corresponding to $\Delta s = 2$ (Ref.6) is connected with general forbiddenness of M1 transitions in the configuration j^n, $T = \frac{n}{2}$, so that forbiddenness with respect to s does not play any significant role (G.Lipkin, private communication).

3) In M3 transitions in the case of a configuration j^n formed by neutrons and protons, $\Delta s = 0$ or 2; in the case when $T = 0$, $\Delta s = 0$.

More detailed investigation of the symmetry properties of j^n states with respect to "pairing" leads to additional s selection rules for electromagnetic transitions.[7]

Application of the shell model to calculation of the energy spectra of light nuclei

The actual situation in light nuclei proves to be intermediate between the extreme cases of LS and jj coupling. This is due to the fact that neither the spin-orbit interaction of the outer nucleons with the nucleons of the filled shells nor the pair interaction of the nucleons with each other is predominant.

The first calculations of the levels in p shell nuclei, carried out in 1953 by Inglis[8], showed that some information on the sequence of levels in such nuclei can be obtained by reasonable extrapolation of the spectra calculated for the extreme LS and jj coupling cases into the intermediate region. At the same time it

became clear that for more detailed determination of the level schemes one must know the specific properties of the effective residual interaction between the outer nucleons.

What is the contribution of different exchange terms in this interaction? Must one take into account tensor forces? Can one reduce spin-orbit interaction of the nucleons to single-particle spin-orbit forces? Despite numerous investigations and some advances in the field, these questions remain largely unsolved.

The most fundamental work on the intermediate coupling model to date is that of Kurath[9] in which there were calculated the energy spectra of p shell nuclei. The actual approximations made in this work are in all cases identical with the approximations of the so-called intermediate coupling model.

According to this model the interaction of the outer nucleons is described by pair central forces and single-particle spin-orbit forces:

$$V = \sum_{i<j} V_{ij} - a \sum_i \mathbf{l}_i \mathbf{s}_i. \tag{1.5}$$

The potential V_{12} of the pair central nucleon interaction is assumed to be the same as for free nucleons; its parameters are chosen so as to satisfy the data on nucleon-nucleon scattering. In his work Kurath uses the Gaussian potential $V_{12} \sim e^{-(r_{12}/a)^2}$; other authors use the Yukawa potential for V_{12}.

V_{12} contains various exchange terms. The contribution from Wigner, Majorama, Bartlett and Heisenberg forces is characterized by coefficients introduced into the expression for V_{12}:

$$V_{12} = [W + MP_x + BP_\sigma + HP_xP_\sigma]\, V(r_{12}), \tag{1.6}$$

where P_x and P_σ are space and spin coordinate exchange operators, respectively.

Assuming that the central interaction consists of 80% Majorama forces and 20% Bartlett forces, Kurath calculates the position of levels in nuclei from Li^7 to C^{13} as a function of the parameter a/K, which is a measure of the ratio of the amplitude of spin-orbit forces to the Slater integral K, which is proportional to the amplitude of V_{12}. The actual calculations are complicated and require the use of a computer. As a result of his computations Kurath obtained good agreement with experiment as regards the order of the low-lying levels; the actual energy values obtained are, however, only approximate.

A quantitative inference from Kurath's calculations is the growth of the amplitude of the spin-orbit interaction a with filling of the shells from 1.6 Mev for Li^6 to 4.8 Mev for C^{13}. This is indicative of the fact that whereas in the lightest nuclei the actual situation is close to the LS coupling limit (thus the magnetic and quadrupole moments of Li^6 virtually coincide with those calculated according to the LS model) with increase of the spin-orbit interaction in going to larger mass numbers we approach the jj coupling limit.

The substance of all subsequent investigations in the framework of the intermediate coupling model[10] is essentially refinement of the parameters characterizing the pair central interaction. Most of these investigations are devoted to Li^6 and Li^7, calculations for which are more simple than calculations for nuclei in the middle of the shell. Thus in the work of Soper[11] on the levels of Li^6, by means of imposition of a certain addition condition, there are determined the exchange parameters of the central potential W, M, B and H and the principal independent integrals L and K, characterizing the amplitude and radial dependence of the potential $V(r_{12})$. The levels in Li^7 calculated on the basis of these results are in fairly good agreement with the experimental data. A characteristic of all such calculations is complete neglect of noncentral pair interaction. At the

same time investigation of such interactions is of undoubted interest.

Pair spin-orbit interaction. Noncentral interaction of nucleons is described in the framework of the usual intermediate coupling model by single-particle spin-orbit forces $V_{sl} = -a\sum_i l_i s_i$. The presence of a single-particle term in the many-particle Hamiltonian can be due only to averaging of the pair interactions. Thus, it can be shown[11] that single-particle spin-orbit forces appear as a result of averaging of pair spin-orbit interactions of the outer nucleon with the nucleons of the filled shells:

$$V_{sl}(1,2) = f(r_{12})(S_{12}L_{12}), \tag{1.7}$$

where S_{12} and L_{12} are the total spin and orbital momentum of the relative motion of two nucleons. Thus in description of nuclei containing one nucleon or one "hole" in the unfilled shell the single-particle and two-particle spin-orbit forces are simply equivalent. In the general case, however, this equivalence does not obtain. In this sense, use of the single-particle potential when the spin-orbit interaction of the outer nucleons with the nucleons of the filled shell is taken into account while their spin-orbit interaction with each other is rejected is inconsistent inasmuch as it does not correspond to any definite physical assumption regarding the potential.

The question is: how critical is rejection of this interaction? Calculations carried out on the basis of the experimental data for the levels of Li^6 (Ref.12) showed that taking into account the pair spin-orbit interaction between the outer nucleons leads to a substantial change in the value of the principal parameters describing the central interaction, which, in turn, substantially affects the position (energy) of calculated levels in other nuclei.

Tensor forces. The success of the "pure" intermediate coupling model, which disregards noncentral forces, naturally suggests that if any tensor forces are present in the effective interaction, their magnitude must be very small. At the same time it may be hypothesized that in a number of specific cases the role of even such "weak" forces may be appreciable. By way of a rather unique fact, presumably indicating the presence of tensor forces, there has been cited the case of the anomalously long lifetime of C^{14} with respect to β-decay. The long lifetime of C^{14} with $\log ft = 9.03$ for a typical allowed transition can be understood only by assuming a substantial reduction of the matrix element for this transition. Such a reduction can be explained by some sort of "accidental" overlapping of the wave functions of the initial and final states. All attempts to obtain such an overlapping, however, come up against the necessity of going outside the framework of the "pure" intermediate coupling model. Then there were introduced tensor forces[13]; this led to agreement with experiment. At first it seemed that the problem was solved, but then it was found that the tensor forces introduced in this case lead to quantitative divergence with experiment in calculating the properties of other nuclei.

Thus, on the one hand, for solution of the problem of C^{14}, one must seek other ways and, on the other hand, the actual role of tensor forces remains unclear.

In addition to taking into account noncentral interactions, there is another possibility of going outside the framework of the "pure" intermediate coupling model. The requirement of general radial dependence of different exchange terms of the central potential

$$V_{12} = [W + M \cdot P_x + BP_\sigma + H \cdot P_x P_\sigma] V(r_{12}) \tag{1.8}$$

is an additional restriction imposed on the central interaction of nucleons, which does not follow either from theory or from experiment. It is impossible to reject it in the framework of the usual theory, inasmuch as this would lead to a great increase in the number of model parameters. It can be done if we go from the ordinary to the so-called "shell" concept[12,14], the independent parameters of which are the matrix elements of the potential under consideration with respect to the basic model functions. The possibility of such improvement of the intermediate coupling model has only been suggested but not explored. The first calculations[12] show that the difference between the radial dependences of forces of different exchange character may be substantial.

All improvements of the model connected with extending the class of interactions require increasing the number of parameters characterizing the interaction. Very often in such cases the physical meaning of the parameters is completely lost in the ensuing complex and cumbersome calculations. Hence it is of interest to determine the basic quantities characterizing pair interaction of nucleons in the nucleus regardless of the specific form of the potential. This approach, which is analogous to the method of phase analysis in scattering, is basic to the method of direct determination of the nucleon-nucleon interaction Hamiltonian proposed in 1956 by Shirokov, Balashov & Tumanov[14]. These authors showed that in the case of oscillator functions for introduction of pair, isotopic invariant interaction between the p shell nucleons one must have 12 independent matrix elements ("phases"); (if one rejects the use of oscillator functions, the number of independent "phases" increases somewhat). No specific assumptions are made regarding the specific properties of the potential (including its exchange character, dependence on spins and velocity, radial dependence, etc.). In the framework of the shell description knowledge of the final number of such "phases" means "complete" knowledge of the effective interaction of the nucleons in the nucleus, sufficient for calculations of the levels and the shell functions of nuclei in the given shell. Unfortunately, experimental data on the levels in light nuclei now available are inadequate for realizing "complete" determination of all the independent "phases".

In connection with this it is of interest to examine a large group of investigations, foremost among which are the works of Talmi et al[15], wherein for description of the ground and low-lying excited states of light nuclei there are also made no particular assumptions regarding the specific properties of pair interaction; however, mixing of states with respect to j is not taken into account, and the state functions are taken for the jj coupling case. Thus, pair interaction, although strong, is considered as a perturbation with respect to the spin-orbit interaction, which is considered to be the principal interaction. It is surprising that this obviously inconsistent approach leads to excellent agreement with experiment and satisfactorily explains the energy variation of the ground states of nuclei within one shell with a given j. Such calculations have been carried out for the $1p_{3/2}$, $1p_{1/2}$, $2s_{1/2}$, $1d_{5/2}$, $1d_{3/2}$, $1f_{7/2}$ shells and for the levels of $p_{1/2}$ shell nuclei, corresponding to excitation of $2s_{1/2}$ states. By way of argument against this model, its opponents cite its inadequacy for calculating electromagnetic transitions and nuclear moments. The proponents of this model do not deny this shortcoming, but assert that the principal problem of theory is reproduction of the level spectrum and not derivation of the wave functions. In any case the undoubted success of this model justifies taking it seriously.

Electromagnetic moments and transitions in light nuclei

The many-particle character of the modern shell model is evinced, in particular, in that the probabilities for electromagnetic transitions, as well as the values of the magnetic and quadrupole moments, calculated according to this model for odd nuclei differ substantially from the respective single-particle values. The familiar and sometimes incorrectly invoked circumstance that the electromagnetic properties of such nuclei are completely determined by the last odd particle are fulfilled only in special cases. The question of when such special cases are realized has been fully solved by the modern shell theory.

For purposes of illustration let us compare the single-particle magnetic moments (Schmidt lines) with the values calculated according to the shell model (jj coupling).[16]

Table 2

Comparison of the single-particle magnetic moments (Schmidt lines) with the calculated values according to the shell model (jj coupling)

Nucleus	Configuration	T, J	μ Single-part.	μ_{ij}	Nucleus	Configuration	T, J	μ Single-part.	μ_{ij}
Li^7	$(p_{3/2})^3$	$1/2, 3/2$	3,79	3,04	F^{19}	$(s_{1/2})^3$	$1/2, 1/2$	2,79	2,79
Be^9	$(p_{3/2})^{-3}$	$1/2, 3/2$	—1,91	—1,16	Mg^{25}	$(d_{5/2})^3$	$1/2, 5/2$	—1,91	—0,64
	$(p_{3/2})^{-1}$		3,79	3,79		$(d_{5/2})^{-1}$		4,79	4,79
B^{11}	$(p_{3/2}^{-3})(p_{1/2})^2$	$1/2, 3/2$	3,79	3,04	Al^{27}	$(d_{5/2})^{-3}(s_{1/2})^2$	$1/2, 5/2$	4,79	3,52
C^{13}	$(p_{1/2})^1$	$1/2, 1/2$	0,64	0,64	Cl^{35}	$(d_{3/2})^3$	$1/2, 3/2$	0,13	0,26
N^{15}	$(p_{1/2})^{-1}$	$1/2, 1/2$	—0,26	—0,26	Cl^{37}	$(d_{3/2}^{-3})$	$3/2, 3/2$	0,13	0,13
O^{17}	$(d_{5/2})^1$	$1/2, 5/2$	—1,91	—1,91	Sc^{45}	$(f_{7/2})^5$	$3/2, 7/2$	5,79	5,10

As will be evident from Table 2, except for the trivial cases of one particle or one "hole" in the closed shell, the values of μ and μ_{ij} also agree in the case of Cl^{37}, which has three proton "holes" in the $d_{3/2}$ shell. This is explained by the fact that the ground state of j^n configurations is characterized by the lowest seniority. In the given $(d_{3/2})^{-3}$ case, seniority $s = 1$, i.e., two of the three "holes" are "paired" in a state with $J = 0$. Inasmuch as for two protons the magnetic moment of such a state equals zero, the moment of all $(d_{3/2})^{-3}$ configurations equals the magnetic moment of one "hole". At the same time, for example, in Cl^{35}, where the seniority also equals one, there may be paired either two neutrons or a neutron with a proton, and, consequently, the magnetic moment of the entire nucleus does not reduce to the magnetic moment of one $d_{3/2}$ neutron.

At present the experimental data on electromagnetic transitions in light nuclei are extremely scattered and with the exception of a few cases are rather inaccurate. However, analysis of these data from the standpoint of the intermediate coupling model[17] allows of drawing the following conclusions.

1) The probabilities for M1 transitions (as well as the values of the magnetic dipole moments) can be explained by the modern shell model. In any case the level of approximation is fully equal to the level of accuracy in the experimental data. By way of weighty substantiation one can cite the analysis by Lane[18] of C^{13} and N^{13}, where for one and the same value of the intermediate coupling parameter there are explained the positions of the level with $J = 3/2^-$, the value of the magnetic moment of C^{13}, the intensity of the magnetic dipole transition in N^{13}, the ft value of $N^{13} \rightarrow C^{13}$ β-decay, and the reduced width of the $3/2^-$ level in N^{13}.

2) Generally the shell model yields underestimates of the matrix elements of E2 transitions and of the quadrupole moments.

Inasmuch as detailed experimental investigation of electromagnetic transitions in light nuclei is a problem for the future, at present it is important to bear in mind the principal qualitative peculiarities of such transitions, which may serve as a guide in planning experiments.

M1 transitions. In 1958 Morpurgo[19] formulated selection rules for M1 transitions in nuclei with Z = N. Analysis showed that transitions between states with isotopic spin $T = 0$ are retarded by a factor of about 100 relative to transitions occurring with change of the isotopic spin. This rule is reminiscent of the familiar selection rule for electric dipole transitions according to which E1 transitions in nuclei with Z = N are strongly forbidden if the isotopic spins of the initial and final states are zero (in this case the dipole moment operator is simply proportional to the total momentum of the nucleus). In the case of M1 transitions the selection rule is approximate and apparently due to "fortuitous" variation of the numerical values of the anomalous magnetic moments of the proton and neutron.

The probability for an M1 transition between states a and b in a nucleus is proportional to the square of the following matrix element:

$$M = \left\langle a \left| \sum_{i=1}^{Z} \mathbf{L}_i + \sum_{i=1}^{Z} \mu_p \vec{\sigma}_i + \sum_{i=Z+1}^{A} \mu_n \vec{\sigma}_i \right| b \right\rangle, \tag{1.9}$$

where L is the orbital momentum and $\vec{\sigma}$ is the spin of the nucleon, and μ_p and μ_n are the magnetic moments of the proton and neutron, respectively. Expressing the nucleon charge in terms of projection of the isotopic spin τ^3 (for a proton $\tau_3 = 1$, for a neutron $\tau_3 = -1$)

$$e_i = e \frac{1 + \tau_3(i)}{2}, \tag{1.10}$$

one can in all three sums extend the summation from 1 to A:

$$M = \left\langle a \left| \sum_{i=1}^{A} \left\{ \mathbf{L}_i \frac{1 + \tau_3(i)}{2} + \mu_p \vec{\sigma}_i \frac{1 + \tau_3(i)}{2} + \mu_n \vec{\sigma}_i \frac{1 - \tau_3(i)}{2} \right\} \right| b \right\rangle. \tag{1.11}$$

In $T_\alpha = 0 \to T_b = 0$ transitions there is involved only the scalar part, with respect to isotopic spin, of the operator, and accordingly, the matrix element is of the form

$$M' = \frac{1}{2} \left\langle a \left| \sum_{i=1}^{A} \{ \mathbf{L}_i + (\mu_p + \mu_n) \vec{\sigma}_i \} \right| b \right\rangle. \tag{1.12}$$

Utilizing the fact that the matrix element of the total nuclear momentum operator $\vec{J} = \sum_{i=1}^{A} \left\{ \mathbf{L}_i + \frac{1}{2} \vec{\sigma}_i \right\}$ for orthogonal states a and b equals zero, we obtain

$$M' = \frac{1}{2} \left(\mu_p + \mu_n - \frac{1}{2} \right) \left\langle a \left| \sum_{i=1}^{A} \vec{\sigma}_i \right| b \right\rangle. \tag{1.13}$$

Inserting the numerical values of μ_p and μ_n, we finally obtain

$$M' = 0.19 \left\langle a \left| \sum_{i=1}^{A} \vec{\sigma}_i \right| b \right\rangle. \tag{1.14}$$

At the same time the matrix element of the transition occurring with change of T, associated with the vector part, with respect to the isotopic spin, of the opera-

tor, is roughly proportional to $\frac{1}{2}(\mu_p - \mu_n) = 2.35$. Thus we obtain

$$\left| \frac{M(T_a = 0 \to T_b = 0)}{M(\Delta\vec{T} = 1)} \right|^2 = 0.65 \cdot 10^{-2}.$$

The value of Morpurgo's rule is that it is not connected with any specific nuclear model and is based only on the property of isotopic invariance of nuclear forces.

E2 transitions. The above mentioned speeding up of E2 transitions and increase of the quadrupole moments given by experiment as compared with the values calculated on the basis of the shell model is usually attributed to collective motions in the nucleus. This effect was taken into account in the case of O^{17} by introduction of an additional effective nucleon charge $e' = \alpha e$, connected with excitation of collective quadrupole oscillations in the nucleus.[20] The O^{17} nucleus contains one neutron outside the filled shell corresponding to O^{16}. By setting $\alpha \approx 0.6$ it proved feasible to explain the anomalously high value of the probability of the $2s_{1/2} \to 1d_{5/2}$ E2 transition and the magnitude of the electric quadrupole moment of O^{17} in the ground state.

The appearance of an effective charge on the neutron owing to excitation of quadrupole oscillations of the core can be understood in the framework of the unified Bohr-Mottelson model[21] in the weak nucleon-nuclear surface coupling approximation. It is significant that this additional effective charge is the same for the proton and the neutron, i.e., the corresponding quadrupole transition operator contains only a scalar component with respect to the isotopic spin. Hence in transitions with change of isotopic spin these collective effects must be excluded and, consequently, it may be assumed that the shell model will give correct (with the same accuracy as for M1 transitions) values of the probabilities for such E2 transitions.[22]

Unfortunately, check of this rule for light nuclei is possible only in a small number of cases. Actually, experimental data are available only for one case: only the probability of the E2 transition from the 16.1 Mev, $J = 2^+$, $T = 1$ level in C^{12} to the ground state is known. Calculation of the probability for this transition on the basis of the shell model led to agreement with the experimental results.[22]

2. Alpha-Association and the Shell Model

Investigations carried out in recent years have shown that the α-model and the shell model are much closer than was assumed earlier. In any case, they are not mutually exclusive. For example, under certain conditions the wave functions for the two models are identical.

For the case of oscillator wave functions of the shell model it can readily be shown[23-25] that in the LS case, for example, the wave function for the lowest levels of Be^8

$$\psi^L_{Sh} = |s^4 | p^4 [\lambda] L \quad S = 0 \quad T = 0\rangle, \tag{2.1}$$

where $[\lambda] = 4$ (greatest possible symmetry of the orbital part of the wave function as a necessary condition) is identical with the α-model wave function. For $L = 0$ this α-particle wave function is of the form

$$A\psi_{\alpha_1}\psi_{\alpha_2}\varphi(R_{\alpha_1} - R_{\alpha_2}), \tag{2.2}$$

where ψ_{α_1} and ψ_{α_2} are the internal wave functions of the α-particle and

$$\varphi(R_{\alpha_1} - R_{\alpha_2}) = (R_{\alpha_1} - R_{\alpha_2})^4 \exp\left\{-\frac{(R_{\alpha_1} - R_{\alpha_2})^2}{b^2}\right\}. \quad (2.3)$$

The role of operator A (antisymmetrizator) is very significant, and without it there would be no agreement of the wave functions, inasmuch as in the given case the "internal dimensions" of the α-association and the mean separation between the α-particles are close.

Analogously the shell model wave functions for the low-lying states of Li^6 with Young's diagram [2] can be written in terms of the wave functions of the α-particle and deuteron. The wave function of O^{16} can be expressed in terms of the wave functions of two Be^8 nuclei, etc. If one does not use oscillator wave functions, qualitatively the picture remains the same. Thus if in a real nucleus the separation between the α-particles is close to the size of the particles, taking into account antisymmetrization, which is essential in this case, yields an α-model wave function close to the shell model wave function.

An undoubted advantage of the α-model is that in it there can naturally be taken into account the spatial correlations of four nucleons in the S state of relative motion. These correlations are in principle very important, as is indicated by the high binding energy of α-particles. In the shell theory for this one must use a number of admixtures of higher configurations, whereas in the α-model the four-particle correlation can be taken into account if the "internal dimension" parameter of α-association is not related beforehand with the magnitude of the mean separation between the α-particles in the nucleus. It is difficult at present to say to what extent use of the "conventional" α-model is justified. Despite the great success of the model in explaining, for example, the level diagram of O^{16} (Ref.26), the formal condition for applicability of the α-model ("dimensions" of α-association much smaller than the mean separation between the levels) is not fulfilled in this case. Investigation of the structure of the wave functions of the excited levels of C^{12} and O^{16} by means of (p,p'), (d,n), (α,α'), (He^3,p) and similar reactions can be helpful in answering the question of the value and validity of the α-model.

In the light of comparison of the two nuclear models let us consider the question of the binding energy of light nuclei. The assertion that the strong dependence of the binding energy of light nuclei on the number of nucleons (α-nuclei have particularly strong binding) is evidence in favor of the α-model (see, for example, Mamasakhlisov[27]) is actually not quite accurate inasmuch as the shell model leads to the same results. In the shell model, particularly in the case of LS coupling, α-nuclei have the greatest binding energy, inasmuch as all the nucleons are broken up into groups of four, in each of which the nucleons are in the S state of mutual motion, i.e., interact most strongly. The identity of Eqs.(2.1) and (2.2) illustrates this. Thus the general shape of the binding energy curve and its close periodicity with respect to "fours" are a rough characterization of the structure of the nucleus, which does not allow of giving preference to either one of the models.

It must be noted that having accepted α-association in the shell model nucleus for purposes of analysis, in addition to the above formal comparison of the models, we are enabled to calculate the reduced widths for α-particles, tritons, etc.

The method of calculation is the following.[28] Let there be given the state $|s^4, 1p^n\ [\lambda] LST\rangle$, where $[\lambda]$ is Young's diagram. By algebraic methods with the aid of genealogical coefficients we separate the wave function of the four particles $|1p^4[4]\ S=0\ T=0\rangle$, so that the wave function of the α-particles is of the form

$|s^4[4]\,L=0\;S=0\;T=0\rangle$, and require that the function of the separated four particles have the same "internal" quantum numbers as the α-particle function, i.e., $[\lambda]=[4]\,S=0\;\;T=0$). Further, we perform linear transformation of the coordinates in the wave function $|1p^4[4],L\,S=0\;T=0\rangle$, separating the motion of the center of mass of the four particles from their internal motion. This can be done rigorously only for oscillator wave functions. The wave function $|1p^4|\,[4]\;S=0\;T=0\rangle$, thus is written as the sum of a number of terms corresponding to internal states with different orbital momenta. Of interest to us will be the coefficient at the term containing the wave function of the ground state of the α-particle, i.e., when the orbital momentum of internal motion $\Lambda = 0$. Thus the expression for the reduced width contains, in particular, two factors: a genealogical coefficient for separating the four particles in the state $|1p^4[4]\;L\,S=0\;T=0\rangle$ and a coefficient indicating the relative weight in this state of the ground state of the internal motion of the α-particle.

Calculation of the reduced width by this method for Be^8, Li^7 (emission of a triton) and Li^6, as might have been expected, yielded reduced widths close to the Wigner limit. This method can also be used in calculating direct nuclear reactions. For example, let us take the $O^{16}(\gamma,pt)C^{12}$ reaction at $E_\gamma \approx 80$ Mev. Here one of the O^{16} α-particles is split by the γ-ray into t + p. The cross section for the reaction with formation of C^{12} in a certain state is equal to the cross section for the (γ,pt) reaction of an α-particle multiplied by a coefficient which might be called "the effective number of α-particles". Calculations for the 0^+, 2^+ and 4^+ levels of C^{12} yield values of 8/27, 40/27 and 72/27, respectively, for the "effective number of α-particles".

3. Collective Motion and the Shell Model

In their respective simple forms the collective model and the shell model are very different. One is based on the concept of a rotating nonspherical body, the other on the concept of a single nucleon moving in a spherical symmetrical potential well. The fact that these simple versions had only limited success led to the creation of more complex variants. Thus in 1955, Nilsson[29] introduced the concept of single-particle states of the nucleons in a deformed potential, which rotates adiabatically. Other investigators introduced into the shell model, as noted above, pair interaction of the outer nucleons and took into account mixing of configurations with close energy, as was done, in the calculations of Elliott & Flowers[20] for F^{19}. To what extent these more complex model versions differ (or are similar) was not clear until recently. Obviously, if in the framework of the shell model one takes into account the admixture of many higher configurations, then by means of this more complete system of functions one can describe collective motion. Another point is of interest: can the collective aspects of motion be described by means of the usual calculations of shell theory taking into account mixing of only very close configurations (for example, $2s$ and $1d$)? It was found that this is the case, inasmuch as use of both models for analysis of the properties of a number of light nuclei yielded equally good results.

We have already spoken above regarding use of the intermediate coupling model for analysis of the properties of nuclei up to F^{19}. For nuclei heavier than Ne^{20} the calculations become extremely cumbersome, inasmuch as the number of mixing states increases rapidly. Nevertheless, it was established for Mg^{24} that the level spectrum is close to rotational. Further, very successful was application of the Nilsson model to analysis of the experimental data for the neighboring Mg^{25} and Al^{25} nuclei.[30] For these nuclei the quantum numbers of more than ten levels are known and they are well described by a series of rotational bands corresponding to different values of K (K is the projection of the total angular

momentum on the nuclear symmetry axis). Nilsson's model correctly predicts the values of K and the K-selection rules given by Nilsson are consistent with the experimental data on transitions. This model was also successfully used by Paul[31] for F^{19} and even for p shell nuclei[32], where the shell model theory proved to be highly successful (see Section 1). The reasons for this success of the Nilsson model were brought out recently in a number of investigations, in particular, in the work of Elliott[33], Moszkowski[34] and others.

These authors attempted to describe the deformation and rotation of nuclei as a result of residual interaction between the nucleons. It has long been known (Ref.35) that for forces that are independent of the spin, the level energy of the $1p^n$ configuration in the LS coupling limit with a given Young diagram $[\lambda]$ is described by the rotational formula $L(L+1)$. This situation obtains, for example, in Be^8 (lowest levels 0^+, 2^+, 4^+). In heavier nuclei the rotational structure of the levels is less clearly pronounced inasmuch as it is disturbed by spin-orbit interaction. It should be noted that these rotational bands, in contrast to the bands of the usual collective model, are cut off at a certain L_{max}.

For other shells arbitrary forces independent of spin no longer give precise rotational bands, but the regular level sequence obtains. One may ask whether for some specific forces there will be realizes a regular rotational structure? On the whole, the question of the relation between deformation and, consequently, rotation of nuclei and the residual interaction remains complicated and unclear. At present only simple interactions have been investigated. Thus Elliott[33], who pioneered in this field, using the methods of group theory considered the $2s$ and $1d$ shells, the energies of which agree with the oscillator potential. He showed that if one neglects the admixture of higher configurations, quadrupole-quadrupole interaction of the form

$$V_{QQ}(r_{12}) = -\frac{4\pi}{5} C \sum_m r_1^2 r_2^2 Y_{2m}(\theta,\ \varphi)\, Y^*_{2m}(\theta_2\varphi_2) \tag{3.1}$$

leads to mixing of the degenerate $2s$ and $1d$ states and that the eigenfunctions obtained as a result yield a rotational level spectrum. Analysis of the work of Elliott would require extensive use of group theory, and we shall not carry it out here. We shall cite only a few illustrations from the work of Moszkowski[34], whose results are generally equivalent to those of Elliott.

The fact that forces of the QQ type produce deformation of the nucleus is evident from the following example. Let us consider the interaction of nucleons on the nuclear surface

$$V_{ik} = -\sum_m C\delta(r_i - R_0)\,\delta(r_k - R_0)\,\frac{4\pi}{5} Y_{2m}(\Omega_i)\, Y^*_{2m}(\Omega_k). \tag{3.2}$$

Assume that the nucleons at every given instant are in single-particle states (for simplicity we disregard the Pauli principle):

$$\psi(1, 2, \ldots, n) = \psi_1(1)\,\psi_2(2), \ldots \psi_n(n).$$

Let us determine the external potential, in addition to the average field, acting on the i-th particle. To this end we must average V_{ik} over the states of the other nucleons; as a result we obtain

$$-\sum_m \frac{4\pi}{5} C\delta(r_i - R_0)\, V_{2m}(\Omega_i) \left\langle \sum_{k\neq i} \delta(r_k - R_0)\, Y^*_{2m}(\Omega_k) \right\rangle, \tag{3.3}$$

where the term in the brackets is the averaged value of the operator.

On the other hand, in the collective model with quadrupole deformation of

the nucleus

$$R(\theta, \varphi) = R_0\left[1 + \sum_m a_{2m} Y_{2m}(\theta, \varphi)\right]$$

the nucleons, in a potential well of depth V_0 and radius R_0, undergo an additional interaction with the nuclear surface of the form

$$-\sum_m V_0 R_0 \alpha_{2m} \delta(r_i - R_0) Y_{2m}(\theta_i \varphi_i). \tag{3.4}$$

The potentials (3.3) and (3.4) agree on condition that

$$\alpha_{2m} = \frac{4\pi}{5} \frac{C}{V_0 R_0} \left\langle \sum_{k \neq i} \delta(r_k - R_0) Y^*_{2m}(\theta_k \varphi_k) \right\rangle. \tag{3.5}$$

It will be evident therefore that pair interaction between nucleons can be taken into account by introducing quadrupole deformation and that the magnitude of the deformation is proportional to the strength of the interaction.

If we consider not only the quadrupole interaction on the surface, but also interaction (3.1), we obtain that the field as seen by the nucleon i is of the form

$$V(r_i) = -\sum_m \frac{4\pi}{5} C r_i^2 Y_{2m}(\Omega_i) \left\langle \sum_{k \neq i} r_k^2 Y^*_{2m}(\Omega_k) \right\rangle, \tag{3.6}$$

i.e., on the average the motion of the particle i with the given state of the other nucleons is described by the Hamiltonian

$$H_i = T_i + \frac{m\omega^2 r_i^2}{2} - \frac{4\pi C}{5} \left\langle \sum_{k \neq i} r_k^2 Y^*_{20}(\Omega_k) \right\rangle r_i^2 Y_{20}(\Omega_i). \tag{3.7}$$

This, of course, is the Hamiltonian of a spheroidal oscillator. This means that if in the zeroth approximation there were used the wave functions of a spherical oscillator, for taking into account the residual interaction (3.1) it is essential to take the spheroidal oscillator wave functions (3.7). As a result there are obtained functions χ_k, having a definite projection K of the momentum on the nuclear spherical axis, but not corresponding to a definite total momentum J. These functions are defined in the system of axes connected with the nucleus (the Z axis is aligned with the nuclear symmetry axis). This is the internal function of the nucleus. To obtain the wave function of the state with momentum J in the laboratory system of coordinates, one can, as is done in the collective model, take into account rotation of the nucleus by multiplying the internal function by the Wigner D-function, which depends on the collective coordinates (the Euler angles ξ, η, ζ):

$$\psi_{JM}(r) = D^J_{MK}(\xi, \eta, \zeta) \chi_k(r_{in}). \tag{3.8}$$

Here, however, there are encountered difficulties associated with the fact that the collective coordinates are "superfluous" degrees of freedom, inasmuch as the internal function depends on the coordinates of all n particles as on independent variables. In the right-hand part of (3.8) the number of degrees of freedom is $3n + 3$, whereas in the left part the number is $3n$. While this difficulty is not serious where heavy nuclei are concerned, for light nuclei it may be significant. Hence a different method of constructing the wave functions in the laboratory system is employed. According to the usual procedure, the component with a given J is separated in the internal functions by means of the Wigner D-function:

$$\psi_{JM}(r) = \int D^{J}_{MK}(R)\,\chi_K(R^{-1}r)\,dR, \tag{3.9}$$

where R is the set of Euler angles. Expression (3.9) is a Hill-Wheeler type integral. Here we have carried out averaging over the orientations of the nuclear axis in space. Moszkowski[34] showed that the wave function (3.9) is a precise eigenfunction of the residual interaction (3.1).

Let us consider the average value of the operator of some physical quantity R over the functions (3.9):

$$\langle \psi_{JM} | E | \psi_{JM} \rangle = \int D^{J+}_{MK}(R')\,\chi^{*}_K(R^{-1}r)\,F D^{J}_{MK}(R)\,\chi_K(R^{-1}r)\,dR\,dR'\,dr =$$

$$= \int DJ^{*}_{MK}(R')\,D^{J}_{MK}(R)\,F_{KK}(R', R)\,dR'\,dR, \tag{3.10}$$

where

$$F_{KK}(R', R') = \int \chi^{*}_K(R'^{-1}r)\,F\chi_K(R^{-1}r)\,dr. \tag{3.11}$$

The value of $F_{KK}(R', R)$ depends on the angle ω between the orientations of the nucleus R' and R; if with increase of this angle the overlapping of the functions $\chi_K(R'^{-1}r)$ and $\chi_K(R^{-1}r)$ decreases rapidly (and this occurs in the case of a large number of particles[37]), we find that $F_{KK}(R', R)$ behaves like $\delta(\omega)$ and for the matrix element we have

$$\langle \psi_{JM} | F | \psi_{JM} \rangle = \int D^{J}_{MK}(R)\,D^{J'}_{MK}(R)\,F_{KK}\,dR, \tag{3.12}$$

i.e., the same situation as is obtained with the functions (3.8) in the framework of the ordinary collective model. Moreover, the functions (3.9) with a residual interaction (3.1) yield a rotational spectrum. Thus it may be asserted that these functions describe the rotational properties of nuclei in the framework of the shell model.

Let us now touch on the question of the role of different multipoles in expansion of the residual interaction:

$$V_{ij} = \sum_{\lambda} f_\lambda(r_i, r_j)\,P_\lambda(\cos\omega_{ij}). \tag{3.13}$$

The functions (3.9) are precise functions only for interaction of the form of (3.1). What will happen in the case of participation of the forces of higher multipoles or for different radial dependence of the forces? This question, although of great interest, has not yet been investigated in detail. Bayman[38] showed that for low multipoles the functions (3.9) yield a rotational spectrum for any radial dependence of the forces. In the case of more complex interaction the functions (3.9) can be used as the starting point for variational computations.[39]

If configuration mixing is neglected, for the p shell there will be significant only terms with $\lambda = 0$ and 2. The matrix elements of the term with $\lambda = 0$ do not depend on L, although they may depend on Young's diagram $[\lambda]$. There remain only the terms with $\lambda = 2$, which leads to the above mentioned cutting off of the rotational spectrum. In the case of the $(2s - 1d)$ shell the situation becomes more complicated inasmuch as terms with $\lambda = 4$ also begin to play a significant role and in the case of a small number of particles there occur deviations from the rotational spectrum.

Inasmuch as for the p shell there will be effective multipoles not higher than quadrupoles, it may be assumed that the functions (3.9) will be a fairly good approximation to the true functions. True, for higher accuracy one must take into account spin-orbit interaction. For this it is better to use by way

of the internal wave functions χ_k in Eq.(3.9) not simply the functions of a spheroidal oscillator but, for example, Nilsson's functions[29] taking into account ls interaction. Such calculations were carried out for p shell nuclei by Kurath & Picman[40], who found that the wave functions (3.9) agree (95-100%) with the intermediate coupling wave functions[9]. In order to obtain agreement it was necessary to attribute a large deformation to the nucleus (ellipsoid semi-axis ratio 2-3; "cigar" shaped nucleus for a small number of particles, disk shaped nucleus for an almost filled shell). It is interesting to note that application to light nuclei ($4 < A < 32$) of the pure collective model[32], i.e., use of the function (3.8) also leads to large deformation of the nuclei with a semi-axis ratio of 1.5-2, which, however, is on the average less than the ratio used by Kurath & Picman.

On the other hand, the functions of Kurath & Picman, being equivalent to the intermediate coupling functions, yield quadrupole moments smaller by a factor of ~2 than the experimental moments, although the deformations are greater. Actually, however, it is difficult to compare directly the results of Kurath & Picman[40] and those of Gonchar, Inopin & Tsytko[32] because the latter took into account configuration mixing with respect to the principal quantum number, i.e., polarization of the core, although they did not use the integral form of (3.9), whereas Kurath & Picman used the integral form of (3.9), but did not take into account mixing of configurations with respect to the principal quantum number, although in the presence of great deformations this is very important in calculating the quadrupole moments. It would be interesting to see calculations carried out without these simplifications. There will probably be obtained fairly large deformations with a semi-axis ratio ≈2.

4. Experimental Problems

The formalism of the modern theory of light nuclei has been developed to a high degree. For checking it and for further development, the scanty and extremely scattered experimental data now available are inadequate. It is essential now to undertake systematic investigation of light nuclei, aimed at clarifying the character of nucleon interaction; this is necessary both for refining the shell model and for determining the relation of this model with other nuclear models.

Such investigation can initially be restricted to a small number of nuclei, but the information obtained regarding their properties must be as comprehensive as possible. This information must include data on the positions, spins, and isotopic spins of the low-lying states up to an energy of ~10 Mev, the values of the radiation widths, reduced widths and (for β-active nuclei) lifetimes. From the standpoint of theoretical value and present experimental possibilities of greatest interest in this respect are nuclei at the end of the p shell with A = = 13, 14 and 15, as well as the already fairly thoroughly investigated nucleus B^{10}.

As for the particular problems in the field of light nuclei, in our opinion, the following are the most urgent and interesting:

1) Levels in Li^7. From the standpoint of checking the theory it would be of particular interest to investigate the 4.63 Mev level in Li^7 which, according to some calculations[12], has spin $7/2^-$, and according to others[41], $5/2^-$. Study of the (d,p) reaction on Li^6 at a number of deuteron energies should prove useful. The angular distribution should differ from the Butler distribution and will probably be characterized by Bowcock's formula[42] for spin-flip stripping. Scattering of H^3 from He^4 through the 4.63 Mev level should occur with $L = 3$.

2) Calculation[43] of the levels of Li^7 leads to the inference that there may exist nuclearly stable β-active He^7. To check this there can be used the following reactions:

$Li^7(n,p)$ $Q \approx -10$ Mev,
$Li^7(t,He^3)$ $Q \approx -11$ Mev,
$Li^7(d,2p)$ $Q \approx -12$ Mev,
$Be^9(\gamma,2p)$ $Q \approx -29$ Mev,
$Be^9(n,He^3)$ $Q \approx -26$ Mev,
$C^{12} + \pi^- \rightarrow He^7 + \alpha + p$; $Li^7 + \pi^- \rightarrow He^7$.

3) Of particular interest is the nature of the 0^+ excited levels in C^{12}, O^{16}, Ne^{20} and other nuclei. These levels are, naturally, treated in the framework of the α-model and apparently cannot be described from the standpoint of the shell model without configuration mixing. The 0^+ level in C^{12} is not excited in elastic scattering of protons, but is excited, for example, in the $Be^9(\alpha,n)C^{12*}$ reaction. For analysis of the structure of wave functions it would be useful to investigate the $B^{11}(d,n)C^{12*}$, $N^{15}(d,n)O^{16*}$ and similar reactions at different energies.

4) It is desirable to investigate E2 transitions in nuclei close to Mg with change of isotopic spin. Here one can expect the collective increase of the transition probabilities to be weakened.[22]

5) There are a number of experimental spectroscopic problems that are of interest from the standpoint of the theory of photonuclear reactions.[44]

A. Deuteron initiated stripping reactions with the formation of single-particle levels the parity of which is opposite to that of the ground state of the final nucleus. An important example would be to find the level corresponding to capture of a $d_{5/2}$ proton by B^{11}. This level, on the assumption of weak binding of the s and d nucleons with the p core[44], should lie close to the threshold for the $C^{12}(\gamma,p)$ reaction, but so far has not been detected.

B. The inverse stripping reaction (p,d) with pick-off of a nucleon from an inner shell in such nuclei as Mg^{24}, where there is a large number of nucleons outside the filled shell. Also of interest would be experiments involving the (p,d) reaction on nuclei with closed shells; for example, it would be desirable to determine the energy of the $d_{5/2}^{-1}$ and $2s_{1/2}^{-1}$ levels in Ca^{39}. Here, apparently, $Q \approx -24$ and -20 Mev, respectively. Similar determinations might be made for Ni^{60}.

C. Elastic scattering of protons of energies up to 8 Mev should give information on single-particle levels of outer shells. In such experiments one must study the angular distributions by means of an instrument with a sufficiently high resolution in order to be able to determine the orbital momenta. An experiment of this type was recently performed by Class, Davis & Johnson[45].

Scientific-Research Institute of Nuclear Physics,
Moscow State University

References

1. S.A.Moszkowski, I.P.Elliott & A.M.Lane, Handbuch der Physik, 39.
2. H.A.Jahn, Proc.Roy.Soc., 201, 516 (1950); A205, 195 (1950); H.A.Jahn & van Wieringen, Ibid., A209, 502 (1951); B.H.Flowers, Ibid., A210, 497 (1951).
3. B.H.Flowers, Proc.Roy.Soc., A212, 248 (1952); A.R.Edmonds & B.H.Flowers, Ibid., A214, 248 (1952).
4. B.H.Flowers, Phys.Rev., 86, 254 (1952); Physica, 18, 1101 (1952).
5. V.G.Neudachin, Zhur.eksp.i teor.fiz., 31, 891 (1956). (Trans.Soviet Physics - JETP.)
6. N.N.Delyagin & M.Preisa, Ibid., 36, 1586 (1959). (Trans.Ibid.)
7. V.V.Balashov, Ibid., 36, 1387 (1959). (Trans.Ibid.)

8. D.R.Inglis, Revs.Mod.Phys., 25, 300 (1953).
9. D.Kurath, Phys.Rev., 101, 216 (1956).
10. S.Meshkov & C.W.Ufford, Phys.Rev., 101, 734 (1956); J.M.Soper, Phil.Mag., 2, 1219 (1957).
11. J.Hughes & K.J.Le Conteur, Proc.Phys.Soc., A63, 1219 (1952); I.P.Elliott & A.M.Lane, Phys.Rev., 96, 1660 (1954).
12. V.V.Balashov, Zhur.eksp.i teor.fiz., 36, 1123 (1959). (Trans.Soviet Physics - JETP.)
13. W.M.Visscher & R.A.Ferrell, Phys.Rev., 107, 781 (1957); T.H.R.Skyrme, Nucl.Phys., 9, 641 (1959).
14. Yu.M.Shirokov, V.V.Balashov & A.K.A.Tumanov, Zhur.eksp.i teor.fiz., 32, 167 (1957) (Trans.Sov.Phys. - JETP.); V.V.Balashov, Thesis, Moscow State University, 1958.
15. I.Talmi & R.Thieberger, Phys.Rev., 103, 718 (1956); I.Unna & I.Talmi, Phys.Rev., 112, 452 (1958).
16. B.J.Blin-Stoyle, Revs.Mod.Phys., 24, 75 (1956).
17. D.Kurath, Phys.Rev., 106, 975 (1957).
18. A.M.Lane, Proc.Phys.Soc., A66, 977 (1953); A68, 197 (1955).
19. G.Morpurgo, Phys.Rev., 110, 721 (1958).
20. I.Elliott & B.H.Flowers, Proc.Roy.Soc., A229, 536 (1955); B.H.Flowers, in "Yadernye reaktsii pri malykh i srednikh energiyakh" (Nuclear reactions of low and medium energies), M., 1958; B.J.Raz, Phys.Rev., 107, 1201 (1957); R.D. Amado, Phys.Rev., 108, 1462 (1957).
21. A.Bohr & B.Mottelson, Kgl.Danske Videnskab.Selskab.Mat.-fys.Medd., 27, No.16 (1953).
22. V.V.Balashov & A.F.Tulinov, Zhur.eksp.i teor.fiz., 36, 615 (1959). (Trans.Soviet Physics - JETP.)
23. T.H.R.Skyrme & I.K.Perring, Proc.Phys.Soc., A69, 600 (1956).
24. B.F.Bayman & A.Bohr, Nucl.Phys., 9, 596 (1959).
25. V.G.Neudachin, Yu.F.Smirnov & N.P.Yudin, Zhur.eksp.i teor.fiz., 37, 1781 (1959). (Trans.Soviet Physics - JETP.)
26. D.M.Dennison, Phys.Rev., 96, 378 (1954).
27. V.I.Mamasakhlisov, Zhur.eksp.i teor.fiz., 24, 190 (1953).
28. H.I.Mang, Z.Phys., 148, 582 (1957); V.V.Balashov, V.G.Neudachin, Yu.F. Smirnov & N.P.Yudin, Zhur.eksp.i teor.fiz., 37, 1384 (1959) (Trans.Soviet Phys. - JETP.)
29. S.G.Nilsson, Kgl.Danske Videnskab.Selskab.Mat.-fys.Medd., 29, No.16 (1955).
30. A.E.Litherland et al, Phys.Rev., 102, 208 (1956); 11, 608 (1958); Nucl. Phys., 2, 136 (1957).
31. E.Paul, Phil.Mag., 2, 311 (1957).
32. V.Yu.Gonchar, E.V.Inopin & S.P.Tsytko, Report presented at the Eighth All-Union Conference on Nuclear Spectroscopy, Leningrad, January, 1958.
33. I.P.Elliott, Proc.Roy.Soc., A245, 128, 562 (1958).
34. S.A.Moszkowski, Phys.Rev., 110, 403 (1958).
35. E.Feenberg & M.Philips, Phys.Rev., 51, 597 (1937).
36. M.G.Redlich & E.P.Wigner, Phys.Rev., 95, 122 (1954).
37. R.Peierls & I.Yoccoz, Proc.Phys.Soc., A70, 381 (1957); J.J.Griffin & J. A.Wheeler, Phys.Rev., 108, 311 (1957).
38. B.F.Bayman, Compt.rendu.Congr.Intern.Phys.Nucl., p.711, Paris, 1959.
39. J.J.Griffin, Phys.Rev., 108, 328 (1957); I.Yoccoz, Proc.Phys.Soc., A70, 388 (1957).
40. D.Kurath & L.Picman, Nucl.Phys., 10, 313 (1959).
41. F.Haig, Nucl.Phys., 7, 429 (1958).

42. J.E.Bowcock, Phys.Rev., 112, 923 (1958).
43. V.V.Balashov, Report presented at the Ninth All-Union Conference on Nuclear Spectroscopy, Khar'kov, 1959; V.V.Balashov, Atomnaya energiya, 9, 48 (1960). (Trans.Soviet Journal of Atomic Energy.)
44. V.G.Neudachin, V.G.Shevchenko & N.P.Yudin (In press).
45. C.M.Class, R.H.Davis & J.H.Johnson, Phys.Rev.Letters, 3, 41 (1959).

* * * * * * *

SHAPE OF THE β-SPECTRUM OF A^{41}

- G.R.Kartashov, N.A.Burgov & A.V.Davydov

Introduction

The Feynman-Gell-Mann[1] universal theory of weak interactions predicts that in some cases the shape of allowed β-spectra must deviate from the usual shape characteristic of allowed transitions. Gell-Mann considered such deviations in the case of the β-spectra of B^{12} and N^{12}.

Recently Dreitlein[2] considered the question of analogous corrections to the shape of the β-spectra associated with unique first forbidden transitions ($\Delta I = 2$, yes).

In view of this we felt it would be of interest to investigate in detail the shape of the β-spectrum of such transitions. As the subject of the present study we chose A^{41}, the decay scheme for which is shown in Fig.1 (Ref.3).

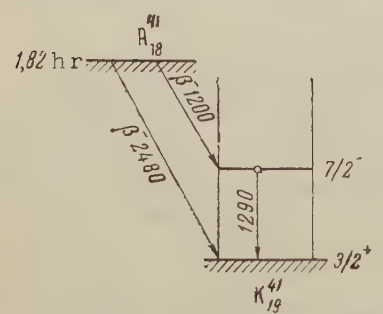

Fig.1. Decay scheme for A^{41}.

In addition to the transition to the excited state of K^{41}, which occurs in ~99% of all decays, there is a relatively weak transition to the ground state of K^{41}. The shape of the β-spectrum of this weak transition was investigated by Schwarzschild et al[4]. These authors concluded that the shape of this β-spectrum is in better agreement with the assumption of a unique first forbidden transition rather than an allowed or nonunique first forbidden transition. However, since the statistical fluctuations in the experiments of Schwarzschild et al were high and the resolution of their spectrometer was relatively low, some details of the spectrum may have escaped their attention.

1. Spectrometer

The measurements were carried out on the large magnetic-lens β-spectrometer described in Refs.5 & 6. For obtaining the β-spectrum we utilized the electrons emitted from the source in the range from 40 to 75° relative to the axis of the instrument. The source was a 10 mm diameter, 10 mm high cylinder covered at the ends with 1.5 mg/cm^2 terilen film and filled to a pressure of 300-400 mm Hg with pile irradiated spectroscopically pure argon. The detector was a plastic scintillator 10 mm in diameter and 10 mm high coupled to an FEU-35 photomultiplier.

The relative line half-width ($\Delta(H\rho)/H\rho$) was 2.4%. The photomultiplier pulses were fed, through a cathode follower, to an integral discriminator and registered by a scaler. The instrument was calibrated with reference to the K conversion line of Au^{198}.

2. Measurements and corrections

The β-spectrum of A^{41} is shown in Fig.2. The horizontal scale is laid off in momenta p in units of m_0c; the ordinates represent the average number of counts. There is clearly discernible a peak corresponding to conversion of the γ-transition in A^{41}. On the basis of our measurements the energy of this transition is

$$E_\gamma = (1290 \pm 4) \text{ kev.} \qquad (1)$$

The error in determining the individual points (calculated from the scatter of the experimental data obtained in different series of measurements) does not exceed 1.5% for the $p < 2.8$ range, is of the order of 0.8% for the $p = 2.8$ to 5.4 interval and is 1.5% for $p > 5.4$.

The internal conversion coefficient calculated from the area under the conversion peak is

$$K_\gamma = (6.8 \pm 0.9) \cdot 10^{-5}. \qquad (2)$$

The integral K + L conversion coefficients calculated using the tabulated data in the literature[7] are $8.7 \cdot 10^{-5}$, $7.2 \cdot 10^{-5}$ and $4.9 \cdot 10^{-5}$ for E3, M2 and E2 transitions, respectively. It follows that the 1290 kev transition is M2. This is consistent with the $7/2^-$ spin assignment for the excited state of K^{41}.

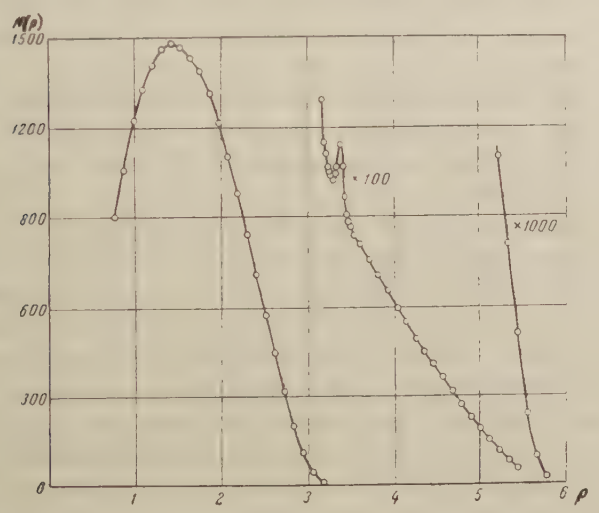

Fig.2. β-spectrum of A^{41}.

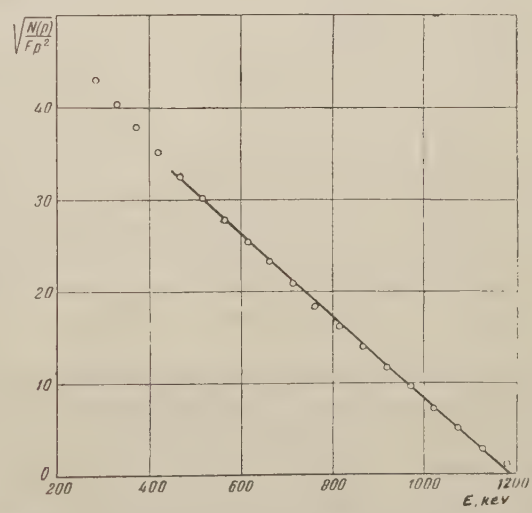

Fig.3. Fermi-Kurie plot for the low energy component of the A^{41} β-spectrum.

The spectrum shown in Fig.2 was corrected for the weak constant background and for the background due to the γ-rays from the A^{41} source. The variation of the background due to the γ-rays from the source as a function of the current in the spectrometer coils was investigated in a separate experiment, in which we utilized the γ-rays of Co^{60}, which are close in energy to the γ-rays from A^{41}. This experiment showed that in the region of high energies ($p > 3.0$) the background decreases linearly with increase of the energy.

In general, this background is not high: it is of the order of 3% of the average number of counts in this energy region.

It will be evident from Fig.2 that the spectrum comprises two β-components.

Analysis of the low energy β-spectrum showed that this spectrum has the allowed shape: the Fermi-Kurie plot (Fig.3) is rectilinear in the energy range above 400 kev. A minor rise is evident in the range below 400 kev, but this can be explained by scattering of electrons in the source and from the spectrometer walls.

The end-point energy of the spectrum determined by extrapolation of the Fermi-Kurie plot is 1195 ± 8 kev. For analysis of the low energy partial spectrum we subtracted the high energy spectrum from the experimental curve. It was assumed that the high energy spectrum has the shape characteristic of unique first forbidden transitions ($\Delta I = 2$, yes), i.e., that

$$N(p)\,dp = AF(Z, W)\,p^2 \times (W - W_0)^2 (p^2 + q^2)\,dp, \quad (3)$$

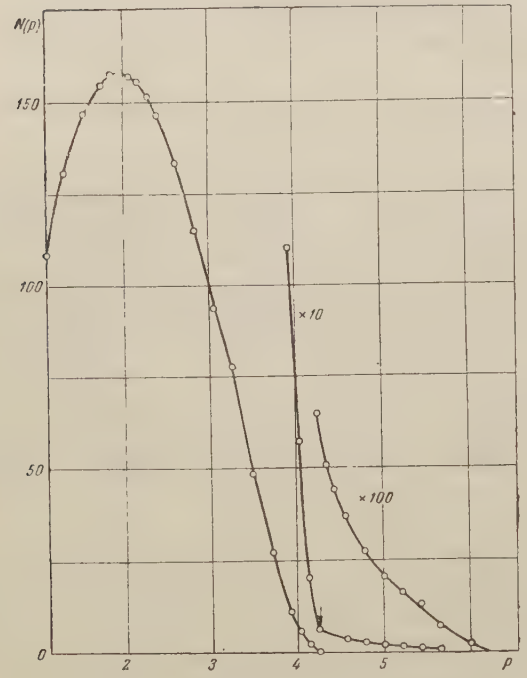

Fig.4. β-spectrum of P^{32}.

where $F(Z, W)$ is the Fermi function, q is the neutrino momentum in units of m_0c, W is the total electron energy in m_0c^2 units, and W_0 is the end-point energy of the β-spectrum in the same units.

Actually, however, since the high energy electrons are emitted in less than 1% of all the β-decays, as far as determination of the end-point energy of the low energy component is concerned the precise correction for the high energy spectrum is unimportant.

In the high energy spectrum there may be present electrons initially of low energy but scattered inside the spectrometer. In order to determine the requisite correction we investigated the spectrum of P^{32}. The P source was prepared of irradiated orthophosphoric acid.

Investigation of this spectrum, which is shown in Fig.4, showed that there actually is present a background of scattered electrons, which are detected by the spectrometer when the current through the spectrometer coils is greater than the current corresponding to the end-point energy of the P^{32} β-spectrum. The spectrum of P^{32} was plotted to a modified momentum scale so that the end-point energy of the P^{32} β-spectrum would coincide with the end-point energy of the intense (low energy) components of A^{41}. The spectra were normalized in area.

From the experimental P^{32} spectrum we determined the corrections to the ordinates of the high energy A^{41} component. The correction for electron scattering amounted to 20% at the beginning of the spectrum, and rapidly fell off to zero. The phosphorus spectrum was recorded with an error of ~1% over its entire range. This error was determined from the scatter of the experimental data in individual series of measurements and did not exceed the statistical uncertainty.

Independent determination of the A^{41} γ-ray energy from the conversion electrons and the end-point energy of the soft spectrum enabled us to calculate the end-point energy of the high energy partial spectrum. We obtained a value of 2485 ± 10 kev.

Using this value of the end-point energy for the corrected partial high energy β-spectrum we plotted the variation of

$$\frac{1}{W-W_0}\sqrt{\frac{N(p)}{p^2F(p,W)(p^2+q)^2}}$$

as a function of W. If the spectrum has the shape described by Eq.(3), this plot should be a straight line parallel to the horizontal axis.

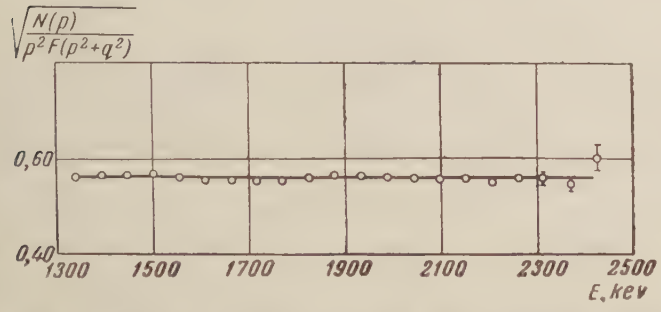

Fig.5. Fierz plot for the high energy component of the β-spectrum of A^{41}.

The Fierz plot is shown in Fig. 5. It follows from the plot that to within 1% the investigated spectrum has the shape defined by Eq.(3) and characteristic of $\Delta I = 2$, yes transitions. The Fermi-Kurie plot in this energy region ($3.5 < p < 6$) cannot be approximated by a straight line without introducing the correction factor $p^2 + q^2$.

The actual relative intensity of the high energy partial β-spectrum proved to be 0.78 ± 0.02%.

Discussion

1. The spin and parity of the A^{41} ground state are $7/2^-$. This follows from the shape of the β-spectrum associated with the transition to the ground state. In view of our experimental data it may be inferred that the assignment for the first excited state of K^{41} is also $7/2^-$.

In particular, it follows from this that the Fermi matrix element in the expression for the probability of the β-transition of A^{41} to the excited state of K^{41} must be nonzero. There is reason to infer that the ground state of A^{41}, the first excited state of K^{41} and the ground state of Ca^{41} have the same isotopic spin.

2. The β-spectrum corresponding to the transition between the ground states of A^{41} and K^{41}, according to our results, is described by Eq.(3) to within 1-2%, i.e., the corrections to this spectrum predicted by the Feynman-Gell-Mann theory are not evinced. According to the calculations of Dreitlein[2], in our case there should be a correction factor of the form $(1 + \lambda W)$, and the Fierz plot (Fig.5) should have a noticeable slope. The value of this correction factor at the end of the spectrum should be 1.02.

3. It must be noted, however, that in our case there may occur compensation of the corrections, inasmuch as in addition to the corrections following from the universal theory of weak interactions, the shape of the β-spectrum may be affected by other corrections. In order to evaluate these corrections one must determine the matrix elements for third forbidden β-transitions. This problem can, in principle, be solved if the calculations are carried out in the framework of the shell model.

We desire to thank I.S.Shapiro for discussion of the results; we are deeply indebted to V.G.Alpatov, Yu.I.Nekrasov and A.I.Zubkov for assistance in carrying out the measurements.

Institute of Theoretical and Experimental Physics,
Academy of Sciences of the USSR

References

1. R.P.Feynman & M.Gell-Mann, Phys.Rev., 109, 193 (1958); M.Gell-Mann, Phys. Rev.,111,362 (1958).
2. J.F.Dreitlein, Phys.Rev., 116, 1604 (1959).
3. B.S.Dzhelepov & L.K.Peker, Skhemy raspada radioaktivnykh yader (Decay schemes of radioactive nuclei), M.-L., 1958.
4. A.Schwarzschild, B.M.Rustad & C.S.Wu, Phys.Rev., 103, 1796 (1956).
5. G.R.Kartashov, A.V.Davydov & N.A.Burgov, Report presented at the Tenth All-Union Conference on Nuclear Spectroscopy, M., Jan.1960.
6. N.A.Burgov, A.V.Davydov & G.R.Kartashov, High luminosity toroidal iron-free β-spectrometer, Nuclear Instruments (In press).
7. Beta- and Gamma-Ray Spectroscopy, edited by Kai Seigbahn, Amsterdam, 1955.

* * * * * * *

CONVERSION ELECTRON SPECTRUM OF THE HOLMIUM FRACTION FORMED IN PROTON BOMBARDMENT OF Ta

- A.S.Basina, K.Ya.Gromov, B.S.Dzhelepov & V.A.Morozov

The conversion electron spectrum of the holmium fraction extracted from a tantalum target bombarded with fast protons in the Joint Institute for Nuclear Research synchrocyclotron was investigated by means of a lens β-spectrometer with a resolution of ~1.9%.

The operation of radiochemical separation of the holmium fraction required approximately three hours, so that measurement of the spectrum started about 3.5 hours after bombardment of the target. We investigated the conversion electron spectrum in the range from 30 to 1000 kev.

The spectrum of the holmium fraction was measured continuously over a period of 20 hours and then further, as was necessary for obtaining the spectra of the long-lived isotopes. Inasmuch as our primary task was to investigate the spectrum of the short-lived isotope of holmium (period ~1 hr) the lines of the long-lived isotopes were of interest to us mainly as a background for subtraction, although in some cases we also identified these lines for the purpose of elucidating the genetic relationships.

We observed in the spectrum of the holmium fraction conversion electron lines with the following periods: ~30 min, ~1 hr, ~2.5 hr, ~5 hr, ~10 hr and several days.

1. T = 5 ± 0.5 hr - Ho^{160}

The conversion lines decaying in intensity with a period of ~5 hrs belonged to the well-known isotope Ho^{160}. We observed groups of conversion electrons associated with transitions of 60, 87, 197, 298, 540, 648, 730, 880 and 963 kev energy, all of which have been observed in earlier studies[1-4]. All these lines were clearly evinced in the spectrum of our activity 6 and more hours after the beginning of measurement, when the lines associated with the decay of the shorter lived isotopes had faded.

2. T = 3 ± 0.5 hr - Ho^{161}

We observed one conversion electron line with this decay period: E_e = 69.0 kev. Mihelich et al[4] identified this as the L-77.5 line of Ho^{161}. We did not observe any other lines belonging to this isotope inasmuch as they are either of low intensity or masked by the stronger lines of the other holmium isotopes.

3. T = 55 ± 5 min - Ho^{156}

The existence of a holmium isotope with a period close to one hour was first reported in the work of Mihelich et al[4]. In the case of bombardment of a target enriched with dysprosium 156 by 22 Mev protons there is observed a transition of 138.1 kev energy in the reaction products; this transition is associated with a 1-hour activity. The 138.1 kev transition was not observed in the case of dysprosium targets enriched in Dy^{158}. On the basis of this observation Mihelich et al arrived at the tentative mass number assignment of 156 for the ~1-hr holmium isotope.

A one-hour activity in the holmium fraction separated from the products of spallation of tantalum with protons was observed by Gromov et al[5]. In addition to the 138 kev transition reported by Mihelich et al, the authors of Ref.5 observed a line with an energy of 214 ± 2 kev (T = 55 ± 2 min), which they identified as the K-268 line; they hypothesized that the 138 and 268 kev transitions form a rotational band in the level scheme of Dy^{156}.

In Table 1 we list our data on the energies, periods and relative intensities of the conversion lines of Ho^{156}.

Table 1

Conversion electrons of Ho^{156}

$H\rho$, Gs, cm	$E_{e\,l}$, kev	$h\nu$, kev	$T_{1/2}$, min	Identification	Relative intensity
1020	84,5	138,3	60±5	*K*138	1420
1292	130,2	139,2	60±5	*L*138	1000
1335	138	140	—	*M*138	300
1720	214,9	268,7	58±3	*K*268	300
1925	259,6	268,3	50±5	*L*268	154
2155	312,6	366,4	52±3	*K*366	31
2349	359	367,6	53±2	*L*366	11
3412	632,3	686	60±5	*K*686	24

In addition to the two above-mentioned transitions, we succeeded in detecting transitions with energies of 366 and 686 kev. Possibly the 366 kev transition occurs between the third and second levels of the rotational band in Dy^{156} (level energies: E_1 = 138, E_2 = 406 and E_3 = 772 kev). The energy ratio E_3/E_1 = 5.6 is somewhat low compared with the theoretical value of 7 for even-even deformed nuclei. This, however, is not surprising inasmuch as Dy^{156} is located close to the boundary of the region of deformed nuclei.

The data on the relative intensities of the K-138, K-268 and K-366 conversion lines do not conflict with the inference that these transitions are of equal intensity and are both E2.

The location of the 686 kev transition in the decay scheme is still unclear; nevertheless in view of its decay period this transition must be attributed to Ho^{156}.

4. T = 30 ± 5 min - Ho^{158}

The conversion electron spectrum of the half-hour (more precisely, 27-minute) activity in the holmium fraction was investigated earlier in the work of Gromov

Table 2

Conversion electrons of Ho^{158}

Hρ, Gs см	E_e, kev	$h\nu$, kev	$T_{1/2}$, min	Identification	Relative intensity
729	44,8	98,6	27±3	*K*98	86
839	58,5	—	33±3	—	115
1062	90,8	99,4	28±3	*L*98	108
1102	97,5	99,5	27±3	*M*98	34
1481	165,9	218,7	32±4	*K*218	26
2102	300,2	354	40±10	*K*356	1,5
3159	565	619	—	*K*619	—
4000	792	846	—	*K*849	—
4365	892	947	—	*K*948	—
4530	940	948	—	*L*948	—
4800	1016	1070	—	*K*1070	—

Table 3

Unidentified conversion electrons emitted by the short-lived Ho isotopes

Hρ, Gs см	E_e, kev	$T_{1/2}$, min	Remarks
908	67,3	—	Poorly resolved from L-77 of Ho^{161}
1658	201,8	34±4	Intensity equal to 20% the intensity of L-98 of Ho^{158}
1813	235	—	
2620	425	—	
2928	504,6	—	
2745	457,6	46±10	
3700	710	50±15	

et al[5] in the 70 to 315 kev region on a spectrometer with a transverse homogeneous magnetic field. These authors observed transitions of 98 and 218 kev energy. In view of their energy ratio it was inferred that the departure levels form a rotational band in this even-even nucleus.

In the work of Dneprovskii[6], devoted to investigation of the erbium fraction on a high resolution instrument, there were observed conversion lines corresponding to transitions with energies of 97.6, 218, 320 and 356.5 kev, the intensity of which fell off with a period of about 2.5 hours. The nuclear charge as evaluated from the K - L and K - M differences for these transitions indicated that they occur in a dysprosium nucleus. From the 98.6 kev energy value for the first excited level of the even-even nucleus there follows the mass number assignment 158 for the holmium isotope in the decay of which these transitions are excited. Thus, apparently there exists the decay chain:

$$Er^{158} \xrightarrow[EC]{2.5\ hr} Ho^{158} \xrightarrow[EC]{27\ min} Dy^{158}.$$

In the spectrum of our holmium fraction we observed a number of conversion lines that decayed with a period close to 30 min. The energies and relative intensities of these lines as well as their decay periods are given in Tables 2 and 3.

In Table 2 we list the conversion electrons of eight transitions including those from the well-known transitions in Ho^{158} with energies of 98.6, 218.7 and 356 kev.[5] We did not observe the conversion electron lines corresponding to the 320 kev transition; apparently these lines are masked by the more intense lines of Ho^{156}. The other lines in Table 2, namely, K-619, K-848, K-947 and K-1070, were observed by Dneprovskii[6] also in the erbium fraction, where they fell off in intensity with a period of 2 to 4 hours.

Only two isotopes of erbium are known which close decay periods: Er^{158} and Er^{161}. These isotopes give rise to the decay chains:

$$Er^{158} \xrightarrow[EC]{2.5\ hr} Ho^{158} \xrightarrow[EC]{0.5\ hr} Dy^{158}\ \text{(stable)},$$

$$Er^{161} \xrightarrow[EC]{3.5\ hr} Ho^{161} \xrightarrow[EC]{2.5\ hr} Dy^{161}\ \text{(stable)}.$$

Inasmuch as the intensity of these lines in the spectrum of the holmium fraction falls off with a period of 0.5-1.0 hr, they must be attributed to Ho^{158}.

This inference would not be altered if there existed Er^{156} with a period of 2-4 hours, inasmuch as in this case there would be observed in the spectrum of the erbium fraction lines corresponding to Ho^{156}, which in reality is not the case.[6,7]

In addition to the lines detected earlier[5,8] in the spectrum of the half-hour Ho^{158} activity, in the conversion electron spectrum of our holmium fraction we also observed an intense line of 58.5 kev energy (T = 33 ± 3 min) (see Table 2). It may be assumed that this is an L line inasmuch as there are no lines that could be interpreted as the L and M lines of the given transition if it is assumed that the 58.5 kev line is the K line. It is not impossible that the weak line at ~67 kev (it decays with a short period), which we have included in the list of unidentified lines, is the M line of a 67 kev transition. A transition of this energy (66.9 kev) was observed by Dneprovskii in this erbium fraction; he determined its period as 135 ± 15 min and interpreted it as an isomeric transition in Ho^{158} (analog of the 60 kev transition in Ho^{160}).

In Table 3 we have collected the conversion lines which were detected in the spectrum of the holmium fraction but not observed in the spectrum of the erbium fraction, i.e., lines which are not associated with decay of Ho^{161} or Ho^{158} and which have a relatively short decay period. Most of these lines were too weak for precise determination of their decay period, but the 201.8 kev line is strong enough for this purpose; its period was found to be 34 ± 4 min.

$$5.\ Ho^{155} \xrightarrow[EC]{46\ min} Dy^{155} \xrightarrow[EC]{10\ hr} Tb^{155} \xrightarrow[EC]{5.6\ d.} Gd^{155}$$

The holmium isotope with mass number 155 is evinced in the holmium fraction in the form of its daughter Dy^{155}. The period of Ho^{155}, as determined by Dalkhsuren et al[8] by repeat separations of Dy from Ho, is close to 45 min. The presence of Dy^{155} in the homium fraction extracted from proton bombarded tantalum was noted in the work of Gromov et al[5].

In the spectrum of our activity there were also clearly discernible lines associated with the 227 kev transition in Tb^{155}, and after the passage of 60-80 hours, when the lines associated with the decay of the short-lived holmium isotopes had faded sufficiently, there became noticeable the conversion lines of transitions of 86, 105, 162, 180 and 262 kev energy in Tb^{155}, the third member in the genetic chain $Ho^{155} \rightarrow Dy^{155} \rightarrow Gd^{155}$.

Our attempt to determine the period of Ho^{155} from the growth in intensity of the K-227 line of the daughter Dy^{155} was not successful inasmuch as during the first hours of measurement the K-227 line is poorly discernible owing to the interference of the neighboring intense lines of the short-lived holmium isotopes. Presumably this problem could be solved with the aid of an instrument with higher resolution.

We did not observe any strong conversion electron lines with a period of 45 min. However, one cannot with certainty deny their existence, inasmuch as they could be among the weaker lines (with short periods) listed in Table 3. As noted above, owing to their weakness we were unable to determine the periods of these lines with any degree of certainty.

We desire to express our gratitude to I.A.Yutlandov and V.A.Khalkin for preparation of the sources and M.A.Dolgoborodova and Ku Za Khek for assistance in the measurements.

References

1. D.Strominger, J.M.Hollander & G.T.Seaborg, Tables of Isotopes, Revs.Mod. Phys., 30, 585 (1958).

2. B.S.Dzhelepov, B.K.Preobrazhenskii, I.M.Rogachev & P.A.Tishkin, Izv.AN SSSR, Ser.fiz., 21, 962 (1957). (Trans.Bulletin, 21, 964.)

3. E.P.Grigor'ev, B.S.Dzhelepov, A.V.Zolotavin, B.Kratsik, B.K.Preobrazhenskii & I.S.Yanchevskaya, Doklady AN SSSR, 117, 53 (1957). (Trans.Soviet Physics - Doklady.)

4. J.W.Mihelich, B.Harmatz & T.H.Handley, Phys.Rev., 108, 980 (1957).

5. K.Ya.Gromov, B.S.Dzhelepov, Zyong Chong Bai & V.G.Chumin, Materialy II Soveshchaniya po yadernoi spektroskopii neitronodefitsitnykh izotopov redkikh zemel' (Transactions of the Second Conference on Nuclear Spectroscopy of Neutron-Deficient Rare Earth Isotopes), Dubna, 1959.

6. I.S.Dneprovskii, Ibid.

7. A.A.Abdurazakov, K.Ya.Gromov & B.S.Dzhelepov, Materialy XI Soveshchaniya po yadernoi spektroskopii (Transactions of the Eleventh Conference on Nuclear Spectroscopy), Riga, 1961.

8. B.Dalkhsuren, I.Yu.Levenberg, Yu.V.Norseev, V.N.Pokrovskii & S.S.Khainatskii, Atomnaya energiya, 8, 248 (1960). (Trans.Soviet Journal of Atomic Energy.)

9. E.P.Grigor'ev & B.S.Dzhelepov, Doklady AN SSSR, 135, 564 (1960). (Trans. Soviet Physics - Doklady.)

Note added in proof: Our results for the conversion electron spectrum of Ho^{156} are substantiated by the data of Grigor'ev & Dzhelepov[9] who measured the spectrum by means of a double focusing $\pi\sqrt{2}$ β-spectrometer.

* * * * * *

RELATIVE INTENSITIES OF SOME GAMMA-LINES IN THE SPECTRUM OF Ta^{182}

- V.D.Vitman, N.A.Voinova, B.S.Dzhelepov & A.A.Karan

Using the Elotron type magnetic spectrometer constructed in the All-Union Scientific Research Institute of Metrology, we investigated the γ-radiation from Ta^{182} in the 850 to 910 and 975 to 1280 kev regions for the purpose of obtaining more accurate values for the relative line intensities. The 850 to 910 kev section of the spectrum was considered in detail in Ref.1.

The experimental Compton recoil curve corresponding to γ-rays in the 975 to 1280 kev region is shown in the accompanying figure. The experimental spectrum was resolved into components taking into account the apparatus line shape, and then the relative intensities of the individual components were determined. The data on all the observed lines together with the results of other authors are listed in the accompanying table. The 1045.9 kev γ-rays were hitherto observed only by Fowler et al[2]; the relative intensity of these γ-rays was determined for the first time in the present study.

"D.I.Mendeleev" All-Union Scientific Research Institute of Metrology &
Physical-Technical Institute of the
Academy of Sciences of the USSR

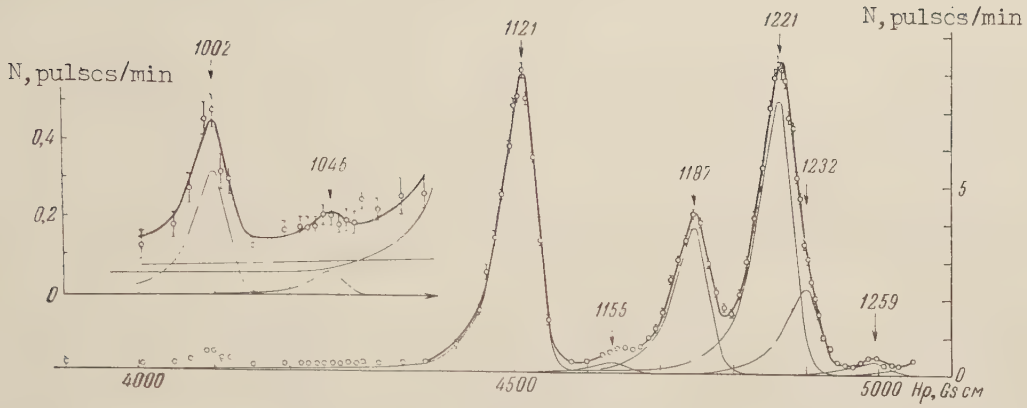

Ta^{182} γ-ray spectrum in the 975 to 1280 kev region, background subtracted; the figures at the peaks are the γ-ray energies in kev.

Energies and relative intensities of the γ-lines in the spectrum of Ta^{182}

E_γ, kev	Relative intensities					
	Crystal spectro. (Ref.3)	$\pi\sqrt{2}$ spect. photoelect. (Ref.4)	Crystal spectro. (Ref.5)	Scint. spectro. (Ref.6)	Magnetic spectr., Compt. recoils (7)	Our data
892,4	—	—	—	—	<1,4	≤0,5
1002	—	—	—	—	9±3	5±2
1046	—	—	—	—	—	$0,9^{+0,9}_{-0,6}$
1121	100	100	100	100	100	100
1155	6,5	—	7,1	—	<4	3,6±1,0
1187	45	—	56,8	21	45±8	44±3
1221	95	—	} 161	(75) } 113	84±8	80±6 } 105±8
1232	50	—	}	(38) }	35±10	25±5 }
1259	—	4	—	—	6±2	4±1

References

1. V.D.Vitman, N.A.Voinova, B.S.Dzhelepov & A.A.Karan, Zhur.eksp.i teor. fiz., 40, 479 (1961). (Trans.Soviet Physics - JETP.)

2. G.Fowler, H.Kruse, V.Keshishian, R.Klotz & G.Mellor, Nucl.Sci.Abstr., 9, No.24B, 102 (1955).

3. J.Murray, F.Boehm, P.Marmier & J.DuMond, Phys.Rev., 97, 1007 (1955).

4. G.Bäckström, Arkiv.Fysik., 10, 387 (1956).

5. O.I.Submaev, Izv.AN SSSR, Ser.fiz., 21, 987 (1957) (Trans.Bulletin, 21, 989); Zhur.eksp.i teor.fiz., 32, 247 (1957). (Trans.Soviet Physics - JETP.)

6. P.Fröman & H.Ryde, Arkov.fys., 12, 399 (1957).

7. N.A.Voinova, B.S.Dzhelepov & N.N.Zhukovskii, Izv.AN SSSR, Ser.fiz., 23, 828 (1959). (Trans.Bulletin, 23, 822.)

RELATIVE INTENSITIES OF GAMMA-RAYS FROM RaC IN THE 1300 TO 2520 kev REGION

- V.D.Vitman, B.S.Dzhelepov & A.A.Karan

The most reliable data published hitherto on the relative intensities of the γ-rays from RaC are contained in Ref.1. The new Elotron type spectrometer of the All-Union Scientific Research Institute of Metrology has a resolution in the >1 Mev region 1.5 times higher than the Elotron of the Radium Institute, which was used in the work of Ref.1. Hence use of this new instrument enabled us to bring out certain new details in the γ-ray spectrum of RaC and to obtain more accurate values for the relative intensities and in some cases for the energies of the γ-lines.

Our source was 4 grams of radium in the form of $RaBr_2$; the shape and size of the source was the same as in the work of Ref.2 (the activity was contained in an array of 24 glass ampoules 4-5 mm in diameter and 40 mm in length enclosed in copper foil).

The background in our measurements amounted to 0.04 coincidences per minute at $h\nu = 1350$ kev and less than 0.01 coincidences per minute in the region above 1500 kev.

After subtraction of the background, the experimental spectrum was resolved into components using the standard line shape which was obtained as a result of studying the shape of the following discrete lines: 1171.5 and 1331.6 kev of Co^{60}, 1367.9 and 2753.5 kev of Na^{24} and 2614.3 kev of ThC". These lines, together with the more intense Ra lines (1120.4, 1509.3, 1764.4 and 2204.2 kev) served for the energy calibration.

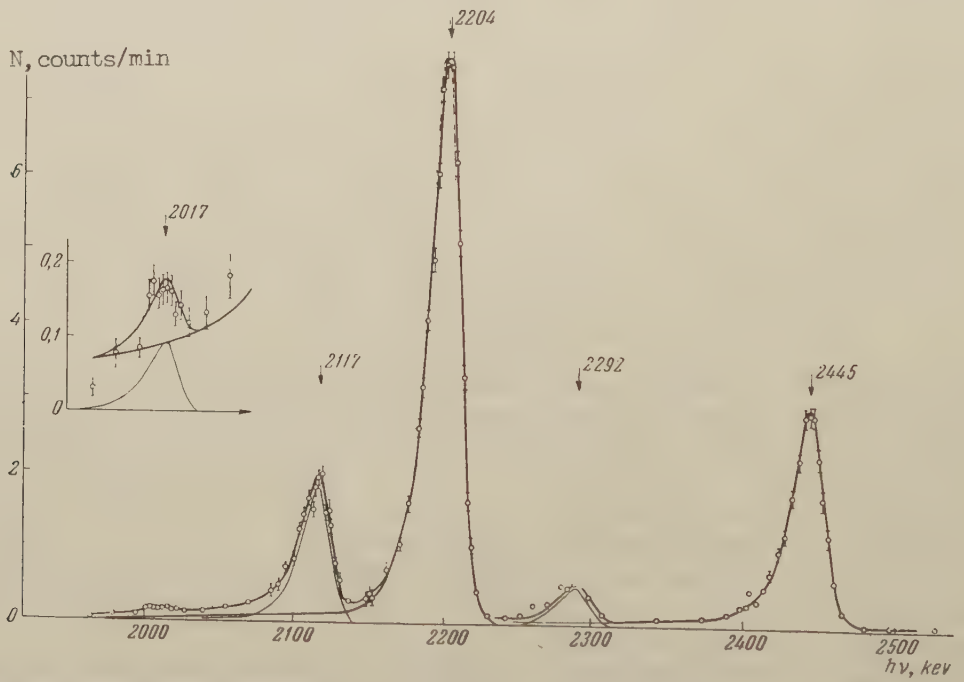

Fig.1. Gamma-ray spectrum of RaC in the 2000 to 2500 kev region (background subtracted). Light lines - resolution into components.

To find the relative intensities we determined the area under each line, reduced to equal $H\rho$ intervals. Then we introduced appropriate corrections for the absorption in the source and instrument walls and the spectral sensitivity of the instrument.

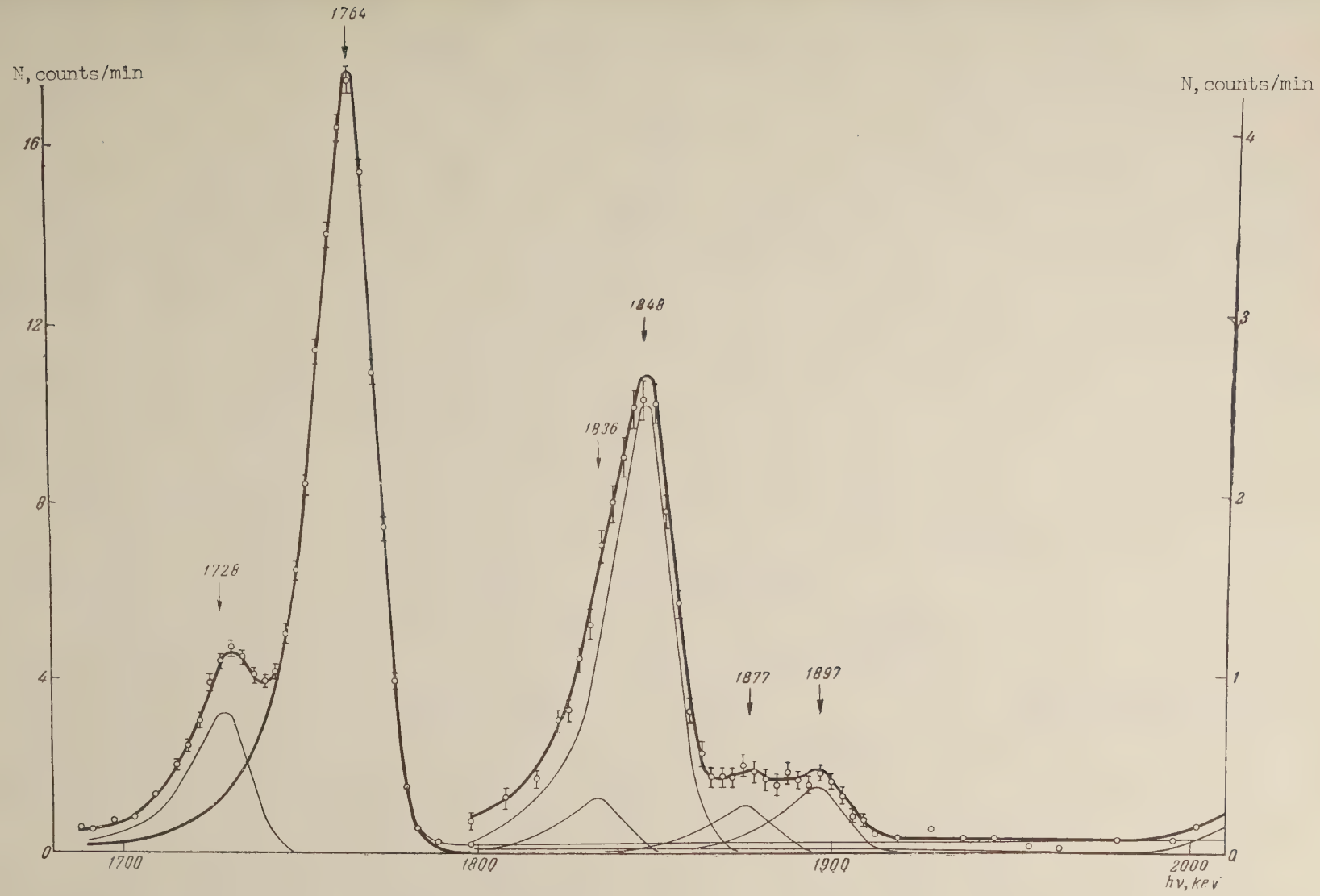

Fig.2. Gamma-ray spectrum of RaC in the 1700 to 2000 kev region (background subtracted). Light lines - resolution into components

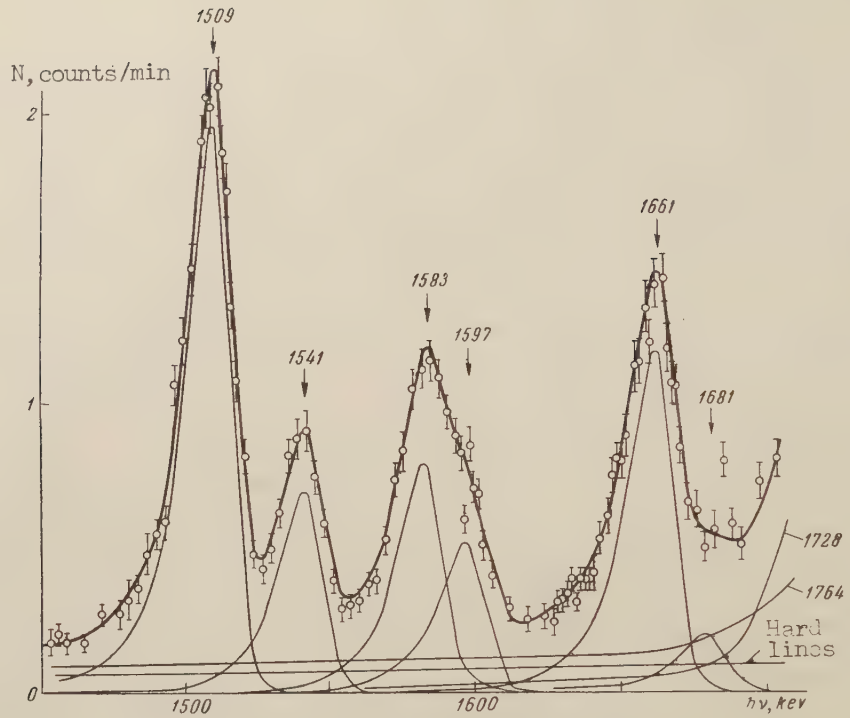

Fig.3. Gamma-ray spectrum of RaC in the 1450 to 1700 kev region (background subtracted). Light lines - resolution into components.

The results of resolution into components are shown by the light lines in Fig.1 through Fig.4. Analysis was started from the high energy side, inasmuch as the lines have appreciably low energy tails.

Fig.1 shows the 2000 to 2500 kev section of the γ-spectrum. In addition to the 2117, 2204, 2292 and 2445 kev lines known earlier, there is clearly discernible in this section of the spectrum a γ-line at 2017 kev, the existence of which was inferred previously from observation of conversion electrons[3]. After plotting and subtraction of all five of these lines there remains in the 2270 kev region an excess of recoil electrons with an intensity of ~1% relative to the 2204 kev line.

Fig.2 shows the 1600 to 2000 kev section of the spectrum. Here the 1728 kev line is clearly separated from the 1764 kev line, which makes it possible to determine its relative intensity more accurately than was feasible in the work of Ref.1. Further, we see a group of unresolved lines. The most intense line of this group has an energy of 1848.5 kev. When this line is inscribed into the experimental spectrum there are revealed the following features:

1) an excess of recoil electrons on the side of high energies, which can be accounted for by one line with an energy of 1836 kev;

2) two γ-lines with energies of 1877 and 1897 kev in the region above 1870 kev; the latter line is already known (this is the 1900 kev line of Refs.1 & 2), while the 1877 kev line has not been observed hitherto. In Refs.1 & 2 there is mentioned a line with an energy of 1862 kev. The resolution of our spectrometer was inadequate to bring out this γ-line. Hence we can only give the upper bound for its intensity: $\gamma_{1862}/\gamma_{2204} < 0.05$.

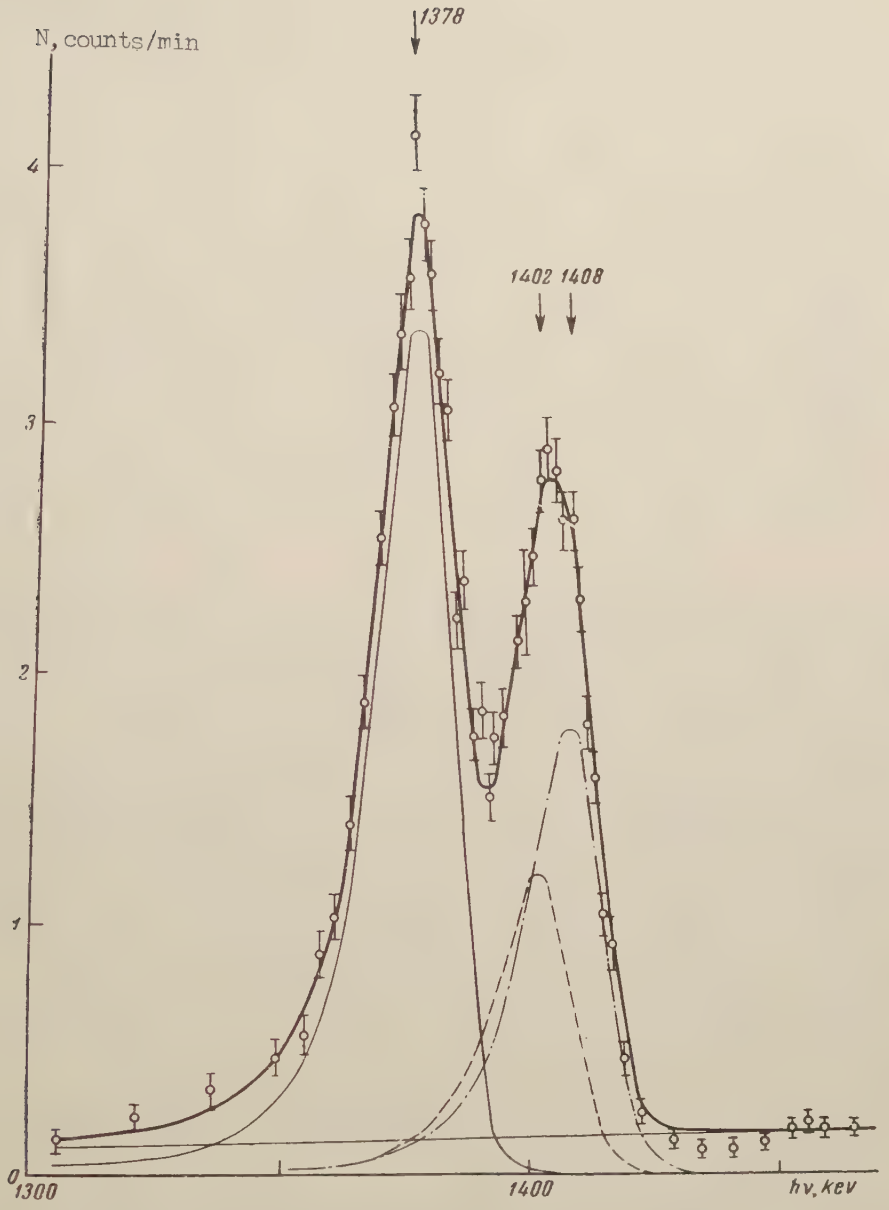

Fig.4. Gamma-ray spectrum of RaC in the 1300 to 1460 kev region (background subtracted). Light lines - resolution into components.

Fig.3 shows the 1450 to 1700 kev section of the spectrum. The 1541 kev line, first observed in the work of Ref.1, is well separated from the 1509 kev line.

The 1583 kev line is almost two times wider than the standard line shape. It is, however, impossible to explain this broadening by the presence of a line with an energy of 1605.5 kev (as was attempted in Ref.1). This broadening can be explained by a line of 1597 ± 4 kev energy; a line of this energy has not been observed hitherto.

The line which in Ref.1 was attributed an energy of 1668.4 kev is actually located at 1661 kev. Conversion electrons associated with a transition of this energy were observed in the work of Mladjenovic & Slätis.[3]

Table 1

Relative intensities of the γ-lines in the spectrum of RaC

E_γ, kev (Ref.3)	Relative intensities		E_γ, kev (Ref.3)	Relative intensities	
	Ref.1	Our data		Ref.1	Our data
1378,2	0,91	0,91±0,09	1728,3	0,45	0,60±0,05
1385,3			1764,4	3,11	3,18±0,13
1391,1			1836±5	—	0,05±0,02
1396,5	0,77	0,78±0,08	1848,5	0,39	0,43±0,03
1401,7		(0,32)	1862,3	0,15	—
1408,0		(0,46)	1877±5	—	0,04±0,01
1438,0		—	1897±5	0,08	0,06±0,01
1509,3	0,42	0,45±0,04	2016,7	~0,02 (excess)	0,014±0,008
1541±3	0,16	0,15±0,02	2085	~0,02 (excess)	—
1582,9	0,21	0,17±0,02	2117,0	0,26	0,25±0,02
1597±4	—	0,11±0,02	2204,2	1	1
1605,2	0,07	—	2270	—	~0,01 (excess)
1660,9	—	0,23±0,02	2292±5	0,08	0,07±0,01
1668,4	0,20	—	2410	~0,03 (excess)	—
1681,0	—	0,04±0,01	2445±5	0,30	0,33±0,01

After all the above-mentioned lines have been inscribed in the experimental spectrum there remains an excess of recoil electrons which can satisfactorily be explained by a 1681 kev line; this line is known from observation of conversion electrons[3] but has not hitherto been observed directly.

Fig.4 shows the 1300 to 1460 kev region of the spectrum. On the basis of the data of Mladjenovic & Slätis[3] on conversion electrons one may expect to observe seven lines in this section of the spectrum: 1378.2, 1385.3, 1391.1, 1396.5, 1401.7, 1408.0 and 1438.0 kev. The 1438 kev line should be well-separated from the first six lines, but it is not discernible in our spectrum ($\gamma_{1438}/\gamma_{2204} < 0.03$). There are clearly evinced two peaks in the spectrum. The first is explained by a 1378 kev line; the second peak is somewhat broader than follows from the standard line shape. It may be inferred that it consists of two lines with energies of 1402 and 1408 kev. These are tentatively indicated by dashed lines in Fig.4; it is at present impossible to resolve them unambiguously.

The relative intensities of the γ-transitions are shown in Table 1 together with the values obtained in the work of Ref.1. The energies of the γ-rays are given according to the data of Mladjenovic & Slätis[3] when the corresponding conversion electrons were observed by these authors; in other cases we give our energy values. It will be evident from the table that in most cases our data agree well with the earlier results of Ref.1.

Mladjenovic & Slätis list a number of unidentified conversion lines. Part of these have now been identified inasmuch as the corresponding γ-rays from RaC have been observed in our experiments. If it is assumed that all the other lines are K conversion lines, then on the basis of our results one can indicate the upper bounds of the corresponding transition intensities. The results of such evaluation are listed in Table 2. In the last column we give the integral intensities of the groups of poorly resolved or completely unresolved lines. Operating the spectrometer under conditions of enhanced transmission we undertook a search for the 2513 kev line mentioned in Ref.1. If this line exists its intensity must be less than $5 \cdot 10^{-5}$ γ-rays per decay.

We desire to express our gratitude to S.A.Shestopalova for her interest in the work and discussion of the results and to P.Galan, graduate student of Leningrad State University, for assistance in carrying out the measurements.

Table 2

Evaluation of the intensities of the γ-rays corresponding to conversion lines not identified in the work of Mladjenovic & Slätis[3]

E_γ, kev (Ref.3)	Relative intensities	Relative intensities of unresolved groups	E_γ, kev (Ref.3)	Relative intensities	Relative intensities of unresolved groups
1385,3	<0,15		1728,3	0,60	
1391,1	<0,13		1749,4	<0,18	3,78±0,15
1396,5	<0,18	0,78±0,08	1764,4	3,18	
1401,7	fm 0,16 to 0,42		1783,8	<0,04	
1408,0	fm 0,40 to 0,48		1790,7	<0,02	
1438,0	<0,03		1836*	0,05	
1582,9	0,17	0,23±0,03	1848,5	0,43	0,58±0,05
1597*	0,11		1862,3	<0,05	
1605,2	<0,04		1877*	0,04	
1645,4	<0,02	0,27±0,03	1897*	0,06	
1660,9	0,23				
1668,4	<0,06				
1681,0	0,04				

*Our line energy values.

"D.I.Mendeleev" All-Union Scientific Research Institute of Metrology

References

1. B.S.Dzhelepov. N.N.Zhukovskii, I.F.Uchevatkin & S.A.Shestopalova, Izv. AN SSSR, Ser.fiz., 22, 841 (1958). (Trans.Bulletin, 22, 835.)

2. B.S.Dzhelepov & S.A.Shestopalova, Ibid., 21, 990 (1957). (Trans.Bulletin, 21, 992.)

3. M.Mladjenovic & H.Slätis, Arkiv.Fysik, 9, 65 (1954).

GAMMA-RADIATION FROM Eu^{146}

- E.E.Berlovich, V.N.Klement'ev, L.V.Krasnov & M.K.Nikitin

The present work was concerned with the γ-radiation emitted by the electron capture nuclide E^{146}. The source was the gadolinium fraction separated chromatographically from a tantalum target bombarded with 600 Mev protons accelerated in the Joint Institute for Nuclear Research Synchrocyclotron. After the decay of the short-lived Gd^{147} (29 hrs) and Gd^{149} (9.3 days), the basic activity was due to Gd^{146} (60 days) and its daughter Eu^{146} (5 days). The contribution of the relatively low-energy radiation from Gd^{146} in the region of the Eu^{146} lines, according to our evaluations, was negligible. In our experiments we used only sources stored for 40 and 180 days.

The measurements were made on a coincidence spectrometer, one arm of which was coupled to a 100-channel AI-100 pulse height analyzer. The radiation was detected by FEU-14 photomultipliers viewing 30 x 40 mm NaI crystals. A schematic of the spectrometer is shown in Figure 1.

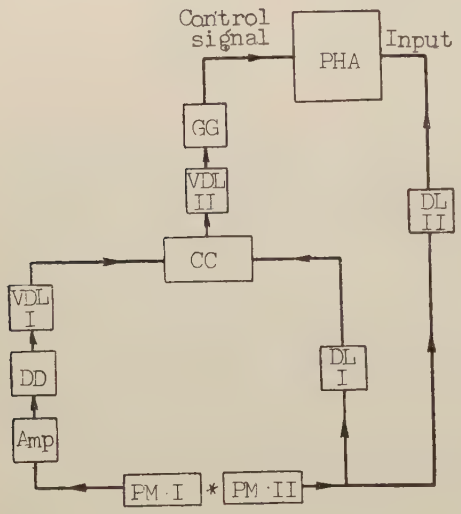

←Fig.1. Block diagram of the apparatus: A - amplifier; DD - differential discriminator; VDL 1 and VDL II - variable delay lines (delay time from 0 to 250 microsec); DL - delay line, RKZ-401 cable, (delay time 2 microsec); DL II - delay line, RKZ-401 cable, (delay time 8 microsec); CC - coincidence circuit with variable resolving time 2τ = 0.2 to 20 microsec; GG - gating pulse generator; PHA 100-channel pulse height analyzer, AI-100-1 ("Raduga") type.

The amplified pulse from photomultiplier PM I is applied to the differential discriminator DD. The pulse from the differential discriminator is fed, through the variable delay line VDL I, to one of the coincidence circuit inputs. The pulse from the anode of the second photomultiplier PM II is fed to the other input through the delay line DL I. The resolving time of the coincidence circuit can be varied from 0.2 to 20 millisecs. The pulse from the coincidence circuit, after passing through the variable delay line VDL II, triggers the gate generator, which in turn triggers the multiple-channel analyzer, the input of which receives pulses from the PM II dynode.

Thus, from among γ-rays detected by the photomultiplier PM II, the multiple-channel analyzer selects only those which coincide with the γ-rays selected by the differential analyzer.

By appropriate adjustment of the variable delay lines one can count either prompt or delayed coincidences.

If the delay introduced by the variable line VDL I is greater than the delay of the fixed line DL I, there are counted the γ-rays emitted later than the γ-rays selected by the differential discriminator. If the delay of the line VDL I is shorter than that of DL I, the γ-rays counted are those emitted earlier than the γ-rays gated by the differential discriminator.

Prompt coincidences are counted when the delay of VDL I equals that of DL I. The compensating delay lines VDL II and DL II provide for correct phasing of the gating pulse with the counting pulse.

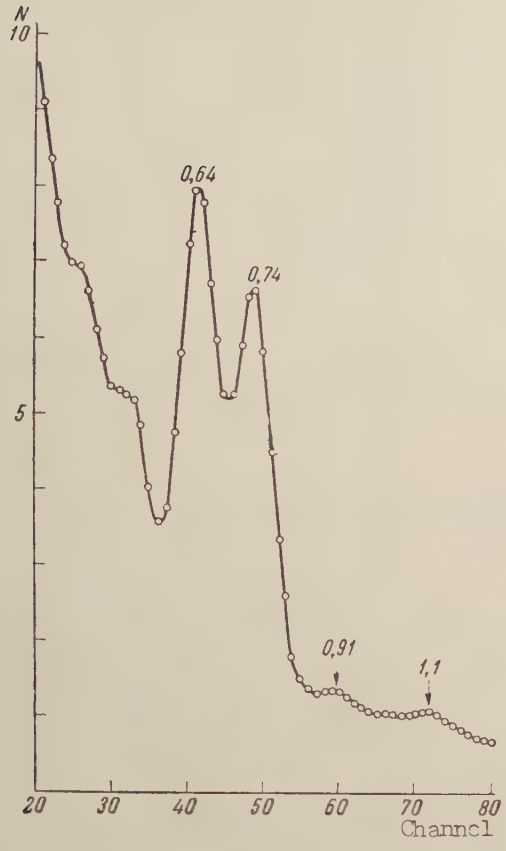

Fig.2. Gamma-ray spectrum of Eu^{146} in the 0.5 to 0.9 Mev region.

Energies and relative intensities of the Eu^{146} γ-rays

E_γ, Mev	I_γ
0,64	~1
0,74	1,00
0,91	0,10
1,1 (1,07+1,17)	0,14
1,3 (1,26+1,31)	0,10
1,5 (1,45+1,56)	0,13
1,8	0,02
2,1 (1,94+2,06+2,19)	0,04
2,4	0,01

Fig.3. Gamma-ray spectrum of Eu^{146} in the 0.9 Mev region.

The decay of Eu^{146} was studied by the Radium Institute group[1,2], who detected 0.63 Mev and 0.74 Mev transitions. In addition, Gorodinskii and his co-workers[3] detected transitions of 0.66 Mev and 0.89 Mev energy.

In the present work we observed a number of γ-transitions appearing in the decay of Eu^{146}. The energies and relative intensities of these transitions are listed in the table. The recorded γ-ray spectrum is shown in Figs.2 and 3.

Inasmuch as the γ-spectrum comprises a number of lines with close energies, we give the integral intensity for each line group together with the mean energy of the group, then in parentheses we list the energies of the individual lines composing the given group.

The relative intensities of the γ-rays were determined by resolving the spectrum into components, assuming a standard line shape in all cases. The intensity of the 0.74 Mev γ-rays was taken as unity. The 0.64 Mev transition is not a single one but is part of a cascade. According to our evaluations the intensity of the 0.64 Mev γ-rays is approximately equal to the intensity of the 0.74 Mev rays. The error in the intensity determinations is estimated as ~30%.

The region of the spectrum above 0.9 Mev was studied using lead absorbers from 6 to 28 g/cm^2 thick in order to eliminate the additive effect due to the intense and coinciding 0.64 and 0.74 Mev γ-rays.

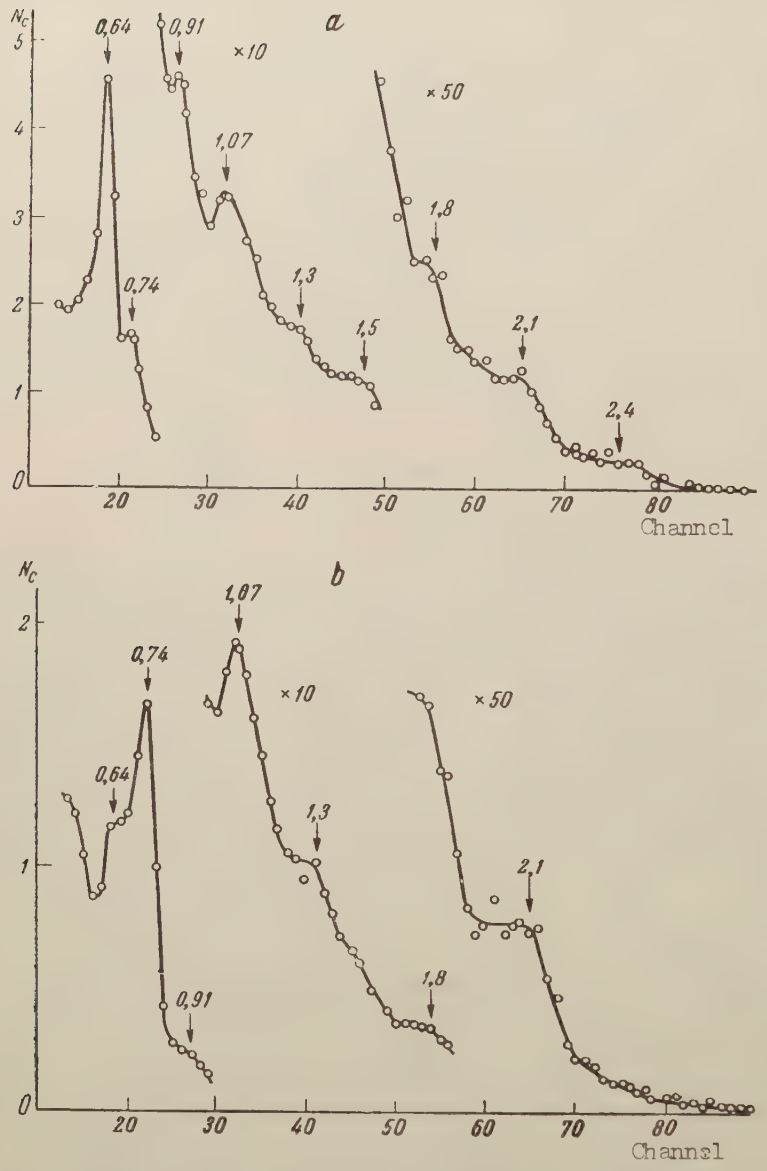

Fig.4. Coincidence spectra: a) with 0.74 Mev γ-rays, b) with 0.64 Mev γ-rays. In both cases 6 g/cm^2 thick lead absorbers were used.

Our experiments confirmed the existence of coincidences between 0.74 and 0.64 Mev gammas.[1] Fig.4 shows the coincidence spectra of these γ-rays. Coincidences were detected between the 0.74 Mev γ-rays and γ-rays of the following energies: 0.64, 0.91, 1.07, 1.3, 1.5, 1.8, 2.1 and 2.4 Mev. We also observed coincidences of the 0.64 Mev gammas with all the γ-rays listed above except the 1.5 and 2.4 Mev ones, and in addition, noted self-coincidences of the 0.64 γ-rays, which would imply the existence of another transition having an energy close to 0.64 Mev.

There are several possible explanations for the observed self-coincidences of the 0.64 and 0.74 Mev γ-rays: a) with the gate of the single-channel analyzer set for the 0.64 Mev or 0.74 Mev peak a portion of the γ-rays belonging to the other peak was passed; b) some of the "self-coincidences" were caused by the Compton distribution from higher energy γ-rays. These reasons are sufficient to explain the self-coincidences of the 0.74 Mev γ-rays, but do not suffice to account for the intensity of the 0.64 Mev self-coincidences.

Control experiments were carried out in order to check whether these self-coincidences were true. The width of the single-channel analyzer gate was reduced, which increased the proportion of γ-rays corresponding to the given transition relative to the distribution from all other γ-rays in the same energy range. Under these conditions the 0.74 Mev γ-ray self-coincidence peak was substantially diminished. This indicates that the "self-coincidences" of 0.74 Mev γ-rays are explained by the reasons adduced above. In the case of 0.64 Mev γ-rays, however, the self-coincidence peak did not diminish noticeably, indicating that these are true coincidences.

In addition, we investigated coincidences with different sections of the high-energy part of the spectrum: the fixed channel was set at 2.4, 2.1, 1.8,

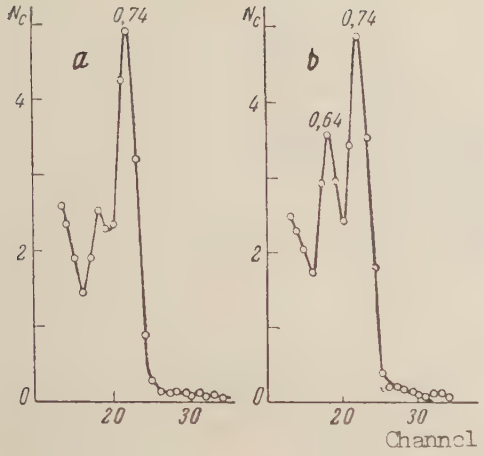

Fig.5. Coincidence spectra: a) with 2.4 Mev γ-rays, b) with 2.1 Mev γ-rays.

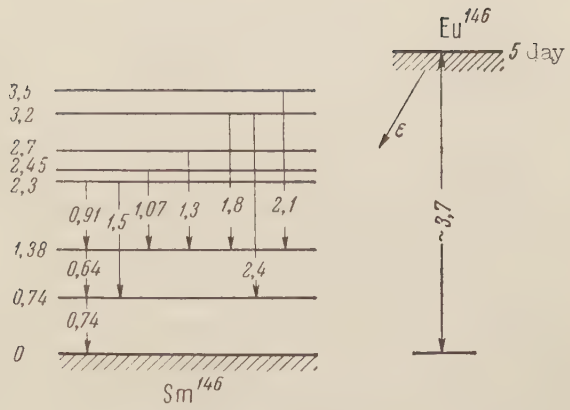

Fig.6. Level diagram for Sm^{146}.

1.5, 1.3, 1.1 and 0.9 Mev. As will be evident from Fig.5, in the spectrum of coincidences with 2.4 Mev γ-rays the 0.74 Mev peak is strongly evinced, while the 0.64 Mev peak is weaker, which agrees with the results of the coincidence experiments with the 0.64 Mev γ-rays. In the spectrum of coincidences with the 2.1 Mev γ-rays, both peaks are present and well defined.

The presence of some 0.64 Mev γ-rays in the coincidence spectrum with the 2.4 Mev γ-rays can be explained by the fact that the gate of the single-channel analyzer when set to 2.4 Mev also passed a number of the 2.1 Mev γ-rays. In this particular experiment it was necessary to use a wide gate in the analyzer because the abundance of 2.4 Mev γ-rays is rather low and the efficiency in detecting them is relatively poor.

Measurements of coincidences with the γ-rays in the 0.9, 1.1 and 1.3 Mev regions give 0.64 and 0.74 Mev peaks of about equal intensity. However, in the spectrum of coincidences with the 1.5 Mev γ-rays there is observed a marked increase in the height of the 0.74 Mev peak, which agrees with the results for coincidences with the 0.64 Mev γ-rays, and gives reason to assume that the 1.5 and 0.64 Mev transitions are not in cascade. It follows that in the 0.64—0.74 Mev cascade the 0.74 Mev transition is the lower one, since the 1.5 Mev and 2.4 Mev transitions go directly to the 0.74 Mev level. Regarding the other transitions, it can be affirmed that they feed the 1.38 Mev level.

Neither in the singles spectrum nor in the coincidence spectra did we observe a cross-over transition from the 1.38 Mev level to the ground state with an intensity > 0.05 that of the 0.74 transition.

In conclusion we propose the version of the decay scheme for Eu^{146} shown in Fig.6; this is consistent with the results of this investigation. The Eu^{146} to Sm^{146} disintegration energy equals 3350 kev according to Cameron's formula and 3700 kev according to Levy's formula[4], which allows the existence of the inferred levels up to 3.5 Mev.

Some of the transitions evinced in the coincidence measurements are probably components of the groups listed in the table (for example, the 1.07 Mev line is presumably a member of the ~1.1 Mev group).

We detected 280 kev γ-rays which yield coincidences with γ-rays in the 115-120 kev region; presumably these γ-rays pertain to the decay of Gd^{146} or Eu^{147}.

"A.F.Ioffee" Physical-Technical Institute,
Academy of Sciences of the USSR

References

1. G.M.Gorodinskii, A.N.Murin, V.N.Pokrovskii & B.K.Preobrazhenskii, Izv. AN SSSR, Ser.fiz., 21, 1624 (1957). (Trans.Bulletin, 21, 1611).

2. N.M.Anton'eva, A.A.Bashilov, B.S.Dzhelepov & B.K.Preobrazhenskii, Zhur. eksp.i teor.fiz., 36, 28 (1959). (Trans.Soviet Physics - JETP.)

3. G.M.Gorodinskii, A.N.Murin, V.N.Pokrovskii, B.K.Preobrazhenskii, & N.E. Titov, Doklady AN SSSR, 112, 405 (1957). (Trans.Doklady.)

4. B.S.Dzhelepov & G.F.Dranitsina, Sistematika energii β-raspada (β-decay energy systematics), M.-L., 1960.

* * * * * * *

LEVELS OF Eu^{147}, Eu^{149} AND Eu^{151}

- E.E.Berlovich, V.N.Klement'ev, L.V.Krasnov & M.K.Nikitin

The level systematics of Eu^{147}, Eu^{149} and Eu^{151} were investigated in the work of Bashilov et al[1] by observation of photoelectrons and internal conversion electrons. The level diagrams of these isotopes have a number of common traits: in particular, all three nuclei presumably have a $h_{11/2}$ level from which there depart M2 type transitions, and E3 type transitions in Eu^{147} and Eu^{149}.

In an earlier study we established the existence of isomeric levels in all three nuclei and measured the lifetimes of these levels (see Ref.2).

In the present work we investigated the level systems of these nuclei by means of a twin scintillation spectrometer. A brief description of the set-up and experimental procedure will be found in Ref.3 (preceding article).

The source was the gadolinium fraction separated chromatographically from the rare earths formed by spallation of a tantalum target with 660 Mev protons in the Joint Institute for Nuclear Research synchrocyclotron.

Eu^{147}

The γ-spectrum of Gd^{147} recorded on a single scintillation spectrometer is reproduced in Fig.1. There are observed the following γ-rays: 230, 380 (370-396), 500, 620, 750, 900, 1100, 1300, 1550 and 1750 kev. To identify these lines the spectrum was recorded at different intervals after irradiation, which enabled us to make a rough evaluation of the decay periods corresponding to the different lines.

Fig.2 shows the spectrum of prompt coincidences with the 230 kev γ-rays of Gd^{147}. There are evident coincidences of the following γ-rays with the 230 kev gammas: 400, 550, 620, 770, 900, 1100, 1300 and 1550 kev. In addition, there were detected prompt coincidences of the 400 kev γ-rays with the 230 kev γ-rays, of the 500 kev γ-region with the 230 kev γ-rays, of the 900 kev γ-rays with the 230 and 620 kev γ-rays, and of the 1550 kev γ-rays with the 230 kev γ-rays. The 1750 kev gammas do not yield coincidences with any of the γ-rays. In the spectrum of coincidences with the 1750 γ-rays there is evident only the K x-ray peak (Fig.3).

We also investigated delayed coincidences. As was shown in Ref.2, the level at 625 kev is an isomeric level with $T = (7.1 \pm 0.4) \cdot 10^{-7}$ sec. It was established

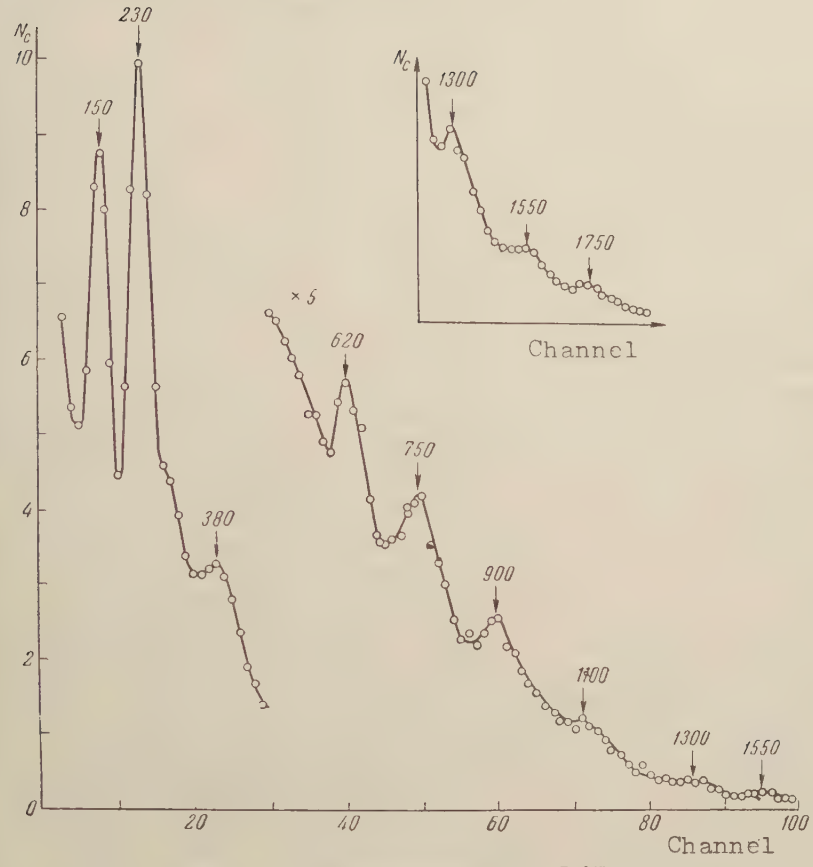

Fig.1. γ-Spectrum of Gd^{147}.

that the 230, 400 and 625 kev γ-rays yield delayed coincidences with the 370 and 930 kev gammas and apparently with γ-rays having energies of about 510 and 570 kev. By way of illustration of coincidences of this type in Fig.4 we reproduce the spectrum of delayed coincidences with the 625 kev gammas. There were observed coincidences of both the 370 kev γ-rays and the 930 kev γ-rays with the 230, 400 and 625 kev gammas. In addition, measurement of the delay coincidences with the γ-rays in the 500 to 600 kev region also showed coincidences with the same 230, 400 and 625 kev gammas. The spectrum of delay coincidences with the 930 kev γ-rays is shown in Fig.5.

Our results are in good agreement with the decay scheme for Gd^{147} proposed by Bashilov et al[1]. However, in view of the complexity of the Gd^{147} decay scheme and owing to the presence of a large number of γ-transitions close in energy, transitions which cannot be resolved by means of a scintillation spectrometer, we were unable to check the location of all the γ-transitions indicated in Ref.1.

Fig.6 shows the level diagram of Eu^{147} consistent with our measurements; this diagram agrees in general with the scheme proposed in Ref.1. No additional levels need be introduced to accomodate the newly detected 1550 and 1750 kev transitions. They can be interpreted as transitions from the 1742 kev level to the first excited state and ground state, respectively. In view of the fact that there were observed prompt coincidences between the 1100 and 230 kev γ-rays, the 1100 kev transition apparently cannot be identified with the 1130 kev transition indicated in the decay scheme proposed by Bashilov et al. In order to insert the 1100 kev transition into the decay scheme one must introduce a new level at 1330 kev.

The existence of prompt 230-400 kev coincidences is in agreement with the results of Dzhelepov & Sergienko[4] on $e^- - e^-$ coincidences. The existence of coincidences of 230 kev γ-rays with the 770 and 900 kev gammas is substantiated by the measurements carried out on a $\beta-\gamma$ coincidence spectrometer (see Ref.5).

Eu^{149}

In the spectrum of Gd^{149} there were observed γ-rays of the following energies: 150, 300, 350, 500, 790 and 940 kev, which is in agreement with the results

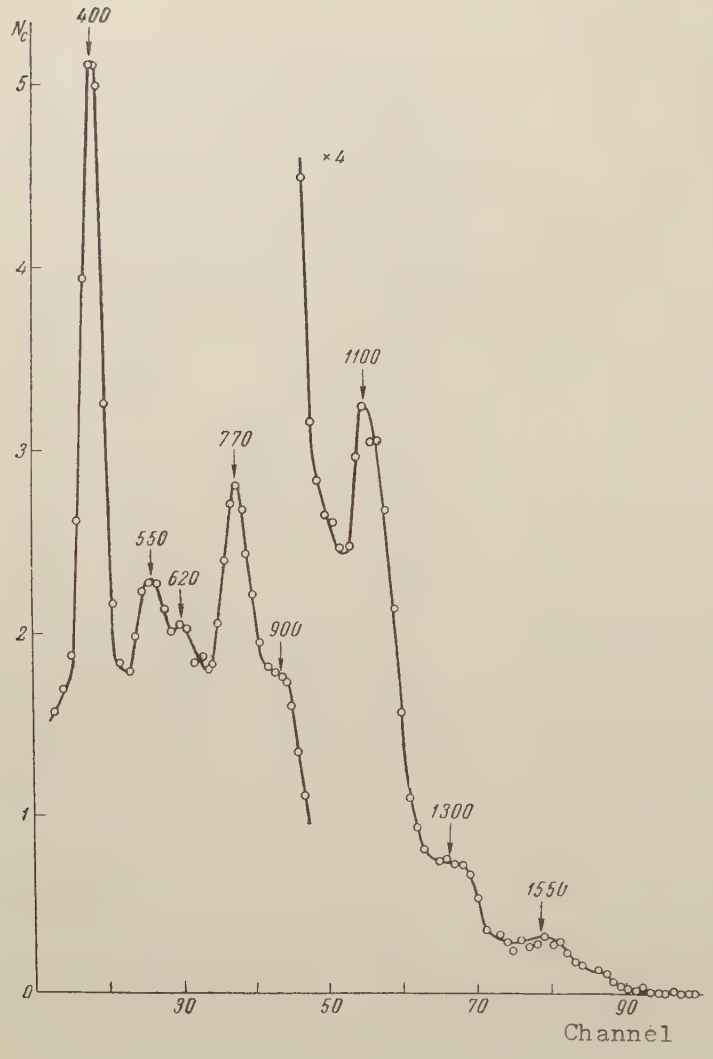

←Fig.2. Spectrum of prompt coincidences with the 230 kev γ-rays of Gd^{147}.

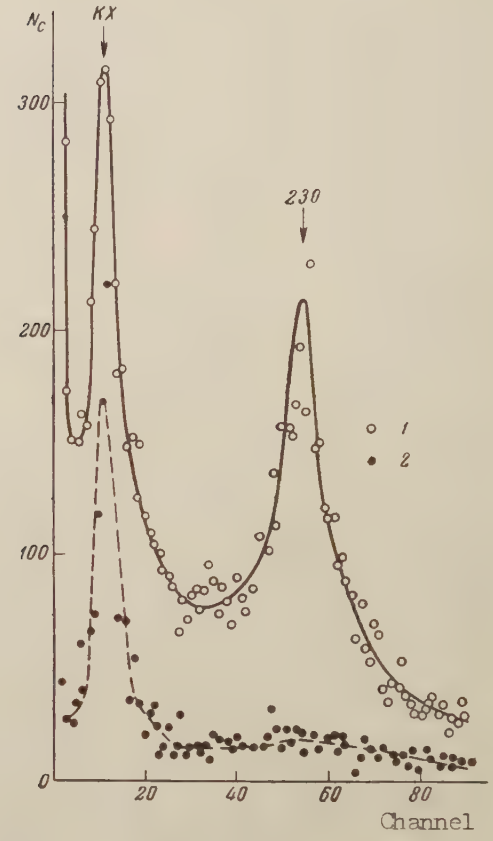

Fig.3. 1) Spectrum of coincidences with the 1550 kev γ-rays of Gd^{147}, 2) spectrum of coincidences with the 1750 kev γ-rays of Gd^{147}.

of Bashilov et al[1]. It was found that the 150 kev γ-rays yield prompt coincidences with the 350, 520 and 790 kev gammas (Fig.7). There were also observed coincidences of the 350, 520 and 790 kev γ-rays with the 150 kev gammas. Coincidences between the 150 and 350 kev γ-rays were also observed in the work of Sergienko[4] and Strominger[6]. Strominger also detected coincidences of the 150 kev γ-rays with the 500 and 750 kev γ-rays; these coincidences probably correspond to the coincidences observed by us between the 150 γ-rays and the 520 and 790 kev gammas. The 750-630 kev coincidences reported by Strominger[6] probably pertain to the decay of Eu^{146} forming from Gd^{146} (see Ref.3).

As was shown in Ref.2, the level at 496 kev is an isomeric level with a lifetime of $(2.48 \pm 0.05) \cdot 10^{-6}$ sec. We also carried out measurements of delayed coincidences. In the spectra of delayed coincidences with the 150, 350 and 500 kev γ-rays there are present 300 kev gammas, but no higher energy γ-rays with an intensity exceeding 5% relative to the intensity of the 300 kev line. By way of illustration in Fig.8 we show the delayed coincidence spectrum with one arm of the spectrometer set on 350 kev. The spectrum of delayed coincidences with the

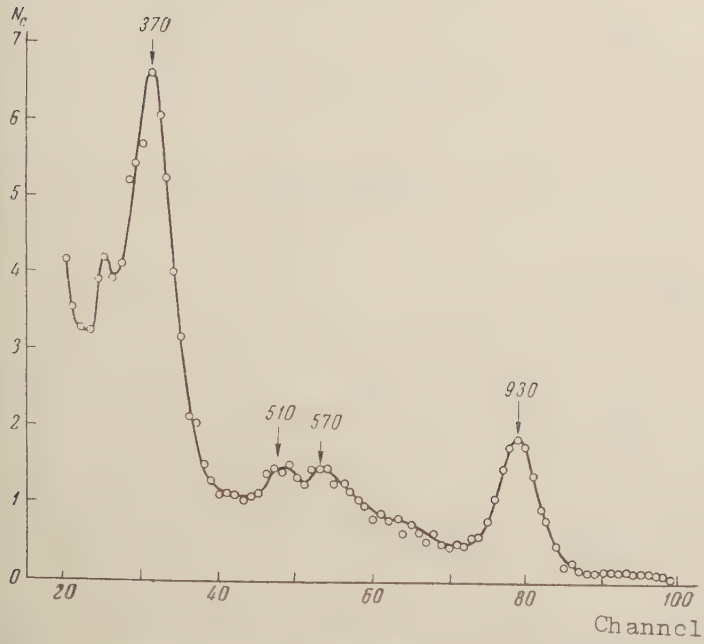

Fig.4. Spectrum of delayed coincidences with the 625 kev γ-rays of Gd^{147}.

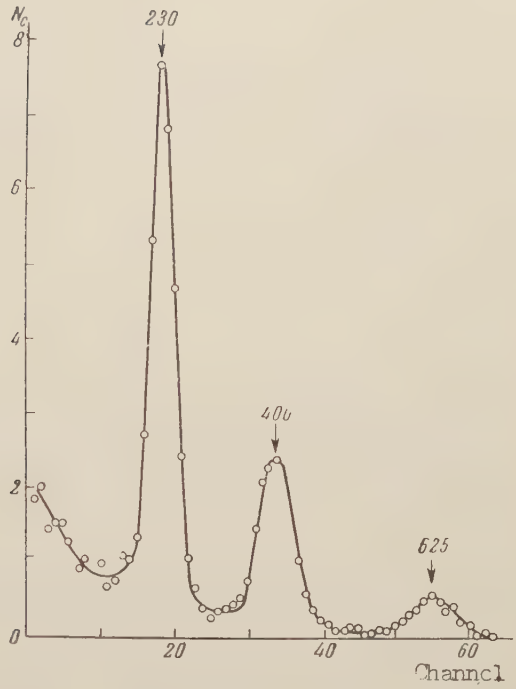

Fig.5. Spectrum of delayed coincidences with the 930 kev γ-rays of Gd^{147}.

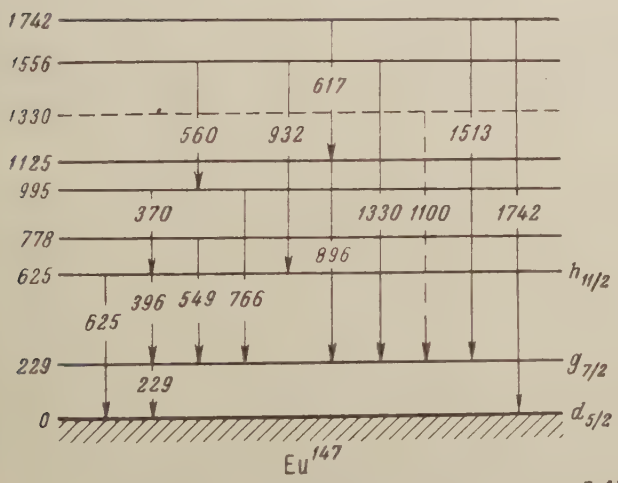

Fig.6. Level diagram of Eu^{147}.

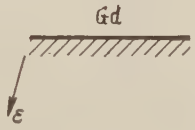

300 kev γ-rays is reproduced in Fig.9. It will be evident from this figure that coincidences are observed with the 150, 350 and 500 kev γ-rays. These measurements clearly indicate that the 300 kev transition is situated above the isomeric level.

Eu^{151}

It was shown in the work of Ref.2 and by Shirley & Rasmussen[7] that the Eu^{151} nucleus has an isomeric level that is situated above the 175 kev transition; according to Ref.2 the lifetime of the isomeric level is $(5.8\pm0.3)\cdot10^{-5}$ sec. Sergienko[4] showed that the 175 kev γ-rays yield coincidences with the 22 kev γ-rays. Thus the energy of the isomeric level is presumably 197 kev.

In the present work we investigated delayed coincidences in Eu^{151}. It was

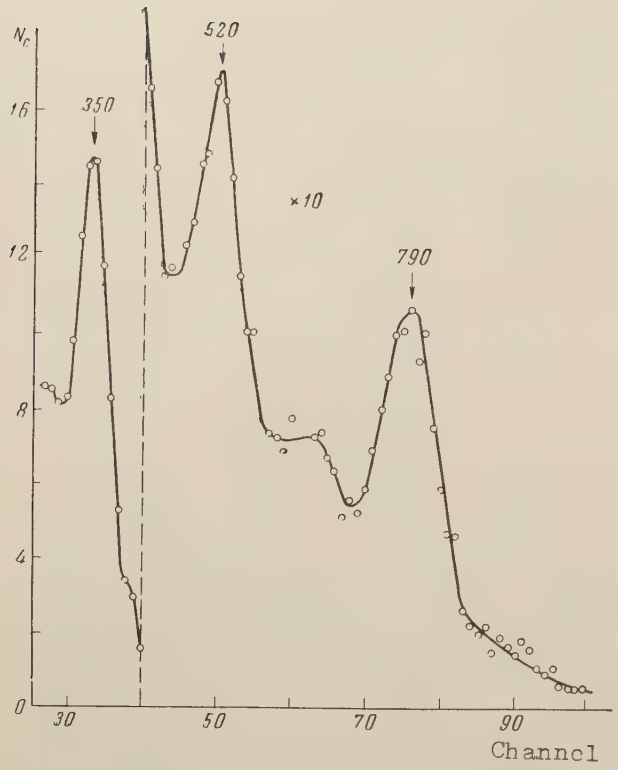

Fig.7. Spectrum of prompt coincidences with the 150 kev γ-rays of Gd^{149}.

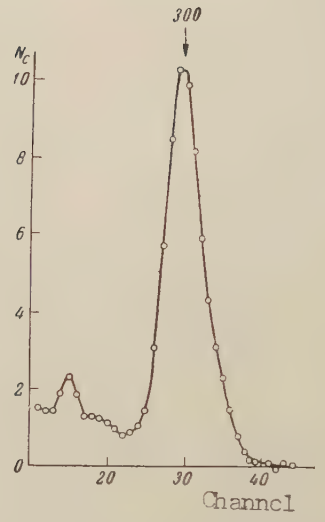

Fig.8. Spectrum of delayed coincidences with the 150 kev γ-rays of Gd^{149}.

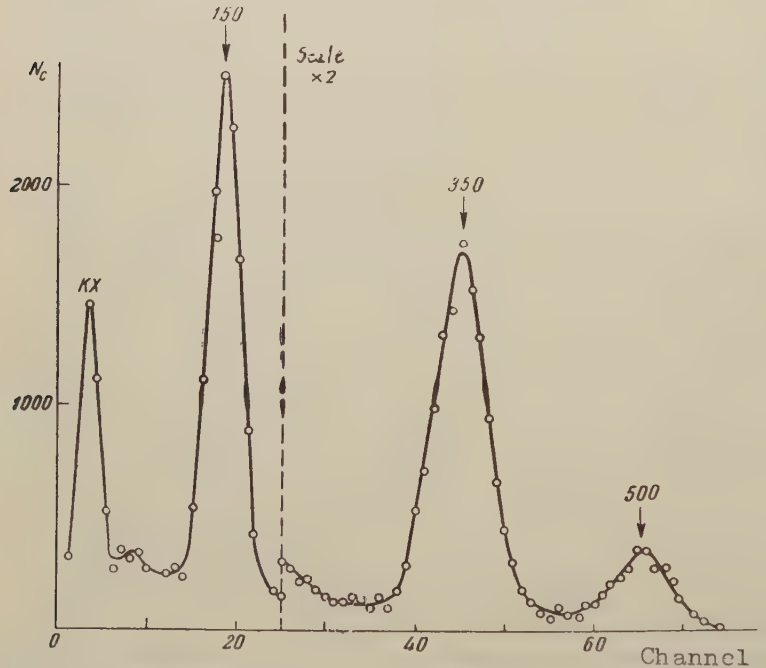

Fig.9. Spectrum of delay coincidences with the 300 kev γ-rays of Gd^{149}.

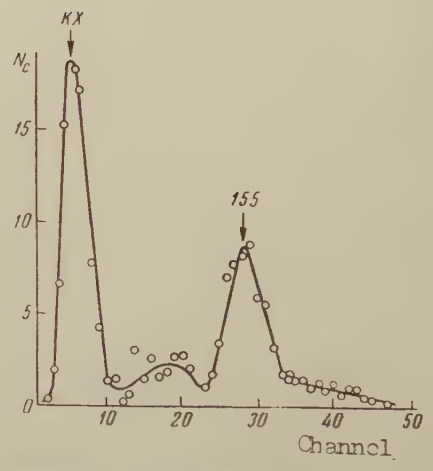

Fig.10. Spectrum of delay coincidences with the 175 kev γ-rays of Gd^{151}.

found that the 175 kev γ-rays yield coincidences with the 155 kev gammas. The spectrum of delayed coincidences with the 175 kev γ-rays is shown in Fig.10.

We observed no delayed coincidences with the 243 kev γ-rays with delays in either arm of the spectrometer, which indicates that this transition is not located above the isomeric level. Moreover, the 243 kev γ-transition is not in prompt cascade with the 175 kev transition inasmuch as in the experiments in which the 155 kev γ-rays were delayed and coincidences with the entire spectra recorded, the 243 kev γ-rays were not evinced.

"A.F.Ioffe" Physical-Technical Institute,
Academy of Sciences of the USSR

References

1. N.M.Anton'eva, A.A.Bashilov, & B.K.Preobrazhenskii, Izv.AN SSSR, Ser. fiz., 22, 895 (1958) (Trans.Bulletin, 22, 889); V.K.Adamchuk, A.A.Bashilov & B.K.Preobrazhenskii, Ibid., 22, 919 (1958) (Trans.Bulletin, 22, 911); N.M.Anton-'eva, A.A.Bashilov, B.S.Dzhelepov & B.K.Preobrazhenskii, Ibid., 22, 135 (1958) (Trans.Bulletin, 22, 134).

2. E.E.Berlovich, V.N.Klement'ev, L.V.Krasnov, M.K.Nikitin & I.Yursik, Doklady, AN SSSR, 133, 789 (1960). (Trans.Soviet Physics - Doklady.)

3. E.E.Berlovich, V.N.Klement'ev, L.V.Krasnov & M.K.Nikitin, Present issue of the Bulletin, p.200.

4. B.S.Dzhelepov & V.A.Sergienko, Izv.AN SSSR, Ser.fiz., 23, 211 (1959) (Trans.Bulletin, 23, 203); Ibid., 23, 219 (1959) (Trans.Bulletin, 23, 211).

5. E.E.Berlovich, M.K.Nikitin, E.N.Tunimanova & D.M.Khai, Ibid., 25, 90 (1960). (Trans.Bulletin, 25, No.1.)

6. D.Strominger, Nucl.Phys., 4, 395 (1957).

7. V.S.Shirley & J.O.Rasmussen, Phys.Rev., 109, 2092 (1958).

Note added in proof: After presentation of this report, we established the existence of a 108-243 kev cascade, which can readily be located between the known 352 kev level and the ground state of Eu^{151}. This involves the introduction of a level at 243 kev, which is populated mainly by K capture in Gd^{151}.

MEASUREMENTS OF THE LIFETIMES OF THE FIRST EXCITED STATES OF Tb^{159} AND Yb^{173} BY MEANS OF A MULTICHANNEL TIME ANALYZER

- E.E.Berlovich, M.P.Bonitz* & V.V.Nikitin

Introduction

Multichannel time analyzers are coming into increasing use for measuring the lifetimes of excited nuclear states.[1-8]

The procedure based on use of a multichannel time analyzer has a number of advantages over the "classical" single-channel time analyzer technique.[9] One of the principal advantages is that the measuring time is appreciably reduced. In addition, the multichannel time analyzer method, based on the principle of conversion of time intervals to corresponding electric pulse amplitudes, differs from the "classical" procedure in a number of important respects.[8] For example, the coincidence counting efficiency does not depend on the energy of the coinciding particles and is always 100%. On the other hand, the time scale is not constant, but requires redetermination with every change in the experimental conditions.

The instrument developed by us and described below satisfies the requirements set for multichannel time analyzers: linearity in the working range, increase in the converter output amplitudes with increase of the delay between the coinciding pulses, unambiguous relationship between the converter output amplitude and the delay between the pulses, and convenient procedure for determining the time scale. Very important is the method employed by us for checking the choice of experimental conditions[8], i.e., the method of eliminating possible apparatus time shifts, which is particularly important in measuring lifetimes of the order of 10^{-10}-10^{-11} sec in the case of low energy transitions.

1. Description of the Time Analyzer

As will be evident from the block diagram reproduced in Fig.1, the apparatus comprises a "slow" part (amplifiers, differential discriminators and a "slow" triple coincidence circuit) and a "fast" part (pulse limiters, shaping cables, variable delay line and time-to-amplitude converter).

Here we shall describe only the "fast" part, which is diagramed in Fig.2. The pulses A and B, shaped in duration and amplitude, the time delay between which is subject to variation, are fed into the spiral delay line.[9,10] The D2V type crystal diode D_1 serves as a converter. In a certain range of delays between A and B, the output amplitude I is a linear function of the delay time (Fig.3). The crystal diode D_2 fulfills the function of a coincidence control circuit; the purpose of this circuit is to reduce the number of chance coincidences by half and to insure an unambiguous relation between the output amplitude of the converter and the delay between pulses. The diodes are cut off for single pulses by means of a positive bias. (Actually, a part of single pulses passes through the diodes; the control procedure described below is based on this fact.) The pulse spectrum from the converter output is applied through an amplifier to the pulse height analyzer, which records the coincidence curves.[11]

To obtain meaningful results the time scale must be determined for the spectrum (curve) obtained by means of the pulse height analyzer. To this end a time delay Δt is introduced between the pulses A and B and the corresponding shift of the coincidence curves is determined (see Fig.3). The described system is extremely convenient for stepless variation of the delay time from 10^{-11} sec to

---

*Dresden Polytechnic Institute.

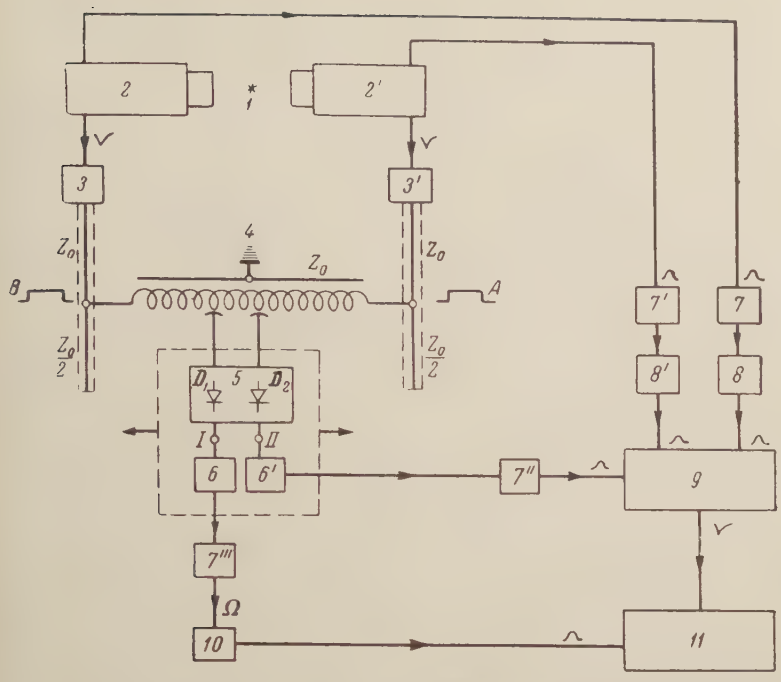

Fig.1. Block diagram of the time analyzer: 1 - investigated source, 2 & 2' - photomultipliers, 3 & 3' - vacuum tube limiters shaping the standard height of pulses A and B, 4 - variable delay line with characteristic impedance Z_o; the duration (width) of pulses A and B is shaped by means of short circuited cables with characteristic impedance $Z_o/2$, 5 - converter-coincidence control circuit system with diodes D_1 and D_2, 6 & 6' - cathode followers, 7,7',7'' & 7''' - amplifiers, 8 & 8' - differential discriminators, 9 - triple coincidence circuit supplying control pulses to the amplitude analyzer, 10 - constant delay insuring the appropriate time sequence of the control and measuring pulses entering the pulse height analyzer, 11 - pulse height analyzer.

several microsec with an accuracy to 10^{-11} sec.

To illustrate the operation of the apparatus "self-coincidence" and "prompt coincidence" curves are reproduced in Figs.4 & 5, respectively. For obtaining the self-coincidence curve the output pulses from one photomultiplier are applied to both limiters and hence pulses A and B always reach the inputs of the delay lines simultaneously. The control pulse for the pulse height analyzer is taken from the output of the corresponding differential discriminator, the gate of which in our case was set on the "hard" part of the Compton distribution in the stilbene crystal receiving the radiation from a Co^{60} source. The given crystal occupied only the central part (15 mm in diameter) of the FEU-33 photomultiplier cathode; the thickness of the crystal was 3 mm. Under these conditions the resolution 2τ was less than $1.5 \cdot 10^{-10}$ sec. With increase of the crystal dimensions to 30 x x 30 mm the resolving time

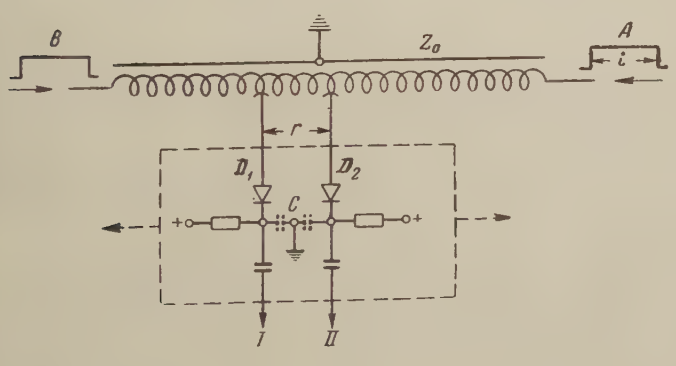

←Fig.2. Diagram of the time-amplitude converter with control coincidence circuit: A & B - coinciding pulses of duration l, Z_o - characteristic impedance of the spiral variable delay line, D_1 - crystal diode of the time-amplitude converter, D_2 - crystal diode of the coincidence control circuit, 4 - time separation between D_1 and D_2, C - stray capacity, I & II - outputs to cathode followers.

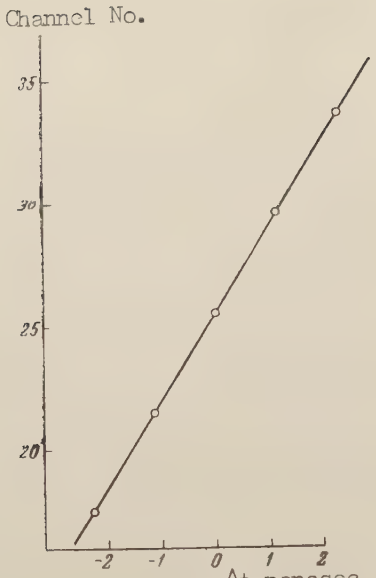

Fig.3

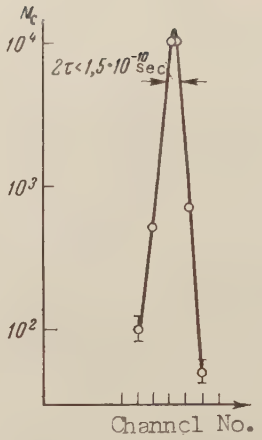

Fig.4

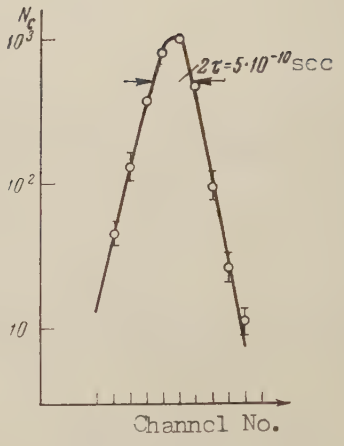

Fig.5

Fig.3. Variation in the position of the coincidence curves with the delay.

Fig.4. Self-coincidence curve in semilogarithmic coordinates. Channel width - $2.11 \cdot 10^{-11}$ sec.

Fig.5. Prompt coincidence curve for the cascade γ-rays of Co^{60} plotted in semilogarithmic coordinates. Channel width - $1.57 \cdot 10^{-10}$ sec.

increased to $3.5 \cdot 10^{-10}$ sec. For the two cascade radiations from Co^{60} under the former experimental conditions (with two separate detectors) there was obtained the prompt coincidence curve with a resolution of $\sim 5 \cdot 10^{-10}$ sec.

This resolution is the optimum one. With larger crystals and lower radiation energies the resolution is impaired. Decrease in the resolution in going to lower energies of the particles in coincidence is due to increase of the scatter in the time $(\overline{\Delta t})^2$ of appearance of the first l photoelectrons on the photomultiplier cathode; according to the formula of Post & Schiff[12]

$$(\overline{\Delta t})^2 = \frac{\tau^2 p^l}{n^2}\left(1 + \frac{2(l+1)}{n} + \ldots\right), \qquad (1)$$

where n is the mean number of photoelectrons appearing in one scintillation, and τ_p is the decay time of the phosphor.

For this reason the coincidence curves obtained in determining the lifetimes of the first excited states of Tb^{159} and Yb^{173} with energies of 58 and 79 kev, respectively, are characterized by a resolution substantially below the optimum one (Figs.6 & 7). In addition to its influence on the resolution, the energy also affects the position of the coincidence curve. The influence of the selected energy intervals of the particles in coincidence and the position of the coincidence curve may be described as follows:

a) With variation in energy (expressed in terms of n) there is a corresponding variation of the instant of the appearance of the l-th photoelectron on the cathode and hence on the anode of the photomultiplier:

$$t = \frac{\tau_p l}{n}\left(1 + \frac{l+1}{2n} + \ldots\right). \qquad (2)$$

This means that transition from one energy of the coinciding particles to a different energy has the same effect as the introduction of an artificial delay, i.e., results in shift of the coincidence curve.

b) In going from one energy to another (which can, for example, be readily realized in the continuous Compton spectrum from γ-rays or a continuous β-spectrum) there occurs a change in the leading and trailing edges of the shaped pulses A and B entering into the coincidence circuit; the lower the energy the longer will be the rise and decay times of the pulses. It will be evident that lower energies will lead to lower amplitudes of the output pulses from the converter and hence to shift of the coincidence curve to the "left".

Measurements of extremely short times are usually carried out by determining the shift of the center of gravity of the coincidence curve for the measured source relative to the center of gravity of the coincidence curve obtained with a reference source (with a vanishingly short or well-known lifetime). It follows that to exclude the apparatus time shifts one must either insure the same energy intervals for the investigated and reference sources[13] or in cases when this is impossible, one must take into account the apparatus shifts, as has been done in a number of investigations[14,15].

In practice, however, even fulfillment of the requirement of equivalence of the energy intervals in measurements with two sources proved to be insufficient: owing to the finite width of these intervals the variation of the spectra inside these intervals for the two sources produces some effect[14,16]. The magnitude of this effect is such that a 2% difference (in the energy scale) in the positions of the centers of gravity of the spectra of the two sources in one of the intervals produces a time shift of the coincidence curve amounting to 10^{-11} sec.

One of the factors giving rise to the apparatus time shift of the coincidence curve is incorrect choice of the intensity of the compared sources. Change in the intensity of the source leads to change in the amplification factor of the photomultipliers and the amplifiers in the side channels. Experiments show that these changes are minimal for close integral intensities of the compared sources.

The influence of the above factors (shape of the spectra in the working interval and the intensity of the sources) can be checked and monitored by means of the following "single pulse curve control" procedure. This procedure consists in utilizing single pulses that pass through the cut-off converter diode owing to the presence of stray capacitance and the finite value of the back resistance of the diode. These pulses after amplification are subjected to pulse height analysis. The pulse height analyzer is set to admit only pulses corresponding to the chosen energy interval. The single pulse curves obtained in this manner vary in shape and position depending on the choice of the spectrum interval: at higher energies there are obtained higher amplitudes of the single pulses and a lesser width of the distribution curves. This is explained by the above-mentioned influence of the energy both on the steepness of the leading and trailing edges of the pulses A and B and on the scatter in steepness. Thus the shape and position of the single pulse curves characterize the amplitude spectrum in the side channel. Obviously, the intensity of the source, because of the above noted influence of the intensity on the amplification, affects the single pulse spectrum in an analogous manner.

Hence for proper performance of the experiment one must do the following:

1. Roughly select the necessary energy intervals for the investigated source.

2. Provide approximately equal integral intensities of the measured and reference sources (if the detected radiation consists of electrons equalization in intensity can be carried out by means of apertures).

3. Adjust and set the position and width of the gates in the side channels so that the position and shape of the single pulse curves for the investigated and reference sources will coincide.

It may be noted that the single pulse control procedure can be carried out very rapidly if, for example, for rapid interchange of sources one uses a light shutter and for the pulse height analyzer an AI-100 type analyzer, on the screen of which one can view the single pulse curves for a sufficient length of time. The above described procedure was rigorously adhered to in carrying out the experiments described below.

2. Description of the Experiments

The 58 kev level of Tb^{159}

The 58 kev transition is the most intense transition in Tb^{159} formed in the decay of Dy^{159} by electron capture. This transition is strongly converted[17,18]; hence it is convenient to measure the lifetime of the 58 kev level by detecting coincidences of the L shell conversion electrons with the characteristic 43 kev x-rays accompanying the electron capture. The gate in the left channel (pulses B, Fig.1) was set on the L electron spectrum, obtained by means of a thin (<1 mm) stilbene crystal. The number of 58 kev γ-rays detected by the crystal is negligibly small. The gate in the right channel (pulses A) was set on the photopeak from the x-rays which is clearly evinced in a thick (30 x 30 mm) stilbene crystal.

One of the experimental difficulties is that the expected shift of the x_{cap}-e delayed coincidence curve is reduced by half because these coincidences cannot be separated from the prompt coincidences between the conversion electrons and the x-rays accompanying them (e-x_{conv} coincidences).

Another difficulty is that the spectrum of Dy^{159} is very "short", while the spectrum of Co^{60}, which we first selected as the reference source, is very "long"; consequently, the expected number of coincidences for Co^{60} in the requisite energy intervals is small. In order to eliminate the influence of possible drift of the electronic circuits one must carry out the measurements alternately for equal times for Dy^{159} and for the reference source, but owing to the low coincidence rate for Co^{60} there would in this case be required an inordinately long experimental time to obtain reliable statistics. It would be desirable, of course, to have a reference source with a "shorter" spectrum and a short level lifetime. However, since level lifetimes generally vary inversely with the transition energy, it was virtually impossible to find the source with a transition energy close to the radiation energy of Dy^{159} and a vanishingly short lifetime of the level, so as a compromise we had to choose Hg^{203}, which decays by emission of β-particles with an end-point energy of 200 kev to the 279 kev level

Table 1

Lifetimes of the 279 kev state of Tl^{203} according to the data of different authors

Method	T, 10^{-10} sec	Refs.
Coulomb excitation	3.6±1.2	19
	3.2±0.4	20
Resonance scattering	2.7±0.5	21
Delay coincidences	2.1±0.7	22
	2.9±0.3	16
	2.5±0.7	23
	2.9±0.2	24
	2.9±0.2	8

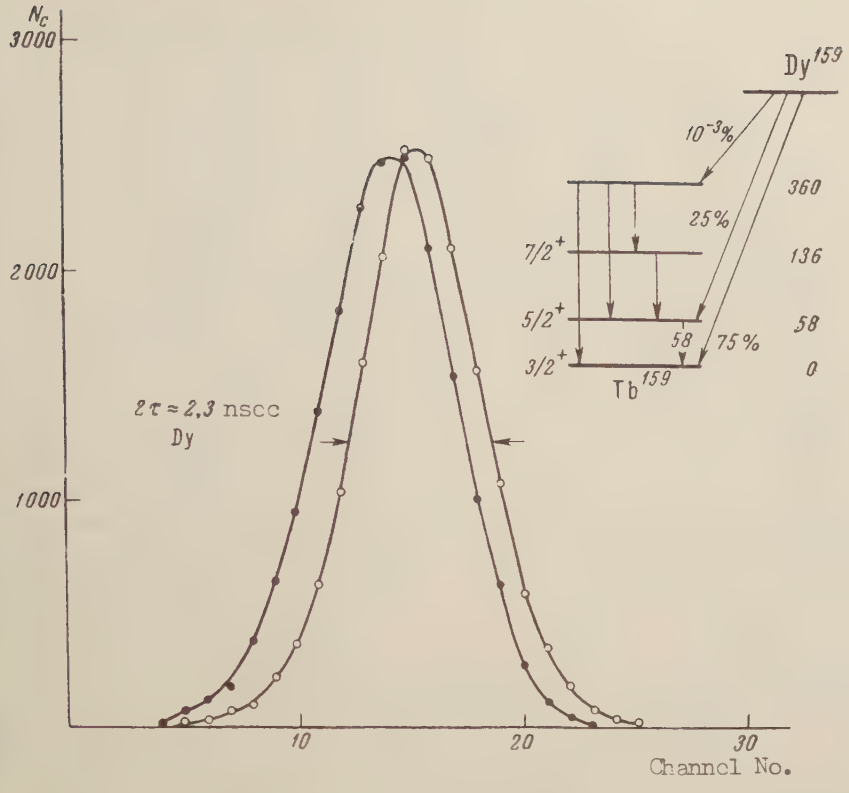

Fig.6. Coincidence curves obtained for determining the lifetime of the first excited state of Tb^{159}. Channel width $1.92 \cdot 10^{-10}$ sec. Open circles - points obtained for the Dy^{159} source; solid circles - points for the Hg^{203} reference source. Insert - decay scheme for Dy^{159}.

of Tl^{203}. The lifetime of this state has been measured by a number of authors (Refs.8,16,19-24) and the results obtained are in good agreement, as may be seen in Table 1. The weighted mean of all the listed values for the half-life of the 279 kev state of Tl^{203} is

$$T = (2.90 \pm \pm 0.12) \cdot 10^{-10} \text{ sec.}$$

The coincidence curves obtained in these experiments are reproduced in Fig.6. The relative shift of the centers of gravity of the curves is the sum $\tau_{Hg} + (1/2)\tau_{Dy}$ because the β-γ coincidences for Hg^{203} and the γ-β coincidences for Dy^{159} have a tendency to shift the curves in opposite directions. In view of the properties of the analyzer described above, the coincidence curve is shifted to the side of the input of the pulses from the preceding radiation. Hence in Fig.6 the curve for the Hg^{203} case is located to the left of the curve for Dy^{159}. Analysis of the experimental curves leads to the following value for the half-life of the 58 kev state of Tb^{159}:

$$T = (1.3 \pm 0.4) \cdot 10^{-10} \text{ sec.}$$

Ketelle & Brosi[18] in studying the decay of Dy^{159} showed that the half-life of the 58 kev level in Tb^{159} is $<10^{-9}$ sec.

The 79 kev level of Yb^{173}

The strongly converted[25] 79 kev transition in Yb^{173} is in cascade with an intense transition of 272 kev energy. A special experiment carried out with an aluminum absorber for stopping the conversion electrons showed that owing to the low efficiency of the stilbene crystal in detecting γ-rays the coincidences of the 272 kev γ-rays with the preceding K x-rays can be neglected. A resonance absorber consisting of 1 mm phosphor bronze was mounted in front of the large crystal in order to decrease the load due to x-rays.

By way of reference source in these experiments we used Co^{60} inasmuch as the

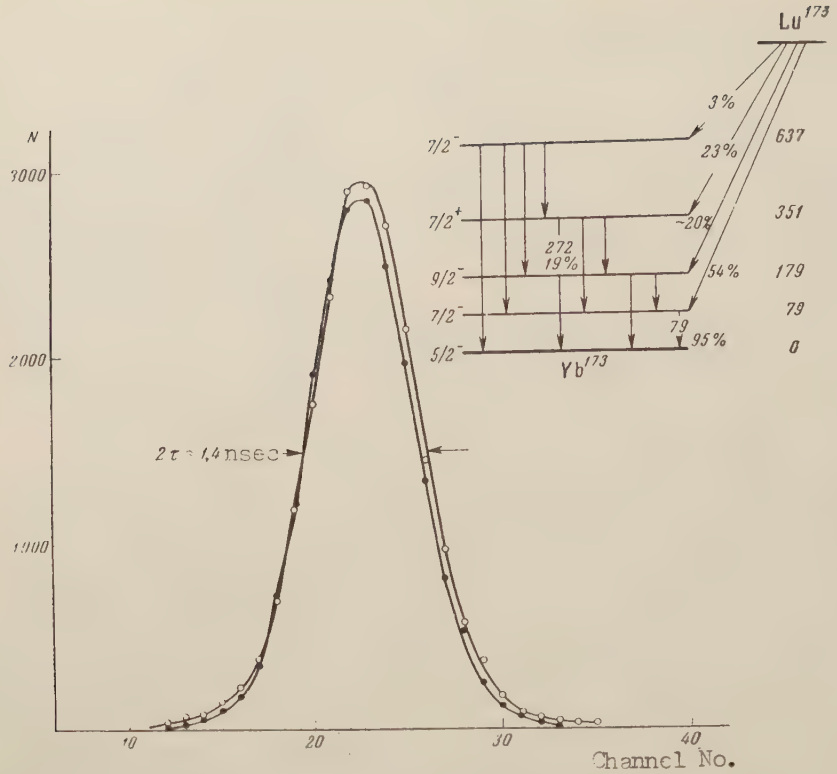

Fig.7. Coincidence curves obtained for determining the lifetime of the first excited state of Yb^{173}. Channel width $2.16 \cdot 10^{-10}$ sec. Open circles - points obtained for the Lu^{173} source; solid circles - points for the Co^{60} reference source. Insert - decay scheme for Lu^{173}.

requisite energy intervals here lie higher than in the case of Dy^{159}; moreover in the case of Lu^{173} only a small fraction of the total load participates in the investigated coincidences, so that the counting rate for the Lu^{173} and Co^{60} sources proved to be approximately equal. The measurement procedure was analogous to that for the Dy^{159} source. The curves obtained in one of several series of measurements are reproduced in Fig.7. Analysis of the results led to the following value for the half-life of the 79 kev level in Yb^{173}:

$$T = (3.8 \pm 0.5) \cdot 10^{-11} \text{ sec.}$$

3. Discussion of the Results

Both the investigated transitions are nearly pure M1. In the case of the 78.7 kev transition in Yb^{173}, according to the most reliable data of Romanov et al[25], the admixture of E2 is 4.5%. There are no precise data on the admixture for the 58 kev transition in Tb^{159}. Mihelich et al[17] give the following ratios for the conversion coefficients: $L_I:L_{II}:L_{III}:M:N = 1000 : 140 : 125 : 305 : 80$.

Attempts to determine the admixture of E2 by using the theoretical values of the L subshell conversion coefficients calculated taking into account finite nuclear size[26] and using M shell conversion coefficients evaluated without taking finite nuclear size into account[27] led to values of the order of 1-2% for the admixture, but it proved impossible to obtain conversion coefficient ratios reasonably close to those cited above by any choice of admixture. Possibly this is connected with inaccuracies in determining the experimental ratios, owing to the low energy of the electrons involved.

Knowledge of the periods for magnetic dipole transitions and of the nuclear magnetic moments μ makes it possible to determine the collective motion and internal motion (single-particle) gyromagnetic ratios g_R and g_K by means of the relationship

$$\lambda(M1) = \frac{16\pi}{9} \cdot \frac{1}{\hbar} \left(\frac{E_\gamma}{\hbar c}\right)^3 B(M1)\downarrow, \qquad (3)$$

where the reduced M1 transition probability

Table 2

Comparison of the reduced transition probabilities, gyromagnetic ratios and values of Q_0 following from the results of the present investigation and from other studies

Nucleus & transition	1 T_{exp}, 10^{-11} sec	2 δ^2	3 α	4 $T_\gamma(M1)_{exp}$ 10^{-11} sec	5 $T_\gamma(M1)_{Weisskopf}$, 10^{-11} sec	6 $\frac{T_\gamma(M1)_{exp}}{T_\gamma(M1)_{Weisskopf}}$	7 $B(M1)\downarrow_{exp}$ $\left(\frac{eh}{2Mc}\right)^2$	8 $B(E2)\downarrow$ $e^2 \cdot 10^{-48}$, cm^4	9 g_K	10 g_R	11 Q_0 10^{-24}, cm^2	Refs.
Tb^{159} 58kev	13	0,02	10,4	150	6,7	23	0,13	1,8	1,6	0,1	6,9	[28]
									1,49	0,25	8,1	[29]
		0,04	10,7	160		24	0,12	2,10	1,37	0,44	7,85	Our data
Yb^{173} 79kev	3,8	0,047	7,05	32	2,5	9	0,25	2,15			7,6	[32]
								2,4	—0,49	+0,31	8,2	[31]
								2,5	—0,52	+0,35	8,4	Our data

$$B(M1)\downarrow = \frac{3}{4\pi}(g_K - g_R)^2 \frac{K^2(I+1-K)(I+1+K)}{(I+1)(2I+3)} \qquad (4)$$

and

$$\mu = g_K \frac{K^2}{I+1} + g_R \frac{I(I+1)-K^2}{I+1}. \qquad (5)$$

In using the Coulomb excitation method the reduced E2 transition probability $B(E2)$ is determined from experiment, while the value of $B(M1)$ is calculated from the intensity ratio $\delta^2 \frac{\lambda(E2)}{\lambda(M1)}$. In cases, however, when the M1 component greatly predominates, determination of the gyromagnetic ratios by the method of Coulomb excitation proves to be unreliable inasmuch as it is based on precise knowledge of the small admixture of E2.

Obviously, in this situation, which is not uncommon, it is expedient to make direct measurements of the level lifetimes by the method of delay coincidences.

In Table 2 we list the results of our measurements together with the data of other authors. Column 4 gives the values of the radiative half-life $T_\gamma(M1)$, while column 7 gives the values of the reduced M1 transition probability $B(M1)\downarrow$, calculated for the E2 admixtures indicated in column 2. In view of the great predominance of the M1 component, minor variation in the admixture has virtually no effect on the calculated values of $T_\gamma(M1)$ and $B(M1)$.

In columns 9 and 10 of Table 2 we list, respectively, the values of g_K and g_R.

For the two assumed admixtures (4% and 2%) for the 58 kev transition in Tb^{159} the gyromagnetic ratios, like the reduced probabilities $B(M1)$, are virtually the same. In contrast, the value of $B(E2)\downarrow$ (column 11) shows a strong dependence on the amount of admixture.

The values of the g factors for Tb^{159} obtained in the work of Huus et al[28] and in the work of Martin et al[29] from Coulomb excitation of the 137 kev level differ greatly from our values.

In order to obtain on the basis of our measurements reasonable values for the internal quadrupole moment of Tb^{159} it must be assumed that the admixture of E2 in the 58 kev radiation is about 4%.

The experimental value of the magnetic moment of Tb^{159} was determined by Baker & Bleaney[30], who give $\mu = \pm 1.5$ n.m., but did not determine the sign from experiment. It may be noted, however, that most odd-Z nuclei have positive magnetic moments; in cases when they are negative the absolute values are small and generally do not exceed 0.2 nuclear magnetons. In view of this the plus sign was chosen. The sign of the ratio $g_K - g_R/Q_0$ was determined from angular correlation experiments[29], consequently of the two sets of values of g_K and g_R obtained in solving Eqs.(4) and (5), one was chosen.

Our values for the gyromagnetic ratios of Tb^{173} are $g_R = 0.35 \pm 0.04$ and $g_K = -0.52 \pm 0.02$; these are close to the values obtained by deBoer et al[31] from Coulomb excitation of the 78.7 kev level. In view of the fact that the admixture of E2 is fairly reliably known to be 4.5% in this case[25], the values of the reduced E2 transition probability $B(E2)\downarrow$ and the internal quadrupole moment Q_0 (8.4 barns) calculated by us are in reasonably good agreement with the corresponding results obtained from Coulomb excitation experiments[31,32].

It is interesting to note that the values of the collective motion gyromagnetic ratios obtained in our experiments, namely, $(g_R)_{Tb^{159}} = 0.44 \pm 0.10$ and $(g_R)_{Yb^{173}} = 0.35 \pm 0.04$, agree within the limits of the experimental error with the evaluations based on the unified nuclear model for uniformly distributed charge, which yield 0.41 for Tb^{159} and 0.4 for Yb^{173}.

"A.F.Ioffe" Physical-Technical Institute,
Academy of Sciences of the USSR

References

1. G.Jones & J.B.Warren, J.Sci.Instr., 33, 429 (1956).
2. C.Cottini & E.Gatti, Nuovo Cimento, 4, 1550 (1956).
3. R.E.Green & R.E.Bell, Nucl.Instr., 3, 127 (1958).
4. A.W.Sunyar, Proceedings on the Second UN Conference on Peaceful Uses of Atomic Energy, 14, 347 (1958).
5. A.G.Khabakhpashev & E.M.Tsenter, Zhur.eksp.i teor.fiz., 37, 991 (1959). (Trans.Soviet Physics - JETP.)
6. R.E.Bell & M.H.Jorgensen, Nucl.Phys., 12, 413 (1959).
7. S.Gorodetzky, R.Manquenouille, R.Richert & A.Knipper, J.Phys.Rad., 21, 439 (1960).
8. M.Bonitz & E.E.Berlovich, Nucl.Instr., 9, 13 (1960).
9. R.E.Bell, R.L.Graham & H.E.Petch, Can.J.Phys., 30, 35 (1952).
10. E.E.Berlovich, Izv.AN SSSR, Ser.fiz.,19,343 (1955). (Trans.Bulletin, 19, 305.)
11. Z.Bay, IRE Transactions of Nuclear Science, NS-3, 12 (1956).
12. R.F.Post & L.I.Schiff, Phys.Rev., 80, 113 (1950).
13. E.E.Berlovich, Izv.AN SSSR, Ser.fiz., 20, 1438 (1956). (Trans.Bulletin, 20, 1315.)
14. E.Bashandy, Nucl.Instr., 6, 289 (1960).
15. E.E.Berlovich, V.V.Il'in, A.I.Kislyakov, M.K.Nikitin & T.Bedike, Izv.AN SSSR, Ser.fiz., 24, 1492 (1960). (Trans.Bulletin, 24, 1483.)
16. E.E.Berlovich & G.V.Dubinkin, Zhur.eksp.i teor.fiz., 32, 23 (1957). (Trans.Soviet Physics - JETP.)
17. J.W.Mihelich, B.Harmatz & T.H.Handley, Phys.Rev., 108, 989 (1957).
18. B.H.Ketelle & A.R.Brosi, Phys.Rev., 116, 98 (1959).
19. T.Barloutand, T.Griebine & M.Riou, Physica, 22, 1129 (1956).
20. F.K.McGowan & P.H.Stelson, Phys.Rev., 109, 901 (1958).

21. F.R.Metzger, J.Franklin Inst., 261, 216 (1956).
22. R.E.Azuma & G.M.Lewis, Phil.Mag., 46, 1034 (1955).
23. G.T.Ewan & R.L.Graham, see Ref.24.
24. E.Bashandy, T.R.Gerholm & I.Lindskog, Arkiv Fysik, 17, 421 (1960).
25. V.A.Romanov, M.G.Iodko & V.V.Tuchkevich, Zhur.eksp.i teor.fiz., 38, 1019 (1960). (Trans.Soviet Physics - JETP.)
26. L.A.Sliv & I.M.Band, Tablitsy koeffitsientov vnutrennei konversii gamma-izlucheniya (Tables of internal conversion coefficients), M.-L., 1958.
27. M.E.Rose, Internal Conversion Coefficients, Amsterdam, 1958.
28. T.Huus, I.H.Bjerregaard & B.Elbek, Kgl.Danske Videnskab Mat.-Fys.Medd., 30, No.17 (1956).
29. M.Martin, P.Marmier & I.de Boer, Helv.Phys.Acta, 31, 435 (1958).
30. I.M.Baker & B.Bleaney, Proc.Phys.Soc., 68A, 257 (1955).
31. I.de Boer, M.Martin & P.Marmier, Helv.Phys.Acta, 32, 1019 (1959).
32. B.Elbek, K.O.Nielsen & M.C.Olesen, Phys.Rev., 108, 406 (1957).

* * * * * * *

DETERMINATION OF THE K FLUORESCENCE COEFFICIENTS OF V^{51}, Mn^{55}, Cu^{65} and Ga^{71}*

- A.A.Konstantinov, I.A.Sokolova & T.E.Sazenova

Knowledge of the precise values of the K fluorescence coefficients are essential for the solution of many problems involving radioactive isotopes. The experimental values of the fluorescence coefficients reported in the literature differ and in most cases diverge from the values obtained by theoretical calculations.[1]

We determined the K fluorescence coefficients of V^{51}, Mn^{55}, Cu^{65} and Ga^{71} by the procedure of determining the absolute number of K Auger electrons and K x-rays emitted by the source by means of a 4π proportional counter. Actually, determination of the absolute number of K Auger electrons emitted by an electron capture isotope by means of a 4π proportional counter is a difficult experimental task. The principal difficulties stem from the fact that Auger electrons with an energy of 5-10 kev have a very short range (80-160 $\mu g/cm^2$) and, consequently, are strongly absorbed in the source itself. Hence to keep self-absorption of the Augers below 1% one must prepare the source with a superficial density of the order of 10^{-8} g/cm^2 (invisible layer). Moreover, the absolute count of the K Auger electrons must be carried out in a 4π solid angle; consequently, the source must be applied to a very thin supporting film (0.07-0.09 microns) so that the absorption of K Augers in the film will not exceed 20%.

Determinations of the absolute number of K x-rays emitted by the electron capture sources were carried out by the method of three fillings of the 4π counter developed by Konstantinov[2].

To insure normal operation of the 4π counter it is desirable to have a source with an activity of about 10^{-8} curie. If one uses a radioactive isotope with a specific activity of 500 mC/g, then in case of application of material with an

---

*The original report was reported at the Tenth All-Union Conference on Nuclear Spectroscopy. The data on the K fluorescence coefficient of Mn^{55} were obtained after the Conference.

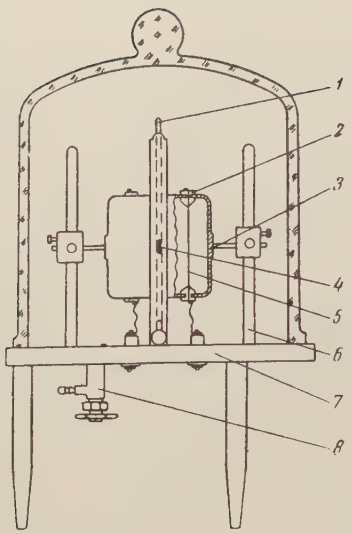

Fig.1. Diagram of the 4π proportional counter: 1) frame with aluminum foil, 2) polystyrene lead-in seals, 3) counter housing, 4) source, 5) filament, 6) stand, 7) brass base plate, 8) valve.

activity of 10^{-8} curie over a surface area of 2 to 7 cm^2, we obtain a superficial density of the active layer of the order of 10^{-8} g/cm^2.

The thin films that served as the backing were prepared of vinyl perchloride and were lightly aluminized on both sides. The active material was applied to the film by vacuum evaporation. In each experiment the prepared source was inserted into the 4π counter (Fig.1) which, as usual, consisted of two 2π counters. The 4π counter was filled with methane at a pressure of 20 cm Hg. At this methane pressure the counter detects only Auger electrons, inasmuch as the K x-rays of $Mn^{55}(Fe^{55})$, $Cu^{65}(Zn^{65})$ and $Ga^{71}(Ge^{71})$ are virtually not absorbed, while the K x-rays of $V^{51}(Cr^{51})$ are absorbed in the methane in an amount not exceeding 1%.

In Figs.2,3 and 4 we reproduce the energy distributions of the Augers from $Ga^{71}(Ge^{71})$ recorded by means of a single-channel differential pulse height analyzer from the first and second halves of the 4π counter and from both halves together. The Auger electron spectra from the first half (the side to which the source is turned) and from both halves of the 4π counter both have two peaks corresponding to L and K Auger electrons. Between the two peaks there is evident a certain amount of K Auger electrons that lost part of their energy in the source itself and also in reflection from the film and gas filling the counter. The energy distribution of Auger electrons in the second half of the 4π counter has only one peak corresponding to K Auger electrons inasmuch as all the L Auger electrons are completely stopped by the supporting film.

For determining the total number N_{12} of K Auger electrons detected simultaneously by both halves of the 4π counter and the number N_1 detected by the first half of the 4π counter one must extrapolate over the energy distribution in order to exclude the L Auger peak. The total number N_2 of K Auger electrons detected by the second half of the 4π counter is determined from the integral count. The following three equations can readily be written for N_1, N_2 and N_{12} :

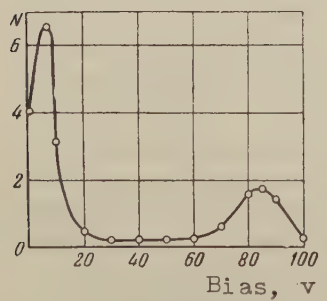

Fig.2

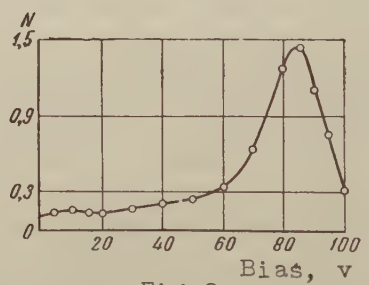

Fig.3

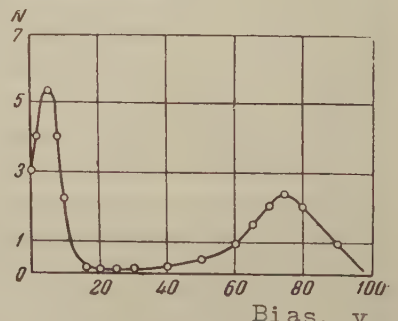

Fig.4

Fig.2. Spectrum of Ga^{71} Auger electrons from the first half of the 4π counter filled with methane at a pressure of 20 cm Hg.

Fig.3. Spectrum of Ga^{71} Auger electrons from the second half of the 4π counter.

Fig.4. Spectrum of Ga^{71} Auger electrons from both halves of the 4π counter.

$$N_1 = \frac{N_0}{2}(1 + k - \beta + f_1), \tag{1}$$

$$N_2 = \frac{N_0}{2}(1 - k - \tau - \beta + f_2), \tag{2}$$

$$N_{12} = \frac{N_0}{2}(2 - \tau - 2\beta), \tag{3}$$

where N_0 is the total number of K Auger electrons emitted by the source in the 4π solid angle, k is the coefficient of reflection of K Auger electrons for the given film, β is the coefficient of self-absorption of the K Auger electrons, f_1 is a coefficient characterizing the increase in the number of K Auger electrons in the first half of the 4π counter owing to reflection from the gas in the second half of the counter, τ is the coefficient of true absorption of the K Auger electrons in the given film, and f_2 is a coefficient characterizing the increase in the number of K electrons in the second half of the counter owing to reflection from the gas in the first half of the 4π counter.

Reflection of the K Auger electrons from the gas filling the counter is explained by the fact that the gas pressure in the counter is such that the range of the 5 to 10 kev Auger electrons is appreciably shorter than the distance from the source to the counter walls.

Below we shall show that self-absorption for sources with a superficial density of 10^{-8} g/cm^2 does not exceed 10% and, consequently, the term β can be neglected so that Eqs.(1), (2) and (3) can be rewritten:

$$N_1 = \frac{N_0}{2}(1 + k + f_1), \tag{4}$$

$$N_2 = \frac{N_0}{2}(1 - k - \tau + f_2), \tag{5}$$

$$N_{12} = \frac{N_0}{2}(2 - \tau). \tag{6}$$

For calculating N_0 from Eq.(6) one must know τ; this coefficient was determined by means of auxiliary measurements with a source which was covered with a film of the same thickness (this is the same procedure as is used in determining the activity of β-active nuclides[3]). In this case the source is located between two identical films. The absorption in each of the films is

$$\frac{N_0}{2}\tau(1 + k + k^2 + k^3 + \ldots) = \frac{N_0}{2}\frac{\tau}{1-k}. \tag{7}$$

Let N_3 and N_4 be the integral counts obtained during a certain period from the first and second halves of the 4π counter, respectively, and N_{34} be the integral count for the two halves; then

$$N_3 = N_4 = \frac{N_0}{2}\left(1 - \frac{\tau}{1-k} + f_3\right), \tag{8}$$

$$N_{34} = \frac{N_0}{2}\left(2 - \frac{2\tau}{1-k}\right). \tag{9}$$

In determining the activity of β-nuclides, when $k \ll 1$, the coefficient of reflection in (9) can be neglected; then, Eqs.(8) and (9) reduce to

$$N_3 = N_4 = \frac{N_0}{2}(1 - \tau + f_3), \tag{10}$$

$$N_{34} = \frac{N_0}{2}(2 - 2\tau). \tag{11}$$

From Eqs.(6) and (11) we readily obtain

$$\tau = \frac{N_{12} - N_{34}}{N_{12} - \frac{N_{34}}{2}}, \tag{12}$$

$$N_0 = 2N_{12} - N_{34}. \tag{13}$$

For 5-10 kev Auger electrons the coefficient of reflection k from films 0.05-0.07 microns thick is approximately 10-25%. One cannot neglect a coefficient of this magnitude in Eqs.(10) and (11) without introducing a substantial error in the determined absolute number of K Auger electrons. But inasmuch as the coefficients f_1 and f_2 in our case are small and their sum does not exceed 10%, we can set $f_1 = f_2$, and then from (4) and (5) we obtain

$$N_1 = \frac{N_1 + N_2 - N_{12}}{2} = N_1 = \frac{N_0}{2}(1 + k), \tag{14}$$

$$N_2 = \frac{N_1 + N_2 - N_{12}}{2} = N_2' = \frac{N_0}{2}(1 - k - \tau). \tag{15}$$

Making use of (6), (9), (14) and (15) to perform the obvious substitutions, we obtain the following relationships:

$$N_0 = \frac{N_1' N_{34}}{N_{34} - N_2'}, \tag{16}$$

$$k = \frac{N_{34} - 2N_2'}{N_{34}}. \tag{17}$$

$$\tau = \frac{2(N_{12} - N_{34})N_2'}{N_{34}N_1'}. \tag{18}$$

For a vinyl perchloride film 0.07-0.09 microns thick (8-10 μg/cm^2) the coefficient of true absorption for the K Auger electrons emitted by the investigated isotopes is 4 to 15%.

The coefficient of self-absorption of K Auger electrons can be evaluated from the coefficient of true absorption: if a film 0.07-0.09 microns thick absorbs 4-15%, an active layer with a superficial density of 10^{-8} g/cm^2 will absorb appreciably less than 1%.

K fluorescence coefficients ω_K of V^{51}, Mn^{55}, Cu^{65} and Ga^{71}

Element	Our results	Calculated by the semi-empirical formulas of	
		Ref.4	Ref.5
V^{51}	0.23±0.02	0.22	0.20
Mn^{55}	0.27±0.02	0.26	0.24
Cu^{65}	0.42±0.02	0.41	0.39
Ga^{71}	0.47±0.02	0.47	0.46

The value of the K fluorescence coefficient ω_K is given by the formula

$$\omega_K = \frac{N_0^x}{N_0^x + N_0}, \tag{19}$$

where N_0^x is the total number of K x-rays and N_0 is the total number of K Auger electrons.

Using the procedure outlined above and Eq.(19), we determined the K fluorescence coefficients of $V^{51}(Cr^{51})$, $Mn^{55}(Fe^{55})$, $Cu^{65}(Zn^{65})$ and $Ga^{71}(Ge^{71})$. The results obtained are listed in the accompanying table.

References

1. E.H.S.Burhop, The Auger Effect and other Radiationless Transitions, Cambridge Univ.Press, 1952.
2. A.A.Konstantinov, PTE, No.1, 67 (1959). (Trans.Instruments & Experimental Techniques.)
3. W.B.Mann & H.H.Seliger, NBS J.Research, 50, 197 (1953).
4. J.Laberrigue-Frolow & P.Radvanyi, J.Phys.Rad., 17, 944 (1956).
5. A.H.Wapstra, G.J.Nijgh & R.van Lieshout, Nuclear Spectroscopy Tables, Amsterdam, 1959.

* * * * * * *

GAMMA-RADIATION FROM Ta^{182}

- N.A.Voinova, B.S.Dzhelepov & Yu.V.Khol'nov

The γ-ray spectrum of Ta^{182} is very complex: it is known to comprise over 70 γ-lines.

The γ-rays emitted by Ta^{182} are clearly separated in energy into two groups: soft γ-rays (<350 kev) and hard γ-rays (850 to 1450 kev). No γ-rays have been detected in the intermediate energy region. The γ-ray spectrum of Ta^{182} in the 850 to 1450 kev region has been investigated in the greatest detail in the work of Voinova et al[1] and Vitman et al[2] on magnetic spectrometers by observation of recoil electrons.

The entire γ-spectrum of Ta^{182} was covered in the measurements of Muller et al[3], Murray et al[4] and Sumbaev[5], carried out on crystal diffraction spectrometers and in the work of Fröman & Ryde[6] performed with a scintillation spectrometer. Bachström[7] investigated the photoelectron spectrum corresponding to the hard γ-rays.

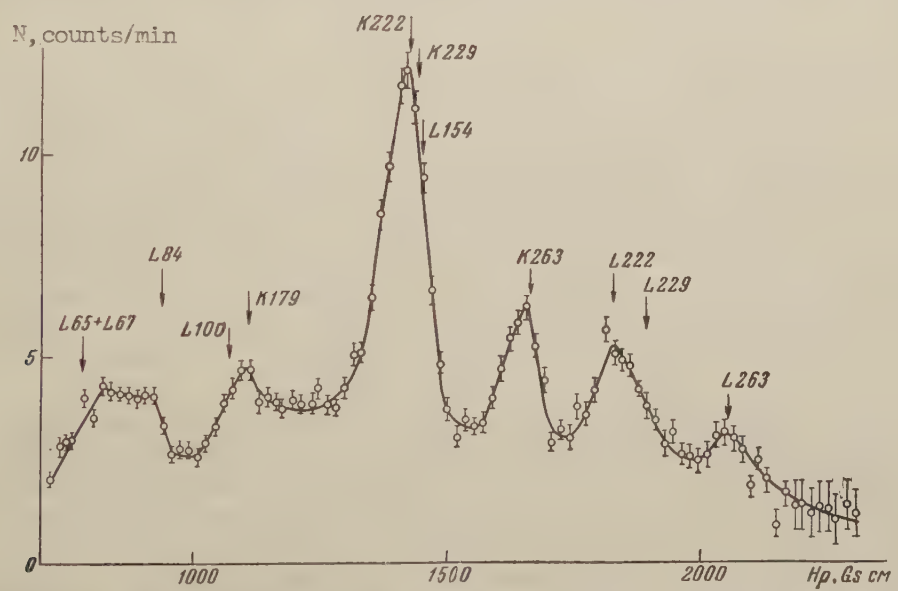

Fig.1. Spectrum of photoelectrons ejected from a bismuth target by Ta^{182} γ-rays.

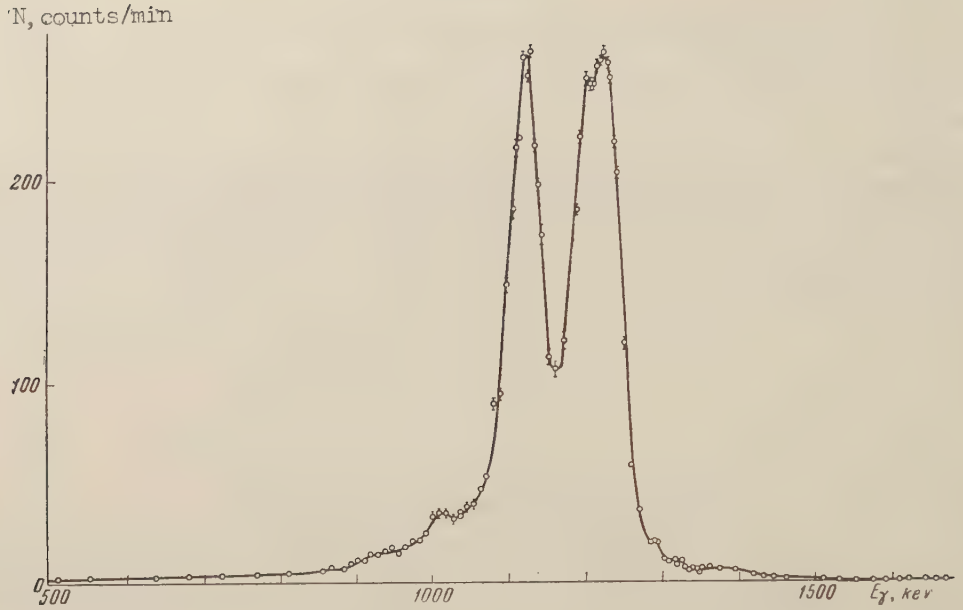

Fig.2. High energy part of the Ta^{182} γ-spectrum (background subtracted).

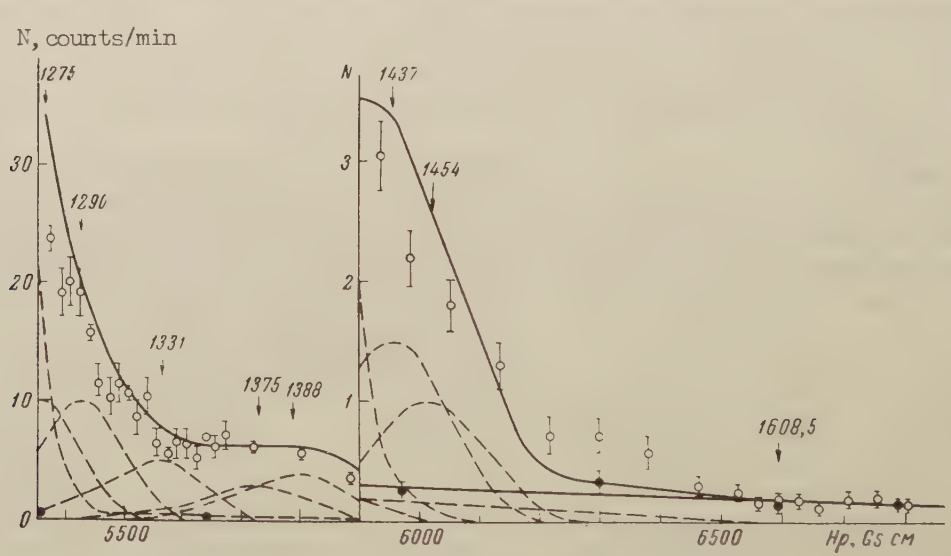

Fig.3. Resolution of the Ta^{182} γ-spectrum (dashed lines) in the 1275 to 1700 kev region into components. Solid points and heavy solid lines - background; open points - effect.

The relative γ-ray intensities determined in the above-mentioned investigations are shown, together with our data, in the table below. There is evident generally good agreement in the high energy region (except for the approximate results of Fröman & Ryde[6]). In contrast there are substantial divergences in the low energy part of the spectrum (Cf.Refs.4 & 6 and 3 & 5).

The purpose of the present work was to investigate the γ-spectrum of Ta^{182} in a wide energy range by means of the ritron[8] and the photoritron[9], using a common intensity scale. The source was a neutron activated tantalum foil weighing 2.8 g. The activity of the source was ~2 curie.

Relative intensities of the γ-rays from Ta^{182}

Transition energy, kev	Relative intensities							
	Ref. 3	Ref. 4	Ref. 7	Ref. 5	Ref. 6	Ref. 1	Ref. 2	Our data
65,71	2,6	7,5	—	—	} —	—	—	—
67,74	28,4	85	—	—	} 130	—	—	—
84,67	1,7	5	—	—	(7)	—	—	—
100,09	13,1	40	—	—	52	—	—	15±7
113,66	2,6	7,5	—	—	}	—	—	—
116,40	0,4	1,7	—	—	} (8)	—	—	—
152,41	12,5	35	—	18,2	} 39 (29)	—	—	} 18±4
156,37	4,0	11,5	—	7,2	} (10)	—	—	} 3
179,36	5,4	16	—	8,7	(12)	—	—	3±1
198,31	2,6	7,5	—	4,5	} 39 (6)	—	—	—
222,05	12,8	35	—	21,4	} (25)	—	—	} 19±3
229,27	6,8	20	—	9,8	(14)	—	—	}
264,09	7,7	22	—	9,1	12	—	—	8±1
892,4	—	—	—	—	—	<1,4	<0,5	—
927	—	—	—	—	—	3±2	—	—
960	—	—	—	—	—	2,5±1,5	—	—
1003	—	—	—	—	—	9±3	5±2	—
1046	—	—	—	—	—	—	0,9±0,9	—
							0,6	—
1121,6	100	100	100	100	100	100	100	100
1155	—	6,5	—	7,1	—	<4	3,6±1,0	—
1189,4	44,6	45	—	56,8	~21	45±8	44±3	43
1220,0	} 95	95 } 145	—	} 161	} 112,5 (75)	84±8	80±6 } 105±8	} 118
1231		50 }	—		} (37,5)	35±10	25±5 }	
1254	—	—	4	—	—	6±2	4±1	—
1275	—	—	3	—	—	3±2	—	~4
1290	—	—	2	—	—	5±2	—	~4
1331	—	—	—	—	—	<0,6	—	(~1,5)
1375(+1388)	—	—	<0,3	—	—	<1,4	—	~2
1437	—	—	<0,3	—	—	<0,05	—	(~0,6)
1454	—	—	<0,3	—	—	—	—	(~0,4)
1608,5	—	—	—	—	—	—	—	<0,05

The experimental photoelectron curve obtained on the photoritron[9] is shown in Fig.1.

We determined the relative intensities of the γ-rays (last column of the table) from the relative intensities of the photopeaks with appropriate corrections for the absorption in the source and the exit window of the instrument and using the spectral sensitivity function derived for the photoritron.

The complex lines were resolved into components using standard line shapes.[9]

It will be evident from the table that our data are in good agreement with the results of Muller et al[3] and Sumbaev[5] and differ significantly from the data of Murray et al[4] and Fröman & Ryde[6].

The high energy part of the γ-spectrum of Ta^{182} was investigated by means of the ritron[8]. The experimental spectrum with the background subtracted is shown in Fig.2. The intensities of the hard lines, evaluated with appropriate corrections for absorption, are listed in the table. The resolution of the ritron does not allow of separating the lines as was done in the work of Refs.1 & 2. Hence, our intensities for the hard lines resolved by using standard line shapes (Fig. 3) are less accurate than the results in Refs.1 & 2. We paid particular attention to the spectrum in the 1600 kev region inasmuch as one group of investigators[10] reported the existence of a line of 1608.5 kev energy (no information regarding the relative intensity of this line was given). It will be evident from Fig.3 that the number of coincidences in the 1600 kev region does not noticeably

rise above the background. Hence it may be asserted that if 1608.5 kev γ-rays do exist their intensity does not exceed 0.05% the intensity of the 1121.6 kev γ-rays

"V.G.Khlopin" Radium Institute,
Academy of Sciences of the USSR

References

1. N.A.Voinova, B.S.Dzhelepov & N.N.Zhukovskii, Izv.AN SSSR, Ser.fiz., 23, 828 (1959). (Trans.Bulletin, 23, 822.)

2. V.D.Vitman, N.A.Voinova, B.S.Dzhelepov & A.A.Karan, Present issue of the Bulletin, p.192.

3. D.Muller, H.Hoyt, D.Klein & J.Du Mond, Phys.Rev., 88, 775 (1952).

4. J.Murray, F.Boehm, P.Marmier & J.DuMond, Phys.Rev., 97, 1007 (1955).

5. O.Sumbaev, Izv.AN SSSR, Ser.fiz., 21, 987 (1957). (Trans.Bulletin, 21, 989.)

6. P.Fröman & H.Ryde, Arkiv Fysik, 12, 399 (1957).

7. G.Bachström, Arkiv Fysik, 10, 387 (1956).

8. B.S.Dzhelepov, N.N.Zhukovskii & Yu.V.Khol'nov, Izv.AN SSSR, 18, 599 (1954) (Trans.Bulletin, 18, 285); B.S.Dzhelepov, V.P.Prikhodtseva, A.I.Feoktistov & Yu. V.Khol'nov, Ibid., 20, 1361 (1956) (Trans.Bulletin, 20, 1245); I.B.Golovanov, B.S. Dzhelepov, L.S.Lebedev, V.P.Prikhodtseva & Yu.V.Khol'nov, Ibid., 21, 985 (1957) (Trans.Bulletin, 21, 987).

9. B.S.Dzhelepov & Yu.V.Khol'nov, Izv.AN SSSR, Ser.fiz., 25, 98 (1961). (Trans.Bulletin, 25, No.1).

10. C.Fowler, H.Kruse, V.Keshishian, R.Klotz & G.Mellor, Phys.Rev., 94, 1082 (1954), cited in Nuc.Sci.Abstr., 9, No.24B, 102 (1955).

A HIGH-RESOLUTION IONIZATION ALPHA-SPECTROMETER

- G.E.Kocharov & G.A.Korolev

One of the chief means of investigating the collective levels of heavy nuclei is by studying the fine structure of their α-spectra. Once the energies and intensities of the fine structure components have been experimentally determined, the distribution and nature of the levels of the daughter nuclei, the nuclear deformation, and other parameters can be ascertained.

Investigation of the fine structure of α-spectra has extended our understanding of nuclear structure and contributed substantially to the formulation of different nuclear models. The progress made so far has been largely due to elaboration and improvement of experimental methods for investigating α-radiation. Improvement of measurement techniques expands experimental potentialities and makes it possible to solve hitherto unapproachable problems. For example, construction of an instrument with high-transmission and high-resolution enabled us to determine the energies and intensities of a number of previously unknown α-lines in the spectra of certain long-lived isotopes.

In recent years several high-transmission magnetic α-spectrometers have been constructed in the Soviet Union.[1,2] Using such a spectrometer, Baranov et al[2] succeeded in studying α-transitions with partial periods of up to 10^{10} years. Studies of alpha fine structure have revealed the need for studying even weaker α-lines from sources with low specific activity, but present day magnetic α-spectrometers are inadequate for this purpose.

In this respect the ionization chamber offers the best prospects. Ionization chambers have a transmission factor several orders greater than that of magnetic spectrometers, but, unfortunately, are definitely inferior as regards energy resolution.

Up to 1955, when the present work was begun, the half-width of α-lines measured with ionization chambers was 50 to 70 kev. Since fine structure α-lines are less than 50 kev apart, it was impossible to investigate them with such resolution; hence a significant increase in resolving power was called for.

This article describes the high-transmission, high-resolution (α-line half-width of 25 to 30 kev) α-spectrometer designed by the authors and constructed in the Physical-Technical Institute.

I. Energy Resolution of a Grid Ionization Chamber

The heart of the α-spectrometer is the ionization chamber shown in Fig.1.

The chamber is filled with the working gas and a potential difference is applied between the electrodes. When electrons move to the collecting electrode, voltage pulses are induced on the high voltage and collecting electrodes (Fig.2). The pulse amplitude on the collector is proportional to the α-particle energy E, and is given by

$$V_1 = -\frac{Ne}{C_1}, \tag{1}$$

where $N = E/u$ is the number of ion pairs produced by the α-particles, e is the electron charge, C_1 is the total capacitance of the collecting electrode with respect to ground, and u is the mean energy required for production of an ion pair. The pulse amplitude on the high-voltage electrode is a function of α-particle emergence angle:

$$V_2 = \frac{Ne}{C_2}\left(1 - \frac{X}{d}\cos\vartheta\right), \tag{2}$$

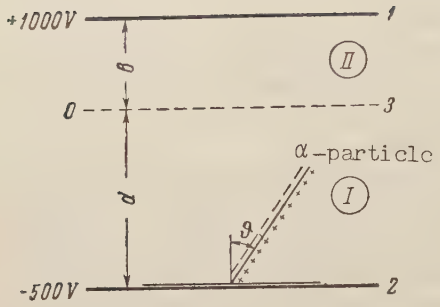

Fig.1. Diagram of grid ionization chamber. 1 - Collecting electrode; 2 - high voltage electrode; 3 - grid.

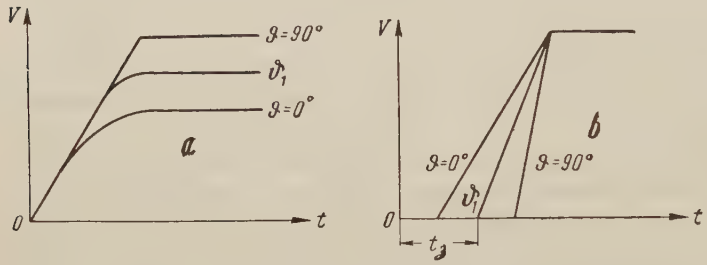

Fig.2. Shape of pulses on ionization chamber electrodes: a) on the high voltage electrode, b) on the collecting electrode. (ϑ_1 is an example of an intermediate angle.)

where ϑ is the α-particle emergence (flight) angle relative to the normal to the electrode, X is the distance of the center of mass of the ions from the start of the track, d is distance between the high voltage electrode and the grid, and C_2 is the total capacitance of the high voltage electrode relative to ground.

Thus it is possible, using the pulses on the collecting and high voltage electrodes, to determine simultaneously the energy and emergence angle of the α-particles.

The resolution of grid ionization chambers depends on the source thickness, gas purity, electronic noise, geometry and operating conditions of the ionization chamber, etc.

To achieve good resolution a detailed study must be made of the causes of poor resolution in order to minimize their effect on α-spectra. The causes of poor resolution can be divided into two groups according to their effects on the α-spectra:

1. Electronic noise and fluctuations of the number of ion pairs produce a Gaussian distribution of pulse amplitudes without shifting the position of the peak.

2. Source thickness, attachment of electrons to electronegative impurities, inadequate screening by the grid, and the finite rise time of the pulse widen the α-line and shift the peak toward lower energies.

We shall characterize the energy resolution by the half-width of the α-line,

$$\Pi = \left(\sum_i \Pi_i^2\right)^{1/2},$$

where the Π_i are the contributions to the α-line half-width due to the diverse factors mentioned above.

Below we shall show that the chief factors influencing the resolution are ionization fluctuations and noise, which produce a Gaussian pulse distribution with half-width $\Pi_G = \sqrt{\Pi_f^2 + \Pi_n^2}$.

We determined each of the remaining Π_i from the shape of the spectrum corresponding to the particular factor. In this way we determined the effect of each Gaussian distribution on the final shape of the spectrum. From these spectra we found the half-width Π_{Gi} and the amount of displacement of the peak. The effective half-width was then calculated by means of the formula $\Pi_i = \sqrt{\Pi_{Gi}^2 - \Pi_G^2}$.

1. Ionization fluctuations

An ionization chamber permits determination of the number of ion pairs formed by an α-particle in the sensitive volume of the chamber. Actually, the total ionization produced by an α-particle fluctuates. The mean square fluctuation in the number of ion pairs $\Delta N^2 = E/u$ when the number of single ionizations obeys Poisson's law. In our case, however, this condition is not fulfilled, so $\Delta N^2 = F\frac{E}{u}$. The corresponding half-width is

$$\Pi_f = 2.35\sqrt{FEu}. \qquad (3)$$

According to the theoretical calculations of Fano[3], F varies in the range from 1/3 to 1/2.

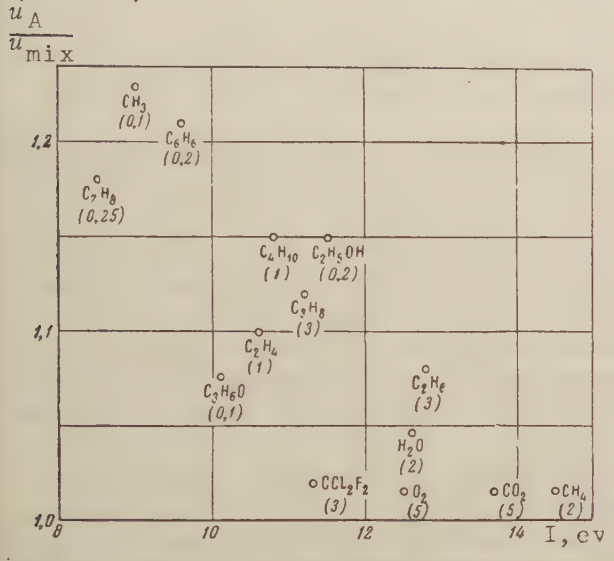

Fig.3. Ratios of the mean energy for ion pair production in argon to the mean energy for pair production in mixtures of gases as a function of the ionization potential of the "impurity" atoms. The figures in parentheses indicate the impurity content in percent.

The parameter F can be determined from our data. Since the resolution of the Po^{210} α-line (half-width 25 kev) is determined chiefly by noise (Π_n = 16 kev) and fluctuation of the number of ion pairs, we find that $\Pi_f \approx 19$ kev and hence $F < 0.43$.

Thus $F \neq 1$, and we have experimentally confirmed Fano's assumption that the number of single ionizations does not obey Poisson's law.

Obviously, to lessen the effect of ionization fluctuation on the line half-width we must reduce the mean energy required for production of an ion pair. By definition the mean energy for pair production is the ratio of the α-particle energy to the total number of ion pairs formed. When a charged particle is stopped, part of its energy goes for excitation of the gas atoms; approximately half of the energy of an α-particle is expended on such excitation. Therefore, to increase the number of ion pairs, we must utilize this energy. This can be done by adding to the usual inert gas, some gas with an ionization potential lower than the excitation energy of the inert gas. An excited atom of the inert gas, for example, argon, can then ionize the "impurity" atoms upon collision. Fig.3 shows the experimental values of the mean pair production energy (referred to the energy in argon) for different gas mixtures.[4,5] Thus, it will be evident that the spectrometer resolution can be improved by using a mixture of gases.

2. Noise

Noise is another important factor affecting the energy resolution. The significant factor where physical measurements are concerned is the signal-to-noise ratio. The signal-to-noise ratio at the output of the amplifier depends upon the

parameters of the first tube of the amplifier and on proper choice of the passband. The last is determined by the time constants T_d and T_i of the differentiating and integrating circuits. The chief components of the noise are shot noise, grid current noise and thermal noise in the resistance of the amplifier input circuit. However, with a sufficiently high input resistance, the thermal noise is minor compared to other noise. For the case of instantaneous rise of the pulse on the collecting electrode Elmore[6] has shown that the signal-to-noise ratio is greatest when

$$T_d = T_i = \sqrt{5kT\frac{C_1^2}{eI_gS}}. \qquad (4)$$

Under these conditions the signal-to-noise ratio is given by

$$\frac{u_s}{\sqrt{\overline{u_n^2}}} = D\frac{S^{1/4}}{I_g^{1/4}C_1^{1/2}}, \qquad (5)$$

where k is the Boltzmann constant, T is the Kelvin temperature, S is the transconductance of the first amplifier tube, I_g is the grid current (the sum of the absolute values of the electron and ion components) of the first tube, and D is a proportionality constant.

Obviously, the chief criterion for selecting the first tube of the amplifier is the ratio of transconductance to grid current S/I_g. Knowledge of I_g and S is also necessary for proper selection of the amplifier passband.

Tests showed that 6Zh1P tubes have the best noise properties.[7] It is most advantageous to operate these tubes at a plate voltage of 50 to 60 v and a filament voltage of 4 to 6 v. Under these conditions the best selected 6Zh1P tubes have a grid current of $2\cdot10^{-11}$ amp and a transconductance of 2.5-3.0 ma/v. The measured[7] grid current is the difference between the electron and ion components, while the noise is determined by their sum. This was taken into account in selecting the tubes for the equipment.

The signal-to-noise ratio increases with decrease of the total capacitance of the collecting electrode. The total capacitance is $C_1 = C_c + C_i + C_v$, where C_c is the capacitance of the collector relative to ground, C_i is the input capacitance of the first amplifier tube and C_v is capacitance due to the chamber. We succeeded in reducing C_1 below 15 pf with $C_i + C_c = 7$ pf.

The noise half-width was experimentally determined with an optimum passband characterized by $T_d = T_i = 18$ μsec. We recorded differential pulse height spectra by feeding standard pulses into the amplifier. The amplitude of the standard signal corresponded to pulses from 4.76 Mev α-particles. The distribution was a Gaussian curve with a half-width of 16 kev.

3. Influence of source thickness on resolution

Particles emerging from the depth of the source or at large angles lose part of their energy in the source itself. Consequently, the α-line half-width increases, and a low-energy tail develops. Analysis of the α-spectrum is hindered in the presence of a large tail in the pulse distribution. Furthermore, the position of the peak is shifted because of finite source thickness.

It is important to know the effect of source thickness on the shape of the spectrum, not only for α-spectroscopy but in general in investigating the emission of particles from targets (studying nuclear reactions, absolute counting, etc.).

Consider an α-source of thickness h (Fig.4) and extensive area. Let us

calculate the number of α-particles with energy E that emerge through a surface area dS. Taking $R = aE^n$, we find that these particles must travel a distance in the source:

$$x = R_0 - aE^n = R_0 (1 - \varepsilon^n),$$

where $\varepsilon = \frac{E}{E_0}$, E_0 is the initial α-particle energy, R_0 is the range in the source of an α-particle with energy E_0, $n \approx 1.5$, and a is a proportionality constant.

a) Thick source ($h \geqslant R_0$)

Suppose a unit volume emits η α-particles per unit time, then the number of particles impinging on the area dS from the spherical shell between x and $x + dx$, will be

$$dN_\varepsilon = dS \frac{\eta dr}{4\pi} \int_0^{2\pi} d\varphi \int_0^{\vartheta_k} \sin\vartheta \cos\vartheta \, d\vartheta = \frac{\eta dr \, dS}{4} \sin^2 \vartheta_k.$$

Recalling that $dx = -R_0 n \varepsilon^{n-1} d\varepsilon$, and integrating over the area of the source, we obtain

$$\frac{dN_\varepsilon}{d\varepsilon} = -\frac{N_0 R_0 n}{4h} \varepsilon^{n-1} + \frac{N_0 R_0 n}{4h} \varepsilon^{n-1} \cos^2 \vartheta_k, \qquad (6)$$

where $N_0 = \eta S h$ is the total number of particles emitted by the source per unit time.

The second term in Eq.(6) appears as a result of collimation, i.e., when only the α-particles in the angular range from 0 to ϑ_c are detected.

b) Thin source

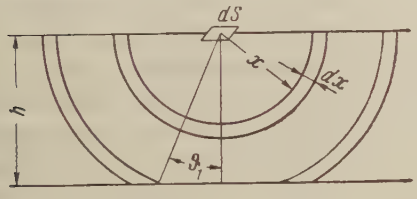

Fig.4. Diagram for calculating the effect of source thickness on the spectrum shape.

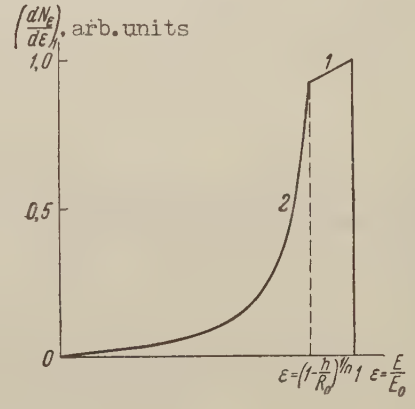

Fig.5. Energy distribution of α-particles emitted from a source: 1 - curve calculated using Eq.(6), 2 - curve calculated by means of Eq.(7).

Equation (6) is valid for α-particles emerging from the source with energies $\varepsilon \geqslant (1 - \frac{h}{R_0})^{1/n}$, which corresponds to $x \leqslant h$. For α-particles with lower energies ($x \geqslant h$) the integration over ϑ must be carried out from ϑ_1 to ϑ_c, where $\vartheta_1 = \arccos \frac{h}{x}$ (Fig.4). This integration gives

$$\frac{dN_\varepsilon}{d\varepsilon} = -\frac{N_0 nh}{4R_0}\frac{\varepsilon^{n-1}}{(1-\varepsilon^n)^2} + \frac{N_0 R_0 n}{4h}\varepsilon^{n-1}\cos^2\vartheta_k. \qquad (7)$$

Haeberli et al[8] deduced analogous formulas for the special case of $\vartheta_c = 90^\circ$ and $n = 1$.

Fig.5 shows the energy distribution of particles emerging from a source.

To determine the shape of experimentally obtained spectra, one must, as noted above, consider the effects producing a Gaussian distribution.

Let us use the subscript 1 to identify quantities ε and $\frac{dN_\varepsilon}{d\varepsilon}$, pertaining to the distribution we considered above (Eqs.(6) and (7)), and the subscript 2 to identify the actual final distribution. Then the final shape of the spectrum will be described by

$$\left(\frac{dN_\varepsilon}{d\varepsilon}\right)_2 = \frac{2{,}35}{\Pi_G\sqrt{2\pi}}\int_0^1 e^{-\frac{2{,}76}{\Pi_G^2}(\varepsilon_2-\varepsilon_1)^2}\left(\frac{dN_\varepsilon}{d\varepsilon}\right)_1 d\varepsilon_1. \qquad (8)$$

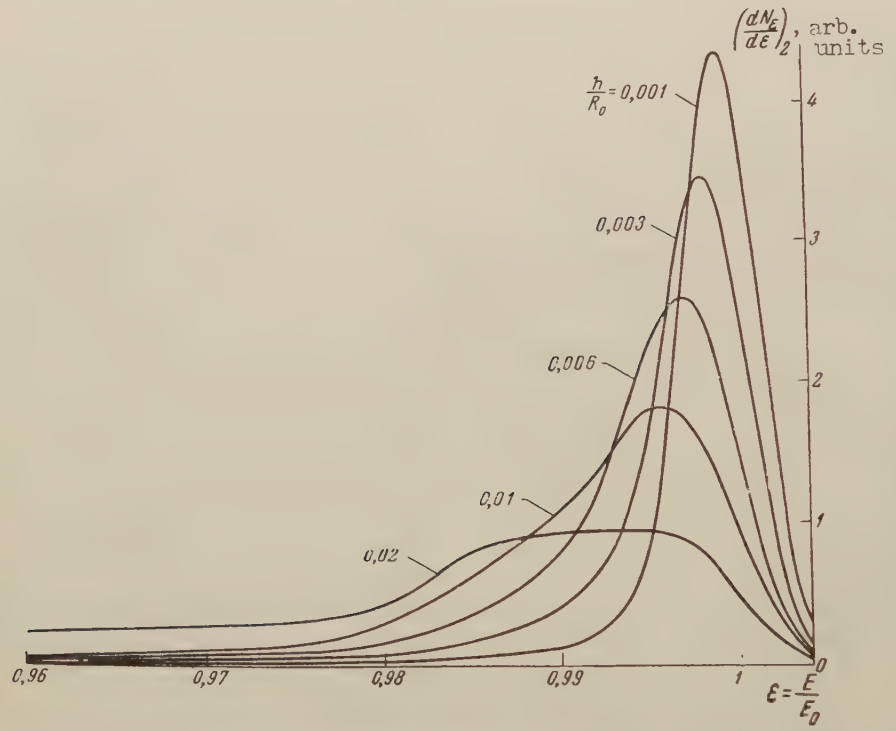

Fig.6. Alpha-spectra shapes as calculated by means of Eq.(8) for different source thicknesses.

Equation (8) was numerically integrated for different values of h. The results of these calculations, neglecting collimation, are shown in Fig.6.

Fig.7 shows how the shift of the peak depends on source thickness for different degrees of collimation. The degree of collimation f is the factor by which a given collimation reduces the transmission. We must know the above dependences in order to correct for the source thickness when measuring α-particle energies.

Fig.8 shows how the half-width Π_t depends on source thickness.

4. Imperfect shielding by the grid

The grid is introduced into the ionization chamber to eliminate the inductive effect of positive ions on the collecting electrode. However, despite the presence of a grid, positive ions still have some effect on the collecting electrode, an effect characterized[9] by the parameter

$$\sigma = \frac{a}{2\pi b}\ln\frac{a}{2\pi r}, \qquad (9)$$

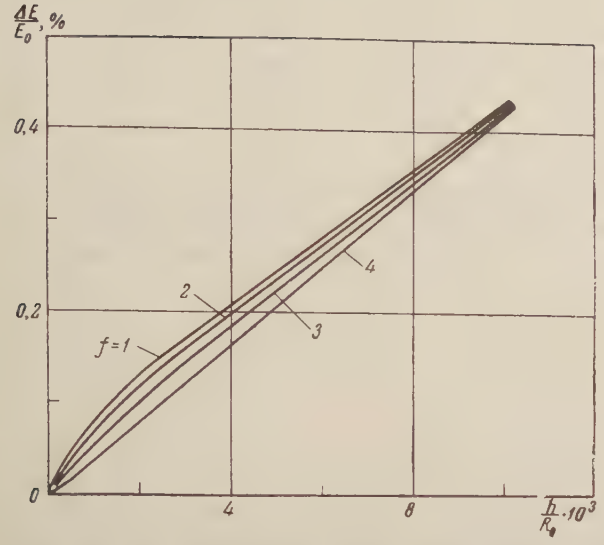

Fig.7. Shift of the line peak as a function of source thickness with different degrees of collimation.

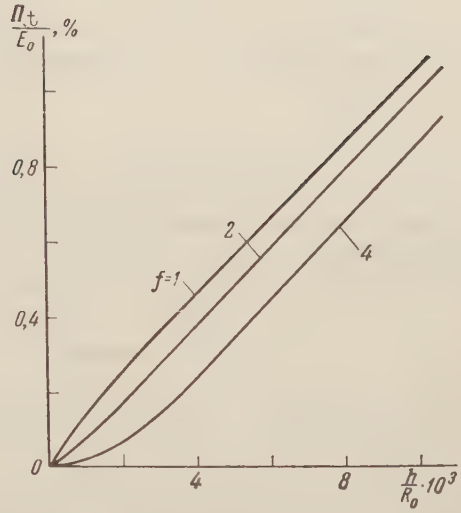

Fig.8. Variation of Π_t with source thickness.

where a is the separation between the grid wires, r is the wire radius, and b is the distance between collecting electrode and grid. A grid can be made more effective by increasing the distance between the collector and grid, by increasing the wire radius, and by decreasing the separation between wires. However, one must also consider the possibility of the electrons settling on the grid and being lost. Incomplete shielding by the grid causes the pulse height on the collecting electrode to depend on α-particle emergence (flight) angle. One should know σ to determine the α-particle energy correctly. Measurements show that the actual values of σ agree with those given by Eq.(9) in the range of grid parameters yielding small values of σ (<0.02) but diverge in the range of large σ.

Let us determine the effect of imperfect shielding on the shape of α-spectra. The pulse height on the collecting electrode, allowing for imperfect shielding, is given by

$$V = V_{\max}\left(1 - \frac{\sigma X}{d}\cos\vartheta\right), \tag{10}$$

where $V_{\max} = -\frac{Ne}{C_1}$. The maximum amplitude $V_{\max}$ corresponds to a pulse from an α-particle moving parallel to the electrode ($\cos\vartheta = 0$), while the minimum amplitude

$$V_{\min} = V_{\max}\left(1 - \frac{\sigma X}{d}\right).$$

corresponds to a pulse from a particle emerging at an angle normal to the electrode ($\cos\vartheta = 1$).

Taking collimation into account, we have

$$V^k_{\max} = V_{\max}\left(1 - \frac{\sigma X\cos\vartheta_k}{d}\right).$$

For an isotropically radiating source the number of particles emitted into the interval between ϑ and $\vartheta + d\vartheta$ is proportional to $d(\cos\vartheta)$, i.e.,

$$dN = Ad(\cos\vartheta). \tag{11}$$

Using Eqs.(10) and (11), we find that the differential pulse height distribution dN/dV is a rectangle bounded by V_{max} and V_{min}:

$$\frac{dN}{dV} = \text{const.}$$

As in the case of the effect of source thickness, it is necessary to take into account all factors contributing to the Gaussian distribution. We then obtain the following expressions for the half-width and shift of the peak due to imperfect shielding:

$$\Pi_S = 0.72\frac{E\sigma X}{df}\sqrt{1 + 0.13\frac{E\sigma X}{df\Pi_G}}, \tag{12}$$

$$\frac{\Delta E}{E} = \frac{\sigma X}{2d}\frac{2f-1}{f}. \tag{13}$$

Buneman et al[9] give a formula for the contribution of imperfect shielding to the half-width. Their formula is not exact, since they do not consider the joint effect of the Gaussian and rectangular distributions. They simply took Π_S to be the width of the rectangle. The Π_S given by the Buneman formula is 1.5 times greater than the true value given by Eq.(13).

5. Electron attachment in the ionization chamber

Electronegative impurities in the working gas of the ionization chamber collect electrons and reduce the number of electrons drifting to the collecting electrode. As a result, the position of the peak is shifted by an amount depending on the α-particle energy, and the α-line is broadened. Damaskinskii et al[10] show that electron attachment can be reduced by 1) purifying the gas of oxygen (the chief electronegative impurity in argon) and 2) operating the chamber under conditions insuring a minimum attachment cross section.

We tried both methods. A sodium purifier was used to scrub the argon. However, since purification takes a long time it is not always feasible to use this procedure. Tests showed that addition of 1% to 3% methane[10,11] to the argon makes it possible to operate the chamber under conditions assuring virtual elimination of diffusion, recombination, electron attachment, and loss of electrons to the grid. The shift of the peak and the half-width Π_a then become negligible.

The best procedure for minimizing electron attachment is the combined one of adding a polyatomic gas and purifying the mixture. This also results in increase of the electron drift velocity. When purification is impossible, the field strength in each region of the chamber must be carefully chosen so that the average electron energy corresponds to the minimum attachment cross section.

6. Effect of different collector pulse rise times on the energy resolution

The pulse rise time on the collecting electrode depends on the α-particle emergence angle and equals

$$t = \frac{b}{w_2} + \frac{R\cos\vartheta}{w_1},$$

where R is the range of an α-particle in the chamber gas, w_1 and w_2 are the drift

Table 1
Total line half-width evaluation

Π_i, kcv	Degree of collimation	
	$f=1$	$f=3$
Π_f	16,4	16,4
Π_n	16	16
Π_s	28	9
Π_t	14	8
Π_r	<1	<1
$\Pi = (\sum_i \Pi_i^2)^{1/2}$	38	26

velocities in the regions between the high-voltage electrode and grid and between the grid and collecting electrode, respectively. In the process of amplification the pulses pass through differentiating and integrating circuits; the pulse height at the output of these circuits depends on the rise time. Consequently, the final pulse height depends on the α-particle emergence angle.

A mixture of argon and methane greatly increases the drift velocity, thereby markedly reducing pulse straggling due to the effect of rise time (Π_r for argon is ~16 kev, while for the methane mixture it is ~1 kev).

7. Total α-line half-width

Let us evaluate the total line half-width for 5 Mev α-particles under the following conditions: the working mixture A + 3% CH_4, d = 4 cm, b = 2.5 cm, p = = 1.5 atm, $h/R_0 = 2 \cdot 10^{-3}$ (Table 1).

Even if the influence of all other factors affecting the resolution could be reduced to zero, the α-line half-width would still be about 15 kev, because the limit of resolution of an ionization chamber is fixed by fluctuations in the number of ion pairs.

II. Electronic Collimation

Collimation is essential to enhance the α-particle energy spectra. Usually a material collimator is used. However, these have a number of shortcomings: 1) some of the electrons produced by the α-particles are lost because of weakening of the electric field in the collimator apertures, and 2) transmission is severely reduced. The difficulty of preparing good uniform collimators is also a substantial drawback.

Electronic collimation is better for studying low intensity α-lines. Electronic collimation makes use of 1) the dependence on the α-particle emergence angle of the time lag between the start of a pulse on the collector and the start of a pulse on the high-voltage electrode - time collimation (Fig.2), or 2) dependence on the α-particle emergence angle of the high-voltage electrode pulse height or grid pulse height - pulse-height collimation.

1. Time collimation

After the α-particle ionizes the gas in the working volume of the chamber, the electrons start to drift toward the grid. At this instant a voltage pulse is induced on the high-voltage electrode; a pulse rises on the collecting electrode only after the first electrons reach the grid. The time lag before the collector pulse begins depends on the emergence angle of the α-particle and is given by

$$t_3 = \frac{d - R\cos\vartheta}{w_1},$$

where R is the α-particle range, w_1 is the drift velocity of electrons between the high-voltage electrode and grid, and d is the distance between the high-voltage electrode and grid.

Pulses with minimum delay time correspond to α-particles traveling perpendicular to the source. Obviously, we can collimate by counting only pulses for

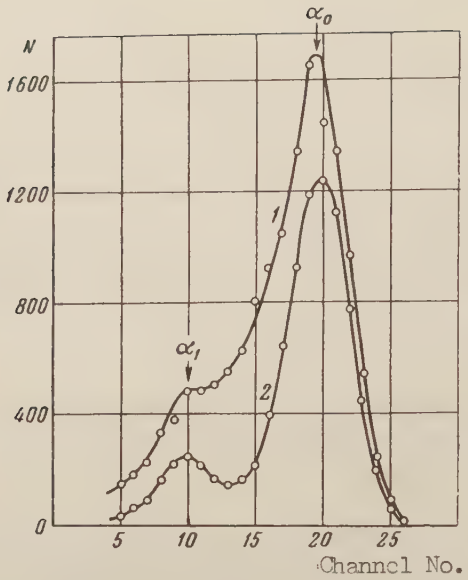

Fig.9. U^{234} α-spectra: 1 - without collimation, 2 - with collimation. The channel width is 5 kev.

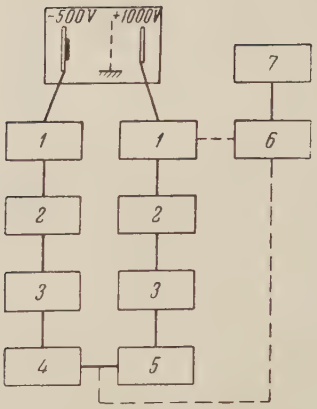

Fig.10. Block diagram of the ionization α-spectrometer: 1) preamplifier, 2) amplifiers, 3) clippers, 4) single channel analyzer, 5) 28 channel analyzer, 6) precision pulse height generator, 7) pulse height meter.

which t_3 is smaller than some t_C. By varying t_C we can control the degree of collimation.

When determining the relative intensities of α-groups, an appropriate correction must be made because the degree of collimation depends on α-particle energy.

2. Pulse height collimation

For pulse height collimation we can use either the pulses on the high-voltage electrode or those on the grid. In the latter case, a second, shielding grid is introduced into the chamber.[12] The principal features of pulse height collimation are described by Bochagov[12] and Valladas.[13]

Fig.9 shows α-spectra of U^{234} recorded with and without collimation. Collimation significantly improves the shape of the spectrum (25 kev half-width), although the transmission goes down by a factor of 3.

III. Description of the α-Spectrometer

The ionization α-spectrometer we built consists of

1) a grid ionization chamber,

2) electronic circuits for amplifying, shaping, selecting, and analyzing the pulses, and

3) a system for evacuating the chamber and filling it with the desired gas mixture.

The ionization chamber is a 22 liter brass cylinder. The collecting electrode is attached to the bottom of the chamber. The grid and high-voltage electrodes are mounted on special sliders so that the distance between the electrodes can be varied. The electrodes are brass discs 4 mm thick. The high-voltage electrode is 220 mm in diameter, and the collecting electrode is 120 mm in diameter.

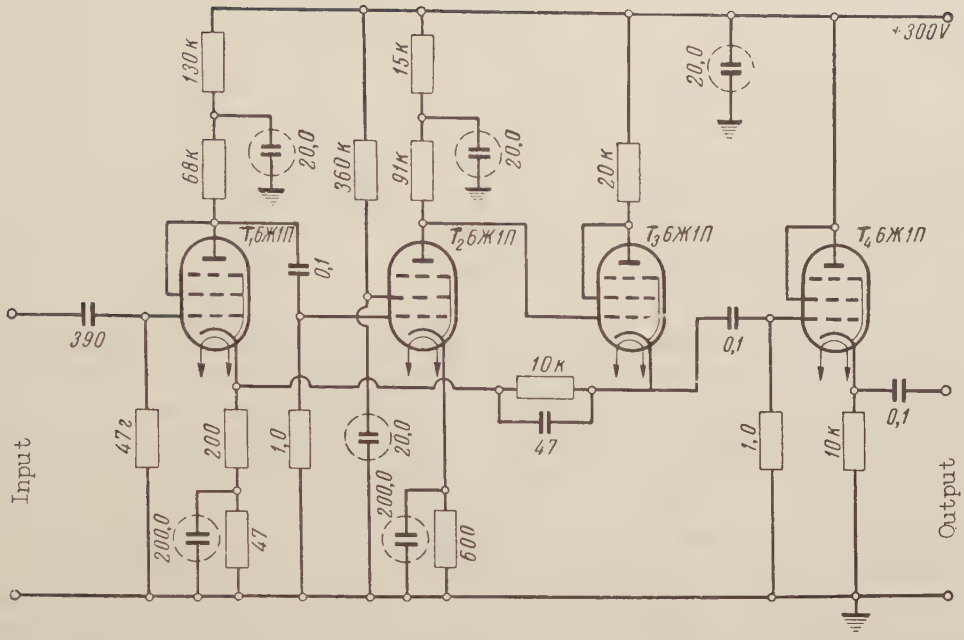

Fig.11. Circuit of the low noise preamplifier.

The grid is made of 0.1 mm diameter nichrome wires spaced 1.5 mm apart and welded to a ring of stainless steel. Special leads into the chamber supply the high-voltage and bring out the pulses. The entire system is pumped down to 10^{-2} mm Hg and then filled with a mixture of A + 3% CH_4 to a pressure of 1.5 to 1.8 atm.

The electrode potentials were chosen to minimize recombination and loss of electrons to the grid.

The pulses rising on the collecting and high-voltage electrodes are first amplified by a low noise level preamplifier and then fed to the main amplifier with a gain of 10^3 (Fig.10). The preamplifier circuit is shown in Fig.11. The preamplifier is supplied by VS-12 (plate circuit) and VS-13 (filament circuit) power units.

The amplifier design was based on Elmore's model 100, except that integrating and differentiating circuits were introduced to allow of varying the passband.

The clipper serves to reduce the analyzer channel width. Pulses fed into the clipper are clipped to a level variable from 0 to 100 v and then amplified by a three-tube stage with variable gain. Changing the amplification factor varies the analyzer channel width from 5 to 50 kev.

A single-channel differential discriminator is used for electronic collimation. Pulses corresponding to different channels (and thus to different angles) come from the amplifier and are fed into the single channel analyzer. For pulse height analysis we use a 28-channel analyzer designed and built in our laboratory.[14]

IV. Selection of the Gas Mixture and Operating Conditions

The working gas and chamber operating conditions should be chosen

1) to eliminate recombination of electrons with positive ions and the loss of electrons to the chamber grid,

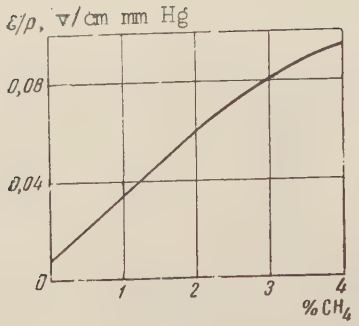

Fig.12

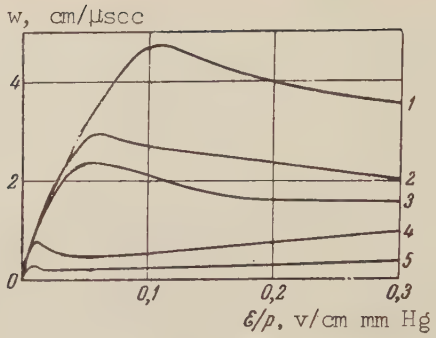

Fig.13

Fig.12. Field strengths corresponding to saturation in different mixtures.
Fig.13. Variation of drift velocity with $\mathscr{E}/p$ for different mixtures: 1) A + + 5.3% CH_4,[15] 2) A + 2.1% CH_4,[15] 3) A + 1% CH_4 (our data), 4) chemically pure argon (A + 0.2% N_2 + 0.02% O_2 + 0.05% CO_2) (our data), 5) spectroscopically pure argon (Ref.16).

2) to minimize the rise time of the pulses on the collecting electrode,
3) to prevent electron attachment to electronegative impurities.

The field intensity at which saturation sets in (i.e., recombination ceases) is usually determined from the variation of the collecting electrode pulse height with field strength in the first region (the region between the high-voltage electrode and the grid). The field strength in the second region is maintained high enough to prevent loss of electrons to the grid.

Adding methane to pure argon raises the field strength at which saturation begins (Fig.12). For values of $\mathscr{E}/p$ in the region above the curve in Fig.12 there is no recombination.

Loss of electrons to the grid can be eliminated by properly selecting the field ratio $\mathscr{E}_2/\mathscr{E}_1$. Usually this ratio should lie between 1.5 and 3.

The finite rise time of the pulses on the collecting electrode affects both the time and the energy resolution of the chamber.

The rise time corresponding to a given chamber geometry depends on the electron drift velocity in the gas. Curves of electron drift velocities for several gas mixtures are shown in Fig.13. The electron drift velocity can be determined from the pulse rise time on the high-voltage electrode or from the time lag of the collecting electrode pulse. The addition of methane markedly increases the electron drift velocity. The rise time can be reduced to 1-2 microsec by using a mixture of A + CH_4. This mixture also minimizes electron attachment.

V. Research Applications of the α-Spectrometer

Investigation of the fine structure of α-spectra

The described spectrometer has been used for studying the fine structure of the α-spectra of thorium and uranium isotopes.[11,17-19] The uranium and thorium sources were prepared from solutions of the nitrates in ethyl alcohol by electrolysis. The anode was a Pt grid; the cathode an Al foil. Sources of up to 200 cm^2 were prepared by this procedure.

Because of the high transmission factor (20 to 30% 4π for sources with areas up to 200 cm^2) and high resolution, it was possible to investigate the α-spectra of the long-lived isotopes Th^{232}, U^{236} and U^{238} and to measure the energies and

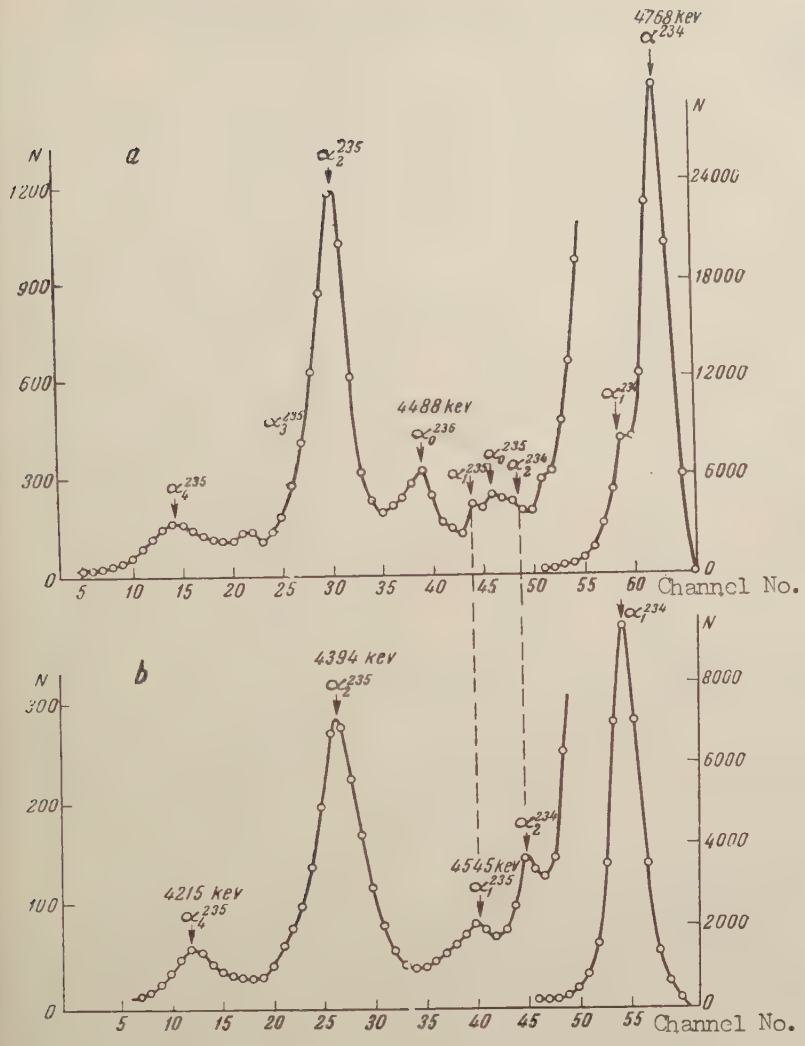

Fig.14. Alpha-particle spectra of U^{234} and U^{235}, obtained a) without coincidences, b) in coincidence with conversion electrons. The right-hand vertical scales pertain to the α_0^{234} and α_1^{234} lines.

relative intensities of α-lines corresponding transitions to the 0^+, 2^+ and 4^+ levels of the daughter nuclei.

We discovered a line in the α-spectrum of Th^{232} (measurement period 90 hours) which corresponds to a partial half-life of 10^{13} years. Hitherto, ionization chambers could not be used to investigate lines corresponding to such long partial periods.

To make spin assignments for detected excited states, one must supplement the α-decay data by observing the accompanying radiations. The most intense of these are usually conversion electrons; therefore we developed an α-e_K coincidence technique for use in conjunction with the ionization α-spectrometer. Because conversion electrons have low energies (tens of kev) their detector must be located inside the ionization chamber. By way of electron detector we used a proportional counter consisting of a sectioned brass cylinder 100 mm in diameter and 200 mm long. The anode was a 50 μ diameter platinum filament. The α-particle source should be thin enough to avoid distorting the conversion electron spectrum. It should also be several square centimeters in area and strong enough to withstand evacuation and contact with the working gas. Film sources prepared as described in our earlier work[22] satisfy these conditions. Since the high-voltage electrode is grounded in measuring α-e_K coincidences, we took the function-of-angle pulses off the grid, and introduced a second, shielding grid into the chamber. In operation, bipolar pulses appear on the grid.

Both the negative and positive parts of the pulse depend on the particle emergence angle. Proper choice of the amplifier passband is very important for work with grid pulses, because the differentiating and integrating circuits have substantially different effects on pulses resulting from particles incident at different angles. Furthermore the angular distribution can be distorted; on the other hand, the passband should be selected for optimum signal-to-noise ratio. The results of our earlier study, described in Ref.23, proved helpful in selecting the amplifier passband.

Table 2

Results of investigation of the α-spectra of Th and U isotopes

Isotope	E, kev	Intensity, %	Energy of excited level, kev	Spin and parity	Half-life, years
			0	$(3/2^+)(5/2^-)$	
Th^{229}	5040±5	8	25		$8,7\cdot10^4$
	4965±10	10	100		$7,0\cdot10^4$
	4890±10	12	180		$6,0\cdot10^4$
	4835±5	60	235	$5/2^+$	$1,1\cdot10^4$
	4805±10	10	267	$7/2^+$	$7,0\cdot10^4$
Th^{232}	4007±5	77	0	0^+	$1,8\cdot10^{10}$
	3948±8	23	60	2^+	$6,0\cdot10^{10}$
	3825±10	0,2	185	4^+	$0,7\cdot10^{13}$
U^{234}	4768	73	0	0^+	$3,4\cdot10^5$
	4718	27	50	2^+	$9,3\cdot10^5$
	4598±8	0,3	173	4^+	$9,0\cdot10^7$
U^{235}	4580±15	4	0	$(5/2^+)$	$1,7\cdot10^{10}$
	4545±10	4	~40		$1,7\cdot10^{10}$
	4394±5	74	185	$5/2^-$	$9,6\cdot10^8$
	4360?	14	220?		
	4215±5	4	370	$7/2^-$	$1,7\cdot10^{10}$
U^{236}	4488±3	74	0	0^+	$3,2\cdot10^7$
	4438±5	26	50	2^+	$9,2\cdot10^7$
	4326±8	0,26	165	4^+	$9,2\cdot10^9$
U^{238}	4195	77	0	0^+	$5,8\cdot10^9$
	4145	23	50	2^+	$2,0\cdot10^{10}$
	4037	0,23	160	4^+	$2,0\cdot10^{12}$

Using the α-e_K coincidence technique, we studied[20,24] the fine structure of the α-spectra of Th^{229}, U^{234} and U^{235}.[20,24]

The α-spectra of U^{234} and U^{235} recorded directly and in coincidence with conversion electrons are reproduced in Fig.14.

The energies and intensities of the α-particles emitted by uranium and thorium isotopes are given in Table 2.

For the even-even nuclei the character of the levels was determined with the aid of the familiar interval rule. The experimental data obtained, when analyzed in conjunction with the theoretical formulas given by Nosov[25], lead to the structure parameters listed in Table 3.

Few comparisons can be made between the deduced quadrupole moments and those determined by Coulomb excitation because there are almost no appropriate data for heavy nuclei. According to Alder et al[26], the quadrupole moments of Th^{232} and U^{238} are 10 and 11 barns, respectively, which is in agreement with our values.

Knowing values of the deformation parameter, we can determine theoretically the probability of a transition to the 4^+ level. The probabilities calculated for the even isotopes of Ra and Th are listed in Table 4.

Our data on α-decay of U^{235} agree well with the results of Baranov et al[27] and Vorob'ev[28] but disagree with Pilger's[29] data.

Further investigation is needed to clarify the nature of the levels of Ra^{225}. Measurements of the conversion electron spectrum in coincidence with separate α-particle groups should prove particularly useful. For such measurements an ionization α-spectrometer might well be used in conjunction with a high-transmission β-spectrometer.

Table 3

Determination of the parameters of even Ra and Th nuclei

Daughter	Nuclear radius, $10^{-13} A^{1/3}$ units	Deformation parameters	Quadrupole moment, barns
Ra^{228}	1,0	0,27	11
	1,4	0,21	17
	1,6	0,19	19
Th^{230}	1,0	0,23	9,5
	1,4	0,19	15
	1,6	0,18	16
Th^{232}	1,0	0,23	9,4
	1,4	0,19	15
	1,6	0,18	16
Th^{234}	1,0	0,21	8,4
	1,4	0,17	14
	1,6	0,15	16

Table 4

Comparison of theoretical and experimental probabilities for α-transitions to the 4^+ level in even Ra and Th nuclei

Daughter	Nuclear radius, $10^{-13} A^{1/3}$ units	Transition probability to the 4^+ level (normalized to the grnd state transition	
		Theo.	Exper.
Ra^{228}	1,0	0,14	
	1,4	0,17	0,26±0,10
	1,6	0,19	
Th^{230}	1,0	0,34	
	1,4	0,38	0,41±0,16
	1,6	0,41	
Th^{232}	1,0	0,29	
	1,4	0,32	0,35±0,14
	1,6	0,36	
Th^{234}	1,0	0,15	
	1,4	0,21	0,30±0,09
	1,6	0,23	

Measurement of α-particle energies

The energy of α-particles is usually measured by comparing the ionization produced by the given α-particle group with the ionization produced by α-particles of known energy. The α-particle energy is related to ionization by the expression

$$E = Nu,$$

where N is the number of ion pairs and u is the mean pair production energy.

It is important to note that the mean energy u depends on the α-particle energy as well as on the working gas in the chamber. The exact E dependence of u is unknown, but numerous experimental data show u to be independent of α-particle energy for energies above 4 Mev. We then get the relation

$$E = Nu_0 + \alpha_0, \tag{14}$$

where u_0 is the average energy needed to produce an ion pair when $E > 4$ Mev, and α_0 is a parameter dependent on the chamber gas. For our mixture of argon and methane $\alpha_0 = 83$ kev.[30] Using relation (14), we can express the energy of the unknown line E_x in terms of the reference line energy E_r and the pulse height ratio for these groups $m = \frac{V_x}{V_r}$ (actually the ratio of ionizations):

$$E_x = mE_r + \alpha_0(1 - m). \tag{15}$$

This method of determining α-line energies requires measurement of m, i.e., we must compare the measured line pulse height with reference line pulse height. To compare these pulse heights, pulses from a precision pulse generator are fed into the preamplifier (Fig.10) and the pulse amplitudes are measured by the method described by Vorob'ev et al[31]. Corrections must be made for shift of the spectrum peak in the direction of small pulse height due to source thickness, imperfect shielding by the grid, and finite rise time of the pulses. The curve shown

in Fig.7 is used to correct for source thickness. Eq.(13) gives the shift of the maximum due to imperfect shielding. The decrease in pulse height due to finite rise time can be determined by means of the familiar expression

$$\frac{\Delta E}{E} = \frac{t_r^2}{24T^2},$$

where t_r is the pulse rise time on the collecting electrode and $T = T_i = T_d$ is the time constant of the integrating and differentiating circuits.

High energy resolution and precise correction for all sources of error permit measurement of α-line energies with uncertainties of 0.05% to 0.1%. For example, we have measured the energy of the main group of α-particles of U^{236} to within ±3 kev.[18]

Use of the ionization α-spectrometer to identify new isotopes

Recent years have seen a remarkable growth of interest in production and investigation of new isotopes. The detection of new elements and new isotopes requires an apparatus with high transmission, good energy resolution and low background.

The background in an ionization chamber arises mainly from contamination of the chamber walls, electrodes and leads. Work in our laboratory has shown that chamber background can be substantially reduced by using pulses appearing on the different chamber electrodes. Coincidence of the collector and high-voltage pulses can be used to avoid counting particles emitted from the walls and electrodes and entering the second region (Fig.1) because such particles do not induce voltage pulses on the high-voltage electrode.

After prolonged operation of the chamber, the grid becomes contaminated by various α-activities. We can avoid counting pulses due to α-particles traveling from the grid into the first region by using delayed coincidences. We have shown above that there is a time lag between pulses from the collecting and high-voltage electrodes. Using the delayed coincidence technique, we can arrange to detect only the particles the pulses due to which on the collecting electrode are delayed a time t_x, thereby excluding particles emitted from the grid because for them $t_3 = 0$. The above-mentioned measures enabled us to reduce the background counting rate to 0.1-0.2 pulses per hour in the 100 kev region. Thus a spectrum interval corresponding to a single α-line receives 0.1 to 0.2 pulses per hour, which makes it feasible to detect α-lines with an intensity as low as 1 pulse per hour.

For a source 200 cm^2 in area and 20-30 $\mu g/cm^2$ thick this intensity corresponds to a decay period of 10^{15}-10^{16} years.

Measurement of decay periods of short-lived α-emitters

We have used our ionization α-spectrometer in conjunction with a 48-channel time analyzer for measuring short decay periods.

The decay period is determined from the time distribution of the pulses due to the investigated isotope, detected in coincidence with the pulses due to the parent α-emitter.

Energy selection of the α-particles and the low background of the ionization chamber markedly reduce the number of chance coincidences, making possible measurement of periods of from 10^{-4} to 10 sec. Furthermore, the results obtained[32] are far more accurate than those yielded by other techniques.

Both the energy and decay period of a given isotope can be simultaneously determined with an ionization α-spectrometer operated in conjunction with multi-

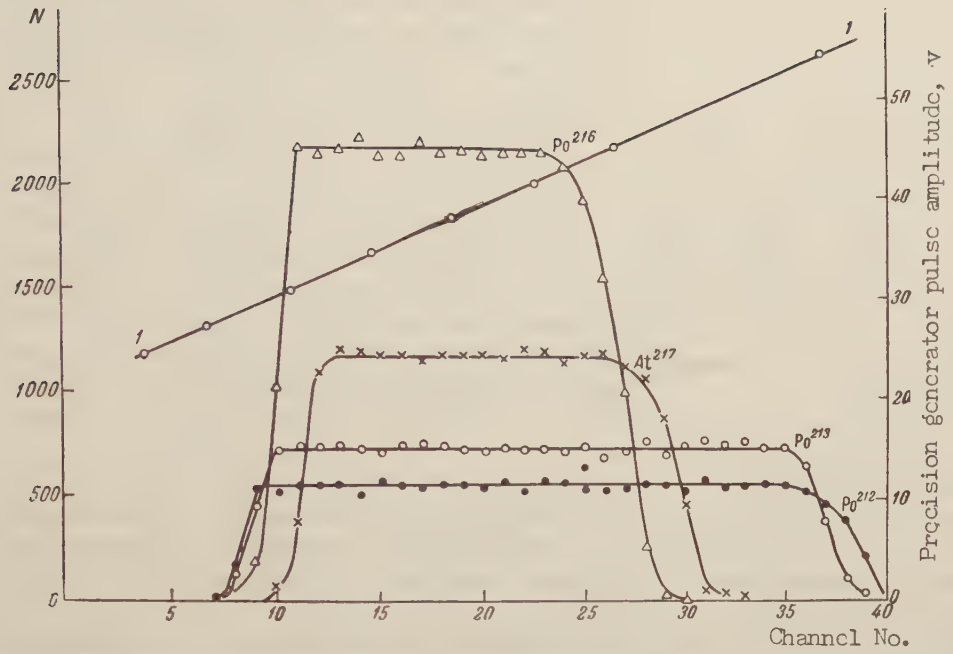

Fig.15. Angular distributions of α-particles from different isotopes. The scale on the right is for the 1-1 line.

channel pulse-height and time analyzers. This is very important where identification of new isotopes is concerned.

Determination of the energy dependence of the range of the center of mass of an α-particle track in argon

For determininag α-particle energies and correcting for the distortion of α-line intensities because of electronic collimation, we must know how the range of the center of mass of the ions is related to the starting point of the α-particle track in argon.

This relation was determined both by calculations (carried out by E.A.Damanskinskii) and by experiment.

For experimental determination we used pulses appearing on the high-voltage electrode. The differential pulse height distribution on the high-voltage electrode is rectangular since

$$V_{\max} = \frac{Ne}{C_2} \text{ and } V_{\min} = \frac{Ne}{C_2}\left(1 - \frac{X}{d}\right).$$

Using the experimentally determined values of $V_{\max}$ and $V_{\min}$ we calculated the range of the ions' center of mass by means of the equation $X = d\left(1 - \frac{V_{\min}}{V_{\max}}\right)$

The accuracy of determination depends on the chamber geometry (d) and the shape of the "rectangle" (accuracy in finding the values of $V_{\max}$ and $V_{\min}$).

Fig.15 shows some "rectangular" pulse height distributions for pulses taken off the high-voltage electrode. To obtain them we set the differential discriminator to a specified group of α-particles and then recorded the corresponding angular distribution. We used the precision pulse height generator (Fig.10) for

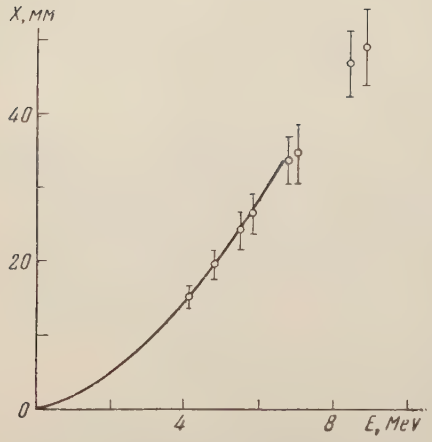

Fig.16. Energy dependence of the range of the ions' center of mass for α-particles in argon. Solid line - calculated curve; points - experimental.

calibration purposes.

The points in Fig.16 give the experimental dependence; the solid line shows the theoretical curve, calculated using the formula

$$X = \frac{\int_0^R r\left(\frac{dN}{dr}\right)_A dr}{\int_0^R \left(\frac{dN}{dr}\right)_A dr}.$$

The Bragg curve for argon $\left(\frac{dN}{dr}\right)_A = f(r)$ was derived from the Bragg curve for air.

Conclusions

This paper describes a high-resolution ionization chamber (the apparatus α-line half-width is ~25 kev) with an effective solid angle of 20 to 30% of 4π).

Detailed consideration of the chief factors affecting the energy resolution enabled us to deduce expressions for determining the line half-widths and the shift of the line peaks. Close attention to details of the operating conditions and careful selection of the first tube of the amplifier resulted in reduction of the noise level to the point where the noise half-width does not exceed 16 kev.

By using a mixture of argon and methane we eliminate attachment of electrons to electronegative impurities. Moreover a significant increase in drift velocity leads to improved time and energy resolution. Electronic collimation allows of improving the resolution of the ionization chamber without serious sacrifice of transmission.

The instrument parameters permit extensive use of the equipment for investigating the fine structure of α-spectra, for isotopic analysis, etc. The spectrometer is especially useful for identifying new isotopes.

The authors thank A.P.Komar for his unflagging interest in this work.

Physical-Technical Institute,
Academy of Sciences of the USSR

References

1. B.S.Dzhelepov, R.B.Ivanov, V.G.Nedovesov & V.G.Chumin, Izv.AN SSSR, Ser. fiz., 23, 782 (1959). (Trans.Bulletin, 23, 780.)

2. S.A.Baranov, A.G.Zelenkov, G.Ya.Shchepkin, V.V.Beruchko & A.F.Malov, Atomnaya energiya, 7, 3, 262 (1959). (Trans.Soviet Journ.of Atomic Energy.)

3. U.Fano, Phys.Rev., 72, 26 (1947).

4. C.E.Melton, G.S.Hurst & T.E.Bortner, Phys.Rev., 96, 643 (1954).

5. G.Bertolini, M.Bettoni & A.Bisi, Phys.Rev., 92, 1988 (1953).

6. C.Elmore, Nucleonics, 2, 16 (1948).

7. B.A.Bochagov, G.E.Kocharov & G.F.Kirshin, PTE (Instruments & Experimental Techniques), No.6, 72 (1957).

8. W.Haeberli, P.Huber & E.Baldinger, Helv.Phys.Acta, 26, 145 (1953).

9. O.Buneman, T.E.Cranshaw & J.A.Harvey, Can.J.Res., 27A, 191 (1949).
10. E.A.Damaskinskii, G.A.Korolev & G.E.Kocharov, Trudy (Proceedings), Leningrad Polytechnical Institute, 1960.
11. G.E.Kocharov, A.P.Komar & G.A.Korolev, Zhur.eksp.i teor.fiz., 36, 68 (1959). (Trans.Soviet Physics - JETP.)
12. B.A.Bochagov, Thesis, Physical-Technical Inst.USSR Ac.of Sci., 1956.
13. G.Valladas, Thesis, Paris, 1955.
14. S.N.Nikolaev, Yu.M.Volkov, A.V.Kulikov & V.A.Kireev, Tsentr. in-t. Tekhn.-ek.inform. (Central Inst.of Tech. & Econ.Info.), No.2 (1960).
15. W.N.English & G.C.Hanna, Canad.J.Phys., 31, 768 (1953).
16. A.A.Vorob'ev, B.A.Ivanov, A.P.Komar & V.A.Korolev, Zhur.tekh.fiz., 29, 1252 (1959). (Trans.Technical Physics.)
17. B.A.Bochagov, A.P.Komar & G.E.Kocharov, Zhur.eksp.i teor.fiz., 32, 1257 (1957). (Trans.Soviet Physics - JETP.)
18. A.P.Komar, G.A.Korolev & G.E.Kocharov, Ibid., 38, 1436 (1960). (Trans. Ibid.)
19. A.P.Komar, G.A.Korolev & G.E.Kocharov, Ibid., 34, 1345 (1958). (Trans. Ibid.)
20. G.E.Kocharov, Thesis, Radium Institute, 1960.
21. A.P.Komar, G.A.Korolev & G.E.Kocharov, Izv.AN SSSR, Ser.fiz., 22, 824 (1958). (Trans.Bulletin, 22, 818.)
22. G.A.Korolev & G.E.Kocharov, PTE, No.5, 112 (1958). (Trans.Instruments & Experimental Techniques.)
23. G.A.Korolev & G.E.Kocharov, Izv.AN SSSR, Ser.fiz., 24, 357 (1960). (Trans.Bulletin, 24, 342.)
24. G.E.Kocharov, A.P.Komar, G.A.Korolev, I.N.Marov & Yu.A.Surkov, Ibid., 23, 855 (1959). (Trans.Bulletin, 23, 847.)
25. V.G.Nosov, Doklady AN SSSR, 112, 3, 414 (1957); Zhur.eksp.i teor.fiz., 33, No.1, 226 (1957). (Trans.Soviet Physics - JETP.)
26. K.Alder, A.Bohr, T.Huus, B.Mottelson & A.Winter, Revs.Mod.Phys., 28, 4, 432 (1956).
27. S.A.Baranov, A.G.Zelenkov & V.M.Kulakov, Reports presented at the Tenth Conference on Nuclear Spectroscopy, M., 1960.
28. A.A.Vorob'ev, A.P.Komar & V.A.Korolev, Ibid.
29. R.C.Pilger,Jr., Ph.D. Thesis, UCRL-3877, July (1957).
30. B.C.Harwey, H.G.Jackson, T.A.Eatwood & G.C.Hanna, Canad.J.Phys., 35, 258 (1957).
31. A.A.Vorob'ev, V.A.Korolev, V.A.Kireev, S.N.Nikolaev & G.E.Solyakin, Tsentral'nyi in-t tekhn.-ekon.inform. (Central Inst.of Tech.& Econ.Info.), No.3 (1960).
32. Yu.M.Volkov, G.A.Korolev, A.P.Komar, & G.E.Kocharov, Report presented at the Eleventh Conference on Nuclear Spectroscopy, Riga, January, 1961.

A MERCURY GAMMA-CALORIMETER

- E.A.Khol'nova

Gamma-spectrometers are often calibrated in intensity with reference to sources the activity of which has been determined beforehand by means of some type of γ-calorimeter. Thus, the "ritron" and "elotron" spectrometers of the Radium Institute and the crystal diffraction spectrometer of the All-Union Scientific Research Institute of Metrology were calibrated in intensity with the aid of the Institute of Metrology lead sphere calorimeters[1]. One of the principal shortcomings of such calorimeters is relatively low sensitivity. Only sources with an activity exceeding 50 mC can be measured by means of such calorimeters.

On the other hand, sources of appreciably lower activity are used in a number of spectrometers. For the purpose of measuring such low activities work was initiated in the All-Union Scientific Research Institute of Metrology in 1956 with a view to developing a new type of sensitive calorimeter, namely, a mercury calorimeter.

As regards principle of operation, the mercury calorimeter is similar to a conventional thermometer. It differs primarily from a thermometer in having a much larger spherical reservoir - "bulb". The mercury filling the reservoir serves simultaneously as the thermometric substance and the γ-ray absorber. The glass spherical reservoir is topped by a long thin capillary which serves as the measuring part of the calorimeter. In order to provide for introduction of the source, the glass reservoir has a cylindrical glass cavity extending approximately to the center of the sphere.

The γ-radiation emitted by the radioactive source is absorbed by the mercury, as a result of which the mercury heats up and expands. The amount of energy absorbed by the mercury is determined by observing the level of the mercury in the capillary.

The calorimeter set-up is diagramed in the accompanying figure. It will be seen that the calorimeter is exceptionally simple in design: it consists of a glass sphere filled with mercury and a long capillary tube. All the other parts of the set-up serve for mounting and for temperature stabilization of the calorimeter.

As may be seen in the figure, the set-up consists of two completely identical γ-calorimeters, each of which operates as a single calorimeter. The source is inserted into one of the calorimeters, while the other serves for temperature control purposes. Such control is very important inasmuch as the calorimeter sensitivity is high and the measuring time is relatively long (approximately 2 hours).

In successive series of measurements the roles of the calorimeters may be interchanged, i.e., the source is inserted into the second calorimeter, while the first serves as the temperature control.

The calorimeter is made entirely of glass: the spherical reservoir of glass No.23, and the capillary of thermometer glass. The spherical reservoir has the following dimensions: outside diameter 61.5 mm, inside diameter 60.0 mm; inside diameter of the source cavity 11 mm, length of source cavity 35 mm. The total length of the capillary is 540 mm; the inside diameter 0.07 mm. At the top the capillary widens to form an expansion cavity with a volume of 0.2 cm^3. Over a length of about 480 mm the capillary tube has a milk glass scale graduated in millimeters.

In preparing the calorimeter each of the reservoir spheres was filled with about 108 cm^3 of chemically pure mercury. The reservoirs were filled so that at

a temperature of 25.1° C the mercury level in the capillaries would be close to the zero graduation. This working temperature (somewhat higher than room temperature) was purposely chosen to exclude the possibility of inflow of heat from the surroundings.

The sensitivity of our calorimeter is indicated by the results of the following simple calculations. With a 0.01° temperature rise the volume of the mercury in the reservoir should change by

$$\Delta V = V\alpha t = 108 \cdot 0.000182 \cdot 0.01 = 196 \cdot 10^{-6} \text{ cm}^3$$

(here α is the coefficient of expansion of mercury relative to glass, equal to 0.000182 degree^{-1}). Inasmuch as the capillary diameter is 0.007 cm, the resultant change in the level of the mercury in the capillary is given by

$$l = \frac{\Delta V}{S} = \frac{\Delta V}{\frac{\pi d^2}{4}} = \frac{196 \cdot 10^{-6} \cdot 4}{3.14 \cdot 49 \cdot 10^{-6}} = 5.11 \text{ cm}.$$

Thus with increase of the mercury temperature by 0.01° the mercury level in the capillary changes by ~51 mm. Since the capillary scale can be read to within 0.5 mm or even better, the given design allows of detecting temperature changes of down to 0.0001°.

Usually γ-calorimeters are calibrated with the aid of an electric heater of known power, which is inserted into the calorimeter instead of a source. In addition to this method, the mercury γ-calorimeter can also be calibrated directly in degrees by comparing its indications with those of a precision thermometer; this procedure allows of establishing the absolute temperature corresponding to any given indication on the capillary scale. We used the second method and found that the zero on the scale of the first calorimeter which has a capillary with a mean diameter of 0.07 mm*, corresponds to a temperature of 25.16° and the 450 mm mark on the scale to a temperature 25.25°; the mean

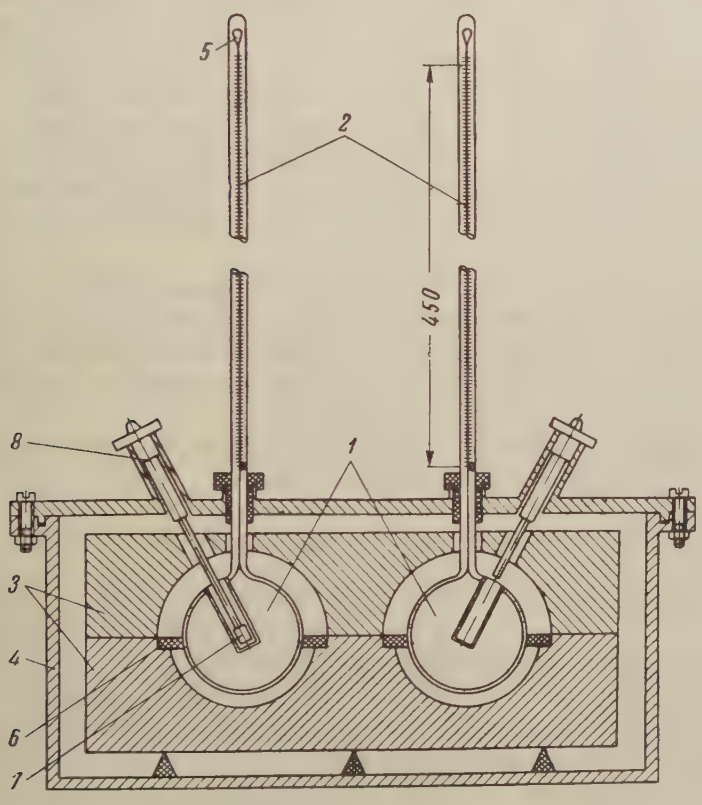

Mercury γ-calorimeter: 1 - spherical reservoir filled with mercury, 2 - capillary tube, 3 - copper block (temperature equalizer), 4 - brass box, 5 - expansion volume, 6 - teflon gasket, 7 - source being measured, 8 - source holder.

---

*The internal diameters of the capillaries and their uniformity over the length of the tubes were investigated by introducing a precisely weighed drop of mercury into the capillary. Then the length of the mercury column formed by the drop in different parts of the capillary was measured by means of a universal microscope. Knowing the weight of the mercury and the length of the column we could readily calculate the capillary diameter.

Comparison of the characteristics of lead and mercury calorimeters

Calorimeter	Diameter, mm	Transfer surface, cm^2	Weight, g	Total heat capacity cal/degree
Lead	70	154	2030	61
Mercury	61.5	121	1497	53

capillary diameter of the second calorimeter is 0.072 mm and its 0 and 450 mm graduations correspond to 25.14° and 25.24°, respectively.

The high sensitivity of the γ-calorimeter imposes rigorous requirements as regards temperature stabilization. It is meaningful to measure the temperature with an accuracy to within 0.0001° only if the "background" temperature of the calorimeter is maintained constant within the same limits during the period of measurement. In the case of our mercury calorimeter, however, this requirement is less exacting, inasmuch as the presence of the second control calorimeter allows of determining and correcting for the background temperature.

For better stabilization of the temperature background both calorimeters are mounted inside a massive copper block, which is a good temperature equalizer. The copper block in turn is enclosed in a brass box and in this form is immersed in a large oil bath, the temperature of which is maintained at 25.16° by a thermostat. The oil bath temperature should be maintained constant to within ±0.002°. A thermostat meeting these requirements is now under construction.

As will be evident from the figure, there is no need to disassemble the box and copper block in order to insert the source. The source, mounted in a special holder, is inserted through a side channel in the copper block and brass box without disturbing the temperature regime of the calorimeter.

The γ-radiation from the measured source encounters a mercury layer 24 mm thick, which is equivalent as regards absorption to 29 mm lead. This was the thickness of the absorbing layer in the No.2 lead sphere calorimeter[1] (outside diameter 70 mm). Calculations of the absorption of γ-radiation of different energies for this calorimeter were carried out earlier.[2] These basic calculations were utilized for the mercury calorimeter.

The absorption capacity of the mercury calorimeter is the same as that of the No.2 lead calorimeter. In contrast, its thermometric characteristics are appreciably better. Thus the heat-transfer surface is smaller and the total capacity of the mercury calorimeter is lower (see table), while the temperature sensitivity is an order of magnitude higher.

Comparison of these data shows that the mercury calorimeter can be used for measuring activities (for example, Co^{60}) of the order of 2-5 mC.

"D.I.Mendeleev" All-Union Scientific Research Institute of Metrology

References

1. K.K.Aglintsev & E.A.Khol'nova, Trudy VNIIM (Proceedings, All-Union Scientific Research Institute of Metrology), No.30 (90), 25 (1957); K.K.Aglintsev, F.M.Karavaev, A.A.Konstantinov, G.P.Ostromukhova & E.A.Khol'nova, Atomnaya energiya, No.2, 55 (1956). (Trans.Soviet Jour.of Atomic Energy.)

2. E.A.Khol'nova, Thesis, VNIIM, L., 1954.

TWO-CRYSTAL SPECTROMETER AND ITS USE FOR INVESTIGATING THE (p,γ) REACTION

- Yu.N.Antuf'ev, V.Yu.Gonchar, E.G.Kopanets, A.N.L'vov & S.P.Tsytko

In studying the energy levels of nuclei by means of the radiative proton capture reaction it is necessary to measure the spectra of the γ-rays emitted by the excited nuclei. Generally this γ-radiation is comparatively weak; hence for measuring the γ-spectrum it is necessary to use a spectrometer with high efficiency.

The most suitable type of γ-spectrometer for investigating the γ-radiation from the (p,γ) reaction is a scintillation spectrometer. In most cases, however, the γ-ray spectrum is so complicated that it is almost impossible to interpret it by means of a single-crystal scintillation spectrometer.

In such cases the most suitable method is investigation of the coincidences between γ-rays emitted in cascade. From the observed coincidence spectra one can infer the energies of the intermediate levels involved in the cascade transitions. Sometimes it is useful to use the method of a summing spectrometer[1,2].

Two-crystal coincidence γ-spectrometers and summing spectrometers can also be used for measuring γ-γ angular correlation. The results of such measurements yield information on the spins of the excited levels.

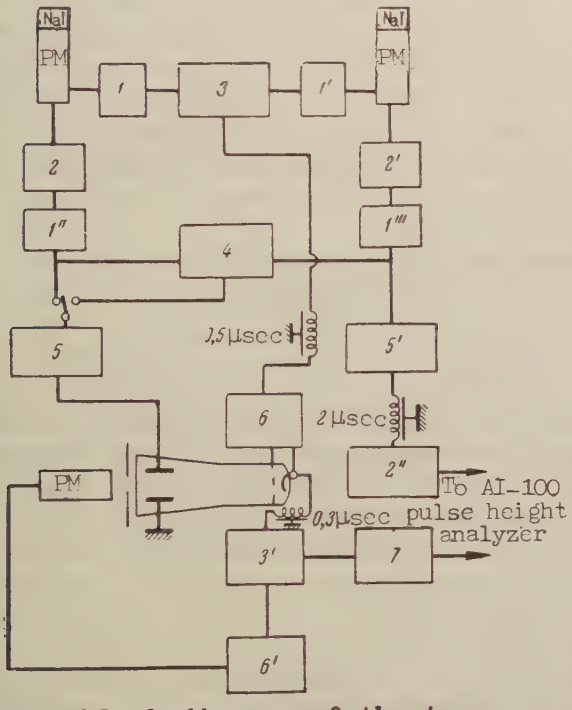

Fig.1. Block diagram of the two-crystal γ-spectrometer: 1,1',1'' & 1''' - pulse shapers, 2,2' & 2'' - cathode followers, 3 & 3' - coincidence circuits, 4 - summing circuit, 5 & 5' - linear amplifiers, 6 & 6' - blocking oscillators, 7 - multivibrator.

In this report we describe a two-crystal γ-spectrometer with a universal type electronic circuit, which makes it possible to use this instrument either as a coincidence spectrometer or as a summing spectrometer. The described spectrometer was constructed in the Physical-Technical Institute of the Ukrainian SSR Academy of Sciences and has been used for over a year for investigating diverse (p,γ) reactions. To illustrate the operation of the spectrometer we give the results of measurements with a Co^{60} source and in investigating the Al^{27} (p,γ)Si^{28} reaction.

A block diagram of the equipment is shown in Fig.1. The radiation detectors are two NaI(Tl) crystals. One of these has a diameter of 70 mm, a thickness of 60 mm and an energy resolution of 11% for 661 kev γ-rays. The second crystal is 70 mm in diameter, 40 mm thick and has an energy resolution of 14%. We also used an NaI(Tl) crystal 40 mm in diameter, 40 mm thick, with a resolution of 9%. The crystals are coupled to FEU-1B photomultipliers developed by Khlebnikov. The crystal-photomultiplier assemblies are mounted on rotatable arms and hence can be set at any angle relative to each other and to the proton beam.

The pulses are taken off the ninth dynodes and fed through cathode followers to shapers. After shaping there are obtained flat topped pulses of 3 microsec duration. These pulses are amplified by linear amplifiers with a maximum amplification coefficient of 100. The amplification can be varied in steps.

The pulses for the fast coincidence circuit are taken off the photomultiplier anodes in order to obtain high pulses. These pulses are shaped by a short-circuited delay line (5 meters of RK-50 cable) which yields pulses of $5 \cdot 10^{-8}$ sec for the coincidence circuit. The coincidence circuit is assembled about a 6A3P tube. Its resolving time is $5 \cdot 10^{-8}$ sec. The pulse from the coincidence circuit goes through a delay line ($T = 5 \cdot 10^{-7}$ sec), which is necessary so that the pulse at the output of the linear amplifier will attain its full amplitude, and triggers a blocking oscillator, which yields a pulse unblanking the cathode-ray tube. During this time the pulse from the output of the linear amplifier controls the sweep of the cathode-ray tube: if the pulse has the necessary height, the beam appears in the opening of the opaque screen and reaches the photomultiplier viewing the tube. The pulse from this photomultiplier triggers a blocking oscillator the pulse from which goes to the coincidence circuit with the delay pulse from the first, cathode-ray tube driving, blocking oscillator. The output pulse from the coincidence circuit triggers a multivibrator which generates a control pulse that is applied to the AI-100-1 type pulse height analyzer. A similar circuit is described in Ref.3. The output from the second linear amplifier through a cutoff and an auxiliary amplifier with a gain of 5 is applied to the input of the pulse height analyzer.

Thus the analyzer opens only in the presence of pulses from both photomultipliers, coinciding in time, and with a given height of the pulse from the linear amplifier controlling the sweep of the cathode-ray tube. A pulse from one of the photomultipliers may be applied to this amplifier - then from the other photomultiplier there will be obtained the spectrum of coincidences with the selected part of the total γ-ray spectrum; there can also be applied pulses equal to the sum of the pulses in both photomultipliers - then there will be obtained the spectrum of γ-rays the sum of whose energies is equal to a set value.

The efficiency of the spectrometer in counting coincidences with the selected section of the spectrum is given by

$$\eta_{coinc} = \theta_1 \eta_1 \cdot \theta_2 \eta_2 \cdot k,$$

where θ_1 is the solid angle viewed by the first crystal and η_1 is its efficiency, θ_2 and η_2 are the solid angle and efficiency of the second crystal, and k is the part of the total spectrum from the second γ-line that is accepted by the fixed channel.

The efficiency of the spectrometer in counting coincidences of two γ-rays the sum of whose energies equal to the set value is given by

$$\eta_{sum} = 2\theta_1 \eta_1 \cdot \theta_2 \eta_2 \cdot k_1 k_2$$

where k_1 and k_2 are the parts of the spectra of the first and second γ-lines, the sum of whose energies is equal to the set energy value.

To illustrate the operation of the spectrometer in Fig.2 we reproduce the spectra obtained for Co^{60}. Fig.2,a is the spectrum of γ-rays yielding coincidences with the 1.33 Mev gammas (the fixed channel was set on the photopeak corresponding to these γ-rays). Fig.2,b gives the γ-ray spectrum of Co^{60} in the case when the channel was set on the sum of the 1.17 and 1.33 Mev γ-rays which form a cascade.

The calculated efficiency of the spectrometer in the first case was $\eta_{coinc} = 0.00017$, assuming $\theta_1 = \theta_2 = 0.048$ and $k = 0.2$. In the second case with $\theta_1 = \theta_2 = 0.048$ and $k_1 = k_2 = 0.2$, the calculated efficiency $\eta_{sum} = 0.00007$. Experimental evaluations of the efficiencies yielded values within ±15% of the calculated value in both cases.

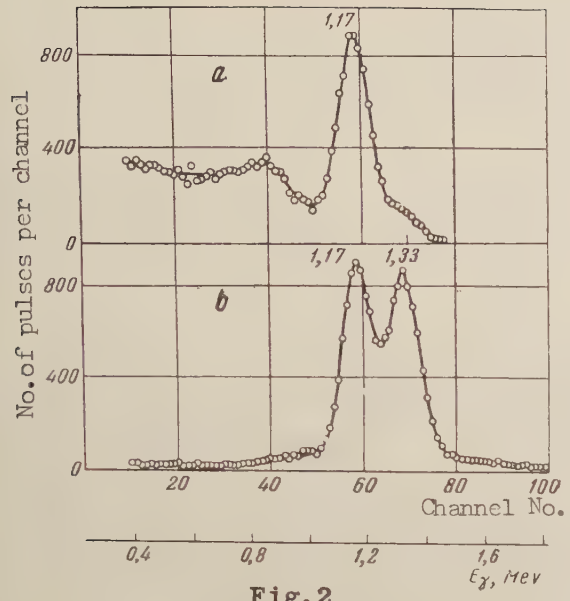

Fig.2

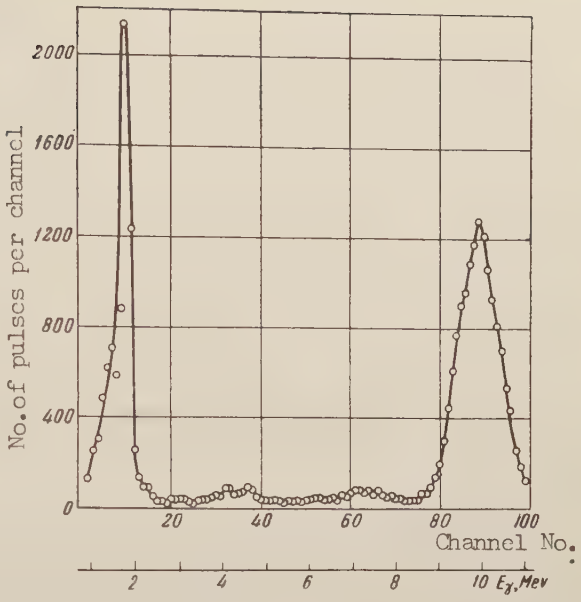

Fig.3

Fig.2. Coincidence spectrum for Co^{60}. a - fixed channel set on the 1.33 Mev line; b - channel set on the total energy of the 1.17 and 1.33 Mev γ-rays.
Fig.3. Spectrum of coincidences of the γ-rays from the $Al^{27}(p,\gamma)Si^{28}$ reaction; fixed channel set on the energy of the excited level of the compound Si^{28} nucleus.

The spectrometer was used for investigating the γ-rays from the $Al^{27}(p,\gamma)Si^{28}$ reaction. Specifically, we investigated the resonance γ-rays emitted at a proton energy of 993.3 kev. The fixed channel in this case was set on the energy of the excited level of the compound Si^{28} nucleus. From the spectrum reproduced in Fig. 3 it will be evident that this state de-excites in two ways: by a cascade transition via a 1.78 Mev level and a cascade transition via a 4.6 Mev level. The intensity of the latter is not more than 5% that of the former; nevertheless, the γ-lines of this cascade are clearly evinced, whereas they are unnoticeable in the spectrum recorded by means of a single-crystal spectrometer.

As noted above, this spectrometer, operated as a summing instrument, can be used for studying γ-γ angular correlation. For test purposes we measured the anisotropy of the γ-γ correlation using a constant Co^{60} source. The fixed channel was set on the energy of the 2.5 Mev level and we measured the number of coincidences with two geometries: a) with an angle of 90° between the axes of the crystals and b) with an angle of 180°. The measured anisotropy agreed within the limits of the experimental error with the theoretical.

The design of the spectrometer makes it possible to use it as a Compton γ-spectrometer, unblocking the pulse height analyzer with a pulse from γ-rays scattered at a certain angle, and as a total absorption spectrometer, blocking the analyzer if a scattered γ-ray is detected.

The spectrometer circuitry comprises 28 tubes, not counting the power supply tubes.

Physical-Technical Institute
Academy of Sciences of the Ukrainian SSR

References

1. J.Kajfocz & J.Kopecky, Cs.Cas., 5, 582 (1958).
2. B.Astrom, Nucl.Instr., 1, 143 (1957).
3. A.J.West & L.G.Mann, Rev.Sci.Instr., 25, 129 (1954).

* * * * * * *

RADIATIVE PROTON CAPTURE BY S^{34}

- Yu.P.Antuf'ev, A.K.Val'ter, V.Yu.Gonchar, E.G.Kopanets, A.N.L'vov & S.P.Tsytko

As reported in our earlier communication[1], we investigated the $S^{34}(p,\gamma)Cl^{35}$ reaction in the proton energy range from 0.6 to 1.9 Mev. Over 40 γ-ray resonances were observed. Investigation of the γ-ray spectra and angular distributions enabled us to draw certain inferences regarding the spins and parities of some of the resonance levels and of the first excited states of Cl^{35}.

In the present work we investigated radiative proton capture by S^{34} at a resonance energy of 1214 kev. The γ-spectra were measured by means of a single-crystal γ-spectrometer and also by means of a two-crystal coincidence spectrometer. We measured the angular distributions and the γ-γ directional correlation. In addition, we determined the γ-ray yield from a thick S^{34} target.

Experimental Procedure and Results

The monoenergetic beam of 1214 kev protons, accelerated in the Physical-Technical Institute of the Ukrainian SSR Academy of Sciences electrostatic generator[2] was directed onto the thin target prepared by knocking S^{34} ions into a tantalum backing.[1,3] The target was located in the center of the chamber and oriented at an angle of 60° relative to the proton beam. The target chamber was mounted at the center of a rotating stand, which carried the γ-spectrometer crystals and photomultipliers. Thus, the NaI(Tl) crystal, 70 mm in diameter and 60 mm thick, could be rotated about the center of the target 150° in either sense relative to the direction of the proton beam.

The associated electronic circuit, which was connected to an AI-100 100-channel pulse height analyzer, made it possible to operate the γ-spectrometer as a conventional single-crystal spectrometer with high efficiency, as a coincidence spectrometer and also as a summing spectrometer. The spectrometer was calibrated with reference to the γ-rays from Cs^{137}, Co^{60} and $MsTh_2$ and from the $Be^9(p,\gamma)B^{10}$ and $Al^{27}(p,\gamma)Si^{28}$ reactions. A description of the instrument will be found in Ref.4 (preceding article).

In measuring the angular distributions and γ-γ correlations by way of monitor we used a CsI(Tl) crystal 30 mm in diameter and 20 mm thick, which was mounted at a fixed angle of 90° relative to the direction of the proton beam. The monitor detected all γ-rays having energies greater than 1.5 Mev.

The proton current was measured by means of a current integrator, the calibration of which was checked before and after each series of measurements.

The singles γ-ray spectrum is shown in Fig.1. As will be evident from the figure, there appear two γ-ray groups with energies of 3.17 and 4.38 Mev. In

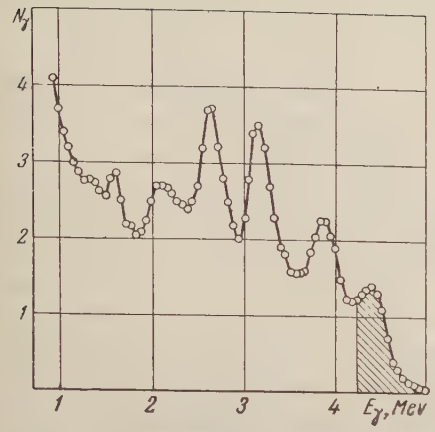

Fig.1. Gamma-ray spectrum obtained by means of the single-crystal spectrometer.

addition, there is present γ-radiation with an energy of 1.63 Mev. This line is probably a background line inasmuch as its intensity varies with time, whereas the yield of the 3.17 and 4.38 Mev γ-rays remain constant.

Fig.2 shows the spectrum obtained by means of the spectrometer operated as a coincidence instrument. The fixed channel was set on the part of the spectrum that corresponds to the total absorption peak for the 4.38 Mev γ-rays (hatched region in Fig.1). There are evident in this spectrum only three peaks from the 3.17 Mev γ-rays.

Fig.3 shows the spectrum obtained by means of the summing coincidence spectrometer. The sum channel was set on the γ-ray energy in the vicinity of 7.55 Mev. There are evident in the spectrum peaks that correspond to γ-rays of 3.17 and 4.38 Mev energy. As might have been expected the total absorption peaks are the most intense.

On the basis of the results obtained in all three series of measurements (singles, coincidence and summing) it may be asserted that the de-excitation of the 7.55 Mev level occurs only by a cascade transition via one intermediate level, the energies of the cascade γ-rays being 3.17 and 4.38 Mev. The cross-over transition to the ground state, if it exists, has a relative intensity $<0.5\%$.

The angular distribution was investigated for the 3.17 and 4.38 Mev γ-rays in the angular range from 0° to 150° clockwise and counterclockwise relative to the direction of the proton beam. Measurements in the indicated angular range allow of excluding the error connected with inaccuracy in determining the distance from the target to the crystal and also facilitate making corrections for the absorption of the γ-rays in the backing and target holder.

For determining the angular distribution of the 4.38 Mev γ-rays we used the total area in the spectrum under the total absorption peaks and the peak associated with emission of one annihilation photon from the crystal. The contribution from the 3.17 Mev γ-rays to the angular distribution curve did not exceed 1-2%.

The angular distribution of 3.17 Mev γ-rays was determined from the total area in the spectrum under the peaks due to ejection from the crystal of one and two annihilation photons. From these areas for each

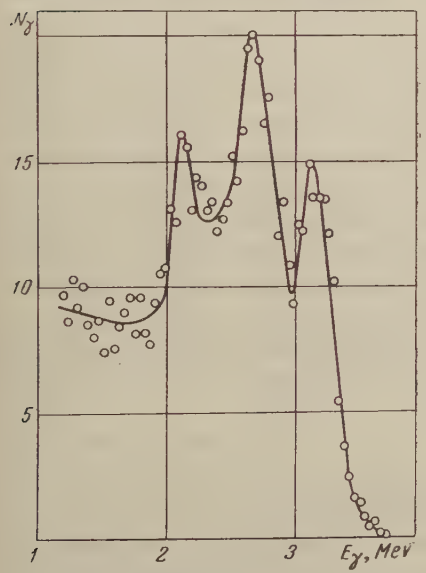

Fig.2. Gamma-ray spectrum obtained by means of the coincidence spectrometer.

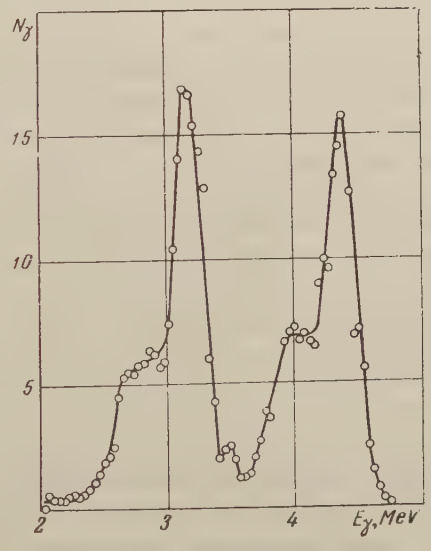

Fig.3. Gamma-ray spectrum obtained by means of the summing spectrometer.

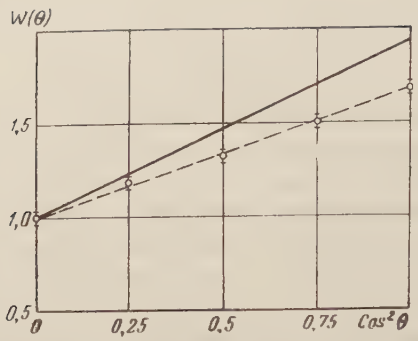

Fig.4. Angular distribution of the 4.38 Mev γ-rays: dashed line - experimental; solid line - theoretical curve.

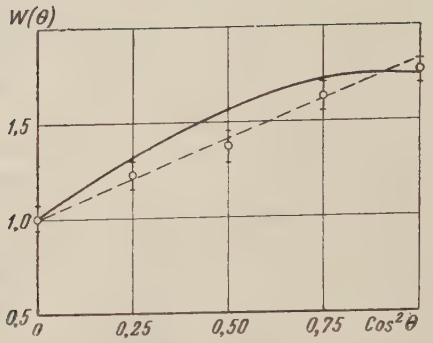

Fig.5. Angular distribution of the 3.17 Mev γ-rays: dashed line - experimental; solid line - theoretical curve.

angle we subtracted the Compton part of the spectrum due to the 4.38 Mev γ-rays.

The experimental data were processed by the method of least squares; the results are shown in Figs.4 and 5.

The γ-γ correlation was measured by means of the spectrometer connected to operate as a summing coincidence spectrometer. The sum channel was set on the energy region of the 7.55 Mev γ-rays. The coincidence counts were recorded for two geometries: a) both crystals oriented at an angle of 90° to the direction of the proton beam (crystals at 180° to each other), and b) one of the crystals at 90° to the proton beam, the second at 0° (angle between crystal axes 90°). Measurements of the coincidence intensities with these two geometries make it possible to determine the γ-γ correlation and compare it with the calculated correlation.

The procedure for measuring the γ-γ correlation by means of the summing spectrometer was checked in earlier experiments with a Co^{60} source, the γ-γ correlation function for which is known with a high degree of accuracy (see preceding article).

In addition to the above experiments, we also determined the absolute γ-ray yield from a thick S^{34} target. These measurements were carried out with a semi-thick ZnS target with a natural isotopic content of S^{34}. The thickness of the target was 20 kev for 1 Mev protons. By way of detector in these experiments we used a 70 mm diameter, 60 mm thick NaI(Tl) crystal. The efficiency of this crystal for detecting 7.4 Mev γ-rays was determined experimentally from the yield of γ-rays from a thick Be^{9} target bombarded with 998 kev protons ($Be^{9}(p,\gamma)B^{10}$ reaction). We then evaluated the efficiency of the crystal in detecting 4.38 Mev γ-rays on the basis of this data. The measured value of the absolute yield of γ-rays from the thick S^{34} target proved to be $2.56 \cdot 10^{-9}$ disintegrations per proton. The error in determining the γ-rays yield is estimated to be $\leqslant 15\%$.

Discussion

The experimental angular γ-ray distributions were compared with the theoretical distributions calculated on the basis of different assumptions regarding the spins of the resonance and intermediate levels and the multipole orders of the γ-transitions. Such comparison shows that best agreement is obtained on the assumption that the spin of both the resonance and the intermediate levels is 7/2. The theoretical curves for a $7/2 \rightarrow 7/2 \rightarrow 3/2^{+}$ cascade are given by the solid lines in Figs.4 & 5.

The measured γ-γ correlation agrees within the limits of the experimental error with the theoretical based on this assumption and thus substantiates the 7/2 assignment.

It should be noted that in the cascade in question the angular distributions of the two γ-rays are very close to each other (cf. Figs.4 & 5). The energies of the γ-rays are also close. This means that our experimental results and inferences do not depend on the sequence of the γ-rays in the cascade, i.e., do not depend on whether the energy of the intermediate level is 3.17 or 4.38 Mev. However, we have assumed throughout that the energy of the intermediate level is 3.17 Mev, inasmuch as a level of this energy in Cl^{35} was observed in the work of Ref.5.

The experimental angular distribution of γ-rays associated with the first transition from the resonance level with spin 7/2 to the intermediate level, which also has spin 7/2, noticeably (in excess of the experimental error) differs from the calculated distribution on the assumption of a pure dipole transition (see Fig.4). Hence it may be inferred that in the given case we have a mixture of M1 and E2 and, consequently, that the parities of the resonance and intermediate levels are the same.

Consideration of the relative probabilities for the transitions from the resonance level to the ground state and to the intermediate state, which have spins $3/2^+$ and $7/2^{\pm}$, respectively, leads to the inference that the parity of the resonance and intermediate levels must be odd and that the multipole order of the transition from the resonance level to the ground state must be M2. Only this assumption regarding the multipole order of the transition and the parity of the levels involved can explain the great inhibition (retardation by a factor of more than 100) of the cross-over transition to the ground state. The appreciable intensity of the resonance at E_p = 1214 kev indicates that of all possible orbital momenta of the picked up proton one must give preference to the lowest value, i.e., to $l_p = 3$, which in turn, substantiates the inferred odd parity of the resonance level.

According to the shell model, the ground state of Cl^{35} is determined by an unpaired proton in the $d_{3/2}$ state, and the low-lying level in the 3 to 4 Mev excitation energy range with spin $7/2^-$ may be due to single-particle excitation with transition of the proton from the $d_{3/2}$ to the $f_{7/2}$ state. However, neither the shell model nor the unified model allows of explaining by means of single-particle excitation the presence close to 7.55 Mev of yet another level with spin $7/2^-$, corresponding to a resonance level. Hence it must be inferred that this level is characterized by two- or multiple-particle excitation.

In connection with this it is interesting to compare the resonance level widths determined from experiment with the widths calculated on the basis of the single-particle model.

As noted above, we measured the absolute γ-ray yield from a semithick target. Assuming the stopping power of ZnS to be $dE/d\xi$ = 150 kev·cm^2/mg, we readily obtain $\Gamma_\gamma\Gamma_p/\Gamma$ = 0.1 ev. If we further assume that $\Gamma_p > \Gamma_\gamma$, we obtain a value of 0.1 ev for Γ_γ. The value of Γ_γ calculated according to the single-particle model for an M1 transition is 2 ev. The great difference between the experimental value of Γ_γ and the calculated value is consistent with the assumption of deviation of the character of the excitation of the resonance level from single-particle excitation, inasmuch as in the case of such deviation the probability for an M1 transition is generally decreased.

We desire to express our gratitude to M.I.Guseva for preparing the isotope targets and to A.A.Tsygikalo and Yu.A.Kharchenko and the personnel of the electrostatic generator for insuring satisfactory operation of the accelerator during the

course of the experiment.

Physical-Technical Institute,
Academy of Sciences of the Ukrainian SSR

References

1. Yu.P.Antuf'ev, A.K.Val'ter, V.Yu.Gonchar, E.G.Kopanets, A.N.L'vov & S.P. Trytko, Izv.AN SSSR, Ser.fiz., 24, 877 (1960). (Trans.Bulletin, 24, 878.)
2. A.K.Val'ter & A.A.Tsygikalo, PTE (Instruments & Exper.Techniques), No.4, 3 (1957).
3. M.I.Guseva, PTE, No.5, 112 (1957).
4. Yu.P.Antuf'ev, V.Yu.Gonchar, E.G.Kopanets, A.N.L'vov & S.P.Tsytko, Present issue of the Bulletin, p.249.
5. P.M.Endt, C.H.Paris, A.Sperduto & W.W.Buechner, Phys.Rev., 103, 961 (1956).

* * * * * * *

MEASUREMENT OF THE NUMBER OF GAMMA-RAYS PER DECAY OF Mo^{99}

- A.N.Silant'ev

In the present work we measured the number of γ-rays per decay of Mo^{99} by the method of $4\pi\beta$-γ coincidences. In employing this method the source is mounted inside a 4π β-counter, which is located near the crystal of a scintillation spectrometer. A block diagram of the set-up is shown in Fig.1. It will be evident from the figure that the multichannel pulse height analyzer detects only the pulses from the scintillation counter that are in coincidence with pulses from the 4π β-counter. The delay line is introduced in order to correlate the β pulses with the pulses from the scintillation spectrometer.

The $4\pi\beta$-γ coincidence method has advantages over other methods in the following cases: 1) in measurement with sources with a short half-life, 2) in measurements with sources having a low activity (10^{-13}-10^{-14} curie), 3) in investigating low probability γ-transitions, 4) in investigating transitions masked by γ-radiation emitted in de-excitation of metastable states, and 5) in the presence of a strong γ-background.

One of the principal advantages of the $4\pi\beta$-γ coincidence method is that it allows of direct measurement of the counting coefficient of the 4π counter for

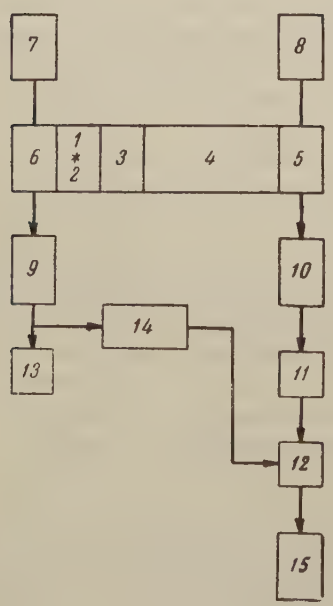

←Fig.1. Block diagram of the $4\pi\beta$-γ coincidence set-up: 1 - source, 2 - 4π β-counter, 3 - scintillation crystal, 4 - FEU-S photomultiplier, 5 & 6 - amplifiers, 7 - VS-9, 8 - VS-16, 9 - "Siren" amplifier, 10 - wide band amplifier, 11 - delay unit, 12 - gating circuit, 13 - "Kalina" scaler, 14 - coincidence circuit, 15 - multiple channel pulse height analyzer.

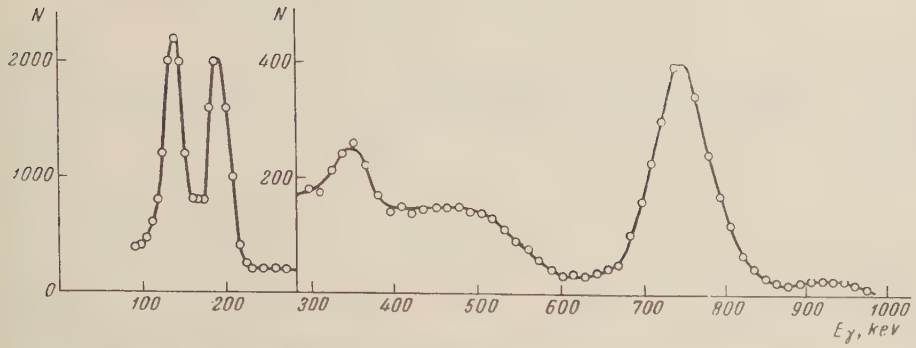

Fig.2. Experimental γ-ray coincidence spectrum (background subtracted).

the β-rays from a given source. To this end one measures separately the singles γ-spectrum and the coincidence spectrum. The ratio of these two quantities gives the efficiency in detecting the β-spectrum in coincidence with the measured γ-spectrum. For a source with a complex β-spectrum one can measure the efficiency for the partial β-spectrum (except for the β-rays to the ground state).

In carrying out such measurements it is essential to take into account the possibility of simultaneous detection by the crystal of two cascade γ-rays.

The set-up was calibrated with reference to the following "standard" sources: Cs^{137}(32 kev), Hg^{203}(71 & 279 kev), Au^{198}(412 kev), Nb^{95}(768 kev) and Co^{60}(1332 kev).

For measuring the number of γ-rays per decay of Mo^{99} the activity was applied to a thin collodion film. The measurements were repeated over a period of several days in order to check the half-life.

The experimental coincidence curve with the background due to chance coincidences subtracted is reproduced in Fig.2. The γ-ray energies and numbers of γ-rays per decay are listed in the accompanying table together with the corresponding data of other authors.

Energies of γ-rays and number of γ-rays per decay

E_γ, kev				No. of γ-rays per decay, %	E_γ, kev				No. of γ-rays per decay, %
Ref. 1	Ref. 2	Ref. 3	Our data	Our data	Ref. 1	Ref. 2	Ref. 3	Our data	Our data
41	40	40,3	—	—	372	390	—	—	—
140	—	140,1	140*	4	740	—	—	750	13
			140	85	780	—	—	920**	1
—	—	142,0	—	—	—	—	—		
181	180	181	180	4					

*γ-Rays not yielding coincidences with the β-rays.

**The 920 kev line may be obtained owing to simultaneous detection by the crystal of the two cascade γ-rays with energies of 180 and 740 kev.

The data obtained in the present study are consistent with the decay scheme proposed by Levi & Papineau[2]. Apparently there is a transition from the level at 922 kev to the ground state, inasmuch as it is difficult to explain the observed intensity for the 920 kev line solely on the basis of simultaneous detection by the crystal of the 180 and 740 kev cascade γ-rays.

"V.G.Khlopin" Radium Institute,
Academy of Sciences of the USSR

References

1. C.E.Mandeville & J.Varma, Phys.Rev., 94, 91, 780 (1954).
2. C.Levi & G.Papineau, Compt.rend., 239, 1782 (1954).
3. N.Vlasov, K.Artemov, A.Sorokina & Yu.V.Yurgenson, Trudy RIAN (Proceedings, Radium Institute of the USSR Ac.of Sci.) 7, No.1, 158 (1956).

* * * * * * *

MEASUREMENT OF THE NUMBER OF GAMMA-RAYS PER DECAY OF Ba^{140} AND Pr^{144}

- B.S.Duznetsov & A.N.Silant'ev

We measured the number of γ-rays per decay of Ba^{140} and Pr^{144} by the method of $4\pi\beta$-y coincidences (see preceding article). The sources were deposited on collodion films and inserted into the 4π β-counter, which was located at a distance of 2 cm from the crystal of the scintillation spectrometer.

The Ba was purified of La by the chromatographic procedure. The amount of La^{140} impurity in the source was evaluated from the intensity of the 1600 kev γ-line. The γ-spectrum corresponding to the La^{140} impurity was subtracted from the experimental spectrum. The La^{140} activity during the time of measurement did not exceed 5% of the total activity of the source. All measurements were carried out within a period of two hours, during which time the build-up in La^{140} activity amounted to no more than 3% of the total Ba activity. Hence the influence of radiation from La^{140} on the Ba^{140} spectrum could be neglected.

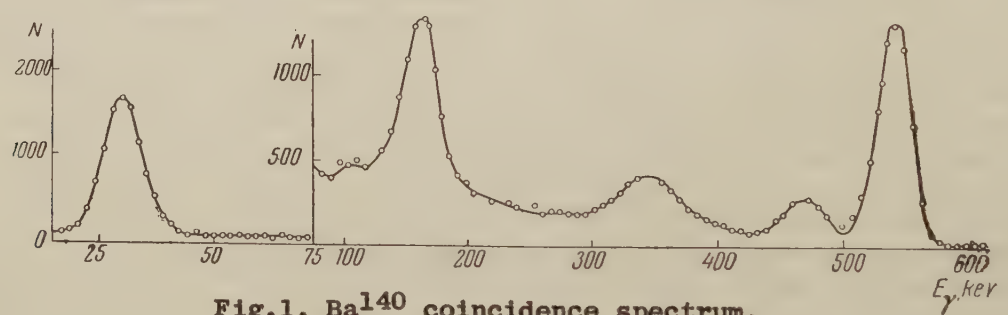

Fig.1. Ba^{140} coincidence spectrum.

The γ-ray coincidence spectrum obtained for Ba^{140} is shown in Fig.1. To bring out the 30 kev γ-line we carried out additional measurements of the γ-ray coincidence spectrum through a copper absorber 1 g/cm^2 thick. For bringing out the 160 kev γ-line we carried out additional measurements through a 1 g/cm^2 thick lead absorber. We compared the spectrum obtained with the spectrum recorded without an absorber and, taking into account the weakening of the hard lines, evaluated the intensity of 160 kev γ-rays.

The values obtained for the number of γ-rays per decay of Ba^{140} are listed in the accompanying table together with the γ-ray energies and relative intensities obtained by other investigators.

The relative intensities found in our work differ from the values reported by Boskma & De Waard[4]. The reason for this divergence is unclear.

Relative intensities and numbers of γ-rays per decay of Ba^{140}

E_γ, kev			I_γ	E_γ kev	I_γ	E_γ, kev	I_γ
Ref.1	Ref.2	Ref.3	Ref.3	Ref.4		Our data	
29,6	30	30	0,7	—	—	30	0,16
118,5	—	—	—	—	—	—	—
131,8	132	—	—	132	3	—	—
162,1	162	160	0,18	162	22	160	0,05
304	304	305	0,12	304	10	—	—
421,8	—	—	—	—	—	—	—
435,8	436	430	0,18	436	10	430	0,05
556,7	537	537	1,0	537	55	537	0,25

According to Boskma & De Waard, the β-spectrum of Ba^{140} consists of four components with end-point energies 480, 590, 830 and 1020 kev. The respective log ft values are 6.9, 7.1, 8.2 and 8.6.

Using the data of the present work and earlier investigations, one can evaluate the relative intensities of the β-components. If we accept the decay scheme given by Silant'ev[3] and take the conversion coefficient of the 162 kev transition to be 0.4 (according to Boskma & De Waard[4] and the tables of Sliv & Band[5,6]), we obtain the following values for the listed β-components: 25, 8, 4 and 63%, respectively.

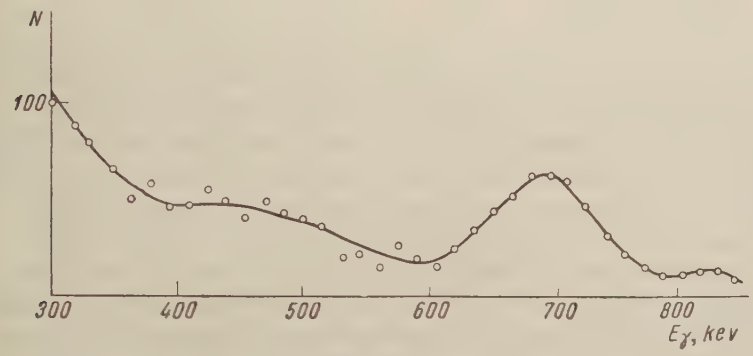

Fig.2. Pr^{144} coincidence spectrum.

Inasmuch as the 162 kev transition occurs in 7% of the decays (5% γ-rays and 2% conversion electrons), it may be inferred that 93% of the disintegrations go to the 30 kev level. Since 15% of all decays occur in the form of γ-rays from this level, it follows that the conversion coefficient for this transition is 5.2. This value indicates that the 30 kev transition is M1.

The number of γ-rays per decay of Pr^{144} was measured under the same conditions. These measurements were carried out both with a source in which Ce^{144} and Pr^{144} were in equilibrium and with a source in which the Pr^{144} was purified chromatographically of Ce^{144}. The results of both series of measurements are in good agreement. We measured the number of 695 kev γ-rays per decay and obtained a value of 0.012.

The measurements with the chemically purified Pr^{144} were started half an hour after the purification operation and terminated on the average after five periods of Pr^{144}. Each measurement took 2-4 min. Inasmuch as the measurements were carried out by the $4\pi\beta$-γ coincidence procedure it was not necessary to introduce any significant correction for the decay of the activity during the time of measurement.

The γ-ray coincidence spectrum obtained for Pr^{144} is reproduced in Fig.2.

"V.G.Khlopin" Radium Institute,
Academy of Sciences of the USSR

References

1. J.Cork, J.Le Blanc, A.Stoddard, D.Martin, C.Branyan & W.Childs, Phys. Rev., 83, 856 (1951).
2. W.Kelly & M.Wiedenbeck, Phys.Rev., 102, 1130 (1956).
3. A.Silant'ev, Zhur.eksp.i teor.fiz., 34, 569 (1958). (Trans.Soviet Physics - JETP.)
4. P.Boskma & H.De Waard, Nucl.Phys., 14, 145 (1959).
5 & 6. L.Sliv & I.Band, Tablitsy koeffitsientov vnutrennei konversii gamma-izlucheniya. Ch.I & II (Tables of internal conversion coefficients, Part I - K shell, Part II - L shell). M.-L., 1956 & 1958.

* * * * * * *

CONVERSION TRANSITIONS ACCOMPANYING α-DECAY OF Th^{229} AND THE LEVEL DIAGRAM FOR Ra^{225} *

- E.F.Tret'yakov, N.I.Pirogova & L.L.Gol'din

Introduction

Until recently there were virtually no investigations of α-decay of Th^{229}. It was known[1] only that the decay proceeds mainly to excited levels of Ra^{225}. The first detailed investigation of Th^{229} α-decay and the excited levels in Ra^{225} was that of Gol'din et al[2]. These authors also reported preliminary data on the conversion transitions accompanying the α-decay. Kocharov et al[3] investigated the decay of Th^{229} by means of an ionization chamber.

In the present work we give the results of investigation of the conversion electron spectrum of Ra^{225}, recorded by means of a more advanced procedure. We studied not only the α-e coincidences, but also γ-e (conversion electrons in coincidence with γ-rays) and e-γ (γ-spectrum in coincidence with electron lines) coincidences. The conversion electrons were detected by a high luminosity toroidal β-spectrometer[4], while the γ-rays were detected by a scintillation spectrometer consisting of an NaI(Tl) crystal, an amplifier and a single-channel analyzer.

Source Preparation and Measurements

The measurements were carried out on Th^{229} obtained by chemical separation of the thorium from long-lived U^{233}. We had available two samples of U^{233}, containing substantially different amounts of Th^{228} and Th^{229}.

The thorium together with the radium and actinium was separated from a solution of uranyl nitrate in lanthanum carrier by the fluoride method.[5] After separation, the thorium was purified of radium with introduction of a barium carrier by repeated precipitation of the thorium, lanthanum and actinium hydroxides by carbon-free ammonia. Separation of microgram amounts of thorium from the carrier (lanthanum) was carried out by triple precipitation of thorium iodate. This also eliminated the actinium impurity.[6] The thorium iodate was dissolved in hot dilute

---

*This report was presented at the Tenth All-Union Conference on Nuclear Spectroscopy held in Moscow January 1960.

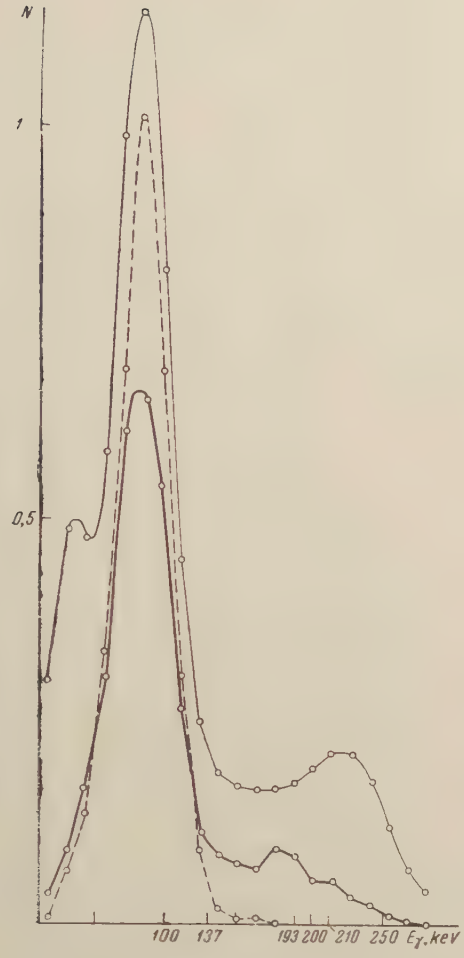

Fig.1

Fig.2

Fig.1. e-γ coincidences. Light solid line - total γ-spectrum of the equilibrium source measured for calibrating the γ-spectrometer. Dashed line - spectrum of γ-rays coinciding with the K conversion electrons of the 193.4 kev transition. Heavy solid line - spectrum of γ-rays coinciding with the L_{III} conversion electrons of the 25.3 kev transition. The curves have been normalized to the number of counts in the γ-e coincidence channel, measured without discrimination of the γ-rays in energy. Clearly evident are coincidences of the L_{III} electrons with γ-rays with an energy of the order of 200 kev.

Fig.2. e-γ coincidences. Light solid line - total γ-spectrum of the equilibrium source measured for calibrating the γ-spectrometer. Dashed line - spectrum of γ-rays yielding coincidences with the K conversion electrons of the 193.4 kev transition. Heavy solid line - spectrum of γ-rays yielding coincidences with the L_{II} and L_{III} conversion electrons of the 75.1 kev transition. Curves normalized in the same manner as the curves in Fig.1. There are evident coincidences of the L_{II} and L_{III} electrons with γ-rays of ~135 kev energy.

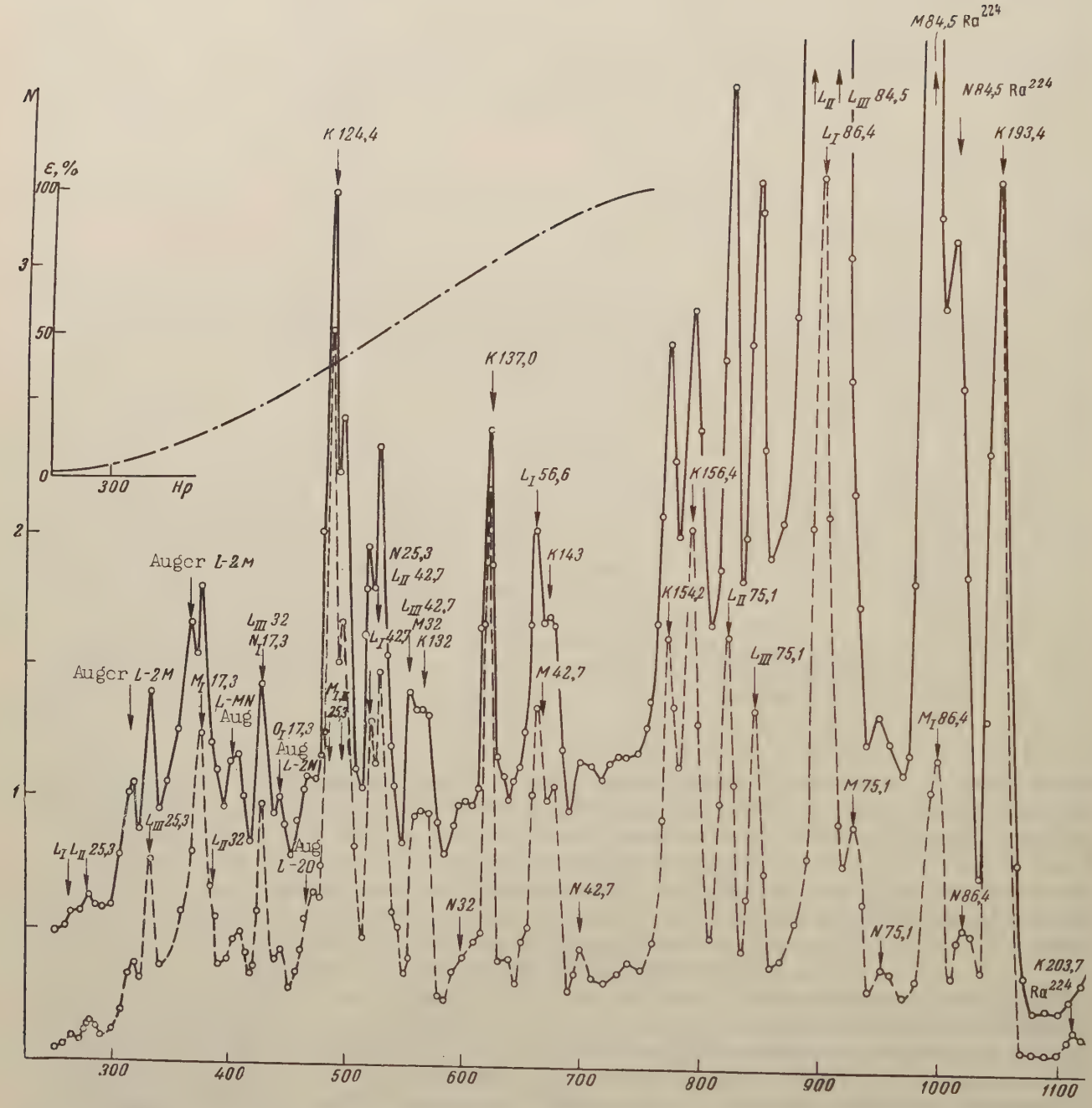

Fig.3. Th^{229} internal conversion electron spectrum. Solid line - internal conversion electron spectrum. Dashed line - spectrum of conversion electrons yielding coincidences with γ-rays without discrimination in the γ-channel. Dot dash line - efficiency of the β-counter.

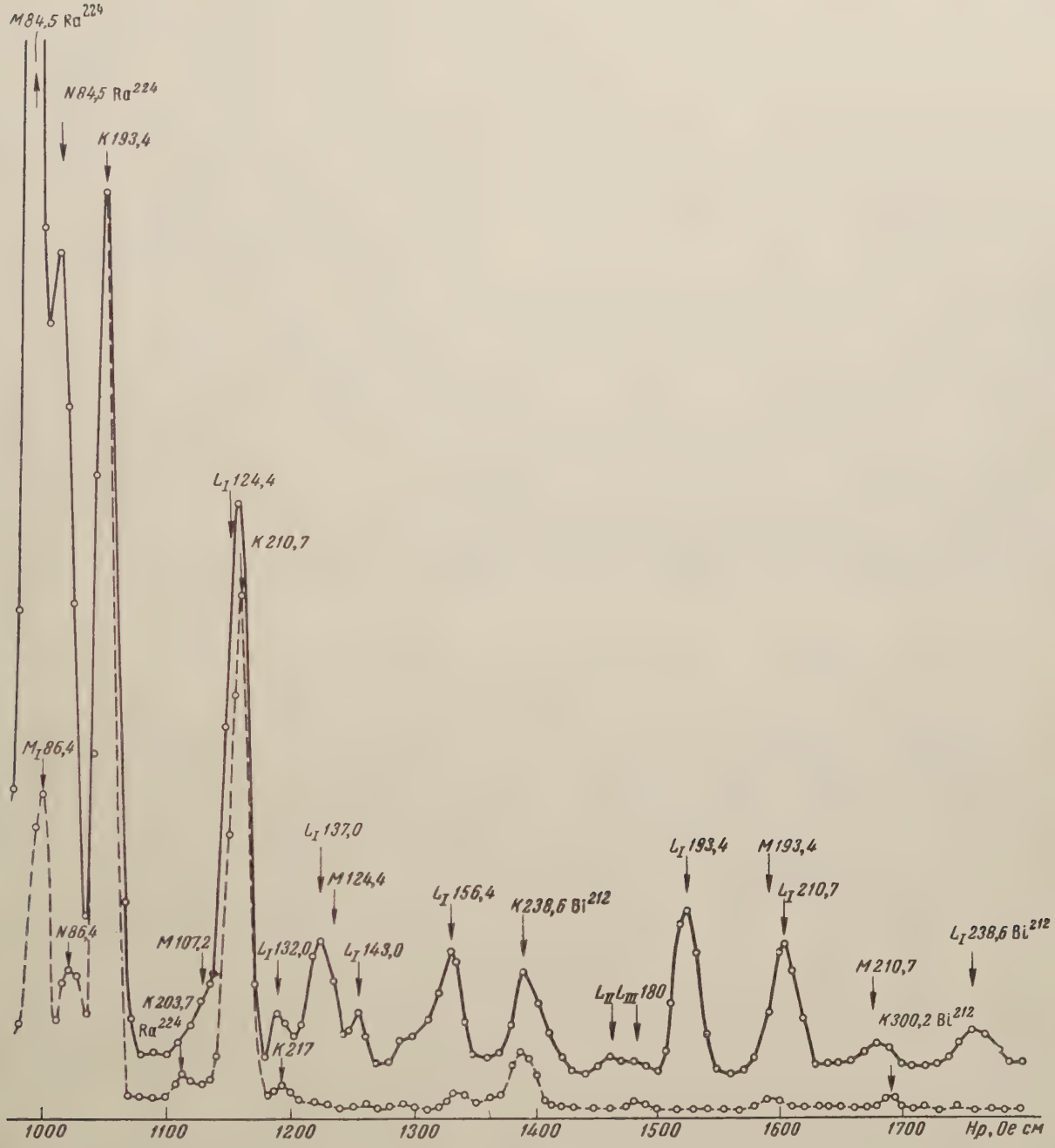
M84,5 Ra224
N84,5 Ra224
K193,4
LI124,4
K210,7
MI86,4
N86,4
M107,2
K203,7
Ra224
LI137,0
M124,4
LI132,0
LI143,0
K217
LI156,4
K238,6 Bi212
LI193,4
M193,4
LI210,7
LIILIII180
M210,7
K300,2 Bi212
LI238,6 Bi212
1000
1100
1200
1300
1400
1500
1600
1700
Hp, Oe cm

Fig.3. (cont.)

hydrochloric acid containing a small amount of sulfuric acid. After dilution with water, the thorium was precipitated from the solution with ammonia and thoroughly washed with water to eliminate the iodate. The thorium hydroxide was converted to the chloride, which was then used for preparing the source.

The chemical purification process was monitored at all stages by measuring the activity of the decay products of Th^{228}. To this end we used a γ-counter with a lead shield which discriminated γ-rays with energies greater than 2 Mev and also a simple "radon" counter (scintillation α-counter in which the α-particles moving along a straight line could not reach the scintillator).

The sources were prepared by vacuum evaporation from a tungsten ribbon filament, the material being deposited on a thin mica support. The sources were attached to the case of the NaI(Tl) crystal which served as the detector of the scintillation spectrometer. This method of mounting the source insured high efficiency for detecting the γ-rays (~30%). The relative half-width of the Au^{198} 412 kev line was 15%.

For the γ-e coincidence measurements the scintillation γ-counter was connected in coincidence with the electron detector (a scintillation counter with a stilbene crystal). The resolving time of the coincidence circuit was about 10^{-7} sec. The trigger level of the circuit was set so that coincidences of the electrons with the L x-rays would not be recorded. Thus in varying the current through the β-spectrometer coil there was measured the number of coincidences of the conversion electrons with the K x-radiation and γ-radiation from the source. Coincidences between the electrons and selected sections of the γ-spectrum could be investigated by introducing additional appropriate discrimination into the γ-channel.

In investigating the spectrum of γ-rays yielding coincidences with selected conversion electrons, i.e., in measuring γ-e coincidences, we almost always encountered strong interference from the strong characteristic x-radiation. It was usually impossible to subtract this reliably from the γ-spectrum. Information on the stronger γ-transitions was therefore obtained simply by comparison of the shape of the γ-spectrum with the shape of the K x-ray line measured in coincidence with some conversion electrons, the emission of which is not accompanied by γ-radiation. It proved highly important that the shape of the K x-ray line and the γ-spectrum be investigated simultaneously. Hence the measurements were carried out in the following manner. At some position of the γ-spectrometer analyzer gate, the β-spectrometer was set first on the investigated line and then on a reference electron line, which could be any K line giving weak coincidences with the γ-rays (for example, the K conversion line of the 193.4 or the 210.7 kev transition). Then the analyzer gate was shifted one step and the measurements were repeated, etc. The γ-ray coincidence spectrum was obtained by subtracting the spectra so recorded (after normalizing). This method of measurement enabled us to separate the coincidences with γ-rays from the coincidences with the x-radiation.

The results of two such series of measurements are shown in Figs.1 & 2. In these figures N is the number of coincidences divided by the total count of γ-e coincidences and hence does not depend on either the recording time or the intensity of the conversion lines.

Results

The conversion electron spectrum obtained in one of the series of measurements is reproduced in Fig.3. The more complicated sections of the spectrum were also investigated with two different levels of discrimination in the γ-channel (these curves are not shown in the figure in order not to complicate it unduly).

The spectrum shown in Fig.3 was not corrected for the energy dependence of the β-counter efficiency, which fell off to 1% at the end of the spectrum (see dot-dash curve in Fig.3). The spectrum shown in the figure was recorded with a new source containing a relatively large admixture of Th^{228}. The conversion electron spectrum is shown up to 240 kev. The higher energy region was also investigated but in it we did not observe any lines belonging to Ra^{225}.

Table 1 lists the detected and identified conversion lines. The energy of the conversion electrons was determined with reference to the K line of the 238.6 kev transition in Bi^{212}, which has been thoroughly studied by Krisyuk et al[7] and others (Bi^{212} is the decay product of Th^{228}; this isotope was always present in our sources in the form of an impurity). The calibration in energy was checked with reference to a number of conversion lines of the daughters of Th^{228} and Th^{229} and proved to be reasonably accurate.

The intensity of the conversion transitions relative to α-decay has been determined with an accuracy of ±20% with reference to the conversion lines of the 84.5 kev transition accompanying α-decay of Th^{228}. The intensity of this transition (28%) is known from the data of Asaro et al[8]. The ratio between the α-activity of Th^{228} and Th^{229}, which is necessary for evaluating the intensities of the Ra^{225} conversion lines, was determined for one of the samples by G.I.Novikov on a magnetic α-spectrometer.

Analysis of the data of Table 1 leads to the list of converted transitions given in Table 2. In cases when it was feasible to determine reliably the multipole order of the radiation, we give the total intensity of the transition. The multipole orders were determined primarily on the basis of the $L_I:L_{II}:L_{III}$ and K:L ratios and from the ratio of the x- and γ-radiations measured in investigating the e-γ coincidences.

Level Diagram

The experimental results obtained enabled us to construct the Ra^{225} level diagram shown in Fig.2. The results of investigation of α-decay of Th^{229}, taken from Ref.2, are given in the left part of the diagram, where we indicate the energies of the levels (α_0, α_{20}, etc.) calculated from the α-spectrum and the population of the levels in percent. At the right we give the level parameters obtained on the basis of analysis of the conversion electron spectrum.

In investigating the γ-radiation and conversion electrons there are evinced transitions between levels that are poorly populated in α-decay. We shall begin our discussion of the Ra^{225} diagram with these levels.

1. As will be evident from Fig.4, it proved necessary to introduce a new level (not evinced in investigating α-decay of Th^{229}) located 25.3 kev below the α_0 level. This was necessary because there was observed a 25.3 kev transition of very appreciable intensity (70%) in cascade with the 17.3 kev transition (17.3 + + 25.3 = 42.6 kev; we note that there is a 42.7 ± 0.2 kev transition). In addition, investigation of the e-γ coincidences showed that the conversion electrons of the 25.3 (Fig.1) and 42.7 kev transitions yield coincidences with γ-rays of up to 200 kev energy.

The necessity of introducing a level below α_0 also follows from consideration of the results of Kocharov et al[3] obtained in investigating the α-spectrum of Th^{229} by means of an ionization spectrometer. These authors used the method of e-γ coincidences for resolving the main group of α-particles (corresponding to α-decay to the ground level of the daughter nucleus). In this case the α-line corresponding to the transition to the ground level should disappear. Examination of Fig.4 of Ref.3 shows, however, that the α_0 line does not completely

Table 1

List of conversion electron lines

No.	E_{e^-}, kev	Uncertainty, kev	Intensity relative to α-decay, %		Identification	Energies of γ-rays yielding coincidences with conv. electrons, kev
			Total No.	Coinc.		
1	2	3	4	5	6	7
1	6,1	0,1	10	7	L_I 25,3	
2	6,87	0,1	13	15	L_{II} 25,35	
3	8,74	0,3	31	7	Auger $L_{II}\,L_{III} - 2M_{I,\,II}$ & L_{III} 23,8	
4	9,83	0,05	38	22	L_{III} 25,27	90,210
5	11,97	0,2	20	7	Auger $L - 2M$	
6	12,40	0,05	25	18	M_I 17,21	190
7	12,83	0,2	—	3	L_I 32,0 or L_{II} 31,3	190 210
8	14,35	0,2	6	2,5	Auger $L - MN$	
9	15,71	0,2	—	1,5	(L_{III} 31,15)	
10	16,06	0,07	10	6	N_1 17,26	190
11	17,02	0,1	3	1,5	O_I 17,22 & Aug-$L - 2N$	
12	18,8	0,2	1,5	1,5	M_I 23,6	
13	19,2	0,2	1,5	1,5	M_{II} 23,7	
14	20,52	0,05	12	11	K 124,45	
15	20,8	0,2	—	8	$M_I + M_{II}$ 25,4	
16	21,49	0,1	—	9	M_{III} 25,27	
17	22,08	0,2	0,6	1,5		
18	23,4	0,1	6	5	L_I 42,6	190
19	24,2	0,1	10	7	L_{II} 42,7 & N 25,4	
20	25,3	0,2	0,8	—		
21	27,21	0,1	3	3	L_{III} 42,66 & M 32	190
22	28,0	0,2	3	3	K 131,9	
23	30,5	0,3	—	0,5	N 31,5	
24	30,9	0,2	0,7	0,4		
25	33,03	0,05	8,0	8,0	K 136,96	
26	34,25	0,3	0,6	0,4		
27	36,06	0,2	—	0,5		
28	34,43	0,07	3,0	2,1	L_I 56,66	150
29	38,0	0,2	—	2,0	M 42,5	
30	39,07	0,1	2,5	2,5	K 143,0	
31	41,40	0,2	0,6	0,6	N 42,4	
32	42,7	0,4	0,3	—		
33	45,8	0,4	—	0,3		
34	49,5	0,3	0,6	?	L_I 68,7	
35	50,28	0,1	3,5	3,0	K 154,21	
36	50,50	0,3	0,7	?	L_{II} 69,0	
37	51,9	0,2	—	1,0	M 56,7	
38	52,54	0,1	5	5	K 156,47	
39	52,54	0,1	0,7	?	L_{III} 69,03	
40	56,58	0,05	7,5	3,6	L_{II} 75,06	135
41	59,7	0,07	6,0	3,0	L_{III} 75,14	135
42	66,0	0,1	Ref.	—	L_{II} 84,48 Ra^{224}	
43	67,12	0,1	11,5	9,0	L_I 86,35	124
44	68,8	0,1	Ref.	—	L_{III} 84,24 Ra^{224}	
45	70,9	0,3	4,0	2,0	$M_{II} + M_{III}$ 75,0	
46	74,1	0,4	0,7	0,5	N 75,1	
47	80,3	0,2	—	—	$M_{II} + M_{III}$ 84,4 Ra^{224}	
48	81,54	0,1	—	2,5	M_I 86,35	
49	83,43	0,2	—	—	N 84,4 Ra^{224}	
50	85,26	0,2	—	0,7	N 86,26	
51	89,46	0,1	9	8.5	K 193,39	

*The intensity of the peak increased with time.

(Table 1 continued)

No.	E_{e^-}, kev	Uncertainty, kev	Intensity relative to α-decay, %		Identification	Energies of γ-rays yielding coincidences with con. electrons, kev
			Total No.	Coinc		
1	2	3	4	5	6	
52	95,3	0,4	0,08	—		
53	99,8	0,5	—	0,08	K 203,7 Ra^{221}	
54	102,4	0,3	0,3	—	M 107,2	
55	105,2	0,2	1,5	—	L_I 124,4	
56	106,8	0,1	5	5	K 210,72	
57	112,8	0,2	—	0,06	K 216,7	
58	113,3	0,2	0,5	—	L 131,8	
59	118,0	0,2	1,4	—	L_I 136,5	
60	120,0	0,5	—	—	M 124,8	
61	123,5	0,5	0,5	—	L_I 142,7	
62	132,0	0,5	0,2	—	M 136,8	
63	136,9	0,2	1,0	—	L_I 156,1	
64	138,2	0,2	—	0,05	K 242,1	
65	148,1	Ref.	—	*	K 238,6 Bi^{212}	
66	149,4	0,5	0,2	—	M 154,2	
67	151,5	0,5	0,2	—	M 156,3	
68	161,5	0,5	0,3	—	L_{II} 180,0	
69	164,4	0,5	0,2	—	L_{III} 179,8	
70	165,3	0,5	—	0,02	K (?) 269,2	
71	174,4	0,2	1,8	—	L_I 193,6	
72	188,8	0,5	—	—	M 193,6	
73	189,8	0,7	—	0,02		
74	191,5	0,5	1,2	—	L_I 210,7	
75	206,9	1,0	0,3	—	M 211,7	
76	209,6	0,3	—	*	K 300,1 Bi^{212}	
77	222,8	0,5	*	—	L_I 239,2 Bi^{212}	

*The intensity of the peak increased with time.

Table 2

Transitions between levels in Ra^{225}

No.	E, kev	Uncertainty, kev	Intensity rel. to α-decay, %	Multipole order	No.	E, kev	Uncertainty, kev	Intensity rel. to α-decay, %	Multipole order
1	17,3	0,1	30	$M1$	12	131,9	0,2	3	
2	23,7	0,3	5		13	137,0	0,1	10	$M1$
3	25,3	0,1	70	$E1$	14	143,0	0,2	3	
4	32	0,7	5÷3	$M1 + E2$	15	154,2	0,2	4	$M1$ (?)
5	42,7	0,2	26	$E1$	16	156,5	0,2	6	$M1$
6	56,7	0,2	3	$M1$	17	179,9	0,5	0,5	
7	68,9	0,3	3	$M1 + E2$	18	193,4	0,1	16	$M1$
8	75,1	0,1	18	$E2$	19	210,7	0,1	10	$M1$
9	86,3	0,1	15	$M1$	20	217,0	0,4	0,7÷0,1	
10	107,2	0,3	1		21	242,2	0,3	0,3÷0,1	
11	124,4	0,2	12	$M1$	22	269	1,0	0,10÷0,05	

disappear, as occurs, for example, in the case of Th^{228} (Fig.3 in Ref.3).

2. It also proved necessary to introduce a level close to the α_{214} level. According to our measurements, the energy of the α_{214} level relative to the α_0 level is 210.7 kev. This value, which is obtained for the cross-over transition, is substantiated by a number of cascades: 17.3 + 193.4 = 210.7; 86.3 + 124.4 =

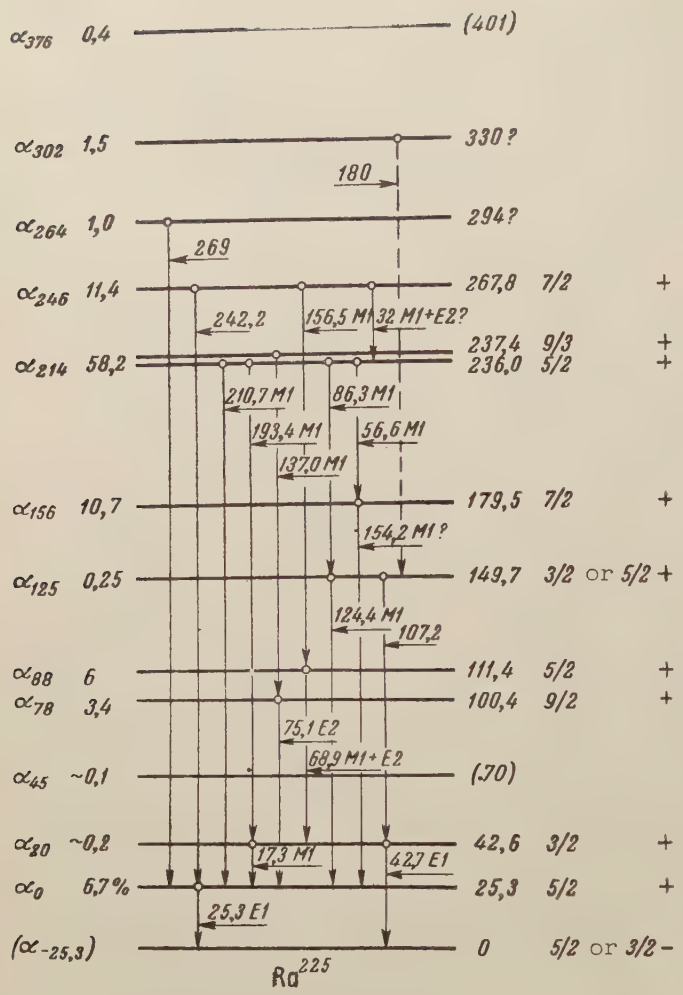

Fig.4. Diagram of the low-lying levels of Ra^{225}. At the left - level energies and α-decay intensities to the indicated levels taken from Ref.2 (except for the $\alpha_{-25.3}$ level). At the right - energies, spins and parities deduced by analysis of the conversion electron spectrum.

= 210.7; 56.6 + 154.2 = 210.8. It was found, however, that the lines corresponding to the intense 75.1 kev transition that is not converted on the K shell, coincide in more than half the cases with the K x-radiation. We investigated the spectrum of γ-rays yielding coincidences with the conversion electrons of the 75.1 kev transition (Fig.2). The energy of the γ-rays coinciding with the L_{II} and L_{III} electrons of the 75.1 kev transition is approximately 135 kev. The only converted transition that can provide this γ-e coincidence intensity has an energy of 137.0 kev. The 137.0 kev (M1) transition is converted mainly on the K shell. Obviously, however, 137.0 + 75.1 = 212.1 and not 210.7. One can advance three different hypotheses: a) the 75.1 kev level is populated from the 154.2 kev level by a weakly converted E1 type transition (the energy of the γ-rays of this transition coincide with the energy of the K x-rays) and also by a weakly converted transition from the α_{214} level, yielding coincidences with the γ-spectrum (E_γ = 135 kev); b) among the excited levels of Ra^{225} there is an $\alpha_{-1.2}$ level; c) there is an $\alpha_{212.1}$ level populated in α-decay of Th^{229}. We chose the last possibility, inasmuch as the first two hypotheses lead to very great difficulties in constructing the level diagram. It should be noted that introduction of such a level is not in conflict with the available data on the α-spectrum of Th^{229}, inasmuch as the resolution of our α-spectrometer was not sufficient to detect 1.2 kev broadening of the α_{214} line.

3. The energy of the 86.3 kev transition almost coincides with the energy of the α_{88} level, observed in investigating the α-spectrum. We deemed it preferable, however, to locate this transition in a different place, namely, between the 210.7 level and the 124.4 level. This decision was prompted by the fact that the 86.3 kev transition almost fully (~80%) coincides with the K x-radiation. This location is possible only with the above described arrangement of the transitions inasmuch as the α_{88} level is strongly populated in α-decay (6%), while α-decay to the α_{125} level is very weak (0.25%). We detected only one transition from the α_{88} level: 68.9 kev (M1 + E2). This transition was found by subtracting the γ-e

coincidence count from the total β-spectrum. The intensity of this transition may actually be greater than indicated, owing to the part of the 68.9 kev radiation that coincides with the x-radiation.

4. It was hypothesized in the work of Ref.2 that the α_{214} and α_{246} levels are the first two levels of a rotational band. In this case there must occur between these levels a relatively intense transition of the M1 + E2 type. Such a transition was observed. Its energy is 32 ± 0.7 kev, and its intensity is of the order of 5%. The e-γ coincidence measurements showed that this transition yields coincidences with γ-rays of up to 210 kev energy. This indicates that this transition occurs between high-lying levels. In the conversion electron spectrum reproduced in Fig.3 the L lines of the 32 kev transition are located on the sides of the M and N lines of the 17.3 kev transition, which yields coincidences with the 193.4 kev γ-rays. This prevented us from determining the multipole order of the 32 kev transition. In all probability it is almost pure M1.

5. The spins and parities of the levels (α_0 and higher) are indicated in Fig.4 on the basis of the data on the multipole orders of the transitions and the relative intensities of the lines. As a point of departure we assumed that the α_{214} level has spin and parity $5/2^+$. This value follows from the fact that the transition from U^{233} to the α_{214} level of Ra^{225} occurs by way of two allowed α-transitions ($\Delta I = 0$, no). The spin of the ground state of U^{233} is 5/2 and the parity is even (see Ref.9).

6. We now turn to the spin and parity of the $\alpha_{-25.3}$ level. The L conversion lines of the 25.3 kev transition from the α_0 level to the $\alpha_{-25.3}$ level lie at the sensitivity threshold of the counter. Hence in order to determine the multipole order we used the M lines. It was assumed that the M subshell conversion coefficients are approximately equal to the L subshell coefficients. The experimental $M_I:M_{II}:M_{III}$ line intensity ratios are 4:6:9, which almost agrees with the theoretical $L_I:L_{II}:L_{III}$ ratios for an E1 transition (4:6.6:9) and is in conflict with the theoretical ratios for all other multipole orders. Hence we accepted the E1 assignment for the 25.3 kev transition. (The M lines of the 25.3 kev transition are not visible in Fig.3, but they were clearly evinced in other series of measurements, when appropriate discrimination was introduced into the γ-channel to bring out the coincidences with high energy γ-rays.)

The intensities of the L lines of the 42.7 kev transition are greatly distorted by superposition of other lines. If, however, one subtracts from the L_{II}-42.7 line the N-25.3 line superimposed upon it (the intensity of the N-25.3 line is known) one can carry out a comparison of the $L_I:L_{II}:L_{III}$ ratios with the theoretical values. The experimental $L_I:L_{II}:L_{III}$ ratios are 5:4:4; the theoretical ratios for an E1 transition are 5:4.3:4.8. In this case, however, we cannot entirely exclude the possibility of other multipolarities inasmuch as a close value of the ratios may obtain for a mixture of M1 + E2. Nevertheless, it seems probable that this transition is predominantly E1.

It follows from the above data and the values inferred for the spins of the α_0 and α_{20} levels that the $\alpha_{-25.3}$ level has spin 5/2 or 3/2 and odd parity.

As was noted above, no transition to the $\alpha_{-25.3}$ level was observed in the α-spectrum of Th^{229}. Presumably α-decay to this level is strongly forbidden owing to the fact that its parity is opposite to the parity of the other levels of Ra^{225}.

We desire to express our sincere gratitude to G.I.Grishuk, V.F.Konyaev, Yu. N.Chernov and S.V.Kalashnikov for assistance in carrying out the experiments.

Institute of Theoretical and Experimental Physics,
Academy of Sciences of the USSR

References

1. F.Hagemann, L.I.Katzin, M.H.Studier, G.T.Seaborg & A.Ghiorso, Phys.Rev., 79, 435 (1950).

2. L.L.Gol'din, G.I.Novikova, N.I.Pirogova & E.F.Tret'yakov, Zhur.eksp.i teor.fiz., 37, 1155 (1959). (Trans.Soviet Physics - JETP.)

3. G.E.Kocharov, A.P.Komar, G.A.Korolev, I.N.Markov & Yu.A.Surkov, Izv.AN SSSR, Ser.fiz., 23, 877 (1959). (Trans.Bulletin, 23, 847.)

4. E.F.Tret'yakov, L.L.Gol'din & G.I.Grishuk, PTE (Instruments & Experimental Techniques), No.6, 22 (1957).

5. V.F.Gillebrand, G.E.Lendel', G.A.Brait & D.I.Gofman, Prakticheskoe rukovodstvo po neorganicheskomu analizu (Handbook on Inorganic Analysis), 568 (1957).

6. N.E.Ballou, National Nuclear Energy Series, Radiochemical Studies. Fission Products, 3, 292, 1673 (1951).

7. E.Krisyuk, A.Vitman, V.Vorob'ev, G.Latyshev & A.Sergeev, Izv.AN SSSR, Ser.fiz., 20, 877 (1956). (Trans.Bulletin, 20, 797.)

8. F.Asaro, F.Stephens,Jr. & I.Perlman, Phys.Rev., 92, 1495 (1953).

9. B.S.Dzhelepov & L.K.Peker, Skhemy raspada radioaktivnykh yader (Decay schemes of radioactive nuclei), M.-L., 1958.

CONCERNING ELECTROMAGNETIC TRANSITIONS OF MULTIPOLE ORDER $L = |J_i - J_f| + 1$

- M.E.Voikhanskii

Experimental data on nuclear level lifetimes for gamma emission are usually compared with the independent-particle model calculations for single-particle transition probabilities.[1,2] According to such calculations, the half-life for a proton EL transition is given by

$$T_{1/2}^{(\gamma)}(EL) = \frac{0.158L\,[(2L+1)!!]^2}{L+1}\left(\frac{L+3}{3}\right)^2\left(\frac{197}{E_\gamma}\right)^{2L+1} R^{-2L}S^{-1}(J_iLJ_f)\cdot 10^{-21}\ \text{sec} \qquad (1)$$

and for an ML transition by

$$T_{1/2}^{(\gamma)}(ML) = \frac{3.65L\,[(2L+1)!!]^2}{L+1}\left(\frac{L+2}{3}\right)^2 \times M_\mu^{-1}\left(\frac{197}{E_\gamma}\right)^{2L+1} R^{-2L+2}\,S^{-1}(J_iLJ_f)\cdot 10^{-21}\ \text{sec} \qquad (2)$$

where $R = r_0 A^{1/3}$ is the nuclear radius in units of 10^{-13} cm.

In Weisskopf's[1] expression for $T_{1/2}^{(\gamma)}(ML)$ the dimensionless factor M_μ is a constant ($M_\mu = 10$). According to Moszkowski[2], however, M_μ is given in terms of the proton magnetic moment μ_p and the multipole order L:

$$M_\mu = \left(L\mu_p - \frac{L}{L+1}\right)^2. \qquad (3)$$

In the framework of this theory, the dependence of $T_{1/2}^{(\gamma)}(EL)$ and $T_{1/2}^{(\gamma)}(ML)$ on the initial and final spins J_i and J_f is given by the statistical factor $S(J_iLJ_f)$. For single-particle states,

$$S(J_iLJ_f) = \frac{Z^2\left(l_i J_i l_f J_f;\ \frac{1}{2}L\right)}{2J_i+1} \qquad (4)$$

for an EL transition. When the transition is a magnetic multipole,

$$S(J_iLJ_f) = \frac{Z^2\left(l_i+1 J_i l_f J_f;\ \frac{1}{2}L\right)}{2J_i+1}, \qquad (5)$$

if $J_i = l_i + 1/2$ and

$$S(J_iLJ_f) = \frac{Z^2\left(l_i-1 J_i l_f J_f;\ \frac{1}{2}L\right)}{2J_i+1}, \qquad (6)$$

if $J_i = l_i - 1/2$.

The function $Z\left(abcd;\ \frac{1}{2}L\right)$ entering into expressions (4)-(6) is a combination of $W\left(abcd;\ \frac{1}{2}L\right)$ Racah and Clebsch-Gordan coefficients.[3]

With the given values of J_i, J_f and L, the statistical factor does not depend on whether the transition is electric or magnetic, or on the kinds of states that are involved in the transition ($J_i = l_i \pm 1/2$, $J_f = l_f \pm 1/2$ or $J_i = l_i \pm 1/2$, $J_f = l_f \mp 1/2$). Therefore, if J_i, J_f and the multipole order L are given, equations (4)-(6) all lead to the same result.

The numerical values of the $S(J_iLJ_f)$ for γ-transitions of multipole order $L = |J_i - J_f|$ are given in Table 1.* One does not usually include $S(J_iLJ_f)$ in rough

---

*Siegbahn's volume[2] gives an incorrect value for $S(J_iLJ_f)$ when $J_i = 5/2$, $J_f = 11/2$. The correct value is 100/33, rather than the 25/33 given there. This error is repeated in other works.

Table 1

Statistical factor $S(J_iLJ_f)$ for EL and ML transitions with $L=|J_i-J_f|$

J_f	J_i = 1/2	3/2	5/2	7/2	9/2	11/2	13/2
1/2	—	1	1	1	1	1	1
3/2	2	—	6/5	9/7	4/3	15/11	18/13
5/2	3	9/5	—	9/7	10/7	50/33	225/143
7/2	4	18/7	12/7	—	4/3	50/33	700/429
9/2	5	10/3	50/21	5/3	—	15/11	225/143
11/2	6	45/11	100/33	25/11	18/11	—	18/13
13/2	7	63/13	525/143	1225/429	315/143	21/13	—

Table 2

Statistical factor $S(J_iLJ_f)$ for EL and ML transitions with $L=|J_i-J_f|+1$

J_f	J_i = 1/2	3/2	5/2	7/2	9/2	11/2	13/2
1/2	1	1	1	1	1	1	1
3/2	2	1/5	2/7	1/3	4/11	5/13	2/5
5/2	3	3/7	3/35	1/7	2/11	30/143	3/13
7/2	4	2/3	4/21	1/21	20/231	50/429	20/143
9/2	5	10/11	10/33	25/231	1/33	25/429	35/429
11/2	6	15/18	60/143	75/429	10/143	3/143	6/143
13/2	7	7/5	7/13	35/143	49/429	7/143	1/65

evaluations of the γ-transition probability, since this factor is generally close to unity. This is true, however, only if $J_i > J_f$ and then only for transitions of the lowest possible multipole order $L=|J_i-J_f|$.

In many cases, in addition to radiation of multipole order $L_1=|J_i-J_f|$ transitions of the next higher order $L_2=|J_i-J_f|+1$ may occur (for instance, M1 + + E2). One usually assumes the factor $S(J_iLJ_f)$ in the expressions for $T_{1/2}^{(\gamma)}$ to be the same for both types of transitions. Calculations show, however, that this is true only if the spin of the initial or final state is 1/2. Otherwise, the values of $S(J_iLJ_f)$ for $L=|J_i-J_f|+1$ transitions are on the average an order of magnitude smaller than the corresponding ones for $L=|J_i-J_f|$ transitions. Table 2 gives the statistical factors for γ-transitions of the higher orders.

Of greatest importance are mixed transitions of the M1 + E2 or E1 + M2 type. Calculation of $S(J_iLJ_f)$ for such transitions will uncover various effects depending on the initial and final spins.

1) If $J_i = 1/2$ or $J_f = 1/2$, but $J_i \neq J_f$ the dipole and quadrupole transitions have the same values of $S(J_iLJ_f)$.

2) If $J_i, J_f \neq 1/2$ and $J_i \neq J_f$ the statistical factor tends somewhat to increase (by a factor of 1.2—1.7) the probability for dipole radiation, and to decrease (by a factor of 20 or greater) the probability for quadrupole radiation.

Table 3

Statistical factor $S(JLJ)$ for transitions with $J_i=J_f\equiv J$

L	J = 1/2	3/2	5/2	7/2	9/2	11/2	13/2
1	1	1/5	3/35	1/21	1/33	3/143	1/65
2	—	1	8/7	25/21	40/33	175/143	16/13

3) For transitions between states with equal spins ($J_i = J_f$), the statistical factor leads to the opposite effect. Namely, the probability for dipole radiation is greatly decreased (by a factor of 50 or more), while the probability for quadrupole radiation remains essential

ly unaltered. This is related to the fact that for the dipole radiation $L = |J_i - J_f| + 1$ for which $S(J_i L J_f)$ is small, while the quadrupole radiation has $L = |J_i - J_f| + 2$ which has a statistical factor close to unity, just as in the ordinary $L = |J_i - J_f|$ case. Numerical values of $S(J_i L J_f)$ for transitions between states with equal initial and final spins are given in Table 3.

Let us consider in somewhat more detail the factor M_μ in Eq.(2). Magnetic radiation of multipole order $L = |J_i - J_f|$ can occur only for transitions of the form $J_i = l_i + 1/2 \to J_f = l_f - 1/2$ or $J_i = l_i - 1/2 \to J_f = l_f + 1/2$. In both types of transitions M_μ is the same and is given by (3). In the case of magnetic multipoles of order $L = |J_i - J_f| + 1$ one must differentiate[4] between $J_i = l_i + 1/2 \to J_f = l_f + 1/2$ transitions and $J_i = l_i - 1/2 \to J_f = l_f - 1/2$ transitions, which have different values of M_μ. For such transitions M_μ depends not only on the magnetic moment of the nucleon and the multipole order of the transition, but also on the initial and final spins. Table 4 gives expressions for M_μ for four possible types of magnetic transitions. In this table $J_>$ denotes the greater, and $J_<$ the lesser of J_i and J_f. When it is a neutron which is undergoing magnetic transition, rather than a proton, one must replace $\mu_p = 2.79$ by $\mu_p = -1.91$ and drop the second term in the brackets.

Table 4

Expressions for M_μ for four possible types of magnetic transitions

J_i	J_f	M_μ
$l_i+1/2$	$l_f-1/2$	$\left[\mu_p L - \frac{L}{L+1}\right]^2$
$l_i-1/2$	$l_f+1/2$	
$l_i+1/2$	$l_f+1/2$	$(J_> + 1)^2\left[\mu_p + \frac{2J_< - 1}{L+1}\right]^2$
$l_i-1/2$	$l_f-1/2$	$J_<^2\left[\mu_p - \frac{2J_> + 3}{L+1}\right]^2$

It would thus seem that for magnetic multipoles of order $L = |J_i - J_f| + 1$ the initial and final spin dependence of the transition is included (according to Moszkowski) not only in $S(J_i L J_f)$, but also in M_μ. The expressions given by Weisskopf give this dependence only in $S(J_i L J_f)$.

Electric and magnetic transitions of multipole orders $L_1 = |J_i - J_f|$ and $L_2 = |J_i - J_f| + 1$ have very different values of the statistical factor $S(J_i L J_f)$ (unless $J_i = 1/2$ or $J_f = 1/2$).

I express my gratitude to L.A.Sliv for his interest in the work.

Leningrad Chemical-Pharmaceutical Institute

References

1. J.M.Blatt & V.F.Weisskopf, Theoretical Nuclear Physics, N.Y., 1952.
2. Beta- and Gamma-Ray Spectroscopy, edited by Kai Seigbahn, Chapt.13, Amsterdam, 1955.
3. L.Beidenharn, J.M.Blatt & M.Rose, Revs.Mod.Phys., 24, 249 (1952).
4. M.E.Rose, Multipole Fields, N.Y., 1955.

DISTINCTIVE FEATURES OF DEFORMED ODD-ODD NUCLEI WITH K = 0*

- D.A.Varshalovich & L.K.Peker

In even-even and in some odd-odd deformed nuclei there are observed states with $K = 0^{\pm}$ as well as rotational levels associated with them.[1-6] In cases when all the nucleons in the nucleus are bound in pairs (this obtains in the ground and collective** excited states of even-even nuclei) the properties of the rotational bands with K = 0 have been investigated thoroughly both theoretically and experimentally. It has been shown, for example, that such a rotational band with $K = 0^+$ comprises levels only with even spins ($I = 0^+, 2^+, 4^+ \ldots$), while the band with $K = 0^-$ consists only of levels with odd spins ($I = 1^-, 3^-, 5^- \ldots$).[1]

Between the levels of one rotational band there occur only E2 type γ-transitions and the energy of these transitions in the first approximation is given by the simple formula

$$E_{\text{rot}} = E_0 + AI(I+1), \tag{1}$$

where $A = \hbar^2/2J$ and E_0 is the internal energy associated with the motion of the individual nucleons. This energy is the same for all the levels of the rotational band.

On the other hand, the properties of rotational states with K = 0 in which there are unpaired nucleons have scarcely been studied, although they should exhibit a number of interesting features. Such states may be encountered in odd-odd nuclei containing an odd proton or neutron and in strongly excited even-even nuclei when the excitation energy is greater than the nucleon pairing energy, i.e., greater than 1 Mev.

Now that there have appeared the first experimental data on such states in some odd-odd nuclei, detailed consideration of their properties is of appreciable practical interest. It must be emphasized that although in the present study we shall be primarily concerned with the properties of the rotational levels of odd-odd nuclei, all the inferences drawn apply fully to excited states of even-even nuclei containing unpaired nucleons.

1. Wave Function

It was shown by Bohr[7] that the wave function of a nucleus characterized by symmetry as regards reflection in the plane perpendicular to the nuclear axis (axial symmetry) can be written in the form

$$\psi(IMK) = \sqrt{\frac{2I+1}{16\pi^2}}\{D^I_{MK}(\vartheta)\,\chi^{\tau}_K + (-1)^{I-j} D^I_{M-K}(\vartheta)\,\chi^{\tau}_{-K}\}, \tag{2}$$

where χ^{τ}_K characterizes the internal nucleon motion and $D^I_{MK}(\vartheta)$ describes the rotation of the nucleus as a whole. The internal motion of the nucleons in an odd-odd nucleus is determined primarily by the states of the odd proton $\chi^{\alpha}_{\Omega_p}(p)$ and neutron $\chi^{\beta}_{\Omega_n}(n)$:

---

*The preliminary results of this investigation pertaining to the distinctive features of Am^{242}, Ta^{180m} and Lu^{176m} were presented at the Tenth All-Union Conference on Nuclear Spectroscopy (Moscow, Jan.1960).

**Among such states one may classify quadrupole vibrational and "pair" levels with $K = 0^+$ as well as octupole vibrational levels with $K = 0^-$.

$$\chi_K(p, n) = \sum_{\substack{\alpha\beta \\ \Omega_p + \Omega_n = K}} C_K^{\alpha\beta} \chi^{\alpha}_{\Omega_p}(p) \chi^{\beta}_{\Omega_n}(n). \qquad (3a)$$

In general nucleon pair correlation can mix states with different values of Ω_p and Ω_n, nevertheless K remains a good quantum number. Hence in expansion (3a) one must take into account only states α and β for which $\Omega_p + \Omega_n = K$* To simplify the notation hereinafter we shall omit the summation sign and write simply

$$\chi_K(p, n) = \chi^{\alpha}_{\Omega_p}(p) \chi^{\beta}_{\Omega_n}(n), \qquad (3b)$$

instead of (3a). For a rotational band with K = 0 $(\Omega_p = -\Omega_n)$ $D^I_{MK}(\vartheta) = D^I_{M-K}(\vartheta) = D^I_{MO}(\vartheta)$ and function (2) is simplified and can be written in the form

$$\psi(IK = OM) = \sqrt{\frac{2I+1}{16\pi^2}} D^I_{MO}(\vartheta) \{\chi^{\alpha}_{\Omega}(p) \chi^{\beta}_{-\Omega}(n) + (-)^{j_p + j_n} \chi^{\alpha}_{-\Omega}(p) \chi^{\beta}_{\Omega}(n)\} \quad \text{(even I)} \qquad (4a)$$

$$\psi(IK = OM) = \sqrt{\frac{2I+1}{16\pi^2}} D^I_{MO}(\vartheta) \{\chi^{\alpha}_{\Omega}(p) \chi^{\beta}_{-\Omega}(n) - (-)^{j_p + j_n} \chi^{\alpha}_{-\Omega}(p) \chi^{\beta}_{\Omega}(n)\} \quad \text{(odd I)} \qquad (4b)$$

Despite the identical states of the odd neutron and proton, the internal wave functions describing levels of the same rotational band will differ for levels with even and odd spin.

2. Rotational Levels

Inasmuch as the functions (4a) and (4b) are nonzero**, there are realized in a rotational band with K = 0 levels with both even and odd spins I = 0,1,2,3, 4,..., and with the same parity. Owing to the difference between the functions (4a) and (4b), however, the internal nuclear energy E_0 is not the same for levels with even and odd I. This I dependence of E_0 can be taken into account by writing (1) in the form

$$E_{\text{rot}} = B(-1)^I + AI(I+1), \qquad (5)$$

where

$$B = \frac{E_{0_{I\,\text{even}}} - E_{0_{I\,\text{odd}}}}{2}. \qquad (6)$$

It follows that rotational levels with even and odd spins are "shifted" relative to each other. Thus the rotational band breaks up into two groups of levels (Fig.1): a group with I = $0^{\pm}$, $2^{\pm}$, $4^{\pm}$ ..., and a group with I = $1^{\pm}$, $3^{\pm}$, $5^{\pm}$ .... The level energies in each group are described by $E = A[I(I+1) - I_0(I_0+1)]$, where I_0 is 0 or 1, respectively.

The parameter $A = \frac{\hbar^2}{2J}$ is the same for both groups. The parameter B may be either positive or negative. Its magnitude depends on the character of the nuclear forces, in particular, on the interaction of the odd proton and neutron,

---

*It can be shown that in most cases a predominant role is played by only one term in the expansion (3a) and that the other terms are small.

**In states of even-even nuclei wherein all the nucleons are bound into pairs in (4) one should write $\chi_{\Omega}(n)$ instead of $\chi_{\Omega}(p)$ (or vice versa). It can be shown that in this case function (4b) vanishes and the corresponding states with odd spins are not realized.

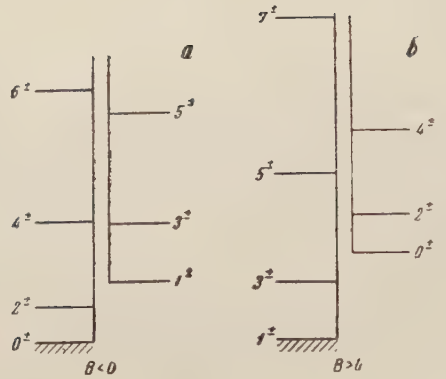

Fig.1. Rotational band of an odd-odd nucleus with $K = \Omega_p - \Omega_n = 0$.

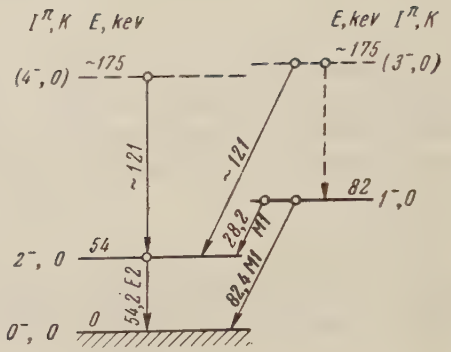

Fig.2. Level scheme of Ho^{166}.

and on the details of the internal wave function.

Using Eq.(5), it can readily be shown that with $B < A$ the level with I = 0 is the lowest level in the band with K = 0. This condition is fulfilled, for example, in $_{67}Ho^{166}$ (T = 27 hr), for which A = 9 kev and B = -32 kev. Recently there have been obtained many experimental data on the properties of the ground state and low-lying excited levels of this nucleus. Data[8] on the character of β^--decay of Ho^{166} and direct measurements[9] of the spin showed that the ground state of this nucleus is described by $I = 0^-$. This agrees with the assigned configuration $p\,^7/_2^-[523]$ and $n\,^7/_2^+[633]$.[10] It follows from the data on the multipole orders and intensities of the γ-transitions accompanying β-decay of Dy^{166} (Fig.2) that the 54 kev level in Ho^{166} has $I = 2^-$ and $K = 0^-$, while the 82 kev level is characterized by $I = 1^-$ and $K = 0^-$.[11-13] These quantum assignments for the 0, 54 and 82 kev levels give reason to assume that these levels belong to one rotational band. A further argument in favor of this is furnished by the results of evaluation of the moment of inertia of the ground state of Ho^{166}. According to the rule set forth in Ref.14, the moment of inertia of an odd-odd nucleus with mass number A may be written in the form

$$J^A_{\text{o.o.}} = J_{\text{e.e.}} + \delta J_p + \delta J_n, \qquad (7)$$

where $J^A_{\text{e.e.}}$ is the "average" moment of inertia of an even-even nucleus with the same A (moment averaged over a number of neighboring even-even nuclei), and $\delta J_{p\,(n)} = J_{\text{e.o.}} - J_{\text{e.e.}}$ is the specific contribution of the odd proton (or neutron), dependent on its quantum characteristics; $\delta J_{p\,(n)}$ can be found by comparing the moments of inertia of even-odd and even-even nuclei.

Using the values of $J_{\text{e.e.}}$ and $J_{\text{e.o.}}$ known from experiments, it can be shown that for a proton in the $^7/_2^-[523]$ state, $\delta J_p = 0.18\,J_{\text{e.e.}}$, while for a neutron in the $^7/_2^+[633]$ state $\delta J_n \approx 0.35 J_{\text{e.e.}}$ and, consequently, $J_{\text{o.o.}} \approx 1.53 J_{\text{e.e.}}$. The energy of the first rotational 2^+ level in the even-even nucleus $_{68}Er^{166}$ is 80.5 kev.[1] Hence it may be inferred that the energy of the first rotational level with I = = 2^- in $_{67}Ho^{166}$ will be lower by a factor of 1.53, i.e., will be equal to ~53 kev. This value is in good agreement with the experimental value of 54 kev and hence substantiates the assumption that this is a rotational level.

The presence in Ho^{166} of a rotational band comprising levels with $I = 0^-$, 1^- and 2^- and the location of the 1^- level above the 2^- level are experimental facts that substantiate the above inference that the band with K = 0 must contain levels

Table 1

β-decay of odd-odd nuclei with I = 1 to levels of the daughter nuclei with I = 0^+ and 2^+ (Refs.3 & 4)

Parent & daughter nuclei	Type transition	$\log ft_{exp}$	A^*_{exp}	$A_{theo.}$ $K=1$	$A_{theo.}$ $K=0$
$_{67}Ho^{164}_{97} \xrightarrow{\beta^-} {}_{68}Er^{164}_{96}$	$1^+ \to 0^+$ $1^+ \to 2^+$	6,4 6,7	+0,3	+0,3	—0,3
$_{69}Tu^{170}_{101} \xrightarrow{\beta^-} {}_{70}Yb^{170}_{100}$	$1^- \to 0^+$ $1^- \to 2^+$	8,9 9,3	+0,4	+0,3	—0,3
$_{73}Ta^{180}_{107} \xrightarrow{\beta^-} {}_{74}W^{180}_{106}$	$1^- \to 0^+$ $1^- \to 2^+$	6,8 6,5	—0,3	+0,3	—0,3
$_{75}Re^{186}_{111} \xrightarrow{\beta^-} {}_{76}Os^{186}_{110}$	$1^- \to 0^+$ $1^- \to 2^+$	7,7 8,0	+0,3	+0,3	—0,3
$_{75}Re^{188}_{113} \xrightarrow{\beta^-} {}_{76}Os^{188}_{112}$	$1^- \to 0^+$ $1^- \to 2^+$	8,1 8,6	+0,5	+0,3	—0,3
$_{93}Np^{236}_{143} \xrightarrow{\beta^-} {}_{94}Pu^{236}_{142}$	$1^- \to 0^+$ $1^- \to 2^+$	6,8 7,1	+0,3	+0,3	—0,3
$_{93}Np^{236}_{143} \xrightarrow{\varepsilon} {}_{92}U^{236}_{144}$	$1^- \to 0^+$ $1^- \to 2^+$	~7,2 ~7,7	~+0,5	+0,3	—0,3
$_{95}Am^{242}_{147} \xrightarrow{\beta^-} {}_{96}Cm^{242}_{146}$	$1^- \to 0^+$ $1^- \to 2^+$	7,1 6,8	—0,3	+0,3	—0,3
$_{95}Am^{242}_{147} \xrightarrow{\varepsilon} {}_{94}Pu^{242}_{148}$	$1^- \to 0^+$ $1^- \to 2^+$	~7,6 ~7,3	~—0,3	+0,3	—0,3

* $A = (\log ft)_{2^+} - (\log ft)_{0^+}$.

with even and odd spins shifted relative to each other.

It is interesting to note that in radiative thermal neutron capture by Ho^{165} there is observed in the spectrum of the daughter Ho^{166} a γ-line of 121 kev energy.[15-17] Inasmuch as this line is rather intense, it may be assumed that the given γ-transition occurs between low-lying excited levels in Ho^{166}. Comparing the energy of this transition with the expected energy for transitions between the levels of the rotational band it can be inferred that this transition may be either $4^- \to 2^-$ transition or a $3^- \to 2^-$ transition (Fig.2). In all probability the observed line is due to both transitions, i.e., the 121 kev line is a double one. It would be of interest to check this experimentally.

An analogous rotational band is encountered in $_{91}Pa^{234}$. According to the data[19] on β-decay of UX_2 (1.2 min Pa^{234}), its ground state has spin zero. Moreover, this state, like the 91 kev level in Pa^{234}, is obtained directly in β^--decay of Th^{234} (UX_1). The decay of Th^{234} is accompanied by emission of γ-rays having energies of 91, 63 and 29 kev.[2,3] There is no β^--transition to the intermediate 29 (or 63) kev level. Inasmuch as in the spectrum of conversion electrons from the 91 and 63 kev transitions the strongest are the lines corresponding to conversion on the L_I subshell, it may be inferred that these transitions are magnetic dipole transitions (in the original investigations[2,3] it was assumed that the 63 kev transition is E1).

Making use of the above rules, we calculated the moment of inertia for the state of Pa^{234} with spin 0, assuming that the 91st proton is in the $^5/_2{}^+$ [642] state (analogous to the proton in Np^{237} and Np^{239}), and the 143rd neutron occupies the $^5/_2{}^+$ [633] level (analogous to the neutron in U^{233}). The energy calculated on the basis of the deduced moment of inertia for the first rotational level with I = 2 is 28 kev, which is in good agreement with the observed transition energy (29 kev).

All these data indicate that in β^--decay of $_{90}Th^{234}$ to $_{91}Pa^{234}$ there are excited 0 (0^+), 29 (2^+), and 91 kev (1^+) levels, which may be interpreted as members of one rotational band with K = 0, A = +4.8 and B = -41 kev.

In the case when $A < B$ the I = 1 rotational level of the band with K = 0 must be located below the I = 0 level (Fig.1,b). Is this arrangement actually realized? It is easiest to check this if the state in question is the ground state or an isomeric state and undergoes β-decay. Hence for analysis[19] we chose a number of odd-odd nuclei for which the experimental data[2,3] directly or indirectly indicate I = 1 (Table 1). Naturally, in the decay of these nuclei there are observed β-transitions both to the ground state of the daughter even-even nucleus with $I = 0^+$ and to its first excited level with $I = 2^+$. Inasmuch as both final states belong to the same rotational band and the β-transitions are of the same type, the ratio of their reduced probabilities $(ft)_{2+}/(ft)_{0+}$ is expressed only in terms of Clebsch-Gordan coefficients which depend on I, L (multipole order of the transition) and K.

In all the cases under consideration the values of I, L and K are known, but for the initial state with I = 1 one must allow for two possible values of K, namely, 0 or 1. Inasmuch as the ratio of the reduced β-transition probabilities is highly sensitive to replacement of K = 0 by K = 1 (it changes by a factor of 4), even a rough measurement of the intensities of the two β-transitions allows of unambiguous determination of K for the odd-odd nucleus.

It will be evident from Table 1 that both $_{73}Ta^{180m}$ (T = 8.15 hr) and $_{95}Am^{242}$ (T = 16 hr) have K = 0.* These values of K for the given nuclei can be explained by means of Nilsson's scheme inasmuch as for them one can expect that $\Omega_p = \Omega_n$ and $K = |\Omega_p - \Omega_n| = 0^-$ (in Ta^{180m} $p\,{}^9/_2^-[514]; n\,{}^9/_2^+[624]$ or $p\,{}^7/_2^+[404]; n\,{}^7/_2^-[514]$); in Am^{242} $p\,{}^5/_2^-[523]$; $n\,{}^5/_2^+[622]$).

A similar band with $K = 0^-$ should occur in $_{71}Lu^{176}$, inasmuch as in the ground state of this nucleus $p\,{}^7/_2^+[404]$ and $n\,{}^7/_2^-[514]$. Apparently this state is identical with the familiar isomeric state (3.7 hr Lu^{176m}) the spin of which according to the decay scheme[2] and the results of direct measurements[22] is 1. It is not impossible that a similar situation obtains in $_{93}Np^{240}$ (T = 7.3 min)[23] which has spin I = 1, inasmuch as its probable configuration $p\,{}^5/_2^+[642]$ and $n\,{}^5/_2^+[622]$ (in Np^{240}) leads to K = 0.**

3. Electric and Magnetic Moments

For nuclei for which there is fulfilled the condition $A < B$ and the ground or isomeric state has I = 1, but K = 0, there can be predicted the absolute values and the signs of the electric quadrupole moments Q and the magnetic dipole moments μ.

For the quadrupole moment, as is known, there obtains the relation[1]

$$Q = \frac{3K^2 - I(I+1)}{(I+1)(2I+3)} Q_0, \qquad (8)$$

where Q_0 is the internal quadrupole moment.

---

*Winocur et al[20] showed by direct measurements that the spin of 16-hr Am^{242} is 1, while Asaro et al[21] found from analysis of β-decay that for this state K = 0.

**In Np^{240} there were detected two close lying levels with $I = 1^+$ (Ref.23). Possibly the indicated configuration and $K = 0^+$ pertain not to the 7.3 min metastable state but to some higher lying level in Np^{240}.

It will readily be evident that in states with K = 0 and I = 1

$$Q = -0.2Q_0. \tag{9}$$

Inasmuch as it may be assumed that deformed nuclei are prolate, we have $Q_0 > 0$ and $Q < 0$. Apparently, this serves to explain the negative sign of the quadrupole moment found experimentally for Am^{242} (Refs.20 & 21).

Using the experimental values of Q_0 found for neighboring even-even or odd nuclei, one can by means of Eq.(9) calculate the absolute values of the quadrupole moments of Lu^{176m}, Ta^{180m} and Am^{242}.

The magnetic moments of deformed nuclei are given by[1]

$$\mu = (g_K - g_R)\frac{K^2}{I+1} + g_R I, \tag{10}$$

where g_K and g_R are the gyromagnetic ratios due to motion of individual nucleons and to the collective motion of the nucleus. For K = 0 and I = 1 we have

$$\mu = g_R I = g_R \approx + \frac{Z}{A}. \tag{11}$$

Thus in cases when K = 0 the magnetic moment is positive and does not depend on the details of the internal wave function. The values of Q and μ calculated by means of Eqs.(9)-(11) for Lu^{176m}, Ta^{180m} and Am^{242} are listed in Table 2.

4. Probability of γ-Transitions Between Rotational Levels

The reduced probability for γ-transitions of multipolarity L between rotational band levels with spins I_1 and I_2 and K = 0 can be represented in the form

$$B(L) = [\langle \chi^{\alpha}_{\Omega}(p)\,\chi^{\beta}_{-\Omega}(n) \mid \hat{W} \mid \chi^{\alpha}_{\Omega}(p)\,\chi^{\beta}_{-\Omega}(n)\rangle \times (1 + (-1)^{\Delta I + L})]^2 \langle I_1 L00 \mid J_1 L I_2 0\rangle^2. \tag{12}$$

For γ-transitions between levels with even (or odd) spins $\Delta I = I_2 - I_1 = 2$, this expression reduces to

$$B(E2) = \frac{5}{16\pi} e^2 Q_0^2 \langle I_1 L00 \mid I_1 L I_2 0\rangle^2, \tag{13}$$

i.e., becomes analogous to the expression for the reduced probability of E2 transitions between the rotational levels of even-even nuclei.[1]

Table 2

Electric quadrupole and magnetic dipole moments of odd-odd nuclei with K = 0, I = 1

Nucleus	Q_0	Q_{theo}	μ_{theo}
$_{71}Lu^{176*}_{105}$	7,8 (per Lu^{175}, Hf^{176}) [1]	−1,6	+0,40
$_{73}Ta^{180*}_{107}$	7,0 (per Ta^{181}, Hf^{180}) [1]	−1,4	+0,41
$_{95}Am^{242}_{147}$	13,7 (per Am^{241}) [24]	−2,74	+0,39

Of particular interest are transitions between levels with even and odd spins. At first glance it would seem that transitions between rotational levels with spins I + 1 and I can be of the M1 + E2 type, if I ≠ 0. It can be shown, however, that for such transitions $B(E2) = 0$, and they must be pure magnetic dipole transitions (M1).

It will be recalled that the Clebsch-Gordan coefficient $\langle I_1 L00 \mid I_1 L I_2 0\rangle = 0$ if $I_1 + I_2 + L$ is odd. The last expression in this case will be odd only if L is even (inasmuch as $I_1 + I_2$ is odd), i.e., only in the case of E2 (or E4...) transitions.

It must be noted that this result is valid not only for transitions between the levels of one and the same rotational band with K = 0, but also for transitions between the levels of two different rotational bands each of which has K = = $0^{\pm}$. Moreover in the case when $\Delta I + L$ is odd, for transitions inside one rotational band the internal matrix element vanishes owing to the presence of the factor $(1 + (-1)^{\Delta I+L})$ in (12). The presence of pair correlation and mixing of states with different Ω but with the same K does not remove this forbiddenness.

This result ($B(E2; I + 1 \rightarrow I) = 0$) is in agreement with the experimental data on the multipole order of the γ-transition between the $I_1 = 1^-$ and $I_2 = 2^-$ levels in Ho^{166}. According to the data on the internal conversion coefficients, this 28 kev transition in Ho^{166} is pure M1 (the admixture of E2, if any, must be <1%).[12,13]

The reduced transition probability for an M1 transition between rotational levels with spins I + 1 and I, as is known, is given by the formula[1]

$$B(M1) = \frac{3}{4\pi}(g_K - g_R)^2 K^2 \langle I_1 100 | I_1 1 I_2 0\rangle^2 \qquad (14)$$

In odd-odd nuclei $g_K K = g_{\Omega_p}\Omega_p + g_{\Omega_n}\Omega_n$. Inserting this expression in (14) and recalling the fact that with K = 0, $\Omega_p = -\Omega_n = \Omega$, we obtain the following formula

$$B(M1) = \frac{3}{4\pi}\left(g_{\Omega_p} - g_{\Omega_n}\right)^2 \Omega^2 \langle I, 100 | I_1 1 I_2 0\rangle^2, \qquad (15)$$

where Ω is the projection of the angular momentum of the odd nucleon and g_{Ω_p} and g_{Ω_n} are the gyromagnetic ratios characterizing the contributions of the odd proton and neutron to the magnetic moment of the nucleus. Inasmuch as $B(M1)$ does not depend on g_R, the collective motion of the nucleons does not make any contribution to the probability of a rotational M1 type transition. It follows from Eq.(15) that with $g_{\Omega_n} \approx g_{\Omega_p}$ the reduced probability $B(M1)$ will be small. This can lead to interesting consequences if the rotational level with I = 1 does not lie very high and can de-excite only to the levels with I = 2 and I = 0. In this case the probability for de-excitation of the I = 1 level will be very small inasmuch as the reduced γ-transition probabilities from it $B(E2) = 0$ and $B(M1) \approx 0$ (or very small) so that it will be evinced as a long-lived isomeric state.

For specific evaluations of $B(M1)$ one can for g_{Ω_p} and g_{Ω_n} use the known values of these ratios in the neighboring odd nuclei with the same odd nucleons.[1,2]

In the case of Ho^{166}, for example, g_{Ω_p} = +1.12 (from Ho^{165}), g_{Ω_n} = -0.26 (from Er^{167}), and Ω = 7/2.

Inasmuch as $g_{\Omega_p} \neq g_{\Omega_n}$, the probability for de-excitation of the 82 kev rotational level in Ho^{166} with $I = 1^-$ will be large and the lifetime of the level will, accordingly, be short. Calculations by means of Eq.(15) show that in this case $T = 4 \cdot 10^{-11}$ sec. It would be of interest to check this result experimentally.

5. Characteristics of the Rotational Band with K = 0 in Light Odd-Odd Nuclei

If the odd proton and neutron in a light nucleus are in the same quantum state ($\chi^{\alpha}_{\Omega_p} = \chi^{\beta}_{\Omega_n}$), which may obtain, for example, in Na^{22} and Al^{26}, the rotational band with K = 0 will exhibit a number of additional distinctive characteristics. In this case one can make use of the isotopic spin formalism and construct the

antisymmetric wave function.

It can readily be shown that actually there will be two such functions. They can be written in the following form.

a) Coordinate-spin part - antisymmetric, and isotope-spin part - symmetric:

$$[\chi_{\Omega}(1)\chi_{-\Omega}(2) - \chi_{-\Omega}(1)\chi_{\Omega}(2)]\,\Phi_{TM_T}(1,2)\,(1-(-)^{I-j_p-j_n})\,(1+(-)^{T-1}).$$

b) Coordinate-spin part - symmetric; isotope-spin part - antisymmetric:

$$[\chi_{\Omega}(1)\chi_{-\Omega}(2) + \chi_{-\Omega}(1)\chi_{\Omega}(2)]\,\Phi_{TM_T}(1,2)\,(1+(-)^{I-j_p-j_n})\,(1-(-)^{T-1}).$$

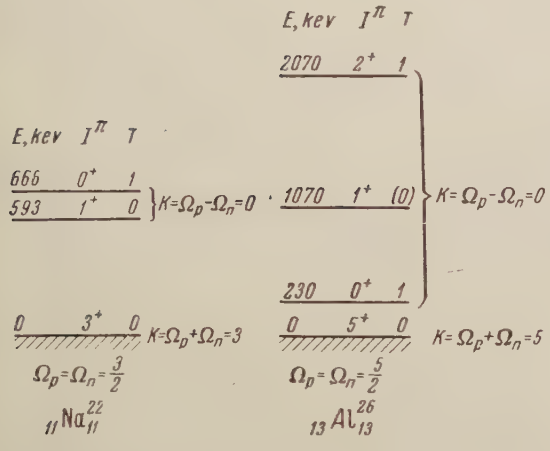

Fig.3. Level diagrams for $_{11}Na^{22}$ and $_{13}Al^{26}$.

The first wave function corresponds to the group of levels with I = 1^+, 3^+, 5^+ ... and is characterized by isotopic spin T = 0. The second wave function corresponds to the group of levels with even spins I = 0^+, 2^+, 4^+ ... and is characterized by T = 1. Levels of this type are analogous to the rotational levels in neighboring even-even nuclei. The experimental data[26,27] on the properties of some of the excited levels of Na^{22} and Al^{26}, which may be interpreted as rotational levels, are in agreement with these inferences (Fig.3). In both nuclei there are states with I = K = 0^+ (T = 1) and I = 1^+ (it has been shown that for this level in Na^{22} T = 0). The interval between the 2^+ and 0^+ levels in Al^{26} is 1.85 Mev or almost equal to the gap ΔE = = 1.83 Mev between the 2^+ and 0^+ levels in the neighboring even-even nucleus Mg^{26} (Ref.27).

6. Rotational Bands in Even-even Nuclei, Associated with "Single-Particle" Excited Levels with K = 0

All the above mentioned distinctive features of rotational bands with K = 0 in odd-odd nuclei are connected only with the fact that the odd nucleons (proton and neutron) in these nuclei are in different quantum states. It can readily be seen that an analogous situation will obtain in even-even nuclei if the bond between one of the neutron or proton pairs is ruptured in the process of excitation. In this case the two protons or two neutrons will end up in different quantum states and if K = 0, the said states will be described by a wave function of the type (4), where instead of $\chi^{\alpha}_{\Omega_p}$ and $\chi^{\beta}_{\Omega_n}$ one should write $\chi^{\alpha}_{\Omega_n}$ and $\chi^{\beta}_{\Omega_n}$ or $\chi^{\alpha}_{\Omega_p}$ and $\chi^{\beta}_{\Omega_p}$.

Just as in the case of odd-odd nuclei, the rotational band connected with this state of the even-even nucleus must contain groups of levels with even and odd spins (I = 0, 2, 4 ... and 1, 3, 5 ...) shifted relative to each other.

This distinctive characteristic of "single-particle" levels in even-even nuclei with K = 0 makes it possible to distinguish them from collective excited levels with K = 0 (β-vibrational and "pair" levels with K = 0^+ and octupole vibrational levels with K = 0^-).

Possibly levels of precisely this type (I = K = 0^+) are observed in Er^{166} (E = 1460 kev)[6], Os^{188} (E = 1086 or 1766 kev) and U^{234} (E = 1045 kev).[28]

Of particular interest is Er^{166}, inasmuch as in this nucleus in β-decay of Ho^{166} (T = 27 hr) in addition to the 0^+ level at 1460 kev there is excited a ~1663 kev level (Fig.3).[2,3,6] Investigation of the character of the excitation and decay of this state shows unambiguously that it is characterized by I = 1 and K = 0. Moreover, according to the data[6], on the angular correlation between the 1582 and 80 kev γ-rays, the 1582 kev transition is virtually a pure dipole transition; the admixture of quadrupole radiation, if any, does not exceed 0.01%. The conjunction of data on the values of I and K and the dipole character of the transition led to the assignment[6] of odd parity for the 1663 kev level (in this case the 1582 kev transition must be E1 with a negligible admixture of M2, if any) and identification of it as an octupole vibrational level with $I = 1^-$ and $K = 0^-$. The 1460 kev level with $I = K = 0^+$ is usually interpreted as a β-vibrational level (see Ref.6). The available experimental data, however, do not conflict with the assignment of even parity to the I = 1 level. Actually, in this case the 1582 kev transition occurs between levels with $I = 1$, $K = 0^+$ and $I = 2$, $K = 0^+$. Such a transition must be M1 inasmuch as for it, as was shown above under Section 4, $B(E2) = 0$.

The data on β-decay are in better agreement with even than with odd parity of the 1663 kev level inasmuch as the β-transition to it is of the $0^- \rightarrow 1$ type and log ft = 6.8, which is more consistent with a once forbidden transition than an allowed one. If we assume that the parity of the 1663 kev level is even (+), it may be inferred that the 1460 ($I = 0$, $K = 0^+$) and 1663 kev ($I = 1$, $K = 0^+$) levels are members of the same rotational band. In this case the 1460 kev level must be interpreted as a single-particle one.

It must, however, be emphasized that at present one cannot make a definitive choice between identifications of the 1460 kev (0^+) level as a collective or as a single-particle one (although we incline to the latter alternative). For positive identification one must ascertain experimentally the parity of the 1663 kev level with I = 1. This can be done by determining the multipole order (M1 or E2) of the 1663 or 1582 kev γ-transition.

Scientific-Research Physical Institute of
Leningrad State University &
Physical-Technical Institute of the
Academy of Sciences of the USSR

References

1. K.Alder, A.Bohr, T.Huss, B.Mottelson & A.Winther, Revs.Mod.Phys., 28, 432 (1956).

2. B.S.Dzhelepov & L.K.Peker, Skhemy raspada radioaktivnykh yader (Decay schemes of radioactive nuclei), M.-L., 1958.

3. D.Strominger, J.M.Hollander & G.T.Seaborg, Table of Isotopes, Revs.Mod. Phys., 30, 585 (1958).

4. I.Marklund, O.B.Nathan & O.B.Nielsen, Nucl.Phys., 15, 199 (1960).

5. O.Nathan, see Nucl.Phys., 15, 533 (1960).

6. I.Marklund, B.van Nooijen & Z.Grabowski, Nucl.Phys., 15, 533 (1960).

7. A.Bohr, Kgl.Danske Videnskab.Selskab.Mat.-fys.Medd., 26, No.14 (1952).

8. R.L.Graham, J.L.Wolfson & M.A.Clark, Phys.Rev., 98, 1173 (1955).

9. L.S.Goodman, W.J.Childs, R.Marrus, I.P.Lindgren & A.Y.Cabezas, Bull. Amer.Phys.Soc., 5, 344 (1960).

10. L.K.Peker, Izv.AN SSSR, Ser.fiz., 21, 1029 (1957). (Trans.Bulletin, 21, 1030.)

11. R.G.Helmer & S.B.Burson, Bull.Amer.Phys.Soc., 4, 427 (1959).
12. J.S.Geiger, R.L.Graham & G.T.Ewan, Ibid., 5, 255 (1960).
13. L.I.Rusinov, A.V.Borovikov, V.S.Gvozdev, G.D.Porsev, S.L.Sakharov & Yu. L.Khazov, Zhur.eksp.i teor.fiz., 39, 1529 (1960). (Trans.Soviet Phys. - JETP.)
14. L.K.Peker, Izv.AN SSSR, Ser.fiz., 24, 365 (1960). (Trans.Bulletin, 24, 350.)
15. V.V.Sklyarevskii, E.P.Stepanov & B.A.Obinyakov, Atomnaya energiya, 4, 22 (1958). (Trans.Soviet Journal of Atomic Energy.)
16. J.E.Draper & A.A.Fleischer, Nucl.Phys., 13, 53 (1959).
17. I.V.Estulin & L.F.Kalinkin, Program of the Tenth All-Union Conference on Nuclear Spectroscopy, M.-L., 1960.
18. G.T.Wood, Phys.Rev., 119, 2004 (1960).
19. L.K.Peker, Program of the Tenth All-Union Conference on Nuclear Spectroscopy, M.-L., 1960.
20. J.Winocur, R.Marrus & W.A.Nierenberg, Bull.Amer.Phys.Soc., 5, 273 (1960).
21. F.Asaro, I.Perlman, J.O.Rasmussen & S.G.Thompson, Ibid., 4, 461 (1959).
22. M.B.White, S.S.Alpert & E.Lipworth, Ibid., 5, 273 (1960).
23. M.E.Bunker, B.J.Dropesky, J.D.Knight, J.W.Starner & B.Warren, Phys.Rev., 116, 143 (1959).
24. T.E.Manning, M.Fred & F.S.Tomkins, Phys.Rev., 102, 1108 (1956).
25. D.A.Varshalovich, Izv.AN SSSR, Ser.fiz., 24, 895 (1960). (Trans.Bulletin, 24, 895.)
26. G.M.Temmer & N.P.Heydenburg, Phys.Rev., 111, 1303 (1958).
27. P.M.Endt & C.M.Braams, Revs.Mod.Phys., 29, 683 (1957).
28. S.Bjornholm, Nucl.Phys., 15, 533 (1960).
29. C.J.Gallagher, Ibid., 16, 215 (1960).
30. F.Asaro, I.Perlman, J.O.Rasmussen & S.G.Thompson, Phys.Rev., 120, 934 (1960).

Note added in proof: Recently we became acquainted with the papers of Gallagher[29] and Asaro et al[30] which are also concerned with the properties of odd-odd nuclei with K = 0 and which arrive at results similar to ours.

CONCERNING SELECTION RULES FOR β- AND γ-TRANSITIONS IN ODD-ODD NUCLEI

- M.E.Voikhanskii & L.K.Peker

In deformed odd-A nuclei the asymptotic quantum numbers N, n_Z, Λ and Σ introduced by Nilsson[1], play an important role as regards classifications of states (Ref.2-4) and interpretation of the β- and γ-transitions[5-7].

The asymptotic quantum numbers have also been used for classification of the angular momenta of the internal states in odd-odd deformed nuclei.[8]

In the present work we consider the asymptotic number selection rules for β- and γ-transitions in odd-odd nuclei. Transitions in such nuclei have a number of distinctive features as compared with transitions in odd-A nuclei.

1. Transition Probabilities and Asymptotic Number Selection Rules

In odd-odd deformed nuclei the last unpaired nucleons - proton and neutron - may be approximately regarded as moving independently in the field of the deformed core. According to Gallagher & Moszkowski[8], the ground state of such nuclei is characterized by the following coupling scheme (rules) for the momenta of the unpaired nucleons, the intrinsic spins are lined up parallel:

$$\Omega = \Omega_p + \Omega_n, \quad \text{if} \quad \Omega_p = \Lambda_p \pm \frac{1}{2}, \quad \text{and} \quad \Omega_n = \Lambda_n \pm \frac{1}{2};$$
$$\Omega = |\Omega_p - \Omega_n|, \quad \text{if} \quad \Omega_p = \Lambda_p \pm \frac{1}{2}, \quad \text{and} \quad \Omega_n = \Lambda_n \mp \frac{1}{2} \tag{1}$$

The wave functions of the system of two nucleons in a deformed nucleus were determined by Gallagher[9] and Varshalovich & Peker[10]. When the coupling scheme or sum of the components of the angular momenta of the two nucleons along the nuclear symmetry axis is $\Omega = \Omega_1 + \Omega_2$, we have

$$\Psi = \sqrt{\frac{2I+1}{16\pi^2}} \{\chi_{\Omega_1}\chi_{\Omega_2} D^I_{MK} + (-)^{I-j_1-j_2}\chi_{-\Omega_1}\chi_{-\Omega_2} D^I_{M-K}\}\,\varphi \tag{2}$$

When the coupling scheme is $\Omega = |\Omega_1 - \Omega_2|$, we have

$$\Psi = \sqrt{\frac{2I+1}{16\pi^2}} \{\chi_{\Omega_1}\chi_{-\Omega_2} D^I_{MK} + (-)^{I-j_1-j_2}\chi_{-\Omega_1}\chi_{\Omega_2} D^I_{M-K}\}\,\varphi \tag{3}$$

The indices 1 and 2 pertain to a proton or neutron.

Beta and γ-transitions in odd-odd deformed nuclei may be divided into two classes[9] depending on whether the transition does or does not involve a change in the coupling scheme of the momenta of the unpaired nucleons. We shall refer to transitions between states with the coupling scheme

$$\Omega_i = \Omega_{1i} \pm \Omega_{2i} \to \Omega_f = \Omega_{1f} \pm \Omega_{2f} \tag{4}$$

as transitions of class I, and to transitions between states with different coupling schemes

$$\Omega_i = \Omega_{1i} \pm \Omega_{2i} \to \Omega_f = \Omega_{1f} \mp \Omega_{2f} \tag{5}$$

as transitions of class II. We assume that emission of a γ-ray or β-particle is connected with change in the state of one nucleon (proton or neutron). β-transitions, like γ-transitions, can be classified as regards multipole order L.[11] We assume that the single-particle transition operator $\mathfrak{M}(L, k)$ is determined in the coordinate system of the nucleus and that this operator acts only on the wave

functions of one nucleon. Then the reduced transition probability between states with the same coupling scheme (for example, $\Omega_i = \Omega_{1i} + \Omega_{2i} \to \Omega_f = \Omega_{1f} + \Omega_{2f}$) is determined by

$$B(L, I_i \to I_f) = \Big| (I_i L K_i K_f - K_i \,|\, I_f K_f) \times$$
$$\times \Big\{ \int \chi^*_{\Omega_{1f}} \chi_{\Omega_{1i}} d\tau_1 \int \chi^*_{\Omega_{2f}} \mathfrak{M}(L, K_f - K_i) \chi_{\Omega_{2i}} d\tau_2 +$$
$$+ \int \chi^*_{\Omega_{2f}} \chi_{\Omega_{2i}} d\tau_2 \int \chi^*_{\Omega_{1f}} \mathfrak{M}(L, K_f - K_i) \chi_{\Omega_{1i}} d\tau_1 \Big\} + (I_i L K_i - K_f - K_i \,|\, I_f - K_f) \times$$
$$\times \Big\{ \int \chi^*_{-\Omega_{1f}} \chi_{\Omega_{1i}} d\tau_1 \int \chi^*_{-\Omega_{2f}} \mathfrak{M}(L, -K_f - K_i) \chi_{\Omega_{2i}} d\tau_2 +$$
$$+ \int \chi^*_{-\Omega_{2f}} \chi_{\Omega_{2i}} d\tau_2 \int \chi^*_{-\Omega_{1f}} \mathfrak{M}(L, -K_f - K_i) \chi_{\Omega_{1i}} d\tau_1 \Big\} \Big|^2 . \qquad (6)$$

An analogous relationship obtains for $\Omega_i = |\Omega_{1i} - \Omega_{2i}| \to \Omega_f = |\Omega_{1f} - \Omega_{2f}|$ transitions.

The reduced probability for transitions between states with different coupling schemes ($\Omega_i = \Omega_{1i} + \Omega_{2i}$ and $\Omega_f = |\Omega_{1f} - \Omega_{2f}|$) is given by

$$B(L, I_i \to I_f) = \Big| (I_i L K_i K_f - K_i \,|\, I_f K_f) \times$$
$$\times \Big\{ \int \chi^*_{\Omega_{1f}} \chi_{\Omega_{1i}} d\tau_1 \int \chi^*_{-\Omega_{2f}} \mathfrak{M}(L, K_f - K_i) \chi_{\Omega_{2i}} d\tau_2 +$$
$$+ \int \chi_{-\Omega_{2f}} \chi_{\Omega_{2i}} d\tau_2 \int \chi^*_{\Omega_{1f}} \mathfrak{M}(L, K_f - K_i) \chi_{\Omega_{1i}} d\tau_1 \Big\} +$$
$$+ (I_i L K_i - K_f - K_i \,|\, I_f - K_f) \times$$
$$\times \Big\{ \int \chi^*_{-\Omega_{1f}} \chi_{\Omega_{1i}} d\tau_1 \int \chi^*_{\Omega_{2f}} \mathfrak{M}(L, -K_f - K_i) \chi_{\Omega_{2i}} d\tau_2 +$$
$$+ \int \chi^*_{\Omega_{2f}} \chi_{\Omega_{2i}} d\tau_2 \int \chi^*_{-\Omega_{1f}} \mathfrak{M}(L, -K_f - K_i) \chi_{\Omega_{1i}} d\tau \Big\} \Big|^2 . \qquad (7)$$

In Eqs.(6) and (7) the integral over the vibrational wave functions $\int \varphi^*_f \varphi_i \, d\tau$ is taken equal to unity, i.e., it is assumed that the state of the surface does not change incident to the transition. If the transition involves a change in the shape of the nucleus, taking this integral into account leads to reduction of the transition probability. It is evident from Eqs.(6) and (7) that emission of a γ-ray or a β-particle is possible in transitions of either the first or the second nucleon. Owing to the orthogonality of the wave functions of the nucleon not participating in the transition, it follows from (6) and (7) that there may occur both single-particle and two-particle transitions. In single-particle transitions one of the nucleons does not change its state. In two-particle transitions, in addition to change of state, for example, of the second nucleon, the angular momentum of the first nucleon "flips", i.e., the projection of its angular momentum on the nuclear symmetry axis is reversed ($\Omega_{1f} = -\Omega_{1i}$). Thus, two-particle transitions of a certain type may occur in the independent particle model. It follows from the properties of the Clebsch-Gordan coefficient $(I_i L K_i - -K_f - K_i \,|\, I_f - K_f)$ in Eqs.(6) and (7) that the corresponding terms are nonzero only for transitions with $K_i + K_f \leqslant L$. Such transitions include, for example, transitions to levels with spin 0 and also transitions characterized by $1 \to 1\,(L = 2)$, $1 \rightleftarrows 2\,(L = 3)$, etc. For transitions of class I, the indicated term in (6) vanishes if the state of both unpaired nucleons changes. This is not the case for transitions of class II.

If the transition involves change in the state of one nucleon and $K_i + K_f > L$ (for transitions of class II), expressions (6) and (7) coincide with the corresponding expressions for the transition probabilities given by Gallagher[9]. Here-

inafter we shall restrict our consideration to single-particle transitions.

The expressions for the transition probabilities contain the products of three factors, one of which is the Clebsch-Gordan coefficient and the other two are integrals over the wave functions of the unpaired nucleons. From the properties of the first factor $(I_i L K_i K_f - K_i | I_f, K_f)$ there follow the K selection rules (K is the projection of the total angular momentum on the nuclear symmetry axis):

$$\Delta K \equiv | K_i - K_f | \leqslant L. \tag{8}$$

For transitions of class I it follows from (4), (8) and the condition $\Omega_{1f} = \Omega_{1i}$ that

$$\Delta K = | \Omega_{2i} - \Omega_{2f} | \leqslant L. \tag{9}$$

Analogously for transitions of class II there must be fulfilled the condition

$$\Delta K = \Omega_{2i} + \Omega_{2f} \leqslant L. \tag{10}$$

For transitions to the ground state of the rotational band this condition is always fulfilled, and such transitions are allowed as regards the quantum number K. For transitions to rotational levels conditions (10) is not fulfilled in many cases. In this case, $\Delta K = \Omega_{2i} + \Omega_{2f} > L$, and the transition is forbidden as regards K.

In addition to the K selection rules, there may apply other inhibitions connected with the integrals over the wave functions of the odd nucleons. The distinctive features of transitions in odd-odd nuclei connected with the integral $\int \chi^*_{\Omega_{1f}} \chi_{\Omega_{1i}} d\tau_1$, were considered by Gallagher[9].

We turn to the integral over the wave functions of the transformed (second) nucleon. For transitions of the first class the integral (see Eq.(6)) has the same form as for transitions in odd-A deformed nuclei. Consequently, for transitions of this type there will be valid the asymptotic number selection rules given by Alaga[5] and Voikhanskii[6] for odd-A nuclei.

For transitions of class II the integral $\int \chi^*_{-\Omega_{2f}} \mathfrak{M}(L, K_i - K_f) \chi_{\Omega_{2i}} d\tau_2$ of interest to us has a different form. Here the projection of the momentum Ω_2 of the transforming nucleon has opposite orientations in the initial and final states. This must lead to new selection rules as regards the quantum numbers N, n_z, Λ and Σ. In order to determine these rules we must approximate the internal wave functions χ_Ω of the deformed nucleus by functions of an anisotropic harmonic oscillator (see, for example, Ref.12). It can readily be shown that for transitions of class II the N and n_z selection rules are the same as for transitions of class I, but that the selection rules as regards orbital angular momentum Λ and spin angular momentum Σ are substantially different. In these cases the restrictions are applied not on the difference between the angular variables $\Delta\Lambda = \Lambda_i - \Lambda_f$ or $\Delta\Sigma = \Sigma_i - \Sigma_f$, but on their sum $\Lambda_i + \Lambda_f$ and $\Sigma_i + \Sigma_f$. For example, for radiative EL transitions of class II the necessary condition is

$$\Delta\Lambda = \Lambda_i + \Lambda_f \leqslant L, \tag{11}$$

while for transitions of class I the analogous condition is

$$\Delta\Lambda = |\Lambda_i - \Lambda_f| \leqslant L. \tag{12}$$

The indicated distinction as regards the selection rules for transitions between states with a different coupling scheme is due to the effect of spin flip, i.e., change in the relative orientation of the projection of the momenta of the unpaired nucleons in the initial and final states. In Table 1 we list the selection rules as regards the asymptotic quantum numbers N, n_Z, Λ and Σ of the affected nucleon in radiative EL transitions of class II. Inasmuch as transitions between states with given K_i and K_f occur with the lowest possible multipole order, we have limited the listing to values of $\Delta\Omega = L, L-1$. For transitions of multipole order $L = 2$, we have also included $\Delta\Omega = L - 2 = 0$.

Table 1

Selection rules for EL type transitions between states with different coupling schemes of the momenta of the unpaired nucleons in odd-odd deformed nuclei

$K_f - K_i$	$\Lambda_f + \Lambda_i$	$\Sigma_f - \Sigma_i$	$N_f - N_i$	$n_{zf} - n_{zi}$	Additional conditions
$\pm L$	L	0	$L, L-2, \ldots -L$	0	
$\pm(L-1)$	$(L-1)$	0	$L, L-2, \ldots -L+2$	1	
			$L-2, L-4, \ldots -L$	-1	
0	0	0	0	0	$L=2$
0	0	0	2	2	$L=2$
			-2	-2	$L=2$

The selection rules for radiative ML transitions and β-transitions of the second class in odd-odd deformed nuclei are not given. They can be deduced from the appropriate tables in Refs.5 & 6, by replacing $\Lambda_i - \Lambda_f$ and $\Sigma_i - \Sigma_f$ by $\Lambda_i + \Lambda_f$ and $\Sigma_i + \Sigma_f$, respectively.

The effect associated with change in the relative orientation of the angular momenta of the odd nucleons should be evinced in the transition probabilities not only for deformed but also for spherical nuclei. Assume that in an odd-odd spherical nucleus the momentum j_1 of one of the unpaired nucleons (for example, of the nucleon not participating in the transition) is aligned in a certain direction. Then the angular momentum j_2 of the second nucleon can be oriented in different ways relative to this direction. Accordingly, the initial and final states of the system, as in a deformed nucleus, may have the same or different coupling schemes. It must, however, be taken into account that the momenta j_1 and j_2 are added vectorially and hence the total momentum $I = j_1 + j_2$ has a number of possible values:

$$|j_1 - j_2| \leqslant I \leqslant j_1 + j_2 \tag{13}$$

Hence one can speak only of predominantly parallel or predominantly antiparallel orientation of j_1 and j_2, depending on the angle between them.

Accordingly, transitions with and without change of the angular momentum coupling scheme will be characterized by different selection rules, analogously to transitions in deformed nuclei.

In actual nuclei the asymptotic quantum number selection rules should be fulfilled only approximately inasmuch as these quantum numbers are not rigorous ones. Forbiddenness with respect to them results in a certain retardation of the transition. For transitions of class I Λ forbiddenness should be observed relatively rarely inasmuch as for such transitions $\Delta\Lambda = \Lambda_i - \Lambda_f$ is usually small. In the case of class II transition the opposite situation obtains. For allowed and once forbidden β-transitions (which are characterized by $L = 0$, 1 or 2) almost always $\Lambda_i + \Lambda_f > L$ or $j_i + j_f > L$. Hence such transitions must be characterized by anomalously high log ƒt values. For transitions of class II there should also be observed a similar effect. However, owing to the fact that a γ-transition

Table 2

β-transitions in deformed nuclei with even-A

Initial & final nuclei	$I_i K_i \pi_i$	$I_f K_f \pi_f$	Level in daughter	log ft
1	2	3	4	5
Allowed Class I transitions $\Omega_1 - \Omega_2 \to \Omega_1 - \Omega_1$				
$_{67}Ho^{164}_{97} \to {}_{68}Er^{164}_{96}$	1 1 +	0 0 +	0	6,4
	1 1 +	2 0 +	91	6,7
$_{66}Dy^{166}_{100} \to {}_{67}Ho^{166}_{99}$	0, 0 +	1 0 +	428	4,8
$_{73}Ta^{178}_{105} \to {}_{72}Hf^{178}_{106}$	1 1 +	0 0 +	0	4,7
	1 1 +	2 0 +	93	4,8
	1 1 +	2 2 +	1480	4,6
$_{93}Np^{240}_{147} \to {}_{94}Pu^{240}_{146}$	1 1 (∓)	1 0 −	597	6,3
Allowed Class II transitions $\Omega_1 + \Omega_2 \to \Omega_1 - \Omega_1$				
$_{63}Eu^{152}_{89} \to {}_{62}Sm^{152}_{90}$	3 3 −	2 2 −	1531	~10
$_{63}Eu^{154}_{91} \to {}_{64}Gd^{154}_{90}$	3 3 −	2 2 −	1400	~10
$_{65}Tb^{160}_{95} \to {}_{66}Dy^{160}_{94}$	3 3 −	2 2 −	1265	8,1
Once forbidden Class I transitions				
$_{66}Dy^{166}_{100} \to {}_{67}Ho^{166}_{99}$	0 0 +	0 0 −	0	7,4
	0 0 +	1 0 −	84	6,0
$_{67}Ho^{166}_{99} \to {}_{68}Er^{166}_{98}$	0 0 −	0 0 +	0	8,1
	0 0 −	0 0 +	1460	7,5
	0 0 −	1 0 (+)	1663	6,8
$_{73}Ta^{180}_{107} \to {}_{74}W^{180}_{106}$	1 0 −	0 0 +	0	6,8
	1 0 −	2 0 +	102	6,5
$_{93}Np^{236}_{143} \to {}_{94}Pu^{236}_{142}$	1 1 −	0 0 +	0	6,8
	1 1 −	2 0 +	44,6	7,1
$_{93}Np^{236}_{143} \to {}_{92}U^{236}_{144}$	1 1 −	0 0 +	0	7,2
	1 1 −	2 0 +	45	7,7
$_{93}Np^{238}_{145} \to {}_{94}Pu^{238}_{144}$	2 2 (±)	2 2 +	1030	6,2
	2 2 (±)	3 2 +	1071	6,6
$_{92}U^{240}_{148} \to {}_{93}Np^{240}_{147}$	0 0 +	1 1 (±)	0	5,7
$_{93}Np^{240}_{147} \to {}_{94}Pu^{240}_{146}$	1 1 (±)	0 0 +	0	6,7
	1 1 (±)	2 0 +	43	7,2
	1 1 (±)	0 0 +	858	6,9
	1 1 (±)	2 0 +	900	7,1
	1 1 (±)	2 (2+)	942	6,8
$_{95}Am^{242}_{147} \to {}_{96}Cm^{242}_{146}$	1 0 −	0 0 +	0	7,1
	1 0 −	2 0 +	42	6,8
$_{65}Am^{242}_{147} \to {}_{94}Pu^{242}_{148}$	1 0 −	0 0 +	0	~7,6
	1 0 −	2 0 +	44,5	7,3
$_{95}Am^{244}_{149} \to {}_{96}Cm^{244}_{148}$	1 1 (−)	0 0 +	0	~6,3
Once forbiddcn Class II transitions				
$_{63}Eu^{152}_{89} \to {}_{62}Sm^{152}_{90}$	3 3 −	2 2 +	1087	9,5
	3 3 −	3 2 +	1235	9,7
$_{63}Eu^{154}_{91} \to {}_{64}Gd^{154}_{90}$	3 3 −	2 2 +	996	11,6
	3 3 −	3 2 +	1128	11,0

Note: Most of the experimental data in Tables 2 through 5 have been taken from Dzhelepov & Peker[14]. Supplementary data have been culled from Refs.15 through 21.

Table 2 (cont.)

Initial & final nuclei	$I_i K_i \pi_i$	$I_f K_f \pi_f$	Level in daughter	log ft
1	2	3	4	5
$_{65}Tb^{160}_{95} \rightarrow {}_{66}Dy^{160}_{94}$	3 3 —	2 2 +	966	9,0
	3 3 —	3 2 +	1049	9,1
$_{69}Tm^{170}_{101} \rightarrow {}_{70}Yb^{170}_{100}$	1 1 —	0 0 +	0	8,9
	1 1 —	2 0 +	84	9,3

may be of multipole order $L = 3$ or 4, forbiddenness with respect to Λ (j or l) will be encountered less frequently than in the case of β-transitions.

2. Discussion of Experimental Data

Beta-transitions

Let us consider in some detail the available data on β-transitions in nuclei with even-A. The coupling scheme in the initial state of odd-odd nuclei can readily be determined if we know the spin of this state and the values of Ω_p and Ω_n in deformed nuclei[8,13] or j_p and j_n (from the Mayer model) in spherical nuclei. In order to have definite information on the angular momentum coupling scheme in the final states we selected β-transitions to the ground state or to collective excited states (vibrational or "pair" levels) of even-even nuclei. In these states all the nuclei are paired so that $\Omega_f = \Omega_1 - \Omega_2 = 0$ or $j_f = j_1 - j_2 = 0$. Thereby we restrict our consideration to transitions of two types

$$a)\ \Omega_1 - \Omega_2 \rightarrow \Omega_1 - \Omega_1,$$
$$b)\ \Omega_1 + \Omega_2 \rightarrow \Omega_1 - \Omega_1.$$

transitions in deformed nuclei and analogous transitions in spherical nuclei.

The experimental data on the probabilities (log ft values) of β-transitions in odd-odd nuclei are listed in Table 2 for deformed nuclei and Table 3 for spherical nuclei. All the data are divided into groups according to the transition class and degree of forbiddenness. In order to bring out more clearly the effect of Λ forbiddenness we have excluded from Table 2 β-transitions forbidden with respect to K. We have also left out data on β-decay of Re^{186} and Re^{188}. Gallagher[9] noted that relatively high values of log ft (8.0-8.6) are characteristics of β-transformations of the 111th and 113th neutrons regardless of whether the mass number is even or odd. We note that in the case of transitions to vibrational levels with $K = 2^+$ or $K = 2^-$ (see Table 2) some increase of log ft may be due to change in the shape of the nuclear surface (owing to change of the integral over the vibrational wave functions φ). It will be evident, however, from comparison of the log ft values for β-transitions of classes I and II arriving at levels of the same type (for example, Tb^{160}, Eu^{154} and Ta^{178}) that in most actual cases the retardation is relatively small ($F \approx 10$). Although the data on β-decay of Na^{22}, Na^{24}, Al^{28} and P^{28} have been included in Table 3 (for spherical nuclei), it is possible that these nuclei should be classed as deformed nuclei.

It will be evident from Tables 2 & 3 that β-transitions of class II, as a rule, are characterized by appreciably higher values of log ft. This is understandable inasmuch as in transitions of class I violation of the Λ (j or l) rule,

Table 3

β-transitions in spherical nuclei with even-A

Initial & final nuclei	$I_i \pi_i$	$I_f \pi_f$	Level in daughter	log ft
1	2	3	4	5
Allowed Class I transitions $j_1 - j_2 + a \rightarrow j_1 - j_1$				
$_5B^{12}_7 \rightarrow {}_6C^{12}_6$	1 +	0 +	0	4,2
	1 +	2 +	4400	5,1
	1 +	0 +	7660	4,2
$_{10}Ne^{24}_{14} \rightarrow {}_{11}Na^{24}_{13}$	0 +	1 +	472	4,4
$_{13}Al^{26}_{13} \rightarrow {}_{12}Mg^{26}_{14}$	0 +	0 +	0	3,5
$_{15}P^{32}_{17} \rightarrow {}_{16}S^{32}_{16}$	1 +	0 +	0	7,9
$_{14}Si^{32}_{18} \rightarrow {}_{15}P^{32}_{17}$	0 +	1 +	0	6,7
$_{15}P^{34}_{19} \rightarrow {}_{16}S^{34}_{18}$	1 +	0 +	0	5,1
	1 +	2 +	2127	4,7
$_{17}Cl^{34}_{17} \rightarrow {}_{16}S^{34}_{18}$	0 +	0 +	0	3,5
$_{19}K^{38}_{19} \rightarrow {}_{18}Ar^{38}_{20}$	0 +	0 +	0	3,4
$_{21}Sc^{42}_{21} \rightarrow {}_{20}Ca^{42}_{22}$	0 +	0 +	0	3,0
$_{21}Sc^{44}_{23} \rightarrow {}_{20}Ca^{44}_{24}$	3 +	2 +	1130	5,3
$_{23}V^{46}_{23} \rightarrow {}_{22}Ti^{46}_{24}$	0 +	0 +	0	3,5
$_{25}Mn^{50}_{25} \rightarrow {}_{24}Cr^{50}_{26}$	0 +	0 +	0	3,5
$_{23}V^{52}_{29} \rightarrow {}_{24}Cr^{52}_{28}$	2 +	2 +	1460	5,5
$_{25}Mn^{52}_{27} \rightarrow {}_{24}Cr^{52}_{28}$	2 +	2 +	1460	5,3
$_{27}Co^{54}_{27} \rightarrow {}_{26}Fe^{54}_{28}$	0 +	0 +	0	3,5
$_{27}Co^{58}_{31} \rightarrow {}_{26}Fe^{58}_{32}$	2 +	2 +	814	6,6
	2 +	2 +	1820	7,5
$_{27}Co^{60}_{33} \rightarrow {}_{28}Ni^{60}_{32}$	2 +	2 +	1330	7,2
$_{29}Cu^{64}_{35} \rightarrow {}_{28}Ni^{64}_{36}$	1 +	0 +	0	5,0
	1 +	2 +	1340	5,6
$_{29}Cu^{64}_{35} \rightarrow {}_{30}Zn^{64}_{34}$	1 +	0 +	0	5,2
$_{28}Ni^{66}_{38} \rightarrow {}_{29}Cu^{66}_{37}$	0 +	1 +	0	3,9
$_{29}Cu^{66}_{37} \rightarrow {}_{30}Zn^{66}_{36}$	1 +	0 +	0	5,4
	1 +	2 +	1050	5,6
$_{31}Ga^{66}_{35} \rightarrow {}_{30}Zn^{66}_{36}$	0 +	0 +	0	7,8
$_{31}Ga^{68}_{37} \rightarrow {}_{30}Zn^{68}_{38}$	1 +	0 +	0	5,2
	1 +	2 +	1020	5,3
$_{31}Ga^{70}_{39} \rightarrow {}_{32}Ge^{70}_{38}$	1 +	0 +	0	5,1
	1 +	2 +	1036	5,6
	1 +	0 +	1210	5,9
$_{35}Br^{78}_{43} \rightarrow {}_{34}Se^{78}_{44}$	1 +	0 +	0	4,4
$_{35}Br^{80}_{45} \rightarrow {}_{34}Se^{80}_{46}$	1 +	0 +	0	4,6
$_{35}Br^{80}_{45} \rightarrow {}_{36}Kr^{80}_{44}$	1 +	0 +	0	5,5
	1 +	2 +	620	5,6
$_{37}Rb^{82}_{45} \rightarrow {}_{36}Kr^{82}_{46}$	1 +	0 +	0	4,3
$_{43}Tc^{94}_{51} \rightarrow {}_{42}Mo^{94}_{52}$	2 +(3+)	2 +	870	5,4
$_{45}Rh^{98}_{53} \rightarrow {}_{44}Ru^{98}_{54}$	2 +	2 +	660	4,9

Table 3 (cont.)

Initial & final nuclei	$I_i \pi_i$	$I_f \pi_f$	Level in daughter	log ft
1	2	3	4	5
$_{45}Rh^{104}_{59} \rightarrow {}_{46}Pd^{104}_{58}$	1 +	0 +	0	4,5
	1 +	2 +	556	5,8
$_{45}Rh^{106}_{61} \rightarrow {}_{46}Pd^{106}_{60}$	1 +	0 +	0	5,2
	1 +	2 +	513	6,4
$_{47}Ag^{106}_{59} \rightarrow {}_{46}Pd^{106}_{60}$	1 +	0 +	0	4,9
	1 +	2 +	513	5,2
$_{47}Ag^{108}_{61} \rightarrow {}_{46}Pd^{108}_{62}$	1 +	0 +	0	4,8
	1 +	2 +	430	6,0
	1 +	2 +	1030	4,8
$_{47}Ag^{108}_{61} \rightarrow {}_{48}Cd^{108}_{60}$	1 +	0 +	0	4,6
	1 +	2 +	637	6,0
$_{49}In^{108}_{59} \rightarrow {}_{48}Cd^{108}_{60}$	2 +	2 +	637	6,0
$_{47}Ag^{110}_{63} \rightarrow {}_{48}Cd^{110}_{62}$	1 +	0 +	0	5,1
	1 +	2 +	656	4,5
$_{49}In^{114}_{65} \rightarrow {}_{48}Cd^{114}_{66}$	1 +	0 +	0	4,6
$_{49}In^{114}_{65} \rightarrow {}_{50}Sn^{114}_{64}$	1 +	0 +	0	4,6
	1 +	2 +	1300	5,7
$_{49}In^{116}_{67} \rightarrow {}_{50}Sn^{116}_{66}$	1 +	0 +	0	5,0
$_{51}Sb^{120}_{69} \rightarrow {}_{50}Sn^{120}_{70}$	1 +	0 +	0	4,5
	1 +	2 +	1180	5,5
$_{53}I^{128}_{75} \rightarrow {}_{52}Te^{128}_{76}$	1 +	0 +	0	5,2
	1 +	2 +	750	5,7
$_{53}I^{128}_{75} \rightarrow {}_{54}Xe^{128}_{74}$	1 +	0 +	0	6,1
	1 +	2 +	460	6,3
	1 +	2 +	990	6,6
$_{55}Cs^{128}_{73} \rightarrow {}_{54}Xe^{128}_{74}$	1 +	0 +	0	4,8
$_{55}Cs^{130}_{75} \rightarrow {}_{54}Xe^{130}_{76}$	1 +	0 +	0	5,1
$_{55}Cs^{130}_{75} \rightarrow {}_{56}Ba^{130}_{74}$	1 +	0 +	0	4,9
$_{59}Pr^{140}_{81} \rightarrow {}_{58}Ce^{140}_{82}$	1 +	0 +	0	4,3
Allowed Class II transitions $j_1 + j_2 - a \rightarrow j_1 - j_2$				
$_{6}C^{14}_{8} \rightarrow {}_{7}N^{14}_{7}$	0 +	1 +	0	9,0
$_{8}O^{14}_{6} \rightarrow {}_{7}N^{14}_{7}$	0 +	1 +	0	7,6
$_{10}Ne^{18}_{8} \rightarrow {}_{9}F^{18}_{9}$	0 +	1 +	0	2,9
$_{9}F^{18}_{9} \rightarrow {}_{8}O^{18}_{10}$	1 +	0 +	0	3,6
$_{11}Na^{22}_{11} \rightarrow {}_{10}Ne^{22}_{12}$	3 +	2 +	1280	7,3
$_{11}Na^{24}_{13} \rightarrow {}_{12}Mg^{24}_{12}$	4 +	3 +	5230	6,8
$_{13}Al^{28}_{15} \rightarrow {}_{14}Si^{28}_{14}$	3 +	2 +	1790	4,9
$_{15}P^{28}_{13} \rightarrow {}_{14}Si^{28}_{14}$	(3 +)	2 +	1790	4,9
$_{15}P^{30}_{15} \rightarrow {}_{14}S^{30}_{16}$	1 +	0 +	0	5,0
	1 +	2 +	2240	5,4
$_{17}Cl^{34}_{17} \rightarrow {}_{16}S^{34}_{18}$	3 +	2 +	2127	6,1
$_{19}K^{38}_{19} \rightarrow {}_{18}Ar^{38}_{20}$	3 +	2 +	2150	5,0
$_{23}V^{48}_{25} \rightarrow {}_{22}Ti^{48}_{26}$	4 +	4 +	2310	6,1
$_{25}Mn^{54}_{29} \rightarrow {}_{24}Cr^{54}_{30}$	3 +	2 +	835	6,1

Table 3 (cont.)

Initial & final nuclei	$I_i \pi_i$	$I_f \pi_f$	Level in daughter	log ft
1	2	3	4	5
$_{25}Mn^{56}_{31} \rightarrow {}_{26}Fe^{56}_{30}$	3 +	2 +	845	7,2
$_{27}Co^{56}_{30} \rightarrow {}_{26}Fe^{56}_{30}$	4 +	4 +	2080	8,6
$_{27}Co^{60}_{33} \rightarrow {}_{28}Ni^{60}_{32}$	5 +	4 +	2160	7,4
$_{29}Cu^{60}_{31} \rightarrow {}_{28}Ni^{60}_{32}$	2 +	2 +	2133	7,4
$_{47}Ag^{110}_{63} \rightarrow {}_{48}Cd^{110}_{62}$	6 +	6 +	2476	8,1
$_{49}In^{114}_{65} \rightarrow {}_{48}Cd^{114}_{66}$	5 +	4 +	1278	7,5
$_{77}Ir^{192}_{115} \rightarrow {}_{78}Pt^{192}_{114}$	(4 +)	4 +	784	8,6
Once forbidden Class I transitions				
$_{17}Cl^{38}_{21} \rightarrow {}_{18}Ar^{38}_{20}$	2 −	2 +	2150	6,9
$_{19}K^{42}_{23} \rightarrow {}_{20}Ga^{42}_{22}$	2 −	2 +	1530	7,5
$_{33}As^{74}_{41} \rightarrow {}_{32}Ge^{74}_{42}$	2 −	2 +	596	7,9
$_{33}As^{74}_{41} \rightarrow {}_{34}Se^{74}_{40}$	2 −	2 +	635	7,5
$_{33}As^{76}_{43} \rightarrow {}_{34}Se^{76}_{42}$	2 −	2 +	550	8,5
$_{37}Rb^{84}_{47} \rightarrow {}_{36}Kr^{84}_{48}$	2 −	2 +	880	7,3
$_{37}Rb^{86}_{49} \rightarrow {}_{38}Sr^{86}_{48}$	2 −	2 +	1080	7,7
$_{37}Rb^{88}_{51} \rightarrow {}_{38}Sr^{88}_{50}$	2 −	2 +	1850	7,9
$_{39}Y^{92}_{53} \rightarrow {}_{40}Zr^{92}_{52}$	2 −	2 +	930	8,0
$_{41}Nb^{94}_{53} \rightarrow {}_{42}Mo^{94}_{52}$	2 −	2 +	870	7,3
$_{45}Rh^{100}_{55} \rightarrow {}_{44}Ru^{100}_{56}$	2 −	2 +	535	8,3
	2 −	2 +	1360	7,7
$_{51}Sb^{122}_{71} \rightarrow {}_{50}Sn^{122}_{72}$	2 −	2 +	1137	7,0
$_{51}Sb^{122}_{71} \rightarrow {}_{52}Te^{122}_{70}$	2 −	2 +	566	7,6
	2 −	2 +	1258	7,7
$_{51}Sb^{124}_{73} \rightarrow {}_{52}Te^{124}_{72}$	3 −	2 +	602	10,5
$_{53}I^{126}_{73} \rightarrow {}_{52}Te^{126}_{74}$	2 −	2 +	650	7,4
$_{53}I^{126}_{73} \rightarrow {}_{54}Xe^{126}_{72}$	2 −	2 +	386	7,9
$_{53}I^{126}_{73} \rightarrow {}_{54}Xe^{126}_{72}$	2 −	2 +	862	7,6
$_{53}I^{132}_{79} \rightarrow {}_{54}Xe^{132}_{78}$	5 −	4 +	1450	7,5
$_{55}Cs^{138}_{83} \rightarrow {}_{56}Ba^{138}_{82}$	3 −	2 +	1426	7,6
$_{57}La^{140}_{83} \rightarrow {}_{58}Ce^{140}_{82}$	3 −	2 +	1596	9,1
$_{59}Pr^{142}_{83} \rightarrow {}_{60}Nd^{142}_{84}$	2 −	2 +	1572	7,4
$_{58}Ce^{144}_{86} \rightarrow {}_{59}Pr^{144}_{85}$	0 +	0 −	0	7,6
$_{59}Pr^{144}_{85} \rightarrow {}_{60}Nd^{144}_{84}$	0 −	0 +	0	6,6
$_{79}Au^{196}_{117} \rightarrow {}_{80}Hg^{196}_{116}$	2 −	2 +	426	7,0
$_{79}Au^{198}_{119} \rightarrow {}_{80}Hg^{198}_{118}$	2 −	2 +	411	7,5
	2 −	2 +	1090	7,8
$_{79}Au^{200}_{121} \rightarrow {}_{80}Hg^{200}_{120}$	1 −	0 +	0	6,9

Table 3 (cont.)

Initial & final nuclei	$I_i \pi_i$	$I_f \pi_f$	Level in daughter	log ft
1	2	3	4	5
$_{81}Tl^{200}_{119} \rightarrow {}_{80}Hg^{200}_{120}$	2 —	2 +	368	7,8
$_{81}Tl^{206}_{125} \rightarrow {}_{82}Pb^{206}_{124}$	0 —	0 +	0	5,2
$_{82}Pb^{212}_{130} \rightarrow {}_{83}Bi^{212}_{129}$	0 +	1 —	0	6,6
$_{82}Pb^{214}_{132} \rightarrow {}_{83}Bi^{214}_{131}$	0 +	1 —	0	6,5
$_{83}Bi^{214}_{131} \rightarrow {}_{84}Po^{214}_{130}$	1 —	0 +	0	7,9

Table 4

Isomeric transitions of class II in deformed odd-odd nuclei

Nuclcus	$T_{1/2}$	E_γ, kcv	Multi-pole order	$\nu = \Delta K - L$	$F = \frac{T_{exp}}{T_{theo}}$
$_{11}Na^{22}_{11}$	$0{,}226 \cdot 10^{-6}$ scc	593	$E2$	1	$\sim 10^2$
$_{11}Na^{24}_{13}$	0,02 scc	472	$M3$	0	~ 1
$_{63}Eu^{152}_{89}$	>9,2 hr	50	$M3$	0	$>5 \cdot 10^6$
$_{65}Tb^{156}_{91}$	5,0 hr	88,4	$E3$	0	$\sim 10^5$
$_{65}Tb^{158}_{93}$	11 scc	111	$M3$	0	$\sim 10^2$
$_{67}Ho^{160}_{93}$	>5 hr	60	$E3$	0	$\geqslant 10^5$
$_{71}Lu^{174}_{103}$	165 days	59	$M3$	2	10^8
$_{95}Am^{242}_{147}$	152 ycars	48,6	$E4$	1	$\sim 10^6$

Table 5

Isomeric M4 type transitions in spherical odd-odd nuclei

Nuclcus	$I_i \pi_i j_{pi} j_{ni}$	$I_f \pi_f j_{pf} j_{nf}$	E_γ, kcv	F
Class I transitions				
$_{81}Tl^{196}_{115}$	$7^+,\ s_{1/2} + i_{13/2}$	$3^-,\ s_{1/2} + f_{5/2}$	120	~ 10
$_{81}Tl^{198}_{117}$	$7^+,\ s_{1/2} + i_{13/2}$	$3^-,\ s_{1/2} + f_{5/2}$	261	~ 10
Class II transitions				
$_{47}Ag^{110}_{63}$	$6^+,\ g_{9/2} + d_{5/2}$	$2^-,\ p_{1/2} - d_{5/2}$	116	10^3

as was already noted, is relatively rare. In both classes of transitions there is a clear distinction between transitions that are allowed or forbidden with respect to Λ (j or l). For example, in β-decay of P^{32}, which is allowed and belongs in class I, the neutron goes over from the $d_{5/2}$ ($l = 2$) level to the $s_{1/2}$ ($l = 0$) level. Here $L = 1$ and $\Delta l = 2$, that is, the transition is forbidden as regards l (log ƒt = = 7.9). Another example is furnished by the transitions $Ne^{18} \rightarrow F^{18}$, $F^{18} \rightarrow O^{18}$ and $P^{30} \rightarrow Si^{30}$, which are transitions of class II and hence should in general be characterized by large values of log ƒt. According to the experimental data, however, these transitions are not retarded as is indicated by the low values of log ƒt (3.5 to 5). This can be readily understood inasmuch as in these data the odd protons and neutrons are in states $s_{1/2}$ ($l_1 = l_2 = 0$) and the transitions are allowed as regards l. It must be admitted that the reason for the low values of log ƒt in Al^{28} and K^{38} is unclear at present.

Gamma-transitions

At present analysis of γ-transitions in odd-odd nuclei is necessarily limited to analysis of isomeric transitions with $L \geqslant 2$ inasmuch as adequate experimental data are available only for such transitions. In most cases these transitions belong in class II, i.e., are accompanied by change in the angular momentum coupling scheme. States with a high spin are, apparently, formed as a result of

addition of the momenta of the unpaired nucleons (Ω or j), while states with low spin are formed by subtraction of the odd nucleon momenta. Isomeric transitions between the end members of multiplets, and in deformed nuclei - doublets, are always accompanied by change of the coupling scheme.

In Table 4 we list the available experimental data on isomeric transitions of class II in deformed nuclei. In Na^{22}, Na^{24}, Tb^{158}, Lu^{174} and Am^{242} these transitions occur between the two members of one doublet.

Except for the γ-transitions in Na^{22} and Na^{24}, where $\Delta\Lambda = \Lambda_i + \Lambda_f \leqslant L$ and, consequently, there is no Λ forbiddenness*, all the other transitions are strongly retarded. This retardation may be due to Λ forbiddenness.**

For γ-transitions of class II in spherical nuclei there should be observed analogous forbiddenness with respect to j or l. For illustration, in Table 5 we list the available data on the probabilities of M4 type transitions where forbiddenness obtains only for transitions involving change of the coupling scheme.

The data listed in Tables 2-5 clearly show the substantial influence of the Λ (j or l) selection rules for β- and γ-transitions in even-A nuclei.

Thus, for the purpose of characterizing the states of odd-odd and even-even deformed and spherical nuclei in addition to I, K and Ω (I and j) there can be used, as in the case of odd-even nuclei, the quantum numbers Λ (j or l). This inference is in agreement with the data of Gallagher & Moszkowski[8], who showed that the introduction of the asymptotic quantum numbers Λ and Σ is important for classification of the states of odd-odd nuclei.

We are grateful to M.A.Listengarten for useful discussions.

Scientific-Research Physical Institute of
Leningrad State University &
Leningrad Chemical-Pharmeceutical Institute

References

1. S.G.Nilsson, Kgl.Danske Videnskab.Selskab, Mat.-fys.Medd., 29, No.16 (1955).

2. B.Mottelson & S.Nilsson, Dan.Mat.Fys.Skr., 1, No.8 (1959).

3. B.S.Dzhelepov & L.K.Peker, Vozbuzhdennye urovni deformirovannykh yader (Excited staes of deformed nuclei), Dubna, 1959.

4. F.Stephens, F.Asaro & I.Perlman, Phys.Rev., 113, 212 (1959).

5. G.Alaga, Phys.Rev., 100, 432 (1955); Nucl.Phys., 4, 625 (1957).

6. M.E.Voikhanskii, Zhur.eksp.i teor.fiz., 33, 1004, 1054 (1957). (Trans. Soviet Physics - JETP.)

7. Yu.N.Gnedin, Izv.AN SSSR, Ser.fiz., 25, No.1 (1961). (Trans.Bulletin, 25, No.1).

8. C.Gallagher & S.Moszkowski, Phys.Rev., 111, 1282 (1958).

9. C.Gallagher, Nucl.Phys., 16, 215 (1960).

10. D.A.Varshalovich & L.K.Peker, Present issue of the Bulletin, p.274.

11. G.Alaga, K.Alder, A.Bohr & B.Mottelson, Kgl.Danske Videnskab Selskab. Mat.-fys.Medd., 29, No.9 (1955).

12. P.M.Morse & H.Feshbach, Methods of Theoretical Physics, Vol.II, Chapt.12, N.Y., 1953 (Cited in Russian trans.).

13. L.K.Peker, Izv.AN SSSR, Ser.fiz., 21, 1029 (1957). (Trans.Bulletin,21,1030.

---

*The retardation of the transition in Na^{22} ($F \approx 10^2$) can be due entirely to weak K forbiddenness: $\nu = \Delta K - L = 1$.

**In Lu^{174} and Am^{242} the retardation may be partially due to K forbiddenness.

14. B.S.Dzhelepov & L.K.Peker, Skhemy raspada radioaktivnykh yader (Decay schemes of radioactive nuclei), M., 1958.

15. G.M.Temmer & N.P.Heydenburg, Phys.Rev., 111, 1303 (1958).

16. N.M.Anton'eva, A.A.Bashilov & E.K.Kulakovskii, ?. (The journal and page citation in the Russian original is nonexistent. Translator.)

17. D.E.Alburger, S.Ofer & M.Goldhaber, Phys.Rev., 112, 1998 (1958).

18. R.G.Helmer & S.B.Burson, Phys.Rev., 119, 788 (1960).

19. B.Jung & G.Andersson, Nucl.Phys., 15, 108 (1960).

20. F.Asaro, I.Perlman, J.O.Rasumssen & S.G.Thompson, Nucl.Phys., 16, 215 (1960).

21. M.E.Bunkder, B.J.Dropesky, J.D.Knight, J.W.Starner & B.Warren, Phys.Rev., 116, 143 (1959).

YIELD OF GAMMA-RADIATION IN INELASTIC SCATTERING OF NEUTRONS FROM ANTIMONY NUCLEI

- D.L.Broder, A.I.Lashuk & I.P.Sadokhin

In the present work we measured the yield of 1.01 Mev γ-rays emitted in inelastic scattering of protons by antimony nuclei.

In the experiments we employed the ring geometry developed by Androsenko et al[1] and diagramed in Fig.1. The scattering specimens were rings 30 mm thick with an outside diameter of 85 mm and an inside diameter of 60 mm. The crystal was shielded from direct radiation from the target by a lead cone 360 mm high with a base diameter of 58 mm. The γ-radiation spectrum was investigated by means of a scintillation spectrometer with a 40 mm diameter, 40 mm thick NaI(Tl) crystal (relative half-width of the Zn^{65} 1.12 Mev line ~9%). The pulse distribution was analyzed by means of a 128-channel pulse height analyzer.

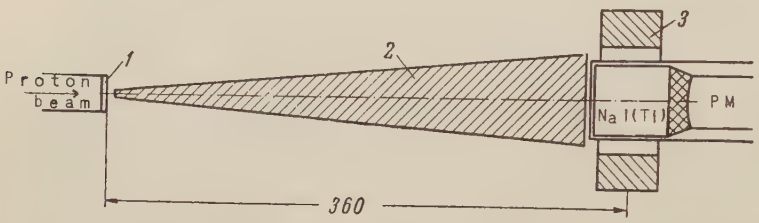

Fig.1. Experimental arrangement: 1 - tritium target, 2 - lead cone, 3 - scattering ring.

The neutrons were obtained by means of the $H^3(p,n)He^3$ reaction, the 1.5 to 3.3 Mev protons being accelerated in an electrostatic generator. The energy width of the neutron beam did not exceed 30 kev. The neutron flux was monitored by a long boron counter and a U^{235} fission chamber.

We carried out two types of measurements: with the specimen in place and without it. The difference between the γ-ray spectra measured at a neutron energy lower than the energy of the investigated level ($E_n < E_i$) with and without the specimen in place yields the pulse spectrum due to elastic scattering of the neutrons, corrected for the ratio of the cross sections for elastic scattering of neutrons at the given energy and scattering of neutrons with an energy lower than the threshold for excitation of the investigated level. No correction for absorption of the γ-rays by the specimen was introduced.

The value of the relative γ-ray yield was calculated by measuring the area under the photopeaks of the amplitude spectra, from which there was subtracted beforehand the contribution from γ-rays of higher energies, if these were present. It was assumed that the anisotropy of the emitted γ-radiation was weak and that the "poor" geometry effected satisfactory averaging over the angular distribution.

For the purpose of obtaining the absolute values of the yield of γ-rays emitted in inelastic scattering as a function of the neutron energy we investigated the yield of 0.84 Mev γ-rays from iron. The observed 0.84 Mev γ-ray yields from iron were matched with the γ-ray yield curve (cross section curve) given by Kiehn & Goodman[2]. The absolute values of the yield of 1.01 Mev γ-rays from antimony were obtained by comparison with the cross section for the yield of 0.84 Mev γ-rays from iron, taking into account the efficiency of the crystal. No correction for neutron absorption by the specimen was introduced.

We obtained an efficiency vs γ-ray energy curve for the NaI(Tl) crystal. To this end we used γ-sources with cascade transitions. The sources were prepared in the form of solutions which were poured into containers of plexiglas of the same size and shape as the ring scatterer, or the same scattering specimens were irradiated directly by 14 Mev neutrons on a neutron generator. The sources[3] and cascades[4] utilized for calibrating the spectrometer are listed in the accompanying

Sources used in calibrating the γ-spectrometer

γ-sources	Cascade transitions, Mev
$Al^{27}(np)Mg^{27}$	0,175—0,834
$Al^{27}(n\alpha)Na^{24}$	2,750—1,380
$K^{39}(n2n)K^{38}$	0,51—2,160
$Ti^{48}(np)Sc^{48}$	1,050—1,320—0,990
$Fe^{56}(np)Mn^{56}$	1,810—0,845; 2,130—0,845
$Cu^{65}(n2n)Cu^{64}$	0,510—1,340
Co^{60}	1,170—1,332

table. In order to obtain a pulse spectrum free of a contribution from Compton scattering we constructed a numerical matrix of the amplitude Compton distributions.[5] We used the following sources with single γ-lines, also of the same shape and size as the scattering rings: Hg^{203}(0.279), Ru^{103}(0.498), Cs^{137}(0.661), Zr^{95}(0.76), Zn^{65}(1.12, Si^{28}(n,p) Al^{28}(1.780), and Mn^{55}(n,α) V^{52}(1.440 Mev).

The data given in the present report are averaged values for two series of measurements of the γ-ray yields.

In the work of other investigators[6-8] there were observed γ-lines of the following energies emitted in inelastic scattering of 3.0, 2.8 and 3.7 Mev neutrons from antimony: 0.49, 0.59, 1.01, 1.32, 1.50, 1.84, 1.96 and 2.16 Mev. According to the decay scheme given in Ref.4, the 0.49 and 0.59 Mev γ-rays are apparently due to de-excitation of 0.506 and 0.573 Mev levels in Sb^{121}. The present measurements which were carried out with neutrons with energies from 0.9 to 2.5 Mev substantiate the existence of these γ-rays. Detailed analysis of the spectrum in the 1 to 1.5 Mev region is hampered owing to the low intensity of the proposed 1.32 Mev line. At present we can only note that excitation of the 1.32 and 1.50 Mev lines occurs as one approaches a neutron energy of 1.5 Mev, which indicates the existence in Sb^{121} or Sb^{123} of a level at 1.50 and possibly a level at 1.32 Mev. It is not impossible, however, that there occurs a cascade transition from the 1.5 Mev level (if it is excited in Sb^{123}) to the level at 0.153 Mev with emission of γ-rays of 1.347 Mev energy.

The appearance in the γ-ray spectrum of a line at 1.01 Mev is observed when the neutron energy is increased through ~1 Mev. This indicates that the antimony nuclei have an energy level in the vicinity of 1 Mev, which is excited in the process of inelastic scattering of neutrons. At a neutron energy exceeding 1.01 Mev there is also evinced in the γ-ray spectrum a line with an energy of about 0.87 Mev. With increase of the neutron energy, owing to inadequate resolution of the spectrometer, this line merges with the 1.01 Mev line (Fig.2). It may be inferred, therefore, that there is another level in antimony in the vicinity of 0.9 Mev. Another possibility, if the 1.01 Mev level belongs to Sb^{123}, is that there occurs a transition from the 1.01 Mev excited state to the level at 0.153 Mev with emission of 0.847 Mev γ-rays. At present, however, it is impossible to assign the indicated levels to a specific antimony isotope.

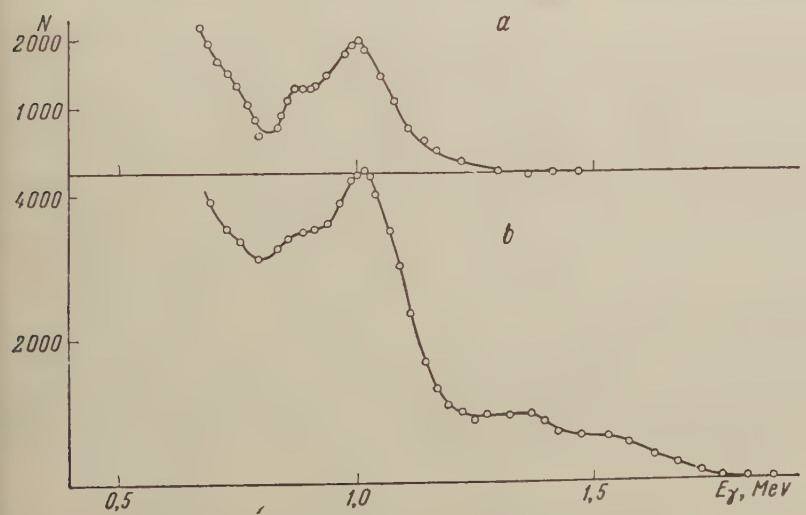

Fig.2. Gamma-ray spectra in the E = 0.5 to 1.5 Mev region: a - E_n = 1.4 Mev, b - E_n = 2.2 Mev.

Fig.3 shows the variation in the yield of 1.01 Mev γ-rays with the neutron energy

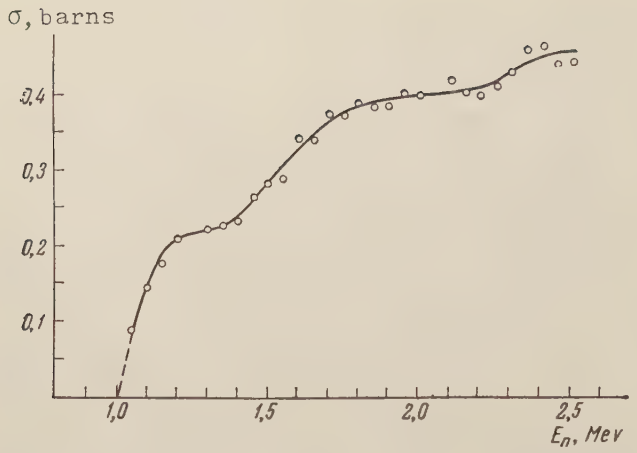

Fig.3. Yield of 1.01 Mev γ-rays emitted in inelastic scattering of neutrons by antimony nuclei.

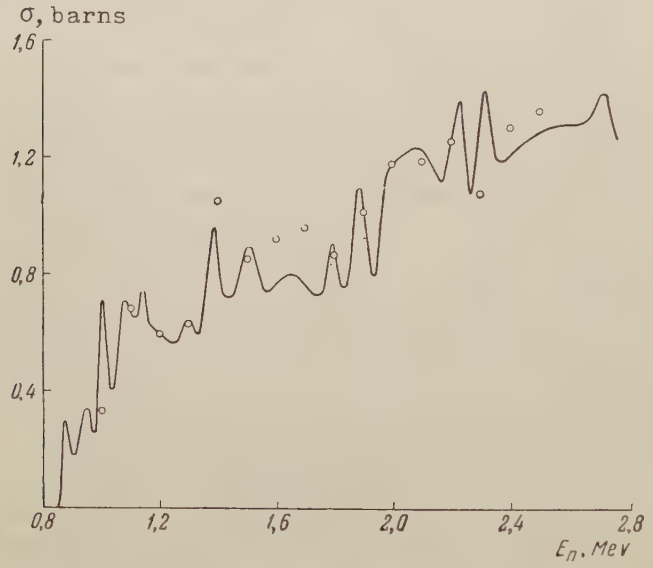

Fig.4. Curve - neutron inelastic scattering cross section of iron according to Kiehn & Goodman[2]; points - our experimental values for the yield of 0.84 Mev γ-rays, normalized to fit the curve at 2.0 Mev energy.

in the range from 1.0 to 2.5 Mev. It may be asserted that for neutron energies from 1.0 to 1.5 Mev this curve corresponds to excitation of the 1.01 Mev level in the antimony nuclei. There can be no cascade transition from the 1.32 Mev level to this level since there has been detected no line with an energy of 0.3 Mev in the γ-ray spectra of antimony. From the proposed 1.50 Mev level there may depart a cascade transition to the 1.01 Mev level or to the level at 0.506 Mev with emission of γ-rays of energies ~0.5 or ~1.0 Mev.

Fig.4 shows the variation in the yield of 0.84 Mev γ-rays emitted in inelastic scattering of neutrons from iron. The curve in this figure is the inelastic scattering cross section curve obtained by Kiehn & Goodman[2]. The points are our experimental values normalized to fit the curve at a neutron energy of 2.0 Mev.

References

1. A.L.Androsenko, D.L.Broder & A.I.Lashuk, Atomnaya energiya, 7, 268 (1959). (Trans.Soviet Jour.of Atomic Energy.)

2. R.M.Kiehn & C.Goodman, Phys. Rev., 95, 989 (1954).

3. N.A.Vlasov, Neitrony (Neutrons), M., 1955.

4. B.S.Dzhelepov & L.K.Peker, Skhemy raspada radioaktivnykh yader (Decay schemes of radioactive nuclei), M.-L., 1958.

5. Yu.A.Kazanskii, PTE, No.4 (1959). (Trans.Instruments & Exper. Techniques.)

6. A.L.Androsenko, D.L.Broder & A.I.Lashuk, Atomnaya energiya (In press). (Trans.Soviet Journal of Atomic Energy.)

7. I.F.Barchuk, M.V.Pasechnik & Yu.A.Tsybul'ko, Atomnaya energiya, February, 1958. (Trans.Soviet Journal of Atomic Energy.)

8. M.A.Rothman, H.S.Hans & C.E.Mandeville, Phys.Rev., 100, 83 (1955).

Bulletin of the Academy of Sciences of the USSR - Physical Series
Vol. 25, No. 2 - February 1961

Transactions of the Eleventh Annual Conference on Nuclear Spectroscopy
(to be continued in Vol. 25, Nos. 7, 9 & 10)

TABLE OF CONTENTS

	Page Orig.	Trans.
Structure of light nuclei - V.V.Balashov, V.G.Neudachin & Yu.F.Smirnov	170	165
Shape of the β-spectrum of A^{41} - G.R.Kartashov, N.A.Burgov & A.V.Davydov	189	184
Conversion electron spectrum of the holmium fraction formed in proton bombardment of Ta - A.S.Basina, K.Ya.Gromov, B.S. Dzhelepov & V.A.Morozov	194	188
Relative intensities of some gamma-lines in the spectrum of Ta^{182} - V.D.Vitman, N.A.Voinova, B.S.Dzhelepov & A.A.Karan	199	192
Relative intensities of gamma-rays from RaC in the 1300 to 2520 kev region - V.D.Vitman, B.S.Dzhelepov & A.A.Karan	201	194
Gamma-radiation from Eu^{146} - E.E.Berlovich, V.N.Klement'ev, L.V.Krasnov & M.K.Nikitin	207	200
Levels of Eu^{147}, Eu^{149} and Eu^{151} - E.E.Berlovich, V.N.Klement'ev, L.V.Krasnov & M.K.Nikitin	212	204
Measurements of the lifetimes of the first excited states of Tb^{159} and Yb^{173} by means of a multichannel time analyzer - E.E. Berlovich, M.P.Bonitz & V.V.Nikitin	218	210
Determination of the K fluorescence coefficients of V^{51}, Mn^{55}, Cu^{65} and Ga^{71} - A.A.Konstantinov, I.A.Sokolova & T.E.Sazonova	228	219
Gamma-radiation from Ta^{182} - N.A.Voinova, B.S.Dzhelepov & Yu.V. Khol'nov	233	223
A high-resolution ionization alpha-spectrometer - G.E.Kocharov & G.A.Korolev	237	227
A mercury gamma-calorimeter - E.A.Khol'nova	257	246
Two-crystal spectrometer and its use for investigating the (p,γ) reaction - Yu.P.Antuf'ev, V.Yu.Gonchar, E.G.Kopanets, A.N.L'vov & S.P.Tsytko	261	249
Radiative proton capture by S^{34} - Yu.P.Antuf'ev, A.K.Val'ter, V.Yu.Gonchar, E.G.Kopanets, A.N.L'vov & S.P.Tsytko	265	252
Measurement of the number of gamma-rays per decay of Mo^{99} - A.N.Silant'ev	270	256
Measurement of the number of gamma-rays per decay of Ba^{140} and Pr^{144} - B.S.Kuznetsov & A.N.Silant'ev	272	258
Conversion transitions accompanying α-decay of Th^{229} and the level diagram for Ra^{225} - E.F.Tret'yakov, N.I.Pirogova & L.L.Gol'din	274	260
Concerning electromagnetic transitions of multipole order $L = \lvert J_i - J_f \rvert + 1$ - M.E.Voikhanskii	283	271
Distinctive features of deformed odd-odd nuclei with K = 0 - D.A.Varshalovich & L.K.Peker	287	274

Concerning selection rules for β- and γ-transitions in odd-odd nuclei - M.E.Voikhanskii & L.K.Peker 297 284
Yield of gamma-radiation in inelastic scattering of neutrons from antimony nuclei - D.L.Broder, A.I.Lashuk & I.P.Sadokhin 309 296

Translated in 1962 by
Columbia Technical Translations
5 Vermont Ave., White Plains, N.Y.

Transactions

of the

Ninth All-Union Conference on Luminescence (Crystal Phosphors)

(Kiev, 20-25 June 1960)

(Continued from Vol.25, No.1; to be continued in Vol.25, No.4)

CONCERNING EXCITATION OF CRYSTAL PHOSPHORS BY IONS

- B.M.Nosenko & N.A.Strukov

Luminescence of phosphors under excitation by atomic particles with energies up to 10 kiloelectron-volts is a phenomenon that has been little studied. The significance of this form of excitation is not limited to questions connected with the ion spot on the screens of cathode-ray tubes and the possibility of measuring weak ion currents and particle energies by observation of the excited luminescence. Ionoluminescence can also serve as the means for investigating the mechanism of interaction of atomic particles with crystals. Our research was concerned mainly with these problems.

We investigated the luminescence and changes in the properties of ZnS:Ag (Type K-5), 55% ZnS·45% CdS:Ag (L-4), 62% ZnS·38% ZnSe:Ag (K-38), 90% ZnS·10% CdS:Cu (L-10), ZnO:Zn (K-20), Zn_2SiO_4:Mn (K-35), $CaWO_4$ and $CaSO_4$:Mn phosphors under excitation by Li, Na, K, Rb and Cs ions with energies up to 6 kev.

1. Luminance under ionic excitation

The ionoluminescence output is proportional to the current density (in the range from 10^{-10} to 10^{-8} amp/cm^2). The variation in brightness E_i as a function of the ion energy, as in the case of cathodoluminescence, is parabolic in the range of low ion energies V and becomes linear in the range of high V. The luminescence threshold energy for different phosphors, which varied from 1.5 to 0.7 kev, was found to be higher for phosphors with a large "dead potential" under electron (CR) excitation (K-5 & K-38). The brightness E_i under ionic excitation was compared with the brightness E_e under CR excitation under equal conditions (same energy and current density). The values of $B = E_i/E_e$ for V = 6 kev are listed in Table 1. These values are only indicative inasmuch as they are strongly dependent on the state of the phosphor surface, particularly in the case of heavy ions.

Table 1

Values of $B = E_i/E_e$ for V = 6 kev (in percent)

Ion	ZnS—Ag	ZnS.CdS—Ag	ZnS.ZnSe—Ag	ZnS.CdS—Cu	ZnO—Zn	Zn_2SiO_4—Mn	$CaWO_4$	$CaSO_4$—Mn
Li^+	2,2	5	3,1	3	5,8	—	6,4	6,7
Na^+	—	1	—	—	5	2,9	2,5	—
K^+	1	1	0,8	2,3	4,5	2	1,8	1,8
Rb^+	0,7	0,35	0,1	—	—	1,3	1,1	1,4
Cs^+	0,15	0,35	0,1	0,95	4,0	0,8	0,7	0,8

It is interesting to note that B for all the investigated phosphors is of the same order of magnitude, whereas the cathodoluminescence output of these phosphors varies by a factor of more than 20 (ZnS:Ag and $CaSO_4$:Mn). The value of B determines the lower bound of the fraction of the ion energy expended on electronic excitation, and comparison of this quantity with the ion range (in the sense of the depth of the excited layer) yields a measure of the excitation produced by collisions of the ions with the atoms of the crystal.

2. Aging (disintegration) of the phosphors

Excitation by ions is accompanied by disintegration of the phosphor, which

is evinced in decrease of the luminance with time (aging or ion burn).

The decrease in brightness depends directly on the bombardment charge $Q = jt$ (t is the bombardment time), which indicates that the process involved is elementary. Aging is the result of disturbance of the crystal lattice owing to elastic collisions of the ions with the atoms of the crystal. The different phosphors differ markedly as regards aging. Thus in the case of 55ZnS·45CdS:Ag and 62ZnS·38ZnSe:Ag (group I) the luminance fell off 50% as a result of irradiation with a charge $Q_{1/2} = 6 \cdot 10^{-8}$ coulomb/cm^2 = $5 \cdot 10^{11}$ particles/cm^2; after bombardment with a charge $5Q_{1/2}$, the brightness amounts to less than 2-5% the initial brightness. In the case of Zn_2SiO_4:Mn, $CaWO_4$ and $CaSO_4$:Mn phosphors (group II) half-disintegration (50% decrease in luminance) occurred with $Q_{1/2} = 4.5 \cdot 10^{12}$ particles/cm^2 with the decrease in brightness being described by the hyperbolic law. The phosphors of group III (90ZnS·10CdS:Cu and ZnO:Zn) underwent rapid initial disintegration ($Q_{1/2} = (0.5\text{-}1.5) \cdot 10^{12}$ particles/cm^2), but then the aging slowed down; after an irradiation charge of $5Q_{1/2}$ the luminance amounted to 15-30% of the initial value.

Thus in the case of phosphors of group I the disintegration rapidly suppresses the ionoluminescence, while in the case of the phosphors of groups II and III complete disintegration is not attained even after relatively prolonged bombardment.

The ion energy and mass proved to be significant factors in the course of the aging process only in the case of ZnO:Zn (the rate of disintegration increased with the ion energy and decreased with the ion mass) and $CaWO_4$ (the rate of disintegration increased with the ion mass).

3. Relation between the excitation depth and disintegration depth

Both the luminescence and the aging of the phosphor are results of inelastic and elastic collisions of the bombarding ions with the atoms of the phosphor crystal. Observation of the luminescence of phosphors bombarded beforehand with ions makes it possible to determine the excitation depth d_E and the disintegration depth d_c.

Obviously, if $d_E > d_c$, the process of aging cannot result in complete suppression of the luminescence. For all the investigated phosphors the luminescence was virtually completely suppressed after sufficiently prolonged bombardment (for phosphors of groups II and III with $Q = 10^{14}\text{-}10^{15}$ particles/cm^2), so that the condition $d_E \leqslant d_c$ was always fulfilled.

Further elucidation of the relation between d_E and d_c was arrived at on the basis of the following experiments: the phosphor samples were subjected to disintegration by ions of energy V_c, and then we measured the luminescence intensity under the influence of ions with energies greater than V_c and determined the luminescence threshold energy V_{0E}.

If $d_E = d_c$, obviously, V_{0E} must be close to V_c; with $d_E < d_c$ the threshold energy should be greater than V_c. These experiments yielded the following results: after irradiation with a charge resulting in close to complete disintegration, V_{0E} agreed with V_c, which is trivial. Further bombardment in the case of phosphors of group I resulted in increase of V_{0E}, i.e., for these phosphors $d_c > d_E$. For ZnS:Ag phosphor bombarded with Li^- ions with $V_c = 1.3$ kev and $Q = 1.5 \cdot 10^{13}$ particles/cm^2, V_{0E} equalled 3 kev; thus $(d_c)_{V=1.3\text{ kev}} = (d_E)_{V=3\text{kev}}$. For phosphors of group II bombarded after complete disintegration $d_c \approx d_E$.

4. Depth of the disintegrated layer

Development of the procedure proposed by us earlier[1] enabled us by comparison of the cathodoluminescence brightness curves of freshly prepared and ion bombarded phosphors ($E_0(V)$ and $E^*(V)$) to determine the variation in depth of the destructive action of the incident ions.

The total disintegration depth d_{0c} is determined from the threshold energy for cathodoluminescence:

$$d_{0c} = l(V_0), \tag{1}$$

where $l(V_0)$ is the range for electrons with energy V_0. The further course of the disintegration process is determined as follows. The brightness under CR excitation

$$E(V) = \int_0^{l(V)} \eta(x)\, W(x, V)\, dx, \tag{2}$$

where $\eta(x)$ is the light yield at a depth x from the surface, and $W(x, V)$ is the electron excitation density at this depth. When $E(V)$, $W(x, V)$ and $l(V)$ are known, this expression may be regarded as an integral equation with respect to $\eta(x)$ and, solving it for $E_0(V)$ and $E^*(V)$, we can characterize the variation in disintegration with depth by the relationship

$$\xi(x) = \frac{\eta^*(x)}{\eta(x)}, \tag{3}$$

where $\eta_0(x)$ and $\eta^*(x)$ are the luminescence outputs of the freshly prepared and ion bombarded phosphors, respectively.

Assuming

$$l(V) = kV^{\alpha} \tag{4}$$

with the values k = 11.2 mg/cm^2 and α = 1.5 (V in kev) obtained by averaging the data of Refs.2 & 5,

$$W(x, V) = {}^3/_2 j / kV^{1/2}\left(1 - \frac{x^2}{b^2V^3}\right), \tag{5}$$

taken from Ref.3 and differing little from the data of Ref.4,

$$E(V) = C(V - V_0)^n, \tag{6}$$

where C, V_0 and n are taken from the experimental values of $E(V)$ for each phosphor, we obtain the solution of Eq.(2) in the form

$$\eta(d) = \frac{C}{3\alpha^2} V^{n-1}\left[(3\alpha - 1)(\alpha - 1)(1 - \Delta)^n + (4\alpha - 1)\, n\,(1 - \Delta)^{n-1} + n(n - 1)(1 - \Delta)^{n-2}\right]; \tag{7}$$

$$\Delta = \frac{V_0}{V}; \quad d = kV^{\alpha}.$$

We determined the values of d_{0c} and $\zeta(d)$ from experiments in which the phosphors were bombarded with ions with energies of 1.3, 3.3 and 6 kev and charges $Q = 2.5 \cdot 10^{12}$ particles/cm^2 (phosphors of group I) and $Q = 10^{14}$ particles/cm^2 (phosphors of groups II and III).

The calculated values of d_{0c} lie in the range from 1 to 40 mg/cm^2. The variation of d_c with the ion energy is given with an accuracy of 5-30% by the relation

$$d_{0c} = bV_n^{\beta}.$$

The values of b and β (with d measured in mg/cm^2 and V in kv) for different phosphors and ions are listed in Table 2.

Table 2

Phosphor	Li		Na		K		Rb		Cs		Average values
	b	β	b	β	b	β	b	β	b	β	β
ZnS — Ag	14	0,72	9,5	0,65	9,5	0,57	7,5	0,5	4,1	0,68	0,64
ZnS.CdS — Ag	5	0,86	3,3	0,87	3,0	0,74	3,0	0,7	3,0	0,7	0,78
ZnS.ZnSe — Ag	8,9	0,74	7	0,68	7	0,64	0,5	7	—	—	0,79
ZnS.CdS — Cu	2,8	1.24	2,4	1,08	3	0,85	1,65	1,1	1,65	0,93	1,0
ZnO — Zn	2	1,15	—	—	1,1	1,1	1,2	0,85	—	—	0,93
Zn_2SiO_4 — Mn	—	—	1,7	1,0	1,4	1,0	1,25	0,92	0,87	1,25	0,95
$CaWO_4$	2	0,92	1,1	0,9	1	0,9	1	0,9	0.85	0,9	0,9
$CaSO_4$ — Mn	3,5	0,95	—	—	1,6	0,95	1,2	0,95	1,0	0,9	0,94
Average values		0,94		0,86		0,84		0,81		0,84	0,86

Calculation of the values of $\zeta(d)$ showed that for phosphors of group II the disintegrated layer has a relatively sharp boundary; the half disintegration depth $d_{1/2}$ ($\zeta(d_{1/2}) = 0.5$) is greater than the complete disintegration depth d_{0c} by a factor of 1.2-1.3. Phosphors of groups I and III do not exhibit such a sharp boundary and for them $d_{1/2}$ exceeds the complete disintegration depth by a factor of 2.5-3.5, and increases with increasing ion energy more rapidly than d_0.

We are of the opinion that the ion range somewhat exceeds d_0 for phosphors of group II and is less than d_0 for phosphors of group I (inasmuch as they are highly sensitive to ion induced disturbances).

This evaluation of the ion range is in reasonable agreement with the data of the relatively few studies[5,6] of penetration of ions into crystals. The appreciable divergence between the present data and the data obtained by us in the work of Ref.1 must be attributed to the incorrect value of the coefficient k used in Eq.(4); the erroneous value was taken from the work of Alden & Koller and Young[4] and led to electron range of values lower by a factor of 7 to 15 compared to those given by more recent studies.[2]

The results of our earlier study[1] recalculated using the new value of k agree with the data obtained in the present investigation.

Chair of Optics,
Tashkent State University

References

1. B.M.Nosenko, N.A.Strukov & M.D.Yagudaev, Optika i spektroskopiya, 3, 351 (1957).

2. J.R.Young, Phys.Rev., 103, 292 (1956); R.O.Lane & D.J.Zaffarno, Ibid., 94, 960 (1954); Yu.M.Vorona, Thesis, Leningrad Polytechnic Institute, 1959; A.Ya. Vyatskin & A.F.Mokhov, Zhur.tekh.fiz., 28, 740 (1958) (Trans.Soviet Physics - Technical Physics); A.R.Shul'man & E.P.Gel', Fiz.tverd.tela, 2, 524 (1960) (Trans. Soviet Physics - Solid State).

3. W.Ehrenberg & J.Franks, Proc.Phys.Soc.B, 60, 1059 (1953).

4. E.D.Alden & L.D.Koller, Phys.Rev., 83, 684 (1951); J.R.Young, J.Appl. Phys., 28, 524 (1958).

5. J.R.Young, J.Appl.Phys., 27, 1 (1956).
6. J.R.Young, J.Appl.Phys., 26, 1302 (1955); M.I.Guseva, E.V.Inotin & S.P. Tsytko, Zhur.eksp.i teor.fiz., 36, 3 (1959) (Trans.Soviet Physics - JETP); M.M. Bredov & H.M.Okuneva, Doklady AN SSSR, 113, 795 (1957) (Trans.Doklady); M.M.Bredov, I.G.Lang & I.M.Okuneva, Zhur.tekh.fiz., 28, 252 (1958) (Trans.Soviet Physics - Technical Physics).

* * * * * * *

THERMOSTIMULATED LUMINESCENCE WITH DIFFERENT FORMS OF EXCITATION

- B.M.Nosenko, L.S.Revzin, V.Ya.Yaskolko & A.R.Krasnaya

In the present work we investigated the light sums stored in $CaSO_4$:Mn, $PbSO_4$:Mn, Zn_2SiO_4:Mn, ZnS:Ag and ZnS:Cu with excitation by electrons (CRE) (V = 0.5 to 7 kev, i = 10^{-5} to 10^{-10} amp/cm^2), β-particle excitation (βE) (S^{35}; 40-500 μ Cu), and photoexcitation (PRK-2 mercury vapor tube, UFS-1 ultraviolet filter plus $NiSO_4$ (PE-1); UFS-4 ultraviolet filter (PE-2). We measured the light sums associated with steady luminescence (S_{st}), the afterglow (S_a) and thermostimulated luminescence (S_t); we also determined the ratios of these quantities to the excitation exposure, i.e., the specific light sums γ_{st}, γ_a and γ_t.*

To bring out the specific characteristics of the different forms of excitation it is convenient to use the relative afterglow light sum $\eta_a = \gamma_a/\gamma_{st}$ and the relative thermoluminescence light sum $\eta_t = \gamma_t/\gamma_{st}$.

The measurements were carried out in the temperature range from -180° to +30°; the heating rates were 60 degree/min and 150 degree/min. Comparison of the excitation density was carried out with reference to the number $\bar{n}$ of ion pairs (excited states) produced in a unit volume per unit time. For CRE and βE the excitation density was also evaluated with reference to the number N_1 of ion pairs produced in a unit volume of track.[1] In a number of cases it proved convenient to consider the mean final density $\bar{N}$, the number of ion pairs forming in a unit volume during the excitation time.

$CaSO_4$:Mn

The principal thermostimulated luminescence peak of $CaSO_4$:Mn is observed at -90° (under strong excitation there also appears a peak at -125°; this is approximately one tenth the height of the main peak). The measurement results with reference to the principal peak are summarized in Table 1.

Table 1

Form of excitation	η_t (T_{st} = 20°)	η_t (T_{st} = -180°)	V_{st}	$\bar{n}$, cm^{-3}sec^{-1}	$\bar{N}$, cm^{-3}	N_1, cm^{-3}
CRE	2.8	1.4	1500	10^{16}	10^{18}	10^{17}
βE	1.4	0.7	15-180	10^{13}-10^{14}	10^{15}-10^{16}	10^{15}

*γ_{st} is directly proportional to the steady state brightness I_{st}.

Table 2

Parameter	T_{st} = 23°	0°	−10°	30°	−40°	−80°	−127°	−170°
γ_t	256	234	228	200	185	158	143	135
γ_{st}	183	164	160	155	147	145	160	173
η_t	1,4	1,42	1,42	1,28	1,25	1,1	0,9	0,78

With increase of T_{st} from -180° to room temperature with βE, γ_{st} at first decreases and then beings to rise; γ_t at first increases slowly and then more rapidly, the inflection point being located in the -80° to -50° region (see Table 2). The temperature dependence of γ_t indicates that the energy storage process needs activation; the variation of γ_{st} with T_{st} is explained on the hypothesis of two-step excitation.

$PbSO_4$:Mn

The glow curve for $PbSO_4$:Mn has only one peak located at -54°. The relative light sums stored with CRE and βE are approximately the same and some 2.5 orders higher than with PE-1. With increase of T_{excit} to room temperature the relative light sum with βE increases by a factor of about 6 owing to decrease of γ_{st}; with PE it increases more rapidly not only owing to decrease of γ_{st} but also because of rise of γ_t (thermal activation of storage). The ratios of γ_{st} at room temperature for βE, PE and CRE were found to be 1:10:50.

The luminescence spectrum contains two bands: an orange manganese band peaking at ~615 mμ and the blue band of "pure" $PbSO_4$ with $\lambda_{max} \approx 425$ mμ. PE-1 yields orange luminescence at all temperatures and orange thermoluminescence. CRE at room temperature yields orange luminescence, which changes to blue with increase of temperature. βE at T_{st} = -180° to +20° gives a blue band with a small admixture of orange, but with increase of T_{st} to 80° the relative intensity of the orange band increases appreciably.

Zn_2SiO_4:Mn

The glow curves for Zn_2SiO_4:Mn have two peaks: the first peak is complex with the principal maximum at -88° and three lower peaks located at -115, -47 and -3°; the relative light sum associated with this peak is of the same order of magnitude with all types of excitation. For the second, blue peak (T_m = 75°) the relative light sum is greatest with βE, and is approximately 5 times smaller with PE-1 and 200 times smaller with CRE. The excitation density $\bar{N}$ with βE equals 10^{14} cm^{-3}, with CRE $\bar{N} = 10^{18}$-10^{20} cm^{-3}, and with PE, $\bar{N} = 10^{15}$-10^{17} cm^{-3}. The values of γ_{st} with PE-1 and CRE are approximately the same, while with βE the value of γ_{st} is 2-3 orders of magnitude lower. The value of γ_t for the second peak decreases with increase in the PE intensity, but not with increase of the excitation time.

ZnS:Cu

The green band of ZnS:Cu was isolated by a 3S-1 filter. There were observed two thermoluminescence peaks, located at -53 and at 22°. The relative afterglow (at -180°) and thermoluminescence light sums and the excitation densities measured for this phosphor are listed in Table 3.

Table 3

Excitation	η_a	η_t	η_{t_1}	η_{t_2}	$\bar{n}$, cm^{-3} scc^{-1}	$\bar{N}$, cm^{-3}	N_1, cm^{-3}
PE-1	0,02	0,04	0,03	—	—	—	—
PE-2	0,04	5,5	1,0	4,5	10^{12}	10^{14}	—
βE	0,03	2,0	—	—	10^{14}	10^{16}	10^{15}
CRE	Not measurable	0,23	0,15	0,07	10^{16}—10^{18}	10^{18}—10^{20}	10^{17}

ZnS:Ag

The glow curves for ZnS:Ag phosphor are characterized by one complex maximum, which may be resolved into two peaks located at -103 and -64°. The relative afterglow (at -180°) and thermoluminescence light sums, the maximum saturation light sums and the excitation densities for this phosphor are listed in Table 4 together with the values of the steady state luminescence and the thickness l of the excited layer. I_{st} increases with the mean excitation density; at the same CRE and PE-2 densities the steady brightnesses referred to a unit volume are equal.

Table 4

Excitation	V, kcv	N_1, cm^{-3}	$\bar{N}$, cm^{-3}	I_{st}, arb. units	l, cm	η_a	η_t	Saturation	S_t, maximum
PE-2	—	—	10^{15}	$3\cdot10^3$	$2\cdot10^{-3}$	0,1	0,3	None	—
	—	—	10^{17}	10^6	$2\cdot10^{-3}$	$2\cdot10^{-3}$	—	For S_t	$2\cdot10^4$
			10^{18}						
CRE	3	10^{17}	10^{18}	$1{,}5\cdot$	$3\cdot10^{-6}$	$5\cdot10^{-3}$	$15\cdot10^{-3}$	None	
			$\cdot10^{21}$	$\cdot10^{-3}$					
	3	10^{17}		—	$3\cdot10^{-6}$	—	—	For I_{st}, S_a, S_t	$2\cdot10^3$
	0,5	10^{17}	$5\cdot10^{21}$	—	—	—	—		$3\cdot10^2$

Working with thin layers of this phosphor, layers virtually transparent to the exciting light, we observed the de-exciting action of cathode rays. The phosphor was excited with ultraviolet light (λ = 365 mμ) to saturation. Irradiation with cathode rays reduced the stored light sum. The effect was weakly dependent on the current density (it showed a tendence to decrease with increase of the density) and increased linearly with the irradiation time at a constant current density. With a charge of $4\cdot10^{-5}$ coulomb/cm^2 up to 30% of the stored light sum was emitted. The depth of the exciting action of electrons in the investigated energy range is 10 to 50 times less than the depth of UV excitation.

Corpuscular forms of excitation (CRE, βE, γ-excitation, etc.) may be distinguished from PE by the following factors: the density and depth of excitation, bands of preferential absorption, magnitude of the de-exciting and quenching influence of the exciting agent, presence and magnitude of general and local heating. Taking into account the different densities and depths of excitation satisfactorily explains the observed[3-5] differences in the values of I_{st} and γ_a with PE, CRE and βE.

By making certain specific assumptions regarding the relation between the de-exciting influence of the exciting agent and the excitation density, one can

explain the variation of γ_t with the exciting agent; unfortunately, the assumptions must be contradictory for zinc sulfide and sulfate phosphors, because for the former the de-exciting influence must increase with the density, while for the latter it should decrease. Taking into account selectivity in the absorption with PE and CRE, one can also explain the effect of redistribution in intensity between the deep ("copper") and shallow peaks in ZnS:Cu. Finally, some complication of the straightforward band diagram (introduction of an activation energy for storage, a thermal barrier[6], etc.) makes it possible to explain the different temperature dependences of the spectral composition of the luminescence of $PbSO_4$:Mn under different forms of excitation. However, part of the observed factors can be satisfactorily explained only by introducing highly particular and specific assumptions. We have in mind, for example, the differences as regards saturation of S_t and the different behavior of the shallow and the deep peaks of willemite with CRE, PE and βE.

In our opinion, the distinctive behavior observed with CRE is connected not only with the above mentioned factors but in many cases with the effect of charging. Although in the region of excitation energies where the secondary emission coefficient is greater than unity the charging is of the order of a volt and is weakly dependent on the current density, in the case of thin layers the field strength proves to be sufficient for inducing electroluminescent effects. These considerations may also serve to explain the strange effect of the de-exciting action of cathode rays on the light sum stored in a photo-excited layer: under excitation by electrons the electric field formed in the volume of the crystal as a result of charging leads to the effect of de-excitation. Obviously, electroluminescent effects connected with the effect of charging will also influence the relaxation processes and the maximum S_t. Thus taking into account the effect of charging should help explain the difference between cathode-ray excitation and excitation by light photons, γ-rays and β-particles.

Chair of Optics,
Tashkent State University

References

1. V.V.Antonov-Romanovskii, Zhur.eksp.i teor.fiz., 21, 269 (1951).
2. N.A.Tolstoi & A.V.Shatilov, Ibid., 30, 109 (1956) (Trans.Soviet Physics - JETP).
3. T.P.Belikova, Zhur.eksp.i teor.fiz., 29, 905 (1955) (Trans.Soviet Physics - JETP).
4. V.L.Levshin & V.F.Tunitskaya, Optika i spektroskopiya, 8, 663 (1960). (Trans.Optics & Spectroscopy.)
5. V.L.Levshin & V.N.Rebane, Ibid., 7, 236 (1959). (Trans.Ibid.)
6. E.I.Alirovich, Nekotorye voprosy teorii lyuminestsentsii kristallofosforov (Some problems in the theory of the luminescence of crystal phosphors), M.-L., 1951.

SINGLE CRYSTAL CATHODOLUMINESCENT SCREENS

- M.A.Vasil'eva, V.V.Kuprevich, I.V.Stepanov & P.P.Feofilov

There is at present an acute need for high resolution cathodoluminescent screens. Such screens, for example, are necessary for investigation of electron optical systems, for adjustment of electron microscopes, and for use in light-electron microscopes.

High resolution cannot be realized in the case of conventional screens with a polycrystalline coating. Somewhat better resolution is exhibited by sublimate phosphors. However, these suffer from reduced image contrast owing to appreciable light scattering in the sublimated layer. Best results can be obtained by using so-called structureless screens and, in particular, single crystal screens. Their high resolving power is due to the absence of macrostructure; their high image contrast - to the virtual absence of light scattering.

We developed and investigated single crystal cathodoluminescent screens of artificial fluorite ($CaFe_2$), strontium fluoride and barium fluoride activated with uranium and different rare earths (Sm, Eu, Tb, Dy, Ho, Er & Tm).

The crystals were grown in vacuum by the procedure developed by I.V.Stepanov[1] on the basis of the Bridgeman[2] technique, as perfected by Stockbarger[3]. The activators were introduced into the intial batch in the form of uranyl fluoride (UO_2F_2) or the rare earth fluoride. Uranium activated crystals exhibited bright green luminescence under electron beam and ultraviolet light stimulation only after heating in air at a temperature of about 900°.[4,5] The luminescence of rare earth activated crystals was observed without preliminary heat treatment both under CR and UV excitation.

The luminescence color of the crystals is generally characteristic of the activating rare earth, but varies somewhat in going from fluorite to strontium fluoride and barium fluoride. Thus the luminescence color can be varied in a wide range by appropriate choice of the activator. The cathodoluminescence spectra of the screens proved to be virtually identical with the corresponding photoluminescence spectra.

Rare earth fluoride crystals have a low surface conductivity. Hence to eliminate build-up of charge on the screens these were coated on the excitation side with a conducting film of silver or aluminum. The cathodoluminescence characteristics were investigated on an electron-optical set-up designed for testing luminescence screens. The emission was observed from the unbombarded side.

The cathodoluminescence characteristics of the different screens are generally similar. Hence by way of typical example one may cite the data for CaF_2:Eu screens. (Data on CaF_2:Eu screens will be found in Ref.5.) The europium in these luminophors is mainly in the divalent state and exhibits bright blue luminescence.[6] Fig.1 shows the variation of the light output of CaF_2:Eu screens as a function of the activator concentration. As will be evident from the figure, the cathodoluminescence intensity increases with increase of the activator concentration up to a weak maximum in the 0.20-0.25% region, and then begins to fall off slightly.

In the case of CaF_2:Eu we did not observe "saturation" of the luminescence brightness with increase of the accelerating potential. In the case of most of the other screens the increase in brightness with increasing beam potential begins to slow down at 15-20 kv. The cathodoluminescence brightness of the screens is proportional to the electron current to the screen, at least up to 10^{-7} amp/cm^2.

The resolution of the single crystal screens was determined with the aid of a small electron microscope and the above mentioned screen test set-up. The resolution of structureless (transparent) screens depends primarily on the depth of

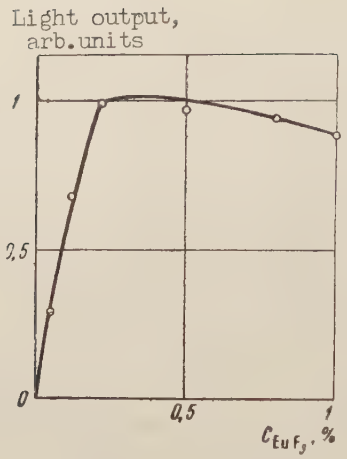

Fig.1. Variation of the cathodoluminescence output of CaF_2:Eu screens as a function of the activator concentration. V = 11 kv; i = 10^{-7} amp/cm^2.

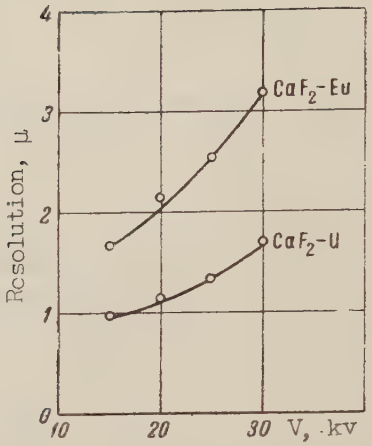

Fig.2. Variation of the resolution of CaF_2:U and CaF_2:Eu screens as a function of the accelerating potential; i = 10^{-8} amp/cm^2.

electron penetration into the luminescing material, and, in the final analysis, on the velocity of the electrons and also on the density of the luminescing medium. Curves characterizing the resolution of CaF_2:U and CaF_2:Eu screens as a function of the accelerating potential are shown in Fig.2. The lower resolving power of europium activated fluorite can be explained partly by the interfering influence of the x-rays generated in the electron bombarded screen and partly by subjective factors (the blue emission of Eu is unfavorable for observation). As noted, the resolution also depends on the density of the crystals. Thus at an accelerating potential of 30 kv the resolution of fluorite screens lies in the range from 2 to 3 μ, that of strontium fluoride screens in the range from 1.5 to 2 μ, while the resolution of barium fluoride screens attains 1 μ.

Temperature quenching of the luminescence and the duration of afterglow were investigated with excitation of the crystals by ultraviolet. Virtually no quenching of the luminescence of the rare earth activated crystal was observed up to 200°, except in the case of CaF_2:Eu, for which temperature quenching begins at 50° (Ref.6). In the case of CaF_2:U crystals, however, the luminescence intensity begins to decrease at 20° and at 50° falls to half the initial value.[5] The persistence τ of the excited state of crystals activated by rare earths lies in the range from 10^{-2} to 10^{-3} sec (for Eu^2 - 10^{-7} sec). For uranium activated crystals, $\tau \approx \approx 10^{-4}$ sec.

An important factor under most operating conditions is stability of the crystals as regards irreversible changes under the influence of electron bombardment. We found that if one uses pure raw materials and takes appropriate precautions to guard against contamination in the process of growth, the resultant screens do not show any loss in luminescence intensity after many hours of electron bombardment (current density 10^{-7}-10^{-8} amp/cm^2).

The developed cathodoluminescent screens are also stable as regards exposure to the atmosphere and heat. The latter is particularly important when the screens are used in vacuum electronic devices that must be heated for outgassing in the process of fabrication. The screens are also mechanically strong and are not affected by dirt.

Some of the high resolution screens have been used in the EM-6 light-electron microscope and in some other electronic instruments.

References

1. I.V.Stepanov & P.P.Feofilov, in "Rost kristallov" (Crystal growth), p.229, M., 1957.
2. P.W.Bridgeman, Proc.Amer.Sci., 60, 306 (1925).
3. D.Stockbarger, J.Opt.Soc.Am., 39, 731 (1949).
4. P.P.Feofilov, Transactions of the Fifth Conference on Luminescence, Tartu, 1957.
5. V.V.Kuprevich, I.V.Stepanov & P.P.Feofilov, Inzh.fiz.zhur. (Eng.-Phys. Journal), 1, No.11, 130 (1958).
6. P.P.Feofilov, Optika i spektroskopiya, 1, 992 (1956).

* * * * * * *

INVESTIGATION OF ACTIVATORLESS ZnS SUBLIMATE PHOSPHORS

- E.Ya.Arapova

The thin zinc sulfide films investigated in the present work were prepared by vacuum evaporation onto heated quartz plates. The zinc sulfide was treated beforehand for 2 hours in a current of H_2S at 1150° and purified of excess sulfur by aging in vacuum. When zinc sulfide is deposited on quartz substrates heated to 200 to 350° there are obtained films with blue luminescence under excitation by ultraviolet (λ = 313 mμ). Films prepared on substrates at higher temperatures emit only a weak red-orange luminescence.

In order to elucidate the nature of the blue luminescence we investigated the absorption and excitation spectra of the ZnS films and also recorded diffraction patterns for them. The x-ray diffraction studies showed that these films have cubic structure; no evidence pointing to the presence of zinc oxide was found.

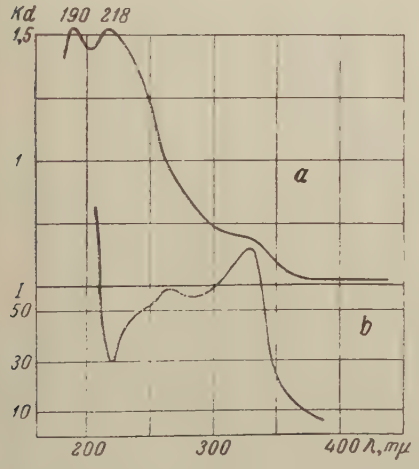

Absorption (a) and excitation (b) spectra of ZnS films.

The absorption and excitation spectra of a ZnS film with blue luminescences prepared by vacuum evaporation onto a substrate heated to 300° are shown in the accompanying figure. It will be seen that strong absorption begins at about 340 mμ, goes through a hump at 325-330 mμ, increases rapidly to 220 mμ and then goes through two maxima at 218 and 190 mμ. Hall[2], in addition to a band at 330 mμ, reports observing an absorption band located at 213.8 mμ. The above mentioned absorption at 190 mμ has not been reported hitherto.

It will be evident from a comparison of absorption and excitation spectra that there is a dip in the excitation curve in the region of the 218 mμ absorption band of the material. This band is inactive. On the other hand, in the region of the 190 mμ absorption peak there is observed a strong increase in excitation. Hence this absorp-

tion band is active.

Analogous effects have been described in the literature[3] for other luminophors.

We tested the stability of the blue luminescing ZnS films as regards repeated heating: the ZnS films were heated in vacuum for 1 hour at temperatures from 400 to 900°. Up to a temperature of 700° the brightness of the blue luminescence is not affected; the absorption spectrum also remains unchanged. As a result of heating to 800° the blue luminescence becomes weaker, and at 900° it vanishes, the film darkens, and exhibits only weak red emission. X-ray diffraction studies showed that at 800 to 900° the cubic ZnS lattice begins to transform to the hexagonal modification.

Thus the results of our experiments substantiate the assertion, made earlier, that the blue luminescence of activatorless zinc sulfide can be obtained in the absence of any coactivator.

We are undertaking further research to determine the influence of coactivator impurities on the blue luminescence of activatorless zinc sulfide.

References

1. E.Ya.Arapova, Transactions of the Seventh Conference on Luminescence, M., 1957.

2. J.F.Hall, J.Opt.Soc.Am., 46, 1013 (1956).

3. Z.L.Morgenshtern, Doklady AN SSSR, 105, 250 (1955).

SOME CHARACTERISTICS OF ZINC SULFIDE-SELENIDE SUBLIMATE SCREENS

- V.V.Golubets

There are two basic procedures for preparing sublimate screens: in employing the first, transparent luminescent layers are obtained as a result of reaction in the gaseous phase between zinc vapor and hydrogen sulfide[1]; the second procedure is based on evaporation under vacuum of previously prepared phosphors and involves additional heating of the sublimate layers[2]. In both cases the luminescence brightness of the resultant screens attains 20-30% of the brightness of the corresponding powdered phosphor.

In the present work we demonstrated that by appropriate choice of the evaporation conditions the brightness of zinc sulfide-selenide sublimate screens can be appreciably enhanced. We also measured some of the characteristics of zinc sulfide-selenide screens under cathode-ray excitation.

Experimental part

For preparing our screens we used 85% ZnS·15% ZnSe:$6\cdot10^{-5}$ Cu. The phosphor was evaporated from a quartz vaporizer onto a preheated glass substrate. After evacuation of the vessel and before evaporation of the phosphor powder, a metered amount of hydrogen chloride was admitted into the reaction space. By means of this preparation procedure there were obtained sublimate screens with a bright green cathodoluminescence.

The luminescence spectra of the sublimate screens were investigated in a demountable cathode-ray tube with excitation by a stationary electron beam. For recording the spectral characteristics we used a UM-2 monochromator with the radiation being detected by an FEU-19 photomultiplier. The duration of phosphorescence was measured in a demountable cathode-ray tube connected into an oscillographic circuit.

Characteristics of sublimate screens

In experiments on sublimation of zinc sulfide-selenide it was established that the spectral composition and brightness of the cathodoluminescence of the resultant sublimate screens depend on the concentration of hydrogen chloride in the gaseous phase. The cathodoluminescence spectra of sublimate screens obtained with different HCl concentrations in the vacuum chamber are shown in the accompanying figure. With increase of the HCl concentration the peak of the spectrum band shifts to the short wavelength side. During sublimation there occurs a partial loss of selenium, owing to thermal dissociation of the zinc sulfide-selenide, as a result of which the relative content of zinc sulfide in the layer increases.[3]

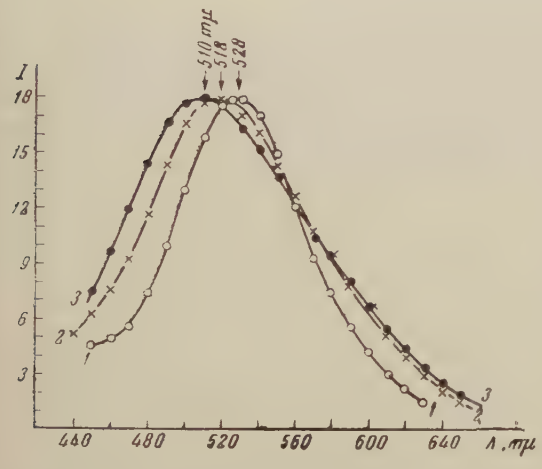

Variation of the spectral composition of the luminescence of ZnS·ZnSe:Cu sublimate screens depending on the concentration of HCl in the gaseous phase: 1) 0.019%, 2) 0.038%, 3) 0.076%. V = 15 kv, i = = 0.03 μa/cm^2.

For determining the variation of the cathodoluminescence intensity as a function of the HCl concentration in the gaseous phase we prepared a series of screens with

the same coating thickness. The brightness was measured with observation from the unbombarded side in a demountable cathode-ray tube. It was found that at first, with increasing HCl concentration the brightness increases linearly; the increase slows down at an HCl concentration of 0.048% and attains a maximum value at 0.057%. With further increase of the HCl concentration the brightness falls off fairly rapidly.

It may be assumed that the effect of hydrogen chloride on the luminescence brightness depends on a number of factors. First, with changes in the amount of HCl in the gaseous phase there are realized different conditions for incorporation of the activator into the host lattice. Thus, Kröger, Hellingman & Smit[4] showed that when ZnS:Cu without flux is heated, the intensity of the green luminescence band depends on the concentration of hydrogen chloride present. Second, hydrogen chloride in the process of sublimation acts as a mineralizer, so that changes in the amount of it present in the gaseous phase may lead to changes in the chemical nature and structure of the sublimate layer. In the present work we were only able to follow the combined influence of these two factors on the cathodoluminescence brightness.

The investigated zinc sulfide-selenide sublimate screens exhibit a persistent phosphorescence. Thus in the case of the sublimate screen obtained with 0.057% HCl in the gaseous phase decay of the brightness to 5% the initial value occurs only at the end of $3 \cdot 10^{-2}$ sec. Such persistent phosphorescence is typical of copper activated zinc sulfide-selenide.

The resolving power of the sublimate screens is 1.5-2 times higher than that of corresponding screens prepared by the conventional method (settling). The brightness of the investigated sublimate screens equals 70-80% the brightness of the corresponding conventional screens.

I desire to thank E.I.Chernovetskaya for preparing the phosphor and M.S. Paramonova and G.A.Zhirnova for assistance in the work.

References

1. F.Studer & D.Cusano, J.Opt.Soc.Am., 45, 493 (1955).
2. C.Feldman & M.O'Hara, J.Opt.Soc.Am., 47, 300 (1957).
3. V.V.Golubets, Transactions of the Seventh Conference on Luminescence, p.353, Tartu, 1959.
4. F.Kröger, J.Hellingman & N.Smit, Physica, 15, 999 (1949).

LUMINESCENCE PROPERTIES OF CERIUM ACTIVATED ALUMINUM OXIDE AND HELENITE UNDER CATHODE-RAY EXCITATION

- T.V. Oranovskaya

The preparation of cathodoluminophors with short persistence is at present one of the most important problems in phosphor research. There are very few such luminophors in industrial use. Recently there have appeared in the domestic and foreign literature a number of reports on the use in cathode-ray tubes of a short persistence phosphor with the crystal lattice of helenite - $2CaO \cdot Al_2O_3 \cdot SiO_2$:Ce - which has a good efficiency, a decay time of $\sim 2 \cdot 10^{-7}$ sec and λ_{max} = 4050-4100 A.[1-3]

The principal raw materials for preparing helenite are usually CaO, SiO_2 and Al_2O_3; the activator is commonly $Ce(NO_3)_3 \cdot 6H_2O$. The first two oxides are available in the luminescence pure grade ($\leqslant 3 \cdot 10^{-3}$% Fe, $\sim 2 \cdot 10^{-4}$% Cu); the aluminum oxide is usually prepared by thermal decomposition of reagent grade aluminum ammonium sulfate ($5 \cdot 10^{-4}$% Fe, $5 \cdot 10^{-5}$% Cu). In the process the impurities convert to Al_2O_3, but there occurs additional contamination of the product, particularly if the heating is carried out in a porcelain or alundum crucible. All this greatly complicates preparation of the phosphors.

In the present work we investigated the luminescence spectra, emission brightness and decay time of $2CaO \cdot Al_2O_3 \cdot SiO_2$:Ce and Al_2O_3:Ce phosphors as a function of the amount of heavy metals (Fe, Cu & Cr) present in the batch.

The aluminum oxide used was in the form of α-Al_2O_3.

All the characteristics were investigated with excitation by a stationary electron beam with V = 15-17 kv and i = 0.1 $\mu a/cm^2$. The spectra were recorded by means of a UM-3 monochromator with the radiation being detected by a photomultiplier with a cesium-antimony or cesium oxide-silver photocathode. The short-lived component of the decay (from 10^{-4} to 10^{-1} sec) was determined by the oscillographic procedure.

Experimental part

The spectral characteristics of $2CaO \cdot Al_2O_3 \cdot SiO_2$:Ce and Al_2O_3:Ce are shown in Fig.1. The emission spectra of these phosphors are stable as regards the location of the peak and do not change with variation of the Ce concentration and the conditions of heat treatment. In a number of cases, however, in the spectra of phosphors prepared from the same initial products there appears, in addition to

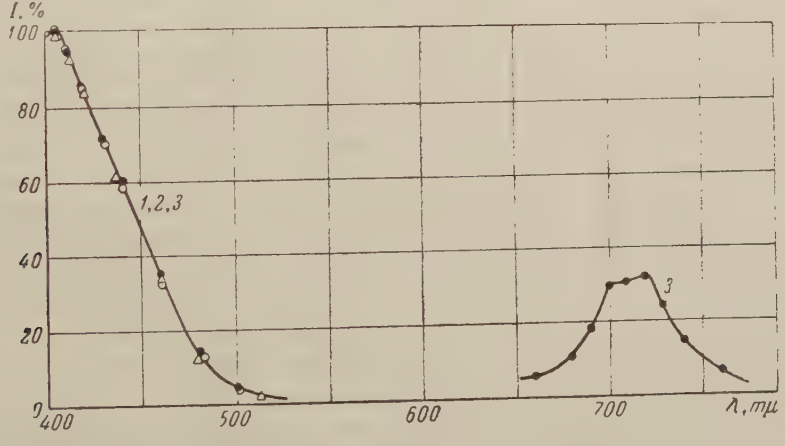

Fig.1. Cathodoluminescence spectra of: 1) Al_2O_3:Ce and 2 & 3) $2CaO \cdot Al_2O_3 \cdot SiO_2$:Ce.

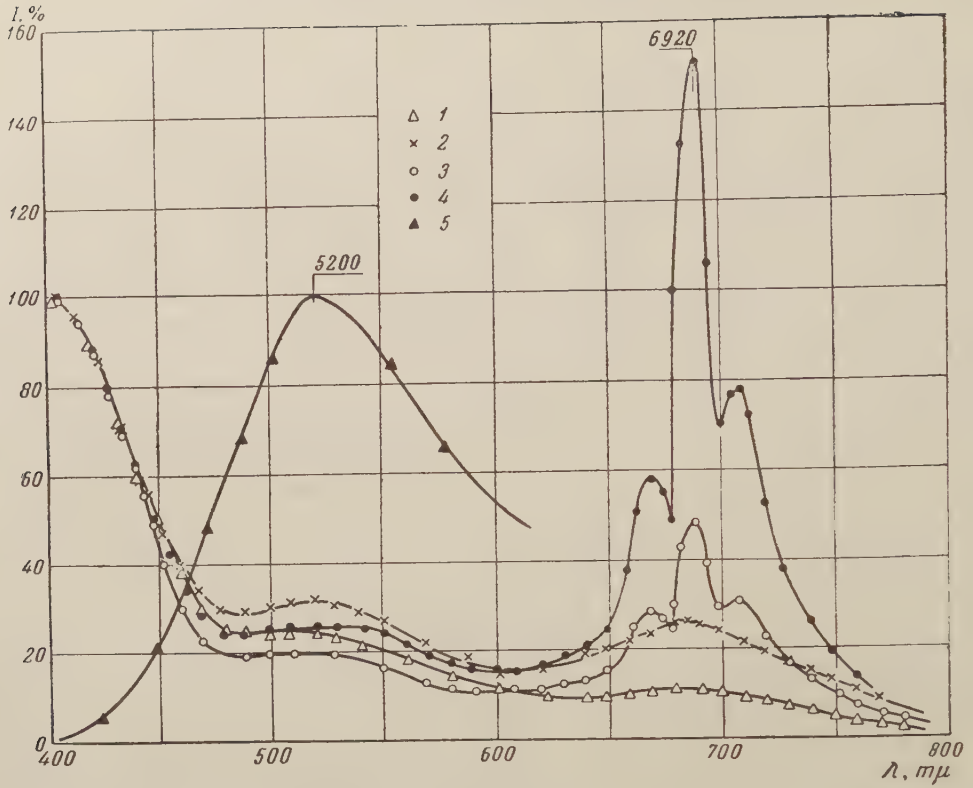

Fig.2. Cathodoluminescence spectra of Al_2O_3:Ce phosphors with different concentrations of iron: 1) 0.0025% Fe, 2) 0.005% Fe, 3) 0.01% Fe, 4) 0.05% Fe; 5) spectrum of Al_2O_3:1% Cr.

the blue band peaking at 4050 Å and corresponding to cerium, a narrow band with λ_{max} = 690 Å, which may be identified with chromium. The intensity of this band varies in a wide range. Specimens containing this red band in their luminescence spectrum are also characterized by a more persistent afterglow and a lower luminescence intensity. These effects are most pronounced in Al_2O_3:Ce; hence most of the investigations were carried out with this phosphor, and only the final results were checked with helenite.

According to the data of spectroscopic analysis, the initial aluminum oxide contained ~$5\cdot10^{-3}$% Fe and ~$6\cdot10^{-3}$% Cr. We investigated the following phosphors: Al_2O_3:Ce:Cr (the additional amounts of Cr being $1\cdot10^{-3}$, $1\cdot10^{-2}$ and $1\cdot10^{-1}$%), Al_2O_3:Ce:Fe (we introduced $5\cdot10^{-3}$, $1\cdot10^{-2}$ and $5\cdot10^{-2}$% Fe), and Al_2O_3:0.1% Cr without cerium.

We measured the luminescence intensity of the individual bands and the decay time of all the luminophors. Our measurements showed that all the Al_2O_3:Fe:Cr and Al_2O_3:Ce:Fe phosphors exhibit in their luminescence spectrum a red band with λ_{max} = 6920 Å, and that the intensity of this band varies, depending on the concentration of Cr or Fe.

With increase of the chromium concentration from 0.006 to 0.1% the intensity of the red band increases by a factor of almost 7; at the same time the intensity of the blue band decreases. At a chromium concentration of ~$1\cdot10^{-2}$% the blue band is completely suppressed, while at a concentration of ~$1\cdot10^{-3}$% the red band has an intensity equal to ~30% the intensity of the blue one. All the specimens

had a persistent afterglow: at the end of 10^{-2} sec, and in some cases at the end of 10^{-1} sec, the residual brightness exceeded 5% the initial value.

Introduction of iron into Al_2O_3:Ce results in substantial decrease of the luminance, and the emission color changes from blue to rose. Measurements of the intensities of the red and blue bands showed that iron is a quencher for both the blue and the red radiation, but that the intensity of the former decreases more rapidly, so that at a certain concentration of Fe the red begins to predominate in the emission spectrum. In addition to changing the color of luminescence, introduction of iron, like introduction of chromium, results in increase of the afterglow persistence. As regards both shape and position of the red band Al_2O_3: :Ce:Cr and Al_2O_3:Ce:Fe are similar to Al_2O_3:Cr (Fig.2). Consequently, it may be inferred that the cause of the red band is contamination of the initial aluminum oxide by chromium; iron only facilitates manifestation of this Cr band.

The luminescence spectrum of Al_2O_3:Fe consists of two bands peaking at 6920 and 5200 Å. The first of these two is the band of chromium. The green band is also present in the cathodoluminescence spectra of Al_2O_3:Ce:Fe phosphors and in specimens of Al_2O_3:Ce:Cr containing chromium in concentrations under 10^{-2}%, but its intensity in these phosphors is relatively low. In the spectrum of Al_2O_3:Fe the intensity of the green band equals about 30% relative to the intensity of the red emission.

According to the data in the literature[2], green luminescence of Al_2O_3 may appear when this substance is activated by copper or manganese. According to spectroscopic analyses, the Mn content in our aluminum oxide specimens was $\leqslant 1.6 \cdot 10^{-4}$%; the copper content varied from $2 \cdot 10^{-5}$ to $1 \cdot 10^{-3}$%. The intensity of the band peaking at ~5200 Å in the spectra of the specimens with the higher Cu concentration is appreciably greater. Al_2O_3:Cu exhibits bright green luminescence with λ_{max} = 5200 Å. Introduction of copper into Al_2O_3:Ce also results in enhanced intensity of the green band. Introduction of copper in the amount of 1% by weight into the initial batch results in a phosphor with a green luminescence band having an intensity equal to ~50% the intensity of the cerium band.

All the phosphors containing Cu have a persistent afterglow: the decay time to 5% of the initial intensity value is 10^{-2} sec.

Investigation of "activatorless" phosphors, i.e., Al_2O_3 without deliberately introduced Cr, Fe, Cu or Ce showed that in their spectra there is also evinced a band peaking at 5200-5300 Å and a band with λ_{max} = 6920 Å. The intensity of these bands depends on the purity of the aluminum oxide; this was checked by spectroscopic analysis of different batches of Al_2O_3 for Cr, Fe and Cu.

The best results as regards short persistence and luminescence intensity were obtained for the specimens prepared of spectroscopically pure aluminum oxide ($<1 \cdot 10^{-3}$% Fe and $<1.3 \cdot 10^{-3}$% Cr).

Comparison of the principal characteristics of Al_2O_3:Ce and $2CaO \cdot Al_2O_3 \cdot SiO_2$: :Ce phosphors prepared of spectroscopically pure and reagent grade Al_2O_3 and aluminum oxide obtained by decomposition of reagent grade ammonium alum showed that use of spectroscopically pure aluminum oxide yields a 20-25% increase in luminescence brightness as compared with phosphors prepared of Al_2O_3 obtained by decomposition of the alum. The decay time of such cathodoluminophors to 5% the initial brightness is $\sim 1 \cdot 10^{-4}$ sec.

I desire to express my deep gratitude to A Ya.Gutner and E.K.Raspletina for carrying out the measurements of the luminescence characteristics of the luminophors, to N.G.Karpel' for spectroscopic analysis of the aluminum oxide samples, and to V.G.Sergeeva for preparing the phosphor specimens.

References

1. A.Bril & H.A.Klasens, Philips Res.Repts., 7, 421 (1952).
2. A.Bril, J.de Gier & H.A.Klasens, Philips Techn.Rev., 15, No.8/9, 233 (1954).
3. T.V.Korovkina, A.V.Morozova & Yu.S.Blank, Certificate No.7749 on Registration with the Committee on Inventions and Discoveries at the Soviet of Ministers of the USSR.
4. A.V.Moskvin, Katodolyuminestsentsiya (Cathodoluminescence), Part 2, M., 1949.

* * * * * * * * *

CATHODOLUMINOPHORS WITH VERY SHORT PERSISTENCE AND EMISSION IN THE BLUE, YELLOW AND RED REGIONS

- Z.I.Klabukova & A.V.Morozova

In preparing CdS:Ag and ZnSe:AgNi phosphors from different batches of raw materials, we often noted a marked lack of reproducibility of the luminescence properties. For our work we used laboratory samples and materials supplied by the Krasnyi khimik (Red Chemist) Plant, rated as luminescence pure. All the batches of CdS were obtained by precipitation with hydrogen sulfide from solutions of $CdSO_4$; all the batches of ZnSe were obtained by the ZnS + SeO_2 reaction ("wet" variant). The batches were heated in the furnace atmosphere for 1 hour at 600° in the case of CdS:Ag and for 1/2 hour at 900° in the case of ZnSe:AgNi; 2% NaCl was used as the flux (in preparing helenite we used 6% LiCl and heated the mixture for 5 hr at 1250°).

For the CdS:Ag phosphors we observed displacement of λ_{max} from 7400-7200 Å (curves 13 and 10 in the accompanying figure) to 6900 Å (curve 9). According to Grillot[1], λ_{max} = 7400 Å. At the same time there was observed an increase in the luminescence brightness and decrease in the size of the phosphor grains. Comparison of the data of chemical and spectroscopic analyses and x-ray diffraction studies showed that different samples of unheated CdS differ mainly as regards the structure of the crystals (sphalerite and greenockite), which is in agreement with the indications in the literature[2]. This presumably explains the observed variation of the properties of CdS and CdS:Ag phosphors.

For the ZnSe and ZnSe:AgNi phosphors we noted significant variation as regards the luminescence spectrum and brightness, and afterglow persistence and thernal stability. It was established that from all the different batches of ZnSe there were obtained essentially two different types of self-activated ZnSe (NaCl) phosphors: phosphors with λ_{max} = 6400 Å and phosphors with λ_{max} = 6100 Å.

Only ZnSe from batch B* proved to be suitable for preparing heat stable ZnSe:Ag:Ni cathodoluminophor with one emission band (λ_{max} = 5700 Å) and a very short persistence ($\sim 2 \cdot 10^{-6}$ sec).

However, the luminescence band of ZnSe(NaCl) prepared of batches A proved to be more stable as regards introduction of Ag, heating in air or vacuum and

---

*B designates ZnSe batches yielding self-activated ZnSe(NaCl) with λ_{max} = = 6100 Å; A designates ZnSe batches yielding ZnSe(NaCl) with λ_{max} = 6400 Å.

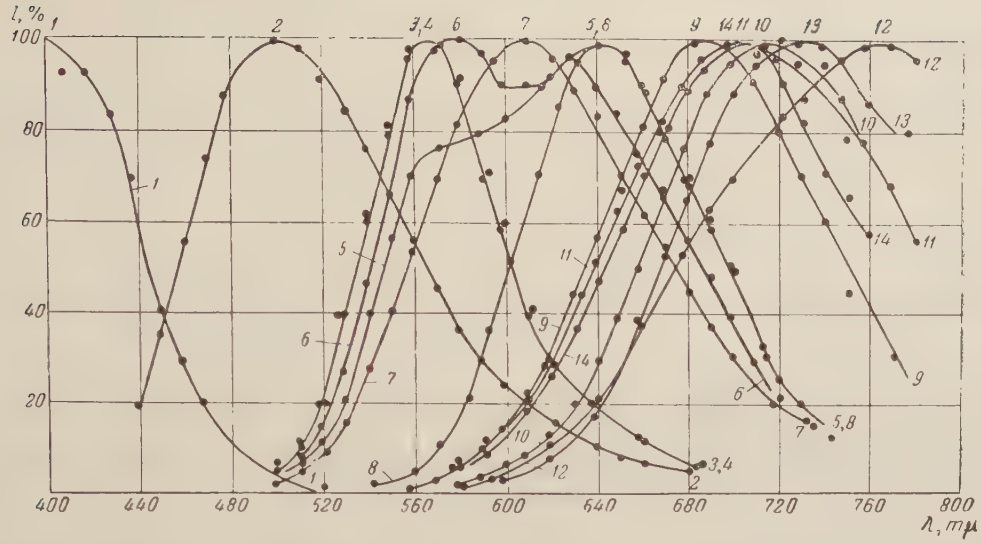

Cathodoluminescence spectra: 1 - 2 $CaO \cdot Al_2O_3 \cdot SiO_2$:1.6% Ce, 2 - ZnO:Zn, 3 - ZnSe:$1 \cdot 10^{-4}$ Ag:$2 \cdot 10^{-6}$ Ni, batch B, 4 - ZnSe:$1 \cdot 10^{-4}$ Ag, batch B, 5 - ZnSe:$1 \cdot 10^{-4}$ Ag, batch A, 6 - ZnSe:$1 \cdot 10^{-4}$ Ag:$2 \cdot 10^{-6}$ Ni, batch A, 7 - ZnSe(2% NaCl), batch B, 8 - ZnSe(2% NaCl), batch A, 9 - CdS:$1 \cdot 10^{-4}$ Ag, batch 1, 10 - CdS:$1 \cdot 10^{-4}$ Ag, batch 6, 11 - CdS(2% NaCl), batch 1, 12 - CdS(2% NaCl), batch 6, 13 - CdS:$1 \cdot 10^{-4}$ Ag, batch 16, 14 - 90% CdS·10% ZnS:$1 \cdot 10^{-4}$ Ag, batch 16. V = 8 kv, i = 15 μa/cm^2.

variation in the excitation conditions. ZnSe:Ag:Ni prepared of A batches of ZnSe, precisely owing to constancy of the λ_{max} = 6400 Å band, is appreciably less stable than the same phosphor prepared from B batches of ZnSe. ZnSe:Ag:Ni phosphors can be decomposed by heating in a current of superheated steam at 400° for 3 hours. As a result of such decomposition there appears in the cathodoluminescence spectrum the band of the self-activated phosphor with λ_{max} = 6400 Å, regardless of whether the phosphor was prepared from an A or a B batch. This result is to some extent in conflict with the data of Refs.3 and 4, where the λ_{max} = 6100 Å band is attributed to the presence of Cl (Ref.4) or zinc oxide (Ref.3). We did not observe any difference as regards ZnO content (ZnO washed out with acetic acid) in the zinc selenide of batches A and B. Introduction of NaCl leads only to an insignificant (~50-70 mμ) shift of λ_{max}.

Inasmuch as the batches of ZnSe used in our experiments had the same crystal structure (sphalerite) and differed significantly only as regards the content of Se, which did not wash out from ZnSe, the observed difference between the luminescence properties of the ZnSe (NaCl) phosphors produced from A and B batches may be attributed to the influence of elemental Se. It will be recalled that selenium goes into the vapor state at the heating temperature (800-900°) and, consequently, can readily affect the process of formation of luminescence centers.

We desire to express our sincere gratitude to V.G.Prokhvatilov for carrying out the x-ray diffraction studies and to F.M.Pekerman for investigating the photoluminescence spectra.

References

1. E.Grillot, J.Chem.Phys., 48, 115 (1951).

2. G.Bauer, Handbuch der präparativen anorganischen Chemie, Stuttgart, 1951-4. (Cited in Russian trans.M., 1956).

3. L.Ya.Markovskii & R.I.Smirnova, Izv.AN SSSR, Ser.fiz., 23, 1341 (1959). (Trans.Bulletin, 23, 1327.)
4. C.Larch, J.Chem.Phys., 21, 756 (1953).

* * * * * * *

CATHODOLUMINESCENCE OF EUROPIUM ACTIVATED STRONTIUM PHOSPHATES

- V.P.Nazarova

The purpose of the present work was to develop new cathodoluminophors with blue emission and a short persistence.

Earlier we showed that α-$Ca_2P_2O_7$:Eu is a bright violet-blue cathodophosphor with a narrow diffuse emission band peaking at 4130 Å and a short decay time ($<10^{-4}$ sec).[1]

Below we give the results of a recent investigation of some of the properties of europium activated strontium phosphates. The cathodoluminescence parameters were determined in a demountable cathode-ray tube with excitation of the phosphor by a stationary electron beam (V = 15-17 kv, i $\approx 10^{-7}$ a/cm^2). The luminescence spectra were investigated by means of a UM-3 monochromator with the radiation being detected by a cesium oxide or a cesium-antimony cathode photomultiplier. The intensity was measured by means of a cesium-antimony photomultiplier with a peak sensitivity at about 4300 Å; the intensity values were evaluated with reference to ZnS:Ag, the intensity of which was taken as 100%. The decay times were measured with excitation by square pulses on an oscillographic set-up.

Cathodoluminescence parameters

The principal cathodoluminescence parameters of the europium activated strontium phosphates are listed in Table 1.

Table 1

No.	Phosphor	Emission during excitation	λ_{max}, A	Half-width of luminescence band, Å	Relative intensity, %
1	$Sr(PO_3)_2$:Eu	Violet	4130	430	1-2
2	β-$Sr_2P_2O_7$:Eu	Violet-blue	4230	580	1.0
3	α-$Sr_2P_2O_7$:Eu	Violet	4150	430	5-8
4	$Sr_3(PO_4)_2$:Eu	Blue	4250	430	25-35

The luminescence spectra of the phosphate phosphors are presented in the accompanying figure. Each phosphor has an individual emission spectrum in the form of a broad structureless diffuse band; the location of the peak (λ_{max}) and the half-width of this band vary with changes in the chemical composition and the crystal lattice of the strontium phosphate.

In the spectra of the above-mentioned samples there were not present the sections of line or narrow-band emission characteristic of phosphors activated by trivalent rare earths.[3]

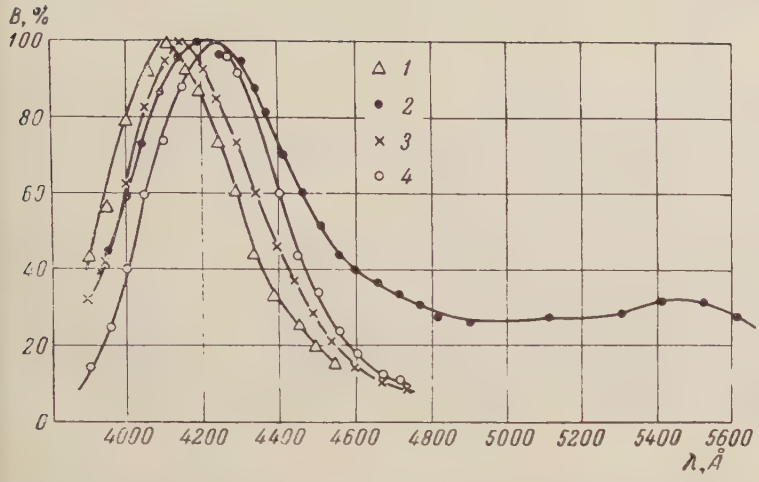

Luminescence spectra of Eu activated strontium phosphates: 1) $Sr(PO_3)_2$:Eu, 2) β-$Sr_2P_2O_7$:Eu, 3) α-$Sr_2P_2O_7$:Eu, 4) $Sr_3(PO_4)_2$:Eu.

Table 2

No.	Rare earth %	Luminescence spectrum, Å (4000 5000 6000 7000 8000 9000)	Relative intensity, %	Decay time to 1% intensity, sec
1	—		100,0	$<10^{-4}$
2	10^{-5} Dy		100,0	$<10^{-4}$
3	10^{-4} Dy		100,0	$<10^{-4}$
4	10^{-3} Dy		98,5	$1\cdot10^{-4}$
5	10^{-2} Dy		90,2	$2\cdot10^{-3}$
6	10^{-1} Dy		12,7	$1\cdot10^{-2}$
1	—		100,0	$<10^{-4}$
2	10^{-5} Sm		100,0	$<10^{-4}$
3	10^{-4} Sm		91,0	$1\cdot10^{-4}$
4	10^{-3} Sm		94,5	$1\cdot10^{-4}$
5	10^{-2} Sm		86,5	$3\cdot10^{-4}$
6	10^{-1} Sm		40,0	10^{-1}
1	—		100,0	$<10^{-4}$
2	10^{-5} Tb		100,0	$<10^{-4}$
3	10^{-4} Tb		100,0	$1\cdot10^{-3}$
4	10^{-3} Tb		100,0	$4\cdot10^{-3}$
5	10^{-2} Tb		95,0	$6\cdot10^{-2}$
6	10^{-1} Tb		82,0	—

The isomorphism of α-$Ca_2P_2O_7$ and α-$Sr_2P_2O_7$ (orthorhombic lattice) is substantiated by the closeness of the luminescence spectra of α-$Ca_2P_2O_7$:Eu and α-$Sr_2P_2O_7$:Eu. In going from the former to the latter phosphor, the band peak λ_{max} remains at 4130-4150 Å, but the half-width of the band increases from 250 Å to 430 Å.

The brightest of the investigated phosphors proved to be $Sr_3(PO_4)_2$:Eu, the luminescence intensity attains 25-35% the intensity of ZnS:Ag.

All the europium activated strontium phosphates have a short decay time (decay to 1% intensity $\leqslant 10^{-4}$ sec).

Influence of rare earth and heavy metal impurities

The experiments on the effect of coactivators were carried out primarily with $Sr_3(PO_4)_2$:Eu. We introduced the nitrates of Dy^{3+}, Sm^{3+} and Tb^{3+}, ions which are known to be energetic activators in other phosphors[1] and often accompany europium in its compounds. The results obtained are summarized in Table 2.

The presence of a second rare earth ion, for example, Dy^{3+} or Sm^{3+}, in the amount of 10^{-5} to 10^{-1}% does not alter the configuration and position of the characteristic luminescence band of $Sr_3(PO_4)_2$:Eu; however, there do begin to appear in addition sections of a narrow-band or line spectrum typical of trivalent rare earth ions in many hosts. With increase in the concentration of the coactivator the intensity of the auxiliary bands increases. In all the investigated samples, however, the intensity of the blue europium band remained predominant up to

a 1 to 50 ratio of europium to the second rare earth.

The change evident in the configuration of the europium band in the spectra of $Sr_3(PO_4)_2$:Eu doped with terbium (Table 2) is due to partial overlapping of the europium and terbium spectra.

The luminescence spectra presented in Table 2 were obtained by photoelectric recording. In the figure the narrow-band or line character of the auxiliary sections of the luminescence spectra, i.e., the sections due to the Sm^{3+}, Dy^{3+} and Tb^{3+}, is not clearly evinced.

The variation of the luminescence intensity and decay time of $Sr_3(PO_4)_2$:Eu as a function of the concentration of the second rare earth activator is shown in Table 2. Quenching of the luminescence begins to be evident at a concentration of 10^{-4}-10^{-3}% of the second rare earth. The weak quenching action of terbium is probably connected with the superposition of its emission on the europium band. The persistence of $Sr_3(PO_4)_2$:Eu phosphors begins to increase noticeably from a second rare earth concentration of about 10^{-3}%.

Conclusions

The best of the investigated phosphors and the one holding the greatest promise for practical application is $Sr_3(PO_4)_2$:Eu. Its emission color is violet-blue with λ_{max} = 4250 Å, and its decay time is less than 10^{-4} sec. Its luminescence intensity amounts to 25-35% the intensity of ZnS:Ag as measured with a Cs-Sb photomultiplier with a peak sensitivity at ~4300 Å.

All the observations of the cathodoluminescence of Eu activated strontium phosphates indicate that the europium is present in these phosphors in the divalent state. This is substantiated by the clear change in the position of λ_{max} of the diffuse luminescence band with changes in the chemical composition of the base or its crystal lattice, and also by the absence of the narrow-band or line emission characteristic of trivalent europium. Reduction of Eu^{3+} to Eu^{2+} in strontium meta-, pyro- and orthophosphates occurs during the heating of the phosphor (this is also known to be the case for calcium phosphates) and does not require a reducing medium. Similar reduction of Eu^{3+} to Eu^{2+} is also known to occur in alkali halide[3,4] and sulfide[5] phosphors.

Our measurements show that the admixture of other rare earths acts to reduce the cathodoluminescence parameters of the Eu activated strontium phosphates. A change in the luminescence spectrum is observed at a 10^{-5}% concentration of the second rare earth, and a noticeable decrease in brightness and increase in decay time begins at a concentration of 10^{-3}%. Hence for practical purposes the content of "accompanying" rare earths in europium activated phosphate luminophors should not exceed 10^{-4}%.

I desire to express my deep gratitude to S.Ya.Gutner and E.K.Raspletina for investigating the cathodoluminescence parameters and to Yu.P.Kozlova for preparing the phosphor samples.

References

1. V.P.Nazarova, Materialy VII Soveshchaniya po lyuminestsentsii (Transactions of the 7th Conference on Luminescence - Crystal Phosphors), Tartu, 1959.

2. P.W.Ranby, D.N.Mesh & S.H.Hendersen, Brit.J.Appl.Suppl., No.4, 18 (1955).

3. P.Pringsheim, Fluorescence and Phosphorescence, N.Y., 1949.

4. L.M.Shamovskii & Yu.N.Zhvanko, Transactions of the 7th Conference on Luminescence, Tartu, 1959.

5. S.A.Fridman & V.V.Shchaenko, Ibid.

COMPREHENSIVE INVESTIGATION OF THE OPTICAL AND THERMOOPTICAL PROPERTIES OF POLYACTIVATED ALKALI-HALIDE CRYSTAL PHOSPHORS

- A.Kh.Khalilov, E.Yu.Salaev, A.P.Mamedov, T.D.Alieva & F.K.Isaev

Investigation of the interaction of activators in polyactivated crystal phosphors is important from the standpoint of development of spectral converters, i.e., luminophors transforming invisible to visible radiation. Comprehensive investigation of the optical and thermooptical properties of such phosphors is essential for clarifying the mechanism of recombination luminescence and the structure of the complex luminescence centers. In the present report we give the results of investigation and measurements of the excitation spectra of individual luminescence bands and the spectral composition of the fluorescence, phosphorescence and thermostimulated luminescence of a number of alkali halide phosphors (see Figs.1 & 2 and table). We also investigated the internal quenching of the visible and

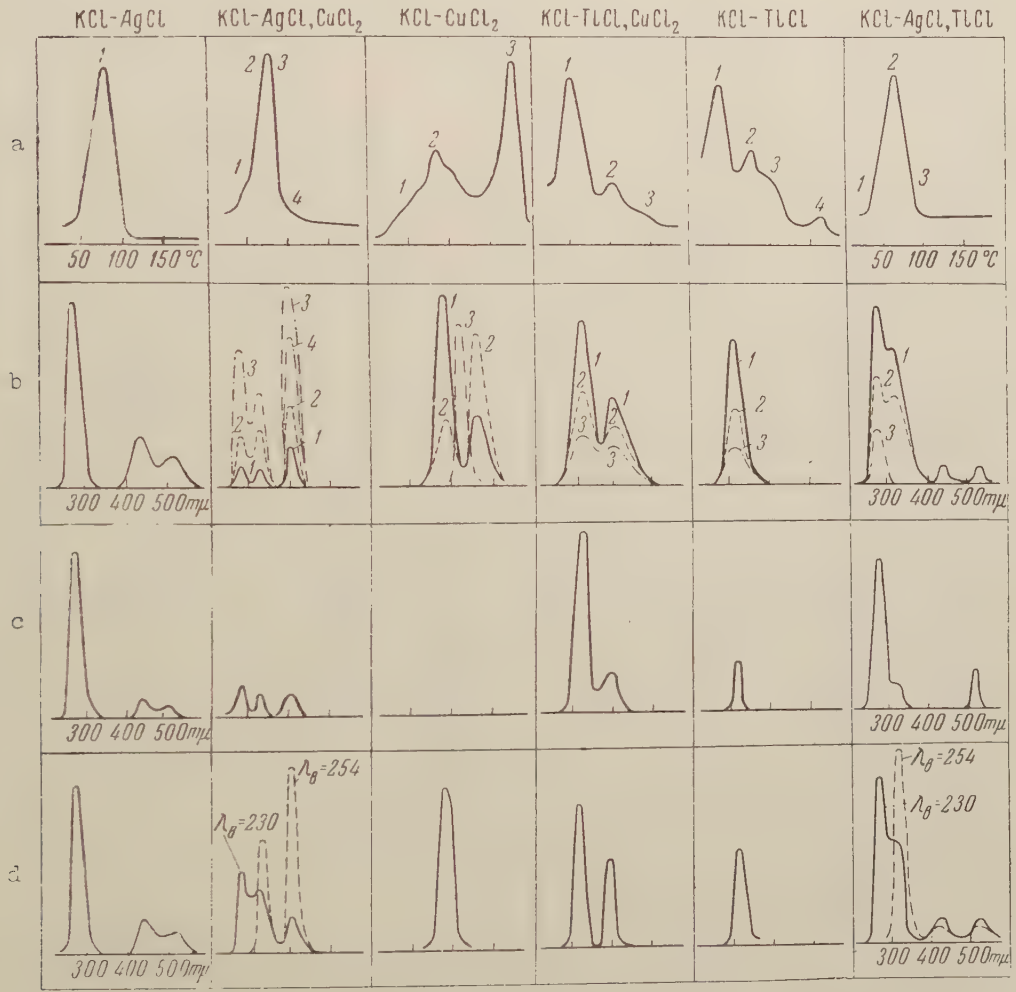

Fig.1. a - Thermostimulation spectra (glow curves); b - spectral composition of the individual glow curve peaks shown in a; c - phosphorescence spectra after excitation with x-rays; d - fluorescence spectra with excitation in the region of the principal absorption bands of the activators. The horizontal scales in all the rows are the same.

Wavelengths of the peaks (in mμ) and the half-width* of the luminescence bands

Phosphor	Fluorescence							Phosphorescence**	Thermostimulation											
									Peak I				Peak II				Peak III			
	λ_{exct} = 230 mμ	248 mμ	254 mμ	265 mμ	275 mμ	280 mμ	302 mμ													
NaCl — AgCl	398						520 0,33	400			400	520 0,40			520					
NaCl — $CuCl_2$			360 0,35	360 0,36						360 0,37			360				360			
NaCl — AgCl, $CuCl_2$	360 400	360 0,37		360 400 520	360	360	520 0,36		360 0,40	400	460	520 0,43	360 0,42	400	460	520		520 0,45		
NaCl — AgCl, TlCl	400	360	360				520		250 0,41	400	460	520			520			520		
NaCl — $CuCl_2$, $MnCl_2$			360*** 570 0,31	360*** 570 0,30	360*** 570 0,33		570		360 0,35				360 0,36	570						
NaCl — $PbCl_2$, $MnCl_2$				315 360 440 570	315 360 440 570	360 570*** 0,28	570													
NaCl — $CuCl_2$, Sb			295*** 360 0,60	295*** 360 0,58					295 0,64	360	480		295 0,65	360	480			360	480	
NaCl — $PbCl_2$, Sb			295*** 360 440 0,58	295 360 440	315 440 360			295*** 360 0,59	295	360			295	360	480		295 0,64	360 0,64	480 0,61	

Table continued

Phosphor	Fluorescence							Phosphorescence**	Thermostimulation									
									Peak I				Peak II				Peak III	
	λ_{exct} = 230 mμ	248 mμ	254 mμ	265 mμ	275 mμ	280 mμ	302 mμ											
$NaCl — MnCl_2$							570			570			570 0,38				570 0,42	
$NaCl — PbCl_2$					360 440				360					360			360	
$NaCl — Sb$		295 0,60	295 0,60	295				295 360	295 0,64	360	480		295 0,65	360	480		295 0,65	360	480
$KCl — PbCl_2$, TlI		306 342 470	306 342 470	342	342							470				470		
$KCl — PbCl_2$, $CuCl_2$		400	400	342 400	342 400					460			400	460			400	
$KCl — PbCl_2$, AgI	310 342 440				310 342 440										460	500		460	500
$KCl — PbCl_2$, $MnCl_2$				342 640	342 640													

* The half-widths are indicated under the peak wavelengths in ev.

**We list phosphorescence data only for NaCl:AgCl, NaCl:Sb and $NaCl:PbCl_2:Sb$; the phosphorescence spectra were not recorded for the other phosphors.

***Where several luminescence bands are present, we list the width only for the bands identified by ***.

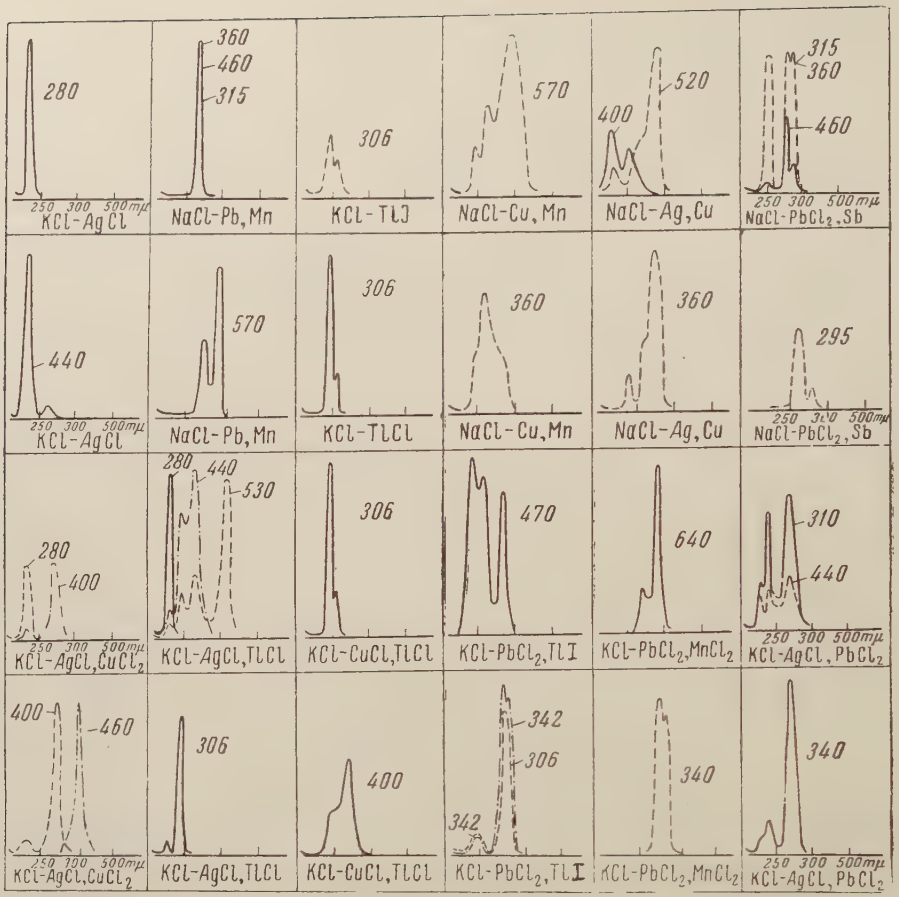

Fig.2. Excitation spectra; the figures at the curves are the wavelengths of the luminescence band peaks. The horizontal scales in each row are the same.

ultraviolet luminescence of the phosphors with excitation by radiation with λ_{max} = = 218, 230, 255 and 272 mμ.

The phosphor single crystals were grown by the Kyropoulos technique with activator concentrations of 0.01 and 1 mole percent in the melt. The fluorescence, phosphorescence and excitation spectra and the spectral composition of the emission corresponding to individual glow curve peaks were investigated on a spectrometer assembled by us using two SF-4 spectrograph monochromators.

The following conclusions may be drawn on the basis of the experimental data:

1. Cu^{2+} ions in KCl:$CuCl_2$ do not yield phosphorescence. In contrast, in KCl:$CuCl_2$:AgCl and KCl:$CuCl_2$:TlCl phosphors in the presence of Ag^+ and Tl^+ ions, Cu^{2+} ions do phosphoresce (Fig.1, curves c, band with λ_{max} = 400 mμ). This is apparently due to the sensitizing influence of Ag^+ and Tl^+, the phosphorescence of which is transmitted to the Cu^{2+} ions and excites their sensitized luminescence.

2. In different phosphors the fluorescence, phosphorescence and thermostimulated luminescence differ as regards spectral composition. For the low temperature glow curve peaks of some phosphors (KCl:Ag, KCl:Ag:Cu, KCl:Ag:Tl and others) the spectral composition of all three forms of luminescence is the same, but for the high temperature glow curve peaks the agreement no longer obtains. Particularly great divergences are observed for KCl phosphors with the activators Cu^{2+}, $Ag^+ + Cu^{2+}$, $Pb^{2+} + Tl^+$ and NaCl phosphors with Sb^{3+}, $Sb^{3+} + Pb^{2+}$, $Cu^{2+} + Mn^{2+}$,

Pb^{2+} + Mn^{2+} and Ag^{+} + Tl^{+}.

3. The individual glow curve peaks and the fluorescence and phosphorescence bands of all the investigated crystal phosphors comprise spectral bands corresponding to the activator ions incorporated in the process of crystal growth into the halide lattice at cationic sites; this substantiates the recombination nature of the afterglow mechanism. In the case of NaCl:Ag:Tl and NaCl:Ag phosphors the short wavelength luminescence bands of the activators are contained in the spectra of all three forms of luminescence, while the long wavelength bands of the activators are present only in the second and third glow curve peaks.

4. In the emission of KCl:Ag:Tl, KCl:Ag:Cu, KCl:Ag and NaCl:Ag there are observed the long wavelength (440 and 530 mμ) luminescence bands of Ag, which are of low intensity in all three spectra. In contrast to the 280 mμ band of Ag, the intensity of these long wavelength bands changes very little in going from the low temperature to the high temperature glow curve peaks. These bands are, apparently, due to association of Ag^{+} ions with lattice defects or with other ions of the same type and ions of the second activator.

5. Comparison of the peak wavelengths and widths of the same luminescence band (see table and Fig.1) in all three forms of luminescence shows that the minimum band width is observed in the fluorescence spectra, i.e., the phosphorescence and thermostimulated luminescence bands are somewhat broadened. Comparison of the peak wavelength λ_{max} and width of the same luminescence band in the spectra of different glow curve peaks shows that for all phosphors λ_{max} and the luminescence band width in going from the first to the last glow curve peak, increases very little, except in the case of KCl:Cu:Tl, in the thermostimulated luminescence of which λ_{max} for the 305 and 400 mμ bands increases by 15 mμ in going from the first to the fourth peak.

6. Contrary to the commonly held view, doubly and triply charged activator ions in general do not phosphoresce, but this is not true in all cases: our experiments showed that Mn^{2+}, Pb^{2+} and Sb^{2+} in the NaCl lattice do phosphoresce.

7. Comparative measurements of the fluorescence spectra excited by different wavelengths (230, 248, 254, 265, 275, 290 and 302 mμ) and the excitation spectra of the different fluorescence bands (see Fig.2) of KCl phosphors with two activators: Ag + Cu, Ag + Tl, Ag + Pb, Tl + Pb and Pb + Mn, and of NaCl phosphors with Ag + Tl, Ag + Cu, Cu + Mn and Sb + Pb (in which as our studies showed, the absorption bands of the first activator overlap little or not at all with the short wavelength edge of the emission bands of the second activator) and the corresponding single activator phosphors prepared and studied under the same conditions enabled us to establish the presence of the effect of energy migration from one activator center to another. Thus we established that in the enumerated phosphors with excitation in the region of the absorption band of Ag with λ_{max} = 230 mμ there is observed intense sensitized luminescence of Cu^{2+}, Tl^{+} and Pb^{2+}, whereas in the corresponding single activator phosphors KCl:$CuCl_2$, KCl:TlCl, KCl:$PbCl_2$, NaCl:$CuCl_2$ and NaCl:TlCl the Cu^{2+}, Tl^{+} and Pb^{2+} ions do not luminesce at all under excitation in the region of the Ag absorption band with λ_{max} = 230 mμ. As will be evident from Fig.2, the sensitized luminescence of Cu^{2+}, Tl^{+} and Pb^{2+} in these phosphors comprises all the luminescence bands of these ions (the 400 and 460 mμ bands of Cu^{2+}, the 310, 340 and 460 mμ bands of Pb^{2+}, etc.). We observed a similar effect in Pb + Sb and Pb + Tl activated phosphors: whereas with excitation in the absorption region of Tl and Sb with λ_{max} = 250 mμ the Pb^{2+} ions in the single activator phosphors KCl:Tb and NaCl:Pb do not luminesce, in two activator phosphors NaCl:Pb:Sb and KCl:Tl:Pb excitation in this region (λ_{max} = 250 mμ) gives rise to sensitized luminescence of the Pb^{2+} ions; this luminescence comprises

all three of the characteristic emission bands of Pb^{2+}: 315, 340 and 460 mμ.

We also observed the effect of sensitized luminescence in NaCl:Cu:Mn, NaCl:Pb:Mn and KCl:Pb:Mn phosphors, the last two of which were first investigated in the work of Refs.2-5. In these phosphors with excitation in the absorption region of Cu^{2+} with λ_{max} = 250 mμ and 260 mμ and of Pb^{2-} with λ_{max} = 272 mμ, there is observed sensitized luminescence of Mn, whereas in the case of KCl and NaCl phosphors containing only Mn no manganese luminescence is observed under excitation at the indicated wavelengths.

8. In order to clarify the nature of the sensitized luminescence in the investigated phosphors we grew and investigated under identical conditions two batches of KCl phosphors containing activator concentrations of 0.01 and 1 mole percent. The measurements showed that for the phosphors with the 0.01 mole percent activator no significant sensitized luminescence was observed. This can be taken as proof that the effect of energy migration between the activators in KCl and NaCl phosphors is not due to reabsorption of the luminescence of one activator by the other (with the longer wavelength absorption band), for the reabsorption should not depend on the activator concentration. Hence there is reason to assume that the sensitized luminescence is due primarily to resonance energy transfer between the activators.

References

1. E.Claffy & C.Klick, J.Electrochem.Soc., 104, 445 (1957).
2. M.Kato, Sci.Papers Instr.Phys.chem.Res.Tokyo, 41, 113 (1943).
3. K.Murata & R.Smith, Am.Mineral., 31, 523 (1946).
4. R.Ginter, J.Electrochem.Soc., 98, 874 (1951).
5. K.K.Shvarts, Trudy IFA AN ESSR (Proceedings, Institute of Physics and Astronomy, Estonian SSR Ac.of Sci.) Vol.II, Tartu, 1960.

ORIGIN OF THE LONG WAVELENGTH LUMINESCENCE BANDS OF ALKALI-HALIDE PHOSPHORS

- N.I.Ivanova, L.I.Tarasova & A.P.Zhukovskii

There is no unanimity among investigators regarding the origin of the diverse luminescence bands of single activator alkali halide phosphors. Thus according to the model proposed by Seitz[1], all the luminescence bands should be attributed to transitions in centers of a single type. Most investigators, however, incline to Pringsheim's[2] hypothesis that there exist at least two different types of luminescence centers. The short-wave luminescence bands characteristic of low activator concentrations are usually attributed to activator ions located at cationic sites of the host lattice; different models are proposed for the centers responsible for the long wavelength bands: pair centers, activator ions located close to defects in the host lattice, etc.

For determining the nature of the luminescence centers in alkali halide phosphors, it is useful to compare the emission of phosphors based on different materials. We undertook such a comparison for alkali halide salts activated by silver and thallium. We found that the number of bands and the dependence of the spectrum on the conditions of preparation differ greatly even for phosphors with close chemical properties. Inasmuch as such comparison is meaningful only for bands of the same nature, we felt it essential to clarify the characteristics of the individual bands in more detail.

To this end we investigated the polarization of the luminescence of a large number of sodium and potassium halide phosphors. On the basis of the results obtained one can draw the general conclusion that in many cases the different bands of the same phosphor as well as the emission bands of different phosphors of similar composition (for example, the visible bands of KCl:TlCl and NaCl:TlCl) should be attributed to different centers.

We also carried out comparison of the luminescence bands in the spectra of series of mixed base material phosphors. In such series there was realized step-by-step change in the composition of the base material, so that one can follow the transformation of the spectrum from one phosphor to the other. In general the changes observed in the spectra of the investigated series were complex in character; however, the principal regularities noted were the following:

1. In some cases one can follow the transition of a luminescence band of one component in the series to the band of another. Usually, however, the band identified with a particular component gradually weakens and disappears, without giving rise to an analog in the spectrum of the second component. In some cases there appeared new bands not present in the spectra of the pure components.

2. In none of the investigated series were there observed band shifts that could be correlated with changes in the lattice constant of the host. Even in the series KCl·KBr:Tl and KCl·RbCl:Tl in which the lattice constant is a linear function of the composition the shift of the bands was nonuniform. The observed changes in the spectra occurred mainly in the region of relatively low concentrations of the heavier elements (both anions and cations). A particularly strong effect was produced by introduction of iodine: the luminescence spectrum changed markedly even at an iodine concentration comparable with the activator concentration.

3. The behavior of the short wavelength luminescence bands was generally analogous to the behavior of the long wavelength bands.

The results obtained, in our opinion, are consistent with the assumptions that a) the different luminescence bands of a given phosphor must be attributed to different centers and b) the centers are formations of the molecular complex type, involving both the base material and the activator.

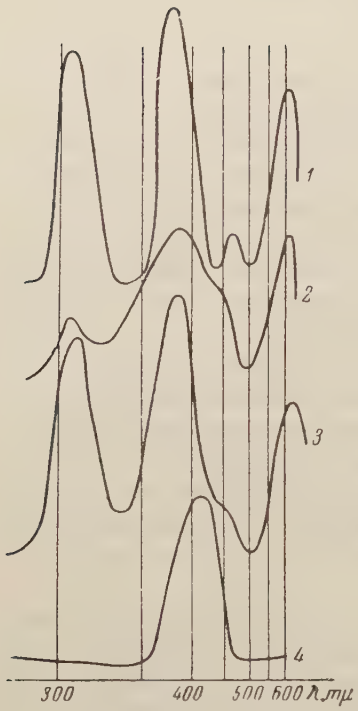

Photometric traces of the luminescence spectra of: 1 - KCl:TlCl(1), 2 - K_2SO_4: :TlCl(0.5), 3 - K_2SO_4: :Tl_2SO_4(0.5). All activator concentration in mole percent.

Apparently centers of this type should be little sensitive to the surroundings. Possibly a regular host lattice is not needed for the luminescence of some centers, the only requirement is conditions insuring the formation of the given complex (compound) and sufficient isolation of the centers from each other. We investigated the luminescence of phosphors activated from the surface, phosphors doped with divalent metals and phosphors based on some nonhalide salts of the alkali metals.

The preliminary results obtained are consistent with the above assumptions. For example (see figure), the following regularities were observed in the luminescence of the sulfates and nitrates of alkali metals: when activated with the sulfate or nitrate of the activator, these salts either do not luminesce or have their own characteristic spectrum. When activated with halide salts of the activator, there is observed an intense luminescence, the bands of which are close in energy to the bands of the corresponding alkali halide phosphor. Introduction of small amounts of alkali halide (amounts comparable to the activator concentration) led to the formation of phosphors similar as regards luminescence spectrum to the corresponding alkali halide phosphor and equal to it in brightness. Here, however, one can hardly expect the formation of alkali halide phosphor with an ordered, typical halide lattice.

The hypothesis that luminescence centers are molecular complexes is not inconsistent with the concept of pair centers or centers located on intercrystalline surfaces or close to microdefects in the host crystal.

Scientific Research Physical Institute,
Leningrad State University

References

1. F.Seitz, J.Chem.Phys., 6, 150 (1938).
2. E.Hirschlaff & P.Pringsheim, J.Chem.Phys., 16, 241 (1948).

DISCUSSION

N.N.Kristofel': I would like to say a few words regarding the so-called "molecular complexes". One can speak of complexes when the forces of interaction between the activator and its nearest neighbors are much greater than the forces between these neighbors and the other ions of the crystal. This situation does not obtain where the regular luminescence centers in alkali halide crystals are concerned. The luminescence centers in these phosphors can be regarded as quasimolecules, but in an entirely different sense. Introduction of the activator leads to the appearance of local vibrations (the amplitude of which falls off rapidly with the distance from the activator), and the centers, in general, include all the ions participating in the local vibrations, with which

the activator interacts. In this sense, the "dimensions" of the center have a vibrational nature, and one can speak of quasimolecules in the crystal. We are in agreement with the opinion of F.D.Klement that the results of Ivanova can be understood on the basis of the usual concepts regarding centers: there is no need to introduce hypothetical "complexes".

* * * * * * *

SENSITIZED LUMINESCENCE OF KCl:Pb:Mn PHOSPHOR

- K.K.Shvarts & G.K.Vale

In the present work, which is a continuation of our earlier investigations[1], we consider resonance energy transfer in KCl:Pb:Mn phosphor. It is known that the electron transitions in Mn^{2+} ions are quadrupole transitions and that these are virtually not evinced in absorption.[2] Energy transfer from Pb^{2+} to Mn^{2+} probably corresponds to dipole-quadrupole resonance.[3]

We measured the absorption, luminescence and excitation spectra of KCl:Pb:Mn phosphor, as well as the quantum luminescence efficiency and its dependence on the excitation frequency and temperature (Figs.1 & 2).

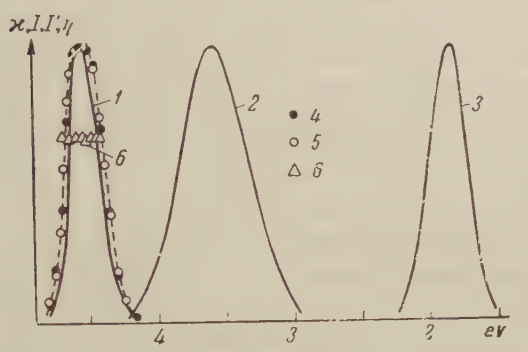

Fig.1

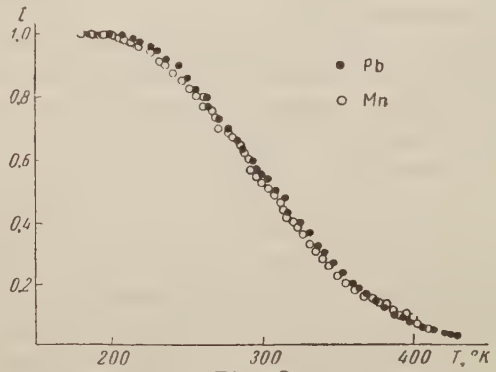

Fig.2

Fig.1. Spectral characteristics of KCl:Pb:Mn phosphor (0.03 mole percent Pb and 0.3 mole percent Mn in the melt): 1) absorption spectrum, 2) Pb luminescence spectrum, 3) Mn luminescence spectrum, 4) Pb excitation spectrum, 5) Mn excitation spectrum, 6) relative quantum efficiency of the Mn luminescence.

Fig.2. Temperature dependences of the luminescence intensities of lead and manganese in KCl:Pb:Mn (excitation by the 265 mμ mercury line).

As will be evident from Fig.1, the excitation spectrum of manganese in KCl:Pb:Mn agrees with the excitation spectrum of lead. It follows therefore that the energy is first absorbed by the Pb ions and is then transferred to the Mn ions. Inasmuch as the excitation spectra of lead in KCl:Pb:Mn and in KCl:Pb coincide, it may be asserted that the presence of manganese in KCl:Pb:Mn in the range of low concentrations ob Pb and Mn (0.03 and 0.3 mole percent, respectively) does not noticeably affect the spectral characteristics of the lead centers.

It was found that the quantum efficiency of luminescence of Mn with excitation in the absorption band of lead, which corresponds to the $^1S_0 - ^3P_1$ transition

in the Pb ions, does not depend on the frequency of the exciting light, i.e., Vavilov's law obtains for the sensitized luminescence of Mn^{2+}.

By special experiments we showed that the luminescence of Mn is also excited in the short wavelength absorption band of the lead centers ($^1S_0 - ^1P_1$ transition).

We felt it would be of interest to determine how the probability for energy transfer from Pb to Mn ions depends on the temperature. To this end we measured the temperature dependences of the quantum efficiency of Pb and of Mn in KCl:Pb:Mn. We found that both dependences agree with each other and with the temperature dependence of the luminescence efficiency of Pb in KCl:Pb (Fig.2). It may be concluded therefore that nonradiative transitions are realized in the lead ions[1,2] and that the energy transfer from the Pb to the Mn ions, in agreement with the theory of Dexter[3], occurs after attainment of equilibrium as regards vibrational energy between the excited lead centers and the surrounding crystal lattice.[5]

In addition, our experiments indicate that the probability for energy transfer from Pb to Mn ions does not depend on the temperature in the range from 180 to 430°K. This may be explained by the fact that owing to the "dense" spacing of the energy levels in Mn^{2+} ions, variation in the luminescence spectra of the Pb ions with temperature does not alter the magnitude of the "overlap integral".

Microscopic observation of the luminescence of manganese in KCl:Pb:Mn phosphor showed that the luminescence of manganese occurs at special defects in the crystal lattice, where the concentration of lead and manganese is higher than the mean concentration of these elements in the crystal. This result shows that for some systems exhibiting sensitized luminescence an important requirement for obtaining a good phosphor, in addition to realization of a solid solution, is its subsequent treatment in order to insure higher local concentrations of the impurity ions (for example, high concentrations near dislocations in the lattice).

We desire to express our deep gratitude to Ch.B.Lushchik for his guidance in the work.

References

1. K.K.Shvarts & U.A.Zirnitis, Trudy IFA AN ESSR (Proceedings, Inst.of Physics and Astronomy, Estonian Ac.of Sci.), No.11, 3 (1960).
2. C.Klick & J.Schulman, J.Opt.Soc.Am., 42, 910 (1952).
3. D.Dexter, J.Chem.Phys., 21, 836 (1953).
4. M.Kato, Sci.Papers.Inst.Phys.Chem.Res.Tokyo, 41, 113 (1943).
5. K.K.Shvarts, G.K.Vale & B.Ya.Zunde, Trudy IFA AN Eston.SSR, No.12, 77 (1960).

DISCUSSION

Ch.B.Lushchik: The interesting effect of sensitized fluorescence of alkali halide phosphors, the effect investigated by Shvarts & Vale, enabled I.V.Yaek (Tartu) to detect in these systems a new interesting effect, which he calls "sensitized" phosphorescence. In NaCl:Tl:Mn crystals after excitation in the absorption band of Tl^{2+} there appears phosphorescence of Mn^{2+}; this phosphorescence persists for many minutes. The excitation spectrum of the Mn^{2+} phosphorescence agrees with the absorption band of Tl^{+} ($^1S_e \rightarrow ^1P_1$ transitions). The effect of "sensitized" phosphorescence may play a significant role in recombination phosphorescence of crystals.

CONCENTRATION AND TEMPERATURE QUENCHING OF LUMINESCENCE IN SOME SILVER ACTIVATED ALKALI-HALIDE PHOSPHORS

- L.A.Rebane

1. It is known that introduction of high activator concentrations into a phosphor generally leads to complication of the spectral characteristics of the phosphor; this is commonly attributed to the formation of more complex centers.[1] The nature of the centers forming at high activator concentrations has not yet been sufficiently studied, but it is obvious that the presence of such centers greatly complicates the processes involved in concentration quenching. In the present work we investigated the phosphors NaCl:Ag and NaBr:Ag, which are characterized by unlimited solubility of the activator salts in the base material. For comparison we took KCl:Ag, in which the limit solubility of AgCl at room temperature is ≤ 0.2 mole percent.

2. Investigation of the variation of the absorption coefficient as a function of the activator concentration in NaCl:Ag and NaBr:Ag showed that the short wavelength absorption bands belong to centers containing one Ag^+ (centers I), while the long wavelength absorption band belongs to centers with two Ag ions (centers II[2,3]). At low activator concentrations, there predominates the luminescence spectra of these phosphors the emission band of centers I. With increase of the activator concentration, the relative intensity of the long wavelength band belonging to centers II rises. Upon further increase of the activator concentration, this band begins to predominate and its long wavelength part is enhanced. The band peak shifts to the long wavelength side. Investigations of the luminescence spectra with excitation at different wavelengths and of the excitation spectra for different parts of the luminescence spectrum showed that we are dealing here with the superposition of two luminescence bands, the excitation for which differs. Apparently, at high concentrations there form new, different luminescence centers (centers III). At least three different types of luminescence centers also form in KCl:Ag, but in this case the dependence of the spectra on the conditions of heat treatment of the samples comes to the fore.

3. For all the concentration series phosphors we measured the relative quantum efficiency by determining the areas under the spectral curves. The results obtained for NaCl:Ag are shown in the accompanying figures (analogous curves were obtained for NaBr:Ag). It will be evident that the concentration behavior of the luminescence output depends on the excitation wavelength λ_{excit} and differs for the different centers. The constancy of the integral output ($\eta_1 + \eta_2$ in Fig.a) with simultaneous decrease of the output from centers I evinced in the range of

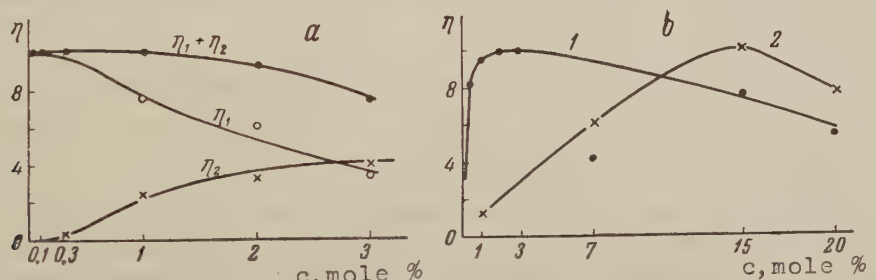

Variation of the luminescence output of NaCl:Ag phosphor as a function of the activator concentration: a - λ_{excit} = 218 mμ; b - λ_{excit} = 228 mμ (1) and 240 mμ (2).

low activator concentration can be explained on the assumption of competition between centers I and centers II as regards absorption of the excitation energy.[3] The decrease of the integral output in the range of high activator concentrations is evidence of concentration quenching in these phosphors. At such high activator concentrations there may obviously occur energy transfer between the different centers, but the decrease of the integral luminescence output may also occur in the process of competition with centers that are in the stage of undergoing temperature quenching.

c, mole %	$T_{1/2}$, °K	Q, ev	c^*
0,03	496	1,06	$6 \cdot 10^{10}$
0,1	499	1,01	$2 \cdot 10^{10}$
0,3	493	1,04	$1 \cdot 10^{10}$
1	481	0,95	$9 \cdot 10^{9}$
2	465	0,78	$3 \cdot 10^{8}$

*Parameter entering into Mott's formula.

4. Investigation of temperature quenching in Ag activated phosphors is complicated by the strong temperature dependence of the absorption.[4] Thus, for example, in the case of NaCl:Ag (0.03 mole percent) increase of the temperature from 20 to 370° increases the area under the absorption curve by a factor of 3.8. Aside from the trivial correction for the temperature dependence of the fraction of adsorbed energy in the case of incomplete absorption, one must take into account the fact that even under conditions of complete integral absorption the ratio of the absorption of centers I and II will vary with the temperature, which, of course, will affect the temperature behavior of the quenching. This is particularly important in the range of high concentrations.

The temperature quenching of centers I obeys Mott's formula. For NaCl:Ag we observed some change in the parameters entering into Mott's formula as a function of the activator concentration (see table). It is not clear at present whether the observed decrease of Q really corresponds to lowering of the energy barrier for thermal activation[5] or is only due to partial superposition of the emission from centers II.

For centers I there is observed independent variation of temperature quenching, the character of which depends on by what absorption band of the centers the phosphor is excited.

References

1. F.D.Klement, Trudy IFA AN ESSR (Proceedings, Instit.of Physics and Astronomy, Estonian SSR Ac.of Sci.), No.1, 3 (1955); N.I.Ivanova, Thesis, Leningrad State Univ., 1952.

2. H.Etzel & J.Schulman, J.Chem.Phys., 22, 1549 (1954).

3. L.A.Rebane, Trudy IFA AN ESSR, No.12, 49 (1960); R.Lushpa, Thesis, Tartu University, 1960.

4. M.Forro, Z.Phys., 56, 534 (1929).

5. F.D.Klement, Izv.AN SSSR, Ser.fiz., 15, No.15, 651 (1951).

DISCUSSION

Z.L.Morgenshtern: Rebane observed a number of luminescence bands in silver activated alkali bromides and chlorides and attributed all these bands to centers containing silver. In our opinion, however, the short wavelength band is not connected with silver activator but belongs to the host lattice. The behavior of this band is analogous to the behavior of the ultraviolet luminescence bands of unactivated alkali iodides (see N.N.Vasil'eva & Z.L.Morgenshtern, Izv.AN SSSR, Ser.fiz., 25, 47 (1961) (Trans.Bulletin, 25, 47)).

The luminescence output in this short wavelength band falls off to zero with increase of the activator concentration. Such behavior is improbable for an activator band but is entirely natural for luminescence due to the host lattice. The luminescence yield in this band falls off with increasing temperature in the same was as for the short wavelength luminescence band of alkali iodides.

* * * * * * *

LUMINESCENCE OF AMMONIUM HALIDE PHOSPHORS

- A.Ya.Pae & L.Ya.Uibo

Ammonium halide crystal phosphors, which were originally synthesized and investigated by Klement[1], Ivanova[2] and Hüniger & Rudolf[3], are in many respects analogs of alkali halide phosphors. At the same time, they display a number of interesting, distinctive features, which are probably connected with the complex structure of the tentrahedral NH_4 ion. Our investigations were concerned primarily with ammonium halide crystals activated by Tl^+ and Sn^{2+}.

X-ray diffraction studies showed that NH_4Cl and NH_4Br form continuous series of substitutional solid solutions with TlCl and TlBr. Vegard's law is fulfilled in these systems, i.e., the variation in unit cell dimensions is linear with change in the composition. The Tl^+ activator ions replace the NH_4 ions in the crystal lattice. Ammonium halide phosphors can be prepared with very high activator concentrations: luminescence is still observed at 70% thallium halide content.[4] NH_4I + TlI constitute a somewhat more complex crystallochemical system.[5]

The luminescence centers in ammonium halide phosphors are the activator ions: Tl^+ and Sn^{2+}. As in alkali halide phosphors[6,8], in ammonium halide phosphors the individual bands in the excitation and absorption spectra can be associated with definite electronic transitions ($^1S_0 \rightarrow {}^3P_{0,1,2}$ and $^1S_0 \rightarrow {}^1P_1$) in the free activator ions. The transition involved in luminescence is $^3P \rightarrow {}^1S_0$. The excitation and luminescence spectra are largely similar to the spectra of the corresponding alkali halide phosphors.[9,10]

At high thallium concentrations the spectral characteristics of ammonium halide phosphors become more complicated: there appear new long wavelength bands in the luminescence spectra, and the corresponding excitation spectra are shifted to the long wavelength side relative to the excitation spectra of the main centers. There apparently exist at least two types of luminescence centers, differing as regards the nearest neighbors of the Tl ions. No analogous complication of the spectra with increase of the activator concentration is observed in the case of activation by Sn^{2+} (cf.Ref.11).

In order to clarify the mechanism of luminescence in ammonium halide phosphors we measured the excitation spectra of the activator luminescence of NH_4:Tl in a wide range including the principal absorption band of the host. We found that the most intense luminescence is stimulated by excitation in the activator bands. Excitation is less effective in the exciton absorption band (~5.15 ev) and in the shorter wavelength absorption region corresponding to band-band transitions (5.8-6.6 ev). This indicates that in ammonium halide phosphors, as in alkali halide phosphors, the absorbed energy can be transferred from the base material to the luminescence centers by exciton and by electron-hole processes.

The persistent luminescence of ammonium halide phosphors is recombination phosphorescence, inasmuch as the luminescence centers and trapping centers associated with the host material are spatially separated.[14]

Some of the characteristics of the trapping centers in ammonium halide crystals differ significantly from the corresponding characteristics of the trapping centers in alkali halide phosphors: the principal absorption peak in ammonium halide phosphors has an appreciably width and its position is independent of the temperature, the host anion, etc.[9,15] We assume that these distinctive attributes are due to the characteristics of the NH_4 ions that surround the electron color centers.

In contrast to alkali halide crystals, ammonium halide crystals are polymorphous. Changes in the crystal lattice incident to the polymorphic transitions exert an appreciable influence on the luminescent characteristics of these phosphors. Substantial rearrangement of the crystal lattice (change of the coordination number from 6 to 8) is accompanied by an abrupt change in the spectral characteristics of the phosphor.[10] In the region of the low temperature polymorphic transition there is observed a change in the characteristics of the trapping centers. Thus in NH_4Cl:Tl at 30.8° there is a marked discontinuity in the value of the energy of thermal ionization of the trapping centers; this abrupt change in ionization energy probably explains the "cold flash" effect observed in NH_4Cl:Tl.[16,17]

Apparently, in the course of our investigations we were the first to succeed in observing in pure form the influence of polymorphic transformations on electron-hole relaxation processes.

Detailed and extensive comparison[18] of the characteristics of ammonium halide and alkali halide phosphors leads to the following inferences:

1. The characteristics and structure of the activator luminescence centers in alkali halide and ammonium halide phosphors are in general similar.
2. However, the electron color centers in ammonium halide crystals differ in a number of respects from the F centers in alkali halide crystals.
3. The attributes of exciton centers in ammonium halide and alkali halide phosphors are similar, and hence the exciton processes occurring in these two types of crystals are analogous.

References

1. F.D.Klement, Izv.AN SSSR, Ser.fiz., 15, 651 (1951).
2. N.N.Ivanova, Thesis, Leningrad State University, 1952.
3. M.Hüniger & J.Rudolf, Z.Phys., 117, 81 (1940).
4. A.Ya.Pae, Trudy, IFA AN ESSR (Proceedings, Institute of Physics & Astronomy, Estonian SSR Ac.of Sci.), No.4, 26 (1956).
5. A.Ya.Pae, Ibid., No.11, 49 (1960).
6. A.S.Andrianov & M.L.Kats, Transactions of the 5th Conference on Luminescence, Tartu, 1957.
7. N.E.Lushchik & Ch.B.Lushchik, Trudy IFA AN ESSR, No.6, 5 (1957).
8. Ch.B.Lushchik, N.E.Lushchik & K.K.Shvarts, Ibid., No.8, 3 (1958).
9. L.Ya.Uibo, Ibid., No.7, 227 (1957).
10. A.Ya.Pae, Ibid., No.8, 47 (1958).
11. T.A.Abdusadykov, Ibid., No.10, 122 (1959).
12. Ch.B.Lushchik & G.G.Liid'ya, Ibid., No.7, 193 (1957).
13. Ch.B.Lushchik, Izv.AN ESSR (Bulletin of the Estonian SSR Ac.of Sci.) 8, No.4, 287 (1959).
14. L.Ya.Uibo & E.V.Yaek, Doklady AN SSSR, 105, 1212 (1955).
15. H.Rüchardt, Z.Phys., 134, 554 (1953).

16. L.Ya.Uibo, Transactions of the 7th Conference on Luminescence (Moscow, 1958). Pub.Tartu, 1959.
17. L.Ya.Uibo, Trudy IFA AN ESSR, No.11, 108 (1960).
18. Ch.B.Lushchik & L.Ya.Uibo, Ibid., No.12, 275 (1960).

* * * * * * *

DETECTION OF LATTICE DEFECTS IN ALKALI HALIDE CRYSTALS BY MEANS OF ELECTROLYTIC COLORING

- V.M.Bezruchko & A.A.Shatalov

Usually the process of coloring in alkali halide crystals is treated as though it occurs in an ideal crystal lattice, i.e., no account is taken of the influence on the color centers of different defects, which are always present in real crystals.

We found that in the process of electrolytic coloring there occurs "development" of different types of imperfections. At points where the crystal lattice is disturbed the energy for thermal activation of the ions and formation of vacancies is much lower than in the other parts of the crystal, and, consequently, color centers are formed more rapidly and in higher concentrations in the vicinity of imperfections. As a result of this selectivity one can "develop" the picture of defects in transparent solids. This pertains not only to major disturbances of the lattice: it is also feasible to develop very fine, minor imperfections. In our laboratory we have observed many cases of "development" by means of coloring of different types of defects. Below we shall discuss one of these.

It was established that in some alkali halide crystals, as a result of appropriate heat treatment, there are produced distinctive deformations consisting in the appearance of formations similar to domains in ferroelectrics. For example, if the crystal is heated to a temperature above 500° and then quenched to room temperature, the inner part of the sample fragments into a series of thin layers oriented parallel to the (110) and ($1\bar{1}0$) planes. The thickness of these layers varies in the range from 0.2 to 0.4 mm in different crystals. If the specimen is observed in the [100] direction by means of a polarizing microscope these layers can be seen in the form of light and dark bands, corresponding to periodic alternation of birefringence. In our experiments we established the temperatures of appearance and disappearance of this structure; these temperatures may be likened to the Curie points of ferroelectric materials. For NaCl the temperature of appearance of polarization lies in the 455 to 460° interval; the temperature of disappearance in the 380 to 390° range.

If a crystal with such a twin formation is colored, the different layers are colored differently by F centers. The twin layering is even more clearly evinced in the case of colloid formation; in NaCl one can realize the situation where the twin layers acquire alternating red and blue colors, discernible even in nonpolarized light (figure a).

As is known, by means of appropriate heat treatment one can obtain colloids of different sizes, which impart different colors to the crystal. In our case there were obtained bands of different color, which is indicative of the presence of centers of different size. From this it may be concluded that in neighboring twinned regions the crystal lattice is in different states. There simultaneously

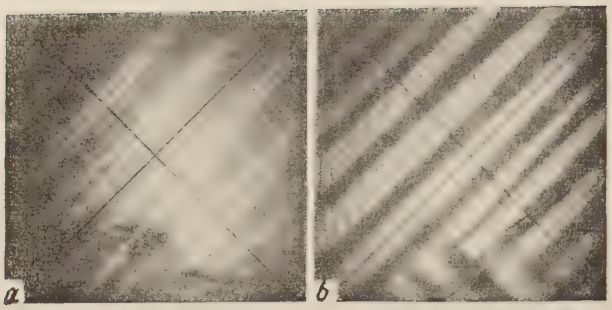

a - Colored crystal with twin formations observed in nonpolarized light (magnification 15 X); b - similar crystal observed between crossed Nicols.

exist two modifications of the lattice; these result in different rates of conglomeration of the F centers, which leads to formation of "red" molecular centers in one set of layers and of "blue" colloids in the alternate layers.

Further, it is found that the two lattice modifications affect not only the rate of coagulation but also the orientation of the new centers. Crystals heat treated and colored by the above described procedure exhibit birefringence when viewed between crossed Nichols (figure b).

Moreover, in these crystals we also detected the effect of dichroism. In measuring the absorption in an individual twin band by means of polarized light there were obtained curves of different height for the two mutually perpendicular directions of polarization.

Special experiments carried out with NaCl showed that the rate of conglomeration depends greatly on the presence of static deformations in the crystal lattice. This substantiates our assumption that the twinned formations are regions of deformation of the crystal lattice.

"T.G.Shevchenko" Kiev State University

STRUCTURAL DEFECTS IN CRYSTAL PHOSPHORS

- L.M.Shamovskii & A.S.Shibanov

It was demonstrated in earlier studies[1-4] that the spectrum of additional absorption and the luminescence spectrum of alkali halide phosphors are determined by the activator ions connected with structural defects. In these studies, however, the character of the defects involved was not elucidated. In order to bring out the nature of these disturbances we used the method[5,6] of decoration of dislocations in the volume of the crystal and the method of selective etching of the crystal surface. The observations were carried out on KCl:Ag and NaCl:Ag phosphor crystals grown by the Kyropoulos technique.

Usually the dislocation structure of crystals is investigated in connection with plastic deformation[5-8]. In contrast, we tried to bring out the structural defects of the crystal lattice connected with introduction of activator impurities. Hence the investigated samples were first carefully annealed near the melting point and then cooled to room temperature at a rate not exceeding 1 degree per min.

The decoration of dislocations was effected by additive coloring of the crystals held at 650-700° for several days, followed by slow cooling. The selective etching was carried out on fresh cleavage surfaces with glacial acetic acid.

The results of our studies showed that 1) etch pits on the crystal surface correspond to rows of dislocations in the volume, decorated by chains of colloidal metal particles, and 2) the density of single dislocations and the dimensions of the dis-oriented mosaic blocks do not depend on the activator concentration in the crystal. In well-annealed samples the mean block size lies in the range from 200 to 500 microns. The density of single dislocations not connected with block faces depends on the heat treatment of the crystal. As a result of annealing it is reduced by 3-4 orders of magnitude.

The coarse dislocational substructure of phosphors cannot be satisfactorily reconciled with the concept of dual distribution of activator and with the idea that the luminescence is localized at structural disturbances of the lattice. In particular, one cannot by the presence of such structure explain the high conversion efficiency of scintillators under excitation by ionizing radiation, inasmuch as the length of the elementary displacements of the carriers in alkali halide crystals is appreciably less than the dimensions of the observed blocks. In connection with this we undertook an attempt to determine whether there is present in alkali halide phosphors a finer defect structure in addition to the coarse mosaic.

Such submicrostructure was observed under high magnifications in additively colored crystals with a higher activator concentration. The fine defect structure was evinced in the form of numerous fine activator metal particles distributed throughout the volume of the crystal (see figure). Segregation of the activator in the form of the pure metal incident to decoration of the fine defect structure cannot be regarded as a result of reduction of the silver from AgCl - separation of the silver into an independent phase owing to decomposition of the solid solution - inasmuch as in our experiments we used crystal phosphors in which the activator concentration did not exceed the limit of solubility (the maximum AgCl concentration was 0.1 mole percent in the KCl crystals and 1.6 mole percent in the NaCl crystals.

The above-mentioned two types of defects are characterized by qualitative differences. The coarse dislocation structure appears incident to plastic deformation of the crystals under the influence of thermal and mechanical stresses. It undergoes changes as a result of high temperature annealing. The fine defect

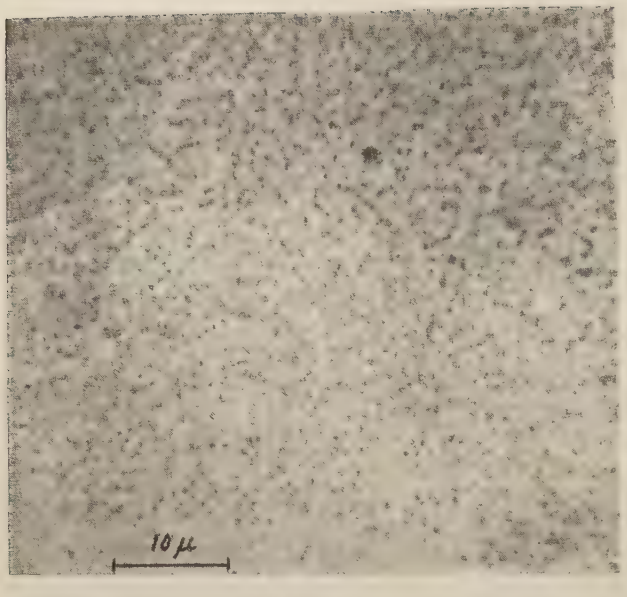

Micrograph of submicrostructure in the volume of an additively colored NaCl:AgCl (0.4 mole %) crystal.

structure, on the other hand, does not change under the influence of mechanical and thermal factors and persists even in well-annealed crystals. Apparently, this submicrostructure is connected with some specific intrinsic characteristics of the crystal phosphors, connected with the dual distribution of activator. The fine defect structure is not brought out by selective etching of the crystal surface.

At present it is difficult to give a precise definition of these microdefects. It may be assumed that the submicrostructure is formed in crystal phosphors either by a three dimensional network of dislocations or by a fine mosaic structure consisting of weakly disoriented blocks with dimensions of the order of 1-5 μ.

Activator impurities on structural defects form deep electron traps. Hence incident to additive coloring they are reduced to atoms and acquire an effective negative charge. The metallic particles increase in size in the process of thermolysis.*

The colloidal silver particles forming in the phosphor bring out the defect structure that existed prior to the additive coloring.

During excitation of the crystal phosphor these activator trapping centers on defects localize electrons and form "atomic" centers. By virtue of their excess negative charge they are effective recombination centers. The energy released in the process of electron-hole recombination is evinced in the form of luminescence having a wavelength characteristic of the given phosphor.

Inasmuch as there exist in phosphors two different types of structural defects - a coarse and a fine mosaic - there are evinced activator excitation and luminescence centers of two types.[9]

References

1. L.M.Shamovskii & Yu.N.Zhvanko, Doklady AN SSSR, 111, 140 (1956). (Trans. Doklady.)
2. L.M.Shamovskii, Optika i spektroskopiya, 1, 407 (1956).
3. L.M.Shamovskii & Yu.N.Zhvanko, Ibid., 3, 267 (1957).
4. L.M.Shamovskii, A.A.Dunina & Yu.N.Zhvanko, Ibid., 2, 599 (1957).
5. S.Amelinckx, Phyl.Mag., 1, No.3, 269 (1956).
6. S.Amelinckx, Acta Metallurgica, 6, No.1, 34 (1958).
7. J.J.Gilman & W.G.Johnston, J.Appl.Phys., 27, No.9, 1018 (1956).
8. D.J.Barber, K.B.Harvey & J.W.Mitchell, Philos.Mag.,2,No.17,704 (1957).
9. T.A.Abdusadykov, Trudy IFA AN ESSR (Proceedings, Inst.of Physics and Astronomy, Estonian SSR Ac.of Sci.), No.10, 97 (1960).

---

*Detailed data on the mechanism of thermolysis will be published elsewhere.

DISCUSSION

Ch.B.Lushchik: Comparing the inferences drawn in the reports of Shamovskii & Shibanov and Gindina it may be concluded that the views of Shamovskii's group have approached the views of the Tartu school. Whereas at the Fifth Conference on Luminescence Shamovskii considered films of the activator salt on the surface of the crystal to be responsible for luminescence, and at the Seventh Conference he attributed the luminescence to activator complexes studding the surface of mosaic blocks, in today's report the luminescence centers are identified as activator particles located in a three-dimensional network of dislocations. It must be emphasized that in coming to this view the authors reject the concept of crystal phosphors as surface activated systems of the adsorbate type. There can be no doubt that impurities interact with dislocations. The possibility of decoration of the volume network of dislocations has been convincingly demonstrated in the work of Dutch physicists,of Gindina, and the present study of Shamovskii & Shibanov. This, of course, does not mean that activator particles located at regular lattice sites cannot absorb light and luminesce. This assertion, repeated by the authors in the present report, appears to me to be completely unfounded. Of course, activator particles located at dislocations can also absorb light and luminesce.

In the work of Gindina, which was presented at the Conference on the Physics of Alkali Halide Phosphors (Tartu, 1959), it was shown that the block boundaries in typical crystals are not the points of preferential distribution of luminescence centers. This is indicated by the convincing data on the uniform distribution of luminescence in crystals. Only in special cases, as in the case of sensitized luminescence, does the emission have a complex point topography.

So far it has not proved feasible by microscopic examination to show that the luminescence is or is not localized at the volume dislocation network. There are, however, indirect proofs in favor of nonlocalization in Gindina's report. I hope that by the time of our next conference someone will be able to furnish direct proof that absorption and luminescence is realized both by activator ions at regular sites and in the region of dislocations, and that the points of view of Shamovskii and of the Tartu physicists will thus be reconciled. In this connection it might be of interest to investigate the behavior of dislocation-free crystal whiskers.

Also promising is the comprehensive investigation of the relation between luminescence centers of different types and activator trapping centers for holes and electrons, initiated by Gindina. From the data obtained so far it follows, for example, that x-irradiation and optical bleaching of phosphors give rise to a large number of new luminescence centers and electron trapping centers. Yet such treatment does not affect the dislocation structure and changes only the number of point defects in the crystal lattice, which, in our opinion, serves as luminescence and trapping centers.

A.S.Shibanov: Admittedly decoration of defects in crystal phosphors alone is not sufficient to infer that luminescence centers are localized at structural disturbances of the lattice, but in the framework of our other studies these investigations are significant. They substantiate our conclusions regarding the dual distribution of activator in phosphors and the fact that the defect structure of phosphors is not healed by annealing. Activator impurities distributed over the submicrostructure give rise to deep trapping levels for electrons, which are not released from these traps by heat. Bleaching of these centers is feasible only by recombination with holes. The same "atomic" centers appear incident to excitation of the phosphors. It was established in our laboratory that during addi-

tive coloring of NaCl:Ag and KCl:Ag not more than 10% of the silver is reduced. Nevertheless, as a result of this treatment the crystals completely lose their characteristic luminescence. This indirectly proves that the Ag ions at the lattice sites do not form recombination centers.

We have no reason to reject the hypothesis of formation of complex compounds of the activator with the ions of the host lattice at structural defects. On the other hand, the concept of complexes "studding" the surface of the blocks should not be attributed to us.

The results of our work differ radically from the investigations of R.I. Gindina. She brought out only the coarse mosaic, which appears mainly as the result of decomposition of supersaturated solid solutions. The defects brought out in our studies apparently exist regardless of the method of decoration. One cannot count on visual means for bringing out the local distribution of luminescence centers, particularly if one bears in mind the presence in crystal phosphors of submicrostructure that is not eliminated by annealing.

* * * * * * *

DECORATION OF DISLOCATIONS AND ACTIVATOR DISTRIBUTION IN UNSTABLE ALKALI HALIDE PHOSPHORS

- R.I.Gindina

In recent years a number of investigators[1-3] have advanced the hypothesis regarding the predominant role in the luminescence of alkali halide phosphors played by luminescence centers and electron traps located at the boundary of mosaic blocks. In the present work we made an attempt to check this hypothesis experimentally.

Our ultramicroscopic investigations of unstable NaCl-$PbCl_2$, KCl-CuCl, KCl-AgCl and KBr-Au solid solutions after different heat treatments showed that the colloidal particles of the impurity salt after annealing at high temperatures segregate and accumulate at dislocations on the surface of blocks, and after heating at low temperatures are localized in the volume dislocation network.

Fig.1 shows a micrograph (focal plane inside the crystal) of a KCl:AgCl (7 mole percent in the melt) phosphor heated for 10 min at 700°C and then cooled slowly over a period of 8 hours to 300°. If such a decorated crystal is again heated to 700°, quenched to room temperature and subjected to decomposition at 230° for 1 hour, it is found that the impurities decorate the three dimensional locational network (Fig.2 - magnification 120 X, scale 0.015:1). Similar results were obtained for the NaCl:$PbCl_2$ system.[4]

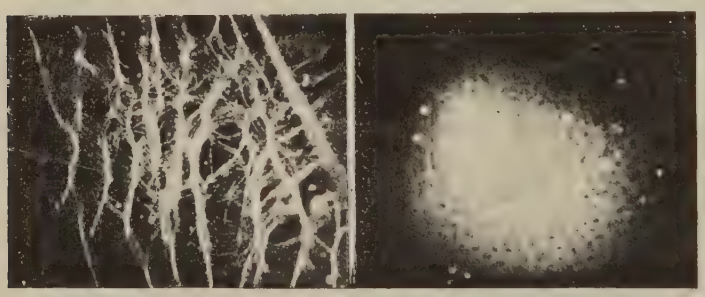

100 μ

Fig.1 Fig.2

Inasmuch as under conditions of high temperature annealing the impurity is segregated over the entire volume of the crystal, it may be inferred that in quenched NaCl-$PbCl_2$ and KCl-AgCl crystals

the boundaries of the blocks, the dimensions of which in this case are of the order of 0.1-0.01 mm, are not the regions of preferential location of the activator.

It is particularly significant that annealing of NaCl-$PbCl_2$ and KCl-AgCl crystals, resulting in accumulation of the impurities on the surface of the blocks, does not lead to increase of the activator absorption and luminescence.

Microscopic investigations by means of an ultraviolet microscope with magnifications of 100 X and 600 X showed that the luminescence of KI:TlI and KCl:CuCl phosphors is uniformly distributed throughout the crystal lattice. There is no discrenible localization of the luminescence in the region of the block boundaries.

As a result of plastic deformation by compression (40-70%) of KCl-TlCl, KI-TlI, KBr-In and NaCl-$PbCl_2$ crystals, leading to increase in the number of dislocations by several orders of magnitude, the activator absorption of the crystals, reduced to the new thickness, virtually does not change.

The results of all these experiments do not agree with the hypothesis that the activator ions responsible for the absorption and luminescence are distributed over the block boundaries.[1,2]

We showed that as a result of plastic deformation of KCl:AgCl (0.3 mole percent in the melt) crystals there are created in the phosphor new luminescence centers (centers II) the absorption bands of which peak at 226 and 236 mμ. Excitation in these bands stimulates luminescence with λ_{max} = 350 mμ. Centers of this type also appear as a result of x-irradiation and bleaching of unstrained crystals. The trapping of electrons at these centers in the process of x-irradiation significantly weakens the luminescence of centers II. In the process there form new atomic centers with λ_{max} = 228 mμ and λ_{max} = 436 mμ; these centers have been investigated by Etzel & Schulman[5] and Kats.[6]

All these data are consistent with the concept[7,8] of centers II as activator ions located next to point defects of the crystal lattice (in this case probably next to anionic vacancies).

In view of the uniform nature of the blue luminescence (observed at magnifications of 100 X and 600 X) of x-irradiated KCl:AgCl phosphor with excitation at 228 mμ, it may be inferred that the trapping centers in this phosphor are not activator ions located on the surface of the mosaic blocks but activator ions located at the lattice sites.

In some cases, however, the block boundaries and the Cottrell[9] circumdislocation clouds may play a significant role in the luminescence. For example, in the case of NaCl:Pb:Mn phosphor after annealing we observed enhancement of the luminescence of the Mn^{2+} ions near the block boundaries and along the glide bands consisting of groups of dislocations. This is probably connected with the fact[10] that there built up near the defects the enhanced local concentrations of Pb^{2+} and Mn^{2+} ions necessary for realization of sensitized luminescence.

References

1. L.M.Shamovskii, Optika i spektroskopiya, 1, No.3, 407 (1956).

2. L.M.Shamovskii & A.A.Dunina, Transactions of the 7th Conference on Luminescence (Crystal Phosphors), Tartu, 1959.

3. L.M.Shamovskii & Yu.N.Zhvanko, Izv.AN SSSR, Ser.fiz., 21, 557 (1957). (Trans.Bulletin, 21, 551.)

4. R.I.Gindina, Trudy IFA AN ESSR (Proceedings, Inst.of Physics & Astronomy, Estonian SSR Ac. of Sci.) No.11, 91 (1960); Program of the Conference on the Physics of Alkali Halide Phosphors, Tartu, 1959.

5. H.W.Etzel & J.H.Schulman, J.Chem.Phys., 22, 1549 (1954).
6. M.L.Kats, Optika i spektroskopiya, 3, No.6, 602 (1957).
7. N.E.Lushchik, Trudy IFA AN ESSR (Proceedings, Inst.of Physics & Astronomy, Estonian SSR Ac.of Sci.), No.10, 68 (1959).
8. T.A.Abdusadykov, Ibid., No.10, 122 (1959).
9. A.H.Cottrell, Usp.fiz.nauk, 46, 179 (1952).
10. K.K.Shvarts, Trudy IFA AN ESSR, No.11, 3 (1960).

* * * * * * *

ELECTRON DIFFRACTION STUDY OF THE INFLUENCE OF GASES ON THE STRUCTURE OF SUBLIMATED LAYERS OF ALKALI HALIDE SALTS

- A.A.Khaav

Klement and his co-workers[1,2] established that layers of a base material and activator deposited by successive vacuum sublimation transform under the influence of air, oxygen and fluorine into phosphors. Other gases (N_2, H_2, water vapor, etc.) do not have this effect. In some systems after admission of fluorine there is observed intense recrystallization in the sublimated layers (appearance of dendrites).

The purpose of the present investigation was to determine whether recrystallization of sublimated layers also occurs under the influence of air and oxygen and what significance this recrystallization has in the process of phosphor formation. Our experiments were carried out with potassium, cesium and thallium halides.

The electron diffraction patterns were recorded by means of a Rumsh[3] electron diffraction camera. In order to determine the influence of the gaseous medium on the structure of the sublimated layers (200-300 Å thick) electron diffractions patterns of the same layers were recorded immediately after sublimation in vacuum and then again after exposure of the layers to the chosen gaseous medium.

If in the course of recrystallization the crystal size increases, the process is evinced by decrease in the half-width of the interference rings on the diffraction patterns.[4] The results obtained show that under the influence of normal (undried) air there does occur recrystallization of the layers: the dimensions of the crystallites increase as will be evident from the following table.

Salt	*hkl*	Mean size of crystallites, Å	
		Immediately after sublimation	After exposure to air
Potassium halides	(200);(220)	50-70	100-140
Cesium halides	(110);(211)	70-100	100-150
Thallium chloride	(110);(211)	~100	~150

In the case of potassium halides there is observed formation of texture; the crystallites are oriented with the (002) face parallel to the substrate. No grain orientation was observed in the case of cesium and thallium halides.

We investigated the following double layers: KCl + TlCl, KBr + TlBr, CsCl + + TlCl, CsBr + TlBr, CsCl + TlI and CsI + TlI. We exposed these layers to dry and moist nitrogen, dry and moist oxygen, and dry and moist air.

It was found that recrystallization of the layers occurred only in the presence of moisture. Inasmuch as according to Klement[1] water vapor does not facilitate formation of luminescing systems from sublimated layers, the observed recrystallization of the two layer films under the influence of moisture should not lead to the formation of a phosphor. At the same time the substantial changes in the structure of the layers in the process of recrystallization should facilitate introduction of the activator into the base material. The absence of luminescence may be explained by the quenching effect of water vapor.

I desire to express my gratitude to F.D.Klement for discussion of the results.

References

1. F.D.Klement, Zhur.fiz.khim., 21, 563 (1947).
2. F.D.Klement, A.F.Malysheva, I.S.Nilova & A.A.Solov'eva, Trudy IFA AN ESSR (Proceedings of the Inst.of Phys. & Astron., Estonian Ac.of Sci.), No.4, 36 (1956).
3. M.A.Rumsh, Zhur.tekh.fiz., 25, 2556 (1955).
4. Z.G.Pinsker, Difraktsiya elektronov (Electron diffraction), M., 1949.

KINETICS OF THE LUMINESCENCE OF PHOSPHORS WITH SEVERAL TYPES OF TRAPS*

- V.V.Antonov-Romanovskii

When there are present in a phosphor electron and hole traps of several types, in addition to the process of recombination, there also occurs, as a rule, the process of redistribution among the traps of the charges divided incident to excitation (retrapping). The simultaneous presence of two processes greatly complicates examination of the kinetics of phosphorescence, inasmuch as the descriptive equations are nonlinear and of complicated form. Actually, however, the situation is often not as hopelessly complicated as might appear at first glance.

The nonlinearity of the kinetic equations is due mainly to nonlinearity of the recombination process, inasmuch as in principle, each electron can recombine with any hole and vice versa. The process of redistribution of charges among traps of both signs is also nonlinear owing to the effect of saturation, i.e., owing to the fact that the number of free traps depends on the concentration of the separated charges.

However, such "double" nonlinearity in most cases reduces to a second order factor owing to the de-exciting action of the exciting light, which hinders storage of a large light sum in the phosphor. As a result the traps are filled only partially, so that the effect of saturation can virtually be neglected. Moreover, since in most cases the relative concentration of separated charges is small compared to the concentration of traps, the probability for recombination proves to be appreciably lower than the probability for retrapping. This allows of further simplification of the kinetic equations.

By virtue of the fact that in the process of excitation, as a result of a number of different factors, the charges are distributed among the traps of different types in a manner not consistent with thermal equilibrium, at the first stages of decay or build-up of luminescence there occurs mainly the process of redistribution of charges among the traps - usually from shallower to deeper traps. As long as this process dominates over the process of recombination, the kinetic equations are approximately linear and hence readily solved. The nonlinear process of recombination can be taken into account by the method of perturbations.

The descriptive formulas are particularly simple if the probabilities for release of charges from traps of different types differ greatly, while the difference between the other trap parameters is relatively minor. Then in the first approximation the process of motion of charges in the case of decay occurs as follows.

Initially the source of free charges of both bands are the shallowest traps of both signs. Then as the traps empty and equilibrium is attained between the population of the traps and the population of the respective bands, i.e., as the traps come to return as many charges to their respective bands as they capture, the sources "supplying" both bands become the deeper traps; this process continues until it is the "turn" of the deepest traps of one sign or the other. At this instant the process of redistribution of charges of this sign among the traps ceases, and the process of recombination of these charges begins to predominate. At this point the kinetics as a whole stops being linear, but by virtue of the fact that the distribution of the charges of one sign among the traps does not vary with time, i.e., is constant, the nonlinear equations can be integrated.

In the case of build-up of luminescence, during its initial stages, the problem also proves to be quasilinear (the linear homogeneous equations for decay are

---

*Review of the investigations described in Refs.1.

supplemented by a constant term taking into account excitation), but, in contrast to decay, the linearity may cease before the deepest traps come into play. This critical instant arrives when recombination removal of charges from some traps (not necessarily the deepest ones) begins to dominate over nonrecombination removal (release of charges). In this case in going to the later stages of build-up of luminescence the problem proves to be appreciably more complicated inasmuch as only part of the electron and hole traps (the shallower ones) are in equilibrium with their band. However, at the late stages of build-up, when the excitation conditions become steady, the kinetics can again be analyzed to the end.

In the case of steady excitation it is feasible to divide the traps of different depth into two groups: thermotraps and recombination traps. The first group is formed by the shallower traps, which are in detailed equilibrium with their band and virtually do not interact by recombination with the other band. The second group is formed by the deeper traps, which do not return the charges captured from their band but yield them by recombination to the other band. In this case there is no detailed equilibrium; rather the role of these traps reduces to that of an "overflow chamber" that fills and empties, inasmuch as the equilibrium becomes cyclic in character. Virtually all the separated charges proved to be concentrated in recombination traps.

This division of the electron and hole traps into two groups depends both on the temperature and on the intensity of the exciting light. With heating or with decrease of the light intensity, the number of types of traps in the first group obviously increases, while that in the second group decreases accordingly. In the limiting case there remain in the recombination group only the deepest traps of one sign. In the case of cooling or increase of the light intensity the opposite situation obtains.

One of the important consequences of linearity of the kinetics during the initial stages of de-excitation is the fact that the decay curves for a phosphor with a complicated system of traps is at first approximately the sum of the corresponding exponential curves. The thermostimulated luminescence curves also are characterized by kinetics of the first order, and only the curve associated with release of charges from the deepest traps is characterized by kinetics of the second order. The fact that the thermostimulated luminescence curves can follow kinetics of the first order is mathematically equivalent to the results of Randall & Wilkins[2], who however, unjustifiably neglected the effect of retrapping.

In exactly the same way the initial stages of build-up of luminescence can be represented in the form of a sum of exponential, essentially independent processes.

An entirely unique situation is realized in the case of steady luminescence. It is found that with increase in intensity of the exciting light or with cooling of the phosphor the concentration of separated charges increases step by step as the successive thermolevels transform to recombination levels. If such a transformation is undergone by an electron level, the concentration of electrons on all the other electron trapping levels decreases somewhat, but so that the total concentration of all trapped electrons still increases, in the same way as the concentration of holes on any type of recombination levels. If such a transition is undergone by a hole level, there is obtained the same picture, but with the roles of the electron and hole traps interchanged.

Thus it follows from the above that if the electron and hole traps differ appreciably as regards the release probability but in other respects are less different, then provided there is fulfilled the condition of not excessively strong excitation, the kinetic of phosphorescence even in the presence of traps

of many types can be calculated approximately.

On the other hand, in the presence of several types of traps of both signs, the probability is great that some of them will differ very appreciably not only as regards the release probability but also as regards other parameters. This can lead to results differing greatly from those inferred above. In practice there may be a great number of different "particular" cases, i.e., many different deviations from the norm; for example, there may be great differences as regards trap concentration, degree of filling of the traps, or, if the traps are close in depth, they may differ appreciably as regards other properties; in other cases one must distinguish between the properties of thermal and optical electrons and holes. Moreover, there may simultaneously occur two or more deviations from the norm. Owing to the great number of such possibilities there is no sense in trying to discuss all of them; we can restrict our consideration to specific experimentally observed cases (or some particularly interesting results).

Some years ago, Tolstoi[3] turned his attention to certain effects observed in zinc sulfide phosphors, effects which presumably could not be explained on the basis of the ordinary semiconductor model of a phosphor. First among these was the superlinear initial rise with time of excitation of photoconductivity and, second, quadratic dependence of the steady photoconductivity as a function of the exciting light intensity. Tolstoi, accordingly, proposed his original "two-step" theory[4] which was supposed to explain these unique effects on the basis of assumptions significantly differing from those commonly accepted and based on the modern band model for semiconductors; for example, Tolstoi postulated that the probability for recombination of a free electron does not depend on the concentration of ionized centers!

It was found, however, that even such exceptional regularities can be interpreted on the basis of the semiconductor model with three levels, for example, with two types of electron and one type of hole levels.

If it is assumed that the exciting light transfers mainly electrons from the filled band to deeper electron traps, the growth of photoconductivity, provided its hole component is negligibly small, will be superlinear. It is immaterial whether the electrons are ejected from traps thermally or optically; what is important is that the lifetime of the electrons in the "supplying" traps be greater than in other traps.

The same semiconductor model for phosphors also allows of explaining the quadratic dependence of the steady photoconductivity as a function of the incident light intensity E, if it is assumed that the electrons from the deeper traps are ejected by the exciting light and from the shallower traps only partially by the light. Then the concentration of electrons in shallower traps will be proportional to E, and the component of the photoconductivity due to ejection of electrons from these traps by light will be proportional to E^2. Although such electrons will amount to a minor fraction of the total number of electrons, owing to their greater energy, their contribution to the photoconductivity will be decisive. It is known, for example, that the effective mass of a low energy electron (polaron) may be two or more orders of magnitude greater than the effective mass of a high energy electron[5] and therefore its contribution to the conductivity will be much smaller.

The band model also allows of explaining the fact that the superlinear initial growth of photoconductivity and the quadratic dependence of the steady state photoconductivity on the incident light intensity are observed only in a certain temperature range.

Let us now turn to another interesting effect which can arise when two types of traps differ little as regards depth. Calculations show that for a certain

relationship between the parameters of these two sorts of traps, when at the initial instant of de-excitation the entire light sum is concentrated in the traps for which the probability for retrapping is much lower than for the traps of the other sort, the luminescence curve will behave in an extraordinary manner. Under isothermal conditions the luminescence can at first build up (!) instead of decaying monotonically with time, while under conditions of thermostimulation the half-width of the thermoluminescence peak in the presence of traps of two types may be appreciably smaller (!) than the "natural" width of the peak when only one type of traps is present.

This concludes our consideration of some of the regularities that may be deduced on the basis of the band model of crystal phosphors. Although this does not exhaust the great possibilities latent in the band model it should be obvious that if properly and thoughtfully utilized this model is capable of explaining many effects.

"P.N.Lebedev" Physical Institute,
Academy of Sciences of the USSR

References

1. V.V.Antonov-Romanovskii, Optika i spektroskopiya, 7, 377, 524, 827 (1959); Ibid., 8, 73 (1960). (Trans.Optics & Spectroscopy.)

2. J.T.Randall & M.H.F.Wilkins, Proc.Roy.Soc.A, 184, 366 (1948).

3. N.A.Tolstoi, Zhur.eksp.i teor.fiz., 30, 171 (1956). (Trans.Soviet Physics - JETP.)

4. N.A.Tolstoi & A.V.Shatilov, Optika i spektroskopiya, 1, 216 (1956); Ibid., 5, 590 (1958); Ibid., 6, 665 (1959). (Trans.Optics & Spectroscopy.)

5. S.I.Pekar, Issledovaniya po elektronnoi teorii kristallov (Studies in the electron theory of crystals), M.-L., 1951.

DISCUSSION

N.A.Tolstoi: Antonov-Romanovskii proposes for explaining some important characteristics of photoconductivity a model which he calls the "simple model with three levels". He affirms that this model illustrates the possibilities for interpretation that are latent in the band model and which have hitherto been neglected. He refers to the band model, particular cases of which he considers, as the "ordinary" model, in some cases, and as the "modern" model in others. Antonov-Romanovskii attributes development of the two-step theory to failure to utilize the possibilities of the band model. I must emphatically state that in contrasting the "model with three levels" proposed recently with the two-step model developed and described by me earlier, Antonov-Romanovskii must be laboring under a misapprehension.

Actually, fundamental to the two-step model is the assumption that the first act of absorption of light transfers the electron to a local level. This is what serves to explain all the paradoxical superlinear effects. Actually, Antonov-Romanovskii in his model repeats the same assumption. There are two alternatives according to the two-step theory (in its published version) as regards the further history of the electron excited to the first level. The electron may be transferred into the conduction band optically or thermally. Superlinear increase of photoconductivity with time is obtained in the case of both optical and thermal further excitation. It is entirely natural that Antonov-Romanovskii, having repeated the initial assumption of the two-step theory, obtained the same consequence,

namely, the possibility of explaining the superlinear increase in photoconductivity. True, he introduced an additional trapping level but this results in only a small change in the form of superlinearity. If this third level is removed, superlinearity still remains.

The two-step theory, assuming the second transition to be optical, obtains superlinearity of the steady photoconductivity. If the second transition is optical-thermal, the superlinearity will be very weak. If the second transition is purely thermal, superlinearity vanishes. Having repeated the initial assumption of the two-step theory, Antonov-Romanovskii again obtains its consequences, that is, he offers an explanation for the superlinearity of steady photoconductivity. True, he tries to make the second transition mixed: optical-thermal, apparently, with a minor optical component. In order to retain strong superlinearity he suggests that optical electrons are two orders of magnitude better current carriers than thermally released electrons. It is significant that the optical part of the second transition in Antonov-Romanovskii's model is entirely unnecessary. Without the optical transition no superlinearity is obtained. This is explained by the fact that Antonov-Romanovskii's model is the same two-step model "diluted" by thermal transitions and extra, unnecessary levels.

Antonov-Romanovskii presented his report as an illustration of the omissions in utilizing the possibilities of the band theory. As we see, these omitted possibilities are possibilities of utilizing the two step theory, that is, its basic assumption regarding the primary transition of an electron to a local level. Inasmuch as the concept of such a primary transition to a local level is not anything exceptional in the band model, at least in its "modern" version which takes into account excitons, the rebuke regarding failure to utilize the possibilities of the band model for explaining superlinearity should be addressed not the the proponents of the two-step theory but to Antonov-Romanovskii himself, for the two-step theory was described in print many years before Antonov-Romanovskii repeated the two-step theory in distorted form.

In conclusion I want to say that I note with great satisfaction the closer approach of the views of Antonov-Romanovskii and myself. This makes it all the more desirable to clear up the misunderstanding I spoke of.

Ch.B.Lushchik: In connection with the question of the reasons for the superlinear effects observed in zinc sulfide phosphors I would like to note the importance of investigating these effects under different excitation conditions. In Tartu, G.Liid'ya and I.Yaek investigated the kinetics of optical flash stimulated in the F absorption band while producing different elementary excitation in alkali halide phosphors. With excitation in the activator absorption bands the kinetics is monomolecular. Quasimonomolecular kinetics obtain in the case of electron-hole excitation as well. However, with excitation in the exciton absorption band there are observed clearly pronounced superlinear effects, which are evidence of the bimolecular character of the kinetics. It should be noted that the character of the interaction of excitons with point defects is such that the electron (or hole) after dissociation of the exciton and trapping of the hole (or electron) at a defect moves through the crystal at a very high velocity and has time to migrate to a great distance from its partner. A consequence of this is bimolecular kinetics. In case of delocalization of the impurity excitations the electron and hole are localized near the impurity ion that gave rise to them.

At first glance the monomolecular character of the processes involved in band-band transitions appears surprising. It is possible that in this case there are produced slow electrons and holes that do not have time to migrate far from each other.

EFFECT OF THE SIZE OF NATURAL AND CRUSHED CRYSTALS ON THE LUMINESCENCE OF ZINC SULFIDE PHOSPHORS

- V.L.Levshin & B.D.Ryzhikov

The strongest effect of mechanical crushing of zinc sulfide phosphor crystals is decrease of their luminescence intensity. It is held[1] that the principal reason for decrease in luminance is decrease of the crystal size and, consequently, increase of the light scattering by the particles.

In order to study the influence of crystal size and mechanical crushing on the optical properties of crystal phosphors we first divided our phosphor samples into fractions according to degree of dispersion (grain size). One of the fractions was then subjected to mechanical crushing and the resultant powder was again divided into fractions. Thus for each investigated phosphor we obtained fractions of crushed and uncrushed crystals with the same degree of dispersion.

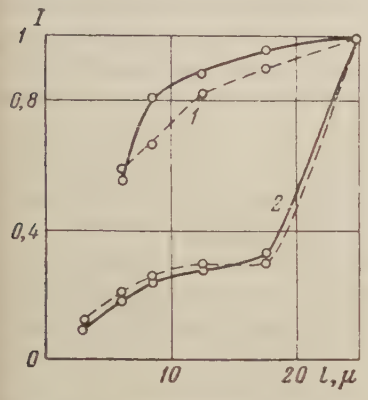

Fig.1. Variation of the luminance of ZnS:Sm phosphors with the particle size for natural (1) and crushed (2) crystals. Solid lines for excitation at 365 mμ; dashed lines for excitation at 312 mμ.

Fig.1 shows the variation in luminance of an infinitely thick ZnS:Sm phosphor layer under steady excitation as a function of the particle size for natural (uncrushed) and crushed crystals. In the case of uncrushed crystals strong decrease in luminance is observed only in the region of small grain size. The curves for crushed crystals are complex in character: at first there is a rapid decrease in luminance, then the brightness changes very little and finally it falls off rapidly. It follows from the present results and from those of experiments with zinc sulfide phosphors of other composition that the grain size dependence of the luminance is greatly affected by the wavelength of the exciting light and by the composition and technology of the phosphor. In addition, the shape of the luminance vs size curves depends on the temperature of measurement and the intensity of the exciting light.

Comparison of the curves reproduced in Fig.1 with the theoretical dependence of luminescence brightness on grain size[2] showed that one cannot explain the decrease in brightness merely by increased light scattering. For uncrushed (natural) crystals the difference between the experimental and theoretical curves is apparently due to differences between the structure of the luminescence and trapping centers in crystals of different size; this is indicated by the difference between their luminescence spectra, glow curves, brightness vs temperature curves, etc. The Debye diffraction patterns for natural crystals of different size are virtually identical, which means that the crystals are free of distortions of the crystal lattice and that the phase composition is the same in crystals of different size.

In order to determine the character of the structural changes occurring as a result of grinding we recorded Debye diffraction patterns for a number of crushed fractions. With decrease in particle size there is observed disappearance of the far lines, weakening and broadening of the diffraction lines, and some increase in background intensity. All this indicates that grinding results in development of internal deformations. However, the relation between the Debye line broadening and the change in line intensity is not consistent with the relation between Debye line broadening and the luminescence intensity of the phosphor. This indicates that not all deformations lead to decrease of luminance: the lumi-

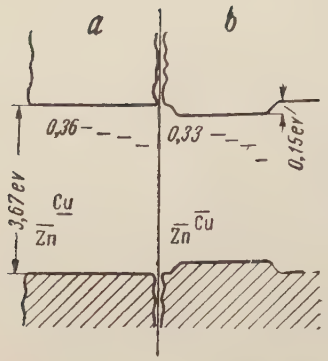

Fig.2. Energy diagram for an undeformed (a) and a deformed (b) phosphor crystal.

nance is reduced only by lattice deformations that affect the luminescence and trapping centers and the mechanism of energy transfer.

Deformation of the lattice in the vicinity of an activator ion results in disturbance of the symmetry of the lattice field at that point, which should lead to change in the shape of the potential curves for the upper and lower states and, consequently, to change in the luminescence spectrum. When the upper and lower state potential curves intersect there develops quenching inside the luminescence centers, the magnitude of which is strongly dependent on the temperature. Experiments showed that crushing results in a significant change of the luminescence spectra, and that the change is the greater, the greater the decrease in luminance. That internal quenching is an important factor in crushed crystals is also indicated by the enhanced sensitivity of crushed crystals to variation in temperature even in the region of low temperatures.

If we take into account the fact that the decrease in the thermal light sums stored in the phosphor is greater than the decrease in intensity under steady excitation, it may be concluded that in addition to internal quenching, external quenching increases in crushed crystals. Apparently, incident to deformation of the crystals there appear regions wherein nonradiative electron-hole recombination becomes possible. Such regions may be dislocations. That the number of dislocations in crushed crystals is greater is indicated by the decrease of photoconductivity.

In addition, there may occur quenching in connection with direct transitions of trapped electrons into the normally filled band. Experiments show that deformation has a strong effect on the trapping levels: it alters the depth of the traps

Assuming in the first approximation that the change in the trap depth is proportional to the change in the width of the forbidden energy band, it follows from the glow curves that the width of the forbidden band is reduced by 0.3 ev (Fig.2). This result is based on rough calculations and naturally requires further checking.

Thus the significant factor involved in the alteration of the diverse luminescence properties of crystal phosphors as a result of crushing is plastic deformation. The decrease in luminance is connected with increase of both external and internal quenching in plastically deformed crystals; there is reason to infer that internal quenching plays the predominant role.

Department of Optics, Physics Faculty,
Moscow State University

References

1. N.Riehl & H.Ortman, Ann.Phys., 29, 556 (1937).

2. Yu.I.Chekalinskaya, Trudy In-ta fiz.i matem.AN BSSR (Proceedings of the Institute of Physics & Mathematics of the Belorussian Ac.of Sci.), 2, 38 (1957).

DISCUSSION

A.M.Gurvich: We carried out the following simple experiment which substantiates the validity of the views of Levshin and Ryzhikova on the reason for the

decrease in brightness of phosphors as a result of grinding. A coarse grain (mean grain size ~30 μ) ZnS·CdS:Ag phosphor, prepared by heating at 1200°, was ground in a porcelain mortar for ~15 min. This did not produce any significant change in the granulometric composition. Yet the photoluminescence brightness (λ_{max} = 3650 Å) was reduced by a factor of 10, while the roentgenoluminescence brightness ($\lambda_{eff} \approx 0.6$ Å) decreased only 50-60%. Increase of light scattering in the phosphor as a result of grinding or increase of the absorption by the activator segregated into an independent phase should have had the opposite effect (greater decrease of the roentgenoluminescence as compared with the photoluminescence), inasmuch as x-rays excite a thicker layer. Obviously, the reason for the observed effect lies in the formation of quenching centers at deformations produced by the grinding. In excitation by x-rays the electron concentration in the conduction band is higher than in photoexcitation owing to the fact that incident to interaction of x-rays with the phosphor material there are raised into the conduction band electrons not only from the upper filled band but also from deeper levels. As a result, the rate of recombination of electrons with holes trapped on activator levels increases, and, accordingly, the probability for migration of holes to quenching centers decreases.

* * * * * * *

KINETICS OF LUMINESCENCE OF ZnS:Cu WITH EXCITATION BY ALPHA-PARTICLES AND SHORT LIGHT PULSES

- T.P.Belikova & M.D.Galanin

Decay of α-scintillations in ZnS:Ag phosphors have been investigated by a number of authors (see, for example, Ref.1). Search of the literature shows that no such studies for ZnS:Cu phosphors have been made, although it is known that in the case of both these phosphors the duration of scintillations produced by α-particles is short compared with the duration of photoluminescence.

The purpose of the present work was to compare the kinetics of α-scintillation with the kinetics of photoluminescence of ZnS:Cu phosphor. For photoexcitation we used a condensed spark in air between iron electrodes (V = 6 kv, C = 700 pf). The light pulses had a duration of 0.5 microsec and a repetition rate of about 10 per sec. The phosphor was excited through a UFS-2 filter (λ_{trans} = 300-400 mμ); the effective energy of each pulse amounted to about 3 ergs per ~0.025 cm^2. The luminescence was detected by means of an FEU-29 photomultiplier coupled to a DESO-1 oscillograph. The curves characterizing the decay of the blue and green α-scintillations of ZnS:Cu (phosphor FK-106, $C_{Cu} = 7 \cdot 10^{-5}$ g/g, heating temperature 1140°C) are shown in Fig.1. In what follows, however, we shall give only the results for the green band.

Analysis of the decay of α-scintillations of the phosphor showed the following: 1) the decay curve is virtually independent of the temperature: in the range from -150 to +200° there was no noticeable change in the shape of the decay curve; 2) the observed short term scintillation represents only the initial part of the decay. Calculation of the number and intensity of the scintillations and comparison with the mean emission brightness showed that in the decay range to 10% the maximum intensity only about 5% of the stored light sum is emitted (cf.Ref.2).

It was found that with gradual increase of the energy density with excitation by light pulses there begins to be evinced a short term decay process, the amplitude of which increases superlinearly with increase of the excitation intensity.

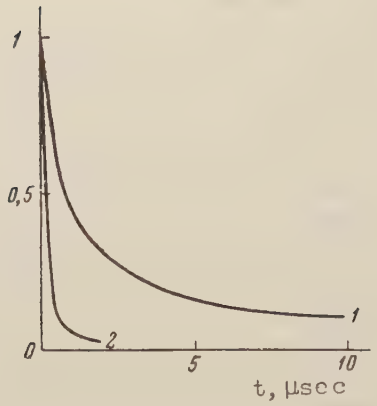

Fig.1. Decay curves for the green (1) and blue (2) bands of ZnS:Cu excited by α-particles.

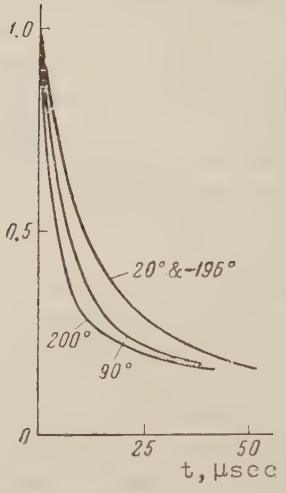

Fig.2. Decay curves of the photostimulated green luminescence of ZnS:Cu at different temperatures.

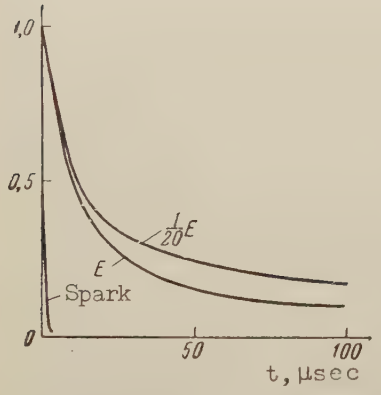

Fig.3. Decay of the green band of ZnS:Cu at different photoexcitation densities and decay of the stimulating light pulse from the spark.

As in the case of α-scintillations, the initial section of the decay curve is weakly dependent on the temperature (Fig.2), and the light sum emitted in the process amounts to not more than 15% (at the highest intensity) of the steady luminescence energy as indicated by the mean photomultiplier current. Thus this short term process* has some traits in common with α-scintillation.

However, the duration of this process is at least ten times greater than the duration of the scintillation process; it is doubtful whether with further increase of the light pulse energy this duration could be reduced to the level of the scintillations: our experiments show that with decrease of the excitation density the initial part of the decay curve changes very little (Fig.3).

Thus the difference between the kinetics of scintillation and the kinetics of photoluminescence cannot be attributed simply to the influence of the excitation density (cf.Ref.4). The luminescence intensity can be described by $I = -\frac{dn}{dt} = pnN$, where n is the concentration of ionized centers, p is the recombination probability, and N is the concentration of electrons in the conduction band. In the investigated process n changes little (not more than 5-15%) and hence can be regarded as virtually constant. Hence the relative change in intensity $\frac{1}{I} \cdot \frac{dI}{dt} \approx -\frac{1}{N} \cdot \frac{dN}{dt}$ is determined by change of N as a func-

*This short term process was apparently observed in the work of Vinakurov et al[3], but contrary to the inference of these authors it cannot be characterized by a single constant τ inasmuch as the decay is essentially nonexponential.

tion of t. The weak temperature dependence shows that, contrary to what usually happens, in this case $N(t)$ is not controlled by thermal release of electrons (or holes) from traps. It may be assumed that the initial change of $N(t)$ is determined by diffusion of electrons towards the ionized centers, accompanied by short term trapping of the electrons in very shallow traps. If this is the case it is possible that the difference between the kinetics of scintillation and photoluminescence depends on the influence of the electric field that is produced along the α-particle tracks (see, for example, Ref.5), if the ejection of electrons and holes is different. Rough evaluations show that the electric field along an α-particle track as compared with the field of an ionized center[6] can accelerate the recombination process by a factor of ~10.

References

1. J.Warnce & H.Neuert, Naturwissenschaften, 47, H.1, 11 (1960). J.P.Antony, J.Phys.Rad., 16, 182 (1955); P.G.Kootz, G.R.Keepin & J.E.Ashley, Rev.Sci.Instru., 26, 352 (1955).

2. J.Broser, H.Kallman & C.Reuber, Z.Naturforsch., 52, 79 (1950).

3. L.A.Vinokurov, L.V.Levshin & E.G.Baranova, Zhur.eksp.i teor.fiz., 21, 236 (1951).

4. M.D.Galanin & A.V.Raevskii, Izv.AN SSSR, Ser.fiz., 23, 1280 (1959). (Trans.Bulletin 23, 1273.)

5. H.Kallman & J.Dresner, Phys.Rev., 114, 71 (1951).

6. V.V.Antonov-Romanovskii, Optika i spektroskopiya, 3, 592 (1957).

* * * * * * *

EFFECT OF HYDROSTATIC COMPRESSION ON THE SPECTRAL CHARACTERISTICS OF ALKALI HALIDE PHOSPHORS

- Ya.Ya.Kirs & A.I.Laisaar

Earlier[1,2] we investigated the effect of pressure on the spectral characteristics of alkali halide phosphors activated by mercury-like ions and europium. On the basis of the results obtained we came to the conclusion that in these phosphors the equilibrium separation between the ion activator and its nearest anion neighbors is smaller in the excited state than in the ground state.

In the present work we investigated the effect of hydrostatic compression on the spectral characteristics of alkali halide phosphors activated by copper and manganese.

The luminescence spectra of Cu activated phosphors at atmospheric pressure and at 6000 atm are shown in the accompanying figure. It will be seen that this pressure produces a 0.6 ± 0.005 ev shift to the shorter wavelength side of the luminescence bands of NaCl:Cu, KCl:Cu and KBr:Cu and of the short wavelength band of KI:Cu. It was found that the magnitude of the shift increases virtually linearly with pressure. The shift of the long wavelength luminescence band of KI:Cu is ~0.13 ev. We investigated the effect of pressure on the long wavelength excitation band of copper activated phosphors mainly in the case of KBr:Cu. Compression of this phosphor shifts the peak of the excitation band (E_{max} = 4.72 ev) some 0.03 ev to the short wavelength side. At the same time the width of the band increases.

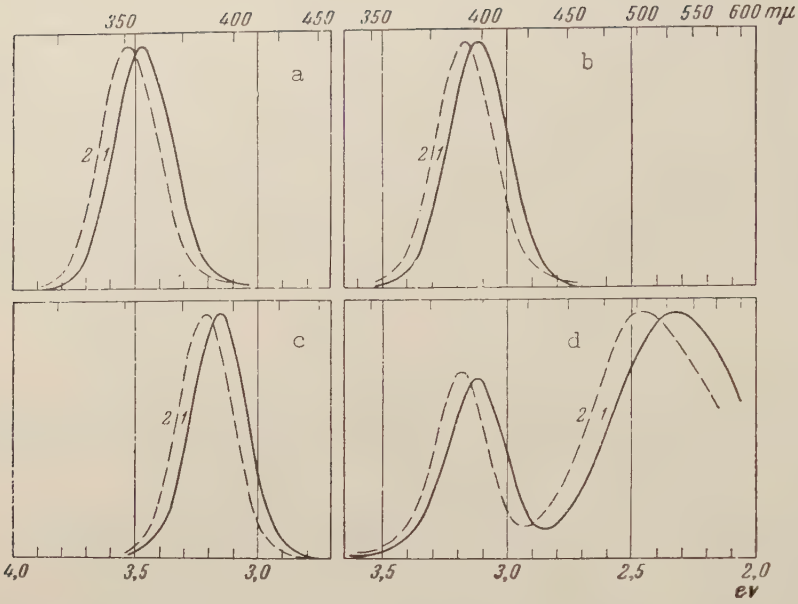

Luminescence spectra of: a) NaCl:Cu, b) KCl:Cu, c) KBr:Cu, d) KI:Cu; 1 - atmospheric pressure, 2 - 6000 atm.

In the case of the manganese activated phosphors we observed shift of the luminescence band to the side of longer wavelengths under hydrostatic pressure. Thus, for example, the emission band of KCl:Mn:Pb (E_{max} = 1.87 ev) shifts to the long wavelength side 0.015 ev with increase of the pressure from atmospheric to 4700 atm.

One can attempt to explain the short wavelength shift of the emission bands of Cu activated phosphors (and the shift of the emission of phosphors activated by mercury-like ions) by pressure induced redistribution of the luminescence centers over energetically close excited states (see Ref.1). However, these shifts can also be understood from the standpoint of the theory proposed by Johnson & Williams[3]. One need only assume that in Cu activated phosphors the equilibrium separation between the activator ion and its nearest neighbors in the excited state is greater than in the ground state. Unfortunately, the small short wavelength shift of the excitation band of KBr:Cu cannot serve as an argument in favor of this assumption owing to the nonelementary nature of this band: the short wavelength shift of the peak of this band may be due simply to redistribution in the relative intensities of its individual components.

From the standpoint of the Johnson-Williams theory the long wavelength shifts of the emission bands of the Mn activated phosphors indicate that in these phosphors the minimum of the potential curve corresponding to the excited state of the luminescence centers is shifted relative to the minimum of the curve corresponding to the ground state to the side of lower values of the configuration coordinate (see, also, Ref.6).

We compared the pressure induced shift of the spectral characteristics of all the investigated phosphors with the behavior of these characteristics in the corresponding homologous series. To this end we calculated the relative, i.e., per unit change of the lattice constant, shift of the emission and excitation bands both under the influence of hydrostatic pressure and in going from one member of the homologous series to the next. It was found that in phosphors activated by copper and mercury-like ions the pressure produced relative shift is at least 2-3 times greater than the shift in the homologous series, while in the phosphors activated by europium it is at least an order of magnitude greater. We believe that the relatively small value of the spectral shift in the homologous series is due to the fact that the interionic separations in the luminescence centers of phosphors with the same activator differ appreciably less than the lattice constants of the corresponding base materials. The structure of the centers is

largely determined by the activator ion.

We also investigated the effect of pressure on the excitation and luminescence spectra of ZnS:Cu phosphors with different activator concentrations. It was established that the excitation spectra of these phosphors are shifted 0.03 ev when the phosphor is subjected to hydrostatic pressure of 6000 atm. This is probably connected with increase in the width of the forbidden energy band with decrease of the interionic separation. The values of the shifts to the short wavelength side of the luminescence spectra of ZnS phosphors with $C_{Cu} = 10^{-6}$ ($E_{max} = 2.64$ ev), 10^{-4} ($E_{max} = 2.28$ ev) and 10^{-3} g/g ($E_{max} = 2.39$ ev) are 0.06, 0.035 and 0.035 ev, respectively.

References

1. Ya.Ya.Kirs & A.I.Laisaar, Trudy IFA AN ESSR (Proceedings, Institute of Physics & Astronomy, Estonian SSR Ac.of Sci.), No.10, 51 (1959).
2. Ya.Ya.Kirs & A.I.Laisaar, Ibid., No.12, 42 (1960).
3. P.Johnson & F.Williams, Phys.Rev., 95, 69 (1954).
4. Ya.Ya.Kirs, Trudy, IFA ESSR, No.4, 108 (1956).
5. N.N.Kristofel', Ibid., No.10, 43 (1959).
6. Ya.Ya.Kirs & A.I.Laisaar, Transactions of the 7th Conference on Luminescence, Tartu, 1959.

* * * * * * *

INVESTIGATION OF PHOTOELECTRIC POLARIZATION OF ZINC SULFIDE PHOSPHORS

- I.K.Vitol & I.A.Tale

1. In investigating the mechanism of recombination in crystal phosphors, in addition to optical measurements, it is expedient to use electric methods designed to determine the polarity of the excited current carriers. Under certain conditions the method of photoelectric polarization[1] can be used for determining not only the polarity of the current carriers but also the ratio of the electron and hole components in the case of mixed conductivity.[2]

2. Surface states have a strong effect on the photoeffect in semiconductors[3-5]. The presence of surface levels can affect both the magnitude and polarity of the experimentally determined photoelectric polarization in crystal phosphors. However, a number of theoretical considerations and experimental facts indicate that owing to the specific characteristics of crystal phosphors[1,2], under certain conditions (excited conductivity much greater than the equilibrium conductivity) the surface levels have no significant influence on the polarity and magnitude of the photoelectric polarization.

3. Light in the region of the fundamental absorption of ZnS phosphors activated by Cu, Ag and Mn excites n-type conductivity. The magnitude of the p component of the conductivity at room temperature is generally below the level of experimental sensitivity, i.e., amounts to less than 5% of the total conductivity (see, also, Refs.2 & 6).

4. With excitation of ZnS:Cu phosphor by steady $\lambda = 312$ mμ light the photoelectric polarization attains a stationary value equivalent to the potential difference. Then when auxiliary light in the region from 350 to 1150 mμ is switched

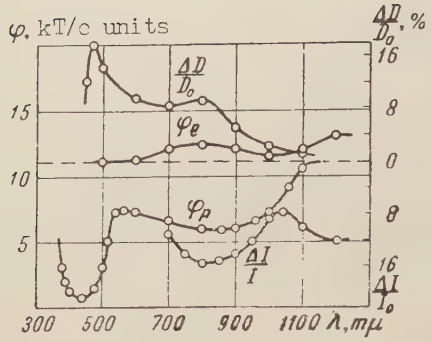

Variation of the prompt (φ_p) and lagging (φ_1) components of the photoelectric polarization (in kT/e units, T = = 293°K) and the relative decrease in luminescence $\Delta I/I$ as a function of the auxiliary illumination wavelength for ZnS:Cu phosphor under continuous excitation by λ = = 312 mμ light producing φ = = 11 kT/e units. For comparison the figure also shows the spectrum of additional absorption $\Delta D/D_0$, according to the data of Antonov-Romanovskii & Shchukin.[7]

on, simultaneously with quenching of the luminescence, the photoelectric polarization drops rather rapidly to φ_p, and then slowly increases to φ_1. The variation of φ_p and φ_1 as a function of the wavelength of the auxiliary illumination is shown in the accompanying figure. The figure also shows the decrease in luminescence intensity $\Delta I/I$ and the increase in absorption $\Delta D/D_0$ of the excited ZnS:Cu phosphor, according to Antonov-Romanovskii & Shchukin[7]. The decrease of the photoelectric polarization in the 500 mμ and 800 mμ auxiliary excitation regions may be due to the following (and/or other) factors: 1) the infrared light releases holes, which recombine with trapped electrons, and thus reduces the electron concentration in the conduction band; 2) the infrared light releases holes, and the photoelectric polarization decreases owing to diffusion of the holes to the side of the unilluminated surface of the specimen. The absence of the effect of decrease of the photoelectric polarization with auxiliary illumination in the 1150 mμ region shows that the quenching of luminescence in this region differs from the mechanisms of quenching with auxiliary illumination in the 500 and 800 mμ regions.

We desire to express our deep gratitude to Ch.B.Lushchik for his interest in the work and valuable discussions.

References

1. I.K.Vitol, Trudy IFA AN ESSR (Proceedings, Inst.of Physics & Astronomy, Estonian SSR Ac.of Sci.) No.8, 175 (1958); Transactions of the 7th Conference on Luminescence, Tartu, 1959.

2. I.K.Vitol & I.A.Tale, Trudy, IFA AN ESSR, No.10, 220 (1959).

3. V.E.Lashkarev, Trudy, In-ta fiz.AN USSR (Proceedings, Inst.of Physics of the Ukrainian SSR Ac.of Sci.), 3, 3 (1952).

4. K.B.Tolpygo, Izv.AN SSSR, Ser.fiz., 16, 46 (1952).

5. V.Kozhevin, Tezisy dokladov na I Vsesoyuznom soveshchanii po fotoelektricheskim i opticheskim yavleniyam v poluprovodnikakh (Abstracts of reports presented at the First All-Union Conference on Photoelectric and Optical Effects in Semiconductors), Kiev, 1957.

6. U.Kh.Nymm & A.K.Aidla, Trudy IFA AN ESSR, No.11, 199 (1960).

7. V.V.Antonov-Romanovskii & I.P.Shchukin, Doklady AN SSSR, 71, 3 (1950).

DIELECTRIC CHANGES IN ZnS:Cu:Fe PHOSPHOR DURING THERMOSTIMULATION

- P.E.Ramazanov

Using the procedure described earlier[1], we investigated the change in conductivity, C, and the dielectric loss tangent, tan δ, of a capacitor filled with ZnS:Cu:Fe phosphor in the process of thermostimulation. Prior to heating the phosphor was excited to the equilibrium state and allowed to decay for 20 min at the initial temperature T_o. Simultaneously with the measurements of Δ tan δ and ΔC (the increments of tan δ and C, respectively) we measured the glow intensity I.

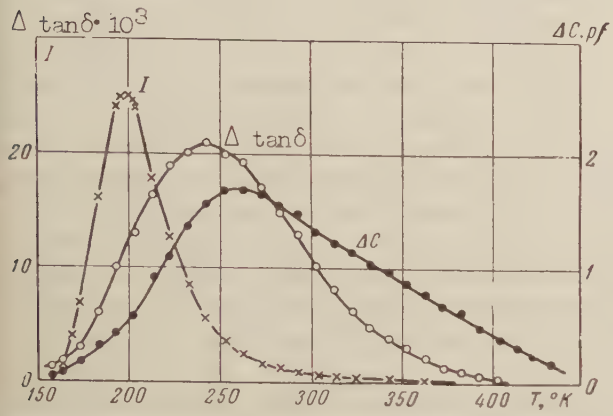

Thermostimulation of ZnS:Cu:Fe phosphor from T_o = 219°K (heating rate 0.23 degree/sec) and the accompanying dielectric changes observed at f = = 2.94 Mc.

The temperature dependences of I, Δ tan δ and ΔC obtained with T_o = 219°K & f = 2.94 Mc are shown in the accompanying figure. It will be seen that both Δ tan δ = f(T) and ΔC = f(T) have clearly pronounced maxima. In all cases the maximum of Δ tan δ precedes the ΔC maximum (see table); the position of the glow peak (I = = f(T) maximum) as a rule does not coincide with the position of either of these maxima. With increase of the frequency the Δ tan δ and ΔC maxima shift to the side of higher temperatures.

Hitherto there has been no satisfactory explanation for the interrelation between the temperature dependences of I, ΔC and Δ tan δ. The model of an inhomogeneous dielectric with one component having a varying conductivity is not suitable, inasmuch as according to this model the position of the ΔC maximum is determined only by the temperature variation of the conductivity and should not depend on the frequency of the measuring field.

We attempted to give a qualitative explanation of the temperature dependences of ΔC and Δ tan δ on the basis of the assumption that the photodielectric effect in the phosphor is due to multiple localization (retrapping) of the electrons, oriented by the external field.[1]

Considering the case of a simple phosphor with trapping levels of one depth U and using the familiar[2] relation defining the concentration of trapped electrons in the process of thermostimulation, one can, on the basis of the general theory of relaxation dielectric losses[3] and on the assumption that Δ tan δ and ΔC are connected with the proposed mechanism of supplementary polarization of the excited phosphor, deduce the following approximate equations:

$$\Delta C \approx \frac{1}{T\left(1+gT^2e^{-\frac{U}{kT}}\right)\left(1+b^2e^{\frac{2U}{kT}}\right)}. \qquad (1)$$

$$\Delta\tan\delta \approx \frac{e^{-\frac{U}{kT}}}{4mT\left(1+gT^2e^{-\frac{U}{kT}}\right)\left(1+b^2e^{\frac{2U}{kT}}\right)+a}, \qquad (2)$$

where

$$a=\frac{n_0q^2x^2}{3k},\quad b=\frac{\omega}{2\nu},\quad m=\frac{\varepsilon_\infty}{4\pi},$$

T_0, °K	f, cps	Position of pcaks, °K			$\nu \cdot 10^{12}$, sec^{-1}
		I	$\Delta \tan\delta$	ΔC	
155	$9{,}02 \cdot 10^4$	206	178	217	3
150	$2{,}82 \cdot 10^5$	174	189	240	2
157	$2{,}94 \cdot 10^6$	199	243	258	5
149	$9{,}69 \cdot 10^6$	197	270	285	5
213	$9{,}02 \cdot 10^4$	251	223	246	1
210	$2{,}82 \cdot 10^5$	246	227	258	8
219	$2{,}94 \cdot 10^6$	252	263	275	7
215	$9{,}69 \cdot 10^6$	255	268	293	4

q is the electron charge, x is the separation between neighboring electron traps, ω is the angular frequency of the measuring field, ν is the intrinsic frequency of oscillation of a trapped electron, n_0 is the concentration of trapped electrons at T_0, and ε_∞ is the dielectric constant of the phosphor as determined solely by processes rapidly attaining equilibrium.

The inhomogeneity of the dielectric medium (phosphor) filling our capacitor, as calculations show, should greatly deform the temperature dependence of $\Delta \tan \delta$ and ΔC pertaining only to the phosphor without, however, changing the position of the ΔC maximum and only slightly shifting the $\Delta \tan \delta$ maximum to the side of lower temperatures. This does not allow of comparing relationships (1) and (2) with the experimental relationships as a whole, but does allow of evaluating, from the maxima of I and ΔC, the frequency ν of the natural oscillations of a trapped electron; we determined this earlier[1] from the frequency shift of the ΔC maximum for the case of steady excitation.

From the condition for the maximum of I, namely, $dI/dT = f_1(U, T_{m1}, g) = 0$, knowing U and T_{m1}, one can determine the parameter g, and then from the conditions for the maximum of ΔC, namely, $d(\Delta C)/dT = f_2(U, T_{m2}, g, b) = 0$, one can determine the parameter b and, consequently, ν. The resultant equations for g and b are of the form

$$g \approx \frac{\frac{U}{kT_{m1}} e^{\frac{U}{kT_{m1}}}}{T_{m1}^2 \left(4 + \frac{U}{kT_{m1}}\right)};$$

$$b^2 = \frac{1 + gT_{m2}^2 \left(3 + \frac{U}{kT_{m2}}\right) e^{-\frac{U}{kT_{m2}}}}{\left(\frac{2U}{kT_{m2}} - 1\right) \cdot e^{\frac{2U}{kT_{m2}}} - gT_{m2}^2 \left(3 - \frac{U}{kT_{m2}}\right) e^{\frac{U}{kT_{m2}}}}.$$

Calculations yielded a mean value of $4 \cdot 10^{12}$ sec^{-1} for ν (see table), which agrees within the limits of the determination error with the value $\nu = 3 \cdot 10^{12}$ sec^{-1} obtained by us earlier. In the calculations, in accord with the results obtained in determining the depth of the electron traps from the glow curves and the activation energy for the photodielectric effect under conditions of steady excitation[1], we assumed $U = 0.3$ ev.

In our opinion the obtained agreement between the values of ν indicates that one can explain the dielectric changes occurring in the phosphor during thermostimulation by means of the earlier proposed mechanism for the photodielectric effect.

References

1. P.E.Ramazanov, Izv.AN SSSR, Ser.fiz., 23, 1290 (1959). (Trans.Bulletin 23, 1281).

2. Ch.B.Lushchik, Trudy IFA AN ESSR (Proceedings, Inst.of Physics & Astron., Estonian SSR Ac.of Sci.) No.3, 3 (1955).
3. G.I.Skanavi, Fizika dielektrikov (Physics of dielectrics), M., 1949.

DISCUSSION

E.B.Aleksandrov: Use of a Q meter for investigating the photodielectric effect is limited by the low accuracy of this instrument (particularly in the range $\tan \delta > 0.02$) and the long measuring time.

We developed two types of set-ups free of these shortcomings, by means of which one can investigate the photodielectric effect in terms of the increments of the components of the complex dielectric constant ϵ. The principal component of the set-ups is an ac bridge supplied from a symmetric oscillator. The investigated capacitor is connected into one arm; the other arm is the balancing arm. Prior to measurements the bridge is balanced. When the specimen is excited an unbalance voltage appears in the bridge diagonal; the components of this voltage are proportional to the increment in the ϵ components. In the first type of set-up the amplified unbalance voltage is applied to a synchronous detector. By appropriate phasing of the reference voltage, one can completely discriminate one of the voltage components. Then the other component is determined by means of a suitable instrument. To extend the frequency range into the region of higher frequencies we had recourse to frequency conversion of the signal taken off the bridge diagonal and of the reference voltage. This set-up has been used in the frequency range from audiofrequencies to 20 Mc and proved capable of detecting capacitance increments equal to 0.01% of the initial ~100 pf capacitance. The time resolution at high frequencies was $5 \cdot 10^{-3}$ sec.

In the second type of set-up for recording one of the voltage components the signal off the bridge diagonal is added linearly to a voltage much greater in amplitude than the last, but coinciding in phase with the component being recorded. As a result of addition, the amplitude of the higher voltage undergoes an increment equivalent to the increment of the detected component multiplied by a constant factor. Further treatment of the signal reduces to detecting and measuring the dc voltage increment. This set-up has a working frequency range from 100 kc to 20 Mc; the measurement accuracy is 0.1% at an initial capacitance of ~100 pf. The time resolution is $\sim 10^{-4}$ sec. This second set-up is appreciably simpler in design, but is characterized by lower accuracy and necessitates imposing more rigorous requirements on the stability of the oscillator and regulation of the supply sources.

TEMPERATURE DEPENDENCE OF THE ROENTGENOLUMINESCENCE AND DARK CONDUCTIVITY OF YAKUTSK DIAMONDS

- K.N.Pogodaev & E.S.Vilutis

There are no references in the domestic literature on investigations of the electric conductivity of diamonds excited by x-rays, and there are only scanty data on the roentgenoluminescence spectra. Yet the importance of such investigations is obvious.

As regards crystal characteristics, the diamond samples investigated by us could be divided into two groups: group I - perfect twins of the spinel type (octahedra flattened to a tetrahedral plate); group II - imperfect flattened twins of the spinel type (faces sculpted with shield-like growth layers, edges of the triangular plates bent, curvature positive).

The principal purpose of the experiments was to determine the temperature dependence of the electric conductivity with a view to evaluating the activation energy for appearance of current carriers. The current was measured by means of a vacuum tube voltmeter in the process of heating the samples at a constant rate of 0.48 degree/sec in the temperature range from 50 to 350°. Typical results for an unexcited diamond are shown by curve 1 in the accompanying figure. At temperatures above 220° the temperature dependence of the conductivity is exponential in all cases. The current carrier activation energy values for different samples, as determined from the slope of the log $\sigma = f(1/T)$ plots lie in the range from 2.05 to 2.82 ev. This scatter must be attributed to variation in the specific properties of the individual specimens.

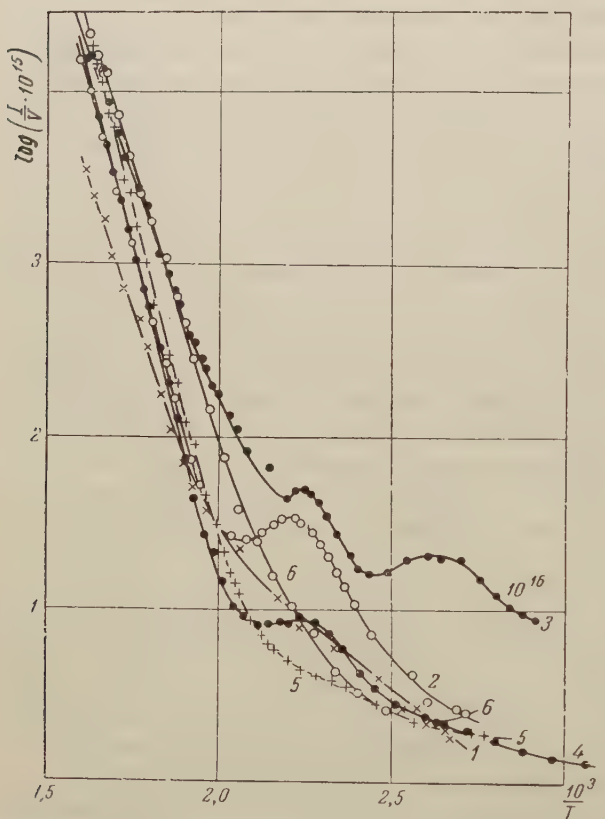

Temperature dependence of the dark conductivity of diamonds: 1) unexcited diamond, 2) x-irradiated diamond of group I, 3) x-irradiated diamond of group II (scale increased by 10), 4) diamond of group I irradiated for 25 hours, 5) diamond of group I irradiated for 1000 hrs, 6) same diamond after annealing at 350°.

Next we investigated the conductivity of x-irradiated specimens. Typical results obtained for diamonds of group I are shown by curve 2 in the accompanying figure. It will be seen that as a result of x-irradiation the conductivity increases substantially in the temperature region below 200° and attains a maximum value at 180°. This maximum is observed in the curves for all specimens. In the case of diamonds of group II, after x-irradiation, in addition to the maximum at 180°, there appears another conductivity maximum at about 110°. After heating to 350° all these conductivity maxima disappear. With subsequent irradiations and heatings the conductivity maxima reappear and disappear in the same way as in the initial cycle.

As was noted above, diamonds of group II differ from the others by a lower degree of perfection of the crystal shape. If this indication, which is indicative of "difficult" conditions

of growth, is connected with internal disturbances of the crystal structure, these specimens should have a greater number of defects than specimens of group I. In investigating the roentgenoluminescence it was established that these specimens also differ from the others by a brighter luminescence; moreover specimens of group II store a substantial light sum during x-irradiation, whereas specimens of group I do not store any significant amount of energy.

The carrier activation energies in the x-irradiated diamonds of group I proved to be 1.44 and 2.64-3.07 ev. The activation energy values for diamonds of group II were 0.96, 1.40 and 2.27-2.78 ev. The activation energy for raising carriers from the deepest level in an x-rayed diamond is always greater than prior to x-irradiation.

Further experiments on measurements on the conductivity of diamonds exposed to the radiation from Tl^{204} showed that the conductivity goes down with increase of the radiation dose (curves 4 and 5) and returns to its initial value after annealing (curve 6). These effects are connected with formation of pairs, presumably consisting of a vacant site and an interstitial atom[1,2], and indicate that the low temperature conductivity in the investigated diamonds is of the n-type.[3-6]

As was established earlier[7], the roentgenoluminescence spectra of diamonds comprise two independent bands: a blue band and an orange one. In view of the arbitrary variation of the intensity of these bands, it may be inferred that in diamonds of group II there are present luminescence centers of two types, each of which is responsible for one of the luminescence bands. Inasmuch as in thermal de-excitation of each band there are evinced two peaks at different wavelengths, it must be inferred that in each of the two types of luminescence centers there are "utilized" electrons from two different trapping levels.

Under excitation by x-rays electrons from the conduction band are partially localized on trapping levels, from which, when the appropriate activation energy is supplied, they can rise to the excitation levels of the luminescence centers. The mean values of the excitation energy obtained from the thermostimulation curves are 0.42 and 0.64 ev for the blue band and 0.36 and 0.80 ev for the orange band.

Thus one may infer that in diamonds of group II there are present two kinds of trapping levels, the depth of which below the conduction band is 0.96 and 1.40 ev, as determined from the experimental $\log \sigma = f(1/T)$ plots. In addition, there are distributed through the crystal luminescence centers of two types. If we assume that the depth of the excitation levels of these crystals is 0.60 ev for the orange band and 0.55 ev for the blue band, it may be inferred that the trapping levels serve as sources of electrons for both processes. In the process of heating of the specimen part of the electrons rise into the conduction band, resulting in conductivity, while other electrons that find themselves in the proximity of luminescence centers go to the excitation levels in these centers, subsequently giving rise to luminescence that is more or less monomolecular in character.

"A.A.Zhdanov" Irkutsk State University

References

1. R.Fletcher & W.Brown, Phys.Rev.,92,585 (1953).
2. W.Brown, R.Fletcher & K.Wright, Phys.Rev., 92,591 (1953).
3. J.Cleland, J.Crawford & D.Holmes, Phys.Rev., 102,722 (1956).
4. O.Curtis, J.Cleland, & J.Crawford, J.Appl.Phys., 29,722 (1958).
5. F.Stochmann, E.Klontz, J.Mackay, H.Fan & K.Lark-Horowitz, Z.Phys.,153,331 (1958).
6. J.Crawford & J.Cleland, J.Appl.Phys., 30,1204 (1959).
7. E.Vilutis, Izv.AN SSSR, Ser.fiz., 23,1379 (1959).(Trans.Bulletin, 23,1365.)

LUMINESCENCE OF THALLIUM CHLORIDE SINGLE CRYSTALS

- N.A.Tolstoi & V.A.Sokolov

We investigated the spectral composition and intensity of the luminescence of thallium chloride single crystals grown in our laboratory and subjected to the influence of different factors. In all cases the emission was excited by 365 mμ light at liquid nitrogen temperature. During the measurements the specimens were maintained in an atmosphere of pure helium.

Our experiments show that thallium chloride may have three luminescence bands: 1) a blue band peaking at ~460 mμ (Fig.1, curve 1), 2) an orange band with a peak near 620 mμ, and 3) a dark red band peaking in the region of 740 mμ (cf.Refs.1-3).

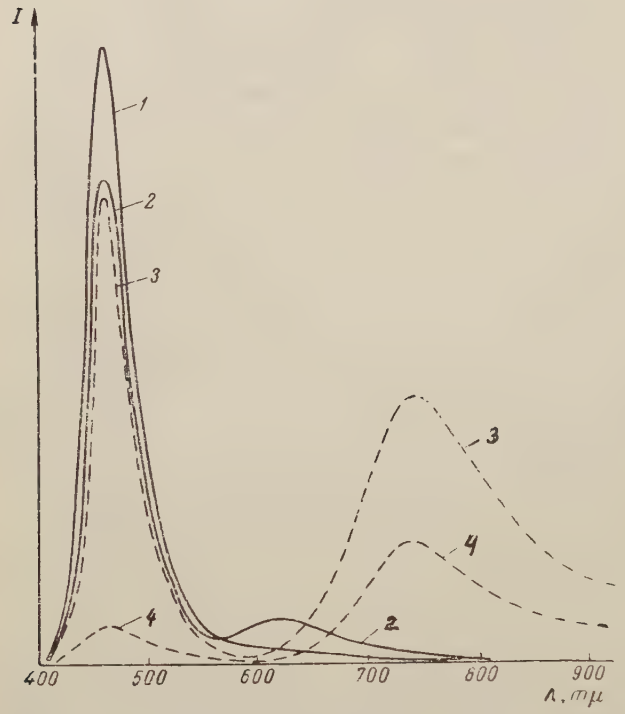

Fig.1. Luminescence spectra of thallium chloride after different treatments.

The thallium chloride single crystals luminesce blue immediately after growth. The orange band appears after plastic deformation of the specimen (Fig.1, curve 2). The dark red band is brought out by heating of the specimens in an atmosphere of pure helium (Fig.1, curve 3).

Prolonged exposure of the specimens to ultraviolet (365 mμ) at temperatures below -150° does not noticeably affect the luminescence. On the other hand, illumination with the same ultraviolet at higher temperatures leads to decrease in intensity over the entire spectrum. The blue luminescence is quenched more rapidly than the long wavelength luminescence (Fig.1, curve 4). Measurements of the variation of the luminescence intensity I at the peak of the blue band with exposure time to λ = 365 mμ light showed that I decreases with increasing t according to the hyperbolic law: $I = I_0/(1 + At)$, where I_0 is the initial intensity, and A is the constant that depends on the temperature and the ultraviolet intensity.

Concurrent measurements of the transmission of 436 mμ light by the crystals showed that the transmission after exposure of the sample to 365 mμ ultraviolet does not change noticeably (Fig.2); consequently, the observed weakening of the luminescence cannot be explained by some sort of "filtering" effect. The decrease in intensity as a result of exposure to ultraviolet is a reversible process: if the exposed specimen is held in the dark the initial luminescence is virtually completely restored. The rate of regeneration increases with increase of temperature.

It may be reasonably assumed that the blue luminescence centers are structural defects in the thallium chloride lattice. The orange luminescence band (λ_{max} = = 620 mμ) appears as a result of development of mechanical defects (dislocations) in the crystal, which is in agreement with the hypothesis advanced by Gobrecht & Becker[2]. The dark red band, presumably, develops as a result of impoverishment of the crystal as regards chlorine, owing to volatilization of this element during

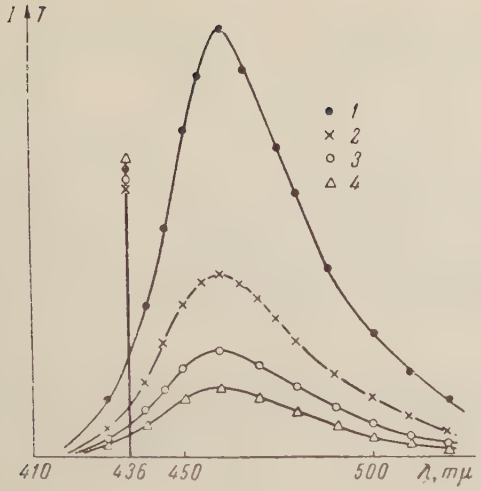

Fig.2. Variation of the luminescence spectrum of and transmission of the 436 mμ mercury line by a thallium chloride single crystal at liquid nitrogen temperature after illumination of the crystal at room temperature with λ = 365 mμ light: 1 - prior to exposure, 2 - after first 5 sec exposure, 3 - after second 5 sec exposure, 4 - after third 5 sec exposure.

heating. Possibly, the electron left behind by the volatilized chlorine atom occupies its place and forms an F center.

References

1. I.T.Randall, Trans.Faraday Soc., 35, 6 (1939).

2. H.Gobrecht & F.Becker, Z.Physik, 5, 553 (1953).

3. A.S.Vysochanskii, Doklady AN SSSR, 112, 228 (1957). (Trans.Doklady.)

CONCERNING THE MECHANISM OF EXCITATION AND DE-EXCITATION OF RECOMBINATION LUMINESCENCE OF ALKALI HALIDE PHOSPHORS

- Ya.A.Valbis, I.K.Vitol & V.E.Zirap

1. Relaxation processes in excited alkali halide crystal phosphors are complex in character, and their nature is still obscure.[1,2] In the present work we used the procedure of comprehensive investigation of the thermostimulated current and thrmostimulated luminescence and of the thermoluminescence spectra, a procedure that has certain advantages in investigating complex processes in alkali halide phosphors. All the measurements were carried out on the "relaxation combine" set-up described in Ref.3.

2. Investigation of the thermostimulated current and thermostimulated luminescence of nonactivated and thallium activated KCl and KBr crystals excited by x-rays showed that in the temperature region from 110 to 340°K a thermostimulated current peak corresponds to each thermostimulated luminescence peak. This is direct substantiation of the assumption made earlier[4,5] and then verified by optical methods[6-8] that the afterglow in crystal phosphors is predominantly recombination phosphor escence.

3. It can readily be shown that in the case of a relaxation process of one polarity the luminescence intensity I is related to the conductivity σ by the simple expression

$$\frac{I}{\sigma} = \frac{\eta\beta}{eu} p, \qquad (1)$$

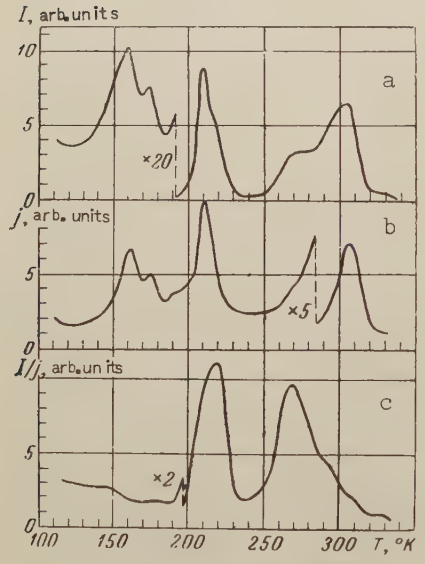

Fig.1. Temperature dependences of the luminescence intensity I (a), the thermostimulated current j (b) and the ratio I/j (c) for x-irradiated (Cu anode, 50 kv, 12 ma, 0.5 hrs) KCl:Tl(0.2 mole percent) phosphor heated at the uniform rate of 0.15 degree/sec.

where p is the concentration of holes in the recombination centers, β is the probability for recombination of a free electron with a trapped hole, η is the luminescence output appearing as a result of recombination, e is the charge of an electron and u is the electron mobility. In the case of a hole recombination mechanism, the above definitions of the quantities entering into Eq.(1) one should read "hole" instead of "electron" and vice versa. Experimental measurements of I/σ can yield results characterizing the change in the mechanism of the many-step relaxation process. If, for example, in a given time interval there are ionized trapping centers of one polarity and different depth and the recombination occurs at the same recombination centers, I/σ will decrease in direct proportion to the concentration of recombination centers. In case of change of the polarity (sign) of the recombination process, I/σ may change appreciably, inasmuch as other values of η and β come into effect.

4. In the case of KCl:Tl there are evinced at least two temperature regions of gradual decrease of the ratio I/σ (Fig.1): the first region extends from 110 to 190°K (probably the region near 240°K is connected with it). Possibly the recombination mechanism is of opposite polarity in the two regions; if this is the case, then according to the data of Refs.9 & 10, the second region corresponds

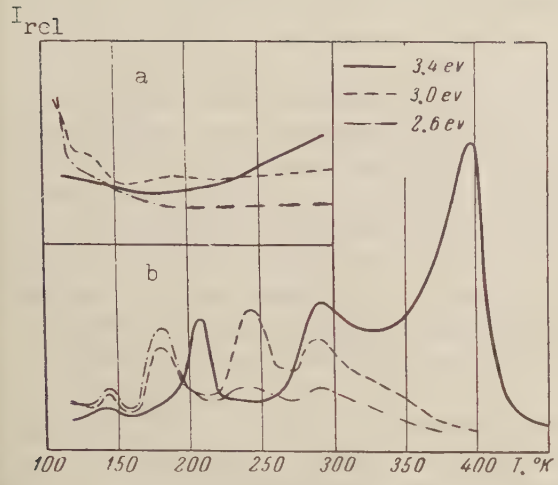

Fig.2. Temperature dependences of the intensities of different luminescence bands (peaks at 2.6, 3.0 and 3.4 ev) of KBr:Tl(0.5 mole percent) crystals: a - roentgenoluminescence (measured while cooling the crystal), b - thermostimulated luminescence (heating rate 0.2 degree/sec).

to the electron recombination mechanism, and the first to the hole recombination mechanism, which is in agreement with the data of Refs.11-13.

5. Changes in the recombination mechanism may affect the luminescence spectra as well; this is substantiated by experiment. Fig.2 shows the variation with temperature of the luminescence intensity of the long wavelength band of thallium (3.4 ev) and of the 2.5 ev and 3.0 ev bands of KBr:Tl(0.5 mole percent). As in the case of crystal phosphors of other composition, a particular group of bands predominates in each thermostimulated luminescence peak. In the roentgenoluminescence and thermostimulated luminescence spectra of deliberately nonactivated crystals, as in the spectra of activated crystals, there appear the following bands: KBr - 2.6 ev and 3.0 ev, NaCl - 2.5 ev and 3.0 ev, and KCl - 2.7 ev. The nature of the luminescence centers responsible for these bands is unknown (see, also, Refs.14-16).

The authors desire to thank Ch.B. Lushchik for helpful discussions and I.I. Lielpeter for assistance in the work.

References

1. Kh.F.Kyaembre & Ch.B.Lushchik, Trudy IFA AN ESSR (Proceedings Inst. of Phys. & Astron., Estonian SSR Ac.of Sci.), No.11, 150 (1960).
2. Ch.B.Lushchik & E.S.Tiisler, Ibid., No.10, 135 (1959).
3. I.K.Vitol, Ch.B.Lushchik & I.V.Yaek, Ibid., No.12, 175 (1960).
4. S.I.Vavilov, Vestnik AN SSSR, No.8, 26 (1933).
5. V.V.Antonov-Romanovskii, Trudy (Proceedings), Physical Institute, USSR Ac.of Sci., 2, 1, 2-3 (1942).
6. Ch.B.Lushchik, Thesis, Leningrad State University, 1954.
7. Ch.B.Lushchik, Trudy IFA AN ESSR, No.3, 1955.
8. Ch.B.Lushchik, Kh.F.Kyaembre & I.V.Yaek, Transactions of the 7th Conference on Luminescence, Tartu, 1959.
9. A.I.Belkind & Kh.F.Kyaembre, Transactions of the 9th Conference on Luminescence (Crystal Phosphors), Kiev, 1960.
10. I.K.Vitol, Transactions of the 7th Conference on Luminescence, Tartu, 1959.
11. G.Chiarotti & N.Inchauspé, Phys.Rev., 109, 2, 345 (1958).
12. P.Pringsheim, P.Yuster & C.Delbeq, Z.Phys., 138, 226 (1954).
13. D.Dutton & R.Maurer, Phys.Rev., 90, 126 (1953).
14. G.Bonfiglioli, P.Brovetto & C.Cortese, Ibid., 114, 951 (1959).
15. Z.L.Morgenshtern, Optika i spektroskopiya, No.6, 345 (1960). (Trans.Optics & Spectroscopy).
16. I.K.Vitol, Ibid., 9, No.4, 535 (1960). (Trans.Ibid.)

INVESTIGATION OF THE EFFICIENCY OF RECOMBINATION LUMINESCENCE OF ALKALI HALIDE PHOSPHORS

- I.V.Yaek

For purposes of comprehensive investigation of nonisothermal relaxation processes we developed equipment which we call a "relaxation combine" and by means of which one can simultaneously record curves characterizing the variation of bleaching $\varkappa$, thermostimulated luminescence I and thermooptical emission I_λ for the same phosphor specimen as a function of temperature (for more details see Ref.1). Hitherto, these different characteristics were usually recorded separately (see, for example, Ref.2). By means of the "relaxation combine", in addition to more detailed investigation of nonisothermal relaxation processes[3], one can measure the characteristic that might be termed the "instantaneous efficiency of thermoluminescence". This characteristic is defined by the formula $\rho(T) = \left[\frac{I}{-dn/dt}\right]_T$ (I is the luminescence intensity and n is the number of color centers).[4]

Experimental determination of this characteristic requires simultaneous measurements of $I(T)$ and $\varkappa(T)$, inasmuch as $n \sim \varkappa_m \sqrt{T}$. In our experiments we measured the efficiency of thermoluminescence of x-irradiated KCl:Tl, KBr:Tl and NaCl:Tl single crystals.

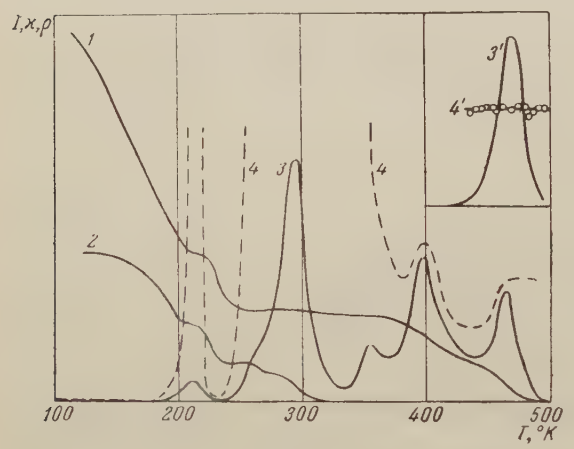

In the accompanying figure we show somewhat schematically (the data obtained in the case of x-raying the phosphor at liquid nitrogen temperature and at room temperature are shown as single curves) the curves characterizing thermal bleaching of the F band (1), the band with λ_{max} = 360 mμ (2), thermoemission (3) (a filter was used to isolate the emission of Tl^+ ions) and $\rho(T)$ for KCl:Tl (4). The temperature variation of the efficiency of thermoluminescence has a complex, step-like character. It may be assumed that the individual steps in the temperature dependence of ρ correspond to different electron and hole stages of the relaxation process. Thus at different elementary stages of the relaxation process the instantaneous efficiency of thermoluminescence has different values ranging from zero to infinity. The infinite values of the thermoluminescence efficiency calculated from bleaching of the F band stem from the fact that in the investigated regions breakdown of F centers virtually does not occur, and the observed thermoluminescence presumably accompanies the process of break up of some other type of color centers. For example, the thermoluminescence peak of KCl:Tl at ~350°K and partially the peak at ~400°K are due to two-stage dissociation of M centers that are produced at room temperature; in the region of the peak at 295°K there occurs another stage of bleaching of the band with λ_{max} = 360 mμ. The very high intensity of the thermoluminescence in this peak gives reason to assume that the recombination in this region occurs at the activator: activator color centers break down. The polarity of this process has not been established so far.

The values of $\rho(T)$ close to zero are connected with the low efficiency of energy transfer from the points of recombination to the luminescence centers and

are usually observed in the hole stages of the relaxation process. Thus, for example, according to the data of Refs.3 & 5, the stage of break-up of V_1 and F centers in KCl:Tl at about 170°K (and probably at 230°K) is due to a hole process. The efficiency of thermoluminescence in these regions is much (~100 times) lower than in the electron stages[6] of the relaxation process that occurs at temperatures above 350°K.

In the accompanying figure we also show the thermoemission curve (3') and efficiency of thermoluminescence curve (4') for KCl:Tl phosphor x-irradiated at room temperature and then heated to 450°K.

In the elementary stage of the relaxation process the instantaneous efficiency of thermoluminescence remains constant. It can readily be shown that this constancy can be regarded as experimental substantiation of the theoretical condition of Andirovich[7] regarding the quasistationary concentration of electrons in the conduction band.

References

1. I.V.Yaek, Trudy IFA AN ESSR (Proceedings, Inst.of Phys.& Astron., Estonian SSR Ac.of Sci.), No.12, 226 (1960).
2. Ch.B.Lushchik, Izvestiya, Estonian SSR Ac.of Sci., 5, 12 (1956).
3. I.K.Vitol, Ch.B.Lushchik & I.V.Yaek, Trudy IFA AN ESSR, No.12, 175 (1960).
4. Ch.B.Lushchik, Ibid., No.3, 3 (1956).
5. Ch.B.Lushchik, Ibid., No.8, 75 (1958).
6. I.K.Vitol, Transactions of the 7th Conference on Luminescence, Tartu,1959.
7. E.I.Adirovich, Nekotorye voprosy teorii lyuminestsentsii kristallov (Some problems in the theory of luminescence of crystals), M.-L., 1951.

* * * * * * *

PHOTO- AND THERMOSTIMULATED ELECTRON EMISSION FROM ALKALI HALIDE PHOSPHORS EXCITED BY ULTRAVIOLET RADIATION

- A.I.Belkind & Kh.F.Kyaembre

For the purpose of clarifying the mechanism and kinetics of the physical processes occurring incident to luminescence and creation of color centers in alkali halide phosphors, we, in addition to the conventional absorption and luminescence procedures widely used in our laboratory (see, for example, Refs.1 & 2), made use of an electric procedure.

Using a point counter (see Refs.3 & 4), we investigated the photostimulated and thermostimulated electron emission (hereinafter PSE and TSE) from excited alkali halide crystals. The experimental technique is described in Ref.5. In contrast to the case in most studies devoted to electron emission from excited crystals (exoelectronic emission), we excited our KBr, KCl, NaCl, KBr:Tl, KCl:Tl and NaCl:Tl crystals with UV light from a spark between aluminum electrodes, isolating the individual lines by means of a monochromator. This enabled us to realize different elementary excitations of the crystal (excitation of the activator ions, anionic excitons, etc.).

In agreement with the data of Refs.6 & 7, the spectrum of emission stimulation for KBr crystals does not repeat the contour of the F absorption band, but

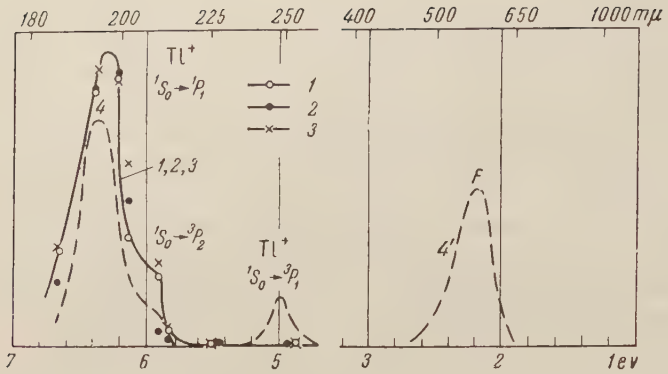

Fig.1. Excitation spectra of PSE (1), luminescence photostimulated in the F band (2) and phosphorescence (3) of a KCl:Tl single crystal; absorption spectrum of KCl:Tl (4) and spectrum of excited absorption (4') of the same phosphor after irradiation with ultraviolet from an Al spark.

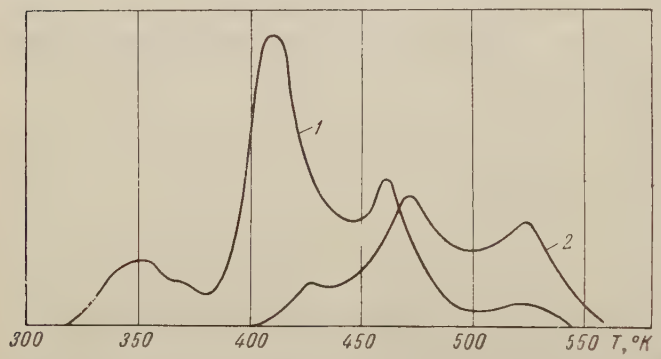

Fig.2. Thermostimulated luminescence (1) and TSE (2) of an NaCl:Tl crystal excited by ultraviolet from an Al spark.

rises rapidly from $h\nu \approx 1.6$ ev to the side of shorter wavelengths. Measurements of the influence of visible light on the PSE of photoexcited KBr show, however, that the observed PSE is undoubtedly realized from F centers (we measured the decrease of PSE after illumination of the excited crystal by monochromatic light of different frequencies). These data substantiate the hypothesis advanced by Apker & Taft[7] regarding direct optical ejection of electrons from F centers into the vacuum. The KBr PSE excitation spectrum attains a maximum at 186 mμ, the region of the peak of the exciton absorption band (we measured the magnitude of the photostimulated emission from F centers after excitation of the crystal by monochromatic radiation of different frequencies).

As will be evident from Fig.1, in the case of KCl:Tl phosphor the PSE excitation spectrum and the spectrum of luminescence photostimulated in the F band repeat the contour of the short wavelength activator absorption band, corresponding to the $^1S_0 \rightarrow {}^1P_1$ transition in Tl^+ ions. The phosphorescence excitation spectrum has the same shape. Thus after repeated vain attempts[8,9] to detect the photoelectric effect incident to excitation in the activator absorption band, on the basis of which Seitz proposed the metastable mechanism of phosphorescence in alkali halide phosphors, we now have direct electric data substantiating the recombination nature of the phosphorescence mechanism in KCl:Tl.

After excitation of an NaCl:Tl phosphor by ultraviolet in the short wavelength activator band we also succeeded in observing TSE(Fig.2). At the same time we also measured the thermal bleaching in the F band, which clearly consists of several stages, or the thermostimulated luminescence. In measuring the TSE of NaCl:Tl crystals (measurements were started 10 min after excitation), we observed that the thermal bleaching stages occurring at 420, 440 and 520°K are accompanied by emission. The stage of thermal bleaching at 520°K was observed by Elango[10] earlier. Inasmuch as emission corresponds to escape of electrons from the crystal, it may be concluded that at least the two or three highest temperature stages of F center bleaching are due to thermal ionization of the centers.

The fact that the low temperature stages of thermal bleaching are not accompanied by emission may be explained on the assumption that the emission is a

surface effect whereas the absorption is a volume effect.

The results of concurrent measurements of TSE and thermostimulated luminescence (Fig.2) indicate close correlation between the TSE and thermostimulated luminescence peaks. This correlation, the relation between the thermoluminescence peaks and the different stages of thermal bleaching observed in the work of Lushchik, and the character of the PSE process discussed above, all substantiate the recombination character of phosphorescence in alkali halide crystals.

Institute of Physics and Astronomy,
Academy of Sciences of the Estonian SSR

References

1. Ch.B.Lushchik, Kh.F.Kyaembre & I.V.Yaek, Transactions of the 7th Conference on Luminescence, Tartu, 1959.
2. Ch.B.Lushchik, G.G.Liid'ya & I.V.Yaek, Izv.AN SSSR, Ser.fiz., 25, 23 (1961). (Trans.Bulletin, 25, 23.)
3. J.Kramer, Z.Phys., 133, 629 (1952).
4. A.Bohun, Chekhosl.fiz.zh. (Czechoslovak Physics Journal), 5, 224 (1955).
5. A.I.Belkin, Trudy IFA AN ESSR (Proceedings, Inst.of Physics & Astronomy, Estonian SSR Ac.of Sci.), No.12, 241 (1960).
6. R.Fleischmann, Z.Phys., 84, 717 (1933).
7. L.Apker & E.Taft, Phys.Rev., 79, 964 (1950).
8. K.Hecht, Dissertation, Göttingen, 1930.
9. J.Ewles & R.Joshi, Proc.Roy.Soc., A254, 358 (1960).
10. M.Elango, Trudy IFA AN ESSR, No.12, 197 (1960).

* * * * * * *

INVESTIGATION OF OPTICAL DISSOCIATION OF F CENTERS IN ALKALI HALIDE CRYSTALS

- I.A.Parfianovich & E.I.Shuraleva

The mechanism of optical dissociation (bleaching) of F centers in photochemically colored alkali halide crystals has been the subject of numerous discussions in the literature. In this connection a number of authors have considered the so-called stability of F centers: some associated it with the presence in the crystal of hole centers with different recombination luminescence[1,2], while others infer the existence of two types of F centers, termed "soft" and "hard" by Oberley[3]. Markham[4], however, proposes a different explanation.

With a view to determining the mechanism of photodissociation of F centers we undertook a detailed investigation of the effect of optical flash and dissociation of F centers in pure and activated NaCl crystals. The F centers were produced by x-rays; the colored crystals were bleached by light in the F band.

It was established that the weakening of the F band under the influence of light in pure crystals is connected primarily with transformation of the F centers into other electron centers (M and F'); as for recombination of free electrons with the holes of V centers, in our estimation, this plays an insignificant role. After attainment of the limiting electron concentration on shallow trapping levels the dissociation of F centers virtually ceases. This is illus-

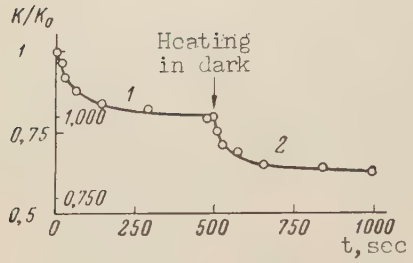

Fig.1. Relative change in the F center concentration in a pure NaCl crystal: under the influence of light: 1 - immediately after x-irradiation, 2 - after subsequent heating at 70° for 7 min.

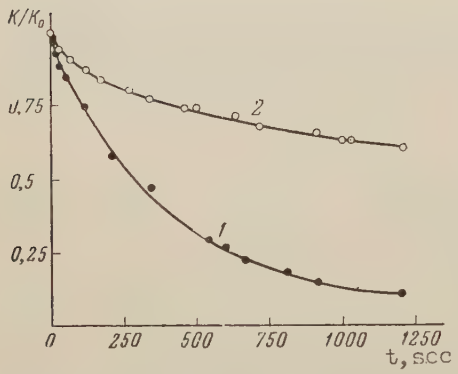

Fig.2. Relative variation of the F center concentration incident to photodissociation in NaCl:Ni phosphor x-irradiated for 20 min (1) and 5 hours (2).

trated by the experimental results presented in Fig.1, which shows the relative changes in F center concentration in the process of their optical dissociation in a pure NaCl crystal. Curve 1 was obtained immediately after x-irradiation; curve 2 after subsequent heating of the crystal in the dark for the purpose of releasing the electrons from the shallow traps.

It will be seen that curve 1 consists of two sections: the initial section characterizes rapid dissociation of the F centers, while the final section indicates virtual cessation of dissociation. But, as will be evident from curve 2, it is sufficient to remove the electrons from the shallow trapping levels for dissociation of F centers to resume at a high rate.

An entirely different situation obtains in crystals containing an activator. As we showed earlier[5,6] for the case of NaCl:Ni phosphors, introduction of an activator leads to reduction of the F center stability. Investigation of the spectra of the additional absorption and simultaneous study of quenching of the optical flash and the photodissociation of F centers under conditions when there could be electrons on shallow trapping levels and under conditions when this was impossible, enabled us to establish the mechanism of F center dissociation in phosphors. True photodissociation of F centers in activator crystals is due primarily to recombination of electrons with ionized luminescence centers, which are present in NaCl:Ni phosphors prior to their excitation, and the number of which decreases as a result of exposure to x-rays. The role of ionized luminescence centers in the process of optical dissociation of F centers is particularly clearly evident from the curves of Fig.2, which characterize the relative changes in the F center concentration in the same NaCl:Ni phosphor specimens but exposed to x-rays for different periods. In the case of short-term x-irradiation (curve 1) the bleaching of the F centers occurs fairly rapidly; in the case of prolonged irradiation (curve 2) there occurs so appreciable a decrease in the number of ionized luminescence centers that the F centers become almost as stable as in a pure crystal.

Thus we see that the different stability of F centers in alkali halide crystals is not due to the presence of centers with different properties ("soft" and "hard" centers), but is determined by the conditions governing the recombination of electrons released from these centers.

Worthy of attention is the fact that the stability of F centers is affected not only by the presence of a divalent activator but also by the presence of a monovalent one. This was demonstrated in the work of Hersh[7] with KI:Tl. In addition, we carried out experiments with NaCl:Cu phosphors. Here again we found that with increase of the activator concentration the optical stability of F centers decreases. It is interesting to note that the activator absorption band

(λ_{max} = 255 mμ) in these phosphors can be weakened as a result of heating the phosphor; at the same time the stability of the F centers is enhanced, i.e., the F centers become more stable as a result of heating. These experiments led us to the conclusion that the stability of F centers is affected not only by the part of the activator that is located at the cationic lattice sites, but also by the part of the activator distributed in special places in the crystal, namely, on block faces and similar surfaces along which it can move with relative ease when the crystal is heated.

"A.A.Zhdanov" Irkutsk State University

References

1. R.Casler, P.Pringsheim & P.Yuster, J.Chem.Phys., 18, 887 & 1564 (1950).
2. P.Pringsheim, Z.Phys., 144, 31 (1956).
3. J.J.Oberly, Phys.Rev., 84, 1257 (1951).
4. J.J.Markham, J.Phys.Chem., 57, 762 (1953); Phys.Rev., 86, 433 (1952).
5. E.I.Shuraleva, Optika i spektroskopiya, 2, 396 (1957).
6. I.A.Parfianovich & E.I.Shuraleva, Optika i spektroskopiya, 7, 518 (1959). (Trans.Optics & Spectroscopy.)
7. H.Hersh, J.Chem.Phys., 30, 790 (1959).

* * * * * * *

OPTICAL PROPERTIES OF ALKALI HALIDE CRYSTALS DOPED WITH O, S, Se AND Te

- O.A.Shmits & Yu.R.Zakis

The properties of alkali halide crystals doped with O, S, Se and Te have scarcely been studied. In the investigations listed under Refs.1-4 there were obtained the absorption and luminescence spectra of some alkali halide crystals with oxygen-containing impurities and the absorption spectrum of KI with S impurity.

The present work is a continuation of the study of the properties of alkali halide crystals doped with O, S, Se and Te, started in 1959 in the Latvian State University.

The doped KCl, KBr and KI crystals were obtained by two procedures, namely, by growing from the melt by the Stockbarger technique and by diffusion of the impurity vapor into the crystal additively colored beforehand.

The absorption spectra of KCl, KBr and KI crystals containing oxygen impurities proved to be similar to those described in the literature[1-4]. The following results were obtained for the crystals with other impurities.

In the absorption spectra of KCl crystals with O, S, Se and Te there is observed a monotonic increase of the absorption starting at about 4 ev and extending to the side of shorter wavelengths without any distinct maxima. All these crystals exhibit a weak photoluminescence in the visible region (we plan to study the characteristics of this luminescence in the future).

In contrast, the absorption spectra of doped KBr crystals exhibit a series of maxima but no monotonic rise of the absorption to the side of shorter wavelengths. The absorption, excitation and photoluminescence (excitation by 313 mμ)

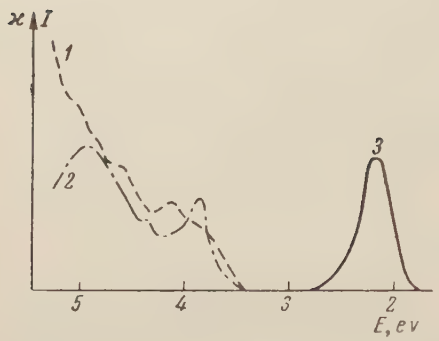

Absorption (1), excitation (2) and photoluminescence (λ_{excit} = 313 mμ) (3) spectra of KBr crystals doped with Se.

spectra of a KBr:Se crystal are shown in the accompanying figure.

In the absorption spectra of KI crystals containing O, S, Se or Te impurity, in addition to the monotonically increasing absorption to the side of shorter wavelengths, there are present several peaks. These crystals also yield photoluminescence in the visible region.

It follows from the results obtained that KCl, KBr and KI crystals doped with O, S, Se and Te have absorption and luminescence spectra characteristic of the impurity contained in the crystal. This is substantiated by the fact that the absorption and luminescence spectra of the crystals do not agree with the spectra of the same crystals containing Cu, Pb and other frequently encountered impurities.

In addition, for some crystals we determined the variation of the absorption spectra with the impurity concentration and found that the absorption at all the peaks decreases with decrease of the impurity concentration.

It may be assumed that the enumerated impurities enter into the crystal lattice in the form of divalent anions. This assumption is in agreement with the experimental data on subtractive and additive coloring of crystals with these impurities.

We note that whereas alkali halide crystals containing cationic impurities are highly hygroscopic (particularly KI), the hygroscopicity of the alkali halide crystals doped with S, Se and Te is substantially reduced.

Latvian State University

References

1. A.D.Lüpke, Ann.Phys., 21, 1 (1934).
2. S.Akpinar, Ibid., 37, 429 (1940).
3. J.Rolfe, Phys.Rev.Letters, 1, 56 (1958).
4. H.W.Etzel & D.A.Patterson, Phys.Rev., 112, 1112 (1958).

DISCUSSION

Ch.B.Lushchik: Most investigations of alkali halide crystals have been concerned with crystals containing cationic impurity luminescence centers. Hence, one should welcome investigations devoted to anionic luminescence centers. It may be noted that for anionic centers in the crystal lattice there should be observed "expansion" of the energy diagrams as compared with free anions. The inverse effect of "compression" of the energy diagrams is familiar for cationic impurities.

INTERACTION OF ACTIVATORS IN ALKALI HALIDE PHOSPHORS

- A.T.Khlevnyuk

Sensitized luminescence of alkali halide phosphors has been studied by Shvartz & Zarnitis[1] and other authors.

The purpose of the present work was to investigate the effect of activator interaction on the electron trapping centers in NaCl:$CuCl_2$:$PbCl_2$ phosphors. The study was carried out by comparison of the thermostimulated luminescence (glow) curves and the additional absorption spectra of x-irradiated one- and two-activator phosphors. The phosphor single crystals were grown by the Kyropoulos technique.

The thermostimulated luminescence of x-irradiated NaCl:Cu phosphors has been investigated by Parfianovich[2,3], Kats[4] and Lushchik[5]. The thermostimulated luminescence of NaCl:Pb phosphors was studied by Lushchik and his co-workers[6]. The spectral characteristics of NaCl:Cu and NaCl:Pb phosphors are described in Refs. 7-9.

Our results as regards the glow curves and additional absorption spectra of NaCl:Cu and NaCl:Pb phosphors agree in general with the data in the literature.

In investigating the two-activator phosphors we obtained the following results. Phosphors with equal molecular concentrations of the activators (for example, NaCl:$CuCl_2$(0.02):$PbCl_2$(0.02))* have glow curves with three peaks located at 40, 58 and 128°; these peaks also appear in the glow curves of NaCl:$CuCl_2$ phosphors.

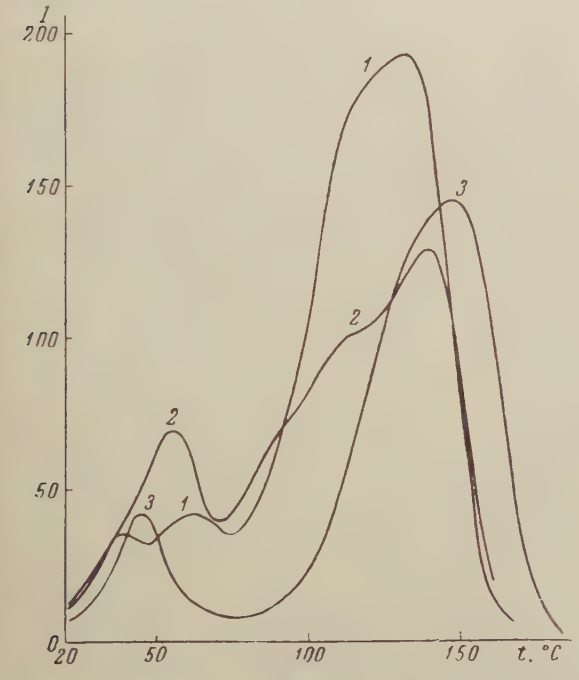

Glow curves: 1 - NaCl:$CuCl_2$(0.02), 2 - NaCl:$PbCl_2$(0.4) (the vertical scale for this curve has been increased by a factor of 2), 3 - NaCl:$PbCl_2$(0.4):$CuCl_2$(0.02).

The deformation of the glow curves of two-activator phosphors with increase of the relative copper concentration is the same as for the curves of NaCl:$CuCl_2$ phosphors with increase of the activator concentration. However, the peak at 220°, characteristic of NaCl:$CuCl_2$ phosphors, does not appear in the glow curves for the two-activator phosphors. Moreover, the light sum stored in the two-activator phosphors is appreciably smaller than that stored in NaCl:$CuCl_2$ phosphors.

In case of minor predominance of lead (for example, for NaCl:$PbCl_2$(0.04):$CuCl_2$(0.02)) the high temperature peak is shifted to the side of higher temperatures and increased in height. At the same time there appears a peak at 110°, which is characteristic of NaCl:$PbCl_2$ phosphors. With an appreciable predominance of lead, the glow curve has two peaks located at 45 and 145° (curve 3 in the accompanying figure). This curve differs greatly from the curves for one-activator phosphors. Both these peaks do not agree with the peaks in the curves for one-activator phosphors (see figure); in fact the second peak is located outside the region of the peaks characteristic of

---

*All the activator concentrations are given in mole percent.

one-activator phosphors.

The additional absorption spectra of two-activator phosphors differ from the absorption spectra of the one-activator phosphors. The optical density at the maximum of the F band (465 mμ) for two-activator phosphors depends on the activator concentration ratio. The optical density in the F band increases with increasing relative copper concentration, but remains virtually constant with increase of the relative lead concentration.

In case of appreciable predominance of lead (for example, NaCl:$PbCl_2$(0.4): $CuCl_2$(0.02)) the maximum of the F band is shifted to 460 mμ, while the M band disappears. The shift of the F band is consistent with the fact that the peak in the glow curve for the given phosphor which corresponds to release of electrons from the F levels is shifted to the side of higher temperatures.

Thus it is apparent that interaction of the activators in NaCl:$CuCl_2$:$PbCl_2$ phosphors definitely affects the conditions of formation of F and M centers.

"V.G.Korolenko" Poltava Pedagogical Institute

References

1. K.K.Shvarts & U.A.Zarnitis, Trudy IFA AN ESSR (Proceedings, Inst.of Physics & Astronomy, Estonian SSR Ac.of Sci.), No.11, 3 (1960).

2. I.A.Parfianovich, Izv.AN SSSR, Ser.fiz., 15, 669 (1951).

3. I.A.Parfianovich, Zhur.eksp.i teor.fiz., 21, 314 (1951).

4. M.L.Kats, Doklady AN SSSR, 85, 757 (1952).

5. Ch.B.Lushchik, Trudy IFA, AN ESSR, No.3, 3 (1955).

6. Ch.B.Lushchik, F.N.Zaitov, V.Ya.Kark, L.A.Teis & I.V.Yaek, Transactions of the 5th Conference on Luminescence, Tartu, 1957.

7. I.A.Parfianovich, Optika i spektroskopiya, 4, 253 (1958); Ibid., 4, 692 (1958).

8. J.H.Shulman, R.Ginther & C.C.Klick, J.Opt.Soc.Am., 40, 854 (1950).

9. Ch.B.Lushchik, N.E.Lushchik, G.G.Liid'ya & L.A.Teis, Trudy IFA AN ESSR, No.6, 63 (1957).

EFFECT OF DIFFERENT GASES ON THE FORMATION OF LUMINESCENCE CENTERS IN SILVER HALIDE

- S.I.Golub & N.A.Orlovskaya

To yield intense luminescence silver chloride sublimate layers, like most alkali halides[1], require heat treatment. The activation occurs as the result of decomposition of the salt particles and formation of a stoichiometric excess of silver. In silver halide sublimate phosphors there are present at least two types of luminescence centers[2]: internal centers responsible for the short wavelength band (blue band in the case of AgCl), and external or superficial centers responsible for the long wavelength band (red). The medium in which the phosphor is heated (300-400°C) has a substantial influence on the effect produced; moreover, the effect differs for different bands.

The results of our measurements are shown in the accompanying figure.

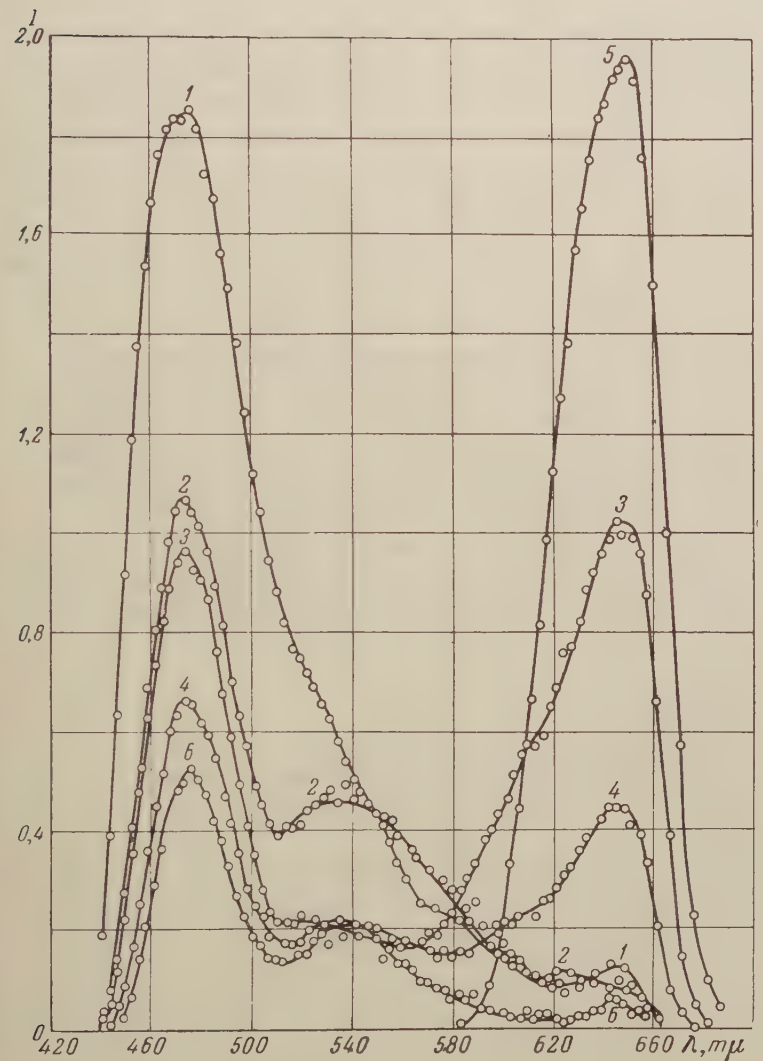

Effect of heating AgCl at 300°C in different media: 1) oxygen, 2) air, 3) vacuum, 4) control (not heated) sample, 5) chlorine, 6) control sample for heating in chlorine.

Blue band

Heating in vacuum with continuous pumping of the container enhances the luminescence by a factor of 2-3. This "pure" effect of heating can be explained on the assumption that, on the one hand, heating leads to ordering of the crystal lattice, and, on the other hand, increases the concentration of surstoichiometric silver atoms, which diffuse through crevices onto the internal surfaces of the crystals and there form new luminescence centers.[3]

Heating in air (furnace atmosphere) increases the luminescence to a greater extent than heating in vacuum, while heating in pure oxygen (p = 2-3 cm Hg) has an even stronger intensifying effect. Consequently, pure oxygen or atmospheric oxygen facilitates diffusion of the activator into AgCl, producing, as in the case of alkali halide phosphors, additional local heating of the host.

Heating in chlorine vapor (p = 20 atm) greatly weakens or even completely quenches the blue luminescence of AgCl. This fact may be interpreted as the result of diffusion of

chlorine into the crevices and over the surfaces of the substructure blocks and oxidation by it of the silver atoms adsorbed on these surfaces. This process results in destruction of the blue luminescence centers.

Red band

Inasmuch as the red luminescence centers are colloidal silver particles, heating, on the one hand, increases the number of centers, inasmuch as it raises the concentration of excess silver, and, on the other hand, decreases the number of centers, because at 300° there begins resorption or dispersion of the colloidal particles. Upon these two effects there is superposed the influence of the medium in which the phosphor is heated. Our experiments yielded the following results.

Heating in vacuum enhances the luminescence: obviously, there predominates the process of formation of new centers because the chlorine evolving in the process of decomposition of AgCl by heat is evacuated.

Heating in oxygen weakens the luminescence. This apparently occurs because oxygen facilitates dispersion of the colloidal particles (the Herschel effect occurs only in the presence of oxygen during heating[4]), so that this process predominates over the process of formation of new centers. In addition, the oxygen oxidizes the silver particles, which also leads to weakening of the luminescence. Heating in air at 300° intensifies the luminescence; here there predominates formation of new centers, while the dispersing effect of oxygen of the air is weaker than that of pure oxygen. It must be noted, however, that heating at 400° in air, as in pure oxygen, completely suppresses the red band.

Heating in chlorine vapor greatly enhances the red band. This might be explained by the fact that the presence of chlorine penetrating through crevices into the crystals, hinders inward diffusion of the silver atoms. Hence the excess silver, forming as a result of thermal decomposition of the AgCl, remains on the external surfaces of the crystals, and as a result of conglomeration the concentration of colloidal silver particles increases. Chlorine interacts weakly (and only on the surface) with colloidal silver particles; hence they are not oxidized. In the absence of oxygen, there is no noticeable dispersion of the colloidal particles. The combined effect of all the above factors is a great increase in the number of red luminescence centers with consequent enhancement of the red luminescence.

References

1. F.D.Klement, Zhur.fiz.khim. (Jour.Physical Chem.) 21, 563 (1947).

2. S.I.Golub, Transactions of the 7th Conference on Luminescence, Tartu, 1959.

3. S.I.Golub & N.A.Orlovskaya, Trudy (Proceedings), Odessa State University, 148, Ser.fiz.nauk, (Phys.science series), No.6, 29 (1958).

4. A.S.Vnukova, Zhur.fiz.khim., 9, 593 (1937).

LUMINESCENCE OF ALKALI HALIDE PHOSPHORS ACTIVATED BY ANTIMONY TRICHLORIDE

- A.S.Andrianov & M.L.Kats

The usual procedure for determining the nature of the luminescence centers in alkali halide phosphors is experimental determination of the regularities obtaining in the activator absorption spectra and comparison of these with the regularities governing the electron transitions between the energy levels of the activator in the free state. From this standpoint it is of interest to investigate alkali halide phosphors activated by ions with identical outer electron shells; a suitable homologous series is represented by In^{+}, Sn^{2+} and Sb^{3+}.

The optical properties of tin and indium activated alkali halide phosphors have been investigated repeatedly.[1-5] Hitherto there has been only one study, by Schleede[6], devoted to alkali halide phosphors activated by antimony; the principal results of this study are summarized in Pringsheim's book[7]. (Some preliminary results on KCl:$SbCl_3$ phosphors will be found in Ref.8.)

For the purposes of the present work we prepared surface-activated single crystal phosphors.

The accompanying figure gives the experimental absorption curves obtained for KCl:$SbCl_3$, KBr:$SbCl_3$ and a layer of $SbCl_3$ deposited on a quartz substrate, as well as the curves characterizing the excitation and fluorescence spectra of KCl:$SbCl_3$.

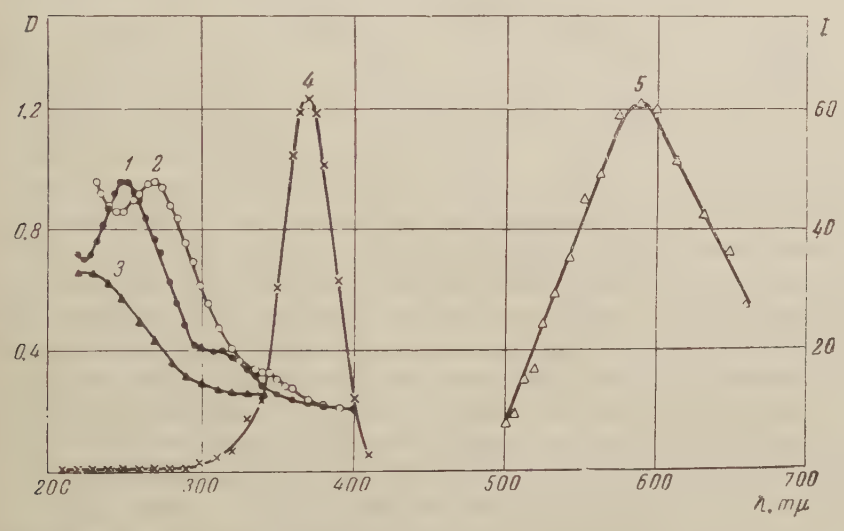

Absorption of KCl:$SbCl_3$ (1), KBr:$SbCl_3$ (2) and an $SbCl_3$ layer on a quartz substrate (3), and excitation (4) and fluorescence (5) spectra of KCl:$SbCl_3$.

It will be evident from a comparison of curves 1 and 2 and the curves characterizing the absorption of alkali halide phosphors activated by Sn and In (Refs.1-5) that they are similar in appearance; hence, presumably, the absorption peaks can be associated with the same electron transitions.

However, there are also substantial differences between the optical properties of the enumerated phosphors. Whereas the activator absorption spectra of In and Sb activated alkali halide phosphors completely agree with the respective fluorescence excitation spectra, no such agreement is observed for the Sb activated phosphors (compare curves 1 and 4).

The noncoincidence of the peaks in the absorption and fluorescence excitation spectra of KCl:$SbCl_3$ indicate that the optical absorption in the bands with λ_{max} = = 250 and 312 mμ and the process of fluorescence in the visible region are associated with different centers. Whereas the optical absorption, as was noted above, is due to electron transitions between levels in Sb^{3+} ions, the fluorescence, apparently, is connected with centers of more complex structure.

It must be noted that the layer of antimony trichloride deposited on a quartz backing does not fluoresce under the influence of ultraviolet. Consequently, a necessary condition for the formation of fluorescence centers appears to be inter-

action of the antimony tetrachloride molecules with the particles of the base material.

Alkali halide phosphors activated by $SbCl_3$ can be obtained at room temperature by simple mixing of the host and activator impurity, without grinding. This suggests that these phosphors belong in the class of surface-activated phosphors.

"N.G.Chernyshevskii" Saratov State University

References

1. M.Huniger & J.Rudolf, Z.Phys., 117, 81 (1941).
2. A.S.Andrianov & M.L.Kats, Transactions of the 5th Conference on Luminescence, Tartu, 1957.
3. M.L.Kats & V.K.Nikol'skii, Optika i spektroskopiya, 4, 354 (1958). (Trans. Optics and Spectroscopy.)
4. L.M.Shamovskii & A.A.Dunina, Transactions of the 7th Conference on Luminescence, Tartu, 1959.
5. N.E.Lushchik & Ch.B.Lushchik, Optika i spektroskopiya, 8, 839 (1960). (Trans.Optics & Spectroscopy.)
6. A.Schleede, Leuchten und Struktur fester Stoffe. Vorträge der Münchner Arbeitstagung, 1942, Berlin, 1943.
7. P.Pringsheim, Fluorescence and Phosphorescence, N.Y., 1949.
8. N.E.Lushchik & Ch.B.Lushchik, Trudy IFA AN ESSR (Proceedings, Instit.of Physics & Astronomy, Estonian SSR Ac.of Sci.), No.6, 5 (1957).

DISCUSSION

N.E.Lushchik: We investigated the absorption, excitation and luminescence spectra at 300°K of KCl:Sb single crystals prepared by the method of diffusion from the gaseous phase. The results obtained (see Trudy IFA AN ESSR - Proceedings, Institute of Physics & Astronomy, Estonian SSR Ac.of Sci.) No.6, 3 (1956), and my Dissertation) agree in general with the results reported by Andrianov & Kats. It must be noted, however, that the inference drawn by Andrianov & Kats regarding the noncoincidence between the absorption and excitation spectra of KCl:Sb are possibly premature, inasmuch as these authors did not investigate the ultraviolet emission of KCl:Sb and did not prove that the impurity absorption must be attributed to the antimony ion. I agree with the opinion of Andrianov that the yellow luminescence of KCl:Sb is probably connected with luminescence centers of type II.

INVESTIGATION OF THE EFFECT OF DOUBLE ACTIVATION BY SILVER AND SAMARIUM ON TRAPPING LEVELS IN AND THE LUMINESCENCE OF ZINC SULFIDE PHOSPHORS

- V.L.Levshin, Yu.V.Voronov, V.B.Gutan, S.A.Fridman & V.V.Shaenko

In phosphors containing two activators there is usually observed strong interaction of the activators, leading to complex distribution of the excitation energy between the individual emission bands.[1-4]

Particularly strong interaction occurs between activators that are rare earth elements. In the present work, which is the first of a series of planned studies on activator interaction, we investigated the interaction of Ag and Sm in zinc sulfide phosphors.

The phosphor samples were prepared in a stream of hydrogen sulfide, so that the intrinsic luminescence of zinc sulfide itself did not appear and the corresponding system of trapping levels did not form. By way of flux we used magnesium chloride, which was added in the amount of 4%. Some of the investigated phosphor samples were prepared without flux, but the quantitative data presented in the report pertain only to phosphors fluxed with $MgCl_2$.

We prepared and investigated phosphors activated only by silver, and only by samarium, phosphors containing Ag in the amount of 10^{-4} g/g and amounts of Sm varying from 10^{-7} to 10^{-3} g/g, and phosphors containing 10^{-4} g/g Sm and varying amounts of Ag in the range from 10^{-7} to 10^{-3} g/g.

1. Luminescence centers

Silver is characterized by emission in a relatively narrow blue band peaking at 430 mμ. The luminescence of samarium consists of three groups of very narrow bands, essentially lines: a green, orange and red group. The last, which is the most intense, is located at about 650 mμ.

One may ask: does the entire emission spectrum of samarium correspond to one type of center or are several types of centers involved[5]? Trapeznikova[6] came to the conclusion that Sm in zinc sulfide phosphors gives rise to at least three different kinds of luminescence centers. In order to answer this question we recorded the spectra of the red group for different phosphors and under different conditions. Analyzing the resultant spectrograms, we compared the variation in intensity of the red lines depending on the concentration of Sm, the presence of Ag and flux and on the temperature.

It was found that the effect of these factors on the intensity of the individual lines differs; this does not necessarily mean, however, that the number of different luminescence centers is equal to the number of lines observed. The varying factors may have different effects on the excitation of the same center, resulting in excitation of different states. Nevertheless, a number of considerations give reason to think that there must be present centers of more than one kind.

2. Trapping levels in ZnS:Ag:Sm phosphors

The next step in our work was investigation of the arrangement of trapping levels in zinc sulfide phosphors with one or two activators, and determining the effect of interaction of the activators on the depth and development of the different trapping levels.

The glow curves obtained for one- and two-activator phosphors in thick layers are shown in Fig.1.

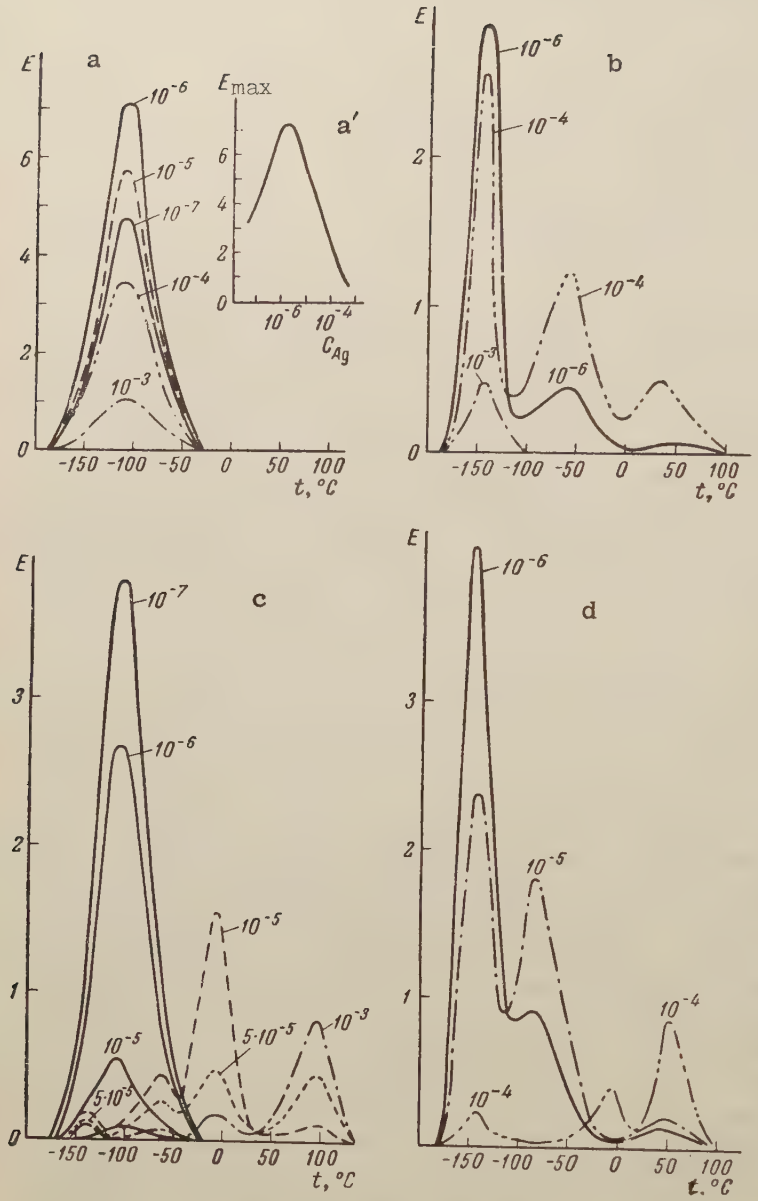

Fig.1. Glow curves for the investigated phosphors; the figures at the curves give the activator concentration. All phosphors prepared with 4% $MgCl_2$ flux.

Fig.1,a gives the glow curves for ZnS:Ag phosphors with different amounts of silver from 10^{-7} to 10^{-3} g/g. It will be seen that all the curves have a peak at about -112°. With increase of the Ag concentration the number of trapped electrons attains a maximum at 10^{-6} g/g and then with further increase of C_{Ag} falls off sharply.

Fig.1,b shows the glow curves for ZnS:Sm phosphors with different samarium concentrations. Here the principal peak lies at -144°; there are also evident two lower peaks at -60° and +30°, which at first increase with increase of the Sm concentration and then disappear at $C_{Sm} = 10^{-3}$ g/g. As in the case of ZnS:Ag phosphors, in the range of high activator concentrations the total energy storage ability decreases.

Fig.1,c shows the glow curves obtained for ZnS:Ag:Sm phosphors ($C_{Ag} = 10^{-4}$ g/g, $C_{Sm} = 10^{-7}$ to 10^{-3} g/g). In the Sm concentration range under $5\cdot10^{-4}$ g/g there is observed the luminescence of both silver and samarium. It will be evident from the figure that the glow curves for silver (solid lines) occupy the same temperature interval as for the phosphors without samarium; however, introduction of even very minor amounts of samarium sharply reduces the energy storage ability of these levels; the release of electrons from these levels yields only the luminescence of Ag. The dashed curves in Fig.1,c represent the glow curves due to the presence of samarium, but deformed by the presence of silver; the luminescence belongs to Sm. Comparison of these glow curves with the curves of Fig.1,b shows that the principal Sm level at -144° disappears almost completely in the presence of 10^{-4} g/g silver. At the same time the level corresponding to the -60° glow peak is weakened and the level emptying at +30° disappears, but there appear two new levels, yielding glow peaks at -10° and +90°. Thus the introduction of silver destroys the initial levels and produces new ones. The total energy storage capacity is reduced.

Fig.1,d shows the variation in the system of levels in ZnS:Sm:Ag with a constant concentration of Sm (10^{-4} g/g and $C_{Ag} = 10^{-6}$, 10^{-5} and 10^{-4} g/g). It will be seen that at $C_{Sm} = 10^{-4}$ g/g the luminescence of Ag disappears. The curves of Fig.1,d illustrate the strong suppressing influence of silver on the luminescence of samarium.

The depth of the trapping levels was determined by means of the formula proposed by Parfianovich[7]:

$$E = \frac{kT_1T_2}{T_2 - T_1}\left(\ln\frac{\beta_2}{\beta_1} + 2\ln\frac{T_1}{T_2}\right), \qquad (1)$$

where β_1 and β_2 are different rates of heating, T_1 and T_2 are the corresponding absolute temperatures of the glow curve peak, and E is the depth of the trapping level.

There were obtained the following values for the depth of the samarium trapping levels:

T,°C	-144	-90	-60	-10	+30	+70	+90
E,ev	0.26	0.37	0.43	0.53	0.61	0.69	0.73

The calculated energy depth of the silver levels is 0.33 ev.

It follows from the described results that the interaction of activators, first, modifies the system of trapping levels, forming new levels (in the table above the three underlined levels pertain to the one-activator phosphor, while the three other levels appear as a result of activator interaction), and, second, interaction of the activators sharply reduces the light sums stored on the original levels: at $C_{Sm} = 5 \cdot 10^{-4}$ g/g the initial levels of Ag are completely destroyed; introduction of 10^{-4} g/g Ag reduces the Sm luminescence light sum by more than half.

From the fact that increase in the number of activator ions leads to reduction of the stored light sums it follows that a trap created by two close activator ions is less efficient that a trap produced by a single ion. This observation applies both to ions of different activators and to ions of the same activator.

Investigations of the decay of Sm luminescence showed that the formation of deep Sm trapping levels with increase of its concentration leads to slowing down of Sm luminescence decay at the later stages of the process.

It must also be noted that the traps formed by samarium and silver are distinctive and give up their electrons only to centers formed by the same activator.

3. Variation of the luminescence spectra of ZnS phosphors under steady excitation with the amount and proportion of Sm and Ag introduced

The luminescence of the investigated phosphors consisted of the emission of Ag - a band between 400 and 500 mμ with a peak at 430 mμ - and a number of narrow Sm bands, among which we investigated only the group of intense lines between 640 and 660 mμ. We investigated the variation of the luminescence spectra under steady excitation as a function of the concentration of the interacting activators and the temperature.

Before turning to a discussion of the experimental results, it may be well to describe the character of the variation in the spectra for a specific case. Fig.2 shows the spectra of phosphors with the same optimum Ag concentration (10^{-4} g/g) and Sm concentrations equal to 0, 10^{-6} and 10^{-5} g/g. As will be evident from Figs.2,a & b, the luminescence of Ag falls off rapidly with increase of the Sm content.

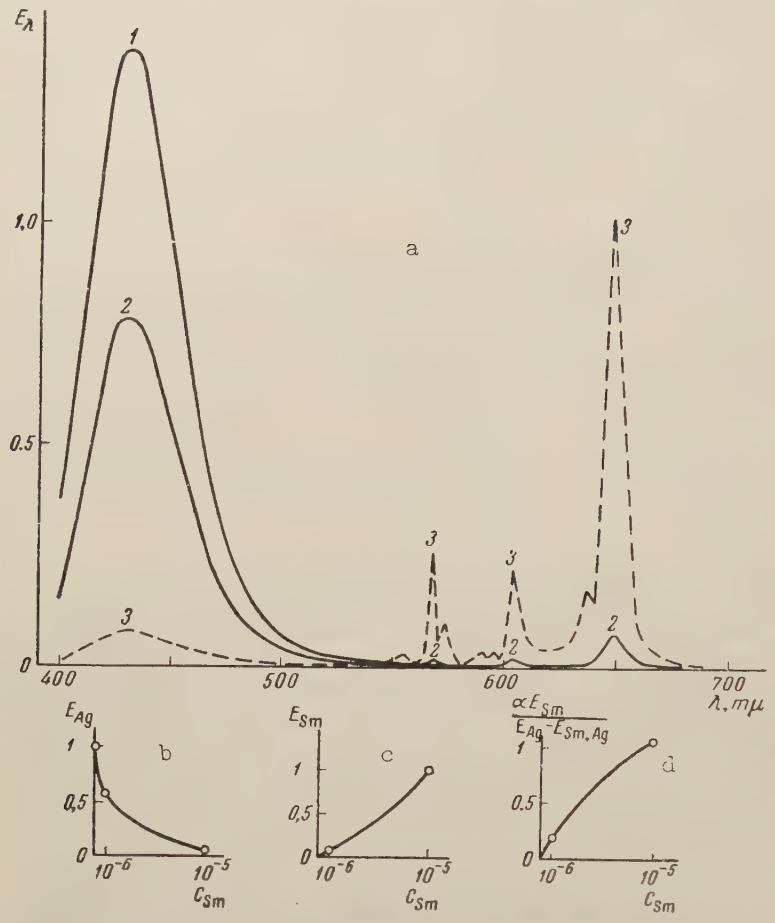

Fig.2. Luminescence spectra: 1) ZnS:Ag(10^{-4}), 2) ZnS:Ag(10^{-4}):Sm(10^{-6}), 3) ZnS:Ag(10^{-4}):Sm (10^{-5}). Excitation by λ = 365 mμ.

The first additions of Sm, although they produce substantial quenching of the Ag luminescence, yield only weak luminescence of Sm itself (Fig.2,c); in small amounts Sm acts mainly as an effective quencher. Further additions of Sm yield more noticeable luminescence. As will be evident from Fig.2,c, the increase in Sm luminescence with increase in Sm content is superlinear.

It is difficult to establish the absolute value of the coefficient of transformation of Ag luminescence to Sm luminescence: however, the relative change in the transformation coefficient, i.e., the value of $\Delta E_{Sm}/\Delta E_{Ag}$ can readily be determined by dividing the area under the Sm luminescence spectrum by the decrease of the area under the Ag spectrum. The rapid increase of the transformation coefficient with increase of Sm concentration is shown by the curve of Fig.2,d. Below we shall show that this curve passes through a maximum.

We now turn to discussion of the resulting curves characterizing the activator interaction. Fig.3 gives a number of curves characterizing the interaction processes at different activator concentrations. This figure is essentially a summary of results of investigation of the variation of the intensity of the luminescence spectra with changes in the activator concentration. The luminescence was excited by λ = 365 mμ.

Fig.3,a shows the variation in intensity of the Ag luminescence in the absence of Sm. It will be seen that the optimum Ag concentration is 10^{-5} g/g.

Fig.3,c shows the variation in the intensity of the luminescence of Sm(C_{Sm} = = 10^{-4} g/g) with different concentrations of Ag. Ag itself in this case does not yield luminescence, i.e., the luminescence of Ag is completely suppressed by the samarium. But it will be seen that the luminescence of Sm decreases with increase of the Ag content. Thus the two activators strongly quench each other. The action of Sm on Ag is stronger than the influence of Ag on Sm: thus the luminescence of Ag completely vanishes at $C_{Sm} \geqslant 10^{-4}$, whereas the introduction of Ag in the amount of 10^{-3} g/g only reduces the luminescence of Sm by a factor of 5.

Fig.3,d shows the variation in the intensity of the luminescence of Ag (left curve) and Sm (right curve) as a function of the Sm concentration. It will be seen that increase of the Sm content rapidly quenches the Ag band, which disappears completely at $C_{Sm} = 5 \cdot 10^{-5}$ g/g. The luminescence of Sm itself at first increases sublinearly, then goes through a maximum and decreases.

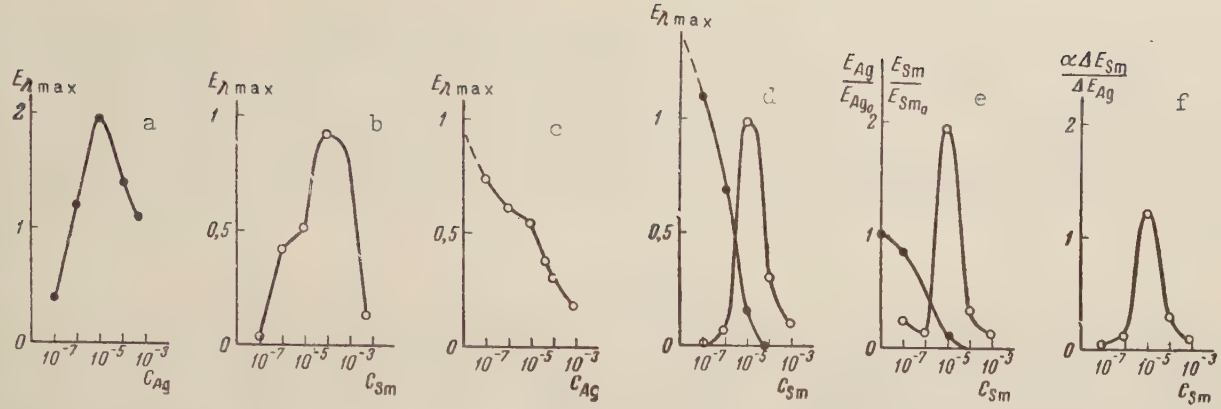

Fig.3. Variation in the luminescence intensity of Ag and Sm in ZnS phosphors (4% $MgCl_2$ flux) as a function of the activator concentrations; λ_{excit} = 365 mμ: a) ZnS:Ag, b) ZnS:Sm, c) ZnS:Sm(10^{-4}):Ag, d) ZnS:Ag(10^{-4}):Sm, e) $E_{Ag}/E_{Ag_0} = f(C_{Sm})$; $E_{Sm}/E_{Sm_0} = f(C_{Sm})$; f) $\Delta E_{Sm}/\Delta E_{Ag} = f(C_{Sm})$. Solid points - Ag; Open points - Sm.

Fig.3,e shows the variation as a function of the Sm concentration of the ratio of the luminescence intensities of Ag and Sm in the two-activator phosphor to the corresponding intensities in the one-activator phosphors. It will be seen that the luminescence of Ag monotonically decreases, while the luminescence of the Sm in the two-activator phosphors at a concentration of 10^{-5} g/g proves to be twice as bright in the single activator phosphor. Here we have a clear case of stimulation of the samarium luminescence by silver.

The coefficient of transformation of the vanishing blue luminescence of silver to the luminescence of samarium was determined in relative units: the variation of this coefficient as a function of the samarium content for ZnS:Ag (10^{-4}):Sm phosphors is given in Fig.3,f. The curve characterizing the transformation coefficient has a sharp maximum at $C_{Sm} = 10^{-5}$ g/g.

Similar investigations of the luminescence of the zinc sulfide phosphors with excitation by the λ = 313 mμ line and by a 10 kv, $5 \cdot 10^{-7}$ a/cm^2 electron beam showed that these two forms of excitation yield very similar results: they differ more appreciably from the results of excitation with λ = 365 mμ than from each other, but on the whole these differences are mainly qualitative.

4. Effect of temperature on the interaction of Ag and Sm

The above described interaction of the Ag and Sm activators was observed at room temperature. The next series of experiments was undertaken with a view to determining the effect of temperature on the activator interaction. Curves characterizing the temperature dependence of luminescence at the moment of excitation by λ = 365 mμ are shown in Fig.4.

Fig.4,a gives the variation in the luminescence intensity of the single activator phosphors: the dashed curve characterizes the luminescence of Ag(10^{-4} g/g); the solid curve - the luminescence of Sm(10^{-4} g/g). It will be seen that the two curves are similar, but that the luminescence curve for Ag has a peak at -20°, whereas the curve for Sm peaks at +20°. In view of this, the luminescence of Ag at temperatures above 60° is greatly weakened, while the decrease in the luminescence intensity of Sm with increasing temperature is relatively slow. A similar temperature variation of the luminescence intensity was observed for the phosphor with $C_{Sm} = 10^{-6}$ g/g.

Fig.4,b shows the temperature variation of the luminescence intensity of Ag

and Sm in ZnS:Ag(10^{-4}):Sm(10^{-6});Ag was taken in a large excess. It will be evident from a comparison of these curves with the curves of Fig.4,a that the shape of the intensity curves for Ag and Sm is greatly altered. The luminescence band persists in the region of low temperatures, and suppresses the Sm lines in this temperature region. In contrast, in the high temperature region the Sm lines are intensified, while the Ag band is suppressed. The intensities in Fig.4 are given in arbitrary units.

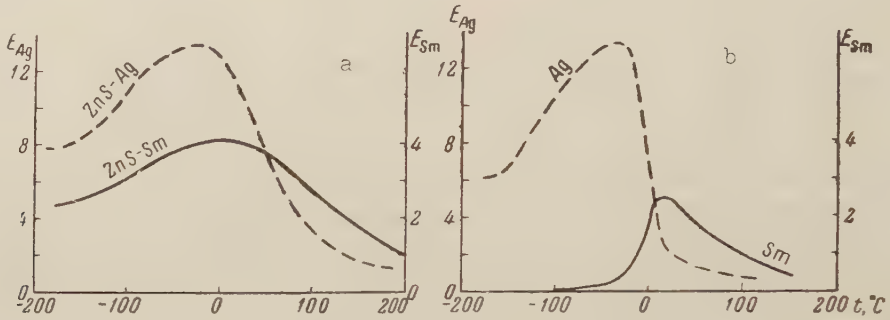

Fig.4. Temperature dependences of the luminescence intensity at the time of excitation by λ = 365 mμ.

In order to clarify the character of the interaction of Ag and Sm we calculated the ratios of the luminescence intensities of the two-activator phosphor bands to the respective intensities in the spectra of the one-activator phosphors. These calculations showed that the interaction of the activators in the investigated range of concentrations leads to quenching at all temperatures. However, the relative effects are reversed in the high and low temperature regions. The silver luminescence is quenched most strongly by Sm at +20°, where the intensity is decreased relative to the intensity for the single activator phosphor by a factor of ~10. At this temperature the quenching of Sm by silver is minimal.

The quenching effect of one activator on the other becomes noticeable at such low concentrations and where the mutual effects are concerned at concentrations differing so radically for the two activators that one cannot logically attribute the effect solely to short range interaction, i.e., to interaction when the respective activator ions are in the immediate proximity of each other.

The strong temperature dependence of the activator interaction is probably connected with variations in the effectiveness of charge carrier transfer through the energy bands. However, in addition, there apparently comes into play resonance energy transfer between the activators, particularly at low temperatures.

The complex character of the temperature variation of quenching is possibly connected with the presence of several different kinds of samarium luminescence centers, so that the observed complexity may be due to the fact that we investigated only the integral luminescence of Sm.

"P.N.Lebedev" Physical Institute,
Academy of Sciences of the USSR

References

1. V.L.Levshin, Zhur.eksp.i teor.fiz., 17, 675 (1947); Ibid., 8, 663 (1960). (Trans.Soviet Physics - JETP.)

2. V.F.Tunitskaya, Trudy FIAN SSSR (Proceedings, Physical Institute, USSR Ac.of Sci.) 7, 107 (1956).

3. V.L.Levshin & V.F.Tunitskaya, Optika ispektroskopiya, 8, No.5, 663 (1960). (Trans.Optics & Spectroscopy.)
4. V.L.Levshin & V.F.Tunitskaya, Ibid., 9, No.2, 223 (1960). (Trans.Ibid.)
5. V.V.Antonov-Romanovskii & Z.A.Trapeznikova, Ibid., 1, No.4, 204 (1956).
6. Z.A.Trapeznikova, Izv.AN SSSR, Ser.fiz., 23, 1319 (1959). (Trans.Bulletin, 23, 1306.)
7. I.A.Parfianovich, Zhur.eksp.i teor.fiz., 26, 696 (1954).

DISCUSSION

V.Ya.Yaskolko: We prepared $CaSO_4$ phosphors and activated them with Mn, Sm, Pb, Zn, Bi and Co, which were introduced in pairs in different concentrations. We investigated the steady luminescence and thermostimulated luminescence spectra and also the trapping levels in these phosphors under x-ray excitation. It was found that for some activator pairs the spectra contained the bands of both activators in steady luminescence and thermostimulated luminescence, while for other activator pairs there was observed only one band, sometimes mixed (Ce and Bi coactivators). The thermoluminescence color for some activator pairs (Mn, Sm and others) changed, so that one could not identify any thermoluminescence band with any given activator on the basis of the characteristic normal luminescence color. For other activators (Pb and Bi) the light sum stored on the trapping levels of one activator was emitted from the recombination centers formed by the other activator. The results obtained cannot be explained if one does not assume that the activator ions, at least in some cases, are arranged in pairs.

* * * * * * *

FLARE-UP OF ZnS PHOSPHORS AND COMPETITION OF THE LUMINESCENCE BANDS

- N.A.Tolstoi, A.M.Tkachuk, V.A.Sokolov, A.V.Burlakov, A.I.Ryskin, Z.S.Mansurova & M.V.Epifanov

The effect of flare-up of phosphors (initial burst of fluorescence) is connected with retrapping of electrons and holes, occurring during the dark interval between two successive excitations.[1] It follows from considerations of neutrality that electron and hole levels must be involved in each trapping, both the first and the second.

Obviously, the minimum number of levels necessary for realization of flare-up must be three, inasmuch as two levels can be common.[2]

Let us assume that the hole levels involved in the first and second trappings are ionized centers responsible, respectively, for the blue and red luminescence, while the electron trapping levels are united or grouped into a single electron sticking level. The proposed scheme is essentially a variant of the familiar Schön-Klasens[3] energy diagram and gives the following picture.

Under steady excitation most of the equilibrium number of holes are located at deep centers (Fig.1). At the same time there are some holes at the red centers (the number of which must be much smaller than the number of blue centers), inasmuch as the red centers are excited by the stimulated light and there is a transfer of holes from the blue to the red centers.

When the exciting light is switched off the movement of holes from the blue

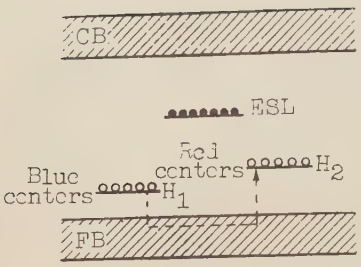

Fig.1. Energy diagram: FB - filled band, CB - conduction band, H_1 - first trapping hole levels, H_2 - second trapping hole levels, ESL - electron sticking levels.

to the red centers continues. Holes ejected by heat from the blue centers into the valence band migrate through this band and (possibly after a number of restickings at blue centers) are caught by the deeper (for holes) red centers. The number of holes at red centers now becomes greater than in the equilibrium state under excitation by light, and, moreover, during the first instants there are no holes capable of catching excited electrons at the blue centers. Thus the situation is ripe for flare-up, and upon switching on the light, the number of recombinations per second with ionized red centers will, during the first instants, be greater than the equilibrium number, i.e., there will be observed a flare-up or flash of fluorescence.

Thus we see that the flare-up effect can be explained without recourse to the concept of the "de-exciting action of the exciting light" (DAEL). This does not exclude the possibility that DAEL does participate in the formation of the flash in the form of an additional flow of electrons released from electron trapping levels; this, however, is difficult to prove, but there can be no doubt that DAEL is evinced in the effect of limitation of the number of electrons and holes involved in the first trapping.

If the stimulating light is not switched on and, consequently, the flare-up is allowed to "over-ripen", the holes trapped at red centers will be released from time to time by heat into the valence band. Now migration of holes in the filled band will lead to the situation where the electrons on sticking levels will recombine with these holes and the phosphor will attain a final equilibrium state. But this process of recombination of migrating holes with trapped electrons must also take place when the holes are released from the blue centers and move toward the red ones, i.e., in the process of ripening. Hence there is reason to assume that the number of holes leaving the blue centers is greater than the number of holes caught by the red centers, i.e., that part of the holes is annihilated in the process of transfer from the blue to the red centers. If we assume that the number of holes reaching the red centers in the process of ripening is equal to the flash light sum and, consequently, is given by the area under the curve characterizing the flare-up, and the number of holes leaving the blue centers is given by the area above the blue flare-up curve, the difference between these two areas should characterize the number of holes lost or annihilated on the way from the blue to the red centers. Experiments show that for such phosphors as ZnS:Ni and ZnS:Co the number of holes reaching the red centers is approximately two orders of magnitude lower than the number of holes leaving the blue centers. In the case of ZnS:Mn phosphors the loss of holes during the first migration is appreciably smaller and under certain conditions may be negligible.

The above described mechanism of over-ripening is not the only possible mechanism that may be hypothesized within the frame-work of the proposed scheme. If the depth of the electron trapping levels is greater than the depth of the blue hole levels, but less than the depth of the red hole levels, the over-ripening will be accomplished by thermal release of the trapped electrons and their recombination with ionized red centers, still firmly retaining their holes.

As is known, in ZnS:Mn phosphors there is evinced a unique competition between the blue and orange bands, which has been investigated in detail in the work of Levshin et al[5-9]. We observed similar competition effects in all phos-

phors that exhibit flare-up.

Let us consider the stationary luminescence of a phosphor of this type.

Red luminescence

Let us assume at first that the temperature is low (in practice, a few degrees below zero centigrade). Then the first trapping levels (in our case the blue centers) are filled to the limit (in the sense of DAEL) by holes at any excitation intensity, but there is virtually no transfer of holes from the blue to the red centers, inasmuch as the thermal energy is insufficient for release of holes into the valence band. The red centers are excited and acquire holes only by relatively weak direct excitation by the incident light. Hence in this case the red luminescence will be of low intensity and will depend linearly on E (curve 1 in Fig.2,a).

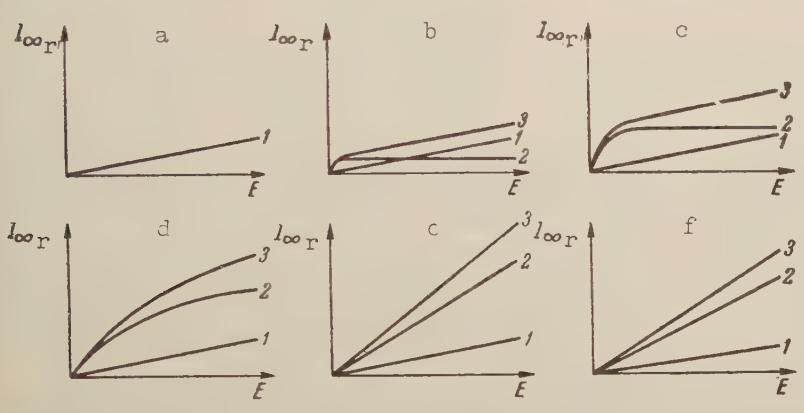

Fig.2. Theoretical dependences of the steady long wavelength luminescence (red band) on the intensity of the exciting light E.

Now let the temperature be a bit higher (room temperature in practice). The first trapping levels will still be filled to the limit at all E, except the weakest, but there will also begin some migration of holes from the blue to the red centers. The number of holes that transfer per second will be proportional to their number at the blue centers and the same for all E, except the weakest intensities. Now the brightness of the red luminescence becomes greater (curve 3 in Fig.2,b) and can be represented as consisting of two components: one, linearly dependent on E (Fig.2,b, curve 1) and the second constant, i.e., independent of E in almost the entire range of variation of E (Fig.2,b, curve 2).

Let us raise the temperature further (in practice, 10-20° above room temperature). Now the first trapping levels will still be completely filled in a wide range of E, but the number of holes that transfer from the blue to the red centers per unit time will be appreciable (curve 2, Fig.2,c). The red luminescence will be greatly increased in intensity, and the dependence of the intensity on E becomes sublinear (curve 3, Fig.2,c); although the curve characterizing the E dependence of the intensity is reminiscent of a curve approaching saturation, actually this does not occur inasmuch as it always comprises a linear component.

Let us increase the temperature a further 10-20°. Now the degree of filling of the first trapping levels will be less than the limiting value, and these levels will lose holes so rapidly that with a slight decrease of E the equilibrium population of these levels will fall (Fig.2,d, curve 2), but the supplement to the linear red luminescence (curve 1) is very appreciable. The resultant curve 3 is sublinear, but is less reminiscent of a curve tending to saturation.

With further increase of the temperature (to ~100°) the holes depart so readily from the first trapping levels that the number of holes on these levels and, therefore, the rate of departure becomes proportional to E (curve 2 in Fig. 2,e). The resultant curve 3 becomes the sum of two linear dependences (curves 1

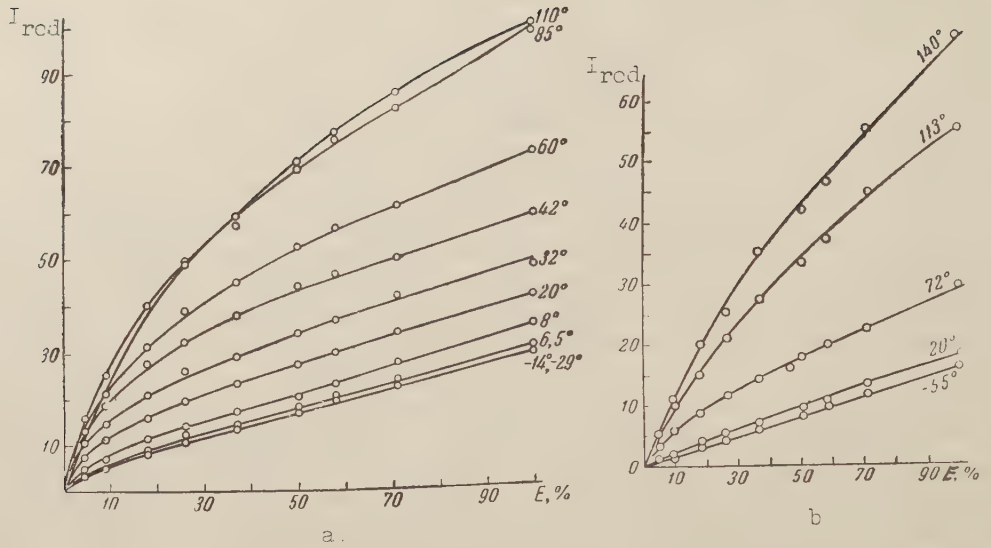

Fig.3. Experimental dependences of the steady long wavelength luminescence on the intensity of the exciting light: a - ZnS:Mn ($C_{Mn} = 7.5 \cdot 10^{-4}$ g/g), b - ZnS: :Ag:Ni ($C_{Ag} = 5 \cdot 10^{-3}$ g/g; $C_{Ni} = 10^{-5}$ g/g).

and 2), i.e., becomes a straight line. Thus the E dependence of the red luminescence is no longer sublinear.

If the temperature is raised still further, the resulting red luminescence intensity, remaining linear, must decrease (owing to temperature quenching). The reasons for this may be different: in particular, there may be a noticeable departure of holes from the red centers prior to radiative recombination of these with electrons; there may also develop nonradiative transitions in the luminescence centers. This is why we have represented curves 1 and 2 in Fig.2,d as straight lines with a smaller slope.

The experimental curves for ZnS:Mn and ZnS:Ag:Ni phosphors are shown in Fig.3.

Summarizing the discussed temperature behavior of the red luminescence of phosphors exhibiting flare-up, we can say that fundamental to the situation are two processes: the process of ripening and the process of over-ripening, both of which occur concurrently with excitation.

If the holes ejected by heat from the blue centers can undergo repeated sticking at these centers before being caught by the red centers, the rate of their final transfer from the blue to the red centers will obviously depend on the concentration of the latter. Increase in the concentration of the red centers will act in the same direction as raising the temperature.

Blue luminescence

We established earlier[2] that the properties of the curves characterizing the build-up of blue and red luminescence are in a sense "contrary": ripening of the flare-up in the red band corresponds to slowing down of the build-up in the intensity of the blue band, i.e., in this band there forms a luminescence deficit.

It is tempting to summarize the situation by saying that a photon is traded for a hole; in other words, departure of a hole from a blue center leads to loss of a "blue photon", while a hole arriving at a red center yields an extra "red

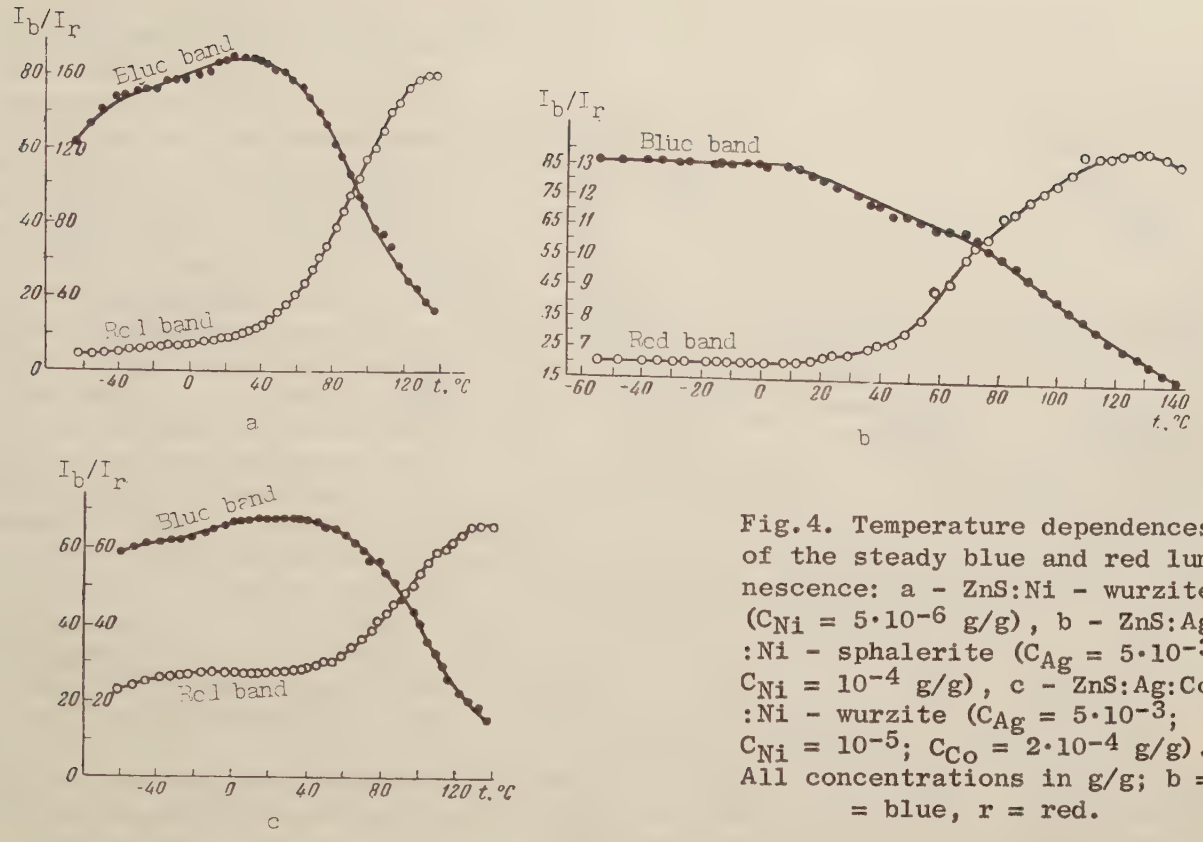

Fig.4. Temperature dependences of the steady blue and red luminescence: a - ZnS:Ni - wurzite (C_{Ni} = 5·10^{-6} g/g), b - ZnS:Ag:Ni - sphalerite (C_{Ag} = 5·10^{-3}; C_{Ni} = 10^{-4} g/g), c - ZnS:Ag:Co:Ni - wurzite (C_{Ag} = 5·10^{-3}; C_{Ni} = 10^{-5}; C_{Co} = 2·10^{-4} g/g). All concentrations in g/g; b = blue, r = red.

photon". We noted above, however, that the number of holes departing from the blue centers may be appreciably greater than the number of holes arriving at the red centers. But if these numbers are at least proportional, we can expect that the loss in steady blue luminescence brightness will be proportional to the increment of red luminescence. Lack of proportionality with maintenance of qualitative "antiparallelism" or competition between the red and blue luminescences would mean that the process of "loss" of holes incident to their migration from the blue to the red centers is not as simple as pictured; for example, it may be hypothesized that the probability for loss of holes will depend on their number, the temperature and other factors. On the other hand, lack of clear-cut proportionality may mean that the luminescence mechanism of centers of one type (for example, blue) is such that for them the loss of a hole does not result in a proportional decrease in luminescence brightness. In any case, the right to assert the simple principle of "a photon for a hole" or the necessity of taking into account various complications can only be determined by experiment. Careful experiments have shown that proportionality between the decrement of blue and the increment of red luminescence is more fortuitous than a physical rule. Nevertheless, there is clear evidence for qualitative parallelism in phosphors exhibiting flare-up (Figs.4 and 5).

Nevertheless, we feel that on the basis of the above data one can judge of the extent to which the red and blue luminescences are "supplementary" or "competing" in phosphors exhibiting flare-up. In the first approximation these emissions are "supplementary", although this is not substantiated in detail by experiment. This provides an answer to the above question of whether one must seek for complications to the simple scheme with migration of holes from the blue to the red centers.

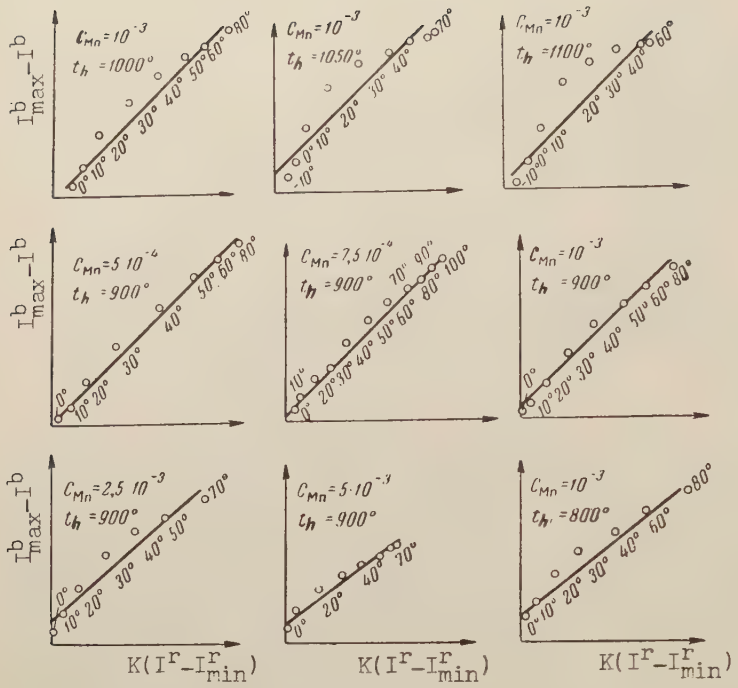

Fig.5. Relation between the decrement of luminescence in the blue band and increment in the red band at different temperatures for ZnS:Mn phosphors. All the vertical and horizontal scales are the same. All concentrations are given in g/g; t_h = heating temperature, r = = red, b = blue.

As we see, analysis of flare-up leads to better understanding of some details of the mechanism of temperature development of luminescence and competition of different bands.

We have already noted that filling of the first trapping levels is limited to some extent by the de-exciting action of the exciting light (DAEL). This is proved by the fact that under normal conditions the flash does not depend on the strength of the preliminary excitation (sometimes in a very wide range of variation thereof), but does noticeably depend on the wavelength of the exciting light. We used wavelengths of 313, 365, 405 and 436 mμ and x-rays. The agreement of the curves characterizing the ripening of the flare-up pre-excited by light of different wavelengths showed that in all cases the same system of trapping levels is involved, and consequently, the dependence of the flare-up on the wavelength is connected with the wavelength dependence of the DAEL. The existence of this effect imposes certain restrictions and imperatives on the possible theories that might be formulated to describe the photoconductive properties of sulfides.

References

1. N.A.Tolstoi, N.N.Tkachuk, Z.S.Mansurov & M.Ya.Tsenter, Optika i spektroskopiya, 1, 719 (1956).
2. N.A.Tolstoi, A.M.Tkachuk & N.N.Tkachuk, Ibid., 2, 759 (1957).
3. M.Schön, Z.Phys., 119, 463 (1942).
4. H.A.Klasens, Nature, 158, 306 (1946).
5. V.L.Levshin, Zhur.eksp.i teor.fiz., 17, 675 (1947).
6. V.L.Levshin, N.S.Borodin & G.P.Neronova, Optika i spektroskopiya, 3, 258 (1957).
7. V.L.Levshin, Doklady AN SSSR, 54, 127 (1946).
8. V.L.Levshin, Ibid., 54, 215 (1946).
9. V.L.Levshin & B.D.Ryzhikov, Optika i spektroskopiya, 4, 358 (1958).

CHARACTERISTICS OF CATHODOLUMINESCENCE AT HIGH EXCITATION DENSITIES

- Yu.M. Popov

In the present contribution we consider theoretically the processes responsible for the two important distinctive characteristics of cathodoluminescence connected with high excitation densities, namely, a) the deviation from linear increase in brightness with increase of the excitation density (effect of saturation) and b) increase in the steepness of the cathodoluminescence afterglow decay curve with increase of the excitation density.

It has been shown experimentally[1] that saturation of the cathodoluminescence intensity is attained at high excitation densities even in the case when temperature quenching (owing to overheating of the phosphor) is absent.

In order to explain the effect of saturation not connected with temperature quenching we must invoke the process of triple recombination[2,3], when after collision of two mobile current carriers, one of them settles on an impurity center, and the energy is transferred to another carrier, which loses it nonradiatively, relaxing with the crystal lattice. Inasmuch as the intensity of this process is proportional to the square of the density of the mobile carriers, while the intensity of the usual processes involved in luminescence (nonradiative and radiative recombination involving impurity centers) depend linearly on the carrier density, at high excitation densities there will predominate the nonradiative process of triple recombination, and this will hold down the linear growth of the luminescence brightness. Our calculations showed that the deviation from linear increase of brightness with excitation density occurs at an excitation density $Q_q \approx 10^{24}$ particles cm^{-3} sec^{-1}, when the concentration of mobile carriers in the band attains a value $N \approx 10^{16}$ cm^{-3}.

In the case of very high excitation densities, the luminescence intensity $L \sim \sqrt{Q_q}$. We calculated the variation of L as a function of Q_q in the intermediate or transition region. The character of the deviation from the linear law obtained agrees with that observed experimentally.[1] If it is assumed that electrons with an energy of 50 kev penetrate to a depth of 10^{-3} cm, the theoretical excitation density at which there should occur deviation from the linear increase in brightness law ($Q_q \approx 10^{24}$ particles cm^{-3} sec^{-1}) is attained at a current density $I \approx 10^{-2}$ amp/cm^2, which is in agreement with experiment.[1]

We now turn to consideration of the possible reasons for increase in the rate of decay of the cathodoluminescence afterglow with increase of the excitation density.

One reason for this effect is the relative increase in the light sum stored on the shallower trapping levels (as compared with the deeper ones) with increase of the excitation density. From the principle of detailed balance in the case of steady luminescence it follows that

$$\frac{n_2}{n_1} = \frac{\nu_2}{\nu_1} \frac{N_{cff} e^{-\frac{\Delta E_1}{kT}} + N}{N_{cff} e^{-\frac{\Delta E_2}{kT}} + N}, \qquad (1)$$

$$N_{cff} = \frac{2(2\pi m^* kT)^{3/2}}{h^3} \approx 4.8 \cdot 10^{15} \left(\frac{m^*}{m} T\right)^{3/2},$$

where n_1 and n_2 are the numbers of electrons per cm^3 on trapping levels of the first and second kinds, respectively; ν_1 and ν_2 are the numbers of impurity centers of the first and second kinds, respectively; ΔE_1 and ΔE_2 are the distances of the respective trapping levels from the bottom of the conduction band; N is

the concentration of electrons in the conduction band; m is the usual and m^* the effective mass of the electrons; T is the temperature of the crystal. The only quantity in (1) dependent on the excitation density is the number of electrons in the conduction band; this can be found by solution of the equations describing the kinetics of luminescence. We shall use the most general dependence of N on the excitation density, i.e., assume monotonic increase of N with increase of the excitation density.

If $\Delta E_2 > \Delta E_1$, then with increase of N the denominator of (1) will increase more rapidly than the numerator and the ratio n_2/n_1 as a whole will decrease, i.e., increase of the excitation density leads to decrease in the relative number of electrons held on deeper trapping levels as compared with shallower trapping levels. Depending on the relation between ν_2 and ν_1, with increase of the excitation density the increase in the relative number of electrons stored on the shallower levels need not necessarily lead to increase of the absolute increment in the number on shallower levels. We note that this effect may obtain for all forms of luminescence, not only cathodoluminescence.

The other reason for the decrease of the light sum stored on deeper levels in cathodoluminescence is ejection of the electrons from trapping levels by fast electrons forming in the conduction band. Inasmuch as the question of the total exchange or utilization of the energy of the primary electrons is complicated, owing to the many-setp character of energy exchange in solids (exchange via secondary, tertiary, etc. electrons) and is still obscure, we shall not consider this process. We assume that for all the electrons in the solid (primary, secondary, etc.) as long as their energy is sufficient for transfer of the electron from the valence band to the conduction band, the fundamental processes are ionization processes. We assume that as a result of action of the primary electron beam there are produced, within a time shorter than all the other characteristic times, electrons with a kinetic energy smaller than the width of the forbidden energy band. For the sake of simplicity we shall assume that the electrons obtained instantaneously as a result of complete ionization are monoenergetic, and denote their energy by $\mathscr{E}_0$. The probability for ejection of an electron from the k-th level as a result of ionization by a fast electron is given by

$$W_i^{(k)} = \int_{I^{(k)}}^{\infty} \sqrt{\frac{2\mathscr{E}}{m}}\, \sigma_i^{(k)}(\mathscr{E})\, f(\mathscr{E})\, d\Gamma, \qquad (2)$$

where $\sigma_i^{(k)}(\mathscr{E})$ is the cross section for ionization from the k-th trapping level by a conduction electron of energy $\mathscr{E}$, $I^{(k)}$ is the ionization potential of the k-th level, and $d\Gamma$ is the level density in the conduction band.

Thus calculation of W_i reduces to finding the distribution function $f(\mathscr{E})$ for electrons in the conduction band. The equation for the distribution function is of the form

$$(a-b)f + q\delta(\mathscr{E}-\mathscr{E}_0) - j + u = 0, \qquad (3)$$

where $(a-b)f$ is the collision integral, j is the flux of electrons leaving the conduction band, and u is the flux of electrons entering the conduction band from the trapping levels.

In the energy region of interest $\mathscr{E} \gg kT$ (we assume that $I^{(k)} \gg kT$) the last two terms in (3) will be small compared with the first two terms and can be discarded. Inserting the solution of (3) into (2), we obtain

$$W_i^{(k)} = \frac{\sigma_0 M a^3 E_R \mathscr{E}_0 Q \ln(\mathscr{E}_0 / I^{(k)})}{\pi m \gamma^2 Z^2 e^4 \ln(4\mathscr{E}_0 / \hbar\omega_0)} \qquad (4)$$

where σ_0 is the maximum cross section for ionization of a hydrogen atom (we assume the hydrogen-like model for the impurity centers); E_R is the Rydberg energy; M is reduced mass of the ions; a is the separation between neighboring ions; Ze is the charge of each ion; Q is the number of electron-hole pairs produced by the electron beam per sec in 1 cm^3; the factor γ differs from unity owing to deformation of the electron shells incident to vibration of the ions.

Assuming the cross section for nonradiative recombination of an electron on a trapping level to be $\sigma_{nr} \approx 10^{-16}$ cm^2, we find from (4) that the probability for ionization ejection of an electron from the k-th level is greater than the probability for thermal ejection when

$$Q \geqslant 10^{28} e^{-I^{(k)}/kT}. \qquad (5)$$

It follows from Eq.(5) that with increase of the electron beam density the effect will be evinced first where the deepest trapping levels are concerned. If $I^{(k)} = 10\ kT$ (T = 300°K) then with an accelerating potential V = 30 kev and a penetration depth $l = 10^{-4}$ cm condition (5) will be fulfilled for $i \approx 10^{-4}$ amp/cm^2. Inasmuch as the common cathodoluminophors are not predominantly heteropolar (ionic) compounds ($\gamma^2 < 1$), the above evaluation for the necessary current density can be reduced to $i \approx 10^{-5}$ amp/cm^2. Thus the described effect imposes a limit on the light sums stored on deep trapping levels, depending on the excitation density.

The probability for ionization from trapping levels does not depend on the temperature, while the probability for thermal ejection decreases exponentially with decreasing temperature. Hence if at a certain temperature and excitation density the probability for ionization from trapping levels is comparable with the probability for thermal ejection of electrons, reduction of the temperature or increase of the excitation density will not result in increase of the light sum stored on these levels.

"P.N.Lebedev" Physical Institute,
Academy of Sciences of the USSR

References

1. P.A.Einstein, Brit.J.Appl.Phys., 8, 190 (1957).
2. L.Bess, Phys.Rev., 105, 1469 (1957).
3. Yu.M.Popov, Zhur.eksp.i teor.fiz., 35, 505 (1958). (Trans.Soviet Physics - JETP.)

EFFECT OF THE CHEMICAL NATURE OF THE FLUX ON THE LUMINESCENCE PROPERTIES OF ZINC SULFIDE AND ZINC-CADMIUM SULFIDE PHOSPHORS

- A.A.Bundel', A.A.Glagoleva, Z.I.Guretskaya, O.A.Danilevskaya, DouNai-Khua & L.N.Sokolova

The purpose of the present work was to check Kröger's hypothesis according to which chlorine ions and trivalent metal ions act as coactivators in the synthesis of sulfide phosphors.

Fixation of the flux cation in sulfide phosphors prepared with a halogen flux was observed by Randall[1] long before Kröger, Helligman & Smit[2] established the fixation of chlorine. We carried out quantitative determinations of Na^+ (by the uranyl acetate procedure), Li^+ (in the form of the sulfate after separation of the zinc with barium carbonate) and Cl^- (nephelometric procedure using AgCl) in ZnS:Zn, ZnS:$5\cdot10^{-4}$ Cu and ZnS:$5\cdot10^{-5}$ Cu phosphors heated at 950° in air with 5% NaCl. After heating, the samples were etched in nitric acid to solution of approximately 20% of the material and then washed with water until tests for Cl^- were negative. The results of the analyses are listed in Table 1.

Table 1

Content of flux anions and cations in synthesized phosphors, in g ion/g ZnS

Phosphor	Cl^-	Na^+	Li^+	Ratio: g Me ion/ g Cl ion
ZnS — Zn(NaCl)	$5{,}16\cdot10^{-6}\pm20$ %	$4{,}55\cdot10^{-6}\pm15$%	—	0,88:1,00
ZnS — Zn(LiCl)	$5{,}10\cdot10^{-6}\pm22$ %	—	5,00±10 %	0,98:1,00
ZnS — $5\cdot10^{-5}$Cu(NaCl)	$1{,}6\cdot10^{-6}\pm15$ %	$2{,}7\cdot10^{-6}\pm13$%	—	1,69:1,00
ZnS — $5\cdot10^{-4}$Cu(NaCl)	$4{,}0\cdot10^{-6}\pm25$ %	$2{,}7\cdot10^{-6}\pm15$%	—	0,68:1,00

Thus it was shown that in the synthesized phosphors, simultaneously with the chlorine ions, there are fixed the monovalent flux cations in an equivalent amount. This proved that the chlorine ions cannot play the role of a coactivator with respect to the introduced activator.

Kröger[3] bases his hypothesis regarding the role of Al^{3+} as coactivator on purported observation of variation of the luminescence spectra of ZnS:Ag:Al phosphors heated in H_2S at 1200° with the ratio of the Al^{3+} and Ag^+ concentrations in the initial batch. Kröger reports that when $C_{Al^{3+}} > C_{Ag^+}$, the characteristic band of zinc is present in the spectrum and that this band weakens with increase of C_{Ag^+}, and disappears when $C_{Al^{3+}} = C_{Ag^+}$. The higher the initial Al^{3+} concentration, the higher the concentration of Ag^+ at which the zinc band is suppressed.

Investigation of the luminescence spectra of ZnS:Ag:Al phosphors prepared precisely by the procedure described by Kröger did not substantiate his observations: the zinc band in the presence of Al is suppressed by heating in H_2S at exactly the same Ag^+ concentration ($1\cdot10^{-4}$ g/g ZnS) as in the case of heating with NaCl in air without Al in the batch. The only fact correctly described by Kröger is that in the presence of aluminum the zinc band does not undergo quenching as a result of heating in H_2S. However, the brightness of this band is substantially lower than in ordinary self-activated phosphors heated in air.

Table 2

Luminescence brightness of self-activated phosphors

Flux	ZnS.Zn		50ZnS.50CdS	
	950°	1100°	950°	1100°
3% NaCl	100	100	100	100
None	3	5	63	88
1% B_2O_3	95	96	95	94
1% $Na_2B_4O_7$	97	67	98	93
0,25% Na_2HPO_4	82	50	142	111

According to Kröger, $Al(NO_3)_3$ added to the batch decomposes with the formation of Al_2O_3, which converts to Al_2S_3; the aluminum sulfide then dissolves in the ZnS, and the Al^{3+} ions are located

at cationic sites, replacing Zn^{2+} ions, and thus compensate the shortage of positive charges resulting from replacement of Zn^{2+} by Ag^{+} ions.

This mechanism, proposed speculatively by Kröger, was checked by us in stages. Al_2O_3, obtained by decomposition of $Al(NO_3)_3$ at 350° was heated in H_2S by the method of a boiling layer for 1 to 3 hours at 1200°. Analysis of the product showed that not more than 1% of the Al_2O_3 transforms to the sulfide. Consequently, Kröger's hypothesis was disproved at the initial stage. It might be assumed that Al_2O_3 is capable of dissolving in ZnS as such. To check this, 50 g of phosphor prepared by heating in H_2S at 1200° from a batch containing $3 \cdot 10^{-4}$ mole $Al(NO_3)_3$ per 1 mole ZnS was dissolved in 15% HCl. The undissolved residue consisted of Al_2O_3, and amounted to approximately 86% of the material.

Thus Al^{3+} cannot be a coactivator in the zinc sulfide phosphors inasmuch as no Al_2S_3 is formed, while Al_2O_3 does not dissolve in ZnS. Despite the fact that the aluminum oxide is present in the form of a separate phase, it does exert a strong influence on the process of crystallization. The mean size of the crystals obtained in the presence of Al_2O_3 in heating in H_2S and in heating in air with NaCl was 4-8 times smaller than in the absence of the aluminum oxide.

It must be noted that phosphors with a normal spectral composition and luminescence yield are also obtained with fluxes that cannot possibly supply coactivator ions; this will be evident from the data of Table 2.

Thus, although we reject Kröger's hypothesis that in zinc sulfide phosphors chlorine and aluminum ions can play the role of coactivators, we cannot at present advance any definitive inferences regarding the mechanism involved in the influence of different additives. Presumably this mechanism consists in action of the additive on the process of formation of the host material.

References

1. J.T.Randall, Trans.Faraday Soc., 35, 2 (1939).
2. F.A.Kröger, J.Helligman & N.Smit, Physica, 15, 990 (1949).
3. F.A.Kröger & J.Dikhoff, Physica, 16, 297 (1950).

DISCUSSION

A.M.Gurevich: It is possible that an appreciable fraction of the chlorine found in analysis of the phosphor belongs to the flux that is not removed fully despite careful and thorough washing of the phosphor. The results of chemical analysis have not hitherto been regarded as decisive proof that chlorine is a coactivator. Proof of this must be sought in investigations of the dependence of the optical properties of phosphors on the conditions of synthesis and, in particular, investigations of ZnS:Cu single crystals and self-activated ZnS sublimate phosphors (see report of E.Ya.Arapova in the present issue of the Bulletin).

It must be borne in mind that the concentration of luminescence centers may be not proportional not only to the total chlorine concentration as given by analysis of the phosphor but also to the number of Cl^- ions that are actually incorporated into the lattice, inasmuch as in all probability associated electric neutral formations of the type $Cl^- \square Cl^-$ or AgCl do not form luminescence centers. (See the work of Prener and Williams.) As for the equivalence in the concentrations of the flux anions and cations disclosed by analysis, first, as will be evident from the data given in the report under discussion, this equivalence at $5 \cdot 10^{-4}$ Cu and also in the case of use of NaCl as flux is disturbed in favor of the anion, and, second, the flux cation may belong not only to the flux but also to the products of its reaction with ZnS.

CONCERNING THE INFLUENCE OF FLUX ON THE OPTICAL PROPERTIES OF ZINC SULFIDE PHOSPHORS

- A.M.Gurvich

At present it may safely be asserted that, contrary to earlier concepts[1], the effects of the chlorides of alkali and alkaline earth metals, commonly employed as fluxes, is not restricted merely to formation of a liquid phase accelerating the recrystallization of the host sulfide.

In the process of heating there occurs formation of zinc chloride[2-4] as well as of the chlorides of cadmium and the metals introduced as activators into the initial batch, for example, AgCl and CuCl. Thermodynamic analysis showed[5] that in most cases there does not occur an exchange reaction between the sulfides of heavy metals and the chlorides of alkali and alkaline earth metals.[2,3] The formation of heavy metal chlorides is a consequence of the oxidizing roasting in which the oxygen of the air participates, for example:

$$ZnS + 2NaCl + 2O_2 = ZnCl_2 + Na_2SO_4. \qquad (1)$$

This is indicated by the presence of a large amount of soluble sulfate in water extracts from sulfide phosphors prepared with flux and not washed to remove the excess flux. This cannot be explained by oxidation of ZnS to $ZnSO_4$, inasmuch as the latter decomposes completely at sintering temperatures with the formation of ZnO.[6] Oxidation of sulfides in roasting without flux usually goes to the respective oxides.[6] Fluxes such as NaCl, on the one hand, act as accumulators of oxygen, owing to the ease with which reactions of type (1) proceed and, on the other hand, covering the surface of the sulfides, they inhibit direct oxidation leading to formation of the oxides.

Our chemical analyses showed that after 20 minute heating of ZnS with 5% by weight NaCl at 1100°, the flux phase has the following molar composition: 0.81 NaCl, 0.07 $ZnCl_2$ and 0.12 Na_2SO_4. The concentrations of $ZnCl_2$ and Na_2SO_4 differ owing to partial volatilization of the former. The flux phase of a luminophor heated under the same conditions for 3-5 min has approximately the same composition.

The interaction of sulfides with halogenous fluxes consists not so much in "eating away" of the sulfide surface, as was assumed by early investigators[2,3], as in formation of the chlorides of the activators (AgCl, CuCl), in which form these are readily incorporated into the ZnS lattice. In contrast to silver and copper sulfides, the monochlorides of these metals have the same chemical formula as ZnS, which is one of the necessary criteria for their isomorphous solution, which can also occur with different valence of the particles (so called mixed crystals of the "new kind"[7]). The relative facility with which solid solutions of such substances form in the case of ionic crystals is conveniently treated from the standpoint of the principle of "charge compensation".[8] In the case of ZnS-CuCl there also obtains similarity of structure, i.e., of coordination and polarity of the bonds.

A significant role is played, probably, by the fact that the chlorides of silver, copper and zinc have, as compared to their respective sulfides, a lower melting point (the melting points of AgCl, CuCl and $ZnCl_2$ are, respectively, 455°, 422° and 283°), which accelerates their diffusion into the depth of the crystal. The fact that ZnS phosphors (including self-activated) form in general even without flux[9] cannot be regarded in the light of the considerations set forth by Bube[10] and Prener & Williams[11] as disproof of the above described role of the flux in formation of crystal phosphors.

Formation of AgCl and CuCl occurs at a relatively low temperature (~300°).[12,1] Once formed, they can enter into exchange interaction with ZnS with the formation

Influence of the nature of the flux on the photoluminescence intensity (λ_{excit} = 365 mμ) of cub.-ZnS:0.1 Ag-20' phosphor

Flux	Flux conc. rel.to ZnS by wt.,%	Luminescence intensity	
		unwashed phosphor*	water washed phosphor**
NaCl	15	94	38
NaCl	5	83,5	53
NaCl	0,5	70	83
$MgCl_2$	7	65	102
KCl	5	44	89,5

*In percent relative to the intensity of the luminophor with the optimum Ag content.

**In percent relative to the intensity of the unwashed luminophor.

of the corresponding sulfides.[5] This process may be retarded to a greater or lesser extent depending on the conditions of synthesis: its duration and temperature, the nature and concentration of the flux, etc.

In the case of ZnS:Ag phosphors this leads to different degrees of change in the intensity of luminescence in going from the optimum Ag concentration to an excess of the activator (see table), inasmuch as Ag_2S forms on the crystal surfaces a filtering layer that absorbs the light emitted by the luminophor (cf Ref.14). The ability of molten rock salt (in contrast to KCl) to dissolve unlimited amounts of AgCl (Ref.15) apparently plays a significant role in retarding the transformation of AgCl to Ag_2S.

We established that the appearance of the blue luminescence band of ZnS:Cu phosphors containing relatively large amounts of copper precedes, as a rule, the appearance of green luminescence (Fig.1). Thermodynamic analysis and comparison of the factors favoring the course of the process

$$2CuCl + ZnS = Cu_2S + ZnCl_2 \quad (\Delta Zn_{1100^\circ C} = -21 \text{ kcal/mole}), \qquad (2)$$

in one direction or the other, with the factors favoring the appearance of the green and blue luminescence bands led us to the conclusion that the transition from green to blue luminescence is connected with reaction (2) proceeding to the side of formation of Cu_2S in the greatly "loosened" ZnS lattice.*

Chlorine is necessary for the formation of the blue copper band in ZnS:Cu only in so far as CuCl is more readily incorporated into the ZnS lattice than Cu_2S. The rate of conversion of CuCl to Cu_2S is the greater, the higher the concentration of Cu and, consequently, of CuCl in the ZnS phase. Process (2) is also accelerated by the presence of flux.

The nature of the flux also has a substantial influence on the process of formation of phosphors and their properties. It was established that $MgCl_2$ has a specific effect on ZnS phosphors, evinced in change in the intensity and spectral composition of their emission (Fig.2) with simultaneous decrease of the average crystal size. Owing to high temperature hydrolysis and also due to oxidation within the first minutes of heating, the predominant part of $MgCl_2$ present in the batch transforms to MgO. Thermodynamic analysis showed, in addition, that in contrast to other chloride fluxes $MgCl_2$ is capable of exchange interaction with ZnS:

$$McGl_2 - ZnS = MgS - ZnCl_2 \quad (\Delta Z^\circ_{1100^\circ C} = -2.9 \text{ kcal/mole}).$$

MgS dissolves in ZnS (see Ref.3), attaining a concentration of the order of 0.6-0.7 mole percent (in heating ZnS with a mixture of NaCl and MgO in an amount equivalent to 7% $MgCl_2$ (relative to the weight of ZnS), the fraction of MgO not washed out by acetic acid amounts to not more than 0.2 mole percent). The small size of

*This matter will be discussed in more detail in a separate publication.

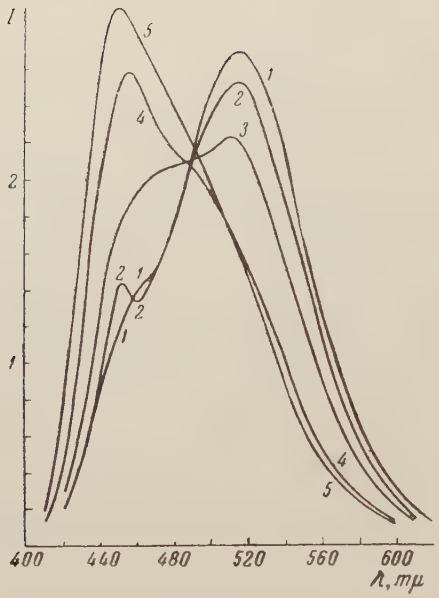

Fig.1. Energy distribution in the roentgeno-luminescence of hex.-ZnS:0.05 Cu (5 NaCl) phosphor heated for 1 - 2 min, 2 - 4 min, 3 - 10 min, 4 - 20 min, 5 - 30 min.

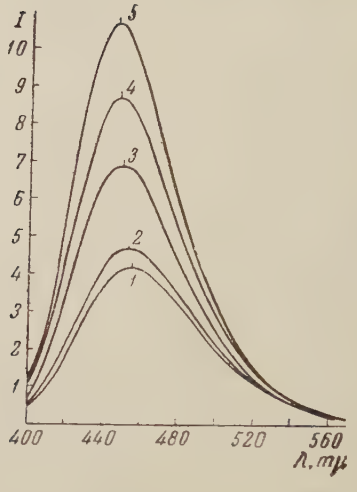

Fig.2. Energy distribution in the photoluminescence spectrum of "self-activated" hex.-ZnS luminophors obtained by heating with fluxes: 1 - 7% NaCl, 2 - 6% NaCl, 1% $MgCl_2$, 3 - 4% NaCl, 3% $MgCl_2$, 4 - 2% NaCl, 5% $MgCl_2$, 5 - 7% $MgCl_2$.

the Mg^{2+} ion facilitates incorporation of the coactivator - Cl^- ions - into the ZnS lattice, counteracting in the process association of oppositely charged defects.* This gives rise to increase of the luminescence intensity owing to increase in the concentration of defects participating in the emission process, for example: $[AgS_4]$, $[CuS_4]$, and $[\boxdot ClS_3]$, ($\boxdot$ denotes a cationic vacancy). At the same time the total concentration of activator and coactivator in the ZnS phase may not increase (cf. Ref.16).

In view of the results of thermodynamic analysis mentioned at the beginning of this report, it is clear that oxygen is necessary for the appearance of luminescence (in the presence of a flux) only in cases when there are not formed in its absence zinc, copper, and silver chlorides that readily incorporate into the ZnS lattice. This is why blue luminescence does not appear as a result of heating ZnS with sodium chloride[4,16,17], whereas in heating ZnS in the presence of Al^{3+} (Ref. 18) or HCl (Ref.17) there forms the normal "self-activated" ZnS phosphor.

On the other hand, in certain cases, acting as a desulfurizing agent, oxygen gives rise to formation of sulfur vacancies which facilitate diffusion of the activator sulfide, for example, Cu_2S, into the ZnS lattice.

Lastly, participating in the reactions of type (1), oxygen facilitates "eating away" of the surface of the ZnS crystals (cf.Ref.3). Only in this sense can one speak of the mineralizing action of oxygen[17].

The solubility in the flux of the chlorides of heavy metals-activators has a substantial influence on their concentration in the host phase. For example, by inhibiting volatilization of $ZnCl_2$, NaCl facilitates saturation of the ZnS phase with zinc chloride and hence contributes to increase of the luminescence

---

*This example shows that detection in the host phase of the flux cation together with its anion cannot be regarded as proof that the anion is not a "coactivator".

brightness. The activator concentration in ZnS depends on the nature of the flux (its anion) also because different halide activators differ from each other as regards volatility.

In the process of washing out the flux with water the chlorides dissolved in it interact with the ZnS and thus produce changes in the optical and other properties of the phosphor owing to the formation of light absorbing sulfides, for example, Ag_2S (Ref.5). In the case of $MgCl_2$ these changes are insignificant or absent (see table) inasmuch as transformation of $MgCl_2$ to MgO is accompanied by evaporation of the excess AgCl; in the case of KCl the changes are also minor because almost all the excess AgCl is converted to Ag_2S in the process of heating.

Thus both the process of heating and the subsequent washing of the phosphor to remove the flux are accompanied by a number of different chemical reactions, the character of which depends on the nature of the flux and which therefore exert different effects on the properties of the final phosphor.

I desire to express my gratitude to T.A.Sokolov for assistance in the work.

State Scientific Research Roentgenoradiological Institute,
Ministry of Health of the RSFSR

References

1. H.W.Leverenz, An Introduction to Luminescence of Solids, p.78, N.Y., 1950.
2. H.Schlegel, Naturwissenschaften, 30, 242 (1942).
3. B.M.Gugel', Izv.AN SSSR, Ser.fiz., 9, 539 (1945).
4. H.Ril' & G.Ortman, Zhur.obshch.khimii, 25, 1057 (1955). (Trans.J.Gen.Chem.)
5. A.M.Gurvich, Izv.AN SSSR, Ser.fiz., 23, 1370 (1959). (Trans.Bulletin, 23, 1356.)
6. D.M.Chizhikov, Metallurgiya tsinka (Metallurgy of zinc), Pub.GONTI, 1938.
7. V.A.Kotovich, Dissertation, Leningrad, 1954.
8. F.A.Kröger & J.E.Helligman, Trans.Electrochem.Soc., 93, 156 (1948).
9. A.A.Bundel', Zhur.fiz.khimii, (J.Phys.Chem.), 30, 2261 (1956).
10. R.H.Bube, J.Chem.Phys., 20, 708 (1952).
11. J.S.Prener & F.E.Williams, J.Chem.Phys., 25, 361 (1956).
12. D.M.Chizhikov, Khlornyi metod pererabotki polimetallicheskikh rud i kontsentratov (Chlorine method of treating polymetallic ores and concentrates), M, 1936.
13. Handbuch der anorganischen Chemie, Gmelin, 8 Aufl.Sist.-Num.60, Teil A, 424 (1955).
14. N.I.Ivanova, Optika i spektroskopiya, 1, 578 (1956).
15. A.I.Belyaev, E.A.Zhemchuzhina & L.A.Firsanova, Fizicheskaya khimiya rasplavlennykh solei (Physical chemistry of molten salts), M., 1957.
16. A.V.Lavrov, Izv.AN SSSR, Ser.fiz., 23, 1351 (1959). (Trans.Bulletin, 23, 1337.)
17. A.A.Bundel', A.I.Rusanova & L.G.Taushkanova, Ibid., 23, 1326 (1959). (Trans. Bulletin, 23, 1313.)
18. N.Riehl & R.Sizmann, Z.Naturforsch., 14a, 394 (1959).

INFLUENCE OF FLUXES ON THE PROPERTIES OF ELECTROLUMINOPHORS

- M.A.Berchenko

Fluxes play a significant role in the process of formation of sulfide, sulfide-selenide and selenide phosphors. The use of fluxes in synthesis of phosphors was proposed many years ago by Lenard and his school[1]. The halogen compounds of alkali and alkaline earth metals when used as a flux or mineralizer serve to reduce the roasting temperature and thus exert an influence on the size of the phosphor particles, favor a more uniform activator distribution and increase the brightness of the phosphor.

Many authors assert that halogen fluxes, penetrating directly into the crystal lattice, play a significant role in producing luminescence centers[2] and also in the formation of charge compensators[3]. It is said that halogen fluxes form impurities of the donor type[4] and may produce disturbances of the lattice[5]. Levshin[6] notes that even in the case of phosphors from which the flux can be washed out, residues of the flux remain in the phosphor and together with the deformations of the crystal lattice produced by the flux affect the luminescence of the phosphor.

Little attention has been paid hitherto to the role of fluxes in determining the color of the emission of Cu activated zinc sulfide phosphors and of other phosphors with a number of emission bands. In an early study by Gugel'[7] there are indications that fluxes can affect the emission spectrum of phosphors and the character of the photostimulated phosphorescence. Whereas, Glaser, Randall & Guntz inferred that the specific influence of fluxes is due to the anions (Cl^-, Br^- and I^-; reportedly, F^- ions are relatively ineffective), Gugel' and the writer[8] showed that different flux cations with the same halogen can significantly alter the emission color of the phosphor under cathode-ray excitation.

Unfortunately, the role played by the flux in determining the emission color of phosphors is far from clear. In fact, at present the choice of flux most suitable for obtaining a phosphor with desired properties is more or less empirical.

The purpose of the present work was to investigate the influence of flux cations and anions on the emission color of phosphors excited by an electric field.

For the purposes of the present investigation we used the following basic batch formulation: ZnS (100%), 0.2% Cu, and 0.025% Al. This basic mixture was heated with chloride, bromide and iodide fluxes in which the cations were the elements of Groups I and II of the periodic table. The batches were heated in quartz tubes following the procedure proposed by Kazankin, Pekerman & Petoshina[9].

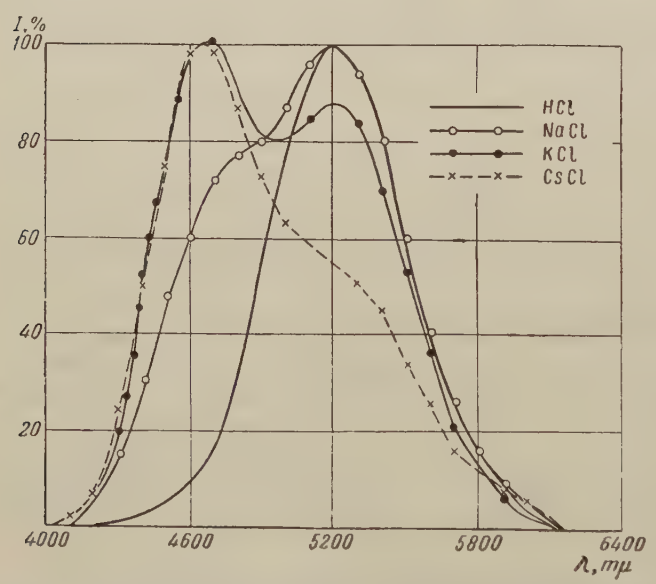

Fig.1. Influence of flux cations (chlorides) on the electroluminescence spectrum.

It is known that the amount of halogen flux introduced into the batch may have a substantial influence on the emission color of electroluminophors.[10] In order to exclude the influence of different amounts of halogen introduced with different fluxes, we added the same proportion of flux to each batch, namely, $3.3 \cdot 10^{-3}$ g halogen per g ZnS.

Under excitation by a 200 v, 400 cps electric field the luminophors obtained with different fluxes yielded green, green-blue and blue luminescence.

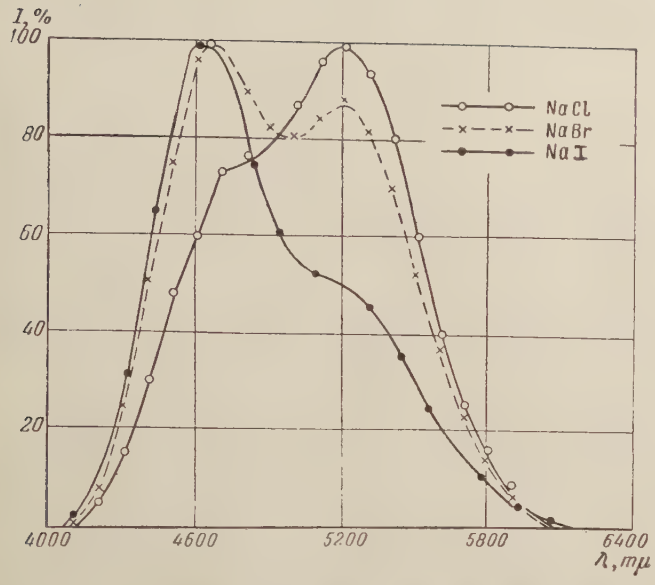

Fig.2. Influence of the flux anions (sodium halides) on the electroluminescence spectrum.

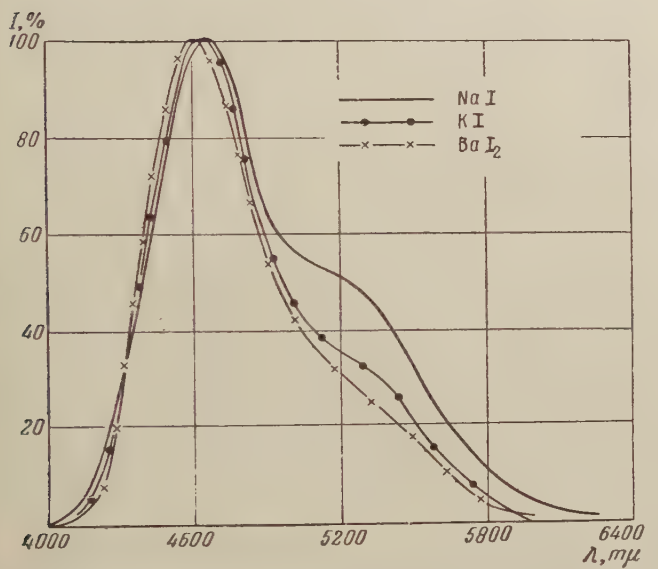

Fig.3. Influence of flux cations (iodides) on the electroluminescence spectrum.

The electroluminescence curves are shown in Figs.1, 2 & 3. It follows from the experimental results that the variation in the color of the phosphors is explained by redistribution of the emission energy between two principal bands and that this redistribution is affected not only by the anion but also by the cation of the flux.

This is clearly evident in the case of chloride fluxes (Fig.1). The spectrum of the electroluminophor obtained with HCl as the flux has one clearly pronounced peak at 5200 Å. The emission color is green. In the case of the phosphor obtained with NaCl flux, in addition to the principal peak at 5200 Å, there begins to appear a second peak at 4650 Å and the overall luminescence is blue. With KCl flux there is obtained a luminophor with the principal emission peak at 4650 Å and, finally with CsCl flux there results a luminophor in the spectrum of which the blue band predominates and the green band is almost completely suppressed. A similar variation is obtained for the chlorides of elements of Group II.

For phosphors fluxed with the bromides of Group I elements there is observed the same regularity in the redistribution of the energy between the bands as a function of the flux cation, but the intensity of the blue band increases more rapidly. Thus with NaBr the principal emission peak, in contrast to the case of NaCl, is in the region of the green rather than the blue band (Fig.2).

Iodide fluxes (Figs.2 & 3) also conform to the above regularity, but with them the green band is suppressed even more than with the bromides. For NaI flux the maximum of the green band amounts to only 50% and for KI flux to only 30% the maximum of the blue band. In the spectrum of the electroluminophor prepared with BaI_2 the green peak is almost completely effaced.

An exception to the above regularity was observed for the electroluminophor obtained with $CaBr_2$. This may be explained as follows. In investigating the influence of fluxes on the lattice constant, Pringsheim[11] showed that in the case of fluxes containing calcium in the presence of sulfate ions there are obtained phosphors with a reduced lattice constant, as in the case of mixed (Ca,Zn)S phosphors, and the luminescence spectrum proves to be similar to that of the mixed

No.	Group	Flux	Color coordinates		Brightness, arb.units
			x	y	
1	I	HCl	0,22	0,59	25,0
2		LiCl	0,20	0,58	20,0
3		NaCl	0,18	0,40	10,0
4		KCl	0,17	0,32	9,0
5		CsCl	0,17	0,26	9,5
6		LiBr	0,21	0,51	17,0
7		NaBr	0,17	0,32	13,0
8		KBr	0,17	0,30	7,0
9		NaJ	0,17	0,24	3,8
10		KJ	0,15	0,20	2,5
11	II	$BeCl_2$	0,20	0,57	20,0
12		$MgCl_2$	0,19	0,56	32,0
13		$CaCl_2$	0,18	0,47	13,5
14		$SrCl_2$	0,17	0,34	5,0
15		$BaCl_2$	0,17	0,32	1,0
16		$ZnCl_2$	0,21	0,61	37,0
17		$CdCl_2$	0,20	0,57	32,0
18		$CaBr_2$	0,20	0,54	17,0
19		SrJ_2	0,15	0,20	7,0
20		BaJ_2	0,15	0,17	4,0
21		NH_4Cl	0,20	0,59	16,0
22		NH_4Br	0,19	0,55	10,7
23		NH_4J	0,15	0,18	3,0

phosphor. This is due to exchange of the calcium and zinc ions, accelerated by the catalytic action of the sulfate ions.

The variation of the spectral characteristics depending on the nature of the halogenous flux can be explained on the basis of the work of Larach[12], who showed that the amount of copper incorporated into the host lattice depends on the halogen of the flux, decreasing in the series Cl—Br—I.

It must be noted that the curves given by Larach for the spectral distribution of the electroluminescence for the Cl—Br—I series do not take into account the influence of the cation, inasmuch as all the halides were introduced with one and the same cation. As will be evident from our curves (Fig.1), however, the character of the luminescence curve is affected not only by the anion but also by the cation.

We calculated the color coordinates for all the synthesized phosphors (see table).

It follows from the values of the color coordinates and the recorded electroluminescence spectra that the flux cations and anions affect the luminescence color of the phosphor as a consistent function of their position in Mendeleev's periodic table.

1. The lower the cation in Mendeleev's table, the greater the shift of the emission to the short wavelength side. For example, the color of the electroluminophor obtained with NaCl flux will be greener ($x = 0.18$; $y = 0.40$) than the color of the electroluminophor obtained with CsCl ($x = 0.17$; $y = 0.26$).

2. The lower the flux anion in the periodic table, the greater the shift of the emitted light to the short wavelength side. For example, the color of the electroluminophor prepared with KCl will be greener ($x = 0.17$; $y = 0.32$) than that of the luminophor prepared with KI flux ($x = 0.15$; $y = 0.20$).

3. The further to the right the cation is situated in the Mendeleev table, the greater the color shift into the long wavelength region.

4. With introduction of different fluxes in which the anion is Cl^{-1} and the cations are elements of Groups I and II, in going down the group columns there is observed repetition in the character of the luminescence curves. Thus the character of the curve of the phosphor prepared with HCl agrees with that for the phosphor prepared with $BeCl_2$; the character of the spectral curve for the phosphor prepared with LiCl is similar to that of the luminophor made with $MgCl_2$, etc. This means that knowing the character of the emission curve for an electroluminophor prepared with a flux the cation of which is an element of Group I, one can identify the corresponding element of Group II which will result in the formation of an electroluminophor with a similar emission curve.

As a result of our experiments we were able to systematize the halogenous fluxes for the ZnS:Cu:Al system from the standpoint of their influence on the

emission color as a function of the positions of the flux cation and anion in the periodic table.

I desire to express my gratitude to M.F.Gorbenko and N.I.Solomko for assistance in synthesizing the luminophors and to V.P.Martynova for carrying out some of the measurements.

Special Design Bureau,
L'vov Electric Lamp Plant

References

1. P.Lenard, F.Schmidt & R.Tomashek, Phosphorescenz und Fluorescenz (Handbuch der Experimental Physik), B.23 (Abt.I,II), Leipzig, 1938.
2. A.L.Smith, J.Electrochemical Soc., 96, 75 (1949).
3. F.A.Kröger & J.E.Hellingman, Ibid., 93, 156 (1948); Ibid., 95, 68 (1949).
4. R.H.Bube & S.M.Thomsen, J.Chem.Phys., 23, 15 (1955).
5. S.Larach & J.Turkevich, Phys.Rev., 98, 1015 (1955).
6. V.L.Levshin, Fotolyuminestsentsiya zhidkikh i tverdykh veshchestv (Photoluminescence of liquids and solids), M., 1951.
7. B.M.Gugel', Izv.AN SSSR, Ser.fiz., 9, 539 (1945).
8. B.M.Gugel' & M.A.Berchenko, Sb.materialov po vakuumnoi tekhnike (Collected reports on vacuum engineering), No.XVI, p.60, M., 1958.
9. O.N.Kazankin, F.M.Pekerman & L.N.Petoshina, Sb.tr.GIPKh, vyp.43, Khimiya i tekhnologiya lyuminoforov (Collected proceedings of GIPKh, No.43, Chemistry and technology of luminophors), p.46, L., 1960.
10. P.Zalm, Philips Res.Rep., 11, 353 (1956).
11. P.Pringsheim, Fluorescence and Phosphorescence, N.Y., 1949.
12. S.Larach, RCA Rev., 20, No.4, 532 (1959).

DISCUSSION

A.M.Gurvich: Our observations also show that the nature of the flux may influence the luminescence of ZnS:Cu phosphors with a high copper concentration. Thus in the case of brief (15-20 min) heating of ZnS + 0.05 Cu with $MgCl_2$ there is obtained a phosphor the luminescence band of which lies in the region of longer wavelengths than the case of the phosphor fluxed with NaCl. Increase of the heating time by a factor of 2-3, however, results in phosphors with similar luminescence characteristics. We assume that these effects are due to the influence of the flux on the kinetics of the process

$$2CuCl + ZnS = Cu_2S + ZnCl_2$$

which is involved in the transition from green to blue luminescence (see our report).

Hence I feel it would be expedient to continue the work reported on by M.A. Berchenko in the direction of more extensive variation of the heating conditions, namely, the duration and temperature of heating, the flux concentration, etc. This may help establish the reasons for the observed effect.

EFFECT OF HIGH PRESSURES ON THE FORMATION OF CRYSTAL PHOSPHORS AND THEIR PROPERTIES

- S.I.Kunenkov

Investigation of the effects of high pressure is of great interest in many fields of science and technology, including that of luminescence. Chemical reactions in all physical states are generally accelerated and the solubility and permeability of substances are increased under pressure. Many substances under high pressures change to other polymorphous forms with entirely different properties. Many cases are known when the structure formed under high pressure persists after removal of the pressure. For example, it has proved feasible by means of pressure to obtain a new modification of quartz - koerzite - which is impervious to the action of even hot hydrochloric acid. White phosphorus with a melting point of 44° under pressure transforms irreversibly to the black modification with t_{melt} = 1000°; the electric conductivity of this phosphor is 10^{11} times higher than that of the white form. Under high pressure wurzite transforms to sphalerite even at room temperature. Diamonds have been synthesized by means of high temperature and high pressure in Sweden and the USA. One can cite many other instances of the preparation of different substances with the aid of high pressures[1,2].

There have been a number of studies of preparation of phosphors under pressure[3-8]. It is reported that at high pressures one can realize phosphors that are not obtainable under the usual heating conditions. Using pressure, Fischer[9] prepared zinc sulfide phosphors in the form of large crystals.

For purposes of the present investigation we chose the phosphor familiar to us from previous work, namely, ZnS·CdS:Ag. In preparing the specimens we used quartz tubes which were connected to the nitrogen tank and a pressure gage by means of a special adapter. In these tubes we prepared phosphors at temperatures up to 1000° and nitrogen pressures up to 60 atm. Batches having the composition 55ZnS·45CdS:Ag(10^{-4} g/g) without flux were heated at temperatures of 450, 500, 600, 700 and 800° for 30 min at a nitrogen pressure of 60 atm. At the same time an identical batch in the same type of tube was heated at the same temperatures, also for 30 min, but at a nitrogen pressure of 1 atm. The results of these experiments are shown in Fig.1; the luminescence was excited by cathode rays; the intensities were compared with that of the yellow K-50 commercial phosphor produced by the "Krasnyi khimik" (Red Chemist) Plant.

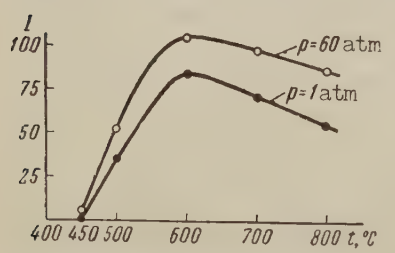

Fig.1. Variation of the luminance with heating temperature for phosphors prepared at different pressures. Batch composition 55ZnS·45CdS:Ag (10^{-4} g/g). The luminances are referred to as industrial K-50 phosphor.

As a result of heating at 450° under high pressure there was obtained a luminescent phosphor, whereas the brightness of the phosphor obtained at the same temperature but at atmospheric pressure was nil. With increase of the heating temperature the brightness of the phosphors obtained at 1 and 60 atm pressure increases, attaining a maximum at a temperature of about 600°. With further increase of the heating temperature the luminance decreases. At all temperatures, however, the brightness of the phosphor prepared under high pressure is greater than that of the corresponding phosphor prepared at atmospheric pressure. The brightest phosphor obtained in our experiments at a pressure of 60 atm, exceeds the brightness of the industrial K-50 phosphor which we used as the reference, but the grain size of the high pressure phosphor is appreciably smaller. The following is the grain-size composition of the phosphors (in microns):

Phosphor prepared at t = 600°, p = 60 atm, (I = 103.7%)		Commercial K-50 phosphor (I = 100%)	
To 0.5	25%	To 0.76	16%
From 0.5 to 0.71	52.6%	From 0.76 to 0.96	25.2%
From 0.71 to 0.88	15.2%	From 0.96 to 1.1	55.1%
From 0.88 to 1.0	7.0%	From 1.1 to 1.5	3.4%

The persistence of these phosphors is short and virtually does not change with the preparation pressure. The maximum of the luminescence spectrum of phosphors heated under pressure at low temperatures (up to 700°) is shifted somewhat to the side of shorter wavelengths. In the case of heating at a temperature of 800° the luminescence spectrum does not change as a result of heating under pressure.

When the batch is heated with flux (2% $MgCl_2$ & 2% NaCl) in nitrogen at a pressure of 60 atm luminescent phosphors form at heating temperatures from ~350°. The luminance versus heating temperature curves for the fluxed phosphors prepared under high pressure and atmospheric pressure do not have a maximum. In all cases the phosphors synthesized under high pressure are brighter than those obtained under atmospheric pressure, but in the range of high temperatures the difference minor.

We also prepared phosphors at higher pressures using a heated steel autoclave into which we placed quartz crucibles containing the test batches. In this manner we prepared 55ZnS·45CdS:Ag(10^{-4} g/g) phosphor without flux at nitrogen pressures from 1 to 1200 atm; the heating temperature in all cases was 450°.

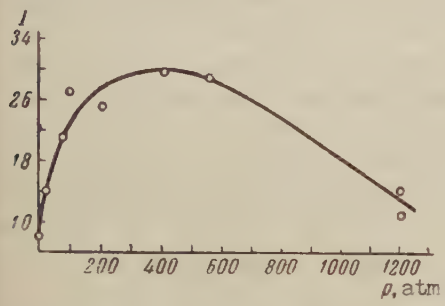

Fig.2. Variation of the luminance of 55ZnS·45CdS:Ag(10^{-4} g/g) phosphors as a function of the synthesis pressure; heating temperature 450°.

The luminance of these phosphors was measured with excitation by 365 mμ ultraviolet. The results are shown in Fig.2. It will be seen that with increase of pressure the brightness of the phosphors rises up to a pressure of 400 atm, and then decreases.

Preliminary experiments involving heating of batches of the same composition at 600° showed that increase of the pressure to 300 atm results in slight increase of the brightness. Further increase of the pressure with this heating temperature has virtually no effect on the brightness, which was high for all samples prepared at this temperature.

On the basis of the present experimental data we cannot venture to give a rigorous theoretical explanation of the influence of pressure on the process of synthesis. In preparation of ZnS·CdS:Ag phosphors without flux at a temperature of 450° pressure undoubtedly affects the structure of the phosphor; this structure persists after removal of the pressure. Comparison of the x-ray diffraction patterns for samples prepared at 450° but different pressures shows that the samples obtained at a pressure of 400 atm have a structure differing from that of samples synthesized at atmospheric pressure. At a heating pressure of 600°, however, pressure does not affect the structure of the phosphor: x-ray diffraction patterns obtained for phosphors prepared at this temperature and different pressures proved to be identical.

I desire to express my gratitude to V.L.Levshin for his interest in the work and N.V.Mitrofanova for assistance in carrying out the experiments.

References

1. P.W.Bridgeman, Recent Work in the Field of High Pressures, Revs.Mod.Phys., 18, 1 (1946).
2. M.G.Gonigberg, Vestnik AN SSSR, No.2, 50 (1957).
3. E.Tiede & A.Schleede, Ber.deut.chem.Ges., 53, 1717 (1920).
4. R.Coustal, Compt.rend., 196, 1306 (1933).
5. L.Wesch & K.Kamm, German Patent No.682660, 1939.
6. L.Wesch, Chem.Ber.Pruf., No.145, July, 1942.
7. E.Streck, Z.phys.Chem., Abt.A, 186, 19 (1940).
8. H.W.Leverenz, USA Patent No.2462517, 1949; H.W.Leverenz, An Introduction to Luminescence of Solid, N.Y., 1950.
9. A.Fischer, Z.Naturforsch., A13, 105 (1958); A.Fischer, J.Electrochem., 106, 838 (1959).

DISCUSSION

B.I.Maksakov: Kunenkov in his report showed that the simultaneous influence of heat and high pressure leads to substantial changes in the properties of substances, distinguished by the ability to dissociate even at low temperatures. Such a substance is zinc sulfide.

In our laboratory there was developed a procedure for crystallization from the melt of cadmium sulfide, a substance that has many properties similar to zinc sulfide. In the experiments we used a pressure of the order of 1500 atm. At these pressures prolonged holding of the material in the molten state does not result in any substantial changes in its stoichiometric composition. Crystallizing the material under these conditions, we did not notice any changes in its crystal structure. The resultant crystals have the same structure as the initial powder, namely, hexagonal. It was found that in order to obtain high quality crystals it is desirable to subject the material to vacuum distillation beforehand. Using cadmium sulfide purified in this manner we were able to perfect large crystals with a high degree of transparency and a resistivity of the order of 10^9 ohm/cm.

* * * * * * *

SPECTROSCOPIC ANALYSIS OF SOME LUMINESCENCE-PURE MATERIALS AND LUMINOPHORS

- L.A.Dvorzhetskaya, L.Ya.Khlebnikova & M.K.Shvaneva

In the present report we give the results of work in the phosphor laboratory in the State Institute of Applied Chemistry on the use of emission spectrum analysis for determining impurities in luminescence pure substances and phosphors. Most of the work was concerned with zinc sulfide. In analyzing this material we used the method of direct spectrum analysis developed by Kibisov and his co-workers[1,2] and the procedure of preliminary chemical enrichment.[3,4] In analyzing the other substances we used only the method of direct spectrum analysis; as far as we know, this is the first time emission analysis has been used for determination of impurities in luminescence-pure materials of this type.

We used the common spectroscopic procedure of complete evaporation of the sample from the crater in a carbon electrode burned in a dc arc. The instrument

Table 1

Analyzed substance	Method	$10^5 \cdot C$, %				
		Cu	Fe	Ni	Co	Mn
ZnS	Direct	0,5	5	5	10	5
ZnS	Chemical enrichment	0,001	0,1	0,2	0,4	—
ZnS	Physical enrichment*	—	—	1	1	—
CdS	Direct	0,7	6	5	10	—
PbS	Direct	3	5	5	10	3
ZnSe	Direct	1	50	20	40	5
CdSe	Direct	1	50	20	40	5
$CaHPO_4$	Direct	5	50	—	—	-
$(NH_4)_2HPO_4$ (27 % solution)	Direct	5	—	—	—	—
$(NH_4)_2CO_3$ (20 % solution)	Direct	5	—	—	—	—

*Physical enrichment of ZnS was carried out by converting the sample to $ZnCl_2$ and subsequent evaporation of this under vacuum; the concentrated deposit was then taken for spectrum analysis.

was a medium dispersion ISP-28 quartz spectrograph with photographic recording. The standards for quantitative analysis were prepared using the purest batch of the given substance. The impurities still present in the "pure" standard sample were determined by the method of additions (i.e., extrapolation of curves obtained using samples with deliberated added known amounts of impurities).

As a result of our experimental work it was established that quantitative spectroscopic analysis of luminescence-pure materials for microimpurities can be carried out with a sensitivity characterized by the minimum concentrations listed in Table 1.

The arithmetic mean deviation for an individual determination is ±15%. The analytic accuracy is highest for copper, and lowest for iron.

Table 2

Phosphor	Element	C, %
SrS base	Cu	$1 \cdot 10^{-4}$-$1 \cdot 10^{-2}$
	Bi	0.001-0.1
$CaHPO_4$ base	Sb	0.1-4.5
FKP-03	Fe	$5 \cdot 10^{-5}$-$1 \cdot 10^{-3}$
K-5	Fe	$5 \cdot 10^{-5}$-$1 \cdot 10^{-3}$
	Cu	$5 \cdot 10^{-6}$-$1 \cdot 10^{-4}$

Industrial FKP-03 phosphors were analyzed for iron; K-5 type phosphors for iron and copper. In the case of the strontium sulfide base phosphor we determined the amounts of copper and bismuth which were introduced as activators. The calcium phosphate base phosphor was analyzed for the antimony content. It was established that in the last two phosphors the concentration of Cu and Bi activators after heating of the batch does not change[5], while the concentration of Sb decreases by a factor of 4. The concentrational sensitivities for the listed elements in the enumerated phosphors are given in Table 2.

We desire to thank L.Ya.Markovskii for valuable advice and interest in the work.

References

1. G.I.Kibisov, M.I.Rezvova & E.N.Vinnichenko, Materialy X soveshchaniya po spektroskopii (Transactions of the 10th Conference on Spectroscopy), Vol.2, p.417, L'vov, 1958.

2. G.I.Kibisov & M.I.Rezvova, Inzh.-fiz.zhur. (Eng.-Phys.Journ.), 6, 47 (1959).

3. V.N.Vasil'eva, L.Ya.Khlebnikova, L.A.Dvorzhetskaya & L.Ya.Markovskii, Izv. AN SSSR, Ser.fiz., 23, 1152 (1950). (Trans.Bulletin, 23, 1146.)
4. V.N.Vasil'eva, L.A.Dvorzhetskaya & L.Ya.Khlebnikova, Trudy Gos.in-ta prikl. khimii (Proceedings of the State Institute of Applied Chemistry), 43, 151 (1960).
5. L.A.Dvorzhetskaya & L.Ya.Khlebnikova, Ibid., 4, 161 (1960).

* * * * * * *

ON THE QUESTION OF RADICAL-RECOMBINATION LUMINESCENCE OF CRYSTAL PHOSPHORS

- V.A.Sokolov & A.N.Gorban'

Back in 1925 Bonhoeffer[1], investigating hydrogen reactions, discovered luminescence of phosphors under the influence of atomic hydrogen. Subsequently, other authors observed emission of luminophors under the influence of free atoms and radicals of other gases. Unfortunately, this extremely interesting form of luminescence has long been neglected.

In the present work we draw a parallel between the luminescence of phosphors in the atmosphere of an active gas and under the influence of chemically active flames, and make an attempt to explain this form of luminescence on the basis of the electron theory of chemical catalysis.

The source of excitation of the luminescence in an atmosphere of active gas is the energy evolved in recombination on the phosphor surface of the atoms and radicals of the gas to form molecules. The surface in this case plays the role of a "partner" without which the formation of molecules becomes impossible; the recombination usually occurs incident to triple encounters, when the recombining atoms and molecules can transfer the released energy to a third particle.

We showed experimentally that the luminescence of phosphors under the influence of a flame, called candoluminescence, is also a consequence of recombination on the phosphor surface of free atoms and radicals, the presence of which in the flame is connected with the chain mechanism of the burning reaction.[2]

The experiments designed to prove the radical-recombination nature of the mechanism of candoluminescence were the following:

1. Determination of the coefficients of recombination of atoms and radicals on some phosphors in a flame. The coefficient of recombination for strongly candoluminescing phosphors proved to be high: in the range from 0.3 to 1.0.[3]

2. Observation of luminescence in the intercone gases of a flame. In this experiment there were eliminated all other excitation factors (corpuscular, ultraviolet radiation from the flame, etc.), so that only recombination of atoms and radicals was significant. To this end we used a zone burner in the flame of which there was an appreciable separation between the inner and outer flame cones. It was found that phosphors held in the atmosphere of the intercone gases luminesced strongly under the influence of the free atoms and radicals contained in the gas.

3. Suppression of luminescence in a flame by means of an active catalyzer. It is known that the surfaces of such metals as platinum, vanadium and copper are excellent catalyzers of the reaction of recombination of atomic hydrogen and radicals. Consequently, by inserting a copper or similar screen into the flame below the phosphor, one can induce the atoms and radicals to recombine on the surface of the screen; this should greatly weaken the luminescence of the phosphor if it is due to the radical-recombination mechanism. Experiments with a catalytic screen

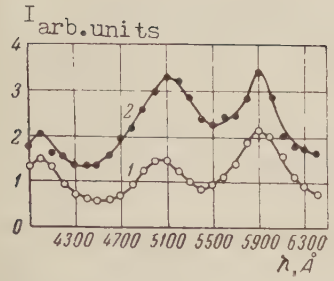

Luminescence spectra of lime in illuminating gas flame (1) and in an atmosphere of the same gas activated by an electric charge (2).

resulted in significant quenching of candoluminescence.[3]

4. Investigation of the luminescence of phosphors under the influence of free atoms and radicals of the same type as those producing candoluminescence in the flame, but obtained by means of an electric discharge. The spectra obtained in the two cases proved to be identical. By way of illustration we reproduce in the accompanying figure the luminescence spectrum of lime in an illuminating gas flame (curve 1) and in an atmosphere of the same gas activated by an electric discharge (curve 2).[4]

The phenomenon of radical-recombination luminescence can be qualitatively explained from the standpoint of the usual mechanism of chemical catalysis on semiconductors. According to the commonly accepted concepts, the recombination of free atoms (or radicals) on the solid surface should take place in three stages, consisting of adsorption of the gas atoms X, formation of molecules X_2 on the surface and desorption of the molecules with release of a recombination energy E.[5] These stages are symbolized by the following formulas:

$$X \rightarrow (X)_{ads}; \quad (X)_{ads} + X \rightarrow (X_2)_{ads}; \quad (X_2)_{ads} \rightarrow X_2 + E.$$

The adsorbed atom will in general form a trapping center for electrons or holes; this is usually represented in the energy diagram by an acceptor or donor level. The electron can arrive at this level either as a result of dropping out of the conduction band or as a result of rising out of the valence band. In the latter case, according to Vol'kenshtein[6], there is produced on the surface an electron-hole pair; the electron is localized (trapped), while the hole remains free and migrates over the surface. It may be hypothesized that in the case of a phosphor-catalyzer, such a hole, appearing near an activator atom, makes possible exothermal ionization of the luminescence center. This can lead to recombination of an electron from the conduction band with the luminescence center, as a result of which there will be emitted a luminescence photon. The electrons are furnished either by the stage of formation of molecules or desorption thereof. As was shown by Vol'kenshtein[7], the energy of recombination of atoms and radicals into molecules can be utilized for raising electrons into the conduction band.

However, in the case of adsorption of an atom or radical on an activator atom, in our opinion, there may occur direct ionization of the luminescence center; owing to distortion of the energy field in the vicinity of the adsorbed particle there occurs "displacement" of the activator level, which may lead to anti-Stokes luminescence.[8]

We desire to express our gratitude to F.F.Vol'kenshtein for his interest in the work and valuable advice.

References

1. K.F.Bonhoeffer, Z.phys.Chem., 116, 391 (1925).
2. N.N.Semenov, Tsepnye reaktsii (Chain reactions), M., 1934.
3. A.N.Gorban' & V.A.Sokolov, Optika i spektroskopiya, 7, 259 (1959). (Trans. Optics & Spectroscopy.)
4. A.N.Gorban' & V.A.Sokolov, Ibid., 7, 569 (1959).
5. G.K.Lavrovskaya & V.V.Voevodskii, Zhur.fiz.khim. 25, 1050 (1951).

6. F.F.Vol'kenshtein, Uspekhi khimii, 27, 1304 (1958).
7. F.F.Vol'kenshtein, Izv.AN SSSR, Otd.khim.nauk, 2, 143 (1957). (Trans. Bulletin of the USSR Academy of Sciences - Div.Chem.Sci.)
8. A.N.Gorban' & V.A.Sokolov, Optika i spektroskopiya, 7, 815 (1959). (Trans. Optics & Spectroscopy.)

* * * * * * *

RECOMBINATION LUMINESCENCE OF Sn^{4+} IN AQUEOUS SOLUTIONS OF LiCl AND HCl AT LOW TEMPERATURE

- M.U.Belyi, B.A.Okhrimenko & B.F.Rud'ko

It is a familiar fact that there is much in common between the optical characteristics of alkali halide crystal phosphors and those of concentrated solutions of the corresponding salts: their absorption spectra are virtually identical and their luminescence spectra have many points of resemblance. Hence, investigation of concentrated halide solutions containing heavy metal atoms can be of help in elucidating the mechanisms of absorption and luminescence of crystal phosphors.

In investigating the temperature behavior of the luminescence of halide solutions containing heavy metal ions, we noted[1] that in the case of aqueous solutions of Sn^{2+} in LiCl (or HCl)* there appears a new red luminescence band at low temperatures. Thus the luminescence spectrum of these solutions at liquid oxygen temperature consists of two bands: a blue band (λ_{max} = 440 mμ) and a red band (curve 3 in the accompanying figure). The present work was concerned with determining the nature of the red luminescence band.

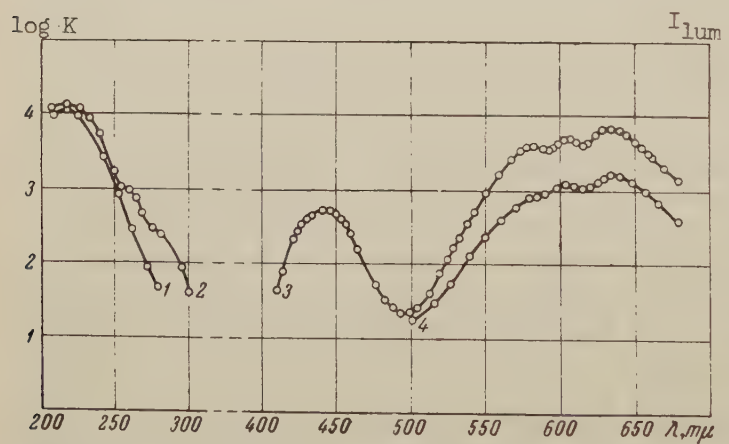

Absorption (1 & 2) and luminescence (3 & 4) spectra of Sn^{4+} + LiCl (1 & 4) and Sn^{2+} + LiCl (2 & 3) solutions.

Careful studies showed that this red luminescence band comprises three peaks located at 585, 605 and 635 mμ. It was established that the blue and red luminescence bands are excited in different parts of the absorption spectrum: the blue band is excited in the fundamental absorption peak at 226 mμ, while the red band is excited in the region of two weak absorption maxima at 262 and 276 mμ.

The absorption curves (1 & 2) shown in the accompanying figure were obtained earlier[2] at room temperature; however, subsequent studies[1] showed that the absorption spectra of such solutions virtually do not shift with decrease of temperature; cooling results only

---

*Virtually identical spectra are obtained in LiCl and HCl solutions; hereinafter we describe LiCl solutions, but the results apply equally to HCl solutions.

in the peaks becoming somewhat narrower and higher.

Investigation of analogous solutions of tetravalent tin at liquid oxygen temperature showed that the absorption spectra of Sn^{4+} + LiCl and Sn^{2+} + LiCl solutions have a common absorption maximum at 226 mμ, but that the two weak peaks (262 and 276 mμ), observed in the spectra of divalent tin solutions, are not evinced in the absorption of tetravalent tin solutions.

The luminescence spectrum of Sn^{4+} + LiCl solutions has only one red band, which exhibits the same triplet structure as the spectrum of Sn^{2+} + LiCl solutions.

Investigation of the excitation spectrum of Sn^{4+} + LiCl solutions showed that the maximum of the excitation function is located on the side of the absorption curve in the region of 300 mμ.

The above experimental fact can be explained on the assumption that the long wavelength absorption peak of the Sn^{2+} + LiCl solutions is due to ${}^1S_0 \rightarrow {}^3P_{0,1,2}$ transitions. In this case obviously, the triplet structure of the red luminescence band of Sn^{2+} must be associated with ${}^3P_{0,1,2} \rightarrow {}^1S_0$ transitions.

The analogous structure of the red luminescence band of Sn^{4+} solutions and the position of the excitation spectrum can be explained as follows. Ultraviolet in the 300 mμ region is absorbed - if only weakly - by the Cl^- ions. The electrons detached from the Cl^- ions can recombine with Sn^{4+} ions, occupying ${}^3P_{0,1,2}$ levels. Accordingly, ${}^3P_{0,1,2} \rightarrow {}^1S_0$ transitions take place and give rise to the red luminescence band of Sn^{4+}. This interpretation is substantiated by the agreement between the peaks in the experimental spectrum and the maximum given by the formula

$$I_{\text{lum}} = I_0 \frac{\alpha C_0 C_x K_x}{K_x C_x + K_0 C_0} [1 - e^{-(K_x C_x + K_0 C_0) d}], \qquad (1)$$

where I_{lum} and I_0 are the luminescence and exciting light intensities, α is the probability for radiative recombination of an electron and an Sn^{4+} ion, K_x and K_0 are the absorption coefficients (at liquid oxygen temperature) of Cl^- and Sn^{4+}, respectively, C_x and C_0 are the Cl^- and Sn^{4+} concentrations, respectively, and d is the thickness of the absorbing layer.

Analysis of Eq.(1) as a function of C_x and C_0 shows that the maximum of I_{lum} corresponds to $\frac{K_0}{K_x} = \frac{C_x^2}{C_0^2}$ (in the calculations it is assumed that $d \rightarrow \infty$), which also agrees with experiment.

Department of Physics,
"T.G.Shevchenko" Kiev State University

References

1. M.U.Belyi & B.F.Rud'ko, Izv.AN SSSR, Ser.fiz., 24, 582 (1960). (Trans. Bulletin, 24, 588.)

2. M.U.Belyi & K.F.Gudimenko, Ibid., 20, 579 (1956). (Trans.Bulletin, 20, 526.)

DISCUSSION

Ch.B.Lushchik: In recent years many investigators have compared the characteristics of free activator ions with those of activator luminescence centers in crystals. In crystals activated by hydrogen-like ions (Ga, Ge, Tm, Sn, Te,Pb)

the principal absorption bands are interpreted as being due to $^1S_0 \rightarrow {}^3P_{0,1,2}$ and $^1S_0 \rightarrow {}^1P_1$ transitions. Obviously, as a result of some mixing of wave functions of the activator ions and the nearest host ions, this interpretation is only approximate. For excited ^3P states this approximation is satisfactory, but for $^1P_1$ states the wave function mixing is appreciable. It leads to the effect (observed in our experiments) of delocalization of the impurity excitations (in crystals only a small fraction of the excitations - ~5% - is delocalized).

The interesting results obtained by Belyi & Rud'ko indicate that the above mentioned approximation is even less valid for solutions of hydrogen-like ions. Whereas for ^3P states it is still applicable, for higher excited states of luminescence centers, it is no longer meaningful to speak of excitation of the activator ion per se. Actually the excitation involves an entire complex. It should be possible to establish a correlation between the difference in the behavior of luminescence centers in crystals as against solutions and the different degrees of overlapping of the absorption spectra of the anions and activator. In solutions the overlapping is appreciably greater.

* * * * * * *

CORRELATION BETWEEN THE THERMAL ACTIVATION ENERGY FOR CONDUCTIVITY AND THE ABSORPTION AND PHOSPHORESCENCE SPECTRA OF SOME ORGANIC SUBSTANCES

- A.T.Vartanyan & L.D.Rozenshtein

In addition to the many familiar inorganic phosphors there exist organic phosphors, the activators in which are usually organic compounds (carbazole, esculin and dyes such as uranin (sodium fluorescein), eosin, fluorescein, etc.). The properties of these compounds as activators are related with their semiconductor properties as evinced in their electric conductivity, photoconductivity and so on. One of the important quantities characterizing the properties of organic activators is the thermal activation energy for conductivity, on the basis of which one can judge of the semiconductor properties of both the activator and the organic phosphor as a whole.

In the present work we measured the thermal activation energy for conductivity for a number of compounds in solid layers. These energy values were determined from the experimental temperature dependence of the conductivity, which for organic semiconductors, as a rule, obeys the law

$$\sigma = \sigma_0 e^{-\varepsilon_T/2kT},$$

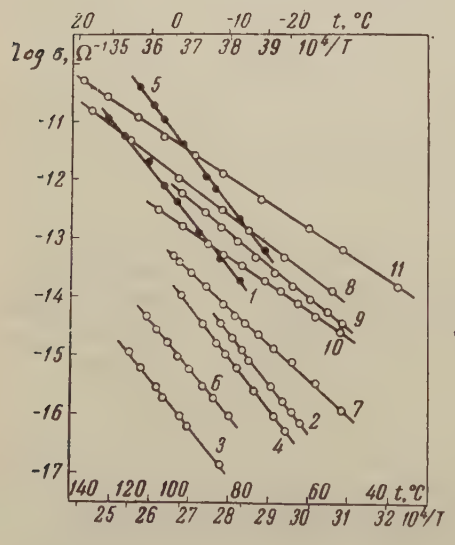

←Temperature dependences of the conductivity of solid layers: 1 - benzophenone (the upper temperature scale pertains to this compound), 2 - anthranilic acid, 3 - phenylanthranilic acid, 4 - 3-acteylamino-N-methylphthalimide, 5 - 3-acetylamino-N-phenylphthalimide, 6 - 3-benzoylamino-N-methylphthalimide, 7 - fluorescein, 8 - uranin, 9 - phosphine, 10 - indigo, 11 - aqueous blue.

Compound	Temp. range, °C	ϵ_T, ev	λ corresp. to ϵ_T, mμ	SAC	EPB
1	2	3	4	5	6
Malachite green	40-112	1.65	749	655-750	
Brilliant green	66-110	1.71	722	659-740	
Fuchsin	40- 85	1.79	690	580-700	
Crystal violet	63-100	1.78	694	630-710	
Aqueous blue	19-147	1.75	706	610-750	
Uranin	54-153	2.05	603	510-605	
Eosin	60-154	2.30	536	520-590	
Erythrosine	64-161	2.22	566	530-600	
Phloxin	60-160	2.07	597	530-600	
Bengal rose	52-153	2.05	603	560-610	
Rhodamine B	52-100	2.10	588	578-630	
Colorless prod. of Rhod. B	100-155	3.70	334	317-350	
Rhodamine 6 G	53-106	2.07	597	555-620	
Fluorescein	51-103	2.44	506	490-530	
Phenosafranine	64-131	2.08	595	570-620	
Trypoflavine	58-100	2.3	536	480-540	
Phosphine	55-100	2.26	546	468-550	
Capri blue	18- 76	1.67	740	700-780	
Nile blue	10-100	1.63	758	680-780	
Thionine	45-118	1.83	675	650-700	
Indigo	40-110	1.75	705	660-720	
Pinacyanol	35- 87	1.90	650	642-720	
Orthochrome T	40- 80	2.05	603	584-640	
Phthalocyanin	60-163	1.7	725	688-790	
Cu phthalocyanin	88-158	1.7	725	685-780	
Zn phthalocyanin	109-160	1.7	725	714-810	
Benzophenone	-23- 14	3.34	370	330-400	2.8*
Anthranilic acid	62- 86	3.38	366	342-400	2.8
Phenylanthranilic acid	87-119	3.30	375	375-430	2.7
3-acetylamino-N-methylphthalimide	67-100	3.46	357	350-390	2.9
3-acetylamino-N-phtnylphthalimide	54-124	3.50	353	340-400	2.7
3-benzoylamino-N-methylphthalimide	84-112	3.28	377	360-410	2.8
3-methoxy-N-methylphthalimide	54- 78	3.18	388	355-390	
3-hydroxy-N-methylphthalimide	60- 91	3.8	325	350-390	
4-aminophthalimide	123-151	2.78	444	410-510	
4-amino-N-cyclohexylphthalimide	73-100	2.90	426	375-440	

SAC - Section of long wavelength side of the absorption curve corresponding to the energy of the singlet-singlet transition (in mμ).

EPB - Energy corresponding to the short wavelength edge of the phosphorescence band of the compound in the solid state (in ev).

*Ref.6.

where ε_T is the thermal activation energy.

We investigated benzophenone, anthranilic and phenylanthranilic acids, a number of phthalimides and dyes of different types (see table). The substances were investigated in the form of layers (up to 10 μ thick) which in most cases were obtained by vacuum (10^{-5} mm Hg) evaporation. Inasmuch as anthranilic and

phenylanthranilic acids and most phthalimides when heated in vacuum to 50-60° begin to sublimate at an appreciable rate, in investigating these we used an atmosphere of spectroscopically pure helium. The sensitivity of the current measuring instrument was 10^{-14} amp.

The temperature dependences of the conductivity for some of the investigated compounds are plotted in the accompanying figure.

In the table (column 3) we list the values of an activation energy as determined from the slope of the conductivity vs temperature plots; in column 4 we list the wavelength corresponding to these energy values. In order to compare these values with the optical characteristics of the compounds we measured the absorption spectra of the solid layers and the phosphorescence spectra of the substances that phosphoresce in the solid state. The absorption spectra were measured on an SF-4 spectrometer. Column 5 in the table gives the section of the long wavelength side of the absorption curve (SAC) for the solid layers, corresponding to the energies of the singlet-singlet transition in the process of absorption. As the short wavelength edge of the sections we took the peaks of the bands. In determining the long wavelength absorption edge we went by the beginning of the sharp rise of the spectral curve.

The phosphorescence spectra were recorded at liquid nitrogen temperature with excitation of the layers by light in the near ultraviolet (where the absorption bands of the investigated compounds are located). The energy values corresponding to the short wavelength edges of the phosphorescence bands (EPB) are given in column 6. These values characterize the energy of the triplet level of the compound in the same state of aggregation as that in which the conductivity was measured (solid layer).

There has been extensive discussion in the literature regarding the mechanism of conductivity in organic semiconductors. According to the new view on the nature of photoconductivity, the internal photoeffect in organic semiconductor crystals occurs with participation of electrons raised to the triplet level.[2-5] The results of our investigation allow of drawing certain inferences regarding the nature of the dark conductivity in organic substances. As will be evident from the table the wavelength corresponding to the activation energy values are in good agreement with the sections of the long wavelength sides of the absorption curves. At the same time for the phosphorescing compounds the heights of the triplet levels proved to be much less than the values of ε_T. Comparison of these results indicates that the free carriers participating in the dark conductivity of the phosphorescing compounds are produced incident to singlet-singlet electron transitions. This inference is also probably valid for the other investigated compounds, including the dyes.

References

1. A.T.Vartanyan, Izv.AN SSSR, Ser.fiz., 20, 1541 (1956). (Trans.Bulletin, 20, 1412.)
2. D.J.Carswell, J.Ferguson & L.E.Lyons, Nature, 173, 736 (1954).
3. A.N.Terenin, Radiotekhnika i elektronika, 1, 1127 (1956).
4. B.Rosenberg, J.Chem.Phys., 29, 1108 (1958).
5. B.Rosenberg, Ibid., 31, 238 (1959).
6. V.L.Ermolaev, Thesis, Leningrad, 1958.

EXCITATION WAVELENGTH DEPENDENCE OF THE BLUE LUMINESCENCE YIELD OF CADMIUM SULFIDE CRYSTALS AT 20°K

- V.L.Broude & V.S.Medvedev

Investigation of the spectral distribution of luminescence is of great interest from the standpoint of establishing the nature of the luminescence of solids and the relation between luminescence and absorption of light. Moreover, if one can determine the relation between the excitation spectrum and the absorption spectrum, the results can be utilized for determining the absorption curves in the regions inaccessible to direct measurement.

Earlier[1] we investigated the excitation spectra for the "green" and "orange" luminescence bands of CdS crystals. In the present work we determined the excitation spectra for the "blue" luminescence of these crystals. The "blue" luminescence is located in the region adjacent to the absorption edge of CdS, and its short wavelength bands coincide with weak absorption lines[2] associated with electronic transitions in the vicinity of defects in the crystal lattice.[3]

The spectral distribution of the luminescence output was measured at 20°K. The exciting wavelengths were isolated by means of a diffraction grating monochromator with a dispersion of 3 Å/mm. The excitation curves obtained for the "green", "red" and "blue" luminescence of one CdS crystal are shown in Fig.1. In the lower part of the figure the arrows indicate the positions of the peaks of the absorption bands, taken from the absorption spectra recorded for relatively thin (0.3-0.4 μ) crystals.

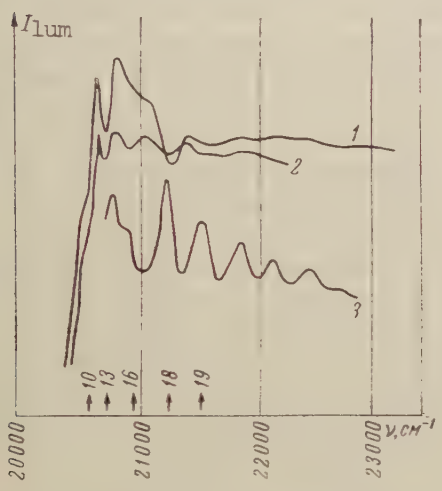

Fig.1. Spectral dependence of the output of "green" (1), "red" (2) and "blue" (3) luminescence of a CdS crystal.

In the excitation spectra for the "green" and "red" luminescence there are observed dips in the luminescence yield at wavelengths corresponding to the peaks of the absorption bands. On the other hand, in the excitation spectrum of the "blue" luminescence, beginning with 21 000 cm^{-1} there is evinced direct proportionality between the luminescence intensity and the absorption coefficient (Fig.1). Thus in the case of the investigated CdS specimens increase in the intensity of the "blue" luminescence with variation of the excitation wavelength is accompanied by decrease in the luminescence intensity in other regions of the spectrum. The "blue" luminescence excitation spectrum is characterized by pronounced structure. Fluctuations of the luminescence output can be observed up to 23 000 cm^{-1} (2.9 ev), i.e., almost to 0.3 ev from the absorption edge. This is evidence of the much stronger dependence of the intensity of the "blue" luminescence on the absorption coefficient, as compared with the dependences of the "green" and "red" emissions.

We made use of the sensitivity of this spectrum to variation of the absorption coefficient in order to establish the character of the absorption curve in the short wavelength region. From the absorption of crystals of different thickness we were able to determine the approximate position of the absorption curve down to 21 500 cm^{-1}. From the excitation spectrum we were able to obtain information in the range from 21 000 to 23 000 cm^{-1}. Combining these data enabled us

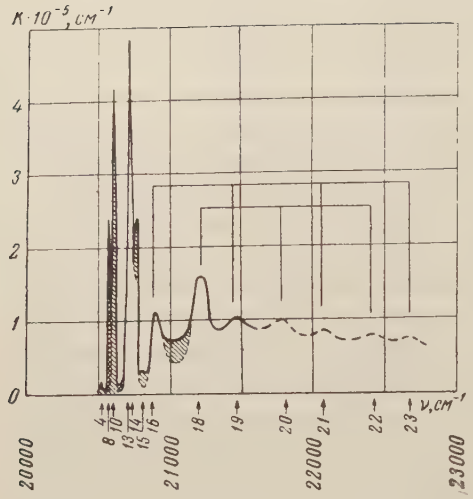

Fig.2. Absorption spectrum of CdS crystal. Double hatched region - polarization $\perp c$; hatched region - polarization predominantly $\perp c$, but $\| c$ component discernible; unhatched region - weak polarization, intensity $\| c$ somewhat higher.

to establish the absorption in the region from 20 400 to 23 000 cm^{-1} (Fig.2).*

One can distinguish three regions in the absorption spectra of CdS crystals. In the 20 400 to 20 560 cm^{-1} interval there are a number of weak ($K \approx 10^2$-10^3 cm^{-1}) narrow (3-5 cm^{-1}) variable absorption bands, polarized perpendicularly to the c axis. The character of these bands was investigated earlier and described in Ref.3.

In the 20 560 to 20 780 cm^{-1} region there are evinced wider (20-40 cm^{-1}), very intense absorption bands. The absorption coefficient at the peak of the 20 700 cm^{-1} band (No.13 in Fig.2) is $5 \cdot 10^5$ cm^{-1}. The polarization of the bands in this region varies. The bands at 20 572 (No.8) and 20 740 cm^{-1} (No.14a) are wholly polarized perpendicularly to c. The bands at 20 589 (No.10), 20 740 (No.14b) and 20 800 cm^{-1} (No.15) are also strongly polarized $\perp c$, but are observed with a low intensity with the incident light polarized parallel to c. The band at 20 700 cm^{-1} (No.13) is intense in both components (somewhat stronger in the component parallel to c). This is the most intense absorption band in the entire investigated region. It must be noted that the No.8 band is also variable, i.e., differs in intensity in the spectra of different crystals (see table). The same thing but to a lesser degree applies to the band at 20 740 cm^{-1} (No.14a). Also unstable as regards intensity (and in some cases as regards wave number) is the 20 589 cm^{-1} (No.10) band in the c component of the spectrum. In the spectra of different specimens its intensity varies by an order of magnitude or more. Bands Nos.8 and 10 and Nos.14a and 14b are highly sensitive to mechanical deformation of the crystal.[5] There is a noticeable redistribution in intensity between these bands (Fig.3) in the spectrum of even weakly stressed specimens. We detected no other changes in the spectra of lightly stressed specimens.**

In the third absorption region (20 850 to 23 000 cm^{-1}) we find a group of broad relatively intense bands. In all we observed eight bands in this region. The absorption coefficient at the peaks is 10^5 cm^{-1} on the average. Between the peaks there is substantial continuous absorption. The polarization of these bands is weak; all of them are somewhat more intense in the c component of the spectrum. These bands form two vibrational series with a separation of 605 ± 20 cm^{-1} between members. The first series, comprising the weaker bands, begins at 20 875 cm^{-1} (No.16) and has four members; the second series begins with the intense band at

---

*The absorption curve for CdS crystals at 20°K was measured in our earlier[4] paper. Being unable to obtain sufficiently uniform thin crystals, we were able to measure this curve only to values of the absorption coefficient $K \approx 10^4$ cm^{-1}. In the region of stronger absorption the curve was extrapolated on the basis of spectrograms photographed for thin specimens. It was found in subsequent studies that in this extrapolation we underestimated the absorption at the peaks of the strongest bands: No.10 (20 589 cm^{-1}) and No.13 (20 700 cm^{-1}) (Fig.2).

**Substantial increase in the deformation of the crystal leads to appreciable alteration of the entire spectrum.[5]

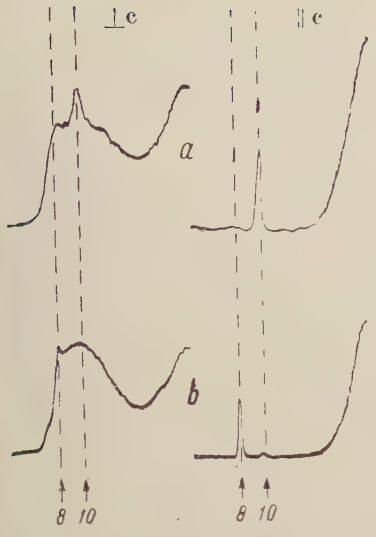

Fig.3. Comparison of the absorption spectra of an unstressed (a) and a stressed (b) CdS crystal.

21 190 cm^{-1} (No.18) comprises four members and is 320 cm^{-1} distant from the first. The absorption background located in the interval between the beginnings of these series, in contrast to the bands, is more intense in the ⊥c component.

As for the general character of the absorption spectrum of the CdS crystals, we want to emphasize its similarity to the absorption spectra of typical molecular crystals. As in the case of molecular crystals, strong intrinsic absorption is preceded by weak narrow polarized bands belonging to impurities in the widest sense of the word (contaminations, distortions of the lattice in the neighborhood of impurity centers, defects and dislocations). In coincidence with these bands are luminescence bands, but intrinsic luminescence is absent or very weak.[6] As in the spectra of molecular crystals, in the initial section of the intrinsic absorption of the crystal there are observed particularly intense sharp bands, partially strongly polarized along the crystallographic axes. Davydov[7] associates these bands with excitation of excitons capable of migrating through the crystal. The absorption bands in the high frequency region combine into vibrational series, the higher members of which have a relatively low intensity and are more diffuse and broad.

Apparently, in interpreting the absorption spectrum of CdS crystals, one should bear in mind the semipolar character of the lattice of this compound; by semipolar we understand a structure intermediate between ionic and molecular.

Characteristics of the absorption bands of CdS crystals

Band No.	Location of peak, cm^{-1}	Absorption coefficient at peak cm^{-1}	Polarization
1	20400—20415	$0—10^2$	
2	20430—20450	$0—10^2$	
3	20 500	$0—10^2$	
4	20513—20525	$10^2—10^3$	⊥c
5	20 530	$0—10^3$	
6	20 545	$0—10^2$	
7	20 550	$0—10^2$	
8	20 572	$10^2—2\cdot10^5$	
9	20 580	$0—10^3$	
10	20 585—20 600	$4\cdot10^5$ (⊥c); $10^2—10^4$ (∥c)	⊥c≪∥c
11	20 625	$\sim10^4$	
12	20 685	$\sim10^5$	∥c>⊥c
13	20 700	$\sim5\cdot10^5$	
14a	20 740	$\sim2\cdot10^5$	⊥c
14b	20 750		⊥c≫∥c
15	20 800	$\sim3\cdot10^4$	⊥c>∥c
16	20 875	$\sim10^5$	c>⊥c
17	20 930	$\sim7\cdot10^4$	⊥c>∥c
18	21 190	$\sim1,5\cdot10^5$	
19	21 456		
20	21 788	$\sim10^5$	∥c>⊥c
21	22 060		
22	22 415		
23	22 670		

Institute of Physics,
Academy of Sciences of the
Ukrainian SSR

References

1. V.L.Broude, V.V.Eremenko & V.S. Medvedev, Zhur.tekh.fiz., 28, 2563 (1958). (Trans.Soviet Physics - Technical Physics.)

2. V.V.Eremenko, Optika i spektroskopiya, 4, 348 (1958).

3. V.L.Broude, V.V.Eremenko & E.I.Rashba, Doklady AN SSSR, 114, 520 (1957). (Trans.Doklady.)

4. V.L.Broude, V.V.Eremenko & N.N.Chikovani, Ibid., 119, 911 (1958). (Trans. Ibid.)

5. V.L.Broude, O.S.Pakhomova & A.F.Prikhot'ko, Optika i spektroskopiya, 2, 323 (1957).
6. V.L.Broude, A.F.Prikhot'ko & E.I.Rashba, Usp.fiz.nauk, 67, 99 (1959). (Trans.Soviet Physics - Uspekhi.)
7. A.S.Davydov, Trudy, IFAN USSR (Proceedings, Inst.of Physics, Ukrainian SSR Ac.of Sci.), No.1 (1951).

* * * * * * *

LUMINESCENCE OF Se ACTIVATED CADMIUM IODIDE

- I.P.Shapiro

When stimulated by near ultraviolet cadmium iodide emits weak yellowish-brown luminescence. This luminescence can be explained (as in the case of ZnS) on the assumption that the emission originates at surstoichiometric atoms in the host lattice, formed by the dissociation mechanism.[1,2] The luminescence of pure cadmium iodide is so weak that attempts to obtain its spectrum failed. Upon the introduction of a minor amount of selenium (10^{-6} g/g) into the CdI_2 lattice, however, the luminescence intensity is greatly increased.[3] Bundel' & Rusanova[3], investigating zinc sulfide-selenide phosphors, observed a band peaking at 600 mμ, which they attributed to Se.

We also observed a selenium band with λ_{max} = 603 mμ in the luminescence of cadmium iodide doped with selenium. This confirms the deductions of Bundel' et al[4] that not only metals but also metalloids can be activators. The luminescence spectra of CdI_2:Se phosphors with different Se concentrations are shown in the accompanying figure. The spectra were obtained by means of an MS-3 glass spectrograph with recording on isopanchromatic film (sensitivity 65 GOST units). At the right we show photomicrograms of spectra 3, 4 and 5, obtained taking into account the spectral sensitivity of the film (determined with the aid of a lamp with a color temperature of 2850°). It will be evident from the reproduced spectra that the luminescence intensity depends on the selenium concentration in the phosphor. The lowest intensity is obtained at $C_{Se} = 10^{-2}$ g/g. It also follows from the experimental data that the luminescence spectra of CdI_2:Se phosphors consist of two bands: a broad band peaking at 640 mμ and less intense, narrow band peaking at 603 mμ.

We also recorded the luminescence spectra of CdI_2-PbI_2, CdI_2-PbI_2:Se, CdI_2::Mn and CdI_2:Mn:Se.

Phosphors activated by Pb and Mn are characterized by one intense luminescence peak at 640 mμ. Mixed phosphors in which selenium is also present exhibit an additional peak at 603 mμ. Thus it may be asserted that the emission band in the spectrum of CdI_2:Se located at 603 mμ belongs to selenium. The peak at 640 mμ may be attributed to the deformed CdI_2 lattice. The stability of the selenium band as regards doping with Pb and Mn is not constant and depends on the selenium concentration in the phosphor. It may be assumed that phosphors of the CdI_2:Se type are systems containing both metal and metalloid activators.

In addition, we made a detailed investigation of CdI_2-PbI_2 phosphors. The experimental data of Klement & Malysheva[5] indicate that the bands in the excitation spectra of CdI_2-PbI_2 phosphors coincide with the bands in their absorption spectra. We obtained analogous results not only for CdI_2-PbI_2 but also for KI-TlCl phosphors. CdI_2-PbI_2 compounds containing up to 90 mole percent PbI_2 lumi-

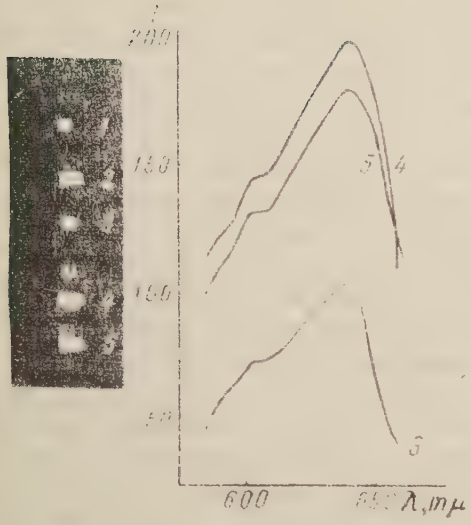

Luminescence spectra of CdI_2:Se phosphors with different Se concentrations (in g/g): 1 - $5 \cdot 10^{-2}$, 2 - 10^{-3}, 3 - 10^{-4}, 4 - 10^{-2}, 5 - $2 \cdot 10^{-3}$. At right - photometric traces of spectra 3, 4 and 5.

nesce yellow under stimulation by near ultraviolet; the highest intensity is obtained for the phosphor with 3-5 mole percent PbI_2. This phosphor has a short persistence: $\tau = 10^{-4}$ sec. Ryvkin[6] used the capacitor technique to determine the photoconductivity of PbI_2 and CdI_2-PbI_2 and the width of the gap in these compounds.

In earlier experiments[7], we found that the photoconductivity of PbI_2 and CdI_2-PbI_2 is predominantly of the p-type. From the values of $\lambda_{1/2}$, corresponding to the half-height of the spectral distribution curve for PbI_2, it follows that the width of the forbidden energy band in PbI_2 is relatively large (E_g = 2.08 ev). Using the procedure of Stepanov et al[8] for determining the absorption spectrum from the diffuse reflection spectrum, we determined[9] the width of the gap in CdI_2 and found E_g = 3 ev. In view of the fact that the radius of the Se ion is small (1.15 Å) compared with the interatomic separation in the CdI_2 lattice (4.24 Å), it may be inferred that the "defects" in the CdI_2 lattice are formed by interstitial selenium atoms that are readily incorporated to the layered CdI_2 lattice in the process of heating (luminescence appears after melting CdI_2 + Se to form a solid solution). This serves to explain why CdI_2:Se, like CdI_2:Pb, luminesces even at very high activator concentrations.

I desire to express my gratitude to B.I.Stepanov for valuable advice and his interest in the work.

References

1. A.Schleede, Z.angew.Chem., 50, 908 (1937).
2. H.Schlegel, Naturwissenschaften, 30, 242 (1942).
3. A.A.Bundel' & A.I.Rusanova, Izv.AN SSSR, Ser.fiz., 13, 173 (1949).
4. A.A.Bundel', E.I.Guretskaya, U.A.Asakhov & T.F.Uvarova, Transactions of the 5th Conference on Luminescence (Crystal phosphors), Tartu, 1957.
5. F.D.Klement & A.F.Malysheva, Trudy IFA AN ESSR (Proceedings, Inst.of Physics & Astronomy, Estonian SSR Ac.of Sci.), Tartu, 1955.
6. S.M.Ryvkin, Zhur.tekh.fiz., 58, 1521 (1948).
7. I.P.Shapiro, Uch.zap.Belorussk.in-t.Ser.Fiz. (Scientific notes, Belorussian Inst., Phys.Series), No.41 (1958).
8. B.I.Stepanov, Yu.I.Chekalinskaya & O.P.Girin, Trudy In-ta fiz.i matem. AN BSSR (Proceedings of the Inst. of Physics & Mathematics, Belorussian SSR Ac. of Sci.) No.1, 1952.
9. I.P.Shapiro, Optika i spektroskopiya, 4, 256 (1958).

IMPROVEMENT OF PHOSPHORS FOR LIGHT SOURCES

- R.A.Nilender & D.P.Troshenskii

Work on the development of "fluorescent lamp" phosphors began in the Soviet Union more than 20 years ago. During Vavilov's time this research was carried out in the laboratory of the Moscow Electric Lamp Plant in collaboration with the Physical Institute of the Academy of Sciences and also by the Light Source Laboratory of the All-Union Electrotechnical Institute. The first phosphor developed for use in lamps was cadmium silicate activated by manganese in mixture with magnesium tungstate. This phosphor was characterized by poor stability and in 1944 was replaced by a mixture of Mn activated zinc-beryllium silicate and magnesium tungstate. An intensive search for new better phosphors began in 1949; Vavilov induced the State Optical Institute to participate in this work.

The result of collaboration of the Physical Institute, the Optical Institute and the Laboratory of the Moscow Electric Lamp Plant was development of calcium halophosphate:Sb:Mn phosphor. Although at first this phosphor did not give an appreciable increase in efficiency, it made it possible to do away with the use of such scarce and toxic materials as tungsten anhydrate and beryllium compounds. Bundel' et al[1] reported on the development of the calcium halophosphate phosphor at the Third Conference on Luminescence in 1951. The halophosphate phosphor was put into production at the "Krasnyi Khimik" (Red Chemist) Plant.

After the death of Vavilov, all collaborative work ceased, and only the laboratory of the Moscow Electric Lamp Plant continued research aimed at development of phosphors for light sources and cathode-ray tubes. From 1955 to 1960 there have been carried out at the plant numerous investigations aimed at increasing the initial brightness of lamp phosphors and reducing the loss in efficiency with time.

Calcium halophosphate:Sb:Mn belongs in the group of sensizied phosphors. Its primary sensitizing activator is antimony. The ultraviolet radiation from the low pressure mercury discharge is absorbed by the antimony, and is partly emitted by it (band with λ_{max} = 4800 Å) and partly transferred to the manganese centers, as a result of which there appears a luminescence band peaking at 5800 A. Calcium halophosphate phosphors activated only by manganese are not excited by ultraviolet, while phosphors activated by only antimony emit only one blue band with a peak at 4800 Å.

Antimony acts as a sensitizer only in the trivalent state.[2] However, depending on the conditions of preparation of the phosphor the antimony may be volatilized to some extent and transform to the pentavalent state, forming inactive calcium antimonate. The content of active antimony in the phosphor depends greatly on the chemical composition of the host and the quality of the raw material.

The brightest halophosphate luminophors are phosphors close in composition to apatite: $3Ca_3(PO_4)_2 \cdot CsF_2$. In an efficient halophosphate luminophor part of the calcium is replaced by antimony and manganese, which are responsible for its luminescence properties. Moreover, part of the fluorine is replaced by chlorine, which results in some shift of the luminescence spectrum. The concentration of trivalent antimony entering into the apatite lattice and forming the luminescence centers proves to be the higher, the lower the content in the batch of hydroxyl apatite, forming as a result of hydrolysis.[2-4]

In order to obtain phosphors with high efficiency there were investigated in our laboratory the conditions of precipitation of disubstituted calcium phosphate; it was shown that for obtaining it without hydroxyl apatite impurity it is essential to carry out the precipitation under rigorously controlled conditions. Other experiments were carried out to optimize the temperature and heating time, the

content of antimony and manganese and the proportion of fluorine to chlorine in the phosphor. With variation of the heating temperature the brightness of the phosphor goes through a flat maximum at 1150°. The optimum content of active antimony lies in the range from 0.7 to 0.8%. Variation in the amount of manganese introduced and variation in the proportion of fluorine to chlorine results in alteration of the spectral composition of the emission, but the stability of the phosphor in lamps is not affected.

There were also carried out in the plant laboratory investigations of the influence on the brightness and stability of the phosphor of the total metal to phosphorus ratio. It was established that the phosphor characterized by greatest brightness and stability contains about 4.9 metal atoms per 3 phosphorus atoms.

As a result of the research there was developed an improved calcium halophosphate luminophor which was put into production and resulted in lamps with 10-20% higher efficiency (48 to 55 lu/w for a 40 watt lamp).

The aging of halophosphate luminophors in fluorescent lamps is connected with breakdown of the antimony centers. It was shown that the presence of a reducing agent in the gaseous medium in contact with the phosphor under the electric discharge conditions leads to weakening of the luminescence owing to reduction of the antimony. When the reduced antimony is oxidized, the luminescence brightness increases.

Such reducing agents as carbon monoxide, hydrogen and hydrogen-containing compounds (water and hydrocarbons) may seep into the tube in process of production or may be released from the coating if the binder is not completely eliminated in the baking operation. Hence there was carried out a careful analysis of the loss in brightness in the process of production.

The phosphor supplied by the "Krasnyi Khimik" Plant is a coarse-grain powder. To obtain a high quality coating it must be ground for preparing the suspension. In the process, as a result of triboquenching, and increase of scattering of ultraviolet by the very small particles, the luminescence brightness falls by approximately 15%. The next greatest loss in brightness - about 6% - is incurred in the operation of burning out the nitrocellulose binder; this occurs for two reasons: first, owing to incomplete burning out and partial carbonizing of the nitrocellulose, and, second, owing to oxidation of the phosphor when heated in contact with air to 500°. There is virtually no loss in brightness incident to sealing off of the lamps. In the operation of evacuation of the lamps, in heating of the phosphor coating without access of air there occurs carbonization of the remaining nitrocellulose, which results in an additional 1-3% loss in brightness. Thus the total decrease in brightness from the initial phosphor to the finished coating in the lamp amounts to 20-24%.

There was developed in our lamp laboratory a method of restoring the brightness of the ground halophosphate luminophor to 95-97% the initial value without substantial increase in grain size by reheating at 1100° for 15-30 min and subsequent treatment of the powder with a weak hydrochloric acid solution to remove the oxidized manganese from the surface of the crystals.

In order to reduce the segregation of harmful impurities in the lamps and enhance the stability of the light flux there was developed an improved procedure for burning out the nitrocellulose; this involves the use of oxygen and reducing the baking temperature. There was also developed a new technique for vacuum treatment of the lamps with continuous pumping and aging of the cathode by a high voltage discharge in mercury vapor.

The lamps fabricated by the new technology had a 2-3% higher efficiency and showed about half the loss in intensity after 3000 hours of operation: 10-14% loss instead of 20-30%.

As a result of all the above mentioned measures we were able to reduce the loss in brightness incident to production of the lamps to 8-10% and thus increase the efficiency of 40 watt lamps to 60-62 lu/w.

The general conclusions that may be drawn on the basis of the research carried out at the plant laboratory are the following: the stability of fluorescent lamps in operation is determined mainly by the production technology; the light output depends primarily on the quantum efficiency of the phosphor and the coefficient of absorption of ultraviolet by the coating.

The ratio of the visible light output (in photons) to the absorbed radiation, i.e., the quantum efficiency, for modern halophosphate phosphors is about 80%. It has been repeatedly noted that further efforts should be directed to developing luminophors with a higher quantum efficiency.

An extremely important factor where the ultraviolet absorption coefficient is concerned is the grain-size composition of the calcium halophosphate phosphor. According to recent data in the literature, it appears that one can obtain lamps with a light output of 75-80 lu/w merely by insuring the optimum grain-size composition of the phosphor and structure of the coating.[5,6] Obviously, research to this end is essential.

Despite the great amount of diversified research being carried out in different laboratories in the field of luminescence, there is virtually no work being done for the practical purpose of increasing the efficiency of fluorescent lamps.

It is imperative to take immediate measures to increase the number of investigations undertaken in scientific research institutes in the field of phosphors for light sources; it would also be desirable to set up new industrial laboratories at enterprises producing phosphors.

References

1. A.A.Bundel', B.I.Vainberg, T.S.Dobrolyubskaya, V.V.Zelinskii, F.M.Peckerman, R.G.Smirnova, A.K.Trofimov & S.P.Frenkel', Izv.AN SSSR, 15, 815 (1951).
2. W.L.Wanamaker, A.H.Hoekstra & M.G.A.Tak, Phil.Res.Rep., 10, 11 (1955).
3. G.R.Fonda, Brit.Appl.Phys., 6, Suppl.4 (1955).
4. M.Doherty & N.Harrison, Brit.Appl.Phys., 6, Suppl.4, 511 (1955).
5. J.L.Ouweltjes, Elektrizitätsverwertung, 1958.
6. K.H.Butler & H.H.Homer, Illum.Eng., 4, No.9, 556 (1959).

DISCUSSION

V.M.Skobelev: It must be admitted that, aside from the report presented by Troshenskii, we have not heard a single report at this Conference concerned with research in the field of lamp phosphors. Thus Troshenskii is justified in asserting that everything that has been accomplished in this field is the result of work at the Moscow Electric Lamp Plant. Scientists in other laboratories are remiss in neglecting the problem. The phosphors developed by the Moscow Electric Lamp Plant Laboratory yield lamps with an efficiency of 55 lu/w, whereas lamps produced abroad have a light output of 70-72 lu/w. This has apparently been achieved by controlling the grain-size composition. This is substantiated by the work of Levshin & Ryzhikov, which, unfortunately, has been carried out on zinc sulfide rather than lamp phosphors. One can, however, welcome the fact that they have developed a suitable experimental technique, and it is to be hoped that it will soon be applied to determining the optimum granulometric composition of calcium halophosphate. Important problems here are problems of technology; un-

fortunately, nobody is studying these problems and yet it will be recalled that the production of phosphors will soon reach hundreds of tons annually. I again call upon the participants in the Ninth Conference on Luminescence to turn their attention to the problems of lamp luminophors.

Ch.B.Lushchik: I want to give my vigorous support to Troshenskii in his call for expanding research on lamp phosphors. I feel that investigation of the physical processes occurring in lamp phosphors is not only of practical interest, but can also yield valuable information on the mechanism of luminescence.

I would like to call attention to the similarity between many characteristics of lamp phosphors and those of "ideal" alkali halide crystals activated by hydrogen-like ions. Groups working on lamp luminophors should carefully study the results obtained in research on alkali halide crystals. Of particular interest, in my opinion, is investigation of the topography of the physical processes occurring in lamp luminophors; this topography for sensitized luminescence is extremely complex.

D.P.Troshenskii: The assertion made by some workers of the VNICI (All-Union Scientific Research Institute of Lighting Engineering) that the loss in brightness of halophosphate luminophors in the process of coating lamps is 30% and in the process of vacuum treatment 20% is far from the truth.

As I noted in the report, there was carried out in the laboratory of the Moscow Electric Lamp Plant a careful analysis of the losses in brightness incurred in the process of preparation of the suspension and fabrication of lamps. It was found that as a result of grinding the luminescence brightness falls by about 15%. The next largest loss in brightness (about 6%) occurs in burning out the nitrocellulose binder. The loss during the operation of sealing off the tube is virtually nil, while the loss connected with the operation of evacuation amounts to 1-4%. Thus, the total loss in brightness from the initial luminophor to the final coating in the lamp amounts to only 20-25% and not 50% as was asserted by V.I.Dolgopolov and other workers of the VNICI.

I spoke of the reasons for the loss in brightness incident to grinding in my report. During the operation of burning out the nitrocellulose the loss in brightness occurs for two reasons: first, owing to incomplete burning out and partial carbonization of the nitrocellulose, and, second, owing to oxidation of the luminophor in the process of heating in air at about 500°. A slight further loss occurs during the operation of evacuation incident to heating of the coating without access of air as a result of carbonization of the remaining nitrocellulose.

As a result of various measures developed in the plant laboratory, namely, use of regenerated, i.e., heated after grinding, phosphor and improvement in the technique of burning out the nitrocellulose, the loss in brightness incident to production of lamps has been reduced to 8-10% and the light output of 40 watt lamps has been increased to 60-62 lu/w.

The workers of VNICI would be better advised to devote their efforts to developing practical measures aimed at further reduction of the loss in brightness in luminophors in the process of lamp production, measures that would result in lamps with a light yield of at least 80 lu/w.

Bulletin of the Academy of Sciences of the USSR - Physical Series
Vol. 25, No. 3 - March 1961

Transactions of the Ninth All-Union Conference on Luminescence (Crystal Phosphors)
(Continued from Vol. 25, No.1; to be continued in Vol. 25, No. 4)

TABLE OF CONTENTS

	Page Orig.	Trans.
Concerning excitation of crystal phosphors by ions - B.M.Nosenko & N.A.Strukov	314	303
Thermostimulated luminescence with different forms of excitation - B.M.Nosenko, L.S.Revzin, V.Ya.Yaskolko & A.R.Krasnaya	318	307
Single crystal cathodoluminescent screens - M.A.Vasil'eva, V.V.Kuprevich, P.P.Feofilov & I.V.Stepanov	321	311
Investigation of activatorless ZnS sublimate phosphors - E.Ya.Arapova	324	313
Some characteristics of zinc sulfide-selenide sublimate screens - V.V.Golubets	325	315
Luminescence properties of cerium activated aluminum oxide and helenite under cathode-ray excitation - T.V.Oranovskaya	327	317
Cathodoluminophors with very short persistence and emission in the blue, yellow and red regions - Z.I.Klabukova & A.V.Morozova	330	320
Cathodoluminescence of europium activated strontium phosphates - V.P.Nazarova	332	322
Comprehensive investigation of the optical and thermooptical properties of polyactivated alkali-halide crystal phosphors - A.Kh. Khalilov, E.Yu.Salaev, A.P.Mamedov, T.D.Alieva & F.K.Isaev	335	325
Origin of the long wavelength luminescence bands of alkali-halide phosphors - N.I.Ivanova, L.I.Tarasova & A.P.Zhukovskii	341	331
Sensitized luminescence of KCl:Pb:Mn phosphor - K.K.Shvarts & G.K.Vale	343	333
Concentration and temperature quenching of luminescence in some silver activated alkali-halide phosphors - L.A.Rebane	345	335
Luminescence of ammonium halide phosphors - A.Ya.Pae & L.Ya.Uibo	347	337
Detection of lattice defects in alkali-halide crystals by means of electrolytic coloring - V.M.Bezruchko & A.A.Shatalov	349	339
Structural defects in crystal phosphors - L.M.Shamovskii & A.S.Shibanov	351	341

Decoration of dislocations and activator distribution in unstable alkali-halide phosphors - R.I.Gindina 354 344

Electron diffraction study of the influence of gases on the structure of sublimated layers of alkali-halide salts - A.A.Khaav 356 346

Kinetics of the luminescence of phosphors with several types of traps - V.V.Antonov-Romanovskii 357 348

Effect of the size of natural and crushed crystals on the luminescence of zinc sulfide phosphors - V.L.Levshin & B.D.Ryzhikov 362 353

Kinetics of the luminescence of ZnS:Cu with excitation by alpha-particles and short light pulses - T.P.Belikova & M.D.Galanin 364 355

Effect of hydrostatic compression on the spectral characteristics of alkali-halide phosphors - Ya.Ya.Kirs & A.I.Laisaar 366 357

Investigation of photoelectric polarization of zinc sulfide phosphors - I.K.Vitol & I.A.Tale 368 359

Dielectric changes in ZnS:Cu:Fe phosphor during thermostimulation - P.E.Ramazanov 370 361

Temperature dependence of the roentgenoluminescence and dark conductivity of Yakutsk diamonds - K.N.Pogodaev & E.S.Vilutis 373 364

Luminescence of thallium chloride single crystals - N.A.Tolstoi & V.A.Sokolov 375 366

Concerning the mechanism of excitation and de-excitation of recombination luminescence of alkali-halide phosphors - Ya.A.Valbis, I.K. Vitol & V.E.Zirap 377 368

Investigation of the efficiency of recombination luminescence of alkali-halide phosphors - I.V.Yaek 379 370

Photo- and thermostimulated electron emission from alkali-halide phosphors excited by ultraviolet radiation - A.I.Belkind & Kh.F.Kyaembre 381 371

Investigation of optical dissociation of F centers in alkali-halide crystals - I.A.Parfianovich & E.I.Shuraleva 383 373

Optical properties of alkali-halide crystals doped with O, S, Se and Te - O.A.Shmits & Yu.R.Zakis 385 375

Interaction of activators in alkali-halide phosphors - A.T.Khlevnyuk 386 377

Effect of different gases on the formation of luminescence centers in silver halide - S.I.Golub & N.A.Orlovskaya 388 379

Luminescence of alkali-halide phosphors activated by antimony trichloride - A.S.Andrianov & M.L.Kats 390 381

Investigation of the effect of double activation by silver and samarium on trapping levels in and the luminescence of zinc sulfide phosphors - V.L.Levshin, Yu.V.Voronov, V.B.Gutan, S.A.Fridman & V.V.Shaenko 392 383

Flare-up of ZnS phosphors and competition of the luminescence bands - N.A.Tolstoi, A.M.Tkachuk, V.A.Sokolov, A.V.Burlakov, A.I.Ryskin, Z.S.Mansurova & M.V.Epifanov 399 389

Characteristics of cathodoluminescence at high excitation densities - Yu.M.Popov 405 395

Effect of the chemical nature of the flux on the luminescence properties of zinc sulfide and zinc-cadmium sulfide phosphors - A.A.Bundel', A.A.Glagoleva, Z.I.Guretskaya, O.A.Danilevskaya, Dou Nai-khua & L.N.Sokolova 408 398

Concerning the influence of flux on the optical properties of zinc sulfide phosphors - A.M.Gurvich 411 400

Influence of fluxes on the properties of electroluminophors - M.A. Berchenko 415 404

Effect of high pressures on the formation of crystal phosphors and their properties - S.I.Kunenkov 419 408

Spectroscopic analysis of some luminescence-pure materials and luminophors - L.A.Dvorzhetskaya, L.Ya.Khlebnikova & M.K.Shvaneva 422 410

On the question of radical-recombination luminescence of crystal phosphors - V.A.Sokolov & A.N.Gorban' 424 412

Recombination luminescence of Sn^{4+} in aqueous solutions of LiCl and HCl at low temperature - M.U.Belyi, B.A.Okhrimenko & B.F.Rud'ko 426 414

Correlation between the thermal activation energy for conductivity and the absorption and phosphorescence spectra of some organic substances - A.T.Vartanyan & L.D.Rozenshtein 428 416

Excitation wavelength dependence of the blue luminescence yield of cadmium sulfide crystals at 20°K - V.L.Broude & V.S.Medvedev 430 419

Luminescence of Se activated cadmium iodide - I.P.Shapiro 434 422

Improvement of phosphors for light sources - R.A.Nilender & D.P. Troshenskii 435 424

Translated in 1962 by
Columbia Technical Translations
5 Vermont Ave., White Plains, N.Y.

Transactions

of the

Ninth All-Union Conference on Luminescence (Crystal Phosphors)

(Kiev, 20 - 25 June 1960)

(Continued from Vol.25, Nos. 1 & 3)

Lithographed in U.S.A. by
EDWARDS BROTHERS, INC.
Ann Arbor, Michigan

DIFFERENT TYPES OF PHOSPHOR CRYSTALLOCHEMICAL SYSTEMS AND THEIR LUMINESCENCE PROPERTIES

- M.A.Konstantinova-Shlezinger

We classify the crystal structure of phosphors into groups on the basis of the conjunction of structural properties that have the strongest effect on the luminescence characteristics, and then compare the luminescence properties peculiar to each phosphor grouping.

We consider the following properties of the crystal structures: the lattice energy and the character of the atomic (ionic) bonds; the melting temperature, which is related to the lattice energy; the readiness with which there form defects; thermal and biographic vacant sites[1] (i.e., vacant sites that are in equilibrium at high temperatures but that persist at room temperature only in the "frozen" state, and such vacant sites as form incident to replacement of the host ions by ions of different valence and persist in the equilibrium state even at absolute zero); the electric conductivity (in the absence of measured mobility values or similar quantitative indices we can only compare the conductivity values of different systems only qualitatively on the basis of indirect data[2]); interaction with a gaseous medium (the chemical stability or more accurately the degree of inertness as regards oxygen, usually present in heating); the absorption region, which to some extent allows of judging of the energy necessary for ejection of electrons from the valence band and production of holes.

In the classification of crystal phosphors on the basis of the enumerated properties there stands out with great distinctness one group, the group of ionic crystals of alkali halide salts, i.e., of binary compounds of ions with the structure of an inert gas. It is characterized by exceptionally low values of lattice energy (230 to 138 kcal/mole) and great readiness to form vacancies. As Schottky[3] and later Mott & Gurney[4] showed, the number n of Schottky defects is related to the lattice energy W by the exponential expression

$$n = B\gamma N e^{-\frac{W}{kT}},$$

where N is the total number of sites, and B and γ are correction factors taking into account the variation in the frequency of oscillation of the ions about the vacant site and the variation in energy connected with changes in volume owing to formation of vacant sites.

This group of crystalline compounds, characterized by minimal lattice energy values, also, naturally, occupies a special place as regards ease of formation of vacant sites both thermal and biographic. The conductivity of members of this group is ionic; the absorption lies in the far ultraviolet.

Crystal phosphors in the alkali halide class are characterized by the formation of F and other centers and the ability to be activated by many different elements: Ga, In, Tl, Mn, Sn, Pb, Ag and others. The electronic structure of free ions is evinced in the luminescence spectra of these phosphors, so that we can attempt to interpret the electronic structure of the luminescence centers by comparison with the spectro-energetic characteristics of the ions.[5]

The enumerated distinctive features of the crystal phosphors in this group are intimately related with the specific characteristics of their crystal structure.

In all other structural groups we have ionic-covalent bonds (with predominance of one or the other), higher lattice energies and high melting points.

The second group in our classification comprises structures of compounds with strongly electronegative anions and doubly or higher charged cations that

are not transition elements. This group includes the oxides of the rare earth elements, Ca, Sr, and Ba, magnesium oxide, aluminum oxide, some spinels, the fluorides of these metals, and certain other compounds. The lattice energy of compounds in this group is some 3-4 times greater than in the first group.

Theoretical calculations of the fraction of equilibrium Schottky defects have been carried out only for alkali halide salts. Nevertheless, it may be asserted that in view of the high lattice energy values characteristic of crystals of the second group, the fraction of Schottky defects should be infinitely small. The conductivity of crystals in this group is low. The absorption lies in the ultraviolet region.

In a number of cases at low temperatures the luminescence bands split into narrow bands, reflecting lattice vibrations. This was observed by Ewles[6] for pure calcium oxide and a number of other phosphors. Tunitskaya[7], in investigating CaO:Bi, showed that the spectrum represents a superposition of lattice vibrations on electronic transitions. Such superposition is also observed, as will be shown below, in the case of other crystal phosphors characterized by high lattice energies, but their crystal structures in view of a number of other indications must be placed in a different group. It is interesting to note that one elementary substance, namely, diamond, is distinguished by an exceptionally high lattice energy and high melting point; the luminescence spectrum of diamond consists of equidistant bands associated with lattice vibrations.

Into the next group we put crystal structures in which, with a high lattice energy, the ions are weakly electronegative, so that the bonding is predominantly covalent. Typical compounds in this group are sulfides and selenides. The lattice energies and melting points of these compounds are exceptionally high. The sulfides of transition elements, zinc and cadmium, sublimate at temperatures much lower than the melting point. Consequently, the bonds in the surface layer are weakened to a greater extent than usual, so that formation of vacant sites is greatly facilitated.

The compounds in this group readily interact with the oxygen of the atmosphere. Their absorption lies in the long wavelength ultraviolet. The crystal phosphors formed by these compounds are characterized by reproducibility; they readily undergo different microreactions. As a result and also owing to the presence of vacant sites in the neighborhood of the activator a number of different bands, i.e., different emission spectra, may be observed for the same activator. As Trapeznikova showed, this applies even to Sm in zinc sulfide.

The luminescence yield of crystal phosphors in this group is not a linear function of the excitation intensity. Many of the phosphors in this group are characterized by a persistent afterglow, i.e., store large light sums. Some luminophors in this group, as for example, CaS:Bi investigated by Tunitskaya[7], yield luminescence spectra in which lattice vibrations are clearly evinced.

We now turn to crystal structures, which like those of compounds in our second and third groups, have high lattice energies, but in distinction to these have bonds of at least two types. These are heterodesmic crystals: silicates, phosphates, tungstates, sulfates, etc.

It must be noted that in these compounds the melting point corresponds in many cases to rupture of only the weakest bonds. Thus, it has been shown by x-ray diffraction studies that in some silicates the SiO_4 tetrahedra persists in the melt. This must be taken into account in evaluating the lattice energy on the basis of the melting point (850 to 2000°). The formation of thermal vacancies in these compounds is hindered not only by the high bond energies but also by the difficulty of ejecting the anions.

We can illustrate the above in the specific case of zinc silicate. In its

structure the SiO_4 tetrahedra are linked by zinc ions. Each oxygen is strongly bound to a silicon (this bond is reported to be 50% covalent) and, in addition, is linked to two zinc atoms. Each zinc atom is surrounded by four oxygen atoms, each of which enters into the oxygen tetrahedron. The principle of electronegativity requires that simultaneously with formation of a vacant zinc site there form a vacant anionic site; yet in melting, the silicon-oxygen tetrahedra remain unaffected, i.e., the oxygens do not break away from the silicon atom. Displacement of the zinc ion to an interstitial site, i.e., formation of Frenkel defects, appears to be little probable. As Schottky showed, the formation of these defects is possible in case of equivalence of the energy of ejection of the cation from its site and its lodging at an interstitial site, as occurs, for instance, in lattices with large anions, for example, in silver bromide.[9] At present we can adduce only the above general arguments, for there have been no precise calculations of the energies involved. The conductivity of crystals in this group is low. The width of the energy gap is large; the crystals absorb in the far ultraviolet. These compounds are stable, and do not normally undergo microreactions when heated in air. The crystal phosphors of this group are readily reproducible.

Within the same crystal modification the spectrum is constant, i.e., the activator forms only one type of luminescence centers. There are only a few suitable activators for each structure; for example, the sole activators for zinc silicate are Mn and possibly Ti. There have been described luminophors the luminescence spectra of which consist of individual bands and reflect lattice vibrations; such, for example, is magnesium arsenate with manganese.

Thus in each group of crystal structures classified according to the above mentioned conjunction of properties we find crystal phosphors exhibiting common luminescence properties. These properties are determined primarily by the crystal lattice rather than by the activator.

As an interesting fact, we note that comparison of the cathodoluminescence properties of crystal phosphors in the different groups shows that compounds of the third group - sulfides - have the highest electric conductivity; cathodoluminophors of this group exhibit a cathodoluminescence efficiency attaining 25%.[10]

Also sometimes used for practical purposes are compounds of the fourth group with heterodesmic structure; however, the quantum efficiency of these luminophors does not exceed 8.5% (this is the value for zinc silicate:Mn; the efficiency of other phosphors in this group is even lower).[10]

References

1. A.Rees, Chemistry of Crystals with Defects (Trans.M., 1956.).

2. H.Gobrecht, D.Hahn & H.J.Kossel, Z.Phys., 136, H.1, 57 (1953); A.F.Ioffe, Fizika poluprovodnikov (Physics of semiconductors), M.-L., 1957; E.Fervein, in "Poluprovodnikovye materialy" (Collected articles on semiconductor materials), M., 1954.

3. W.Schottky, Z.Phys.Chem., 29, 335 (1935).

4. K.Hauffe, Reakionen in und an festen Stoffen, Berlin, 1955; C.Kittel, Introduction to Solid State Physics, N.Y., 1953 (Cited in Russian trans.).

5. N.E.Lushchik & Ch.B.Lushchik, Trudy, IFA AN ESSR (Proceedings, Inst.of Physics and Astronomy of the Estonian Ac.of Sci.), 6, 5 (1957).

6. J.Ewles, Proc.Roy.Soc.A. 167, 94 (1938).

7. V.F.Tunitskaya, Thesis, Physical Inst., USSR Ac.of Sci., 1954.

8. V.L.Levshin, Fotolyuminestsentsiya zhidkikh i tverdykh veshchestv (Photoluminescence of liquids and solids), M., 1951.

9. H.Schmalzried, Z.Phys.Chem., 22, H.3-4, 199 (1959).

10. F.A.Kröger, Ergebnisse der exakten Naturwissenschaften, S.111, Berlin, 1956.

11. A.Classens & A.Brill, Invited Lecture, Eindhoven, Extrait de Optica, Vol.5, Numero special, 1958.

* * * * * * *

THERMODYNAMICS OF THE MECHANISM OF ACTIVATION OF SULFIDE AND SULFIDE-SELENIDE PHOSPHORS

- A.A.Bundel', Z.I.Guretskaya & L.B.Taushkanova

The present communication is devoted to comparison of experimental data with the deductions following from general thermodynamic considerations. We have pointed out earlier that to produce a luminophor it is sufficient to bring into contact at a sufficiently high temperature an appropriately formed crystal of the base material with an activator taken in the elemental state. The formation of luminescence centers occurs incident to penetration of the neutral activator atoms into the crystal.

In order to check this, crystals of previously formed self-activated zinc sulfide luminophors were exposed at 950° to molecular beams of cadmium, mercury, phosphorus, selenium and tellurium. The resultant specimens yielded luminescence spectra with new bands characteristic of the introduced elements.[1]

These experiments substantiated our assertion. They could not, however, yield results suitable for thermodynamic consideration owing to the presence of concentration and temperature gradients in the experimental system.

In the luminophor preparation procedure, i.e., introduction of an activator salt into the initial batch, there immediately forms the sulfide of the activator. At the usual heating temperatures the activator sulfides undergo thermal dissociation with the formation of neutral atoms.

Of great interest is elucidation of the mechanism of self-activation of zinc (and cadmium) sulfide and selenide phosphors. Earlier we showed that to obtain self-activated ZnS it is sufficient to heat pure ZnS in a closed space devoid of temperature gradients to a temperature high enough to insure a reasonably high rate of diffusion in the solid phase. From the thermodynamic standpoint there must occur the following processes:

1. Transformation of part of the sulfide to the vapor state to attainment of saturated vapor pressure of ZnS molecules in the system.

2. Dissociation of the sulfide in the gaseous state according to the formula

$$ZnS_{vap} \rightleftarrows Zn_{vap} + S_{vap},\ K_{ZnS} = \frac{p_{Zn}\, p_S}{p_{ZnS}}.$$

Inasmuch as at the same time there occurs association of the sulfur atoms into sulfur molecules, one can with fair approximation describe the process of dissociation by the formula

$$2ZnS_{vap} \rightleftarrows 2Zn_{vap} + S_{2vap},\ K_{ZnS} = \frac{p_{Zn}^2\, p_{S_2}}{p_{ZnS}^2}.$$

3. The neutral dissociation products must be distributed between the gaseous phase and the crystal; upon attainment of equilibrium there must obtain the relations:

$$C_{Zn}^{n_{Zn}} = L_{Zn}\, p_{Zn} \text{ and } C_S^{n_{S_2}} = L_{S_2}\, p_{S_2},$$

where the C are the concentrations of the indicated elements in the crystal, the L are the coefficients of distribution, and n_{Zn} and n_S are factors indicating the number of particles forming in the crystal incident to penetration into it of one particle from the gaseous phase.

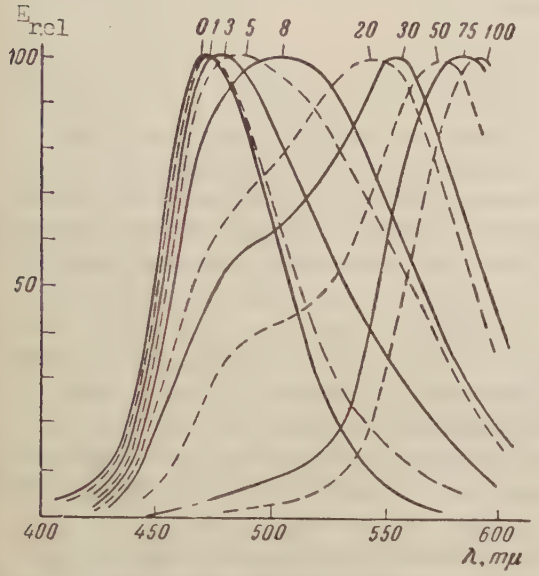

Fig.1. Luminescence spectra of ZnS·ZnSe at -196°. The figures at the curves indicate the percent by weight of ZnSe in the phosphor.

At each temperature, assuming equilibrium is attained, there must exist in the crystal certain definite concentrations of neutral zinc and sulfur atoms. If, as we hypothesized, neutral atoms result in the formation of luminescence centers, then in the spectrum of self-activated zinc sulfide, in addition to the zinc band, there must be present a band due to sulfur. However, hitherto, there has been no convincing proof of this.[2]

Recently we succeeded in realizing introduction of sulfur under controlled conditions; the brightness of the sulfur band in the luminescence spectra of the samples is comparable to the brightness of the bands of zinc and other common activators. The sulfur was introduced into the system by heating ZnS, de-oxidized beforehand by heating in H_2S and in NH_3, with 1% NaCl and sulfur in tubes sealed under vacuum. After heating at temperatures of 1050° and higher there appears in the luminescence spectrum a new band peaking at 590 mμ.[3] The brightness of this sulfur band increases with increase of the sulfur vapor pressure. Complete suppression of the zinc band occurs at p_{S_2} = 40 atm.

Thus the results of these experiments are in accord with the above mentioned thermodynamic requirements. The reason why the sulfur band is not observed under the usual conditions of preparation of self-activated phosphors is the great difference between the values of the zinc and sulfur distribution coefficients L_{Zn} and L_S; an additional reason is the strong variation of L_S with temperature. The value of L_{Zn} can be evaluated on the basis of the estimate of C_{Zn} given by Brill and the data of Pogorelov on the vapor pressure of zinc in the products of dissociation of ZnS. Evaluations yield $L_{Zn} \approx 10^{-2}$. L_S can be evaluated only approximately[4]; it appears to be of the order of 10^{-4} at 1100° and varies greatly with temperature. The last has a simple explanation: L_S, as any equilibrium constant, is a function of the temperature: $\frac{dL}{d\tau} = \frac{Q_S}{RT^2}$, where Q is the thermal effect of solution in the solid phase. Inasmuch as the zinc vapor is monatomic, the total thermal effect can be regarded as consisting of two components:

$$Q_{Zn} = \lambda_{Zn} + Q'_{Zn},$$

where λ_{Zn} is the heat of condensation of zinc vapor, and Q'_{Zn} is the heat of reaction with the lattice.

In the case of sulfur, in addition to the above two components, one must add a third:

$$Q_S = \lambda_S + Q'_S + Q_{dis},$$

where Q_{dis} is the heat of dissociation of the S_2 molecules into atoms. Inasmuch as this is always an appreciable quantity, we have

$$Q_S \gg Q_{Zn} \quad \text{and} \quad \frac{dL_S}{d\tau} \gg \frac{dL_{Zn}}{d\tau}.$$

More convenient for checking the validity of the proposed concept are the self-activated phosphors of the series Zn(S,Se). We carried out a detailed investigation of the spectra of a number of compositions at different excitation intensities and in the temperature range from -196° to 120° and also of the phosphorescence spectra with a view to detecting the band of selenium in pure form and determining the variation in the intensity of the zinc band with increase of the ZnSe content. Some of the results are shown in Fig.1.

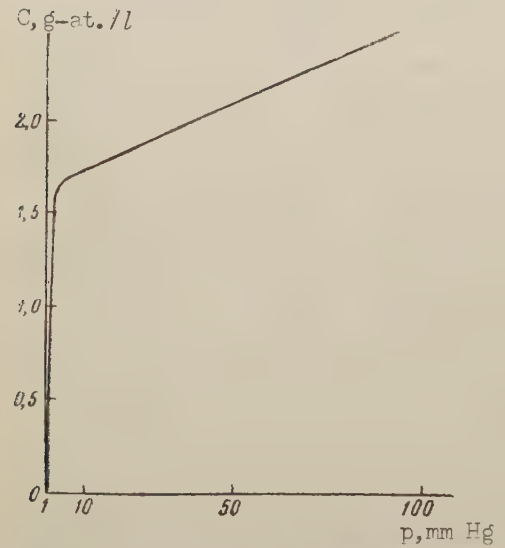

Fig.2. Variation of the selenium concentration in the phosphor with the Se pressure in the gaseous phase.

As will be evident from the figure, the zinc band is present, although in very weak form, in the spectrum of pure ZnS. Thus the requirements for the dissociation mechanism of self-activation are substantiated in this case as well.

The ease with which ZnS is activated by selenium enabled us to determine directly the selenium distribution coefficient L_{Se}. Self-activated ZnS, prepared by heating at 950°, was exposed in sealed tubes at 950° to selenium vapor at different pressures to attainment of equilibrium. The time to equilibrium varied from 5 to 30 hrs depending on p_{Se}.

The resultant specimens were analyzed for Se and we recorded their luminescence spectra. The band of selenium was observed in each spectrum. The position of the band peak is close to its position in the spectra of phosphors obtained by heating ZnS + ZnSe and ZnS + SeO_2 with the same selenium concentration.

The variation of C_{Se} with p_{Se} is shown in Fig.2. It will be seen that the curve has two different sections: a steep section corresponding to the p_{Se} range from 10^{-3} to 1 mm Hg and a flatter section corresponding to the range from 1 to 87 mm Hg. This indicates that the mechanisms of incorporation of Se differ at high and low vapor pressures. In Fig.3 we show the initial section of the curve to an enlarged scale. For determining the values of the exponent n^{Se}, the values of C are plotted as a function of $\sqrt[m]{p}$ for three different values of m. It will be seen that the curve becomes a straight line for $m = n^{Se} = 4$. This means that in the process of incorporation of the selenium into a crystal there form four particles from each Se_2 molecule. A similar relationship was established earlier

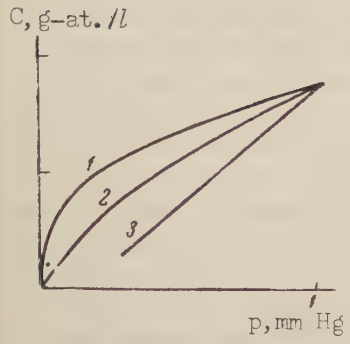

Fig.3. Variation of the selenium concentration in the phosphor with the Se pressure in the gaseous phase in the range $p_{Se} \leqslant 1$ mm Hg: 1) $C = f(p^1)$, 2) $C = f(p^{1/2})$, 3) $C = f(p^{1/4})$.

for the intrusion of O_2 into ZnO. This indicates that the process of incorporation of selenium can be described by the equation

$$Se_{2\,gas} + \boxed{Lattice} \longrightarrow 2\boxed{Se}_a + 2\boxed{\ }_k$$

Thus it must be inferred that the selenium atoms are lodged at anionic sites with formation of positive holes and cationic vacancies. This inference was substantiated by determination of the sign of the current carriers by the method of Ryvkin. With excitation by light with λ = 400 to 450 mμ there obtains n-type conductivity, while with excitation by wavelengths from 500 to 1000 mμ, p-type conductivity predominates. For the section of the $C_{Se} = f(p_{Se})$ curve corresponding to large p_{Se} best results are obtained for $n^{Se} = 2$, which corresponds to the reaction

$$2ZnS + Se_2 \rightarrow 2ZnSe + S_2.$$

Thus introduction of selenium into ZnS in the range of low Se vapor pressures appears to be primarily a process of solution. Only at high pressures and, accordingly, large C_{Se} does there begin to predominate chemical reaction of the atomic selenium with the S^{2-} ions. In the process the sulfur is expelled from the crystal, while the Se atoms are inactivated and enter into the composition of the host material.

Further substantiation of the proposed dissociation mechanism of activation is the possibility of quantitative explanation from this standpoint of the great differences in concentration at which the zinc band is suppressed by different activators. The observed difference in the effectiveness of different activators in zinc sulfide is determined by the values of the pressure of dissociation of their sulfides and the solubility of the activator sulfide in zinc sulfide.

In the case of unlimited solubility the effectiveness of the activator is determined only by its dissociation pressure. Analysis of this question and comparison of the results of analysis with experimental data will be found in Ref.5.

Thus on the assumption that activation is realized through intrusion of neutral atoms into the crystal, simple thermodynamic consideration allows of explaining a number of the important relationships obtaining between the spectral composition of luminescence and the conditions of synthesis of phosphors.

References

1. A.A.Bundel', Trudy, Mosk.khim.-tekhnol.in-ta (Proceedings, Moscow Chem-Tech.Inst.), No.31, 8 (1960).

2. A.A.Bundel' Thesis, Moscow State University, 1956.

3. A.A.Bundel' & L.B.Taushkanova, Trudy, Gos.in-ta prikl.khimii (Proceedings, State Inst.of Appl.Chem.), 43, 120 (1960).

4. A.A.Bundel' & L.B.Taushkanova, Ibid., 1961.

5. A.A.Bundel', Trudy Mosk.khim.-tekhnol.in-ta., 31, 3 (1960).

DISCUSSION

A.M.Gurvich: In my opinion thermodynamic analysis of the formation of crystal phosphors is an extremely promising approach to investigation of phosphors, for it is one of the ways in which one can avoid the purely empirical approach to the chemistry of phosphors. Although I am strongly in favor of this approach, I want to note a number of specific shortcomings in the actual investigation.

1. The authors of the report consider their phosphor system as consisting only of sulfides and the products of their dissociation. This simplification is probably inapplicable inasmuch as heating of sulfides alone, as a rule, yields poor phosphors. Under normal conditions of synthesis of sulfide phosphors there are also present in the system flux, oxygen and other ingredients, instrumental in the appearance of luminescence. In the process of synthesis there occur different chemical reactions (see our report), compared with which the dissociation of ZnS plays a secondary role.

2. The conclusion given in the abstract of the report to the effect that "the ability of self-activated phosphors to luminesce is the result of appearance of neutral atoms in the host lattice" does not follow from the thermodynamic arguments set forth in the report itself.

3. The optimum concentration of an activator whose sulfide is poorly soluble in ZnS is appreciably lower than the optimum concentration of an activator forming a sulfide readily soluble in ZnS. To explain this, Bundel' invokes the hypothesis according to which the activator is incorporated into the ZnS lattice in the form of atoms, and then carries out his thermodynamic analysis on the basis of this hypothesis (this part of the work was published in the Proceedings of the Moscow Chemical-Technological Institute, No.31, 1960). But this experimental fact can be more easily and simply explained if it is assumed that the activator enters into the lattice in ionic form (see the article of N.I.Ivanova cited in our report, and the report of M.A.Konstantinova-Shlezinger presented at the Fifth Conference on Luminescence).

* * * * * * *

INFLUENCE OF OXYGEN ON THE LUMINESCENCE PROPERTIES OF ACTIVATORLESS ZINC SELENIDE

- L.Ya.Markovskii & R.I.Smirnova

The luminescence of zinc selenide was first investigated by Leverenz[1,2] who gives the spectral distribution curves for phosphors synthesized at 780° with 2% NaCl without activator (λ_{max} = 643 mμ) and with silver (λ_{max} = 570 mμ), copper (λ_{max} = 650 mμ) and manganese (λ_{max} = 650 mμ). Larach[3] gives somewhat different values for λ_{max} for the spectral-distribution curves of ZnSe and shows that use of a flux and introduction of trivalent cations results in a significant shift of the spectral distribution curves. He infers that activatorless zinc selenide actually has two luminescence bands peaking at 637 and 602 mμ. Blazhnova[4], in her report, lists slightly different data on the luminescence of zinc selenide. The divergences between the results of different authors suggests that the luminescence of ZnSe depends to some extent on the method of preparation of the phosphor. In particular, it was shown in our report[5], presented at the Seventh All-Union Conference on Luminescence, that the presence of oxides in zinc selenide

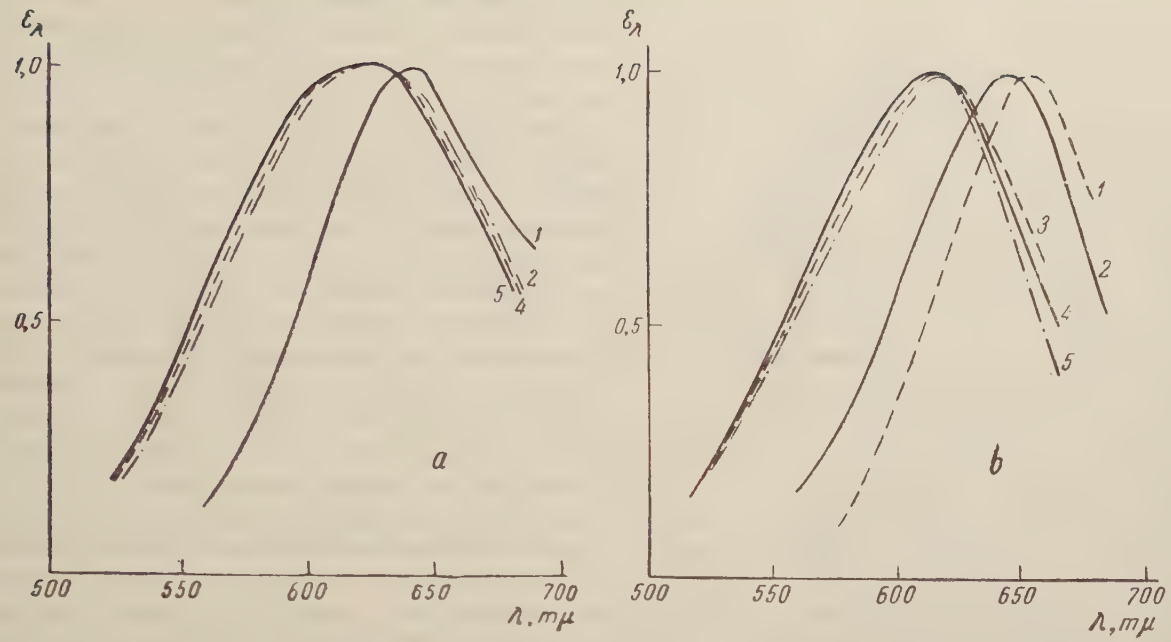

Fig.1. Spectral distribution curves of the emission of oxygen-free zinc selenide specimens and specimens subjected to different degrees of oxidation in the process of synthesis: a - CR excitation, b - photoexcitation, λ = 365 mμ: 1 - ZnSe without ZnO, 2 - 0.5% ZnO, 3 - 2% ZnO, 5 - 10% ZnO.

shifts the spectral distribution curve to the side of shorter wavelengths. In view of the great practical importance of this phosphor, we felt it would be of interest to investigate in detail the luminescence properties of pure, activator-less zinc selenide and to determine the effect of oxygen on its behavior.

Recognizing the fact that none of the commonly employed synthesis procedures for zinc selenide (hydrogen selenide[6], seleno-sulfate[6] and zinc-sulfide-selenite[7]) insures obtaining zinc selenide entirely free of oxygen impurity, we employed synthesis from the elements for obtaining our experimental raw material. The synthesis was carried out in the gaseoue phase at 950° under static conditions in an atmosphere of purified nitrogen and 20% hydrogen following a procedure similar to that described by Pashenkin et al[8]. There was obtained stoichiometric ZnSe, which according to the data of chemical analysis, contained no oxygen and had a cubic lattice with a = 5.657 kX.

Then by admission of metered quantities of air into the reaction space there were obtained under the same conditions specimens containing different amounts of oxygen. The photo- and cathodoluminescence spectra of oxygen-free and oxygen-containing specimens of zinc selenide are shown in Fig.1.

The cathodoluminescence spectra were recorded in a demountable electron beam tube with sweep (modulated) excitation with V_a = 9 kv and I_a = 2 μa/cm^2; the radiation was detected by an FEU-22 photomultiplier. The resultant data show that the presence of even 0.5% oxide is sufficient to produce a noticeable displacement of the peak of the spectral distribution curve to the short wavelength side. Further increase of the oxide concentration from 2-4 to 10% ZnO has no noticeable effect on the spectral distribution curves. For these curves λ_{max} = 615 mμ, i.e., they are shifted 30 mμ to the short wavelength side compared to the curve for

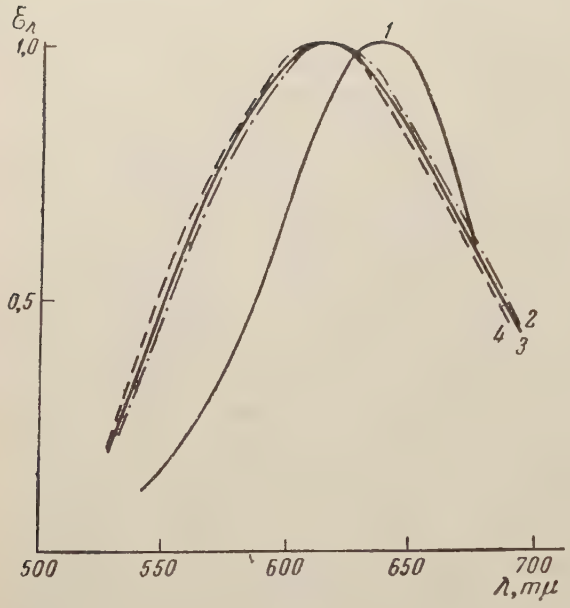

Fig.2. Variation of the spectral distribution of the emission of zinc selenide with the degree of oxidation (CR excitation): 1 - ZnSe without ZnO, 2 - 0.5% ZnO, 3 - 10% ZnO, 4 - 20% ZnO.

oxide-free zinc selenide.

Similar results were obtained when the initial oxygen-free zinc selenide was oxidized by heating at 900° in air. As will be evident from Fig.2, the spectral distribution curves for specimens containing 0.5, 10 and 20% ZnO are shifted 25-30 mμ to the side of shorter wavelengths. Complete oxidation of zinc selenide in air yields the earlier described[9] phosphor ZnO:Se with λ_{max} = 610 mμ, a value close to λ_{max} for oxidized zinc selenide specimens. However, the short wavelength branch of this phosphor is shifted to the left. Hence it will be evident that when zinc selenide is oxidized to an appreciable degree, i.e., contains substantial quantities of ZnO, there is superimposed on the spectrum of activatorless ZnSe the emission spectrum of ZnO:Se, as a result of which the short wavelength branch of the spectral-distribution curve is displaced upward. The curves of Fig.3, which were recorded at different temperatures (20 and -70°) show that reduction in temperature does not result in "resolution" of the spectral distribution curves: λ_{max} is shifted 20 mμ to the left both for oxidized and for oxygen-free ZnSe specimens.

In Fig.4 we give the spectral distribution curves of the emission of commercial zinc selenide specimens synthesized by the zinc-sulfide-selenite procedure and heated in nitrogen at 850°. As was shown earlier[7], this preparation procedure leads to the formation of appreciable quantities of zinc oxide, which, naturally, shifts λ_{max} to 615-620 mμ; it must also be noted that heating of these specimens

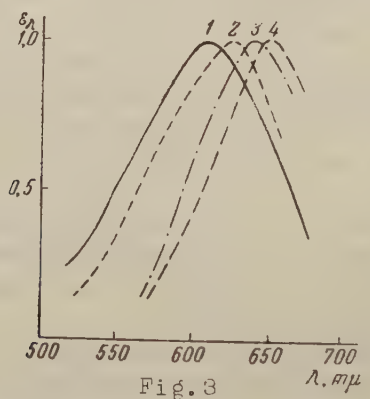

Fig.3

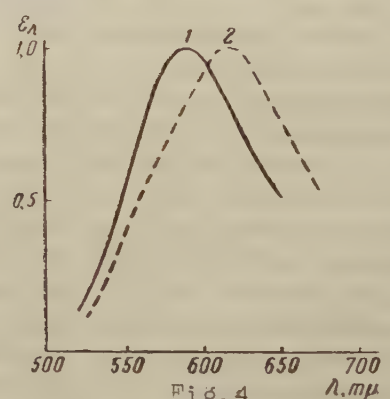

Fig.4

Fig.3. Spectral distribution curves for oxygen-free and oxidized specimens of zinc selenide recorded at different temperatures (photoexcitation): 1 - ZnSe + 1.5% ZnO (-70°), 2 - ZnSe + 1.5% ZnO (20°), 3 - ZnSe without ZnO (-70°), 4 - ZnSe without ZnO (20°).

Fig.4. Spectral distribution curves for specimens of commercial zinc selenide (CR excitation): 1 - 2% NaCl, 2 - prepared without flux.

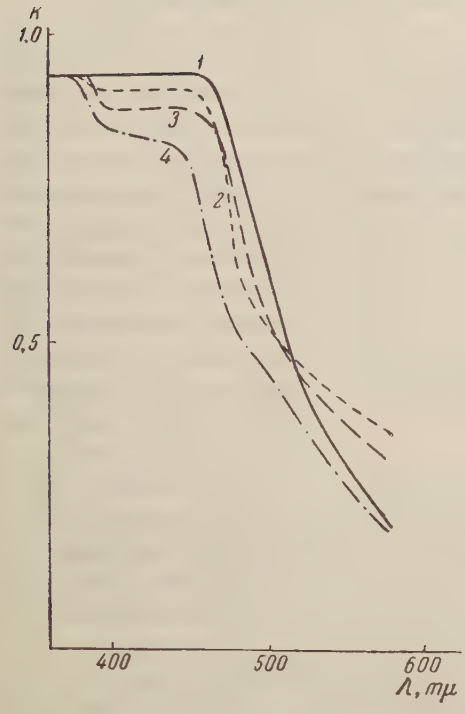

Fig.5. Absorption spectra of zinc selenide with different zinc oxide concentrations: 1 - ZnSe without ZnO, 2 - 4% ZnO, 3 - 10% ZnO, 4 - ZnO:Se.

with flux (2% NaCl) leads to further shift of λ_{max} to 590-600 mμ.

Thus our experimental data clearly demonstrate the role of oxygen in the luminescence of activatorless zinc selenide. The absorption spectra of ZnSe specimens with different amounts of ZnO are compared with the absorption spectrum of ZnO:Se phosphor in Fig.5. It will be seen that with increase of the ZnO content the absorption in the short wavelength region decreases significantly. As follows from the results of x-ray diffraction studies carried out by Kondrashev, in the process of oxidation of ZnSe there form ZnSe-ZnO substitutional solid solutions with resultant contraction of the lattice.

On the basis of the data obtained by Kondrashev it may be asserted that approximately 1-1.5% ZnO dissolves in ZnSe; at higher oxide concentrations the ZnO is evinced in the diffraction patterns in the form of a separate phase. Thus one can correlate the variation in the luminescence properties of zinc sulfide in the process of oxidation with the formation of a new phase: ZnSe-ZnO solid solution. It may, therefore, safely be assumed that the differences between the luminescence characteristics of activatorless zinc sulfide reported by different authors are connected with differences in the degree of oxidation of the specimens studied.

We desire to express our gratitude to Yu.D. Kondrashev for measuring the lattice parameters of the zinc selenide specimens and to thank M.Z.Aleksandrova for assistance in preparing and analyzing the specimens.

References

1. H.W.Leverenz, E.J.Wood, R.E.Shrader & S.Lasof, "Zinc:Cadmium-Sulphide:Selenide Phosphors" in Preparation and Characteristics of Luminescence Materials, N.Y., 1948.

2. H.W.Leverenz, An Introduction to Luminescence of Solids, p.200, N.Y.,1950.

3. S.Larach, J.Chem.Phys., 21, 756 (1953).

4. E.I.Blazhnova, Transactions of the Seventh All-Union Conference on Luminescence, Tartu, 1958.

5. L.Ya.Markovskii & R.I.Smirnova, Izv.AN SSSR, Ser.fiz., 23, 1341 (1959). (Trans.Bulletin, 23, 1327.)

6. G.S.Klebanov & E.I.Kochugova, Sbornik referatov GIPKh po khimii i tekhnologii lyuminoforov (Collection of reports of the State Institue of Applied Chemistry on the Chemistry and Technology of Phosphors), 1955-1956.

7. L.Y.Markovskii & R.I.Smirnova, Zhur.neorgan.khim. (J.Inorg.Chem.), 2, 2752 (1957).

8. A.S.Pashinkin, G.N.Tishchenko, I.V.Korneeva & B.N.Ryzhenko, Kristallografiya, 5, 261 (1960). (Trans.Soviet Physics - Crystallography.)

9. L.Ya.Markovskii & N.S.Orshanskaya, Optika i spektroskopiya, 9, 77 (1960). (Trans.Optics & Spectroscopy.)

CONCERNING THE VALENCE OF Sn AND Mn ACTIVATORS IN CRYSTAL PHOSPHORS

- N.A.Gorbacheva & V.V.Osiko

The purpose of the present work was to investigate the variation of the luminescence properties of Sn and Mn activated luminophors with the activator valence.

The valence of Sn was determined by the polarographic procedure; the valence of Mn by the method of calorimetric and iodometric analysis. Obviously, there were determined the average values of the effective valence V_{av} of the activator in the phosphor system. Detailed results for phosphors with manganese are given in Ref.1. Here we recall that as regards correlation between the luminescence properties and V_{av} of Mn activator the investigated phosphors fell into three groups.

Phosphor	Luminescence	Heating conditions	$E_{1/2}$*	Valence
$(Sr,Mg)_3(PO_4)_2$:Sn	Orange	1200° in NH_3	0.56	2
$Ba_2P_2O_7$:Sn	Rose	1000° in NH_3	0.56	2
$Sr_2P_2O_7$:Sn	Blue	1000° in NH_3	0.56	2
$(Mg,Ca)_2PO_4F$:Sn	Violet	1000° in air	0.56	2
$(Mg,Ba)_2PO_4F$:Sn	Yellow	950° in air	0.56	2

*$E_{1/2}$ is the Sn half-wave potential measured in polarographic analysis.

In investigating the valence of tin we worked with a group of phosphate phosphors. The results obtained are shown in the accompanying table. It will be evident that despite differences as regards their luminescence spectra, the tin was present in all these phosphors in the divalent state. Oxidation of the tin, that is, conversion of it to the tetravalent state; and reduction of the tin to the elemental state resulted in disappearance of the luminescence. It was also found that a reducing atmosphere was not necessary in all cases to obtain Sn in the divalent state: some of the phosphors were obtained by heating in air of a batch containing a reducing agent (ammonium salts which at t = 1000° decompose (with evolution of hydrogen)[2].

To clarify the character of the correlation between the activator valence in the phosphor system and the heating temperature and atmosphere and the activator concentration we investigated the "model phosphor" system ZnO-MnO-O_2. The specimens, consisting of intimate mixtures of ZnO and MnO_2, were heated at different temperatures in a stream of oxygen or pure nitrogen.

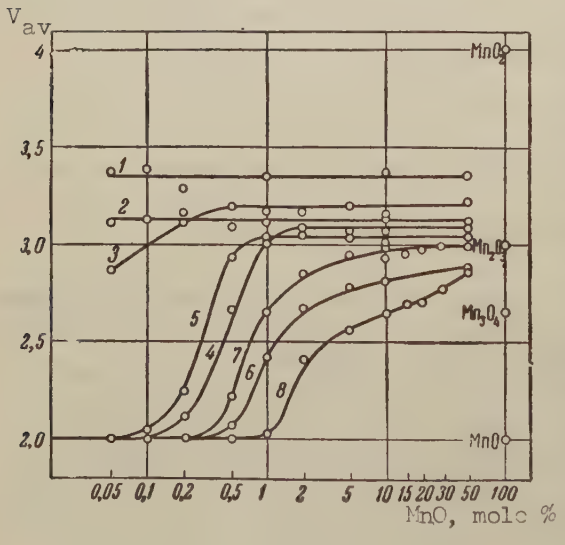

←Variation of the average valence of manganese as a function of the Mn content, and the heating temperature and atmosphere; heating time in all cases 30 min: 1 - 600° in O_2, 2 - 600° in N_2, 3 - 800° in O_2, 4 - 300° in N_2, 5 - 1000° in O_2, 6 - 1000° in N_2, 7 - 1200° in O_2, 8 - 1200° in N_2.

The values of the average valence of Mn in the resultant specimens are shown in the accompanying figure. It will be seen that, other conditions being equal, V_{av} is strongly dependent on the manganese content. It will also be evident that up to a certain Mn concentration $V_{av} = 2$ regardless of the heating atmosphere; this means that in this case the Mn valence is wholly determined by the crystallochemical structure of the base material. Thus it follows that the average manganese valence may differ in the same phosphor heated under the same conditions, depending on the manganese concentration. It must also be borne in mind that change in the valence state of the activator is, as a rule, accompanied by change in the phase composition of the phosphor. Thus we showed that in the case of heating in oxygen of ZnO-MnO solid solutions with a high manganese content these single phase systems stratify: next to the (Zn,Mn)O phase (the manganese content in which is reduced) there appears a manganese oxide phase, which can readily be distinguished under a microscope.

References

1. V.V.Osiko & G.V.Maksimova, Optika i spektroskopiya, 9,478 (1960). (Trans. Optics & Spectroscopy.)

2. N.A.Gorbacheva, Izv.AN SSSR, Ser.fiz., 23, 1310 (1959). (Trans.Bulletin, 23, 1299.)

* * * * * * *

PHOSPHATE LUMINOPHORS FOR FLUORESCENT LAMPS WITH IMPROVED COLOR CHARACTERISTICS

- N.A.Gorbacheva, B.M.Gugel', M.A.Konstantinova-Shlezinger, E.S.Lapir & T.G.Rutshtein

In view of the ever expanding use of fluorescent lamps the problem of developing lamps with emission characteristics insuring correct color rendition has become actue. For such lamps one must have phosphors with wide luminescence spectra so that the radiation produced by a mixture of two or three phosphors will approximate "white light". In addition, the phosphors should have a high quantum efficiency, both initial and during the service life of the lamp. Among such phosphors are barium-titanate phosphate[1,2] (BTP) and Sn activated strontium-magnesium phosphate[3] (SMP). In the present work we investigated these phosphors. In addition, we established that introduction of B_2O_3 into SMP yields a phosphor with a high temperature stability of luminescence; hence the phosphor is suitable in principle for correcting the color of high-pressure mercury lamps. The BTP was prepared by baking a mixture of $BaHPO_4$, TiO_2 and BaF_2 at 1075° for 3 hours. The $BaHPO_4$ was obtained by precipitation at different pH. We tested batches of different composition with $2BaO:P_2O_5$ ratios from 1.9:1 to 2.1:1 but with a constant TiO_2 concentration (~0.26 mole/mole BTP). The experimental data on the brightness and emission stability of the phosphor specimens are listed in Tables 1 and 2. In Table 1 we also give data on the quenching effect of Mn impurity in BTP. The spectral composition of the luminescence of the phosphate luminophors is shown in Fig.1.

It will be evident from the data of Table 1 that the brightness of BTP rapidly decreases with introduction of excess BaO; on the other hand, an excess of P_2O_5 (up to 5 mole percent) has no noticeable effect. This substantiates the

Table 1

Characteristics of barium-titanate phosphate phosphors (BTP)

Phosphor	Relative Brightness	Relative Stability	Quantum efficiency, %	Light output 15 watt lamp, lu/w
$2BaO \cdot 0.26\ TiO_2 \cdot P_2O_5$	100	From 79 to 100 for different samples	75	36
$2.1\ BaO \cdot 0.26\ TiO_2 \cdot P_2O_5$	77	64	--	--
$2.2\ BaO \cdot 0.26\ TiO_2 \cdot P_2O_5$	71	93	--	--
$1.95\ BaO \cdot 0.24\ SiO_2 \cdot P_2O_5$	102	75	--	--
$1.95\ BaO \cdot 0.22\ TiO_2 \cdot P_2O_5$	68	75	--	--
$2\ BaO \cdot 0.26\ TiO_2 \cdot P_2O_5$ + 0.003% Mn	95	--	--	--
$2\ BaO \cdot 0.26\ TiO_2 \cdot P_2O_5$ + 0.01% Mn	68	--	--	--
$2\ BaO \cdot 0.26\ TiO_2 \cdot P_2O_5$ + 0.03% Mn	63	--	--	--
$2\ BaO \cdot 0.26\ TiO_2 \cdot P_2O_5$ + 0.1% Mn	44	--	--	--
$2\ BaO \cdot 0.26\ TiO_2 \cdot P_2O_5$ + 0.3% Mn	41	--	--	--

Table 2

Characteristics of strontium-magnesium phosphate phosphors (SMP)

Phosphor	Method of preparation	Relative stability in lamps	Quantum efficiency, %	Light output 15 watt lamp, lu/w
$(Sr_{2.63}Mg_{0.34})(PO_4)_2Sn_{0.04}$	1. Three-stage heating; reduction of Sn in NH_3.	106	~100	32
	2. Two-stage heating; reduction of Sn in NH_3 or with carbon.	104	~100	32
	3. Three-stage heating; Sn in the form of $H_3C \cdot SnOOH$ without reducing atmosphere.	91	~100	--
$(Sr_{2.7}Mg_{0.3})(PO_4)_2Sn_{0.04}$ - $[B_2O_3]$	Heating with carbon or in an atmosphere of 96% N_2 + 4% H_2.	100	~100	--

data of Harrison[2] on the existence in BTP of a nonluminescing BaO rich phase absorbing UV radiation (in contrast, an excess of P_2O_5 should not lead to absorption of ultraviolet). It is interesting to note that with a large excess of BaO the phosphor, although less bright, is characterized by good stability, possibly better than the normal BTP phosphor. As is known, the emission stability of phosphors in fluorescent lamps is determined by a) the concentration of the main activator (the stability increases with main activator concentration) and b) the specific intensity of the exciting ultraviolet (mainly 185 mμ) (the stability decreases with increasing UV intensity).

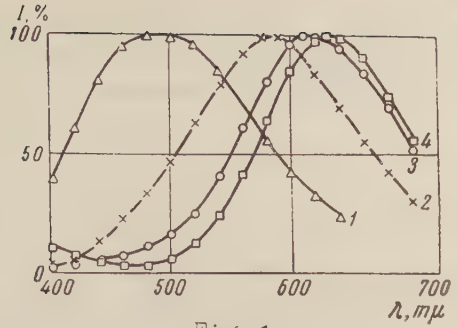

Fig.1

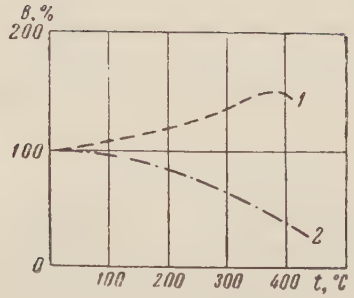

Fig.2

Fig.1. Luminescence spectra of phosphate phosphors with excitation by 2537 A: 1 - $2BaO \cdot 0.26TiO_3 \cdot P_2O_5$, 2 - $(Sr_{2.7}Mg_{0.3})(PO_4)_2Sn_{0.04}[B_2O_3]$ at 300°, 3 - same at 20°, 4 - $(Sr_{2.63}Mg_{0.34})(PO_4)_2Sn_{0.04}$.

Fig.2. Temperature dependence of the luminescence brightness of strontium-magnesium phosphate luminophors with excitation by λ = 365 mμ: 1 - $(Sr_{2.7}Mg_{0.3})(PO_4)_2Sn_{0.04}[B_2O_3]$ 0.4 2 - $(Sr_{2.63}Mg_{0.34})(PO_4)_2Sn_{0.04}$.

In the presence of excess BaO there forms the compound $4BaO \cdot 3TiO_2 \cdot P_2O_5$, as a result of which the concentration of Ti activator is effectively reduced and owing to absorption of UV by this compound, the intensity of excitation of the activator is diminished. This explains why with the introduction of excess BaO the stability of BTP phosphors is first reduced and then enhanced.

The SMP phosphors were prepared by heating $SrCO_3$, $MgCO_3$, $(NH_4)_2HPO_4$ and SnO_2. Three different procedures were employed: 1) heating at 600° for 1 hour in air; then after grinding repeat heating at 1200° for 2 hours in air and, finally, heating at 1200° for 30 min in NH_3; 2) heating from room temperature to 1200° (holding time 1 hour) and second heating at 1200° for 30 min in NH_3 or in contact with carbon; 3) heating of the phosphate and carbonates (without Sn) from 20 to 1200° (holding time 1 hour), grinding with the addition of $H_3C \cdot SnOOH$ and final heating in a sealed tube for 30 min at 1200°. In general the resultant phosphor is a mixed strontium-magnesium orthophosphate with the composition $(Sr_{2.63}Mg_{0.34})(PO_4)_2$-$Sn_{0.04}$.

The spectral distribution of the emission of this phosphor is shown in Fig. 1. Data on the influence of the method of preparation on the quality of the phosphor are given in Table 2. With introduction into the phosphor of 0.4 mole B_2O_3 and increase of the SrO content to the orthophosphate level there is obtained mixed Sr-Mg borophosphate. Heating of this phosphor was carried out at 1050° in the presence of carbon or in an atmosphere of 96% N_2 + 4% H_2. The quantum luminescence efficiency of this phosphor is ~100%.

Data on the emission stability in lamps are given in Table 2; data on the temperature stability in Fig.2. The brightness of the phosphor with B_2O_3 under excitation by 313 mμ photons is 125% referred to the brightness of a sample of $(Sr,Zn)_3(PO_4)_2$:Sn obtained from the GIPKh (State Institute of Applied Chemistry).

The SMP phosphors have a high quantum efficiency and good stability, and can therefore be recommended for use in fluorescent lamps.

A mixture of 50% BTP and 50% SMP was used for preparing test 15-watt fluorescent lamps with improved color rendition; these lamps had a color temperature of 4500°K, a Harrison factor of 86% and a light output of 34 lu/w. For purposes of comparison we recall that similar lamps prepared from a mixture of calcium halophosphate, calcium silicate and willimite[4] with the same light output had a Harrison factor of 83%. Using a mixture of 70% L-38 phosphor (Sb activated calcium

halophosphate) and 30% SMP one can obtain lamps with a color temperature of 6500°K and a Harrison factor and light output equal to those of commercial fluorescent lamps fabricated from a mixture of 85% L-39 phosphor (Sb and Mn activated calcium halophosphate) and 15% L-37 phosphor (Mn activated magnesium-arsenate).

References

1. S.T.Henderson & P.W.Ranby, J.Electrochem.Soc., 98, 478 (1951).
2. D.E.Harrison, Ibid., 107, 217 (1960).
3. H.Koelemans & A.P.Cox, Ibid., 104, 442 (1957).
4. R.A.Nilender, Izv.AN SSSR, Ser.fiz., 23, 1393 (1959). (Trans.Bulletin, 23, 1377.)

* * * * * * *

EFFECT OF REPLACEMENT OF THE BASE MATERIALS OF PHOSPHORS ON THEIR LUMINESCENCE PROPERTIES

- M.-L.Yu.Allsalu

In recent years there have appeared in the literature numerous descriptions of phosphors in which the base material is not a single compound but a mixture. The heightened interest in such complex systems is not fortuitous. By replacing part of the atoms or ions of the host by foreign atoms or ions one can realize different and in many cases useful effects.

The main base material used in the present study was Mn activated $SrSb_2O_6$. Despite the fact that the emission band of this phosphor lies in the blue region ($\lambda_{max} \approx 470$ mμ), a location unusual for Mn, we have every reason to assume that this luminescence does belong to manganese.

In the substitution experiments we replaced components in both the cationic and anionic parts of the phosphor. The composite phosphors were prepared by heating mixtures of the powders, usually at 1100° (in some cases, 1200°). We synthesized a number of compositions in the $SrO \cdot Sb_2O_5$-$BeO \cdot Sb_2O_5$ system, the end members of which differ markedly as regards their luminescence properties. The data obtained for the phosphors of this system are shown in Figs.1 and 2 (curves 1 and 1'). It was found that introduction of fairly large amounts of the small and strongly polarizing Be ion does not affect the cathodoluminescence spectrum of $SrSb_2O_6$:Mn; only at very high concentrations of Be ($\geqslant 50$ mole percent) does there begin to form the characteristic independent band of $BeSb_2O_6$:Mn ($\lambda_{max} = 545$ mμ). Apparently, introduction of Be facilitates ordering of the $SrSb_2O_6$ lattice; this is indicated by the character of the excitation spectra, the substantial increase in luminescence brightness and the general appearance of the powders. Noteworthy is the great difference between the luminescence spectra under cathode-ray as compared with long wavelength ultraviolet excitation. In the latter case there predominates an orange-red band (observed for $BeSb_2O_6$:Mn), the brightness of which decreases with decrease of the Be concentration. In this system one can obtain phosphors with pure white emission thanks to the favorable conjunction of the blue and yellow bands of Mn.

With replacement of the host cation by calcium, the luminescence band of $SrSb_2O_6$:Mn is broadened and shifted to the side of longer wavelengths; this indi-

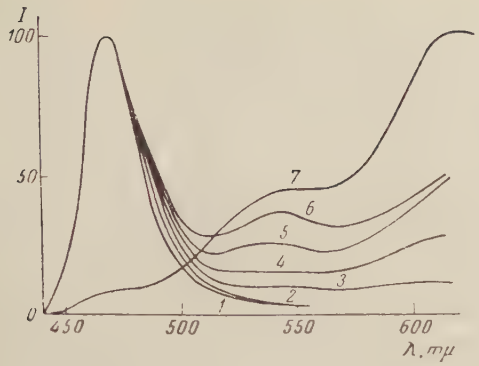

Fig.1. Cathodoluminescence spectra of $(SrO \cdot BeO)Sb_2O_5$:Mn phosphors: 1 - $SrO \cdot Sb_2O_5$, $(0.9\ SrO \cdot 0.1\ BeO)Sb_2O_5$, $(0.75\ SrO \cdot 0.25\ BeO)Sb_2O_5$; 2 - $(0.5\ SrO \cdot 0.5\ BeO)Sb_2O_5$; 3 - $(0.25\ SrO \cdot 0.75\ BeO)Sb_2O_5$; 4 - $(0.15\ SrO \cdot 0.85\ BeO)Sb_2O_5$; 5 - $(0.1\ SrO \cdot 0.9\ BeO)Sb_2O_5$; 6 - $(0.05\ SrO \cdot 0.95\ BeO)Sb_2O_5$; 7 - $BeO \cdot Sb_2O_5$. In all cases $T_{heat} = 1100^o$; $C_{Mn} = 0.1\%$.

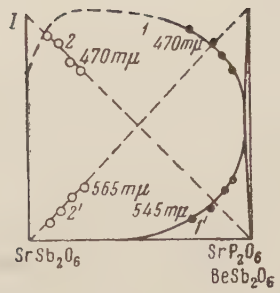

Fig.2. Composition dependence of the intensity of the emission bands of individual components: - 1 - $(SrO \cdot BeO)Sb_2O_5$:Mn; 2 - $SrO(Sb_2O_5 \cdot P_2O_5)$:Mn.

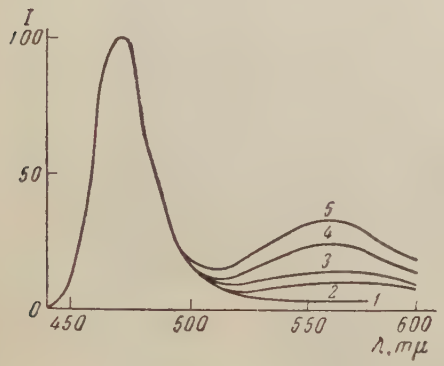

←Fig.3. Cathodoluminescence spectra of $SrO(Sb_2O_5 \cdot P_2O_5)$:Mn phosphors: 1 - $SrO \cdot Sb_2O_5$; 2 - $SrO(0.9\ Sb_2O_5 \cdot 0.1\ P_2O_5)$; 3 - $SrO(0.85\ Sb_2O_5 \cdot 0.15\ P_2O_5)$; 4 - $SrO(0.8\ Sb_2O_5 \cdot 0.25\ P_2O_5)$; 5 - $SrO(0.75\ Sb_2O_5 \cdot 0.25\ P_2O_5)$.

cates the formation of a solid solution in the system. Na, Ba, Mg and Zn can be introduced into the lattice in very large amounts (up to 50 mole percent) without substantial effect on the emission spectrum. Introduction of these elements in concentrations of 5 to 15 mole percent even enhances the luminescence brightness of $SrSb_2O_6$:Mn. Introduction of Tl (5 weight percent) increases the luminescence brightness by a factor of 3 without significant alteration of the luminescence and excitation spectra.

Effects analogous to those observed with introduction of Be are observed when the Sb is replaced by As in the anionic part of the phosphor. The independent band of $SrAs_2O_6$:Mn ($\lambda_{max} \approx 575$ mμ) appears only at high As concentrations. Smaller amounts of arsenic do not produce any change in the spectrum of $SrSb_2O_6$:Mn, but only increase the luminescence intensity by increasing the degree of crystallization of the material.

When the antimony oxide is replaced by phosphorus oxide there appear in the luminescence spectrum two independent bands peaking at 470 and 565 mμ even at a relatively low P concentration (Fig.3 and curves 2 and 2' in Fig.2). A nearly white luminescing phosphor can be obtained by proper combination of the two components. There is virtually no smearing out of the 470 mμ band with introduction of phosphorus. This indicates that there are present in this phosphor two independent crystal phases, which do not form a solid solution. Introduction of P_2O_5 also improves the crystalline structure of the host phosphor.

Replacement of part of the oxygen in the phosphor by fluorine (up to 16.7 mole percent) has no effect on the shape of the luminescence spectrum. In contrast, a substantial change is observed in the excitation spectrum: the long wavelength tail of the excitation curve broadens and there gradually forms an independent peak at 300 mμ. As a result the phosphor begins to luminesce rather brightly even with stimulation by long wavelength ultraviolet (UFS-2 filter).

It is significant that in the case of introduction of fluorine, for obtaining a uniformly luminescing powder and formation of the long wavelength peak in the excitation spectrum a high heating temperature (to 1200°) is required. This is probably connected with the circumstance that incident to replacement of divalent oxygen by monovalent fluorine in the lattice there forms an excess charge which must be compensated for by elimination of part of the antimony. This occurs only at high temperature by evaporation of the antimony in the form of Sb_2O_3. Specimens obtained at a lower temperature luminesce orange-red under long wavelength ultraviolet excitation. This luminescence is probably due to an excess of Sb_2O_4 forced out of the lattice.

Replacement of Sb by Bi leads to coloring of the phosphor and suppression of its luminescence.

Iron is a strong quencher of the luminescence of $SrSb_2O_6$:Mn. Pb and Cu exert a weaker but noticeable quenching effect.

I desire to express my deep gratitude to A.V.Moskvin for his guidance in the work.

LUMINESCENCE OF LANTHANIDES IN THORIUM OXIDE

- A.K.Trofimov

The basic procedure in luminescence microanalytic determination of rare earth elements consists in observation of the luminescence of crystal phosphors containing the determined elements as activators. Among the numerous compounds that are suitable for use as the base material in preparing such phosphors, thorium oxide stands out as regards brightness of the luminescence. Yet the luminescence properties of rare earth activated ThO_2 phosphors have scarcely been investigated. There are no detailed data in the literature on the luminescence spectra and no information on the limiting concentration detectable by observation of the luminescence.[1-3] The present work was concerned with investigation of the luminescence spectra of trivalent lanthanides in thorium oxide for the purpose of evaluating the possibility of utilizing the spectra for analytic purposes.

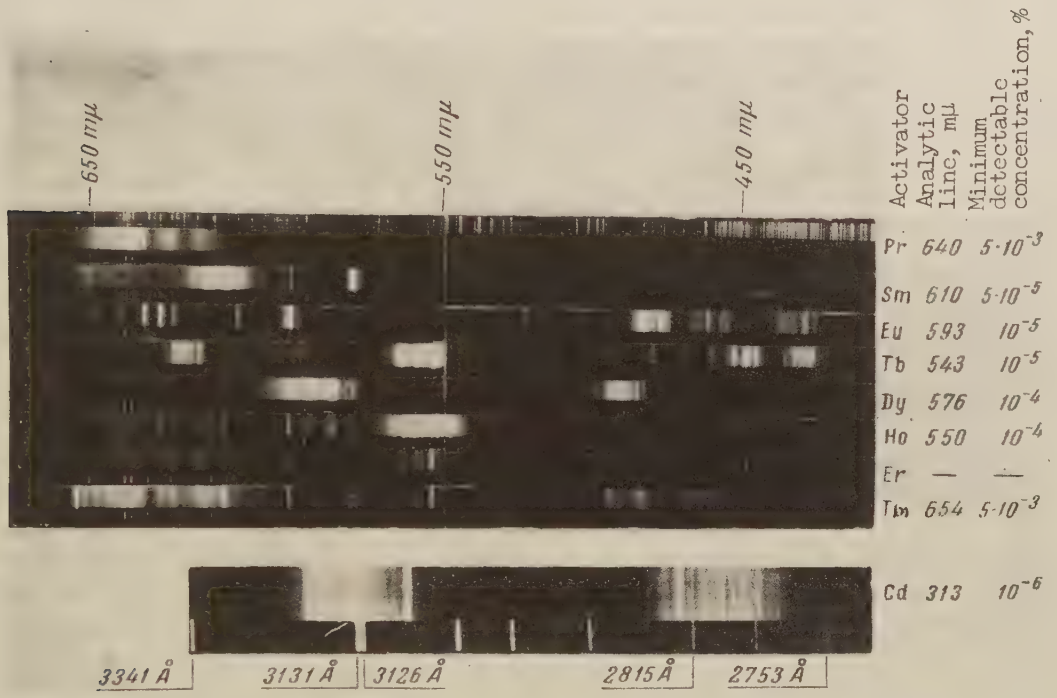

Luminescence spectra of rare earths in thorium oxide.

The luminescence of the phosphors was excited primarily by short-wave ultraviolet. The use of a GOI (State Optical Institute) spark phosphoroscope[4] as the excitation source enabled us to observe the luminescence in any part of the spectrum without using light filters, which is particularly important where observation of the ultraviolet emission of Gd is concerned. The luminescences of Pr, Sm, Eu, Tb, Dy, Ho, Er and Tm and of ThO_2 lies mainly in the visible region. The luminescence spectra of thorium oxide phosphors activated by the investigated rare earth elements are reproduced in the accompanying figure. It will be seen that most of the spectra are predominantly line spectra. For almost all of them one can indicate a bright line that can conveniently be utilized as the analytic line. The wavelengths of these analytic lines are listed at the right in the figure.*

---

*A detailed description of the spectra of all the investigated lanthanides in thorium oxide will be published elsewhere.

It is difficult to choose an analytic line for ThO_2:Er because the group of brightest lines of Er (550-520 mμ) coincides in wavelength with groups of bright lines due to Ho and Tb. The last two elements can be identified not only by means of their analytic lines but also from their characteristic luminescence: yellow-green (560-550 mμ) for Ho and green (430-440 mμ) for Tb.

In the figure we also list the minimum concentration of each element detectable under the usual conditions of photographing luminescence spectra. Increase of the activator concentration for all phosphors leads to a proportional increase in the luminescence intensity up to a content of about 0.1%, which is the upper concentration bound for quantitative determination of these elements by the luminescence procedure. The luminescence of Nd and Yb is located in the infrared[5] and could not be recorded by our photographic materials.

Crystalline thorium oxide is not only a good host for rare earth phosphors, but, as was shown earlier[6], is an excellent acceptor of lanthanide ions. The effect of directed thermal diffusion of rare earth elements into thorium oxide was utilized by us in developing an entirely new technique for quantitative determination of gadolinium in metallic beryllium.[7] It should be possible to use this technique for microchemical determination of lanthanides in minerals containing low concentrations of these elements.

I desire to thank P.P.Feofilov for his guidance in the work.

References

1. E.L.Nichols & F.G.Wick, J.Opt.Soc.Am., 22, 357 (1932).

2. F.G.Wick & C.G.Troupp, Ibid., 25, 57 (1935).

3. A.V.Moskvin, Katokolyuminestsentsiya (Cathodoluminescence), Part II, p. 240 (1948).

4. E.M.Brumberg, Opt.-mekh.prom-st' (Optical-mechanical Industry), No.11 (1936).

5. P.P.Feofilov, Optika i spektroskopiya, 5, 216 (1958).

6. A.K.Trofimov, Izv.AN SSSR, Ser.fiz., 21, 757 (1957). (Trans.Bulletin, 21, 754.)

7. E.Ya.Arapova, E.G.Baranova, V.L.Levshin, T.V.Timofeeva, A.K.Trofimov & P.P.Feofilov, Trudy Komissii po analit. khimii (Proceedings of the Commission on Analytic Chemistry), 12, 344 (1960).

INFLUENCE OF THE SYNTHESIS CONDITIONS ON THE LUMINESCENCE OF ZINC OXIDE

- Ya.M.Zelikin

The visible part of the luminescence spectrum of zinc oxide, in addition to a green band peaking at ~510 mμ, generally includes a yellow band at about 610 mμ. Different authors have expressed divergent and sometimes contradictory opinions regarding the nature of the centers responsible for the yellow band. For example, attempts have been made to attribute the yellow band to excess zinc.[1,2] This hypothesis must, however, be rejected if only because the yellow band disappears after heating of the zinc oxide in a reducing or inert medium and reappears or is intensified as a result of heating in an oxidizing medium.

More justified, we feel, is the assumption[3-5] that excess oxygen is responsible for the yellow luminescence. It is not impossible, however, that the yellow luminescence centers may be formed by some extraneous impurity and that the oxygen, which quenches the green band, only favors the yellow luminescence. Randall[6], for example, attempted to attribute the activating effect to manganese. However, Osiko[5] conclusively showed that manganese is not an activator of ZnO. In order to identify the effective impurities we investigated the influence of different metals on the yellow band. We found that only in the case of divalent cadmium and magnesium and trivalent aluminum, gallium and indium is there a noticeable enhancement of the yellow band. All our attempts to obtain by thorough purification ZnO that would not yield a yellow band after heating at high temperature in an oxidizing medium failed. In view of this it may be inferred that the yellow luminescence is an attribute of pure ZnO.

It has been hypothesized[1,7] that the yellow band is associated with a high temperature modification of ZnO. This hypothesis is plausible in view of the data in the literature and the results of our observations, in particular, the fact that the yellow band appears at temperatures close to the temperature of the hypothesized polymorphous transformation of zinc oxide. It must be noted that the available crystallographic data on the existence of two modifications of ZnO are contradictory. Some authors[8,9] report the existence of two modifications, while others[10-12] indicate that there is only one. X-ray diffraction studies carried

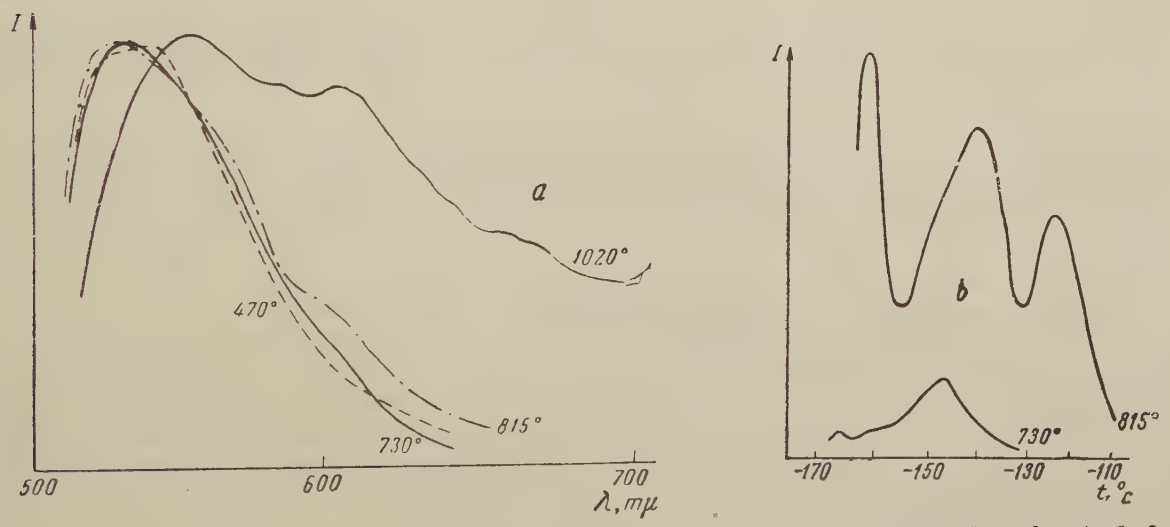

Luminescence spectra (a) and glow curves (b) of zinc oxide samples heated for 40 min in a stream of oxygen. The heating temperatures are indicated at the curves. In (a) the ordinates of the peaks of all the spectra are normalized to unity.

out at room temperature on samples heated at different temperatures show the same wurzite structure.[13] This, in our opinion, cannot be taken as proof of nonexistence of high temperature modification, inasmuch as this may be unstable at room temperature. Thus, it is entirely possible that upon cooling to room temperature the lattice as a whole assumes the normal, stable structure, but that there persist defects, which serve as yellow luminescence centers, about small residues of the high temperature modification. In order to check this hypothesis, we recorded Debye diffraction patterns for ZnO at room temperature and at 900°. The preliminary results did not show the presence of a high temperature modification in ZnO.

Our experiments convinced us that no yellow luminescence centers are formed in zinc oxide as a result of heating in the absence of oxygen (with or without impurities) at temperatures in the range from 500 to 1200°. The presence of oxygen is a necessary condition for the formation of yellow luminescence centers. Further, the experiments show that in the presence of oxygen the zinc oxide must be heated to a temperature of not less than 700° for yellow luminescence centers to form. Even 20 hours heating at 60° did not result in the formation of yellow luminescence centers. Apparently, a further essential condition is the presence of a certain defect structure. The above mentioned intensifying influence of some metals is consistent with the assumption of a defect structure in zinc oxide specimens luminescing yellow. Possibly the role of the metals reduces mainly to the formation of defects which, however, may also form in the pure oxide under appropriate conditions.

Data on the thermostimulated luminescence of ZnO samples heated at different temperatures in a stream of oxygen indicate that the specimens exhibiting a yellow luminescence band are also characterized by the presence of an additional glow curve peak (see figure). In general, specimens with yellow luminescence store a larger light sum. This is further evidence in favor of the assumption that specimens with yellow luminescence have a structure with more defects.

Scientific-Research Physical Institute,
Leningrad State University

References

1. K.V.Shalimova, Dissertation, Physical Institute, USSR Ac.of Sci., 1952.
2. G.A.Konovalov, Trudy (Transactions), Siberian Phys.-Tech.Institute, No. 24, (1953).
3. F.A.Kröger & H.J.Vinc, J.Chem.Phys., 22, 250 (1954).
4. A.N.Shekhter, I.A.Myasnikov & S.Ya.Pshezhetskii, Materially V Soveshch. (Transactions of the Fifth Conference on Luminescence) Tartu, 1954.
5. V.V.Osiko, Optika i spektroskopiya, 7, No.6, 770 (1959). (Trans.Optics & Spectroscopy.)
6. Randall, Trans.Faraday Soc., 35, 2 (1939).
7. J.Tafel, Ann.Physik, 14, 206 (1904).
8. A.F.Wells, Structural Inorganic Chemistry, Oxford 1950. (Cited in Russian translation.)
9. G.B.Bokii, Vvedenie v kristallokhimiyu (Introduction to crystallochemistry), M., 1954.
10. V.F.Ormont & I.A.Goryunova, et al, Izv.AN SSSR, Ser.fiz., 21, 133 (1957). (Trans.Bulletin, 21, 128.)
11. Strukturberichte, Leipzig, 1941.
12. Wyckoff, The Structure of Crystals, N.Y., 1935.
13. A.B.Shekhter & Yu.M.Moshkovskii, Doklady AN SSSR, 72, No.2 (1950).

QUENCHING AND STIMULATION OF THE LUMINESCENCE OF ZINC OXIDE UNDER THE INFLUENCE OF ADSORBED AND CAPILLARY-CONDENSED VAPORS AND GASES

- K.V.Tagantsev

Investigation of the influence of vapors and gases on the luminescence of crystal phosphors is of interest from two standpoints. On the one hand, such investigations allow of determining the extent to which surface levels are involved in the luminescence and, on the other hand, they serve to elucidate the course of the physical-chemical processes (adsorption, catalysis, chemical and photochemical reactions) occurring on the phosphor surface. The present work was a continuation of the research undertaken in collaboration with A.N.Terenin[1] and reported on at the Fifth Conference on Luminescence in Tartu.

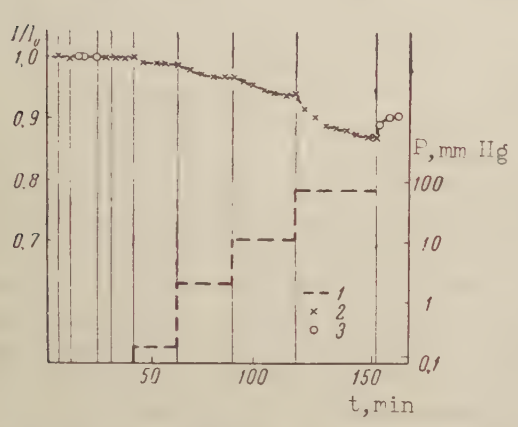

Fig.1. Quenching of luminescence of ZnO with time during dark adsorption of NO (short-term illumination) and stimulation of the luminescence under prolonged illumination: 1 - NO pressure, 2 - luminescence under short-term illumination, 3 - luminescence under continuous illumination.

For the purpose of the present investigation we took zinc oxide which was prepared by burning zinc in air; in some cases the specimens were subjected to further treatment. All the specimens had either exclusively or predominantly a green luminescence band peaking at 510 mμ. Prior to the experiments the zinc oxide was aged in high vacuum for 4 hours at 200°. The luminescence was excited by the light from a PRK-4 mercury tube through a UFS-3 ultraviolet filter. The luminescence intensity was measured by means of a differential photoelectric photometer built in our laboratory. In order to exclude the influence of light on the adsorbent-adsorbate system the luminescence was observed during the period of short-term light flashes (usually 10 sec) with dark pauses of not less than 5 min between flashes. We also investigated the effect of continuous illumination. The following results were obtained.

1. Nitric oxide (NO), even at a pressure of a few tenths of a millimeter Hg quenches the luminescence under short-term illumination; upon transition to prolonged illumination the quenched luminescence is partially restored (Fig.1).

2. Acetone and benzene vapors have a similar effect.

3. N_2O, CO and CO_2 in the gaseous state have no discernible influence on the luminescence.

The variation in intensity of luminescence with the pressure of different gases and vapors is shown in Fig.2.

What is the mechanism of the observed effect?

According to the most widely held view[2,3], the photoconductivity and green luminescence centers in zinc oxide are thermally ionized excess Zn atoms. Emission of light (luminescence) occurs as a result of recombination of these centers, which are probably ionized by the exciton mechanism, with conduction electrons.[2] The mechanism of luminescence quenching of ZnO by nitric oxide is apparently the same as the mechanism proposed[1,4] for quenching by oxygen, namely, the adsorbed nitric oxide molecules in the dark trap electrons from the conduction band, which leads to upward curvature of the energy bands and electron depletion of the conduction band at the surface. The last reduces the probability for recombination of the ionized centers with conduction electrons, and is evinced in the form of weakening of the luminescence.

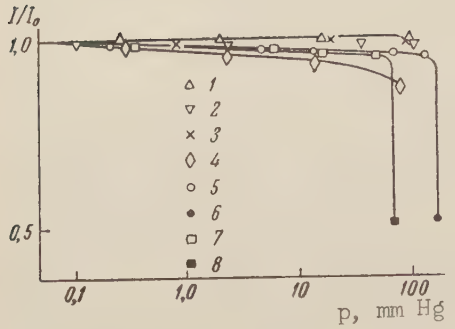

Fig.2. Variation of the luminescence intensity with the pressure of different vapors and gases under short-term illumination: 1 - CO_2, 2 - CO, 3 - N_2O, 4 - NO, 5 - adsorbed acetone, 6 - capillary-condensed acetone, 7 - adsorbed benzene, 8 - capillary-condensed benzene.

This hypothesis regarding the trapping of electrons by the adsorbed nitric oxide molecules is substantiated by the experiments of Filimonov[5] in our laboratory; he observed the infrared absorption of thoroughly degassed zinc oxide and found that it extends from 3.5 μ into the long wavelength region. This absorption is due to electron transitions to the conduction band. Upon admission of O_2 or NO into the experimental chamber the absorption is weakened, which indicates trapping of electrons from the conduction band or from local levels (traps) by the adsorbed O_2 or NO molecules.

In absorption of light by a crystal having upon its surface adsorbed molecules part of the excitons produced by the incident light are broken up on the adsorbed molecules, leading to release of their electrons and desorption of the molecules under the influence of the excess energy. This process must lead to reduction in the upward curvature of the bands and to increase in the concentration of electrons in the conduction band near the surface, which is evinced in transition from short-term to prolonged illumination in the form of enhancement of the luminescence.

The mechanism of luminescence quenching by benzene is probably somewhat different. As was shown by Vilesov & Terenin[6] by measurements of the photoelectric work function, in the case of adsorption of benzene on zinc oxide there occurs polarization of the benzene and the negative ends of the dipoles are turned to the side of the zinc oxide. This must lead to increase in energy of the electrons in the surface layer, i.e., to upward bending of the energy bands which, in accord with the proposed mechanism, should lead to weakening of the luminescence.

As will be evident from Fig.2, capillary-condensation of acetone and benzene vapors results in great weakening of the luminescence. One could attempt to interpret this effect by means of a mechanism similar to that described above. It must be noted, however, that the "quenching" of luminescence by benzene and acetone in the condensed state is also exhibited by specimens of zinc oxide and uranyl glass, the luminescence of which is not quenched by the respective vapors. It follows, therefore, that the observed weakening of luminescence as a result of capillary-condensation of acetone and benzene is connected mainly with change in the conditions of diffuse scattering of light. This is substantiated by measurements of the attenuation of visible light scattered by ZnO as a result of capillary-condensation of benzene; this attenuation is of the same order of magnitude as the "quenching" of luminescence.

It was noted in Ref.1 that dry oxygen produces quenching of luminescence in the case of a number of specimens, while in the case of other specimens it is effective only in the presence of water. Repetition of the experiments under conditions of higher purity substantiated the above mentioned observations and also the hypothesis that the quenching of luminescence by oxygen in the presence of water occurs owing to lowering of the acceptor level of oxygen upon approach to it of dipole molecules. If this hypothesis is correct, the lowering of the acceptor level and, consequently, the quenching of luminescence must be particularly noticeable at high concentrations of dipole molecules, i.e., in the case of capillary concentration. Our new experimental data substantiate this:

Water vapor pressure, mm Hg	State of the water on the adsorbant	Oxygen pressure, mm Hg	Additional quenching of luminescence by the oxygen,%
14	Adsorbed	80	2
10	Capillary-condensed	50	12

I desire to express my deep gratitude to A.N.Terenin for his guidance in the work.

Photocatalysis Laboratory,
Leningrad State University

References

1. K.V.Tagantsev & A.N.Terenin, Optika i spektroskopiya, 2, 355 (1957); Izv.AN SSSR, Ser.fiz., 21, 525 (1957). (Trans.Bulletin, 21, 523.)

2. H.Weiss, Z.Phys., 132, 335 (1952); G.Heiland, Z.Physik, 142, 415 (1955); Ibid., 138, 459 (1955); Ibid., 132, 367 (1952).

3. E.Mollwo & Stöckmann, Ann.Phys., 3, 340 (1948); F.I.Vergunas & T.P.Konovalov, Zhur.eksp.i teor.fiz., 23, 712 (1952).

4. A.N.Terenin, Elektronnyi obmen poluprovodnikov c adsorbirovannymi molekulami. Fotoelektricheskie i opticheskie yavleniya v poluprovodnikakh (Electron exchange of semiconductors with adsorbed molecules. Photoelectric and optical effects in semiconductors), p.255, Kiev, 1959.

5. V.N.Filimonov, Optika i spektroskopiya, 5, 709 (1958).

6. F.I.Vilesov & A.N.Terenin, Doklady AN SSSR, 125, 1053 (1959). (Trans. Doklady.)

INVESTIGATION OF THE THERMAL ACTIVATION ENERGY FOR OPTICAL QUENCHING OF SOME CRYSTAL PHOSPHORS

- V.L.Levshin & B.M.Orlov

The present work was devoted to investigation of optical quenching of crystal phosphors, which, as is known, depends on the temperature[1,2]. As far as we know, the effect has not been studied quantitatively. Hence we felt it would be of interest to determine how the activation energy for quenching depends on the wavelength of the quenching light and the depth of the trapping levels.

If we use S_0 to denote the area under the glow curve corresponding to a single trapping level, recorded without preliminary quenching of the phosphor by IR light, and S_T to denote the area under the curve recorded after quenching with IR at a temperature T, we can write

$$\Delta S_T = S_0 - S_T = Ae^{-E/kT}, \qquad (1)$$

where A is a constant and E is the quenching activation energy.

From (1) it follows that

$$2.3 \log \Delta S_T + B = -\frac{E}{kT}, \qquad (2)$$

where B is a constant; i.e., the logarithm of the quenched light sum varies linearly with $1/T$. From the slope of the log $\Delta S_T = f(1/T)$ plot one can calculate the activation energy for quenching.

In the present investigation we used three different phosphors with traps of different depth, namely, ZnS, ZnS:Co and CaS:Bi.

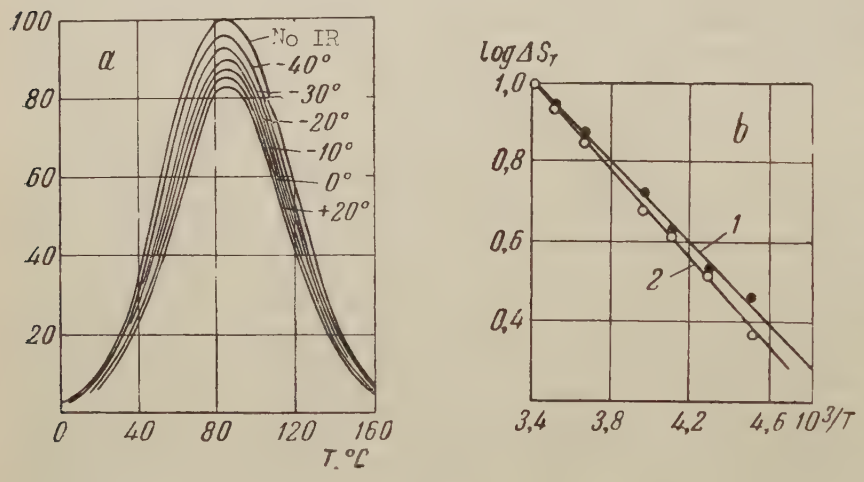

Fig.1

In the case of pure ZnS, the value of ΔS_T for the level corresponding to the glow curve peak at -60° varied very slowly with temperature. Hence we could not calculate E for the given level inasmuch as the value of the energy is apparently close to the experimental uncertainty. One can only say that in this case for all λ_{IR} the activation energy E is smaller than 0.02 ev.

ZnS:Co yields a glow curve with a peak at 90°. Fig.1,a shows a series of curves for this level, recorded after quenching the phosphor with λ = 1.3 μ light at different temperatures. Line 1 in Fig.1,b represents the experimental variation of log ΔS_T with $1/T$ for this case; from the slope of this line we calculated E.

Similar measurements were carried out using other IR wavelengths: 0.8, 0.9, 1.0 and 1.2 μ (see table). The average value of the quenching activation energy E for this level was found to be 0.098 ev.

More detailed investigations showed, however, that the calculated value of E depends somewhat on the magnitude of the quenched light sum. In the experiments

Summary of experimental results: values of E_{av}

Phosphor	λ=0,7μ	0,8 μ	0,9 μ	1,0 μ	1,1 μ	1,2 μ	1,3 μ	E_{av}
ZnS	<0,02	<0,02	<0,02	<0,02	<0,02	<0,02	<0,02	<0,02
ZnS — Co (ΔS_T =15%)	—	0,092	0,105	0,096	—	0,096	0,101	0,098
ZnS — Co (ΔS_T =50%)	—	0,104	0,106	0,107	—	0,105	0,110	0,106
CaS — Bi	0,27	0,33	0,29	0,30	—	—	—	0,30

mentioned above the maximum quenching did not exceed 15% of S_0. If the quenching is increased to approximately half the total light sum stored, the variation of log ΔS_T with $1/T$ for λ = 1.3 μ is given by straight line 2 in Fig.1,b. In this case E_{av} = 0.106 ev, i.e., is 8% larger than the value of E_{av} adduced above.

CaS:Bi phosphor has a glow curve with a peak at 230°. As a result of experiments with this phosphor we obtained values of E equal to ~0.3 ev for all IR wavelengths used.

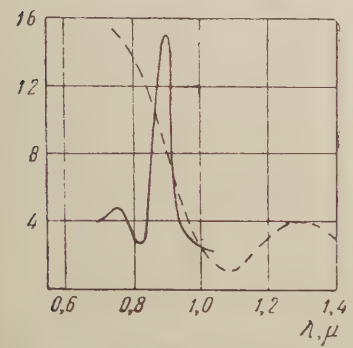

Fig.2

All the experimental results are summarized in the accompanying table.

It follows from these data that for any given level E does not depend on λ_{IR}. Moreover, the deeper the trapping level, the greater E. This explains the increase of the activation energy for quenching with increase of IR irradiation shifts the glow curve peak to the side of higher temperatures inasmuch as it depopulates mainly the shallower traps. The value of E calculated in this case characterizes the deeper trapping levels and, hence, is somewhat greater than the true average.

Earlier[3] we obtained similar regularities for the thermal activation energy of optical flash of ZnS:Cu:Pb phosphors; the activation energy for levels of the same depth was found to be approximately two times greater than the above values.

It must not be assumed that because E does not vary with λ_{IR}, IR irradiation of different wavelengths actually has the same quenching effect. The IR quenching spectra for CaS:Bi (solid line) and ZnS:Co (dashed line) are reproduced in Fig.2. These curves clearly illustrate the selective nature of the IR quenching effect.

Physics Faculty,
Moscow State University

References

1. C.Peyrou, Ann.phys., 3, 459 (1948).

2. E.I.Adirovich, Nekotorye voprosy teorii lyuminestsentsii kristallov (Some problems in the theory of luminescence of crystals), M., 1956.

3. V.L.Levshin & B.M.Orlov, Optika i spektroskopiya, 7, 530 (1959). (Trans. Optics & Spectroscopy.)

DISCUSSION

Ch.B.Lushchik: V.V.Antonov-Romanovskii and N.A.Tolstoi have published a number of contributions describing their investigations of the de-exciting action of exciting light (radiant release of stored energy by incident light). Nevertheless, the physical essence of the processes involved in this de-exciting action is still unclear. In recent years in Tartu we have been carrying on detailed investigations of the de-exciting action spectra. We measured the decrease in the number of electrons localized on definite trapping levels after additional exposure of the excited crystal to equal numbers of photons of different frequencies. We judged of the decrease of electrons in the traps from the change in absorption, thermostimulated luminescence, optical flash, photostimulated emission, photoelectric polarization, stored light sum, etc.

It was found that decrease in the number of F centers occurs not only as a result of their photothermal ionization but also incident to photothermal release of holes from trapping levels, incident to ionization of the F centers by exciton impact, in the process of sensitized de-excitation by resonance energy transfer to the F centers from other electron color centers, etc. Actually all these elementary de-exciting action mechanisms depend on temperature. The temperature dependence is particularly strong in the case of photothermal release of electrons and holes from trapping levels. We feel that at least in the case of alkali halide crystals there is realized mainly photothermal (rather than thermooptical) ionization of the centers. This is substantiated by parallel investigations of infrared fluorescence of color centers and their photothermal stability. The attributes of most potential wells, serving as electron and hole traps, are such that, in addition to the ground state of the center, there may also be an excited state. Only in the case of F centers does there occur direct optical ionization.

In general, the values of the activation energy for thermal ionization of excited optical centers differ for different centers. There is no unique relationship between the position of the center absorption band and the magnitude of the activation energy.

The quantum efficiency of the de-exciting action is constant within the range of the elementary absorption bands. After optical excitation of centers there was first established equilibrium distribution of the centers over vibrational energies and only then was there realized their thermal ionization. Photothermal ionization of centers cannot be properly considered in the framework of the electron-hole model of phosphors. To interpret this effect correctly one must invoke the concept of electronic-vibrational processes.

CONCERNING THE PARAMETERS OF STICKING CENTERS WHICH DETERMINE THE KINETICS OF PHOTO-THERMOSTIMULATED EFFECTS

- V.E.Khartsiev

In conjunction with experimental investigations of thermostimulated current (t.c.) which have been carried out for many different substances (see, for example, Ref.1), it is of interest to consider theoretically a new class of nonisothermal relaxation effects, called photo-thermostimulated (p.t.) effects. These consist of changes in the conductivity of a crystal phosphor under different nonisothermal conditions under the influence of different initial excitations and irradiations. For the sake of simplicity we shall restrict our consideration to the case of unipolar conductivity, one type of sticking centers with concentration M and a trapping coefficient γ. Assume that there are two irradiations: the first with intensity i gives rise to impurity conductivity, and the second produces interband transitions. The heating rate is an arbitrary function of time. The balance of transitions per unit time, shown in the accompanying figure, leads to the set of equations (1)-(2) for the time varying concentration of electrons in the conduction band $n(t)$ and in the sticking centers $m(t)$. In the quasi-stationary approximation

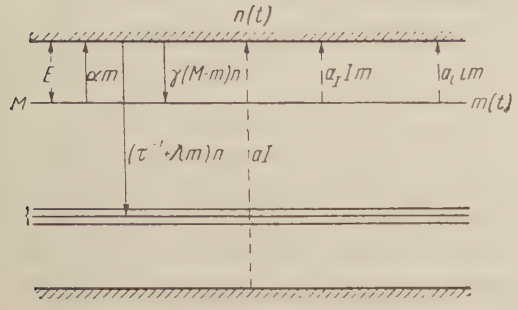

Balance of transitions determining the kinetics of photo-thermostimulated effects in the case of one type of sticking centers. The dashed lines represent optical transitions.

$$n(t) = (\bar{\alpha}m + aI)[\tau^{-1} + \gamma M + (\lambda - \gamma)m]^{-1}$$

and the set of equations has a precise solution (3) in the vicinity of the p.t. current maximum, for $\tau^{-1} \gg \lambda m$, where

$$\varphi(t) = (\bar{\alpha} + \gamma n_{max})(1 + \gamma M\tau)^{-1},\ \delta_t = \gamma M(\tau^{-1} + \gamma M)^{-1};$$

$$n'(t) + m'(t) = -[\tau^{-1} + \lambda m(t)]n(t) + aI(t); \qquad (1)$$

$$m'(t) = -\bar{\alpha}m(t) + \gamma[M - m(t)]n(t);$$

$$\int_{t_0}^{t} \bar{\alpha}[T(t)]\,dt = \int_{t_0}^{t} [\alpha + a_i i + a_I I]\,dt = a(t); \qquad (2)$$

$$n(t) = aI(t)\tau(1 + \delta_t) + \varphi(t)\tau\left[m_0 + \int_{t_0}^{t} a\delta_t I \exp\left(\int_{t_0}^{t} \varphi(t)\,dt\right)dt\right] \times \exp\left(-\int_{t_0}^{t} \varphi(t)\,dt\right). \qquad (3)$$

The recombination term in (1) is a generalized term for mono- and bimolecular recombination.[2-6] For $I = 0$, neglecting weak temperature dependence of τ, γ and λ, we can obtain a precise solution of Eqs.(1)-(2) in implicit form (4), which for $p > q$ can be represented approximately in the explicit form (5):

$$(1 + p)\ln\frac{m}{m_0} + (p - q)\ln\left[1 - r_0\left(1 - \frac{m}{m_0}\right)\right] = a(t);$$

$$p = \gamma M\tau;\ q = \gamma/\lambda; \qquad (4)$$

$$r_0 = \frac{\lambda m_0}{\tau^{-1} + \lambda_{m_0}} < 1; \quad \frac{m}{m_0} = \exp\left(-\left\{\frac{a(t)}{1+p} + \left(1 - \frac{1+q}{1+p}\right) \times \right.\right.$$
$$\left.\left. \times \left[\left[1 - (1-r_0)^{-1}\left(1 - e^{-\frac{a(t)}{1+p}}\right)\right]\right\}\right). \qquad (5)$$

The adduced solutions of the equations characterizing the kinetics of p.t. current*, which take into account strong filling of the sticking centers, irradiations, variation of the lifetime as a function of the carrier concentration on the sticking centers, and nonequilibrium in the system sticking centers-conduction band, generalize the results of the t.c. theory developed in Refs.2-6 and provide additional possibilities for investigating the conjunction of sticking center parameters E, M, a_i and m_{max}, particularly when $\tau^{-1} \gg \lambda m$.

In addition to the earlier proposed[2,3] method of determining the thermal activation energy E for sticking centers, analysis of the solutions shows that, in accord with the results of Ref.6, the existence of a noticeable temperature dependence of γ and τ gives rise to an addition to the value of E. Comparison of the results of measurements carried out by a nonisothermal procedure with the results obtained by some isothermal method can yield information on the temperature dependences of γ and τ. The kinetics of t.c. is connected with the parameter $c = \gamma/(1 + \gamma M\tau)$, which can easily be determined from the position of the t.c. maxima. In the strong trapping approximation $(\tau^{-1} \ll \gamma M)$ one can obtain evaluations of M for known τ, and then, by fitting the experimental to the theoretical curves, obtain an estimate for γ. The values of a_i can be obtained by means of a formula connected with the temperature position of the p.t. current maxima at different heating rates $s = T_i'$:

$$\alpha \frac{Es}{kT^2_{max}} = (1 + \gamma M\tau)^{-1} [\alpha + a_i i]^2.$$

Finally, for the temperature corresponding to the p.t. current maximum we have the precise relationships: for $\tau^{-1} \gg \lambda m$

$$n^2_{max}(1 + \gamma M\tau) = \alpha^2 m^2_{max} \tau^2 \frac{Es}{kT^2_{max}}$$

and

$$\alpha \frac{Es}{kT^2_{max}} = c\gamma\left(N_c e^{-\frac{E}{kT_{max}}} + n_{max}\right)^2,$$

and for $\lambda m \gg \tau^{-1}$

$$m_{max}\, \alpha \frac{Es}{kT^2_{max}} = n^2_{max}\, q\lambda^2 M.$$

In the presence of several types of sticking centers and sufficiently large energy separations between them the kinetics of p.t. effects can with some approximation be considered independently for each type of center.

The results obtained can be applied directly to investigation of the kinetics of nonisothermal recombination luminescence, which is of interest in connection with the considerations set forth in Ref.7.

In conclusion we note that the principal results of the most recent theoreti-

---

*For the sake of brevity we do not give other more general solutions in explicit form or the consequences following from Eqs.(3)-(5) under various simplifying assumptions.

cal investigation[8] of t.c. kinetics are actually contained in Refs.2 & 3.

Physical-Technical Institute,
Academy of Sciences of the USSR

References

1. E.N.Arkad'eva & S.M.Ryvkin, Fiz.tverd.tela, 1, 1379, 1460 (1959). (Trans. Soviet Physics - Solid State.)
2. V.E.Khartsiev, Transaction of the 7th Conf.on Luminescence, 1958.
3. V.E.Khartsiev, Fiz.tverd.tela, 1, 104 (1959). (Trans.Sov.Phys. - Solid State.)
4. K.W.Böer, S.Oberlander & J.Voigt, Ann.Phys., 2, 130 (1958).
5. V.E.Khartsiev, Transactions of the All-Union Conference on the Theory of Semiconductors, L'vov, 1959.
6. I.I.Boiko, E.I.Rashba & A.P.Trofimenko, Fiz.tverd.tela, 2, 109 (1960). (Trans.Soviet Physics - Solid State.)
7. K.K.Rebane, Ibid., 2, 273 (1960). (Trans.Ibid.)
8. R.Haering & E.Adams, Phys.Rev., 117, 451 (1960).

* * * * * * *

INVESTIGATION OF TRAPPING LEVELS IN CaS PHOSPHORS BY THE METHODS OF EXOELECTRONIC EMISSION AND THERMOSTIMULATED LUMINESCENCE

- V.L.Levshin & P.A.Pipinis

The method of thermostimulated luminescence (glow curves) is one of the basic procedures for investigating trapping levels in crystal phosphors. This procedure cannot, however, give a complete picture of the traps in a phosphor, inasmuch as the released electrons do not always yield luminescence. Another procedure, which supplements the glow curve method, is that of exoelectronic emission. This method can be used even when the released electrons do not yield luminescence in the process of recombination. The method of exoelectronic emission was first utilized for investigation of electron trapping levels in crystals by Lepper[1] and Bogun[2] in 1955.

In employing the emission method, the phosphor is first excited and then there is measured the electronic emission from the surface of the crystal in the process of gradual warming. As in the case of glow curves, there are observed at certain temperatures electronic emission peaks, which are associated with trapping levels in the crystal. This procedure is most effective when used in conjunction with investigation of glow curves. One cannot expect complete coincidence of the electronic emission peaks and the thermostimulated luminescence peaks, for obviously a certain energy, equal to the work function, is required for emergence of the electron from the conduction band into the vacuum. In view of this, the electronic emission peaks may be shifted to the side of higher temperatures relative to the glow curve peaks. Moreover, the electronic emission may be influenced by the surface state of the crystal. There may also be present surface trapping levels, which will give rise to additional electronic emission peaks. On the other hand, there may be evinced in the glow curves hole trapping levels,

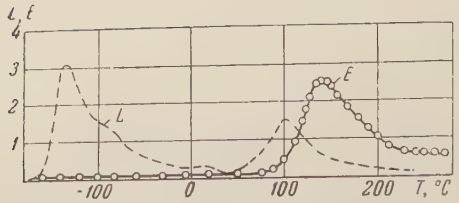

Fig.1

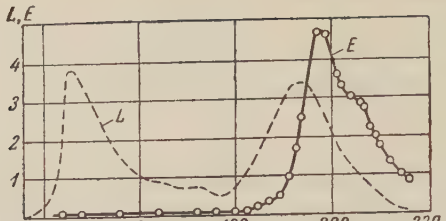

Fig.2

Fig.1. Thermostimulated luminescence (L) and electronic emission (E) curves recorded for CaS:Bi (10^{-2}%) phosphor; heating rate 0.1 degree/sec.
Fig.2. Glow curves and electronic emission curves for the same phosphor as in Fig.1 but heated at 1150° in air for 15 min.

electronic emission from which is obviously impossible.

In the present work we used the method of exoelectronic emission in conjunction with the method of thermostimulated luminescence for investigating trapping levels in crystal phosphors. We constructed a special high vacuum set-up by means of which we could concurrently record glow curves and exoelectronic emission curves in the temperature range from -160 to +300°. A vacuum of $5 \cdot 10^{-7}$ to $5 \cdot 10^{-6}$ mm Hg was maintained in the experimental tube. The phosphor was excited by a cathode beam from an electron gun operated at 6 kv. The electronic emission was recorded by a special electron multiplier sealed into a branch in the main tube. The multiplier signal was applied, via a wide band amplifier, to a pulse integrator. Using this set-up, we investigated the trapping levels in a number of zinc sulfide, calcium sulfide, strontium sulfide and alkali halide phosphors.

By way of illustration, in Fig.1 we show the glow curves and electronic emission curves for a specimen of CaS:Bi (10^{-2}%) phosphor recorded after CR excitation at -160°. There are evinced in the glow curves two low temperature peaks at -130 and -90° and a higher temperature peak at 100°, which can be juxtaposed with the first electronic emission peak at 130°. The electronic emission curves for all CaS phosphors do not have low temperature peaks. This can be explained either on the assumption that the levels involved are hole levels or by the fact that the electrons do not have sufficient energy at low temperatures to emerge from the crystal.

Fig.2 gives curves for the same phosphor but heated beforehand at 1150° for 15 min in air. Here the high temperature glow curve peak and the electronic emission peaks have been shifted 60° to the side of higher temperatures. The close location of the peaks leads to the inference that in both thermostimulated luminescence and exoemission the electrons are released from the same trapping levels. This inference is substantiated by the equal shift of both peaks after heating of the phosphor at 1150°. The small difference (~30°) between the positions of the peaks is explained by the emergence energy of the electrons or by the difference between the kinetics of the two processes.

Physics Faculty
Moscow State University

References

1. J.Lepper, Z.Naturforsch.B, 10, 47 (1955).
2. A.Bogun, Chekhosl.fiz.zh. (Czechoslovak.Physics Journal), 5, 64, 294, 429 (1955).

ON THE POSSIBILITY OF THERMAL ACTIVATION OF CURRENT CARRIER TRAPPING IN CRYSTAL PHOSPHORS

- Yu.L.Lukantsever & F.N.Zaitov

The possibility of thermal activation of the process of current carrier trapping in crystal phosphors has been discussed by Blokhintsev[1] and others. A number of experimental results obtained for different phosphors has been explained from this standpoint.[2-5]

In the present report we give new results indicating that such activation is possible. The subjects of investigation were ZnS:Cu (10^{-4} g/g), NaCl:Ca (0.5 mole %), and KCl:Ag phosphors and unactivated NaCl. We made use of the methods of thermostimulated luminescence and analysis of the decay curves in and near the region of temperature quenching of luminescence (in the case of ZnS:Cu phosphor) and the methods of thermal bleaching and analysis of the spectra of excited absorption (in the case of alkali halide phosphors). The procedures have been described earlier in Refs.6 & 7.

ZnS:Cu phosphor

1. It was found that in excitation of ZnS:Cu at different temperatures the light sum stored on each of the three groups of electron trapping levels in this phosphor varies nonmonotonically. With increase of the temperature in the 140 to 150°K interval the light sum stored on the shallowest group of trapping centers (ϵ = 0.12 ev) decreases, while the light sum stored in the deeper traps (ϵ = 0.18 ev) remains virtually constant. With increase of the excitation temperature from 200 to 250°K the light sum stored on the medium depth levels decreases markedly, while the light sum stored on the deepest group of levels (ϵ = 0.30 ev) increases. This is direct proof of the fact that thermal activation is essential for the process of electron trapping.

2. In investigating the temperature dependence of the ratio of the trapping probability to the electron recombination probability $\gamma = A_t/A_r$ by the method based on analysis of the decay curves in and near the temperature quenching region[8], it was found that the function $\gamma = f(T)$ passes through a maximum. Near the quenching region there is observed growth of γ (from 5.5 at T = 298°K to 9.6 at T = 392°K); in the quenching region γ decreases, falling almost to zero.

The behavior of the parameter γ in the quenching region can be explained on the basis of the elementary decay theory proposed by Adirovich and Vergunas[9]. However, the growth of γ close to the quenching region (also observed by Hsü Haü-Yung[10] for ZnS:Cu:Co phosphor) cannot be explained with the aid of this theory, according to which the parameter γ should be constant in the region close to quenching.

The variation of γ with temperature near quenching can be explained if we assume that thermal activation is necessary for electron trapping.

If, following Vergunas[9], we assume that

$$\gamma = \frac{A_t}{A_r^r + A_r^n} = \frac{\gamma_0}{1 + Ce^{-\Omega/kT}} \qquad (1)$$

(where A_r^r and A_r^n are, respectively, the probabilities for radiative and nonradiative recombination, Ω is the activation energy for the process of nonradiative recombination, and γ_0 and C are constants) and postulate that

$$A_t = fe^{-\frac{\Delta}{kT}} \qquad (2)$$

where f is a constant, Δ is the activation energy for the process of electron trapping by sticking levels, the behavior of $\gamma = f(T)$ in the temperature interval near quenching can be explained as follows.

In accord with (2), Eq.(1) can be written in the form

$$\gamma = \frac{e^{-\frac{\Delta}{kT}}}{B + C' e^{-\Omega/kT}}, \tag{3}$$

where

$$B = \frac{A_r^r}{f};$$

$$C' = \frac{A_r^n}{f}.$$

Investigation of the expression for γ leads to the conclusion that the temperature corresponding to the maximum of $\gamma = f(T)$ is

$$T_m = \frac{\Omega}{k \ln \frac{C'(\Omega - \Delta)}{B \cdot \Delta}}. \tag{4}$$

It will be evident from (4) that the function $\gamma = f(T)$ can pass through a maximum if there is fulfilled the condition

$$\Delta < \Omega. \tag{4a}$$

Alkali halide phosphors

Investigation of the thermal bleaching curves for alkali halide phosphors (see, for example, Ref.7) showed that the stability of F centers is strongly dependent on plastic deformation of the phosphor and the presence of impurities in the crystal. This behavior, in view of the quasimonomolecular kinetics of destruction of F centers, must be connected with changes in the mechanism and conditions of destruction of F centers under the influence of different factors acting on the phosphor.

The ion mechanism of destruction of F color centers in alkali halide crystals was considered in Refs.11 & 12. At present the mechanism of ionic destruction of F color centers can be described as follows:

1. At a certain point in the crystal lattice there form free point microdefects. The probability of freeing of these microdefects is given by

$$P_{0\nu} = P_{0\nu} e^{-Q_\nu/kT},$$

where Q_ν is the activation energy.

If n_ν is the number of possible points of formation of free microdefects, the number of free microdefects will be $n_\nu P_{0\nu} e^{-Q_\nu/kT}$.

2. These point microdefects interact with the F centers and destroy them. We denote the number of F centers by n_F and the cross section for interaction of microdefects with F centers by $\sigma_r = \sigma_{0r} e^{-Q_r/kT}$, where Q_r is the activation energy for the process of trapping of a microdefect by an F center.

3. Point microdefects interact with dislocation breaks and are "trapped" by them. We denote the number of dislocation breaks by N, and the cross section for trapping by $\sigma_t = \sigma_{0t} e^{-Q_t/kT}$, where Q_t is the activation energy for the trapping process.

Represented schematically the process is

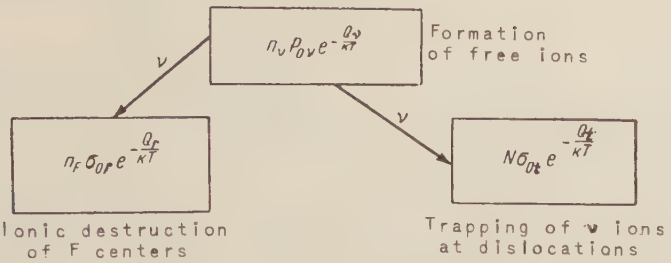

Using the above defined notation, we can write the following expression for ionic destruction of F centers:

$$-\frac{dn_F}{dt} = P_\nu n_\nu \frac{\sigma_r n_F}{\sigma_r n_F + \sigma_t N}, \tag{5}$$

or

$$-\frac{dn_F}{dt} = \frac{P_{0\nu} n_\nu e^{-\frac{Q_\nu}{kT}}}{1 + \gamma_0 \frac{N}{n_F} e^{-\frac{Q_t - Q_r}{kT}}}. \tag{6}$$

Inasmuch as dislocation breaks are "sinks" for point microdefects, the probability for trapping of mobile ions capable of destroying F centers by these sinks will be greater than the probability for interaction of these ions with F centers. Then on condition that $\gamma_0 \frac{N}{n_F} e^{-\frac{Q_t - Q_r}{kT}} \gg 1$ from Eq.(6) we obtain

$$-\frac{dn_F}{dt} = P_{0\nu} \frac{n_\nu}{\gamma_0 N} n_F e^{-\frac{(Q_r + Q_\nu) - Q_t}{kT}}. \tag{7}$$

In this kinetic equation the factor $C = P_{0\nu} \frac{n_\nu}{\gamma_0 N}$ depends on the conditions of preparation of the phosphor (n_ν and N) and can assume an anomalously high value, exceeding the ion vibration frequency $\nu \approx 10^{14}$ sec^{-1}.

By appropriate treatment of the phosphor to obtain different values of n_ν and N one can vary the rate of dissociation of F centers $-dn_F/dt$. Equation (7) agrees in form with the equation of Adirovich[5] for the electron mechanism of ionization of color centers, if we assume that

$$(Q_r + Q_\nu) - Q_t > 0,$$

i.e.,

$$Q_r + Q_\nu > Q_t. \tag{8}$$

Noteworthy is the close similarity or universality of the results obtained for different phosphors as regards the relation between the activation energy for trapping processes and recombination of current carriers (see Eqs.(4a) and (8)). The actual degree of universality of these results is still not clear. There is need for further investigation of carrier (electron, ion, hole) trapping levels in different types of crystal phosphors.

References

1. D.I.Blokhintsev, Izv.AN SSSR, Ser.fiz., 9, No.4-5 (1945).

2. V.V.Antonov-Romanovskii, V.L.Levshin, Z.L.Morgenstern & Z.A.Trapeznikova, Ibid., 13, 75 (1949).
3. Z.L.Morgenstern, Doklady AN SSSR, 58, 783 (1947).
4. D.T.Randall & M.H.F.Wilkins, Proc.Roy.Soc.A, 184, 366 (1945).
5. E.I.Adirovich, Nekotorye voprosy teorii lyuminestsentsii kristallov (Some problems in the theory of luminescence of crystals), M., 1951.
6. Yu.L.Lukantsever, Thesis, Tomsk, 1959.
7. F.N.Zaitov, Thesis, Tartu, 1957.
8. F.I.Vergunas & Yu.L.Lukantsever, Optika i spektroskopiya, 5, 156 (1958).
9. F.I.Vergunas, Ibid., 1, 416 (1956).
10. Hsü Hsü-yung, Doklady AN SSSR, 103, 586 (1955); Ibid., 106, 818 (1956).
11. F.N.Zaitov & V.Ya.Kark, Trudy IFA AN ESSR (Proceedings, Inst.of Physics & Astronomy, Estonian SSR Ac.of Sci.), No.6, 82 (1957).
12. Ch.B.Lushchik, Ibid., No.8, 75 (1958).

DISCUSSION

Ch.B.Lushchik: A few years ago we discovered that for many classes of nonmetallic crystals prolonged storage of the light sum is impossible at temperatures higher than half the absolute melting temperature. This interesting effect is connected with ionic processes that occur at these temperatures, processes that vitiate the spatial separation of electrons and holes. Ionic processes, in general, lead to many interesting effects and situations. In particular, they make possible exceptionally narrow glow peaks. In Tartu we observed peaks for which $T_m/\delta = 20\text{-}25$, where T_m is the temperature of the peak and δ is its half-width. The factor p_o in the expression $p = p_o \exp(-\epsilon/kT)$ attains a value of 10^{20} sec^{-1}. Zaitov showed theoretically that the values of p_o can be very large. This is the point of greatest interest in his report. I would like to call attention of all investigators engaged in analysis of data on thermostimulated luminescence that in most cases they have to deal with nonelementary peaks. Before attempting to calculate the activation energy and other parameters one must carefully check the nature of the peak. The relation $T_m/\delta \approx 10$ cannot serve as a criterion for establishing whether the peak is elementary.

RATE OF PHOSPHORESCENCE DECAY AS A FUNCTION OF FILLING OF ELECTRON TRAPS AND TEMPERATURE

- N.V.Zhukova, G.K.Evdokimova & V.L.Levshin

The aims of the present work were to investigate the filling of electron traps under excitation of the phosphor at different temperatures, to establish the relation between the rate of decay of phosphorescence and the release of electrons from traps of different depth, and to elucidate the role of retrapping in the process of natural decay.[1,2]

For the experiments we chose ZnS:Cu($6\cdot10^{-5}$ g/g):Co(10^{-5} g/g) phosphor[3], which has one broad (~180°) thermostimulated luminescence band peaking at ~75°. The shape of the glow curve is shown in Fig.1,a.

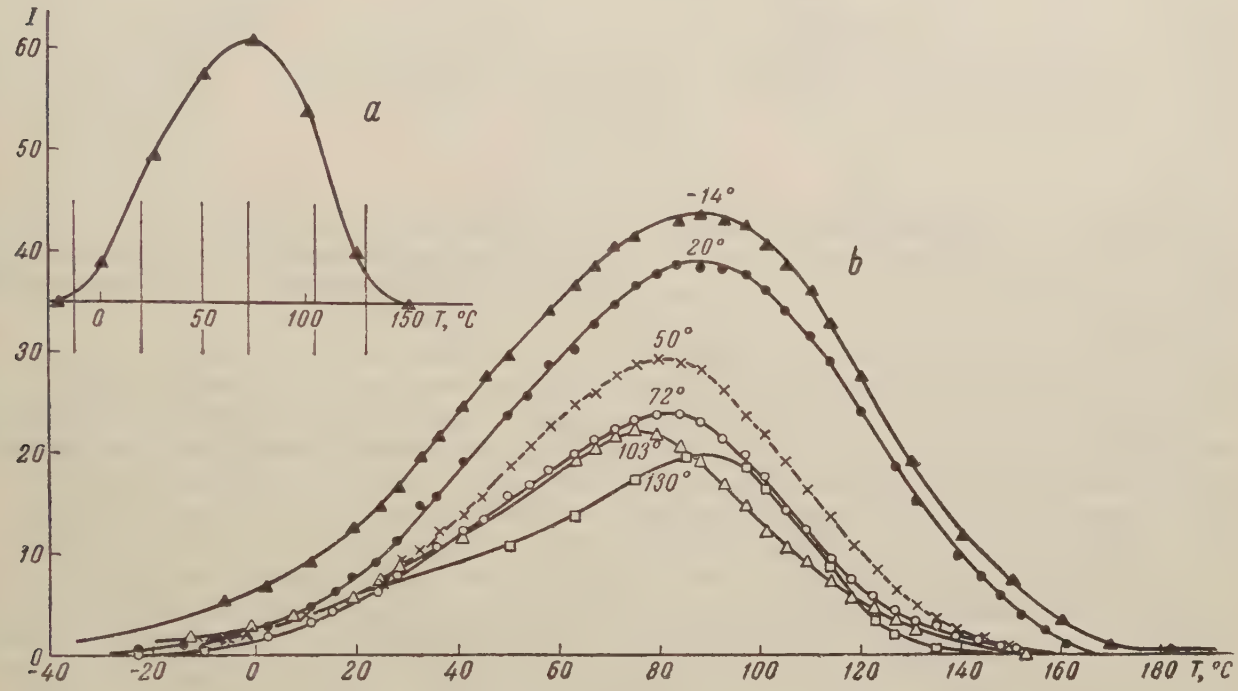

Fig.1

In investigating the filling of the trapping levels, we excited the phosphor simultaneously by the 366 and 436 mμ lines from a mercury tube for 10 min at different temperatures in the range from -14 to +130°. Immediately after excitation the specimen was immersed in liquid nitrogen. The excitation temperatures employed in the experiment are indicated by the bars on the temperature scale in Fig.1,a. The glow curves obtained in this manner are shown in Fig.1,b. It will be seen that with increase of the excitation temperature the light sum stored by the phosphor decreases and the glow curves are deformed.

In excitation of the phosphor at any temperature there occurs population by electrons of a wide band of trapping levels, including levels that lie 150° below the excitation temperature. The filling of the shallower levels proceeds more intensely then of the deeper levels, which indicates that the shallow levels are characterized by a larger trapping cross section. Thus in the early stages of natural decay there must participate electrons ejected from shallow levels, T_{max} for which is appreciably lower than the excitation temperature.

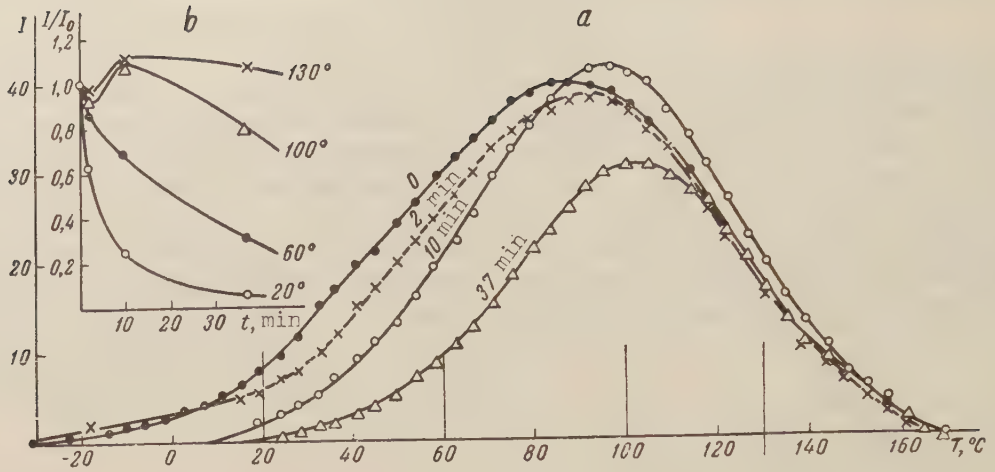

Fig.2

In order to determine which levels are de-excited in the individual stages of decay, we excited the phosphor at 18° and then after allowing it to decay for different periods from 0 to 37 min, recorded the thermostimulated luminescence curves (Fig.2,a).

With decrease of the stored light sum the peak of the glow curve is shifted to the side of higher temperatures, inasmuch as in the process of decay first the shallowest and then the increasingly deeper traps are emptied. In addition, there obviously occurs electron migration, i.e., retrapping: the electrons from shallow levels migrate to deeper ones, so that the number of electrons in deep traps in some cases even increases during the decay period. This result is presented in Fig.2,b, where we show the variation in the population of trapping levels of different depth in the process of decay. The level depths are characterized by the temperatures indicated at the ends of the respective curves.

Further we determined what range of levels participates in different stages of decay. It was found that in the process of natural decay trapping levels in a wide range of depths (~130°) take part in each stage. At late stages of decay there is noticeable transfer of electrons from shallow to deeper levels. However, the increment in number of electrons in deep traps is always smaller than the number of recombining electrons: at no stage in decay did the number of electrons in deep traps exceed 0.6 the number that had undergone recombination.

Moscow Avaiation Institute &
Moscow State University

References

1. N.V.Zhukova, Doklady AN SSSR, 103, No.6, 101 (1955).
2. V.Levchine, J.phys.et radium, 17, 684 (1956).
3. Hsü Hsü-yung, Optika i spektroskopiya, 1, 264 (1956).

VARIATION OF THE STEADY-STATE LUMINESCENCE OF ZnS PHOSPHORS WITH THE EXCITATION INTENSITY

- K.-S.K.Rebane

Investigation of equilibrium processes in phosphors involving transfer of the excitation energy by migration of holes and electrons in the crystal is of great interest. Some aspects of this problem have been investigated in the studies of Ref.1-7.

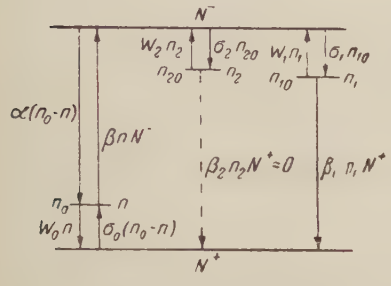

Trapping level scheme

In the present work we consider a band scheme comprising three trapping levels, one of which is a hole level and two are electron levels. The possible transitions between these are indicated in the accompanying figure. In solving the system of equations describing the behavior of this model we take into account the possibility of complete filling of the hole levels. We consider the region of weak and medium intensity excitations, wherein one can assume $n_1 + n_2 \approx n$). We further assume the number of trapping centers for electrons is much greater than the number of trapping centers for holes. Also, we postulate $\beta_2 \ll \beta_1, \beta$. In this case the following equation may be written for the number of ionized luminescence centers (for trapped holes) (also see Ref.7):

$$n = -\frac{1}{2}\cdot\frac{C\alpha+D}{A\alpha-B}\alpha + \sqrt{\left(\frac{1}{2}\cdot\frac{C\alpha+D}{A\alpha-B}\alpha\right)^2 - \frac{E-F\alpha}{A\alpha-B}\alpha}. \qquad (1)$$

Here α is a quantity proportional to the excitation intensity, and $A,\ldots,F$ are quantities that do not depend on α as long as $W_i(T) > W_i(\alpha)$, if the probabilities for release of electrons and holes are written in the form

$$W_i(\alpha, T) = W_i(T) + W_i(\alpha)^*. \qquad (2)$$

Further we obtain

$$N^- = \frac{\alpha + \left(W_1 - \frac{\alpha}{n_0}\right)n}{\delta_1 + \delta_2\frac{W_1}{W_2} + \beta n}. \qquad (3)$$

The luminescence intensity is proportional to the number of recombination events:

$$I = \beta n N^-. \qquad (4)$$

For small α, when $W_i(T) \gg W_i(\alpha)$, n increases in proportion to $\sqrt{\alpha}$. If also $\left(W_1 - \frac{\alpha}{n_0}\right)n \gg \alpha$, we will have $N^- \sim \sqrt{\alpha}$. In this region the quantum yield is constant:

$$q = \frac{\beta}{\beta_1}\cdot\frac{W_1}{W}\cdot\frac{\delta}{\delta_1} = q_1. \qquad (5)$$

With increase of α the first term in Eq.(3) becomes larger than the second, and in this region N^- becomes proportional to α. The quantum yield q increases. The growth of q continues as long as $n \to \text{const}$. As will be evident from Eqs.(1)

---

*As usual, we assume $W_i(\alpha) = k_i\alpha$, where k_i is a constant.

and (3), in principle, one can obtain a very sharp increase of $I(\alpha)$. Actually, it follows from (1) that under certain conditions $n \sim \alpha$. If $n \sim \alpha$ in the region of α, where $W_1(T) < W_1(\alpha)$, then $I \sim \alpha^3$. In this case $N^- \sim \alpha^2$.

In the region of variation of α, where $W_i(T) < W_i(\alpha)$ all the α in (1) cancel, and $n = \text{const}$, $N^- \sim \alpha$, $I \sim \alpha$ and $q = q_2$. Obviously, $q_2 > q_1$.

Inasmuch as the release probability depends on the temperature, we can readily obtain the temperature dependences of n, N^- and I. It can readily be shown that the region of nonlinear growth of I as a function of α shifts with increase of the temperature T to the side of higher values of α. I does not depend on T in the region which is defined by the condition $W_i(T) < W_i(\alpha)$. Under certain conditions one can obtain increase of I with growth of T. The region of temperature quenching is shifted to the side of higher temperatures with increase of α. A similar shift is obtained if we take into account the influence of infrared light. These results are in good agreement with the experimental data[8-12]. For the region of strong temperature quenching $q \approx W^{-1/2}$. If we assume that $W \sim \exp(-E/kT)$ where E is the depth of the hole traps, we obtain

$$q \sim \exp(E/2kT). \qquad (6)$$

There is no difficulty in principle in taking into account high concentrations of free holes and electrons in the crystal (see, for example, Ref.7), but this will add nothing significant to the above analysis.

References

1. L.A.Vinokurov & M.V.Fok, Optika i spektroskopiya, 1, 248 (1956).
2. M.Fock, Halbleiter und Phosphore, s.593, Braunschweig-Berlin, 1958.
3. M.Schön, Techn.Wiss.Abhandl.Osram.Ges., 7, 185 (1958).
4. H.A.Klasens, J.Phys.Chem.Solids, 9, 185 (1959).
5. C.A.Dubov, Brit.J.Appl.Phys.Suppl., 47, 107 (1955).
6. N.A.Tolstoi, Optika i spektroskopiya, 6, 665 (1959); Ibid., 1, 216 (1956).
7. K.-S.K.Rebane, Trudy In-ta fiz.i astron.AN EstSSR (Proceedings of the Institute of Physics and Astronomy of the Estonian SSR Ac.of Sci.), No.10, 209 (1959).
8. K.-S.K.Rebane, Optika i spektroskopiya, 4, 211 (1958).
9. K.-S.K.Rebane, Proceedings of the Institute of Phys. & Astron. of the Estonian SSR Ac.of Sci., No.8, 105 (1959).
10. N.R.Nail, F.Urbach & D.Pearlman, J.Opt.Soc.Amer., 29, 690 (1949).
11. P.S.Litvinova, Izv.vyssh.uchebn.zaved.Fizika (Bulletin of Higher Schools. Physics), No.2, 73 (1958).
12. K.-S.K.Rebane & E.Sakarinen, Optika i spektroskopiya, 4, 545 (1960). (Trans.Optics & Spectroscopy.)

DISCUSSION

Ch.B.Lushchik: It is of interest to compare the variation of the quantum yield of luminescence by ZnS phosphors as a function of the intensity of the stimulating light, investigated by Rebane, with the analogous variation of the photoelectric polarization of ZnS crystals observed by I.K.Vitol. It presumably follows from the data of Vitol that in the region of both low and high excitation intensities the sign of the process is the same (the process is probably electronic). Hence there is no justification in interpreting these results to invoke the hypothesis of sensitized energy transfer from hole and electron recombination centers to luminescence centers. Rebane's theory explains this effect without recourse to "sensitized effects".

INVESTIGATION OF RARE EARTH ACTIVATED SrS PHOSPHORS BY THE METHOD OF ELECTRON PARAMAGNETIC RESONANCE

- V.V.Antonov-Romanovskii & V.G.Dubinin

1. In an earlier study[1] the method of electron paramagnetic absorption was used for investigating the state of the activator in phosphors. In SrS:Eu:Sm phosphor there was observed a decrease of the paramagnetic absorption of Eu^{2+} with excitation of the phosphor in the optical absorption band of Eu^{2+}. The decrease in paramagnetic absorption amounts to ~15%, which is in agreement with the decrease of the intrinsic absorption coefficient of Eu^{2+}. At the same time there were carried out absolute measurements of the number of quanta emitted by the excited phosphor; the results of the measurements substantiated the paramagnetic absorption data. Thus it may be asserted that in the process of excitation of SrS:Eu:Sm phosphor there occurs ionization of the europium activator ($Eu^{2+} \rightarrow Eu^{3+}$).

2. The paramagnetic absorption technique was also used for determining the influence of flux on the concentration of Eu activator in the phosphor. To this end there were investigated phosphors with the same amount of Eu in the initial batch, but prepared with LiF or $SrCl_2$ flux and without flux. It was found that in the phosphor prepared with flux the paramagnetic absorption of Eu^{2+} is greater by a factor of 1.5. This gives reason to assume that the Eu activator concentration in SrS:Eu:Sm phosphor prepared with flux exceeds the concentration of this activator in the phosphor prepared without flux by 30-40%.

3. Inasmuch as all the rare earth elements enter as activators into the SrS lattice mainly in the trivalent state (except for Eu^{2+}), we felt it would be of interest to investigate the influence of flux on trivalent activators. It was obviously necessary to select an activator that would exhibit paramagnetic absorption. Gd^{3+} proved to be suitable, inasmuch as its ground state is $^8S_{7/2}$ and for it paramagnetic absorption is observed at room temperature.

There were prepared SrS:Eu:Gd phosphors without flux and with LiF flux. It was found that under the influence of the flux the concentration of Eu increases by a factor of approximately 3, while the concentration of Gd increases by a factor of ~20. In the single activator phosphor SrS:Gd, the Gd concentration under the influence of LiF flux increases by a factor of ~10. On the basis of the experimental data it may be concluded that for incorporation of Gd^{3+} into the host lattice there must be fulfilled the principle of charge compensation.

4. Having determined from measurements of the paramagnetic absorption of the activator the light sum stored by the phosphor and having calculated the absolute number of quanta emitted by the excited phosphor in process of de-excitation, one can, taking into account the different concentrations of activator entering into the lattice in the process of synthesis of the phosphor, determine the loss of the energy stored by the phosphor in the process of emission. It was established that in SrS:Eu:Sm phosphor only half the stored energy is emitted in the form of light during de-excitation; the remainder is converted to heat after recombination.

"P.N.Lebedev" Physical Institute,
Academy of Sciences of the USSR

Reference

1. V.V.Antonov-Romanovskii, V.G.Dubinin, A.M.Prokhorov, Z.A.Trapeznikova & M.V.Fok, Zhur.eksp.i teor.fiz., 11, 1466 (1959). (Trans.Soviet Physics - JETP.)

DISCUSSION

V.V.Antonov-Romanovskii: The paramagnetic absorption technique is a very powerful research tool inasmuch as it enables us to obtain a direct answer to some questions regarding the structure of luminescence centers and the kinetics of phosphorescence. Luminescence centers are highly complex formations, and the method of paramagnetic absorption enables us to determine of what atoms or ions these centers consist, what is the valence of the constituent ions and atoms and how the valence changes as a result of excitation.

At the Fifth All-Union Conference on Luminescence, which was held in 1956 in Tartu, we called attention to the great potentialities of the paramagnetic absorption technique. The report presented today shows that this prediction was correct. In the present work there was obtained a very important result: it was shown that in the excitation of SrS:Eu:Sm phosphor it is the europium rather than any other component of the luminescence centers that transforms from the divalent to the trivalent state. At the same time there were also obtained interesting data on the degree of incorporation of the activators Eu and Gd into the host lattice, depending on the conditions of preparation of the phosphor.

Undoubtedly, when measurements of paramagnetic absorption are realized at low temperatures, where the number of substances exhibiting noticeable paramagnetic absorption is much greater, there will be obtained new, interesting results.

E.B.Aleksandrov: We also carried out measurements similar to those described in the presented report; the purpose of our experiment was to determine the change in the valence state of Mn in $CaSO_4$:Mn phosphor in the process of light sum storage. Detection of such changes would have enabled us to draw certain conclusions regarding the responsibility of the activator for the formation of deep traps in the phosphor. Unfortunately, we did not observe any systematic variation in the intensity or character of the Mn^{2+} absorption lines in the process of de-excitation of the phosphor, although measurements of the number of quanta emitted by the phosphor in the process of de-excitation showed that the absolute sensitivity of our spectroscope was inadequate. It may be assumed that the major part of the Mn in the phosphor does not play any role in the process of light sum storage, and that changes in the spectrum connected with change in the valence of the "active" Mn cannot be detected against the background of the intense lines of the inactive Mn.

In the line of continuing research in this field we believe it may be promising to investigate luminophors with activators that are diamagnetic in the unexcited state and that upon excitation will become paramagnetic as a result of ionization.

In this case the measurements will be essentially of the null type, which should make it possible to realize the full sensitivity of the radiospectrometer and obtain significant results.

INVESTIGATION OF ELECTROLUMINESCENCE PULSES EMITTED BY ZnS:Cu:Al PHOSPHORS WITH A HIGH Cu CONCENTRATION

- A.M.Bonch-Bruevich & V.A.Molchanov

1. The purpose of the work was concurrent investigation of the characteristics of the green and blue luminescence of ZnS:Cu:Al phosphors with a high copper concentration (~0.2 g/g).*

Most of the work was carried out on samples of the phosphor mixed with cable oil and placed in a capacitor with one transparent electrode (the thickness of the luminophor layer was of the order of 60 microns). Unipolar square voltage pulses with a repetition rate of 10^{-2} sec were applied to the capacitor; the pulse rise and decay times were of the order of 2-3 microsec. The pulse duration t' and pulse amplitude U_m could be varied in a wide range.

We employed the oscillographic procedure to observe the kinetics of decay of the luminescence peaks accompanying the leading and trailing edges of the voltage pulses (hereinafter voltage-on and voltage-off light pulses) and the amplitudes I_{m_1} and I_{m_2} of these light pulses. The light sum L emitted under the influence of each voltage pulse was determined by graphic and electrical integration. All measurements were carried out at room temperature.

In addition, we investigated the luminescence of ZnS:Cu:Al single crystals with linear dimensions of the order of 60-80 microns under a microscope. These single crystals were polymerized with two needle electrodes in a mixture of melaminoformaldehyde and resil resins, and mounted in the focal plane of the microscope. An aperture in the focal plane was used to isolate the emission of individual regions about 10 μ in diameter. The signal taken off the photomultiplier coupled to the microscope was applied to a special storing device, which reduced the fluctuation level without distorting the shape of the signal.[1-3] The set-up and its characteristics are described in Ref.4, which also contains reproductions of typical emission pulse oscillograms for individual regions. Thus it was possible to observe on the oscillograph screen the kinetics of luminescence pulses originating in individual regions of the single crystal.

2. As was noted earlier by several authors[5,6], the decay of the voltage-on and voltage-off luminescence pulses in both emission bands does not follow an exponential or hyperbolic law. Hence without regard to the specific law involved, here we will evaluate the rate of decay by the time required for the intensity to fall off by 50% (half-decay time $\tau^{(1/2)}$).

In the green luminescence band the half-decay time for voltage-on pulses ($\tau_1^{(1/2)}$) does not depend on the pulse duration in the range $t' \geqslant 30$ microsec. For shorter t' the voltage-on pulse does not have time to fall off to $I_{m_2}/2$, but the kinetics of initial luminescence decay remains the same as long as t' exceeds the time necessary for build-up of the electroluminescence (~10 microsec).

The half-decay time for voltage-off pulses in the green band also does not depend on the duration of the voltage pulses provided these exceed ~30 microsec, despite the fact that in this case there is superimposed on the voltage-off pulse an appreciable part of the decaying voltage-on pulse (Fig.1). Up to t' of the order of 20-30 microsec (or even 40 microsec for some phosphors prepared under different heating conditions) the voltage-off luminescence pulse amplitude also remains virtually constant. At the same time the light sum L begins to decrease for t' of the order of 100-150 microsec (or even a longer pulse duration for some of the investigated luminophors) (Fig.1).

---

*The investigated phosphors were made available by F.M.Pekerman, whom we take this opportunity to thank.

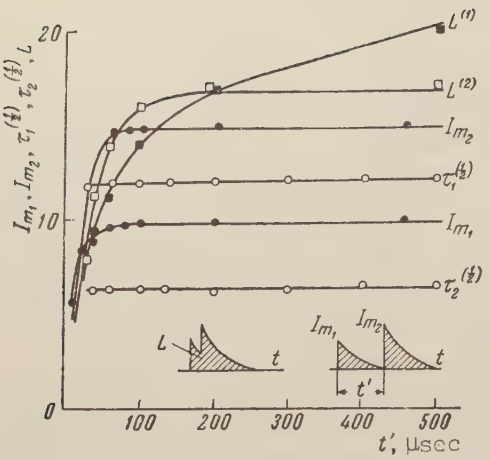

Fig.1. Variation of the half luminescence decay time of voltage-on ($\tau_1^{(1/2)}$) and voltage-off ($\tau_2^{(1/2)}$) luminescence pulses, their amplitudes (I_{m_1} and I_{m_2}) and light sum L ($L^{(1)}$ and $L^{(2)}$ apply to two different specimens) with the pulse duration t'. Data for the green luminescence band. The hatched diagrams show the shape of the luminescence pulses at different values of t'.

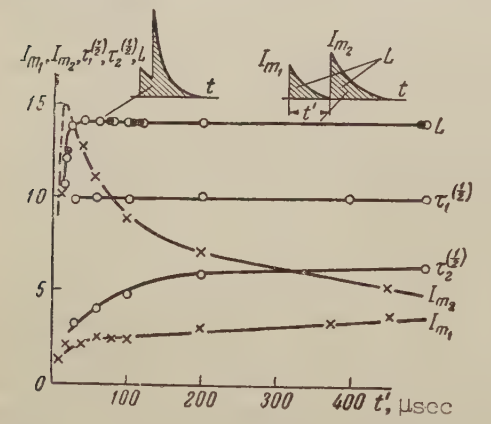

Fig.2. Variation of $\tau_1^{(1/2)}, \tau_2^{(1/2)}, I_{m_1}, I_{m_2}$ and L with t' for the blue luminescence band. The hatched diagrams show the shape of the emission pulses for different t'.

Thus the experimental data indicate that cut-off of the voltage is accompanied by diminution of the luminescence in the green band, excited at the instant of application of the voltage to the capacitor.[7] In our opinion this effect is not in conflict with the commonly proposed mechanism of electroluminescence, according to which most of the luminescence is associated with return of electrons into the region of strong ionization of the luminescence centers in the region near the cathode.[8-11] If the external voltage is cut off before virtually all the luminescence centers have time to recombine with electrons, then under the influence of the polarizing field an appreciable number of electrons will again be drawn out of the ionization zone and, naturally, the emitted light sum will be reduced. As for the time of formation of the polarizing field, in view of the observed regularities it may be concluded that this field forms in the luminophor in a time of the order of 30 microsec.[7]

In the blue luminescence band the light sum L remains virtually constant up to t' of the order of 30-40 microsec, while in the range of appreciably longer pulse durations the decay of luminescence of the voltage-off pulses is accelerated and at the same time the amplitude of these pulses in increased (Fig.2). This indicates that in the blue luminescence band there is no diminution of the emission in the above mentioned sense. Excitation of luminescence in the blue band is not connected with recombination of electrons, which can be drawn out of the zone of strong ionization in the vicinity of the cathode and into which they can return upon reversal of the electric field acting on the crystal. At the samt time, as in the green band, "preparation" of the voltage-off luminescence in the blue band occurs upon application of the electric field. This follows from the fact that the probability or tempo of decay of the luminescence of the blue centers depends substantially on the pulse duration, although the total number of de-exciting pulses does not depend on t'.

Further investigations are necessary to elucidate the mechanism of the blue luminescence, which cannot be interpreted from the standpoint of the simple scheme of excitation of electroluminescence. As far as we know there are no references in the literature to the absence of an explicit relationship between the variation of the light sum in the green and blue bands and the effect of diminution of lumi-

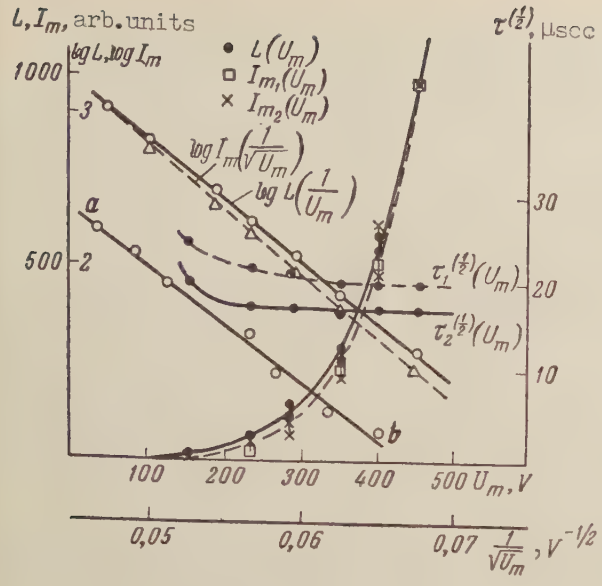

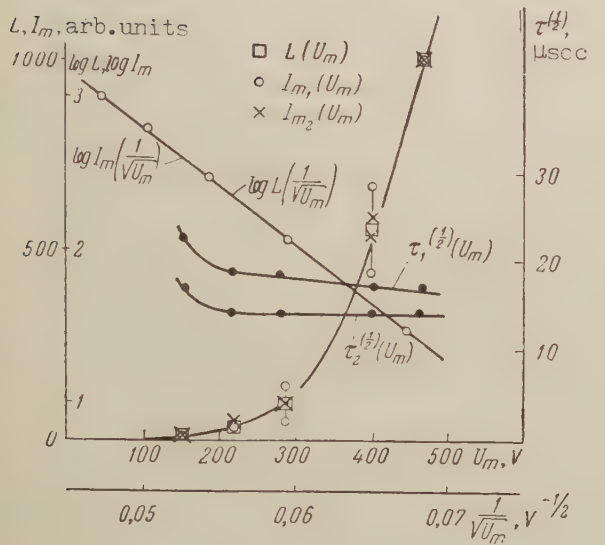

Fig.4. Variation of $\tau_1^{(1/2)}$, $\tau_2^{(1/2)}$, I_{m_1}, I_{m_2} and L for the blue luminescence band with U_m. The indicated spread indicates the scatter of the experimental data for different pulse durations.

←Fig.3. Variation of $\tau_1^{(1/2)}$, $\tau_2^{(1/2)}$, I_{m_1}, I_{m_2} and L for the green luminescence band with the pulse voltage U_m. The indicated spread characterizes the scatter of the experimental data for different pulse durations. The line ab represents the variation of log I_{m_2} as a function of $1/\sqrt{U_m}$ for a ~10 μ section of a single crystal.

nescence in the green band; also we have found no mention of the above described distinctive behavior of the blue band.

3. There is evinced a certain parallelism between the variation of the luminescence in the blue and green bands with variation of the voltage pulse amplitude; this is complicated, however, by different t' dependences of the light sum and voltage-off emission pulse amplitudes in the two bands: first, in both bands the values of $\tau_1^{(1/2)}$ and $\tau_2^{(1/2)}$ are weakly dependent on U_m, increasing only slightly with decrease of the field strength on the capacitor (Figs.3 & 4), and, second, in both bands the U_m dependence of the light sum is characterized by the law

$$L = Ae^{-\frac{B}{\sqrt{U_m}}}, \qquad (1)$$

the values of the coefficient B for both bands are virtually equal ($B \approx 190$-200). The value of the coefficient A for the blue band does not depend on the pulse duration t' in the $t' \geqslant 30$-40 microsec range. In contrast, in the green band, the value of A depends substantially on t' this dependence is characterized by the L vs t' plots in Fig.1. Moreover, the variation of I_{m_2} with U_m in both luminescence bands follows a law similar to (1), namely,

$$I_{m_2} = A'e^{-\frac{B'}{\sqrt{U_m}}}, \qquad (2)$$

The value of the coefficient B' for both bands is virtually the same and agrees within the limits of the measurement error with the value of B in Eq.(1). The value of the coefficient A' (in contrast to that of coefficient A in Eq.(1)) does not depend on t' in the green band (for $t \geqslant$ 30-40 microsec) but does depend on t' in the blue band. This dependence is characterized by the $I_{m_2} = f(t')$ curve in Fig.2.

Relationships of the type of Eq.(1) have been repeatedly discussed in the

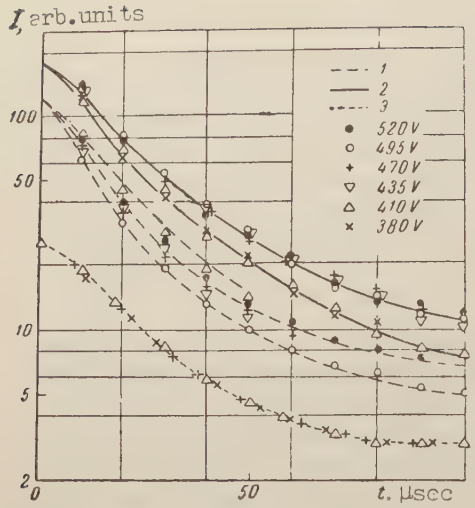

Fig.5. Kinetics of luminescence decay of a section of a single crystal (1), of an entire single crystal (2) and of an electroluminescent capacitor (3) at different values of the applied voltage (green band).

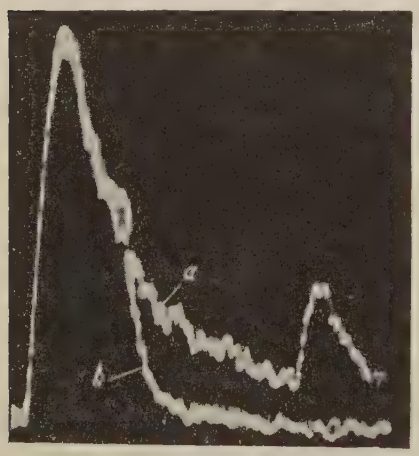

Fig.6. Oscillograms of luminescence pulses in the green band obtained for different durations of the voltage pulses: a - 120 microsec, b - 40 microsec.

literature in connection with considerations of the conditions of ionization of luminescence centers.[8,9,12-14]

It is worth noting that this relationship appears to be valid for both the luminescence bands. This indicates that the processes of ionization of both blue and green luminescence centers have traits in common, even though the regularities characterizing the de-excitation of these centers and the processes occurring in them during the interval between excitation and de-excitation are substantially different. The fact that relationships (1) and (2) are of the same form is in agreement with the weak dependence of the kinetics of decay on the amplitude of the voltage pulses.

4. The use of a storing device in the set-up for microscopic observation of the luminescence enabled us to follow the kinetics of electroluminescence of single crystals and of the emission from the regions in the neighborhood of the electrodes. The luminescence kinetics proved to be as complicated (neither exponential nor hyperbolic decay) as in the case of polycrystalline specimens, and generally similar to the latter (Fig.5). In particular, the half-decay time of areas of single crystals, like that of electroluminescence capacitors, is very weakly dependent on the amplitude of the voltage pulses. The slight differences between the rates of decay of an individual single crystal and a polycrystalline specimen can be attributed to inhomogeneity of the crystals in the capacitor-filling mixture.

The other regularities characterizing the emission observed under a microscope are similar to the regularities for polycrystalline specimens. Thus, for example, the variation in the amplitude of the green band voltage-off pulses observed for individual sections of the crystal as a function of U_m agrees with the variation observed for the electroluminescence of the capacitor (Fig.3).

Our microscopic set-up also enabled us to observe the diminution of luminescence in the green band with change in the direction of the field in the crystal. This is illustrated by the luminescence-pulse oscillograms obtained for voltage pulses of different duration and reproduced in Fig.6. It will be seen that with decrease of t' from 120 to 40 microsec, cut-off of the voltage is accompanied by an appreciable increase in the rate of decay of the luminescence induced by application of the voltage. It will be evident that with decrease of the pulse duration the light sum corresponding to a voltage pulse is also reduced.

Thus microscopic observations show that the above described regularities characterizing the electroluminescence are not complicated by the use of polycrystalline electroluminescent capacitors, i.e., the polycrystalline effect are truly representative of the "microscopic" effects.

References

1. D.Steinhais, H.Grosswhite & G.Dieke, Spectrochimica Acta, 5, 436 (1953).
2. B.A.Mamyrin, Zhur.tekh.fiz., 26, 652 (1956). (Trans.Soviet Physics - Technical Physics.)
3. B.A.Ermakov & A.A.Mak, PTE, No.3, 95 (1959). (Trans.Instruments & Experimental Techniques.)
4. A.M.Bonch-Bruevich, Ya.E.Karis & V.A.Molchanov, Optika i spektroskopiya, 11, (1961). (Trans.Optics & Spectroscopy.)
5. S.Nudelman & F.Matossi, J.Electrochem.Soc., 101, 546 (1954).
6. F.Matossi & S.Nudelman, Phys.Rev., 99, 1100 (1955).
7. A.M.Bonch-Bruevich & O.S.Marenkov, Optika i spektroskopiya, 8, 855 (1960). (Trans.Optics & Spectroscopy.)
8. W.Piper & F.Williams, Phys.Rev., 87, 151 (1952).
9. P.Zalm, Philips.Res.Reports, 11, 353 (1956).
10. C.Hanke, J.Appl.Phys., 28, 117 (1937).
11. D.R.Frankl, Phys.Rev., 100, 1105 (1955); Ibid., 111, 1540 (1958).
12. G.Destriau & H.Tvey, Proc.IRE, 43, 1911 (1953).
13. V.A.Chuenkov, Izv.AN SSSR, Ser.fiz., 22, 369 (1958). (Trans.Bulletin, 22, 369.)
14. L.V.Keldysh, Zhur.eksp.i teor.fiz., 37, 713 (1959). (Trans.Soviet Physics - JETP.)

INVESTIGATION OF THE ELECTROLUMINESCENCE OF ZnS:Cu AND ZnS:Cu:Mn PHOSPHOR LAYERS WITH EXCITATION BY DC AND PULSE VOLTAGES

- V.N.Favorin, G.S.Kozina & I.D.Anisimova

1. Luminescence in a dc field

The luminescence of ZnS electroluminophors in conducting media in a dc field has been described by a number of authors.[1,2] In 1958 one of us (G.S.Kozina) discovered that ZnS:Cu:Mn phosphor in a solid dielectric medium (for example, a mixture of melamineoformaldehyde and alkyd-resyl resins) exhibits bright luminescence with a band characteristic of manganese (λ_{max} = 580 mμ).[3] Typical brightness vs voltage curves for the yellow electroluminescing ZnS:Cu:Mn phosphor are shown in Fig.1 (curves 1 and 2). Curve 3 in this figure shows the variation with voltage in an ac field.

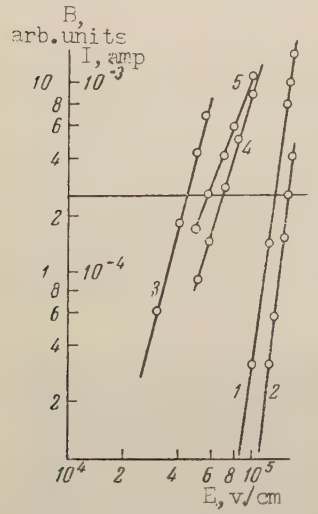

Fig.1. Variation of the brightness B (1,4) and conduction current I (2,5) with the applied dc voltage for ZnS:Cu:Mn layers in a solid dielectric after aging in an electric field (1,2) and before aging (4,5); curve 3 - B = f(E) in an ac field.

The behavior of this electroluminophor is characterized by the following regularities:

1. In the investigated range of brightness, currents and voltages, all the observed dependences are characterized by relationships of the type $B \sim V^n$ and $I \sim V^m$.

2. The nonlinearity indices (exponents) for the brightness (n) and the current (m) are close, and, consequently, the variation of brightness as a function of the current - $B = f(I)$ - is nearly linear.

3. The nonlinearity index $n_{=}$ for the luminophor luminescing in a dc field is appreciably higher than the index for the same luminophor luminescing in an ac field: $n_{=} \approx 10$ while $n_{\sim} \approx 3$-4.

Thus it may be assumed that the characteristic of luminescence of the layer is intimately related with the characteristics of its conductivity.

The brightness and current characteristics for the green luminescing (ZnS:Cu) electroluminophor are similar in character. Just as in the case of the yellow manganese luminophor, the nonlinearity index for a dc field is higher than for an ac field ($n_{=}$ = 10-12; $n_{\sim}$ = 3-4), and the indices for the current and brightness in a dc field are close.

The principal difference between the yellow and green luminophors is that the brightness of the yellow luminophor is at least two orders of magnitude **greater than that of the green, and attains several millistilb.**

A characteristic of the investigated layers is that the brightness and current vary with time in the process of aging, i.e., holding the layer in a field. In the process of aging the nonlinearity indices n and m increase; the current nonlinearity index increases more rapidly than the brightness index (see curves 4 and 5 in Fig.1 for the layer before aging). It follows from the data of Fig.1 that with the same current the brightness of the aged specimen is higher than that of the unaged one, which indicates increase of the effective voltage on the luminophor crystals in the aged layer. This increase in effective voltage, however, does not correspond to the growth of the mean voltage on the layer, which is explained by change in the distribution of the voltage between the phosphor crystals and the dielectric strata.

Similar results are observed for the green luminophors.

Thus the electroluminescent layer may be represented in the form of a nonlinear resistance consisting of two nonlinear resistances with different nonlinearities, namely, the luminophor and the dielectric.

Flow of current through the luminophor leads to excitation of its luminescence, the brightness of which is determined by the magnitude of the current flowing through it, while the nonlinearity of the voltage dependence of the brightness depends primarily on the nonlinearity of the resistance of the layer.

2. Luminescence with excitation by a pulse field

Excitation of luminophors with a bright luminescence in a dc field (for example, ZnS:Cu:Mn) with square voltage pulses should lead, on the one hand, to luminescence of the Destriau type associated with the rise and fall of the pulse, and, on the other hand, to luminescence associated with actual flow of current during the period of the pulse. Possibly these two excitations interact to some extent. Thus the "brightness wave" will consist not only of two brightness peaks but also of a plateau between them, corresponding to the "steady" (dc) luminescence during the period of the pulse.

We investigated the excitation of ZnS:Cu:Mn electroluminescent layers by unipolar voltage pulses of duration τ_p = 7 millisec and having a repetition rate of 100 pps.

The brightness waves recorded at two values of the pulse voltage are shown in Figs.2,b & c. It will be evident from a comparison of the figures that the heights of the brightness peaks increase more slowly with increasing voltage than the level of the luminescence plateau. At even higher voltages there are obtained "square" brightness waves. The variation of the amplitudes of the peaks (B_1 and B_2) and the height of the plateau (B_0) with the pulse voltage is shown in

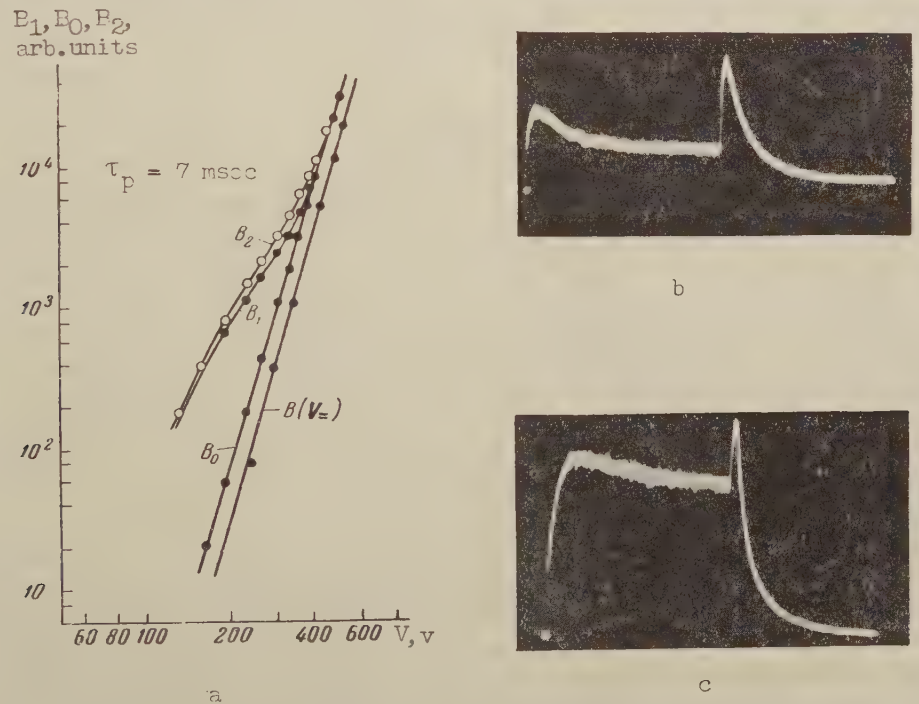

Fig.2. a - Variation of the elements of the brightness waves of ZnS:Cu:Mn (the leading and trailing edge peaks B_1 and B_2 and the plateau B_0) with voltage; b - brightness wave with V_p = 300 v; c - brightness wave with V_p = 400 v.

Fig.2,a. As will be evident from this figure, the level of the plateau increases according to the law for luminescence in a dc field: $B = f(V_{=})$. The amplitudes of the peaks reckoned from the zero level increase according to the luminescence law in an ac field with $n_{\sim} < n_{=}$. With increase of the pulse amplitude $n_{\sim} \rightarrow n_{=}$, and the brightness waves tend to become "square".

These variations in the shape of the brightness waves also lead to change in the variation of the integral brightness as a function of the ac voltage: at higher voltages the brightness tends to vary according to the $B = f(V_{=})$ law.

3. Luminescence under the joint influence of a dc field and a pulse voltage

It was found back in 1958 that the simultaneous application of a dc and ac voltage on solid layers of ZnS:Cu:Mn luminophor in a dielectric medium leads to increase of the brightness in the yellow region of the spectrum.[3] Investigation of the integral luminance[4] and the brightness waves[5] under the influence of simultaneously acting ac and dc fields showed that such luminophors are characterized by a great increase of brightness in the combined field as compared with the sum of the brightnesses in separate equivalent fields. Enhancement of the brightness of specially prepared layers under the joint influence of ac and dc fields has also been described by Thornton[6].

Subsequent investigations showed that the effect of enhancement of brightness under the joint influence of ac and dc voltages is observed not only for yellow but also for green luminophors in a dielectric medium.

In the case of simultaneous application of square pulses and a dc voltage to yellow and green electroluminophors there are observed two effects leading to increase in the integral luminosity of the layer: increase in the height of the brightness peaks and increase of the steady (plateau) luminescence, arising as a result of action of the field consisting of the sum of the dc bias and the pulse

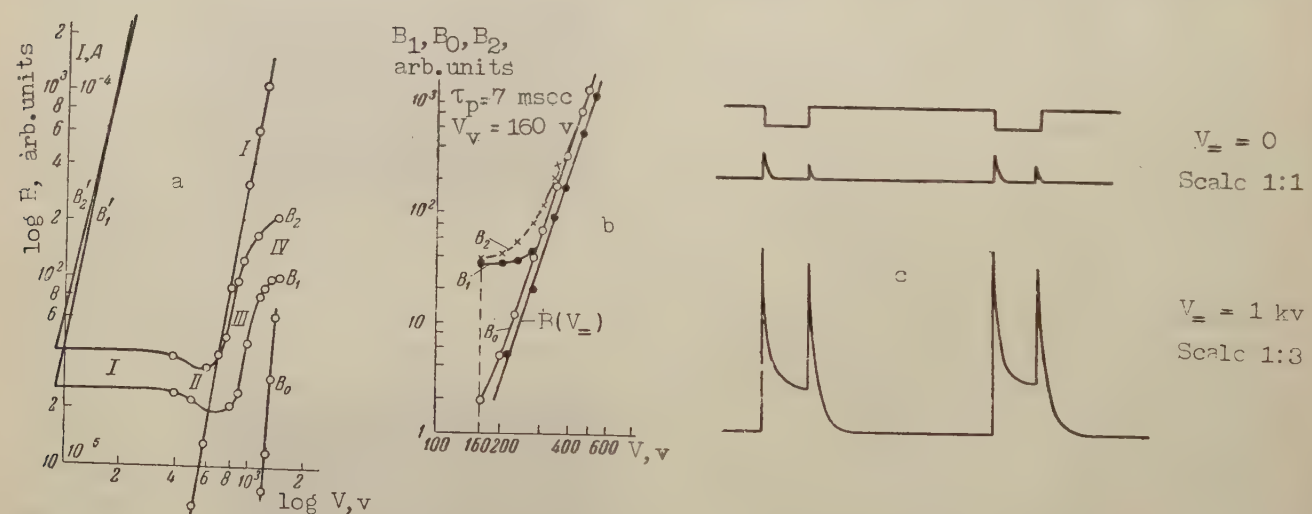

Fig.3. a - Variation of the elements of the brightness waves of ZnS:Cu with the dc voltage at a constant value of the applied ac field; b - variation of the elements of the brightness wave of ZnS:Cu:Mn with the constant voltage at a constant value of the applied ac field; c - ZnS:Cu:Mn electroluminescence brightness waves at a constant value of the ac field and different values of the dc field.

voltage. These effects are illustrated by the oscillograms reproduced in Fig.3,c.

The character of the variation of the height of the brightness wave peaks B_1 and B_2 and the level of the plateau B_0 is shown in Figs.3,a & b.

The conductivity of the layer increases rapidly with increase of the dc voltage (curve 1 in Fig.3,a). The instant of increase in the height of the peaks is associated with a certain value of the conduction current (10^{-5}-10^{-6} amp/cm^2). The similarity observed between the character of the growth of the peaks with increase of the dc voltage (section III in the curves for B_1 and B_2 in Fig.3,a) and the character of the growth of the peaks owing only to the ac voltage (curves B_1' and B_2' in Fig.3,a) suggests that the effect of the dc voltage in this intereval reduces to increase of the nonlinearity of the conductivity, leading to change of the impedances of the phosphor grains and the dielectric strata, as a result of which the ac voltage acting on the phosphor crystals increases. In this case, section I of the curve corresponds to a dc voltage and current insufficient for noticeable change of the impedances, i.e., corresponds to the state $(1/\omega c) \ll R$; section II is apparently due to the fact that the constant voltage is insufficient for redistribution of the impedances but is already sufficient to hinder recombination. In section III, where $(1/\omega c) \approx R$, there already occurs redistribution of the impedances. In section IV the Destriau effect is weakened owing to broadening of the depletion band and relative decrease of the acting gradients. At the same time, there becomes evident the dc field luminescence (B_0).

The proposed explanation for the observed regularities calls for more detailed and careful quantitative investigation.

The character of the analogous curves for ZnS:Cu:Mn phosphors is somewhat different (Fig.3,b). At low values of the dc voltage the heights of the peaks B_1 and B_2 do not depend on the dc voltage. Increase of the dc bias leads to a sharp increase of the luminescence, i.e., rise of the level of the plateau B_0. The luminescence peaks rise only slightly, the increase being characterized by the ac field luminescence law, as in the case of the green luminophor; with further increase of the voltage the peaks merge with the luminescence associated with the conduction current, and the integral luminance increases according to the dc luminescence law.

Conclusions

Thus in general in applying a dc and an ac voltage to a phosphor layer in a dielectric one can observe the effect of additive enhancement of the integral luminance, when the luminescence brightness in an ac field there is added the electroluminescence in a dc field at the instants of addition of the voltages. This additive enhancement is strongly evinced in the case of the yellow luminophors, which have a high electroluminescence brightness in a dc field, but is only weakly evinced in the case of the green luminophors, whose electroluminescence in a dc field is weak.

In addition to the additive enhancement there is also observed the effect of true nonadditive increase in the height of the luminescence peaks in an ac field under the simultaneous influence of a dc field. This effect is particularly clearly evinced in the case of the green luminophors in the region of low brightnesses (corresponding to regions of conductivity of the layer) and is only weakly evinced in the case of the yellow luminophors, inasmuch as in these there rapidly develops the intrinsic dc luminescence.

The region of additive enhancement of the luminance of yellow luminophors is evinced at brightness values in the range from 10^{-1} to 1 millistilb in the 10^{-5} to 10^{-3} amp/cm^2 conductivity region. The region of nonadditive enhancement

of the brightness of the green luminophors is evinced at low luminances ($\sim 10^{-2}$ millistilb) and corresponds to a layer conductivity of 10^{-6}-10^{-5} amp/cm^2.

The brightness of green luminophor layers in an ac field can be increased by a factor of several hundred by the application of a dc biasing field (mainly owing to nonadditive enhancement), while in the case of yellow layers the luminance can be increased only by a factor of 10-20 (owing to additive enhancement).

Most of the observed regularities can, apparently, be explained in terms of the electric properties of the layers consisting of a luminophor and a dielectric, primarily by the nonlinear characteristics of the resistances. The differences between the behavior of the green and yellow luminophors are connected with the differences between their sensitivity to dc current and require further investigation under conditions excluding the nonlinearities introduced by the dielectric strata.

We desire to acknowledge our indebtedness to F.M.Pekerman and her co-workers for developing and preparing the magnesium activated luminophors intensely luminescing in a dc field. We also desire to express our gratitude to Z.A.Trapeznikova and her colleagues for making available the phosphor specimens in which the observed effects were first observed and also to L.K.Tikhonova and A.V.Kapitonov for preparing and measuring the characteristics of the layers.

References

1. P.Zalm, Philips Res.Reports, 11, 353, 417 (1956).
2. J.B.Taylor & G.F.Alfrey, Brit.J.Appl.Phys.Suppl., 4, 44 (1955).
3. V.N.Favorin, G.S.Kozina & L.K.Tikhonova, Optika i spektroskopiya, 7, 703 (1959). (Trans.Optics and Spectroscopy.)
4. G.S.Kozina & L.P.Poskacheeva, Ibid., 8, 215 (1960). (Trans.Ibid.)
5. G.S.Kozina, V.N.Favorin & I.D.Anisimova, Ibid., 8, 218 (1960). (Trans. Ibid.)
6. W.A.Thornton, Phys.Rev., 113, 1187 (1959).

DISCUSSION

G.S.Kozina: In our report there was described the case of weak electroluminescence of green phosphors in a dc field. We also observed bright electroluminescence in a dc field of coatings of electroluminescent enamel loaded with green phosphor (first observed by L.P.Poskacheeva). The enamel layers with a high luminophor concentration had one electrode (backing) of tin oxide. Their other surface was irradiated with an electron flux, which charged the surface to a certain potential relative to the tin oxide backing. With a certain polarity of the voltage on the layer (tin oxide positive), there was observed conductivity of the layer and bright emission consisting of numerous individual, steady (non-scintillating) points. The brightness amounted to 1 millistilb and higher, and increased with increase of the potential on the layer. With opposite polarity, the conductivity was low and no luminescence was observed regardless of the voltage (up to breakdown of the layer).

The cited case shows the possibility of preparing layers with bright electroluminescence in a dc field. In view of the strong voltage dependence of the luminance, it is undoubtedly of interest to continue research on the preparation of green electroluminophors that luminesce in a dc field.

EXPERIMENTAL INVESTIGATION OF THE POSSIBILITY OF REALIZING MULTIPLE COMPONENT ELECTROLUMINESCENT DEVICES EMPLOYING FERROELECTRIC MATERIALS

- I.Ya.Lyamichev, I.N.Orlov, G.G.Pershin & N.I.Taborko

The present work was concerned with the problems of realizing multiple component electroluminescent devices of two types: flat screens for displaying images and flat image intensifiers (converters) employing photoconductors.

The principal difficulties[1] in the way of realizing devices of the first type are, first, the impossibility of obtaining an acceptable image contrast on matrix screens without introducing additional electronic elements (diodes[2] or nonlinear resistances[3,4]) and, second, the low luminescence intensity of electroluminophors when the image is formed by successive excitation of luminous points without "storage" of the incoming information.[5]

Flat image intensifiers employing photoconductors and electroluminophors suffer from the impediment of a limited amplification coefficient[6] connected with inefficient utilization of the high sensitivity of photoconductors and the impossibility of increasing the luminescence output by increasing the frequency of the exciting voltage by means of a resistor-capacitor divider.

Incorporation into devices of both types of auxiliary luminescence brightness control elements allows of combining the necessary parameters of the incoming signals with the optimum conditions of excitation of electroluminescence and thus obviating the above mentioned difficulties. By way of such control elements there have been proposed ferroelectric capacitors[5] and ferromagnetic elements (transfluxors)[7]. In our work we investigated the possibility of utilizing some ferroelectric materials, namely, single crystal triglycine sulfate[8] and "Varikond" type ferroelectric ceramics[9].

Ferroelectric type control devices

In an ac circuit consisting of a ferroelectric and an electroluminescent capacitor the magnitude of the voltage on the electroluminophor (and, consequently, its emission brightness) is determined by the capacitance of the ferroelectric capacitor, which varies under the influence of the received signal. The electric circuits of such control elements incorporating a ferroelectric are similar to the circuits of dielectric amplifiers, except that in this case the load on the amplifier is the capacitance of the electroluminescent capacitor and the output signal is the luminescence of the electroluminophor. The electroluminescent and ferroelectric capacitors may be connected either in series or in parallel. In our work we only used series coupling, inasmuch as parallel connection impairs the characteristics of brightness control and complicates the design.

Fig.1,a shows the basic circuit employed for the control elements and utilized for measuring the characteristics of the ferroelectric. The control characteristics, i.e., the variation of the ac current through the ferroelectric as a function of the alternating and control voltages, for triglycine sulfate and Varikond capacitors are shown in Figs.2,a & b. Inasmuch as triglycine sulfate is characterized by more pronounced nonlinearity, this material was chosen for the experimental multiple component devices.

The specific characteristics of triglycine sulfate make it possible to carry out simplified calculations of the optimal parameters for a "ferroelectric-electroluminophor" circuit on the basis of two parameters of the ferroelectric, namely, the maximum capacitance difference and the half-width of the hysteresis loop. The graphic-analytic procedure is illustrated in Fig.2,c. Here the broken lines OAB and ODB are the idealized characteristics of triglycine sulfate, and the line AC

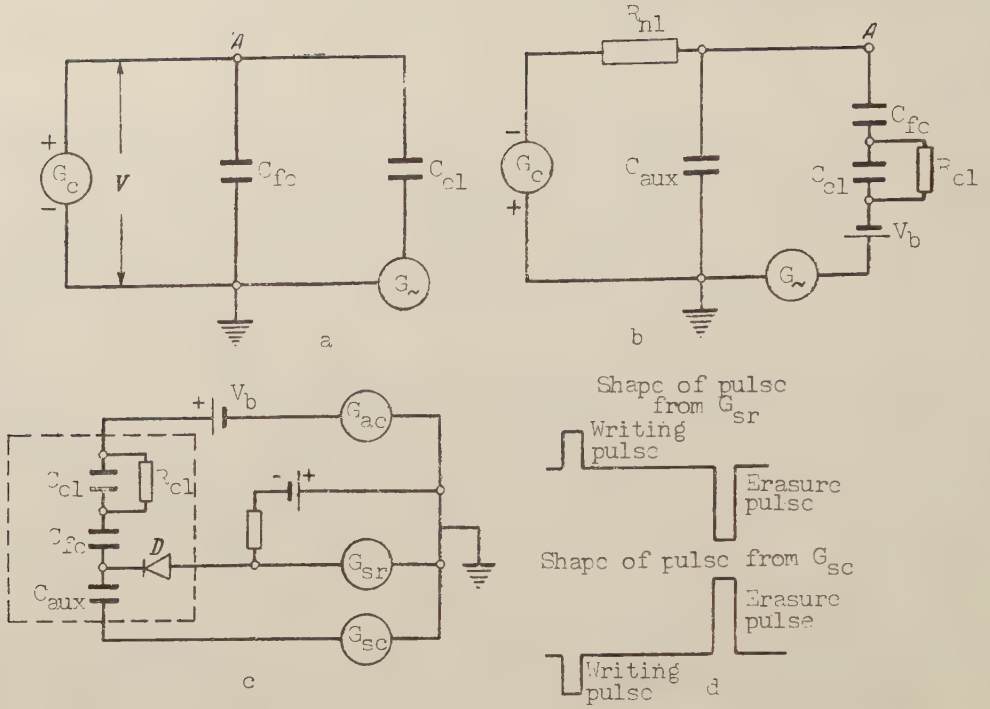

Fig.1. Circuits for display of images: a - basic circuit, b - circuit without forced erasure of information, c - circuit with erasure. C_{el} - electroluminescent capacitor, C_{fe} - ferroelectric capacitor, C_{aux} - auxiliary capacitor, G_{ac} - ac voltage source, G_c - control signal generator, G_{sr} - generator of signals fed to screen rows, G_{sc} - generator of signals fed to screen columns, R_{nl}(D) - nonlinear element (diode), R_{el} - electroluminescent layer leakage resistance.

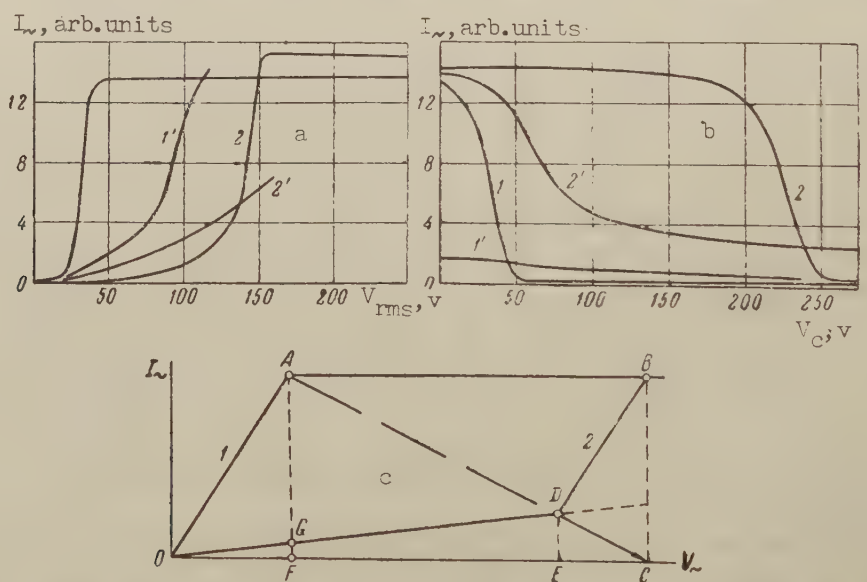

Fig.2. Control characteristics of ferroelectrics: a - $I_\sim = f(V_\sim)$; 1 & 2 - triglycine sulfate; 1' & 2' - Varikond (V_c = 0 and 100 v). b - $I_\sim = f(V_c)$; 1 & 2 - triglycine sulfate, 1' & 2' - Varikond ($V_\sim$ = 50 and 200 v). c - diagram for determining the parameters of the ferroelectric-electroluminophor circuit.

is the load characteristic of the electroluminophor. The intercepts CE and CF on the horizontal axis correspond to the minimum (V_{min}) and maximum (V_{max}) ac voltages on the electroluminophor. The intercept OF = V_o corresponds to the voltage necessary for radical change of the capacitance of the ferroelectric and is determined by the half-width of the hysteresis loop of the given ferroelectric material. The ratio AF/GF = L characterizes the maximum capacitance difference for the given ferroelectric capacitor. From the similarity of triangles ACF and DEC we obtain the following relationship between the principal parameters of the "ferroelectric-electroluminophor" element:

$$\Delta V = \frac{V_o(L - K)}{K} \qquad (1)$$

where $\Delta V = V_{max} - V_{min}$ determines the maximum brightness of the electroluminophor and $K = V_{max}/V_{min}$ characterizes the contrast of the image. Equation (1) allows of determining the maximum values of brightness and contrast of the image produced by a multiple component device employing the given ferroelectric. For triglycine sulfate ($L \approx 40$ and $V_o \approx 90$ v) at the necessary level of contrast of ~100 ($K = 5$), the maximum voltage on the electroluminophor at a frequency of 10-15 kc produces a brightness of about 150 nit. An equal brightness level when employing Varikond ceramics (at a frequency of about 5 kc and $L = 5$-8) is attainable only at a considerable sacrifice of image contrast ($K \leqslant 2$). The frequency of the alternating voltage does not enter into the design formula. Choice of the optimum frequency must be based on the fact that the luminescence brightness of the electroluminophor increases with increase of frequency up to about 20 kc, while the optimum of the control characteristics (maximum value of L and greatest steepness of the control curve) lies in the region from 5 to 10 kc for triglycine sulfate. Hence the supply voltage frequency should lie in the range from 5 to 15 kc.

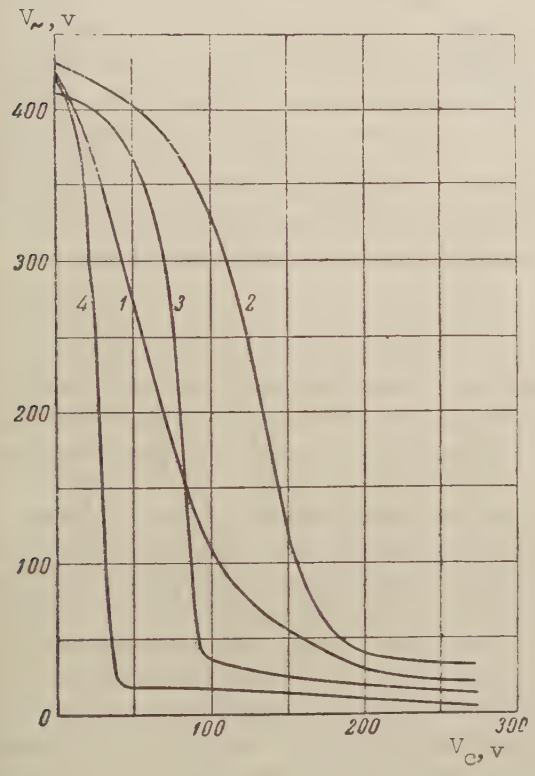

Fig.3. Variation of the voltage drop over the electroluminophor with the control voltage on the ferroelectric with sinusoidal (1) and pulse (2-4) excitation; pulse repetition frequency: 2) 0.6, 3) 1.0, 4) 5.0 millisec.

For a sinusoidal ac voltage the relationship between the voltage differential across the electroluminophor and the magnitude of the polarizing (control) voltage is given by

$$V_c \approx 1.4\,\Delta V, \qquad (2)$$

which is in good agreement with the experimental characteristics of triglycine sulfate (curve 1 in Fig.3).

An acceptable brightness of the electroluminophor is obtained at a value of ΔV of the order of hundreds of volts. In connection with the desirability of utilizing semiconductor devices in switching circuits for the described elements, there arises the problem of lowering the control voltage. In this respect a sub-

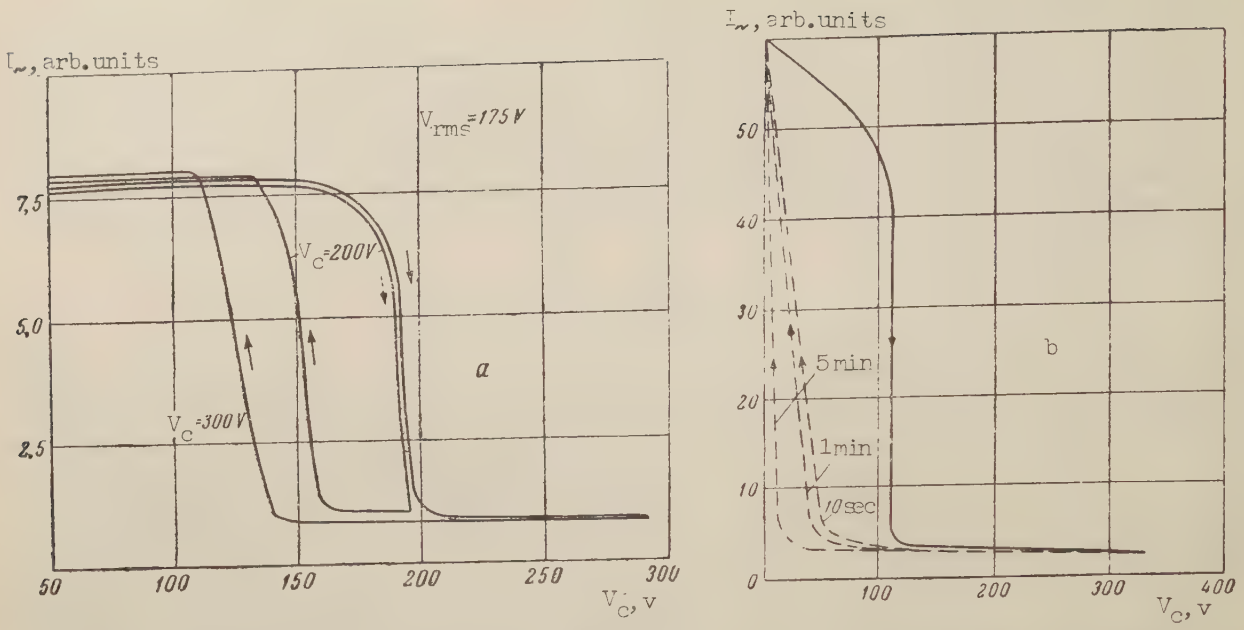

Fig.4. Effect of "memory" in triglycine sulfate: a) for two different values of the control voltage; b) for different periods of application of the same control voltage.

stantial advantage is gained by using pulses instead of a sinusoidal voltage. Curves 2 through 4 in Fig.3 show that in the case of pulse excitation the steepness of the control curve increases and the same value of ΔV can be assured by a polarizing voltage some 3-5 times lower than with a sinusoidal voltage in the circuit.

Unfortunately, in the case of large control signal amplitudes there arises in the ferroelectric the effect of "memory" as regards the polarizing voltage. As will be evident from Fig.4,a, in this case the depolarization curve of the ferroelectric with decreasing V_c does not coincide with the polarization curve; the resultant "loop" is the wider, the greater V_c and the longer the polarizing voltage is allowed to act on the ferroelectric (Fig.4,b). Moreover the effect of memory is the stronger, the higher the frequency of the alternating voltage. (It may be worthwhile to study this particular "memory" effect inasmuch as it may prove useful for realizing information storage devices, for in principle, it allows of simplifying the design of such devices.)

Actual image display circuits

The basic circuit pictured in Fig.1 is not suitable for use in actual multiple component devices for the following reasons:

a) it does not solve the problem of prolonged preservation of the capacitance of the ferroelectric capacitor at the level set by a short control signal, which is necessary for obtaining an adequate brightness of the element;

b) the ac and control voltage networks are not separated in this circuit, which may result in distortion of the control signals;

c) this circuit has "negative" coupling between the magnitude of the control voltage and the brightness of the luminophor, i.e., the brightness decreases with increase of the control signal.

A circuit free of these shortcomings is shown in Fig.1,b. Here for separation of the ac and control voltage networks there is introduced an additional linear capacitance C_{aux} ($C_{aux} \gg C_{ef}C_{fe}$), the nonlinear element R_{nl} (nonlinear resistor, diode, or the like) which provides for "storage" of the information and eliminates coupling between the elements of the device (i.e., insures the necessary image contrast), and a constant bias V_b which provides "positive" coupling between the brightness of the luminophor and the amplitude of the signal.

In this circuit, however, the storage time of the signal is determined by the initially chosen values of V_{aux} and R_{nl} and cannot be regulated in the course of operation. In most devices, however, it is necessary to provide for the possibility of erasure of the written information at any given instant. This problem can be solved by applying special erasing pulses either through an auxiliary nonlinear network or through the signal writing circuit. In the latter case realization of erasure does not require substantial complication of the circuit. One solution of this problem is the circuit shown in Fig.1,c, in which the same crystal diode is used both for writing and for erasure. For erasure there is utilized the distinctive property of silicon diodes to break down in the reverse direction under the influence of short high-amplitude pulses. At the instant of such reverse breakdown there occurs recharging of the capacitor C_{aux}, and the element goes into the unexcited state. We used 220 elements of this type to assemble a prototype electroluminescent display panel for experimental verification of the suitability of circuits of this type.

The interconnection of the individual components (subassemblies) into an array is shown in Fig.5,a. In tests on this prototype we obtained the following parameters: luminescence brightness up to 50 nit; storage time about 5 min with pulses of $\sim$50 microsec duration; erasure time about 1 millisec.

The complexity of the individual component (unit) circuits gives rise to a number of design and technological difficulties in attempting to realize a multiple component device for display of sharp images (resolution comparable to that of television screens). For one thing there are not readily available at present materials with appropriate electrical and technological parameters (powder nonlinear resistances and diode layers of large area, powder or ceramic ferroelectric materials, etc.). Moreover, serious difficulties arise in interconnecting the subassemblies in view of the complex circuits involved. Almost all the prototype multiple component devices described in the literature have been assembled by electrical connection of individually prepared components. The projected design employing nonlinear resistances[10] or a diode layer, shown schematically in Fig.5,b, allows in principle of realizing a compact screen (display panel) into which all the subcomponents are incorporated in the process of fabricating the layer.

Light intensifiers

In electroluminescent light intensifiers employing photoconductors and constructed on the principle of a resistor-capacitor voltage divider, the amplification coefficient as regards light flux does not exceed 1000. In a recent publication[5] it was asserted without substantiating experimental data that the use of ferroelectric materials allows of increasing the intensification factor one or two orders of magnitude. Our experiments with a single element intensifier employing triglycine sulfate substantiated this possibility.

Fig.6,a shows the diagram of a light intensifier element employing a ferroelectric. The photoconductor here is connected into a dc circuit so that its sensitivity is higher than in a resistor-capacitor divider. Moreover, here it no longer serves for transmission of the exciting power to the electroluminophor

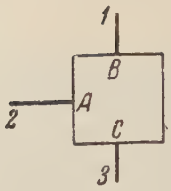

a

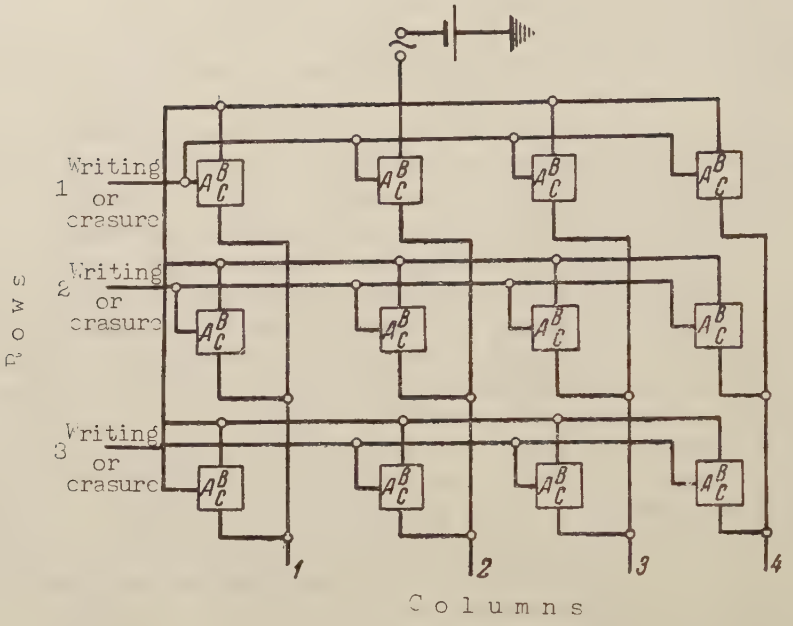

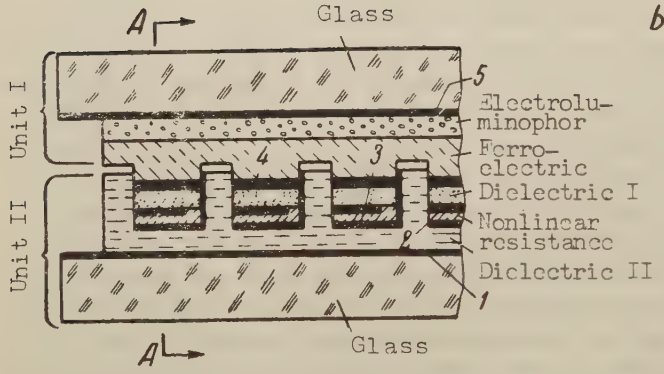

b

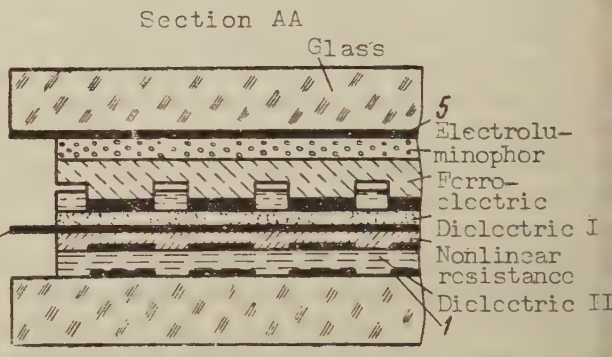

Fig.5. a - Connection of elements in multiple component array: 1 - continuous excitation; 2 - input of writing and erasing pulses; 3 - input of pulses synchronous with pulses in channel A but of opposite polarity, b - design of screen with nonlinear resistance and ferroelectric: 1 - strip electrode for "column" pulses; 2 - strip electrode for "row" pulses; 3 & 4 - mosaic electrodes (auxiliary capacitance-nonlinear resistance-ferroelectric); 5 - continuous transparent electrode to which ac voltage is applied.

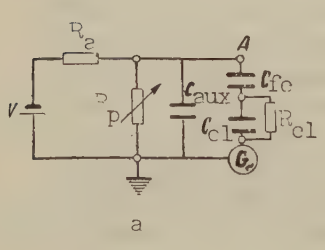

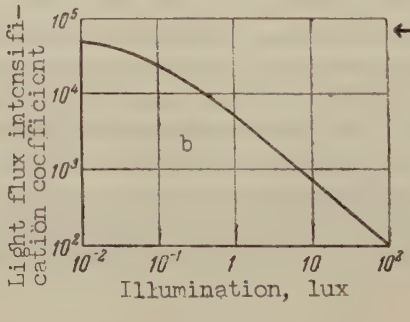

←**Fig.6. a - Circuit of light intensifier employing a ferroelectric; b - variation of the light flux intensification coefficient as a function of the illumination of the photoconductor in a single element light intensifier. Circuit parameters: $V_{\sim}$ = 450 v, f = = 2 kc, $V_{=}$ = 600 v, R_a = 68 megohm.**

and hence does not limit the useful range of frequencies, i.e., in this circuit one can use the optimum frequency for exciting the luminescence. The additional resistance R_a in the dc circuit provides for positive coupling between the illumination of the photoconductor and the luminescence brightness of the electroluminophor, inasmuch as in this case the polarizing potential at the point A is the lower, the lower the resistance of the photoconductor (i.e., the higher the intensity of the incident illumination). Calculations and tests showed that R_a must be of the same order of magnitude as the dark resistance of the photoconductor. The auxiliary capacitance C_{aux} plays the same role as in the circuit of Fig.1,b. With an illumination of about 0.01 lux incident on the photoconductor the intensification factor may attain 50 000 (Fig.6,b). Practical realization of multiple element image intensifiers, in addition to the above mentioned design and technological difficulties, is also hampered by the lack of short-lag photoconductors and ferroelectrics, i.e., materials that would reunite the electric properties of triglycine sulfate with the technological and operational properties of barium titanate ceramic.

Our preliminary research has shown that as regards their electric and optical parameters currently available materials are suitable for the realization of individual components of electroluminescent devices of both types with acceptable output characteristics. Some of these materials have not quite satisfactory technological and operational properties (ferroelectrics and diodes). Nevertheless, in our opinion, the main problem is not so much improvement of the specific properties of various raw materials and component elements, as elaboration of the principles of design of compact multiple component devices and development of special technological means for realizing such designs.

In the present article we have not discussed the question of creating special switching and selector devices for multiple element screens, inasmuch as this is a specialized field and requires separate discussion.

References

1. I.Ya.Lyamichev & I.N.Orlov, Transactions of the 7th Conference on Luminescence, 1959.

2. D.C.Livingston, U.S.Patent 2,774,813 (1956); S.C.Peek,Jr., U.S.Patent 2,818,531 (1957).

3. I.Ya.Lyamichev, I.N.Orlov & V.P.Poruchikov, Tekhnika kino- i televideniya, (Motion picture and television engineering), No.11, 43 (1957).

4. D.H.Mash, J.Scient.Instrum., 37, No.2, 47 (1960).

5. E.A.Sack, Proc.IRE, 46, 1694 (1958).

6. I.N.Orlov & N.I.Taborko, Optika i spektroskopiya, 9, No.5, 626 (1960). (Trans.Optics & Spectroscopy.)

7. J.A.Rajchman, G.R.Briggs & A.W.Lo, Proc.IRE, 46, 1808 (1958).

8. I.S.Zheludev, V.V.Gladkii, L Z.Rusakov & I.S.Rez, Izv.AN SSSR, Ser.fiz., 22, 1465 (1958). (Trans.Bulletin, 22, 1458.)

9. T.N.Verbitskaya & L.M.Aleksandrova, Ibid., 22, 1534 (1958). (Trans.Ibid. 22, 1525.)

10. I.Ya.Lyamichev, I.N.Orlov, I.S.Rez & L.Z.Rusakov, Inventor's certificate No.127696, 3 March 1959.

ON ENHANCING THE EFFICIENCY OF A SCINTILLATION TYPE SLOW NEUTRON DETECTOR

- B.S.Grebenskii, T.V.Timofeeva, S.P.Khormushko & O.S.Tsvetkov

In the present article we describe dispersed slow neutron detectors prepared of ZnS(Ag) and H_3BO_3, both natural and B^{10} enriched. The detectors were prepared by the method of heating mixtures of ZnS(Ag) with H_3BO_3 (Ref.1) and for comparison by the procedures described in Refs.2 & 3 (ZnS(Ag) in boron plastic). The B_2O_3 + ZnS(Ag) sinter obtained after heating the phosphor and boric acid mixture was ground and separated into fraction according to granule size.

The slow neutron detecting efficiency η_n for such a detector is described by

$$\eta_n = \alpha \cdot \epsilon \cdot \epsilon_s,$$

where α is the efficiency of thermal neutron capture by the detector with the formation of an α-particle[5], which is determined by the B^{10} content in the detector and the cross section for interaction of B^{10} with thermal neutrons (σ = 3900 barns); ϵ is the efficiency of entry of the α-particles into the phosphor grains with transfer of an energy sufficient to produce a scintillation (σ depends on the weight ratio of B_2O_3 to ZnS(Ag) and the phosphor grain size); ϵ_s is the efficiency of emergence of the scintillations from the detector and depends on the intensity distribution of the scintillations and the optical transparency of the detector. The optical transparency of the detector for the scintillation radiation is determined by the absorption coefficient and the coefficient of scattering at the interfaces, both between the granules and air and between the ZnS(Ag) and B_2O_3 grains.[6] The number of interfaces depends on the ratio of B_2O_3 to ZnS(Ag), the granule size and the size of the AnX(Ag) grains. Increase of the granule size with a given composition and layer thickness decreases the light scattering, owing to reduction in the number of scattering surfaces, and thus enhances the transparency, which makes it possible to increase the optimum layer thickness. However, this is accompanied by decrease of the average scintillation intensity owing to weakening of the scintillations in the granule, which limits the increase in efficiency in going to granule-monolayer detectors. On the other hand, the optimum granule layer thickness is limited by weakening of the neutron flux attaining the internal layers.

We determined the variation of the efficiency η_n as a function of the granule size and thickness of the detector layer with different contents of boric acid enriched to different percentages of B^{10}; we also recorded the differential pulse height distribution curves for slow neutrons and γ-rays.

The results are summarized in the accompanying table and in Figs.1 and 2; in the table and figures l is the thickness of the detector, l_o is the optimum thickness of the detector (in mg/cm^2), I is the efficiency referred to detector III with 34% natural H_3BO_3, a thickness of 80 mg/cm^2 and a grain size of 185 microns, the efficiency of which in detecting slow neutrons was found to be 5.4 ± 0.4%, i.e., $\eta_n = I \cdot 5.4\%$. The neutron capture efficiency α was calculated on the basis of the B_2O_3 content remaining after heating.

It will be seen that the efficiency increases with increase of the boric acid content, passes through a maximum, which lies in the range from 30 to 35% H_3BO_3 by weight (depending on the degree of enrichment), and then falls off. (Compare detectors I, III and V).

With increase of the layer thickness the efficiency η_n also passes through a maximum; this peak is more pronounced and is shifted to the side of lower thicknesses with decrease of B^{10} enrichment (see Fig.1). For a detector with a given

Granule size, μ	Detector I: 16% H_3BO_3 with 19% B^{10}				Detector II: 16% H_3BO_3 with 85% B^{10}				Detector III: 34% H_3BO_3 with 19% B^{10}				Detector IV: 34% H_3BO_3 with 85% B^{10}				Detector V: 89% H_3BO_3 with 19% B^{10}			
	l_0, mg/cm^2	I	α	I/α	l_0, mg/cm^2	I	α	I/α	l_0, mg/cm^2	I	α	I/α	l_0, mg/cm^2	I	α	I/α	l_0, mg/cm^2	I	α	I/α
800±150	190	1,6	0,33	4,85	150	3.0	0,72	4,2	160	2,0	0,56	3,6	110	4,2	0,89	4,7	100	0,69	0,82	0,84
470±180	—	—	—	—	120	2,5	0,64	3,9	130	1,7	0,49	3,5	90	3,3	0,85	3,9	70	0,57	0,71	0,80
185±100	100	0,9	0,20	4,5	80	1,7	0,51	3,3	80	1,0	0,35	2,9	60	2,5	0,73	3,4	55	0,43	0,63	0,68

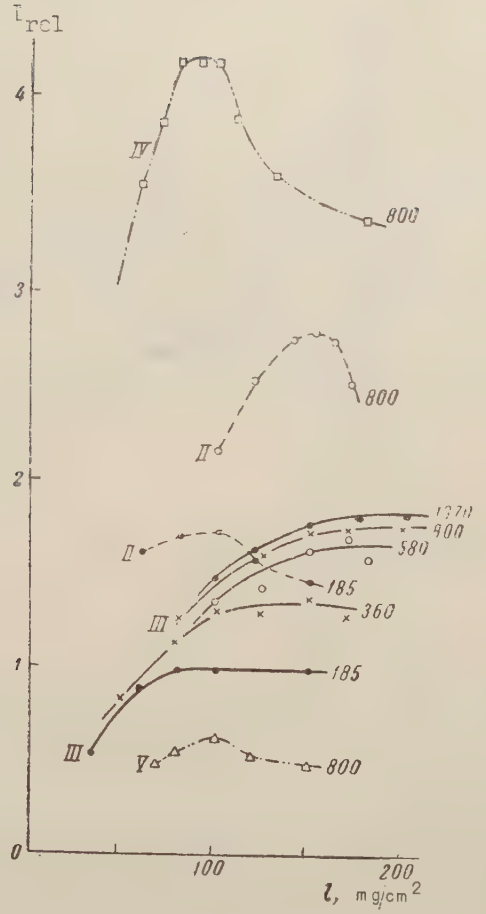

Fig.1. Variation of the relative slow neutron counting efficiency as a function of the layer thickness for detectors II, III & IV (see table). The figures at the curves indicate the granule size in microns.

layer thickness and weight content of H_3BO_3 η_n increases with increase of granule size and then tends to saturation at 800-1100 μ (see Fig.1). For example, for detectors containing 30% H_3BO_3 (B^{10} content 87%) and a layer thickness of 100 mg/cm^2 the efficiency η_n increases from 5 to 14 to 25% with increase of the granule size from 50-100 to 150-300 and 750-1000 microns. At the same time the optimum thickness increases from 40 to 110 mg/cm^2. For detectors of the same composition but with natural H_3BO_3 the optimum thickness for a granule size of 750-950 microns increases to 160 mg/cm^2. In the case of the detectors listed in the table use of the optimum thickness with increase of the granule size from 185 to 800 μ enhances the efficiency by a factor of 1.6 to 2.0. For the same variation of granule size, the optimum thickness for each detector increases by a factor of 1.9-2.0.

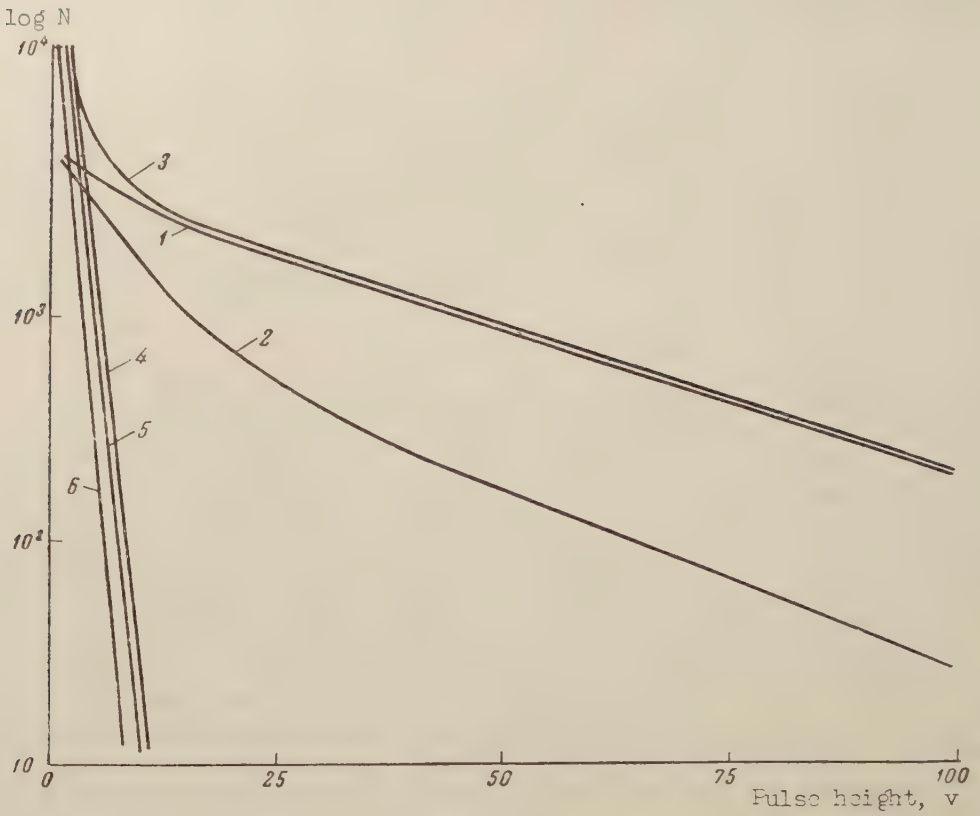

Fig.2. Differential amplitude distribution of pulses from slow neutrons and γ-rays 1 - distribution of pulses from slow neutrons for a detector containing 30% H_3BO_3, enriched with B^{10} to 87%; l = 100 mg/cm^2, granule size 750-1000 μ, η_n = 25%; 2 - same but for detector containing 34% natural H_3BO_3, l = 200 mg/cm^2, granule size 750-1000 μ, η_n = 10%; 3 - integral distribution of pulses from neutrons and γ-rays for detector I; 4,5 & 6 - distribution of pulses due to γ-rays from RaTh (E_γ = = 2.62 Mev), Ra (E_γ = 1.76 Mev) and Cs^{137} (E_γ = 661 kev).

The probability for emergence of a scintillation per absorbed neutron I/α decreases with the granule size; it changes little with increase of the H_3BO_3 content up to the optimum value, but then falls off sharply with further increase of the boric acid concentration (for example, by a factor of 5-6 for detector V). This must be due to impaired energy transfer from the α-particles to the zinc sulfide, inasmuch as in detector V there are five molecules of B_2O_3 per molecule of ZnS(Ag) instead of one molecule B_2O_3 per two molecules ZnS(Ag) at the optimum H_3BO_3 content (detectors III and IV).

Disperse detectors of the described type have a low sensitivity for γ-rays owing to the relatively low specific ionization by secondary electrons forming as a result of interaction of the γ-rays with the detector material as compared with the specific ionization produced by recoil neutrons and α-particles forming in the $B^{10}(n,\alpha)Li^7$ reaction.

Fig.2 shows the differential distributions of pulses from Cs^{137}, Ra and RaTh γ-rays and slow neutrons obtained by means of a 100-channel AI-100 "Raduga" pulse height analyzer. Experimental determination and calculation of the efficiency η_n in detecting 2.62 Mev γ-rays with discrimination of the pulses from 1.76 Mev γ-ray

shows that η_2 is three orders of magnitude lower than η_n. The efficiency η_n was determined with discrimination of the pulses from the 2.62 Mev γ-rays at flux levels not producing superposition of the γ-ray pulses. The relative discrimination threshold B does not depend on the intensity of the γ-ray flux. In case of detection of neutrons against a strong γ-radiation background of the order of 50-100 mC/sec there occurs superposition of the γ-ray pulses so that the time resolution of the detector, which is determined by the characteristics of the ZnS(Ag), corresponds to $\sim 10^{-5}$-10^{-4} sec, which leads to increase of the discrimination threshold and decrease of the neutron detecting efficiency η_n. In this case it is more advantageous to use a detector corresponding to curve 1 in Fig.2, inasmuch as the ratio of efficiencies η_n for detectors prepared with enriched H_3BO_3 (curve 1) and natural H_3BO_3 (curve 2) increases with increase of B.

In conclusion, it must be noted that the different preparation procedures[1-3] result in detectors with close values of η_n, η_γ, the ratio of ZnS(Ag) to B_2O_3 and distributions of pulses from neutrons and γ-rays.

References

1. T.V.Timofeeva & S.P.Khormushko, Izv.AN SSSR, Ser.fiz., 22, 14 (1958). (Trans.Bulletin, 22, 13.)

2. K.Sun, P.Malmberg & F.Pecjak, Phys.Rev., 95, 600 (1954); Nucleonics, 14, No.7, 46 (1956).

3. M.Vorisek, Czechosl.J.Phys., 7, No.6, 757 (1957).

4. G.V.Goshkov, B.S.Grebenskii, S.P.Khormushko & O.S.Tsvetkov, Present issue of the Bulletin, p.505.

5. T.V.Timofeeva & S.P.Khormushko, Izv.AN SSSR, Ser.fiz., 23, 1283 (1959). (Trans.Bulletin 23, 1275.)

6. A.P.Ivanov, Zhur.eksp.i teor.fiz., 30, 196 (1956). (Trans.Soviet Physics - JETP): Optika i spektroskopiya, 4, 225 (1958).

DISPERSED FAST NEUTRON DETECTOR

- G.V.Goroshkov, B.S.Grebenskii, S.P.Khormushko & O.S.Tsvetkov

In the present contribution we describe a detector for fast neutrons consisting of grains of ZnS(Ag) phosphor uniformly dispersed in a hydrogenous medium. The protons scattered in the medium produce recoil electrons which, upon entering the phosphor grains, give rise to scintillations that are detected by a photomultiplier. The complete assembly consists of a detector, a photomultiplier, an amplifier, an integral and differential discriminator and a pulse register.

Detectors of this type have been described by a number of authors[1-6]. Our detectors were prepared by polymerization of styrene and methyl methacrylate with ZnS(Ag). The preparation procedure developed allows of obtaining detectors of different size (1 to 300 mm) and shape (hollow sphere, cylinder, hemisphere, etc.). The ZnS(Ag) phosphor had the following characteristics: grain size 12-25 μ, decay time $\tau \approx 10^{-4}$ sec, intrinsic emission maximum 4100-4500 Å, which matches the maximum spectral response of photomultipliers with a cesium-antimony photocathode.

The neutron detecting efficiency by a disperse detector may be written as

$$\eta = \epsilon_\sigma \cdot \epsilon_p \cdot \epsilon_s, \qquad (1)$$

where ϵ_σ is the efficiency as regards neutron scattering[7]; ϵ_p is the efficiency as regards entry of protons produced by neutrons of energy E_n into the ZnS(Ag) grains, and ϵ_s is the efficiency with which the instrument detects the scintillations arising in the detector; ϵ_s is determined by the intensity distribution of the scintillations, the optical properties of the detector and the discrimination threshold B.

According to Ivanov[8], the transparency of the detector to its intrinsic radiation is determined by the scattering factor S for the intrinsic radiation in the detector material and the absorption coefficient K, which depends on the index of refraction of the scintillator and the hydrogenous medium, the grain size and concentration of ZnS(Ag). With increase of the ZnS(Ag) concentration ϵ_s decreases. The amplitude distribution of the scintillations depends on the neutron energy E_n, the phosphor grain size, its weight concentration C_w and the specific ionization of zinc sulfide by protons. With increase of E_n the proton range in the material increases and, consequently, so does the probability of a proton passing through an entire ZnS(Ag) grain, but the maximum intensity of a scintillation produced in one ZnS(Ag) grain is limited by the size of the grain. With increase of C_w the probability for passage of a recoil proton through several ZnS(Ag) grains increases. It is difficult to determine the scintillation intensity distribution as a function of E_n and the detector parameters. The discrimination threshold B is chosen so as to eliminate, in so far as possible, pulses due to γ-radiation. At high γ-flux levels, however, there occurs superposition of γ-ray pulses and B must be increased. Thus for a detector of thickness l = 10 mm (C_w = 25%) the efficiency in detecting neutrons from a Po-Be source is 1.2% of the bias set to discriminate $3 \cdot 10^4$ γ-rays cm^{-2} sec^{-1} ($h\nu$ = 2.6 Mev), while with discrimination equal to $3 \cdot 10^5$ γ-rays cm^{-2} sec^{-1} the efficiency ϵ = 0.4%. By determining the efficiency as regards neutrons from Po-Be and RaThγ-Be sources with different detector thicknesses and different ZnS(Ag) concentrations one can evaluate the relative variation of ϵ_s with variation of C_w. On the basis of this evaluation of ϵ_s one can determine the character of the variation of ϵ_p with C_w (in our experiments C_w was varied from 10 to 70%). The experimental variation of ϵ_p as a function of C_w and E_n is characterized by a "saturation" curve and is described by

$$\epsilon_p = 1 - e^{-k(r)\, C_V R_n}, \qquad (2)$$

where C_V is the volume concentration of ZnS(Ag), R_n is the range in the scintillator material of protons produced by neutrons of energy E_n, and $k(r)$ is a coefficient that depends on the energy distribution of the proton recoils and the dimensions of the scintillator grains.

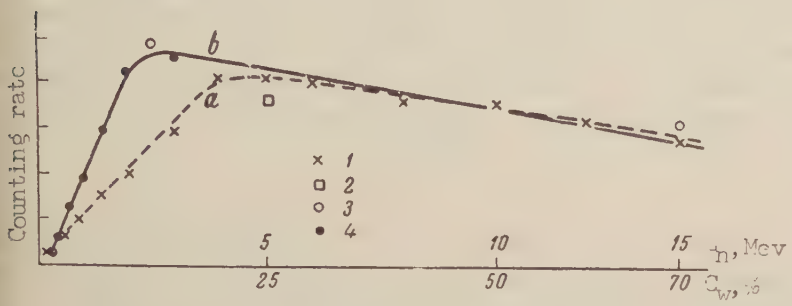

a - Variation of η with C_w for $l \geqslant l_0$ (1 - experimental points; dashed line - calculated curve). b - variation of η with neutron energy (experimental points for curve b: 2 - neutrons from Po-Be source, 3 - neutrons from linear accelerator, 4 - neutrons obtained by means of a Van de Graaff generator).

It will be evident that η increases with increasing thickness l of the detector only to a certain optimum value l_0 which depends on the optical properties of the detector, E_n and B. For a detector with C_w = 25%, in recording the neutrons from a Po-Be source and discrimination of the γ-flux to the extent of $3 \cdot 10^4$ γ-rays cm^{-2} sec^{-1}, the optimum thickness l_0 = 10 mm.

For detectors with $l \geqslant l_0$ the detecting efficiency η will have a maximum at a certain C_w, inasmuch as ϵ_p increases with increase of C_w, while the product $\epsilon_\sigma \cdot \epsilon_s$ decreases. The accompanying figure shows the variation of η with C_w with $l \geqslant l_0$ for neutrons from a Po-Be source with discrimination of the 2.6 Mev γ-radiation equal to $3 \cdot 10^4$ γ-rays cm^{-2} sec^{-1} (curve a); η depends on the neutron energy E_n; ϵ_p increases with increase of E_n, in accord with Eq.(2) and approaches saturation at a certain value of E_n; ϵ_s increases owing to change in the intensity distribution of the scintillations, while ϵ_σ decreases with increase of E_n.

It will be evident from the character of the E_n dependences of ϵ_σ, ϵ_p and ϵ_s that the η vs E_n curve must have a maximum.

The rate of change of η with E_n and the position of the η maximum depend on B and l. In the accompanying figure we also show the variation of η with E_n for a detector with C_w = 25%, l = 10 mm and B set to discriminate $3 \cdot 10^4$ γ-rays cm^{-2} sec^{-1} (2.6 Mev γ-rays) (curve b). It will be evident from the presented data that the given detector can detect neutrons with energies from 0.5 Mev.

References

1. Hornjak, Rev.Sci.Instr., 23, 264 (1952).
2. Kirkbride, Nature, 171, 564 (1953).
3. W.S.Emmerich, Rev.Sci.Instr., 25, 69 (1954).
4. Koontz, Keepin & Ashley, Ibid., 26, 352 (1955).
5. Vsesoyuznaya promyshlennaya vystavka. Stsintillyatsionnye neitronnye radiometry RN-3 i RN-4 (All-Union Industrial Exposition. Scintillation neutron radiometers RN-3 and RN-4), Atomizdat, 1958.
6. Yu.A.Tsirlin, Zhur.tekh.fiz., 29, 531 (1958). (Trans.Soviet Physics - Technical Physics.)
7. N.A.Vlasov, Neitrony (Neutrons), M., 1955.
8. A.P.Ivanov, Optika i spektroskopiya, 4, 225 and 236 (1958).

SELECTION OF PHOSPHOR COATINGS FOR X-RAY SCREENS

- A.M.Gurvich & R.V.Katomina

X-rays of different penetrating power (hardness), generated at different potentials on the x-ray tube, are used in medical and industrial roentgenology, depending on the scientific problem involved.

We investigated the variation in luminescence intensity of screens prepared of the principal industrial roentgenoluminophors as a function of the effective wavelength in the range from 0.11 to 1.8 amp (7 to 114 kv_{eff}). The intensity was measured for layers 70 mg/cm^2 thick by the "through" procedure, i.e., by observation from the nonirradiated side by means of a photoelectric photometer with cesium-antimony photocells. In other respects the experimental conditions were the same as described in Ref.1.

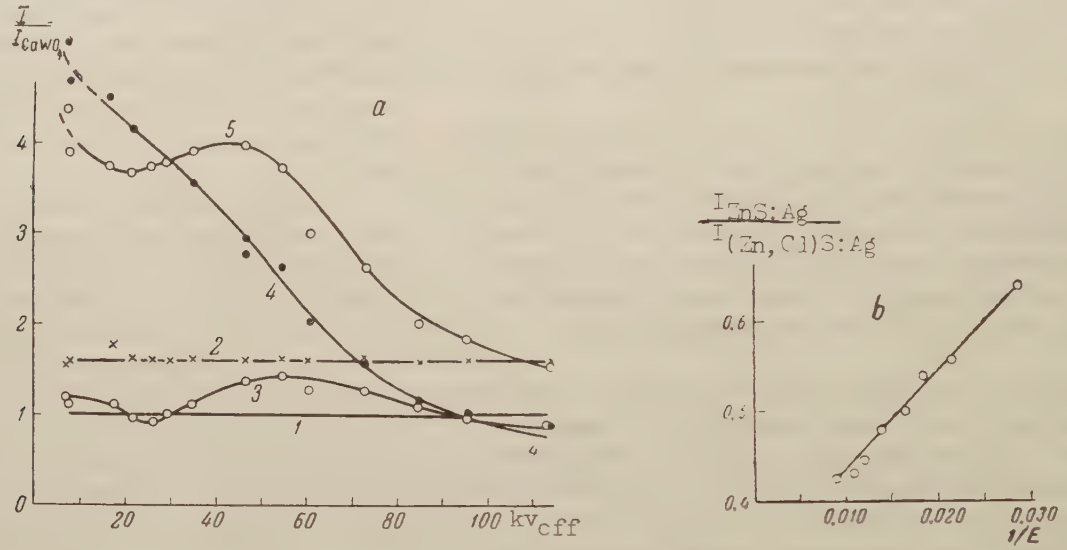

Fig.1. a - Variation of the relative luminescence intensity of screens (70 mg/cm^2) observed from the back as a function of the x-ray energy (tube potential): 1 - $CaWO_4(Na_2HPO_4)$ - standard (the intensity of its luminescence was taken as unity); 2 - $CaWO_4(CaCl_2)$ - UVD (ultraviolet detector) phosphor; 3 - $(Ba\text{-}Pb)SO_4(Na_2SO_4,\text{-}NaHSO_4)$; 4 - cub.ZnS:0.02%Ag($MgCl_2$,NaCl); 5 - hex. 54ZnS·46CdS:0.01Ag(NaCl). b - variation of the ratio between the intensity of a ZnS:0.02%Ag screen and the intensity of a (Zn,Cd)S:Ag screen as a function of 1/E (the reciprocal of the x-ray energy).

Fig.1,a shows the results of measurements of the relative luminescence intensity of different screens as a function of the x-ray energy with a wavelength of λ_{eff}, the value of which was determined by measuring the half-value layer. As was shown earlier[1], the maxima in the luminescence intensity curves for (Ba, Pb)SO_4 and (Zn,Cd)S:Ag phosphors are due to the characteristic absorption of x-rays by barium and cadmium. It should be noted that the intensity ratios shown in Fig.1 change somewhat if one uses screens with optimum phosphor loadings (Fig. 2).

The results of the present investigation, which was carried out under conditions close to those obtaining for the screens in electron-optical image intensifiers[2], show that the most efficient phosphor for screens in such intensifiers in a wide range of values of the x-ray energy E is (Zn,Cd)S:Ag. Above 30 kv_{eff}

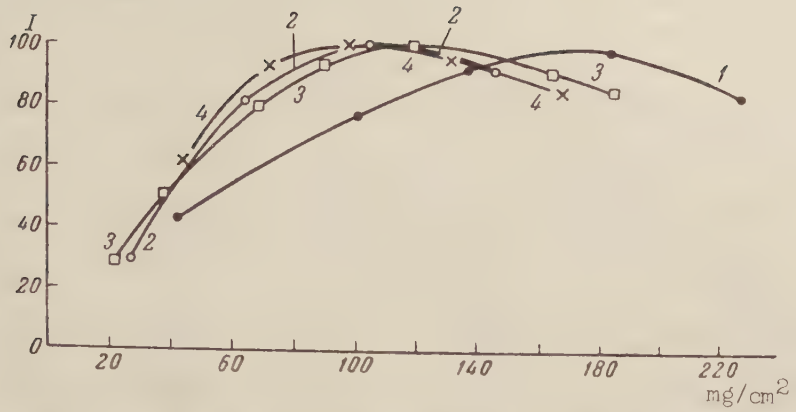

Fig.2. Variation of the luminescence intensity of screens with the phosphor loading in the screen measured from the nonradiated side: 1 - $CaWO_4$ - UFDM phosphor (mean grain size $\bar{d}$ = 12.7 μ), 2 - $(Ba,Pb)SO_4$ ($\bar{d}$ = 18.0 μ), 3 - (Zn, Cd)S:Ag ($\bar{d}$ = 12.5 μ), 4 - ZnS:Ag ($\bar{d}$ = 9.5 μ). All the screens were excited by x-rays with a potential of 80 kv_{max} on the tube and a 0.4 mm Cu absorber ($E = 47\ kv_{eff}$).

the advantage of (Zn,Cd)S:Ag screens as regards luminescence intensity over ZnS: :Ag screens increases with increase of E. It also follows that the amplification (intensification) factor of electron-optical converters with ZnS:Ag screens as determined with reference to a conventional (Zn,Cd)S:Ag fluoroscopic screen, decreases with increase of E. Using the data shown in Fig.1,b we obtain K_a = $= \alpha\left(0.333 \div \frac{10.44}{E}\right)$ for the amplification coefficient of an electron-optical converter in the energy range E = 35 to 115 kv_{eff}. Having measured K_a at a certain value of E, one can readily calculate the coefficient α.

In the case of measurements using a Cs-Sb photocathode to detect the radiation the optimum CdS content in (Zn,Cd)S:Ag screen phosphors is 40% of the total sulfide weight. With decrease of the CdS concentration the effective light yield B_{eff}* decreases, owing to decrease of the roentgenoluminescence yield B, while with increase of the CdS content the effective yield decreases owing to increasing noncorrespondence between the spectral sensitivity S_λ of the radiation detector and the spectral composition I_λ of the emission of the phosphor (by way of criterion for the spectral correspondence one can use the quantity $K = \int S_\lambda I_\lambda d\lambda \Big/ \Big/ \int I_\lambda d\lambda$ (see Ref.1). In the case of fluorographic screens, when the radiation detector is PF-3 panchromatic film, the optimum CdS content lies between 40 and 50%. The peak of the sensitivity band associated with the film lies at 590 mμ (Ref.3), while with 50% CdS the luminescence peak lies at 554 mμ; increase of the CdS content above 50%, however, results in decrease in the value of K and a corresponding reduction of B_{eff}, which is substantiated by experiments (see table).

---

*The variation of B_{eff} with λ_{eff} for screens with a phosphor loading of 300 mg/cm^2 can be obtained if one multiplies the values of $I/\Delta P$ given in Ref.1 by the electron conversion factor.

Variation of the efficiency of (Zn,Cd)S:0.01Ag(NaCl) phosphor with the CdS content in the batch and the spectral response of the radiation detector

CdS content, % of total sulfide weight	Emission λ_{max}, mμ	Coefficient of spectral corresp. with sensitivity of Cs-Sb photocathode	Reading of photometer at 80 KV λ_{max} & 0.4 mm Cu absorber, arb.units	Coefficient of spectral correspondence with RF-3 film	Calculated effective yield R_{eff} with respect to RF-3 film	Optical density on exposed RF-3 film
25	493	83,8	71,5	47,3	57,0	1,04
35	516	74,3	92,6	47,5	83,7	1,40
40	528	64,2	100,0	47,0	99,0	1,48
45	540	55,3	87,0	46,6	100,0	1,50
50	554	48,5	78,5	45,7	99,5	1,50
60	584	27,1	51,4	35,1	89,5	1,40

The scattering of luminescence light and x-rays in the screen depends on the nature of the phosphor, and this in turn affects the resolving power of the screen and the position of the maximum in the curves giving the variation in luminescence intensity as a function of the phosphor loading (Fig.2) (cf.Ref.4).

State Scientific-Research Roentgeno-Radiological Institute,
Ministry of Health of the RSFSR

References

1. A.M.Gurvich & R.V.Katomina, Novosti med.tekhniki (Medical technology news), No.1, 47 (1961).

2. M.M.Butslov, Izv.AN SSSR, Ser.fiz., 23, 552 (1959). (Trans.Bulletin, 23, 535.)

3. Svoistva fotograficheskikh materialov na prozrachnoi podlozhke (Properties of photographic materials on a transparent support), p.125, edited by Yu.N. Gorokhovskii & S.S.Gileva, M., 1955.

4. A.M.Gurvich, Novosti med.tekhniki (Medical Technology-News), No.6, 48 (1960); A.M.Gurvich & R.V.Katomina, Program of the Ninth Conference on Luminescence, p.34, M., 1960.

USE OF STRONTIUM SULFIDE PHOSPHORS FOR MAKING LUMINOUS SIGNS

- T.A.Krasnova

Hitherto, use of strontium sulfide:Bi:Cu phosphors[1], which have persistent afterglow, for preparation of identification signs and similar devices has been limited owing to the great decrease in luminance with time because of hydrolytic decomposition of the phosphor host. However, the excellent qualities of these phosphors justify all attempts to realize their practical use.

In the present report we give the results of experiments aimed at obtaining luminescent devices prepared by incorporating the phosphor into synthetic materials (plastics) in different ways. The data on the phosphorescence brightness before and after test exposures are summarized in the accompanying table. It will be evident from the data presented that there have been found ways of preparing signs with satisfactory stability over a prolonged period. The results show that luminescent signs prepared of strontium sulfide phosphor in combination with synthetic materials can be used for practical purposes.

References

1. T.A.Krasnova, Sb.tr.Gos.in-ta prikl.khimii (Collected reports, State Institute of Applied Chemistry), No.43, 79 (1960).

Brightness of strontium sulfide phosphor devices before and after test exposures

Material and method of incorporation of phosphor	Test (exposure)	Duration of test	Afterglow brightness referred to fresh powder, %	
			before test	after test
Polymethylmethacrylate				
Phosphor in binder between plexiglass plates	Roof test spring-summer	10-50 days	95	73
	Storage in room	9 months	95	70
Powder in sealed plexiglas container	Storage in room	3 months	80	80
Phosphor with binder on dial of sealed instrument	Storage in room	5 months	80	80
Pressure molded with heat	Storage in building	9 months	100	45
		16 months	100	36
Polyethylene				
Low pressure molding with phosphor	Storage in room	100 days	90	85
		2.5 years	90	50
	Roof test Spring-summer	30 days	80	65
		60 days	80	50
Pressure molding	Roof test	30 days	13	13
Phosphor powder in sealed polyethylene tube	Storage in room	1 year	100	100
Powder compressed between polyethylene plates	Storage in room	1 year	100	100
Thermosetting plastic TS-3				
Molded	Storage in room	9 months	80	40
Same but prerolled	Storage in room	9 months	50	30
Epoxy resin				
Luminescent coating on metal surfaces	Sign held under water	30 days	62	50
	Roof test	30 days	62	52
	Same, large sign	30 days	64	61
Silicate enamels				
Applied to metal surface	Storage in room	3 years	30	30

PHOTOELECTRIC PHOTOMETER FOR DETERMINATION OF URANIUM IN SODIUM FLUORIDE BEADS

- Z.M. Sverdlov

The usual procedure commonly employed in recent years for quantitative determination of uranium in fused sodium fluoride is based on visual photometry by means of the LYuF-51 luminescence photometer[1] with the luminescence of the NaF beads being excited by 366 mμ ultraviolet.*

The method of photographic photometry, which has been used by a number of authors[2,3], for quantitative determination of uranium in fused sodium fluoride, has not gained acceptance in analytic practice owing to the laborious nature of the procedure and the bulky character of the equipment involved.

In recent years, thanks to advances in electronic engineering, it has become feasible to design photoelectric equipment for quantitative determination of uranium in fused sodium fluoride.[4]

We have developed and used for quantitative determination of uranium in NaF beads a new instrument, the FAS-1 photoelectric photometer, by means of which one can enhance the sensitivity and accuracy of analysis over those obtainable in employing the visual LyuF-51 instrument.

The electric system of the FAS-1 instrument (Fig.1) consists of a UFO-4A tube, which serves as the light source, an FEU-19 photomultiplier, a dc amplifier and a power supply.

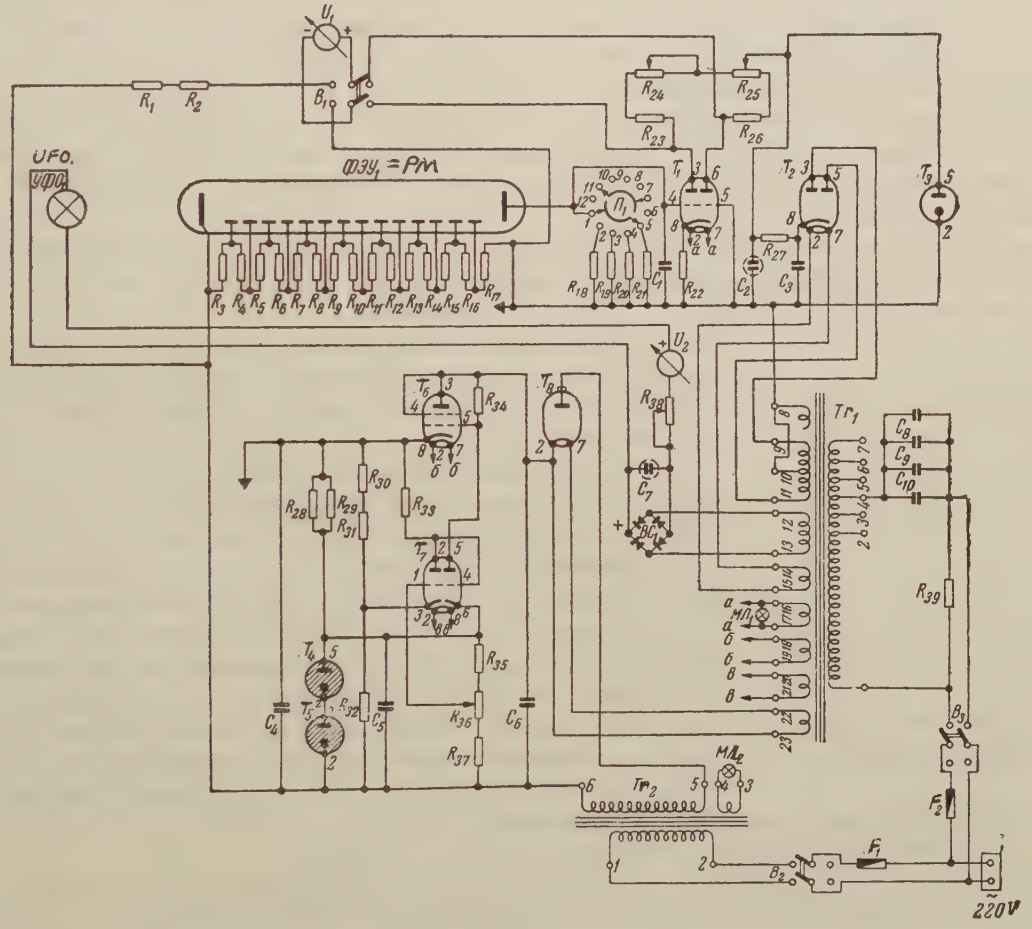

Fig.1. Electric circuit of the FAS-1 photoelectric photometer.

---

*The preparation of uranium-containing sodium fluoride beads weighing 4-5 mg for determination of uranium in ores and minerals is described in Ref.1.

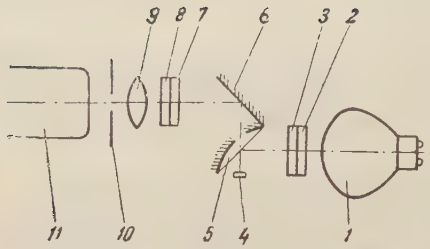

Fig.2. Optical system of the FAS-1.

The UFO-4A tube is a low power source yielding a mercury spectrum. The UFO-4A requires a voltage of 24-28 v and draws a current of 300-350 ma. The FEU-19 photomultiplier has a cesium-antimony semitransparent photocathode and its spectral sensitivity lies in the 3500 to 6000 Å range. The dc amplifier serves for amplifying the output of the FEU-19 and is assembled about a 6N7 dual triode. The output current of the amplifier is measured by means of a microammeter.

The power supply of the instrument consists of a ferroresonance voltage regulator, a rectifier for supplying the amplifier, an electronic voltage regulator for supplying the photomultiplier and a rectifier for supplying the UFO-4A tube. The optical system of the instrument is shown in Fig.2. The ultraviolet light from the UFO-4A tube 1, after passing through the SZS-10 and UFS-3 light filters 2 and 3, is focused by means of the convex aluminized mirror 5 onto the test bead 4. (Instead of being aluminized, mirror 5 may be coated with an interference layer reflecting 366 mμ ultraviolet rays and passing visible luminescence.) The luminescence passes through the opening in mirror 5, is reflected from mirror 6 and after passing through the ZhZS-6 and ZhS-18 light filters 7 and 8 is focused by lens 9 onto the photocathode of the FEU-19 photomultiplier 11. The iris diaphragm 10 mounted in front of the photomultiplier is used to regulate the amount of light incident on the photocathode.

The instrument was calibrated with reference to NaF beads containing known amounts of uranium. In analytic measurements alternately with the test beads the operator observes the luminescence intensity of a standard, a luminescent plate of constant brightness.

By way of illustration in Fig.3 we give the working curve for determination of uranium in sodium fluoride beads in the concentration range from $1 \cdot 10^{-9}$ to $1 \cdot 10^{-8}$ g uranium in a 4 mg bead.

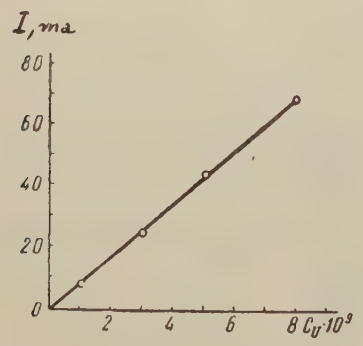

Fig.3. Working curve for the FAS-1 photometer.

We carried out a comparison of the sensitivity limits in determining uranium in NaF beads by means of the FAS-1 instrument and by means of the LYuF-57 photometer*.

It was found that the limiting sensitivity for determinations on both instruments is $1 \cdot 10^{-10}$ g uranium in a 4 mg NaF bead. The reproducibility in repeat measurements on the same bead is the same for both instrmuents and lies within 2% of the measured quality.

In contrast to the LYuF-57 instrument which is intended exclusively for determination of uranium in NaF beads, the FAS-1 instrument is equipped with interchangeable attachments by means of which one can carry out measurements of the luminescence intensity of solutions excited by 366 mμ ultraviolet and 405 or 436 mμ visible rays and gage the absorption of individual lines of mercury (253.7, 313, 366, 405, 436 and 579 mμ) in solutions and solids.

Thus by means of the FAS-1 instrument one can investigate the energy distribution in the luminescence spectra of solutions and solid specimens. To this end

---

*The LYuF-57 photometer employes a balancing circuit; the ultraviolet source is an SVD-120A burner; the light detectors are two alkaline photocells connected in opposition.

the instrument is equipped with a set of ten interference filters for isolating individual regions of the luminescence spectrum.

The production shop of the Leningrad Physical-Mechanical Technical School is setting up batch production of the FAS-1 photometer and these instruments should be available to laboratories and research institutes in 1961.

All-Union Scientific-Research Geological Institute

References

1. Z.M.Sverdlov, Optika i spektroskopiya, 3, 356 (1957).
2. K.Hernegger & B.Karlik, Zitzungsberichte Akad.Wiss., Wien, 144, 217 (1935).
3. J.Hoffman, Sprechsaal f. Keramik, Glas u.verw.ind. Fach U.Wirt.Blatt, 73, 153 (1940).
4. M.H.Fletcher, I.May & M.Slavin, Collected Papers on Methods of Analysis for Uranium and Thorium. Geological Survey Bulletin, 1006, 85 (1954).

INSTRUMENT FOR DETERMINING THE PARAMETERS OF FLUORESCENT SCREENS

- B.I.Pochtarev, K.K.Raspletin & D.V.Fetisov

The PRS instrument was developed for the purpose of investigating and measuring the principal characteristics of cathodoluminescing screens and phosphors. The latest PRS instrument is a universal electron-optical apparatus which employs a system of electrostatic lenses (Fig.1). By means of this instrument one can carry out investigations of the resolution, the light output, the spectral composition of the emission and the cleanliness of the surface of screens with excitation thereof by a stationary electron beam. Under standard conditions the screens are observed from the unbombarded side, but by means of a special attachment, which is mounted on top of the measurement chamber, one can investigate different phosphor powders or screens by observation from the bombarded side.

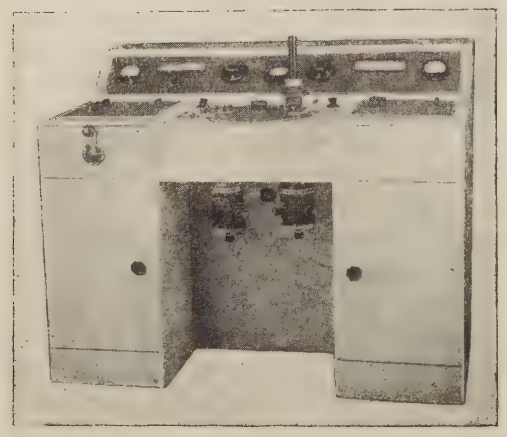

Fig.1. PRS instrument for measuring the parameters of fluorescent screens.

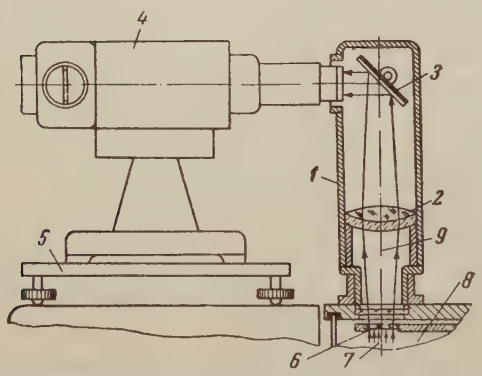

Fig.2. Diagram of the spectrographic attachment: 1) tube, 2) lens, 3) mirror, 4) spectrograph monochromator, 5) stand, 6) screen, 7) electron beam, 8) measurement chamber, 9) light flux from the screen.

The ultimate resolving power of the instrument, evaluated by means of a phosphor single crystal, is 700 lines per mm. The accelerating voltage can be varied from 0 to 30 kv, the beam current can be regulated in the range from $2 \cdot 10^{-8}$ to $3 \cdot 10^{-6}$ amp. For special experiments the current can be increased to $1 \cdot 10^{-5}$ amp.

The electron spot on the screen (phosphor) has a constant diameter of 20 mm. The working pressure in the chamber is $(1\text{-}3) \cdot 10^{-4}$ mm Hg. From 8 to 30 screens or up to 20 cells with phosphor powders can be loaded into the measurement chamber. The light outputs of yellow-green and blue screens (phosphors) are measured by means of selenium and cesium-antimony photocells, respectively. The principle of operation of the instrument, its design and the measurement procedure for the resolution and light output have been described in Ref.1.

Measurement of the Spectral Composition

Measurement of the spectral composition of the emission of the screens or phosphors with observation from the unbombarded or bombarded side is simple because the emission spectrum virtually does not depend on the excitation conditions. The instrument employs a spectrograph (or monochromator) to obtain the spectral distribution curves.

For measurement of the emission spectra a rotatable optical system, diagrammed in Fig.2, is mounted over the viewing window. The system consists of a metal tube 1, housing a lens 2 and mirror 3, which directs the light beam from the screen to the spectrograph or monochromator 4, mounted on the special stand 5.

Under certain conditions the luminescence intensity may be very weak, hence there is provision to use a photomultiplier for amplifying the signal when necessary.

We desire to express our gratitude to Yu.M.Kushnir and M.A.Meerov for valuable advice, assistance and constant interest in the work.

Reference

1.B.I.Pochtarev, K.K.Raspletin & D.V.Fetisov, Izv.AN SSSR, Ser.fiz., 23, 462 (1959). (Trans.Bulletin, 23, 445.)

* * * * * * *

ATTACHMENT FOR THE PRS INSTRUMENT FOR INVESTIGATING PHOSPHORS FROM THE BOMBARDED SIDE

- B.I.Pochtarev

In laboratories and manufacturing plants for preliminary evaluation of the quality of phosphor powders it is the practice to use the method of investigating the luminescence characteristics by observation from the bombarded side. Such investigation of cathodoluminophors is the first stage in controlling their quality and monitoring their parameters.[1]

For the purpose of investigating the properties of phosphor specimens we developed an attachment to the PRS instrument (see preceding article) by means of which one can measure the light output and the spectral composition of luminophors and screens from the bombarded side.

The luminescence of the phosphor or screen is excited by a steady electron beam incident on the surface at an angle of 45°. The accelerating voltage can be varied in the range from 0 to 30 kv, the beam current in the range from $2 \cdot 10^{-8}$ to $3 \cdot 10^{-6}$ amp. The diameter of the electron spot is 20 mm. The instrument chamber can contain up to 20 cells with sample phosphors or screens.

The light from the excited phosphor is measured by means of a selenium photocell corrected to match the sensitivity curve of the human eye, or by a cesium-antimony photocell, depending on the spectral composition of the radiation, or is analyzed by means of a spectrograph.

In measurement by observation from the bombarded side there are employed the same procedures for determining the light output and emission spectra as in investigating screens by observation from the unbombarded side.[2,3]

The attachment, which is diagramed in the accompanying figure, consists of a separate electron-optical system and is mounted on top of the measurement chamber of the PRS instrument in place of the top cover. The electron-optical system, which consists of an electron gun 1 and an electrostatic lens 2, produces and shapes an electron beam of uniform intensity, which is limited by the aperture 3. The high voltage and cathode heater current are supplied to the gun by the armored cable 4.

The investigated phosphor samples are placed in special cells in the rotating drum 5, which is mounted in the measurement chamber 6 of the instrument. To insure a uniform electron beam, a secondary electron collector 7 is mounted along the beam path. The photocell 8 (or the optical system for deflecting the light

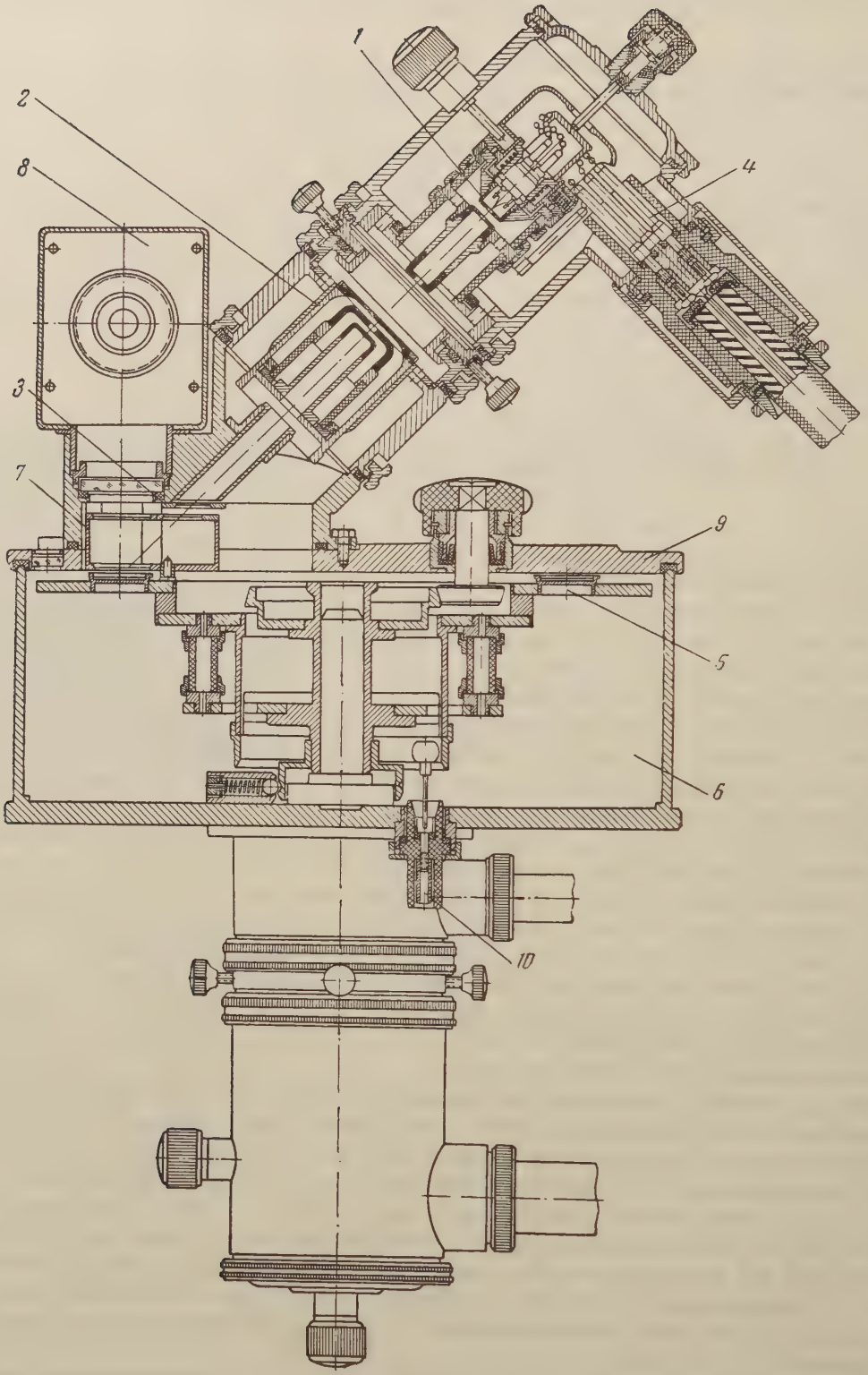

Instrument chamber with attachment for observation of phosphors from the bombarded side: 1) electron gun, 2) electrostatic lens, 3) aperture, 4) armored cable, 5) drum, 6) instrument chamber, 7) secondary electron collector, 8) photocell, 9) cover, 10) connector.

flux to the spectrograph) is mounted directly above the luminescing surface of the phosphor or screen.

I take this opportunity to express my deep gratitude to M.A.Meerov for assistance and constant interest in the work.

References

1. A.V.Moskvin, Katodolyuminestsentsiya (Cathodoluminescence), Part II, M., 1948.

2. B.I.Pochtarev, K.K.Raspletin & D.V.Fetisov, Izv.AN SSSR, Ser.fiz., 23, 462 (1959). (Trans.Bulletin, 23, 445.)

3. B.I.Pochtarev, K.K.Raspletin & D.V.Fetisov, Present issue of the Bulletin, (preceding article.)

Discussion Following the Reports of Z.M.Sverdlov; B.I.Pochtarev, K.K.Raspletin & D.V.Fetisov; B.I.Pochtarev:

B.I.Maksakov: The PRS instrument described by Pochtarev can be used for carrying out diverse investigations of the properties of fluorescent screens: the resolving power, light output, spectral composition of the emission, etc. I would like to suggest that in future models there be provision for exciting the screens not only by means of an electron beam but also by x-rays. However, even in its present form this instrument is highly useful for routine control of the quality of screens particularly under industrial conditions. I move that the Conference recommend that this instrument be put into production.

Regarding the report of Z.M.Sverdlov. The use of photoelectric photometry for investigating luminescence is undoubtedly important in the development of instruments. As for the FAS-1 instrument (photoelectric photometer) described by Sverdlov it must be borne in mind that at present there is another instrument for the same purpose, the LYuF-57, which is being produced by our industry. For a new instrument to be introduced it must possess better technical qualities. Comparison of the LYuF-57 and FAS-1 instruments shows, however, that their basic parameters are virtually identical.

INVESTIGATION OF THE ELECTROLUMINESCENCE OF ZINC SULFIDE SINGLE CRYSTALS

- V.E.Oranovskii

In our earlier studies[1,2] of electroluminescence of ZnS:Cu:Cl single crystals it was shown that the luminescent stripes or striae break up in length into sections characterized by different phases of the brightness wave and different reaction of the luminescence to introduction of positive or negative current carriers. On the basis of the experimental results obtained on excitation of electroluminescence by electric fields directed at different angles relative to the direction of the stria it was inferred that the crystals are anisotropic as regards excitation by an electric field and that this anisotropy is connected with anisotropy of conductivity. There was deduced a formula describing the voltage dependence of the brightness, taking into account the field angle.

The purposes of our present work, which is a continuation of our earlier studies, was to determine in more detail the properties of an elementary section of a stria and to elucidate the mechanism of excitation and influence of injected current carriers. To this end we obtained for ZnS:Cu:Cl crystals indicatrices of the brightness at different positions of the photoprobe (UV light spot) relative to the observed section. In all these measurements the photoprobe was directed onto sections of the crystal outside the field of view. We recorded brightness indicatrices for a uniform section of an electroluminescing stria under the following excitation conditions: 1) without additional photoexcitation by the probe, 2) with the photoprobe to one side or the other, i.e., above or below, the stria, 3) with the probe spot along the direction of the stria and to the right of the observed section, and 4) with the probe spot in the direction of the stria and to the left of the observed section (see diagram of Fig.1).

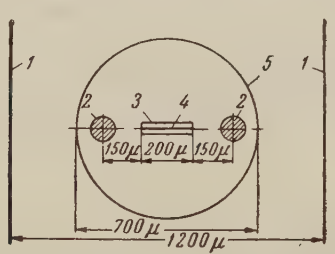

Fig.1. Arrangement for determining the effect of ultraviolet radiation on the electroluminescence of zinc sulfide crystals: 1 - capacitor plates, 2 - ultraviolet spot (100 μ diameter) 3 - slit, 4 - observed section of stria, 5 - boundary of field of view.

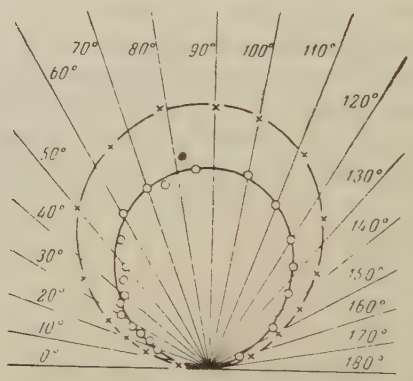

Fig.2. Brightness indicatrices observed under the influence of additional ultraviolet excitation and without such excitation.

The indicatrices obtained in cases 1 and 2 virtually coincide; the result obtained in case 3 is shown in Fig.2. Here the smaller loop is the indicatrix without additional photoexcitation; the larger loop is the indicatrix with additional ultraviolet excitation. Transfer of the photoprobe spot to the opposite side of the observed section of the stria leads to decrease rather than increase in the size of the indicatrix loop; that is, the change can again be represented as in Fig.2 but in this case taking the large loop as the initial one. The ratio of the radius vectors of the indicatrices under the exciting influence of the UV probe and without it is constant for all angles between the field and the direc-

tion of the stria, except for angles close to 90°, where there is observed a large scatter of the experimental points; this is probably connected with the fact that the measured brightnesses are greatly reduced and a substantial role begins to be played by distortions of the field introduced by the crystal itself. Examination of the indicatrices shows that they can be obtained one from the other by simple increase or decrease of the factor A in the following formula describing the relation between the brightness and the field:

$$B = Ae^{-\frac{b}{\sqrt{V\cos\alpha}}}.$$

In view of this it may be inferred that the additional current carriers penetrating into the observed regions of the crystal under the influence of the photoprobe do not participate or even affect the processes associated with field concentration.

Further experiments were carried out on single crystals activated with manganese in addition to copper. The single crystals were prepared by reaction in the gaseous phase between zinc and hydrogen sulfide. The principal activation by copper and manganese was realized during growth of the crystals (part of the copper was introduced additionally afterwards).

The distribution of electroluminescence in the case of these crystals is of the same character as in the crystals investigated earlier[1,2]. The luminescence is concentrated in separate parallel striae, which differ in color depending on the activator involved. The striae in which the manganese emits are red; those in which the luminescence is due to copper are blue.

In view of the relatively low sensitivity of our photomultipliers in the red part of the spectrum, we were unable to carry out quantitative measurements, similar to those described above, for the "manganese striae". Visual observations showed, however, that the manganese striae, in contrast to the copper ones, do not react or react only very weakly to the influence of the UV photoprobe when it is directed onto the crystal outside the field of view. When the photoprobe is incident within the field of view, i.e., directly on the observed section of the stria, in some cases there is observed even increase in the brightness of the stria instead of quenching as in the case of copper activation.

In these experiments there were obviously evinced the distinctive properties of manganese as an activator. It is known that manganese is not ionized in the process of excitation of the crystal. Taking into account the fluorescence character of the emission of manganese it may be concluded that it emits during the excitation half-cycle, that is, that the fluorescence coincides with the excitation half-cycle. This means that the fact that the luminescence of manganese is independent of the action of the photoprobe substantiates the inference that the luminescence of copper occurs during the voltage half-cycle following the excitation half-cycle. This also substantiates the above inference that in a wide range the processes of field concentration are independent of the number of additional injected charge carriers. This also confirms the deduction that the excitation of electroluminescence centers in these crystals occurs in the range of high field intensities.

References

1. V.E.Oranovskii, E.I.Panasyuk & B.T.Fedyushin, Inzh.-fiz.zhur. (Engineering-Physics Journal), 2, 39 (1959).

2. V.E.Oranovskii & B.A.Khmelinin, Optika i spektroskopiya, 7, 542 (1959). (Trans.Optics & Spectroscopy.)

3. W.Piper & F.Williams, Usp.fiz.nauk, 70, 621 (1960).

ELECTROLUMINESCENCE AND SURFACE PROPERTIES OF CRYSTAL PHOSPHORS

- I.K.Vereshchagin

A number of phenomena reported by investigators bear evidence for the significant role of surface effects in the processes of excitation of electroluminescence of powdered phosphors. It was found, for example, that the catalytic activity of ZnO, which is known to be a surface effect, varies congruently with the electroluminescence as a result of change in the conditions of preliminary heating.[1]

It is also known that adsorbed gases have a strong influence on the electroluminescence of ZnO and many polycrystalline specimens of ZnS and (Zn,Cd)S phosphors.[2] Upon removal of part of the adsorbed molecules, for example, by evacuating the container, the mean luminescence brightness usually increases. The influence of ultraviolet light in vacuum (~10^{-2} mm Hg) leads either to further increase of the steady luminescence or to some decrease thereof, which can be explained by photodesorption or photoadsorption of the gas.[3,4] Under the same conditions the intensity of photoluminescence changes very little, while the changes in photoconductivity are commensurate with the changes in electroluminescence. The photo-emf on the contrary, goes down as a result of removal of the adsorbed molecules by evacuation.

In the accompanying figure we present curves characterizing the effect of adsorption of gases on some of the properties of ZnO. Owing to curvature of the energy bands[5] at the surface of ZnO with adsorbed oxygen, the barrier (back) photo-emf will predominate over the diffusion photo-emf, and the magnitude of

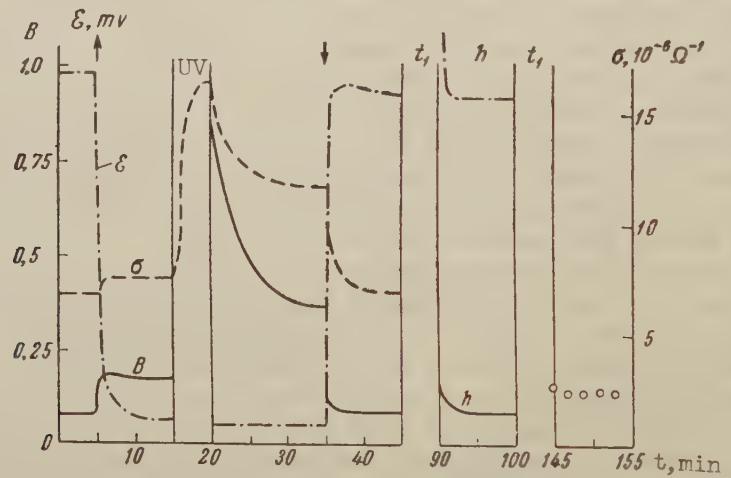

Variation of the electroluminescence B, conductivity σ and photo-emf ϵ of zinc oxide in air and in vacuum as a function of the time t and the experimental conditions. The mean brightness B is given in arbitrary units. The arrows indicate the instants of beginning of evacuation and admission of air (similar changes in the properties are observed with O_2 and CO_2). UV - time of action of ultraviolet light in vacuum (10^{-2} mm Hg); h - photo-emf ϵ and brightness B peaks after an interruption t_1 in excitation with light (400 watt incandescent lamp; frequency of light modulation 100 cps) or with an electric field (200 v, 1 cps). The points indicate the values of B with switching on the field for 10 sec at intervals of 2 min.

the emf will be determined primarily by the height of the barrier at the surface. This is the reason for the decrease of the photo-emf with removal of the adsorbed gas. In cases when evacuation does not affect the electroluminescence of sulfide phosphors, changes in the photo-emf are also usually negligible (predominance of the role of the crystal-second solid phase interface).

Inasmuch as even ordinary evacuation at room temperature, which cannot remove tightly bound oxygen, leads to strong changes in the electroluminescence and photo-emf, it may be assumed that the weak binding between the outer layers of gas molecules and the crystal is chemical in nature and covalent in character. In this case the adsorbed molecules may give rise to surface levels, the existence and filling of which will be evinced in the magnitude of the surface conductivity and the rate of recombination, and then as regards the height of the barrier.[6]

Since the luminescence brightness increases with evacuation despite some lowering of the barrier, a significant factor where electroluminescence is concerned is the rate of surface nonradiative recombination. Increase in the rate of recombination on the surface is usually taken into account in considering the photoconductivity of sulfides.[7-9] Electroluminescence must be very sensitive to surface recombination inasmuch as under the influence of an alternating field the barrier is periodically lowered and electrons emerge to the surface.

In addition, both electroluminescence and the photo-emf depend on the filling of the surface levels (traps). In the case of unexcited ZnO specimens there is observed a rapid initial rise of the electroluminescence and photo-emf, which is apparently connected with release of electrons from surface traps. The height of these initial peaks depends equally on the time the ZnO is kept in the dark or in the absence of a field (gradual filling of the surface levels).

Thus the conditions obtaining on the surface of electroluminophors are significant where electroluminescence is concerned; this must be taken into account both in developing the theory of electroluminescence and in preparing phosphors for practical purposes.

Chernovits State University

References

1. I.K.Vereshchagin, Izv.vyssh,uchebn.zav.Fizika, (Bulletin of higher schools. Physics), 2, 31 (1960).

2. I.K.Vereshchagin, Optika i spektroskopiya, 8, 420 (1960). (Trans.Optics & Spectroscopy.)

3. A.N.Terenin, Probl.kinetiki i kataliza (Problems of kinetics and catalysis), 8, 23 (1955).

4. A.Kobayashi & S.Kawaji, J.Phys.Soc., Japan, 10, 270 (1955).

5. F.I.Vilesov & A.N.Terenin, Doklady AN SSSR, 125, 1053 (1959). (Trans. Doklady.)

6. G.W.Pratt & H.H.Kolm, Semiconductor Surface Physics, p.23, N.Y., 1957.

7. R.H.Bube, J.Chem.Phys., 21, 1409 (1953).

8. S.H.Liebson, J.Electrochem.Soc., 101, 362 (1954).

9. A.N.Terenin, Fotoelektricheskie i opticheskie yavleniya v poluprovodnikakh (Photoelectric and optical effects in semiconductors), p.255, Kiev, 1959.

REGARDING THE POSSIBILITIES OF STIMULATING THE ELECTROLUMINESCENCE PROPERTIES OF CRYSTALS

- I.S.Andreev, G.B.Arzumanyan & L.V.Zyrina

Below we report on the results of our research which had the following principal aims.

I. To determine the influence of conditions of preparation of ZnS:Cu electro luminophors on their brightness, emission spectrum and frequency dependence.

II. To study the kinetics of emission of ZnS:Cu crystals under the influence of an alternating voltage.

III. To elucidate the character of the relaxation processes occurring in powdered phosphors under the influence of pulse excitation.

IV. To search for new ways of synthesizing ZnS electroluminophors.

I. Investigation of the influence of the conditions of preparation (temperature and heating time, type of gaseous medium and kind of solvent used in washing) on the characteristics of the resultant phosphor yielded to the following results:

1. The spectra of ZnS:Cu phosphors prepared in media not containing HCl (for example, in an atmosphere of N_2 (or 20% H_2S + 80% N_2) are somewhat shifted to the short wavelength side as compared with the spectra of phosphors prepared in media containing HCl (for example, 20% H_2S + 80% HCl).

2. The frequency dependence of the electroluminance under the influence of a sinusoidal voltage differs somewhat for phosphors prepared in different media; this dependence is steeper and is linear in a wider frequency range for phosphors sensitized in a medium consisting of 20 H_2S + 80% HCl.

3. Both the spectrum of the phosphor and the frequency dependence change with increase of the heating temperature: the higher the temperature, the more pronounced the "green" (5200 Å) peak in the spectrum; with increase of the heating temperature the frequency dependence coefficient increases and passes through a maximum corresponding to a temperature of about 1200°.

4. Increase of the heating time alters the spectrum and the frequency dependence in approximately the same way as increase of the heating temperature; the optimum heating time is ~2 hours.

5. Different solvents used in washing (water, ammonium, potassium cyanide and acetic acid) have different and often significant effects on the brightness, spectrum and frequency dependence of the phosphors; particularly great changes in the spectrum are produced by potassium cyanide, which tends to enhance the "blue" peak at the expense of the "green" peak.

II. Investigation of the electroluminescence of phosphor single crystals in the field between four mutually perpendicular electrodes (needles to which a sinusoidal voltage was applied) showed the following:

1. The absence of anisotropy of the electroluminescence properties.

2. Significant influence of contact of the phosphor with the electrode on the brightness of the brightness waves, particularly when the luminescent bands are nonuniformly distributed over the crystal.

3. This contact effect is not connected with flow of current through the crystal.

4. The shape of the brightness waves can be explained by assuming, in accord with Oranovskii & Khmelinin[1], that emission at different points in the crystal occurs at different times during the voltage cycle.

III. Investigation of the brightness peaks under the influence of square voltage pulses applied to a capacitor containing only the phosphor (no dielectric) showed the following:

1. Both the "leading edge" peak and the "trailing edge" peak in the case when the potential on the transparent electrode remains higher than the potential of the second electrode, develop at the same rate as the rate of change of voltage, i.e., during the rise or decay time (~10 microsec), which is in agreement with the data of Bonch-Bruevich & Marenkov[2].

2. The rate of decay of the luminescence is an order of magnitude lower than the rate of rise of luminescence, and for the "leading edge" peak the rate is somewhat higher than for the "trailing edge" peak.

3. With opposite polarity on the electrode (potential on the transparent electrode always lower than the potential of the second electrode) both the "leading edge" peak and the "trailing edge" peak can be represented by two parts: in the first part the brightness increases as before with the rate of rise or decay of the voltage, while in the second part the rate of rise is 2-3 times slower.

IV. We investigated the possibility of using electrolysis for activating ZnS electroluminophors.

The ZnS powder was loaded into a quartz tube equipped with electrodes of the desired activator material and heated for a certain time at not excessively high temperatures in an atmosphere of nitrogen with simultaneous passage of current through the powder (temperature 700 to 1000°; current 0.4 to 15 ma).

We used the method of radioactive tracers to elucidate the relative roles of electrolysis and diffusion in the process of transfer of the activating substance and the process of activation. A small weighed sample of ZnS:Ag* (Ag* = = radioactive silver) was placed in the bottom of the tube (anode end) with electrodes of ordinary silver. The rest of the tube was filled with unactivated ZnS. After heating with passage of current all the fractions showed a relatively bright electroluminescence; the distribution of radioactivity, shown below, clearly indicates the predominant role of electrolysis.

Fraction	Activity, pulses/min
Anode	--
Phosphor near anode	628
Phosphor in middle of tube	116
Phosphor near cathode	837
Cathode	4576

In order to bring out the relative roles of electrolysis and diffusion in the process of activation per se, a sample of ZnS was subjected to electrolysis between a copper electrode (anode) and a tagged silver electrode (cathode). The resultant product was separated into nine fractions starting from the anode. The first six fractions yielded a bright green electroluminescence peaking at 5200 Å. The luminescence of the ninth fraction was blue-green with a peak at 4850 Å. The activity distribution was the following:

Fraction:	Anode	I	II	III	IV	V	VI	VII	VII	IX	Cathode
Activity, pulses/min	-	-	3	13	14	14	20	22	170	582	10630

For the same purpose we also performed another experiment in which we heated two tubes with copper electrodes only one pair of which was connected to a dc source. Whereas the product obtained with electrolysis yielded bright green electroluminescence, the nonelectrolyzed material virtually did not luminesce.

We felt it would be of interest to test this procedure for the purpose of "purifying" the initial product. To this end we subjected copper activated ZnS to electrolysis with nickel electrodes. The color of the resultant powder was bright yellow at the anode and shaded to white at the cathode. Weak photoluminescence was observed only for the last two of the four separated fractions. None of the fractions exhibited electroluminescence. After tests for photo- and electroluminescence, the phosphor was again loaded into a tube and subjected to electrolysis with copper electrodes. The initial appearance of the powder was restored as was its electroluminescence.

In view of the results of this experiment, we prepared a batch of ZnS without taking any particular precautions with regard to purity and subjected it to electrolysis. At the same time we heated a control tube with the same ZnS and copper plates. The phosphor from the first tube had a brightness equal to that of the best ZnS:Cu electroluminophors, while the brightness of the phosphor from the second tube was at least one order of magnitude lower.

Analysis of the results obtained in the above described experiments led us to think that the role of electrolysis is not limited merely to more rapid transfer of the activating element. We believe that the passage of current results in the formation of some type of inclusions or produces other changes in the phosphor favoring electroluminescence. In order to check this we determined the concentration of silver in electrolytically prepared ZnS:Ag* phosphors (from their radioactivity), which proved to be 10^{-4} g Ag/g ZnS, and prepared a batch of ZnS: :$AgNO_3$ with the same silver concentration. This batch was subjected to heating under the same conditions as used for preparing the electrolyzed phosphor, but without passage of current. Both phosphors exhibited bright blue photoluminescence. The phosphor prepared by heating only showed no electroluminescence, whereas the phosphor obtained by electrolysis exhibited electroluminescence characterized by the following data:

Voltage, v	300	400	500	600	700	900
Brightness, arbitrary units	2	5.5	9.5	13	24	48

Thus the described electrolysis procedure undoubtedly has potentialities for the preparation of electroluminophors.

Chair of General Physics,
"V.I.Lenin" Central Asian State University

References

1. V.E.Oranovskii & B.A.Khmelinin, Optika i spektroskopiya, 7, 542 (1959). (Trans.Optics & Spectroscopy.)
2. A.M.Bonch-Bruevich & O.S.Marenkov, Ibid., 8, 855 (1960). (Trans.Ibid.)

EFFECT OF ULTRAVIOLET IRRADIATION ON THE LUMINESCENCE CHARACTERISTICS OF AN ELECTROLUMINOPHOR

- I.P.Shapiro & N.I.Kuznetsov

Vinokurov & Fok[1] showed that the effects of photo- and electroexcitation are in general not additive: in some cases the integral luminescence brightness under combined excitation may be greater than the sum of the brightnesses for both forms of excitation (positive nonadditivity), while in other cases the integral luminescence may be lower (negative nonadditivity). At a certain relation between the photo- and electroexcitations one can obtain precise additivity. In view of the fact that there may exist a number of processes that can lead to nonadditivity of photo- and electroexcitation, we undertook experiments aimed at determining the effect of the combined influence of ultraviolet irradiation and an electric field on ZnS:Cu phosphor under different conditions.

Experimental procedure and results*

Fine-grain, green-emitting ZnS:Cu electroluminophor, suspended in liquid melamine formaldehyde resin, was sandwiched between a glass and a quartz plate; the internal surfaces of the plates were covered with a thin transparent layer of SnO_2. The assembled capacitor was irradiated from the quartz plate side with UV radiation from a PRK-4 tube operated from a rectifier with a ripple filter. The radiation emitted by the phosphor was detected by an FEU-19 photomultiplier coupled to an oscillograph.

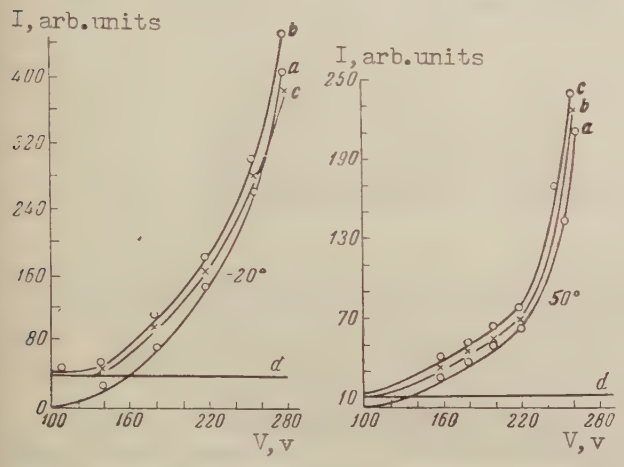

Electroluminescence and photoluminescence of ZnS:Cu phosphor at different temperatures.

In investigating the electroluminescence we observed both positive and negative nonadditivity under the influence of photo- and electroexcitation. The results of our investigation show that with increase of the UV intensity, the transition from negative to positive nonadditivity occurs at increasingly higher field values.

It also follows from the experimental results that the sign of the nonadditivity depends on the temperature of the phosphor.

The variation of the electroluminescence brightness as a function of the applied field at -20° and +50° is shown in the accompanying figure. Curve a in each case corresponds to pure electroluminescence (excitation by an ac field only); curve b represents the sum of the brightnesses of electroluminescence and photoluminescence; curve c represents combined electrophotoluminescence, i.e., the luminescence under the joint influence of ultraviolet and an ac field; line d characterizes the luminescence intensity of the phosphor under the influence of ultraviolet alone.

---

*N.Pesenko, student at the Belorussian State University, participated in the experimental part of the work.

It will be evident from the figure that decrease of the phosphor temperature leads to the appearance of negative nonadditivity.

One of the significant characteristics of electroluminophors is the frequency dependence of electroluminescence brightness. The brightness is a function of not only the amplitude of the applied field but also of the phosphor temperature. Experiments show that the frequency dependence of the luminescence brightness at 20^{o} is characterized by positive nonadditivity.

At -20^{o} the variation of electroluminescence brightness with the frequency of the applied voltage is characterized mainly by negative nonadditivity; precise additivity in this case is observed at low frequencies (up to 300 cps).

Thus we come to the conclusion that increase of the phosphor temperature leads to positive nonadditivity, while reduction of the temperature results in negative nonadditivity of the effects of photo- and electroexcitation.

We also obtained experimental data on the effect of auxiliary UV irradiation on the magnitude and shape of the brightness waves. The experimental results show that auxiliary UV irradiation changes the character of the brightness waves produced in excitation of the phosphor by pulses of different shape.

We desire to thank M.V.Fok for this interest in the work and valuable suggestions.

Reference

1. L.A.Vinokurov & V.I.Fok, Optika i spektroskopiya, 7, 241 (1959). (Trans. Optics & Spectroscopy.)

* * * * * * *

INVESTIGATION OF THE ELECTROLUMINESCENCE OF SOME PHOSPHORS WITH EXCITATION BY UNIPOLAR PULSES

- V.L.Rabotkin & V.A.Sokolov

In the present work we investigated the shape of the electroluminescence brightness waves of ZnS:Mn and ZnS:Cu:Pb phosphors excited by unipolar sine pulses and dc voltage. The luminescence was detected by an FEU-19M photomultiplier connected via a dc amplifier to the input of an MPO-2 oscillograph.

The ZnS:Mn phosphor specimens were prepared by heating batches containing luminescence pure ZnS with appropriate amounts of $MnCl_2$ in glass tubes for 30 min at 1200^{o}. The concentrations of metallic Mn in the batch were 10^{-3}, 10^{-2} and 10^{-1} g/g. Under ultraviolet stimulation (3600 Å) the first phosphor had an intense blue band, the second a blue and orange band, and the third an intense orange band. Under excitation by an electric field (pulse and dc) there was evinced only the orange band, the brightest luminescence being observed in the vicinity of the cathode. The shape of the brightness waves is shown in Fig.1 (a & c). In the first case there was a cellophane film liner between the cathode and the castor oil suspension of the phosphor; in the second case the solid dielectric liner was a sheet of mica. Thus the second peak in the brightness wave can be explained by the effect of polarization of the dielectric by the field. Fig.1 also shows how the luminescence brightness of the capacitor cell with a cellophane liner (b) and a mica liner (d) changes with change of the polarity of the exciting pulses from

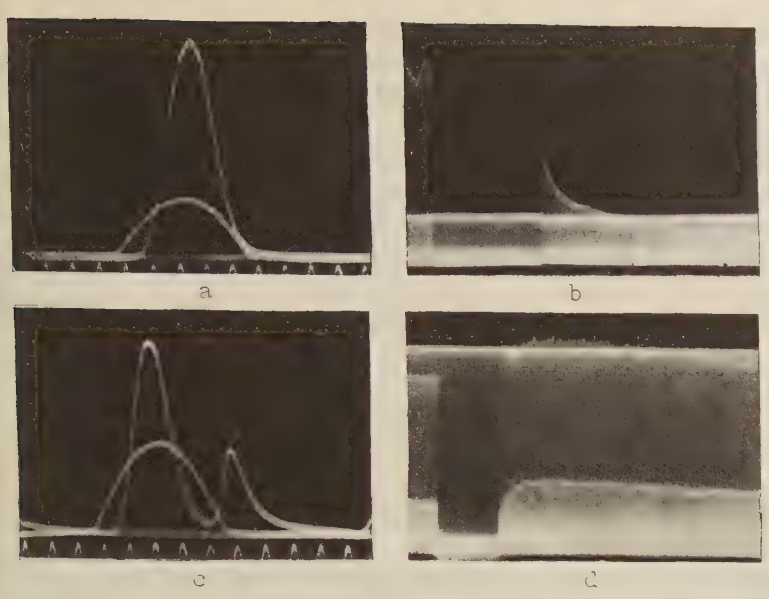

Fig.1

negative to positive (relative to the transparent electrode). It will be evident from Fig.1,b that in the case of the cellophane liner the luminescence is almost completely quenched. Fig.1,d shows the behavior of both peaks: the second polarization peak appears gradually.

The shape of the brightness wave of ZnS:Cu:Pb phosphor is shown in Fig.2 and is reminiscent of the shape of the brightness wave of ZnS:Mn reproduced in Fig.1,c. The shape of the brightness wave changes little with different solid dielectrics between the castor oil suspension and the cathode, but does change substantially with change

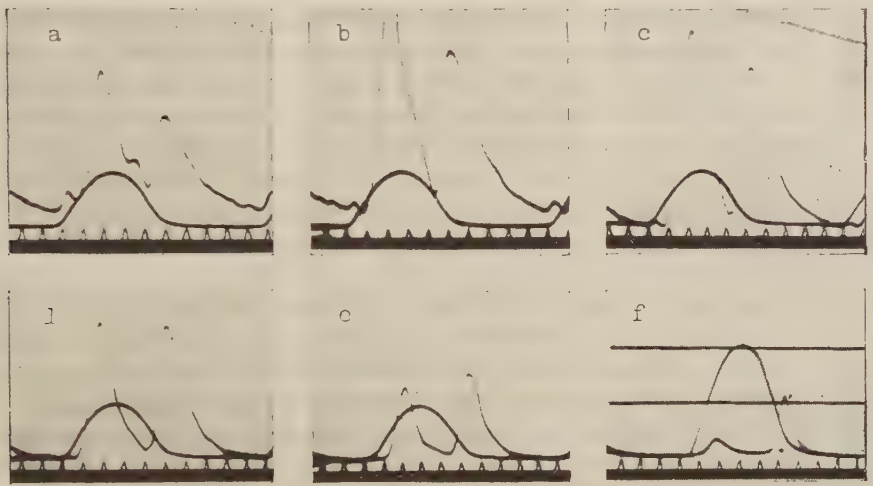

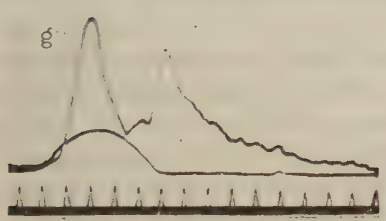

Fig.2. Brightness waves of ZnS:Cu:Pb phosphor at different temperatures.

of temperature. The oscillogram of Fig.2,a was recorded at 25°; for each of the succeeding oscillograms b through f the temperature was increased 50°. Interesting is the presence of two low peaks which disappear with increase of temperature (Fig.2,b-f) and with change of the duty factor without change of the pulse height and duration (Fig.2,g).

If the solid dielectric liner is removed (leaving the phosphor suspended in castor oil) or if one changes the distance between electrodes (or the specific volume of the phosphor as compared with the case of the dielectric layer present), the relation between the heights of the principal peaks changes. This also occurs if the castor oil is replaced by a less viscous dielectric and if the amplitude of the exciting pulses is increased.

Analysis of the experimental data leads to the following conclusions:

1. The mechanism of excitation of electroluminescence of ZnS:Mn and ZnS:Cu:Pb phosphors differs, presumably owing to the different dielectric properties of the phosphor grains.

2. The shape of the brightness wave of ZnS:Cu:Pb phosphor is determined to some extent by the ability of the grains of this phosphor to form "chains" extending from one electrode to the other under the influence of the applied field; these "chains" persist when the field is removed and are responsible for the ability of this phosphor to luminesce in a dc field.

We desire to than Z.A.Trapeznikova for supplying the ZnS:Cu:Pb phosphor.

* * * * * * *

SOME RESULTS OF AN INVESTIGATION OF THE DETERIORATION OF PHOSPHORS DURING ELECTROLUMINESCENCE

- N.N.Grigor'ev & Yu.A.Kulyupin

We investigated the process of deterioration of ZnS·ZnO:Cu:Al:Cl phosphor in the course of electroluminescence. The phosphor, suspended in silicone oil, was contained in a capacitor, which had provision for changing the position of the phosphor particles without disturbing the conditions of excitation and observation. This insured strong deterioration of the phosphor in an appreciable volume of each crystal, which was accompanied by significant decrease in the electroluminescence brightness. The photoluminescence brightness remained unchanged, although the expected decrease in brightness should have amounted to ~22%. This value was obtained on the assumption that strong deterioration occurs in about 5% the volume of an individual crystal during each half-cycle of the field (the ~5% figure is not an excessive estimate for the conditions of our experiment). Thus it may be concluded that the photoluminescence properties of a phosphor deteriorating under electroluminescence remain unchanged.

The increase in the relative intensity of the green band as compared with the blue, observed in the process of deterioration, gives reason to assume that the damage occurs in the phosphor itself, rather than in the surrounding dielectric. The fact that the electroluminescence brightness is partially restored when the position of the particles is changed indicates that the damage is local in character. Apparently, the deterioration occurs in regions of concentration of positive space charge, produced in the crystal under the influence of the applied field. The decrease in electroluminescence brightness can be explained by broadening or diffusion of the space charge region, leading to decrease in the space charge density and thus reduction of the internal field in the crystal.

On the assumption of such diffusion of the space charge one can also explain the observed changes in the frequency characteristics and voltage dependence of the brightness occurring in a deteriorating phosphor. This change in the extent of the space charge region should also produce changes in the shape of the electroluminescence brightness waves. Our experimentally observed increase in the ratio of the varying component of the brightness wave to the constant component and the increase in the height of the additional brightness wave peak relative to the height of the principal peak are consistent with our hypothesis. This hypothesis is not in conflict with some difference between the behavior of the

blue and green electroluminescence brightness waves, leading to gradual "greening" of the phosphor in the process of deterioration.

At present, the reason for diffusion of the positive space charge region is obscure; probably it is connected with the appearance of new defects in the crystal, defects containing trapping levels substantially deeper than were present in the crystal prior to damage. This follows from the observed increase of the photoluminescence light sum stored in a phosphor that has been forced to electroluminescence for some time as compared with a fresh undeteriorated phosphor.

* * * * * * *

USE OF ELECTROLUMINESCENCE FOR CHARACTER INDICATORS

- F.V.Sorkin, A.P.Belyaeva & N.S.Borodin

The high luminance of new electroluminophors makes it possible to utilize the phenomenon of electroluminescence for electroluminescent (EL) character indicators, which may be used as output units for computers, display panels in conjunction with various electronic devices that give figure indications, etc.

In our development work on EL indicators we used green luminescing GIPKh phosphor with the following composition: ZnS:Cu(0.2%):Al(0.05%).

1. Design development

The usual EL character indicator is a flat screen or panel (capacitor), one electrode of which is a transparent conducting coating of SnO_2 and the other electrode is metallic, made in the form of a number of strips (segments), formed by thermal evaporation of Al or Ag under vacuum through a suitable templet. The individual panels are lighted-up by applying a voltage to the common (transparent) electrode and the appropriate segment.

In order to enhance the serviceability of indicators we proposed the following new method of preparing the metallic electrode: vacuum sputtering of a thin layer of copper on the EL coating, electroplating upon this a thicker (10-15 μ) copper layer and subsequent use of appropriate printed circuit techniques for forming the connections.

EL indicators fabricated in this manner have rugged metallic electrodes of electroplated copper to which the voltage carrying leads are attached by soldering, which is particularly convenient for subsequent hermetic sealing of the element.

The above described procedure can also be used for preparing electroluminescent matrix and mosaic screens and other EL devices.

Life tests showed that the proposed technology does not impair the aging characteristics of the EL elements (Fig.1,d).

2. Increase of the character contrast

The basic criterion for distinguishability of symbols on an EL indicator is the contrast characterized by $K = (B_c - B_b)/B_b$, where B_c is the brightness of the character and B_b is the brightness of the background.

The causes of contrast-reducing background luminance are halos and external illumination. The best results as regards reduction of contrast are obtained by

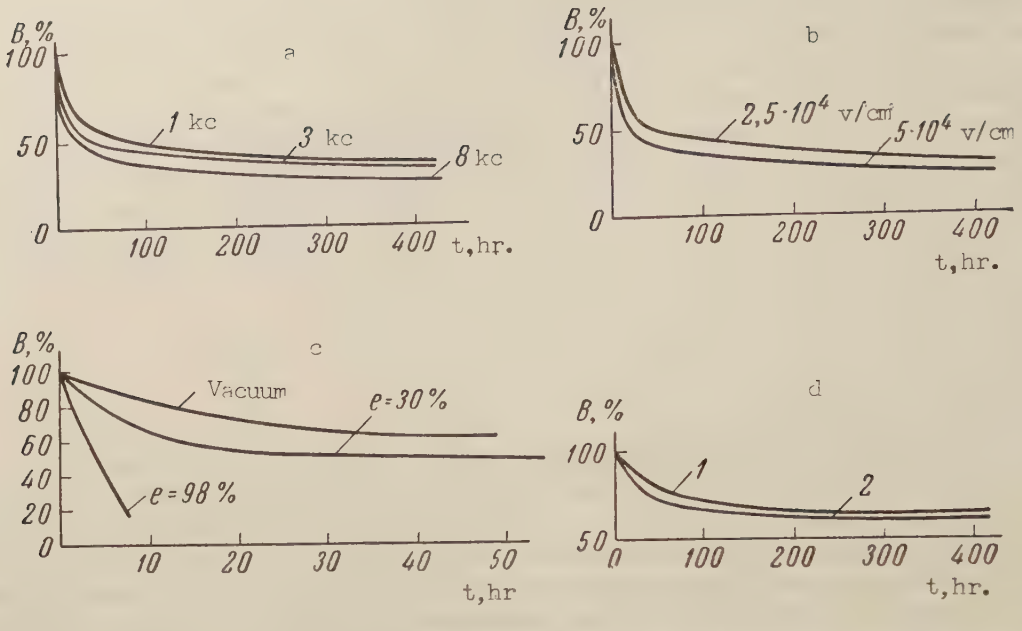

Fig.1. Aging characteristics of EL elements: a - at different excitation frequencies ($E = 2.5 \cdot 10^4$ v/cm); b - different potential gradients ($f = 3$ kc); c - different ambient humidities ($V = 250$ v, $f = 1$ kc); d - vacuum sputtered electrode (1) and hermetically sealed electrode of electroplated copper (2).

reducing the reflection factor ρ of the indicator panel. Calculations show that with a constant level of external illumination the contrast increases rapidly with decrease of ρ.

EL indicators with a low reflection factor have a thin (25-30 μ), almost transparent electroluminophor layer (phosphor suspension in plastic), covered with an absorbing plastic layer colored with nigrosine (aniline black). The use of sublimate phosphors appears to be promising for such indicators.

The advantage of the above described procedure for increasing contrast over the use of light filters is that, in addition to reducing the background brightness produced by external illumination, this procedure completely suppresses halos

Character indicators of this type (Fig.2) can be used at high levels of external illumination (200 to 500 lux).

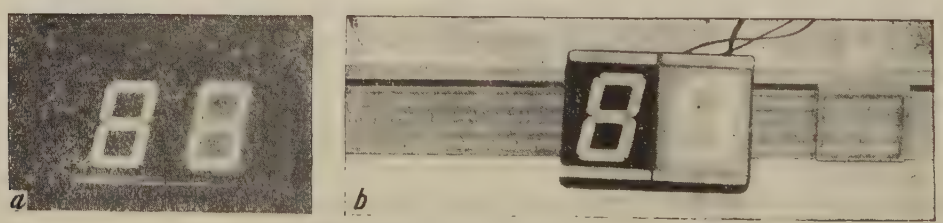

Fig.2. Appearance of EL indicators with white and black backing layers at different levels of external illumination: a - 10 lux, b - 200 lux.

3. Service life tests

For evaluating the service life of EL indicators we carried out aging tests on luminophors in solid dielectrics (Epoxy EP-096).

It was found that prolonged storage of unsealed elements under room conditions leads to some decrease of the initial brightness. Over a period of 8 months storage the brightness of the electroluminescent elements fell off by an average of 15-20%.

We also investigated the aging of EL elements as a function of the frequency; the aging curves obtained at frequencies of 1, 3 and 8 kc are shown in Fig.1,a. It will be evident that the excitation frequency is not a significant factor.

Fig.1,b gives the aging characteristics for EL elements operated at different potential gradients. It will be seen that a two-fold increase of the operating voltage has a more deleterious effect on the deterioration in brightness than a two-fold increase of frequency.

In order to determine the influence of moisture, we investigated the aging characteristics of elements operated in vacuum and in an atmosphere with 98% relative humidity. It was found that if no voltage is applied to the element, exposure to 98% humidity air for a period of 48 hours does not result in any significant decrease of the initial luminance. Under voltage, however, the decrease in brightness with time in an atmosphere of high humidity is more rapid than in vacuo (Fig. 1,c). Moreover, under conditions of high humidity the material darkens rapidly and its electric strength deteriorates.

The results of the present experiments substantiate the data reported earlier by one of us[1] and by other authors[2,3] to the effect that moisture plays a very important role in the process of aging. The rapid decrease in luminance can be explained by electrochemical alteration of the luminophor under the influence of the electric field in the presence of moisture.

Our experiments proved the importance of hermetic sealing of EL indicators for enhancing their service life. The requisite protection can be provided by covering the EL indicators on the luminescent layer side with epoxy compound. The aging characteristics of elements protected in this manner are shown in Fig. 1,d.

References

1. F.V.Sorkin, Voprosy radioelektroniki (Questions of radioelectronics) No.4, 52 (1960).
2. S.Roberts, J.Appl.Phys., 28, No.2, 262 (1957).
3. G.Diemer, H.Klasens & P.Zalm, Philips Techn.Rev., 19, No.1 (1957).
4. P.Zalm, G.Diemer & H.Klasens, Philips Res.Repts., 9, 81 (1951).

MEASUREMENT OF LOSSES IN AN ELECTROLUMINESCENT CAPACITOR

- E.E.Bukke

Measurement of the energy output or efficiency of electroluminescence is of interest both from the practical standpoint and for better understanding of this effect. To determine the efficiency one must measure two quantities, namely, the energy emitted by the phosphor and the energy absorbed by it. The energy emitted by an electroluminescent capacitor (EC) can be measured using the same procedures as those employed in studying photoexcitation. Measurement of the absorbed energy amounts to measuring the power loss in the EC.

Many methods have been developed for measuring the loss in capacitors and the instrument building industry produces a number of fairly sensitive instruments. However, these instruments are, in general, not suitable for measuring the loss in electroluminescent capacitors in view of the fact that owing to nonlinear effects in the electroluminophor the shape of the current curve (with a sinusoidal voltage applied to the EC) differs substantially from a sine curve.

The best instrument for measuring the loss in an EC would be a dynamic wattmeter, in which, as is known, the deflecting force is proportional to the product of the currents in the moveable and stationary coils. The instruments of this type produced by our industry, however, are not sufficiently sensitive for carrying out measurements with small EC of the type commonly used in laboratory experiments. Moreover, the commercial instruments usually cannot be employed at frequencies above 100 cps.

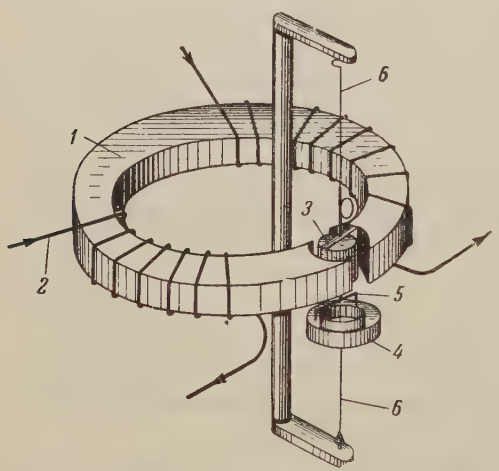

Diagram of wattmeter: 1) ferrite core, 2) stationary coil, 3) moveable coil, 4) oil bath, 5) damping yoke, 6) suspension.

We built and tested a dynamic wattmeter free of these shortcomings; this is diagrammed in the accompanying figure. In order to enhance the sensitivity of the instrument we used a suspension system similar to that employed in mirror galvanometers. The stationary coil (through which there flows a current proportional to the voltage applied to the EC) is made fairly large (3200 turns of 0.31 mm diameter wire) so that, using an amplifier, one can feed in an appreciable power (up to 50 watt).* To improve the magnetic characteristics, the core is made of a ferrite ring 100 mm in diameter.

In order to extend the frequency range, the moveable coil consists of only two turns and has a low inductance (0.3 μh). Up to a frequency of 200 kc there is no significant phase shift in the circuit of this coil if it is connected in series with a 500 ohm resistance. The phase difference between the current and voltage in the stationary coil is compensated by a phase shifter.

The natural oscillation period of the moveable system (in air) is ~2 sec. The system is damped by means of a yoke attached to the moveable coil; the two ends of the yoke are bent downward and immersed in an oil bath.

The principal characteristics of the instrument are the following. At a power level of 2.5 watts in the circuit of the stationary coil the sensitivity of the

---

The winding of this coil is sectioned so that its impedance can be matched with the input impedance of the amplifier at any working frequency.

instrument allows of measuring a current of 10^{-6} amp in the moveable coil (accordingly, at a power of 25 watt the measureable current is 10^{-7} amp). This provides for a thousand-fold reserve of sensitivity in measuring the loss in an EC with an area of 4 cm^2, operating under optimum conditions. The frequency range in which the instrument does not introduce any noticeable distortion (up to the third current harmonic) extends from 50 cps to 50 kc.

* * * * * * *

INVESTIGATION OF THE LUMINESCENCE OF CdS SINGLE CRYSTALS AT LOW TEMPERATURES

- E.F.Gross & M.A.Yakobson

It has been noted in our earlier publications[1,2,5] and in the work of other authors[3,4] that in the spectrum of CdS single crystals at 4.2°K there is observed in the vicinity of the absorption edge a complex absorption and emission structure consisting of narrow lines and bands of different intensity. It was also established[6] that the frequencies, intensities and number of lines in the 4889 to 4860 Å region vary from crystal to crystal. In contrast, the bands in the 4853 to 4800 Å region, which are characterized by a high absorption coefficient, are stable.

In general, one can distinguish two regions in the luminescence of CdS crystals: a long wavelength region extending from 5100 to 4860 Å (blue luminescence), which has been investigated by many authors[3-5,7], and a short wavelength region (λ = 4853 to 4800 Å), which was observed[2] at 77.3°K. As noted earlier[2,5] some of the luminescence lines are in resonance with absorption lines: the luminescence lines are generally shifted to the long wavelength side by approximately the line width (1-2 Å).

Recently we investigated the short wavelength group of luminescence lines corresponding to the short wavelength absorption of CdS single crystals at 4.2°K. A spectrogram of the luminescence of a CdS crystal is reproduced in the accompanying photograph. It will be seen that the short wavelength bands (λ = 4788, 4824 and 4852 Å) are relatively weak owing to reabsorption. With these short wavelength bands, if one considers them to be head bands, one can associate satellites at a distance of 300 cm^{-1}; these satellites do not enter into the vibrational series identified in the long wavelength luminescence.[5,7]

We undertook experiments aimed at determining the nature of the defects responsible for the long wavelength group of luminescence lines. To this end we exposed CdS crystals to S and Cd vapor. It was found that as a result of treatment in S vapor the long wavelength luminescence and absorption disappear completely, while after treatment in Cd vapor the absorption and luminescence spectra remain virtually unaltered. In view of the fact that normally CdS crystals grow with an excess of Cd, it may be inferred on the basis of the above experimental results that the absorption and luminescence are connected with a deficiency of S, so that treatment in sulfur vapor "improves" the stoichiometry of the crystal, which leads to annihilation of the centers responsible for the long wavelength luminescence. This is substantiated by the partial restoration of the luminescence and absorption as a result of heating S-vapor-treated crystals in CdS vapor.

The following deductions may be drawn on the basis of the described experimental results.

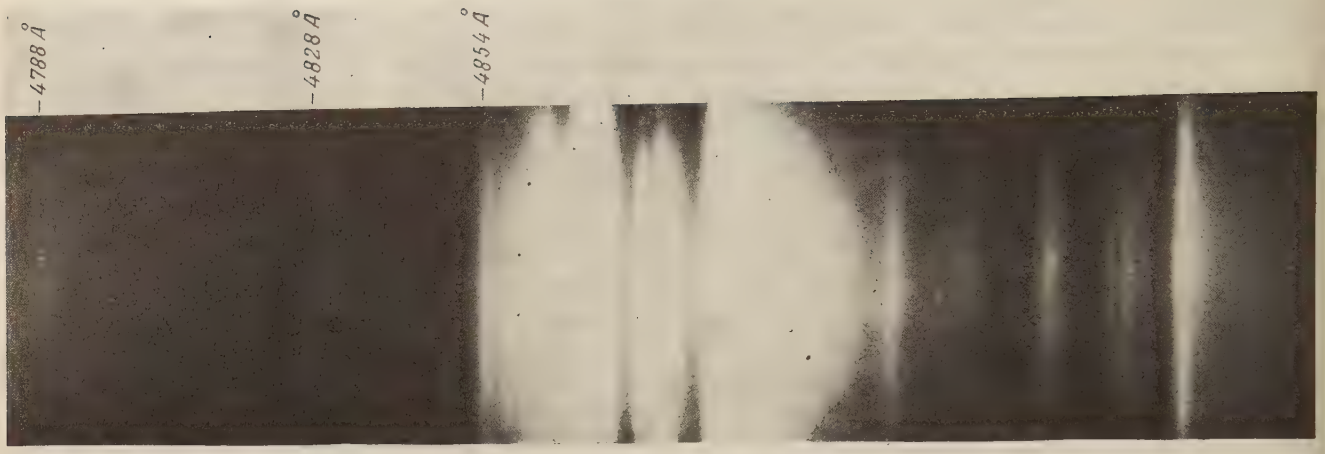

Luminescence spectrum of CdS single crystal

The short wavelength luminescence lines (and the corresponding absorption bands) can be attributed to exciton annihilation (creation) in the crystal lattice under the influence of incident light.

The origin of the long wavelength blue luminescence can be connected with the presence of defects (cf. Refs.5 & 7) in the crystal lattice. The fact that the long wavelength luminescence lines are not distant from the short wavelength lines gives reason to hypothesize that the defects here are evinced by influence on the exciton levels, i.e., the transitions responsible for the long wavelength emission may be regarded as occurring in the lattice itself close to different defects.

Accordingly, we feel justified in advancing the hypothesis that the group of long wavelength lines in both the absorption and blue luminescence spectrum of CdS single crystals is associated with excitation and emission of ortho-excitons forming in excitation with light under the influence of the perturbing action of defects. The short wavelength group of lines, both in the absorption and in the luminescence, must then be associated with para-excitons.

Physical-Technical Institute,
Academy of Sciences of the USSR

References

1. E.F.Gross & M.A.Yakobson, Doklady AN SSSR, 102, No.7, 485 (1955).
2. E.F.Gross & M.A.Yakobson, Zhur.tekh.fiz., 26, 1369 (1956). (Trans.Doklady.)
3. F.A.Kröger, Physica, 7, 1 (1954).
4. V.R.Furlong & C.F.Ravilious, Phys.Rev., 98, 954 (1955).
5. E.F.Gross & M.A.Yakobson, Tr.I Vsesoyuznogo soveshchaniya po fotoelektricheskim i opticheskim yavleniyam v poluprovodnikakh (Transactions of the First All-Union Conference on Photoelectric and Optical Effects in Semiconductors), Kiev Nov., 1957, p.63, Pub.AN Ukrainian SSR, Kiev, 1959.
6. E.F.Gross, B.S.Razbirin & M.A.Yakobson, Zhur.tekh.fiz., 27, 1149 (1957). (Trans.Soviet Physics - Technical Physics.)
7. V.V.Eremenko, Optika i spektroskopiya, 4, 348 (1958).

INVESTIGATION OF THE ABSORPTION AND LUMINESCENCE OF ZnS AND ZnSe SINGLE CRYSTALS

- E.F.Gross & L.G.Suslina

Continuing the program of research on the optical and photoelectrical properties of nonactivated sulfide and selsnide crystals undertaken in our laboratory, we investigated the absorption, reflection and luminescence spectra of ZnS and ZnSe single crystals in the vicinity of the fundamental long wavelength absorption edge at liquid helium temperature.

The ZnS and ZnSe crystals were obtained in the form of plates by sublimation of the powders in an atmosphere of neutral gas. These crystals are hexagonal with the sixth-order symmetry axis in the plane of the plate. The maximum dimensions of the crystals were 25 x 5 x 0.1 mm in the case of ZnS, and 7 x 1.6 x 0.1 mm in the case of ZnSe.

The spectra were recorded photographically in polarized light using specimens of different thickness.

The spectrograms disclose that the long wavelength absorption edges of ZnS and ZnSe crystals have a complex structure; at T = 4.2°K there are evinced several intense narrow polarized absorption lines. Near the absorption edges of both crystals there is observed line luminescence, the shorter wavelength lines of which coincide in frequency with the longer wavelength absorption lines. The positions of the centers of the absorption and luminescence lines and the polarization of the lines in the spectra of ZnS and ZnSe are shown in the accompanying figure.

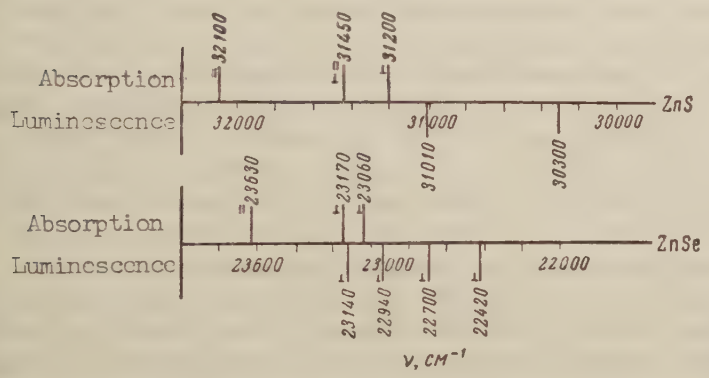

Location and polarization of the absorption and luminescence bands in the spectra of ZnS and ZnSe crystals.

There is evident a considerable similarity between the spectra of the isomorphous ZnS and ZnSe crystals as regards relative position, polarization and width of the lines. In view of the location of the lines at the absorption edge, their stability, and appreciable absorption coefficient ($\sim 10^4$-10^5 cm^{-1}), we infer that the observed features are due to absorption in the lattice of the host, i.e., to production of excitons.

The luminescence spectrum of ZnS was obtained at 77.3°K for fine crystalline powders.

In the luminescence spectra of ZnSe single crystals at 4.2°K we observed an intense line structure, which includes a group of equidistant bands, reminiscent of the band group observed in the spectra of a number of oxide and sulfide crystals. The separation between the equidistant bands (~ 260 cm^{-1}) agrees in order of magnitude with the vibrational energy of the ZnS lattice.

In view of the resonance coincidence of the short wavelength luminescence lines of ZnS and ZnSe with the long wavelength absorption lines it may be inferred that the line emission of these crystals is due to radiative annihilation of excitons in the crystal lattice.

CONCERNING INTERACTION OF THE ACTIVATOR WITH NOT FULLY SYMMETRICAL LOCAL VIBRATIONS

- N.N.Kristofel'

Luminescence centers in alkali halide phosphors may be regarded as quasi-molecules in the crystal. Investigation[1] showed that in nondegenerate electronic states the activator interacts only with fully symmetrical local vibrations, while in orbitally degenerate states it also interacts with certain not fully symmetrical vibrations. This leads to reduction of the symmetry of the center and removal of the degeneracy (analog of the so-called Jahn-Teller effect[2]).

To take into account the interaction of the activator with not fully symmetrical vibrations we used perturbation theory, separating out the corresponding linear term of the expansion and linear coordinates of the electronic energy operator in the adiabatic approximation. Numerical calculations were carried out for the $^3P_1$ state of the luminescence center in KCl:Tl, taking into account the shift only of nearest neighbors of the activator.

The frequencies of the local vibrations were calculated by means of the procedure outlined in Ref.1, where we give the one-oscillator calculation. The frequencies of the "transverse" vibrations, in contrast to the frequencies of the "longitudinal" vibrations, increase as a result of excitation of Tl^+. Using the criterion of Opik & Pryce[3], we showed that the minimum adiabatic potential corresponds to vibrations of E_g symmetry (normal coordinates y_1 and y_2) and the symmetry of the center is reduced to D_{4h}. There are three similar equilibrium configurations, which differ as regards the direction of the fourth order symmetry axis, along which the "dumbbell" of the 6p function of Tl^+ is directed. Along this axis the Cl^- ions move away from Tl^+ by 0.110 Å, while in the perpendicular directions the Cl^- ions approach the Tl^+ ion by 0.055 Å. In the equilibrium configuration there is present one nondegenerate and one twice degenerate level with relative energies of -0.065 and 0.13 ev, respectively. This splitting is less than the multiplet splitting. At the point $y_1 = y_2 = 0$, corresponding to the equilibrium ground state configuration, all three "sheets" have a common value equal to zero.

The magnitude of the Jahn-Teller effect depends on the electronic radius of the center; at first with increase of the radius the effect increases, but then begins to decrease. The Jahn-Teller effect is apparently absent in the case of centers of large radius, interacting with vibrations of the crystal.

The results of the present calculation allow of explaining the low temperature polarization of the $^3P_1 \rightarrow {}^1S_0$ radiation in KCl:Tl, observed by Klick & Compton[4]. At low temperatures an excited center may be in one of three equilibrium configurations of D_{4h} symmetry. With increase of the temperature there begin to occur nonradiative transitions between these configurations*; the polarization must disappear when the transition probability becomes greater than $1/\tau_{opt}$, inasmuch as this leads to loss of anisotropy. The height of the energy barrier equals 0.065 ev, which gives a correct evaluation** for the temperature of disappearance of polarization, namely, ~73°K. Thus the polarization of the radiation from impurity centers may be vibrational in character.

Under certain conditions, as a consequence of the Jahn-Teller effect, there may be observed nonelementarity of the emission bands, and possibly, splitting in the absorption spectrum (for example, if the Condon approximation is violated).

---

*It is meaningful to speak of the Jahn-Teller effect only when the frequency of such a "resonance" is lower than the frequency of oscillation of the ions.

**If there does not occur pumping of the excess vibrational energy from the fully symmetrical to the not fully symmetrical vibrations.

	E_m^x	E_m^I	$E_m^x - E_m^I$	δ_x	δ_I
One oscillator approximation	4,64	3,90	0,74	0,23	0,45
Taking not fully symmetrical vibrations into account	4,66	3,76	0,90	0,25	0,50
Experiment	5,02	4,06	0,96	0,23	0,51

Calculations show that the attempt of Kamimura & Sugano[5] to explain on the basis of the Jahn-Teller effect the presence of two emission bands at 3050 and 4750 Å for the $^3P_1$ state in KCl:Tl is not justified.

Using the adiabatic potentials in the one-oscillator approximation obtained in Ref.1 (in ev and Å),

$$I(^1S_0) = 18.0\,(q - 0.093)^2$$

and

$$I(^3P_1) = 4.34 + 11.4\,(q + 0.065)^2$$

and the results of the present work, we calculated the spectral characteristics of the $^1S_0 \leftrightarrow {}^3P_1$ bands in KCl:Tl taking into account the not fully symmetrical vibrations (in ev - see table). These make a contribution of ~18% to the Stokes losses ($E_m^x - E_m^I$) and ~10% to the half-widths δ so that it is evident that in alkali halide phosphors of the given type the activator interacts much more strongly with the fully symmetrical local vibrations. This explains the good applicability of the one-oscillator approximation, which, however, may prove to be inadequate in considering finer effects.

In investigating the effect of hydrostatic pressure[6] in the framework of the quasimolecular model it is not necessary to take into account the not fully symmetrical vibrations inasmuch as their effect does not lead to any significant change in equilibrium values of the corresponding vibration coordinates.

I desire to express my deep gratitude to M.I.Petrashen' and K.K.Rebane for many valuable suggestions.

Institute of Physics & Astronomy
Academy of Sciences of the Estonian SSR

References

1. N.N.Kristofel', Trudy IFA, Est.SSR(Proceedings of the Inst.of Physics & Astronomy, Estonian SSR), No.10, 3 (1959); Ibid., No.11, 180 (1960).
2. H.Jahn & E.Teller, Proc.Roy.Soc.A, 161, 220 (1937).
3. U.Opik & M.Pryce, Ibid., 238, 425 (1957).
4. C.Klick & W.Compton, J.Phys.Chem.Solids, 7, 170 (1958).
5. H.Kaminmura & S.Sugano, J.Phys.Soc.Japan, 14, 1612 (1959).
6. N.N.Kristofel', Trudy IFA, Est.SSR (Proceedings, Inst.of Physics & Astronomy Acad.of Sci.Estonian SSR), No.10, 43 (1959).

CONTRIBUTION TO THE THEORY OF ELECTRONIC-VIBRATIONAL TRANSITIONS IN CRYSTALS AND MOLECULES

- K.K.Rebane & O.I.Sil'd

We deduced the following formula for the l-th moment of the transition probability distribution in an arbitrary quantum system:

$$S_l = \sum_{p=0}^{l} (-1)^p \binom{l}{p} \int (\hat{P}\Psi_n)^* \hat{H}_{II}^{l-p} \hat{P} \hat{H}_I^p \Psi_n d\tau; \qquad (1)$$

here $\hat{P}$ is the operator of the perturbation producing the transition, $\hat{H}_I$ and $\hat{H}_{II}$ are the Hamiltonians of the initial and final states, respectively, and Ψ_n is the wave function of the initial state. From Eq.(1) one can obtain results for different specific systems, in particular, for atoms, molecules and crystals.

Application of Eq.(1) in the dipole approximation ($\hat{P} = D$, where D is the projection of the dipole moment of the system on the direction of the electric vector of the light wave) to an atom leads with $l = 1$, to the familiar theorem on the sum of the oscillator strengths[1], while with $l = 2$, 3 and 4 it leads to the sum rules established by Vinti[2]. Rejecting the dipole approximation ($\hat{P} = \sum_p \exp(i\mathbf{k}\mathbf{r}_p) \frac{\partial}{\partial x_p}$, where k is the wave vector of the photon and $\mathbf{r}_p$ is the radius vector of the p-th electron), we obtain formulas generalizing the above mentioned familiar results.

In considering a molecule or luminescence center in a crystal, we introduce the adiabatic approximation. Then Eq.(1) for an electronic-vibrational transition from state n to state n' becomes

$$S_l = \sum_{p=0}^{l} (-1)^p \binom{l}{p} \int \varphi_{n\alpha}^* M_{n'n}^*(\mathbf{R}) \hat{H}_{n'}^{l-p} M_{n'n}(\mathbf{R}) \hat{H}_n^p \varphi_{n\alpha} d\mathbf{R}; \qquad (2)$$

here $\varphi_{n\alpha}$ is the vibrational wave function number α in the electronic state n, $M_{n'n}(\mathbf{R})$ is the electronic matrix element of the $n \to n'$ transition, which depends on the nuclear coordinates R, $\hat{H}_n$ and $\hat{H}_{n'}$ are the Hamiltonians describing the vibrations of the nuclei in states n and n', respectively.

After averaging (2) over vibrational states α of the initial electronic state, we obtain (for $n \neq n'$) a formula agreeing with the result of Lax[3].

By means of this formula, which is fundamental to description of the contours of electronic-vibrational bands by the method of moments, in collaboration with Purga & Khizhnyakov[4], we carried out a number of calculations for different models of the vibrating system: a luminescence center in a crystal or molecule. Choice of the model is tantamount to specifying the adiabatic potentials and the vibrating masses in both electronic states of the system.

There were calculated (in the Condon approximation, and also for linear and exponential dependences of the electronic matrix element on the nuclear coordinates) the first four moments of the spectral bands of the system, the vibrations of which in the initial electronic state are described by quasi-independent normal vibrations. Subsequently, using the method of effective curvature[5], we also took into consideration the anharmonicity of the vibrations in the final electronic state. The calculations reduced to transformation of expression (2) to an integral containing the quantum mechanical coordinate distribution function. As a result there were obtained simple integrals of the Poisson type.

The deduced quantum mechanical formulas for the moments enabled us to carry out a detailed comparison of the many-coordinate and quansimolecular models.

For one oscillator there was also carried out a calculation taking into account the anharmonicity of the vibrations in the initial state. In this case the

problem was solved by the method of moments in the energy representation.[4]

We carried out a general investigation of the effect of hydrostatic pressure on the spectrum bands of crystal phosphors.[6]

Detailed comparison of the theoretical results with experiment requires substantial increase in the accuracy of experimental determination of band contours. Quantum mechanical and certain other effects are evinced the more clearly, the lower the Stokes losses expressed in the terms of the number of vibrational quanta. Hence from the standpoint of detailed comparison with theory it is, apparently, promising to investigate rare earth activated alkali halide crystals of small atomic weight, i.e., systems of the NaCl:Eu type.[7]

References

1. W.Kuhn, Z.Phys., 33, 408 (1925); F.Reiche & W.Thomas, Ibid.34, 510 (1925); H.A.Bethe, Quantenmechanik der Ein und Zwei Elektronenproblem, Berlin, 1933; V. Fock, Z.Phys., 89, 744 (1934).

2. J.P.Vinti, Phys.Rev., 41, 432 (1932).

3. M.Lax, J.Chem.Phys., 20, 1752 (1952).

4. K.K.Rebane, A.P.Purga, O.I.Sil'd & V.V.Khizhnyakov, Trudy IFA AN ESSR (Proceedings, Inst.of Physics & Astronomy, Ac.of Sci.Estonian SSR), No.14 (1961).

5. K.K.Rebane & O.I.Sil'd, Inzh.-fiz.zhur. (Engineering-Physics Journal), 2, 60 (1959); Izv.AN SSSR, Ser.fiz., 24, 539 (1960) (Trans.Bulletin 24, 545); Trudy IFA, AN ESSR, No.12, 3 (1960).

6. K.K.Rebane, Optika i spektroskopiya, 9, 557 (1960). (Trans.Optics & Spectroscopy.)

7. A.Niilisk, Thesis, Tartu State University, 1960.

* * * * * * *

CONTRIBUTION TO THE THEORY OF LUMINESCENCE OF ACTIVATED PHOSPHORS

- A.M.Ratner & G.E.Zil'berman

Pekar & Krivoglaz[1-3] calculated the optical characteristics of impurity luminescence centers and the probability for thermal transitions on the assumption of conservation (invariance) of the elastic constants of the lattice incident to the electronic transition. In the case of strong coupling of the impurity atom electrons, this assumption is usually not fulfilled, as is evinced by deviation from the law of mirror symmetry.

In earlier contributions[4-7] the writers calculated the shape of the absorption and luminescence bands of impurity centers and the probability of thermal (nonradiative) transitions, taking into account change of the elastic constants of the lattice incident to the electron transition.

In the classical case ($kT \gg \hbar\omega_D$, where ω_D is the Debye frequency of the crystal), for calculating the optical characteristics there are introduced the variables q_i in terms of which the expressions for the potential energy of the lattice in the ground and excited electronic states are simultaneously brought to diagonal form:

$$U_0 = \frac{1}{2}\sum_{i=1}^{N} K_i q_i^2, \qquad U_s = E^{(0)} + \frac{1}{2}\sum_{i=1}^{N} K_i' (q_i - q_{0i})^2$$

(N is the number of degrees of freedom of the crystal lattice; the variables q_i are not its normal coordinates).

It can be shown that in the case of strong coupling (when incident to the electronic transition there is a change in the interaction only between the impurity atom and its nearest neighbors) only the first M variables q_{0i} are nonzero and

$$\delta_i = (K_i - K_i')/K_i,$$

where M is of the order of a few units.

The quantities K_α, K_α' and $q_{0\alpha}$ ($\alpha = 1,\ldots, M$) are determined directly by the interaction of the impurity atom with its nearest neighbors; the optical characteristics of the impurity luminescence centers and the probability for thermal transitions are expressed in terms of these quantities. Change of the elastic constants of the lattice incident to the electronic transition leads to disturbance of mirror symmetry and to deviation of the absorption and luminescence bands from the Gaussian shape. Change of the elastic constants incident to the transition has a very substantial effect on the thermal transition probability (the probability for thermal transitions from the excited state to the ground state increases greatly if for some α $K_\alpha' < K_\alpha$).

For calculation of the optical characteristics, when treating the ion motion from the quantum mechanical standpoint, it is essential to use normal lattice coordinates, which do not coincide for different electronic states for the impurity atom. However, in the quantum mechanical case the results are greatly simplified if they are expressed in terms of the variables K_α, K_α' and $q_{0\alpha}$ used in the classical case. It is found that at temperatures $kT > \frac{1}{5}\hbar\omega_D$ (usually of the order of 10-20°K), as in the classical case, the optical characteristics are expressed in terms of the elastic constants of interaction of the impurity atom with the nearest neighbors, and are not directly connected with the vibrational motion of the crystal lattice. In particular, local lattice vibrations do not affect the shape of the absorption and luminescence bands. At lower temperatures the law of dispersion of normal vibrations (corresponding to an ideal lattice) becomes significant.

References

1. S.I.Pekar, Zhur.eksp.i teor.fiz., 22, 641 (1952).
2. M.A.Krivoglaz & S.I.Pekar, Trudy In-t fiz.AN USSR (Proceedings of the Institute of Physics, Ukrainian SSR Ac.of Sci.), 4, 37 (1953).
3. M.A.Krivoglaz, Zhur.eksp.i teor.fiz., 25, 191 (1953).
4. A.M.Ratner & G.E.Zil'berman, Fiz.tverd.tela, 1, 1697 (1959). (Trans. Soviet Physics - Solid State.)
5. A.M.Ratner, Ibid., 1, 1707 (1959). (Trans.Ibid.)
6. A.M.Ratner & G.E.Zil'berman, Ibid., 3, 687 (1961). (Trans.Ibid.)
7. A.M.Ratner, Ibid., 3, 704 (1961). (Trans.Ibid.)

DISCUSSION

K.K.Rebane (regarding the report of Ratner & Zil'berman): The idea of Ratner and Zil'berman to consider displacements rather than local normal oscillations is correct; we used the same approach. Displacements of the nearest neighbors should occur in the case of centers of small radius, and this is sufficient for appear-

ance of a different half-width of the absorption and luminescence bands. Local vibrations cannot be involved. However, in considering not normal vibrations but displacements, the entire difficulty shifts to the statistical part of the problem. I did not quite understand how the averaging was carried out, when there were not introduced normal vibrations even in the classical case. In our work there are given in explicit form the formulas derived as a result of quantum mechanical calculations taking into account mixing of the normal vibrations, which may occur at all temperatures. It would be expedient to check on the basis of these formulas the deductions of the authors regarding the insignificant role of local vibrations. There must be cases when local vibrations play a substantial role.

* * * * * * *

LUMINESCENCE OF COPPER-ACTIVATED GLASSES

- G.O.Karapetyan

Copper is one of the most common activators of crystal phosphors[1-5] and is also extensively used for coloring glasses and enamels[6,7]. Precise interpretation of the behavior of copper in glass and crystals is hampered, however, by the fact that copper readily changes its valence and coordination state.

We investigated the properties of different glasses activated by copper, depending on the composition of the glass, the founding conditions, the copper concentration and exposure to ionizing radiation. Investigation of phosphate, borate and silicate glasses of simple composition showed that copper in all cases can be present in the atomic, monovalent and divalent states. With the aid of electron paramagnetic resonance we were able to relate the 800-880 mμ absorption band with the presence of copper in the divalent state. Transition of the copper under the influence of a reducing agent (carbon, ammonium fluoride, metallic tin, etc.) to the monovalent state leads to weakening or complete suppression of this band (Fig.1); at the same time the glass begins to luminesce under ultraviolet stimulation. Characteristic of monovalent copper in glasses is an absorption peak in the vicinity of 250 mμ, which appears when the divalent copper is reduced by carbon or ammonium fluoride. Further reduction brings the copper to the atomic state, which is evinced in the case of the investigated glasses by the appearance, as a result of repeat heating, of colloidal metallic copper particles, which color the glass red. The composition of the glass has a strong effect on the position of the Cu luminescence peak (Fig.2); this is probably connected with the appreciable enhancement of the interaction between this activator and the surrounding medium in going from phosphate glasses to borate and silicate glasses.

This interpretation is consistent with the results of our earlier investigations of glasses with cerium.[8,9] Increase in the concentration of the basic oxides in the glass, as well as increase of the copper concentration, favors transition of the copper to the divalent state. The luminescence spectrum also depends to an appreciable extent on the wavelength of the exciting radiation, which is, probably, connected not only with the Stokes cutoff, but in a number of cases, with the presence of a number of different types of luminescence centers.

In the case of reduction of the copper by metallic tin, there are observed in the luminescence spectrum two well resolved peaks, the location of which is only

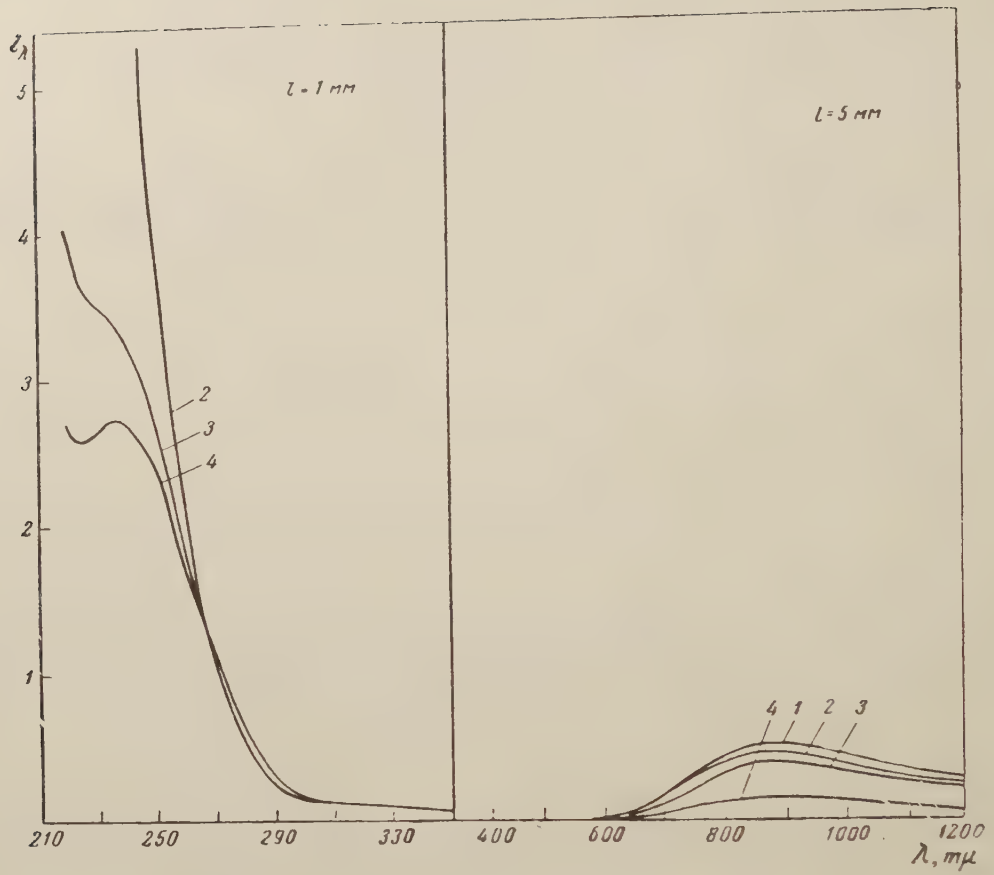

Fig.1. Changes in the spectral absorption of $Na_2O \cdot 1.5\ CaO \cdot 2.5\ P_2O_5$:0.1% Cu glass depending on the founding conditions: 1) neutral conditions, 2) 0.1% carbon, 3) 0.5% carbon, 4) 2% carbon.

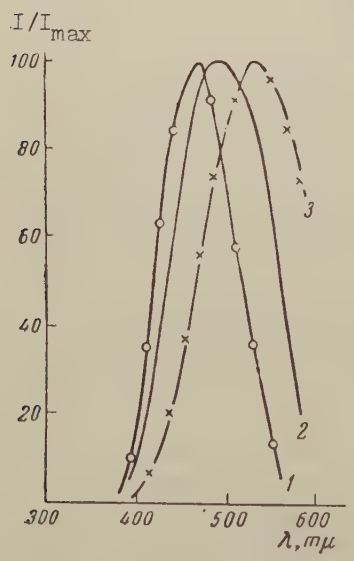

Fig.2

←Fig.2. Luminescence spectra of glasses: 1) $Na_2O \cdot 1.5\ CaO \cdot 2.5\ P_2O_5$:0.1% Cu (2% NH_4F), 2) $Na_2O \cdot CaO \cdot 2.5\ B_2O_3$:0.1% Cu (4% NH_4F), 3) $Na_2O \cdot CaO \cdot 5\ SiO_2$:0.1% Cu. λ_{excit} = 313 mμ.

weakly dependent on the position of the glass. Special experiments showed that the luminescence spectra of glasses with Sn but without Cu differ from the spectra of the glasses with Sn and Cu. Stimulation of phosphate glasses with Sn and Cu by 254 mμ photons leads to emission peaking at 440 mμ (blue luminescence), while stimulation in the 365 mμ region results in emission at 580 mμ (yellow luminescence). Such glasses can be used as indicators for radiation of the indicated frequencies. The luminescence efficiency depends greatly on the compo sition of the glass, the wavelength of the exciting radi tion and the Cu concentration; the maximum quantum effi ciency attains 50%.

In the case of excitation of silicate glasses with

copper by radiation of wavelength shorter than 250 mμ, there is observed both fluorescence and persistent phosphorescence.

Glasses with copper luminesce intensely not only under UV excitation but also under excitation by ionizing radiation.

In special experiments we established the possibility of obtaining glass screens with a 100-200 mμ thick luminescing layer by the diffusion procedure.

References

1. P.Pringsheim, Fluorescence & Phosphorescence, N.Y., 1949.
2. V.L.Levshin, Fotolyuminestsentsiya tverdykh i zhidkikh tel (Photoluminescence of solids and liquids), M., 1951.
3. T.I.Veinberg, Trudy (Proceedings of the) Session Held in Memory of S.I. Vavilov, p.134, M., 1953.
4. T.I.Veinberg, Izv.AN SSSR, Ser.fiz., 13, 203 (1949).
5. E.W.Claffu & H.J.Schulman, J.Electrochem.Soc., 98, 403 (1951).
6. V.V.Vargin, Proizvodstvo tsvetnogo stekla (Production of colored glass), M.-L., 1940.
7. W.Weyl, Coloured Glasses. Sheffield, 1951.
8. W.W.Wargin & G.O.Karapetjan, Glasstechn.Ber., 32, 443 (1959).
9. G.O.Karapetyan, Trudy III Vsesoyuznogo soveshchaniya po stekloobraznomu sostoyaniyu (Transactions of the 3rd All-Union Conference on the Vitreous State), M.-L., 1960.

DISCUSSION

I.B.Keirim-Markus: The data on thermal luminescence reported by Karapetyan overlaps to some extent with the results of our investigations. I am pleased to note that we agree as regards the inferences that the trapping centers are connected with the base material, that the emission of Cu is due to monovalent copper and that a reducing medium is necessary to create favorable conditions for luminescence. According to our data, the luminescence spectrum depends not only on the type of glass (silicate or phosphate) but also on its particular composition. Glasses with monovalent ions (K, Na) luminesce in the blue region, while those with divalent ions (Ca, Sr, Mg, Zn, etc.) luminesce in the red. Apparently, this is connected with the fact that the Cu^+ ion neighbors on these ions. We also note the fact that introduction of Cu results in quenching of the intrinsic luminescence of the glass, which is usually evinced at higher temperatures.

* * * * * * *

INVESTIGATION OF PHOTOLUMINESCENCE AND SCINTILLATION OF SILICATE GLASSES

- S.M.Brekhovskikh & N.F.Shapovalova

The purpose of the present work was to develop formulations for glasses exhibiting a strong enough scintillation effect to justify their use as γ-ray detectors.

We chose cerium as the activator, inasmuch as this element in silicate glasses gives rise to only blue luminescence, lying in the region of the maximum response of most commercial photomultipliers.

To investigate the influence on the luminescence yield of elements of Group I, we synthesized two-component silicate glasses with lithium and sodium.

In comparing the luminescence of these glasses under UV stimulation it was

Chemical composition of glasses SZ-56 and Z-56-8

Glass	Oxide content, % wt.				In excess of 100%	
	Li_2O	SiO_2	BaO	Al_2O_3	CeO_2	NH_4F
				In excess of 100%		
SZ-56	6,43	77,14	16,43	3	0,8	2,0
Z-56-8	9,68	64,81	18,21	7,29	0,8	2,0

found that in the case of lithium the luminescence yield is six times higher and is shifted to the side of shorter wavelengths. Thus in the case of glass with 14% Li_2O the luminescence peak at 410 mμ has an intensity of 133 (arbitrary units), while in the case of glass with 14% Na_2O the peak located at 440 mμ has an intensity of 21.3. The luminescence properties of sodium-silicate glasses changed little with introduction of a third component. The scintillation effect under bombardment by Cm α-particles proved to be so low in the case of glasses with sodium that it was undistinguishable from the noise of the photomultiplier. The high luminescence yield of lithium-silicate glasses remained virtually unaltered as a result of introduction of Mg, Ca or Ba oxide as the third component. The scintillation intensity of these glasses under α-particle stimulation amounted to 1.5-3% relative to the scintillation of our reference NaI(Tl) crystal.

Inasmuch as it is known that glasses to be sensitive to γ-radiation must contain appreciable amounts of heavy elements oxides, we decided to test glasses containing large quantities of barium oxide. We synthesized glasses containing 50% and more BaO. It was found, however, that these glasses were decidedly basic, and it was impossible to reduce the cerium present in them to the luminescing trivalent state even by means of so strong a reducing agent as antimony trioxide. These glasses were yellowish in color with very low transmission in the region of luminescence of Ce^{3+}. As a result of absorption of the cerium luminescence inside the glass, the emerging light was very weak and its spectrum was shifted into the long wavelength region. Thus we were unable to obtain a good luminescence and scintillation yield for heavily barium loaded glasses.

The glasses designated SZ-56 and Z-56-8 (see table) proved to have good luminescence properties and to be suitable for use as γ-radiation detectors. The technical scintillation efficiency of these glasses under excitation by scattered γ-rays from a Co^{60} source equaled 2% relative to the yield of our NaI(Tl) crystal; the efficiency for Cm α-particles, referred to the same crystal, was 3%.

Conclusions

The presence of lithium in glasses has a positive effect on the luminescence yield.

Equivalent replacement of one oxide by another in the basic composition of the glass has a relatively weak effect on the luminescence spectrum and intensity. However, Sb, Ge, As, Ta and Tl sharply reduce the luminescence yield in the investigated glasses, while Cd, Bi, Pb and Ti quench the luminescence completely.

The acidity of the glass has a decisive influence on the luminescence efficiency. With decreasing acidity the luminescence yield decreases, and the peak in the luminescence curve shifts into the long wavelength region (from 390 mμ to 470 mμ).

The luminescence spectrum is intimately related with the transmission spectrum: in the case of all glasses tested the luminescence peak coincides with the transmission peak.

Some of the synthesized glasses can be used as detectors of γ-radiation in scintillation counters.

State Scientific-Research Institute of Glass
under the RSFSR State Planning Committee

LUMINESCENCE OF CRYSTALS SURFACE-ACTIVATED WITH URANYL IONS

- G. I. Kobyshev

As is known, the luminescence of compounds containing uranyl ions is comprised of the emission of discrete centers. However, a number of authors[1-4] have reported cases in which the uranyl ion plays the role of a luminescence activator, forming "crystal phosphor type" luminescence centers.

We undertook an investigation of the luminescence spectrum of the uranyl cation coordinately linked with water molecules when applied to the surface of a crystal (for example, magnesium oxide). In contrast to the case of ordinary crystal phosphors, in this case the activator is on the surface or in the surface layer and hence subject to external influences. We have investigated the luminescence of the uranyl cation on the surface of both inorganic polymers[5], devoid of crystalline structure, and on crystalline solids.

Below we give the results obtained in the experiments with magnesium oxide. The magnesium oxide powder (or gel) was roasted at 600-700°C for 5-6 hours. The activator was introduced in the form of a solution (10^{-3} mole per liter) of an appropriate uranyl salt (tests showed that the nature of the anion is unimportant). Next the specimens were aged at a pressure of 10^{-5} mm Hg with simultaneous heating to 170-200°C, which assured elimination of capillary-condensed, adsorbed and coordination bound water.

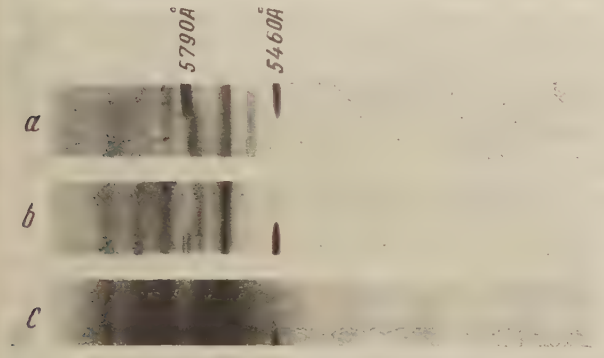

Luminescence spectra: a - two-dimensional uranyl nitrate crystal on magnesium oxide at 290°K; b - same but at 77°K; c - same plus uranyl ion coordinately bound with water in the state of adsorption on the magnesium oxide at 77°K.

In vacuum at low temperature (77°K) there is observed the spectrum reproduced in Fig.b. It must be noted that in the 16 000 to 18 000 cm^{-1} region there is observed weak luminescence with a continuous spectrum which belongs to the uranyl cation that has lost its coordination bound water. In addition to the continuous spectrum, in the same region there is observed only on the surface of crystalline solids a quasiline spectrum which is substantially different from the spectrum of uranyl salt crystals and is due to the luminescence of crystalline formations on the surface of the magnesium oxide. Introduction of the activator does not require heat treatment of the phosphor, which is indicative of the surface nature of the crystal formations. The "lines" in the quasiline spectrum are described by the series formula

$$\nu = 17\ 650 - 700\ \nu_1 + 370\ \nu_2.$$

Admission of vapor or gas (H_2O, NH_3) into the vacuum chamber does not produce any significant changes in this spectrum, whereas the continuous spectrum is transformed into a band spectrum with a frequency interval of about 770 cm^{-1} in the 17 000 to 21 000 cm^{-1} region (Fig.c). The changes produced by the gases are completely reversible: upon evacuation of the gas the band spectrum disappears, and reappears when the gas is readmitted. Earlier in a similar case, we showed that these changes are due to the formation on the surface of a complex compound involving coordinate linkage of the uranyl cation with electron donor molecules of the admitted gas.[5]

As is known, discrete structure in the luminescence spectra of uranyl compounds is in general observed only at low temperatures. Here we must call attention to the surprising fact that the discrete structure in the quasiline spectrum with sharply pronounced vibrational structure persists with increasing temperature up to room temperature (Fig.a). Increase of the temperature leads to decrease in the intensity of the luminescence, redistribution in the relative intensity of the "lines" and the appearance of another shorter wavelength component. The presence in the quasiline spectrum of pronounced vibrational structure at 20°C and the absence of deformation frequencies may be taken as evidence of weak interaction of the excited electronic state with the vibrational energy of the lattice. In our opinion, this effect can be explained by the formation of two dimensional crystals on the surface, crystals that complement the structure of the magnesium oxide crystal.

We established earlier that enhancement of the electron donor properties of the addends in uranyl complexes results in decrease of the frequency of the fully symmetrical valence vibrations of the uranyl oxygens from 880 cm^{-1} (NO_2) to 700 cm^{-1} (pyridine), i.e., reduction of the frequency by approximately 20%. Consequently, in the given case, when there is observed the same low frequency, it may be assumed that the oxygen ions in the magnesium oxide lattice have a high electron donor ability. In the investigated two dimensional crystal there occurs an appreciable equalization of the U—O bonds (uranyl and coordination), which in all probability should be explained by rupture of the double bonds and formation of sesqui-linkages.

Thus, on the one hand, the uranyl cation plays the role of an activator of the luminescence of magnesium oxide, and, on the other hand, only as a result of coordination of the uranyl ion with the oxygens of the host is there observed the luminescence characteristics for the coordinated state of uranyl. In this case the luminescence of the uranyl ion may be regarded as intermediate in origin between the luminescence of a crystal phosphor and luminescence of the molecular type.

In conclusion, we note that as regards structure the investigated quasiline spectrum is similar to the luminescence spectra of the uranyl cation introduced into calcium oxide[3] and sodium fluoride[2]. All these crystals have approximately equal lattice constants (4.5 Å), which indicates the necessity of geometric correspondence between the host crystal and the activator.

I desire to express my deep gratitude to A.N.Terenin for useful advice and suggestions in connection with the work.

References

1. P.P.Feofilov, Materialy V Soveshchaniya po lyuminestsentsii (Transactions of the Fifth Conference on Luminescence), p.3, Tartu, 1957.

2. W.A.Runciman, J.Phys.Chem., 17, 645 (1956); Proc.Roy.Soc., 237, 39 (1956) Brit.J.Appl.Phys.Suppl., 4, 78 (1955).

3. J.Ewles & N.Lee, J.Electrochem.Soc., 100, 392 (1953).

4. E.L.Nichols & M.K.Slattery, J.Opt.Soc.Am., 12, 449 (1926).

5. G.I.Kobyshev, Doklady AN SSSR, 127, 373 (1959). (Trans.Doklady.)

LUMINESCENCE OF LiF CRYSTALS ACTIVATED BY URANYL NITRATE

- E.P.Alekseeva

We investigated the absorption and luminescence spectra and the glow curves of LiF crystals activated by uranium salts. The crystals were excited by x-rays from a tungsten anode tube with beryllium windows, operated at 50 kv and 20 ma.

The absorption spectra were studied on an SF-4 spectrophotometer. Activator absorption bands were observed with peaks at $\lambda_1 = 2500$ Å and $\lambda_2 < 2100$ Å. With increase of the activator concentration the 2500 Å peak shifts to the side of longer wavelengths (to 2600 Å) and there appears a new band peaking at $\lambda_3 = 3150$ Å. The last band was observed by Belyaev et al[1] in investigating the absorption spectra of LiF doped with uranyl salts.

The fluorescence spectra of activated LiF were recorded in an ISP-53 spectrograph with an FEP-1 recorder. The phosphor was excited by the light from a PRK-2 mercury tube through a UFS-2 filter. The fluorescence spectra at room temperature comprises a series of individual bands in the green region; the most distinct bands peak at 5210, 5240, 5290, 5330, 5360, 5380 and 5420 Å. With variation of the activator concentration the general shape of the spectrum remains the same but the relative intensities of the individual bands vary. Comparing the results obtained for the activated lithium fluoride crystals with the luminescence spectra of CaF_2:U^{6+} reported by Feofilov[2], we note that the characteristic wavelengths in both spectra coincide fairly well. This gives grounds for interpreting the luminescence of phosphors activated by uranyl salts as the emission of the uranium ion, transformed by the crystal lattice. The luminescence center model proposed by Feofilov[3] presupposes isomorphous replacement of the Li^+ ion by a hexavalent uranium ion, U^{6+}, with the excess positive charge being compensated by isomorphous replacement of five of the six neighboring F^- ions by O^{2-} ions.

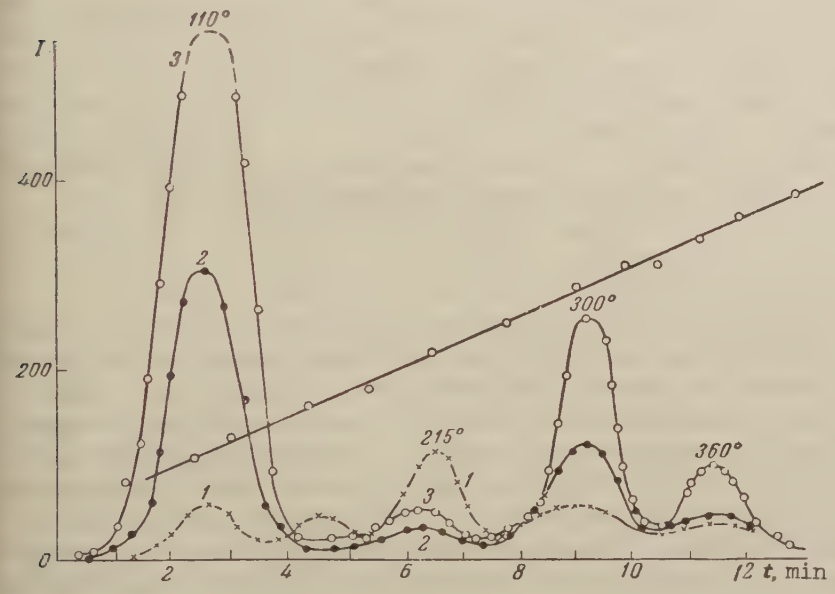

Glow curves for pure and doped LiF crystals: 1) 0.2% $UO_2(NO_3)_2$, 2) 0.01% $UO_2(NO_3)_2$, 3) undoped LiF.

It is known that under the influence of ionizing radiation there appear in pure LiF crystals[4,5] F, M, R, F' and N bands. Excitation of LiF phosphors with uranyl impurity with x-rays leads to the formation of the same color centers. If the activator concentration is sufficiently high (~0.2%), there appears a new absorption band centered at 5700 Å, which colors the crystal violet. This band is stable and persists for several months when the crystals are stored at room temperature. A similar faint color may be observed in crystals with a low impurity concentration subjected to x-irradiation and subsequent heating. The band peaking at 5700 Å is undoubtedly connected with the introduction of the activator, inasmuch as it does not form in pure crystals even after heavy doses of x-irradiation.

During excitation of the phosphors some of the energy is stored by electrons captured in traps. This energy can then be released in the form of "thermolumi-

nescence". The spectral composition of the "thermoluminescence" of pure LiF crystals[5-7] differs from the emission characteristic of the activator. We investigated the thermostimulated luminescence of pure and activated crystals. The activator luminescence was separated by means of a special light filter. The results are shown in the accompanying figure from which it will be evident that the glow curve 3 characteristic of nonactivated LiF crystals has a number of peaks corresponding to temperatures of 110, 163, 215, 300 and 360° (heating rate $\beta = 0.7$ degree per sec). Introduction of uranyl nitrate impurity does not result in the appearance of new glow curve peaks (curves 1 & 2), but only changes the relative height of the peaks. Introduction of the activator significantly increases the peak at 110° and quenches the peaks in the 160-200° region. With increase of the uranyl impurity concentration from 0.01 to 0.2% the height of the peak at 110° increases more than the height of the other high temperature peaks. For samples that are already colored violet repeat excitation yields the same distribution of electrons over trapping levels. Consequently, activation of the crystals results in the change of the relative height of the glow curve peaks but does not lead to the appearance of new peaks. This gives reason to infer that the light sums here, as in other alkali halide crystals[8], are stored in traps of the host material.

Irkutsk University

References

1. L.M.Belyaev, G.F.Dobrzhanskii, V.V.Chadaeva, V.P.Panova, Z.B.Perekalina & V.N.Varfolomeeva, Kristallografiya, 4, 795 (1959). (Trans.Crystallography.)
2. P.P.Feofilov, Materialy V Soveshchaniya po lyuminestsentsii (Transactions of the Fifth Conference on Luminescence), Tartu, 1957.
3. P.P.Feofilov, Optika i spektroskopiya, 7, 842 (1959). (Trans.Optics & Spectroscopy.)
4. C.Delbeck & P.Pringsheim, J.Chem.Phys., 21, 5 (1953).
5. E.Morehead & F.Daniels, Ibid., 27, 6 (1957).
6. J.Sharma, Phys.Rev., 78, 3, 535 (1952).
7. D.F.Saunders, F.Morehead & F.Daniels, J.Amer.Chem.Soc., 75, 3096 (1953).
8. I.A.Parfianovich, Izv.AN SSSR, Ser.fiz., 15, 670 (1951).

DISCUSSION

Z.B.Perekalina: In the Institute of Crystallography there were grown luminescent LiF crystals activated by uranyl salts. The crystals were grown by the Kyropoulos technique in air. The crystals grown in vacuum did not luminesce. This indicates that for the formation of luminescence centers in activated LiF a necessary condition is the presence of hexavalent uranium ions. We investigated the luminescence and absorption spectra of LiF:U crystals as a function of the uranium concentration. In the concentration range from 0.1 to 0.2 percent by weight in the melt there occurs a redistribution in intensity among the luminescence bands: the initial blue-green luminescence becomes yellow-green. At the same time there occur changes in the absorption spectrum: the absorption bands are shifted to the long wavelength side. The results of this investigation were reported at the Conference on the Physics of Alkali Halide Crystals held in Tartu, July 1959.

INFLUENCE OF INFRARED LIGHT ON THE LUMINESCENCE OF SILVER CHLORIDE

- V.M.Belous & N.G.D'yachenko

We investigated the effect of infrared light (isolated by KS-19 and IKS-3 filters) on the blue luminescence of fused AgCl layers. The luminescence was excited by the 366 mμ line of mercury with the specimens cooled to liquid air temperature. The blue luminescence was separated by an SZS-18 filter and detected by an FEU-19 photomultiplier which was connected to an ENO-1 oscillograph.

It was found that under steady UV excitation switching on infrared (IR) leads to flash stimulation and then to quenching of the luminescence. Switching off the IR is followed by a brief decrease in brightness (negative "flash") and then slow growth of the luminescence to the steady state value. An oscillogram characterizing these processes is shown in the accompanying figure. If the excitation of the phosphor is stopped and then sometime later the IR is switched on there is observed a flash of blue luminescence of ~10^{-1} sec duration. Repeat switching on of the IR does not lead to this effect if the intensity of this radiation exceeds a certain limiting value. (In determining the limiting intensity one must bear in mind the duration of the exposure to IR; in the described experiments the exposure was 2 sec.)

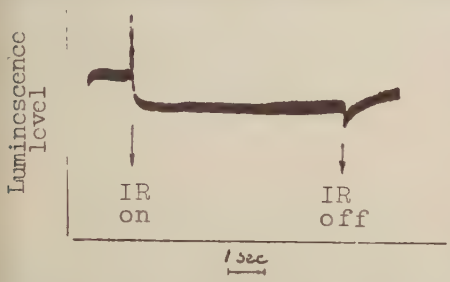

Oscillogram of blue luminescence of AgCl as IR light is switched on and off.

On the basis of these first results one can draw the following conclusion. In AgCl phosphor under the influence of exciting ultraviolet light part of the electrons recombine with subsequent radiation, while part are captured on sticking levels (in traps). When the infrared light is switched on, the release of the electrons from the traps presumably leads to the flash of blue luminescence. If the intensity of the IR is sufficient to empty the traps completely, the magnitude or strength of the flash will to a certain degree be a measure of the number of electrons stored on the sticking levels (held in the traps).

The variation of the flash strength as a function of the dark time (the period between switching off the exciting UV and switching on the IR) is hyperbolic (the intensity of the IR in these experiments always exceeded the limiting value).

We also investigated the variation of the flash strength with the intensity of the exciting light. It was found that in the range of low UV intensities the flash strength during the time of excitation and for a 10 second dark period increases linearly with the intensity of the exciting light; in the range of higher intensities the flash strength decreases. The linear decrease of the flash strength with increase of the UV intensity can, in our opinion, be explained by the de-exciting action of the exciting light.[1]

In the course of determining the variation of the flash strength during the time of excitation as a function of the IR intensity it was found that within the range of intensities employed in our experiments the flash strength depends linearly on the IR intensity.

It is interesting to note that in the case of heat treated silver chloride specimens we observed green luminescence which can be quenched by IR light but without an initial flash.

The orange luminescence of fused AgBr layers is also quenched by IR (IKS-3 filter), but no initial flash is observed upon switching on the IR. Upon switching off the IR, the brightness of the orange band of AgBr rises much more rapidly than the intensity of the blue band of AgCl.

These results not only substantiate the inference[2] that different centers are responsible for the blue and green bands of AgCl but also give reason to infer that the luminescence mechanism involved in emission of the blue band of AgCl differs from the mechanism giving rise to the green band of AgCl and the orange band of AgBr.

We thank T.Ya.Sëra and S.I.Golub for their interest in the work.

Institute of Physics,
Odessa State University

References

1. V.V.Antonov-Romanovskii, Izv.AN SSSR, Ser.fiz., 13, 91 (1949).
2. S.I.Golub & N.O.Orlovs'ka, Pratsi ODU (Proceedings, Odessa State University), 148, 29 (1958).

LUMINESCENCE OF URANIUM ACTIVATED SODIUM AND LITHIUM FLUORIDE SINGLE CRYSTALS

- L.M.Belyaev, G.F.Dobrzhanskii & P.P.Feofilov

The exceptionally bright luminescence of lithium and sodium fluorides activated by uranium has attracted the attention of many investigators. One of the reasons for this is the importance of sodium fluoride beads in luminescence analysis for uranium. All the investigations[1-3] published to date, beginning with the work of Nichols & Slattery[1], have been performed on either beads or powdered phosphors.

Recently there were prepared LiF:U and NaF:U phosphors in the form of comparatively large single crystals.[4] Although the investigation of such basic characteristics as the spectra and kinetics of luminescence can be carried out equally well on powders and polycrystalline beads, investigation of single crystals opens new possibilities particularly where utilization of polarization methods is concerned.

Below we give some data on the luminescence properties of lithium fluoride and sodium fluoride single crystals activated by uranium.

1. Specimens

Lithium and sodium fluoride in crystallizing form a cubic lattice of the rock salt type. The investigated single crystals were grown from melts by the Kyropoulos technique. The activator was introduced into the initial batch, as a rule, in the form of uranyl nitrate. Introduction of the activator in the form of other salts (sulfate or acetate) led, in general, to the same results, which is apparently connected with complete decomposition of all these salts to the oxide (U_3O_8) at temperatures lower than the melting point of the crystals (870° for LiF and 980° for NaF). The activator concentration was varied from 0.01 to 0.3%.

2. Absorption Spectra of LiF:U and NaF:U Single Crystals

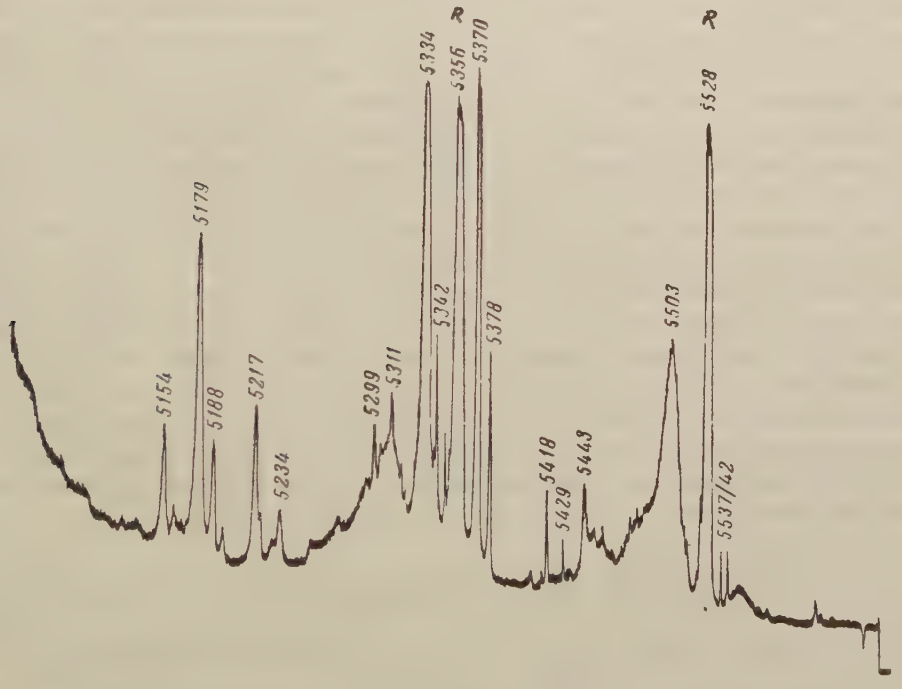

Fig.1. Absorption spectrum of NaF:U at -196° (0.3% $UO_2(NO_3)_2$).

At room temperature the absorption spectra of the investigated single crystals consist of weak bands with clearly discernible structure in the visible region of the spectrum and strong absorption with several diffused peaks in the ultraviolet region. For LiF:U crystals the absorption peaks are located at about 520, 505, 405(?) and 310 mμ; for NaF:U at about 555, 535, 430, 365 and 275 mμ. The last two bands are close in wavelength to the bands recently observed by Le Roux[3] in the spectrum of NaF beads containing uranium.

Upon cooling of the crystals to liquid nitrogen temperature the long wavelength absorption bands split up into an excpetionally large number of very narrow lines (Fig.1).

3. Luminescence Spectra of LiF:U and NaF:U Single Crystals

The luminescence of LiF:U and NaF:U single crystals can be excited either in the region of the long wavelength absorption bands or in the ultraviolet region. Structure in the luminescence spectra is clearly evinced even at room temperature. Upon deep cooling the luminescence spectra become extremely rich in detail: there appear numerous lines, the width of which frequently does not exceed a fraction of an angstrom.

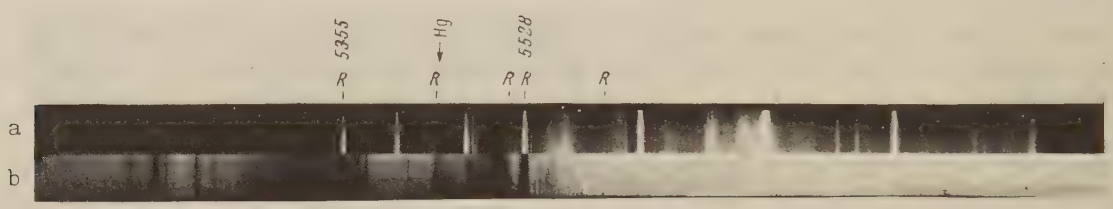

Fig.2. Absorption (a) and luminescence (b) spectra of NaF:U single crystal at -196

Many of the discrete lines are observed both in the absorption spectrum and in the luminescence spectrum (Fig.2), i.e., may be identified as resonance lines (they are identified by the letter R in Fig.2). The presence of a large number of resonance lines, distributed in a rather wide spectral range (about 1800 cm^{-1} for LiF:U and about 800 cm^{-1} for NaF:U), is evidence of the complex structure of the sublevels of the excited state and of the relatively weak interaction of these sublevels, interaction that hinders the attainment of thermal equilibrium within a time of the order of 10^{-4} sec (the lifetime of the excited states of these phosphors). Further evidence of this is the possibility of selective excitation of individual line groups. Thus, for example, in excitation of NaF:U crystals by the 546 mμ line of Hg there is observed bright luminescence, the spectrum of which is distinguished by the absence of not only the shorter wavelength lines (Stokes cut-off) but also of individual lines located in the Stokes region.

The only regularity that can be definitely established at present in the low temperature luminescence spectra of LiF:U and NaF:U is the presence of equally spaced line series into which one can group the principal brightest lines that are always observed in the spectra. We succeeded in distinguishing two series in the spectra of each of the uranium activated fluorides:

$$\left.\begin{aligned} \nu_{ek}\,(cm^{-1}) &= 19\,286 - 800\,k \\ \nu_{mk}\,(cm^{-1}) &= 18\,947 - 800\,k \end{aligned}\right\} \text{for LiF:U } (k = 0, 1, 2)^*$$

*The meaning of the subscripts e and m will be made clear below.

and

$$\left.\begin{aligned}\nu_{ek}\ (\mathrm{cm}^{-1}) &= 18\ 093 - 708\ k\\ \nu_{mk}\ (\mathrm{cm}^{-1}) &= 17\ 743 - 708\ k\end{aligned}\right\}\ \text{for NaF:U } (k = 0, 1, 2, 3).$$

There can also be tentatively identified in the luminescence spectra of LiF:U and NaF:U other sequences with $\Delta\nu$ equal to 800 and 708 cm^{-1}, respectively; these comprise weaker lines as well as lines observed only in the spectra of individual specimens.

4. Polarization of the Luminescence of LiF:U and NaF:U Single Crystals

The luminescence of LiF:U and NaF:U single crystals excited by linearly polarized light is in general partially polarized; the degree of polarization is clearly dependent on the relative orientation of the crystallographic axes and the electric vector of the exciting light (azimuthal dependence), on the wavelength of the exciting light (polarization spectrum) and on the wavelength in the luminescence spectrum.

A. Azimuthal dependence and luminescence center model*

Investigation of the azimuthal dependence of the polarized luminescence makes it possible, as was shown earlier[8], to establish uniquely the character of the orientation of the anisotropic luminescence centers in cubic crystals. Application of this method of investigation enabled us[6-8] to propose a model for the structure of the luminescence centers.

Utilizing the previously proposed scheme[6], we carried out an investigation of the azimuthal dependence of the polarization of the luminescence of plates cleaved from crystals parallel to the (100) planes. Inasmuch as the purpose of the present stage of the study was to establish the character of the orientation of the centers, we carried out our observations in undispersed light, neglecting the rather pronounced dependence of the degree of polarization on the wavelength in the emission spectrum. The results of measurements carried out at room temperature are shown in Fig.3.

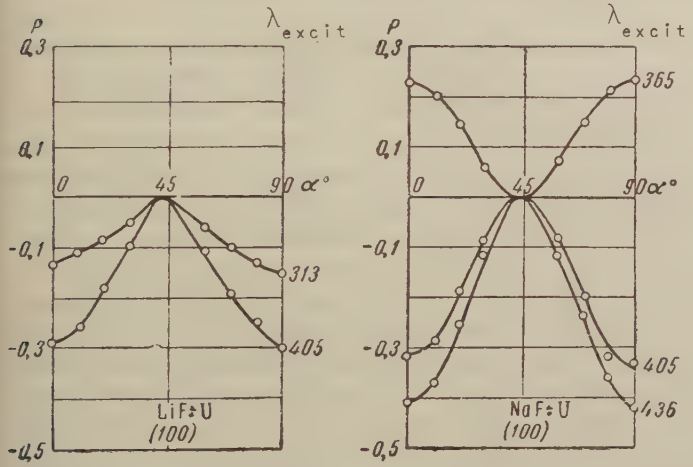

Fig.3. Azimuthal dependence of the polarization of the luminescence of LiF:U and NaF:U at room temperature.

Comparison of the experimental azimuthal dependences (Fig.3) with the calculated dependences[6] clearly indicates that the luminescence centers in MF:U crystals are definitely oriented along a fourth order symmetry axis.

In view of this fact and on the basis of the principle of local charge compensation one can propose a model for the luminescence centers in the investigated crystals. In constructing the model one should also bear in mind the hexavalent state of the uranium atoms and the presence of oxygen as a necessary condition for the appearance of luminescence of hexavalent uranium in these crystals. The last condition was noted earlier by one of us[9] for CaF_2:U by

---

*The preliminary results of this investigation for LiF:U were published in Ref.5.

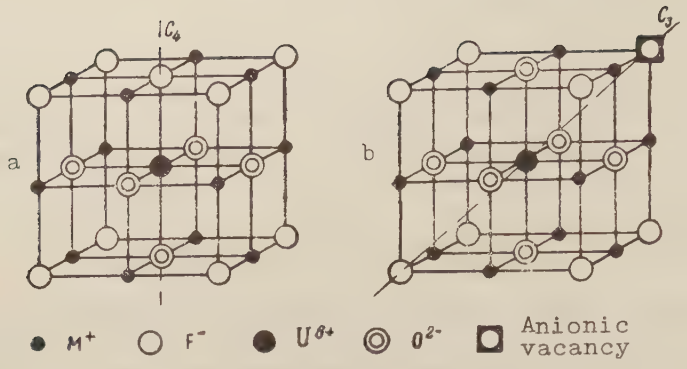

Fig.4. Model of luminescence centers in Mf:U: a - according to Feofilov, b - according to Runciman.

Runciman[2] and Le Roux[3] for NaF:U and Shapiro[10] for a number of uranium activated alkali halides.

The proposed model[5] is shown in Fig.4,a. The U^{6+} ion isomorphously replaces a monovalent alkali metal cation. The resultant excess positive charge (5+) is compensated by isomorphous replacement of five of the six F^- ions surrounding the U^{6+} ion by O^{2-} ions. It can readily be shown that the resulting luminescence center will be an anisotropic formation with a distinctive direction oriented along one of the C_4 axes. This amorphous replacement of F^- by O^{2-} can readily be realized owing to the fact that the radii of these ions are nearly equal.

It should be noted that Runciman[2] proposed a different model for the luminescence centers in NaF:U (Fig.4,b). It can easily be shown, however, that this model in which all six F^- ions surrounding the activator ion are replaced by oxygen and the compensation of charges is realized by an anionic vacancy in the second coordination sphere is not consistent with our polarization data. Runciman's model implies a distinctive direction aligned with a third order axis (C_3). Yet the azimuthal dependences of the polarization of luminescence unambiguously indicate that the luminescence centers in MF:U crystals are oriented along a fourth order symmetry axis.

This example once more demonstrates the importance of the results of polarization measurements as a criterion in judging the validity of any proposed model for luminescence centers.

B. Variation of the polarization over the luminescence spectrum

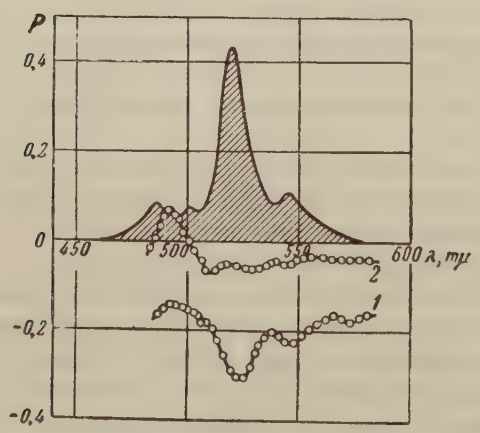

Fig.5. Variation of the degree of polarization with the wavelength in the luminescence spectrum of LiF:U with λ_{excit} = 405 mμ (1) and 365 mμ (2).

As noted above, the degree of polarization in the spectra of LiF:U and NaF:U varies with the wavelength in the luminescence spectrum. This wavelength dependence is not surprising if one recalls the complex character of the luminescence bands, evinced even at room temperature. Some of the curves characterizing the variation of P with λ_{lum} for different specimens excited by light of different wavelengths are reproduced in Figs.5 & 6.* The characteristic but still imperfectly understood shape of these curves can hardly be the subject of serious discussion at present, inasmuch as it represents a highly complex pattern forming as the result of superposition of a number of elementary radiations that are clearly evinced in investigating deep cooled crystals.

---

*The curves were obtained on the polarization set-up of P.I.Kudryashov, whom we take this opportunity to thank.

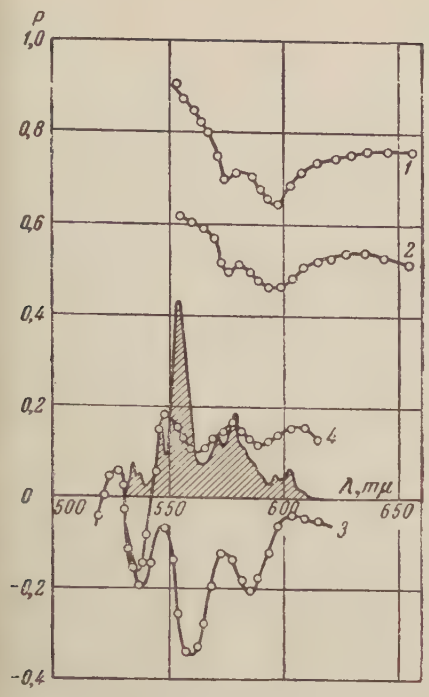

←Fig.6. Variation of the degree of polarization with the wavelength in the luminescence spectrum of NaF:U. $UO_2(NO_3)_2$ concentration: 1, 3 & 4) 0.1%, 2) 0.3%; λ_{excit}: 1 & 2 - 546 mμ, 3 - 436 mμ, 4 - 365 mμ.

C. Polarization luminescence spectra

The fact that the degree of polarization varies with the luminescence wavelength precludes speaking of the polarization spectrum of MF:U crystals in the sense employed in investigating complex molecules. Strictly speaking, one must deal separately with the polarization spectrum associated with each individual spectrum line or at least each narrow spectral interval. Nevertheless, we deemed it worthwhile to carry out measurements of the variation in the degree of polarization of the luminescence as a function of the exciting wavelength, observing the luminescence in a sufficiently wide spectral range. Such "averaged" (over the luminescence spectrum) polarization spectra, measured at room temperature, are shown in Fig.7.

It is interesting to note that as regards their general character these polarization spectra are highly reminiscent of the polarization spectra of most organic dyes.

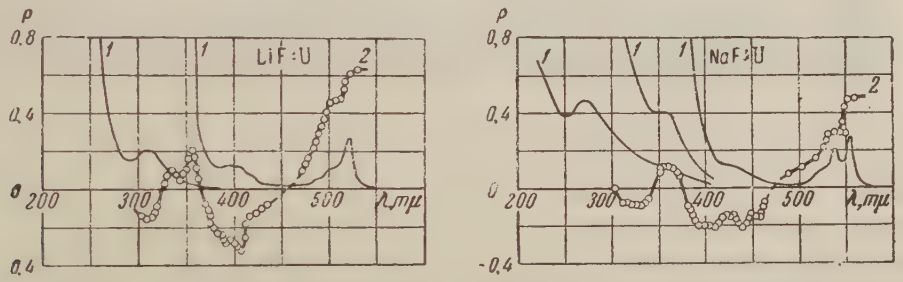

Fig.7. Absorption (1) and polarization of luminescence (2) spectra of MF:U single crystals at room temperature.

5. Polarization in the Low Temperature Luminescence Spectra and the Nature of the Elementary Radiators of the Uranium Ion*

As noted above, the luminescence spectra of LiF:U and NaF:U single crystals cooled to liquid air temperature comprise a large number of extremely narrow lines. Polarization studies show that under certain conditions of excitation and observation the polarization of the radiation differs for individual spectrum lines and for some of them approaches 100%. The presence of highly polarized lines in the luminescence spectrum of the investigated crystals enabled us to apply to these crystals the method of polarization diagrams proposed by Vavilov[9] and developed by one of us[12] for the case of activated cubic crystals. This method makes it possible to establish, in most cases unambiguously, the nature (multipolarity) of the elementary oscillators.

---

*Preliminary results of this investigation for LiF:U were published in Ref.9.

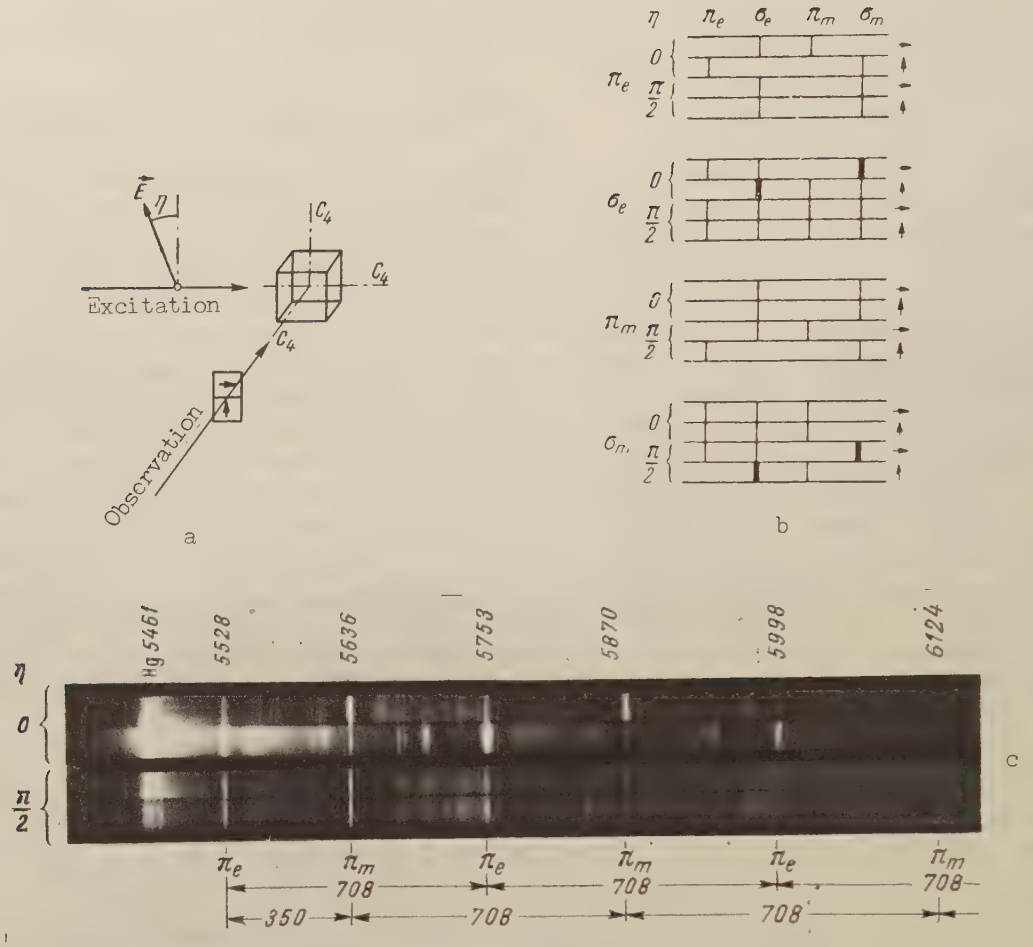

Fig.8. a) Diagram of the experiment for determining the multipolarity of the elementary radiators in MF:U single crystals. b) Patterns corresponding to different combinations of absorbing and radiating dipole oscillators. c) Luminescence spectrum of NaF:U at -196°; λ_{excit} = 546 mμ.

The question of the nature of the elementary oscillators involved in the luminescence of compounds of hexavalent uranium was first raised by Vavilov[13] in connection with the necessity of reconciling the spontaneity of the luminescence of uranyl salts with a long persistence with the dipole character of the emission indicated by the polarization diagrams plotted for the luminescence of uranium glasses[14]. Interference and polarization experiments carried out at that time[15] did not yield a definitive answer to this question. Accordingly, we attempted to answer it making use of the investigated fluoride crystals containing uranium.

The procedure applicable in this case for determining the multipolarities of the elementary radiators has been described earlier[9]. A diagram of the experiment, the patterns that should be observed for different combinations of absorbing and radiating dipole oscillators and a typical spectrogram, obtained for NaF:U under the conditions illustrated are shown in Fig.8.

The results of determination of the multipolarities of the elementary radiators are summarized in the accompanying table. It will be seen from the table that the long wavelength parts of the luminescence spectra are due to linear oscillators of the π_e and π_m types. The short wavelength group of lines in the spectru

Nature of elementary oscillators at -183°

A. In LiF:U luminescence spectrum

λ, A	Type osc.	λ, A	Type osc.	λ, A	Type of oscill.
4828	σ_e	5017	σ_m	5210	π_e
4882	σ_e	5024	σ_m	5240	π_m
4920	σ_e	5052	σ_m	5245	π_e
4941	σ_e	5057	σ_e	5278	$\pi_m\,(m_0)$
4948	σ_m	5067	σ_m	5285	π_e
4993	σ_m	5136	σ_e	5410	$\pi_e\ (e_1)$
5002	σ_m	5185	$\pi_e\ (e_0)$	5511	$\pi_m\,(m_1)$
5012	σ_m	5195	π_m	5655	$\pi_e\ (e_2)$
				5764	$\pi_m\,(m_2)$

B. In NaF:U luminescence spectrum

λ, A	Type of oscill.	λ, A	Type of oscill.
5528	$\pi_e\ (e_0)$	5944	π_e
5636	$\pi_m\,(m_0)$	5970	π_m
5676	π_e	5977	π_e
5699	π_e	5998	$\pi_e\ (e_2)$
5703	π_e	6066	π_m
5753	$\pi_e\ (e_1)$	6087	π_m
5818	π_m	6124	$\pi_m\,(m_2)$
5836	π_m	6229	π_e
5870	$\pi_m\,(m_1)$	6263	$\pi_e\ (e_3)$

of LiF:U is associated with circular oscillators: σ_e and σ_m.

Thus in the case of luminescence of uranium ions, just as in the case of luminescence of rare earth ions[16], we encounter, in addition to electric, magnetic dipole radiators. The intensities of the lines associated with the magnetic and electric dipoles are comparable. This indicates that the transitions accompanied by radiation from the electric dipoles are forbidden and that we are dealing with forced dipole radiation. Noteworthy is the scarcely fortuitous circumstance that the degree of removal of inhibition from the electric dipole transitions, as in the case of rare earth ions, is just sufficient for the probability for the forced electric transitions to be equal in order of magnitude to the probability for spontaneous magnetic transitions.

Thus the results of our investigation show that the luminescence of hexavalent uranium ions should be regarded as the surposition of forced electric and magnetic dipole radiations.

Before concluding, we would like to mention another point that may be important in interpreting the spectra of uranium ions in alkali halide crystals. Examination of Fig.8 shows that there is a regular alternation of the sign of the polarization of the most intense luminescence lines. This alternation of the polarization must be interpreted as alternation of the type of radiators: electric and magnetic dipoles. It is found that of the two principal electronic vibrational series observed in the spectra of each of the investigated crystals, one is formed by electric dipoles and the other by magnetic dipoles. The additional series detected in the spectrum of NaF:U must also be formed by radiators of one type: either electric or magnetic.

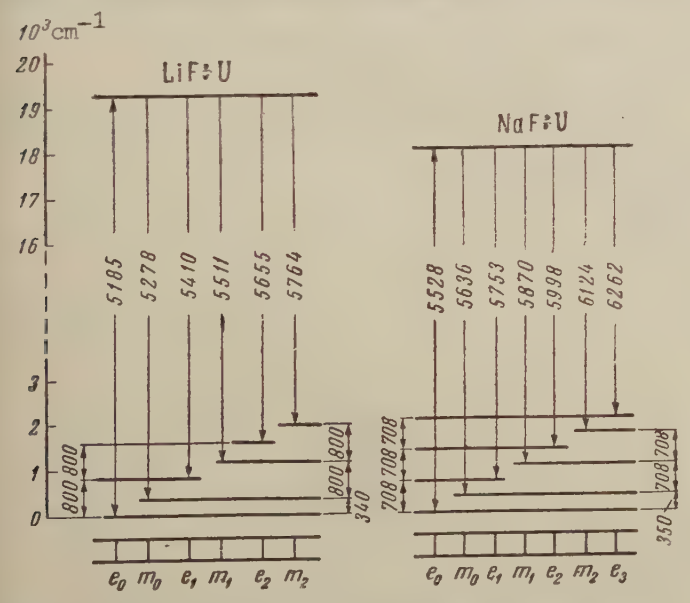

Fig.9. "Electric" and "magnetic" series in the luminescence spectra of LiF:U and NaF:U.

Thus there can be plotted the energy level diagrams for LiF:U and NaF:U shown in Fig.9; these incorporate the principal lines in the long

wavelength part of the spectra of these crystals, beginning with the longest wavelength resonance lines.

References

1. E.L.Nichols & M.K.Slattery, J.Opt.Soc.Am., 12, 449 (1926); Ibid., 19, 175 (1929); E.L.Nichols, H.L.Howes & D.T.Wilver, Cathodo-luminescence and luminescence of incandescent solids, Wash., 1928; F.Hernegger, Anz.Osterr.Akad.Wiss.Math.-naturwiss.Kl.Wien, No.2, 16 (1933); F.Hernegger & P.Karlik, Sitzungsber.Akad. Wiss.Math.-naturwiss., 144, 217 (1935); J.Hoffman, Sprechsaal, 73, 153 (1940); G.R.Price, R.J.Ferretti & S.S.Schwartz, Anal.Chem., 25, 322 (1953); T.S.Dobrolyubskaya, Zhur.analit.khimii, II, 3 (1956) (Trans.J.Analyt.Chem.); E.M.Sverdlov, Optika i spektroskopiya, 3, 356 (1957).

2. W.A.Runciman, Nature, 175, 1082 (1955); Proc.Roy.Soc.A237, 39 (1956); J. phys.et radium, 17, 645 (1956).

3. H.Le Roux, Nature, 183, 1180 (1959).

4. L.M.Belyaev & G.F.Dobrzhanskii et al, Tezisy dokladov na Soveshchanii po fizike shchelochno-galoidnykh kristallov (Program of the Conference on the Physics of Alkali Halide Crystals), Tartu, 1959.

5. P.P.Feofilov, Optika i spektroskopiya, 7, 842 (1959). (Trans.Optics and Spectroscopy.)

6. P.P.Feofilov, Zhur.eksp.i teor.fiz., 26, 609 (1954); Polyarizovannaya lyuminestsentsiya atomov, molekul i kristallov (Polarized luminescence of atoms, molecules and crystals), M., 1959.

7. P.P.Feofilov, Izv.AN SSSR, Ser.fiz., 18, 688 (1954) (Trans.Bulletin, 18, 371); L.I.Tarasova & P.P.Feofilov, Optika i spektroskopiya, 4, 696 (1958) (Trans. Optics and Spectroscopy).

8. P.P.Feofilov, Materialy V Soveshchaniya po lyuminestsentsii (Transactions of the Fifth Conference on Luminescence), p.3, Tartu, 1957.

9. P.P.Feofilov, Optika i spektroskopiya, 8, 824 (1960). (Trans.Optics & Spectroscopy.)

10. I.P.Shapiro, Ibid., 7, 126 (1959). (Trans.Ibid.)

11. S.I.Vavilov, Zhur.eksp.i teor.fiz., 10, 1363 (1940); Collected works, Vol. 2, 58, 1952.

12. P.P.Feofilov, Optika i spektroskopiya, 1, 131 (1956).

13. S.I.Vavilov, Vestnik, Leningrad State University, No.1, 5 (1946); Collected works, Vol.2, 252 (1952); Trudy GOI (Proceedings, State Optical Institute), 20, 132, 4 (1950); Collected works, No.2, 260, 1952.

14. A.N.Sevchenko, Doklady AN SSSR, 42, 349 (1944).

15. P.P.Feofilov, Ibid., 55, 407 (1947).

16. P.P.Feofilov, Ibid., 99, 975 (1954).

INVESTIGATION OF THE RELAXATION TIME OF THE PHOTODIELECTRIC EFFECT IN ZnS:Cu:Co PHOSPHOR

- G.M.Malkin

One of the more important characteristics of the photodielectric effect (PDE) is the relaxation time θ, which determines the position of the dispersion region due to excitation of the crystal phosphor. The relaxation time can be determined experimentally from the condition $\omega_{max}\theta = 1$, where ω_{max} is the angular frequency of the electric field at which the peak value of the dielectric loss factor is observed.

Theory yields different expressions for θ depending on the hypothesized nature of the PDE. If the effect is assumed to be due to conductivity, taking into account diffusion of free electrons, we can write[1]

$$\theta = \frac{C_0}{\sigma}, \qquad (1)$$

where σ is the conductivity and C_0 is the increment in the dc field capacitance of the phosphor as a result of excitation.

If it is assumed that trapped electrons are responsible for the PDE:

$$\theta = \frac{\varepsilon_0 + 2}{\varepsilon_\infty + 2} \cdot \frac{1}{2p_0} e^{\frac{U}{kT}}, \qquad (2)$$

where ε_0 and ε_∞ are the values of the dielectric constant at $\omega = 0$ and $\omega = \infty$, respectively, p_0 is the natural vibration frequency of the trapped electrons, and U is the height of the internal potential barrier on the trapping levels. Ramazanov[3] suggested that U has the physical meaning of the usual trap depth, rather than the height of the internal barrier on the trapping levels.

Both Roux[2] and Ramazanov[3] note that for explaining the experimental data one must assume that there are present in the phosphor several different types of levels with different U. This makes if impossible to check Eq.(2) experimentally as long as the distribution of the trapping levels is not known. One can, however, find a temperature region where the phosphorescence is due to levels of one depth (Ref.4 & 5); and in this region one can establish which of the equations - (1) or (2) - gives a better fit to the experimental data.

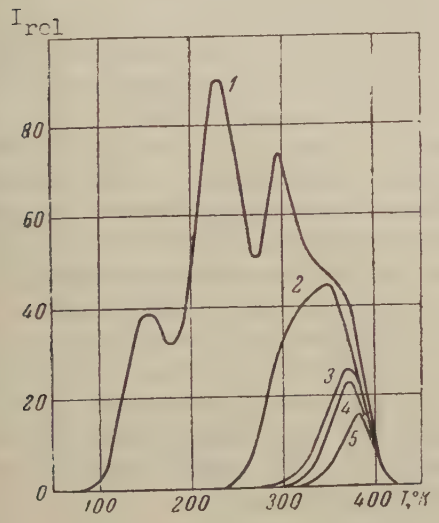

←Fig.1. Glow curves for ZnS:Cu:Co phosphor: 1) after excitation at liquid nitrogen temperature, 2) after excitation at 20°, 3,4 & 5) after 1,2 and 12 hours decay, respectively, at 20°.

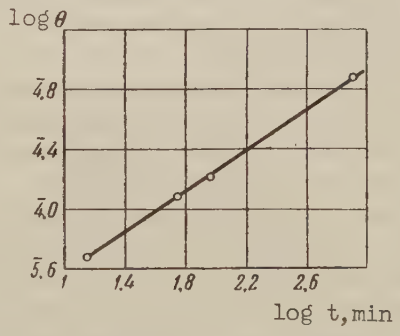

Fig.2. Variation of θ with phosphorescence decay time.

Accordingly, we recorded the thermostimulated luminescence (glow) curves for ZnS:Cu($3\cdot10^{-5}$ g/g):Co(10^{-6} g/g) phosphor; these are reproduced in Fig.1. As will be evident from the figure, this phosphor has four sets of trapping levels. Excitation at room temperature leads to electron population of the trapping levels that yield the glow peaks at 20 and 78° (curve 2). At the beginning of decay there are emptied the levels that are responsible for the peak at 20°. At subsequent stages of decay release of electrons occurs only from the deeper trapping levels. Glow curves 3,4 & 5 were recorded 1,2 and 12 hours after excitation. On the basis of these curves, using the method proposed by Antonov-Romanovskii[6], we calculated the depth of the trapping levels participating in the phosphorescence at different stages of decay. For all three curves we obtained a trap depth of 0.5 ev. Thus in our phosphor release of electrons at 20° during at least the first 11 hours occurs from levels of one depth. For this case Eq.(2) gives either a constant value of θ or a small decrease of θ inasmuch as ε_0 decreases slightly during decay. Increase of θ with the decay time according to Eq.(2) can occur only as a result of departure of electrons from levels having smaller U and consequent increase of the relative significance of trapping levels with larger U. According to (2), the presence of a set of internal potential barriers even for levels of one depth should not give rise to change of θ, inasmuch as the electron release probability does not depend on the height of this barrier, but is determined by the depth of the trapping levels, and, consequently, decay does not change this distribution.

Fig.2 shows the variation of θ with decay time obtained for our ZnS:Cu:Co phosphor. It will be evident that despite the release of electrons from traps of one depth, θ does increase substantially with time, instead of remaining constant or decreasing as is required by Eq.(2). It also follows from Fig.2 that the variation of θ with decay time is described by the hyperbolic law. This is in agreement with (1) and the results of Vergunas & Lukantsever[7], who showed that in the process of phosphorescence decay the concentration of free electrons, which is proportional to the photoconductivity σ, decreases according to the hyperbolic law. C_0 in (1) virtually does not change with decay time at 20°.[1]

Another, independent check of (2) is furnished by the temperature dependence of θ. If this is plotted in log θ, 1/T coordinates there should be obtained a straight line, from the slope of which one can determine the depth of the traps or, according to Roux[2], the height of the internal potential barrier.

To determine the temperature variation of θ, we excited the phosphor at 20° and then after holding it for 12-14 hours at this temperature, heated it slowly. The resultant curves are shown in Fig.3; as will be evident from the figure, the center of the PDE dispersion region shifts to the side of higher frequencies. We plotted the temperature dependence of θ on the basis of the data of Fig.3; the resultant curve is shown in Fig.4. It will be seen that the experimental points do not lie on a single straight line; at higher temperatures the slope of the curve is less steep than at temperatures near room temperature, whereas if there is present a set of U, according to Roux[2] and Ramazanov[3], the opposite should obtain: with increase of the temperature there should at first be evinced levels with smaller U and then, with gradual emission of the light sum, levels with larger U.

In addition, decrease of θ should be accelerated at higher temperatures by decrease of ε_0, owing to release of trapped electrons. On the other hand, Eq.(1) satisfactorily describes the variation of θ in this case as well, inasmuch as heating of the phosphor leads to increase of the conductivity. Thus, even if there are filled trapping levels of one depth in the phosphor, Eq.(2) cannot satisfactorily describe the decay time and temperature dependences of θ.

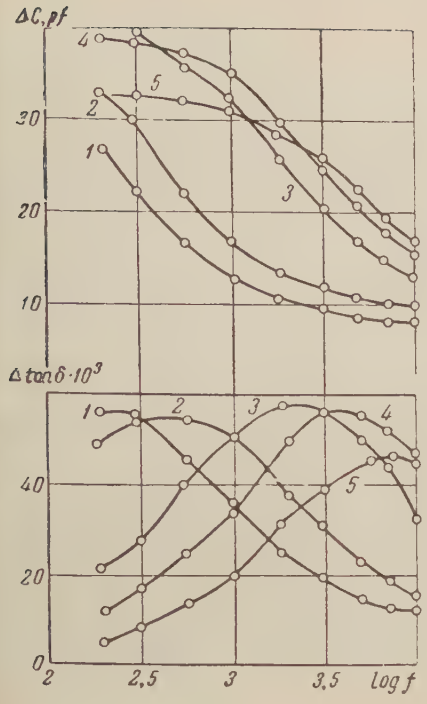

Fig.3. Displacement of the PDE dispersion region with heating of the phosphor at late stages of phosphorescence decay: 1) 20°, 2) 30°, 3) 50°, 4) 69°, 5) 89°.

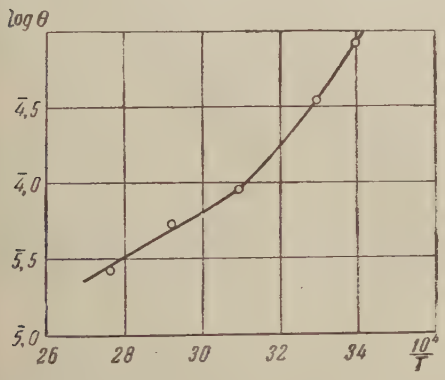

Fig.4. Variation of θ with temperature at late stages of phosphorescence decay.

We also investigated the variation of the PDE relaxation time at liquid nitrogen temperature. It was established that after cessation of excitation at this temperature θ increases more than an order of magnitude. Yet at this low temperature the number of trapped electrons does not change after cessation of excitation and, consequently, there is no redistribution of electrons among trapping levels. Hence Eq. (2) cannot explain the observed increase of θ.

All these experimental results substantiate the inference made earlier[1] that the photodielectric effect in ZnS:Cu:Co phosphor is due to conduction electrons.

I desire to express my deep gratitude to F.I.Vergunas for her guidance in the work.

Gor'kii Physical-Technical Research Institute

References

1. F.I.Vergunax & G.M.Malkin, Fiz.tverd. tela, 2, 2322 (1960). (Trans.Soviet Physics - Solid State.)

2. J.Roux, L'effet photodielectrique dans le sulfure et dans l'oxyde de zinc, Paris, 1956.

3. P.E.Ramazanov, Izv.AN SSSR, Ser.fiz., 23, 1290 (1959). (Trans.Bulletin 23, 1281.)

4. F.I.Vergunas & Yu.L.Lukantsever, Optika i spektroskopiya, 5, 156 (1958).

5. F.I.Vergunas & L.R.Krasovskaya, Ibid., 5, 162 (1958).

6. V.V.Antonov-Romanovskii, Izv.AN SSSR, Ser.fiz., 10, 477 (1946).

7. F.I.Vergunac & Yu.L.Lukantsever, Ibid., 23, 1294 (1959). (Trans.Bulletin, 23, 1285.)

CONCURRENT INVESTIGATION OF THE PHOTODIELECTRIC EFFECT AND THE LIGHT SUM STORED IN ZnS:Cu:Co PHOSPHOR

- G.M.Malkin

It is known that the emission and decay of crystal phosphors with a recombination mechanism is accompanied by change of their dielectric properties. This photodielectric effect (PDE) has been investigated by many authors, primarily by observation of the variation of the dielectric constant and dielectric loss factor as a function of the excitation intensity, the frequency of the applied electric field, the temperature and other factors. It was found that most of the observed regularities can be explained by associating the PDE with trapped electrons or conduction electrons in grainy specimens; both hypotheses lead to equations of the Debye type.[1,2] It must be noted, however, that there have been very few studies involving parallel investigation of the PDE and the optical characteristics of the phosphor, despite the fact that such investigations could yield direct proof of the participation of trapped or conduction electrons in the PDE.

One such study is that carried out by Garlick & Gibson[3], who investigated the decrease of the increment in the dielectric constant $\Delta\varepsilon$ and the stored light sum L during the phosphorescence decay time t. These authors cite the observed parallelism between the log $\Delta\varepsilon$ vs log t and log L vs log t curves as proof that trapped electrons are responsible for the PDE. This inference, however, is erroneous because $\Delta\varepsilon$ is not proportional to the number of polarizing complexes. Actually, the Debye equation for $\Delta\varepsilon$ gives

$$\log \Delta\varepsilon = \log (\varepsilon_0 - \varepsilon_\infty) - \log (1 + \omega^2\theta^2), \qquad (1)$$

where ε_0 and ε_∞ are the values of the dielectric constant measured at frequencies $\omega = 0$ and $\omega = \infty$, respectively, and θ is the relaxation time of the PDE. It will be evident from (1) that $\Delta\varepsilon$ for measurements at a constant frequency is a function of two variables, namely, $\varepsilon_0 - \varepsilon_\infty$ and θ, which, in turn, vary in the process of decay of the phosphor. It is known that θ increases during the decay time. Thus, Roux[1] gives data for ZnS:Cu phosphor from which it follows that during the decay time from 10 sec to 5 min θ increases by two orders of magnitude, while $\varepsilon_0 - \varepsilon_\infty$ decreases by about 50% during the same period.

In our experiments we found that for ZnS:Cu:Co phosphor θ changes from $4 \cdot 10^{-7}$ sec during excitation to $8 \cdot 10^{-4}$ sec after 12 hours decay, i.e., increases by more than three orders of magnitude. For the same phosphor $\varepsilon_0 - \varepsilon_\infty$ decreased by 11.5% during the same decay period. Consequently, the decrease of $\Delta\varepsilon$ during the decay period with $\omega = \text{const}$ occurs mainly due to shift of the dispersion region to the side of lower frequencies. Hence the shape and slope of the $\Delta\varepsilon$ vs t curve plotted in double logarithmic coordinates is determined not only by the variation of $\varepsilon_0 - \varepsilon_\infty$ but also by the particular decay time dependence of θ. It is also obvious that change of the measurement frequency ω should be evinced in the shape of this curve owing to inconstancy of θ.

The influence of ω on the law characterizing the decrease of $\Delta\varepsilon$ was noted by Roux[1]. Roux, however, infers that the persistence of the PDE at liquid nitrogen temperature is evidence of the participation of trapped electrons in the PDE, although this effect may also be due to variation of the measurement frequency. Thus, for example, we obtained the effect of "freezing" of the PDE for ZnS:Cu:Co phosphor at room temperature, that is, we found that the PDE might persist for hours at one frequency and fall off rapidly at another. In the accompanying figure we show curves giving the increment in capacitance measured at two different frequencies at 50°. Curve 1 may serve as an example of "freezing" of the PDE,

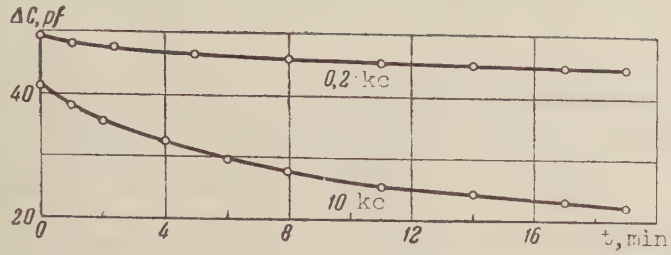

Decrease of ΔC measured at different frequencies with the phosphorescence decay time for ZnS:Cu:Co phosphor at 50°.

while curve 2 illustrates the case of decrease of the PDE at the same temperature.

Thus comparison of the variation of the stored light sum with $\Delta\varepsilon$ should not be carried out with a substantially varying relaxation time. The effect of inconstancy of θ can be avoided, however, in the limit as $\omega \to 0$, i.e., by using a dc field. In this case, parallelism between the variation of $\Delta\varepsilon = \varepsilon_0 - \varepsilon_\infty$ and the stored light sum could be taken as direct proof of the participation of trapped electrons in the PDE.

For determining $\varepsilon_0 - \varepsilon_\infty$ or $C(\varepsilon_0 - \varepsilon_\infty)$ (C is the geometric capacitance of the specimen) one can make use of the circular diagrams of Cole & Cole[4]. Inasmuch as we are interested only in the effect resulting from excitation of the specimen, the circular diagram should be plotted for $C\varepsilon' = C\Delta\varepsilon$ and $C\varepsilon'' = C\varepsilon' \tan\gamma$, where ε' is the increment in the dielectric constant owing to excitation, ε'' is the dielectric loss factor due to the appearance of an absorption current during excitation, and γ is the angle between the absorption current and its reactive component. It can be shown that

$$\tan\gamma = \tan\delta_e + \frac{C_T}{\Delta C}\Delta\tan\delta,$$

where $\tan\delta_e$ is the dielectric loss tangent of the excited specimen, $\Delta\tan\delta$ is the increment in the loss tangent and ΔC is the increment in capacitance as a result of excitation, and C_T is the capacitance of the unexcited specimen.

This presentation of the dispersion data is clear and graphic, and eliminates the possible error connected with "dark" values of the dielectric loss factor and capacitance at different frequencies.

We plotted circular diagrams for ZnS:Cu:Co phosphor during excitation and at different instants during phosphorescence decay at 20°.[2] Concurrently with these measurements, we recorded the glow curves immediately after cessation of excitation at 20° and after different decay periods at the same temperature. From the areas under the glow curves we determined the light sums stored and remaining in the phosphor as a function of the decay time. The following are the data obtained on the increment in static (dc) capacitance and stored light sums:

Decay time, hrs	0	1	2	12
Increment in static capacitance, pf	56.6	50	50	50
Stored light sum, arbitrary units	100	34	29	14.4

It will be seen that during the first hour of decay the light sum falls off by a factor of about 3, whereas the static capacitance decreases only slightly. During the subsequent hours the number of trapped electrons continues to decrease, while the static capacitance remains virtually constant.

Thus it will be evident that for ZnS:Cu:Co phosphor at room temperature, at any rate, there is no parallelism between the decrease of the light sum and $\varepsilon_0 - \varepsilon_\infty$

This is consistent with the inference drawn earlier[2] that in this phosphor the PDE is due mainly to conduction electrons. From this standpoint one can easily explain the small decrease in static capacitance during the initial decay period, inasmuch as this quantity, depending on the conduction electron concentration, rapidly attains saturation.[2] Apparently, the concentration of conduction electrons that obtains in the phosphor during persistent phosphorescence of the phosphor at room temperature is sufficient for the static capacitance to attain saturation.

I desire to express my deep gratitude to F.I.Vergunas for her guidance in the work.

For'kii Physical-Technical Research Institute

References

1. J.Roux, L'effet photodielectrique dans le sulfure et dans l'oxyde de zinc, Paris, 1956.

2. F.I.Vergunas & G.M.Malkin, Fiz.tverd.tela, 2, 2322 (1960). (Trans.Soviet Physics - Solid State.)

3. G.F.Garlick & A.F.Gibson, Proc.Roy.Soc.A, 188, 485 (1947).

4. K.S.Cole & R.H.Cole, J.Chem.Phys., 9, 341 (1941).

DISCUSSION

Ya.A.Oksman: Despite the great potentialities of photodielectric methods they have not yet achieved their merited place in the arsenal of means of investigating semiconductor processes. This is connected with the fact that until now interpretation of the experimental data has been based on the a priori properties of the investigated substances, which naturally leads to ambiguous results. In the report we have just heard, in line with this tendency, there are made inadequately founded assumptions regarding parallelism between the light sum and the static capacitance, regarding the photodielectric effect of the first order being due to trapping levels of one type, etc.

In connection with this I would like to put forward some general considerations regarding the direction of research concerned with the photodielectric effect. First, new data on the properties of trapped and free charges can be obtained only on the basis of formal, rigorously substantiated methods of investigation and analysis of the experimental results. In this respect the method of taking into account the polarization field described by Vergunas appears to be very interesting, inasmuch as it allows of excluding from consideration the detailed distribution of space charges.

The next consideration pertains to the subjects of investigation. Until the precise character of the complicated photodielectric effects has been clarified, it would be preferable to carry out experiments on single crystals rather than on powdered phosphors; this is essential for elucidating the mechanism of the photodielectric effect of the first order and for checking present concepts concerning diffusion effects.

CLOSING ADDRESS

- V.L.Levshin

The Ninth Conference on Luminescence, devoted to crystal phosphors, has completed its work. The Conference has been very successful; there have participated in its work 325 delegates from many scientific and industrial organizations.

In my closing remarks I would like to share with you my impressions of the work accomplished. It seems to me that the Ninth Conference differs in some respects from preceding conferences on luminescence.

First, it must be noted that in many reports there was evinced much deeper penetration into the essence of the investigative processes than was possible earlier. The use of new, improved methods of investigation which I mentioned in my opening address, and which had scarcely been used earlier, has yielded worthwhile results.

Investigation of structureless spectra with wide luminescence bands and of strongly scattering powders hindering precise determination of absorption is gradually giving place to investigation of the luminescence of single crystals and sublimated films. In working with cubic crystals at low temperature it has proved feasible to observe fine line structure in the luminescence spectra and splitting of the luminescence and absorption bands. Absorption spectra with discernible fine structure have also been obtained in investigating sublimated films. These new data have been utilized for elucidating the nature and structure of luminescence centers, the character of elementary emitting systems and of the mechanism of luminescence.

Detailed investigation of the effect of impurity centers in organic crystals, connected with determination and investigation of the fine structure of these spectra, have made it possible to establish the similarity between many luminescence processes in organic luminophors and inorganic crystals.

The possibility of detailed investigation of luminescence centers, highlighted in a number of reports presented at the Conference, is a great step forward.

Another distinctive feature of the Ninth Conference is the tendency to give more profound theoretical interpretations of observed processes. We have heard a number of theoretical communications, the purpose of which was to clarify the kinetics of phosphor luminescence. This is to be applauded. One must, however, note a certain degree of abstraction in the theoretical studies. Most of these investigations are confined to ideal cases of luminescence and do not extend to direct application of the theoretical results to quantitative explanation of experimental data.

Experimenters on their side fail to utilize the calculations of theoretical scientists, partly because use of the new formulas requires carrying out special experiments aimed at determining various constants and partly because the approximate theoretical formulas are not directly applicable to quantitative explanation of experimental data obtained under nonideal conditions for nonideal phosphors.

Despite this, the appearance of a number of theoretical contributions on the kinetics and structure of luminescence centers, on the one hand, and of highly refined experimental studies, on the other hand, gives reason to hope that in the future experimental and theoretical investigations will draw closer together and that we will attain a deeper understanding of the processes occurring in crystal phosphors.

Turning to research involving individual classes of crystal phosphors, we cannot fail to note the significant advances in the investigation of alkali halide phosphors. This is explained, on the one hand, by the favorable properties of phosphors of this class, and, on the other hand, by the concentrated attention of

a number of groups of scientific workers to luminophors of this type.

Less attention in recent years has been paid to phosphors of the zinc sulfide type. Yet this class of luminophors came under investigation in the Soviet Union before alkali halide phosphors and is more important from the practical standpoint. However, owing to the great complexity of the problem, investigation of the luminescence of zinc sulfide has proceeded more slowly. Practical considerations indicate that research on the development of ZnS luminophors must be emphasized. Undoubtedly the advances made in the field of alkali halide phosphors will be of help in understanding the more complex problem of the luminescence of ZnS phosphors. Zinc sulfide phosphors, however, have a number of distinctive characteristics and one cannot simply extend the results obtained for alkali halide phosphors to this class of luminophors.

Even less attention in recent years has been given to study of other classes of luminophors. One can only regret the inadequate development of work on lamp phosphors, in particular, halophosphate phosphors. In view of the ever increasing use of fluorescent lighting, it is essential to give great attention to the investigation of processes occurring in lamp luminophors and to synthesis of new luminophors of this type.

In the field of chemical investigation of crystal phosphors one may note the gradual transition from empirical methods of obtaining luminescent compounds to development of new theoretical ways of arriving at the synthesis of luminophors, taking into account thermodynamic considerations and the specific properties of different crystal structure.

The Conference reports reflect substantial development of research in the field of electroluminescence; it must also be noted that the character of the investigations in this field has changed. Earlier the work in this field was purely technical in character and aimed at developing sufficiently bright electroluminophors and investigating the basic properties of electroluminescence, whereas now the center of gravity has been transferred to investigation of the nature of the effect and the kinetics of the processes involved in electroluminescence.

Finally, one must regretfully note the fact that there is a significant decrease, as compared with previous conferences, in the number of reports on practical applications of crystal phosphors. Yet the number of unsolved questions in the field of practical application of luminescence has increased rather than decreased. We should have expected new proposals on uses of crystal phosphors, reports on development of various new industrial luminophors and descriptions of new equipment for testing phosphors. Unfortunately, there have been very few reports on these topics. Even a number of familiar applications of luminescence have not been touched upon in any of the reports presented at the Conference.

In their report on fluorescent lighting, the representatives of the Moscow Electric Lamp Plant (D.P.Troshenskii) and of the All-Union Light Engineering Institute (V.I.Dolgopolov) expressed sharp disagreement as regards their views on the present state of the question of measures to be taken towards improvement of fluorescent lamps.

It seems to me that questions of technology of luminescent screens and layers for different practical purposes and also questions of coating and deposition of luminophors play a significant role where the potentialities of practical utilization of luminophors are concerned. Hence it is to be hoped that industrial institutes and laboratories will pay due attention to the development of new luminophors for lamps, color television, cathode-ray tubes and the like and to development of methods of deposition and fabrication of high quality screens; it may also be hoped that there will be developed better coordination between industrial and scientific organizations. The Council on Luminescence and its commissions on practical prob-

lems should give serious attention to this matter.

Comrades! Representatives from a large number of different organizations from all parts of the Soviet Union have been gathered at our Conference. The Conference gave a clear general picture of the present state of work in the field of crystal phosphors in the Soviet Union, which should be of great value for every scientific worker and every researcher in industry in choosing the direction of his further work. The Conference will undoubtedly have a favorable effect on concordance of activities in individual laboratories with the general work on luminescence and on rapid assimilation of the new methods of investigation described in the various reports presented at the Conference. In view of the wide scope of investigations in the field of luminescence in the Soviet Union exchange of views and experience is extremely important and the role of our conferences in this respect is impossible to overrate.

Allow me to thank, in the name of all those gathered here, our hosts, the physicists of Kiev, who have expended much effort on insuring the success of the Conference. Our thanks go particularly to Prof.A.A.Shishlovskii, member of the Organizing Committee and head of the Department of Physics of Kiev State University, and I.T.Shvets, Director of Kiev State University, who made it possible to meet in the University halls. We also want to thank the directors of the Physical Institute of the Ukrainian SSR Academy of Sciences for permission to inspect the Laboratory of the Institute.

Finally, we want to express our sincere gratitude to the Secretariat of our Conference who worked so hard to insure its success and who have made our stay in Kiev not only useful in the scientific sense but also pleasant for all participants in the Conference.

Bulletin of the Academy of Sciences of the USSR - Physical Series
Vol. 25, No. 4 - April 1961

Transactions of the Ninth All-Union Conference on Luminescence (Crystal Phosphors)
(Continued from Vol. 25, Nos. 1 and 3)

TABLE OF CONTENTS

	Page Orig.	Trans.
Different types of phosphor crystallochemical systems and their luminescence properties - M.A.Konstantinova-Shlezinger	442	435
Thermodynamics of the mechanism of activation of sulfide and sulfide-selenide phosphors - A.A.Bundel', Z.I.Guretskaya & L.B.Taushkanova	445	438
Influence of oxygen on the luminescence properties of activatorless zinc selenide - L.Ya.Markovskii & R.I.Smirnova	449	442
Concerning the valence of Sn and Mn activators in crystal phosphors - N.A.Gorbacheva & V.V.Osiko	454	446
Phosphate luminophors for fluorescent lamps with improved color characteristics - N.A.Gorbacheva, B.M.Gugel', M.A.Konstantinova-Shlezinger, E.S.Lapir & T.G.Rutshtein	455	447
Effect of replacement of the base materials of phosphors on their luminescence properties - M.-L.Yu.Allsalu	458	450
Luminescence of lanthanides in thorium oxide - A.K.Trofimov	460	453
Influence of the synthesis conditions on the luminescence of zinc oxide - Ya.M.Zelikin	461	455
Quenching and stimulation of the luminescence of zinc oxide under the influence of adsorbed and capillary-condensed vapors and gases - K.V.Tagantsev	464	457
Investigation of the thermal activation energy for optical quenching of some crystal phosphors - V.L.Levshin & B.M.Orlov	466	460
Concerning the parameters of sticking centers which determine the kinetics of photo-thermostimulated effects - V.E.Khartsiev	469	463
Investigation of trapping levels in CaS phosphors by the methods of exoelectronic emission and thermostimulated luminescence - V.L.Levshin & P.A.Pipinis	471	465
On the possibility of thermal activation of current carrier trapping in crystal phosphors - Yu.L.Lukantsever & F.N.Zaitov	473	467
Rate of phosphorescence decay as a function of filling of electron traps and temperature - N.V.Zhukova, G.K.Evdokimova & V.L.Levshin	476	471

Variation of the steady-state luminescence of ZnS phosphors with the excitation intensity - K.-S.K.Rebane 479 473

Investigation of rare earth activated SrS phosphors by the method of electron paramagnetic resonance - V.V.Antonov-Romanovskii & V.G. Dubinin 481 475

Investigation of electroluminescence pulses emitted by ZnS:Cu:Al phosphors with a high Cu concentration - A.M.Bonch-Bruevich & V.A.Molchanov 482 477

Investigation of the electroluminescence of ZnS:Cu and ZnS:Cu:Mn phosphor layers with excitation by dc and pulse voltages - V.N. Favorin, G.S.Kozina & I.D.Anisimova 487 482

Experimental investigation of the possibility of realizing multiple component electroluminescent devices employing ferroelectric materials - I.Ya.Lyamichev, I.N.Orlov, G.G.Pershin & N.I.Taborko 492 487

On enhancing the efficiency of a scintillation type slow neutron detector - B.S.Grebenskii, T.V.Timofeeva, S.P.Khormushko & O.S.Tsvetkov 500 494

Dispersed fast neutron detector - G.V.Gorshkov, B.S.Grebenskii, S.P. Khormushko & O.S.Tsvetkov 504 498

Selection of phosphor coatings for x-ray screens - A.M.Gurvich & R.V.Katomina 506 500

Use of strontium sulfide phosphors for making luminous signs - T.A.Krasnova 508 503

Photoelectric photometer for determination of uranium in sodium fluoride beads - Z.M.Sverdlov 510 505

Instrument for determining the parameters of fluorescent screens (PRS) - B.I.Pochtarev, K.K.Raspletin & D.V.Fetisov 512 508

Attachment for the PRS instrument for investigating phosphors from the bombarded side - B.I.Pochtarev 514 509

Investigation of the electroluminescence of zinc sulfide single crystals - V.E.Oranovskii 516 512

Electroluminescence and surface properties of crystal phosphors - I.K.Vereshchagin 518 514

Regarding the possibilities of stimulating the electroluminescence properties of crystals - I.S.Andreev, G.B.Arzumanyan & L.V.Zyrina 520 516

Effect of ultraviolet irradiation on the luminescence characteristics of an electroluminophor - I.P.Shapiro & N.I.Kuznetsov 523 519

Investigation of the electroluminescence of some phosphors with excitation by unipolar pulses - V.L.Rabotkin & V.A.Sokolov 524 520

Some results of an investigation of the deterioration of phosphors during electroluminescence - N.N.Grigor'ev & Yu.A.Kulyupin 526 522

Use of electroluminescence for character indicators - F.V.Sorkin, A.P.Belyaeva & N.S.Borodin 527 523

Measurement of losses in an electroluminescent capacitor - E.E.Bukke 529 526

Investigation of the luminescence of CdS single crystals at low temperatures - E.F.Gross & M.A.Yakobson 531 527

Investigation of the absorption and luminescence of ZnS and ZnSe single crystals - E.F.Gross & L.G.Suslina 532 529

Concerning interaction of the activator with not fully symmetrical local vibrations - N.N.Kristofel' 533 530

Contribution to the theory of electronic-vibrational transitions in crystals and molecules - K.K.Rebane & O.I.Sil'd 535 532

Contribution to the theory of luminescence of activated phosphors - A.M.Ratner & G.E.Zil'berman 537 533

Luminescence of copper-activated glasses - G.O.Karapetyan 539 535

Investigation of photoluminescence and scintillation of silicate glasses - S.M.Brekhovskikh & I.F.Shapovalova 541 537

Luminescence of crystals surface-activated with uranyl ions - G.I. Kobyshev 542 539

Luminescence of LiF crystals activated by uranyl nitrate - E.P.Alekseeva 545 541

Influence of infrared light on the luminescence of silver chloride - V.M.Belous & N.G.D'yachenko 547 543

Luminescence of uranium activated sodium and lithium fluoride single crystals - L.M.Belyaev, G.F.Dobrzhanskii & P.P.Feofilov 548 545

Investigation of the relaxation time of the photodielectric effect in ZnS:Cu:Co phosphor - G.M.Malkin 556 553

Concurrent investigation of the photodielectric effect and light sum stored in ZnS:Cu:Co phosphor - G.M.Malkin 559 556

Closing address - V.L.Levshin 562 559

Translated in 1962 by
Columbia Technical Translations
5 Vermont Ave., White Plains, N.Y.

Transactions

of the

Symposium on Thin Ferromagnetic Films

(Krasnoyarsk - 4-7 July 1960)

Lithographed in U.S.A. by
EDWARDS BROTHERS, INC.
Ann Arbor, Michigan

THIN MAGNETIC FILMS IN PRESENT DAY PHYSICS AND ENGINEERING

- K.M.Polivanov & A.L.Frumkin

The term "thin magnetic films" is used to describe layers of ferromagnetic substances with a thickness of the order of 10^3 Å and possessing a number of distinctive magnetic properties differing from those of bulk specimens of the same substances. The principal distinctive features of thin magnetic films are the following.

1. Ferromagnetic films are only one domain thick, and under static conditions the magnetization vector lies in the plane of the film.

2. The demagnetizing factor of films in their plane is very small (of the order of 10^{-4}-10^{-5}), and in the direction normal to the film equals unity.

3. No eddy currents exist in thin films, at least up to super-high frequencies.

4. Owing to the distinctive character of the domain structure, the natural ferromagnetic resonance frequency in films is 10 to 100 times higher than in equivalent bulk ferromagnets; accordingly, the permeability of films remains great at high frequencies.

5. Ferromagnetic films are characterized by a high switching rate in pulsed and sinusoidal fields, and the switching loss is low.

6. Many films are characterized by pronounced magnetic anisotropy in their plane.

7. Many films have a rectangular hysteresis loop.

The thickness range from 60 to 6000 Å is noteworthy in being a transition range in that at higher thicknesses ferromagnetic layers as regards magnetic properties approach bulk specimens, while for smaller thicknesses ferromagnetism gradually disappears.

The development of nonmetallic ferromagnets (ferrites) was the culmination of one line of research in the field of high-frequency magnetic materials, that directed at obtaining ferromagnets with a maximum resistivity. Analogously, the development of ferromagnetic films was the culminating point of another line of research, namely, the preparation of thin-layer ferromagnetic materials. In both cases the absence of significant eddy currents greatly extended the potential scope of applications in radio and high-frequency engineering. But in view of their distinctive features, particularly their domain structure and switching dynamics, thin films opened a new avenue of research both as regards investigation of basic physical regularities and as regards unusual practical applications.

There are a number of reasons for the present exceptional interest in the physics of thin films.

In thin films the substance is essentially in a "two dimensional" state, i.e., one of the dimensions is much smaller than the other two. As a result, in the case of thin films we encounter new physical effects, investigation of which allows drawing deductions important for solid state theory in general and for the physics of ferromagnetic phenomena in particular. Thanks to the "two dimensional" character of thin films one can employ experimental procedures that are inapplicable for bulk ferromagnets. Among these, for example, are investigation of domain structure by passing polarized light through semitransparent films. A number of physical effects have been discovered or investigated more thoroughly in experiments with ferromagnetic films. Such, for example, are spin waves in films and the appearance of a constant voltage on the ends of the film in a super-high frequency field, selective transparency of thin layers, the phenomenon of ordering of the crystal structure of a metal deposited on a thin film, etc.

Of great interest from the standpoint of solid state theory is investigation of the mechanism involved in the influence of magnetic fields on a film during its formation, i.e., the mechanism leading to uniaxial anisotropy. Among the most important technical applications of thin films are their use as memory and logic elements in high-speed computers. A particular but highly promising case is the use of such elements in devices operating on the principle of parametric excitation. An advantage of film memory elements as compared with ferrite components is their high speed. There have already been described in the literature film type storage devices with an access time of 0.5-1 μsec, and the possibility for further reduction of the access time has not been exhausted. At the same time, the use of films brings to the fore a number of new problems. For example, the necessity of detecting and utilizing very week magnetic fluxes makes it necessary to develop highly sensitive equipment, reduce air inductances, etc. In connection with magnetic films it is not only logical but frequently necessary to use printed circuits, film transistors and similar components. In principle, films make it possible to realize computers and similar systems with a great storage capacity, high reliability and capabilities for continuous and fully automatic production control. In addition to qualitative improvement of the parameters of extant computers, thin films in conjunction with other miniaturized memory and control elements offer great possibilities for designing systems of much greater intricacy and complexity than now available. The realization of such devices, approaching the potential capacity of the human brain, will be a significant jump forward in computer technology and science in general.

The great advances made in the investigation and application of thin films are in no small measure due to improvement in the methods of preparing such films. At present thin films of ferromagnetic metals on insulating or metal substrates as well as in the free state are prepared by vacuum or electrolytic deposition. Each procedure has its own advantages and, when advanced techniques are employed, yield films of equal quality. There are, however, possibilities of further improvement of both procedures. Moreover, there is reason to expect development in the near future of new and radically different methods of preparing thin films.

Among the different films, the most thoroughly studied (but still inadequately) are thin films of Permalloy type alloys, which have already found extensive practical application. There have been prepared and used to some extent films of other metallic alloys and ferrites (the last are generally of somewhat greater thickness). Under intensive study are magnetically hard films of Mn-Bi alloy which allow of realizing (on the basis of a different principle of operation from that obtaining in the case of Permalloy films) memories with a great capacity.

It may be said without exaggeration that present achievements in the field of thin films are one of the major break-throughs of modern science, comparable to such achievements as the development of semiconductor electronics and the introduction and use of ferrites and solid state amplifiers (masers). There can be no doubt that thin films will be a determining factor in the future technical development of radio engineering and computer technology.

The bibliography at the end of this article, which includes contributions in the field of physics, methods of investigation, technology and use of thin films, is far from exhaustive. Unfortunately, investigation of films carried out in the USSR are still not adequately represented in the scientific literature. The present collection of reports is intended to help fill this gap.

Bibliography

1. Fizika ferromagnitnykh oblastei (Physics of ferromagnetic domains, Edited by S.V.Vonsovskii (translated articles), M., 1951.

2. Magnitnaya struktura ferromagnetikov (Magnetic structure of ferromagnets). Edited by S.V.Vonsovskii (translated articles), M., 1959.

3. Conference on Magnetism and Magnetic Materials, Washington, 1957. (J. Appl.Phys., 29, No.3, 1958.)

4. Conference on Magnetism and Magnetic Materials, Philadelphia, 1958. (J. Appl.Phys., 30, No.4, Suppl., 1959.)

5. C.A.Neugebauer, Structure and Properties of Thin Films, Wiley, N.Y., 1959.

6. IBM Journal, 4, No.2, 1960. (Issue devoted to thin films.)

7. Conference on Magnetism and Magnetic Materials, (J.Appl.Phys., 31, No.5, Suppl., 1960).

8. L.Valenta, Izv.AN SSSR, Ser.fiz., 21, 879 (1957). (Trans.Bulletin, 21, 879.) (Towards a theory of spontaneous magnetization of thin films.)

9. R.L.Conger & F.S.Essig, Phys.Rev., 104, 915 (1956). (Resonance and reversal phenomena in ferromagnetic films.)

10. E.Bradley & M.Prutton, J.Electronics and Control, 6, 81, 1959.

11. K.M.Polivanov, in "Ferrity. Fizicheskie i fiziko-khimicheskie svoistva" (Ferrites. Physical and physical-chemical properties), Minsk, 1960. (Analysis of technical magnetization processes and their influence on its dynamics.)

12. R.Coren & H.J.Juretschke, J.Appl.Phys., 28, 806 (1957). (Hall effect and ferromagnetism of very thin nickel films.)

13. M.Prutton & E.M.Bradley, Proc.Phys.Soc., 75, 557 (1960). (Evaporated films of nickel-iron alloys.)

14. A.S.Mil'ner & L.I.Tatarinova, Fizika metallov i metallovedenie, (Trans. Physics of Metals and Metallography), 9, 673, 1960.(Electric and magnetic properties of nickel films deposited on glass.)

15. A.Corciovei, Czech.Phys.J., B 10, 568 (1960). (On ferromagnetism of thin layers.)

16. C.Kooy & U.Enz, Philips Res.Repts., 15, No.1, 7 (1960). (Experimental and theoretical study of the domain configuration in thin layers of $BaFe_{12}O_{19}$.)

17. M.S.Blois, Electronics, No.6, 210 (1955). (Evaporated magnetic materials.)

18. I.W.Wolf, 44-th Annual Tech.Proc.Am.Electroplaters Soc., 121, Discussion, 166 (1957). (Further studies on nickel-iron alloy electrodeposits.)

19. P.S.Zyryanov, Fizika metallov i metallovedenie (Trans.Physics of Metals & Metallography), 8, 801 (1959). (Electric conductivity of ferromagnetic metals in a radiofrequency field.)

20. M.I.Kaganov, Ibid., 7, 288 (1959). (Selective transparency of thin films.)

21. P.Tannenwald, IRE Wescon Conv.Rec., 3, Part 1, 134 (1959). (Properties of thin magnetic films for microwave applications.)

22. P.Tannenwald & M.Seavey, J.phys.et radium, 20, 323 (1959). (Microwave resonance in thin ferromagnetic films.)

23. A.Van Itterbeek and others, J.phys.et radium, 21, No.2, 81 (1960). (Ferromagnetic resonance in Permalloy films.)

24. D.Fraitova, Czech.Phys.Journal, B 10, 74 (1959). (Theory of ferromagnetic resonance in thin films.)

25. R.J.Heritage & M.T.Walker, J.Electronics & Control, 7, 542 (1959). (Chemically deposited nickel-cobalt films as high-speed storage elements.)

26. Electronics, 32, No.46, 92 (1959). (Parametric amplifier uses thin films.)

27. A.V.Pohm & E.N.Mitchell, Trans.IRE, EC-9, 308 (1960). (Magnetic films memories, a survey.)

28. E.V.Bradley, J.Brit.IRE, 20, No.10, 765 (1960). (A computer storage matrix using ferromagnetic thin films.)

INFLUENCE OF THE TECHNIQUE OF PREPARATION AND THICKNESS OF THIN FERROMAGNETIC FILMS OF Fe-Ni-Mo ALLOY ON THEIR DOMAIN STRUCTURE

- L.V.Kirenskii & V.A.Buravikhin

Thin ferromagnetic films are of interest from the standpoint of both theoretical physics and practical application. They are essentially two-dimensional and their properties differ from the properties of bulk, three-dimensional specimens. Specially prepared ferromagnetic films possessing uniaxial anisotropy, rectangular hysteresis loops and low coercive force, and characterized by a much higher rate of magnetization switching than ferrite cores can be used as storage elements in computers and control systems.

The rectangularity of the hysteresis loops of thin ferromagnetic films and the variation in their intrinsic coercivity with thickness are largely explained by the distribution of the magnetization vectors in the domains and the method of their preparation. The direction of the easy magnetization axis in films can readily be determined from the orientation of the domain structure.

Hence detailed investigation of the domain configuration of ferromagnetic films as a function of the conditions of preparation, thermomagnetic annealing, chemical composition and thickness, and study of the behavior of their domain structure in a magnetic field can be of help in choosing the most suitable and efficient elements for storage devices.

Some questions involved in the theory of the domain structure of thin ferromagnetic films have been considered in the work of Kittel[1] and Kaczer[2]. A number of authors have developed techniques for observing domain structure[3,4] and studying magnetization reversal[5-8] in thin ferromagnetic films. Aside from the work of Williams & Sherwood[8], there have been relatively few studies of the influence of the conditions of preparation and the thickness of ferromagnetic films on the domain configuration. In the present work we investigated the influence of the conditions of preparation, the thickness and magnetic annealing on the domain structure of films of 80% Ni + 17% Fe + 3% Mo alloy.

Experimental procedure

The films were prepared by volatilization of the Ni-Fe-Mo alloy from tungsten crucibles. Each crucible charge was completely vaporized. The films were deposited in a vacuum of $7 \cdot 10^{-6}$ mm on polished glass plates measuring 1 x 10 x x 40 mm. Prior to evaporation, the substrates were cleaned by means of a soap solution, potassium bichromate and alcohol, and outgassed by heating in vacuum to 450-500°. Most of the films were deposted in the presence of a magnetic field produced by a pair of Helmholtz coils. The field was aligned with the plane of the film. There were prepared films:

a) on substrates heated to 350° in the presence of magnetic fields of 125, 100, 75, 50, 25 and 4 oersted,

b) in an orienting field of 100 oe on substrates heated to 420, 350, 150 and 50°, and

c) films of thickness varying from 6150 to 140 Å at a substrate temperature of 350° in a magnetic field of 100 oersted.

The thickness of the films was measured by the optical procedure developed by Shklyarevskii[9]. The domain structure was brought out by the powder technique, the powder patterns being observed and photographed with an MBI-6 microscope.

The direction of easy magnetization in the films coincided with the direction of the magnetic field applied during the deposition.

Effect of the angle between the demagnetizing field and the axis of easy magnetication

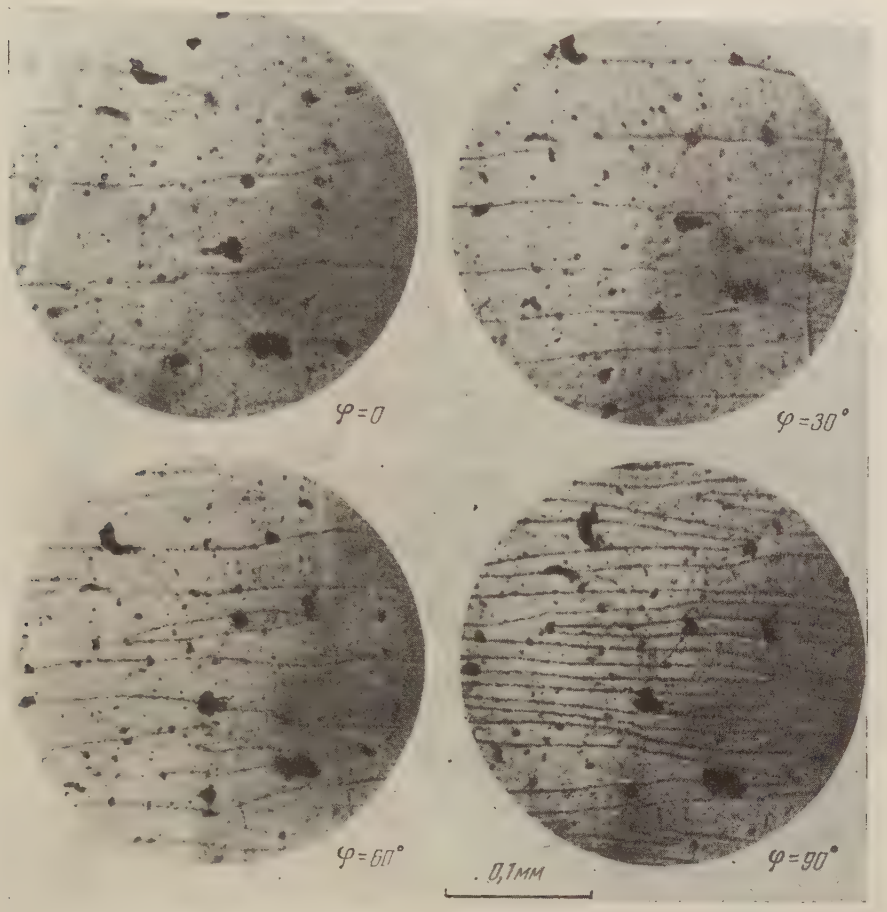

Fig.1. Influence of a demagnetizing field on the domain structure of a 1200 Å film. Film prepared in a 100 oe field; substrate temperature 350°; easy magnetization axis horizontal.

Fig.1 shows Bitter figures obtained on a film of 1200 Å thickness after demagnetization by an alternating field of decreasing amplitude, applied at angles of 0, 30, 60 and 90° to the easy direction. It will be evident from the photographs that the number of domain walls increases with increase of the angle between the demagnetizing field and the axis of easy magnetization, while the orientation of the walls remains the same, i.e., parallel to the orienting field applied during deposition.

Effect of the preparation field on the domain structure

The influence of the magnetic field applied during preparation of the films on the domain configuration was investigated on films of approximately the same thickness deposited on substrates heated to 350° in the presence of magnetic fields of different strength. It will be evident from the photographs reproduced in Fig.2 that in the film prepared in the presence of a 125 oe field the walls are parallel to this field. The parallelism of the walls extends over virtually the entire film, a slight curvature being discernible only at the edges. In the

Fig.2. Influence of the magnetic field applied during deposition on the domain structure. Substrate temperature 350°; easy magnetization axis vertical.

film prepared in the presence of a 100 oe field there is evident some bending of the walls, but none of the walls merge within the area of the film. The walls are also relatively parallel in films obtained in fields of 75 and 50 oe, but in this case there are breaks in the walls and there appear wedge-shaped domains. The undulation of the walls is appreciable in the film prepared in a 50 oe field. In the film obtained in a 25 oe field the walls become still more sinuous and in fact intersect each other.

In the film deposited in the absence of an orienting field there is still an easy magnetization direction which is apparently associated with the field produced by the substrate heater and vaporizer. Our measurements showed that this field equals approximately 4 oe, and in the film prepared in this field there is evident even greater distortion and interweaving of the walls.

Influence of substrate temperature on the domain structure

The films for these experiments were prepared in an applied field of 100 oe onto substrates heated to different temperatures. It will be evident from the photographs reproduced in Fig.3 that at substrate temperatures of 420, 350, 150 and 50° there were obtained films with a clearly evident domain structure oriented parallel to the applied field. In each case the domain structure was photographed 1 hour after preparation of the film. Films prepared on substrates heated to under 100° are mechanically unstable and oxidize rapidly. After the passage of 10 days the domain structure of these films is poorly evident or disappears entirely. In contrast, in the case of films deposited on substrates heated above 200° the domain structure is clearly discernible both immediately

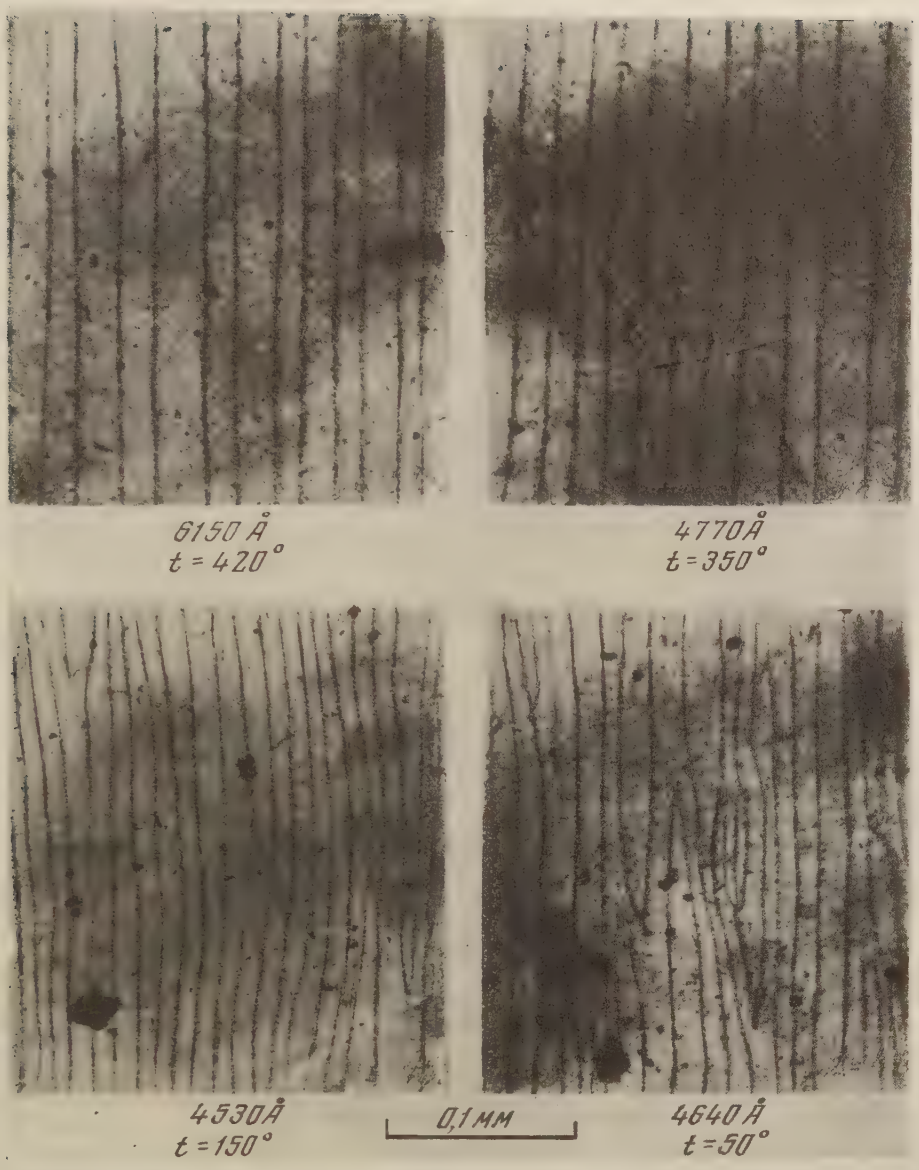

Fig.3. Influence of the substrate temperature on the domain structure of thin films. Preparation field 100 oe; easy magnetization axis vertical.

after deposition and three months later. These films are chemically stable and mechanically strong.

Influence of film thickness on the domain configuration

The thickness is one of the principal factors affecting the ferromagnetic properties of thin films, in particular the domain configuration. In this part of the study we observed the powder patterns on films up to 6150 Å thick. The photographs reproduced in Fig.4 show the domain structure of films of different thickness prepared on substrates heated to 350° in a 100 oe field. It will be

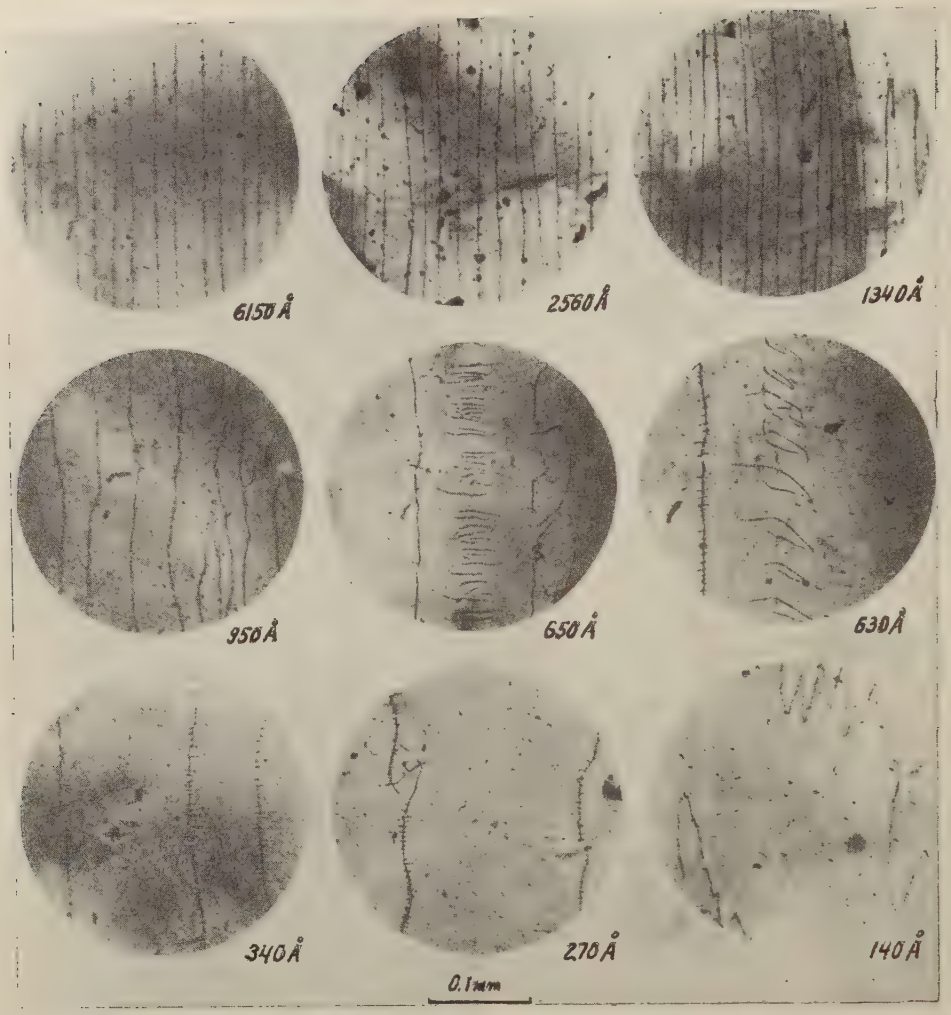

Fig.4. Domain configuration of films of different thickness. Films prepared in a 100 oe field; substrate temperature 350°; easy magnetization axis vertical.

evident from the photographs that the domain walls in films from 6150 to 1340 Å thick are almost parallel lines oriented in the direction of the applied field. In films of 1200 to 800 Å thickness, in addition to the more or less parallel walls, there are present curving walls, i.e., there appear domains in the form of wedges and loops. With further decrease of the film thickness, the walls become even more distorted and there are frequently observed zigzag boundaries. Moreover, in the thickness range from approximately 800 to 200 Å in films of the investigated alloy there are observed 180° walls traversed at definite intervals by "cross-ties", short transverse streaks with free ends. The spacing of these cross-ties and their length depend on the thickness of the film. The cross-ties are more closely spaced and become shorter with decrease in the film thickness. In 200 to 140 Å thick films the walls are greatly distorted; in this thickness range there are observed domains of different size and shape.

The curvature of the walls and the appearance of walls in the direction of difficult magnetization with decreasing film thickness can be explained by weakly

pronounced uniaxial anisotropy, low saturation magnetization, greater inhomogeneity of the films at the edges as compared with the central portion and by local stresses, which naturally are more strongly evinced at the edges of the films.

Effect of thermomagnetic annealing on the orientation of the easy magnetization axis

Films 530, 880 and 1200 Å thick prepared on an unheated substrate in the presence of a 100 oe field had their axis of easy magnetization parallel to this field. These films were then annealed in a vacuum of $2 \cdot 10^{-5}$ mm Hg for an hour at 450° in a 500 oe field. The annealing field was aligned with the plane of the film and directed at different angles relative to the easy magnetization axis. In all cases the powder patterns showed that heat treatment in the magnetic field changed the direction of the easy magnetization axis, reorienting it in the direction of the field applied during annealing.

Institute of Physics,
Siberian Branch of the USSR Academy of Sciences &
Krasnoyarsk State Pedagogical Institute

References

1. C.Kittel, Phys.Rev., 70, 965 (1946).
2. J.Kaczer, Ceskosl.casop.fys., 7, 516 (1957).
3. C.A.Fowler & E.M.Freyer, Phys.Rev., 104, 552 (1956).
4. M.Prutton, Philos.Mag., 4, 1063 (1959).
5. C.A.Fowler, E.M.Fryer & Z.Stevens, Phys.Rev., 104, 645 (1956).
6. R.W.Olmen & E.N.Mitchell, J.Appl.Phys., 30, 258 (1959).
7. C.E.Fuller, J.Phys.et radium, 20, No.2-3, 310 (1959).
8. H.Williams & R.Sherwood, J.Appl.Phys., 28, 548 (1957).
9. I.N.Shklyarevskii, Optika i spektroskopiya, 5, 617 (1958).

DOMAIN WALLS IN THIN FERROMAGNETIC FILMS

- L.V.Kirenskii & V.A.Buravikhin

In recent years there have been published a number of studies devoted to the structure and energy of domain walls in thin ferromagnetic films.[1-10]

It has been established theoretically that in the relatively thick ferromagnetic films the behavior of the magnetization vector in the wall layer is the same as in bulk ferromagnetic crystals. In the case of 180° neighbors the magnetization vector (in the process of reversal) gradually changes its direction from 0 to 180°, while remaining in the plane of the wall layer. In accord with the established terminology we shall refer to walls of this type as Bloch walls.

In thinner ferromagnetic films the magnetization vector in a 180° wall may not lie in the plane of this layer. Such walls may exhibit diverse types of structure. For brevity, we shall call walls of this type Néel walls.

In some cases there is observed twinning of the walls, i.e., formation of double boundary layers which consist of a system of two close walls. To both sides of such a wall the magnetization is oriented in the same direction. Upon the application of a field in the opposite direction, the field splits and there form domains of opposite magnetization.

In the present work we investigated the polarity of the walls in thin ferromagnetic films of different composition and thickness.

Most of the experiments were carried out with thin ferromagnetic films of 80% Ni + 17% Fe + 3% Mo alloy. The films were prepared by vacuum ($2 \cdot 10^{-5}$ mm Hg) evaporation onto glass substrates heated to 350°. Uniaxial anisotropy was realized by application of a 100 oersted field during deposition. The thickness of the films was determined on a universal UM-2 monochromator by means of lines of equal chromatic order (Shklyarevskii's technique[11]). The walls were observed by the magnetic suspension method (powder patterns) with the aid of an MBI-6 microscope. Prior to investigation the films were demagnetized.

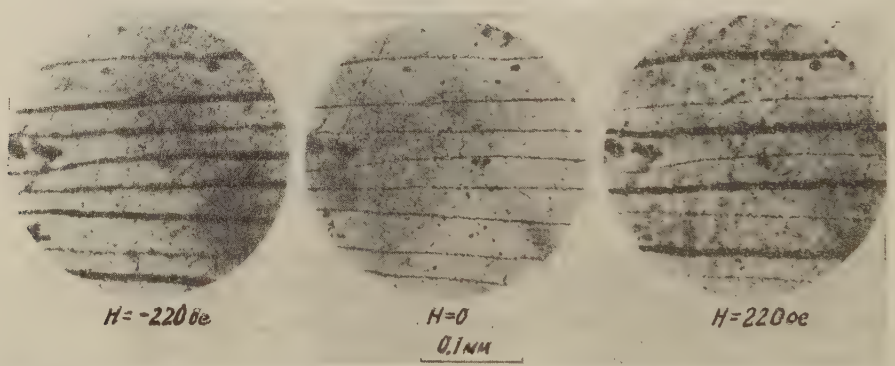

Fig.1. Wall polarity evinced as a result of application of a magnetic field normal to the plane of the film. Fe-Ni-Mo alloy film 1450 Å thick.

The domain structure of an Fe-Ni-Mo film 1450 Å thick is shown in Fig.1. In the absence of a field the domain structure of this film consists of almost plane-parallel domains with clearly evinced thin walls. Upon the application of a 220 oe field normal to the plane of the film the magnetic powder particles collect preferentially at every other wall. Upon reversal of the applied field the walls which were weakly evident become sharp and vice versa. This behavior was observed for a large number of different specimens and is evidence of the alternating

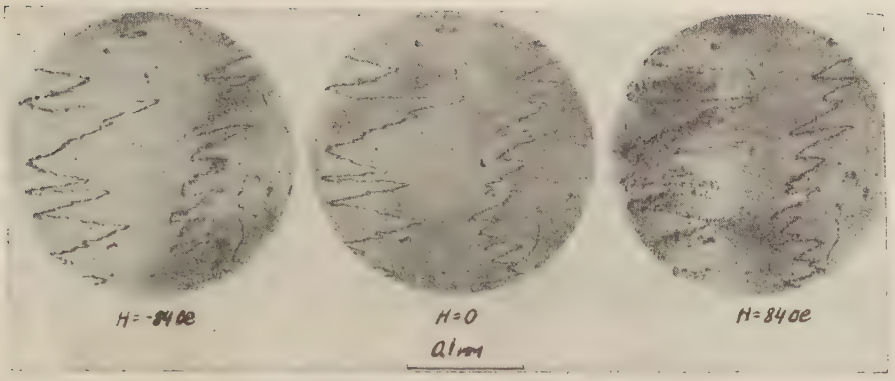

Fig.2. Alternation polarity of zigzag boundaries in a 1230 Å thick iron film.

polarity of Bloch walls in thin ferromagnetic films, which in general is not observed for bulk ferromagnetic crystals.

Alternating polarity of neighboring walls is observed not only in the case of rectilinear or almost rectilinear walls but also in the case of zigzag walls. This is shown for an iron film 1230 Å thick in Fig.2.

A different case is shown in Fig.3. Here the walls in a cobalt film 470 Å thick upon application of a 300 oe or higher field normal to the plane of the film do not exhibit the above mentioned alternating polarity. The same behavior was observed in the case of cobalt and Fe-Ni-Mo film less than 500 Å thick and iron films less than 250 Å thick.

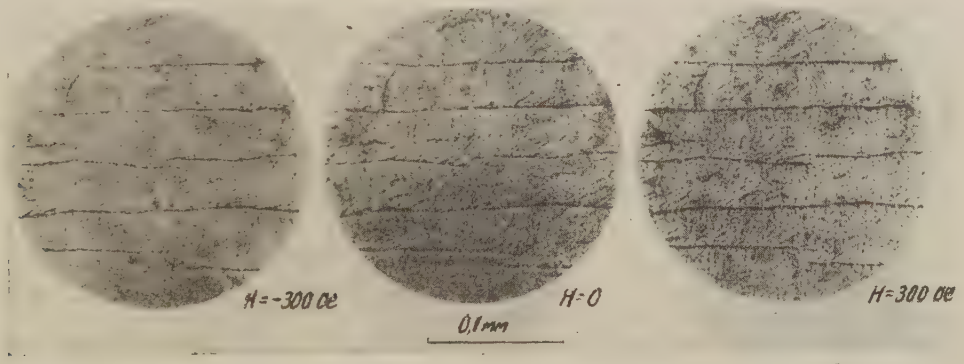

Fig.3. Same polarity of walls in a cobalt film 470 Å thick.

Obviously, the structure of the wall layers in such films is different from that in thicker films: here we are dealing with Néel type walls. In the case of such walls upon the application of a normal field there is sometimes observed an increase in the sharpness of all the walls, while sometimes the sharpness of the walls in the powder patterns remains virtually the same.

Fig.4 shows the domain structure of a 560 Å thick Fe-Ni-Mo alloy film with characteristic double walls. In the absence of a normal field the pattern consists of almost straight rather heavy lines. Upon the application of a normal field, it becomes evident that the double wall layer actually consists of two walls of different polarity. In a -10 oe field all the upper boundaries are

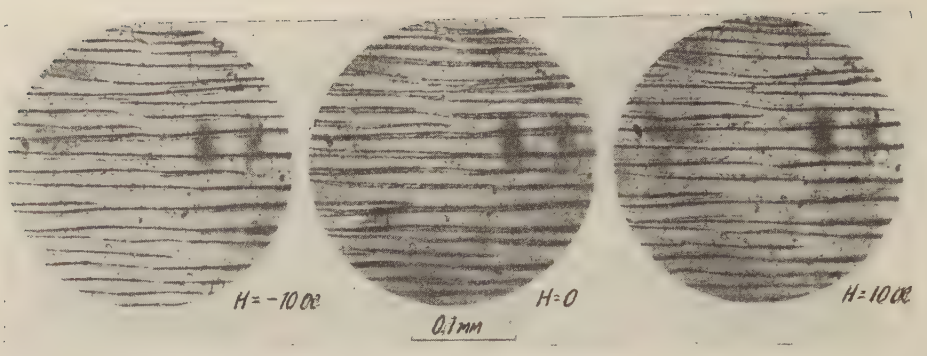

Fig.4. Double walls in an Fe-Ni-Mo alloy film 560 Å thick.

sharply evinced, while the lower ones are barely distinguishable. In a +10 oe field, on the contrary, the lower boundaries stand out sharply while the upper ones become faint. Thus, in accord with Kaczer's theory[5] the double boundary layer consists of a system of two close Bloch walls of opposite polarity.

Conclusions

1. Twin interdomain boundaries in thin ferromagnetic films are Bloch walls of opposite polarity.

2. Bloch walls in thin ferromagnetic films have alternating polarity, which makes it possible to detect the presence of such walls by application of a field normal to the film and changing the polarity of this field.

3. With decrease in the film thickness, beginning with a certain critical value depending on the composition of the film, there are formed Néel type walls. These walls do not exhibit alternating polarity and upon the application of a normal field of either polarity may become more clearly evinced.

Institute of Physics,
Siberian Branch of the USSR Academy of Sciences &
Krasnoyarsk State Pedagogical Institute

References

1. F.Bloch, Z.Phys., 74, 295 (1932).
2. L.Néel, Comp.rend., 241, 533 (1955).
3. H.Williams & R.Sherwood, J.Appl.Phys., 28, 548 (1957).
4. E.Huber, D.O.Smith & J.B.Goodenough, Ibid., 29, 294 (1958).
5. J.Kaczer, Ibid., 29, 569 (1958).
6. H.Stephani, Wiss.Z.Friedrich-Schiller-Univ., Jena, 7, H.4/5, 373 (1957/58).
7. H.W.Fuller & H.Rubinstein, J.Appl.Phys., 30, 84 (1959).
8. R.M.Moon, Ibid., 30, 82 (1959).
9. B.I.Gomi & J.Odani, Phys.Soc. (Japan), 15, 535 (1960).
10. H.Rubinstein, H.W.Fuller & M.E.Hale, J.Appl.Phys., 31, 437 (1960).
11. I.N.Shklyarevskii, Optika i spektroskopiya, 5, 617 (1958).

DOMAIN STRUCTURE AND COERCIVITY OF THIN FERROMAGNETIC FILMS

- L.V.Kirenskii, V.A.Buravikhin & A.G.Zvegintsev

There have been published a number of theoretical and experimental investigations of the thickness dependence of the magnetic properties of thin ferromagnetic films.[1-9]

The present work was concerned with experimental investigation of the domain dynamics of ferromagnetic films in a magnetic field as a function of the thickness and of the correlation between the coercive force and the character of the domain dynamics. It was established that the coercivity and the direction of easy magnetization are affected by annealing in a magnetic field. The investigation was carried out on films of 80% Ni + 17% Fe + 3% Mo alloy.

Experimental Procedure

The ferromagnetic films were prepared by evaporation of the Ni-Fe-Mo alloy in a vacuum of $8 \cdot 10^{-6}$ mm Hg from a tungsten crucible onto polished glass slides measuring 1 x 10 x 40 mm. Each crucible charge was fully vaporized within 30-40 sec. In view of this it may be asserted that the composition of the deposited film could differ only insignificantly from the initial composition. The evaporation was carried out in a 100 oersted field produced by a pair of Helmholtz coils. The field direction was parallel to the plane of the films. The easy magnetization axis in the films was aligned with this field. The ferromagnetic films intended for investigation of the domain structure and coercive force as a function of the film thickness were deposited on glass substrates heated to 300°. The other tilms were prepared on substrates at room temperature. The film thickness was measured on a universal UM-2 monochromator by means of lines of equal chromatic order.[10] An MBI-6 microscope was used for observing and photographing the powder patterns. The films were demagnetized by means of a decreasing ac field aligned with the axis of easy magnetization. In the annealing experiments the annealing was carried out in a vacuum of $2 \cdot 10^{-5}$ mm Hg in a 500 oe field parallel to the plane of the film. The coercive force was measured by the ballistic technique.

Experimental Results

Dependence of the domain structure, its variation in a magnetic field and the magnitude of the coercive force on the film thickness

The domain structure of a series of cobalt films of different thickness in the demagnetized state is shown in Fig.1. It will be evident from the photographs that with decrease in the film thickness the size of the domains increases and the walls show a greater tendency to distortion. In the 150 Å thick film there was visible only one wall dividing the film into two domains. In films thinner than 150 Å no domain structure was observed, although films 110 and 80 Å thick exhibited ferromagnetic properties. Probably these were single domain films.

The variation of the domain structure of cobalt films in a magnetic field may be described as follows.

1. Up to a certain critical field, the magnitude of which depends on the film thickness, the domain structure does not change.

2. In fields above the critical value the magnetization of films 800 Å and more thick is realized by wall motion.[8]

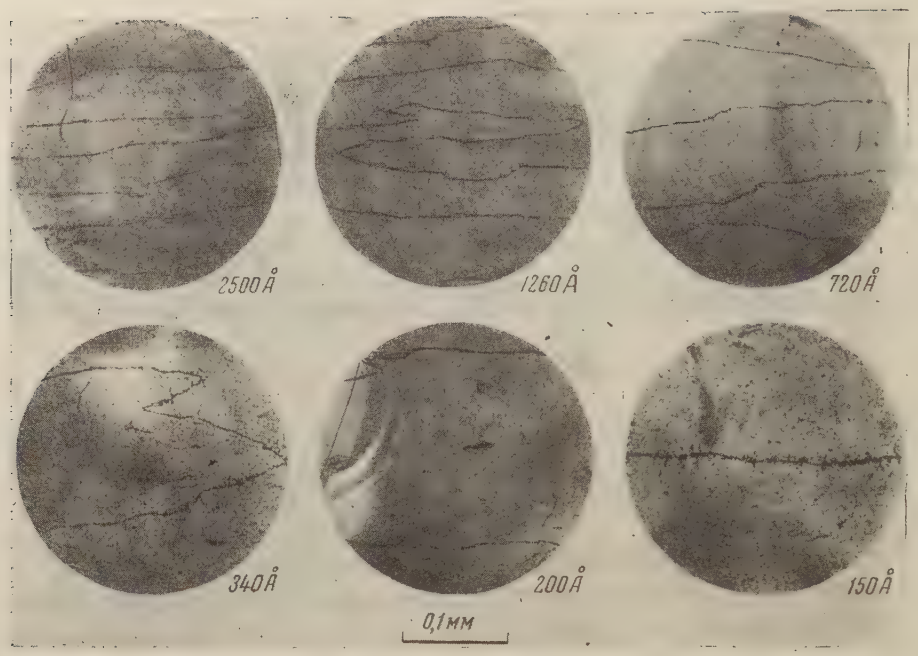

Fig.1. Domain configuration of cobalt films of different thickness. Films deposited on glass substrate heated to 300° in a 100 oe field; easy magnetization axis horizontal.

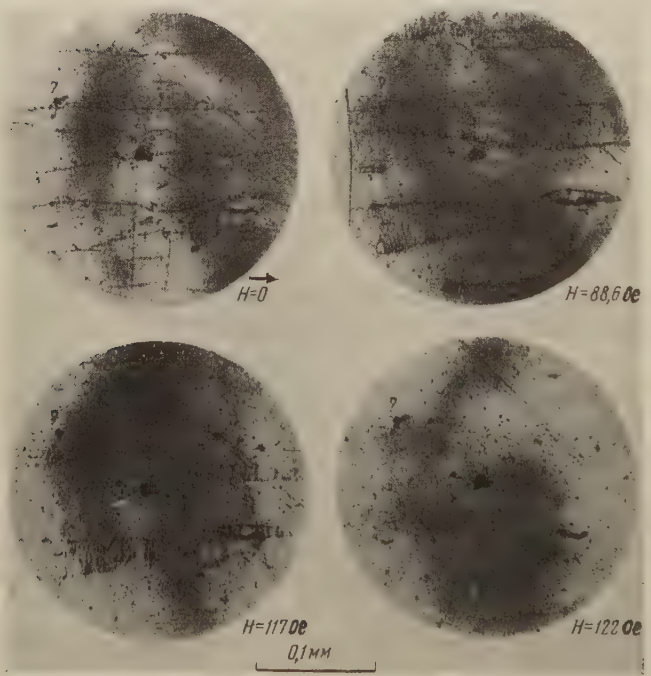

Fig.2. Variation of the domain structure by wall movement and rotation processes in a cobalt film 720 Å thick prepared by deposition on a substrate heated to 300° in a 100 oe field. Applied field and axis of easy magnetization horizontal.

3. In films from ~800 to 500 Å thick upon increase of the field above the critical value there appear in the domains disadvantageously oriented relative to the field new walls at right angles to the principal walls. This apparently occurs because individual parts of the disadvantageously oriented domains undergo changes in the magnetization vectors by rotation and the forming subdomains are separated by new walls. With further increase of the field there is a barely noticeable displacement of the walls and abrupt, discontinuous break-up of these domains to the point of complete disappearance. The successive steps in this process in the case of a 720 Å thick cobalt film are shown in Fig.2.

4. In the case of films ~500 to 150 Å thick no wall

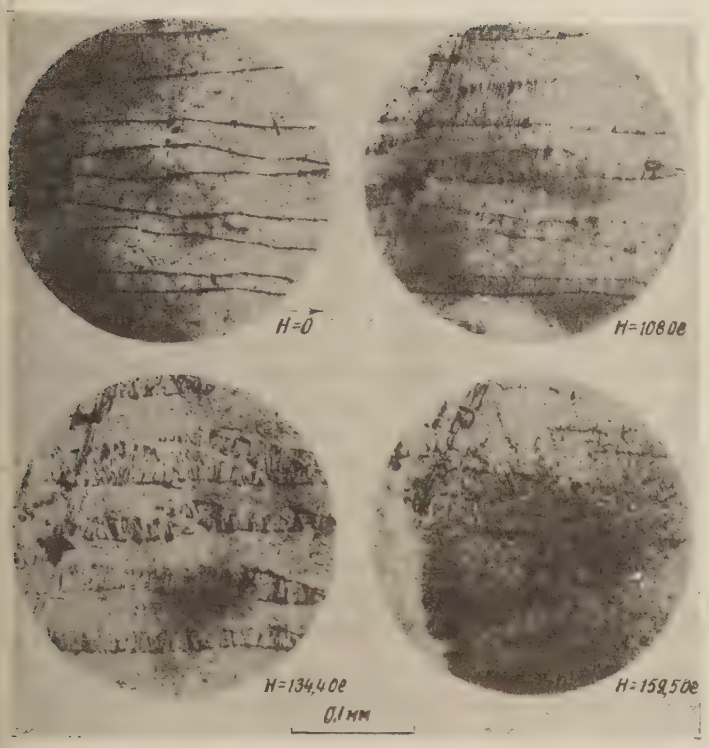

Fig.3. Variation of the domain structure by rotation processes in a 480 Å thick cobalt film deposited on a substrate heated to 300° in a 100 oe field. Applied field and axis of easy magnetization horizontal.

motion is observed, but at a certain field value there appear in the disadvantageously oriented domains new walls perpendicular to the principal walls. Reversal of the magnetization of these domains proceeds by break-up, i.e., apparently by rotation. The behavior of the domain structure in the case of a 480 Å cobalt film is illustrated in Fig.3. Magnetization reversal in single domain films also apparently occurs by uniform rotation of the magnetization vector.

The variation of the coercive force of cobalt and iron films as a function of their thickness is shown in Fig.4. From the above data on the behavior of the domain structure and the data of Fig.4 it follows that when the magnetization of the film is realized by wall movement, the increase in coercive force with decrease in film thickness is relatively slow. In cases when, in addition to barely noticeable wall motion, magnetization is realized primarily by rotation processes, the coercive force rapidly increases with decreasing thickness. It attains a maximum value in single domain films. With further decrease in the film thickness, the coercive force decreases. This can be explained by the general decrease of the magnetization itself. This correspondence between the coercive force and the behavior of the domain structure in a magnetic field as a function of the film thickness was also observed in the case of iron films and films of 80% Ni + 17% Fe + 3% Mo alloy. The film thickness dependence of the coercive force for Fe-Ni-Mo is shown in Fig.5.

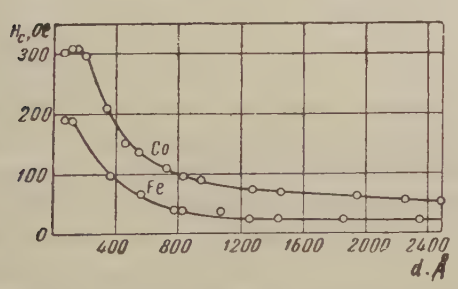

Fig.4. Variation of the coercive force of Co and Fe films with the film thickness.

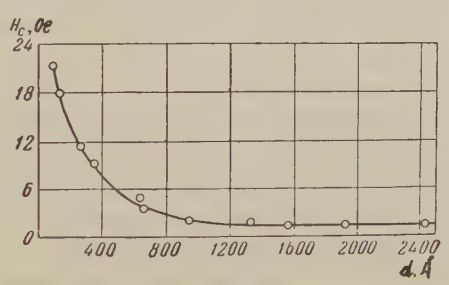

Fig.5. Variation of the coercive force of Fe-Ni-Mo alloy films with thickness.

Effect of vacuum annealing in a magnetic field on the coercive force and the orientation of the easy magnetization axis

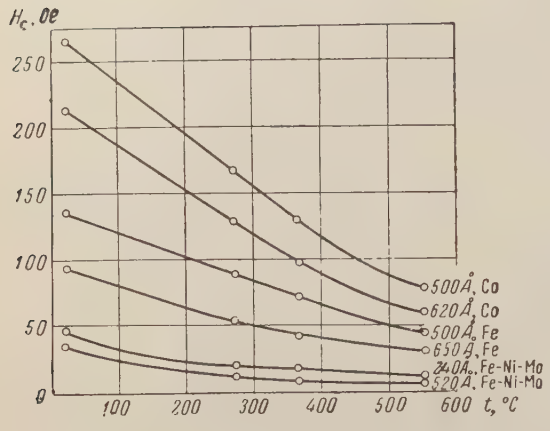

Fig.6. Variation of the coercive force of iron, cobalt and Fe-Ni-Mo alloy films as a function of the annealing temperature in a 500 oe magnetic field.

The variation of the coercive force of thin iron, cobalt and Fe-Ni-Mo alloy films deposited on unheated substrates as a function of the annealing temperature in a 500 oe field is shown in Fig.6. The holding time at the indicated temperature in each case was 1 hour. It will be evident from the figure that the coercive force decreases with increase of the annealing temperature; this can be explained by partial relief of the internal stresses, which are particularly high in films prepared on an unheated substrate. If the direction of the magnetic field during annealing does not coincide with the easy magnetization axis, the initial axis "disappears" and there appears a new easy axis parallel to the applied field.

Institute of Physics,
Siberian Branch of the USSR Academy of Sciences &
Krasnoyarsk State Pedagogical Institute

References

1. C.Kittel, Phys.Rev., 70, 965 (1946).
2. L.Néel, J.phys.rad., 17, 250 (1956).
3. L.Reimer, Z.Phys., 148, 527 (1957).
4. L.Reimer, Z.Naturforsch., 12a, 1014 (1957).
5. J.Kaczer, Ceskoslov.casop.fys., 7, 516 (1957).
6. Stephani, Wiss.Z.Friedrich-Schiller-Univ., Jena, Math.-naturwiss.Reine, 7, No.4-5, 373 (1957-1958).
7. C.A.Fowler, Jr., E.M.Fryer & Z.Stevens, Phys.Rev., 104, 645 (1956).
8. H.Williams & R.Sherwood, J.Appl.Phys., 28, 548 (1957).
9. C.E.Fuller, Phys.et radium, 20, No.2-3, 310 (1959).
10. I.N.Shklyarevskii, Optika i spektroskopiya, 5, 617 (1958).

DOMAIN STRUCTURE OF FERROMAGNETIC FILMS PREPARED BY CATHODE SPUTTERING

- G.V.Spivak, I.G.Sirotenko & R.D.Ivanov

At present there is need for preparing high quality ferromagnetic films with specified parameters. Usually ferromagnetic films are prepared either by vacuum evaporation or by electrolytic deposition. The principal shortcomings of the first procedure are significant deviation of the chemical composition of the film from that of the crucible charge and difficulty in controlling the film thickness. The electrolytic technique generally results in some degree of contamination of the formed films.

Reimer[1] prepared nickel films by cathode sputtering and investigated the thermal transformations in such films by electric measurements and electron microscopic observation. Siddall[2] considered the characteristics of cathode sputtering for preparing oxidized films and films of noble metals and developed a method of cathode sputtering in an alternating field.

It must be noted that earlier experiments[3] aimed at obtaining films by cathode sputtering were not free of faults. The sputtering was realized with weak currents in a glow discharge at pressures from 0.1 mm to several centimeters Hg. Owing to the short free path of the sputtered atoms, part of the sputtered material returned to the cathode because of back diffusion. The current densities in glow discharges in the inert gases were not high. Hence it was difficult to avoid the formation of contaminating layers on the sputtered surface and a long time was required for obtaining films of the desired thickness, which also led to some contamination and oxidation of the formed film.

In our experiments we carried out sputtering in the plasma of an intense, low pressure ($2 \cdot 10^{-2}$ to 10^{-3} mm Hg) discharge. Under these conditions the free path of the sputtered ions was substantially greater than the distance from the bombarded target to the substrate.

The sputtered specimens were introduced into the plasma in the form of a third electrode maintained at a high (~1 kv) negative potential. To increase the discharge current, and consequently, the ion density, we used a hot cathode. The discharge current was usually of the order of an ampere; the current to the sputtered specimen of the order of a milliampere.

The films were formed on glass substrates located at a distance of 2-3 cm from the target.

The sputtered specimens were disks of ~1 cm^2 area. The relative sizes of the sputtered target and the substrate insured relatively uniform formation of the film in thickness. Our apparatus had provision for successively sputtering on several (up to 6) films without interrupting the sputtering process. The film thickness could readily be controlled by varying the sputtering time. Hence in employing cathode sputtering one can, without difficulty, obtain films of any desired thickness. The thickness of the films was measured in a MII-5 microinterferometer.

The thickness of Mo-Permalloy (79% Ni, 17% Fe and 4% Mo) films increased linearly with time (up to 30-35 min) under the following sputtering conditions: specimen potential 800 v, discharge current 0.75 amp, current density 1.6 ma/cm^2, pressure $9 \cdot 10^{-3}$ mm Hg. The glass substrates were heated to 100-125°, the temperature being monitored by a thermocouple. The films were deposited in a 175-200 oe magnetic field in the plane of the film. A significant point is that this magnetic field also acted to concentrate the plasma in the region of the sputtered specimen. The films were not subjected to magnetic annealing.

It is known that in the case of deposition by evaporation the composition of the films differs to an appreciable extent from that of the initial material.

Fig.1. Domain structure of silicon iron film 1000 Å thick. Magnification 250 X.

In contrast, chemical and spectroscopic analyses of the films prepared by cathode sputtering showed that their composition virtually did not differ from that of the initial material (the difference did not exceed some tenth of a percent).

We observed the Bitter figures on a 800 Å thick cobalt film, demagnetized by a decreasing alternating field. The direction of easy magnetization agreed with the direction of the forming field.

Sputtering of silicon iron was carried out under the following conditions: specimen potential 700 v relative to the cathode, current density 6 ma/cm^2, discharge current 1 amp, pressure $8 \cdot 10^{-3}$ mm Hg, sputtering time 30, 20 and 10 min.

On films of silicon iron (3.3% Si) 1000 Å thick there were first evinced

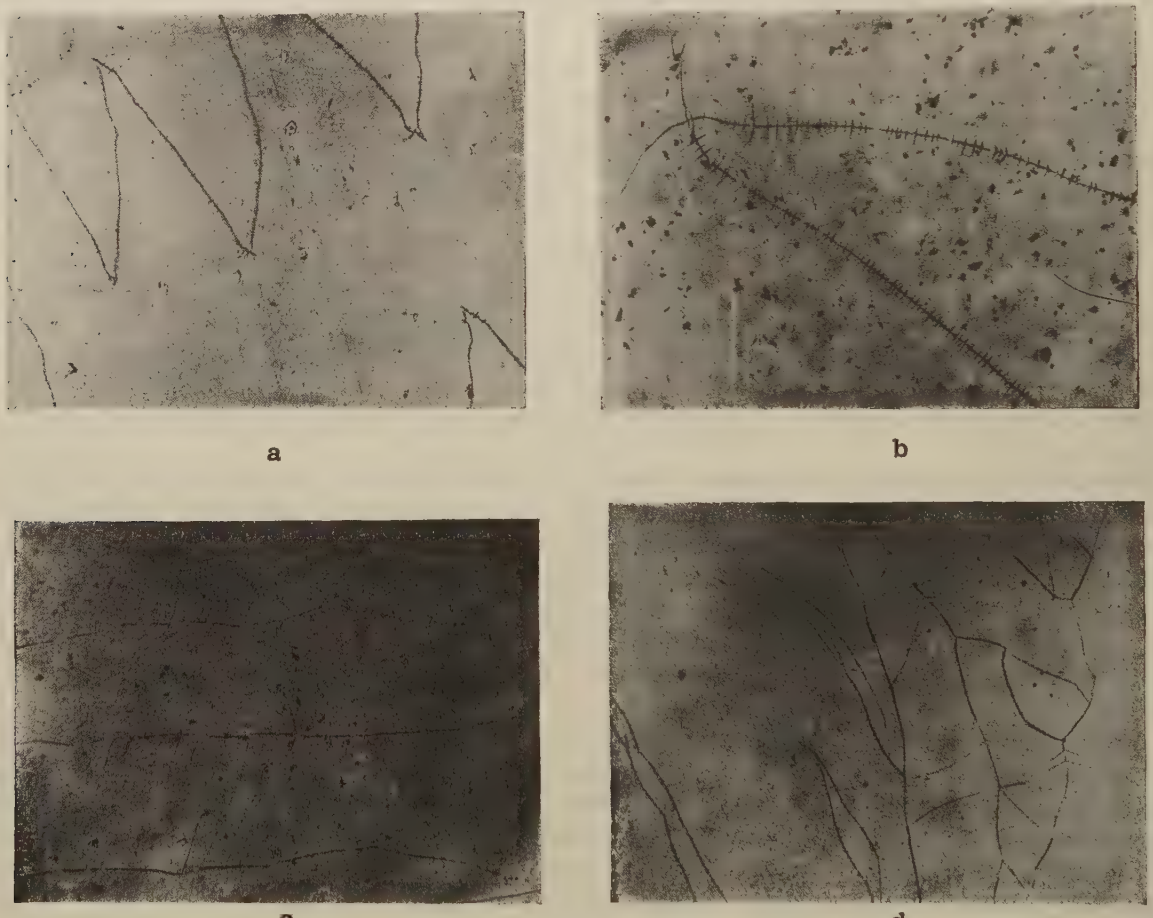

a b c d

Fig.2. Powder patterns on Mo-Permalloy films: a) 800 Å, b) 1200 Å, c) 2500 Å, d) 3000 Å thick. Magnification 250 X.

wedge-shaped domains oriented in the direction of the field (Fig.1). The principal domain walls are interrupted by short transverse boundaries.

Films of the 79% Ni + 17% Fe + 4% Mo alloy were sputtered on under conditions of linear increase of thickness with time. However, sputtering can also be realized under "forced" conditions, under which the rate of deposition increases sharply: discharge current 1 amp, specimen potential 1.2 kv, current density on specimen 2.6 ma/cm^2, pressure $8 \cdot 10^{-3}$ mm Hg. The Bitter figures appearing on the surface of Permalloy films of different thickness are shown in Fig.2.

Huber et al[4] and Moon[5] studied the variation of the domain structure of Fe-Ni alloys films as a function of thickness. The former proposed a model for the formation of domain structure with transverse (cross-tie) walls interrupting the main domain boundaries.

We followed the variation of the domain structure with increase of the film thickness up to 3000 Å.

At a thickness of 500 Å there begins breaking up of the principal domain boundaries by transverse walls spaced at approximately equal intervals. With increase of the thickness (Fig.2,a & b) the domain structure becomes somewhat coarser; the spikes extend along the field, forming "whiskers" at the ends. The formation of the short cross-ties on the principal wall can be explained by means of the mechanism proposed by Huber et al[4]. Further increase of the film thickness (Fig.2,c) leads to evening out of the spikes into parallel walls extending over the entire length of the film in the direction of the field. The cross-tie walls also grow, but not perpendicularly to the main walls: they branch off at the main wall and extend in the direction of motion of the last. In some cases the transverse walls extend to connect the main boundaries. With further increase of the film thickness to 3000 Å (Fig.2,d) there occurs complete fragmentation of the principal walls. The wall configuration becomes complex with no predominant direction. It is difficult at present to interpret the observed domain dynamics by means of the model proposed by Huber et al.

Fig.3. Powder patterns at points of mechanical damage and inclusions in Permalloy film 2500 Å thick. Magnification 250 X.

Williams & Sherwood[6] showed that various defects (scratches or inclusions) in the case of small film thicknesses remain inside the walls or the walls border on the scratches. But with increase of the film thickness (Fig.3) defects become the nuclei of new domain walls, the configuration of which differs in different cases[7].

Conclusions

1. Materials with any melting point may be subjected to cathode sputtering.
2. Films of different thickness may be prepared under controlled conditions by cathode sputtering.
3. Through appropriate choice of sputtering conditions uniform deposition is assured.
4. A particular advantage of cathode sputtering is that by this procedure

one can obtain films differing little in composition from the composition of the initial material.

Physics Faculty
Moscow State University

References

1. L.Reimer, Z.Phys., 149, 425 (1957).
2. G.Siddall, Proc.Inst.Electronics, 3, 1, 34 (1958).
3. G.Wehner, Advances Electronics and Electron.Phys., 7, 239 (1955).
4. E.E.Huber, D.G.Smith & J.B.Goodenough, J.Appl.Phys., 29, 294 (1958).
5. R.M.Moon, J.Appl.Phys., 30, 4, 82 (1959).
6. H.Williams & R.Sherwood, J.Appl.Phys., 28, 548 (1957).
7. Y.Gomi & Y.Odani, J.Phys.Soc.of Japan, 15, 3, 535 (1960).

INVESTIGATION OF THE MAGNETIC STRUCTURE OF THIN FERROMAGNETIC FILMS BY MEANS OF THE KERR MAGNETO-OPTICAL EFFECT

- L.V.Kirenskii, S.V.Kan & I.F.Degtyarev

Magneto-optical techniques for observing the domain structure of bulk specimens, based on application of the Kerr effect, were developed only a relatively short time ago.[1,2]

By coating the specimen with a layer of dielectric or semiconductor one can facilitate visual observation of the domain structure.[3,4]

Fowler, Fryer & Stevens[5] carried out successful studies of the magnetic structure of thin films, making use of a complicated negative-positive superposition procedure.

In 1959 Prutton[6] published a brief report describing a procedure and set-up for visual observation of the domain structure of ferromagnetic films. However, Prutton does not give any significant data on the behavior of the domains. Thus, there have been few investigations of the domain structure of films by magneto-optical techniques. Published data on the domain structure of thin films have been obtained primarily by the powder technique, which has a number of serious shortcomings.

1. The resolving power of this procedure in some cases is limited by the size of the powder particles. For example, the width of the powder lines cannot be considered to be equal to the width of the domain walls, inasmuch as the particle dimensions are commensurate with or may even be greater than the thickness of the investigated ferromagnetic film. Hence it is difficult to say to what degree the observed powder patterns represent the true magnetic structure of the film.

2. It is impossible by means of powder patterns to reveal Néel interdomain boundaries owing to the absence of a field component along the normal to the surface of the film.

3. It is difficult or impossible to observe the dynamics of rapid domain processes owing to inertia of the powder particles.

4. The powder technique can be used only in a narrow temperature range limited by the freezing and boiling points of the suspension.

Hence there is definite interest in investigating the magnetic structure of thin ferromagnetic films by other methods, inasmuch as these may prove to be free of some or all of the above shortcomings. In the present work we studied the magnetic structure of thin ferromagnetic films by the longitudinal Kerr magneto-optical technique.

Specimens and Experimental Procedure

The thin ferromagnetic films for observation were prepared by vacuum (10^{-5} mm Hg) evaporation of 17% Fe + 80% Ni + 3% Mo alloy onto polished glass substrates heated to 350°C. To realize uniaxial magnetic anisotropy a magnetic field of 100 oersted parallel to the surface of the substrate was applied during deposition.

To permit visual observation and photographing of the domains a thin dielectric layer of zinc sulfide was applied by vacuum evaporation onto the films heated to 250°. In order to minimize the deranging effect of heating on the anisotropy of the films, a magnetic field of 70 oersted in the same direction as during deposition of the metal was applied during evaporation of the zinc sulfide. The dielectric layer significantly increases the angle of rotation of the plane of polarization, as a result of which the contrast between neighboring domains is increased sufficiently to permit visual observation. The clearest figures are

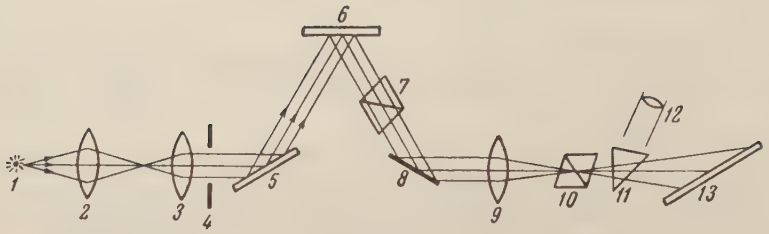

Fig.1. Diagram of the optical part of the set-up: 1) light source, 2) condensing lens, 3) collimator, 4) aperture, 5 & 6) mirrors, 7) polarizer, 8) specimen, 9) lens, 10) analyzer, 11) prism, 12) viewing eyepiece, 13) photographic plate.

observed when the ferromagnetic film is coated with a zinc sulfide layer of such thickness that the coating appears light brown. In repeat observations of the specimens three months after preparation no significant changes in the behavior of the domains and the zinc sulfide coating were noticed.

The domain structure observations were carried out on films in the form of rectangles measuring 8 x 36 mm and circular disks from 2 to 8 mm in diameter. In the case of the rectangular films, the field of observation was limited to the central 7 x 5 mm region. The thickness of the ferromagnetic films was determined by the optical method developed by Shklyarevskii[7].

The experimental set-up was assembled about an MIM-8M metallographic microscope. A diagram of the optical part of the set-up is shown in Fig.1. Inasmuch as the MIM-8M microscope is assembled on a vertical stand, while for observation of the longitudinal Kerr effect one must have oblique incidence of the light, the set-up incorporated mirrors (5 & 6 in Fig.1) oriented to direct the light onto the specimen at an angle of 60°. The specimen stage was designed so that the specimen could be displaced in two mutually perpendicular directions in its plane and rotated about an axis normal to its surface. The set-up also has provision for rotation of the electromagnet by means of which a magnetic field was applied to the specimen.

Polarized light passing through the lens 9 and analyzer 10 was reflected from the mirror face of prism 11 and entered the viewing eyepiece 12. For photographing the patterns the prism was swung out of the way and the light was directed onto the photographic plate 13 tilted at an appropriate angle to obtain a sharp image of the patterns. The photographing was usually carried out with fivefold magnification; visual observation, by interchange of the eyepieces, could be carried out at magnifications up to 30 x.

Results of Observation

The magnetic properties of different batches of film prepared under identical conditions proved to be different. We attribute this to the influence of a number of uncontrollable factors operating during deposition of the metal film.

The direction of the axes of easy and difficult magnetization was determined by observation of the domain structure realized in demagnetized films. Other conditions being equal, the domains in the case of demagnetization along the easy magnetization axis assume the shape of elongated formations with parallel edges and increase in size. Upon the application of an increasing constant field at an angle of 90° to the direction of easy magnetization, there is observed decrease of the contrast between neighboring domains without any noticeable change in their configuration (in the case of correct determination of the easy direction) or

growth of the more advantageously oriented domains (in case of inaccurate determination of the easy direction). Thus by observation of the domain behavior during the magnetization one can readily determine the direction of the easy and difficult axes.

Effect of the conditions of demagnetization on the domain structure

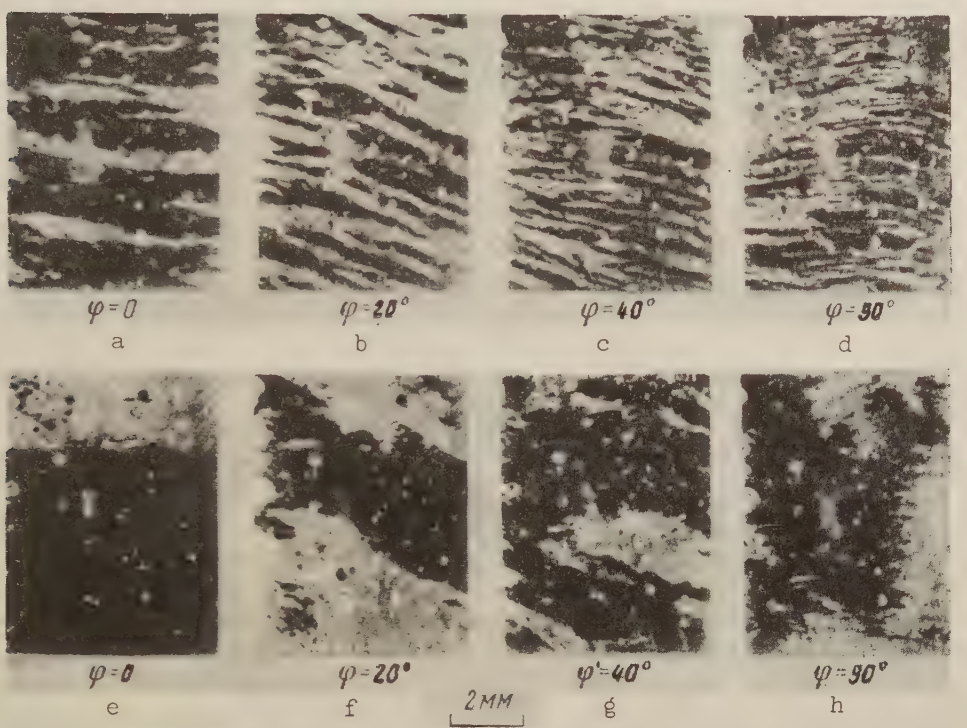

Fig.2. Patterns on a 580 Å thick film obtained with different conditions of demagnetization: top photograph - slow demagnetization; bottom photograph - rapid demagnetization. Axis of easy magnetization horizontal.

Films prepared in an orienting magnetic field usually remain in the saturated state and without preliminary demagnetization no domain structure is revealed. For observation the films were demagnetized by an alternating field of decreasing amplitude.

Photographs of the same section of film demagnetized at different angles relative to the easy axis and at different rates of decrease of the alternating field are reproduced in Fig.2. According to Fowler et al[5], very thin films (500 Å) are usually single-domain specimens and are very difficult to force into the demagnetized state. The film under consideration, which had a thickness of 580 Å, however, was readily demagnetized, which is probably due to its inhomogeneity. One can judge of the inhomogeneity of this film from the character of the variation of the magnetic structure during magnetization (see below). With increase of the angle between the direction of the demagnetizing field and the easy axis in the case of slow demagnetization the figures become finer, more irregular and chaotic (Fig.2,a-d) and may assume a slight inclination (Fig.2,b, c,f & g) relative to the easy direction. Analogous domain behavior was observed for a number of films. In the case of rapid demagnetization (~100 oe/sec) the

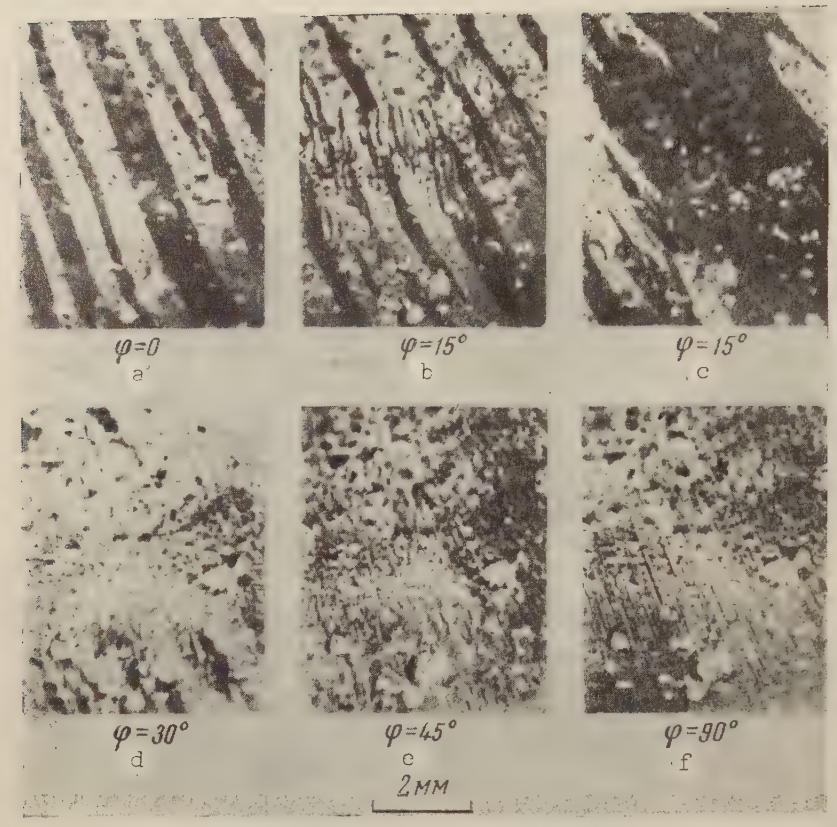

Fig.3. Figures on a 1100 Å thick films obtained during demagnetization at different angles.

figures are appreciably larger in size (Fig.2, e-h) than in the case of slow (~0.6 oe/sec) demagnetization (Fig.2, a-d). This difference was observed for all the investigated films.

The strong influence of the demagnetizing conditions of the domain configurations will be evident from the photographs of Fig.3. The photographs reproduced in this figure (except c) were obtained with slow demagnetization. With an angle $\varphi = 15^{\circ}$ between the demagnetizing field and the easy direction, the antiparallel domains in the central part of the specimen are fragmented into fine figures (Fig. 3,b); such figures do not appear in the case of rapid demagnetization in the same direction (Fig.3,c). With increase of the angle φ the process of fragmentation of the domains is intensified and extends to the edges of the film. In Fig.3 at opposite edges there can still be discerned relatively large dark figures. In the φ range from 45 to 90° the entire surface of the film exhibits a fine, chaotic structure with weak contrast. It may be noted that in the case of demagnetization along the difficult magnetization axis there is established a structure consisting of fine straight bands parallel to the easy axis (Fig.3,f). The figures shown in Fig.3 (except c) are satisfactorily reproduced in repeat demagnetizations.

Variation of the domain structure during magnetization

Six stages in the magnetization of a 580 Å thick film with the magnetizing field in the direction of the easy axis are shown in Fig.4.

Upon application of an increasing field, the domain structure in the range from 0 to 6 oersted does not undergo any noticeable changes. At a field strength somewhat exceeding 6 oersted, the domains magnetized along the field (light figures) begin to absorb the antiparallel domains (dark figures) in small discrete steps. In the illustrated case, this process of absorption begins in the upper right-hand corner of the film and, upon attainment of a field of 6.4 oersted, an appreciable part of the upper domain (Fig.4,b) undergoes abrupt magnetization reversal. With further increase of the field, the process of discontinuous reversal of the domains magnetized against the field extends downward (Fig.4, c-f),

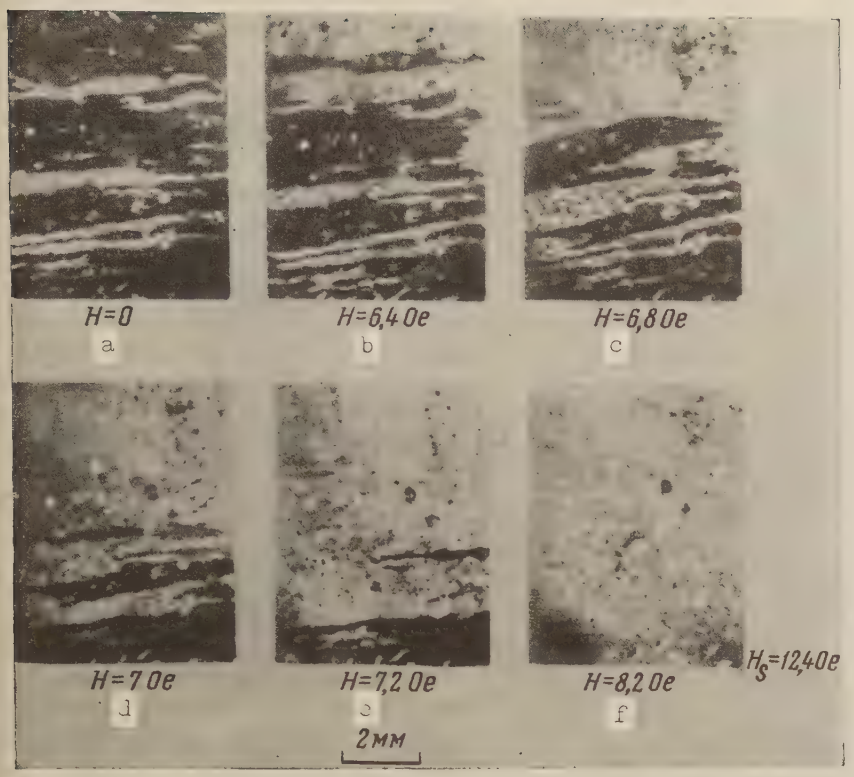

←Fig.4. Stages in magnetization of a 580 A thick film in the direction of the easy magnetization axis (horizontal). H_S = saturation field.

Fig.5. Process of magnetization of an 800 Å thick film at different angles relative to the easy axis. H_S = saturation field. ⟶

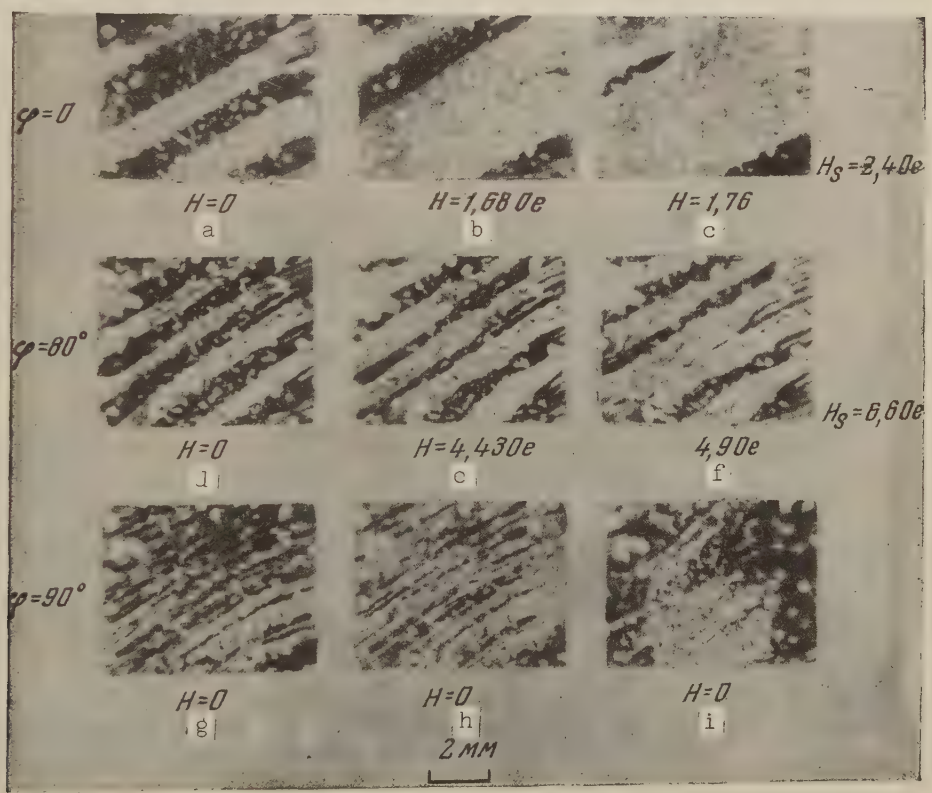

which is presumably indicative of inhomogeneity of the film in thickness. In Fig.4,f, in the lower left-hand corner, there are discernible small unswitched islets blocking the walls of the reversed domains. These islets are probably associated with inclusions.

A distinctive feature of this film is that in it there are no discernible wall displacements.

An entirely different picture is observed in the case of magnetization of a uniform film 800 Å thick. It proved very difficult to demagnetize this specimen in the direction of the easy magnetization axis. For the most part this film behaves as a single-domain specimen, persisting in the state of saturation.

The photographs reproduced in Fig.5 illustrate the process of magnetization of this film at different angles φ relative to the easy magnetization axis (the light spots in the photograph are due to defects in the zinc sulfide coating). In the demagnetized state the structure of this film consisted of antiparallel domains (Fig.5,a,d & g) oriented roughly along the direction of easy magnetization, regardless of the direction of demagnetization (in the case of demagnetization in the easy direction there is rarely established a structure of straight antiparallel domains). As will be evident from the photograph, with increase of the angle φ the domain structure becomes increasingly fine.

The process of magnetization is realized by smooth movement of the walls (Fig.5, a-f). This is clearly evident from a comparison of Fig.5,d and e: the domains magnetized against the field (dark figures) have become narrower than the same domains in the absence of a field. With increase of the angle φ from 0 to 80° the general character of the magnetization process does not change, but the wall motion is realized more smoothly and in stronger fields. In the case of magnetization in the difficult direction no wall movement is observed. With increase of the field strength the contrast between neighboring domains

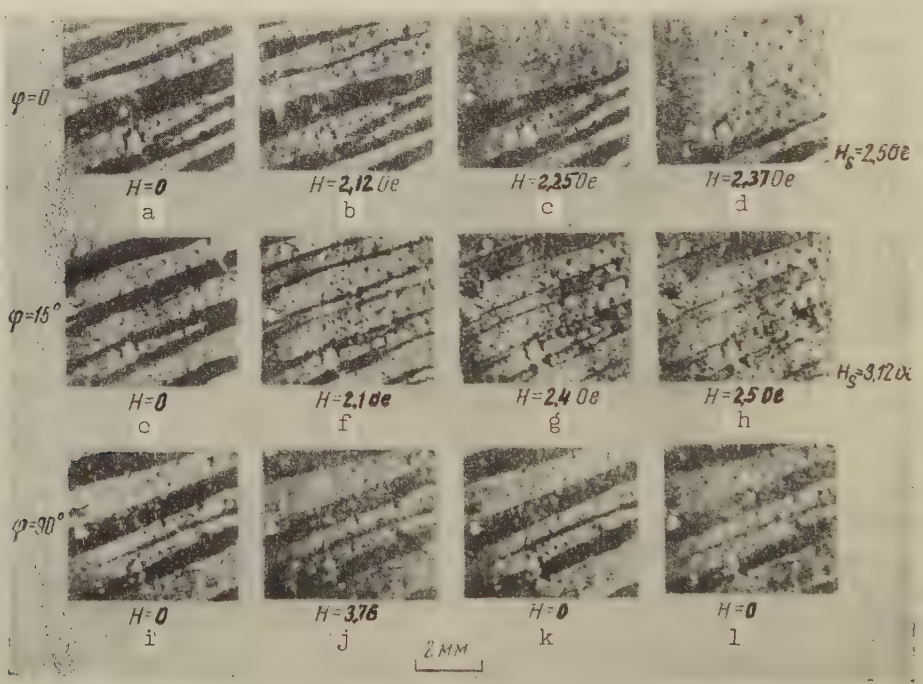

Fig.6. Process of magnetization of a 1100 Å thick film at different angles to the easy magnetization axis, which approximately coincides with the direction of the figures in photograph a.

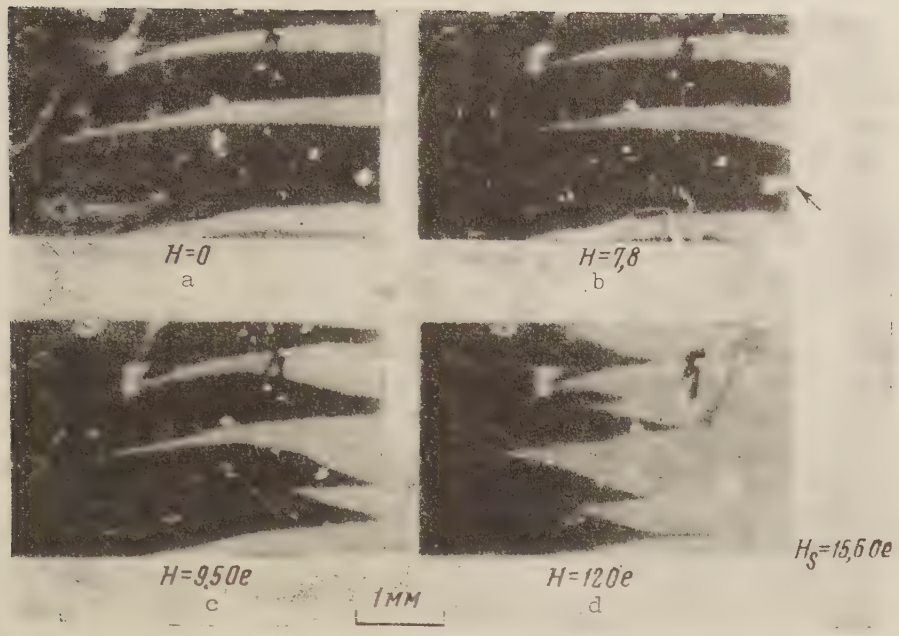

Fig.7. Process of magnetization of a 1750 Å thick film in the direction of the easy magnetization axis.

decreases but their configuration does not change, which is apparently due to rotation of the magnetization vector I_s inside the domains.[6] When the magnetizing field reached a value of 6.5 oersted, the figures became almost unnoticeable, but upon removal of the field the structure shown in Fig.5,h was re-established; this differed, however, from the initial structure (Fig.5,g) in that the dark strips became shorter at the right edge of the film. Upon removal of a magnetizing field of 20 oersted there is revealed an entirely different and less contrasting structure (Fig.5,i); an analogous structure is established upon removal of fields of up to 500 oersted.

The photographs reproduced in Fig.6 show the process of magnetization of a 1100 Å thick film. As a result of demagnetization in the easy direction there is established a structure consisting of straight antiparallel domains (Fig.6,a,e & i).

The process of demagnetization in directions close to the axis of easy magnetization is realized approximately in the same way as in the case of the preceding film. At angles φ close to 45° the process of magnetization is entirely different. With gradual increase of the magnetizing field there is observed lightening of the dark bands; this lightening begins at the center of the domains and extends smoothly towards the edges, as a result of which, instead of the dark band there are obtained two dark lines separated by a light gap (Fig. 6,f). With increase of the field strength this process continues and the lines become thinner (Fig.6,g & h). At a certain field strength these lines disappear, and upon removal of the field are not re-established. It should be noted that the configuration of the domains does not change, and in case of reversal of the magnetizing field direction there is observed an analogous picture with light bands instead of dark.

In case of magnetization in directions close to the axis of difficult magnetization there occurs decrease (equalization) of the contrast of the figures, i.e., the dark figures become somewhat lighter, while the light figures become darker, but the shape of the domains does not change. This will be evident from a comparison of Figs.6,i and j. Upon removal of the magnetizing field the contrast between the domains is re-established (Fig.6,k). When the field strength was brought up to 18 oersted the figures became almost unnoticeable, but upon removal of the field they reappeared (Fig.6,l), only the contrast between neighboring domains became weaker. After removal of a 100 oersted field the figures were not re-established.

The process of magnetization along the easy axis of a section of 1750 Å film having the form of a 6 mm diameter disk is shown in Fig.7.

A predominant role in the magnetization of this film is played by the appearance and growth of advantageously oriented domains in the form of spikes. Thus at a field of 7.8 oersted at the base of the lower dark band (Fig.7,b) at the right edge there appears a nucleus of reverse magnetization in the form of a light small wedge (arrow). With increase in the field strength, the number of spikes increases and they grow by smooth motion of the walls (Fig.7, c & d) in the direction of the tips of the spikes. With increase of the angle, the spikes become finer and are inclined at a slight angle to the field direction.

Conclusions

Investigation of the domain structure of thin films of 17% Fe + 80% Ni + 3% Mo alloy showed that their magnetic structure is greatly affected by the conditions of demagnetization. Observations showed that there obtained the following regularities.

1. With increase of the angle between the direction of demagnetization and the easy magnetization axis there is established a finer domain structure.

2. In the case of rapid demagnetization there is revealed, as a rule, a structure consisting of large domains, generally of irregular shape. In the case of slow demagnetization there is established a fine structure of relatively regular domains.

In investigating the process of magnetization the following was observed.

1. In thin (500-600 Å) and inhomogeneous films the growth of domains more advantageously oriented relative to the applied field is realized discontinuously, i.e., by jumps, without discernible smooth wall movement.

2. With increase of the film thickness and of the angle between the applied magnetic field and the easy magnetization axis and with increase in homogeneity of the films, wall movement becomes increasingly smoother. With magnetization in the difficult magnetization direction the configuration of the domains does not change but the contrast between neighboring domains is gradually effaced (equalized) to the point of complete disappearance upon the attainment of saturation. Upon removal of the magnetizing field the contrast between domains is partially re-established.

3. In case of application of the magnetizing field at an angle $\varphi = 45^{\circ}$ there is observed lightening of the dark bands (or darkening of the light bands), which begins from the center of the domains and extends towards their edges (to the walls), terminating in the formation of two lines coinciding with the walls.

Institute of Physics,
Siberian Branch of the USSR Academy of Sciences &
Krasnoyarsk State Pedagogical Institute

References

1. H.J.Williams, F.A.Foster & E.A.Wood, Phys.Rev., 82, 119 (1951).
2. C.A.Fowler & E.M.Fryer, Ibid., 94, 52 (1954).
3. L.V.Kirenskii & I.F.Degtyarev, Zhur.eksp.i teor.fiz., 35, 584 (1958). (Trans.Soviet Physics - JETP.)
4. I.Kranz & W.Drechsel, Z.Phys., 150, 632 (1958).
5. C.A.Fowler, E.M.Fryer & T.Stevens, Phys.Rev., 104, 645 (1956).
6. M.Prutton, Philos.Mag., 4, 45, 1063 (1959).
7. I.N.Shklyarevskii, Optika i spektroskopiya, 5, 617 (1958).

BEHAVIOR OF THE DOMAIN STRUCTURE OF THIN FERROMAGNETIC FILMS IN THE PROCESS OF SLOW MAGNETIZATION REVERSAL

- L.V.Kirenskii & S.V.Kan

In recent years, particularly after publication of the theoretical work of Kittel[1], there have been carried out extensive studies of the magnetic properties of thin ferromagnetic films. One of the core problems in investigating thin films is study of the process of magnetization reversal or switching, since this is of great practical importance from the standpoint of utilizing such films as computer storage elements. Many properties of thin films including the process of magnetization reversal are connected with changes in their magnetic structure. At present there is a considerable amount of information in the literature on the structure of thin ferromagnetic films, but these data have been obtained primarily by the powder pattern technique. There have been few investigations of the domain structure of ferromagnetic films by magneto-optical procedures; in fact, there has been only one relatively detailed study[2] in which the authors used a complicated negative-positive superposition technique for recording the domain structure.

Recently there appeared a brief report by Prutton[3] giving a description of a set-up and procedure for visual observation of domains, but the report does not give any significant data on the domain behavior.

In the present work we investigated the behavior of the domain structure of ferromagnetic films in the course of slow magnetization reversal by means of the longitudinal Kerr effect. Although it is possible that rapid switching and slow reversal differ significantly, we believe that our data may give a general idea of the character of the processes involved in magnetization reversal.

The experiments were carried out on films of different thickness prepared by the procedure described in Ref.4 (preceding article). Although certain consistent changes are observed with increase in the film thickness, it must be noted that often even very similar specimens exhibit entirely different properties. This can be explained by the fact that many of the properties of thin films are determined by so far uncontrollable factors operating during evaporation of the metal. Thus for as yet unknown reasons the magnetic properties of different batches of film obtained under ostensibly identical conditions proved to be different. Judging from the literature it may be concluded that the problem of controlling the quality of thin films has not yet been solved and is in fact one of the urgent problems in the technology of information storage devices.

Moreover, the same films behave differently depending on their initial state. Thus in the case of uniform films saturated in a very strong field (> 500 oersted) domain structure does not become evident in the process of magnetization reversal, and the reversal is realized entirely by rotation of the magnetization vector I_s; in the case of inhomogeneous films, in contrast, magnetization reversal always begins with the appearance of reverse magnetization nuclei.

In films saturated in a very strong field both rotation of I_s and appearance of reverse magnetization nuclei begin in stronger fields than in films saturated in a weak field (5-20 oersted). This is probably due to the fact that in saturation in a strong field most of the incipient reverse magnetization nuclei are destroyed.

The photographs reproduced in Fig.1 illustrate four stages in the process of magnetization reversal of a 580 Å thick film in the direction of easy magnetization. With gradual increase of the applied field there appear at the upper right-hand edge of the film magnetization reversal nuclei in the form of small light wedges or spikes, which grow by small discrete jumps (Fig.1,a). With further in-

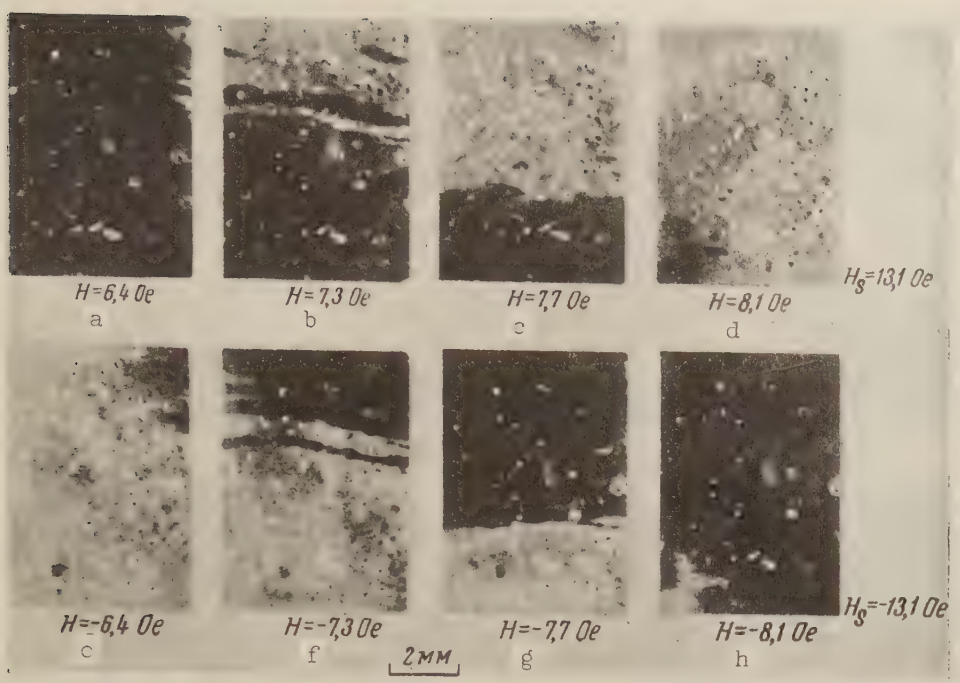

Fig.1. Four stages in magnetization reversal of a 580 Å thick film in the direction of easy magnetization. H_s - saturation field. Axis of easy magnetization horizontal.

crease of the field, reversal is realized not over the entire right-hand edge of the film but by abrupt forward jutting of successive spikes from right to left across the entire film. This character of magnetization reversal is apparently due to the inhomogeneity of the film in thickness. Superficial comparison of Figs.1,b & c gives the impression of wall displacement; actually, however, no smooth wall motion was observed. It is interesting to note that in Fig.1,d there is a small section for reversal of which an appreciable increase in field strength was required (by 5 oersted, whereas the rest of the film underwent reversal upon increase of the field by only 1.7 oersted). This can be explained by appreciable inhomogeneity of the film. Comparing Figs.1,a-d with Figs.1,e-h, respectively, it may be inferred that in the case of return reversal the domain structure is fairly accurately reproduced (light figures have been replaced by dark ones and vice versa, inasmuch as the vector I_s in the domains changed its direction to the opposite).

Upon removal of a saturation field there do not appear magnetization reversal nuclei in the film: it remains in the state of saturation. Thus the behavior of the domain patterns shows that the process of magnetization reversal is strongly dependent on the degree of homogeneity of the film.

An entirely different picture was observed in the case of reversal of a uniform film approximately 800 Å thick. Upon application of a field in the easy direction, upon attainment of a certain field strength, the entire film abruptly reversed magnetization, i.e., by rotation of the vector I_s. In the case of this film it was difficult to obtain reverse magnetization nuclei. To do this it was necessary first to demagnetize the film by repeat application of an alternating field of decreasing amplitude. Then upon application of a slowly increasing reverse field to the barely saturated film there appeared magnetization reversal

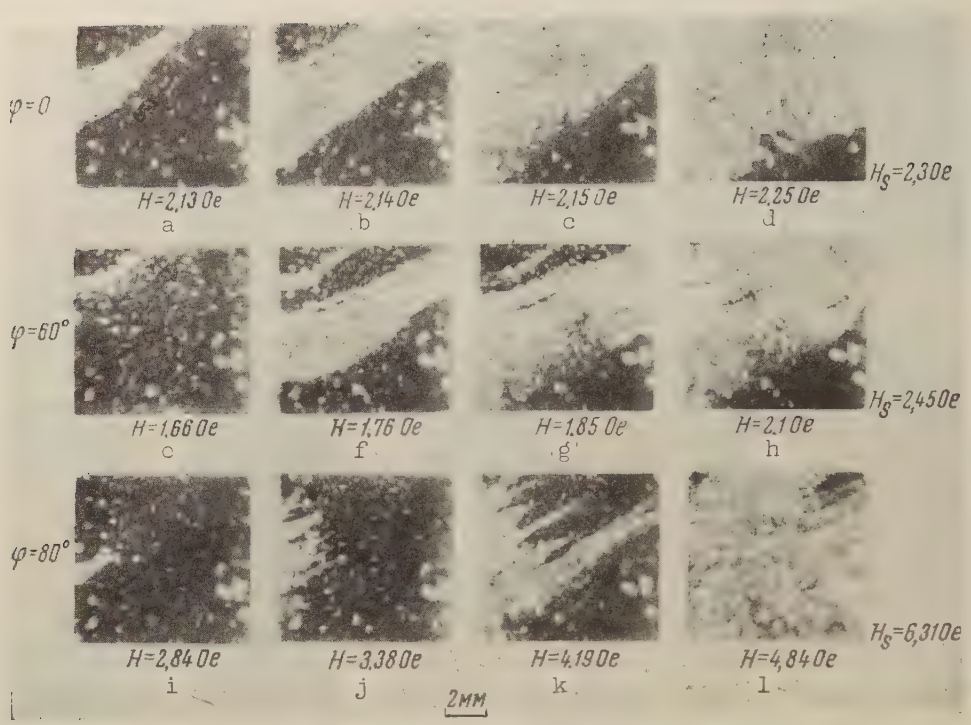

Fig.2. Domain behavior in the process of magnetization reversal of a homogeneous 800 Å thick film with the magnetic field applied at different angles φ relative to the axis of easy magnetization, the direction of which is approximately parallel to the domain walls in photograph c.

nuclei. The magnetization reversal of such a uniform film is illustrated in Fig.2 (the light spots in the photograph are due to defects in the zinc sulfide coating). Upon increase of the field by some hundredths of an oersted, the walls begin to move (Fig.2,b-e). When the field is applied at a certain angle φ relative to the easy magnetization axis, reverse magnetization nuclei appear more easily; also with increase of the angle φ wall motion is realized more smoothly and saturation of the film is attained in stronger fields.

It should be noted that if the film was saturated in a very strong field then with the reversing field applied at an angle φ = 20-40° magnetization reversal is realized by rotation of the vector I_s and no discernible domain structure appears.

The process of magnetization reversal retains approximately the same character up to φ = 60°; at φ = 80° with increase in the field, the number of spikes along the edge of the film increases as does their size (Fig.2,i,j) and only at H = 4.19 oersted does one spike finally penetrate across the film. In the ~800 Å thick film the domains were oriented approximately parallel to the easy magnetization axis regardless of the angle φ.

In the case of a 1100 Å thick film with increase of the angle φ there was observed a marked change in the shape of the figures and in the contrast between domains. As a result of slow demagnetization by a decreasing alternating field applied along the easy axis there was established in this film a structure consisting of straight antiparallel domains.

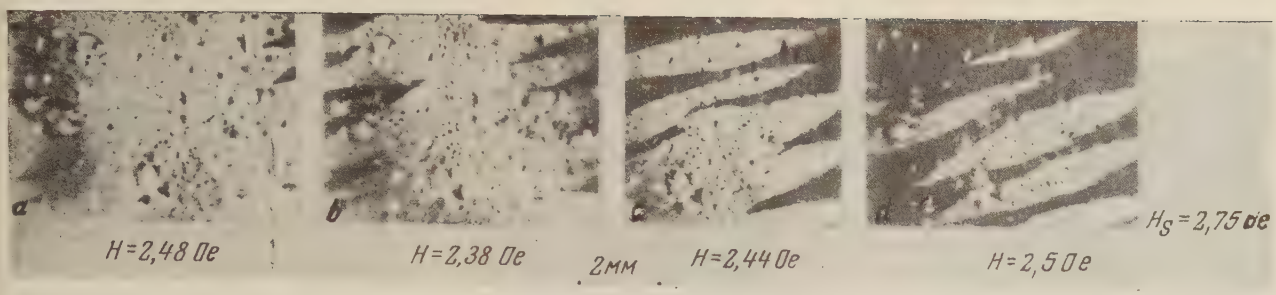

Fig.3. Process of magnetization reversal in 1100 Å thick film with the reversing field applied in the direction of the easy magnetization axis (axis approximately horizontal).

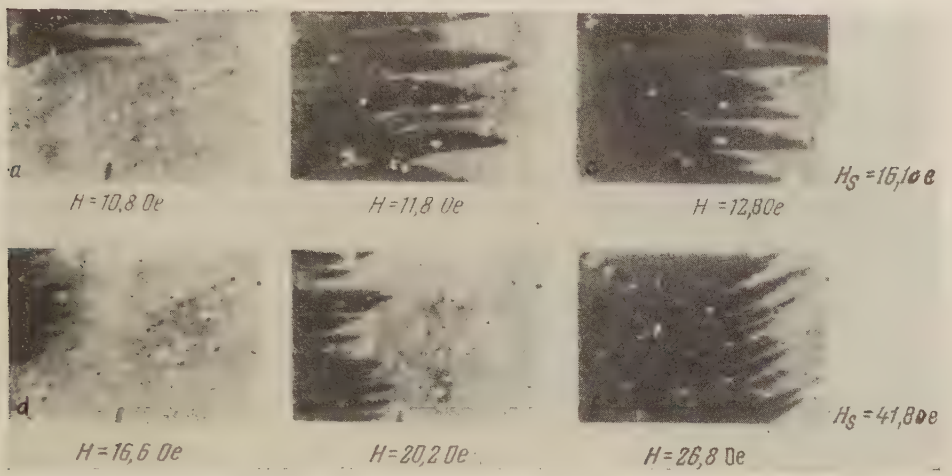

Fig.4. Magnetization reversal in 1750 Å thick film under the influence of fields applied at different angles relative to the easy magnetization axis (axis approximately horizontal).

Magnetization reversal along the easy axis begins with the appearance of spike-shaped reverse magnetization nuclei at the edges of the film (Fig.3,a); these grow by smooth wall movements (Fig.3,b) and finally merge (Fig.3,c). The unswitched regions in the form of elongated light islands (Fig.3,d) are gradually absorbed by the domains oriented along the field.

The photographs of Fig.4 illustrate the process of magnetization reversal in part of a 1750 Å thick film in the shape of a disk 6 mm in diameter. A predominant role in magnetization reversal of this specimen is played by the appearance and growth of spikes. At H = 10.8 oersted there appeared two spikes. With increase of the field the number and size of the spikes increased (Fig.4, b). With further increase of the field the individual spikes by smooth wall displacement traverse the entire film (Fig.4,c) until saturation is attained in a field of 16.1 oersted. Upon application of a field at an angle φ relative to the easy axis the spikes become smaller and tend to be inclined relative to the easy magnetization axis (Fig.4, d-f), but the character of the magnetization reversal process remains essentially the same.

Olmen & Mitchell[5] observed slow domain motion in a uniform Permalloy (78% Ni) film 1500 Å thick in a constant magnetic field. They observed continuous domain wall movement up to complete saturation of the film. The rate of move-

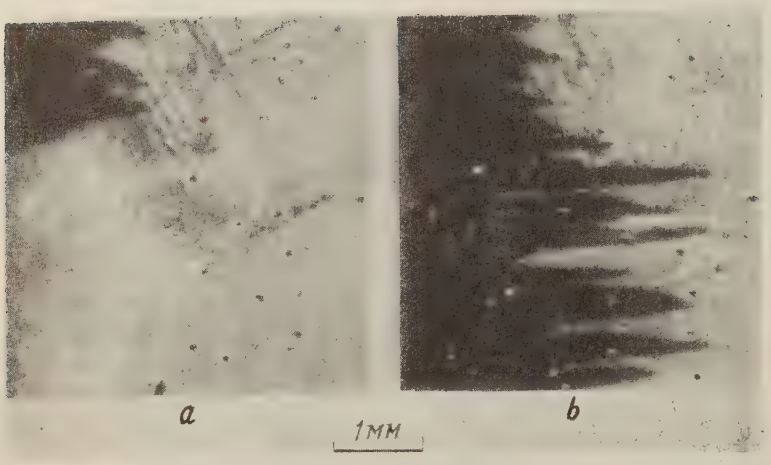

Fig.5. Appearance of spike domains in a 1750 Å thick film in a constant field.

ment was found to depend linearly on the external field; the temperature dependence was characterized by a power law with an exponent greater than 1 but smaller than 2.

We, also, in the case of all films, except the 580 Å thick film, observed slow wall displacement at a fixed value of the applied field. In the case of an inhomogeneous film the wall motion ceased before attainment of saturation. Actually, wall motion is not always realized by the appearance and growth of a single magnetization reversal nucleus, but may occur in conjunction with the appearance of a number of new nuclei (spikes). In Fig.5,a there are visible nuclei which appeared at a field value of 9.8 oersted. When the field was rapidly increased to 11.1 oersted and kept constant at this value for 20 min 13 sec there appeared new spikes (Fig.5,b) which grew by smooth wall movement. The process of appearance of new spikes slows down with time. This will be evident from the following data on the interval between the appearance of new spikes (the spikes are numbered beginning with the lowest in Fig.5,b):

Spike No.	1	2	3	4	5	6	7
Time	20 min 13 sec	15 min 5 sec	13 min	13 min 40 sec	24 sec	5 sec	2.5 sec

Investigation of the domain structure of thin ferromagnetic films showed the following:

1. An inhomogeneous film 580 Å thick undergoes magnetization reversal in a wide range of fields by small discrete jumps without discernible smooth wall motion.

2. A uniform film 800 Å thick with the field applied in the direction of easy magnetization usually behaves as a single-domain specimen. However, with increase of the angle between the direction of the applied field and the easy axis the magnetization reversal is more often realized by the appearance of reverse magnetization nuclei and wall displacement.

3. In the case of all films, except for the thinnest, 580 Å film, there was observed slow movement of the walls in a fixed constant field.

4. With increase in the film thickness and the angle between the direction of the field and the easy magnetization axis wall movement is realized more smoothly and there is also observed better reproducibility of the domain patterns in the case of repeat reversal.

Institute of Physics,
Siberian Branch of the USSR Academy of Sciences

References

1. C.Kittel, Phys.Rev., 70, 965 (1946).
2. C.Fowler, E.Fryer & L.Stevens, Phys.Rev., 104, 645 (1956).
3. M.Prutton, Philos.Mag., 4, 45, 1063 (1959).
4. L.V.Kirenskii, S.V.Kan & I.F.Degtyarev, Present issue of the Bulletin, p.589.
5. R.W.Olmen & E.N.Mitchell, J.Appl.Phys., 30, 4, 258 (1959).

VARIATION OF THE DOMAIN STRUCTURE OF THIN FERROMAGNETIC FILMS IN A MAGNETIC FIELD

- L.V.Kirenskii, V.A.Buravikhin & M.K.Savchenko

In recent years there have been published a number of reports describing the behavior of the domain structure of different ferromagnetic films in the process of magnetization and magnetization reversal. The observations were carried out by the powder pattern technique[1-3] and by means of the Kerr magneto-optical effect.[4-5] These studies, however, do not give anything like a complete picture of the complex variation of the domain structure of thin films in magnetic fields.

The present work was concerned with the behavior of the magnetic structure of films of 80% Ni + 17% Fe + 3% Mo and 50% Fe + 50% Ni alloys in the process of magnetization and magnetization reversal with the field applied along the easy magnetization axis. We also studied the variation in the domain structure during magnetization in fields applied at different angles to the easy axis.

Experiment

The films were prepared by the evaporation procedure described in Ref.6.

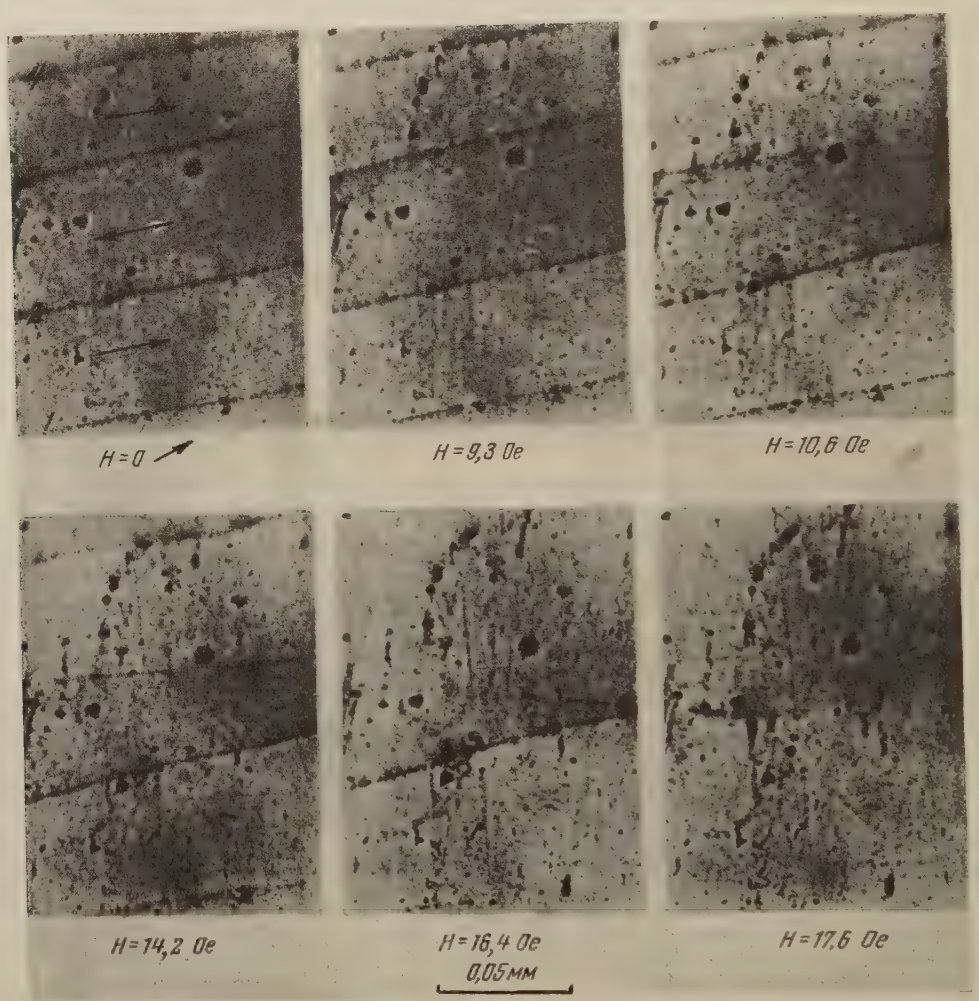

Fig.1. Domain wall motion in a 2470 Å thick Fe-Ni alloy film.

The domain structure was observed by the powder pattern technique by means of an MBI-6 microscope. For purpose of further study we recorded motion pictures of the domain dynamics at the rate of 12 frames per sec.

A series of frames from the film recording the variation of the domain structure in a 2470 Å thick Fe-Ni alloy film in the process of magnetization along the easy axis is reproduced in Fig.1. The initial structure was obtained by demagnetization in the same direction. The direction of the easy magnetization axis and that of the applied field is given by the arrow under the first photograph, while the directions of the magnetization vectors in the domains are indicated on the photograph. It will be evident from the photographs that there is no change in the domain structure with increase of the applied field up to 9.3 oersted. This is a distinguishing feature of magnetization of thin films, as compared with the process of magnetization of bulk ferromagnetic specimens, in which wall movement begins in very weak fields.

With further increase of the field wall motion begins; the rate of movement of the different walls differs and the movement itself is not smooth but jerky. Saturation is attained in a field of 17.6 oersted.

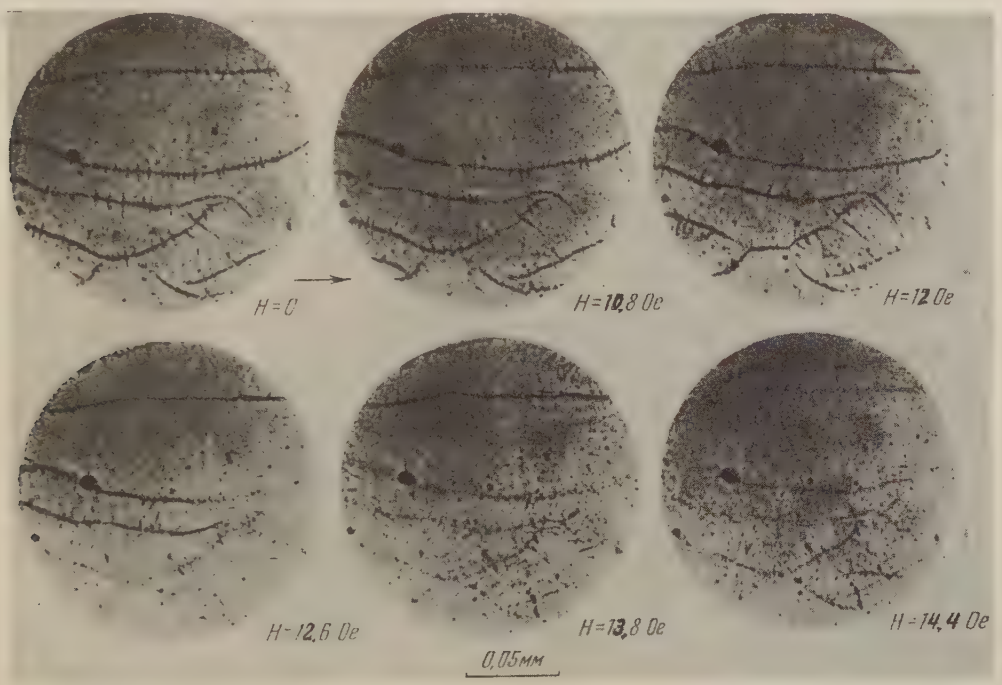

Fig.2. Variation of the domain structure of a 760 Å thick Fe-Ni alloy film in the course of magnetization in the direction of the easy magnetization axis. (Axis horizontal.)

Some frames from the film exposed in the process of magnetization of a 760 Å thick film of the same alloy are reproduced in Fig.2. In the film in the demagnetized state there are discernible domains bounded by walls with cross-ties of the type observed by Huber, Smith & Goodenough[7]. Upon application of a field in the direction of the easy axis no noticeable changes occur up to a field value of 10.8 oersted. With further increase of the field the cross-ties begin to disappear, although there is no noticeable displacement of the main walls. In domains disadvantageously oriented relative to the field there appear cross boundaries, which develop mainly from the few persisting cross-ties. This apparently

occurs because in individual parts of the disadvantageously oriented domains the magnetization vectors change direction, and the formed "subdomains" became separated by new walls. Upon further increase of the field the disadvantageously oriented domains break up, and disappear completely in a field of 14.4 oersted.

Magnetization Reversal Along the Easy Axis

The process of magnetization reversal of a 1200 Å thick film of Fe-Ni alloy is shown in Fig.3. At first the film was magnetized to saturation. Upon removal of this field no domain structure appeared. Then a reverse field was applied. The field of view in these photographs corresponds to the central portion of the film. No domain structure appeared up to a reversing field value of -3.4 oersted. When the field was increased to -3.5 oersted, there appeared a sawtooth boundary dividing domains of opposite magnetization. With further increase of the field to -6.5 oersted, there was no noticeable change in the structure. At -7 oersted there began growth of spike domains, the magnetization of which was aligned with the field. With further increase of the field these spikes continued to grow by smooth wall motion at the expense of spikes magnetized opposite the field. In a field of -16 oersted the domain structure disappeared both from the field of view and from the entire surface of the film.

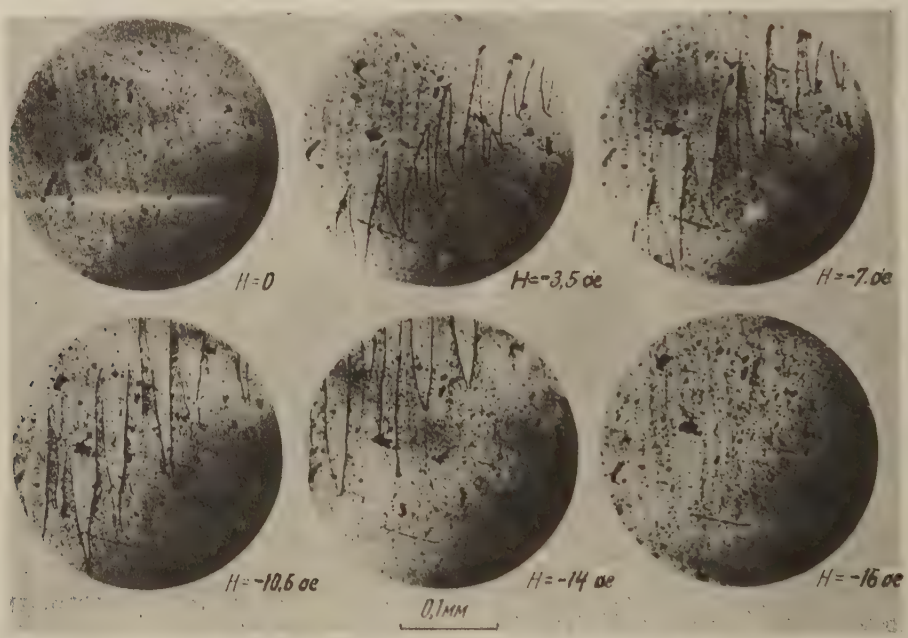

Fig.3. Change in the domain structure of a 1200 Å thick Fe-Ni alloy film by wall movement. The field applied during preparation of the film was vertical.

Magnetization at Different Angles Relative to the Easy Axis

The photographs of Fig.4 show the variation of the domain structure of a 1200 Å thick film of Fe-Ni-Mo alloy in a magnetic field oriented at angles of 0, 45 and 90° relative to the easy magnetization axis. The initial structure in all cases was obtained by demagnetization of the film at an angle of 45° relative to the easy axis.

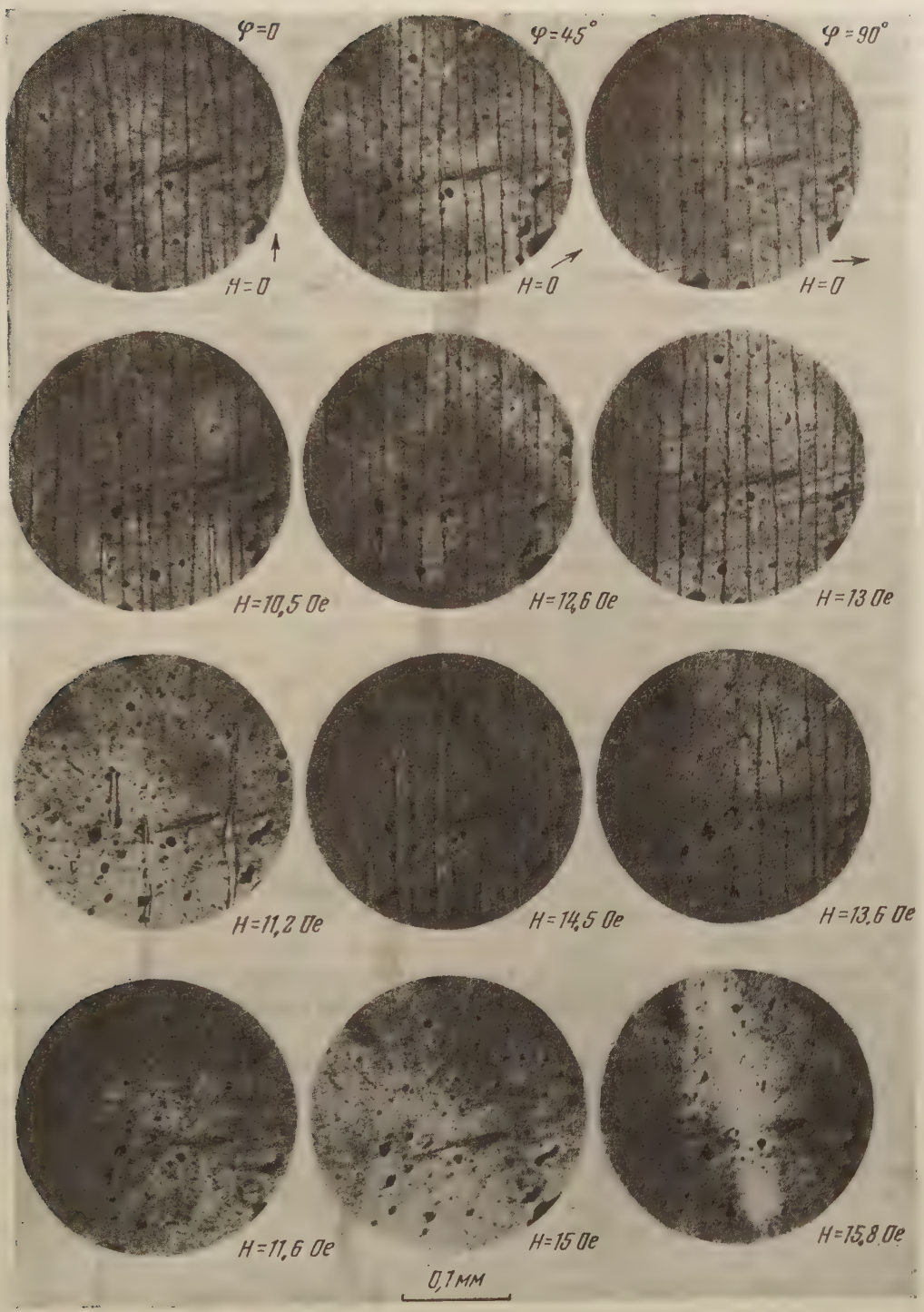

Fig.4. Domain structure of an Fe-Ni-Mo film 1200 Å thick in a magnetic field directed at angles of 0, 45 and 90° to the easy magnetization axis (vertical in the photograph).

No domain structure was observed up to a field of 10.5 oersted in the first case, 12.6 oersted in the second, and 13 oersted in the third. Then in a narrow field interval in the first and second cases there was observed some wall displacement; with further increase of the field there was observed rapid magnetization reversal of parts of those domains in which the magnetization vector was directed opposite to the applied field. In the third case almost no wall movement was observed with increase of the field; the magnetization of this film was apparently realized primarily by rotation processes. Saturation of the film was attained at 11.6 oersted in the first case, 15 oersted in the second and 15.8 oersted in the third.

The following conclusions may be drawn from the results of our investigation of the domain structure of Permalloy films.

1. In the case of all ferromagnetic films the domain structure remains stable up to a certain critical field value. This was observed for films of different thickness prepared of Permalloy alloys and cobalt.

2. In relatively thick ferromagnetic films magnetization is realized by wall movement: this movement begins above a certain critical field value, which differs for films of different materials and thicknesses. The wall movement is generally not smooth, but discontinuous.

3. With decrease of the film thickness magnetization in a certain field range proceeds by barely noticeable wall displacements and by rotation processes.

In thinner films magnetization occurs by rapid magnetization reversal in individual parts of the domains disadvantageously oriented relative to the applied field. Such magnetization reversal is obviously realized by abrupt rotation of the magnetization vectors of the switching sections of the domains.

Institute of Physics
Siberian Branch of the USSR Academy of Sciences &
Krasnoyarsk State Pedagogical Institute

References

1. H.Williams & R.Sherwood, J.Appl.Phys., 28, 548 (1957).
2. G.E.Fuller, J.phys.et radium, 20, 310 (1959).
3. H.W.Fuller & H.Rubinstein, J.Appl.Phys., 30, 84 (1959).
4. C.A.Fowler, Jr., E.M.Fryer & J.R.Stevens, Phys.Rev., 104, 645 (1959).
5. R.W.Olmen & E.N.Mitchell, J.Appl.Phys., 30, 258 (1959).
6. L.V.Kirenskii, V.A.Buravikhin & A.G.Zvegintsev, Present issue of the Bulletin, p.581.
7. E.E.Huber, D.O.Smith & J.B.Goodenough, J.Appl.Phys., 29, 294 (1958).

NEW PROCEDURE FOR MEASURING THE THICKNESS OF DOMAIN WALLS BY MEANS OF THE KERR EFFECT

- V.I.Sinegubov & M.K.Savchenko

Of particular importance from the standpoint of the theory of ferromagnetism is determination of the thickness of domain walls and the surface energy associated therewith, inasmuch as variation of these quantities plays a substantial role in the process of technical magnetization. Solution of this problem can also help clarify such questions of theory as determination of the numerical value of the exchange integral, the nature of the coercive force and hysteresis, and the appearance of reverse magnetization nuclei. A number of authors have carried out theoretical calculations in this field; for example, Landau & Lifshits[1] calculated the width of the boundary layer and the distribution of the magnetization vector I_s therein in the framework of the quasiclassical approximation.

On the other hand, there have been very few experimental determinations of the width of the boundary layer (wall thickness). For measuring the wall thickness, Bean[2] used a cylindrical wire in which axial anisotropy was produced by mechanical stress. The boundary layer was produced by the action of a pulse field on the magnetized wire. Craik[3] made an attempt to measure the thickness of the boundary layer by observing deposits of magnetic powder over the wall by means of an electron microscope. But, as was shown by A.A.Shvarts, the wall thickness cannot be determined by the powder technique inasmuch as the apparent width of the deposit also depends on the magnetic moment of the powder particles and the so-called blackening density. Kirenskii & Veter[4] utilized the polar Kerr effect for observing domains, but owing to inadequacies of their set-up they were not able to make direct measurements of the wall thickness.

Herein we propose a new procedure by means of which one can obtain a clear record of domain walls. This procedure is also based on the polar Kerr effect.

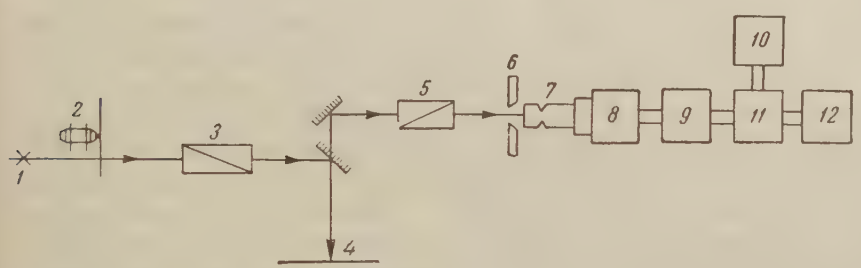

Fig.1. Diagram of set-up for measuring domain wall thickness: 1) light source, 2) rotating shutter, 3) polarizer, 4) specimen, 5) analyzer, 6) micrometric slit, 7) photomultiplier, 8) preamplifier, 9) amplifier, 10) multivibrator, 11) phase detector, 12) recording potentiometer.

A diagram of the set-up is shown in Fig.1. The specimen is mounted on the stage of an MBI-6 microscope. The beam from the light source is modulated by the rotating shutter; after passing through the polarizer the light falls on the specimen and, after reflection from it, passes through the analyzer and then enters the micrometric slit and falls on the cathode of the photomultiplier. The signal from the photomultiplier, after appropriate amplification, enters the phase detector. At the same time a reference signal from the multivibrator, precisely in phase with the useful signal, is also fed into the phase detector. The phase detector is coupled to a potentiometer.

The mechanical stage holding the specimen is advanced at a slow steady rate. The domain structure of the specimen is examined beforehand by the powder technique, and then the powder is carefully removed from the selected section to be

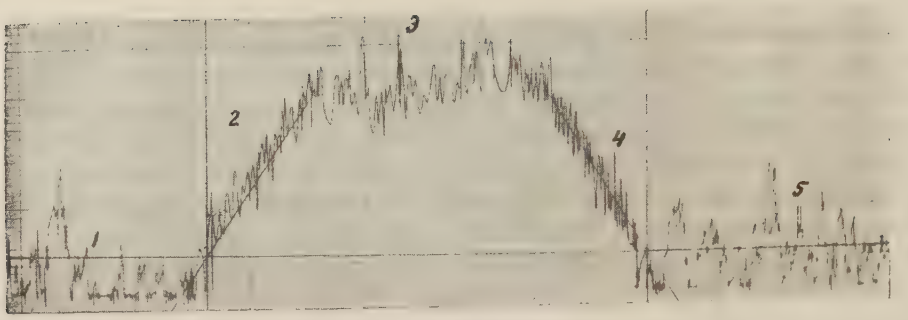

Fig.2. Curve recorded by the potentiometer during scanning of the boundary between domains in a 2500 Å thick film of Mo-Permalloy.

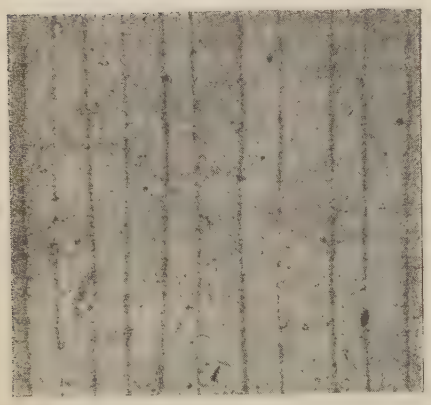

Fig.3. Domain structure of the 2500 Å thick Mo-Permalloy film. Magnification 280 X.

scanned. The modulated polarized light flux reflected from the specimen produces an image of the surface of the specimen in the plane of the micrometric slit. When the polarizer and analyzer are crossed, the analyzer field is dark and if the slit is not viewing a wall, no signal, except noise, appears at the phase detector output. A typical potentiometer chart record is shown in Fig.2. Section 1 corresponds to the time when the slit is not viewing a wall; section 2 corresponds to the instant when a wall is reached; section 3 corresponds to passage of a wall through the scan area; section 4 corresponds to departure of a wall from under the slit; section 5 is again a record of the photomultiplier noise only. By measuring the width of sections 2 and 4 and knowing the rate of motion of the potentiometer chart and specimen, one can readily determine the wall thickness.

Using the described procedure we measured the width of a boundary on a 2500 Å thick Mo-Permalloy (80% Ni, 17% Fe, 3% Mo) film prepared by vacuum ($4.5 \cdot 10^{-5}$ mm Hg) evaporation onto a glass substrate heated to 300°. The domain structure of such a film as brought out by the powder technique is shown in Fig.3. It will be seen that the structure consists of regular 180° domains. The wall thickness in this specimen was found to be 0.7 microns. In making the measurement the specimen was carefully oriented so that the wall would be rigorously parallel to the micrometric slit.

Thus the developed procedure allows of direct measurements of the thickness of domain walls. Further improvement of the sensitivity of the set-up should make it possible to observe not only static walls but also walls in the process of variation under the influence of external factors acting on the ferromagnetic specimen.

Institute of Physics,
Siberian Branch of the USSR Academy of Sciences

References

1. L.D.Landau & E.M.Lifshits, Sow.Phys., 8, 153 (1935).
2. C.P.Bean (Abstract), Izv.AN SSSR, 21, 8, 1183 (1957). (Trans.Bulletin 21, 1174.)
3. D.J.Craik, Proc.Phys.Soc., 69, 6, 438 (1956).
4. L.V.Kirenskii & V.V.Veter, Doklady AN SSSR, 125, 526 (1959). (Trans. Doklady.)

BARKHAUSEN EFFECT IN THIN Mo-PERMALLOY FILMS

- N.M.Salanskii, A.M.Rodichev & M.K.Savchenko

Description of the Experiments

The present investigation was concerned with the Barkhausen effect in thin Mo-Permalloy films. The film was placed in a measuring coil connected to the input of a wide-band amplifier. The magnetization of the film was reversed by smooth variation of the current through the windings of the magnetizing solenoid, which was coaxial with the measuring coil; the rate of increase of the field could be varied in a wide range. After amplification, the Barkhausen pulses were integrated by a special integrating device with adequate resolution. Then the pulses were sorted as regards magnetic moment by an 8-channel electronic integral pulse height discriminator and recorded by PS-100 scalers. The set-up was capable of recording magnetic moments from $0.56 \cdot 10^{-6}$ cgsm units up.

The films of 80% Ni + 17% Fe + 3% Mo alloy were prepared by vacuum ($4 \cdot 10^{-5}$ mm Hg) evaporation onto cover glass substrates heated to 300°. After deposition the films were annealed at 350° in vacuum. By this procedure there were prepared eight films in the form of 25 x 2 mm strips. Four films - 600 Å thick (No.1), 750 Å (No.2), 850 Å (No.3) and 1200 Å (No.4) - were annealed only in the natural field in the laboratory; three films - 600 Å (No.5), 750 Å (No.6) and 1200 Å (No. 7) - were annealed in a magnetic field of 100 oersted applied parallel to the long side of the film; film No.8, 1200 Å thick, was annealed in a 100 oersted field applied perpendicularly to its long side. In addition, there was prepared film No.9 in the form of a disk 11 mm in diameter; this was also annealed in a 100 oersted field in the direction AB marked on the film. (For this film there was prepared a special flat measuring coil). All the films, except No.8, were characterized by uniaxial anisotropy with the easy magnetization axis parallel to the long side of the film. Film No.8 had the easy axis perpendicular to its long side; in disk No.9 the easy axis was in the AB direction.

The films were placed in the measuring coil with the long side of the film parallel to the coil axis, so that the direction of magnetization reversal for films Nos.1 through 7 coincided with the easy magnetization axis, while for film No.8 it was perpendicular to this axis. In the experiments with the disk the reversing field was applied both along the easy direction and perpendicular to it.

Results

The moment distribution of the jumps proved to be similar to the distribution in metallic ferromagnets observed by Tebble et al[1] not only as regards general character but also as regards absolute values of the magnetic moments. The integral moment distributions for films Nos.2 and 6 are shown in Fig.1. If it is assumed that the region of a jump extends through the entire thickness of the film, we find that for a 600 Å thick film, jumps ranging in magnitude from $0.6 \cdot 10^{-6}$ to $9.0 \cdot 10^{-6}$ cgsm units occupy an area of 0.01-0.15 mm^2 on the surface of the film. The distribution of jumps in moment for all the investigated films is well described by the formula

$$N = N_0 e^{-\alpha m^{1/2}}, \qquad (1)$$

where N_0 and α are constants for a given film. The upper right-hand insert in Fig.1 shows the variation of the logarithm of the number of jumps as a function of $m^{1/2}$ for some of the investigated films. The linearity of these plots demon-

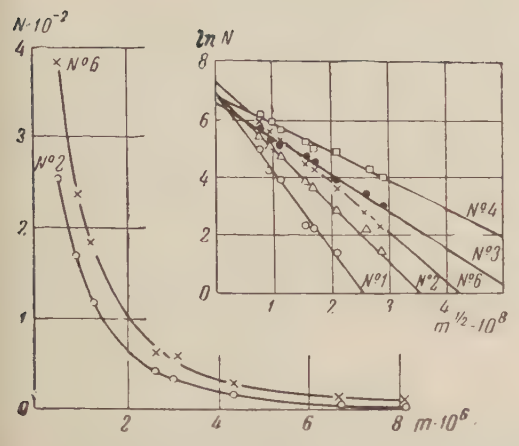

Fig.1. Distribution of jumps as regards magnetic moment.

strates the validity of Eq.(1). Our m dependence of the number of jumps with large moments differs from the dependence obtained by Ford & Pugh[2] by means of the magneto-optical method: the exponent at m in the work of Ford & Pugh was close to unity.

It was found that the average moment of the jumps is strongly dependent on the film thickness (see Fig.2) and in the investigated thickness range increases linearly with the thickness as though the dimensions of each region reversed by a jump remain constant in the plane of the film but increase only in thickness. Apparently this thickness dependence of $\bar{m}$ is to some extent due to variation of I_s with film thickness.

We observed no clear dependence of the average jump moment on whether the specimen was annealed in the presence or absence of a magnetic field: thus for films Nos.2 and 6 the values of the average moment were $1.81 \cdot 10^{-6}$ and $1.85 \cdot 10^{-6}$ cgsm, respectively.

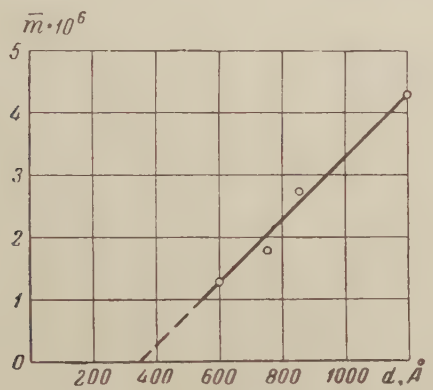

Fig.2

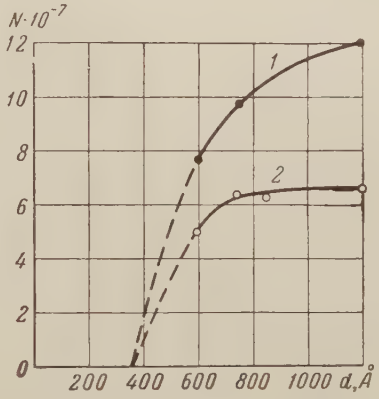

Fig.3

Fig.2. Variation of the average jump moment as a function of the film thickness.
Fig.3. Variation in the number of jumps with the film thickness: 1) films annealed in a magnetic field, 2) films annealed in zero field.

The variation in the number of jumps (per unit volume) with the film thickness is shown in Fig.3. Back in 1948 Drigo & Pizzo[3] were among the first to study this dependence with a view to determining the thickness at which the single domain state is attained; they estimate that the Barkhausen effect should disappear at a thickness of 1000 Å. Approximate extrapolation of the curves of Fig.3 gives a value of 350 Å for disappearance of the Barkhausen effect. However, if it is borne in mind that the size of the jumps decreases with decrease in film thickness and that part of the jumps falls below the sensitivity of the set-up, it must be inferred that the 350 Å thickness is somewhat greater than the single domain criterion. True, on the other hand, it must be noted that with approach to the single domain state the curves may slope more steeply towards zero.

The distribution of jumps according to field values is shown in Fig.4. In contrast to bulk ferromagnets in which reversal jumps, as a rule, begin in the

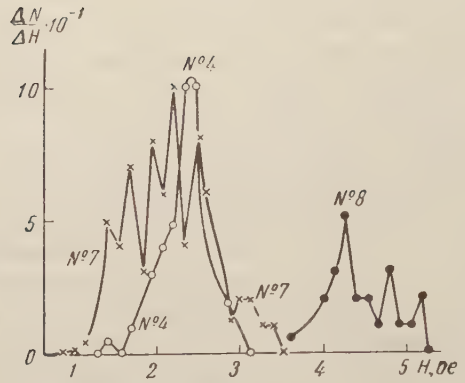

Fig.4

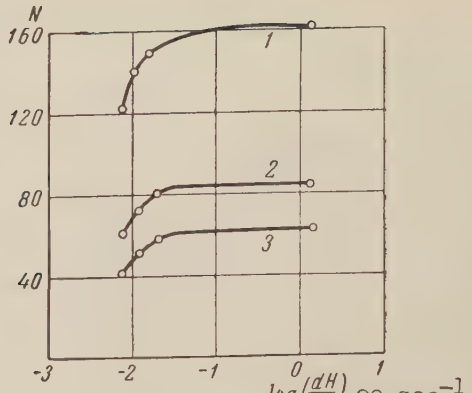

Fig.5

Fig.4. Jump distribution as a function of the field.
Fig.5. Variation in the number of jumps with different magnetic moments as a function of the rate of variation of the field: 1) jumps with moment greater than $0.56 \cdot 10^{-6}$ cgsm units, 2) jumps with moment greater than $0.88 \cdot 10^{-6}$ cgsm units, 3) jumps with moment greater than $1.24 \cdot 10^{-6}$ cgsm units.

range of negative field values (the field is assumed to be varied from negative to positive), in films the jumps begin only in the range of positive fields and, moreover, the range of fields in which jumps occur is appreciably narrower (than in bulk specimens). In films annealed in a magnetic field the jumps begin somewhat later (film No.7 was an exception) and continue into the range of stronger fields as compared with films annealed in zero field. Moreover, the intensity of the Barkhausen effect in magnetically annealed films is appreciably more irregular. Noteworthy is clustering of the jumps: after occurrence of a group of jumps, there may be an interval in which there are no jumps. The total number of jumps in the case of films annealed in a magnetic field is higher (see Fig.3).

Fig.4 also shows a curve for film No.8, the axis of easy magnetization of which was perpendicular to the reversing field. It will be evident from the curve that the critical field value for this film is approximately two times higher than for films of the same thickness but with the reversing field applied in the easy direction. A similar situation is observed for film No.9 (the disk) with the field parallel and perpendicular to the easy magnetization axis: the field intervals in which jumps occur are 0.35 to 4.20 oersted and 1.75 to 4.5 oersted, respectively. The total number of jumps, however, in both cases, was approximately the same.

The variation in the number of jumps depending on the rate of change dH/dt of the magnetic field for film No.1 is shown in Fig.5. The form of the N vs log (dH/dt) curves may be explained as follows. As the moment distributions of the jumps at different dH/dt show, the average moment of the jumps increases with increase of dH/dt in the rate interval shown in Fig.5 from $1.18 \cdot 10^{-6}$ to $1.34 \cdot 10^{-6}$ cgsm units. Owing to increase in the magnitude of the jumps, an increasing fraction of the Barkhausen pulses comes to exceed the sensitivity threshold of the set-up and the total number of jumps recorded increases to a certain limit. If extended further, the curves might fall off owing to inadequate resolution of the set-up in the range of high rates of field variation.

In conclusion, we would like to call attention to the possibility of using some characteristics of the Barkhausen effect as one of the criteria for the rate of pulse magnetization reversal of films. Obviously, the most rapid switching

of a film occurs by a single jump. Nonsimultaneity in the reversal of individual parts of the film leads to increase of the magnetization switching time. If there are many jumps, it would be desirable from the standpoint of rapid switching for all of them to have a critical field of nearly the same value. This would lead to a large number of delayed jumps (in the investigated films greatly delayed jumps were individual events). Lastly, we believe that the duration of the jumps may be intimately connected with the characteristics of pulse magnetization reversal, and investigations in this field may be highly useful.

Institute of Physics,
Siberian Branch of the USSR Academy of Sciences

References

1. R.S.Tebble, I.C.Skidmore & W.D.Corner, Proc.Phys.Soc., A 63, 739 (1950).
2. N.C.Ford & E.W.Pugh, J.Appl.Phys., 30, 4, Suppl.270 (1959).
3. A.Drigo & M.Pizzo, Nuovo cimento, 5, 1 (1948).

NUCLEATION AND THE BARKHAUSEN EFFECT IN FERROMAGNETIC FILMS

- V.F.Ivlev & V.S.Prokopenko

In slow magnetization reversal of ferromagnetic films with a rectangular hysteresis loop the change in magnetization is wholly realized by irreversible jumps.[1] Such important characteristics of the films as the shape of the hysteresis loop and the switching time depend on how these jumps are distributed in field and in size and duration of the jumps.

Ford & Pugh[1] established experimentally that in the case of magnetization reversal of a section of film by motion of one wall the distribution of magnetization jumps in size is described by a function of the form

$$N = N_0 e^{-\lambda M}. \tag{1}$$

For complete reversal of the film the distribution in size is described by the following more complex relation, which is characteristic of bulk ferromagnets:

$$N = N_0 A e^{-kM^{1/n}} \tag{2}$$

where M is the size of the jump, N_0 is the total number of jumps, N is the number of jumps greater than M, and λ, k, n and A are constants.

The size distribution (1) is satisfactorily described by the magnetization reversal model according to which the probability for stopping of a moving wall at a distance dx is proportional to dx. Ford & Pugh[1], generalizing this model to the case of complete magnetization reversal of a ferromagnet, suggest that relation (2) may be regarded as the result of superposition of numerous distributions of type (1), which, obviously, can be done only on the assumption that all the magnetization jumps are due to the process of wall displacements. Observations of domain structure show, however, that a substantial role in reversal of magnetization in films is played by the process of formation of reverse magnetization nuclei.[2-4] Clearly for jumps due to nucleation the distribution in size may be different than for jumps due to wall motion. A resultant distribution of type (2) for complete magnetization reversal in a film is also possible in this case, but inasmuch as nucleation precedes wall displacement, the character of the jump distribution in size in the process of magnetization reversal will change.

The present work was undertaken with a view to clarifying the relation between the process of nucleation and the Barkhausen effect in ferromagnetic films. For our investigation we chose cylindrical iron films for two reasons. In cylindrical films the influence of chance imperfections at the edge of the film on nucleation can be minimized. Moreover, there is reason to assume[5,6] that cylindrical films of iron base alloys are the most promising as regards practical applications. The present work is part of an extensive research program concerned with the properties of films of this type.

The film preparation technique differed from that commonly employed.[7] The evaporator was an iron solenoid mounted by means of a mica frame inside the glass vacuum chamber. The film was deposited on the surface of a glass filament stretched along the axis of the solenoid. Prior to deposition the surface of the filament was outgassed and then cleansed by a gas discharge at a pressure of $\sim 10^{-2}$ mm Hg. At the instant of beginning of evaporation the pressure in the vacuum chamber did not exceed $8 \cdot 10^{-6}$ mm Hg. With the solenoid heated by direct current there were obtained films with uniaxial anisotropy, the easy magnetization axis

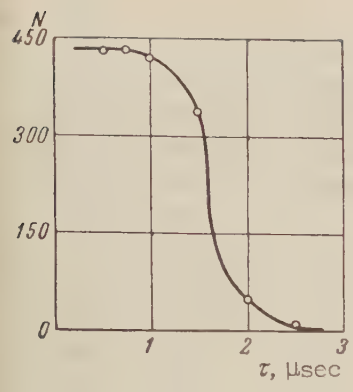

Fig.1

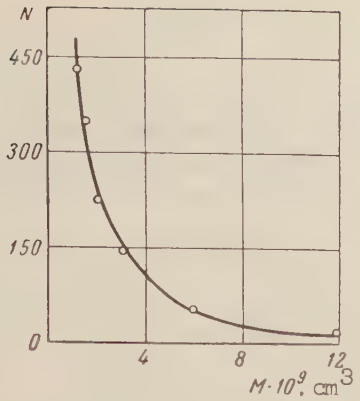

Fig.2

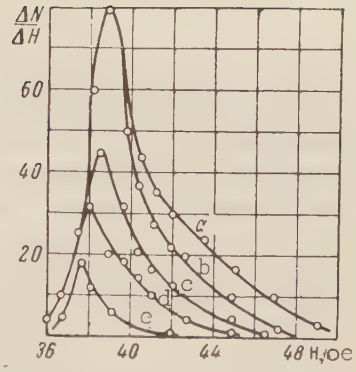

Fig.3

Fig.1. Magnetization jump distribution in duration.
Fig.2. Jump distribution in size for complete magnetization reversal of the film.
Fig.3. Jump distribution as a function of the field.

being aligned with the axis of the solenoid. The field produced by the evaporator-solenoid at the surface of the film did not exceed 20 oersted.

The experimental procedure does not differ in principle from that commonly employed in investigating the Barkhausen effect in bulk ferromagnets.[8] By way of the main amplifier we used a standard wide-band USh-10 amplifier. The parameters of the input circuit of the amplifier were chosen so that the output pulses for all jumps would have approximately the same duration; this was facilitated by the character of the distribution of the magnetization jumps in duration (Fig. 1). The sensitivity of the set-up allowed of reliable recording of magnetization jumps in volumes greater than $1.2 \cdot 10^{-9}$ cm^3.

Below we give the results obtained for films 5000 Å thick deposited on a 0.3 mm diameter filament. The reversing field was applied in the direction of the easy magnetization axis and was varied at the rate of 0.02 oersted/sec. In the course of each complete reversal cycle the jumps were observed twice in the field interval from 36 to 49 oersted with increase of the field.

In the case of complete magnetization reversal of the investigated film the resultant distribution is of type (2) (Fig.2). The recorded distribution of jumps of different size as a function of the field is shown in Fig.3; here curves a, b, c, d and e are plotted for jumps greater than $1.2 \cdot 10^{-9}$, $1.5 \cdot 10^{-9}$, $2 \cdot 10^{-9}$, $3 \cdot 10^{-9}$ and $6 \cdot 10^{-9}$ cm^3, respectively. It will be evident that in the process of magnetization reversal the character of the size distribution of the jumps in the films changes. Up to a field of 37.5 oersted there are no jumps smaller than $3 \cdot 10^{-9}$ cm^3. Up to a reversing field of 39.5 oersted there were recorded no jumps smaller than $1.5 \cdot 10^{-9}$ cm^3. Beginning with the 39.5 oersted field, when 80% of the substance of the film had already switched, the jump distribution in size conforms to Eq.(1) (see Fig.4, where N_0' is the number of jumps of all sizes recorded after increase of the field above 39.5 oersted).

Explanation of this type of distribution of jumps of different size as a function of the field is difficult in the framework of the model proposed by Ford & Pugh[1], which is not surprising in view of the fact that this model fails to take into account the process of nucleation.

Conger & Essig[9] calculated the switching time of films in fields weaker than the anisotropy field and obtained good agreement with experiments on the basis of the following assumptions regarding the character of the field distribution of the magnetization reversal nuclei:

$$N = N_0\left[1-\left(\frac{H_k - H}{H_k - H_0}\right)^p\right]; \qquad (3)$$

here H_0 is the field at which the first nucleus appears in the film, H_k is the anisotropy field of the film, N_0 is the possible number of nuclei in the field interval $H_k - H_0$, N is the number of nuclei forming in the film up to the field H, and p is the nucleation probability density, which is assumed to be constant in the reversal field interval.

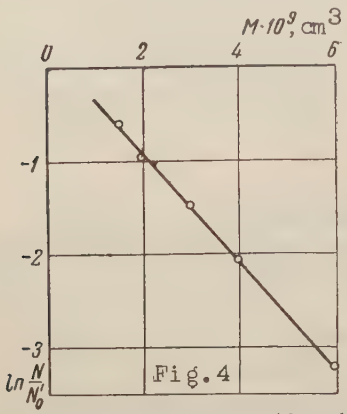

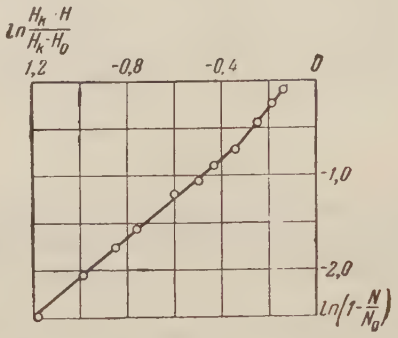

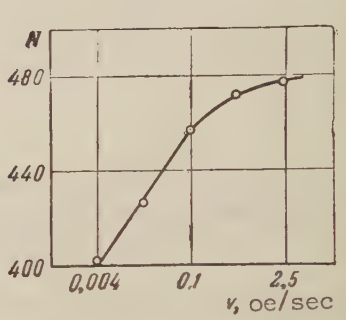

Fig.4. Distribution of jumps in size after a field of 39.5 oersted.
Fig.5. Jump number distribution as a function of the field on the assumption that all the jumps are due to nucleation.
Fig.6. Variation in the number of jumps with the rate of change of the reversing field.

If it be assumed that all the observed magnetization jumps are due to processes of nucleation, the plot of $\ln\left(1-\frac{N}{N_0}\right)$ vs $\ln\left(\frac{H_k - H}{H_k - H_0}\right)$ should be a straight line. Such a graph plotted on the basis of our data is shown in Fig.5. The break in the plot corresponds to a field of 39.5 oersted. The difference in the values of p for the two sections of the plot indicates that there is a difference between the conditions for the appearance of magnetization jumps in fields lower and higher than 39.5 oersted. Close to completion of the reversal process there obtains for the investigated films distribution (1), which is characteristic for cases when the magnetization reversal is realized by displacement of one wall. It is entirely probable that this is how slow magnetization reversal of cylindrical films is consummated: by motion of an annular wall formed by merging of growing nuclei. The fact that the distribution of magnetization jumps in field in this case is analogous to the distribution of reverse magnetization nuclei gives reason to assert that the magnetization jumps observed in films incident to wall motion are due to formation of nuclei immediately at the walls. Thus, it is feasible to identify each Barkhausen jump with the appearance of a reverse magnetization nucleus in the film. It is interesting to note that with increase in the rate of variation of the reversing field the total number of jumps per reversal cycle increases (Fig.6). This may in equal measure be a consequence of increase in the number and growth in the size of the reverse magnetization nuclei with more rapid variation of the applied field.

Krasnoyarsk State Pedagogical Institute

References

1. N.Ford & E.Pugh, J.Appl.Phys.(S), 30, 270 (1959).
2. H.Williams & R.Sherwood, J.Appl.Phys., 28, 548 (1957).
3. C.Fowler, E.Fryer & J.Stevens, Phys.Rev., 104, 645 (1956).
4. M.Prutton, Phil.Mag., 4, 45, 1063 (1959).
5. D.Meier, J.Appl.Phys., 30, 122 (1959).
6. D.Meier, J.Appl.Phys.,(S), 30, 45 (1959).
7. M.Blois, J.Appl.Phys., 26, 975 (1955).
8. V.F.Ivlev, Izv.AN SSSR, Ser.fiz., 16, 664 (1952).
9. R.Conger & F.Essig, J.Appl.Phys., 28, 855 (1957).

INVESTIGATION OF THE DURATION OF BARKHAUSEN JUMPS IN AN IRON FILM

- G.M.Rodichev & P.D.Kim

In magnetization reversal of ferromagnetic films much more appreciable regions relative to the total volume of the specimen are reversed by Barkhausen jumps as compared with bulk ferromagnets. Hence investigation of the Barkhausen effect should yield a better understanding of the mechanism of magnetization reversal in thin films. Of particular interest is investigation of the time characteristics of the Barkhausen effect, in particular the duration of the jumps. Such investigation can yield information on the reversing time of individual regions of the film under the influence of a slowly varying field.

The present work was concerned with investigation of the distribution in duration of Barkhausen jumps in an iron film.

The sensing element in our set-up was a measuring coil surrounding the specimen undergoing magnetization reversal in a slowly varying field. The coil was connected to the input of an amplifier. The voltage pulses, induced by the magnetization jumps, were fed into a converter circuit that yielded pulses of amplitude proportional to the duration of the input pulses. The pulses were then sorted in amplitude by a pulse height discriminator and counted by appropriate scalers.

Hitherto the distribution of Barkhausen jumps in duration has been investigated only by Rodichev, Salanskii & Sinegubov[1] for bulk specimens of Ni-Cr alloys. The set-up used by these authors was triggered only by pulses of duration exceeding 2 μsec. The set-up used in our investigation is capable of detecting pulses with durations from 0.2 μsec.

Except for the pulse length-to-height converter, the components used in our set-up are those ordinarily employed in apparatus for investigating the Barkhausen effect. The circuit of the converter (Fig.1) was designed so that by means of it one can investigate not only the distribution of pulses in duration but also integrate the Barkhausen jump pulses, i.e., investigate the distribution in magnetic moments.[2]

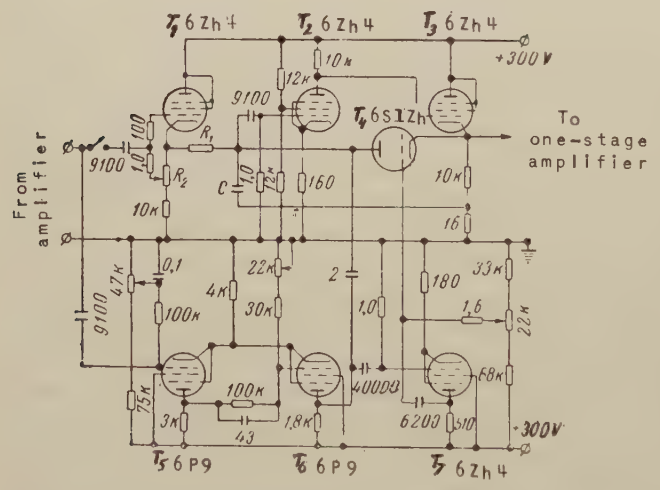

Fig.1. Circuit of pulse length to height converter.

In investigating the distribution of pulses in duration the grid of the cathode follower tube T_1 is disconnected from the input terminal. The voltage on the cathode of T_1, by means of potentiometer R_2, is set higher than the voltage on the cathode of T_3. Since the resistance of resistor R_1 is much higher than the resistance of the triode T_4, the voltage on the capacitor C is close to the voltage on the cathode of tube T_3.

A pulse arriving at the input of the converter trips the trigger circuit (tubes T_5 and T_6), which yields a positive square pulse equal in duration to the input pulse. The positive square pulse is converted by tube T_7 into a negative one, which is applied to the grid of triode T_4 and cuts off this tube. While the tube is cut off, there occurs integration of the dc voltage by the circuit

R_1C. The voltage on capacitor C increases linearly. Owing to the amplification of tube T_3 there is applied to the cathode of tube T_2 a pulse much greater than the pulse on the capacitor and of opposite polarity.

When the input signal dies down, the trigger circuit returns to its initial state, the triode T_4 is unblocked and the capacitor rapidly discharges to the initial potential. The large negative pulse on the cathode of triode T_4 facilitates rapid discharge of the capacitor. Thus the converter output pulses are sawtoothed and have an amplitude proportional to the duration of the input pulses.

In order to go over to investigation of the distribution in magnetic moments, one need only connect the grid of the cathode follower T_1 to the input terminal and equalize the voltages on the cathodes of tubes T_1 and T_3.

Before being fed into the discriminator the output pulses from the converter were amplified by a one-stage amplifier. The amplitude discriminator consists of a system of triggers, similar to the trigger circuit employed in the converter (tubes T_5 and T_6).

The set-up was calibrated by means of an MGI-1 square pulse generator. Applying pulses of known duration to the input of the converter and varying the threshold of one of the channels of the pulse height discriminator, we adjusted it to the point where the scaler connected to this channel began to count; then we increased the duration of the signal pulse, set the threshold of the next channel, etc.

The amplifier installed before the converter had a passband from 0.5 kc to 2.5 Mc. Its gain could be varied in a wide range; the maximum amplification factor was $5 \cdot 10^5$. Before measurements the gain of the amplifier was set just below the point where the first channel of the pulse height discriminator responded to the amplifier noise.

For our experiments we chose an iron film prepared by vacuum evaporation on a glass plate measuring 0.5 x 20 x 0.2 mm. The film thickness was 2000 Å. The axis of easy magnetization was parallel to the length of the plate and in the measurements was aligned with the common axis of the magnetizing solenoid and the measuring coil.

Design calculations show that the shape and duration of the voltage pulses at the amplifier input depend on the time constant of the measuring coil. For the duration of the voltage pulse to be representative of the time of change of the magnetic flux one must use a coil with a sufficiently small time constant. The time constant of the coil depends on the inductance, resistance and capacitance of the coil. Usually larger coils have larger time constants. One can reduce the time constant by reducing the cross section of the coil form and also the diameter and length of the winding.

In winding our coils we used 0.02 mm diameter enameled wire. The coils were would on glass tubes of a diameter just sufficient to admit the specimen. Further decrease of the time constants could be attained only by reducing the number of turns, which, however, can lead to undesirable decrease in the magnitude and number of the pulses. Hence we carried out a series of exploratory measurements using a number of different coils with a view to choosing a coil that would have a sufficiently small time constant and yet would yield pulses of sufficient amplitude.

In testing a series of coils of decreasing size we found a coil beginning with which further decrease of the coil size did not change the character of the duration distribution curves. Two such curves, obtained for coils Nos.1 and 2 (see table below) are shown in Fig.2; N is the number of pulses having a duration greater than the corresponding value on the horizontal scale.

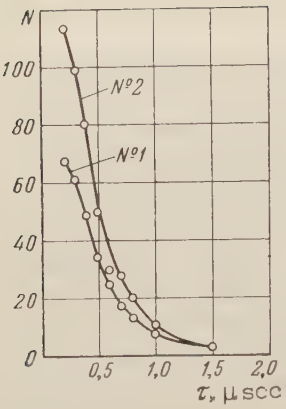

Fig.2. Integral distributions of pulses in duration obtained with two different coils.

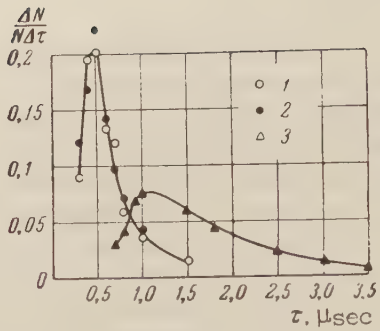

Fig.3. Differential distribution of pulses in duration: 1) specimen - film (coil No.1); 2) specimen - film (coil No.2), 3) specimen - iron wire (coil No. 1).

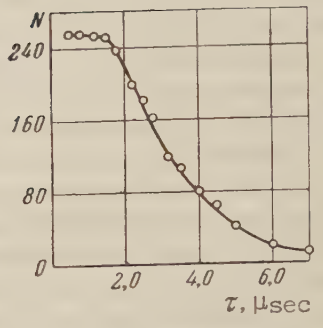

Fig.4. Integral distribution of pulses in duration. Specimen - film (coil No.3).

Despite the fact that these two coils differ appreciably (100 and 290 turns, respectively) the two curves are similar in appearance. The fact that a larger number of jumps was recorded with coil No.2 is explained by the fact that it has a larger number of turns and a greater length so that with it there are recorded some jumps that are missed in using coil No.1.

Coil No.	Number of turns	Length, mm	Inside diameter of winding, mm
1	100	0.4	0.80
2	290	2	0.82
3	10 000	10	0.85

The differential distribution curves obtained with these two coils virtually coincide (curves 1 and 2 in Fig.3). Thus the influence of these coils on the pulse duraction is insignificant and hence the curves obtained characterize the actual distribution in duration of the magnetization reversal jumps. Curve 3 in Fig.3 gives the differential distribution in duration of magnetization jumps in an iron wire 0.2 mm in diameter as obtained by means of coil No.1

We shall not give the data obtained for all the tested coils, but to show to what extent the pulse duration depends on the coil parameters, in Fig.4 we give the distribution curve obtained by means of coil No.3. It will be obvious that the character of this curve differs from that of the curves obtained with coils Nos.1 and 2 (Fig.2).

It will be evident from the curves shown in Figs.2 & 3 that in an iron film 2000 Å thick very few jumps have a duration exceeding 1.5 μsec. The peak in the jump duration distribution lies at about 0.5 μsec, whereas in the case of a bulk specimen of relatively small diameter (influence of eddy currents negligible) the maximum in the number of jumps corresponds to a duration of approximately 1 μsec.

Krasnoyarsk Polytechnic Institute

References

1. A.M.Rodichev, N.M.Salanskii & V.I.Sinegubov, Izv.Sinegubov, Izv.Sibirsk. otd. AN SSSR, (Bulletin of the Siberian Branch of the USSR Ac. of Sci.), No.3, 123 (1960).

2. K.M.Polivanov, A.M.Rodichev & V.A.Ignatchenko, Fizika metallov i metallovedenie, 9, 778 (1960). (Trans.Physics of Metals & Metallography.)

CONTRIBUTION TO THE THEORY OF HIGH FIELD MAGNETIZATION REVERSAL IN THIN FILMS

- A.M.Rodichev

Experiments have shown that magnetization reversal of thin ferromagnetic films is not controlled by eddy currents. Hence the process can be described without recourse to Maxwell's equations. It is commonly assumed that in high fields a thin film reverses by uniform motion, i.e., rotation of the "rigid" magnetic moment of the film. The process has been considered by a number of authors[1-7]; the point of departure is usually the equation of Landau & Lifshits[8] or of Gilbert[9] describing uniform procession.

Theory of magnetic reversal by uniform rotation

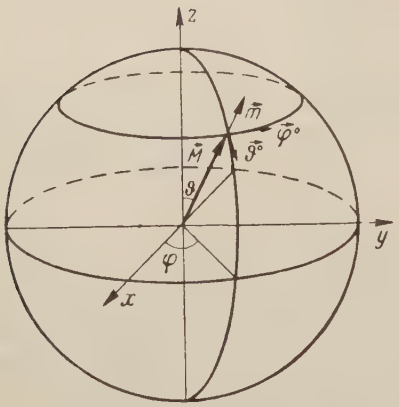

Fig.1. Coordinate system used in the calculations.

Let us attempt to solve the problem in the most general form on the assumption of uniform rotation.

We consider a thin ferromagnetic film lying in the plane xy and magnetized in the x direction (Fig.1).

The anisotropy field in the plane of the film is given by $H_{ax} = \frac{2K}{M_s}\cos\varphi = n_1\cos\varphi$, where K is the anisotropy constant*, M_s is the saturation magnetization and φ is the azimuthal angle measured from the x axis. The normal anisotropy field is of the form $H_{az} = -N_\Phi M_s\cos\vartheta = -n\cos\vartheta$, where ϑ is the polar angle measured from the z axis, and N_Φ is the demagnetizing factor in the z direction. Applied to the film are a reversing field $H_e = -H_x$ greater than the anisotropy field, and a small field H_y in the y direction.**

We start with Gilbert's equation

$$\dot{\mathbf{M}} = \gamma[\mathbf{HM}] + \frac{a}{M}[\mathbf{M}\dot{\mathbf{M}}]. \qquad (1)$$

The position of the vector M is described by two equations following directly from (1):

$$\dot{\vartheta} = \gamma(\vec{\varphi}^0\mathbf{H}) - a(\vec{\varphi}^0\dot{\mathbf{m}}), \qquad (2)$$

$$\sin\vartheta\dot{\varphi} = -\gamma(\vec{\vartheta}^0\mathbf{H}) + a\dot{\vartheta}, \qquad (3)$$

where $\vec{\vartheta}^0$, $\vec{\varphi}^0$ and $\dot{\mathbf{m}}$ are unit vectors forming an orthagonal trihedral ($\vec{\vartheta}^0$ is directed along the meridian, $\vec{\varphi}^0$ - along the parallel and $\dot{\mathbf{m}} = \frac{\mathbf{M}}{M}$).

---

*As measurements of anisotropy of thin films show, the anisotropy energy is satisfactorily described by the formula $E = K\sin^2\varphi$, which corresponds to the equation given for the anisotropy field.

**A small constant field H_y in the y direction has been used in a number of experiments, and resulted in a substantial acceleration of the reversal process and decrease of the critical rotation fields.

We insert in (2) and (3) the vector sum of all the field components and combine the resultant equations. Further, in view of the large value of the demagnetizing factor along the z axis ($n \gg H_e, H_y, H_{ax}$), we assume that the angle ϑ remains close to $\pi/2$ in the process of magnetization reversal. We write

$$\vartheta = \pi/2 + \beta, \quad \beta \ll 1, \quad \dot{\vartheta} = \dot{\beta}, \quad \cos\vartheta \approx -\beta, \quad \sin\vartheta \approx 1.$$

As a result of these operations we obtain

$$\frac{1+a^2}{\gamma}\dot{\beta} = H_e \sin\varphi - n_1 \cos\varphi \sin\varphi + H_y \cos\varphi + a\beta(H_e \cos\varphi - n_1 \cos^2\varphi - n - H_y \sin\varphi), \quad (4)$$

$$\frac{1+a^2}{\gamma}\dot{\varphi} = -\beta(H_e \cos\varphi - n_1 \cos^2\varphi - n - H_y \sin\varphi) + a(H_e \sin\varphi - n_1 \cos\varphi \sin\varphi + H_y \cos\varphi). \quad (5)$$

Further precise solution of these equations is possible only by numerical methods. Hence to obtain a solution we will use a rough approximation: we assume that in the process of rotation the angle β corresponds to the position of dynamic equilibrium and that the variation in the angle is insignificant everywhere except at the beginning and end of the process, i.e., we set $\beta = 0$*; then β can be found from (4). Inserting its value into (5), we obtain

$$\dot{\varphi} = \frac{\gamma}{a}(H_e \sin\varphi - n_1 \cos\varphi \sin\varphi + H_y \cos\varphi). \quad (6)$$

The same equation was obtained by Olson & Pohm[5] by a different method. Inasmuch as $\dot{M}_x = -M_s \sin\varphi\dot{\varphi}$, the shape of the reversal pulse must be described by

$$\dot{M}_x = -M_s \frac{\gamma}{a}\sin\varphi(H_e \sin\varphi - n_1 \cos\varphi \sin\varphi + H_y \cos\varphi). \quad (7)$$

Let us consider a number of particular cases.

1. $H_y = n_1 = 0$. Integrating (6) from φ_0 to $\pi - \varphi_0$, we obtain for the reversal time

$$t = \frac{a}{\gamma H_e} \ln \operatorname{ctg}^2 \frac{\varphi_0}{2}. \quad (8)$$

If we carry out the calculations on the basis of Gilbert's equation as before, but neglect the demagnetizing factor and the anisotropy, then for the reversal time we obtain

$$t = \frac{1+a^2}{a} \cdot \frac{1}{\gamma H_e} \ln \operatorname{ctg}^2 \frac{\varphi_0}{2}. \quad (9)$$

Thus the presence in the film of a large demagnetizing factor along the z axis accelerates the process by a factor of $\frac{1+a^2}{a^2}$.**

2. $H_y = 0, n_1 \neq 0$. In this case integration of Eq.(6) for the same initial and final conditions, i.e., between the same limits, yields

---

*This approximation was used by Smith[4] and Polivanov[7]; Conger & Essig[1] used the approximation $\frac{d^2\varphi}{dt^2} = 0$.

**The physical meaning of this acceleration was first considered by Polivanov.[7]

$$t = \frac{a}{\gamma (H_e^2 - n_1^2)} \left(H_e \ln \operatorname{ctg}^2 \frac{\varphi_0}{2} - n_1 \ln \frac{H_e + n_1 \cos \varphi_0}{H_e - n_1 \cos \varphi_0} \right). \qquad (10)$$

Similar equations for this case were obtained by Conger & Essig[1] and Polivanov[7]. The variation of the reciprocal of the reversing time with H_e for different n_1 and φ_0 is shown in Fig.2.

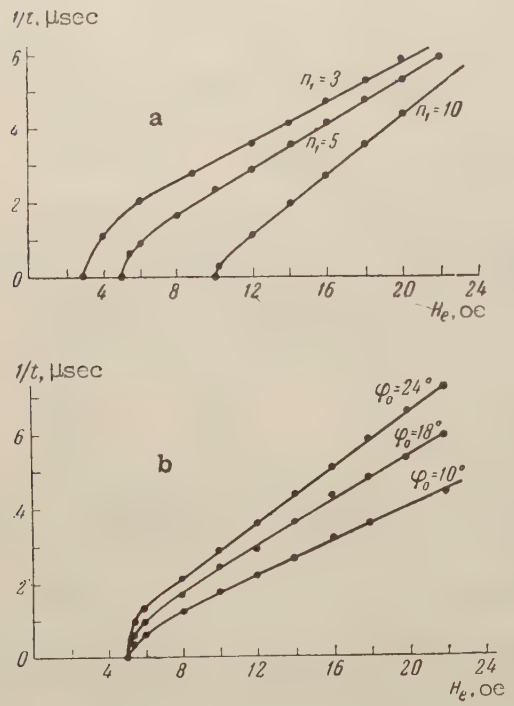

←Fig.2. a) Variation of $1/t$ with H_e for constant φ_0 ($\varphi_0 = 18^\circ$) and different n_1; b) same but for constant n_1 and different φ_0.

3. $H_y \neq 0$, $n_1 = 0$. Obviously, calculations for this case must be carried out on the assumption that the fields H_e and H_y are applied simultaneously. If the integration of (6) is carried out with the same initial and final conditions both in the case of absence and in the case of presence of H_y, φ_0 and $\pi - \varphi_f$ must be smaller than arc tan (H_y/H_e) and the corresponding reversal times prove to be equal, as might have been expected.

4. $H_y \neq 0$, $n_1 \neq 0$. Let us first consider the influence of a small constant field H_y on the initial and final states of a thin film. The magnetization vector in the presence of H_y will be oriented so that the moments of the anisotropy field and the field H_y are equal:

$$n_1 M_s \cos \varphi \sin \varphi = H_y M_s \sin (\pi / 2 - \varphi).$$

Whence

$$\sin \varphi_0 = \frac{H_y}{n_1}. \qquad (11)$$

Correspondingly, the final position will be given by

$$\sin \varphi_f = \frac{H_y}{H_e + n_1}. \qquad (12)$$

We integrate (6) between the limits defined by 1/10 and 9/10 of the total change in M_x (in accord with the usual experimental conditions).* For purposes of comparison let us find the reversal time in the absence of H_y by means of Eq.(10) for the same limits of integration. We take our numerical data from the work of Humphrey & Gyorgy[10]: H_e = 6 oersted, n_1 = 4.8 oersted and H_y = 0.2 oersted. Our calculations showed that the reversal times in the presence of H_y and in its absence are equal within the limits of the computational error (Eq.(6) was integrated graphically). Thus theoretical calculations show that a field H_y of the order of the field commonly used in experiments has no significant influence on

---

*It must be noted that for practical purposes what is important is not so much the reversal time calculated in the above manner as the time between application of the driving field H_e and completion of the reversal process. This parameter should be the subject of careful investigation.

the initial conditions and the reversal time.

Comparison of Theory with Experiment

1. Comparison of the experimental and theoretical $1/t$ vs H_e curves shows that in weak fields the experimental curve has a second derivative opposite in sign to that of the theoretical curve. This character of the experimental curve is explained by the theory of wall movement.[11] The existence of wall motion has been confirmed by a number of authors. In high fields one can by appropriate choice of a fit the theoretical curve to the experimental one. The values of a found in this manner for different films in the experiments of Conger & Essig[1] proved to be 5.17, 10.97 and 28.34; in the experiments of Hanzel & Conger[12] there were obtained values of 9.68 and 24.65; in the experiments of Humphrey & Gyorgy[10] a value of about 5. In some cases, however, it proved impossible for a given n_1 to fit the experimental curves for any value of the constant a.

Thus the value of a found by fitting the experimental curves appears to vary in the range from 1 to 30.

The same constant found from ferromagnetic resonance experiments has a value of the order of 0.01-0.1. It is important to note that calculations from ferromagnetic resonance and pulse magnetization reversal measurements are based on the same equation comprising constants that are apparently highly characteristic of each given material. And if in the case of resonance there does actually obtain uniform precession, the great divergence between the values of a may be taken as evidence that the process of pulse magnetization reversal does not involve uniform precession and cannot be accurately calculated on the basis of this concept.

This is the principal argument against coherent rotation.

2. There is evidence from experiments in which a field H_y was applied that the critical rotation field $H_к$ decreases significantly with increase of H_y. Utilizing the concept of coherent rotation of a "rigid" magnetic vector, one can readily calculate the H_y dependence of $H_к$.

The value of $H_к$ can be found from the condition of equality of the moment of the anisotropy field and the field $\mathbf{H}_e + \mathbf{H}_y$ or by setting the time derivative of the angle φ equal to zero. Both conditions yield the following expression

$$H_e = \frac{n \cos\varphi \sin\varphi - H_y \cos\varphi}{\sin\varphi}.$$

The value of the critical field $H_к$ will be given by the maximum of this expression, the condition for which is

$$\sin^3\varphi = \frac{H_y}{n_1}. \qquad (13)$$

Here we have $H_к = H_y \operatorname{ctg}^3\varphi$. We introduce the notation $\frac{H_y}{n_1} = m$. Consequently,

$$H_к = H_y \frac{(1 - m^{2/3})^{3/2}}{m}.$$

Dividing by n_1, we obtain

$$\frac{H_к}{n_1} = (1 - m^{2/3})^{3/2}. \qquad (14)$$

Fig.3 shows the theoretical dependence (14) (curve 1) and the curves based on experimental data[10,13,14]. It will be evident from the figure that the experimental curves lie far from the theoretical one.

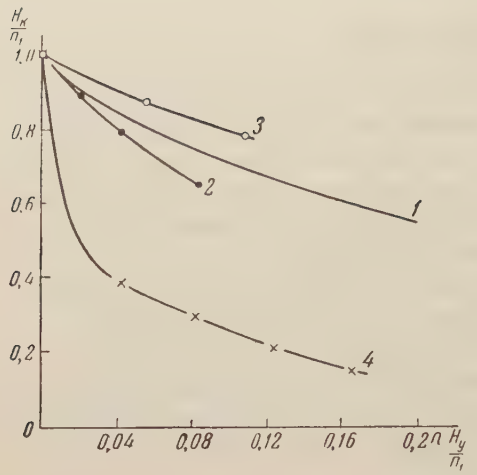

Fig.3. Variation of $H_к/n_1$ with H_y/n_1: 1) theoretical curve, 2) curve calculated according to the data of Humphrey & Gyorgy[10], 3) curve calculated according to the data of Hagedorn[13], 4) curve calculated according to the data of Kobelev & Efimov[14].

3. Thus our theoretical calculations show that the presence of a small constant field H_y should not accelerate the reversal process. Actually, however, numerous experiments indicate that such a field results in a substantial decrease of the switching time. Thus in the experiments of Humphrey & Gyorgy[10] with H_e = 6 oersted and n_1 = 4.8 oersted, application of a field H_y = 0.2 oersted reduced the reversal time by a factor of 8.

These facts are further arguments against the theory of uniform rotation.

Conclusions

It would appear that the process of magnetization reversal in thin ferromagnetic films, as well as in bulk ferromagnets, is much more complicated than would follow from the concepts now commonly held. The initial state of a ferromagnetic film (or ferrite) is characterized by a certain spin wave distribution appropriate to the given temperature.[15] Bulaevskii et al[16] showed that if the angle ϑ between H and M is greater than $\pi/2$, the spin waves will built up irreversibly, and that the waves associeated with different ϑ build up at different rates. In a thin film, by virtue of the large demagnetizing factor along the z axis there will build up only the spin waves, the wave vector of which lies in the plane of the film. Inasmuch as the vectors of different spin waves are directed to the left and to the right relative to the x axis, there will be present "right-hand" and "left-hand" parts of the magnetization. This phenomenon was observed by Olson & Pohm[5].

Naturally, under these conditions, in the presence of fields of the form $q\nabla^2 M$, the mutual influence of out-of-phase reversing parts of the ferromagnet leads to the reversal time being appreciably shorter than in the case of uniform precession, and to the effective damping constant a being appreciably larger. Upon application of H_y the symmetry of the process is disturbed and one direction of rotation of the magnetic moments becomes favored. Factors tending to slow down the process are therefore to some extent suppressed or diminished.

I take this opportunity to thank K.M.Polivanov as well as V.V.Kobelev and I.A.Efimov for making available the results of their work in manuscript form.

References

1. R.L.Conger & F.C.Essig, Phys.Rev., 104, 915 (1956).
2. P.R.Gilette & K.Oshima, J.Appl.Phys., 29, 529 (1958).
3. P.R.Gilette & K.Oshima, Ibid., 29, 1466 (1958).
4. D.O.Smith, Ibid., 29, 264 (1958).
5. C.D.Olson & A.V.Pohm, Ibid., 29, 274 (1958).
6. R.K.Kikuchi, Ibid., 27, 1352 (1956).
7. K.M.Polivanov, Ferrity (Ferrites), p.332, Minsk, 1960.

8. L.D.Landau & E.M.Lifshits, Sow.Phys., 8, 153 (1935).
9. T.L.Gilbert, Phys.Rev., 110, 1243 (1955).
10. F.B.Humphrey & E.M.Gyorgy, J.Appl.Phys., 30, 935 (1959).
11. R.L.Conger & F.C.Essig, Ibid., 28, 855 (1957).
12. A.L.Hanzel & R.L.Conger, Ibid., 30, 1932 (1959).
13. F.B.Hagedorn, Ibid., 30, 254 (1959).
14. V.V.Kobelev & I.A.Efimov, Present issue of the Bulletin; I.A.Efimov, Present issue of the Bulletin, p.639; 647.
15. A.I.Akhiezer, V.G.Bar'yakhtar & M.I.Kaganov, Uspekhi fiz.nauk, 71, 4, 533 (1960). (Trans.Soviet Physics - Uspekhi.)
16. L.N.Bulaevskii, V.M.Fain & G.I.Freidman, Zhur.eksp.i teor.fiz., 39, 516 (1960). (Trans.Soviet Physics - JETP.)

APPARATUS FOR INVESTIGATING PULSE SWITCHING OF THIN FERROMAGNETIC FILMS

- T.N.Nikitina & R.V.Telesnin

1. Nanosecond Pulse Generator

To investigate the pulse characteristics of thin magnetic films it is essential to have a generator yielding square reversing pulses with a rise time not exceeding $(4-5)\cdot10^{-9}$ sec.[1,2]

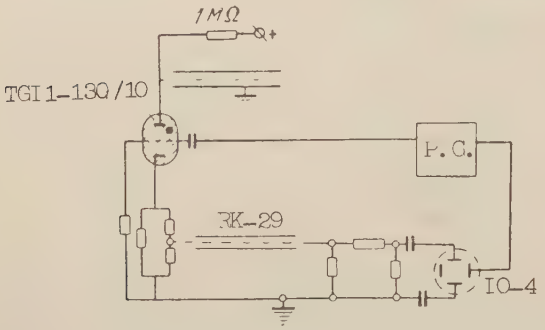

Fig.1. Circuit of pulse generator.

For purposes of such investigations we developed and constructed a generator operating on the principle of discharge of a long line through a hydrogen thyratron, type TGI1-130/10 (Fig.1). The generator is designed in the form of a coaxial line which provides for matching of the shaping line with the load and allows of reducing the parasitic parameters of the circuit to a minimum (Fig.2).

The thyratron is installed in a gap in the central conductor. The condition for matching is

$$R_T = R_L = Z,$$

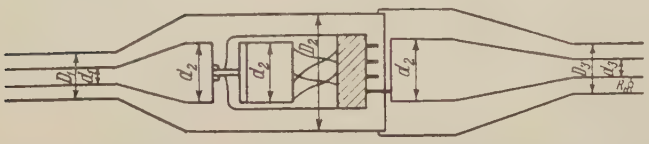

Fig.2. Installation of thyratron in coaxial line. $Z = 60 \ln (D_1/d_1) = 77$ ohm; $Z_L = R_L = 60 \ln (D_3/d_3) = 38$ ohm.

where R_T is the resistance of the thyratron, R_L is the resistance of the load in the thyratron cathode circuit, and Z is the characteristic impedance of the line. Hence at the point of the gap the characteristic impedance must change by R_T. This is realized if over the entire length of the line

$$Z = 60 \ln \frac{D_1}{d_1} = 60 \ln \frac{D_2}{d_2} = 60 \ln \frac{D_3}{d_3}$$

(D_1, D_2 and D_3 are the inner diameters of the outside tubes and d_1, d_2 and d_3 are the outside diameters of the inner tubes).

The overall length of the line is 3.5 meters. The pulse rise time is 4-5 nanosec (equivalent to a steepness of 10 amp/nanosec), the pulse duration is 40 nanosec, the maximum obtainable pulse current is 60 amp. In studying pulse switching of ferromagnetic films one must provide a "reset" pulse between each working pulse in order to bring the film to the initial state.

In order to avoid building a second pulse generator, which would have to be synchronized with the main pulse generator, we utilized part of the main pulse passing through the delay line; this automatically shifts the reset pulse the required interval relative to the main pulse. The magnetizing winding surrounding the specimen is connected to the cathode circuit of the thyratron. The reset pulse is taken off a resistor in the cathode circuit and fed through an RK-6 cable 28.5 meters long to a second winding about the specimen (Fig.3). Owing to the appreciable length of the cable, the reset pulse is delayed $140\cdot10^{-9}$ sec relative to the main pulse (the delay introduced by the RK-6 cable is 5 nanosec/meter).

Oscillograms of a reversing and a reset pulse are shown in Fig.4. In this case for purposes of comparison the reset pulse was applied in the same direction as the reversing pulse.

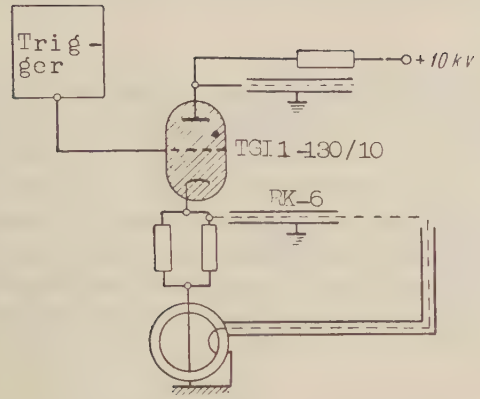

Fig.3. Diagram of reset pulse circuit.

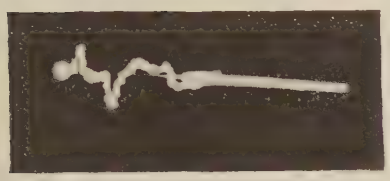

Fig.6. Oscillogram of magnetization reversal pulse recorded for a KVP steel disk 80 μ thick and 15 mm in diameter.

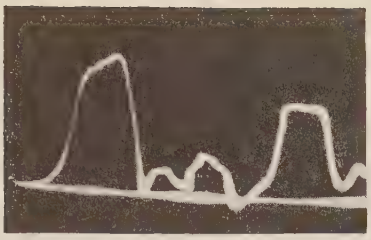

Fig.4. Oscillogram of reversing and reset pulses.

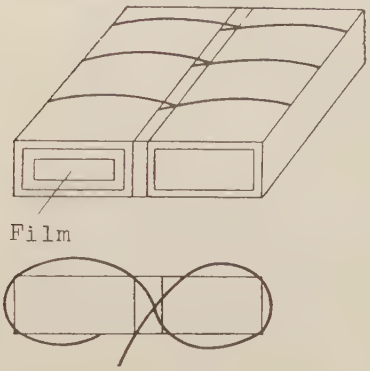

Fig.5. Specimen coil with compensating winding.

To observe the signals we used an I0-4 oscillograph modernized as follows:

1. The 13L037 cathode ray tube was replaced by a 13L03 tube which has direct leads from the deflecting plates brought out through the envelope, which substantially reduces the input capacitances and inductances.

2. The minimum sweep time was reduced from 1 to 0.2 μsec. The sweep was calibrated by means of a sinusoidal voltage from a high frequency LMS-551 oscillator modulated with square pulses from another special generator. According to this calibration 1 mm on the screen corresponds to $2 \cdot 10^{-9}$ sec.

2. Magnetization Reversal of Ferromagnetic Materials

In reversing thin films with a magnetic flux of about 0.02 maxwells, an important problem is elimination of cross interference induced in the secondary winding by a pulse in the primary winding. The secondary winding consists of two halves wound in opposition. Moreover, so that the winding would not "ring" like an inductance, the secondary winding was made of very thin conductor with high resistance (180 ohm/meter). Further to reduce the self-capacitance of the winding it was applied so that $(t/d) \approx 4.5\text{-}5$ (t is the pitch of the turns and d is the diameter of the conductor). The secondary winding was applied in figure eights, i.e., one turn was wound on one half the frame and then an opposed turn was placed on the second half of the frame. Both halves of the frame in both windings were made as identical as possible (Fig.5). The primary winding is wound on the same frame assembly at a distance of 5 mm from the secondary winding.

The entire assembly was placed in a copper shield, the dimensions of which satisfied the ratio $(D_s/D_o) = 3$ (D_o is the diameter of the winding and D_s is the diameter of the shield).[13]

In the preliminary tests we inserted a 15 mm diameter disk of cold rolled KhVP steel 80 μ thick into the coil assembly and recorded the reversal pulses. The pulses from the secondary winding (four turns) were applied directly to the plates of the I0-4 oscillograph. The oscillogram of a reversal pulse for the disk is shown in Fig.6.

The pulses obtained in reversing the magnetization of a very small toroid with an inside diameter of 0.9 mm and an outside diameter of 1.5 mm were very appreciable: the trace rose almost to the edge of the oscillograph screen (without amplification). Pulses from thin films naturally require amplification by means of a wide-band amplifier such as the UR-4.

Chair of General Physics,
Physics Faculty Moscow State University

References

1. J.A.D.Lewis & F.H.Wells, Millimicrosecond Pulse Techniques, N.Y., 1954. (Cited in Russian trans.)

2. G.V.Glebovich & L.A.Morgulin, Formirovanie impul'sov nanosekundnoi dlitel'nosti (Shaping of nanosecond pulses), M., 1958.

3. G.Kaden, Electromagnetic Shields, M., 1957.

NANOSECOND CURRENT PULSE GENERATOR FOR INVESTIGATING THE BEHAVIOR OF FERROMAGNETIC FILMS

- O.S.Kolotov & T.N.Nikitina

For investigating the switching time of thin films it is essential to have a pulse generator yielding current pulses with an amplitude of several amperes and a rise time of the order of 10^{-9} sec. Mercury relay type generators (for example, the GKI-4 generator) which are sometimes employed in such experiments, although they do provide a short rise time (<1 nanosec), have a low repetition rate and have a relatively low peak current rating.[1,2] Moreover, such generators cannot be trigger operated, which may give rise to difficulties in synchronizing the operation of the generator with the operation of the other equipment.

A high pulse repetition rate (greater than 1000 pps) can be obtained only by means of circuits employing electronic tubes. Actually, using even common types of tubes one can obtain current pulses with a rise time of less than 2 nanosec with a rather appreciable current.

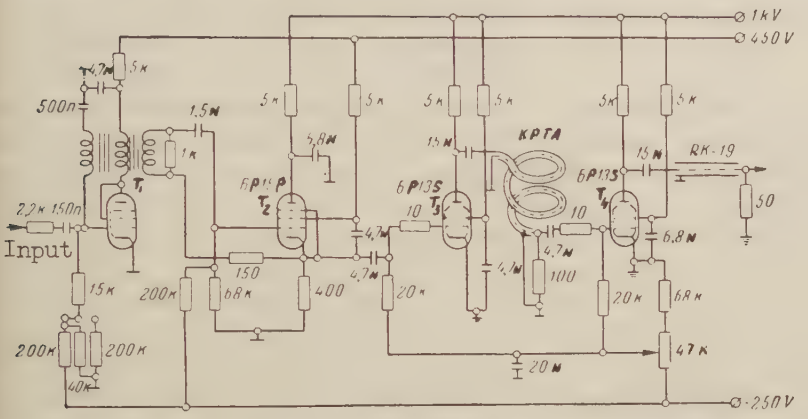

Fig.1. Nanosecond pulse generator circuit.

Fig.1 shows a pulse generator circuit employing the principle of successive limiting and amplification of the signal.

The blocking oscillator, assembled about a 6P14P tube (T_1) produces pulses with a rise time of 20 nanosec, a duration of 100 nanosec and an amplitude of 180 v. This pulse voltage is taken off the secondary of the transformer and applied to the input of the cathode-loaded amplifier (tube T_2) operating as a limiter. The pulses taken off the cathode of T_2 have an amplitude of 350 v and a rise time of 10 nanosec. They are applied to the input of the next nonlinear amplifier (tube T_3). This stage limits the pulses and at the same time acts as a power amplifier, so that on the 70 ohm load (coaxial inverter) there appears a pulse of 320 v amplitude with a rise time of 4 nanosec. This pulse has negative polarity. In order to reverse the polarity, we employ a coaxial inverter, the operating principle of which is described in Refs.3 & 4. The inverter consists of a section of KPTA coaxial cable wound (8 turns) on a ferrite (Oksifer 2000) ring. The core has a diameter of 30 mm and a cross section of 6 x 6 mm. The inductance provided by the outer braiding of the cable is sufficient to invert square pulses of up to 0.1 μsec duration without distortion of their flat top. The plate load in the output stage is a section of RK-19 coaxial cable with a characteristics impedance of 50 ohm; this cable carries the reversing pulse to the coil surrounding the ferromagnetic film specimen. The peak pulse amplitude attains 280 v, which corresponds to a current of 5.6 amp.

The pulse duration, which is determined by the capacitance of the capacitor in the grid circuit of the blocking oscillator, was chosen to be constant and equal to 100 nanosec. The rise of a pulse is shown in the oscillogram reproduced in Fig.2. It will be evident from the figure that the rise time (from 0.1 to 0.9 the pulse height) is less than 2 nanosec.

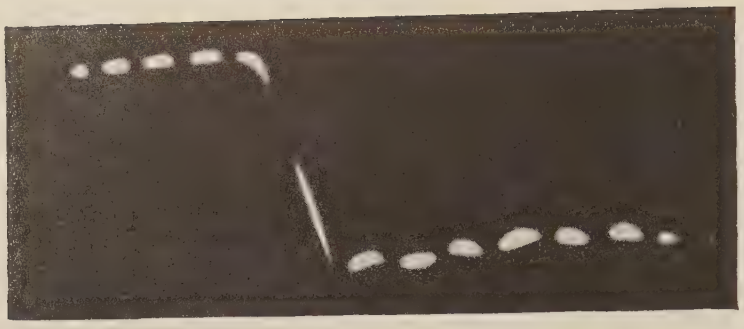

Fig.2. Oscillogram of the leading edge of a pulse (time markers at 2 nanosec interavls).

The generator is driven by an external positive pulse of 40 v amplitude and a rise time of 0.1-0.2 μsec. If necessary the generator can be operated as a self-excited oscillator with a pulse repetition rate of up to 5000 pps. In building the circuit it is essential to reduce all parasitic parameters to a minimum. In order to reduce the inductance of the plate circuit the 6P13S tube was enclosed in a 45 mm diameter metal cup. The entire circuit is assembled of standard commercial components; in particular we used KSO type capacitors and VS type resistors. Since in the main, the tubes are cut off, the current drawn by the plate circuits is small. The mean power dissipated by the tube electrodes does not exceed the rated values.

I desire to thank R.V.Telesnin for his interest in the work

Physics Faculty,
Moscow State University

References

1. J.A.D.Lewis & F.H.Wells, Millimicrosecond Pulse Techniques, N.Y., 1954. (Cited in Russian trans.)

2. G.V.Glebovich & L.A.Morgulin, Formirovanie impul'sov nanosekundnoi dlitel'nosti (Shaping of nanosecond pulses), M., 1958.

3. O.S.Kolotov, Yu.N.Lobanov, A.S.Obukhov & N.M.Polev, No.3, 73 (1960). (Trans.Instruments & Experimental Techniques.)

4. O.S.Kolotov, Yu.N.Lobanov & Z.Shil'berskii, Ibid., No.3 (1961). (Trans. Ibid.)

AMPLIFICATION OF NANOSECOND PULSES

- O.S.Kolotov & T.N.Nikitina

In oscillographic observation of different physical processes, for example, pulses associated with switching of thin films, it is frequently necessary to amplify extremely brief signals, i.e., pulses with a duration of 10^{-8}-10^{-9} sec. To assure a clear oscillogram the amplifier utilized must provide an amplification factor of the order of 1000 with the output signal amounting to some tens of volts in amplitude. Conventional designs of wide-band amplifiers possessing these parameters require the use of a large number of tubes, and such amplifiers are complex and hence difficult to build and adjust.

In a number of cases the problem of amplifying short pulses can be solved by pulse operation of the amplifier tubes.[1-3] This is accomplished by applying a square voltage pulse to one of the tube electrodes, for example, the screen grid, thereby "forcing" the operation of the tube for a brief interval including the time of arrival of the signal to be amplified. As a result of application of the forcing or "supply" pulse there occurs an increase of the plate current and the transconductance during the period of the pulse. At the same time the section of the grid characteristics over which the transconductance is constant is broadened. This makes it possible to obtain under forced operation higher values of the output voltage for the same plate load as compared with ordinary operation. Obviously, the duration of the "supply" pulse must be greater than the duration of the signal.

Moverover, the "supply" pulse must be applied sufficiently in advance of the signal to permit settling of the electrode voltages. This type of operation is particularly convenient when the above sequence can be produced by the investigated effect; in other cases it is necessary to introduce an appropriate delay line to retard the signal.

Pulse Characteristics of the Tubes Employed

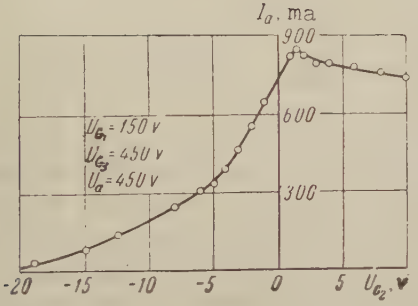

Fig.1. Pulse characteristic of 6Zh22P tubes.

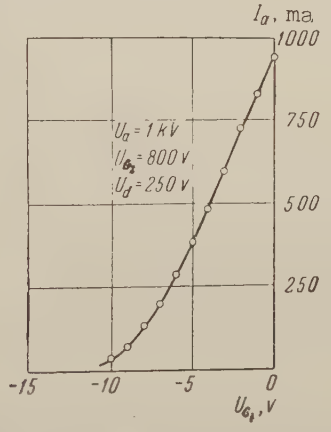

Fig.2. Pulse characteristic of 6V1P tubes.

For our experimental amplifiers we used 6Zh22P and 6V1P tubes which under normal operating conditions have a grid characteristic with a slope of ~30 ma/v.

We investigated the operation of these tubes under pulse conditions by means of the pulse generator described in Ref.2. On the basis of the series of recorded pulse grid characteristics we chose the optimum conditions for supplying the tubes, conditions characterized by a maximum value of the transconductance within

the range of allowable voltages on the tube electrodes.

For the 6Zh22P tubes (Fig.1) we chose the following operating conditions: voltage on plate and screen grid 450 v, amplitude of pulse applied to the control grid 150 v. Increase of the "supply" pulse above 150 v does not produce any noticeable increase of the transconductance, but does increase the power dissipated by the grid. The maximum slope of the grid characteristic of the 6Zh22P tube under the above operating conditions is 80-90 ma/v. The important point is that this value remains virtually constant over the grid voltage range from -4 to +1.5 v (Fig.1).

The transconductance of the 6V1P tube in pulse operation attains an even greater value - 100-120 ma/v (Fig.2) - and remains constant over a grid voltage interval of 6 v (plate voltage 1000 v, voltage on screen grid 800 v, voltage on dynode 250 v). It is particularly convenient to use tubes with secondary electron emission in cases when it is necessary to have a symmetrical voltage at the output. When this is required the output signal is taken off the plate and dynode.

Nanosecond Pulse Amplifier Circuits

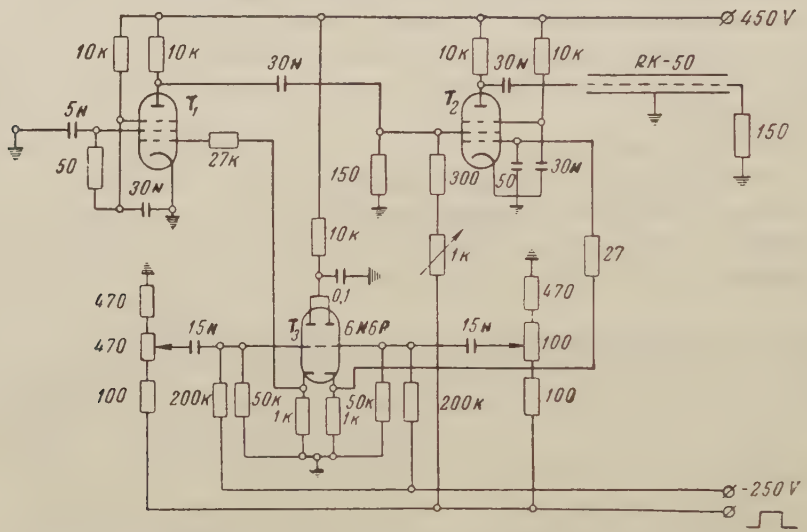

Fig.3. Two-stage amplifier employing 6Zh22P (6Ж22П) tubes. (6Н6П = 6N6P).

Substantial increase of the plate current and the slope of the grid characteristic (transconductance) made it possible to obtain a high amplification factor with relatively low values of plate load resistance (of the order of 30 to 150 ohm), which insures the requisite wide band characteristics of the amplifier. The circuit of a two-stage amplifier employing 6Zh22P tubes is shown in Fig.3. The voltages on the plates and screen grids are constant and equal to 450 v. In the absence of a voltage on the control grid, the plate current is nearly zero. The tubes are brought into operation by application of a positive pulse of 0.6 μsec duration and 150 v amplitude to their control grid. This pulse is taken off the cathode follower T_3. Upon cutting in of one of the amplifier tubes there appears on the plate load of this tube a negative pulse - a pedestal pulse - corresponding to the "supply" pulse. The amplitude of the pedestal pulse may attain 100 v. In case of cascading of several amplification stages one must provide for compensation of the pedestal pulse arriving together with the signal on the grid of the next tube. Such compensation is realized by applying part of the

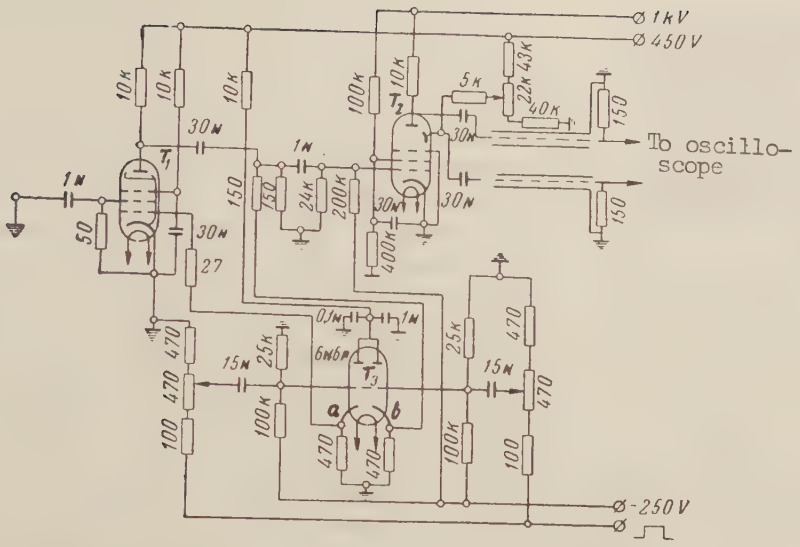

Fig.4. Two-stage amplifier using 6Zh22P (6Ж22П) and 6V1P (6В1П) tubes. (6Н6П = 6N6P).

positive voltage arriving on the control grid to the grid of the next tube by means of a variable voltage divider.

The magnitude of the compensating voltage is chosen so that the operating point on the grid characteristic will correspond to the sign of the amplified signal. The pedestal pulse at the amplifier output is not compensated inasmuch as its presence leads only in parallel displacement of the entire oscillogram on the screen. The load for the first stage is the circuit of the compensating divider with a resultant effective resistance of 75 ohm. The output stage is loaded by a coaxial cable with a characteristic impedance of 150 ohm.

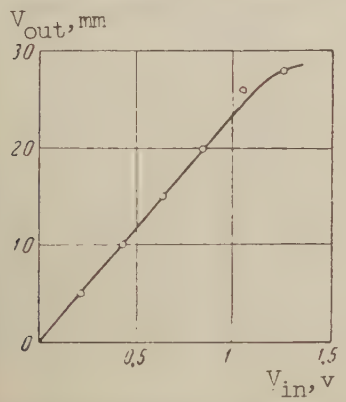

Fig.5. Dynamic characteristic of the amplifier with the 6Zh22P and 6V1P tubes.

The amplifier has a gain of 60 with an intrinsic rise time less than 3 nanosec. The maximum output signal amplitude is 50 v.

To obtain a symmetrical voltage on the amplifier output one can use a tube with secondary electron emission. Such an amplifier assembled about 6Zh22P (T_1) and 6V1P (T_2) tubes is shown in Fig.4. The load of the first tube is the circuit of the divider with cathode follower T_{3-b}. At the same time this circuit performs the following functions: 1) unblocks the tube T_2 initially cut off by the control grid, 2) compensates the negative pedestal pulse arriving from the plate of T_1 to the grid of T_2 and 3) selects the operating point on the grid characteristic of T_2 in accord with the polarity of the amplified signal. The equivalent load resistance of this circuit with respect to T_1 is 100 ohm.

The dynamic characteristic of this amplifier is shown in Fig.5, where the vertical scale is laid off directly in millimeters deflection of the oscilloscope trace. The sensitivity of the cathode ray tube is 0.15 mm/v. It will be

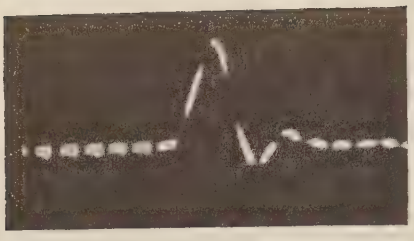

Fig.6. Oscillogram of output pulse from the amplifier with the 6Zh22P and 6V1P tubes. (Time markers = 2 nanosec.)

evident from the curve that the amplification factor of the circuit equals 150 with a maximum voltage of 160 v. The oscillogram of a 3 nanosec (length at half-height) output pulse is shown in Fig.6.

Obviously, with increase in the number of stages it becomes more difficult to compensate the pedestal pulse. First, the "supply" pulse must have an ideally flat top and a high degree of stability, inasmuch as even small variations in the amplitude and shape of the pulse will be amplified from stage to stage and can result in appreciable distortion of the signal. Second, aging of the tubes and fluctuation in the supply voltage can lead to shift of the operating points on the grid characteristic and, consequently, to instability of the amplification factor.

We succeeded in constructing a stably operating four-stage amplifier based on the above described circuits. By way of loads for the first two stages we chose short circuited sections of coaxial cable with a matching impedance. In this case there appear on the grid of the following tube two short pulses corresponding to the edges of the pedestal pulse. In the interval between these pulses the grid voltage is virtually zero and consequently does not depend on the power supply or aging of the tube. Choice of a zero working point is still possible inasmuch as the 6Zh22P tube has a linear section of the grid characteristic even in the range of positive grid voltages (to 2 v).

Obviously, use of short circuited cables (owing to reflection in them) leads to limiting of the amplified signal.

In the first stage we used a section of RK-50 cable with a characteristic impedance of 150 ohm; in the second stage, a section of RK-1 cable with a characteristic impedance of 75 ohm. Obviously, the equivalent load for the first stage is 75 ohm; that for the second stage, 37.5 ohm. The length of the cables (6 meters) corresponds to a maximum duration of the amplified signal of 60 nanosec. The amplification factor of the four-stage amplifier is 1600 with a rise time shorter than 3 nanosec.

The amplifier was tested and found to have stable characteristics up to a pulse repetition rate of 1000 pps; the current drawn from the plate voltage supply does not exceed a few milliamperes.

I am deeply grateful to P.V.Telesnin for his interest in the work and valuable suggestions.

Physics Faculty,
Moscow State University

References

1. A.I.Veretennikov, V.Ya.Averchenko, A.G.Egorov & Yu.A.Spekhov, Report presented at the Fourth Scientific-Technical Conference on Nuclear Radioelectronics, 1959.

2. O.S.Kolotov & Yu.N.Lobanov, PTE, No.2, 94 (1961). (Trans.Instruments & Experimental Techniques.)

3. O.S.Kolotov, A.A.Sanin & Z.Shil'berskii, Ibid., 1961.(Trans.Ibid.)

DOMAIN STRUCTURE OF UNIAXIAL FERROMAGNETIC FILMS

- V.V.Kobelev & A.A.Korsunskii

By now there is an extensive literature on the structure of ferromagnetic films. Most studies of the domain structure of films have been carried out by the powder technique (see, for example, Ref.1). This technique, which allows of substantial magnification of the observed image, is useful for investigation of individual sections on the surface of a magnetic films and observation of individual walls. At the same time, the powder technique has a number of shortcomings: it involves an inertial factor inasmuch as under dynamic conditions the powder particles must follow the wall motion; it is not generally suitable for observation of the overall domain pattern on relatively large specimens; it involves applying a magnetic suspension to the surface of the film which can obviously lead to changes in the magnetic properties of the film.

In present study we used the Kerr magneto-optic effect for observing the magnetic structure of films. As compared with the powder technique, this procedure is lag-free and allows of observing the domain structure of large specimens but has serious limitations as regards magnification of the image.

The optical system of our set-up, which is similar to that described by Fowler & Fryer[2], is shown in Fig.1. A beam of linearly polarized monochromatic light is incident on the surface of the specimen 7 at an angle of 60°. The light reflected from the specimen, after passing through the analyzer, is focused by lens 9 to form an image on the tilted screen or photographic plate. The screen or plate must be tilted at the same angle as the incident beam in order to obtain an undistorted image.

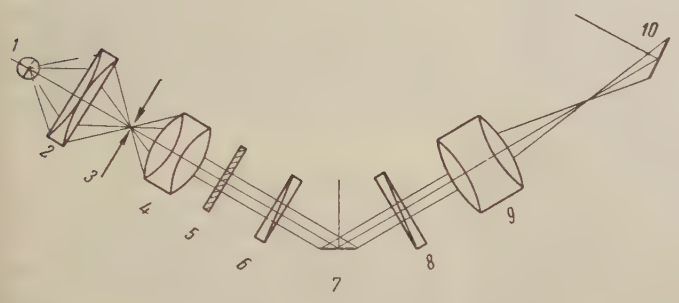

Fig.1. Optical system of the set-up for observing the domain structure of ferromagnetic films: 1) light source, 2) condensing lens, 3) aperture, 4) collimator, 5) interference light filter, 6) polarizer, 7) specimen, 8) analyzer, 9) lens, 10) viewing screen or photographic plate.

Our light source was a high pressure krypton-xenon tube (GSVD-120). Polaroid films were used for the analyzer and polarizer.

The uniform magnetic field in the region of the specimen is produced by a system of two pairs of square coils, mounted perpendicular to each other along the sides of a cube. One of the coil pairs produces a field H_z in the plane of incidence of the light; the other pair produces a field H_x perpendicular to the plane of incidence. The specimen is mounted in the center of the cube so that the field produced by the coils is always in the plane of the film.

The ferromagnetic films were prepared by vacuum ($3 \cdot 10^{-5}$ mm Hg) evaporation of the appropriate ferromagnetic material onto a heated (300°C) glass substrate in a magnetic field of the order of 50 oersted aligned with the plane of the substrate. By way of substrates we used 18 mm cover glasses 0.2 mm thick. We prepared films of Permalloy type alloys containing from 80 to 83% nickel. Through the use of a masking arrangement up to 9 specimens 1 cm in diameter could be deposited simultaneously.

Specimens prepared by this procedure have pronounced uniaxial anisotropy; the easy axis is aligned with the field direction during deposition.

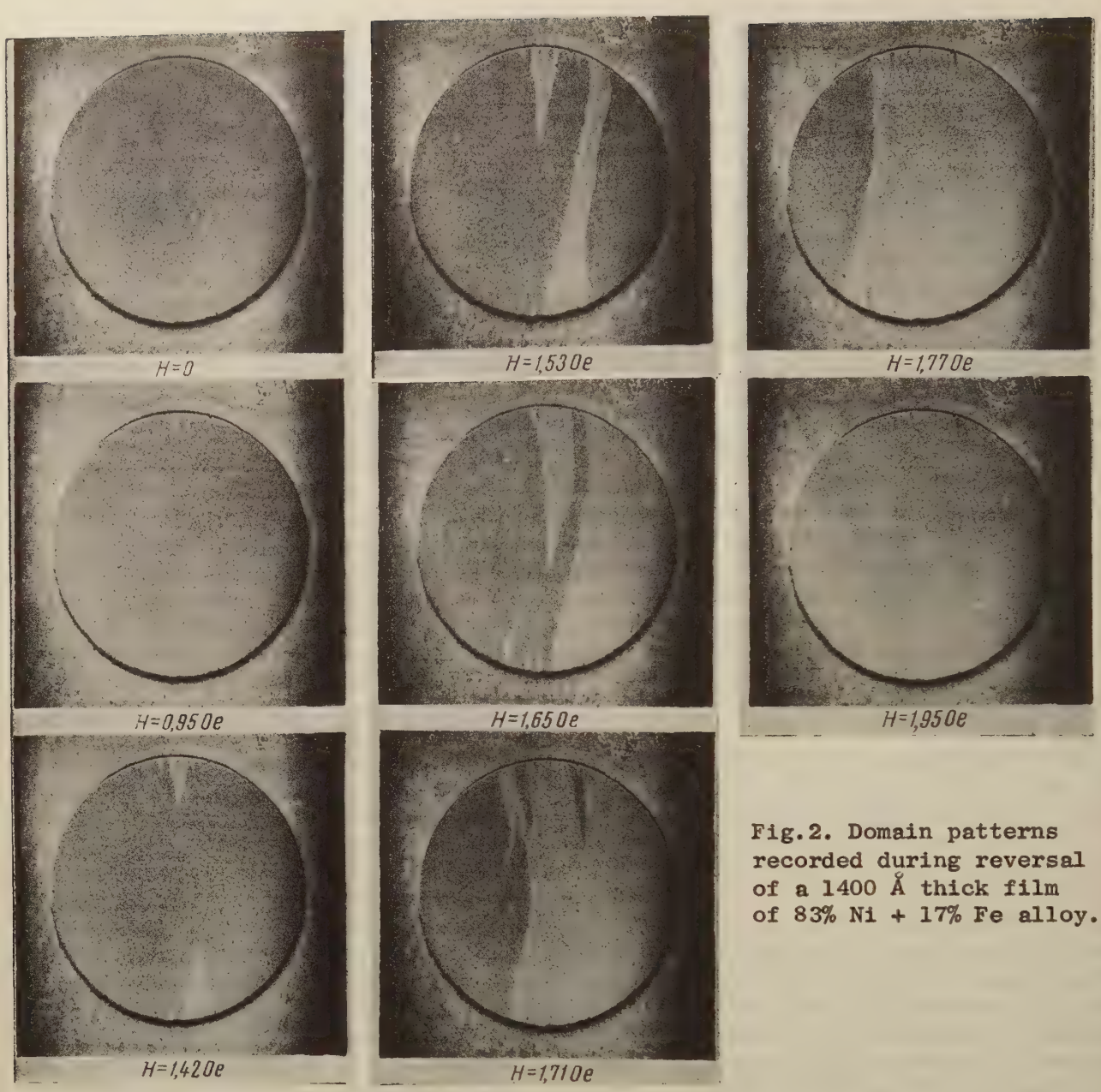

Fig.2. Domain patterns recorded during reversal of a 1400 Å thick film of 83% Ni + 17% Fe alloy.

In our experiments no dielectric coatings were applied to the ferromagnetic films, although it is reported[3] that by means of such coatings one can enhance the Kerr magneto-optic effect.

The domain structure appearing as a result of magnetization reversal of uniaxial films specimens with the field parallel to the easy axis is generally of the same type, provided the magnetic anisotropy of the specimens is pronounced. We did not observe complicated patterns like those described by Fowler, Fryer & Stevens[4] and any effects of aging.

By way of illustration in Fig.2 we show the successive stages of magnetization reversal of specimen No.315 prepared by evaporation of 83% Ni + 17% Fe alloy. The thickness of this specimen according to interferometer measurements was 1400 Å.

The specimen was mounted so that the easy axis was in the plane of incidence of the light. The reversal was produced by a field H_z in the same plane. First, by means of a strong negative field H_z the specimen was brought to the saturated state[3], then the negative field H_z was gradually decreased to zero, and then reversed and increased. Successive photographs of the domain structure were made at different increasing field values.

The amount of light incident on the film is so small that the domain structure can barely be distinguished visually. Hence for photographing the patterns, we used a fast film (180-250 GOST units) and exposure times of from 1 to 3 min.

In decreasing the field from the saturation value to zero, as a rule, no domain structure was observed. If nuclei were present their size must have been inferior to 0.1 mm.

In a positive field of 1.0 oersted there appear near the upper and lower edges of the film small domains in the form of light spikes. With increase of the positive field these spikes at first increase slowly, then more rapidly, until they finally merge and the new phase covers almost the entire surface of the specimen. Usually at the right or left edge there persists for some time an island within which the wall movement is slowed. Usually this island disappears abruptly, and the specimen attains the saturated state.

When the specimen is almost completely saturated, there still persist at the edges of the specimen nuclei of the old phase. These are clearly discernible in the two last photographs of Fig.2. It will be seen that the spikes do not have even straight walls characteristic of crystals. The walls have minor indentations or bulges, which indicate the presence of a number of imperfections, apparently more or less uniformly distributed over the area of the film. In all cases without exception nuclei of the new phase appear at the edge of the film, which is understandable inasmuch as the reversing field is strongest in these regions.

Inasmuch as in the photographs of Fig.2 the magnetization is directed parallel to the easy axis and is opposite in direction in the light and dark domains, we can construct the hysteresis loop, by which we understand the variation of the total magnetic moment of the specimen as a function of the external magnetic field. It can readily be shown that the magnetic moment is proportional to the ratio of the difference between the areas of the light and dark regions to the total area.

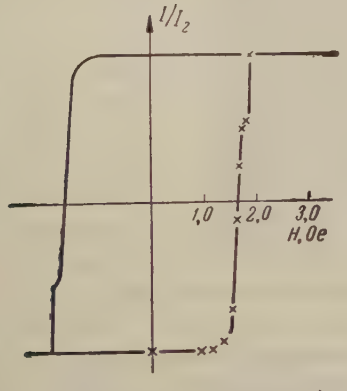

Fig.3. Static hysteresis loop for specimen reversed with the magnetic field along the easy axis.

The hysteresis loop corresponds to the photographs of Fig.2 is shown in Fig.3. The "integration" of light and dark areas was carried out by the simple expedient of cutting the photographic prints along the domain walls and weighing the pieces on an analytic balance.

The complementary part of the hysteresis loop, corresponding to reversal in going from negative to positive fields, was plotted on the basis of symmetry.

The high degree of rectangularity in the hysteresis loop shown in Fig.3 is not at once evident from superficial examination of Fig.2. This is because the photographs of Fig.2 were not taken at equal intervals of H_z. The photographs are spaced closer together in the region of steepest rise of the loop.

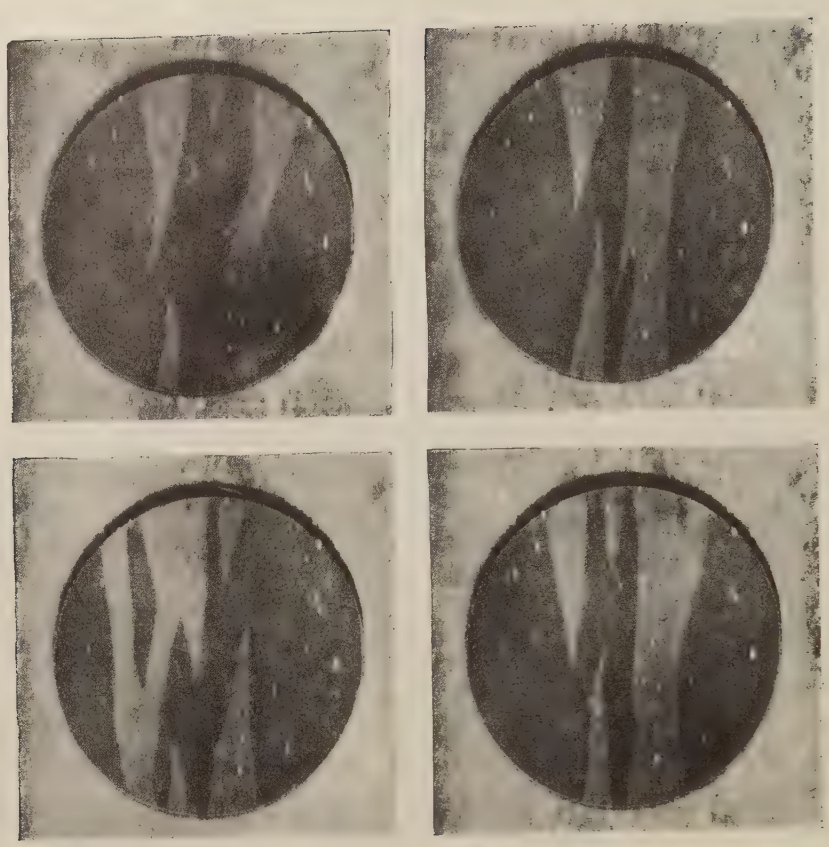

Fig.4. Equivalent states of the same specimen in repeat reversals.

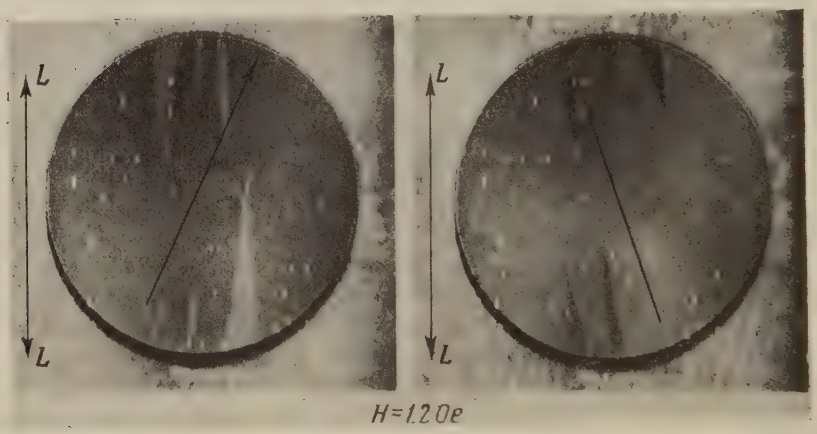

Fig.5. Direction of spike domains in mutually perpendicular fields.

As Prutton[5] noted earlier, in repeat magnetization reversal of a film specimen the domain structure repeats only in a general way. For example, in the case of specimen No.315 (Fig.2) it always goes to completion on the right side earlier than on the left, but the shape of the spikes and their number vary from one reversal to another to an appreciable extent. The photographs of Fig.4 (specimen No.311, prepared in the same batch with No.315) show the domain structure obtained in repeat reversals at approximately the same field value, i.e., corresponding

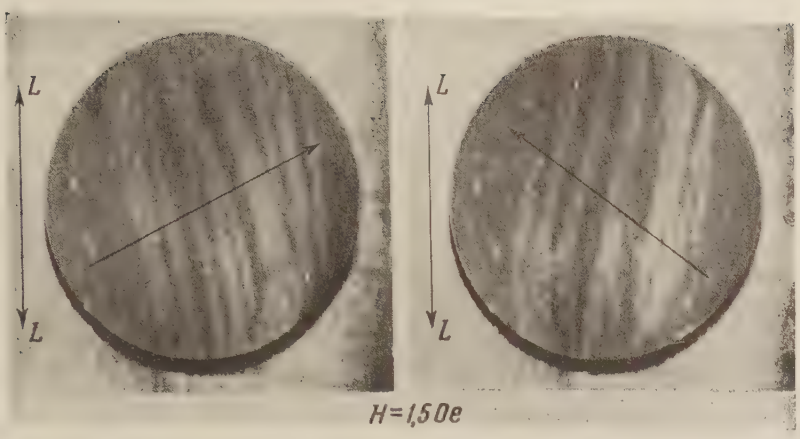

Fig.6. Inclination of spike domains with the perpendicular field H_x in opposite directions.

to the same point on the vertical part of the hysteresis loop. Of course it is impossible to assert that the field value was precisely the same, but careful examination of the photographs shows that they are not successive stages of the same process.

If a domain structure is produced by applying an external field, and then the field is removed, the domain walls do not change position, i.e., do not "retreat". The walls also do not move if the field is brought back up to the given value. Instead, there appear at the edges of the film domains in which the magnetization is directed along the field; with increase of the applied field these domains grow and eventually absorb all the domains of opposite magnetization.

The domain structure obtained in reversing by means of a field directed along the easy axis with simultaneous application of a field along the difficult axis does not differ radically from that described above. There are, however, some minor but significant differences. Thus the stronger the field H_x in the difficult direction, the lower the value of H_z at which domains begin to appear and grow. The field H_z corresponding to the end of reversal (saturation or complete disappearance of walls) also decreases with increase of H_x, but more slowly. It is interesting to note that the first spikes are inclined relative to the easy axis in the direction of the resultant applied field; this will be apparent from Fig.5 in which the arrows indicate the direction of the external field and the mean orientation of the spikes. The angle between the direction of the spikes and the direction of easy magnetization is smaller than the angle between the easy axis and the external field $(H_x + H_z)$. With growth of the domains this inclination of the spikes becomes less noticeable and near the center of the specimens the walls run roughly parallel to the easy axis.

With increase of the transverse field H_x the first spikes become narrower and longer. Simultaneously with increase in the number of domain walls there is observed another interesting effect: the walls are deflected away from the easy axis, the tilt being not in the direction of the field but in the opposite direction. The two photographs of Fig.6 show the domain structure obtained in the course of reversal in the presence of a field H_x of the same value but applied in opposite directions. Clearly apparent is a fine domain structure with the walls tilted in opposite directions.

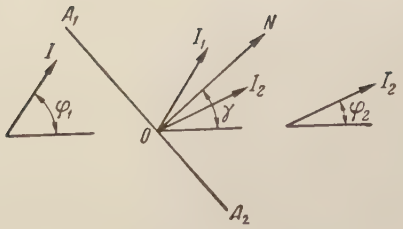

Fig.7. Orientation of magnetization vectors in the vicinity of a wall.

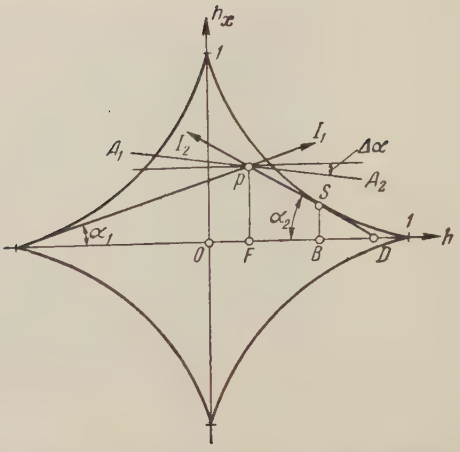

Fig.8. Diagram illustrating the inclination of a domain wall in a uniaxial film.→

In order to explain this at first glance puzzling phenomenon we must analyze theoretically the case of a film specimen divided by a straight wall (A_1A_2 in Fig. 7) into two domains with arbitrary directions of magnetization.

Assume that in one region the magnetization I_1 is directed at an angle φ_1 relative to the horizontal, and that in the second region the magnetization I_2 forms an angle φ_2 with the horizontal axis. We place our origin 0 on the wall, and draw a normal N to the wall at this point.

Then the projections of I_1 and I_2 on the normal N will be

$$\left.\begin{aligned} I_{1N} &= I\cos(\varphi_1-\gamma),\\ I_{2N} &= I\cos(\varphi_2-\gamma). \end{aligned}\right\} \tag{1}$$

If $I_{1N}\neq I_{2N}$, there will appear at the wall magnetic poles of density m:

$$m=(I_{1N}-I_{2N})\,\delta, \tag{2}$$

where δ is the thickness of the film. The presence of free magnetic poles results in a large magnetostatic energy. Hence there will be a tendency for this energy to decrease, i.e., for the wall to move so there will be no magnetic poles on it.

The angle γ corresponding to absence of poles on the wall is not equal to zero for any values of φ_1 and φ_2. Actually the condition for absence of poles on the wall is of the form

$$I_{1N}=I_{2N} \quad \text{or} \quad \cos(\varphi_1-\gamma)=\cos(\varphi_2-\gamma), \tag{3}$$

from which it follows that either

$$\varphi_1-\gamma=\varphi_2-\gamma, \tag{4a}$$

or

$$\varphi_1-\gamma=-(\varphi_2-\gamma). \tag{4b}$$

Condition (4a), obviously, cannot be realized. Hence γ is defined by (4b):

$$\gamma=\frac{\varphi_1+\varphi_2}{2}. \tag{5}$$

Consequently, N is directed along the bisector of the angle between I_1 and I_2.

For example, in the case of antiparallel domains ($\varphi_1 = 0^\circ$ and $\varphi_2 = 180^\circ$), we obtain $\gamma = 90^\circ$. Consequently, the wall is parallel to the magnetization vectors; this is the typical case of 180° walls in a uniaxial film in the absence of an external field.

When $\varphi_1 = 0$ and $\varphi_2 = 90^\circ$, we obtain $\gamma = 45^\circ$, which represents the typical case of a 90° wall in a uniaxial film in zero field.[7]

Now let us consider in more detail the case of a uniaxial film fragmented into domains and located in an arbitrary external field. We assume that condition (3) is satisfied.

Then the poles associated with a wall rapidly weaken in going away from the wall, and the direction of the magnetization in each individual domain is determined only by the influence of the external field and the anisotropy field. As was shown by Proebster et al[8] the direction of magnetization in a uniaxial film can be determined by drawing the tangent from the point characterizing the external field to the arc of an astroid (Fig.8). It can readily be demonstrated that a domain structure can exist only at fields corresponding to points lying within the astroid, inasmuch as from these points one can draw two tangents to the astroid, and, consequently, there are two stable equilibrium states for the magnetization.

Assume that the wall is moving in fields h_z and h_x which corresponds to point P inside the astroid. We define the directions of I_1 and I_2 by the acute angles α_1 and α_2; in this case we measure α_1 in the opposite direction from that assumed in deriving Eq.(5). Consequently, in Eq.(5) we must substitute α_1 for φ_1 and α_2 for $\varphi_2 - 180^\circ$. Then

$$\gamma = \frac{\alpha_1 + 180^\circ - \alpha_2}{2}. \tag{6}$$

Obviously, the angle $\Delta\alpha$ between the wall and the easy axis equals $\gamma - 90^\circ$:

$$\Delta\alpha = \frac{\alpha_1 - \alpha_2}{2}. \tag{7}$$

Even without finding the precise analytic expressions for α_1 and α_2, it is clear that $\Delta\alpha$ cannot be large. It is obvious that on the horizontal and vertical axes $\Delta\alpha = 0$. Near the right and left cusps of the astroid $\Delta\alpha$ is small, inasmuch as α_1 and α_2 are small. Near the upper and lower cusps of the astroid, $\Delta\alpha$ is small inasmuch as here α_1 and α_2 are both close to 90°, while their difference is small.

In order to determine the maximum possible value of $\Delta\alpha$, let us find the analytic expressions for α_1 and α_2. From the equation for an astroid it follows that $BC = \sin^3\alpha_2$, $OD = \cos\alpha_2$ and $OB = \cos^3\alpha_2$. From similarity of the triangles SBD and PFD we have

$$\frac{SB}{BD} = \frac{PF}{FD} \quad \text{or} \quad \frac{\sin^3\alpha_2}{\cos\alpha_2 - \cos^3\alpha_2} = \frac{h_x}{\cos\alpha_2 - h_z}. \tag{8}$$

Transforming the above, we obtain

$$\sin\alpha_2 - \operatorname{tg}\alpha_2 h_z = h_x. \tag{9}$$

Proceeding analogously we obtain

$$\sin\alpha_1 + \operatorname{tg}\alpha_1 h_z = h_x. \tag{10}$$

Thus we must find the maximum of $\Delta\alpha$ under the conditions of (9) and (10) in the region defined by

$$\left.\begin{aligned} h_x^{2/3} + h_z^{2/3} &\leqslant 1; \\ h_x &\geqslant 0; \\ h_z &\geqslant 0. \end{aligned}\right\} \tag{11}$$

In terms of our angles this corresponds to $0 \leqslant \alpha_1 \leqslant 90°$ and $0 \leqslant \alpha_2 \leqslant 90°$. The extremum values of $\Delta\alpha$ in the region (11) can readily be found by Lagrange's method of multipliers. Accordingly, we add to Eq.(7) Eqs.(9) and (10), multiplied by λ_1 and λ_2, respectively, and seek the extremum values of the function

$$\Phi = \frac{\alpha_1 - \alpha_2}{2} + \lambda_1(\sin\alpha_1 + \operatorname{tg}\alpha_1 h_z - h_x) + \lambda_2(\sin\alpha_2 - \operatorname{tg}\alpha_2 h_z - h_x). \tag{12}$$

Taking the partial derivatives of Φ with respect to the variables α_1, α_2, h_x, h_z, λ_1, and λ_2, and equating them to zero, we obtain a set of equations for finding the maximum and minimum values of $\Delta\alpha$.

We shall not write out this cumbersome set here, particularly since it has a single trivial solution, $\alpha_1 = \alpha_2 = h_x = h_z = 0$, corresponding to an inflection point. There are no maxima or minima inside the region. Consequently, the maximum of $\Delta\alpha$ is located on the boundary of the region (11).

The maximum of $\Delta\alpha$ on the boundary can be found if we express h_x and h_z in terms of α_2 : $h_z = \cos^3\alpha_2$ and $h_x = \sin^3\alpha_2$. Inserting these expressions in (10), we obtain

$$\sin\alpha_1 + \frac{\sin\alpha_1}{\cos\alpha_1}\cos^3\alpha_2 = \sin^3\alpha_2. \tag{13}$$

The above equation can readily be brought to the form

$$\sin(\alpha_1 - \alpha_2) = \frac{1}{2}\sin 2\alpha_2. \tag{14}$$

The angle difference on the left is $2\Delta\alpha$. Hence its maximum can readily be found by differentiating (14) with respect to α_2, which yields

$$\alpha_2 = 45° \quad \text{and} \quad \Delta\alpha_{\max} = 15°. \tag{15}$$

It follows from the above that the domain wall must be deflected relative to the easy axis to the side opposite the direction of the external field, and that the angle of inclination cannot be large.

The above described tilt of the domain walls substantiates the hypothesis that in the first approximation rotation of magnetization inside domains is independent of the location and movement of the domain walls.

Institute of Precise Mechanics and Computing Technology,
Academy of Sciences of the USSR

References

1. H.Williams & R.Sherwood, J.Appl.Phys., 28, 548 (1957).
2. C.A.Fowler & E.M.Fryer, Phys.Rev., 94, 52 (1954).
3. J.Kranz, Naturwissenschaften, 43, 370 (1956).
4. C.A.Fowler, E.M.Fryer & J.R.Stevens, Phys.Rev., 104, 645 (1956).
5. M.Prutton, Philos.Mag., 4, 1063 (1959).
6. M.Prutton, Britt.J.Appl.Phys., 11, 335 (1960).
7. B.Elschner & D.Unagst, Z.Naturforsch,a, 11, 38 (1956).
8. W.E.Proebster, S.Nathfessel & C.O.Kinberg, UNESCO (NS)ICIP/K2.

INVESTIGATION OF THE SWITCHING TIME OF FERROMAGNETIC FILM ELEMENTS

- I.A.Efimov

Depending on the external conditions, the switching time of ferromagnetic film elements may vary from as much as a second down to a few nanoseconds.

Since rapid switching is required for practical applications, we made an attempt to investigate the faster processes lying in the range from 500 to 30 nanosec. The lack of superwide band equipment made it impossible to observe shorter processes.

1. Set-up for reversal of film elements by a longitudinal field

The switching of film elements in a longitudinal field (field parallel to the easy axis) in the simultaneous presence of a transverse field was carried out on a special set-up designed and built in our institute.

The reversing and return of the film element to the initial state of saturation is realized by two consecutive pulses well separated in time. The magnetic fields produced by these pulses act on the film element in opposite directions.

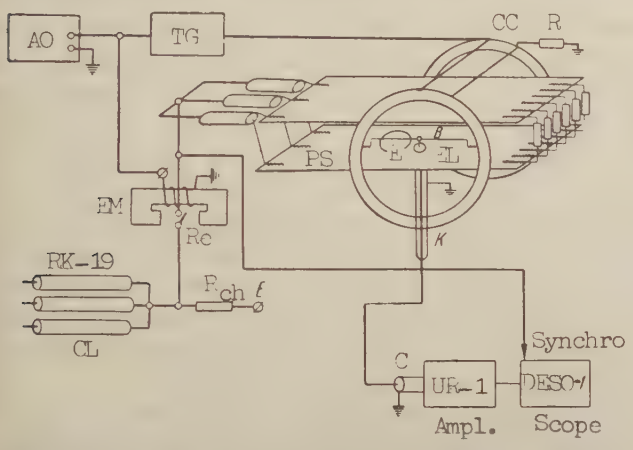

Fig.1. Set-up used to study magnetization reversal of film elements.

A diagram of the set-up is shown in Fig.1. The reversing or driving pulses are generated by discharge of the coaxial line CL through the mercury relay Re, and are sent down the strip transmission line PS consisting of two parallel plates. The investigated film element E is located in a pick-up loop between the strips, the width of which is sufficient to assure the necessary uniformity of the field.

The signals from the audio-oscillator AO go to the winding of the electromagnet EM actuating the armature of the mercury relay and simultaneously to the thyratron generator TG; the pulse from this generator goes to the system of two circular coils CC which produce the resetting field that brings the element to the initial state (of saturation).

The film element E is placed in one arm of the pick-up loop PL. The output signal is carried by the coaxial cable K to the input of the UR-1 amplifier and then goes to the amplifier of the DESO-1 oscillograph, and is viewed on the screen.

The described system of two parallel plates assures a field directed parallel to the plane of the strips. The field at any point between the strips can be calculated by means of the formula

$$H = \frac{0.2I}{l}(\varphi_1 + \varphi_2),$$

where φ_1 and φ_2 are the angles at which the strips are viewed from the given point, I is the amplitude of the current pulse and l is the width of the strips.

The set-up is designed for testing specimens 1 cm in diameter; accordingly, to meet the requirements as regards uniformity and strength of the reversing field

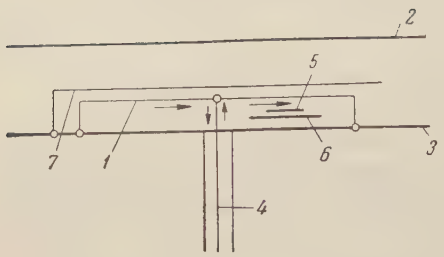

Fig.2. Pick-up loop.

the strips are made 14 mm wide and are separated by a 2.5 mm gap. The length of the strips is 150 mm.

With the given geometry, the field intensity from the center of the strips to the edge falls off by about 5%.

The strips were made of plates of laminated insulation lined with 50 μ thick foil. The central parts of the strips, where the element is located, are subdivided into substrips 1 mm wide with 0.3 mm intervals between them. This subdivision of the strips reduces the eddy current loss in the foil.

The design of the two-arm balanced pick-up loop, modeled after that employed by Smith[1], is shown in Fig.2. Here 2 and 3 are the upper and lower strips. The loop of thin manganin wire 1 is attached at two points to the lower strip; the points of attachment are 48 mm apart along the length of the strip and are at equal distance from its edges. The resistance of the wire is 7.2 ohms. The signal is taken off the midpoint of the wire by the coaxial cable 4, the inner conductor of which is connected to the midpoint of the loop, while the outer braid is connected to the lower strip. Thus there are formed the two loops necessary for compensation of the interference induced by air coupling between the loops formed by the manganin wire and the lower strip, one of which closes the magnetic circuit of the element 5, lying on the glass support 6. In view of the equal resistance of each arm of the loop, a signal of only half the full amplitude is picked up. In order to avoid a shorted loop, it is essential to use a wire with a high resistance per unit length. The polarity of the output signal changes to the opposite if the specimen is transferred from one arm to the other of the loop. In our experimental work the element was always placed in the same arm, while the other arm was used for controlling the interference level. The pick-up loop was shielded by an arch of 50 μ thick foil 7. The purpose of this shielding is to reduce the interference connected with variation of the electric field.

In the described set-up the amplitude of the driving pulses could be varied from small values up to 12 amp, which is equivalent to variation of the field intensity from low values to 10 oersted.

To obtain these pulse amplitudes the discharge line was made of three parallel sections of RK-19 coaxial cable (characteristic impedance 50 ohm), each 15 meters in length. Use of this discharge line made it possible to limit the charging voltage to 400 v.

The duration of the driving pulse is 150 nanosec. The pulse rise time in discharge of the line through the mercury relay is usually less than 1 nanosec. Such a pulse duration is permissible in view of the low resistance of the relay contacts in the closed state.

The strips were terminated by a 50/3 ohm load. The parallel RK-19 cables are also used for carrying the pulses to the strips.

The mercury relay and its magnet are identical with those used in the GKI-4B mercury relay generator.

The repetition rate of the reversing pulses is determined by the resonance frequency of the relay armature and usually lies in the range from 150 to 200 pps. As noted above, the investigated element is returned to its initial state by a pulse through the two circular coils (CC in Fig.1). The current pulse produced by a discharge of a capacitor through the thyratron, flowing through the coils,

produces a field of the order of 10 oersted, which is sufficient for returning the element to the initial state of saturation.

The constant transverse field is produced by a pair of square coils (not shown in Fig.1), located to either side of the strips. The maximum value of the transverse field is ~9 oersted.

The switching signal is observed on the screen of the DESO-1 oscillograph, the sweep of which is triggered by the driving pulse, as shown in Fig.1.

The procedure used for measuring the switching time is the following. First, the free arm of the pick-up loop is adjusted in height so as to obtain a minimum value of the air coupling signal at maximum amplitude of the driving pulses. Inasmuch as one cannot fully compensate or suppress the interference, the interference pulse is first photographed for each test amplitude of the driving pulses. Then the film element is inserted in the pick-up loop and the output signals at different driving pulse amplitudes and values of the transverse field are recorded. The resultant series of photographs is processed as follows: 1) the signal and corresponding interference pulses for each driving pulse amplitude are transferred to a sheet of drawing paper by means of a diascope; 2) the test time interval is divided into a certain number of strips and the ordinates of the interference are subtracted from the ordinates of the signal to obtain the signal minus interference curve; 3) the resultant signal curve is integrated; 4) from the resultant curve, characterizing the time variation of the magnetic flux, the switching time is determined as the time for change of magnetization from the 0.1 to the 0.9 level.

2. Experimental results

As noted above, with a pick-up loop of the described design it is impossible to compensate completely the interference signal due to air coupling. An oscillogram of the picked up signal in the absence of an element is shown in Fig.3. The peak interference amplitude is 5-7 mv. The shape of the trace shows that the interference is oscillatory.

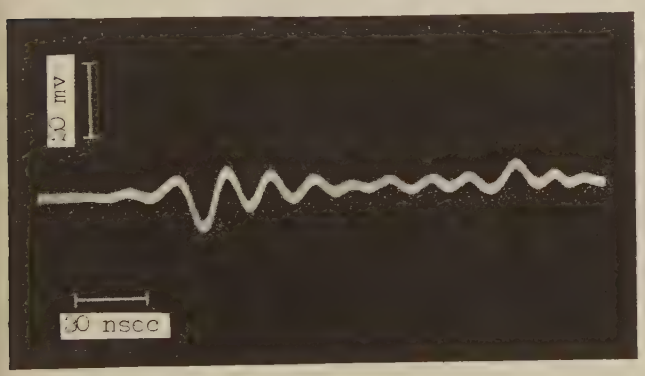

Fig.3

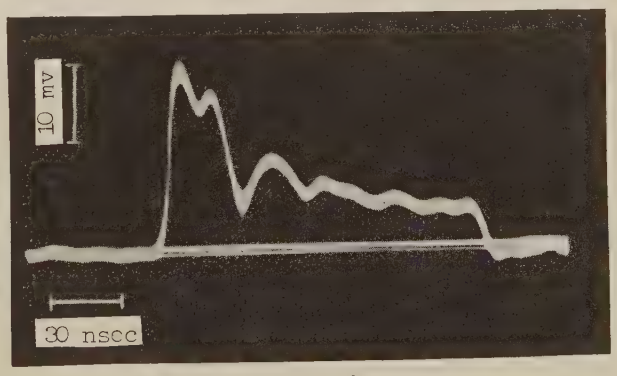

Fig.4

While so high an interference level hampers investigation, one can still draw certain deductions regarding the processes occurring in elements reversed by a longitudinal field on the basis of the observed signals.

The reproduced oscillograms illustrate the characteristic signals obtained under different reversal conditions. Figs.4 & 5 show oscillograms obtained in cases when complete switching is not realized during the time of the driving

pulse. Fig.6 shows an oscillogram obtained in the case of complete reversal of the element; Fig.7 illustrates the case of rapid switching.

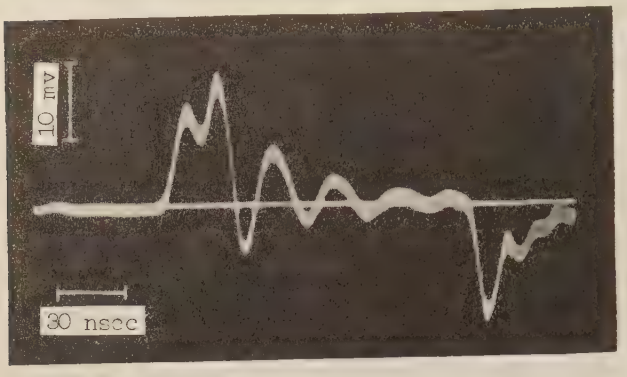

Fig.5

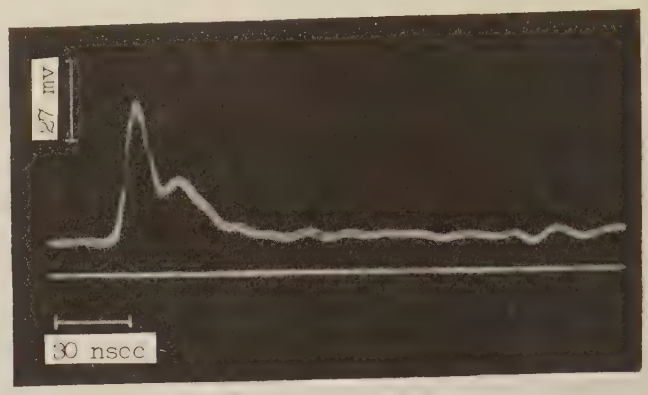

Fig.6

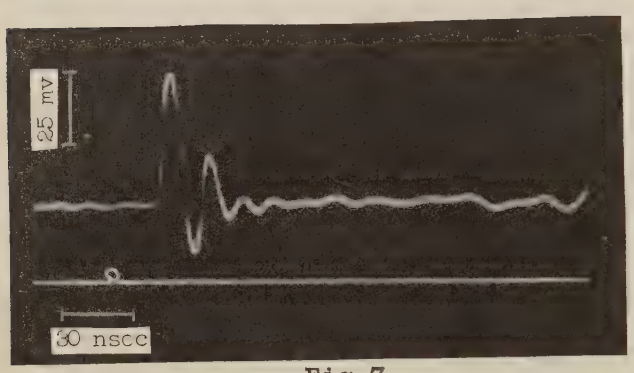

Fig.7

The reproduced oscillograms were photographed with a sweep time of 300 nanosec, while the duration of the driving pulse was 150 nanosec.

Using the above procedure for measuring the switching time, we determined for one of the test specimens, which had a thickness of 1400 Å, the variation of the reciprocal of the switching time ($1/\tau$) as a function of the longitudinal driving field H with different values of the transverse field. The results are shown in Fig.8. In the same figure we also give the corresponding static hysteresis loops.

It will be evident from the figure that increase of the transverse field leads to more rapid switching of the film element. The calculated values of the switching coefficient S_w for the indicated increasing values of the transverse field are 0.185 (zero field), 0.182, 0.15, 0.13 and 0.12 oe-μsec.

The amplitude of the observed pulses depends on the reversing conditions. For a reversal time of about 30 nanosec the amplitude is approximately 40 mv. It must be borne in mind that with the given loop design only half the signal goes to the amplifier. Thus, a film element 1 cm in diameter switching in a time of the order of 40 nanosec yielded an emf of the order of 80 mv in one arm of the pick-up loop. Taking this into account we find that for the investigated element the total (i.e., double) value of the remanent flux is approximately 0.12 maxwells.

Conclusions

Magnetization reversal of film elements along the easy axis occurs rapidly only at relatively high values of the driving field (~10 oersted). In the presence of a transverse field the duration of the reversal processes is reduced.

It must be borne in mind, however, that at the same time the coercive force of the element is also diminished. The switching times in fields equal to twice

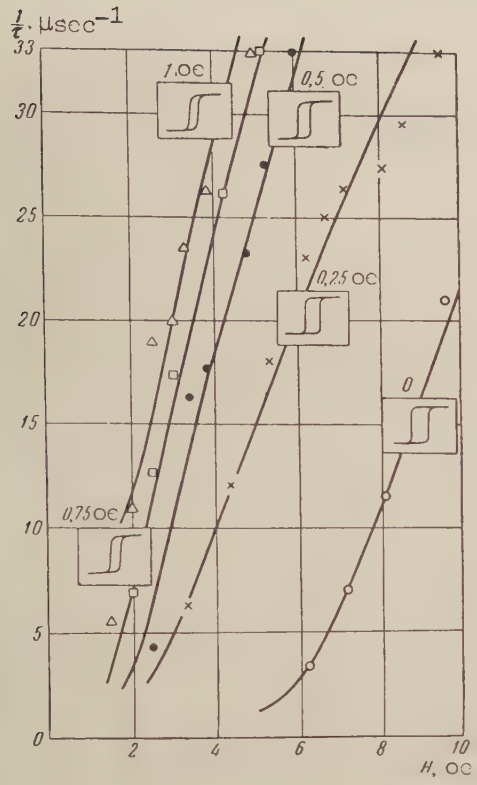

Fig.8. Variation of the reciprocal of the switching time as a function of the longitudinal field H at different values of the transverse field.

the coercive force are 500, 120, 100, 80 and 70 nanosec at values of the transverse field used in recording the curves shown in Fig.8. The protraction of the reversal time in low transverse fields is explained by the slowness of wall motion processes.

Hence in designing storage devices employing film elements, one must try to provide operating conditions under which wall motion does not occur, i.e., conditions conducive to rotation reversal.

Institute of Precision Mechanics and
Computing Technology,
Academy of Sciences of the USSR

Reference

1. D.O.Smith, Phys.Rev., 104, 1280 (1956).

FERROMAGNETIC RESONANCE IN THIN FILMS

- L.V.Kirenskii, V.A.Ignatchenko & O.G.Baklanov

The effect of ferromagnetic resonance (FMR) has been utilized by a number of authors for investigating some of the magnetic characteristics of thin films.[1-3] Where thin films are concerned the FMR technique has some advantages over other procedures, in particular, it allows of obtaining a higher sensitivity and accuracy by relatively simple means.

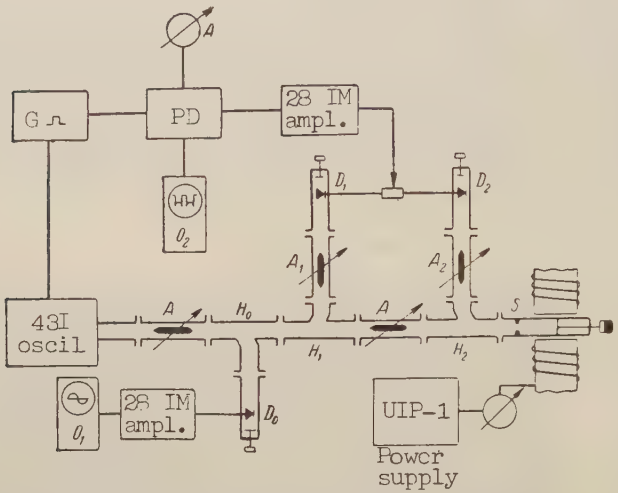

Fig.1. Block diagram of the apparatus.

We used FMR to determine the saturation magnetization and anisotropy constants of thin ferromagnetic films. The experimental arrangement is diagramed in Fig.1. Microwave oscillations, generated by the standard 43I oscillator, are modulated by square pulses produced by the square pulse generator G. The subcircuit consisting of the directional coupling H_o, the detector D_o, the 28IM amplifier and oscillograph O_1 serves to monitor the operation of the generator. Most of the microwave power is incident on the slit S coupling the resonant cavity with the waveguide. The cavity is cylindrical and is excited in the TE_{11} mode. The specimens, in the form of disks, are mounted on the back wall of the cavity. The diameter of the disks is substantially smaller than the diameter of the cavity so that one can neglect deviation from parallelism of the lines of force of the magnetic component of the microwave field. The apparatus has provision for rotation of the film specimen in its plane. The quantity measured is the reflected power arriving at detector D_1 through coupler H_2. In order to enhance the sensitivity of the set-up the initial level of the signal taken off detector D_2 is compensated by a signal arriving in antiphase from detector D_1. The difference between these signals is applied to the amplifier and then to the detector synchronized by pulses arriving from the generator G. The amplified and detected signal is recorded by the galvanometer A. Oscillograph O_2 serves for monitoring the operation of the phase detector and compensator. The resonance chamber is placed between the pole pieces of an electromagnet, which is supplied from a regulated UIP-1 source. The applied field is parallel to the plane of the film and perpendicular to the magnetic component of the microwave field.

The thin films were prepared by cathode sputtering at a vacuum of ~10^{-5} mm Hg. They were deposited on 18 mm diameter cover glasses heated to about 300°C. During deposition a field of ~100 oersted was applied in the plane of the film to produce artificial anisotropy. So far we have investigated a number of Permalloy films and one cobalt film. In the former case, the composition of the initial alloy was 80% Ni + 17% Fe + 3% Mo; the composition of the film was not checked. The thickness of the film was measured by the Shklyarevskii[4] technique on an UM-2 monochromator.

As was first shown by Kittel, the position of the FMR peak for an ellipsoidal ferromagnet is given by the expression

$$\left(\frac{\omega}{\gamma}\right)^2 = (H + H_1^a)(H + H_2^a), \tag{1}$$

where ω is the angular frequency, γ is the gyromagnetic ratio, H is the applied magnetic field, H_1^a and H_2^a are the effective demagnetizing fields due to anisotropy of shape, elastic stresses and crystallographic structure ($H^a = H^{as} + H^{ae} + H^{ac}$). With good approximation a thin film may be regarded as a greatly flattened ellipsoid. Then

$$H_1^{as} = 4\pi I_s, \quad H_2^{as} = 0, \tag{2}$$

where I_s is the saturation magnetization.

As noted above, the films were sputtered on at high temperatures. In view of nonequality of the thermal expansion coefficients of the metal and substrate, upon cooling there are set up in the film radially symmetric elastic stresses. The associated effective demagnetizing fields were calculated by MacDonald[5] and Griffiths[1]:

$$H_1^{ae} = \frac{3\lambda E}{(1-\sigma) I_s}(\alpha_m - \alpha_s)\Delta T, \quad H_2^{ae} = 0, \tag{3}$$

where λ is the isotropic magnetostriction, E is Young's modulus, σ is Poisson's ratio, α_m and α_s are the temperature coefficients of expansion of the metal and substrate, and ΔT is the temperature difference. Since the parameters of the metal entering into this equation are known only approximately, one can make only a rough evaluation of the contribution from elastic stresses. However, in view of the fact that H_1^{ac} is small compared with H_1^{as}, this does not introduce any appreciable error into the final results.

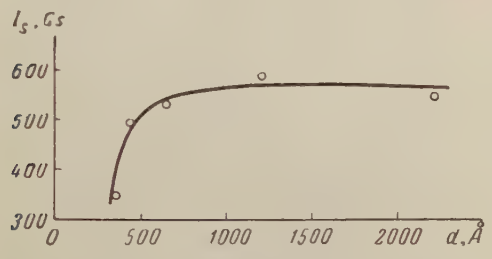

Fig.2

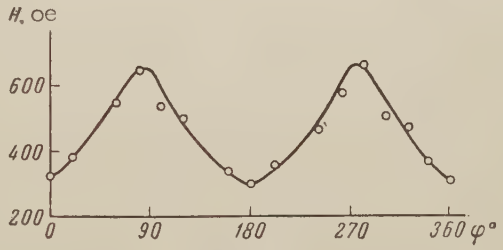

Fig.3

Fig.2. Variation of I_s of Permalloy films as a function of thickness.

Fig.3. Variation of the resonance field with the angle of rotation of a cobalt film.

General expressions for the effective crystallographic anisotropy field in a single crystal were deduced by MacDonald[5]. For the particular case of a hexagonal crystal the expressions are

$$\begin{aligned} H_1^{ac} &= \frac{2}{I_s}[(K_1' + [2K_2')(\gamma_{31}^2 - \gamma_{21}^2) + 2K_2'(3\gamma_{21}^2 - \gamma_{31}^2)\gamma_{31}^2], \\ H_2^{ac} &= \frac{2}{I_s}[(K_1' + 2K_2')(\gamma_{31}^2 - \gamma_{11}^2) + 2K_2'(3\gamma_{11}^2 - \gamma_{31}^2)\gamma_{31}^2]. \end{aligned} \tag{4}$$

Actually the anisotropy of thin films is not of crystallographic origin, but formally it can be described by expressions of the above form, where K_1' and K_2' are the effective anisotropy constants.

The results of measuring the saturation magnetization of thin Permalloy films are shown in Fig.2. Our curve is qualitatively similar to that obtained by Tannenwald & Seavey[3] for 80% Ni + 20% Fe films; however, in our case the sharp drop in saturation magnetization occurs at film thicknesses one order of magnitude greater. This may be due to the difference in chemical composition, but more likely is attributable to inadequate homogeneity of our films. We did not detect anisotropy effects in the case of our Permalloy films; hence the anisotropy does not exceed 10^3 erg/cm^3.

In the case of the cobalt films (3200Å) we observed a pronounced variation of the resonance field with the angle of the film (Fig.3). Using Eq.(4) one can readily calculate the value of the effective anisotropy constant K_1', if we set $K_2' = 0$. We obtain $H^a = 2K_1'/I_s = 175$ oersted. If we further assume that $I_s = 1.42 \cdot 10^3$, we find $K_1' = 1.24 \cdot 10^5$ erg/cm^3.

I take this opportunity to thank T.A.Stepanova for assistance in carrying out the work.

Institute of Physics,
Siberian Branch of the USSR Academy of Sciences

References

1. J.H.E.Griffiths, Physica, 17, 253 (1951).
2. R.L.Conger & F.C.Essig, Phys.Rev., 104, 915 (1956).
3. P.E.Tannenwald & M.N.Seavey, J.phys.et radium, 20, 323 (1959).
4. I.N.Shklyarevskii, Optika i spektroskopiya, 5, 617 (1958).
5. J.R.MacDonald, Proc.Phys.Soc., 64, 968 (1951).

MEASUREMENT OF THE HYSTERESIS LOSS IN THIN FILMS IN A ROTATING MAGNETIC FIELD

- N.I.Sudakov, M.K.Savchenko, E.K.Zagirova & I.I.Starostin

Many investigators[1-6] have measured the anisotropy constant and the hysteresis loss in a rotating magnetic field by means of a torquemeter or similar instrument. But in these investigations the specimens were either single crystals or grain oriented substances in the form of a sphere or disk of considerable volume.

Where investigation of thin ferromagnetic films by the torque method is concerned, one can cite only two studies: the first, by Kotel'nikov[7], is devoted to the anisotropy of electrolytically deposited iron films; the second[8] gives a description of a sensitive anisometer for direct measurement of the magnetic anisotropy in thin layers, an analysis and evaluation of the effect of different parasitic factors on anisotropy measurements and suggestions on eliminating measurement errors.

Experimental Procedure and Specimen Preparation

In the present paper we give the result of measurements of the hysteresis loss in a rotating magnetic field and of the anisotropy constants of thin Permalloy films by the torque method.

The magnetic field was supplied by a special electromagnet designed in the Physics Laboratory of the "M.I.Kalinin" Krasnoyarsk Institute of Nonferrous Metals and built by the Krasnoyarsk Heavy Machine Building Plant.

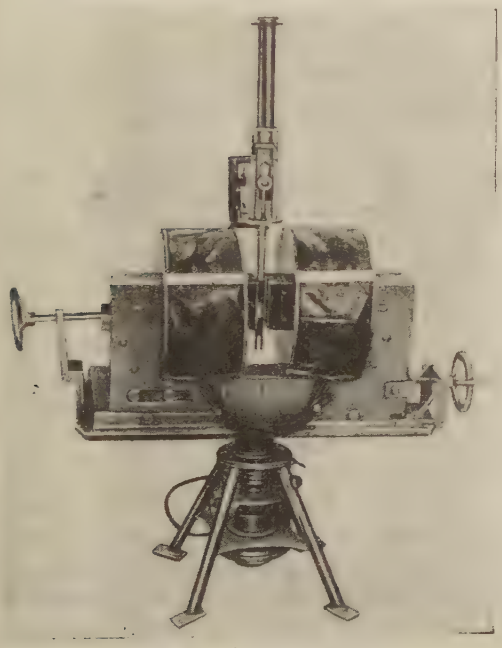

Fig.1. Anisometer.

The values of the mechanical torque resulting from action of the magnetic field on the ferromagnetic film was measured by means of an Akulov type anisometer with a somewhat modified gage. High sensitivity of the anisometer was attained by using a thin (0.1 mm) and long (0.5 meters) suspension filament made of tungsten wire. The scale for reading the angle (light spot reflected from the anisometer mirror) was located at a distance of 4.05 meters from the instrument.

To protect it from air currents the entire torsion system was enclosed in a dural hood with a glass window for passage of the light beam. A general view of the apparatus is given in Fig.1.

Most of the experimental observations were carried out on three Mo-Permalloy films 400, 800 and 1300 Å thick. The films were prepared by vacuum ($4 \cdot 10^{-5}$ mm Hg) evaporation of Mo-Permalloy (80% Ni, 17% Fe & 3% Mo) onto glass substrates heated to 300° in a 90 oersted magnetic field produced by a pair of Helmholtz coils. The substrates were 18 mm diameter cover glasses.

Results and Analysis

The electromagnet employed in the experiments had square pole pieces (19 x 19), and a gap of 4 cm. The magnet field was calibrated and checked for uniformity

by means of a ballistic set-up. Square pole pieces were chosen to assure a uniform field. Prior to each series of observations the suspension was carefully cleaned to remove possible contaminants containing ferromagnetic substances; the angle of inclination of the substrate relative to the horizontal was measured both in zero field and in the presence of a strong field.

Inasmuch as during rotation of the magnetic field about the specimen, in addition to the rotational moment (torque) due to anisotropy of the film, the set-up detected parasitic torques due to any field gradient at the edges of the pole pieces, the presence of para- and diamagnetic components and partial asymmetry of the suspension system, we first recorded the torque curves for each field value with an uncoated substrate in the specimen holder. These curves were recorded by the method of visual observation of the deflection of the light spot from the zero division as the magnet was rotated 360° first one way and then the other. The deflections, proportional to the torque, were read every 10° rotation of the electromagnet. These observations gave us the "tare" torque curves for clockwise and counter-clockwise rotation of the magnet.

Then using the same procedure we recorded the torque curves with specimens in place. The appropriate "tare" curve was then subtracted from each of the specimen curves.

Errors introduced by eccentricity of the specimen can be eliminated by harmonic expansion of the experimental dependences. As a result we obtained a curve of the torque due to anisotropy of the film. The specimen, "tare" and difference curves obtained in a 700 oersted field are shown in Fig.2. Fig.3 shows the component curves obtained by harmonic analysis of the difference curve.

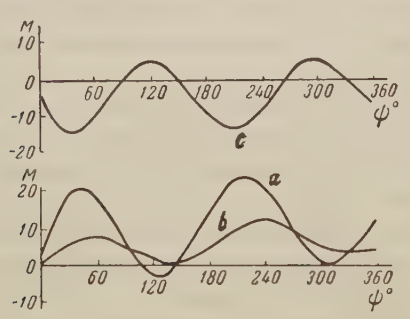

Fig.2

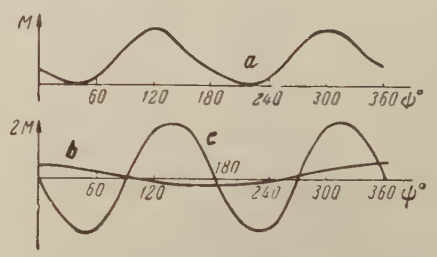

Fig.3

Fig.2. Torque curves obtained in a 700 oersted field: a) without specimen (uncoated cover glass), b) with specimen, c) difference curve.

Fig.3. Resolution of the torque curve by Fourier analysis: a) difference curve, b) component with period 2π, c) component with period π (this is the true torque curve due to anisotropy of the film).

As will be evident from Fig.3 the function with the greatest amplitude has a period π, which indicates the presence of uniaxial anisotropy. Using the data arrived at in the same manner for all three films in an 8500 oersted field, we calculated the anisotropy constants and obtained $K = 1.4 \cdot 10^3$ (1300 Å film), $K = 0.85 \cdot 10^3$ (800 Å) and $K = 0.75 \cdot 10^3$ (400 Å).

The values of the hysteresis loss per cycle in the rotating field were calculated from the areas between the torque curves by means of the formula

$$Q_\tau = \int M d\psi,$$

where M is the torque and ψ is the angle of rotation of the field. The areas were determined by means of a planimeter.

Conclusions

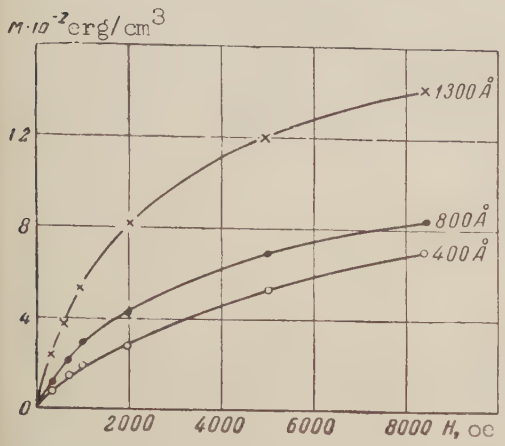

Fig.4. Variation of the maximum torque as a function of the external magnetic field and the film thickness.

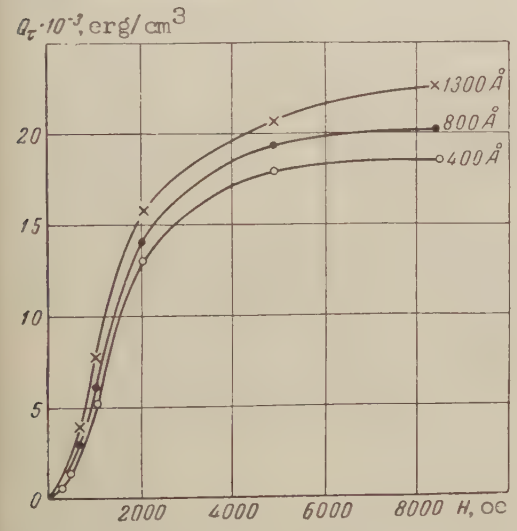

Fig.5. Variation of the hysteresis loss in a rotating magnetic field as a function of the applied field and the thickness of the Mo-Permalloy film.

Analysis of the difference torque curves and the results of hysteresis loss measurements for each of the Mo-Permalloy films point to the following conclusions.

1. There is no change in the period of the sinusoidal torque curves with increase of the rotating field. In the experimental field range from 50 to 8500 oe the main torque curves have a period equal to π, i.e., all the investigated films possess uniaxial anisotropy.

2. The magnitude of the maximum torque with increase of the applied field varies in the same way as in the case of crystallographic anisotropy of single crystals, but the increase in the magnitude of the torque in the range of medium fields is slower in the case of films.

3. The maximum torque in the entire investigated field range increases with increasing film thickness (Fig.4).

4. The hysteresis loss in a slowly rotating magnetic field increases with increase of the field in the same way as the loss in cyclic magnetization reversal (Fig.5). This character of the field dependence of the hysteresis loss in a rotating field is in sharp conflict with the theoretical predictions of N.S.Akulov deduced for rotational hysteresis in single crystal bulk specimens. According to Akulov's theory, with increase of the field the hysteresis loss should at first increase, go through a maximum and then drop to zero in fields approaching the saturation field.

5. The hysteresis loss depends on the film thickness: with increase in thickness the loss increases somewhat.

6. As regards anisotropy, films deposited in the absence of a field from the Helmholtz coils do not differ from films prepared in the presence of a magnetic field. This is shown by a series of curves recorded for films prepared in the presence and absence of a field at different values of the rotating field. Two such curves are reproduced in Fig.6. Apparently a very weak field is sufficient to produce anisotropy; this might be the field produced by the heater coil of the evaporator or the Earth's magnetic field.

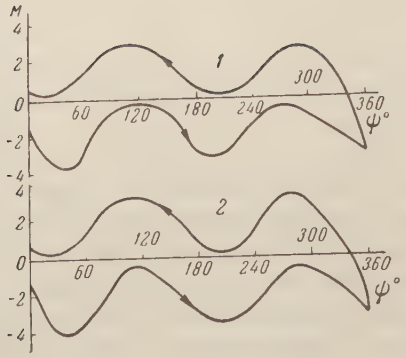

Fig.6. Clockwise and counterclockwise rotation torque curves recorded in a 2000 oersted field: 1) for a film deposited in zero field (laboratory field), 2) for a film prepared in a 90 oe field.

"M.I.Kalinin" Krasnoyarsk Institute of Ferrous Metals &
Institute of Physics of the Siberian Branch of the USSR Academy of Sciences

References

1. A.A.Baskakov & N.L.Bryukhatov, Zhur.eks.pi teor.fiz., 9, 984 (1939).

2. J.Brailsford, J.Inst.of Electr.Eng. (London), I, 566 (1938); Ibid., 2, 399 (1939).

3. P.S.Sarapkin, Trudy (Proceedings), Siberian Physical-Technical Institute at Tomsk University, No.28, 215 (1949).

4. N.I.Vtyurin, Uch.zapiski (Scientific notes), Moscow State University, No.162, Book 6, 161 (1952).

5. N.L.Bryukhatov, Izv.AN SSSR, Ser.fiz., 21, 1268 (1957). (Trans.Bulletin, 21, 1257.)

6. N.V.Kirenskii, Ibid., 12, 121 (1949).

7. V.N.Kotel'nikov, Doklady AN SSSR, 113, 97 (1957) (Trans.Doklady); Fizika metallov i metallovedenie, 6, 222 (1958). (Trans.Physics of Metals and Metallography.)

8. W.Schuppell, O.Stemme, V.Andre & Z.Malek, Fizika metallov i metallovedenie, 6, 837 (1959); Ann.Physik, 5, 211 (1960).

USE OF THIN FILMS FOR MEASUREMENT OF MAGNETOSTRICTIVE AND OTHER STRAINS

- V.A.Yugov & G.P.D'yakov

In recent years a great deal of attention has been given to preparation, investigation and use of thin films. Among other applications, thin films can be used for investigating magnetostrictive strains and other deformations.

Earlier[1] we proposed a new type of strain gage (a film strain gage) for measuring magnetostriction. Wire resistance strain gages[2-4], hitherto used for measuring magnetostriction, are simple and have a number of advantages over other instruments, but they also have a number of shortcomings. As is known, conventional resistance strain gages consist of a thin wire of high resistivity material cemented to a strip of paper with acetone cement or some similar adhesive; for magnetostrictive measurements, the paper mounted wire is cemented to the specimen. The elongation of the specimen (magnetostriction) is found from the relative change in resistance of the gage. Depending on the shape and size of the investigated specimens, the gage is made zigzag or in the form of a single wire. A shortcoming of zigzag elements is that at the bend the change in length of the gage is of opposite sign to the measured magnetostriction. This introduces a substantial error into the results. The use of a paper liner and cement for attaching the strain gage restricts the useful temperature range, i.e., precludes measurements at high and low temperatures. Remote gages are not wholly free of the above shortcomings and require the use of specimens of special shape and size. Such gages cannot be used for measuring the magnetostriction of thin disks, strips, wires and the like.

We developed a new type of strain gage that does not have the shortcomings enumerated above. In these gages the strain-sensitive resistance elements are thin films of constantan or other material applied by vacuum evaporation. The first experiments were carried out on an oxidized nickel disk. The insulating oxide layer was formed by heating the disk in an electric furnace to 800-850°, holding it at this temperature for 30-40 min, and then rapidly cooling in air. The resulting oxide layer has good insulating properties and adheres firmly to the nickel. Tests[5] showed that the presence of such a layer does not impair the physical properties of the material.

Prior to deposition of the film, the oxidized nickel disk is covered with a mica or foil mask with an appropriate cut-out. In this manner one can obtain a strain gage of any desired shape.

Providing good contacts for the leads presented some difficulties. We used auxiliary silver or gold electrodes applied by vacuum evaporation to the ends of the strain-sensitive film. The leads were soldered to the silver spot electrode with Wood's alloy, onto the gold electrodes with a gallium alloy.

A series of test measurements of magnetostriction showed that this new type of gage yields satisfactory results.

For measurement of the magnetostriction the film strain gage deposited on the oxidized nickel disk was connected into one of the arms of a dc bridge. The indicator in the bridge diagonal was a sensitive mirror galvanometer. First, the bridge was balanced in the absence of a magnetic field. Then upon application of a magnetic field owing to magnetostriction the dimensions of the specimen changed and with it the resistance of the strain-sensitive element. The magnetostriction was calculated on the basis of the galvanometer deflection by means of the formula

$$\lambda = \frac{\Delta R_C}{(1+2\sigma)R} \cdot \frac{\alpha}{\beta},$$

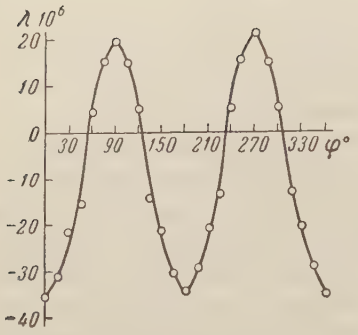

Fig.1. Angular distribution of magnetostriction (nickel disk specimen).

where ΔR_c is the calibrating resistance, β is the deflection of the galvanometer produced by the calibrating resistance, R is the resistance of the straing gage, σ is Poisson's ratio for the strain gage material and α is the deflection of the galvanometer due to magnetostriction.

The results for one of the disks are shown in Fig.1. The magnetostriction was measured in different directions relative to the applied field.[6] As will be evident from Fig.1, the nickel specimen conforms to Akulov's second rule for even effects, according to which the longitudinal magnetostriction should equal twice the negative value of the transverse magnetostriction.

The successful tests of film strain gages for measuring the magnetostriction of nickel[1,6] enabled us to develop this method further for work with ferrites. In fact, some of the characteristics of ferrites - high heat-resistance, high resistivity and appreciable hardness - made it possible to improve and at the same time simplify the strain gage design. In developing the strain gages we had to solve the problems of choosing a suitable material for the strain-sensitive film, providing leads between the film and the measuring instrument, and assuring reliable contacts between the leads and the film.

By way of materials for the strain-sensitive films we first chose nichrome and constantan. Owing to their high resistivity films of nichrome and constantan with the required resistance must be relatively thick (thickness appreciably greater than the critical value). Moreover, the necessary appreciable thickness of the films makes it possible to apply essentially continuous coatings despite the fact that the surface of ferrites even after careful polishing is relatively rough (unevennesses of the order of a micron). Thus in view of the film thickness it may be assumed that the properties of the strain-sensitive layer are identical with the properties of the bulk material. The films were deposited by vacuum evaporation by means of a Bochkareva[7] linear evaporator. The fine (0.1-0.3 mm) nichrome or constantan wire is wound onto a heavy (0.8-1.2 mm) tungsten heater wire; uniformity of the deposited film is assured by using fine wire of constant diameter. The evaporating temperature must be carefully maintained within a certain range to minimize selective evaporation and hence change in the proportions of the alloy components.[8]

The leads to the measuring instrument were attached in the following manner. First (prior to deposition), silver spot electrodes were fired onto the surface of the ferrite specimen at the locations of the ends of the strain-sensitive film. Then wire or ribbon conductors were soldered to these spots. Then, after thorough cleaning of the surface, the sensitive film was deposited. The thickness of the deposited film is monitored by measuring its resistance and the deposition process is stopped when the required value of resistance is attained.

Tests showed that if no further measures are taken the electric contact between the fired on silver and the nichrome film is not sufficiently stable and that sometimes the contact resistance exceeds the resistance of the film. To eliminate this it was necessary to apply additional contact layers. These were also applied by vacuum evaporation and were usually several times thicker than the strain-sensitive film. To insure good contact between the nichrome or constantan and the silver spot electrodes we used aluminum and nickel (one can also

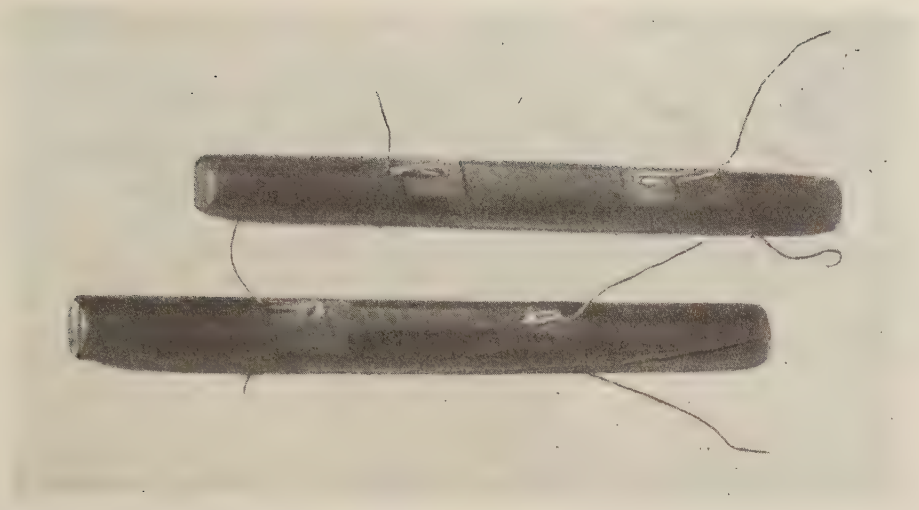

Fig.2. Film strain gages on ferrite specimens.

use nichrome or constantan, but in this case if the layer is made fairly thick it tends to scale off). Finally, the gage assemblies are artificially aged to stabilize their characteristics. This is done by heating the specimens at 200-300° for from 8 to 4 hours and then passing a 10-20 ma current through them for 8 hours. Two ferrite specimens with film strain gages are shown in Fig.2.

After stabilization, measurements were carried out by the procedure described in Ref.9. To eliminate the possible influence of "flexure" oscillations, we applied two strain gages of equal resistance to opposite sides of each specimen. The strain gages were calibrated with reference to standard strain gages on nickel rods and disks, and the results were further compared with the results obtained by means of wire strain gages.

The following data were obtained for the ferrite specimens shown in the accompanying photograph:

Specimen No.7: $MgFe_2O_4$ ferrite; $\rho > 10^9$ ohm cm; film strain gage of nichrome; normal gage resistance 828 ohm; magnetostriction $-6.25 \cdot 10^{-6}$; $I_s = 85$ gauss.

Specimen No.73: $NiFe_2O_4$ ferrite; $\rho > 2 \cdot 10^8$ ohm cm; film strain gage of nichrome; normal gage resistance 285 ohm; magnetostriction $-11.0 \cdot 10^{-6}$; $I_s = 240$ gauss.

It is interesting to note that even in the presence of relatively large temperature fluctuations the film strain gages operate in a stable manner. In view of the fact that the sensitive layer is applied directly to the ferrite surface (without cement and liners) the accuracy of measurement is not affected by heating as is frequently the case for conventional wire type strain gages.

Inasmuch as films of nichrome and more recently tested films of platinum-iridium and other alloys showed an exceptionally high temperature stability, it has become possible to investigate the magnetostriction of ferrites in a wide temperature range (from -190 to 300°) and the striction of piezoelectric specimens as a function of temperature. The results of these measurements will be published at a later date.

Chair of General Physics,
Faculty of Physics,
Moscow State University

References

1. G.P.D'yakov & V.A.Yugov, Vestnik, Moscow State Univ., No.5, 229 (1957).
2. J.E.Goldman, Phys.Rev., 72, 529 (1947).
3. N.S.Akulov & D.I.Volkov, Vestnik, Moscow State Univ., No.10, 29 (1949).
4. N.S.Akulov & D.I.Volkov, Ibid., No.6, 21 (1950).
5. N.L.Bryukhatov & G.P.D'yakov, in "Primenenie ul'traakustiki k issledovaniyu veshchestva" (Use of Ultrasonic Techniques for Investigation of Matter), No.7, 111 (1958).
6. G.P.D'yakov & V.A.Yugov, Vestnik, Moscow State Univ., No.3, 237 (1958).
7. V.A.Bochkareva, Inventor's Certificate No.16907, 18 April 1941.
8. L.Holland, Vacuum Deposition of Thin Films, London, 1956.
9. G.P.D'yakov, Izv.AN SSSR, Ser.fiz., 21, 1133 (1957). (Trans.Bulletin, 21, 1118.)

PREPARATION OF SINGLE CRYSTAL FILMS

- N.G.Nifontov

For many applications of thin films it is undoubtedly of advantage to have films with single crystal structure. One of the most interesting methods of obtaining such films is thermoevaporation of the desired metal under high vacuum onto a single crystal substrate.[1,2] The use of this method does not require as exacting a choice of substrates with a suitable crystal lattice as does preparation of oriented layers from solutions. Thus, for example, we readily succeeded in obtaining an oriented layer (and even double layers) of silver or copper on the cleavage faces of rock salt. The oriented silver layer on rock salt in turn serves as the substrate for a parallel oriented single crystal copper layer (values of the lattice constant a: NaCl - 5.64 A, Ag - 4.08 Å, and Cu - 3.62 Å).

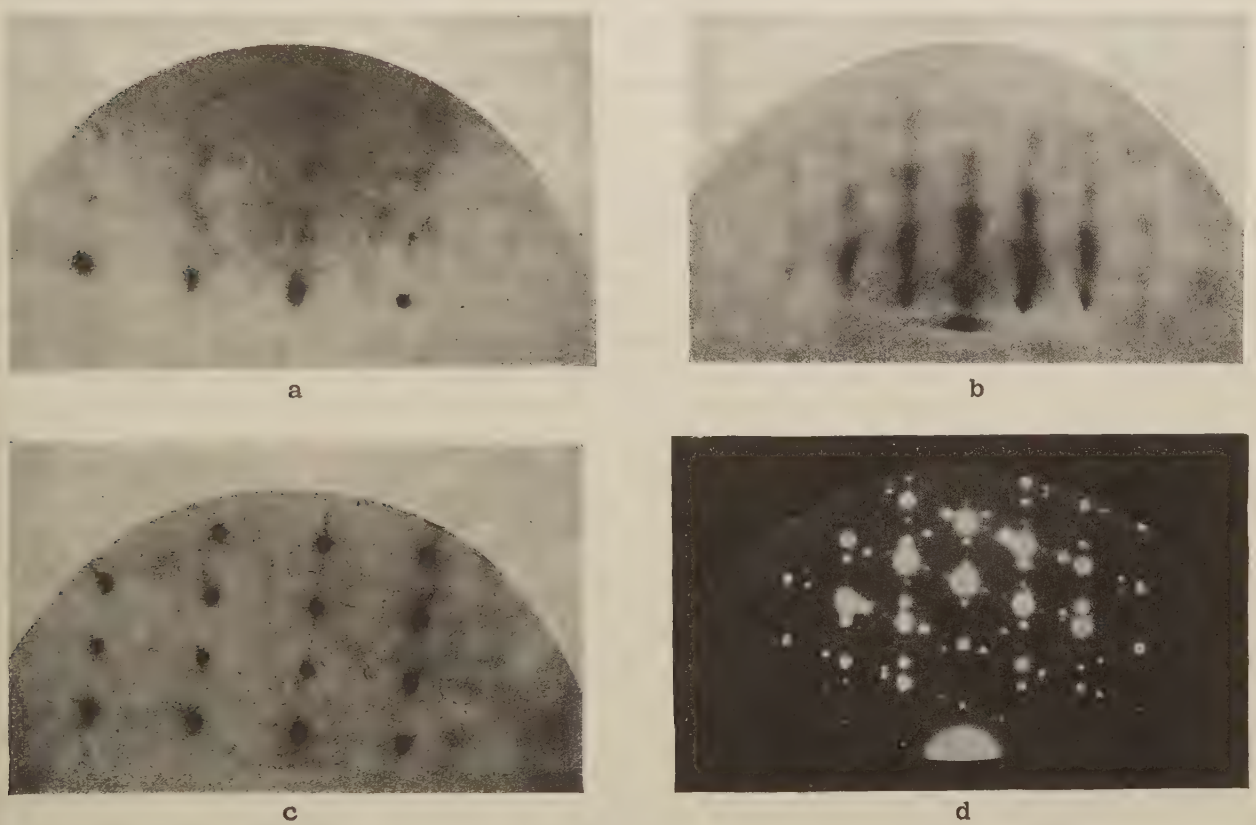

a b c d

Electron diffraction patterns obtained by reflection from the surface of a (111) face of calcium fluoride (a & b) and from a layer of germanium deposited on this face (c & d): a & c - electron beam in the [211]; b & d - beam in the [110] direction.

The problem becomes somewhat more difficult, however, when it comes to preparation of oriented films of germanium. Heavens & Collins[3] described their preparation of such films on rock salt; however, in order to obtain oriented crystallization of the germanium they found it necessary to heat the substrate during deposition to a temperature of 500°. At this temperature rock salt begins to vaporize under vacuum.

To eliminate this difficulty we used a substrate of calcium fluoride. CaF_2 has a crystal structure rather similar to that of germanium, a close value of the lattice constant a (Ge - 5.66 Å, CaF_2 - 5.46 Å) and withstands higher temperatures than rock salt. The experiments[4] were carried out in a specially designed chamber of an electron diffraction instrument equipped for evaporation in the body of the instrument and allowing of continuous observation of the specimen during deposition. The chamber was equipped with a heated substrate holder and a 10 kv ion gun which served both to cleanse the surface of the instrument and for gradual removal of the deposited layer to permit investigating its structure in thickness. Experimental conditions were recorded by means of a six-channel automatic potentiometer.

With this equipment we were able to obtain on a (111) cleavage face of calcium fluoride crystal parallel oriented germanium layers up to several microns in thickness. These layers yielded very sharp point diffraction patterns (see figure). Unfortunately, there also appear additional spots (mainly a distance 1/3 or 2/3 of that between the normal spots); these indicate the formation of twins in the thickness of the film (similar twins were observed by Pashley[2] in silver films on mica). We are carrying out further experiments to determine the evaporation conditions that will preclude the formation of twins.

References

1. Z.G.Pinsker, Difraktsiya elektronov (Electron diffraction), M. 1949.
2. D.W.Pashley, Phil.Mag., 4, 316 (1959).
3. O.S.Heavens & L.E.Collins, Proc.Phys.Soc., B, 825 (1952).
4. J.Marucchi & N.Nifontoff, Compt.rend., 249, 435 (1959).

SOME ELECTRIC PROPERTIES OF VERY THIN METAL FILMS

- N.G.Nifontov

In connection with use and investigation of thin metal films it is of interest to know their electric properties.

It is known that on the basis of the behavior of their resistance thin metal films prepared by vacuum evaporation onto an amorphous substrate may be divided, depending on their thickness, into three types.[1] In relatively thick films (type I) the resistance immediately after deposition at first decreases but soon attains a stable value. Calculations of the effective resistivity of such films yield values slightly higher than for the corresponding metal in the bulk state. (These films have a more or less pronounced hole structure and their thickness is less than the electron free path in the metal, which is the reason for enhanced electron scattering.)

In somewhat thinner films (type II) (thickness of the order of 100 Å for silver) the resistance immediately after evaporation increases rapidly and then stabilizes to some extent. If a slowly varying voltage is applied to such a film it is found that its resistance depends more or less reversibly on the voltage (nonlinear resistance, deviation from Ohm's law). Finally, in very thin films (type III) the resistance increases so rapidly after deposition that it soon becomes virtually impossible to measure. Electron micrographs show that films of the last two types are grainy and consist of crystals located at some distance from each other on the surface of the substrate.

How can one explain the conductivity of such films? Usually it is attributed to transition of electrons from one crystal to the next as a result of field or thermionic emission (at room temperature).[2,3] But field emission (the tunnel effect) cannot explain the temperature dependence of the resistance, while thermionic emission would yield current values may orders of magnitude lower than are actually observed, or would imply work function values smaller than 0.1 ev.[3] Earlier we advanced the hypothesis[4] that the electrons may migrate from one crystallite to another not directly but via a conducting layer on the surface of the substrate, a layer consisting of adsorbed gas and water molecules, local contaminations and the first deposited groups of more or less oxidized atoms of the evaporated metal. As for the deviations from Ohm's law, it can readily be shown that they are not due simply to heating by the current flowing through the film. On the contrary, they can be explained by field or thermionic emission and also related with the presence of a surface layer having more or less semiconductor properties.

Our experiments were carried out on thin films of gold, silver, copper and germanium. The first three metals belong to the same group (I) of the periodic table but have increasing chemical activity; the fourth is a typical semiconductor. The films were deposited on chemically cleaned amorphous quartz substrates with optically polished surfaces. The evaporator design provided for first depositing a pair of electrodes with a gap of about 0.01 mm between them and then depositing the experimental film over this gap and the electrodes without disturbing the vacuum ($\sim 5 \cdot 10^{-6}$ mm Hg). The crucible with the metal charge was first heated under a special retractable shutter. The deposition of the film was stopped upon attainment of the desired resistance by closing the shutter. The resistance of the film was monitored by comparing the current-voltage characteristic of the film with the characteristic of an appropriate standard resistance on the screen of a two-gun oscilloscope. The films were stored for many days in the same rigorously maintained vacuum, while their resistance was measured by means of a recording ohmmeter. After the resistance had reached a stable value,

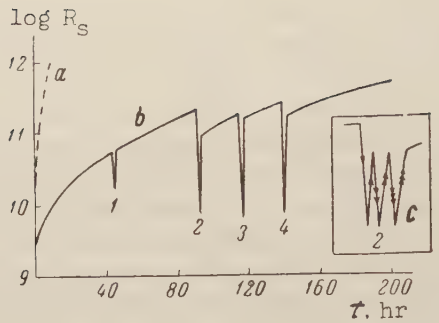

Fig.1. Variation of the resistance of silver films with time: a) film of type III, b) film of type II (deposited over a preliminary light coating of silver), c) detail of series 2 on curve b.

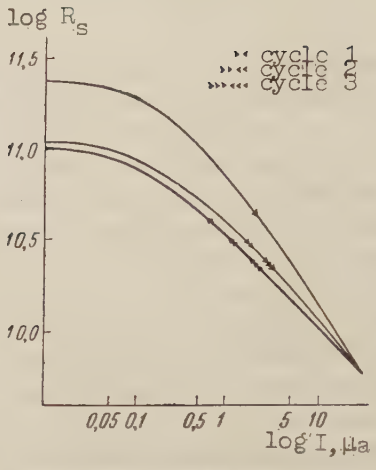

Fig.2. Current-resistance characteristics for the same series of measurements as in Fig.1.

from time to time we measured the deviation from Ohm's law by gradually increasing and decreasing a dc voltage applied to the film (several repeated voltage cycles in each series of measurements). The resistance was measured by means of a special bridge circuit. At the same time we also measured the low-frequency noise level in these films (measurements were carried out in the range from 500 to 10 000 cps).

Silver films were studied in greatest detail.[5] At first the films obtained were not always stable and their resistance frequently increased very rapidly (type III). Experiments showed, however, that if before the actual deposition of the film the substrate is coated by a very thin layer of silver (so thin that the resistance across the gap is virtually unaffected) the final film deposited in this subcoating is stable (type II). Curve b in Fig.1 shows the aging of such a film. The curve also shows the changes obtained during measurements of the deviation from Ohm's law. Curve c in the insert gives the detailed results of one such series of measurements. It shows that during the first measurement cycle, i.e., the first increase of the voltage on the film, there occurs an irreversible change of the resistance; in further cycling of the voltage (within the same series of measurements) the effect is entirely reversible. This is also evident from Fig.2 which gives the R_s vs I (R_s is the specific surface resistivity of the film and I is the current) curves for the same series of measurements. All the reversible characteristics obtained in different series of measurements on the same film are of similar shape.

Gold films deposited directly on the substrate in the normal manner[6] are highly unstable and are characterized by a rapidly increasing resistance (curve 1 in Fig.3). Films prepared by deposition on a preliminary thin coating of gold are more stable (curve 2); gold films deposited over a preliminary silver coating are just as stable as the above described silver films (curves 3 & 4).

Copper films are very stable even without a preliminary thin coating. Their resistance increases more slowly than that of silver and gold films; the deviations from Ohm's law are also smaller at the same voltages. No irreversible processes are observed in copper films. These properties are even more clearly pronounced in germanium films[7], the resistance of which rises to a virtually constant value within a few hours (Fig.4). Measurements of the intrinsic low-

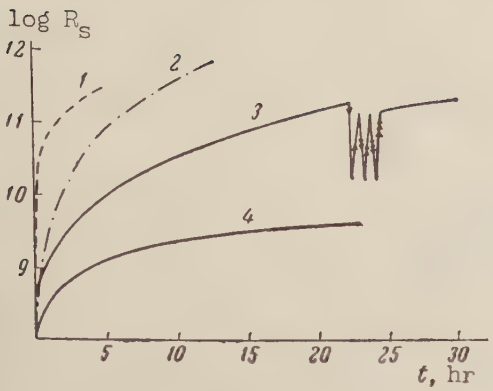

Fig.3

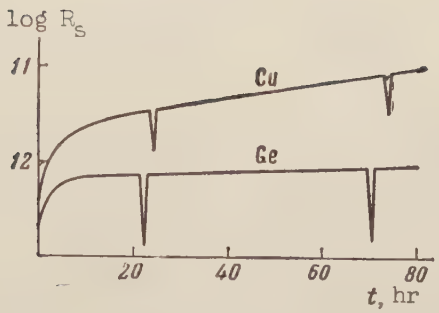

Fig.4

Fig.3. Variation of the resistance with time of gold films: 1) film deposited directly on the substrate (type III), 2) film deposited on a preliminary thin gold coating (type III), 3 & 4) gold films deposited over a preliminary thin silver coating (type II).

Fig.4. Variation of the resistance of copper and germanium films (deposited directly on the substrate).

frequency noise (1/f spectrum) showed that the variation in noise level is correlated with the variation in resistance; again there were obtained reversible and irreversible characteristics. The noise was strongest for gold films, weaker for silver and at the threshold of measurement for copper and germanium.

Thus, the significant effect of a preliminary atomic layer (the atoms apparently react with the surface of the substrate and become firmly attached to it, forming a conducting layer) and the important role of the chemical activity of the investigated metal would seem to substantiate our hypothesis regarding the influence of a surface layer on the conductivity of films. We also note that the described technique makes it possible to obtain stable nonlinear thin-layer resistances.

References

1. M.Perrot & J.P.David, Compt.rend., 234, 1753 (1952); A.Colombani & G. Ranc. Ibid., 232, 1344 (1951); Ibid., 233, 47 (1951).
2. Ya.I.Frenkel', Zhur.eksp.i teor.fiz., 16, 316 (1946).
3. N.Mostovetch, Ann.Phys., 8, 61 (1953).
4. N.Nifontoff, Compt.rend., 238, 1870 (1954); A.Blanc-Lapierre & N.Nifontoff, J.Phys.et Radium, 17, 230 (1956).
5. C.Uny & N.Nifontoff, Compt.rend., 246, 906 (1958).
6. C.Uny, Ibid., 248, 1655 (1959).
7. C.Uny, Ibid., 249, 645 (1959).

MAGNETIC PROPERTIES OF NICKEL DEPOSITS OBTAINED BY CHEMICAL PLATING

- N.V.Kotel'nikov & V.I.Gachegov

At present increasing use is being made of the method of chemical nickel plating (deposition of nickel without an electric current). However, the magnetic properties of coatings prepared in this manner have scarcely been investigated.[1]

It is known that such nickel deposits contain from 3 to 15% phosphorus, depending on the composition and state of the bath. Hence it is natural to assume that the magnetic properties of nickel deposits prepared by the chemical procedure must differ from the properties of nickel coatings obtained electrolytically. Assuming that the variation in the magnetic properties of nickel as a function of the phosphorus content is similar to the variation obtaining for alloys of nickel with antimony[2], we come to the conclusion that at 12 atomic percent P the saturation magnetization should drop to zero. Dependence of the saturation magnetization on the phosphorus content could, for example, be utilized for determining the phosphorus in such deposits. Such a magnetic procedure would be simpler and hence more economical than chemical methods of analysis.

Investigation of the magnetic properties of nickel deposits obtained by the chemical method is also of interest from other standpoints: for example, it may be possible to develop magnetic techniques for determining the thickness of such coatings, it may be feasible to prepared nickel deposits free of ferromagnetism that can be used as protective and decorative coatings on equipment where ferromagnetic properties are undesirable, etc.

Moreover, investigation of the magnetic properties of the Ni-P system is of undoubted interest where the theory of ferromagnetism is concerned.

Specimen preparation and experimental procedure

The nickel coatings were deposited chemically on the outside walls of sealed copper tubes 4 mm in diameter, mounted vertically in the chemical bath. The nickel was deposited on a 100 mm length of the copper tube, the area of deposition being limited by the end of the vinyl tube into which the upper end of the copper was inserted.

The chemical bath was in the form of a cylinder with an inside diameter of 25 mm. To prevent evaporation of the solution the bath was closed with a stopper with a small hole to allow escape of the gases evolving during the plating process.

Prior to deposition the copper tubes were cleansed in the same manner as in preparation for electrolytic plating. In order to initiate the plating process on copper[1] a small strip (1 x 3 mm) of aluminum foil was inserted into the vinyl holder alongside the copper tube. For all specimens the deposition was carried out for a period of 10 hours with the solution being replaced by a fresh one every hour in order to assure a more uniform structure of the deposit in thickness. A fresh solution (100 g) was poured into a bath which was then heated to 87° by immersion into thermostated water, then the stopper together with the vinyl holder and specimen was transferred from the old bath to the new one. Two solutions of different composition (see table) were used. In all we prepared and investigated six specimens (three in each series).

The ferromagnetic properties of the specimens were investigated by recording the magnetization curves and hysteresis loops by the ballistic method. The measuring coil had a length of 50 mm, an inside diameter of 4.5 mm and an outside

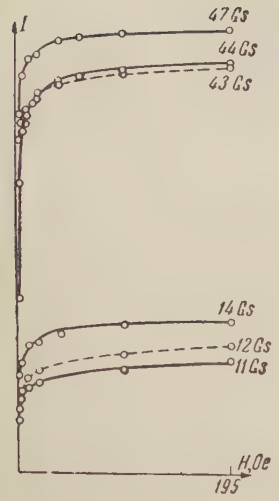

Fig.1

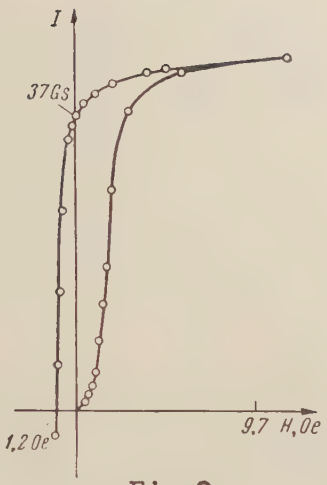

Fig.2

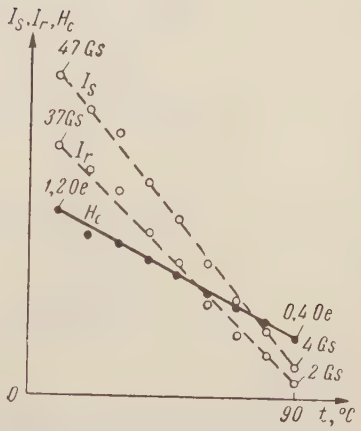

Fig.3

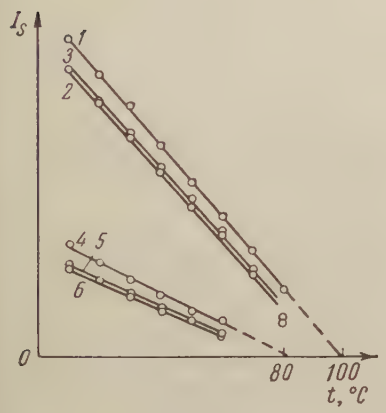

Fig.4

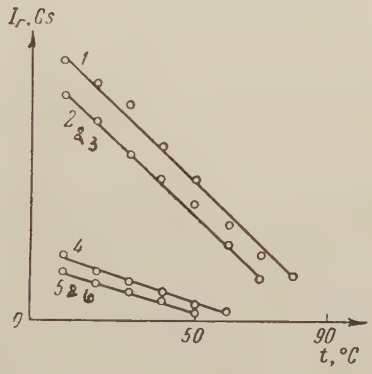

Fig.5

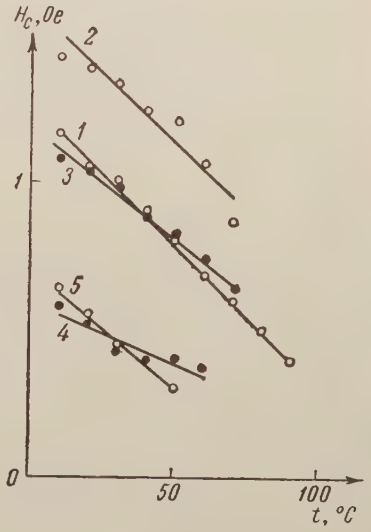

Fig.6

diameter of 16 mm. The difference between the numbers of opposed turns was 2035. The appreciable thickness of the deposits (over 100 microns) and the large difference between the number of opposed turns, made it possible to investigated the weak (compared with pure nickel) ferromagnetic properties of the nickel deposits.

Results

The compositions of the bath solutions and the parameters of the specimens are listed in Table 1. The amount of deposit was determined by weighing the copper tubes before and after plating. The thickness and cross section area of the specimens were calculated from the weight of the deposits and the density, which was assumed to be equal to that of pure nickel (8.9 g/cm^3).

It must be noted that the density of the chemically deposited nickel depends on the composition of the plating bath and its operating conditions and may differ appreciably from the density of pure nickel.[1] Hence the values of saturation magnetization I_S and remanence I_r calculated on this basis are presumably too high. Correct values are obtained in calculating the magnetization

Table 1

Series No.	Bath composition, g/liter	Specimen No.	Weight, g	Cross section area, cm^2	Thickness, microns
I	Nickel sulfate - 30	1	1.3	0.0146	116
	Sodium hypophosphite - 10	2	1.302	0.0146	116
	Sodium acetate - 10	3	1.310	0.0147	117
II	Nickel sulfate - 30	4	1.470	0.0165	131
	Sodium hypophosphite - 15	5	1.466	0.165	131
	Sodium acetate - 10	6	1.458	0.0164	130

per gram of deposit.

Fig.1 shows the magnetization curves recorded at 10° in fields up to 195 oersted. The top three curves pertain to specimens of Series I; the lower curves to specimens of Series II.

Both the magnetization curves and the hysteresis loops for all specimens are similar in shape. The magnetization curve and part of the hysteresis loop recorded at 10° in fields to 11.7 oersted for specimen No.1 of Series I are shown in Fig.2. The temperature dependences of I_s, I_r and H_c for the same specimen are shown in Fig.3. Fig.4 gives the temperature dependences of the saturation magnetization for all six specimens plotted to the same scale. The temperature dependences of the remanence and coercive force are shown in Figs.5 & 6. In these figures the numeration of the curves corresponds to the specimen designation in Table 1 (the curve for specimen No.6 is not shown in Fig.6; it lies close to the curve for specimen No.4).

Discussion and results

As noted in the introduction, the ferromagnetic properties of the Ni-P system have scarcely been studied. There are no experimental data on the solubility of phosphorus in nickel and on the Curie point.[2] It follows from theory that the maximum solubility of phosphorus in nickel should be about 5%. According to Gorbunova & Nikiforova[1], the phosphorus content in specimens of Series I should be 6.87%. Hence, part of the phosphorus in the chemically reduced nickel should be present in the form of intermetallic compounds such as Ni_3P, Ni_2P_5 and Ni_2P (it is not known whether these compounds are or are not ferromagnetic). Gorbunova & Nikiforova note that chemically reduced nickel is an amorphous substance and that in addition to the solid solution of phosphorus in nickel, it may contain inclusions of the above mentioned intermetallic compounds.

Table 2

Specimen No.	Magnetization (gauss) in 195 oe field			Remanence, gauss			Coercive force, oe		
	$t = 10°$ C	$t = 60°$ C	$T = 0$ °K (extrap.)	$t = 10°$ C	$t = 60°$ C	$T = 0$ °K (extrap)	$t = 10°$ C	$t = 60°$ C	$T = 0$ °K (extrap)
1	47	24	196	37	15	162	1,2	0,7	3,98
2	43	18	188	32	11	154	1,55	1,07	4,23
3	44	19	190	32	11	154	1,14	0,74	3,33
4	14	5	69	9	2	54	0,56	0,36	1,73
5	12	4	62	7	0	47	0,64	—	3
6	11	3	59	7	0	47	0,64	—	3

The presence of phosphorus in nickel leads to alteration of its magnetic properties, which have partially been investigated by Polukarov (see Ref.1).

As out measurements showed, deposits of chemically reduced nickel at room temperature are weakly ferromagnetic compared to pure nickel (Figs.1 & 2). Magnetic properties of the deposit exhibit a strong temperature dependence; at temperatures above 100° the ferromagnetism vanishes (Figs.3-5). The temperature dependences of I_s, I_r and H_c are linear (Figs.4-6). It is evident from the experimental curves that the coercive force falls off with temperature more slowly than the remanence. As is evident from Figs.4-6 and Table 2, the values of the coercive force are not proportional to the magnetization: thus, whereas the magnetization curve for specimen No.2 (Fig.4) lies below the curves for specimens Nos.1 & 3, the coercive force curve for this specimen (curve 2 in Fig.6) lies above the H_c curves for the other specimens.

If for pure nickel we take $\sigma_0 = 57.5$ and $n_0 = 0.604$, by linear extrapolation to 0°K we obtain for our specimens (Series I) $\sigma_0 = 24.2$ and $n_0 = 0.254$ magnetons per atom.

Assuming provisionally that the chemical deposit is a uniform solution of phosphorus in nickel and that the concentration dependence of the magnetic properties of the Ni-P system is similar to the dependence obtaining for the Ni-Sb system, on the basis of the above value for n_0 we find that the phosphorus content in the deposit is equal to ~4%. This lower value compared with that given in the literature (6.97%) may be due either to errors in extrapolating to absolute zero or to the fact that the behavior of the Ni-P system is different from that of the Ni-Sb system. Possibly the divergence should be attributed to the complex structure of the deposit, in particular to the presence in it of intermetallic compounds.

The weaker ferromagnetism of specimens of Series II is probably due to a higher phosphorus content, inasmuch as the sodium hypophosphite content in the second bath was 50% higher than in the first (Table 1).

Our experimental results may be summarized as follows.

1. The ferromagnetic properties of chemically deposited nickel differ radically from the properties of the pure nickel, which is in agreement with the data of other authors[1].

2. Increase of the hypophosphite concentration in the plating bath leads to weakening of the ferromagnetic properties of the deposits.

3. The saturation magnetization I_s, remanence I_r and coercive force H_c of all the specimens decreases linearly with increasing temperature.

4. The Curie point of the nickel deposits lies appreciably below the Curie

point of pure nickel; this is probably due to the presence of phosphorus in the deposits.

Perm State University

References

1. K.M.Gorbunova & A.A.Nikiforova, Fiziko-khimicheskie asnovy protsessa khimicheskogo nikelirovaniya (Physics and chemistry of chemical nickel plating), M. 1960.

2. R.M.Bozorth, Ferromagnetism, N.Y. 1951 (Cited in Russian trans.).

3. G.T.Bakhvalov, L.N.Birkgan & V.P.Labutin, Spravochnik gal'vanostega (Electroplater's Handbook), p.155, GNTIL Series on ferrous and nonferrous metallurgy, 1954.

Bulletin of the Academy of Sciences of the USSR - Physical Series
Vol. 25, No. 5 - May 1961

Transactions of the Symposium on Thin Ferromagnetic Films

TABLE OF CONTENTS

	Russ. page	Trans. page
Thin magnetic films in present-day physics and engineering - K.M.Polivanov & A.L.Frumkin	566	569
Influence of the technique of preparation and thickness of thin ferromagnetic films of Fe-Ni-Mo alloy on their domain structure - L.V.Kirenskii & V.A.Buravikhin	569	572
Domain walls in thin ferromagnetic films - L.V.Kirenskii & V.A.Buravikhin	574	578
Domain structure and coercivity of thin ferromagnetic films - L.V.Kirenskii, V.A.Buravikhin & A.G.Zvegintsev	577	581
Domain structure of ferromagnetic films prepared by cathode sputtering - G.V.Spivak, I.G.Sirotenko & R.D.Ivanov	581	585
Investigation of the magnetic structure of thin ferromagnetic films by means of the Kerr magneto-optical effect - L.V. Kirenskii, S.V.Kan & I.F.Degtyarev	584	589
Behavior of the domain structure of thin ferromagnetic films in the process of slow magnetization reversal - L.V.Kirenskii & S.V.Kan	592	598
Variation of the domain structure of thin ferromagnetic films in a magnetic field - L.V.Kirenskii, V.A.Buravikhin & M.K. Savchenko	596	604
New procedure for measuring the thickness of domain walls by means of the Kerr effect - V.I.Sinegubov & M.V.Savchenko	599	609
Barkhausen effect in thin Mo-Permalloy films - M.M.Salanskii, A.M.Rodichev & M.K.Savchenko	602	612
Nucleation and the Barkhausen effect in ferromagnetic films - V.F.Ivlev & V.S.Prokopenko	606	616
Investigation of the duration of Barkhausen jumps in an iron film - G.M.Rodichev & P.D.Kim	610	620
Contribution to the theory of high field magnetization reversal in thin films - A.M.Rodichev	614	624
Apparatus for investigating pulse switching of thin ferromagnetic films - T.N.Nikitina & R.V.Telesnin	619	630

Nanosecond current pulse generator for investigating the behavior of ferromagnetic films - O.S.Kolotov & T.N. Nikitina	622	633
Amplification of nanosecond pulses - O.S.Kolotov & T.N. Nikitina	624	635
Domain structure of uniaxial ferromagnetic films - V.V. Koboelev & A.A.Korsunskii	628	639
Investigation of the switching time of ferromagnetic film elements - I.A.Efimov	634	647
Ferromagnetic resonance in thin films - L.V.Kirenskii, V.A.Ignatchenko & O.G.Baklanov	640	652
Measurement of the hysteresis loss in thin films in a rotating magnetic field - N.I.Sudakov, M.K.Savchenko, E.K.Zagirova & I.I.Starostin	643	655
Use of thin films for measurement of magnetostrictive and other strains - V.A.Yugov & G.P.D'yakov	647	659
Preparation of single crystal films - N.G.Nifontov	651	663
Some electric properties of very thin metal films - N.G. Nifontov	652	665
Magnetic properties of nickel deposits obtained by chemical plating - N.V.Kotel'nikov & V.I.Gachegov	655	668

Translated in 1962 by
Columbia Technical Translations
5 Vermont Ave., White Plains, N.Y.

Transactions

of the

Third All-Union Conference on Electron Microscopy

(Leningrad, 24-29 October 1960)

Publication Note

Part of the reports presented at the Conference will be published in "Radiotekhnika i elektronika" (Radio Engineering & Electronics).

CALCULATION OF ELECTRON LENS FIELDS

- A.G.Vlasov and D.M.Krupp

The calculation of electrostatic fields, as well as of magnetostatic fields of iron-clad coils and permanent magnets reduces to solution of the Dirichlet problem. This problem may be formulated as follows: find a function satisfying Laplace's equation

$$\Delta\varphi = 0 \qquad (1)$$

inside a given region and taking on given values at the boundary of the region.

It may happen that the region one is dealing with can be broken up into subregions or cells whose boundary surfaces are the coordinate surfaces of some curvilinear orthogonal coordinate system in which Laplace's equation can be integrated by separation of variables. In this case the Dirichlet problem may be solved analytically in the following way.

By separating the variables one obtains a particular integral of Laplace's equation. Using this integral, one constructs a solution of Laplace's equation for each cell as a sum of several series with arbitrary coefficients. The boundary conditions are applied to the solution thus constructed on those faces of the cells which are sections of the original boundary. The conditions that must be satisfied at the other, intercell boundaries are continuity of the potential and of its normal derivative. This latter condition implies the requirement of term-by-term differentiability of the series forming the solutions in the separate cells, right through to the boundary.

We have shown earlier[1] that in the general case of a cell with six faces, twelve edges and eight vertices, a solution with enough undetermined elements to satisfy all the necessary conditions on the faces, edges and vertices will consist of six double and twelve simple series with arbitrary coefficients in addition to a solution in closed form containing eight arbitrary constants.

The boundary and continuity conditions then lead to an infinite set of linear algebraic equations for the coefficients of the series.

In the case of electron lenses, the Dirichlet problem is axially symmetric, and it is natural and convenient to use cylindrical coordinates. The cells are then solid or hollow cylinders with three or four faces, two or four edges, and no vertices. Then the solution for each separate cell becomes much simpler: the double series corresponding to the cell faces degenerate into simple series, the simple series corresponding to the edges become solutions in finite closed form, and the solution corresponding to the vertices vanishes.

The infinite set of linear algebraic equations for the coefficients of the series then becomes entirely regular, and it can be solved by a reduction method.

The figure shows a cross section through the meridian plane of a two-electrode cathode lens. The electrodes are ideally conducting hollow cylinders with infinitely thin walls. The cylinder on the left, closed at its left end by a plane base, is the cathode. The anode is the cylinder on the right, closed at its right end by a plane base.

We wish to obtain the potential distribution, assuming the cathode to be at zero potential and the anode at unit potential. We shall use a cylindrical coordinate system whose axis coincides with the symmetry axis of the lens and whose origin lies at the center of the base of the cathode. All the dimensions of the electrodes are indicated in the figure.

While it would be feasible to find the potential through all space, we shall restrict our problem to finding the exact potential only in the neighborhood of

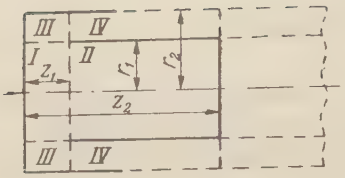

Cross section through the meridian plane of a two-electrode lens.

the axis inside the lens. In this case the calculation reduces to solving the internal Dirichlet problem, assuming that the potential varies logarithmically in the $z = z_2$ plane between the cylinders:

$$\varphi(z, r) = \frac{\ln \frac{r}{r_2}}{\ln \frac{r_1}{r_2}} \quad \text{for} \quad r_1 \leqslant r \leqslant r_2. \tag{2}$$

We then use the $z = z_1$ plane and the cylindrical surface $r = r_1$ to divide the region into the cylindrical cells I, II, III and IV, as shown in the figure.

We write the solutions of the Laplace equation for the different cells in the forms

$$\varphi_{\mathrm{I}} = \sum_{n=1}^{\infty} a_n^{\mathrm{I}} \frac{I_0\left(\frac{n\pi r}{z_1}\right)}{I_0\left(\frac{n\pi r_1}{z_1}\right)} \sin \frac{n\pi z}{z_1} + \sum_{m=1}^{\infty} C_m^{\mathrm{I}} \frac{\operatorname{sh} \alpha_m z}{\operatorname{sh} \alpha_m z_1} J_0(\alpha_m r) + \frac{z}{z_1};$$

$$\varphi_{\mathrm{II}} = \sum_{m=1}^{\infty} C_m^{\mathrm{I}} \frac{\operatorname{sh} \alpha_m (z - z_2)}{\operatorname{sh} \alpha_m (z_1 - z_2)} J_0(\alpha_m r) + 1;$$

$$\varphi_{\mathrm{III}} = \sum_{n=1}^{\infty} a_n^{\mathrm{I}} \frac{I_0\left(\frac{n\pi r_2}{z_1}\right) K_0\left(\frac{n\pi r}{z_1}\right) - K_0\left(\frac{n\pi r_2}{z_1}\right) I_0\left(\frac{n\pi r}{z_1}\right)}{I_0\left(\frac{n\pi r_2}{z_1}\right) K_0\left(\frac{n\pi r_1}{z_1}\right) - K_0\left(\frac{n\pi r_2}{z_1}\right) I_0\left(\frac{n\pi r_1}{z_1}\right)} \sin \frac{n\pi z}{z_1} + \sum_{m=1}^{\infty} C_m^{\mathrm{III}} \frac{\operatorname{sh} \xi_m z}{\operatorname{sh} \xi_m z_1} W_0(\xi_m r) + \frac{\ln \frac{r}{r_2}}{\ln \frac{r_1}{r_2}} \frac{z}{z_1}; \tag{3}$$

$$\varphi_{\mathrm{IV}} = \sum_{m=1}^{\infty} C_m^{\mathrm{III}} \frac{\operatorname{sh} \xi_m (z_2 - z)}{\operatorname{sh} \xi_m (z_2 - z_1)} W_0(\xi_m r) + \frac{\ln \frac{r}{r_2}}{\ln \frac{r_1}{r_2}};$$

where I_0 and K_0 are Bessel functions of an imaginary argument,

$$W_0(\xi_m r) = Y_0(\xi_m r_1) J_0(\xi_m r) - J_0(\xi_m r_1) Y_0(\xi_m r), \tag{4}$$

and the α_m and ξ_m are the positive roots of the equations

$$J_0(r_1 \alpha) = 0, \quad Y_0(r_1 \xi) J_0(r_2 \xi) - J_0(r_1 \xi) Y_0(r_2 \xi) = 0. \tag{5}$$

Equations (3) already satisfy the boundary conditions and the continuity conditions on the intercell faces.

Now using continuity of the normal derivatives, we arrive at the equations

$$\left[\frac{I_1\left(\frac{n\pi r_1}{z_1}\right)}{I_0\left(\frac{n\pi r_1}{z_1}\right)} - \frac{I_1\left(\frac{n\pi r_1}{z_1}\right) K_0\left(\frac{n\pi r_2}{z_1}\right) + I_0\left(\frac{n\pi r_2}{z_1}\right) K_1\left(\frac{n\pi r_1}{z_1}\right)}{I_0\left(\frac{n\pi r_1}{z_1}\right) K_0\left(\frac{n\pi r_2}{z_1}\right) - I_0\left(\frac{n\pi r_2}{z_1}\right) K_0\left(\frac{n\pi r_1}{z_1}\right)}\right] \times$$

$$\times a_n^{\mathrm{I}} (-1)^n = \frac{2}{z_1} \sum_{m=1}^{\infty} \left[\frac{W_1(\xi_m r_1) \xi_m}{\xi_m^2 + \left(\frac{n\pi}{z_1}\right)^2} C_m^{\mathrm{III}} - \frac{\alpha_m J_1(\alpha_m r_1)}{\alpha_m^2 + \left(\frac{n\pi}{z_1}\right)^2} C_m^{\mathrm{I}}\right] + \frac{2}{z_1} \frac{\left(\frac{z_1}{n\pi}\right)^2}{r_1 \ln \frac{r_2}{r_1}};$$

$$\sum_{n=1}^{\infty} a_n^{\mathrm{I}} \frac{\pi (-1)^{n+1} \left(\frac{n\pi}{z_1}\right)^2 \xi_m^2}{\left[\frac{J_0^2(\xi_m r_1)}{J_0^2(\xi_m r_2)} - 1\right]\left[\xi_m^2 + \left(\frac{n\pi}{z_1}\right)^2\right]} + C_m^{\mathrm{III}} \xi_m \operatorname{cth} \xi_m z_1 - \frac{\pi}{z_1} \frac{1}{\frac{J_0^2(\xi_m r_1)}{J_0^2(\xi_m r_2)} - 1} = C_m^{\mathrm{III}} \xi_m \operatorname{cth} \xi_m (z_2 - z_1); \tag{6}$$

$$\frac{2\alpha_m}{r_1 J_1(\alpha_m r_1)} \sum_{n=1}^{\infty} a_n^{\mathrm{I}} \frac{(-1)^n \frac{n\pi}{z_1}}{\alpha_m^2 + \left(\frac{n\pi}{z_1}\right)^2} + \frac{2}{z_1} \frac{1}{r_1 \alpha_m J_1(\alpha_m r_1)} = C_m^{\mathrm{I}} \alpha_m [\operatorname{cth} \alpha_m (z_1 - z_2) - \operatorname{cth} \alpha_m z_1].$$

The coefficients C_m^{I} and C_m^{III} can be expressed in terms of the a_n^{I}. Eliminating C_m^{I} and C_m^{III} from Eq.(6), we obtain the infinite set of equations

$$a_n^{\mathrm{I}} = \sum_{k=1}^{\infty} r_{nk} a_k^{\mathrm{I}} + b_n \qquad (n = 1, 2, \ldots, \infty), \tag{7}$$

where the r_{nk} and b_n are known quantities.

Analysis shows that Eqs.(7) form a completely regular set. The equations have been solved by means of a reduction method.

We have used this method to perform several electron-lens calculations for more complicated configurations; in all cases the infinite set of equations to which the solution reduces proved to be completely regular.

References

1. A.G.Vlasov, Optiko-mekhanicheskaya promyshlenost' (Optical-mechanical industry), 1, 18 (1959).

CONCERNING ABERRATION OF ELECTRON-OPTICAL SYSTEMS

- P.P.Kas'yankov & K.P.Dutova

The formulas of Glaser or Scherzer, often given in textbooks (see, for instance, Glaser[1]) for calculating the aberration of a homogeneous magnetic field may lead to misapprehensions. In particular, it is found that in a homogeneous field coma, curvature, astigmatism and distortion aberrations fail to vanish, while from a direct investigation of electron trajectories it is evident that all third-order aberrations, other than spherical aberration, go to zero in a homogeneous magnetic field. Since there is no reason to doubt the validity of the formulas for the constants of third-order aberration as derived by different authors, the resulting situation can be explained only by the inference that one of the assumptions used in the derivation is not valid. Seman[2], who first pointed out this fact, offers as explanation the fact that in the present case the object itself is in a magnetic field, i.e., that the entire system is a magnetic-immersion one.

A careful study of the derivation of the formulas for the aberration coefficients by either the eikonal method or by following the trajectories shows that the conclusions remain valid whether or not the object is in a magnetic field.

Further, it is known that in an electron microscope the object is usually in a magnetic field, nevertheless no errors have been discovered in the calculations based on the usual aberration formulas.

An electron lens whose focusing field is a homogeneous magnetic field differs from the objective lens of a microscope in that in a microscope the beams are defined by special apertures, whereas trajectory calculations of the aberration due to a homogeneous magnetic field assume the absence of any limiting apertures. These considerations have impelled us to seek a different explanation of the error obtained in using the usual formulas to calculate aberration in the case of a homogeneous magnetic field.

Beam definition in electron optical systems

The basic conditions for the applicability of the third-order aberration formulas are the requirements that the distance of the electrons from the symmetry axis and the angles between the tangents to the electron trajectories and the axis be sufficiently small. This means that the beams of electrons participating in the formation of each point of the image must be limited. In some electron optical systems, such as the electron microscope, this limiting is realized by special diaphragms, called apertures. In cathode lenses, however, beams with apertures as large as $2\beta = 180^{\circ}$ may participate in forming the image of a point of the cathode. But only some of the electrons in this beam, namely, those whose angle of emission α with respect to the normal of the cathode surface is less than 90°, produce a detectable image. Unfortunately, we know of no accurate data on the aperture dependence of the intensity of a beam from which one could estimate the aperture angle α. Cathode lenses usually have no special limiting aperture. A cathode lens in which the focusing field is a homogeneous magnetic field is an example of a system without an aperture.

In order to calculate the aberration of a beam of electrons one need not know the mechanism by which this beam is limited. One requires only that the beams originating at different points of the object be characterized by the same parameters. Therefore any system containing apertures can be treated, for the purposes of aberration calculations, as a special case of a system without apertures. For this it is sufficient to allow that the principal rays of the beams may not be

normal to the object plane, and to assume that they can be chosen so as to intersect the symmetry axis at the same point.

In a homogeneous magnetic field the principal rays are parallel to the optical axis. Therefore a homogeneous magnetic field cannot be treated as a special case of a system with limiting apertures, since in the latter the principal rays intersect the axis. From the fact that a homogeneous magnetic field is a unique kind of system without apertures, we arrive at the following conclusion: from the point of view of aberration calculations, systems without apertures are a general class of electron-optical systems which include, as a special case, systems with apertures, but not vice versa.

In deriving the formulas for the aberration constants, given in the textbooks, one assumes that the beams are defined by special apertures. It will be evident from the above-said that such formulas cannot be used to calculate aberration in systems without limiting apertures, and, in particular, in the case of a homogeneous field.

Derivation of the third-order aberration constants for a system without limiting apertures

We start with the known equations for the electron trajectories in a stationary Cartesian coordinate system x, y, z, in which the z axis is the symmetry axis of the system. Expanding the field potentials as series in x and y, we obtain the trajectory equations up to terms of third order, namely,

$$\left.\begin{aligned} x'' + \frac{1}{2}\frac{\Phi'}{\Phi}x' + \frac{\Phi''}{4\Phi}x + \sqrt{\frac{e}{2m\Phi}}Hy' + \frac{1}{2}\sqrt{\frac{e}{2m\Phi}}H'y = f_1, \\ y'' + \frac{1}{2}\frac{\Phi'}{\Phi}y' + \frac{1}{4}\frac{\Phi''}{4\Phi}y - \sqrt{\frac{e}{2m\Phi}}Hx' - \frac{1}{2}\sqrt{\frac{e}{2m\Phi}}H'x + f_2, \end{aligned}\right\} \quad (1)$$

where $\Phi = \Phi(z)$ and $H = H(z)$ are the electric potential and magnetic field strength on the symmetry axis, f_1 and f_2 are the third order terms in x and y, and x' and y' can be expressed in terms of Φ, H, x, y and their derivatives with respect to z. If we set $f_1 \equiv f_2 \equiv 0$ in Eq.(1), we obtain the paraxial equations. The solutions x_1, y_1 of the paraxial equations with given initial conditions x_0, y_0, x_0', y_0' can be expressed in terms of the two linearly independent solutions r_1, r_2 of the equation

$$r'' + \frac{\Phi'}{2\Phi}r' + \left(\frac{1}{4}\frac{\Phi''}{\Phi} + \frac{e}{8m\Phi}H^2\right)r = 0 \quad (2)$$

and the function χ defined by

$$\chi = \frac{1}{2}\int_{z_0}^{z}\sqrt{\frac{e}{2m\Phi}}H\,dz. \quad (3)$$

A solution x_3, y_3 of Eqs.(1) satisfying the same initial conditions as the solutions x_1, y_1 of the corresponding paraxial system can be expressed in terms of these latter solutions.

The differences

$$\Delta x = x_3 - x_1,$$
$$\Delta y = y_3 - y_1,$$

calculated in the Gaussian plane, are expressed in terms of third order with respect to the initial conditions x_0, x_0', y_0' (y_0 is assumed to be zero):

$$\Delta x = B_1 (x_0'^2 + y_0'^2) x_0' + x_0 [F_1 (3x_0'^2 + y_0'^2) + 2f_1 x_0' y_0'] + [(2C_1 + D_1) x_0' + c_1 y_0'] x_0^2 + E_1 x_0^3; \quad (4)$$

$$\Delta y = B_1 (x_0'^2 + y_0'^2) y_0' + x_0 [2F x_0' y_0' + f_1 (x_0'^2 + 3y_0'^2)] + D_1 y_0' + c_1 x_0') x_0^2 + e_1 x_0^3.$$

The coefficients of these forms are the third-order aberration constants and can be written as integrals of functions whose arguments are Φ, Φ', Φ'', Φ''', Φ^{IV}, H, H', H'', r_1, r_2, r_1', r_2'.

When Eqs.(4) are used to calculate aberrations in a homogeneous magnetic field, the result obtained is correct.

Equations (4) are of the same form as formulas (120.5) in Chapter 18 of Glaser's book[1], except that we express the aberration in terms of the initial conditions x_0, x_0', y_0' of the principal ray taken in the stationary Cartesian coordinate system, while Glaser gives the initial conditions in the rotating coordinate system. The relation between these different initial conditions is given by Glaser's equations (118.5). Using these to transform Glaser's initial conditions to the stationary coordinate system, we obtain the relation between our coefficients B_1, C_1 and D_1 and Glaser's B_r, C_r and D_r.

We express our gratitude to A.G.Vlasov, Yu.V.Vorob'ev and O.I.Seman for helpful discussions.

References

1. W.Glaser, Grundlagen der Elektronoptik (Fundamentals of Electron Optics), Berlin, 1952.

2. O.I.Seman, Radiotekhnika i elektronika (Radio engineering & electronics), 3, 283 (1958).

ELECTRON OPTICS OF PROBE SYSTEMS

- G.G.Dutov

At present probe systems are used in a number of different electron-optical instruments: in an x-ray microanalyzer, in a double condenser electron microscope and in an x-ray microscope. The purpose of these systems is to produce a small spot (the probe), which is a demagnified image of the electron source. Generally, the parameters of the system are chosen so that at a given accelerating potential and probe radius the current in it will be maximum. A number of authors have investigated and analyzed probe systems.[1-3]

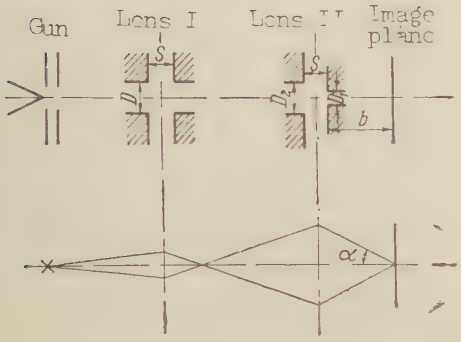

Fig.1.

The usual probe system (Fig.1) consists of an electron source (gun) and two electron lenses designed to yield demagnification. As has been shown by Castaing[1] and Solov'ev & Vertsner[3], for a given size of the probe the maximum probe current is determined by the brightness of the electron source and the spherical aberration constant of the system:

$$I_{\max} = \frac{9}{64}\pi^2 \frac{d^{8/3}}{(2C_S)^{2/3}}\beta, \qquad (1)$$

where d is the probe diameter, C_S is the spherical aberration constant of the system and β is the brightness of the electron source.

It is assumed that both the electron source and the image are located on the optical axis of the system and that astigmatism and chromatic aberration are absent. The spot is considered in the plane of best adjustment, where the radius of the circle of confusion due to spherical aberration is given by the expression

$$\Delta r_S = \frac{1}{4} C_S \alpha^3 \qquad (2)$$

where α is the aperture of the beam in the plane of the image.

Equation (1) shows that in order to enhance the current in the probe one must try to reduce the spherical aberration constant of the system. If the final image is located close to the last lens, this can be achieved by increasing the optical strength of the lenses. However, in certain types of probe systems (for example, in the above mentioned x-ray microanalyzer and double condenser electron microscope) the final image cannot be located arbitrarily close to the last lens, but must be situated at a finite, specified distance from it. Following Mulvey[2], we shall call this distance (b in Fig.1), measured from the inner surface of the last pole piece, the working distance. Accordingly, the second lens must either have a focal length of the order of the working distance of the system or must be operated with a magnification close to unity. In both cases, for precise calculation of the system with a view to obtaining the maximum probe current, one must know the variation of the spherical aberration constant in the image plane as a function of the focal length and the magnification.

Detailed analyses of the properties of the magnetic lenses as a function of the excitation parameter and the geometry of the pole pieces will be found in Refs. 4-7. But the dependence of the spherical aberration constant on the magnification has been investigated only by Archard[8] and Mulvey[2] solely for unit magnification and by Durandeau et al[9] for arbitrary magnification but only for the case of weak lenses.

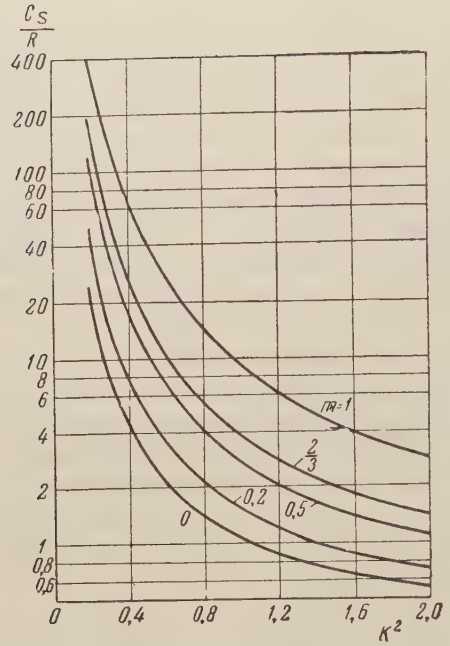

Fig.2

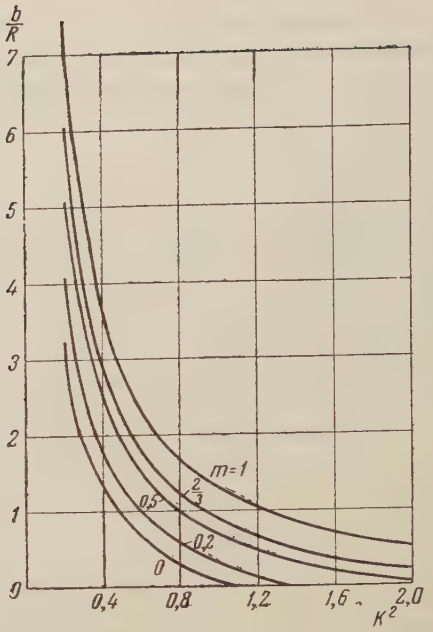

Fig.3

We carried out numerical calculation of the spherical aberration constant as a function of the excitation parameter and the magnification for two lenses with symmetrical and asymmetrical pole pieces. The geometric parameters of the lenses and the excitation parameter were taken close to those commonly encountered in practice. The results are shown in Figs.2 through 7, and can be used to judge of the magnification dependence of the spherical aberration constant and to select appropriate parameters for probe systems.

Figs.2 and 3 give the variation of the spherical aberration constant and working distance for a symmetrical magnetic lens as a function of the magnification m and the excitation parameter for which we took the quantity

$$K^2 = 8.676 \cdot 10^{-3} \frac{(NI)^2}{V}, \qquad (3)$$

where NI is the number of ampere-turns and V is the accelerating potential in volts.

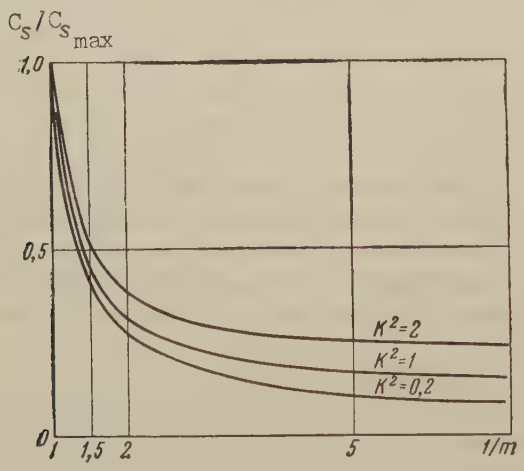

Fig.4

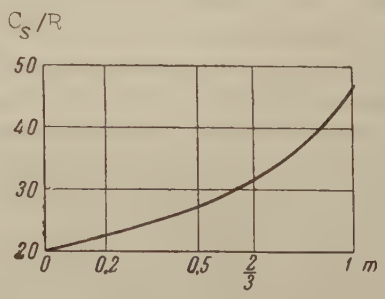

Fig.5

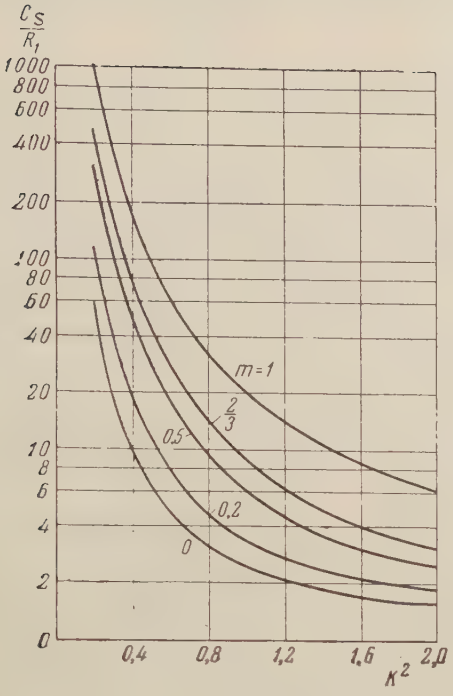

Fig.6

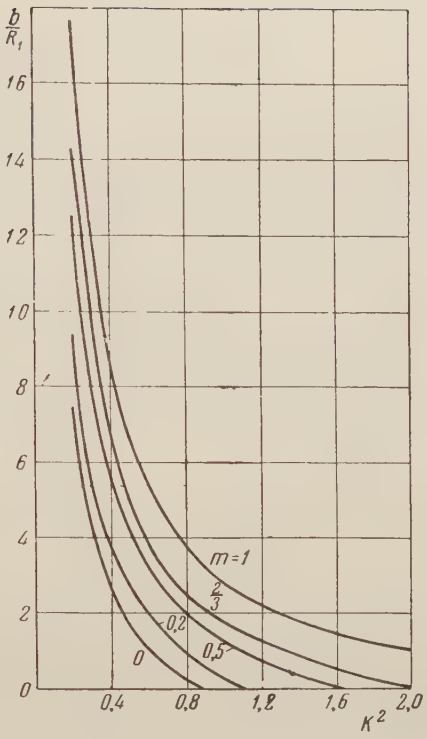

Fig.7

The geometry of the pole pieces is characterized by the ratio S/D = 0.857, where S is the width of the gap and D = = 2R is the diameter of the bore. For $m = 0$ (image in the focal point) our values of the spherical aberration constant agree with the data of Liebmann & Grad[4] and Durandeau & Fert[5].

Fig.4 shows the variation of the spherical aberration constant as a function of the magnification at a given excitation (i.e., given focal length). These curves enable one to judge of the dependence of the spherical aberration constant in the image plane on the value of the spherical aberration constant in the focal point with $m = 0$. The latter constant can readily be calculated from the data of Liebmann[4,6] and Durandeau[5,7].

Fig.5 shows how the spherical aberration constant varies with the magnification at a constant value of the working distance (in Fig.5 $b = 3R$). It will be evident from this figure that, whereas in the range of magnifications close to unity the spherical aberration constant varies appreciably, in the range of demagnifications greater than 2.5-3 the constant differs little from its minimum value in the focal point. This means that as far as increasing the probe current is concerned it is not expedient to increase the dimensions of the system with a view to obtaining a stronger demagnification by means of the last lens.

To obtain similar evaluations for an asymmetrical lens we carried out numerical calculations of the spherical aberration constant and working distance for a lens in which the bore ratio is given by $D_1/D_2 = 3/8$ with a gap to bore ratio $S/D_2 = 1$. The demagnified image is assumed to be on the side of the small bore D_1. The results of these calculations are shown in Figs.6 & 7. They indicate that with the same magnification and working distance and equal diameters of the bore on the image side, the asymmetrical lens has a smaller spherical aberration constant than the symmetrical lens. This is in agreement with the results of

Refs.6 & 7, obtained for the image in the focal point. We note that knowing the spherical aberration constant for $m<1$, one can readily determine its value for $m>1$ by means of the formula[8]:

$$C_S\left(\frac{1}{m}\right)=\frac{C_S(m)}{m^4}. \qquad (4)$$

Substantial decrease of the spherical aberration constant and, consequently, increase of the probe current is theoretically possible if instead of the second lens one makes use of a nonaxially symmetric system composed of quadrupole lenses and Scherzer[10] type correctors. As an analysis made by Grivet & Septier[11] and our calculations show, correction of the spherical aberration in a magnetic lens system of this type is feasible. In this case solution of the correction problem is facilitated by the fact that the last lens operates with a magnification close to unity, which makes it possible to use relatively weak excitation. We also note that in the case of probe systems correction of spherical aberration is an easier matter than in the case of a conventional electron microscope, inasmuch as the maximum probe current $I_{\max}\sim\frac{1}{C_S{}^{2/3}}$, whereas the resolution of an electron microscope $d\sim\sqrt[4]{C_S}$, i.e., a decrease in spherical aberration that is insignificant as regards the resolution of an electron microscope results in nearly an order of magnitude increase of the probe current. Preliminary calculations show that using quadrupole lenses and correctors one can assemble a number of different systems corrected for spherical aberration. Which of these possible designs is the best can only be determined by experiment.

References

1. R.Castaing, Ph.D.Thesis, Univ.of Paris, 1951. Publication O.N.E.R.A.No. 55.
2. T.Mulvey, J.Scient.Instrum., 36, 8 (1959).
3. A.M.Solov'ev & V.N.Vertsner, Present issue of the Bulletin, p.706.
4. G.Liebmann & E.M.Grad, Proc.Phys.Soc., B, 64, 956 (1951).
5. P.Durandeay & C.Fert, Rev.optique, 36, 5 (1957).
6. G.Liebmann, Proc.Phys.Soc., B, 68, 737 (1955).
7. J.Barthere, J.Dugas & P.Durandeau, Compt.rend., 250, 21 (1960).
8. G.Archard, Rev.Scient.Instrum., 29, 11 (1958).
9. P.Durandeau, B.Fagot & C.Fert, Compt.rend., 248, 7 (1959).
10. A.Scherzer, Optik, 2, 2 (1947); Ibid., 5, 8/9 (1949).
11. P.Grivet & A.Septier, Nuclear Instr. & Methods, 6, 2 (1960); Ibid., 6, 3 (1960).

ACHROMATIZATION OF LENSES IN MULTIPLE-LENS MAGNETIC ELECTRON MICROSCOPES

- P.A.Stoyanov

The intermediate lens in multiple-lens microscopes serves for variation of the magnification. Hence this lens generally has a large radial chromatic aberration (magnification aberration). The coefficient of this aberration varies, and over an appreciable section of the working range exceeds the coefficients of the field aberrations of the objective and projector lenses. The rotational field aberration of the intermediate lens in the range of small and medium magnifications is minor.

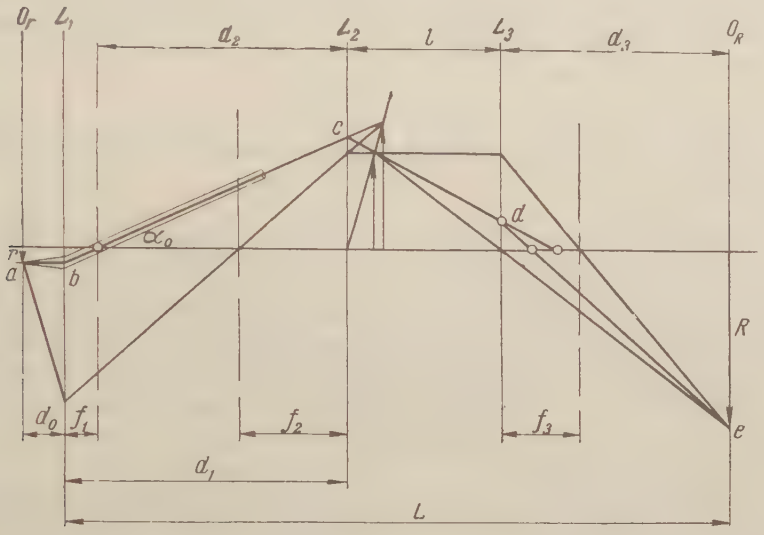

Fig.1. Trajectory of the principal ray *abcde* of the electron beam in a microscope system with two intermediate lenses L_2 and L_3; r is the coordinate of the point of departure of the beam in the object plane; R is the coordinate of the image of the same point in the object plane of the projector lens.

It will be evident from the above that among the different field aberrations of the microscope lenses, radial aberration of the intermediate lens is the most serious and should be the first to be compensated in achromatizing an electron microscope.

The problem of achromatization of an electron microscope consisting of two lenses has been thoroughly studied.[1,2] The designers of the Hitachi HU-5 electron microscope succeeded in eliminating almost completely the influence of field chromatic aberrations on the resolution.[5] True, this has been realized for only a particular operating condition of the lenses, so that good achromatization is obtained only for a constant magnification.

Achromatization of a microscope which employs an intermediate lens is really worthwhile only when in accomplishing it one still retains the possibility of using different magnifications. This last condition greatly complicates the problem.

Below we give the results of achromatization of a multiple-lens magnetic microscope, which we succeeded in realizing by means of two intermediate lenses in a way that allows of operating the microscope at different magnifications.[4] The optical system of the microscope is shown in Fig.1; here L_1, L_2 and L_3 are the principal planes of the objective lens and the two intermediate lenses, re-

spectively, (the projector lens is not shown); O_r and O_R are the object planes of the objective and projector lenses. For calculating the achromatization conditions for the double intermediate lens we considered the principal ray of an arbitrary beam *abcde*. The magnitude of the segment R in the object plane of the projector lens (Fig.1) is given by

$$R = \alpha_0 \left\{ \frac{d_2 l}{f_2} + d_3 \left(\frac{d_2}{f_2} - \frac{d_2 l}{f_2 f_3} + \frac{d_2 + l}{f_3} - 1 \right) - d_2 - l \right\}. \quad (1)$$

The meaning of the symbols in (1) is made clear in Fig.1.

The net chromatic aberration of the two intermediate lenses will be zero if with minor variations in the electron velocity the length of the segment R remains constant. Consequently, there must be fulfilled the condition

$$dR = 0. \quad (2)$$

Inserting (1) into (2) and solving for the focal length of the second intermediate lens yields

$$f_3 = \frac{2d_3 l}{d_3 + l} - \frac{d_3}{d_3 + l} \frac{d_2 + l}{d_2} f_2. \quad (3)$$

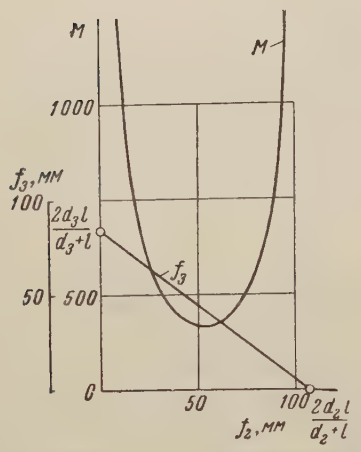

Fig.2. Variation of the focal length f_3 of the second intermediate lens as a function of the focal length f_2 of the first intermediate lens with compensation of the chromatic magnification aberration of the intermediate lenses. M is the corresponding magnification in the object plane of the projector lens.

Thus the condition of achromatization of the double intermediate lens reduces to linear dependence of the focal length of the two-component intermediate lenses. Condition (3) is presented by the straight line in Fig.2. The intercept on the horizontal axis ($f_3 = 0$) gives the segment $\frac{2d_2 l}{d_2 + l}$; the intercept on the vertical axis ($f_2 = 0$) gives $\frac{2d_3 l}{d_3 + l}$.

In varying the magnification of the microscope one should simultaneously change the focal length of both lenses so that Eq.(3) will hold.

The effect of operation of the intermediate lenses can be followed in Fig.3. Here F_1F_1 is the back focal plane of the objective lens, F_2F_2 is the front focal plane of the first intermediate lens, and F_3F_3 is the back focal plane of the second intermediate lens. The trajectory of the principal ray of the electron beam leaving the point A in the object is given by ABCDE. If as a result of instability (fluctuation) of the high voltage there occurs a change in the electron velocity, the focal lengths of the intermediate lenses will change (for example decrease) by Δf_2 and Δf_3 and the principal ray will follow the trajectory indicated by the dashed line. As will be evident from the figure, as a result of decrease of the focal length of the first intermediate lens L_2 the principal ray will be deflected further from the axis and, consequently, will intersect the plane of the second intermediate lens L_3 at the point D_1. Inasmuch as point D_1 is located closer to the lens axis, the ray will be refracted in the lens L_3 through a smaller angle than the preceding case, despite the fact that the refracting power of this lens has increased ($\Delta f_3 < 0$). Hence the

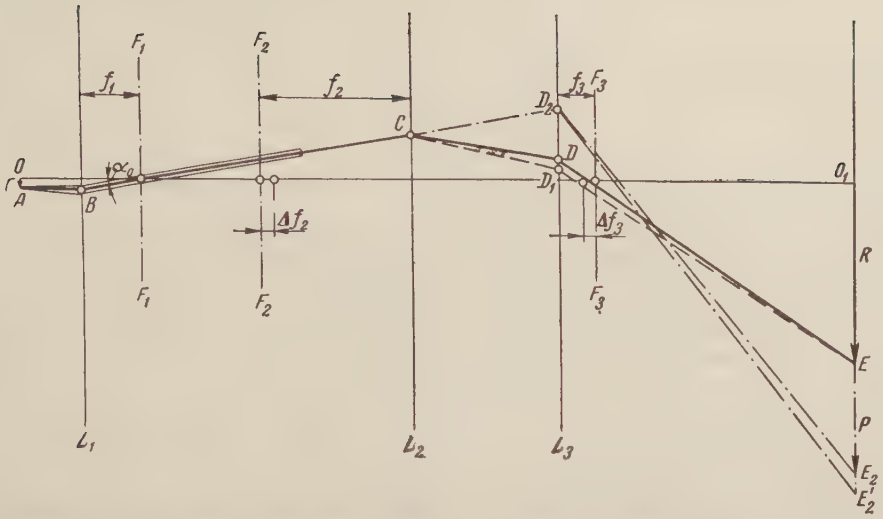

Fig.3. Trajectory of the principal ray: 1 - with operation of the two intermediate lenses (ABCDE); fluctuation of the accelerating potential alters the trajectory so that the principal ray $ABCD_1E$ still intersects the plane OP at the point E; 2 - with operation of only one (the second) intermediate lens the ray trajectory is $ABCD_2E_2$; now fluctuation of the accelerating potential alters the ray trajectory so that the principal ray intersects the plane OP at the point E_2'.

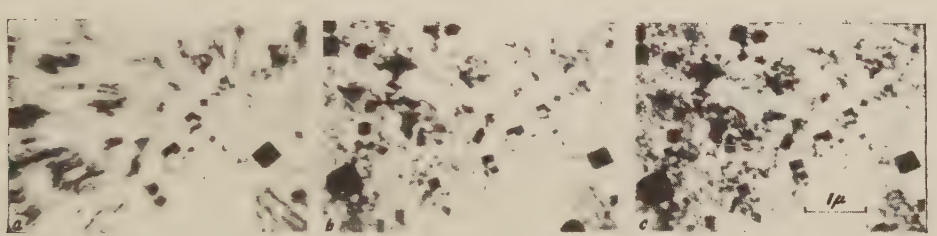

Fig.4. Micrographs of MGO crystals obtained under the following conditions: a - alternating component superimposed on the high voltage; only one intermediate lens operating; b - alternating component superimposed on the high voltage but both lenses operating in the achromatization regime; c - no ac component superimposed on the high voltage.

ray will still intersect the object plane of the projector lens at the same point E (no aberration).

For comparison, in Fig.3 we also show the path $ABCD_2E_2$ of the principal ray when only one (the second) intermediate lens is operating. In this case the ray intersects the object plane of the projector lens at the point E_2. Now in case of fluctuation and change in the focal length of this lens the principal ray will intersect the object plane of the projector lens at the point E_2', i.e., there will appear chromatic aberration of the magnification, represented by the segment E_2E_2'.

Let us see within what range one can vary the magnification without loss of achromatization. The magnification of the object r by the three lenses L_1, L_2 and L_3 in the object plane O_R (Fig.1) of the projector lens is given by

$$M = \frac{1}{d_0}\left\{\frac{d_1(d_3+l)}{f_2} + \frac{d_3(d_1+l)}{f_3} - (d_1+l+d_3) - \frac{d_1 l d_3}{f_2 f_3}\right\}. \qquad (4)$$

The following approximate equalities obtain for the electron microscope: $d_1 \approx d_2$ and $f_1 \approx d_0$ (f_1 is the focal length of the objective lens). These quasi-equalities make it possible to simplify (4) by means of Eq.(3) and yield the following final formula for the magnification

$$M = \frac{d_1 l d_3}{f_1 f_2 f_3} - \frac{L}{f_1}; \qquad (5)$$

here $L = d_1 + l + d_3$.

The curve in Fig.2 shows the variation of the magnification as a function of the focal length of the intermediate lens for the microscope used in the achromatization experiments. This microscope comprised an objective lens, two intermediate lenses and one projector lens. The field aberrations of the objective and projector lenses were mutually compensated. The excitation currents in the intermediate lens coils were varied simultaneously; their value was chosen so that the radial chromatic aberration of both lenses would be nil. The absence of radial chromatic aberration was checked by superimposing on the regulated high voltage an alternating component with a frequency of 50 cps and an amplitude equal to about 1.5% the value of the dc voltage. The effect of radial chromatic aberration in the absence and in the presence of achromatization is illustrated by the micrographs of Figs.4,a and b, respectively. Fig.4,c is a micrograph obtained in the absence of an alternating component in the high voltage circuit. Satisfactory achromatization was realized with different magnifications.

References

1. N.Morito, J.Appl.Phys., 25, 8, 986 (1954).
2. S.Katagiri, J.Electromicroscopy, 1, No.1, 13 (1953).
3. S.Katagiri, Rev.Scient.Instrum., 26, No.9, 870 (1955).
4. P.A.Stoyanov, Inventor's Certificate No.122822, 5 February 1959.

DESIGN OF MAGNETS FOR THE LENSES OF MAGNETOSTATIC ELECTRON MICROSCOPES

- G.V.Der-Shvarts & V.P.Rachkov

Design of magnets for the lenses of magnetostatic electron microscopes is predicated on completion of the preliminary purely optical calculation. To this end one can use the work of Durandeau[1]. Knowing the accelerating potential and the magnification of the lens, one can relate the design parameters of the pole piece with the magnetomotive force. Thus the magnetomotive force can be determined from the strength of the magnetic field in the gap. The magnetomotive force is one of the basic parameters of the magnet. The magnet should be made of a material such that it will operate under conditions of maximum specific internal energy of the material. Otherwise the magnet becomes unnecessarily bulky and heavy.

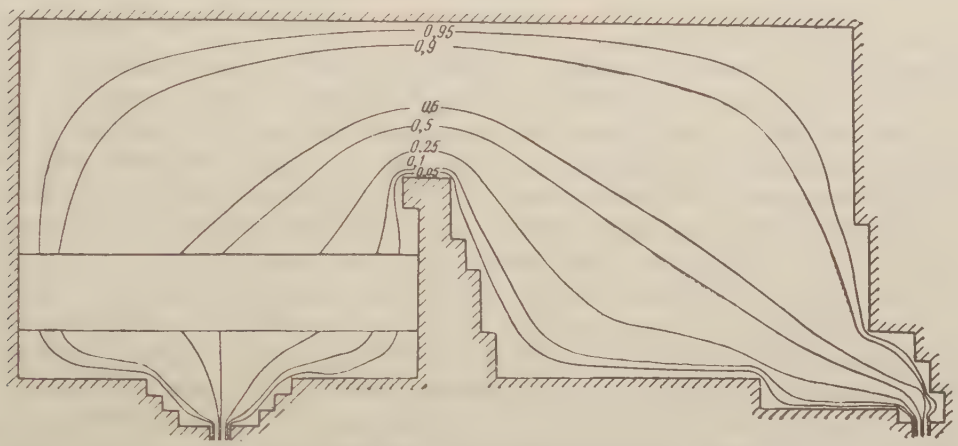

Fig.1. Calculation of magnetic flux penetrating the neutral cross section of an axial magnet.

Another basic parameter is the magnetic flux penetrating the central cross section of the magnet. This flux cannot be calculated analytically, inasmuch as the flux through the magnetic circuit, which is readily calculated, comprises only a small fraction of the total flux. Thus closure of the main part of the flux occurs not in the ferromagnetic part of the magnetic circuit but in the air. This stray flux can rapidly be determined by means of an electrointegrator.

We used an electrointegrator, developed by us[2,3], for calculating focusing systems with permanent magnets in which the magnet simultaneously supplies two lenses (in parallel) and determined the most expedient manner of arranging the magnets in the lens housing and the best shape of the magnet. Design calculations of the magnet dimensions was based on the assumption that the magnet is magnetized uniformly. This assumption, in its rigorous sense, is questionable in view of the fact that the shape of an actual magnet is far from spheroidal and the magnet itself is mounted inside a space bounded by ferromagnetic walls and in the vicinity of the ferromagnetic fittings (yoke) comprised in the focusing system of the microscope. However, the entire calculation is based on the limiting demagnetization curve, which is recorded for a uniformly magnetized magnet. Unfortunately, there are no other standard characteristics for permanent magnets.

Assuming the magnet to be uniformly magnetized, we calculated the magnetic flux through the internal and external walls of the ferromagnetic lens yoke (Fig. 1). These fluxes are not equal. If the magnet were absent as a ferromagnetic

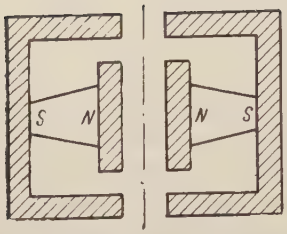

Fig.2. Radial arrangement of magnets in magnetostatic lens.

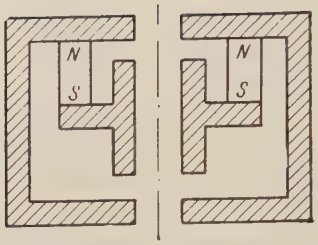

Fig.3. Axial arrangement of magnet in magnetostatic lens.

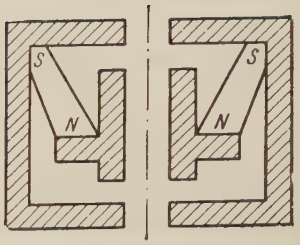

Fig.4. Inclined arrangemen of magnet in magnetostatic lens.

body and there were present only its effect in the form of a magnetic potential difference applied to the oppositely polarized yokes, the magnetic fluxes through the internal and external yoke walls would be rigorously equal. The inequality of these fluxes is due to the fact that closure through the magnet, the yoke wall and the air gap obtains only for a certain, essentially useless magnetic flux. This flux only increases the weight and volume of the magnet. We have called thi flux the "exchange flux" and have introduced the "exchange coefficient", which is equal to the ratio of twice the difference to the sum of the inside and outside fluxes.

We have been able to show that the smallest exchange coefficient (~15%) corresponds to radial arrangement of the magnet (Fig.2). In the case of axial arrangement of the magnet (Fig.3) the exchange coefficient equals ~35%. In the cas of inclined arrangement of the magnet (Fig.4) the exchange coefficient may be as large as 60%. It follows the conical magnet design is not expedient.

If one determines the entire flux that emerges from the outer surface of the yoke and housing in relative units, one can also determine its true value, inasmuch as the flux penetrating the ends of the pole pieces is known from the optica calculation. Then one can also determine the principal dimensions of the permanent magnet.

The exchange coefficient is not the only criterion determining the choice of magnet shape. This choice also depends on the characteristics of the material of which the magnet is made. In connection with this it is appropriate to say a few words regarding the magnetic materials of which magnets are prepared. Among the domestic materials available for fabrication of magnets the most suitable for microscope lens magnets are ANKO-4 alloys and compressed dust core material MBA (magnet, barium, anisotropic). The MBA material is best used for radial magnets, inasmuch as this material has a characteristic demagnetization curve and a high field strength with a relatively low induction, corresponding to the optimum oper ting conditions of the magnet (Fig.5). In view of this the magnet has a small ra dial length, but a large cross section. In designing magnetic microscopes it is always expedient to use magnets that will not greatly increase the radial size of the lens.

Unfortunately, there are many technological difficulties that have to be ove come before MBA material can be used in practice for fabricating radial magnets for electron microscopes. One of the greatest difficulties is that such magnets should be magnetized in the direction of compression directly in the die. Yet it is at present virtually impossible to produce a radially directed field in a compacting die.

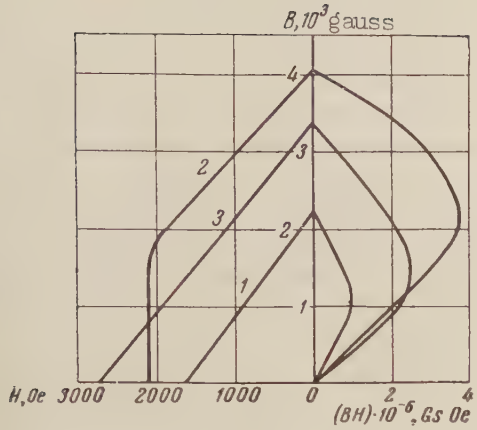

Fig.5

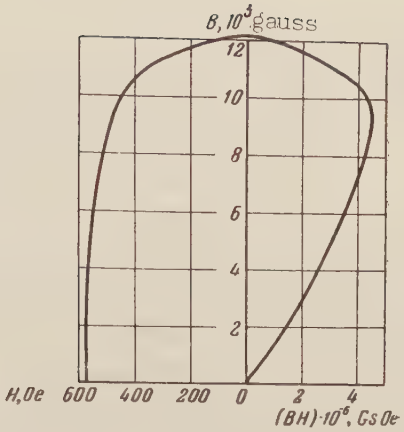

Fig.6

Fig.5. Demagnetization and magnetic energy curves: 1) MBA material, 2) MBA in direction of compression, 3) MBA-1 material. MBA parameters: B_r = 3500-4000 gauss; H_c = 1800-2600 oersted.

Fig.6. Demagnetization and magnetic energy curve for ANKO-4 alloy.

ANKO-4 alloy (Fig.6) is suitable for fabrication of axial magnets, inasmuch as its induction corresponding to $(BH)_{max}$ is very high (over 10 kilogauss), while the field intensity under these conditions is relatively low (about 500 oersted). For adjustable magnetic lenses it is desirable to have a material with a very steep and stable demagnetization curve (partial cycles). No material now available meets this requirement. Thus, for example, the limiting change in magnetic flux in adjustment of a magnet of ANKO-4 alloy does not exceed 20%.

Adjustment of the optical strength is realized in all magnetostatic microscopes by one of the following three methods: by means of an additional winding through which a relatively weak current is sent[4], by means of mechanical variation of the gap or thickness of the magnetic components[5], or by means of redistribution of the magnetic flux between two lenses or the pole pieces. The first two methods can be used only for relatively minor variation of the optical strength (for example, for final focusing of the objective). The third method is usually used for regulating the magnification of projector, condenser and intermediate lenses[6,7]. In connection with adjustment of magnetostatic microscopes two-slit pole pieces have proved to be of great value. In regulating the optical strength, the magnetic fluxes through each of the slits are varied so that when one increases, the other decreases. This makes it possible to vary the optical strength of the system in a wide range.

The optical properties of two-slit lenses have not yet been adequately studied. We are now investigating such lenses by means of an electronic model (MN-7) with integrating, inverting, multiplying and nonlinear units. In our opinion, such models can be adopted for calculating trajectories and determining aberration. Electronic models can accurately integrate trajectory equations and equations with a term on the right-hand side. We checked these possibilities by integrating the differential trajectory equation for the case of a Glaser magnetic lens (bell shaped field). The model computing arrangement is diagramed in Fig.7. The results of our preliminary tests were highly encouraging. Thus the maximum divergence between the trajectories determined by means of the model and the trajectories calculated analytically did not exceed 4%. Differential equations with

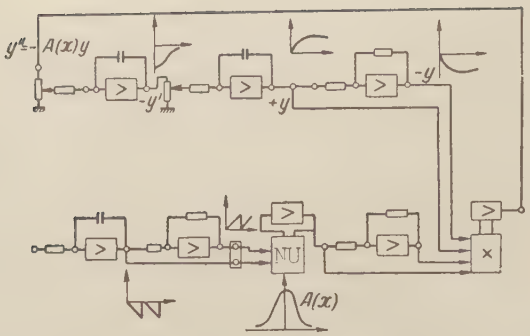

Fig.7. Block diagram of computing elements for solving the equation $y + A(x)y = 0$. NU - nonlinearity unit, X - multiplication unit.

a right-hand side can be integrated with the same accuracy. Work in this direction is continuing, but we can already assert that two-slit lenses are of great interest and potential value, inasmuch as they are free of chromatic rotational variation and for them chromatic variation of the magnification equals zero for relatively low values of the optical lens strength parameter.

References

1. P.Durandeau, Thesis, Toulouse, 1957.

2. G.V.Der-Shvarts, Radiotekhnika i elektronika (Radio Engineering & Electronics), 2, 262 (1958).

3. G.V.Der-Shvarts & K.A.Netrebenko, Izv.AN SSSR, Ser.fiz., 23, 506 (1959). (Trans.Bulletin, 23, 488.)

4. H.Kimura, Optik, 16, No.1, 50 (1957).

5. K.Müller, Z.wiss.Mikrosk., 63, No.5, 303 (1957).

6. G.Langner, Optik, 12, No.12, 554 (1955).

7. H.Kimura, Proceedings of the First Regional Conf.in Asia and Oceania, p.108,Tokyo, 1956.

OPTICS OF THE ÉM-5 AND ÉM-7 ELECTRON MICROSCOPES

- V.N.Vertsner, Yu.M.Vorona, Yu.V.Vorob'ev, G.A.Bogdanovskii & Yu.V.Chentsov

The ÉM-5 microscope has been in batch production for a number of years; our industry is now preparing to put into production the ÉM-7. The electron optical system of these instruments has a number of distinctive features.

The illuminating system of the ÉM-5 and ÉM-7 microscopes utilizes a short focus three-electrode gun and one condenser lens. The crossover in the vicinity of the cathode has a half-width of the order of 20-25 μ. The position of the condenser lens is chosen so that it will image the crossover in the object plane of the objective lens with a demagnification of 1:3. Hence the half-width of the focused electron spot on the object is 6-8 μ. This is essentially the diameter of the illuminated section of the object in a Class I microscope with a double condenser, for example, the Japanese JEM-5Y electron microscope. The effective opening of the illuminator is determined mainly by the condenser aperture. With the condenser focused and an aperture 0.07 mm in diameter, the illuminating system opening equals $5 \cdot 10^{-7}$ rad, i.e., the optimum aperture. This illuminating system is simple in design and easy to adjust.

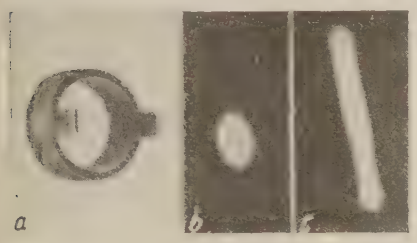

Fig.1

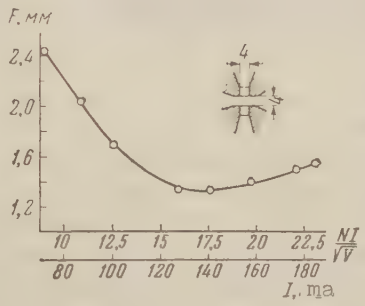

Fig.2

Often the condenser lens in electron microscopes has appreciable astigmatism: the astigmatic focal length difference in some cases attains 500 μ. The astigmatism of the illuminator leads to increase in the size of the irradiated area and decrease in the intensity of the beam. In designing the microscope, for correcting the astigmatism of the illuminating system we employed a simple nonadjustable stigmator (compensator). The stigmator (Fig. 1,a) is a brass cylinder with two symmetrical nickel plated lugs. By varying the position of the stigmator in the condenser lens (screwing it in or out) one can regulate its "strength". The direction of the introduced astigmatism is determined by the aximuthal orientation of the stigmator lugs. Photographs of the beam spot in the object plane of the objective lens with the stigmator (b) and without it (c) are reproduced in Fig.1.

The image forming system consists of an objective, an intermediate and a projector lens. The objective lens employs symmetrical pole pieces of the sleeve type. It has been shown by Glaser[1] and a number of other investigators that increase of the lens excitation, up to a certain limit, leads to noticeable decrease of both spherical and chromatic aberration. Recently, Morito[2] showed experimentally that increase of the excitation also leads to reduction of the astigmatic focal length difference. Tests showed that it was expedient to increase the excitation in the objective lens of the ÉM-5 and ÉM-7 microscopes to 3600 ampere-turns, which corresponds to IN/ V = 16. This was realized in the ÉM-5 series microscopes produced since 1960. This modification resulted in reduction of the residual astigmatism, increase in the image contrast and enhancement of the focal depth owing to transition to a flatter section of the focal length vs excitation curve (Fig.2). This facilitates focusing and insures better quality micrographs. The residual astigmatism of the objective lens is corrected by an electromagnetic stigmator developed by the writers[3]. The intermediate lens of the ÉM-5 and ÉM-7 microscopes

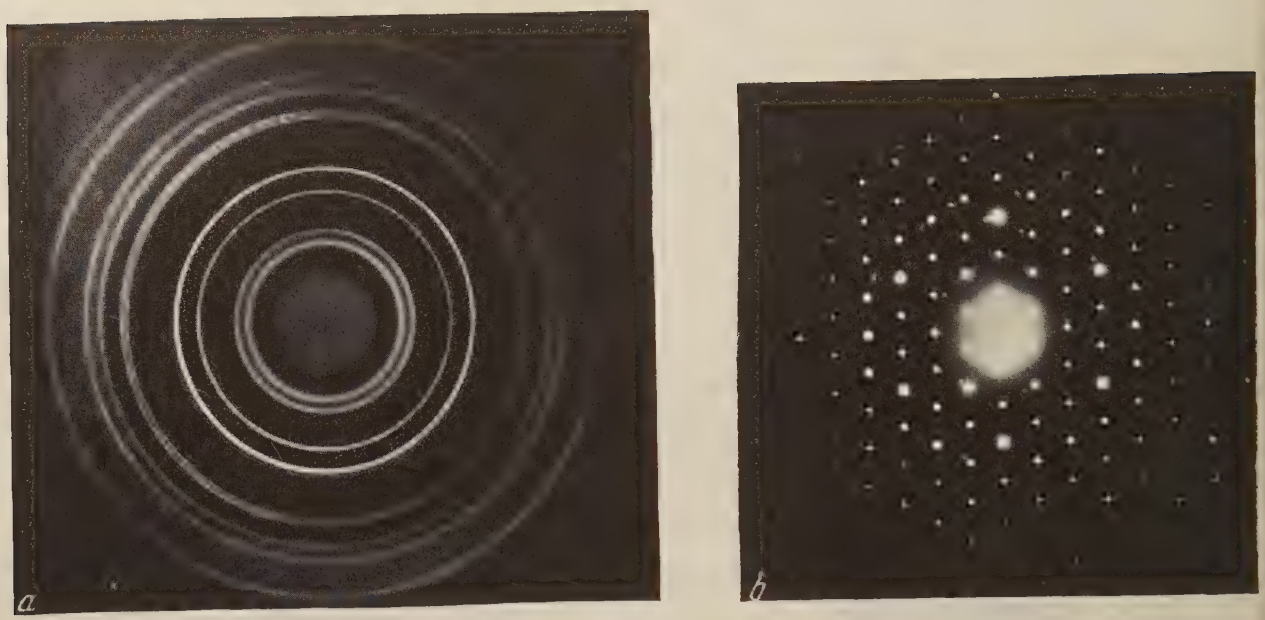

Fig.3

has centerable pole pieces.

Astigmatism of the intermediate lens generally reduces the quality of electron diffraction patterns; hence in some high resolution microscopes the intermediate lenses are corrected by a nonadjustable stigmator. For example, in the Siemens Elmikroskope I such a stigmator is used to reduce the astigmatism to a value corresponding to $\Delta I/I = 3 \cdot 10^{-3}$, where ΔI is the astigmatic current difference. For similar correction, Stoyanov[4] used an adjustable electromagnetic stigmator. However, with careful fabrication of the intermediate lens high quality microdiffraction can be realized without correction, as had been done, for example, in the JEM-5Y electron microscope. In the ÉM-7 microscope the astigmatism of the intermediate lens is corrected by a stigmator similar to that employed in the condenser. This stigmator reduces the initial astigmatism by a factor of 4, which is sufficient for obtaining high quality electron diffraction patterns. Microdiffraction patterns from gold (a) and coalinite (b) obtained using this stigmator are reproduced in Fig.3. In the case of the gold the object was a replica from a 600 lines per mm diffraction grating, shaded with gold.

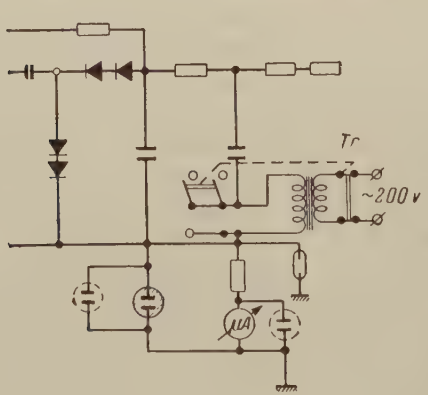

Fig.4

The projector and objective lenses of the ÉM- and ÉM-7 microscopes are designed as an integral unit. An electromagnetic deflecting system is used for adjustment of the objective lenses. The electromagnetic adjustment is realized by means of two pairs of mutually perpendicular coils located under the objective pole piece. As laboratory tests showed, by careful, high quality fabrication of the pole pieces one can dispense with additional adjustment of the objective lens and use the deflecting system for adjusting the intermediate lens. The rated resolution can be attained without recourse to mechanical adjustment of the pole pieces of the intermediate lens.

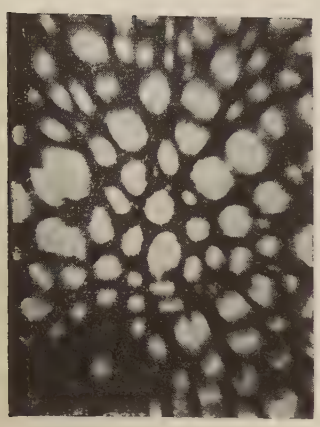

Fig.5

Fig.6

In order to facilitate adjustment of the illuminating system relative to the objective lens, the power supply system of the ÉM-7 has provision for superposing an alternating component on the accelerating potential. The ac voltage supply circuit for the ÉM-5 microscope is diagramed in Fig.4 (the voltage in the secondary of the transformer Tr is ~2 kv). The illuminating system is aligned with the objective at working magnification. The voltage center, i.e., the central point of the image which remains stationary with variation of the accelerating potential (Fig.5), is brought to the center of the screen by tilting the illuminating system. In this case the apex of the caustic or the point without coma virtually coincides with the center of the screen. The position of the apex of the caustic is checked by observing the symmetry of the diffraction fringe about an opening in a carbon film with underfocusing (Fig.6). As the criterion for the quality of adjustment one should take the distance (referred to the object) between the voltage and magnetic centers (the magnetic center is the point of the image that remains stationary with variation of the current in the objective lens coils). For qualitative evaluation of the adjustment the voltage center is first aligned with the center of the screen. In this case, as was noted earlier, the apex of the caustic or the point without coma virtually coincides with the center of the screen. The apex of the caustic of the intermediate lens is then aligned with the center of the screen by means of the deflecting coils.

Usually as a result of change of current in the objective the image is defocused and shifted. Inasmuch as for the chosen excitation the coefficients of the field chromatic aberrations of the magnification (C_{m0}) and rotation ($C_{\theta 0}$) of the objective lens are known, one can determine the distance R_I between the center of the screen and the magnetic center even at large magnifications. According to Vorob'ev[5], Δr_I, the displacement of the point of the image, referred to the object, corresponding to a relative change of the current in the objective lens $\Delta I/I$, equals

$$2\sqrt{C_{m0}^2 + C_{\theta 0}^2} R_I \frac{\Delta I}{I}.$$

Fig.6, which represents two photographs made on the same plate, shows the displacement Δr_I of an opening in a carbon film, resulting from 15 ma increase of the current in the objective. Calculations by means of the above formula give $R_I = 3$ μ.

For the ÉM-5 microscope with the intermediate lens operating in the demagnifying regime (the least advantageous condition as regards chromatic distortion) calculations yield the following tolerances as regards adjustment. So that impairment of the resolution produced by each of the three kinds of aberration separately (coma, and field chromatic errors owing to instability of the accelerating potential and also of the current in the objective lens) will not exceed 2 Å, the distance (referred to the object) from the center of the screen to the voltage center and the point without coma must be less than 2 μ, and the distance to the magnetic center must be less than 3 μ.

By careful alignment and adjustment of the ÉM-5 microscope one can obtain a resolution of the order of 15 Å.

References

1. W.Glaser, Grundlagen der Elektronoptik (Fundamentals of Electron Optics) Berlin, 1952.
2. N.Morito, J.Electronmicroscopy, 7, 4 (1959).
3. V.N.Vertsner and others, Izv.AN SSSR, Ser.fiz., 23, 485 (1959). (Trans. Bulletin, 23, 468.)
4. P.A.Stoyanov, Ibid., 23, 467 (1959). (Trans.Bulletin, 23, 449.)
5. Yu.V.Vorob'ev, Radiotekhnika i elektronika, 6, No.8 (1961). (Trans.Radio Engineering & Electronics.)

* * * * * * *

MIRROR ELECTRON MICROSCOPE FOR STUDYING THE STRUCTURE OF SURFACES

- G.V.Spivak, I.A.Pryamkova, D.V.Fetisov, A.N.Kabanov, L.V.Lazareva & A.I.Shilin

In the present report we describe an all metal mirror electron microscope t represents an advance in the development of instruments of this type. The micro scope design is noteworthy in that the high resolution of the instrument measure up to theoretical expectations.

The mirror electron microscope belongs in the class of instruments that per mit direct observation of the structure of specimens. Its chief operating chara teristics are the following: 1) the specimen is not bombarded by charged particl 2) the electron-optical system has a high sensitivity to surface microfields ina much as these fields interact with slow electrons, and 3) in the case of electri microfields the picture contrast is considerably enhanced as compared with emiss microscopes.

In the mirror microscope, the electrons, after being focused and accelerate by the electron gun, move along the system's axis of symmetry and then are furth retarded by the counter electric field of the "reflecting" electrode. Owing to the fact that the electrons are slowed down and stopped near this electrode and then begin to move in the opposite direction, the beam is extremely sensitive to microfields on the reflecting electrode.

Incident to reflection the electron beam is scattered, and then focused by the immersion objective and successive lenses of the instrument to yield an imag of the microfields. In view of this mechanism, one can expect a resolution of t order of 80-100 Å.[1] Image contrast is due to redistribution in density of the r flected electron beam.

An electric surface microfield gives rise to local distortion of the equipo tential planes. The tangential component of this field[2] broadens or narrows the electron beam. Contrast is higher than in an emission microscope by virtue of t fact that the tangential component acts on the beam twice (during forward and re verse motion).

A magnetic microfield (observed in a mirror for the first time* by Spivak e al[4]) interacts only through its normal component with the radial component of th electron velocity vector: its radial component produces no effect, owing to inte action with the normal component of the electron velocity vector. Inasmuch as t

---

*See also Ref.3.

latter component changes polarity incident to reflection, the forward and reverse effects cancel each other.[5]

The present instrument finds specific application in investigation of the surface of bulk specimens having some sort of electric or magnetic topography.

The instruments described in Hottenroth's[6] and Orthuber's[7] first works were constructed of glass and had low magnifications (20-30 X), yet they served to demonstrate the possibility of imaging the microgeometry and electric field distribution on the surface of semiconductors. The returning beam was separated from the primary beam and deflected onto a fluorescent screen by a magnetic field. The magnetic microstructure of the ferromagnetic domains of cobalt[4,8], and then of silicon iron and meteoric iron[3], was brought out with magnifications of 400 to 800 X. Two years later (1957) Mayer[5] repeated these experiments and extended visual observation of magnetic microstructures to ferrites, magnetic tape and other materials[9], using magnifications in the range from 50 to 1200 X. Subsequently Spivak et al[10] demonstrated the possibility of bringing out the electric domain structure of ferroelectrics, e.g., barium titanate, with a magnification of 1000 X. At the International Semiconductor Conference (Czechoslovakia, August 1960), E.Ingras reported on his observation of a germanium p-n junction by means of an electron mirror. At the Physical Section of the Third Conference on Electron Microscopy, Kormilitsyn et al[11] reported on "photographing" such junctions in silicon and germanium. Spivak et al[12] have published data on the observation of "patch fields" on the emitters of electron multipliers, and examined in detail the mechanism of contrast formation in electron mirrors.[2]

The design of mirror microscopes is being gradually perfected. Whereas the first models were of glass[4,6,7], subsequent models have been of metallic design. The authors of Ref.3 used an EM-4 electron diffraction instrument to produce a narrow electron beam. Mayer[5,9] designed a relatively simple instrument for observing ferrites and magnetic tapes with one stage of imaging by an immersion objective. Heydenreich[13] recently published a description of a metal instrument with voltages up to 20 kv and one stage of magnification; the screen is set at an angle of 45° relative to the instrument axis, which not only does not hamper observation (owing to the great depth of definition of the mirror) but even improves picture quality incident to external photography.

At present a number of laboratories are engaged in developing mirror electron microscopes and extending their range of application.

Design of the Mirror Electron Microscope

Our electron microscope comprises the following components: an electron gun, a condenser lens, a camera, an intermediate lens, an electron mirror, a specimen stage and displacement mechanism, a vacuum system and a power supply.

The metal construction of the mirror provides for the necessary adjustments of the optical system without disturbing the vacuum. For purposes of increasing the relative aperture and, partially, the resolution, the design of the electron mirror provides for "magnetic diaphragming" of electrons in the vicinity of the reflecting electrode[14]. The field strength on the investigated surface can be controlled in a wide range. The specimen in its holder can be displaced along three coordinate axes relative to the system of electrodes forming the electron mirror, which affords the possibility of observing individual sections as well as the microfields at different elevations above the surface.

The design of the instrument includes a supplementary electrostatic lens for the further magnification of the image yielded by the first stage of the mirror. To permit observation of the surface structure of emitters, we provided for a

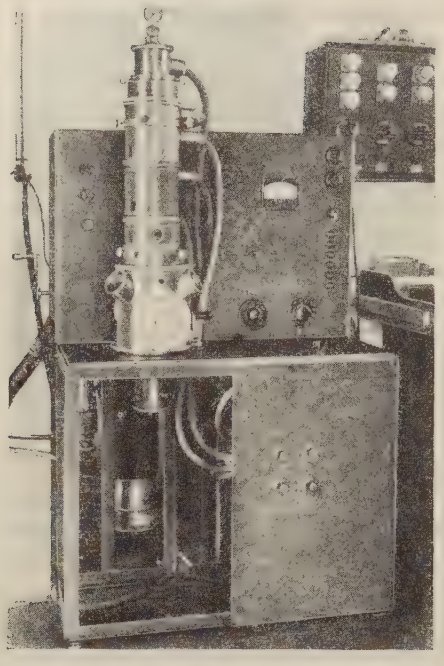

Fig.1. General view of the mirror electron microscope.

vacuum of the order 10^{-6} mm Hg. The design also provides for heating the specimen and connecting to thermocouples monitoring its temperature.

Power is supplied by a high-voltage (45 50 kv) rectifier and a cathode heater supply The electric circuit has two voltage divider for regulating the electrode potentials of the gun, the electron mirror and the intermediate lens: one an oil divider with contin ous voltage control, which serves to set the range and permissible jumps in potential, an the other of conventional design, which serv for stepless control of the voltage within a given range.

A photograph of the instrument is repro duced in Fig.1. The inidividual components are arranged as follows. The electron gun i located at the bottom of the assembly. Its design is based on a conical control electro which insures a high beam intensity. For pu poses of alignment the gun has provision for tilting and for lateral displacement of the entire system. The beam is tilted by displa ing the conical electrode; this tilting arrangement is basically similar to that employed in the illuminating system of the MES 40 electrostatic electron microscope[15].

The illuminating aperture of the gun is mounted on a movable stage and can adjusted by cranks. It can also be withdrawn from the beam for adjustment of th mirror. Horizontal displacement of the entire gun insures displacement of the electron beam parallel to the optical axis. The gun housing is attached to the volumn by a threaded flange.

In adjusting the gun for this instrument, we found that a supplementary con denser lens in the illuminating system is very useful, inasmuch as the electron beam, on its forward and reverse paths, goes through a considerable number of apertures with the result that its intensity is reduced.

An outline of the instrument column is shown in Fig.2. The camera differs markedly from those generally employed in electron microscopes owing to the fact that the electron beam must pass through it (since gun and object are located on different sides of the camera). The camera magazine is a metal box with three compartments for cassettes; the electrons pass through an opening in the cassett Two 4.5 X 6 cm photographic plates are loaded into each cassette. Exposure is e fected by raising the screen. The magazine is positioned in the camera by means of special shutter. The cassettes are inserted into the right-hand compartment through a vacuum lock; they are lifted by a conical spring and successively intr duced into the middle compartment by a special mechanism; after exposure they ar ejected into the left-hand compartment. The cassettes are moved by an external crank, which turns the camera shaft. Two forks fastened to the shaft displace the lid of the magazine, and only the top cassette is picked up for transfer.

Two windows are provided for observation of the image on the fluorescent screen. The camera forms the base of the electron mirror, and the tubing to the vacuum system is connected to it. The condenser and electron gun are mounted on

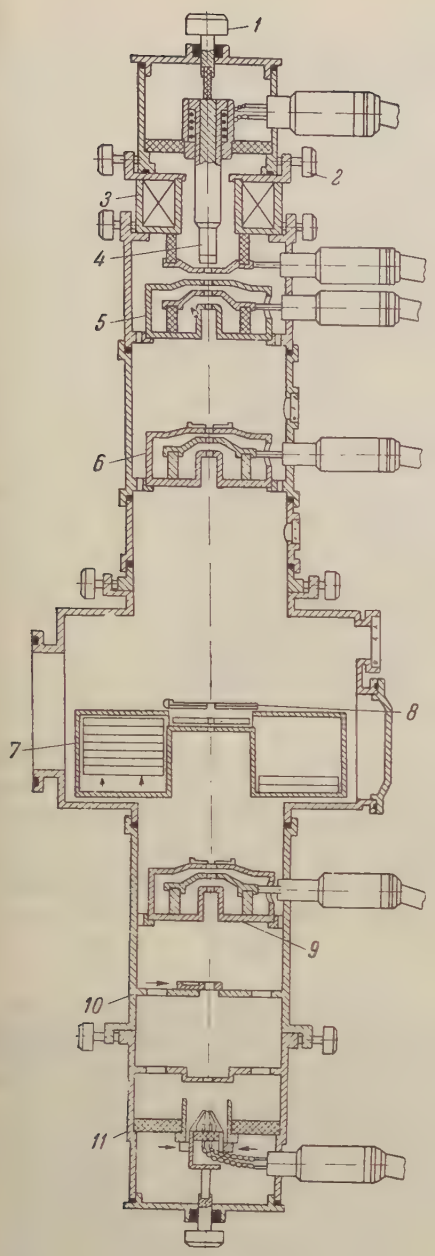

Fig.2

←Fig.2. Diagram of the microscope: 1) mechanism for displacing the object in the vertical plane, 2) mechanism for displacing the object in the horizontal plane, 3) magnetization and "magnetic diaphragming" coil, 4) object-mirror cathode, 5) five-electrode immersion objective, 6) lens for second stage of magnification, 7) camera with opening for beam, 8) fluorescent screen for visual observation, 9) condenser, 11) gun illuminating object (4).

the base of the camera.

The design of the camera is shown in Fig.3. The intermediate lens is an electrostatic lens. The fluorescent screen is located at the upper part of the lens. The design of the instrument column provides for varying the position of the intermediate lens, which is mounted in a sectioned cylindrical tube. The tube sections are fashioned so that they can be interchanged, and one of them can be inverted in assembling the instrument. In this way, by chainging the places of the tube sections, reversing or omitting a section entirely, the intermediate lens can be set in any one of six different positions, which substantially increases the experimental possibilities.

The electron mirror itself is designed as follows. The specimen is mounted on a steel rod. The reflected electrons can be diaphragmed by an externally controlled magnetic field, which can also serve to magnetize the specimen. The first mirror electrode is mounted on an insulator in front of the specimen, and the high voltage from the divider is applied to this electrode. The electrostatic single lens is installed under the electrode. By means of a standard lead a control voltage is brought to the middle electrode. Together with the specimen this system forms a five-electrode electron mirror. This single lens, constituting a part of the mirror, is characterized by the fact that its upper electrode has the form of a plate, and the middle and lower electrodes are brought up close to it. This electrode arrangement provides for positioning the lens close to the first electrode of the mirror. All the electrodes are replaceable, which facilitates maintenance. Inasmuch as the electron beam passes through the opening in the cassette, insertion of a cassette might disturb the adjustment. To provide for easy readjustment the upper part of the mirror column can be displaced in the horizontal plane by special screws.

As noted above, the instrument incorporates a specimen displacement mechanism. The specimen is displaced horizontally by moving the entire specimen chamber. In addition, the metal rod - the object holder - is fastened to a sliding cylinder riding in an insulator and can be displaced along the instrument's optical axis by means of a special crank. A spring insures return movement. Specimen replace-

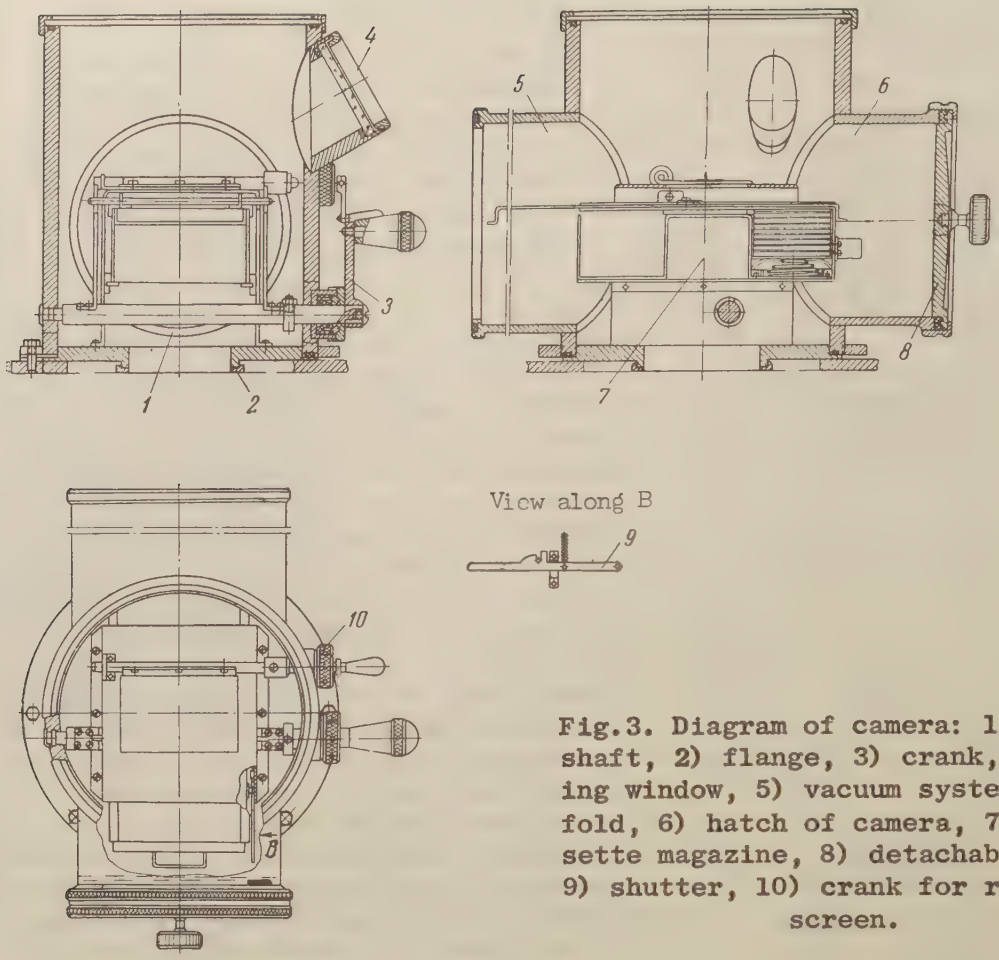

Fig.3. Diagram of camera: 1) crank shaft, 2) flange, 3) crank, 4) viewing window, 5) vacuum system manifold, 6) hatch of camera, 7) cassette magazine, 8) detachable lid, 9) shutter, 10) crank for raising screen.

ment is carried out via a lock at the end of the instrument. The specimen chamb has a high voltage lead-in with four contacts. These provide for applying a potential to the object and connections to the heater and thermocouple.

The design of the vacuum system of the mirror differs little from that used in the electron velocity analyzer described in Ref.16. To provide a vacuum of 10^{-6} mm Hg, we used an oil diffusion pump with a capacity of 500 liters per sec and a rotary pump of appropriate power for the fore-vacuum. The vacuum system comprises a liquid nitrogen vapor trap.

The supply unit consists of a voltage-doubler type 50 kv rectifier employin selenium elements. The gun filament is supplied from a separate 50 cps rectifie located in the same tank and equipped with a filter.

The electron mirror potentials are controlled by dividers. Each voltage di vider is an oil-filled tank of plexiglas with three plates. One is grounded; th second is connected to the high voltage source; the desired voltage is taken off the third, moveable plate.

Principle Operating Conditions of the Mirror Electron Microscope

In working with the present instrument, as well as earlier[3], we observed tw types of images.

We note that for the three- and five-electrode mirror objectives that we

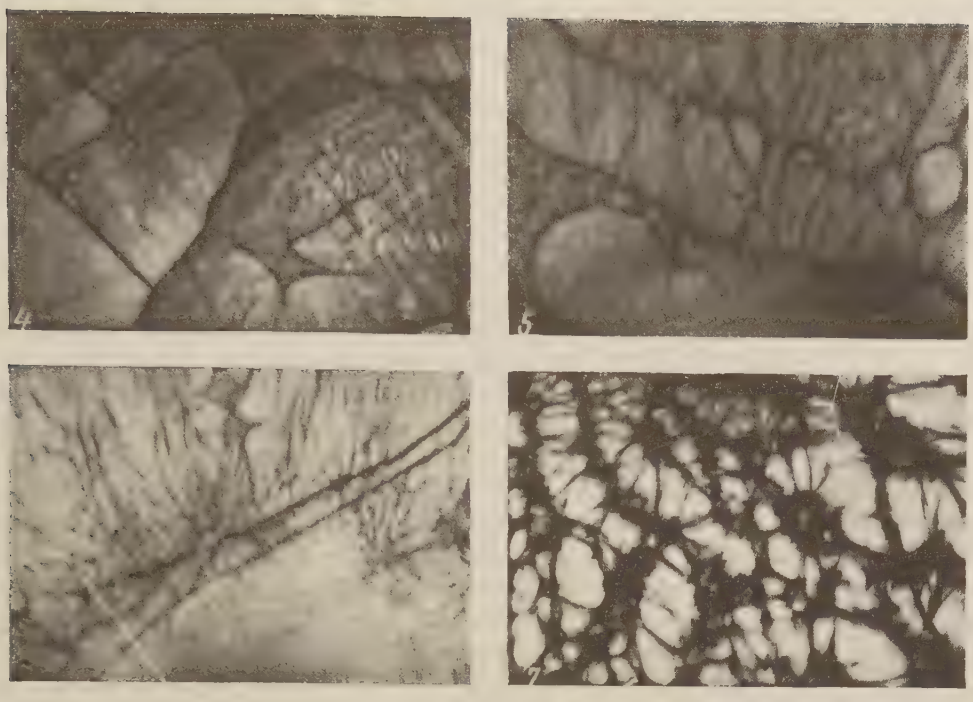

Fig.4. Copper etched by ion bombardment. 600 X.
Fig.5. Small-angle linear dislocation on a (111) face of germanium, brought out by ion bombardment. 600 X.
Fig.6. Domain structure (parallel lines) on annealed Si-iron single crystal. 600 X.
Fig.7. Domain structure of ferrite single crystal (magnetoplumbite). 600 X.

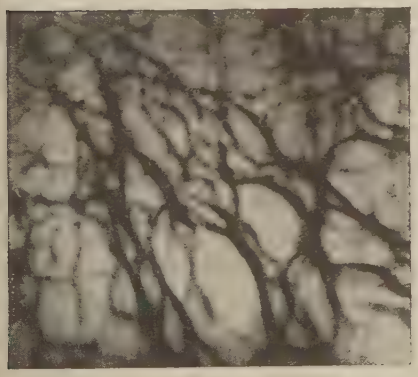

Fig.8. Domain structure on hexagonal face of a cobalt single crystal. 600 X.

used there exists a range of cathode aperture voltages in which no image is observed. Consequently, this no-image region divides the range of voltage values on the focusing electrode (in the case of the three-electrode objective) into two regions and, accordingly, the operation of the objective into two operating regimes. We investigated the character of the image under both regimes. At an anode voltage of 20 kv the first operating regime obtains for the three-electrode objective at a focusing electrode potential of 0 to +1 kv relative to the mirror cathode, while the second operating regime sets in at a potential of +3.5 kv. No image is present in the range from +1 to +3.5 kv. Provisionally, we designate this region the "region of inflection". Under the first operating condition the image is erect and becomes smaller with increase of potential on the focusing electrode; then it shrinks to a point, i.e., vanishes, and then begins to grow again, but is now inverted.

The character of the image is substantially different under the two regimes. Under the second operating condition the "secondary emission spot" accompanying the mirror image appears in the form of a diffuse bright patch at the center of

the image, while under the first condition it has the appearance of a bright ring Application (relative to the gun cathode) of a low positive bias (~0.1 v) to the mirror cathode appreciably weakens the secondary emission spot or even suppresses it altogether.

Our observations show that the second operating regime secures the imaging of microfields that spread out from the object to considerably lesser distances than those fields that can be observed under the first regime. The latter is ver convenient for comparison of thermionic and mirror images, inasmuch as the object ive under this condition has the same focal length for both types of imaging.

To elucidate the electron-optical nature of the image formation, we calculated the electron trajectories for the three-electrode objective under both oper ting conditions. It turned out that the scattering field in the anode-focusing electrode region is considerably weaker under the second operating condition than under the first. This explains the lesser scattering of the electron beam in the second regime and the greater "entry aperture"* in the anode-focusing electrode region. The field of the cathode has a stronger collecting region under the second condition and therefore the electron trajectories, which have a smaller radia velocity component than under the first condition, approach closer to the cathode (~0.01 mm as compared with ~0.1 mm under the first condition) and come up against a stronger retarding-reversing field. Our calculations show that the focal lengt of the system under the second condition is about one order of magnitude less tha under the first (f = 0.02 mm for the second as compared with f = 0.2 mm for the first regime). Thus the focal length under the first regime is of the same order of magnitude as for a thermoelectronic system. This agrees with the experimental fact of concomitance of mirror and thermionic images under the first condition.[2]

Figs.4 to 8 show a number of photographs obtained by means of the microscope

The design of the present instrument differs in a number of respects from that of earlier similar microscopes. The camera with the electron beam passing through it permits photography of electron images in vacuo. Illumination is enhanced by a condenser and a magnetic field on the specimen. The intermediate le can be set at different distances from the immersion mirror objective, permitting immediate high electron-optical magnification, which is crucial for direct method of investigation. The heating of the specimen and measurement of its temperature permit investigation of the structural changes occurring at phase transition poi Finally, the instrument has adequate provisions for making all necessary adjustments.

By now methods for direct microstructural investigations by means of reflec ing, scanning and immersion microscopes have been thoroughly worked out. The us ful magnification provided by the electron mirror cannot in principle exceed the possibilities of these systems. However, the higher sensitivity of the electron mirror to conditions at the surface of the object augurs well for its applicatio and development.

References

1. D.Wiscott, Optik, 13, 463, 481 (1956).

2. G.V.Spivak, I.A.Pryamkova & N.N.Sedov, Izv.AN SSSR, Ser.fiz., 24, 640 (1960). (Trans.Bulletin, 24, 648.)

3. G.V.Spivak, I.A.Pryamkova & E.Igras, Izv.AN SSSR, Ser.fiz., 23, 729 (195 (Trans.Bulletin, 23, 723.)

---

*This can be determined from the distribution in potential and value of the radial velocity component in the electron beam.

4. G.V.Spivak, I.N.Prilezhaeva & V.K.Azovtsev, Doklady, AN SSSR, 105, 965 (1955).

5. L.Mayer, J.Appl.Phys., 28, 975 (1957).

6. G.Hottenroth, Z.Phys., 103, 460 (1936); Ann.Phys., 30, 689 (1937).

7. R.Orthuber, Z.angew.Phys., 1, 79 (1949).

8. G.V.Spivak, N.G.Kanavina, I.S.Sbitnikova, I.N.Prilezhaeva, T.N.Dombrovskaya & V.K.Azovtsev, Izv.AN SSSR, Ser.fiz., 21, 1177 (1957). (Trans.Bulletin, 21, 1169.)

9. L.Mayer, J.Appl.Phys., 28, 259 (1957); 26, 1228 (1955).

10. G.V.Spivak, E.Igras, I.A.Pryamkova & I.S.Zheludev, Kristallografiya, 4, 123 (1959). (Trans.Soviet Phys. - Crystallography.)

11. D.V.Kormilitsyn & Oshchepkov, Abstracts of reports presented at the Third All-Union Conference on Electron Microscopy, Leningrad 1960.

12. G.V.Spivak, I.A.Pryamkova & V.N.Lepeshinskaya, Doklady AN SSSR, 130, 751 (1960). (Trans.Soviet Physics - Doklady.)

13. J.Heydenreich, Exp.Techn.Phys., 8, 49 (1960); G.Bartz, G.Weissenberg & D.Wiscott, Proc.Intern.Conf.on Electron Microscopy, London 1954.

14. G.V.Spivak & V.I.Lyubchenko, Izv.AN SSSR, Ser.fiz., 23, 697 (1959). (Trans. Bulletin, 23, 691.)

15. D.V.Fetisov, V.I.Milyutin & others, Zavodskaya laborator., 1, 92 (1958); V.I.Milyutin, D.V.Fetisov & others, Izv.AN SSSR, Ser.fiz., 23, 454 (1959). (Trans. Bulletin, 23, 438.)

16. A.N.Kabanov, PTE, No.4, 23 (1960). (Trans.Instruments & Experimental Techniques.)

SOME QUESTIONS ARISING IN THE DEVELOPMENT OF AN X-RAY MICROANALYZER

- A.M.Solov'ev & V.N.Vertsner

The electron-optical system of an x-ray microanalyzer is essentially a probe system with a probe (electron spot) diameter of 1 micron. Naturally, with so small a focal spot the question of the intensity of the electron beam (and consequently the intensity of the excited x-radiation) becomes important inasmuch as this factor determines the sensitivity of local x-ray analysis.

Fig.1

Generally a demagnifying system consisting of two lenses is used for producing the electron probe (Fig.1). The diffusion of the electron spot is determined primarily by the aberrations of the second lens, which include spherical aberration, astigamtism and coma.

The diameter of the circle of diffusion due to spherical aberration in the "sharpest image" plane is given by[1]

$$d_S = \frac{1}{2} C_S \alpha_{ex}^3 , \qquad (1)$$

where C_S is the spherical aberration constant of the second lens, and α_{ex} is the exit aperture of the electron beam. It will be evident from this formula that to minimize the circle of diffusion the second lens should have the lowest possible spherical aberration constant, i.e., should be a "strong" lens.

Actually, however, in choosing the electron-optical system for a microanalyzer one must take into account a number of other specific requirements in addition to that of a minimum spherical aberration constant. In particular, one must provide for the insertion of relatively bulky specimens and make provision for light-optical observation of the surface of the specimen with a magnification equal to that of a good metallographic microscope, or one must find place for a deflecting system for scanning the specimen surface with the electron beam. Lastly, one must take into account the influence of ferromagnetic specimens on the field of the second lens.

To satisfy these different requirements it becomes necessary to make the second lens a long focus one (f = 10 to 30 mm), i.e., to use a lens that is appreciably weaker than the lenses employed in electron microscopes and hence characterized by a spherical aberration constant appreciably larger than that of electron microscope lenses.

If the second lens is chosen on the basis of the above mentioned requirements i.e., if the spherical aberration constant is predetermined by the other factors, there arises the question of choice of the exit aperture for this lens, inasmuch as this also affects the size of the circle of diffusion.

The geometric size of the electron probe is the sum of the diameter of the gaussian image and the diameter of the circle of diffusion due to spherical aberration (we provisionally neglect other aberrations), that is,

$$d = d_{gauss} + d_S . \qquad (2)$$

The greater the exit aperture α_{ex}, the greater the probe current, but also the greater d_S. Consequently, to obtain a specified probe diameter d, one must reduce d_{gauss}, i.e., have recourse to a greater demagnification of the electron-

optical system, which leads to decrease of the current density per unit aperture angle.

Obviously, there must be an optimum demagnification for which one can obtain a maximum value of the probe current with a given probe diameter d.

Inasmuch as the data in the literature[2,3] concerning the optimum demagnification conditions and values of the probe current are conflicting, we carried out a mathematical analysis of the operation of the electron-optical system of an x-ray microanalyzer in order to determine the coefficients relating the maximum current with the principal parameters of the system.

As a result there was obtained the formula

$$I_{\max} = \frac{9}{64}\frac{\pi^2}{2^{2/3}}\beta\frac{d^{8/3}}{C_S^{2/3}}, \qquad (3)$$

where d is the probe diameter, and $\beta = \frac{i_0 eV}{\pi kT}$ is the brightness of the gun.

This expression for the maximum current agrees with the formula given by Castaing[2]. We also showed that under optimum conditions the system must operate with a magnification

$$m = \frac{3}{4}\frac{d}{d_{\text{true}}}, \qquad (4)$$

there simultaneously being fulfilled the condition

$$d_S = \frac{1}{4}d. \qquad (5)$$

Fig.2 shows the variation of the probe current as a function of the magnification of the electron-optical system.

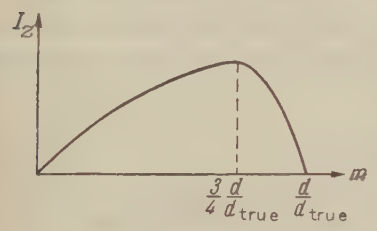

Fig.2

Another possible aberration is astigmatism arising in the system owing to imperfection of the optics and the presence of contaminants along the beam path; in the case of microanalyzers, however, astimatism can be eliminated by means of compensators and, consequently, should not diffuse the electron probe.

Owing to inaccuracies in fabrication and adjustment, in addition to spherical aberration and astigmatism, there may arise in the system coma aberration, due to passage of the electron beam not exactly through the center of the lens, which also leads to diffusion of the electron spot. To eliminate diffusion of the probe due to coma, the instrument should have provisions for adjustment to align the electron beam with the center of the lens. In addition to elimination of diffusion, adjustments are necessary for realizing the maximum probe current.

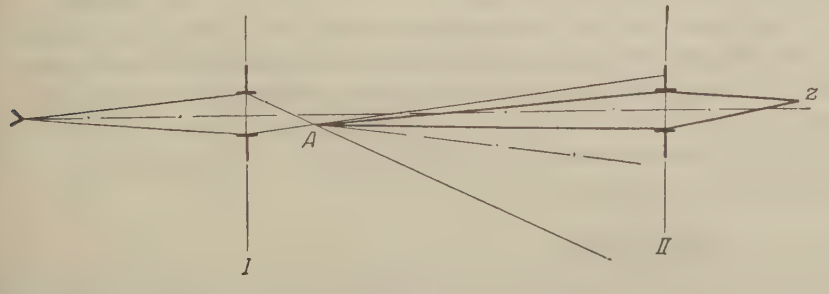

Fig.3.

Let us consider the question of adjustment of the probe system. Fig.3 shows the electron path in a two-lens system consisting of three optical elements, which should be susceptible of adjustment relative to each other.

Inasmuch as the first lens does not produce the

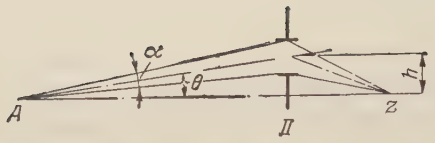

Fig.4

final image and is operated to give demagnification, all its aberrations have no significant influence on the diffusion of the final spot. Hence the only purpose of adjustment of the gun relative to the first lens is alignment of the electron beam from the gun with the center of the lens aperture, in order to obtain the maximum beam intensity after the lens. This can be realized by displacing the gun filament together with the Wehnelt cylinder. As a result of such adjustment the intermediate image is formed at a point which may not lie on the axis of the second lens, so that the axis of the beam will not coincide with the center of the second lens.

If the aperture of the second lens is located at its center, it will cut off a side cone from the beam diverging from point A (Fig.4); hence to obtain the maximum probe current one must align the gun axis with the center of the aperture. Thus there must be provision for another adjustment: either tilting of the beam or displacement of the lenses relative to each other. In this case one can realize the maximum probe current in accord with Eq.(3). However, the center of the second beam aperture may not coincide with the center of the lens (Fig.4), which will give rise to coma.

For the sake of simplicity we shall consider here the case when the intermediate image A is located on the axis of the second lens. The radius of the circle of scattering, due to aberration of this lens in the image plane, will be given by

$$r_S = \frac{1}{2} C_S \left[(\theta + \alpha)^3 + (\alpha - \theta)^3\right] = \frac{1}{2} C_S \left(2\alpha^3 + 6\alpha\theta^2\right) = C_S \left(\alpha^3 + 3\alpha\theta^2\right). \qquad (6)$$

It is evident from this formula that noncoincidence of the center of the aperture with the center of the lens leads to an aberration that is added to the spherical aberration. If it be required that this additional aberration not exceed 10%, there must be fulfilled the conditions

$$3\alpha\theta^2 \leqslant \frac{1}{10}\alpha^3; \quad \theta^2 \leqslant \frac{1}{30}\alpha^2; \quad \theta \leqslant \frac{\alpha}{5.5}; \qquad (7)$$

whence we obtain the following specification for the accuracy of adjustment of the aperture

$$h \leqslant \frac{r_{\text{apert}}}{5.5}. \qquad (8)$$

The absence of data on the extent of the noncoincidence of the geometric center of the lens with its optical center leads to the necessity of having provision for displacing the aperture of the second lens, although in itself the tolerance as regards the value of h is not rigorous.

Thus for alignment and adjustment of the probe system of an x-ray microanalyzer there must be provisions for three adjustments; these three adjustments, as described above, are necessary and sufficient for realizing a minimum probe diameter and maximum probe current.

The question of elimination of spherical aberration of the second lens may be solved by using nonaxially symmetric optics.

References

1. I.Archard, J.Sci.Instruments, 29, 11 (1958).
2. R.Castaing, Ph.D.Thesis, Univ.of Paris, 1951. Publication O.N.E.R.A. ,No.55.
3. T.Mulvey, J.Sci.Instruments, 36, 350 (1959).

SCANNING ELECTRON MICROSCOPE AND X-RAY MICROANALYZER

- Yu.M.Kushnir, D.V.Fetisov, K.K.Raspletin, B.I.Pochtarev, F.U.Spektor, A.N.Kabanov & V.F.Anisimov

In recent years considerable work has been done in the USSR and abroad on development of instruments combining an electron microscope with an x-ray microanalyzer.[1-7] By means of these instruments one can simultaneously obtain an electron image and an x-ray spectroscopic trace of the investigated surface. The electron beam image is of interest not only because this can have a better resolution than obtained by means of a metallographic microscope but also because it allows of observing certain specific processes and effects (for example, one can visualize the boundary in p-n junction transistors and similar devices). The x-ray image, which can be correlated and compared with the electron image (both images are obtained on the screens of two cathode-ray tubes) allows of determining the distribution of a given element over the surface.

Although at present the electron microscope—x-ray microanalyzer is only used for metallographic and mineralogical studies, it has great potential interest for chemists and biologists as well. The present paper is a preliminary report on the development of an instrument of this type.

A scanning electron microscope—x-ray microanalyzer is a very complicated instrument comprising a large number of independent units and assemblies. A block diagram of the instrument is shown in Fig.1.

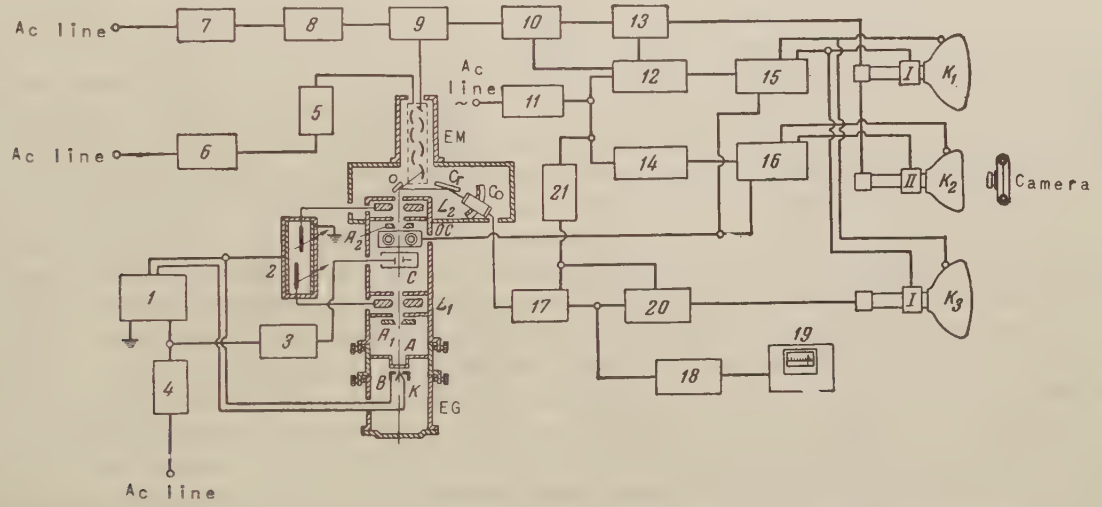

Fig.1. Block diagram of the scanning electron microscope with x-ray microanalyzer: 1) high voltage and cathode supply, 2) oil voltage divider, 3) stigmator (compensator) supply, 4) line voltage regulator, 5) multiplier supply unit, 6) line voltage regulator, 7) line voltage regulator, 8) preamplifier supply, 9) preamplifier, 10) video signal amplifier, 11) line voltage regulator, 12) visual observation sweep supply unit, 13) gamma corrector, 14) slow scan supply, 15) visual observation scan unit, 16) slow scan unit, 17) amplifier, 18) scaler, 19) recorder, 20) discriminator, 21) amplifier and discriminator supply unit.

The electron optical system for obtaining a narrow electron beam (probe) consists of two electrostatic lenses L_1 and L_2, a stigmator (compensator) C and an electron gun EG. Adjustable and interchangeable apertures A_1 and A_2 are installed

in front of each of the electrostatic lenses. The focal length of the first lens is ~3 mm; that of the second is 25 mm. The total magnification (demagnification) produced by the electron-optical system is 1500 X, which makes it possible to obtain an electron probe 0.2-0.4 μ in diameter with a current of $(0.6\text{-}0.8)\cdot10^{-9}$ amp.

The accelerating voltage for the electron gun and lenses is supplied by a low frequency 50 kv half-wave rectifier 1 employing selenium elements in a voltage doubler circuit. The rectifier filter incorporates an additional buffer capacitance of 0.3 μf, which, in addition to suppressing ripple, insures a high operating stability of the optical system forming the probe, inasmuch as the electron trajectories in the electrostatic lenses do not change incident to slow fluctuations of the supply voltage. Focusing of the electron beam is realized by variation of the potential on the two lenses by means of an oil voltage divider 2.

The electron beam focused on the surface of the investigated object O is swept by an electromagnetic deflecting system OC located in front of the second lens (0.1 x 0.1 mm raster). The secondary electrons ejected from the object go to the input of the electron multiplier EM with an amplification factor of 10^7-10^8.

The dynode system of the multiplier consists of 16-17 emitters made of activated beryllium bronze. A multiplier of this type can operate for a prolonged period at a vacuum of $1\cdot10^{-4}$ to $5\cdot10^{-5}$ mm Hg, withstands systematic contact with the atmosphere and has a low sensitivity to x-rays.

To protect the multiplier from oil vapor the vacuum system has two liquid nitrogen traps, installed in front of the high vacuum and fore vacuum pumps. The multiplier is supplied from a regulated 5 kv "Orekh" type rectifier 5. The voltage ripple is smoothed by an additional choke-capacitor filter.

In the prototype instrument we used electron multipliers developed by Akishin[8] and Tyutikov[9].

The signal voltage appearing on the load resistance connected into the multiplier collector circuit is amplified by the wide band amplifiers 9 and 10 with a passband from 25 cps to 6-8 Mc and an amplification factor of ~10 000. The amplifiers are supplied from the regulated rectifiers 7, 8, 11 and 12.

The amplified signal is applied to the modulator of the kinescope K_1. The instrument incorporates a gamma corrector 13 with a nonlinear amplitude characteristic; this unit corrects the nonlinearity of the modulation characteristic of the kinescope. By means of the gamma corrector one can regulate the image contra

The instrument has two scan units: one of these (15 in Fig.1) serves for visual observation of the image with a resolution of 300-350 lines; it yields 50 fram per sec (sweep frequency 15625 cps) and operates in conjunction with a 35LK2B kin scope (K_1); the other scan unit (16 in Fig.1) is a slow sweep unit (scan time per frame 0.2 sec) and operates with a 13LM kinescope with a persistent afterglow; this unit is intended for photographic recording of the image by means of a camer (sweep frequency 5 cps). The two scanning units are supplied from separate recti fiers 12 and 14 with electron regulation.

The x-ray spectroscopic equipment consists of two assemblies: a universal x-ray spectrometer with a recording system and a television circuit incorporating a kinescope K_3, an amplifier 17, a pulse height discriminator 20 and a supply unit 21.

The spectrometer is installed inside a cylindrical vacuum chamber and has pr vision for interchange of the analyzer crystals Cr and gas counters Co during ope tion of the instrument. The spectrometer design employs a Johann mount (reflection). The kinematic system of the spectrometer provides for an operating range of glancing angles from 13 to 45°, which makes it possible to carry out determina tions of metals from magnesium (Z = 12) to uranium (Z = 92). To this end there are provided two quartz single crystals with reflection from the $(13\bar{4}0)$ and $(10\bar{1}0$

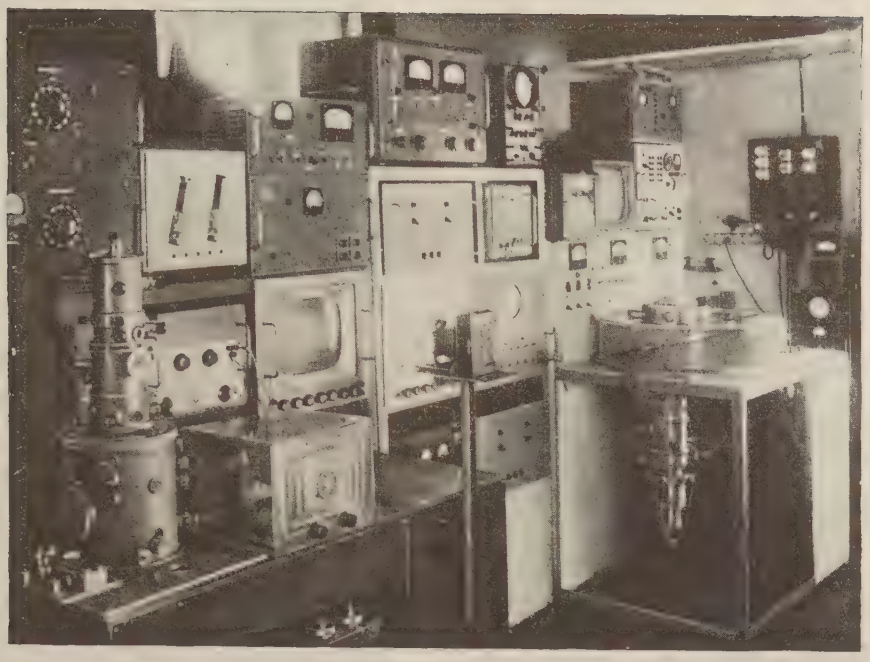

Fig.2. General view of the scanning electron microscope—x-ray microanalyzer.

planes and a mica single crystal with reflection from the (001) face. The crystals are bent to a radius of 400 mm. Thus the range of analytic wavelengths is 0.7 to 10 Å.

This spectrograph allows of making quantitative determination of the chemical composition of metals and alloys in a volume of a few cubic microns. However, the principal function of the instrument is to investigate the distribution of different metals over the surface of the specimen.

In this case the electron probe, somewhat increased in diameter, is swept over the surface of the specimen, and the spectrograph is successively set to detect the different components of the alloy in question. The signals from the counter Co go to the amplifier 17 and after passing through the pulse height discriminator 20 modulate the beam of kinescope K_3, the raster of which is synchronized with that of kinescope K_1.

Thus the instrument allows of simultaneous observation (and/or photography) of the electron beam image of the selected surface of the specimen and recording of the distribution of a selected element over the surface of the specimen.

A general view of the prototype instrument is shown in Fig.2. We have carried out a number of preliminary tests and have obtained electron images of different specimens with a resolution of 300 lines at a frame frequency of 50 per sec.

Micrographs of a number of metal surfaces obtained with a magnification of 700 X are reproduced in Fig.3. The maximum resolution in the recording micrographs is 0.1 μ. It is interesting to note that the resolved distance in the micrographs is usually 1.5-1.7 times smaller than the diameter of the probe. This is, apparently, explained by the character of the current intensity distribution over the probe cross section: the most intense central portion of the probe is primarily responsible for formation of the image.

It will be seen that the recorded images are characterized by good contrast and good rendition of the surface topography.

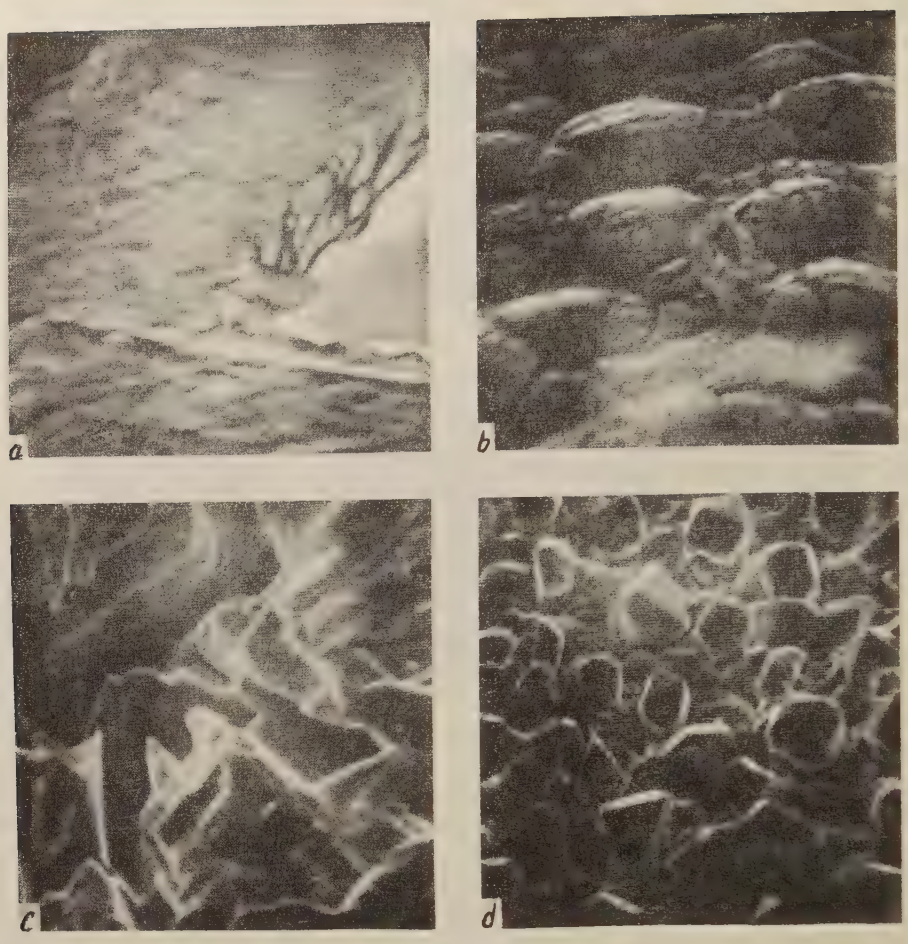

Fig.3. Electron micrographs of a) electrolytic copper screen, b) No.10 steel, c) etched germanium, d) sputtered germanium, e) antimony surface. Magnification - 700 X.

Of great interest is the possibili ty of direct investigation of p-n junc- tion transistors. By way of illustratio in Fig.4 we show a micrograph of the su face of a silicon junction transistor be fore and after application of a potentia difference. The line of the p-n junctio becomes evident even at a potential dif- ference of about 2 v at an electron probe enerty of 25 kev, which indicates that the image in the scanning microscope is formed mainly by slow electrons.

It also proved possible to examine and photograph a number of organic speci- mens by means of the scanning microscope. A micrograph of a fly wing is repro- duced in Fig.5.

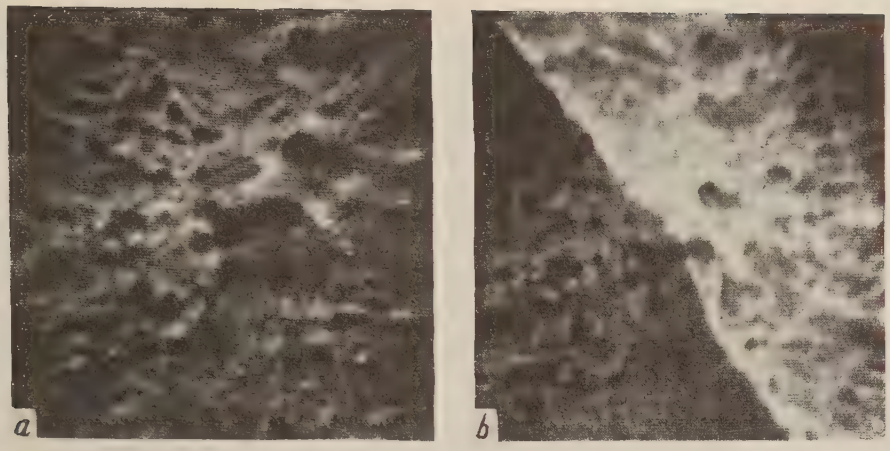

Fig.4. a - pulled silicon p-n junction; b - same junction transistor with a voltage applied to it.

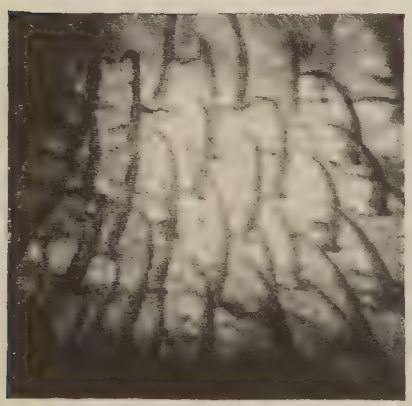

Fig.5. Fly wing. 700 X.

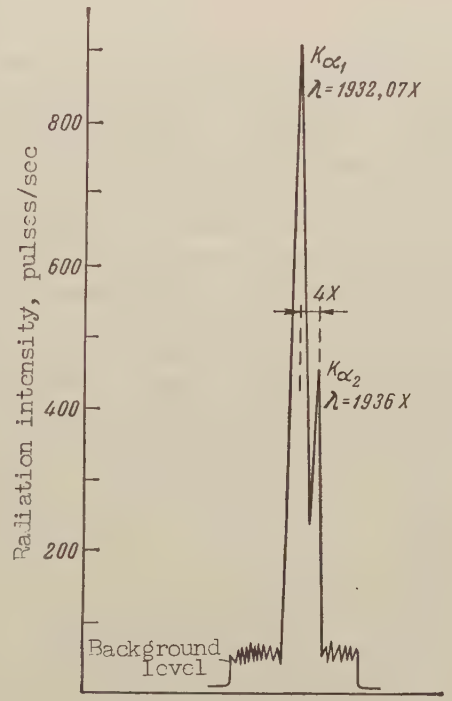

Fig.6. Spectrogram of the Kα doublet of iron.

In addition to investigation of the scanning microscope part of the instrument we have also carried out preliminary tests of the x-ray spectrographic units. In these tests we used an MSTR-4 counter for detecting the x-radiation.

Fig.6 presents the spectrogram of the Kα doublet of iron recorded with the $(10\bar{1}0)$ reflecting plane quartz crystal in the spectrograph. It will be evident from this spectrogram that the instrument is capable of resolving the Kα doublet of iron, the lines of which have a separation of 4 X. Similar spectrograms were obtained for other specimens.

In testing the x-ray spectroscopic apparatus in conjunction with the video-control equipment there was obtained the image of a nickel-iron contact weld (Fig. 7). With alternate setting of the spectrometer on the Kα line of iron and the Kα line of nickel the light and dark halves of the image changed places.

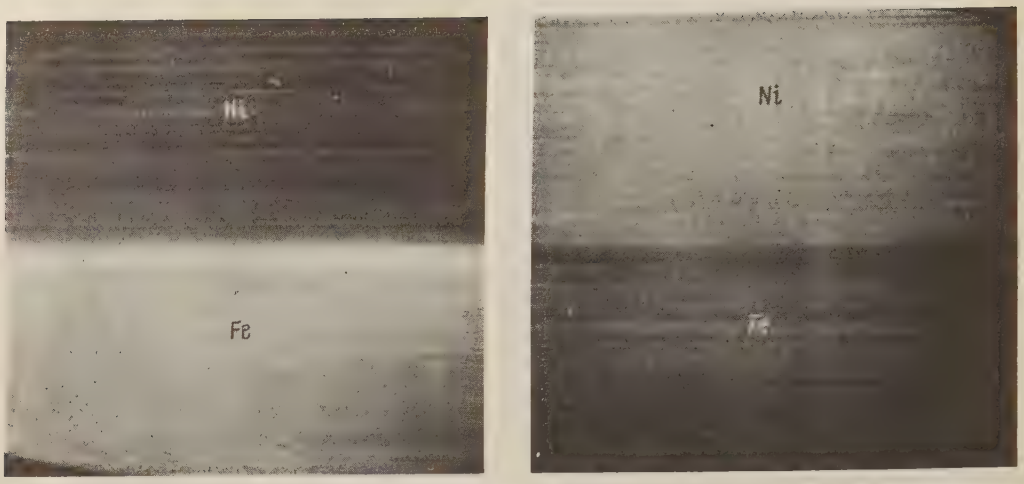

Fig.7. Iron-nickel contact weld.

References

1. V.E.Cosslet & P.Duncumb, Proc.of the Stockholm Conference on Electron Microscopy, p.12, 1956.

2. V.E.Cosslet & P.Duncumb, Nature, 177, 1172 (1956).

3. P.Duncumb & V.E.Cosslet, Proc.of Conference on X-ray Microscopy and Micro radiography, p.374, 617. Academic Press, N.Y.1957.

4. P.Duncumb, Thesis, Cambridge University, 1957.

5. P.Duncumb, Brit.J.Appl.Phys., 10, 420 (1959).

6. M.A.Melford & P.Duncumb, Metallurgia, 205, May, 1960.

7. Scanning Electron-probe X-ray Microanalyser, Cambridge Instrument Company Temporary List, 177/1.

8. A.I.Akishin, Thesis, Moscow, 1958.

9. A.M.Tyutikov, Radiotekhnika i elektronika, 4, 11 (1959). (Trans.Radio Engineering and Electronics.)

USE OF GAS MICROCELLS IN ELECTRON MICROSCOPY

- I.G.Stoyanova

Invention of the electron microscope greatly extended the possibilities of investigating microstructure in that the resolution of even the first electron microscopes was of the order of 100 Å as compared with 2000 Å in the case of light microscopes. Further advances into the submicroscopic world were made both along the line of improving the resolution (from 100 to 10 Å) and along the line of developing new specifically electron microscopic techniques (microdiffraction, dark field, etc.) and preparative procedures (carbon replicas, fixation of biological specimens, ultrasectioning, etc.). The necessity for developing new preparative procedures stems from the fact that the advantages of electron microscopic investigation could not be utilized in the case of a number of objects in view of the specific characteristics of the electron microscope which stem from the fact that it is a high vacuum instrument and utilizes electrons as the source of illumination. Thus there was immediately excluded the possibility of direct observation of biological specimens in the moist state and live cells. Despite the fact that during the initial stages of development of electron microscopy much attention was given to this problem, it was not successfuly solved. As a result, until recently, electron microscopes could be used only for studying static (dried and stationary) objects.

The recent development of the gas microcell procedure[1] made it possible to realize in an electron microscope conditions that permit direct investigation of the kinetics of chemical reactions between solid, liquid and gaseous phases[2], study of live microorganisms and observation of the dynamics of morphological changes[3] occurring in different specimens under the influence of diverse factors including ionizing radiation[4] (this last is facilitated by the fact that the electron beam itself constitutes ionizing radiation).

The possibility of investigating live cells by means of the UÉMB-100 electron microscope is realized by means of a special objective lens with a specimen microcell which is installed instead of the standard specimen chamber, and is equipped with a valve system for controlling the pressure and composition of the gas in the cell. A specimen can be maintained in the natural moist state by virtue of the fact that it is kept in an atmosphere of water vapor (or suitable gas) at a pressure minimizing evaporation.

The space in which the object is located is bounded by two films (1 and 2) covering the openings in the rings 3 and 4. These films prevent the escape of gas or water vapor into the microscope column. The films are of formvar, coated with a hydrocarbon layer, and are thus sufficiently strong to withstand a pressure differential of 1 to 7 under electron bombardment, and at the same time are sufficiently thin not to produce any significant distortion of the electron trajectories. Good vacuum seals between the cell components prevent the leakage of gas or water vapor into the vacuum space of the microscope. The gas channel 5 is located inside the object holder, and is connected at one end with the microcell and at the other with the valve system. Thus in operating the vacuum lock to insert the specimen into the microscope, it is not necessary to evacuate the microcell, which is particularly important in investigating live and moist specimens. The valve system allows of regulating

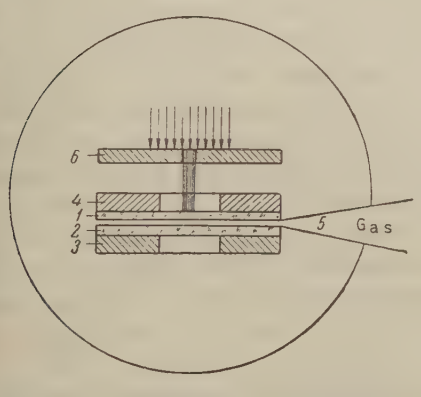

Fig.1. Diagram of microcell.

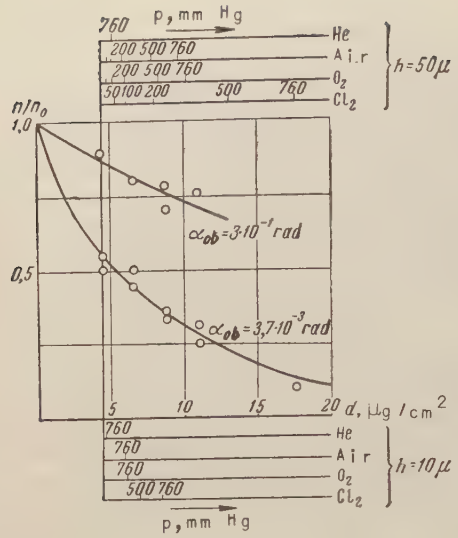

Fig.2.

the composition of the gas in the microcell and of varying the gas pressure from 760 to 10^{-2} mm Hg. The diaphragm 6 with a 10-20 μ aperture is located in the immediate proximity of the specimen and serves to shield all but the observed section of the specimen from the electron beam.

Additional scattering of electrons by the second film of the microcell and the atoms of the gas filling it has a substantial influence not only on the quality of the image (resolution and contrast) but also on the processes occurring in the object (ionization, heating, charging, etc.). In view of this we investigated the influence of the gas and the second film on the quality of the image (influence on the electron beam) and also the effect of the electron beam on the investigated object mounted in the gaseous medium. Our purpose was to find means for protecting live cells from damage by the electron beam. Finding such means would also make it possible to carry out investigations of the kinetics of life processes with the aid of an electron microscopy. Similar problems arise in electron microscopic investigation of the kinetics of chemical reactions.

The contrast of the electron image of objects investigated in the gas microcell was evaluated from the distribution in density of the electrons in the image under different conditions. Changes in the electron density distribution in the presence of two films over the ring apertures and with filling of the cell with gas was determined by means of the procedure described in Ref.5.

Fig.2 shows the variation of n/n_0 as a function of d, obtained with the cell covered by hydrocarbon coated formvar films 2.2 μg/cm^2 thick films (here n is the density of electrons passing through the microcell within the limits of the aperture angle of the objective lens, n_0 is the density of electrons incident on the object, and d is the superficial density of the object). We give curves for two values of the objective aperture, namely, $3.7\cdot10^{-3}$ and $3\cdot10^{-1}$ radians at an accelerating potential of 60 kv. The focal length of the objective lens was 6.5 mm. The observed electron density distribution inside the aperture angle is satisfactorily described by the semi-empirical formula $n = noe^{-sd}$ (Refs.6 & 7); here s - th scattering cross section - equals $12\cdot10^4$ cm^2/g for $\alpha_{ob} = 3.7\cdot10^{-3}$ rad and $3.7\cdot10^4$ cm^2/g for $\alpha_{ob} = 3\cdot10^{-1}$ rad. An idea of the change in the electron density distribution as a result of admission of different gases at different pressures into th cell for two values of the thickness of the gas layer (h = 50 μ and 10 μ) is give by the gas scales located above and below the graph. The zero of the gas scale on the horizontal axis is located opposite the superficial density value corresponding to the total thickness of the two covering films. The scales are plotte on the assumption that at equal superficial thicknesses the scattering in the gas layer is the same as the scattering in the layer of the substance. From these curves there were found the superficial density Δd of the specimen, corresponding to minimum contrast. It was found that there could be detected biological object in the cell if their superficial density is not less than 0.8 μg/cm^2 with an aperture angle $\alpha_{ob} = 3.7\cdot10^{-3}$ rad and 3 μg/cm^2 with $\alpha_{ob} = 3\cdot10^{-1}$ rad. It was postulated that the minimum contrast $K_{min} = 0.1$.

The experimentally determined resolution of the electron microscopic image of objects in the gas microcell attained 50 Å.

Investigation of the characteristic energy loss of the electrons passing through the gas filled microcell[8] enabled us to establish that when the cell is filled with almost any gas except oxygen there appear in the loss spectrum for the covering films lines corresponding to the ionization or excitation potentials of the given gas, and the total loss spectrum consists of the sum of the spectra of the losses in the covering films and gas. In the case of oxygen, however, in addition to the loss lines at 8.2 and 12.8 ev, corresponding to the excited and ionized state of O_2 molecules, respectively, there appears a loss line at 17 ev, which is evidence of change in the structure of the films under the influence of electron bombardment in the presence of oxygen in contact with the films. It should be noted that we observed no significant change in the structure of different objects as a result of short term electron radiation in an atmosphere of gas.

Investigation of the thermal effect of electrons on specimens in the electron microscope makes it possible to obviate deterioration of the specimen as a result of heating by electrons.

Investigation of the conditions leading to appearance of electric charges on nonconducting and semiconducting (dry) biological specimens led us to the conclusion that when the microcell is filled with gas to a pressure of 1 mm Hg this effect is virtually nil, and that in this case one can discount the possibility of damage to the specimen owing to field emission from it.

Elimination of the above enumerated deleterious effects of electrons on the investigated specimen does not, of course, obviate the danger of radiation damage of the specimen connected with the fact that when the electrons pass through matter they produce ionization and excitation of the atoms and molecules leading under certain conditions to irreversible changes in the material. The extent of the radiation damage depends on the properties of the specimen, the current density, the composition of the medium surrounding the specimen, etc. Investigation of the radiation damage to live microorganisms under different conditions (gases of different composition and at different pressure, amount of moisture, etc.) enabled us to select optimum conditions under which most microorganisms remain alive at least for the period of a single exposure[3,4]. The principal life-maintaining measures were the following.

1. The current density on the object was reduced to the minimum possible value consistent with obtaining adequate blackening of the photographic plate ($i_{object} = 10^{-5}$ amp/cm^2, $i_{plate} = 10^{-12}$ amp/cm^2, t = 10 sec); this, obviously, reduced the probability of damage.

2. In adjusting and focusing the instrument we shielded the entire specimen except for a 10-20 μ section, which reduced the radiation dose received by the specimen up to the instant of photographing.

3. The presence of a layer of ionized gas on the surface of the specimen minimized destruction of the specimen owing to field emission, arising under the influence of the field of the electrostatic charges that appear on a nonconducting object when it is irradiated under vacuum with electrons[10].

4. We reduced the oxygen content in the medium surrounding the object at the time of electron bombardment, which lessened the sensitivity of the microorganism to the effect of ionizing radiation.

5. We removed excess moisture, which also reduced the effect of ionizing radiation owing to decrease in the number of active radicals, forming as a result of break up of the water molecules, on the protein molecules of the investigated material.

6. Electron irradiation was carried out in the presence of certain chemical substances that tend to increase the radiation resistance of microorganisms.

7. Where possible we reduced the temperature of the specimen in order to slow down the spread of damage.

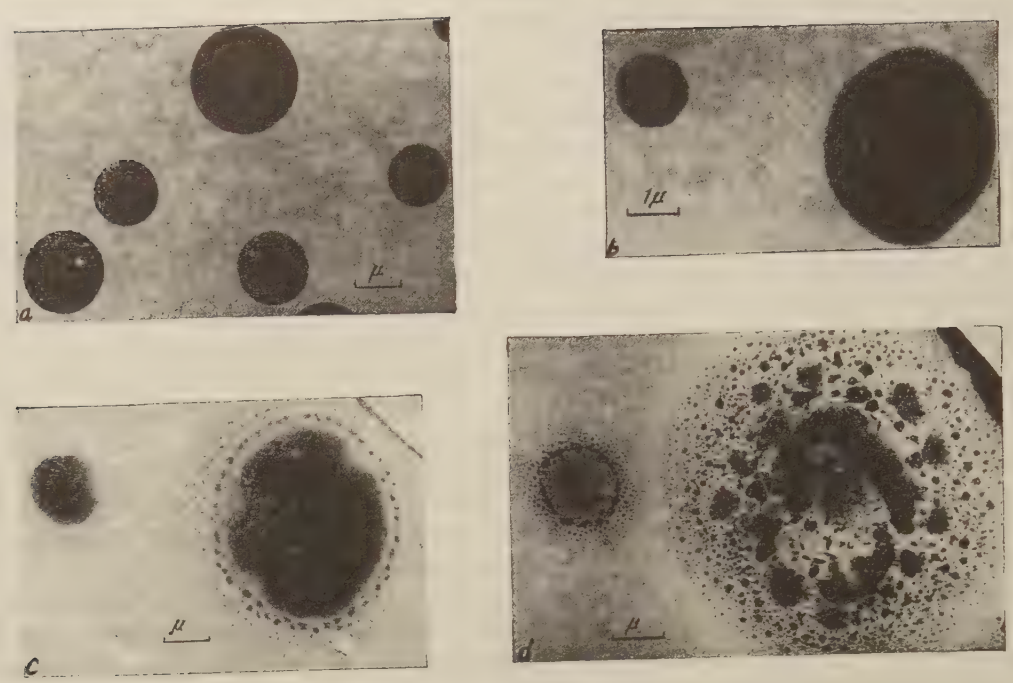

Fig.3

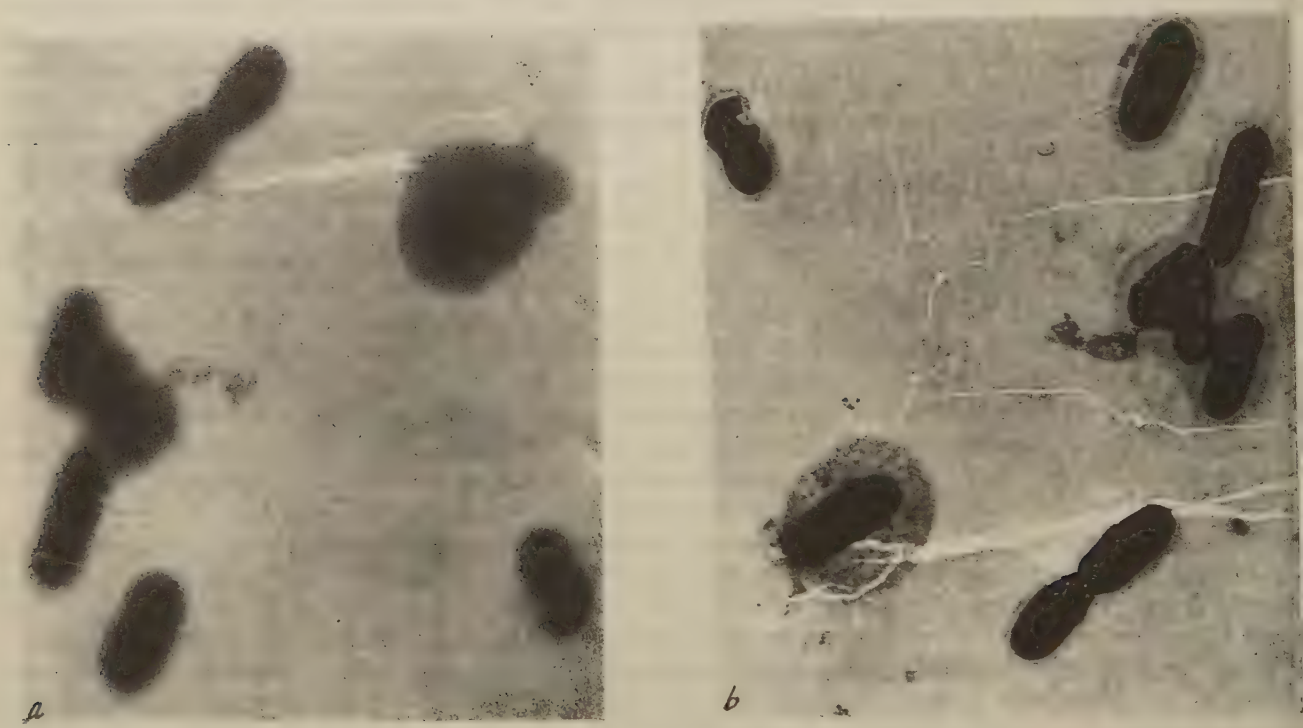

Fig.4. Electron micrographs of cells recorded at different pressures in the micro cell: a) p = 60 mm Hg and b) p = 10^{-2} mm Hg. 7000 X.

8. We tried to reduce the thermal effect of the bombarding electrons on the specimen by reducing the current density on the object to 10^{-4} amp/cm^2 and limiting the area of the bombarded section to 10-20 μ. The temperature of the object did not increase by more than 1-2°.

Simultaneous application of all the above measures, except 6 and 7, made it possible to realize micrographing conditions under which even live microorganisms withstand a single exposure without noticeable damage. This enabled us to expand the range of applications of the electron microscope and to observe a number of interesting phenomena, including the following: the process of chemical reaction between solids and gases, for example, between Ag and H_2S and O_2 (Ref.2); droplets of liquid, for example, H_2SO_4* (Fig.3,a) and the process of its evaporation with reduction of pressure in the microcell (Fig.3,b,c & d); aerosols; changes in bacteria incident to drying (Fig.4); changes in specimens under the influence of ionizing radiation, for example, bacterial cells and collagen[4]; changes in different specimens under the influence of various reagents which are sometimes indicative of the distribution of different components in the specimen; live bacterial cells and the changes in them in the process of development, including interaction between the cells at different stages of their development; the process of development of noncellular and other forms, which is important for understanding the basic nature of life processes[3].

The use of the gas microcell in microbiology may be illustrated by the following example. In investigating live B.mycoides we observed how as a result of interaction between the cell protoplasts there occurred grouping of the cells leading to the formation of large clusters, which are familiar to microbiologists (Refs.11 & 12) and have been frequenctly observed by means of a light microscope. We were not able to detect any morphological differences between the cells entering into the observed interaction; the cells had an entirely normal appearance. The tendency to establishment of contact in one of the periods of the life cycle of the bacteria varied dependong in the conditions under which they were cultured. If the cells were free to move, contact was established when the cells touched each other. In this case one could observe that the protoplasts of the contacting cells approached each other, moving from the initial central position towards the common wall. If free motion of the cells was hindered (by thickening the culture medium or partial drying) in the period when the grouping occurs, contact was still established either through appreciable elongation of the contacting cells or by means of a filiform cytoplasmic formation, starting from the protoplast of one cell and growing in length in the direction of the other cell until it reaches its protoplast (Fig.5,a & b). At the point of contact of the filament with the protoplast there forms a fusiform swelling. The diameter of the cytoplastmic formation is the same over the entire length between the cells, but then abruptly changes at the cell wall. The length of the connecting filaments attains 20 μ in individual cases; the diameter of the filaments varies from 0.04 to 0.1 μ. Control photographs recorded for specimens that had simultaneously gone through all the stages except for observation in the initial state in the electron microscope (i.e., single exposure) substantiated the results obtained with the gas microcell (Fig.5,c): here one can also observe similar filiform cytoplasmic formations connecting the cells as well as the fusiform swellings in the cells at the point of contact. Moreover, in the control photograph there is discernible the end of one of the cytoplasmic formations. This has a very pointed tip; the size of the filiform formation is at the limit of resolution. Hence it may be assumed that there

---

*The sulfuric acid fog was studied in collaboration with M.E.Kuperman and T.A.Nekrasova.

Fig.5. Micrograms of live B.mycoides cells, 48 hour culture: a) section of the specimen in the initial state, b) same specimen after 1.5 hours in the culture medium, c) control experiment cells after 40 min in the culture medium. 5000 X.

is an even finer section at the tip of the filament, since there is a degree of lightening observable in the direction of continuation: the invisible tip has apparently pushed aside the broth particles that settled on the film.

The results obtained show that the observed effect cannot be regarded as a purely mechanical process, as is inferred by some authors. Thus the formation of the fusiform swelling at the point of contact of the filament with the cell may be taken as an indication of reaction of the cell to the irritation produced in it by the substance of the other cells. Hence the phenomenon must be regarded as a physiological process. The fact that the contact is selective in character gives reason to infer that this selectivity may be attributed to heterosexuality of the contacting cells and that the filiform cytoplasmic formations realize the transfer of chromosome material from a cell of one sex to a cell of the opposite sex.

Thus the gas microchamber procedure allows of expanding the region of application of the electron microscope particularly in the direction of investigation of live cells. It must be emphasized that the potentialities of this procedure have not been fully explored as yet. Our aim in the future is to investigate radiation damage in various specimens as a result of electron bombardment, to find means of protecting sepcimens against the influence of ionizing radiation and of increasing their stability and resistance, and to improve the design of the electron microscope itself.

References

1. I.G.Stoyanova, P.V.Zaitsev & S.V.Bezlepkin, Inventor's Certificate No. 118563 (1957); I.G.Stoyanova & G.A.Mikhailovskii, Biofizika, 4, 483 (1959). (Trans.Biophysics.)

2. I.G.Stoyanova, Doklady AN SSSR, 118, 325 (1958). (Trans.Doklady.)

3. I.G.Stoyanova & T.A.Nekrasova, Ibid., 134, 227 (1960). (Trans.Ibid.)

4. I.G.Stoyanova, T.A.Nekrasova & A.L.Zaides, Ibid., 130, 1366 (1960) (Trans. Ibid.); I.G.Stoyanova, T.A.Nekrasova & V.I.Biryuzova, Ibid., 131, 195 (1960) (Trans.Ibid.).

5.I.G.Stoyanova & A.I.Frimer, Ibid., 94, 459 (1954).

6. C.E.Hall, Introduction to Electron Microscopy, London - N.Y., 1953.

7. I.G.Stoyanova, Zhur.tekh.fiz., 24, 990 (1956). (Trans.Soviet Physics - Technical Physics.)

8. I.G.Stoyanova & A.N.Kabanov, Izv.AN SSSR, Ser.fiz., 23, 719 (1959). (Trans.Bulletin, 23, 714.)

9. I.G.Stoyanova & E.M.Belavtseva, Ibid., 23, 754 (1959). (Bulletin, 23, 748.)

10. H.Mahl & W.Weitsch, Naturwissenschaften, 46, 487 (1959).

11. F.Lönnis, J.Agricult.Res., 6, 675 (1916); 23, 401 (1923); Zbl.Bakteriol. II, 56, 529 (1922).

12. A.A.Imshenetskii, Stroenie bakterii (Structure of Bacteria), M.-L., 1940.

THE UIT-3 UNIT FOR ETCHING METALS, SEMICONDUCTORS AND DIELECTRICS BY ION BOMBARDMENT

- G.V.Spivak, F.F.Kushnir & V.E.Yurasova

In this report we describe a new improved model of a unit for etching metals semiconductors and dielectrics by ion bombardment. The original models of the unit - designated UIT-1 and UIT-2 - have been described in Refs.1 and 2.

The new unit - designated UIT-3 - has provision for the following operations 1) heating of the specimen up to 1200°, 2) cooling of the specimen by circulating water in the process of etching, 3) observation of the surface of the specimen in the process of etching or evaporation by means of a metallographic microscope, 4) compression or elongation of the specimen during ionic etching or evaporation, and 5) deposition of silica or metal films (replicas) immediately after ionic etching.

We also give some examples illustrating the application of the ion bombardment procedure for bringing out the boundaries of grains and the submicroscopic structure inside them, obtaining oriented figures indicative of the crystal symmetry and detection of the points of emergence of dislocations.

Ionic etching is a convenient method of bringing out the structure of substances[1-4] and has a number of advantages over the methods of chemical etching and vacuum evaporation. In the case of ionic etching the surface of the metal is not covered by an oxide film as occurs in the case of chemical etching. Hence one can readily obtain good surface replicas for electron microscopy.

One of the important advantages of the ion bombardment procedure is the possibility of investigating structure in a wide temperature range. Of greatest interest is ionic etching at temperatures ranging from room temperature to 0.6 the melting temperature, when neither chemical etching nor thermal evaporation under vacuum can be employed.

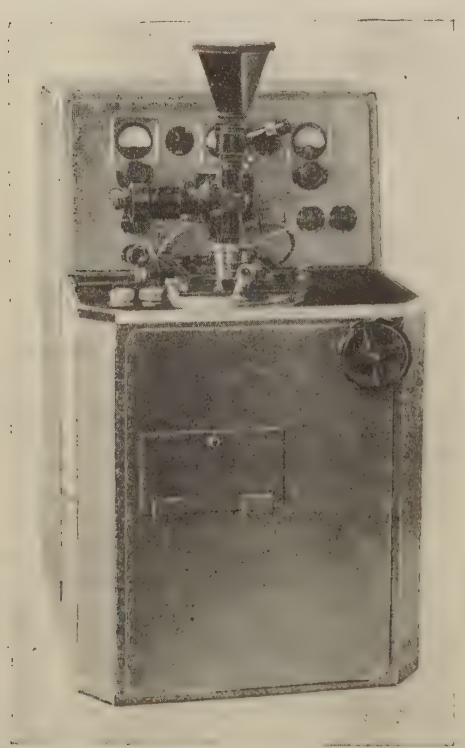

Fig.1. UIT-3 ionic etching unit.

It is desirable to have the possibility of observing the surface of the specimen in the process of etching in the indicated temperature range. Through such observation, for example, one can follow the dynamics of transformation in alloys and obtain information on the structure of the specimen and the changes occurring therein at the etching temperature.

For the purpose of investigating the surface structure of different substances under conditions analogous to those encountered in operation, ionic etching can be combined with mechanical deformation (elongation or compression). As noted above, the UIT-3 ionic etching unit has provision for exposing the specimen to various external factors in the process of etching.

A photograph of the unit is reproduced in Fig.1. The principal assemblies and components of the UIT-3 are a vacuum system, a power supply, a control panel, a device for stretching or compressing the specimens, a metallographic microscope, and equipment for ionic etching and heating of the specimens.

The vacuum system of the UIT-3 unit is

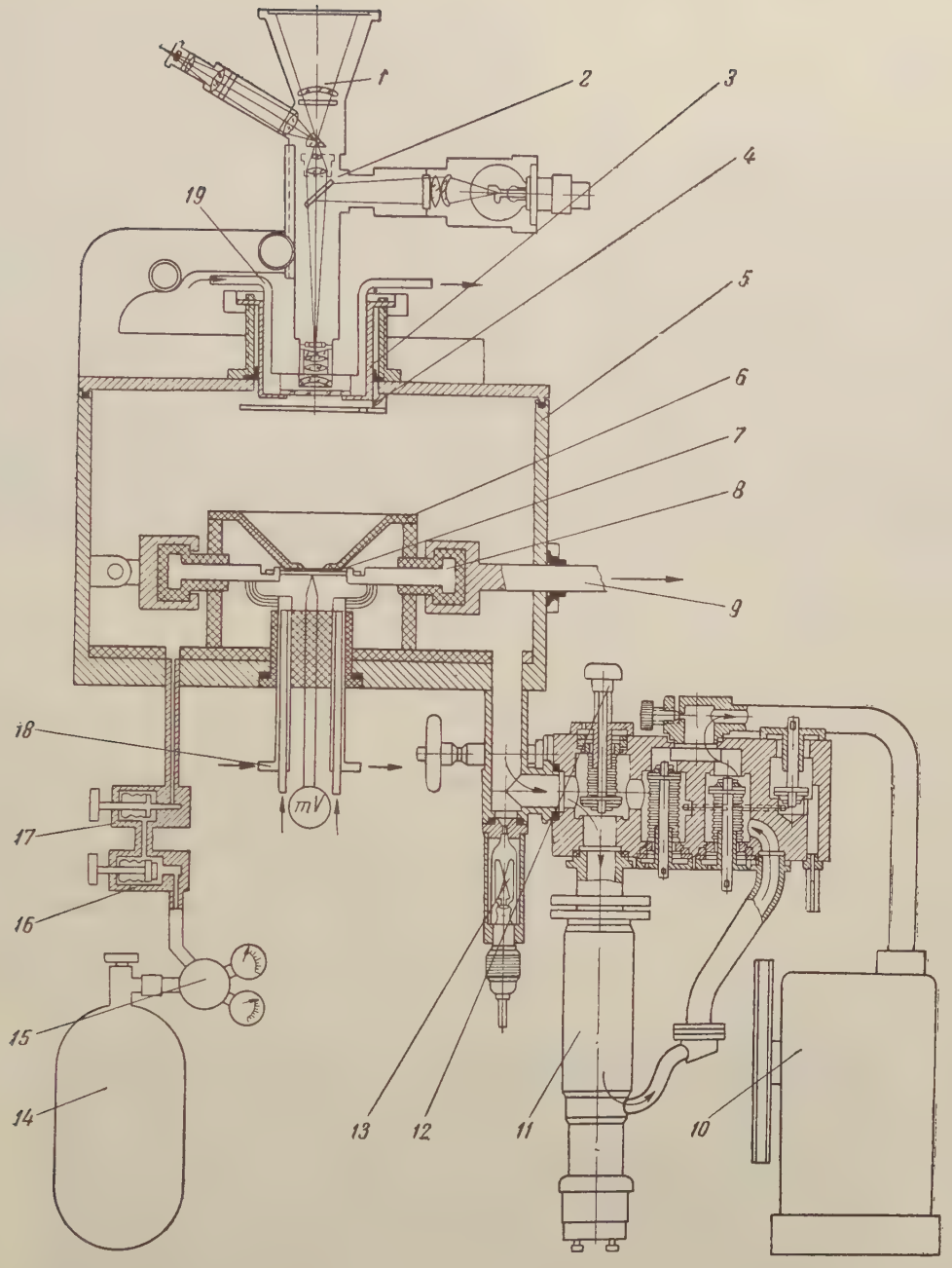

Fig.2. Diagram of the UIT-3 unit: 1) MFN-2 microphotographic attachment, 2) MVT metallographic microscope, 3) movable cup with a quartz window, 4) protective shield, 5) working chamber, 6) ceramic shield for specimen, 7) specimen with thermocouple, 8) specimen holder with insulator, 9) rod for stressing the specimen, 10) VN-461 fore pump, 11) TsVL-100 oil diffusion pump, 12) vacuum limiter, 13) LT-2 vacuum gage tube, 14) tank with inert gas, 15) reducing valve, 16) gas valve, 17) needle valve, 18) cooling contacts for specimen, 19) cooling of quartz window.

similar to the system employed in the original UIT-1 model. A VN-461 fore vacuum pump and a TxVL-100 oil diffusion pump can provide a vacuum down to $1 \cdot 10^{-4}$ mm Hg

in the working space. Flexible control of the vacuum is provided by a system of valves and a vacuum distributor. Etching is best realized at a pressure of $1 \cdot 10^{-}$ $-1 \cdot 10^{-2}$ mm Hg in a current of inert gas or air. The necessary pressure in the vacuum chamber is maintained by controlling the inflow of inert gas and regulatin the pumping. The inert gas, which is stored in a steel tank at a pressure of 100 atm, is admitted through a reducer and a needle valve.

The electric system of the unit comprises the following components: 1) a 10 kv, 50 ma high voltage rectifier, 2) a filament transformer (7 v, 250 amp) with switches to supply the voltage either to the specimen for heating or to the vapor izer, 3) a platinum-platinorhodium or chromel-alumel thermocouple connected to a suitably calibrated millivoltmeter, 4) a pump starting and control system and gages for monitoring the vacuum, and 5) a system of interlocks and release valves to insure the safety of the operator and equipment.

The arrangement of the ionic etching apparatus is diagramed in Fig.2. The specimen, if not subjected to stress, may be of arbitrary shape. It is desirable that the maximum size of the specimen not exceed 30 x 30 x 8 mm. If the specimen must be heated up to 1200° during etching, its size should not exceed 20 x 20 x 2 mm. Specimens with a maximum cross section of 20 mm^2 and a length of up to 60 mm can be subjected to a tensile or compressive loads of up to 400 kg in the process of etching.

For normal etching the specimen is mounted in the steel working chamber whic is made in two parts. The upper removable part of the chamber has a viewing wind for observing the process of etching. When microscopic observation of the specim surface is desired the upper part of the chamber is replaced by a special attachment which incorporates a metallographic microscope with a long focus objective (f = 15-16 mm; magnification up to 300 X).

The main difference between the present attachment and those used in earlier models of the unit is that the viewing quartz window is movable: the distance of the window from the surface of the specimen can be varied from 10 to 60 mm. During ionic etching or deposition of films by evaporation the viewing window is raised by means of a special mechanism controlled from the outside. At the same time the window is automatically covered by a shutter which simultaneously serves as the anode in the process of sputtering (the specimen is the cathode).

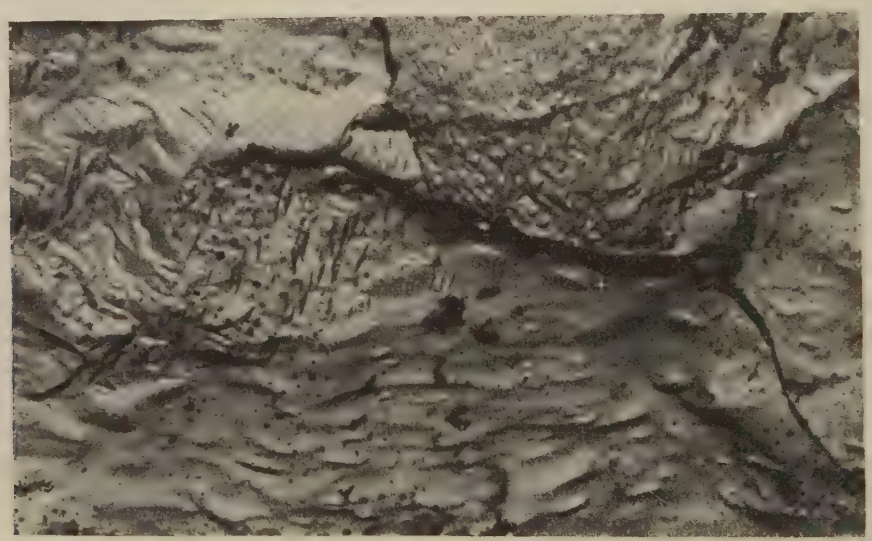

Fig.3. Steel surface subjected to ion bombardment (carbon replica). 10 000 X.

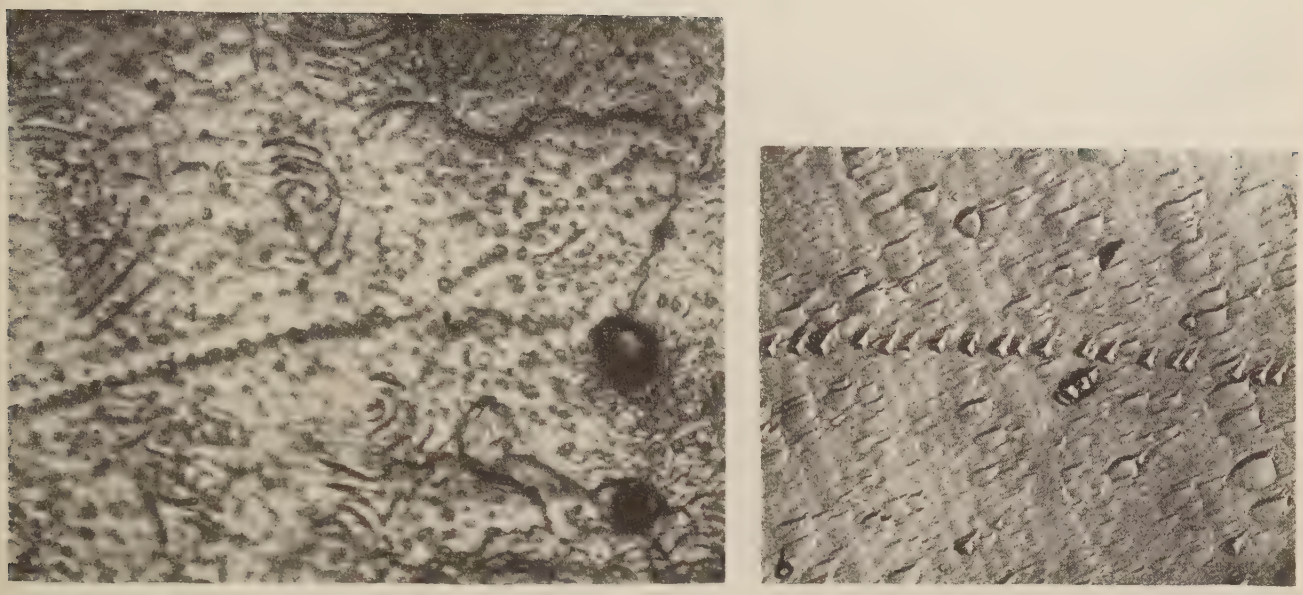

Fig.4. Dislocation chains on surface of cadmium (a) and germanium (b) brought out by ionic etching. Photograph b was obtained by I.G.Sirotenko.

Lead-ins are provided in the bottom of the working chamber for high and low voltage to the specimen and for the leads to the thermocouple. The leads are brought in through a porcelain plug sealed with a rubber gasket. The lead-ins and base of the chamber are protected by ceramic.

The device for loading the specimen is built into the walls of the chamber; the loading is realized by means of two steel rods insulated from the high voltage. One rod is fixed; the other goes out through a rubber diaphragm and is linked to a lever that can be loaded with weights. (We have also developed a pneumatic loading device.)

Specimens not subjected to mechanical stress are heated by means of a molybdenum spiral. Specimens subjected to loads can be heated up to 1200° by passing a suitable current directly through the specimen (the contacts are water cooled). For accelerated etching and also for etching at room temperature the specimen can be mounted in a special water cooled copper holder. Use of this cooling arrangement makes it possible to carry out ionic etching at high current densities (up to 15 ma/cm^2) without danger of fusing the surface. Etching under the forced cooling conditions greatly reduces the time necessary for bringing out the surface structure of metals.

As noted above, immediately after ionic etching one can deposit a silica, metal or carbon film on the surface of the specimen; this replica can then be examined in an electron microscope. By way of illustration in Fig.3 we reproduce a micrograph of a carbon replica from an ion etched steel surface. It will be seen that as a result of ion bombardment there have been clearly brought out the grain boundaries and the submicroscopic relief inside the grain.

Under the influence of ionic etching there may form on the faces of single crystals etch pits with the symmetry of the given face. In the process of cathode sputtering there form on the crystal surface oriented figures with a symmetry corresponding to the face on which they are located; this can be utilized for determining the Miller indices of the crystal faces.

The potentialities of the ionic etching technique are also illustrated by the photographs reproduced in Fig.4: micrograph a shows a branching chain of dislocations on a cadmium crystal; micrograph b shows dislocations brought out by ionic etching on a small-angle face of a germanium single crystal.

The use of ionic etching for bringing out dislocations appears highly promising; this technique should be particularly useful in the case of heated specimens when chemical etching is impossible.

Physics Faculty,
Moscow State University

References

1. G.V.Spivak, V.E.Yurasova, F.F.Kushnir & I.N.Prilezhaeva, PTE (Instruments & Experimental Techniques) No.2, 106 (1957).
2. V.E.Yurasova, G.V.Spivak & F.F.Kushnir, Izv.AN SSSR, Ser.fiz., 23, 744 (1959). (Trans.Bulletin, 23, 739.)
3. McCuthen, J.Appl.Phys., 20, 414 (1949).
4. T.R.Padden & F.M.Cain, Metal Progr., 66, 108 (1954).

* * * * * * *

MAGNETIC OBJECTIVE LENS FOR AN EMISSION ELECTRON MICROSCOPE

- A.M.Rozenfel'd & P.V.Zaitsev

The results of experimental studies[1] carried out a few years ago, led us to the conclusion that further improvement of the resolution of the ÉÉM-50 emission microscope could be attained by replacing the electrostatic objective, used as the first magnification stage in this microscope, by a magnetic lens. Subsequently, Fert & Simon[2] working independently came to a similar conclusion and developed a magnetic objective for a microscope used for investigating secondary emitters. Below we describe the design and some of the characteristics of the magnetic objective which was developed for use in the ÉÉM-50 emission microscope for investigating thermionic and secondary emitters.

Design of the Magnetic Objective

The magnetic objective lens is diagramed in the accompanying figure. This lens consists of an iron housing 1, with a ring 2 of nonmagnetic material, a winding 3 and a holder 4 with a conical end for receiving the pole piece with the anode aperture 5. The holder 4 also serves as the mount for the mechanism 6 for displacement of the diaphragm (aperture) 7, both along the axis of the lens and in the plane normal to it. This diaphragm divides the internal volume of the microscope into two parts, in one of which (including the specimen chamber) there is maintained a relatively high vacuum (10^{-6} mm Hg). In addition, under certain conditions, mainly in studying secondary emitters, the diaphragm can help enhance the resolution of the objective.

The magnetic objective lens is connected directly with the specimen chamber inside which is located the stage 8 with a mechanism for displacing the specimen

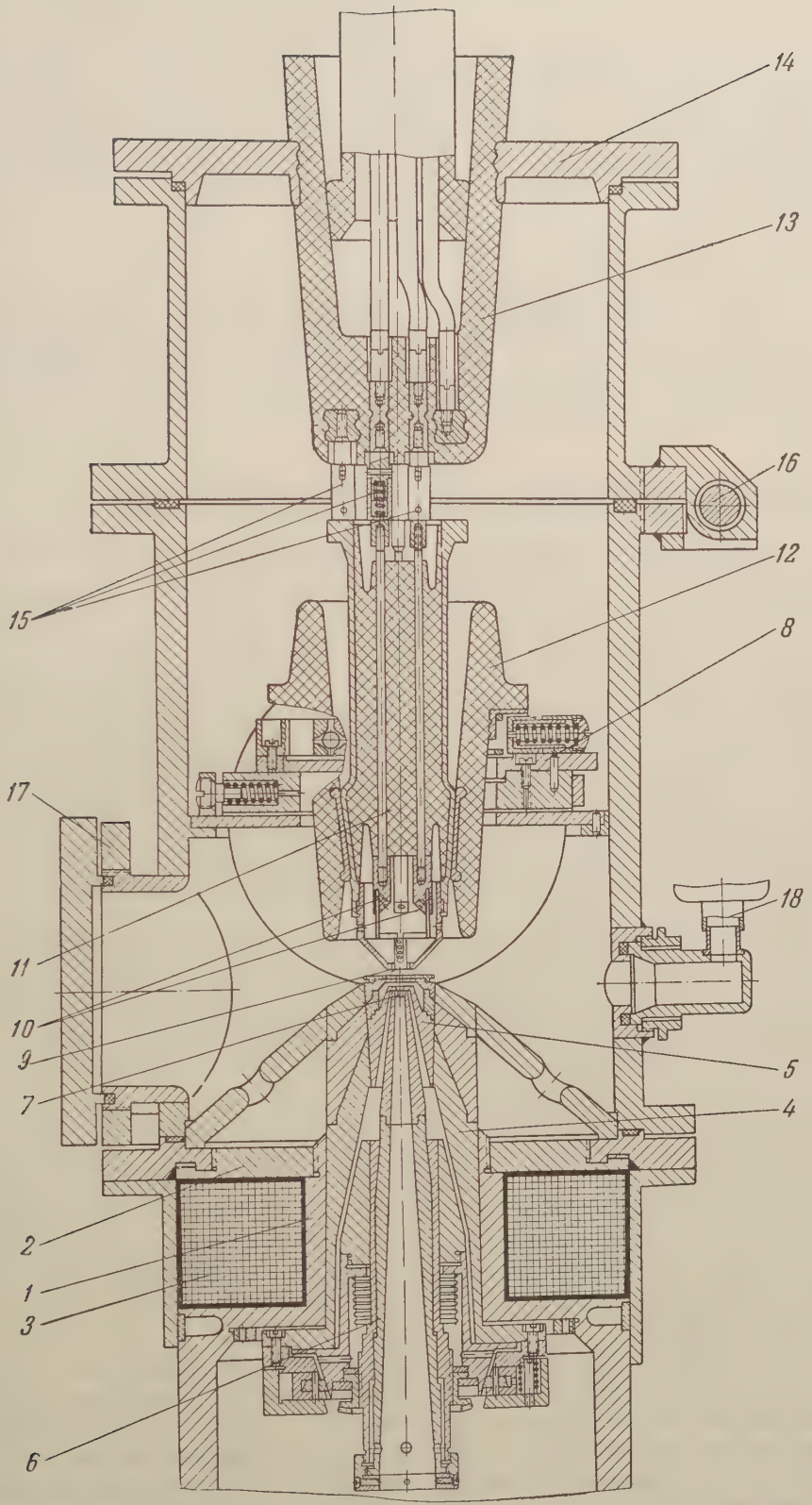

Section diagram of the magnetic objective lens: 1) housing, 2) nonmagnetic ring, 3) winding, 4) pole piece holder, 5) pole piece with anode aperture, 6) mechanism for displacing aperture 7, 8) specimen stage, 9) specimen, 10) current-carrying rods, 11) specimen holder, 12) insulator, 13) duct insulator, 14) cover, 15) spring contacts, 16) hinge, 17) flange, 18) pressure gage sensing element.

9 in the plane perpendicular to the beam axis (in two mutually perpendicular directions). The specimen 9 is mounted on the current-carrying rods 10 of holder 11, which by means of insulator 12 is insulated from the grounded components of the stage mechanism. The high voltage and the voltage for supplying the specimen heater are brought in through the high-voltage insulator 13, mounted on the cover 14 of the specimen chamber. This insulator is equipped with sliding spring contacts 15, which insure good electrical contact with the current-carrying rods of holder 11 in all positions of the specimen stage. For interchange of specimens one must open the upper part of the chamber, which swings on the hinge 16, and pull the specimen holder 11 out of the insulator.

The specimen chamber has a flange mounted port, which serves for attaching an ion or electron source in cases when it is desired to use the microscope for investigating bulky secondary emitters.

The vacuum in the specimen chamber is measured by means of an ionization gage, the sensing element of which communicates directly with the inside of the chamber.

Parameters and Properties of the Objective Lens

The above described magnetic objective lens was installed and tested as the first stage of magnification in an ÉÉM-50 electron microscope.

It was established that if certain conditions are satisfied, in particular if the vacuum in the specimen chamber is of the order of 10^{-6} mm Hg and the shape and state of the surface of the cathode (i.e., specimen) generally meet the requirements set for the shape and state of the surface of high-voltage electrodes, then with a separation of 2-2.5 mm between the cathode and anode one can operate with an accelerating potential as high as 40 kv. In this case the field gradient at the cathode is of the order of 160 000 v/cm, i.e., has a value at which theoretically there may be attained a resolution of 100 Å. The attainable resolution in practice is better than 500 Å; it may therefore be asserted that the resolutic of the magnetic objective is better than the resolution attainable with the norma electrostatic objective lens.

On the basis of the test results one can identify the causes that stand in the way of attaining in practice the maximum theoretical resolution (100 Å).

1. The first cause is inadequate stability of the accelerating potential source and certain shortcomings in the system regulating the excitation current. These difficulties are not a matter of principle and can undoubtedly be overcome by improving the design of the circuit components.

2. The second cause is distortion of the image due to edge effects and noncoaxiality of the cathode section and the magnetic lens. Tests show that the quality of the image produced by the magnetic objective changes substantially, depending on the position of the cathode (specimen) relative to the lens. The quality of the image is best when the axis of symmetry of the cathode is aligned with the axis of the lens. An objective criterion for coaxiality is no change in the position of the image on the screen with changes in the excitation curren in the lens winding (focusing).

Thus in working with the given magnetic objective we encounter a difficulty of principle, i.e., a difficulty inherent in the design of the lens: in practice one can obtain a high quality image only of a small area of the specimen. This area corresponds to the position of the specimen stage for which the axis of sym metry of the cathode section coincides with the lens axis. Any displacement of the stage for the purpose of examining other areas of the specimen is accompanie by disturbance of the coaxiality and, consequently, impairment of the image qual

Further studies are necessary to determine how and to what extent this difficulty can be obviated.

3. The third cause is different types of roughnesses and unevennesses of the specimen surface, which give rise to so-called microlenses that distort the topography of the electric field between the cathode and the anode and impair the resolution of the objective lens. Such unevennesses and microfields are inherent in the emission procedure in general and are always present regardless of the type of optics used for imaging the surface being investigated in an emission electron microscope.

References

1. A.M.Rozenfel'd, Thesis, Scientific Research Institute of the Ministry of the Radio-Engineering Industry, M., 1955.

2. C.Fert & R.Simon, J.phys.et radium, 18, 875 (1957).

INVESTIGATION OF THE MAGNETIC CIRCUITS OF ELECTRON MICROSCOPE LENSES

- P.A.Stoyanov & L.Yu.Vol'fson

Adjustment of electron microscopes is complicated by the presence of asymmetrical stray magnetic fields in the column of the instrument. The asymmetry of the stray fields may be due to inhomogeneity of the magnetic material, particularly, to the presence of cracks; it may also be caused by nonsymmetrical arrangemen of the various magnetic components, such as permalloy shields, iron parts of the specimen stage, etc. A significant role is also played by nonsymmetrical locatio of holes in the magnetic fittings and nonuniform clearances between mating parts (pole pieces, flanges, housing, etc.).

There are two ways in which the effect of stray fields on the electron trajectories can be minimized. These are 1) symmetrical arrangement of the ferromagnetic parts, symmetrical location of all holes therein and careful finishing of all the contacting surfaces, as well as the use of magnetic materials that are as homogeneous as possible, and 2) reduction of the stray fields per se. One of the factors giving rise to stray fields is the drop of the magnetic potential along the magnetic circuit. The magnitude of this drop depends on the geometry of the magnetic circuit and the properties of the material employed. The usual material used at present for magnetic circuits is pure iron which after annealing commonly at a temperature of 900-950°, has a maximum permeability of 3000-3500 gauss/oe and a coercive force 1.3 oe. Use of a material with a greater permeability should make it possible to weaken the stray fields.

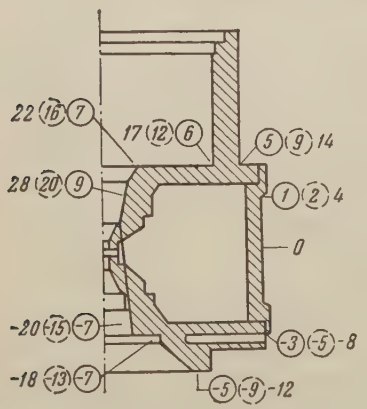

Fig.1. Drop of magnetic potential (in ampere-turns) along the shell (cladding) of the lens circuit of nonannealed iron at different values of the magnetomotive force (2000, 4000 and 6000 ampere-turns).

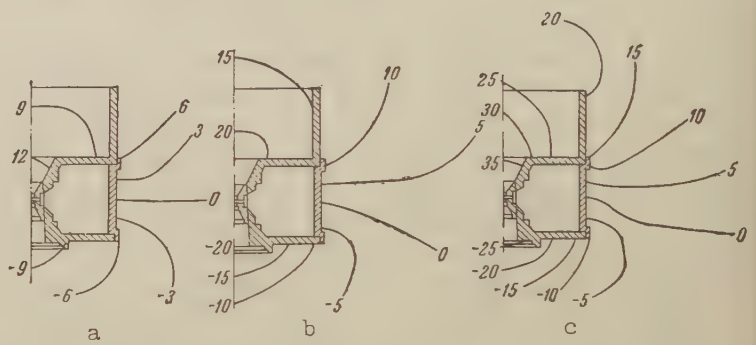

Fig.2. Equipotential surfaces of the stray fields and the magnetic potential drop along the shell of the lens with a circuit of annealed iron at different values of the magnetomotive force: a) 2000, b) 4000 and c) 6000 ampere-turns.

The purpose of the present work was to evaluate Mo permalloy 79NM as a potential material for magnetic circuits. Mo-permalloy has a maximum permeability of 100 000 to 200 000 gauss/oe for large cross sections. We constructed and tested three objective lenses for the UÉMV-100 microscope; these had magnetic circuits of Mo-permalloy, annealed iron and nonannealed iron. The relatively low saturation magnetic inductance of Mo-permalloy (7500-8000 gauss) required a somewhat larger cross section of the magnetic circuit components than in the case of iron. The Mo-permalloy circuit was designed so that the flux density would not exceed 5000 gauss at a magnetomotive force of 5000 ampere-turns.

In view of the high sensitivity of permalloy to mechanical stresses, parti-

cular attention was given to annealing in order to eliminate the effects of stresses arising as a result of machining. The effect of each mechanical operation on the properties of the permalloy was determined by tests. We settled on a two-stage annealing process. The components, machined with a suitable allowance, were first annealed at 1100° and then again, after final machining, at 900°. This procedure resulted in optimum magnetic properties and minimized warping of the components as a result of annealing to relieve residual stresses. Nevertheless it must be noted that appreciable forces were applied to the lens components in the process of assembly which, according to tests, led to some deterioration of the magnetic properties.

The drop of magnetic potential along the circuits was studied by means of the ballistic method, using a highly sensitive magnetic potential meter (Rogovskii belt). The magnetic potential was measured at various points along the magnetic circuit as well as in the space surrounding the lens. The magnetic potential at points on the periphery of the shell in the central plane of the lens was taken as zero. The measurements were made at values of the magnetomotive force equal to 2000, 4000 and 6000 ampere-turns, and in the case of the permalloy component lenses also at 5000 ampere-turns. Since it has been shown that the stray fields in magnetic lenses made of iron depend on the magnetic history of the components, all the test lenses were magnetized with a magnetomotive force of 6000 ampere-turns prior to measurement. This created conditions close to those prevailing during normal operation.

Fig.1 shows the potential drop along the shell of the lens with a magnetic circuit of nonannealed iron. Three values of potential are given for each point: the figures in solid circles are for 2000 ampere-turns, those in dashed circles are for 4000 ampere-turns and those not circled are for 6000 ampere-turns. It will be seen that the dependence of the magnetic potential drop on ampere-turns is almost linear.

The results for the lens with magnetic circuit components of annealed iron are shown in Fig.2. Here, in addition to the potential drop along the magnetic circuit, we show the shape of the equipotential surfaces in the space surrounding the lens. Comparison of these data with those for the lens with nonannealed iron components shows that annealing has no effect on the potential drop in the magnetic circuit and, consequently, on the magnitude of the stray fields. In fact, the potential drop in the nonannealed iron circuit is somewhat lower than in the annealed iron one, which may be explained by the appreciable scatter in the properties of the material.

The most interesting results were obtained in the case of the Mo-permalloy component lens (Fig.3). The potential drop along the magnetic circuit at 2000 ampere-turns (solid circles), 4000 ampere-turns (dashed circles) and 5000 ampere-turns (dash-dot circles) is very small. At 2000 ampere-turns the values of the potentials are at the threshold of sensitivity of the potential meter. At 5000 ampere-turns the total potential difference is of the same order of magnitude as in the case of the iron lens with excitation equal to 2000 ampere-turns. With increase of the magnetomotive force to 6000 ampere-turns the situation changes radically. The drop of potential in this case is considerably greater than in lenses with iron components at the same value of the magnetomotive force. This is due to the fact that in this range the permalloy approaches saturation. It should be noted, however, that the maximum value of the magnetomotive force during normal operation usually does not exceed 5000 ampere-turns; as noted above, the design of the magnetic circuit was based on this value. Consequently, the experimental data show that the design calculations were basically correct.

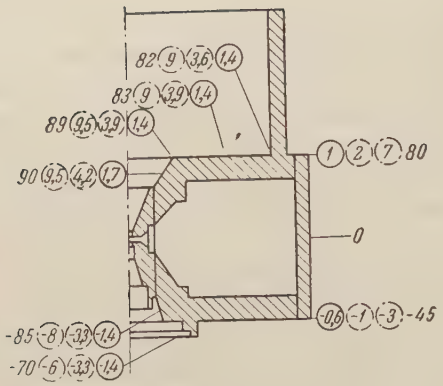

Fig.3. Drop of magnetic potential along the lens shell for the Mo-permalloy circuit at different values of the magnetomotive force: 2000, 4000, 5000 and 6000 ampere-turns.

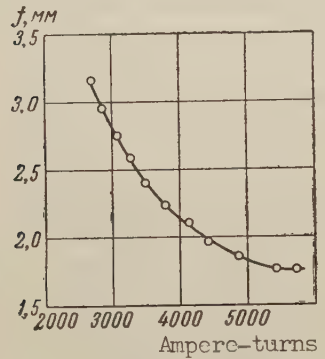

Fig.4. Variation of the focal length with the magnetomotive force for the permalloy component lens.

The lens with the permalloy components was tested in the microscope. We determined the variation of the focal length with the magnetomotive force (Fig.4). With increase in the number of ampere-turns, the focal length decreases monotonically; it does not, however, go through a minimum in the test range of ampere-turn values. This agrees with the results described above, and attests to the possibility of using lenses with permalloy circuit components at high values of magnetomotive force.

Another advantage of the lens with permalloy circuit components was brought out during the tests in the microscope: because of the small coercive force (~0.015 oe) and, consequently, the narrow hysteresis loop of permalloy, the optical characteristics of the lens are determined almost uniquely by the strength of the magnetizing current.

Thus the use of Mo-permalloy for the magnetic circuit components of objective lenses has the following advantages: 1) a considerable reduction of the stray fields and 2) a virtually single-valued dependence of the optical properties of the lens on the magnetizing current.

References

1. M.E.Haine & P.S.Page, Proc.of the Stockholm Conf.on Electron Microscopy, p.32 (1956).

2. B.Borries, F.Lenz & G.Opfer, Optik, 10, N 1/3, 132 (1953).

MODERNIZATION OF THE UÉM-100 ELECTRON MICROSCOPE

- G.V.Der-Shvarts, Yu.M.Kushnir, L.B.Rozenfel'd, P.V.Zaitsev & S.V.Bezlepkin

The UÉM-100 microscope was in production from 1952 to 1957; during this period over 60 instruments were built and sold. Many users note that the UÉM-100 electron microscope is very dependable in service and simple to maintain.

According to the classification established by Kushnir[1] and Vertsner[2], this instrument is a Class III microscope. Borovyagin & Kuptsov[3], however, showed that by making certain modifications which can be realized in any well equipped laboratory, the resolution of the instrument can be increased to 15-20 Å. In other words, the microscope can be converted to a Class II instrument.

A number of users of the UÉM-100 microscope, mainly metallurgists, have expressed a desire to see this instrument adapted for microdiffraction studies.

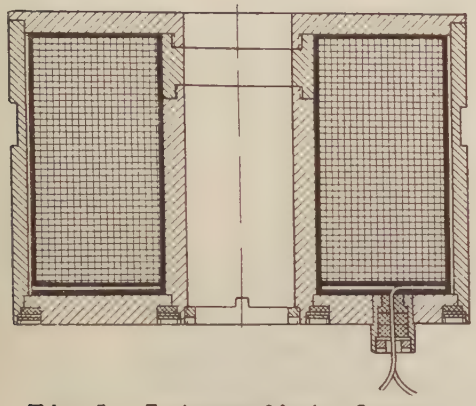

Fig.1. Intermediate lens.

This can be done by introducing an intermediate lens (Fig.1), which should be located in the tube of the objective lens. The shell and leads of the intermediate lens are provided with seals so that the vacuum in the instrument column is not disturbed by the intermediate lens. The dimensions of the lens must be small in view of the limited space available in the objective tube. This lens is installed on the flange of a stage mounted on the pole piece holder of the projector lens. The intermediate lens is centered by means of three knobs on screw shafts brought out through the objective tube through suitable rubber seals. Since this lens operates only for demagnification, the necessary magnetomotive force is relatively small (maximum 1000 ampere-turns). The lens is supplied from a 12 volt battery (for example, two 6ST-128 cells). A special cat's eye type selector aperture is built into a special cover which replaces the standard cover of the objective lens tube. The selector aperture can be displaced in the plane perpendicular to the optical axis by a special mechanism located on the cover. In addition, the aperture can be tilted relative to the axis. This tilting changes the size of the triangular opening in the selector aperture. Its edges are so wide that they overlap the opening of the lens bore. Hence there is no need for an additional background suppressing aperture in the intermediate lens.

An intermediate lens and selector aperture of the above-described design were installed in a UÉM-100 microscope and tested extensively by investigating pyrolytic carbon films (by M.L.Petrova).

Fig.4 is a micrograph of a section of an antimony film defined by the triangular selector aperture; Fig.5 is an electron diffraction pattern recorded from this section.

In addition to the intermediate lens and selector aperture, it is desirable to build into the UÉM-100 microscope a mechanism for adjusting the illuminating (gun) aperture. A diagram of this mechanism is shown in Fig.6. The illuminating aperture is adjusted by means of two knobs that are brought out on the housing of the condenser lens above its winding. The return springs of the mechanism are mounted inside the anode housing.

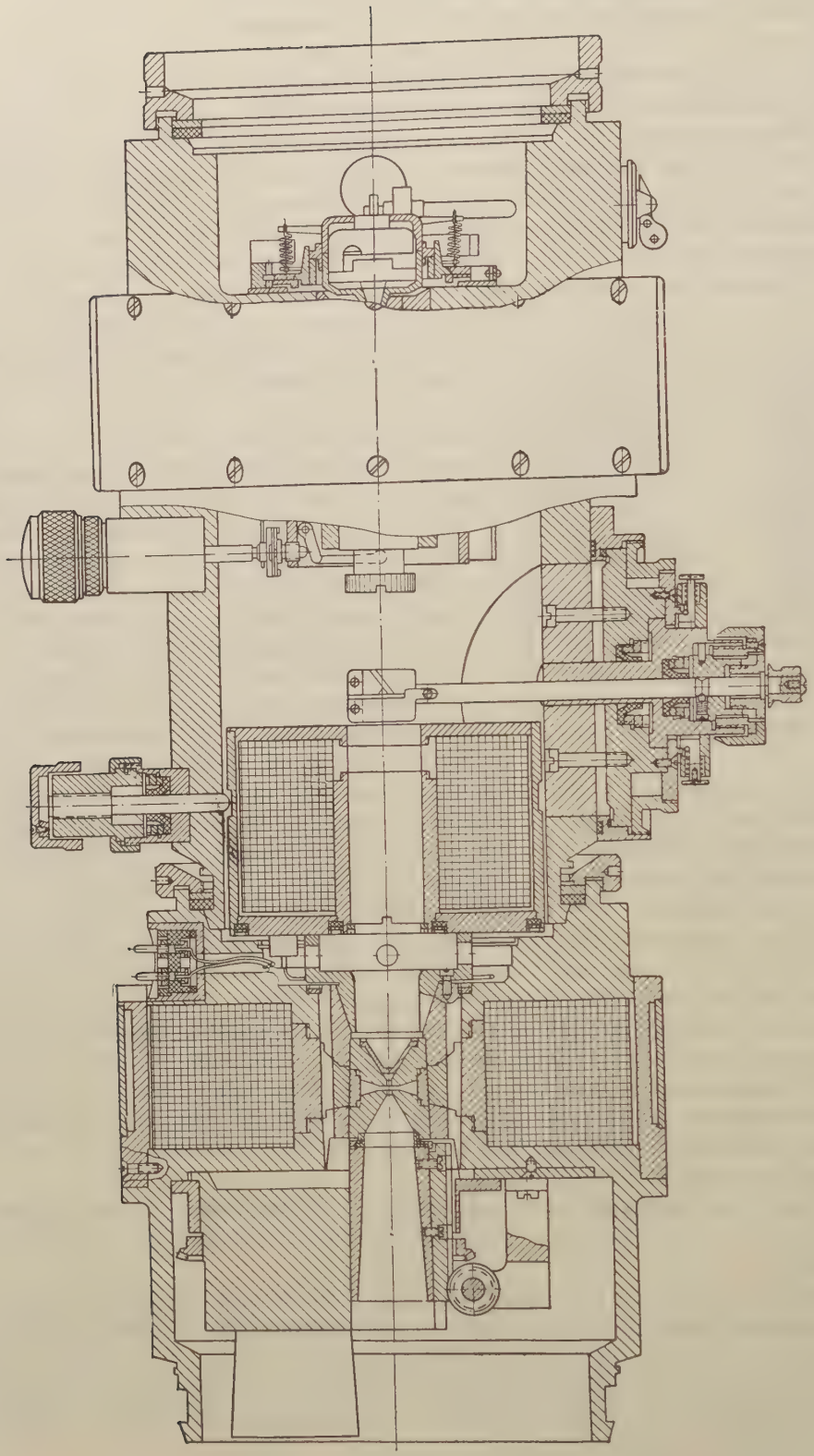

Fig.2. Location of the intermediate lens and selector aperture in the column of the UEM-100 microscope.

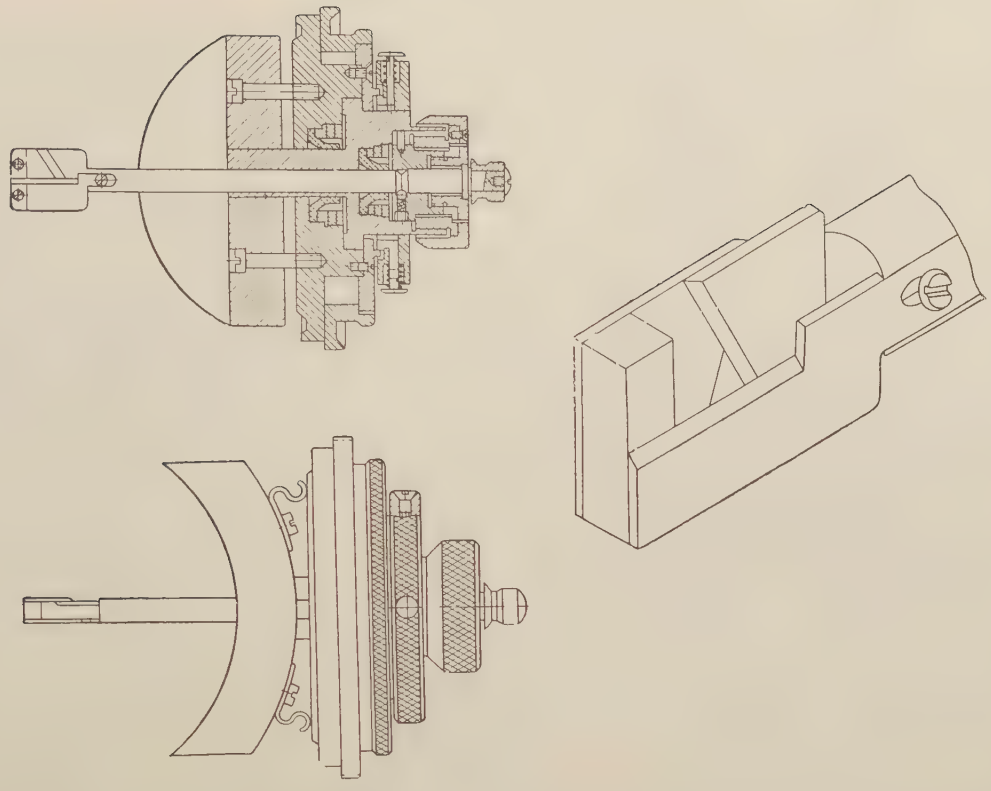

Fig.3. Selector aperture mechanism.

Fig.4. Section of an antimony film isolated by the selector aperture.

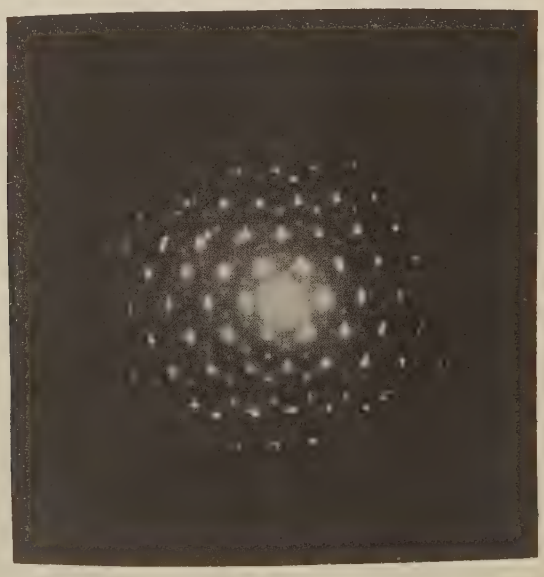

Fig.5. Electron diffraction pattern from the section of the antimony film shown in Fig.4.

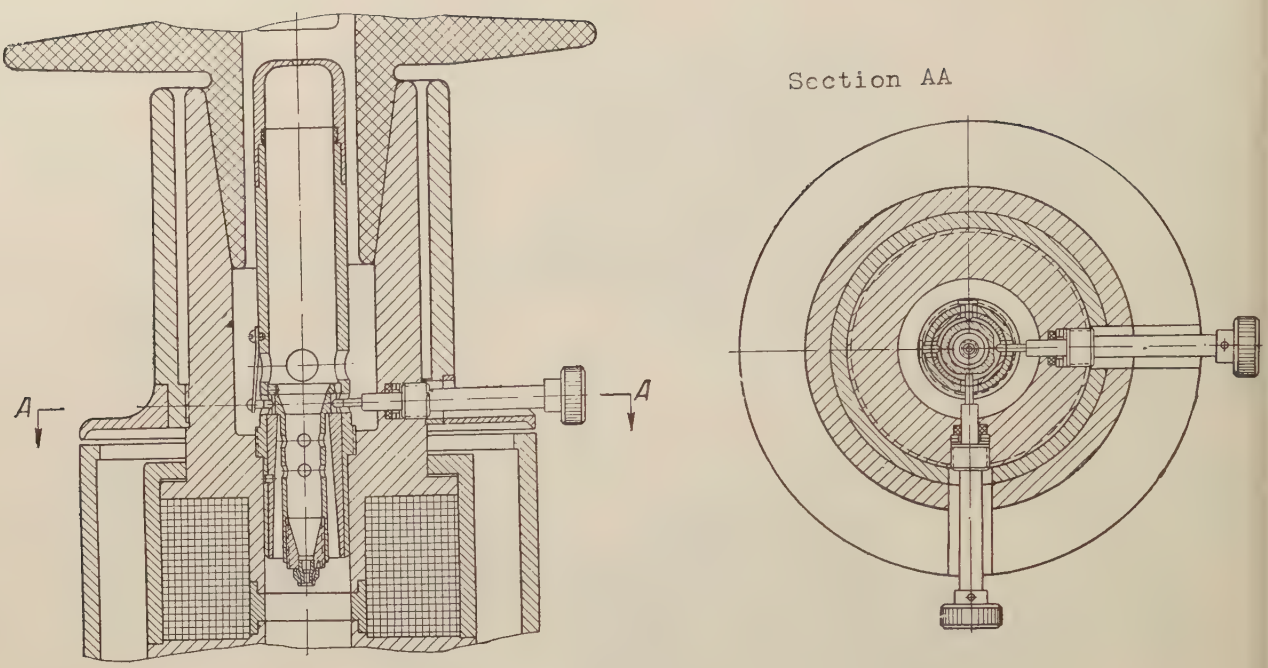

Fig.6. Illuminating aperture adjustment mechanism.

References

1. Yu.M.Kushnir, PTE, No.4, 3 (1958). (Trans.Instruments & Experimental Techniques.)

2. V.N.Vertsner, Izv.AN SSSR, Ser.fiz., 23, 426 (1959). (Trans.Bulletin, 23 413.)

3. V.L.Borovyagin & M.G.Kuptsov, Biofizika, 5, No.3, 366 (1960). (Trans. Biophysics.)

ELECTRON-OPTICAL MEASUREMENTS OF ELECTRIC AND MAGNETIC MICROFIELDS ON SURFACES

- N.N.Sedov, G.V.Spivak & N.F.Isaeva

In the present work we carried out experimental investigations of the relationship between the magnitude of the local microfield on the surface of an electron emitter and the contrast of the picture in the image plane in an emission electron microscope. Knowing this relationship, in addition to observing the electric and magnetic microfields on the surface of an emitter, one can be means of an emission electron-optical system determine the intensity of the local microfields.

In earlier contributions[1-4] we showed that in utilizing secondary and photoemission and also an electron mirror in emission and quasiemission systems, one can observe surface electric and magnetic microfields. We note that the "dark field" electron-optical procedure allows of observing and measuring the microfields only at the edges of the specimen and not over its entire surface.[5]

By means of a secondary emission attachment to the ÉÉM-75 emission electron microscope we investigated the structure and topography of efficient thermionic cathodes. The use of the secondary attachment gave two advantages as compared with the case of utilizing only thermionic emission. First, the contrast of the secondary emission picture owing to local variation of the secondary emission coefficient yields valuable information on the structure of the specimen*; second, the temperature range of investigation is greatly expanded. As a result of such observations there can be established a correlation between the structure of the thermionic emitter and its emission.[6] Similar inferences can be drawn on the basis of combined observation of photo and thermionic emission in the same emission microscope.[3]

The possibility of observing microfields is due to the interaction with them of the slow electrons emerging from or reflected from the surface. Even in the range of relatively small magnifications the electron-optical procedure for recording and measuring microfields has a distinct advantage over the methods of an induction coil or a bismuth wire (for magnetic fields), inasmuch as the dimensions of these sensing elements can be reduced only to a certain extent, so that they are incapable of distinguishing fine details.

A distinctive feature of observation of microfields in an emission or quasiemission system is the fact that the focal plane for them does not coincide with the geometric surface of the cathode.[1] This is understandable if we consider the mechanism of formation of contrast under the influence of local microfields. The initial density distribution of the electrons from the emitting surface changes with increasing distance from the cathode surface. At a certain distance from the cathode the contrast, owing to the effect of the microfields, attains a maximum, and then falls off owing to blurring because of increase of the electron velocities.

If the cathode surface is smooth, there can be distinguished two focusing planes: the plane of the geometric surface and the plane of the microfields, corresponding to maximum contrast of the image. In the case of a rough cathode, it is difficult to speak of precise focusing of the image of the surface, i.e., no

---

*The contrast of the thermionic picture is determined by the value of the work function at the given point and its surroundings (patch fields); the work function has a lesser effect on the magnitude of the secondary emission when a lesser role is played by the thin surface layer, and the contrast of the secondary emission picture is determined to an appreciable extent by the structure of the substrate.

Fig.1

single focusing position gives the true distribution of the emission from the cathode surface.

Thus it may be asserted that in general for complete interpretation of the image one must obtain and study not only the sharpest focus image but a series of images corresponding to displacement of the focal plane within a certain range Δ near the surface of the specimen (Fig.1).

In other words, in studying the state of the surface of a specimen in an electron microscope, one must obtain not some one image but a set of images in different planes near the surface of the specimen. In general the image is affected by the following factors: the microgeometry of the cathode, the emission distribution over the surface, patch fields, magnetic microfields and the microlenses formed by space charges. In general, therefore, interpretation of the image, i.e., separation of the effects of all these factors, is very complicated. The problem is simplified, however, if some of these factors are absent or negligible.

Quantitative evaluation of magnetic microfields

Let us consider the simple case when the surface of the cathode is smooth, the emission is uniform and patch fields are absent. There are present an external (close to the surface) electric field and magnetic microfields. This case corresponds to an inhomogeneously magnetized ferromagnet observed using secondary or photoemission.[1,2] If it is assumed that the radius of the spiral trajectory of an electron in the magnetic field of strength H is much smaller than the dimensions l of the magnetic field inhomogeneities, i.e.,

$$\frac{c}{H}\sqrt{m\varepsilon} \ll l, \tag{1}$$

where ε is the initial electron energy, it may be assumed that the electrons will approximately follow the magnetic lines of force, winding about them. In this case simple calculations show that with focusing in the plane of maximum contrast one can expect the following relation to obtain for the electron flux densities

$$j_1 / j_2 = H_2 / H_1, \tag{2}$$

where the indices 1 and 2 pertain to field and electron flux density values over different sections of the specimen. This simple relationship can obviously be utilized for measuring inhomogeneous magnetic fields of very small size, provided the magnetic field over some one section of the specimen is known.

It is of interest to compare the formation of "magnetic" contrast in emission and mirror electron-optical systems. Whereas in the first case under certain conditions (described above), we can assume for the sake of simplicity that the slow electrons will wind about the magnetic lines of force, i.e., that both the normal (H_z) and the radial (H_r) components of the field will be effective, in the second case, when the electrons first approach and then move away from the surface of the specimen, only the normal component participates in the formation of the contrast. The effects of the radial component cancel each other over the forward and reverse paths of the electrons.

By focusing directly on the smooth surface of the cathode one can measure the density of the current from individual sections of the cathode, if one neglects the influence of patch fields. As was shown in Ref.3, patch fields produce distortion of the equipotential surfaces, and the tangential component of the patch

fields affects the contrast of the image (it was assumed that the external field is strong and compensates the normal component of the patch fields). The tangential component of the patch field in the case of a smooth surface will not be compensated by the external field; the error involved, however, will be the smaller, the stronger the external field (rapid convergence of the electron beam).

The microscope used in the present work was in general similar to that described in Ref.3. This is a combined metal-glass instrument, the vacuum in which with good outgassing attained $(3-5)\cdot10^{-7}$ mm Hg. The magnification ranged from 50 to 500 X. The present instrument differed from that described in Ref.3 by the presence of a Faraday cup located at the center of the screen. This enabled us to measure the density of the current to the screen. In addition, this instrument was constructed in several variants to permit observation of photoemission and of secondary emission from the surface of the specimen. In the last case, instead of the usual illuminating device, the microscope had a branch with an electron gun by means of which the specimen could be bombarded with ~100 ev electrons. Thanks to the incorporation of a heater, it was also feasible to observe the thermionic emission picture of appropriate cathodes.*

The possibility of measuring local magnetic fields was checked by observation of a number of artificial specimens consisting of alternating magnetic and nonmagnetic strips (for example, copper and iron). The end face of these specimens was polished, and the specimens were magnetized by an external magnetic field.

We compared the magnetic field distribution over the specimen and the density of the current to the screen with focusing on the plane of the magnetic inhomogeneities. For measuring the current density over different sections of the specimen the image was shifted by means of Helmholtz coils.

In a number of cases measurements were also made on the basis of the brightness of the screen, which was determined by means of an FEU-19 photomultiplier enclosed in a lightproof housing. This housing had an end opening 1 mm in diameter, which served to isolate the emission from a corresponding section of the cathode. The photomultiplier assembly could be shifted to scan the screen.

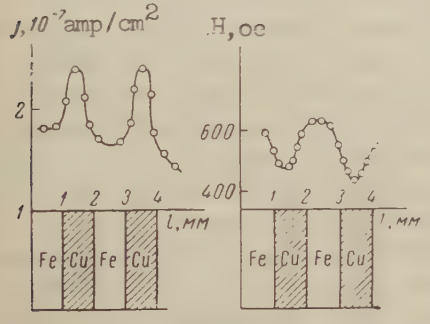

Fig.2. Current density to the screen and the magnetic field intensity over the surface of a specimen consisting of alternating strips of iron and copper.

The results obtained in measuring the brightness of the screen and from direct measurements of the current density to the screen agreed, inasmuch as in the range of current densities obtaining in the experiments the brightness of the screen was proportional to the current density. For control purposes, the magnetic field over the specimen was also measured by monitoring the resistance of a thin bismuth wire (50 to 100 mμ in diameter). This bismuth element was mounted in a fluoroplastic holder and could be moved over the surface of the specimen, insulation being provided by a thin layer of plexiglas dissolved in acetone. This microfieldmeter was calibrated by means of a coil with a known current dependence of the magnetic field.

Typical curves characterizing the variation of the magnetic field over the

---

*We take this opportunity to thank student E.Sh.Gasparyan who participated in the work.

surface of the specimen and the results of measuring the current in the electron microscope are shown in Fig.2, from which it will be seen that sections with a maximum field value correspond to minimum current densities, and vice versa. These measurement results show that relationship (2) holds to within 5-10% (the actual accuracy depends on the care with which the experiment is carried out, mainly on uniformity of illumination of the specimen). Thus by means of this procedure one can measure with reasonable accuracy microfields of very small area, i.e., of a size that defies measurement by other techniques.

We also carried out a number of measurements of magnetic fields over artificial inhomogeneities of the order of a tenth of a millimeter. At present we are using the described procedure for measuring natural magnetic microfields on different specimens.

Electric microfields on the surface of thermionic cathodes

We also investigated the surface of efficient thermal emitters. The surface of oxide-coated cathodes is usually very rough, hence results of measurements of the current density from different sections of the cathode do not correspond to the actual emission current density. In contrast, compressed nickel-oxide cathodes have a relatively smooth surface. In this case, in the absence of diaphragming of the beam[7], we can with an accuracy to the effect of the tangential component of the patch field determine the distribution in density of the emission current from individual sections of the cathode.

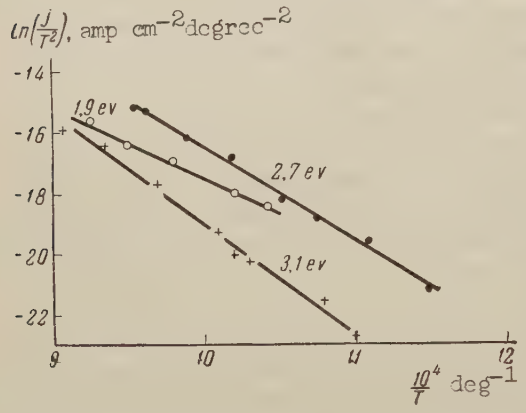

Fig.3. Richardson plots for individual microsections of a compressed cathode.

We measured the density of the current from individual sections of compressed cathodes in the temperature range from 600 to 800°C. The lower temperature bound was determined by the magnitude of the thermionic emission; the upper bound by blurring of the image under the influence of space charge.

On the basis of the temperature dependences of the current density we constructed Richardson plots for individual microsections (Fig.3). The values of the work function, determined from the slope of the Richardson lines, lay in the range from 1.9 to 3.1 ev. Most of the emitting patches had a work function close to the lower value.

Knowing the separation between patches and the magnitude of the contact difference of potentials, determined from the difference between work functions, one can evaluate the intensity of the patch fields. Our calculations show that the intensity is of the order of several kilovolts per centimeter.

Thus by means of emission electron-optical systems one can carry out not only qualitative observations but also quantitative evaulations of the magnetic and electric microfields on different surfaces.

Physics Faculty,
Moscow State University

References

1. G.V.Spivak, N.G.Kanavina, I.N.Chernyshev & I.S.Sbitnikova, Doklady AN SSSR, 92, 541 (1953); Ibid., 105, 706 (1955); G.V.Spivak, I.N.Prilezhaeva & V.K. Azovtsev, Ibid., 105, 965 (1955); G.V.Spivak, I.A.Pryamkova & E.Igras, Izv.AN SSSR, Ser.fiz., 23, 729 (1959) (Trans.Bulletin, 23, 723); I.S.Sbitnikova, G.V. Spivak & I.M.Saraeva, Ibid., 23, 734 (1959) (Trans.Bulletin, 23, 729); G.V.Spivak, E.Igras, I.A.Pryamkova & I.S.Zheludev, Kristallografiya, 4, 123 (1959) (Trans.Soviet Physics - Crystallography).

2. G.V.Spivak, T.N.Dombrovskaya & N.N.Sedov, Doklady AN SSSR, 113, 78 (1957). (Trans.Doklady.)

3. G.V.Spivak, I.A.Pryamkova & N.N.Sedov, Izv.AN SSSR, Ser.fiz., 24, 640 (1960). (Trans.Bulletin, 24, 648.)

4. G.V.Spivak, I.A.Pryamkova & V.N.Lepeshinskaya, Doklady AN SSSR, 130, 751 (1960). (Trans.Doklady.)

5. L.Marton & S.H.Lachenbruch, J.Appl.Phys., 20, 1171 (1949); L.N.Malakhov & Yu.V.Vorob'ev, Doklady AN SSSR, 125, 315 (1959) (Trans.Doklady); Izv.AN SSSR, Ser.fiz., 23, 765 (1959) (Trans.Bulletin, 23, 759); L.N.Malakhov, V.N.Vertsner & A.A.Lebedev, Izv.AN SSSR, Ser.fiz., 23, 770 (1959) (Trans.Bulletin, 23, 763).

6. I.S.Sbitnikova, E.M.Dubinina, G.V.Spivak & D.V.Fetisov, PTE No.5, 78 (1959) (Trans.Instruments and Experimental Techniques); Radiotekhnika i elektronika, 3, 1077 (1958) (Trans.Radioengineering & Electronics).

7. A.V.Druzhinin & B.N.Popov, Izv.AN SSSR, Ser.fiz., 23, 522 (1959). (Trans. Bulletin, 23, 502.)

PROCEDURE FOR DETERMINING THE WORK FUNCTION OF MICROSECTIONS ON THE SURFACE OF THERMIONIC CATHODES

- A.V.Druzhinin

Experimental procedure

The work function distribution over the surface of a thermionic emitter determines the size and extent of the contact microfields, which have a significant influence on the characteristics of the cathode current: the anomalous Schottky effect under saturation conditions[1], the magnitude of perveance under space charge conditions[2], and the deficit of slow electrons in the region of initial velocities[1]. Investigation of the work function distribution can also yield valuable information on the structure and nature of active centers.

Some data on the work function distribution can be obtained in investigating the integral current from the entire cathode surface as a function of the applied voltage under conditions of saturation or initial velocities. However, one cannot always draw unambiguous inferences from the results of such experiments. For example, for determining the magnitude of the inhomogeneities from the Schottky effect one must a priori know the form of the distribution function. From measurements of retarding potential curves[3], also, one cannot obtain the form of the work function distribution over the surface and, moreover, the low field intensity at the cathode in such measurements precludes determining the entire work function spectrum.

Electron-optical methods of investigation of thermionic cathodes in the case of inadequate resolution of the instrument allow only of determining the approximate size of the "patches" and their distribution over the surface of the specimen. It is, however, difficult to obtain quantitative data regarding the work function of individual patches by means of many electron-optical instruments. For example, the electron mirror procedure[4], while indicative of the emission distribution, does not allow of detailed interpretation of the electron-optical picture. The method of an electron probe[5] is unsuitable for the investigation of thermionic cathodes, owing to its low resolution and the necessity of investigating the cathode under conditions when the thermal emission is low.

The emission electron microscope is, probably, the most suitable instrument, for it provides for both visualization and quantitative measurements. Initially, emission images were interpreted quantitatively by photometry of individual sections of the micrographs.[6] Obviously, this procedure could not yield high accuracy. More precise investigations were carried out by measuring the currents in the plane of the image, which made it possible to determine the contact differences of potential at the cathode surface.[7,8] Hitherto, there was no simple procedure for determining the absolute value of the work function. Hence, experimenters did not have the possibility of correlating microscopic data with the results obtained in conventional emission studies.

Below we show that under conditions of good focusing and small aberrations of the emission image, using the values of the local current, the electron-optical magnification and the temperature of the cathode, one can unambiguously determine the work function of an isolated section of the surface.

Let us consider the trajectories of the electrons emitted by an element of the cathode located close to the optical axis of the emission microscope. As is known, the electron trajectories close to the cathode in an immersion objective lens have the form of elongated parabolas. The maximum diameter of the beam under the usual conditions does not exceed 20 microns; consequently, if there is no limiting diaphragm, all the electrons emitted by the central section are collected

without loss in the plane of the image of the immersion objective. The angle β of divergence of the electron beam can be calculated by the Abbe formula, the validity of which for an immersion objective was demonstrated by Artsimovich[9]:

$$\sin\beta = \sin\alpha \sqrt{\frac{\varepsilon}{U_a}} \frac{1}{N},$$

where N is the magnification of the immersion objective, U_a is the anode voltage, ε is the electron velocity, and α is the angle of the electron trajectory relative to the axis at the cathode.

Setting $N = 30$, $U_a = 25 \cdot 10^3$ v, $\varepsilon = 0.1$ ev and $\alpha = 90^\circ$, we obtain $\beta = 6 \cdot 10^{-5}$. With so small a divergence angle all the electrons will pass without loss through the projector lens of the microscope. For example, with a field of view of 50 mm and magnification of the projector lens equal to 50 X, the exit pupil of the projector lens will be 1 mm, which greatly exceeds the width of the beam in any ordinary instrument. Thus all the electrons emitted from the central section of the cathode will be collected in the plane of the image.

Measurement of the current from an element of the image is most easily realized by locating the electron collector behind an opening made in the center of the microscope screen. In this case the measured current is emitted by a section of the cathode, the area of which is determined by the diameter of the opening in the screen and the magnification of the microscope. From the calculated current density one can readily find the isothermal work function Φ_T of the corresponding section of the cathode, assuming that the emitted current is described by Richardson's equation

$$j = A(1 - \bar{R}) T^2 \exp[-e\varphi_T / kT].$$

It follows from thermodynamic considerations that A is a universal constant and does not depend on the type of emitter[10]; for pure metals it is usually assumed that $A = 120$ amp cm^{-2} deg^{-2} and $\bar{R} = 0$. The method of determining φ_T by means of Richardson's formula is now extensively used in investigating patchy emitters. However, Φ_T determined from the integral current does not have a clear physical meaning; in particular, the temperature coefficient of Φ_T is explained only by redistribution of the currents taken off different patches and not by growth of the potential barrier. Calculation of Φ_T by means of Richardson's formula in the case of measurements in an electron microscope is more justified, inasmuch as in this case there is investigated a homogeneous section, i.e., a patch.

The resolution of an emission microscope and, consequently, of the proposed procedure is determined mainly by the chromatic aberration of the immersion objective $\rho \approx \Sigma/E = 0.05$ μ for $\varepsilon = 0.1$ ev and a field intensity at the cathode surface $E = 20 \cdot 10^3$ v/cm) and aberration due to distortions of the field in the vicinity of the cathode surface. Surface roughnesses can give rise to appreciable distortions of the field. Even in the case of an absolutely smooth surface, however, the equipotentials near the cathode will be somewhat warped due to the perturbing influence of the patch field.[11] The influence of the perturbing field on the resolution was considered in detail by Bertain[12]. True, in the work of Bertain the perturbing field was produced by unevennesses of the cathode surface, but this does not affect the basic deductions. In order to make use of Bertain's formula, we assume that the cathode has active strips of width a with a separation l between them. We assume further that the work function of the active strips is $\Delta\varphi$ volts lower than the work function of the separating gaps and that the potential in the vacuum in the vicinity of the strips is zero. Then the zero equipotential will be located a maximum distance $\Delta z \approx \Delta\varphi/E$ from the surface of the cathode. It is obvious from

physical considerations that the electron trajectories will not change if the cathode surface coincides with the zero equipotential and is uniform as regards work function. For qualitative evaluation of the equipotentials one can approximate the surface by a cosine curve of period l and height Δz, and thus calculate the resolution for a wavy cathode. In this case we will have

$$\rho = \frac{\pi}{\sqrt{2}} \sqrt{\frac{\varepsilon}{E}} \frac{\Delta\varphi}{El}.$$

Inserting $\varepsilon = 0.1$ ev, $E = 20 \cdot 10^3$ v/cm, $l = 4 \cdot 10^{-14}$ cm and $\Delta\varphi = 1$ v, we obtain $\rho = 0.12$ μ. Thus the aberration due to the patch field will be more than twice as great as the chromatic aberration.

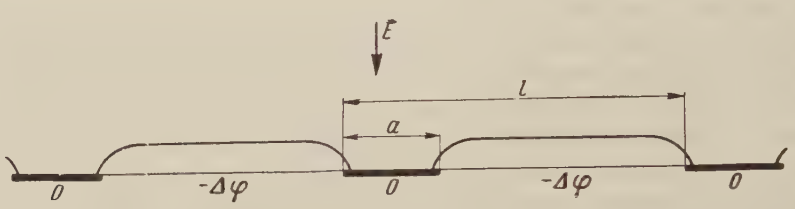

Fig.1. Position of the zero equipotential, measured in an electrolytic bath: $a = 1$ μ, $l = 4$ μ and $E = 20 \cdot 10^3$ v/cm.

Fig.1 shows the position of the zero equipotential determine in an electrolytic bath under the following conditions: $a = 1$ μ, $l = 4$ μ, $\Delta\varphi = 1$ v, and $E = 20 \cdot 10^3$ v/cm. As will be evident from the figure, the sections of the active strip located at a distance of 0.1 μ from the edge are blocked by the negative potentials of the patch field. Similar effects of partial blocking and even of complete "absorption" of the patches were investigated by Rutkevich[13]. It would appear, therefore, that no significant errors will be involved in measurements of the current from the central portion of a patch about 1 micron in diameter or more. Measurements of currents from smaller patches, however, when one cannot neglect edge effects, will be less reliable.

Further enhancement of the resolution of emission microscopes is possible only incident to increase of the field strength at the cathode surface, which is necessary for reducing the aberrations and for preventing "absorption" of the patches. If technical difficulties can be overcome and the field strength at the cathode in emission microscopes can be appreciably increased, the maximum resolving power will be determined by the limitations connected with the Heisenberg uncertainty principle and the potential energy[1]. For regions of the order of a few hundred angstroms the electrochemical potential is no longer a function of the state of the given region per se and, consequently, this quantity determines the minimum size of the cathode region from which it is meaningful to determine the work function.

Investigation of Thermionic Cathodes

A. Compressed tungstate cathodes

Our emission studies of cathodes were carried out in the electrostatic emission microscope described in Ref.8 at a vacuum of the order of $5 \cdot 10^{-7}$ mm Hg, using a special aperture that limited bombardment of the cathode by residual gas ions.

The compressed cathodes[14] were made of powdered barium-calcium tungstate (9.5% wt.), aluminum (0.5% wt.) and tungsten. It is usually assumed that the active substances arrive on the surface of a compressed cathode from fine-scale

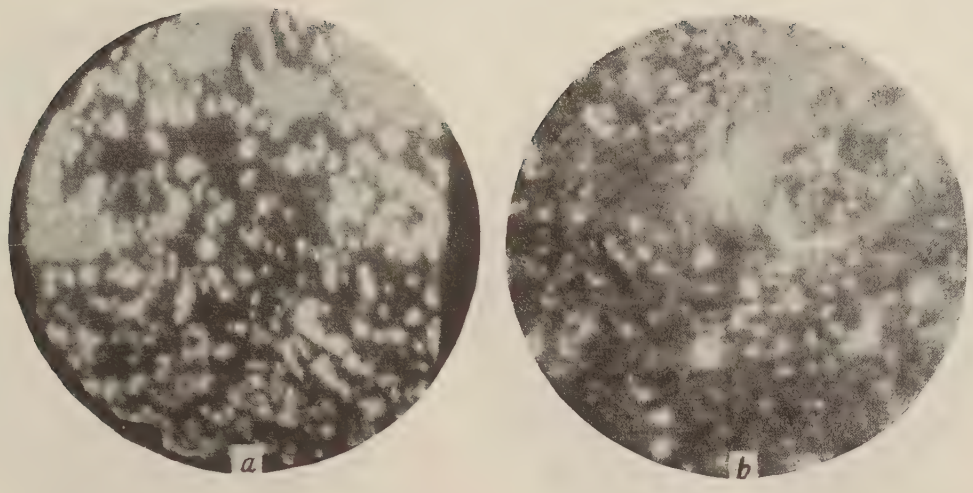

Fig.2. Emission image of a compressed tungstate cathode (magnification 1800 X): a - observation temperature 1100° (after holding at 1280°); current density from active patches 0.45 amp/cm^2 (φ_T = 2.3 ev); current density from sections between patches 10^{-2} amp/cm^2 (φ_T = 2.75 ev); b - observation temperature 940° (after holding at 1250°); current density from active patches $7 \cdot 10^{-2}$ amp/cm^2 (φ_T = 2.25 ev); current density from sections between patches $1.2 \cdot 10^{-3}$ amp/cm^2 (φ_T = 2.65 ev).

sections with dimensions of the order of the diameter of the pores or the particles of the active mass (in our case about a micron). Our emission microscope studies showed, however, that in addition to the fine-scale distribution of the emission and work function, there is observed some variation in the average level of emission in regions of macroscopic size (of the order of tens of microns). In some cases, the macroscopic variation of the emission is connected with the manner of preparation of the cathode; for example, near the edge of the compressed cathode there is observed a 10-20 micron zone of enhanced thermionic activity. At reduced temperatures (900-1000°) the active substances give rise to drop-like formations some tens or hundreds of microns in diameter with an actively emitting rim; these formations exhibit a distinctive behavior as regards evaporation, ion bombardment, etc. The results of these observations of the macroscopic distribution of emission will be described elsewhere. Below we consider only the fine-scale distribution of the emission and work function in typical regions of the cathode.

Inasmuch as the quality of the emission image is impaired when heavy currents are taken off the cathode, owing to the influence of space charge, the studies were carried out at reduced temperatures. Before observation the cathodes were activated at the operating temperature while taking off a pulse current (square pulses of 2 microsec duration were applied to the focusing electrode of the immersion objective). After attainment of a certain level of thermionic activity, the heater voltage was reduced and as soon as thermal equilibrium was attained (observation temperature 940-1100°) the accelerating potential was switched on. The emission of the compressed cathodes reached a steady value about 1 minute after attainment of thermal equilibrium; during this period the emission fell off by a factor of about 10.

Emission images of a compressed cathode are reproduced in Fig.2. The active patches (φ_T = 2.2-2.3 ev) are about 1 micron in diameter. Possibly the work function of the active patches is somewhat increased owing to the poisoning effect of the residual gases during the period of transition to the reduced, observation temperature. The sections of the cathode between the active patches are characterized

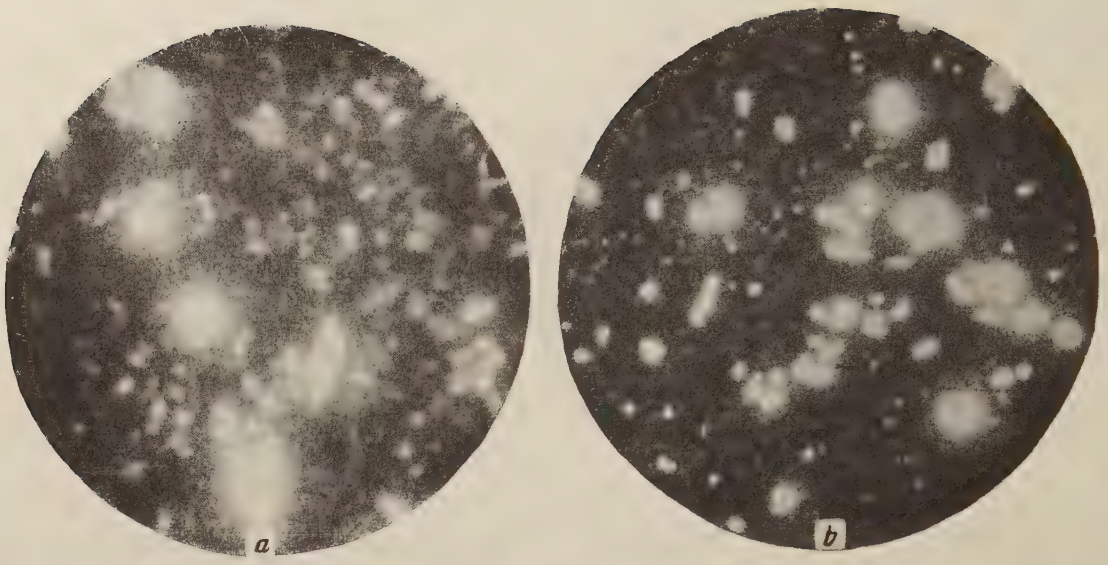

Fig.3. Emission image of an L cathode (magnification 2000 X): a - observation temperature 945° (after holding at 1175°); current density from particularly active patches 40 amp/cm^2 (φ_T = 0.6 ev); b - observation temperature 1175°; current density from particularly active patches 0.3 amp/cm^2 (φ_T = 2.5 ev); current from patches of lower activity $3 \cdot 10^{-3}$ amp/cm^2 (φ_T = 3.1 ev); current from sections between patches $6 \cdot 10^{-4}$ amp/cm^2 (φ_T = 3.3 ev).

by a substantially (40-70 times) weaker emission (φ_T = 2.6-2.8 ev). We note that on the surface of a compressed cathode there are no sections with a high work function, such as are characteristic of the surface of a tungsten cathode with little barium filling. Apparently, in the process of preparation of the cathode the surface of the tungsten grains is covered by chemical compounds with a relatively low work function.

B. L cathodes

The emission image of an active L cathode (emission current density about 20 amp/cm^2 at T = 1175°) was investigated at an observation temperature of about 950 Measurements carried out immediately after attainment of temperature equilibrium (Fig.3,a) gave a current density of about 40 amp/cm^2 from particularly active patches (φ_T = 1.6 ev), about 1 amp/cm^2 from patches of medium activity (φ_T = 2.0 ev) and not more than $8 \cdot 10^{-4}$ amp/cm^2 from the sections between patches ($\varphi_T \geq$ 2.75 ev) The last value is approximate and only an upper bound inasmuch as the measurement were carried out using the most sensitive scale of the electrometric amplifier an misleadingly high values may have been recorded owing to scattered electrons from patches of high activity. We note that in case of L cathodes we were unable to obtain steady emission after cooling: the emission of the cathode continued to fa off and after about 10 minutes the brightness of the screen became inadequate for observation of the emission image. Apparently, the decrease in emission is due t poisoning of the cathode by residual gas ions. An emission image of a "poisoned" cathode could be observed at the operating temperature (Fig. 3,b). With the passage of time there occurs some activation of the cathode; however, normal thermio ic activity with the accelerating potential on could not be attained. At the sam time, pulse measurements which were carried out some 20 sec after switching on th

accelerating potential, showed normal thermionic activity. The rapid restoration of the emission upon switching off the accelerating potential is probably due to change in the surface concentration of the active substances. Hence in investigating L cathodes in an electron microscope one must take into account the possible changes in distribution of the work function owing to ion bombardment of the surface. Despite this one can note a number of respects in which the surface of L cathodes differs from that of compressed cathodes: presence of particularly active patches with φ_T = 1.6 ev, large separation between the active patches, and great contrast as regards the emission intensity of different sections of the cathode (the range of variation of the current density is as much as 1 to 10^3).

References

1. C.Herring & M.Nichols, Thermionic Emission (Cited in Russian trans., M. 1950).

2. A.V.Druzhinin, Elektronika, 10, 79 (1960).

3. D.G.Bulyginskii & L.N.Dobretsov, Zhur.tekh.fiz., 26, 1141 (1956). (Trans. Soviet Physics - Technical Physics.)

4. G.V.Spivak, I.A.Pryamkova & V.N.Lepeshinskaya, Doklady AN SSSR, 130, 751 (1960) (Trans.Doklady); G.V.Spivak, I.N.Prilezhaeva & V.K.Azovtsev, Ibid., 105, 965 (1955).

5. Ya.P.Zingerman & V.A.Morozovskii, PTE (Instruments & Exper.Techniques), No.3, 65 (1956).

6. A.Ahearn & J.Becker, Phys.Rev., 54, 446 (1938).

7. D.Schenk, Ann.Phys., 23, 240 (1935); G.V.Spivak & E.M.Dubinina, and others, Radiotekhnika i elektronika, 3, 1077 (1958).

8. A.V.Druzhinin & B.N.Popov, Izv.AN SSSR, Ser.fiz., 23, 522 (1959). (Trans. Bulletin, 23, 502.)

9. L.A.Artsimovich, Ibid., 8, No.6, 313 (1944).

10. L.N.Dobretsov, Trudy (Proceedings), Physical-Technical Institute, Ukrainian SSR Ac.of Sci., 5, 26 (1953).

11. G.V.Spivak, I.A.Pryamkova & N.N.Sedov, Izv.AN SSSR, Ser.fiz., 24, 640 (1960).(Trans.Bulletin, 24, 648.)

12. F.Bertain, J.phys.et radium, 14, 235 (1953).

13. M.Rutkevich, Zhur.eksp.i teor.fiz., 9, 1332 (1939).

14. A.I.Mel'nikov, A.V.Morozov, B.N.Popov & A.A.Maklakov, Radiotekhnika i elektronika, 3, 322 (1958).

ELECTRON MICROSCOPIC INVESTIGATION OF SEMICONDUCTOR WHISKERS

- I.G.Sirotenko, G.V.Spivak, I.G.Stoyanova & Z.N.Osad'ko

In an earlier contribution[1] we showed that a system of semiconductor (tungsten oxide or molybdenum oxide) whiskers grown by condensation from the vapor phase is capable of yielding a field emission of the order of several tens of microamperes. In this case we were dealing with a "brush" consisting of a large number of field emitters, so that the loss or destruction of an individual whisker or two had no significant effect on the integral emission. We felt it would be of interest to investigate the shape of the whiskers and of their tips in a transmission electron microscope. At first, the whiskers mounted on a carbon support were examined in a UÉM-100 electron microscope; in this case, however, owing to deformation of the whiskers, it was difficult to judge of their true shape. Hence further investigations of tungsten oxide and molybdenum oxide whiskers were carried out in the experimental model transmission microscope developed by Stoyanova & Zaitsev[2] for investigating objects in a gaseous medium.

The tungsten or molybdenum wire loop with the whiskers grown on it was mounted in a special specimen chamber designed for electron microscopy and electron diffraction studies. We investigated the shape and degree of perfection of the surface of the filiform semiconductor crystals, and also the shape of their tips.

Electron diffraction studies showed that the tungsten oxide and molybdenum oxide whiskers are perfect single crystals.

There is little published information regarding the cross section and perfection of whiskers grown from the vapor phase. Coleman & Cabrera[3] found that whiskers of cadmium and zinc grown in an inert gas at atmospheric pressure have a diameter ranging from 1 to 10 microns and a length of 1-2 mm, and appear smooth and straight at magnifications up to 1000 X.

Fig.1. Tungsten oxide whiskers. Magnification 2000 X.

A micrograph of tungsten oxide whiskers is reproduced in Fig.1. They appear straight and of constant cross section. The tips are flat; the sides are smooth in the case of whiskers of large diameter. Careful examination shows, however, that on the side surfaces of some whiskers there appear small protuberances arranged in an orderly manner. They are more noticeable in Fig.2, where they appear to form a spiral about the whiskers. In Fig.1 on the left one can see a twisted whisker, reminiscent of the silver whiskers produced by chemical reduction, observed by Brenner[4].

The tungsten oxide whiskers are characterized by an appreciable scatter both as regards cross section and length. Apparently, first, there occurs axial growth up to a certain length then radial growth begins, leading to thickening; new growth layers apparently start at the base.

The number of molybdenum oxide whiskers growing on a unit surface of the base wire is appreciably smaller than in the case of tungsten oxide, and the shape of the whiskers is different. This difference may be due to differences in condition of growth.

Fig.3 is a micrograph of molybdenum oxide whiskers; these are also straight with smooth side surfaces. The tip is bounded by regular planes, as will be evident in Fig.4. Occasionally there are encountered whiskers of conical shape and with a sharp tip (see Fig.5).

To investigate the field emission, tungsten oxide and molybdenum oxide whiskers grown on a wire loop were mounted in an autoelectronic projector. A prelimi

Fig.2

Fig.3

Fig.4

Fig.2. Filiform tungsten oxide crystals. Magnification 7500 X.
Fig.3. Molybdenum oxide whiskers. Magnification 1500 X.
Fig.4. Tip of molybdenum oxide whisker. Magnification 7800 X.

Fig.5. Conical molybdenum oxide whisker. 7600 X.

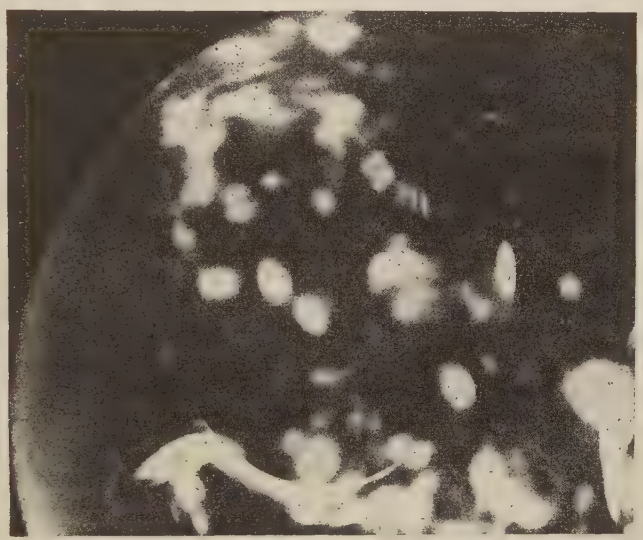

Fig.6. Image of tungsten oxide whiskers obtained in the autoelectronic projector.

ary vacuum of 10^{-7} mm Hg was provided by a forevacuum pump and a mercury diffusion pump equipped with vapor traps; this vacuum was then increased by flashing a titanium getter. At a potential of 4-7 kv there appeared on the screen of the autoelectronic projector individual luminous spots, corresponding to the emission of separate whiskers. With increase of the voltage the picture may change, the images of individual whiskers (those if smaller diameter) disappear, but there appear the images of other whiskers. The whiskers withstand prolonged heating by passage of current through the tungsten or molybdenum loop (red heat). As a result of heating of the whiskers, the same emission current is observed at a higher voltage, but the individual emission images disappear (the entire screen glows uniformly). Apparently, incident to heating, the tips of the whiskers are rounded off and the images of the individual whiskers overlap.

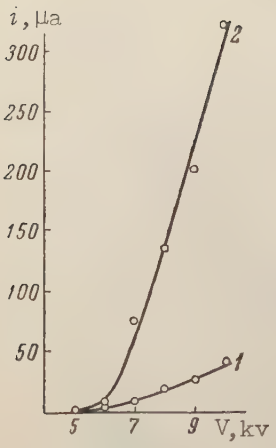

Fig.7. Variation of the integral field emission current as a function of the voltage before (1) and after (2) ion bombardment.

Frequently there were observed on the projector screen images consisting of four separate luminous spots (Fig.6); sometimes there was observed slow rotation of the image 90° about the central axis; this presumably occured under the influence of ion bombardment. However, on the basis of the present experiments one cannot assert that the observed images really represent the structure of the whiskers.

In a few cases with increase of the voltage there occurred abrupt rotation of the image with subsequent disappearance of the image from the screen. Possibly such rotation is connected with emission from twisting whiskers; the image may disappear because the whisker is pulled off by the field. Examination of the whiskers after the field emission experiments showed that their tips are sharpened under the influence of ion bombardment. Ion bombardment is known to be the principal reason for instability of field emission cathodes.[5]

Krylov & Fedorov[6] proposed preparation of field emission cathodes of fine tungsten wires. In this case ion bombardment results in gradual shortening of the wires, but the radius of curvature of the rounded tips remains unchanged. From such cathodes there was obtained stable field emission over a period of many hours. The stability of the emission current is determined by the micropoints on the emitting tips; these may appear and disappear in the process of ion bombardment[7].

In view of this one can expect stable emission from whiskers, which are essentially straight needles of small diameter. In order to investigate the effect of ion bombardment on the emission properties of whiskers, whiskers grown on wire loops were mounted in a tube similar to a Muller projector with an annular anode. The tube was evacuated to 10^{-6} mm Hg, and then filled with neon to $3 \cdot 10^{-2}$ mm Hg. A glow discharge was initiated between the cathode (the wire loop with the whiskers) and the anode, and ion bombardment was carried on for 15 minutes at $V \approx 1$ kv and $i \approx 0.5$ ma. Then the tube was again evacuated and the variation of the integral field emission current as a function of the voltage recorded. It was found that as a result of ion bombardment the field emission current increases several fold and may attain 300 μa (Fig.7). Moreover, the stability of the field emission after ion bombardment is enhanced. At the same time there appeared on the screen of the tube a larger number of four-loop images. The conditions under which the field emission current from a given whisker specimen remained constant was determined experimentally.

Physics Faculty,
Moscow State University

References

1. I.G.Sirotenko, G.V.Spivak & A.Groman, Radiotekhnika i elektronika, 5, No.8 (1960). (Trans.Radioengineering and Electronics.)

2. I.G.Stoyanova & P.V.Zaitsev, PTE, No.3, 138 (1959). (Trans.Instruments & Experimental Techniques.)

3. R.V.Coleman & N.Cabrera, J.Appl.Phys., 28, 1360 (1957).

4. S.S.Brenner, Acta metallurgica, 4, 62 (1956).

5. M.I.Elinson & G.V.Vacil'ev, Avtoelektronnaya emissiya (Autoelectronic emission), M., 1058.

6. K.I.Krylov & V.L.Fedorov, Izvestiya (Bulletin), Leningrad Electrotechnical Institute, 36, 67 (1958).

7. M.B.Ben'yaminovich, B.G.Smirnov & G.N.Shuppe, Zhur.tekh.fiz., 23, 1690 (1953).

* * * * * * *

STRUCTURE AND EMF OF PHOTOVOLTAIC PbS LAYERS PREPARED BY VACUUM SUBLIMATION

- R.Ya.Berlaga & M.I.Rudenok

There have been numerous investigations of the formation and structure of thin metal layers. As far back as the early 1930s there were advanced hypotheses regarding the mechanism of formation and structure of such layers, which were subsequently substantiated by experiment. The possibility of experimental study of thin layers was greatly enhanced by the development of the electron microscope.

In contrast to the case of thin metal layers, there have been relatively few studies of thin semiconductor layers, despite the fact that such layers, produced by vacuum evaporation, are extensively employed as photoresistances. Hence there is particular interest in investigating the structure of such layers.

In our earlier work[1-5] we prepared photovoltaic layers of lead sulfide, i.e., layers in which an electromotive force appears under illumination. These layers were prepared by vacuum (10^{-4} mm Hg) sublimation of lead sulfide onto glass substrates heated to 240-250°C and were not subjected to any orienting treatment. The photo-emf in freshly prepared specimens was very low - of the order of thousandths of a volt.After heating to 500-600° in air, however, the photo-emf increased to several volts. In layers not subjected to heat treatment, the photo-emf did not depend on the direction of the incident light beam. Pronounced directional dependence of the photo-emf became evident after heat treatment. In the case of some layers a photo-emf of opposite polarity appeared as a result of illumination of the layer from the deposit side and from the side of the glass substrate. In some specimens also the magnitude and polarity of the photo-emf varied with the direction of incident of the light flux. Usually we were able to identify an incident light direction (direction of inversion) at which the photo-emf was nil; it increased, with opposite polarity, with increase of the angle in one sense or the other.

Electron microscopic studies of the photovoltaic layers by means of the method of replicas and the method of profile micrographs made it possible to detect on the layer surface formations oriented approximately parallel to the molecular beam (see Fig.1).

It is useful to compare the structure of the layers with their photoelectric properties, for establishment of a correlation between the structure and photoelectric properties should make it feasible to design and prepare photocells for various specific technical purposes.

In our earlier work we investigated the structure of only the surface of the layers, whereas, actually, in many cases it was of interest to know what occurs inside the layer.

Fig.1. Crystalline formations on the surface of a thin polycrystalline layer of lead sulfide.

In the present work we investigated, by means of an ÉM-3 electron microscope, the cross section of a lead sulfide layer approximately 1 micron thick, deposited on a glass substrate. Our attempts to obtain a section of a lead-sulfide element by means of a UMT-2 ultramicrotome were not successful. Hence we developed a simpler method of investigating the cross sections of semiconductor layers. Our procedure was the following: a zinc sulfide layer was deposited by vacuum sublimation onto a glass substrate, which was then broken (together with the layer). Then there was deposited on the broken surface by vacuum evaporation a very thin, transparent (100-200 Å) layer of aluminum, and on top of this a layer of carbon. The carbon film was applied so that it would cover both the break and the adjacent surface of the layer. Then the aluminum was dissolved in hydrochloric acid, freeing the carbon film, which after careful washing was transferred to a specimen grid and examined in the electron microscope. This procedure yields a replica of both the cross section and the adjacent surface of the layer.

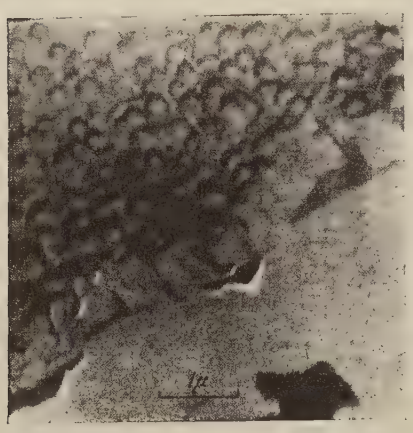

Fig.2. Micrograph of the surface and break cross section of a polycrystalline lead sulfide layer before heating.

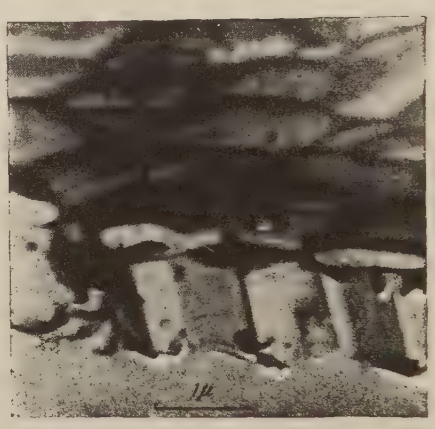

Fig.3. Micrograph of the surface and cross section of a polycrystalline lead sulfide layer after heating in air to 640°.

Typical micrographs of zinc sulfide layers before and after heating in air to 640° are reproduced in Figs.2 and 3.

On the basis of examination of numerous micrographs it may be concluded that the cross section of layers, like their surface, consists of crystalline formations, the direction of growth in which generally agrees with the direction of the molecular beam; with increase of temperature the formations become more distinct and coarse.

At present we are investigating the position of the inversion lines as a function of the direction of the crystalline formations. The preliminary results indicate that there is a definite relation between the inversion lines and the direction of the crystalline formations composing the layer.

References

1. R.Ya.Berlaga & L.P.Strakhov, Zhur.tekh.fiz., 24, 943 (1954).
2. R.Ya.Berlaga, M.A.Rumsh & L.P.Strakhov, Ibid., 25, 1878 (1955).
3. R.Ya.Berlaga, M.A.Rumsh & L.P.Strakhov, Radiotekhnika i elektronika, 2, 287 (1957).

4. R.Ya.Berlaga, M.I.Rudenok & L.P.Strakhov, Zhur.tekh.fiz., 24, 3 (1956). (Trans.Soviet Physics - Technical Physics.)
5. R.Ya.Berlaga, Izv.AN SSSR, Ser.fiz., 23, 676 (1959). (Trans.Bulletin, 23, 672.)

* * * * * * *

ELECTRON MICROSCOPIC OBSERVATION OF MAGNETIC MICROFIELDS BY MEANS OF REPLICAS

- L.V.Lazareva & G.V.Spivak

In the present report we describe an electron microscopic procedure by means of which one can correlate the surface geometry of a ferromagnet with its micromagnetic structure. The procedure is based on the fact that the replica is made directly from the specimen, rather than from a coating of magnetic powder spread over its surface.

Usually investigation of magnetic microstructure by means of an electron microscope is restricted to observation of replicas made of powder patterns on the surface of the ferromagnet[1] or to direct observation of the magnetic structure of thin ferromagnetic films transparent to electrons[2].

The proposed procedure has the following distinctive features: 1) the replica made directly from the specimen does not depend on the magnetic and geometric characteristics of the powder and, consequently, makes it possible to use appreciably higher magnifications and obtain better resolution, and 2) the procedure allows of concurrent investigation of the magnetic properties and the microgeometry of the material.

The microgeometry of specimens was investigated by means of carbon and silica replicas in a transmission electron microscope. At the same time, using the powder pattern technique, we studied the magnetic structure corresponding to each state of the specimen (annealed, mechanically or electrolytically polished, stressed). In all cases there was observed a correspondence between the microgeometry and the magnetic structure.

The analogous relation between the microtopography and the distribution of electric inhomogeneities was utilized earlier for observing the domain structure of ferroelectrics.[3] In this case verification of the fact that there is actually observed the domain structure is furnished by chemical etching, which occurs preferentially at the points of electric inhomogeneities and domain walls.[4]

The usual methods of bringing out the micromagnetic and regular domain structure of ferromagnets may be classified as direct or indirect. Direct methods include optical methods (for example, the procedure utilizing the magneto-optical Kerr effect[5]) and electron-optical methods (procedures utilizing the shadow technique[6], secondary electron emission, the photoeffect, the electron mirror technique[7], thin films transparent to electrons[2], etc.). Indirect methods are the powder pattern technique[8] and electron microscopic methods that generally involve making replicas either from powder patterns or directly from the surface of the specimen.

For the present investigation we chose textured (grain-oriented) silicon iron (3% Si). It is known that the magnetic properties of silicon iron are highly sensitive to stresses.[9,10] As a result of mechanical or heat treatment (for example, grinding or tempering) there arise appreciable stresses in the specimen.

Fig.1

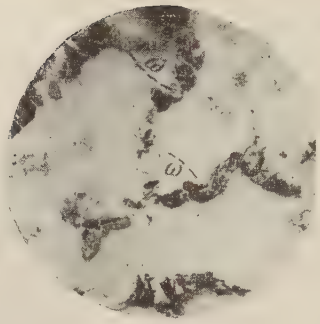

Fig.2

Fig.1. Magnetic structure on the surface of a stressed specimen, brought out by magnetic powder and observed under an optical microscope. Magnification 200 X.

Fig.2. Electron micrograph of powder patterns on the surface of a stressed silicon iron specimen. Magnification 2000 X.

If the specimen is heated to above 900°, its lattice transforms from cubic body-centered to cubic face-centered. If the specimen is allowed to cool slowly the lattice transforms back to body-centered. If, on the other hand, the cooling is rapid (specimen quenched) the reverse transformation is only partially realized, and stresses develop inside the specimen. If the specimen is held for some time at a sufficiently elevated temperature and then slowly cooled, these stresses are relieved. Mechanical working gives rise to plastic deformations that result in impairment of the magnetic properties, owing to the strong anisotropy of the magnetostrictive characteristics of the crystallites. Thus, according to the data in the literature[8], in silicon iron single crystals the maximum magnetic permeability in the [100] direction is 624 000, while in the [111] direction it is only 19 300.

In all we studied about ten different specimens of grain-oriented silicon iron. The results were consistent and hence may be regarded as typical. In studies[10] of textured silicon iron specimens it was established that in the plane of rolling, the crystallites are arranged in a plane close to the (110) plane and are oriented with the [100] direction approximately in the direction of rolling; the [100] direction is the easy magnetization direction in silicon iron.

The single crystals used in our work were extracted from individual large crystallites by etching with nitric acid. The crystallographic orientation was determined from x-ray diffraction patterns. The specimens were selected so that in each case the investigated surface lay in the plane of rolling, which was inclined at an angle of 2-3° to the crystallographic (110) plane. The investigated specimens were of different geometric shapes (disks, rectangles and polygons) with an area from 0.5 cm^2 to several square centimeters. The thickness of the specimen varied in the range from 0.3 to 1.5 mm. The single crystals were polished mechanically. The powder patterns observed on the surface of such specimens by means of an optical microscope (Fig.1) were typical of the (110) plane in the presence of stresses.

The appearance of the mosaic depends on the direction of polishing and, apparently, is not characteristic of the structure of the internal domains. It is known[11], that the mosaic boundaries are zigzagged. In the micrograph reproduced in Fig.2, which was obtained in an electron microscope using a replica made from a powder covered surface, we note a structure with the same zigzag angle* ($\omega \approx 80$-$90°$). Before discussing the common characteristics of the three different types of images of magnetic microstructures, it may be useful to dwell briefly on the distinctive features and origin of the zigzag walls.

The direction of magnetization on either side of a zigzag wall can be determined by the method of scratching[12]. From one side of the wall to the other the

---

*The zigzag angle is the angle between two neighboring sections of a zigzag boundary or wall on the surface of a crystal (Fig.3).

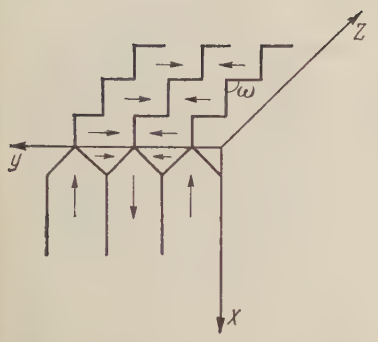

Fig.3. Structure of mosaic domains appearing on a stressed specimen. The arrows indicate the direction of magnetization.

direction of magnetization changes 180°, as is shown by the arrows in Fig.3. The appearance of such magnetic microstructures is explained by the presence of "depth" domains with magnetization vectors normal to the surface of the crystal (Fig.3).[10] The investigated surface of the specimen lies in the YZ plane (so-called Y domains). "Depth" domains form in the XY plane (X domains). The X and Y domains are separated by 90° walls, i.e., the magnetization vector changes its direction by 90° in going from the X to the Y domains. The appearance of these "depth" domains is connected with internal stresses that develop incident to mechanical treatment of the specimen. There is a definite relation between the minimum surface energy and the zigzag angle ω.

For the stable zigzag angles in the domain walls of silicon iron investigators[11] obtained a value of 106°. This value of ω is a common constant for cubic ferromagnets with the easy magnetization direction in the (100) plane, regardless of the magnitude and form of the magnetic anisotropy. In the presence of strong internal stresses in the crystal the zigzag angle becomes smaller than 106°. Our measurements (Figs.2 and 4) yielded zigzag angles in the range from 80 to 110° for specimens with different stresses, which is in good agreement with theory.

Having established the character of the magnetic structure on the surface of stressed specimens in this manner, we then made carbon replicas from the clean (powder-free) surface. A typical replica micrograph obtained by means of the UÉM-100 transmission microscope is reproduced in Fig.4. It will readily be seen that the surface of the stressed specimen is broken up into a number of large regions divided by zigzag walls. The zigzag angles are of the same order of magnitudes (90-100°). Moreover, all the large regions (for example, region a in Fig.4) are subdivided into smaller domains, also separated by zigzag walls. (A similar fragmentation into a finer magnetic structure inside the zigzag domains is revealed by powder patterns - see Fig.1.)

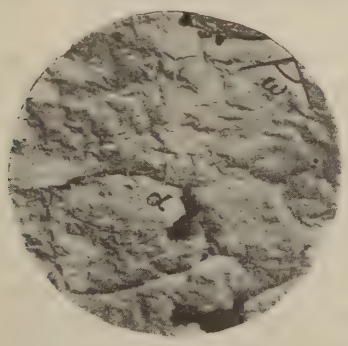

Fig.4

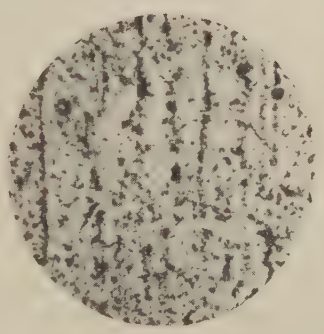

Fig.5

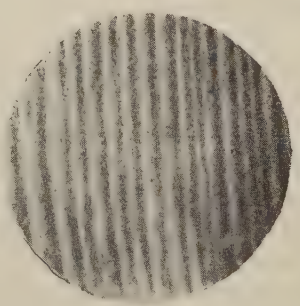

Fig.6

Fig.4. Microgeometry on the surface of a stressed specimen; carbon replica from a clean surface (electron microscope). Magnification 2000 X.

Fig.5. Magnetic microstructure on the surface of an anneal specimen (powder pattern; optical microscope). Magnification 200 X.

Fig.6. Microgeometry on the surface of an annealed specimen (electron microscope). Magnification 8500 X.

The replicas in this case characterize only the microgeometry of the specimen surface. It will be evident from a comparison of Figs.2 and 4 that in the case of stressed silicon iron specimens there obtains complete correspondence between the surface microgeometry and the character of the magnetic structure.

For investigating specimens free of stress, we first carefully polished their surface electrolytically and then annealed the specimens in vacuum for 3-5 hours at 1000°, with subsequent slow cooling. The specimens were then studied in the same way as before.

The powder patterns, which render the magnetic structure of the annealed specimen (Fig.5), consist of parallel lines intersecting the entire surface and are characteristic of the (110) plane of silicon iron.

Using the powder pattern technique, Shur & Abel's[13] established that for demagnetized and annealed crystals, the surface of which is parallel to the (100) or (110) plane, the entire magnetic structure consists of domains in the form of parallel bands separated by 180° walls. Closure domains appear only at the edges of the specimen. Kirenskii & Veter[14] utilized the Kerr effect to evaluate the width of the walls between the domains in silicon iron and found that it varies from 0.6 to 0.89 microns. We made carbon replicas of annealed specimens free of mechanical stresses. A typical micrograph is reproduced in Fig.6. It will be seen that the entire surface of the specimen is striped with parallel bands the width of which varies from 0.1 to 0.3 microns (light bands) and that these are separated by "walls" (dark bands) with a width from 0.05 to 0.1 microns. The transitions from the dark to the light bands are gradual rather than abrupt. This type of structure was observed on all electrolytically polished and then annealed specimens.

We have seen no reports in the literature describing a microgeometry of this type on silicon iron specimens with the surface close to the (110) plane.

From stereoscopic pairs recorded in the electron microscope we established that the wide (light) regions are raised (convex), while the separating narrower dark regions are depressed (concave). Minor defects produced by electrolytic polishing and extraneous inclusions do not affect the character of the microrelief (Fig.6). It may be assumed that this striped or "ribbed" microrelief is due to cold rolling of the material, necessary for producing magnetic structure, and that the line character of the magnetic domains in annealed specimens (Fig.5) is connected with the character of this microstructure.

To substantiate the inferred correlation between the microgeometry and the magnetic structure we carried out the following experiment. An annealed specimen with a typical ribbed microrelief (Fig.6) was rapidly heated in vacuum ($5 \cdot 10^{-5}$ mm Hg) to a temperature appreciable above the Curie point. Naturally, at this temperature the specimen lost its ferromagnetic properties. A carbon replica was deposited onto the surface of the heated specimen. An electron micrograph obtained from this replica is shown in Fig.7. It will be seen that the ribbed relief has disappeared and that there has formed a new microrelief reminiscent of the fine structure observed inside the large domains in stressed specimens (compare with Fig.4). Obviously, in the case of rapid heating there appear internal stresses. The carbon replica made from the surface of such a recrystallized specimen after cooling differs little from the replica taken off a heated specimen (Fig.7).

There is good reason to assume that strong internal stresses produced by heat treatment greatly alter the magnetic structure. Investigations of the magnetic structure of heat treated specimens substantiated this assumption. Fig.8 shows the powder patterns photographed by means of an optical microscope on the surface of such a specimen. Here again there are evident domains separated by zigzag walls and subdivided into smaller sections (compare with Fig.1).

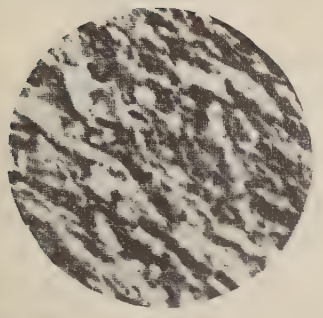

Fig.7

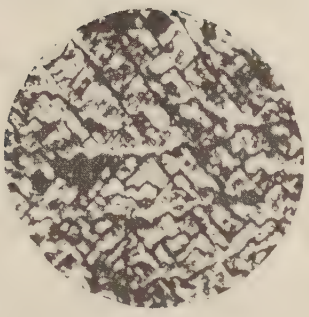

Fig.8

Fig.7. Microgeometry on the surface of a specimen heated above the Curie point (electron microscope). 8500 X.

Fig.8. Micromagnetic structure on a surface of a partially recrystallized specimen (powder pattern; optical microscope). 200 X.

The appearance of similar zigzag magnetic domains on silicon iron specimens heated in vacuum to a temperature above the Curie point was observed earlier by Bates[15]. Bates attributed the appearance of these domains to stresses arising incident to rapid change of temperature (even at temperatures below the Curie point). In addition, Bates assumed that the number of zigzag walls depends on the rate of cooling through the Curie point. In carrying out analogous experiments we noted that there is a dependence between the character of the relief produced by recrystallization and the rate of transition through the Curie point. Thus in the case of repeat annealing of a specimen with a pronounced ribbed relief, followed by slow cooling (3-5 hours), the microgeometry virtually did not change. On the other hand, in the case of repeat annealing followed by rapid cooling (0.5-1 hour), the geometry of the surface was greatly distorted: "cross-ties" appeared on the initial strips. In the case of even more rapid cooling of the reannealed specimen (5-10 min) there formed on its surface a microrelief similar to that shown in Fig.7.

Thus as a result of our experiments we have established a definite correspondence between the microgeometry on the surface of silicon iron specimens and the character of their magnetic structure. It is obvious that the stresses that arise in the material as a result of mechanical or heat treatment produce changes in the microgeometry of the surface, which can be explained by anisotropy of the strictive properties. The net changes occurring in the specimen owing to anisotropy of the mechanical and magnetic properties lead to the appearance of the specific magnetic structure characteristic of the given state of the material.

Physics Faculty,
Moscow State University

References

1. A.Eckardt & B.Elschner, Naturwissenschaften, 39, 566 (1952); D.I.Craik, Proc.Phys.Soc.B, 69, 647 (1956); W.Schwartze, Ann.Phys., 19, 322 (1957); D.I. Craik, Brit.J.Appl.Phys., 9, No.7, 279 (1958).

2. H.Boersch, Naturwissenschaften, 20 (1959).

3. G.V.Spivak, E.Igras & I.S.Zheludev, Doklady AN SSSR, 122, 54 (1958). (Trans.Doklady.)

4. W.I.Merz, Phys.Rev., 95, 690 (1954).

5. G.S.Krinchik, Fizika metallov i metallovedenie (Physics of Metals & Metallurgy), No.3, 549 (1950); C.A.Fowler & E.M.Fryer, Phys.Rev., 94, 52 (1954).

6. L.Marton & S.H.Lachenbruch, J.Appl.Phys., 20, 1171 (1949).

7. G.V.Spivak, N.G.Kanavina, N.I.Chernyshev & I.S.Sbitnikova, Doklady AN SSSR, 92, 541 (1953); G.V.Spivak, T.N.Dombrovskaya & N.N.Sedov, Ibid., 113, 78

(1957) (Trans.Doklady); G.V.Spivak, I.N.Prilezhaeva & V.K.Azovtsev, Ibid., 105, 965 (1955); G.V.Spivak & I.A.Pryamkova and others, Present issue of the Bulletin, p.698.

8. S.V.Vonsovskii & Ya.S.Shur, Ferromagnetizm (Ferromagnetism) Ch.3, M., 1948; E.S.Borovik & A.S.Mil'ner, Lektsii po ferromagnetizmu (Lectures on Ferromagnetism), Ch.XII, Khar'kov University, 1960.

9. A.S.Zaimovskii & L.A.Chudnovskaya, Magnitnye materialy (Magnetic materials), M., 1957.

10. L.V.Kirenskii, Ferromagnetizm i ego primenenie (Ferromagnetism and its applications), M., 1957.

11. S.Chikazumi & K.Suzuki, J.Phys.Soc.Japan, 10, 523 (1955); Magnitnaya struktura ferromagnetikov (Magnetic structure of ferromagnets), p.204, Collected articles and translations edited by S.V.Vonsovskii, M., 1959.

12. Fizika ferromagnitnykh oblastei (Physics of ferromagnetic domains), Collected articles and translations edited by S.V.Vonsovskii, M., 1951.

13. Ya.S.Shur & V.R.Abel's, Doklady AN SSSR, 104, 209 (1955).

14. L.V.Kirenskii & V.V.Veter, Ibid., 125, 526 (1959). (Trans.Doklady.)

15. L.F.Bates, J.Inst.Met., 82, 417 (1954).

OBJECTIVE METHOD OF RECORDING ELECTRON ENERGY SPECTRA WITH AN ELECTROSTATIC ANALYZER

- A.N.Kabanov, Yu.M.Kushnir & D.V.Fetisov

In using electrostatic electron velocity analyzers[1] the energy spectra are usually recorded photographically. Experimenters in the field are familiar with the difficulties that arise in evaluating the line intensities. In addition, inasmuch as in using the photographic method of recording the process of measurement of energy losses is a two-step one, the accuracy in determining loss values is reduced. In addition to the above shortcomings, in using the photographic recording method the analyzer must operate in a regime under which the resolution does not remain constant: the optics of the analyzing lens distorts the true intensity distribution.

Möllenstedt & Dietrich[2] proposed a method by means of which one can obviate the above shortcomings. Subsequently, this method was employed in a 35 kv electrostatic analyzer designed by Dietrich[3]. At approximately the same time we also employed this method in a 75 kv analyzer. The fundamentals of the method are made clear in Fig.1. Fig.1,a shows the trajectories of electrons with energies U and $U - \Delta U$ in the case of photographic recording. The dispersing element of the analyzer consists of one slit and the analyzing lens. The relation between the accelerating potential U and the potential U_l on the middle electrode of the analyzing lens is chosen so that the analyzer will operate in the optimum regime. This regime, as is known[4], corresponds to the maximum resolution, minimum differential magnification and maximum dispersion. In this case the electron trajectories are shown by the solid line in Fig.1,a.* If with a constant potential on the middle electrode the electron energy is reduced by ΔU, as is usually the case in measuring electron energy losses by this procedure, the optimum regime is disturbed (the trajectory is now given by the dashed line in Fig.1,a). The optimum regime voltage ratio $R_{opt} = U/U_l$ also changes and becomes $R = \frac{U-\Delta U}{U_l}$. This is accompanied by broadening of the slit image, i.e., reduction of the resolving power, and a change in the intensity of the image owing to change of the optical strength of the analyzing lens. Both these shortcomings can be easily eliminated by maintaining the optimum regime of the analyzing lens for electrons of different energies. In other words, one should maintain R_{opt} constant for all electron energies. Then the optical properties of the analyzing lens remain unchanged, as do the resolution and intensity of the slit image.

The constant voltage ratio arrangement is shown in Figs.1,b & c. In contrast to the case shown in Fig.1,a, here there is introduced a second slit located below the analyzing lens and at such a distance from it that there will pass through it only electrons with energies that satisfy the optimum regime condition. In the first case (Fig.1,b) this regime obtains for electrons with energy U ($R_{opt} = U/U_l$), in the second case (Fig.1,c) the regime obtains for electrons with energy $U - \Delta U$ ($R_{opt} = \frac{U-\Delta U}{U_l - \Delta U} = U/U_l = \text{const}$). The value of R_{opt} is maintained constant by varying

---

*The 75 kv analyzer operates under conditions for which the optimum regime of the analyzing lens is the second working region. The electron trajectory corresponding to this regime has been called the telescopic path of the rays in the second working region.

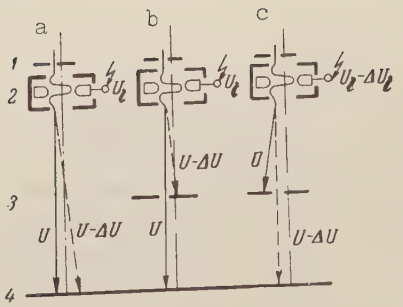

←Fig.1. Electron trajectory in the analyzing lens in using the photographic (a) and the objective (R_{opt}= const) methods (b & c) methods of recording energy spectra. b - $R_{opt} = U/U_l$, c - $R_{opt} = \frac{U - \Delta U}{U_l - \Delta U_l}$. 1 - first slit, 2 - analyzing lens, 3 - second slit, 4 - screen.

the potential on the middle electrode of the analyzing lens. Thus the image of the slit in this case can only change in intensity but remains stationary on the screen.

As a rule, electrostatic analyzers are used in measuring the energy loss of 30 to 75 kev electrons. For most solids the loss is generally of the order of tens of electronvolts. Thus there enters into the analyzing lens through the upper slit an electron beam, the electrons in which have a relatively small energy spread. Having set the optimum regime for elastically scattered electrons and then varying the potential on the middle electrode and each time measuring the number of electrons passing through the second slit, one can readily obtain the sought information on the energy loss and intensity of the lines in the spectrum.

The apparatus is greatly simplified by using a semitransparent fluorescent screen, a photomultiplier and a recording electronic voltmeter (EPP-0.9 potentiograph). The light signal from the fluorescent screen is converted and amplified by the photomultiplier, the output of which is connected to the recording voltmeter. The deflection of the recorder pen is proportional to the intensity of the stationary image of the slit. The variation of the potential on the middle electrode of the analyzing lens should be synchronized with advance of the recorder chart. Then every displacement of the chart will be proportional to the change in electron energy. Thus there will be automatically recorded on the voltmeter chart the electron energy spectrum with constant resolution of the analyzer. The errors in measuring line intensities introduced by use of a fluorescent screen are so small as to be negligible. The brightness of a fluorescent screen is proportional to the electron current density and the accelerating potential to the n-th power; in most cases n does not exceed 2. In view of the fact that the accelerating potential in our case changes by less than a fraction of a percent, the resultant variation in screen brightness can be neglected.

Fig.2 shows a diagram of the dispersing element together with an electron gun and the device for objective recording of electron energy spectra. (Other components of the 75 kv universal analyzer such as the condenser, objective, intermediate camera are not shown in this figure.) The geometric and electron-optical parameters of the analyzing lens have been discussed in Ref.5. Both slits in the apparatus are adjustable in width. The second slit can be opened to a width sufficient for passage of the entire energy spectrum; this can be photographed by means of the camera without disturbing the vacuum. The fact that the film magazine is movable makes it possible to shift from one type of recording to the other without difficulty.

The electron beam passing through the second slit falls on the semitransparent fluorescent screen. This screen has a short persistence and an emission color corresponding to the maximum sensitivity of the 1S type photocathode of the photomultiplier. The photomultiplier is supplied from a regulated VS-9 rectifier. The screen is optically coupled to the photomultiplier by a plexiglass lightpipe. The

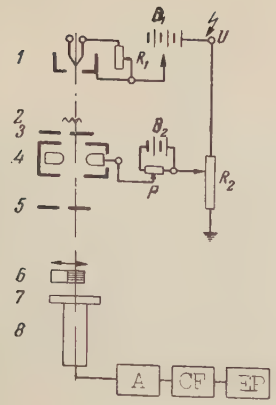

←Fig.2. Diagram of the dispersing element of the analyzer together with the device for objective evaluation of loss line intensities: 1 - electron gun, 2 - specimen, 3 - first slit, 4 - analyzing lens, 5 - second slit, 6 - movable film magazine, 7 - fluorescent screen, 8 - photomultiplier, A - amplifier, CF - cathode follower, EV - recording electronic voltmeter, R_1 - bias variable resistor, R_2 high voltage divider, B_1 - calibrating battery, B_2 - supply battery, P - potentiometer.

output signal from the photomultiplier is preamplified by the dc amplifier A and goes to the input of the cathode follower CF. This serves to match the output impedance of the amplifier with the input impedance of the recording electronic voltmeter EV.

The potential on the middle electrode of the analyzing lens is varied by means of a circular type PL potentiometer. The total resistance of this potentiometer is 20 kilohm; the linearity 0.1%. The potentiometer shaft is rotated by an SD-54 motor through a reduction gear at the rate of 1 revolution per 3 min. Tests showed that this arrangement insures adequate synchronization of the rotation of the potentiometer shaft with the advance of the recorder chart. The potentiometer is supplied from a 150 v battery B_2. The voltage divider R_2 allows of setting the requisite regime of the analyzing lens depending on the electron beam current. The small battery B_1, connected into the electron gun circuit, is intended for impressing calibration markers on the recorder chart to provide an energy scale for the energy spectra. The bias of the electron gun is set by means of the variable resistor R_1.

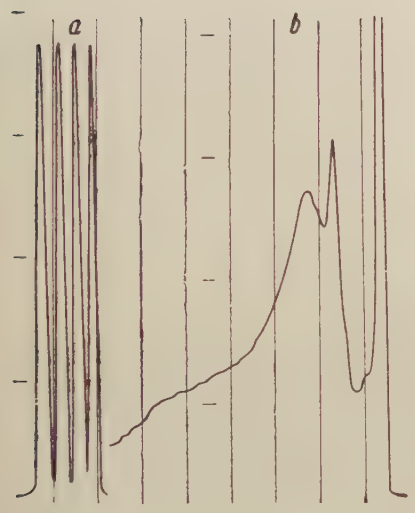

Fig.3. Typical chart showing calibration markers (a) and energy spectrum of 70 kev electrons passing through a thin aluminum film (b).

Fig.3 shows the calibration marks recorded on the voltmeter chart with increase of the accelerating potential in 5 v jumps and the energy spectrum of 70 kev electrons passing through a thin aluminum film. This record was made with the second 20 mm slit adjusted to a width of 2-3 μ. Under these conditions the resolution of the analyzer is of the order of 140 000:1; the dispersion - 0.02 mm/ev.

The results of measurements carried out by means of the above described analyzer will be described elsewhere (see next article).

References

1. V.I.Milyutin & A.N.Kabanov, Uspekhi fiz.nauk, 11, 673 (1957).
2. G.Möllenstedt & W.Dietrich, Optik, 12, 246 (1955).
3. W.Dietrich, Z.Phys., 152, 306 (1958).
4. A.N.Kabanov & V.I.Milyutin, Radiotekhnika i elektronika, 4, 109 (1959). (Trans.Radio Engineering and Electronics.)
5. A.N.Kabanov, V.I.Milyutin & D.V.Fetisov, Izv.AN SSSR, Ser.fiz., 23, 459 (1959). (Trans.Bulletin, 23, 443.)

USE OF AN ANALYZER FOR INVESTIGATING THE ENERGY DISTRIBUTION OF ELECTRONS REFLECTED FROM METALS

- Yu.M.Kushnir & A.N.Kabanov

In addition to the characteristic energy loss of electrons incident to passage through thin films of different substances, it is of interest to investigate the energy loss of reflected electrons. In particular, such measurements are important for determining the optimum operating conditions of a reflecting electron microscope. Commonly, reflecting microscopes employ an accelerating potential of from 70 to 100 kv. In view of this, we carried out measurements of the energy loss of 70 kev electrons reflected from different metals.[1] These measurements were carried out on the universal electrostatic analyzer described in Ref.2, using the photographic method of recording the energy spectra.

In the present work similar measurements were carried out using the objective method of recording.[3] (See preceding article.)

The measurements were made at pressures of the order of 10^{-5} mm Hg in the analyzer column. In all the experiments the glancing and observation angles were constant and equal to 4°. The specimens were thin plates 3-4 mm wide and 0.08-0.10 mm thick. Such specimens could be adequately heated simply by passage of dc current (usually 15-20 amp). This method of heating not only provided for elimination of the carbon contaminant films forming on the surface, but also allowed of measuring energy losses at different temperatures up to above 1000°. The temperature was monitored by means of an optical pyrometer.

The experimental results are given in the table below. The listed loss values are in good agreement with the values obtained earlier in using the photographic method of recording[1].

Substance	Energy loss, ev						
Al	7,8	16,1	22,0	30,0	44,6	—	—
Pb	7,1	16,0	23,2	—	—	—	—
Ta	—	15,5	22,1	29,1	38,3	46,0—51,0	57,0
Ni	9,5	19,0	—	27,5	37,0	—	—
Mo	5,4	16,5	27,0	—	38,0	—	—
Nb	9,1	15,3	24,5	—	38,1	46,1	68,2

In Ref.4 it was shown that in the case of pure iron the characteristic energy loss depends on the temperature: an abrupt change in the value of the loss occurs at the temperature of the α-γ transition (940°), when body-centered α-iron (a = 2.86 Å) transforms into face-centered γ-iron (a = 3.60 Å). In the case of substances that do not undergo such transitions, for example, nickel and molybdenum, we did not observe temperature dependence of the characteristic loss. Using the objective method of recording, we checked the temperature dependence of a different material, namely, titanium. At room temperature and up to 900° titanium has a hexagonal lattice (a = 2.95 A; c = 73 A), while at 900° it has a cubic body-centered lattice (a = 3.32 A). Accordingly, we designate these two forms as α-titanium and β-titanium, respectively.

The electron energy spectra were recorded on the voltmeter chart of the analyzer at temperatures of 20, 500 and 1050°. The voltmeter traces are reproduced in the accompanying figure. It will be evident that in all three cases there are evinced only two peaks, corresponding to inelastically scattered electrons. Incident to transition from α- to β-titanium both peaks are shifted some 2-3 ev to the side of lower loss values. It is noteworthy that the reflected beam consists to the extent of more than 50% of inelastically scattered electrons. Such "demonochromatization" of the electron beam must have a significant effect on the resolution of reflecting electron microscopes.

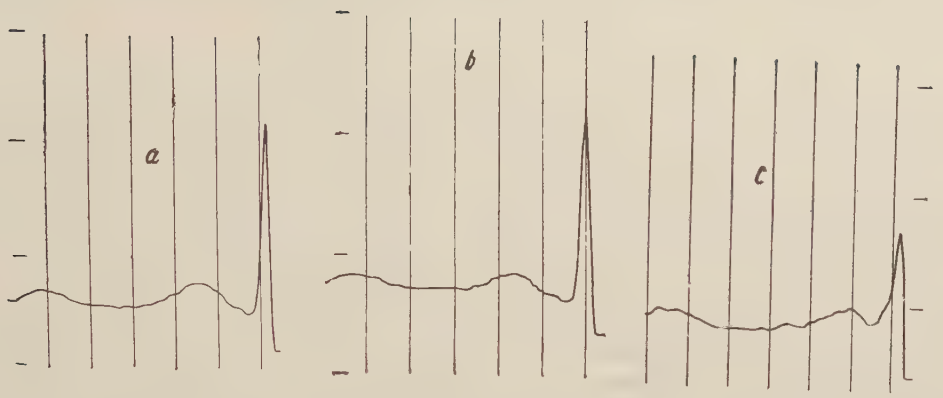

Energy spectra of electrons reflected from titanium: a) T = 20°, b) 500°, c) 1050°.

The following are the values of the electron energy loss (in ev) in α-titanium, measured in our work, in the experiments of Watanabe[5] and calculated by Vyatskii[6] on the basis of the theory of pair collisions:

Our data (exp.)	Watanabe[5] (exp.)	Vyatskii[6] (calc.)
24.0	24.0	23.2
48.0	50.0	50.0

As will be evident from these data, the experimental and calculated values for α-titanium are in good agreement. For β-titanium the calculated electron energy loss value is 27.2 ev, which is in conflict with the results of our experiment. We obtained a similar discrepancy in the case of electrons reflected from iron. This illustrates the difficulty of theoretical interpretation of characteristic energy losses. Further investigations of energy losses are in progress.

References

1. A.N.Kabanov & Yu.M.Kushnir, Radiotekhnika i elektronika, 5, 1703 (1960). (Trans.Radio Engineering and Electronics.)

2. A.N.Kabanov, PTE, No.4, 23 (1960). (Trans.Instrument & Exper.Techniques.)

3. A.N.Kabanov, Yu.M.Kushnir & D.V.Fetisov, Present issue of the Bulletin, p. 759.

4. I.B.Borovskii, A.N.Kabanov, Yu.M.Kushnir & V.V.Shmidt, Zhur.eksp.i teor. fiz., 38, 1383 (1960). (Trans.Soviet Physics - JETP.)

5. H.Watanabe, J.Phys.Soc.Japan, 10, 321 (1955).

6. A.Ya.Vyatskii, Zhur.tekh.fiz., 28, 2217 (1958). (Trans.Soviet Physics - Technical Physics.)

ION-OPTICAL TECHNIQUE FOR PREPARING SMALL DIAMETER APERTURES

- L.B.Rozenfel'd & A.I.Makarov

In constructing various laboratory instruments it is frequently necessary to make openings ranging from a few microns to some tenths of a millimeter in diameter. One way of piercing such openings is "drilling" by means of a focused ion beam. This method has a number of advantages over other drilling procedures: there is no necessity of making a drill bit of appropriate diameter; the ion beam can perforate the hardest materials; the opening itself and the surface in its vicinity are cleansed of contaminants in the process of drilling.

The authors developed a simple apparatus for "drilling" holes by means of a focused ion beam. Tests showed that this apparatus is not critical as regards adjustment and is capable of drilling openings from 2-3 microns to a fraction of a millimeter in diameter in different materials.

The ion gun employed in the instrument (Fig.1) operates on the principle of a channel-beam gas discharge ion source. It consists of a stationary anode with a cylindrical cavity 7 mm in diameter and 22 mm in length, covered with a disk with a 3 mm aperture, and a cathode with an opening for the exit of the beam. The anode-to-cathode distance can be varied by screwing the cathode into the gun housing. For convenience of operation the gun housing (and, consequently, the cathode and perforated piece) are grounded, while the anode is insulated by means of a ceramic insulator.

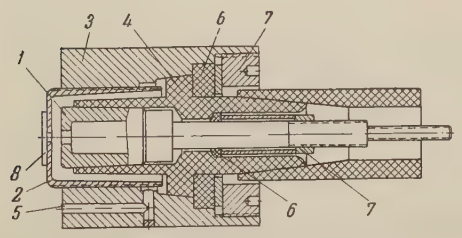

Fig.1. Ion gun: 1) anode, 2) cathode, 3) gun housing, 4) insulator, 5) channel connecting discharge gap with vacuum system, 6) rubber seal, 7) retaining nut, 8) perforated piece.

Usually the anode-to-cathode distance is set in the range from 0.25 to 2.5 mm, and a pressure of the order of 10^{-1} mm Hg is maintained in the discharge gap. At this pressure the electron free path is appreciably greater than the separation between the electrodes at all points except near the axis of the system, so that when a high voltage is applied to the anode the gas discharge forms only in the axial region. The arrangement of electrodes employed in the gun gives rise to autofocusing. As a result, the ion beam is focused to a thin pencil. Inasmuch as the gas discharge is concentrated at the axis of the system, the beam diameter is very small. Consequently, after passing through the minimum cross section plane (crossover), the beam diverges very weakly. This makes it possible to "drill" dielectrics, locating them in front of the opening in the cathode aperture.

The perforating apparatus is diagramed in Fig.2. The piece 2 to be perforate is mounted in the working chamber. The chamber cover 7 is sealed by a rubber gasket (not shown in the figure). The apparatus is then evacuated to 10^{-2} mm Hg. Next, the high voltage is applied to the gun anode and the needle valve 5 is opene Owing to the inflow of gas the pressure in the system rises to about 10^{-1} mm Hg. The discharge is ignited and the "drilling" begins. The discharge current depends on the voltage applied to the anode and the pressure in the system, which depends on the valve setting. The appearance of the opening on the top side of the perforated piece is observed through the glass window 3.

When it first appears, the opening is generally 2-3 microns in diameter. If the operation is continued, the opening increases in diameter. By continuing the operation (boring) one can obtain an opening of any desired diameter. An adequate

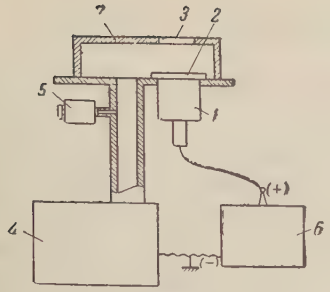

←Fig.2. Diagram of perforating apparatus: 1) ion gun, 2) perforated piece, 3) glass viewing window, 4) vacuum pump, 5) needle valve, 6) high voltage rectifier, 7) cover.

vacuum in the system can be maintained by a fore-vacuum pump (for example, the VN-461). The gun can be supplied from an ordinary high voltage rectifier capable of yielding 2 ma current at up to 25 kv. No filtration or regulation is necessary. The discharge current is stabilized by means of a limiting resistor (VS-10-100 kilohm).

We have used the described equipment to pierce openings in different materials: nichrome, tantalum, molybdenum, stainless steel, diamond and others. Data on the operating conditions and rate of drilling of different materials are summarized in the table.

Material	Thickness, mm	Voltage, kv	Discharge current μa	"Drilling" time	"Boring" time	Opening diameter, microns
Tantalum	0.075	15.5	440	7 min 20 sec	10 sec	14
	0.075	15.5	440	7 min 5 sec	18 sec	21
Nichrome	0.03	15	100	1 min 40 sec	30 sec	28
Molybdenum	0.06	19.5	160	4 min 50 sec	2 min	40
Steel 1Kh18N9T	0.2	13	180	52 min	30 sec	7
Diamond	0.5	20	200	38 min		40

The perforation rates listed in the table are only indicative. The perforation rate increases with the voltage on the cathode and the discharge current, and is limited only by the power dissipation of the gun. Obviously, the "drilling" rate also depends on the thickness of the piece and the material.

The quality of the opening depends on the properties of the material. If the material is homogeneous and fine grained, the edges of the opening are usually even and fairly smooth. If, on the contrary, the material is coarse grained, the opening tends to be ragged.

Apertures pierced in the above-described equipment have been used in a number of electronic instruments, including electron microscopes. Very interesting results are obtained by N.M.Popov in an electron microscope with an accelerating potential of 400 kv in using such apertures with a diameter of a few microns as selector (defining) apertures.

We desire to express our deep gratitude to Yu.M.Kushnir for his interest in the work and to G.V.Der-Shvarts for valuable advice.

References

1. M.Ardene, Elektronen-Übermikrosckopie, p.162, Berlin, 1940.
2. L.B.Rozenfel'd & A.I.Makarov, Author's certificate No.120403, April 15, 1958.

INVESTIGATION OF SOME TYPES OF PHOTOGRAPHIC PLATES SUITABLE FOR USE IN ELECTRON MICROSCOPY

- I.S.Renskii & P.A.Stoyanov

Photographic emulsions for use in electron microscopes, particularly in high resolution microscopes must meet a number of specific requirements. They should have a high sensitivity to electrons, adequate contrast and resolution. The high sensitivity requirement is particularly important inasmuch as one must often employ low current densities and short exposure times. The high contrast requirement is based on the fact that the fine details of objects tend to merge with the background in the electron image.

Generally, the most suitable photographic materials for electron microscopy are electron diffraction and some nuclear photoplates, which are characterized by high sensitivity of the individual fine grains. Type MR (MP) nuclear plates are sensitive to electrons with energies in the range employed in electron microscopes.[1,2]

The present investigation was concerned with MR type photoplates. We compared their properties with the well known characteristics of type III electron diffraction plates.[3,5-7] We shall not describe in detail the procedure and equipment for investigating the plates (see Ref.4).

The photographic plates were investigated on an appropriately modified UÉM-100 electron microscope. The beam current was measured by means of a Faraday cup mounted at the location of one of the pole pieces of the projector lens. By rotation of the projector lens one could introduce the Faraday cup for measuring current or the normal pole piece for the photographic exposure. The current was measured by means of a differential cathode-follower type dc amplifier with a sensitivity of $3 \cdot 10^{-12}$ amp per scale deflection.

The sensitograms were recorded by varying the exposure time while maintaining a constant current density. The current density was chosen to correspond to operation of the microscope with a magnification of 100 000 to 150 000; under these conditions it equaled 10^{-13} to 10^{-12} amp/cm^2. The accelerating potential was 80 kv. Several plates were exposed simultaneously to insure uniform and consistent exposure conditions. The illumination of the plates was uniform to within ±2.5%.

The electron diffraction plates, which served as the "standard", were processed in developer No.1 following the recommendations of the manufacturing plant. The nuclear emulsions were developed in metol hydroquinone developer also in accord with the recommendations of the manufacturer. Comparison of the densities showed that the characteristic curves of the nuclear plates lie below the characteristic curves of the electron diffraction plates. The sensitivity of the nuclear plates proved to be 40% lower than that of the electron diffraction coatings.

We determined the optimum developing time for obtaining the maximum sensitivity. Comparison of the characteristic curves (Fig.1) showed that increase of the developing time up to 10 min substantially increases the sensitivity of the plates. Further increase of the developing time gives rise to noticeable fog.

The characteristic curves of the electron diffraction plates and nuclear MR plates developed for 10 min are compared in Fig.2. In this case the sensitivity of the nuclear plates was 50% higher than that of the electron diffraction plates and their contrast was 20-30% better than that of the electron diffraction plates. The sensitivity of the nuclear plates can be increased a further 10% by developing them by the procedure for electron diffraction plates (Fig.3). At the same time the development process is simplified. Thus by developing nuclear plates for 10 min in developer No.1 one can enhance their sensitivity by a factor of 2. The

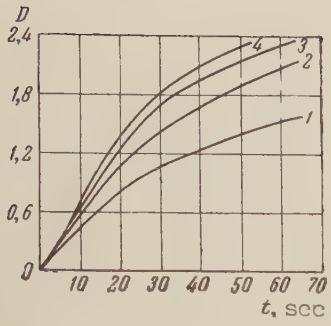

Fig.1

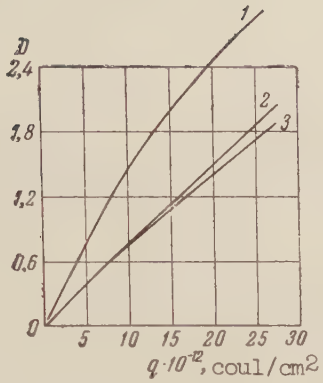

Fig.2

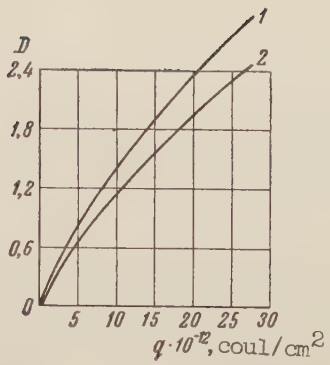

Fig.3

Fig.1. Characteristic curves for MR nuclear photoplates with different developing times: 1 - 4 min, 2 - 6 min, 3 - 8 min, 4 - 10 min. Accelerating potential 80 kv; current density 10^{-12} amp/cm^2; t = exposure time.

Fig.2. Characteristic curves for different plates: 1 - MR type nuclear (Moscow Tech.Photoplate Plant), 2 - electron diffraction, 3 - MR type nuclear (NIKFI). Accelerating potential 80 kv; current density $0.82 \cdot 10^{-12}$ amp/cm^2; developing time 10 min.

Fig.3. Characteristic curves for MR type nuclear plates processed in different developers: 1 - developer No.1, 2 - developer for nuclear plates (metol hydroquinone). Accelerating potential 80 kv; current density $0.82 \cdot 10^{-12}$ amp/cm^2.

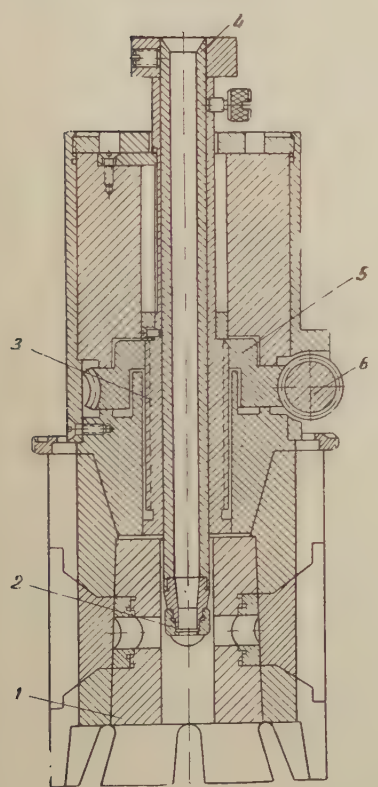

above results pertain to nuclear plates produced by the Moscow Technical Photoplate Plant.

Increase in the sensitivity of the nuclear plates as a result of increasing the developing time is, unfortunately, accompanied by deterioration of their resolution. It is known[8] that electrons are deflected from their initial direction in photographic coatings. If the thickness of the emulsion layers is commensurate with the electron range in the material, the deflection attains values one to two orders of magnitude greater than the size of the emulsion crystals. Despite the fact that the emulsion coating of MR plates is relatively thin, electron scattering in it is appreciable, inasmuch as the concentration of the silver halide in this emulsion is 85-86%.[1] This leads to impairment of the resolution as a result of prolonged development, when the developer not only acts on the surface layer, but also has time to react with the deeper layers.

The resolution of the tested photographic plates was determined by means of the attachment diagramed in Fig.4, using a diffraction grating replica. The specimen holder with the grating replica was mounted

←Fig.4. Microscope attachment for determining the resolution of photographic plates.

in the object plane of the projector lens of the UÉM-100 microscope. A special pole piece 1 (Fig.4) was mounted in the projector lens; this was designed to operate at different magnifications from 3 to 60 X. The position of the specimen 2 on the optical axis could be varied in a wide range by means of a mechanism consisting of a threaded bushing 3, an internal tube 4, and a worm 5 and a worm gear 6. The shaft of the worm was brought out through a vacuum seal. Thus by rotating the worm, tube 4 could be raised or lowered together with the specimen. For each position of the specimen, we calculated the excitation current corresponding to sharp focusing. The appreciable focal depth of the microscope, operating under the described conditions, guaranteed a minimum measurement error owing to noncoincidence of the calculated and actual values of the excitation current for obtaining an accurately focused image.

The preliminary results of measurements by the described procedure show that increase in the sensitivity of MR type plates is accompanied by deterioration of the resolution to 30-40 lines/mm.

References

1. K.S.Bogomolov, M.Yu.Deberdeev, A.A.Sirotinskaya & V.M.Uvarova, Trudy NIKFI (Proceedings, Motion Picture and Photography Scientific Research Institute) No.11 (21), 87 (1957).

2. K.S.Bogomolov, Ibid., No.11 (21), 6 (1957).

3. I.A.Kovner, Zhur.eksp.i teor.fiz., 20, 401 (1950).

4. N.G.Sushkin, I.A.Kovner & E.N.Vtorov, Izv.AN SSSR, Ser.fiz., 15, 395 (1951).

5. N.G.Sushkin & E.N.Vtorov, Ibid., 15, 403 (1951).

6. N.G.Sushkin & I.A.Fomina, Zavodsk.laboratoriya, 22, 961 (1956).

7. I.A.Fomina & K.S.Bogomolov, Ibid., 26, 1015 (1960). (Trans.Industrial Laboratory.)

8. K.S.Bogomolov & S.B.Stefanov, Trudy NIKFI, No.32, 68 (1959).

SOME CHARACTERISTICS OF CARBON AND SILICA REPLICAS MADE FROM POLISHED SURFACES

- L.V.Lazareva & T.F.Filippova

The present work was concerned with the behavior of carbon and silica films, ranging from 100 to 1000 Å in thickness, deposited on different smooth surfaces: the natural growth faces of ferrite single crystals, mirror metal surfaces and polished optical glass. It was found that films of a certain thickness do not always truly replicate the structure of the specimen but deform and exhibit a distinctive intrinsic structure.

The carbon and silica films were prepared by the conventional technique used in making electron microscopic replicas, namely, vacuum evaporation[1]. Carbon films were deposited on the (0001) face of a magnetoplumbite $PbO(Fe_2O_3)_6$ single crystal. X-ray diffraction studies showed that the natural growth surface of plumbite single crystals coincides with the hexagonal [0001] direction. Magnetoplumbite was chosen as the substrate because the natural growth surface of these single crystals is an almost ideal mirror.

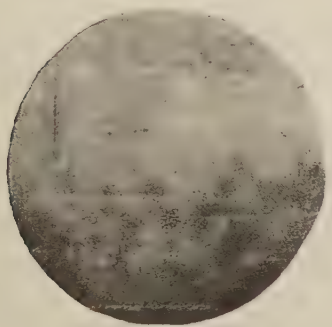

Fig.1

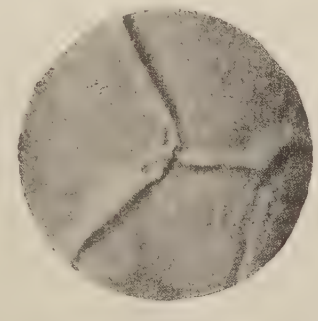

Fig.2

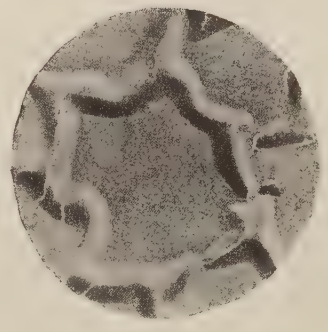

Fig.3

Fig.1. Micrograph of the surface of a magnetoplumbite single crystal. 8500 X.
Fig.2. Center of nucleation of "relief" on a carbon replica. 8500 X.
Fig.3. Characteristic "relief" forming on carbon films. 8500 X.

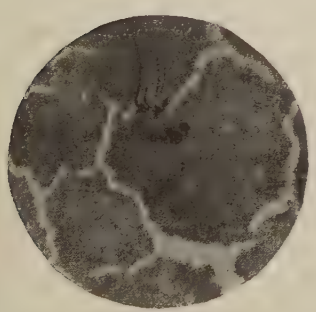

Fig.4

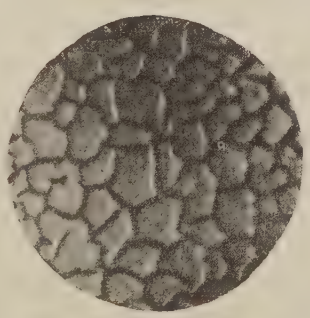

Fig.5

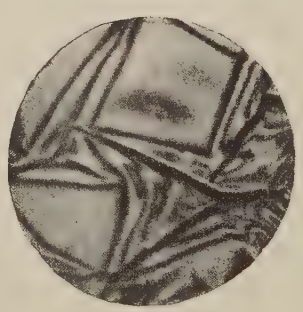

Fig.6

Fig.4. Fragmentation of thick carbon films into regions separated by microcracks. 8500 X.
Fig.5. "Relief" formed by a carbon film on an optically polished glass surface. 2000 X.
Fig.6. "Relief" formed by a silica film on an optically polished glass surface. 2000 X.

Fig.1 shows a micrograph obtained by means of a collodion replica; the horizontal bands discernible in the micrograph are crystal growth bands. A carbon replica made from such a mirror surface, however, instead of the growth bands, evinces a distinctive intrinsic "microstructure" (Fig.2). The character of this "microstructure" depends on the thickness of the carbon film. In the case of films 100 to 300 Å thick in some sections there appear distinctive centers of nucleation of the intrinsic relief. Examination of stereoscopic pairs of such sections showed that these regions are convex, i.e., ridges rising above the general surface of the film and radiating from the "center" at angles of about 120°. A typical center is visible in Fig.2. With increase of the film thickness to 300-500 Å the number of centers increases. The convex regions or ridges departing from individual centers intersect and form a complex topography on the surface of the film (Fig.3). As a result of this development of relief the entire surface of the film is broken up into individual small closed microregions of different size, at the boundaries of which the film is swollen.

In Fig.3 one can clearly see how on such swollen boundaries there form microfissures, disrupting the continuity of the film (narrow light lines extending along the ridges).

With further increase of the film thickness to 500-1000 Å an entirely different picture is observed. The cracks that began to appear along the boundaries in thinner films, now cover the entire area of the boundaries, and the convex boundaries between individual regions are split by relatively wide cracks. A micrograph of a thick film of this type is reproduced in Fig.4. Films of this thickness tend to crumble.

We note that the dimensions of the microregions often lie below the limit of resolution of optical microscopes, and hence cannot be detected in monitoring the quality of the film by means of an optical microscope. It was found that silica and titanium films deposited on mirror surfaces display similar characteristics.

Fig.5 shows an electron micrograph of a carbon film and Fig.6 of a silica film deposited on the surface of optically polished glass. The character of the figures formed by the quartz and carbon films differs: in the case of quartz the larger regions are separated by wedge shaped boundaries, while in the case of carbon the character of the regions is reminiscent of the picture observed on films deposited on the faces of plumbite crystals. The important fact, however, is that in both cases the films exhibit an intrinsic microgeometry. The fact that some films deposited on rough surfaces behave in a different manner than films on mirror surfaces will be evident from the results of the following experiment.

The mirror surface of one of the plumbite crystals was first coated with magnetic suspension of the type used for investigating the domain structure of ferromagnets (Akulov-Dekhtyar and Bitter powder pattern procedure[2]). This suspension was allowed to dry thoroughly (the dry suspension could not readily be rubbed off) and then a carbon film 400 Å thick was deposited on the surface. At the same time a similar film was evaporated onto a clean mirror surface. Examination of the replicas in an electron microscope showed that the film deposited on the rough surface replicated the relief formed by the magnetic suspension (Fig.7), while the control film evinced an intrinsic structure analogous to that shown in Fig.3.

As long as the film remains relatively thin (up to 150-200 Å) it adheres to the surface of the substrate, replicating its microrelief. With further increase in the film thickness, however, there appear at individual points, which may coincide with "accidents of topography" on the substrate, regions in which the adhesion between the film and the substrate becomes weaker than the cohesion between the particles constituting the film. At such points the film rises above the surface of the substrate, forming a distinctive relief (see Fig.2) but still remains

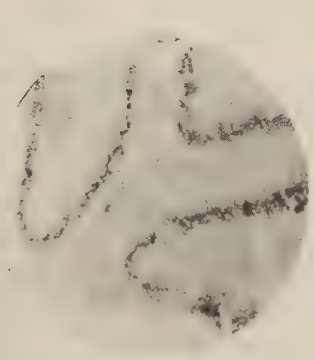

Fig.7. Carbon replica from a magnetoplumbite surface coated beforehand with magnetic powder suspension; the replica renders the structure of the suspension. 8500 X.

continuous, i.e., does not break up into separate regions. In Fig.3 one can see that this microrelief, which is present on the surface of magnetoplumbite in the form of crystal growth bands (row of parallel light bands running horizontally in the figure), as rendered by a thin film, flows smoothly over the convex boundaries between the individual sections of the film, i.e., at these boundaries the film simply stands away from the surface of the substrate. Then with further increase in the thickness of the film, the film breaks along the sections raised above the surface of the substrate. As noted above, on the convex regions there begin to appear cracks, which with further increase of the film thickness leads to general crumbling of the film.

A similar process of fragmentation may occur in the case of thin films that remain whole while still under vacuum but begin to deteriorate upon exposure to the atmosphere. Apparently, water vapor present in the atmosphere facilitates scaling of the films from mirror substrates. This frequently leads to the appearance of microcracks on the surface of even thin films. If the substrate is not mirror smooth, but has some roughnesses as, for example, in the case of the experiment with magnetic suspension, the adhesion of the film to the surface of the substrate increases and the film does not form an intrinsic microrelief, but truly replicates the structure of the substrate.

The above described phenomenon of formation of an intrinsic relief obviously can hamper interpretation of electron micrographs of replicas from various surfaces.

The magnetoplumbite crystals were grown in the laboratory of the Institute of Crystallography of the USSR Academy of Sciences and made available to us by V.A.Timofeeva, whom we take this opportunity to thank.

Physics Faculty,
Moscow State University

References

1. V.M.Luk'yanovich, Elektronnaya microskopiya v fiziko-khimicheskikh issledovaniyakh (Electron microscopy in physical-chemical studies), Chapt.II, 1960.
2. S.V.Vonsovskii & Ya.S.Shur, Ferromagnetizm (Ferromagnetism), M., 1948.

EVALUATION OF THE PERFORMANCE OF THE UMT-2 ULTRAMICROTOME

- Ya.Yu.Komissarchik & V.F.Mashanskii

One of the important factors in successful submicroscopic investigation of tissues is the availability of a reliable ultramicrotome. Many laboratories still find it difficult to select a microtome from among the large number available, particularly, if one includes imported ultramicrotomes. This is due, on the one hand, to the lack of valid criteria for judging the performance of microtomes, and, on the other hand, due to the fact that final evaluation can be made only after extensive work with a given instrument. An important factor, of course, is skill acquired with practice on a given instrument. Thus, in the literature one can find both poor and good examples of work done on a given model. For example, the LKB microtome, developed by Sjöstrand, has gained wide acceptance in Soviet laboratories, yet experience in our laboratory showed that this instrument does not meet present day requirements for ultrathin sectioning. The sliding bearing employed as the basic feed element in this instrument has a number of serious shortcomings: the presence of lateral and radial play some orders of magnitude greater than the requisite feed, and significant wear of the working surfaces without provision for suitable compensation.

In the microscopy laboratory of the Institute of Cytology we have, over a

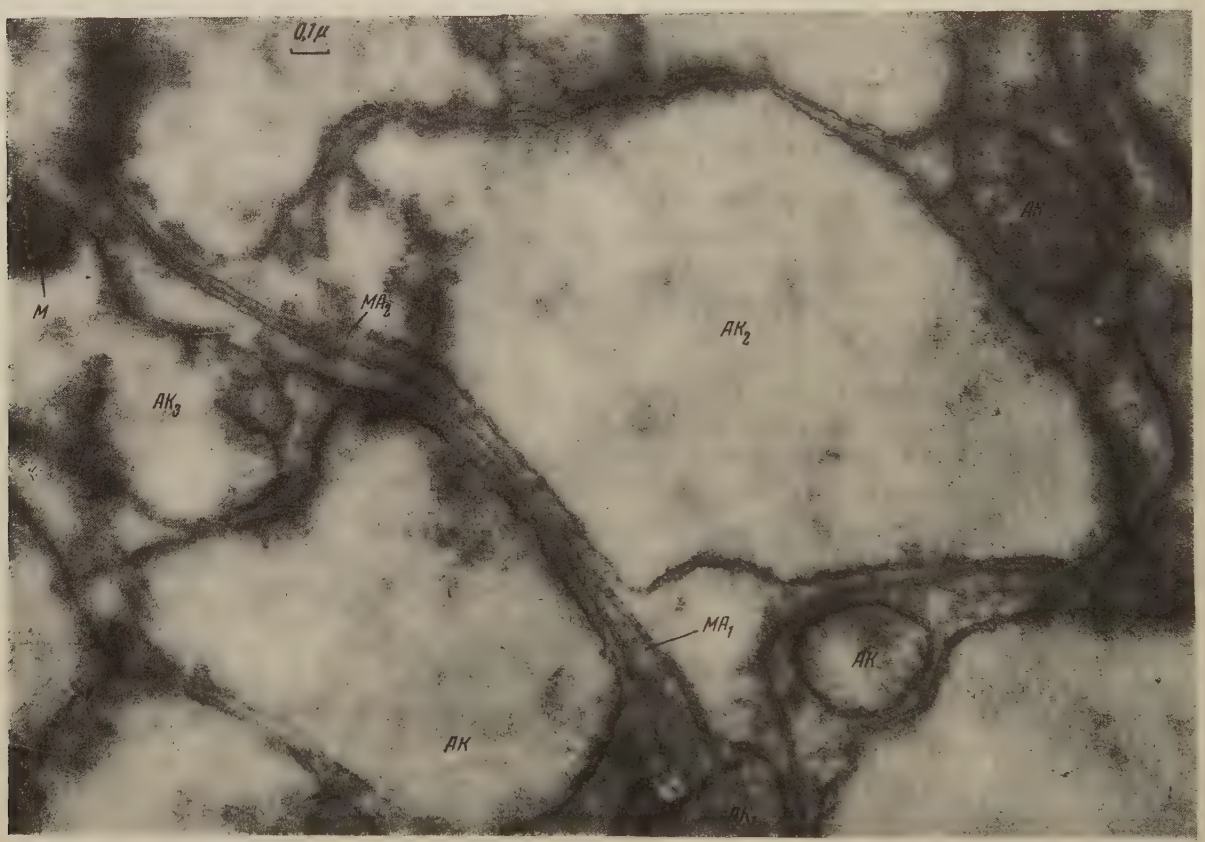

Fig.1. Transverse section of a peripheral nerve of a crab. Discernible in the micrograph are the axons AK of the Remak fibers. One can also follow the mesaxons MA_1 and MA_2 passing from one fiber to another. At the boundary of the axon AK_3 one can discern a mitochondria M with resolved internal structure. 70 000 X.

Fig.2. a - Transverse section through sciatic nerve of a frog. At the center is the axon AK of the medullated nerve fiber. There is also resolved the periodicity of the lipoprotein layers in the medullary sheath MO. Mitochondriae M are visible in the axon and in the cytoplasm of the Schwann cell. At the left - a wall of a blood vessel CK. Between the myelinous fibers one can see collagenous fibers CF. 70 000 X; b - section of the medullary sheath of the central myelinous fiber. In addition to the main period there is brought out the central line C. 280 000 X.

number of years, carried out investigations on ultrathin sections prepared on the UMT-2 ultramicrotome, the design of which is described in Ref.1. At the same time, we made a point of evaluating the performance of this model. To this end there were prepared sections of different tissues, fixed and imbedded in different ways. Specifically, we investigated peripheral nerve fibers and cells of nerve ganglia, epithelial tissues, single cell organisms, blood components, and fractions of homogenized cells. The specimens were imbedded in methacrylate of different density and also in agar-agar with subsequent impregnation in methacrylate.[2] Both glass and ruby knives were used for cutting.[3] In a number of cases we obtained series of sections of uniform thickness with an area of up to 2 mm^2.

By means of the UMT-2 ultramicrotome it is feasible to cut sections only 100 Å thick. With a knife edge of good quality and correct choice of the angle, the sections are not wrinkled as a result of deformation, which makes subsequent flattening unnecessary. Flattening or smoothing by means of xylene or chloroform vapor gives satisfactory results only as evaluated by means of the binocular microscope of the ultramicrotome. Actually, upon examination of these sections in the electron microscope there become evident appreciable changes in the submicroscopic

structure, connected, apparently, with partial solution of the material by the methacrylate vapor. The feed system employed in the design of the UMT-2 ultramicrotome (in which the specimen is moved) insures complete rigidity between the block, the feed rod and the microtome stand, and the absence in this linkage of oil films and bearings; this reduces the possibility of irregularity in advance of the specimen. In view of the rigidity of the design and the great weight of the cast stand. the microtome can be used on an ordinary bench, and does not require a special base or table.

The use of an equi-strength feed rod of varying cross section made it possible to reduce the stress in it during displacement relative to the knife edge and yet provide a sufficient movement of the specimen for slicing.

It must be noted, however, that in the process of work with the instrument there came to light certain design shortcomings. Among these are poor location of the motor and a noisy reduction gear, and an inadequate number of specimen holders supplied with the microtome. It would be desirable to modify the design to provide for variation in the cutting speed in a wide range; it would also be helpful to replace the incandescent lighting bulb by a daylight fluorescent tube of the type now provided with most imported microtome.[4,5]

At the present level of electron microscopic investigation of organic tissues, interpretation is hindered by lack of three dimensional views of the specimen. This difficulty can be obviated to some extent by investigating sections made in series. Many modern ultramicrotomes, including the UMT-2, can provide for this. In the case of the UMT-2, however, series sectioning requires certain accessories: 1) a device for accurate shaping of the block to the form of a truncated regular pyramid (the manual cutting now employed is not satisfactory), and 2) special supporting grids with elongated mesh to minimize the chance of a wire coming under the specimen.

On the basis of our experience and the results obtained we are of the opinion that the UMT-2 ultramicrotome does satisfy modern requirements for ultrathin sectioning and can be made to yield satisfactory sections of biological specimens for examination in high resolution microscopes. With a view to demonstrating the possibilities of the UMT-2 ultramicrotome we reproduce herewith two electron micrographs of sections of different tissues.

Microscopy Laboratory,
Institute of Cytology,
Academy of Sciences of the USSR

References

1. Ya.Yu.Komissarchik, V.N.Vertsner & L.S.Gol'din, Izv.AN SSSR, Ser.fiz., 23, 473 (1959). (Trans.Bulletin, 23, 456.)

2. V.F.Mashanskii & B.O.Beznosikov, Tsitologiya (Cytology), 3, 117 (1961).

3. V.F.Mashanskii, Ya.Yu.Komissarchik, M.A.Rybin & L.N.Vinnichenko, Ibid., 2, 376 (1960).

4. H.Sitte, Microscopie, 10, 365 (1956).

5. Type LKB 48000 Ultratome, Operation manual.

ARMORED HIGH-VOLTAGE LEAD-IN

- D.V.Fetisov & A.N.Kabanov

Electrical connections to high-voltage instruments are commonly realized by a high-voltage lead-in to insure safety of the operating personnel and stability of the voltage supply, which is particularly important in the case of electron microscopes, electron diffraction instruments and similar equipment.

The insulating filler used in cable lead-ins is generally some type of resin or oil. When resin is used the high-voltage lead-in becomes difficult to disassemble, which is frequently an inconvenience, particularly in the case of vacuum instruments. The use of oil is undesirable inasmuch as owing to its reaction with the rubber insulation and electrolysis of the oil, the service life of the connector is reduced.

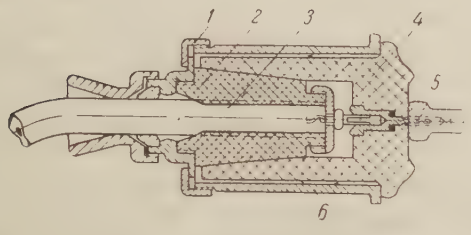

Fig.1. Cross section of the armored vacuum sealed lead-in.

Fig.2. External view of the armored lead-in.

We designed a compact demountable high-voltage lead-in for use in conjunction with electron microscopes and similar equipment. A sectional view is shown in Fig.1. The high-voltage cable 3 with rubber insulation is firmly inserted into the threaded opening in the tapered bushing 2 made of suitable insulating material. The internal diameter of the thread must be 1.5-2 mm smaller than the diameter of the inner rubber sheath of the cable (armor and graphite layer removed). For ZKVR-55 type cable we used standard 1 inch thread. The conical bushing is shaped to fit the mating opening in the duct insulator 4, and before insertion is coated with vaseline.[1] Over the duct insulator there fits the metal shield 6 onto which there is screwed the nut 1, which insures firm contact of the cable armor with the housing of the instrument and retention of the busing with the cable in the duct insulator. The conductors are soldered into plugs, which enter into receptacles in the insulator 5. An external view of the lead-in connector with cable is shown in Fig.2.

Breakdown tests on the lead-in showed that adequate insulation for 110 kv dc is assured with a tapered busing length of 45-50 mm and a threaded opening depth of 30 mm. The criterion for electric strength in the tests was the absence of unstable leakage currents with an amplitude greater than 10^{-8} amp at a voltage of 110 kv.

The described armored lead-in design is convenient for use under laboratory conditions. Actually, instead of a regular cable one can use vacuum rubber tubing covered with suitable metal braid. For voltages up to 75 kv one can use standard vacuum rubber tubing 22 mm in diameter; for voltages up to 100 kv, one should use tubing 27-30 mm in diameter.

The cable (or rubber tubing with the conductors threaded through it) is inserted into the busing in the following manner. The cable is stripped down to the rubber insulation (armor and graphite layer removed) to a length of 120-140 mm and then the end 60-80 mm section is reduced in thickness so as to enter the

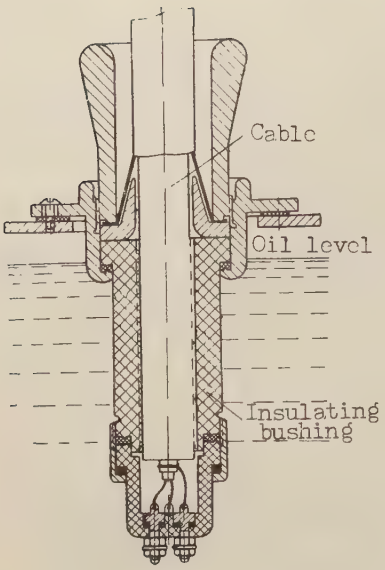

Fig.3. Section of armored lead-in connected to oil filled device.

opening in the bushing. The cable is coated with vaseline, stretched slightly and inserted through the plug. The excess, protruding cable is cut off.

In the case of supplying oil filled equipment, the design of the lead-in is simplified. In this case one need only have a bushing of cylindrical shape (Fig.3), which is mounted on the cover of the rectifier tank in a special fitting. The lead-out contact is insulated by oil resistant rubber to protect the cable from contact with the transformer oil.

The described lead-in has been successfully used in different types of high-voltage equipment, including an electron velocity analyzer[2], and has been employed as a standard component in the commercial MÉSM-40 and UÉMB-100 electron microscopes and their power supplies.[3,4] The small dimensions of the lead-in and the simplicity of its design make it adaptable for use in plug-jack type cable connectors.

We desire to thank A.M.Kondrashov for helping perfect some of the components and the assembly technique.

References

1. D.V.Fetisov & A.N.Kabanov, Inventor's certificate No.106870, 1957.
2. A.N.Kabanov, V.I.Milyutin & D.V.Fetisov, Izv.AN SSSR, Ser.fiz., 23, 459 (1959). (Trans.Bulletin, 23, 443.)
3. V.I.Milyutin, D.V.Fetisov, K.K.Raspletin, F.U.Spektor & B.I.Pochtarev, Ibid., 23, 454 (1959). (Trans.Bulletin, 23, 438.)
4. P.A.Stoyanov, G.A.Mikhailovskii & V.V.Moseev, Ibid., 23, 442 (1959). (Trans.Bulletin, 23, 427.)

HIGH-VOLTAGE SOURCE WITH A HIGH DEGREE OF REGULATION

- A.V. Iz"yurov

In designing high-resolution electron microscopes, one of the most difficult problems is provision of a highly regulated accelerating-potential source. According to the data in the literature[1], the allowable voltage instability-fluctuation plus ripple - for a high-resolution microscope should not exceed 0.0005%. At present the most advanced Soviet electron microscope - the UÉMV-100 - has a low-frequency potential source with an instability of 0.003%. Certain improvements made in this power unit reduced the high voltage fluctuation to 0.0007%, which in sum with the ripple gives an instability of 0.0012-0.0016%. Development work on the low-frequency source for the UÉMV-100 showed that to reduce the instability it is necessary to employ less filtering, which in turn increases the ripple. This conflicting effect led us to explore the possibility of utilizing high-frequency rectifying circuits with a view to further reduction of the instability.

High-frequency rectifier with voltage multiplication

High-frequency voltage sources, as compared with low-frequency units, have the following advantages: 1) better stabilization possibilities in principle, because the rectifier-filter combination has a smaller time constant, 2) reduced dimensions and lower weight, and 3) increased safety in servicing.

The most important part of a high-frequency voltage source is the rectifying and voltage-multiplying network (Fig.1). Multiplication is essential because the primary voltage is limited to 20-25 kv owing to corona effects in the step-up transformer. The principal characteristics of multiplying circuits are the internal voltage drop and the output ripple.

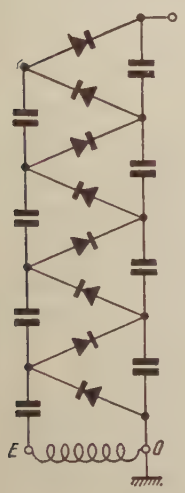

Fig.1. Voltage multiplying network.

To determine the best number of multiplication stages, the operating frequency and the capacitors in the multiplication circuit, we evaluated all the forms of voltage loss. The calculations showed that most of the voltage loss (~70%) in a multiplying circuit intended for electron microscopes, i.e., a high voltage circuit with a small current (a few hundred microamperes) is independent of the operating frequency and of the load current. These losses are due to the stray shunt capacitances in the wiring and circuit elements and to the interelectrode capacitances of the rectifiers.[2] The calculated results were used to plot voltage loss versus the number of stages for different operating frequencies (Fig.2). The curves show that the number of stages should not exceed 5 or 6 and that the frequency should not be less than several kilocycles. The upper frequency limit is imposed by the rectifier parameters and is usually 300 kc.

The high frequency ripple is also determined primarily (80-90%) by the stray capacitance and the capacitance of the rectifiers. The ripple due to the discharge of the output capacitance into the load becomes noticeable only at frequencies of the order of several kilocycles.

With the above considerations in mind, we constructed a prototype high-frequency rectifier with voltage multiplication. For the design we chose ZTs16S kenotrons (peak back voltage 35 kv) and KOB-3 capacitors (2500 pf, 30 kv). We chose an operating frequency of 40 kc, and decided on four multiplication stages. The high-voltage source was a self-excited oscillator incorporating GU-50 tubes

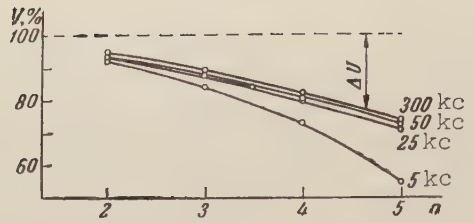

Fig.2. Voltage loss versus number of stages for different operating frequencies.

and a parallel resonance circuit with a high voltage secondary. The peak voltage in the secondary was 12-14 kv. Ferrite cores were used in the coils to insure optimum coupling. The prototype rectifier delivered up to 400 μa at 100 kv.

Regulation of the high voltage

As noted above, the main problem in designing power supply units for an electron microscope is stabilization of the high voltage. In the prototype model stabilization was realized by means of a feedback loop that included the entire high-voltage source. The feedback circuit comprised a wire wound voltage divider, a reference voltage source and a dc amplifier. Control of the output voltage was effected by varying the bias on the screen grid of the oscillator tubes.

Calculations show that to reduce the instability to 0.0005% when the line voltage fluctuates up to 0.5% and the voltage divider ratio is 0.001, the gain required in the feedback circuit is of the order of 10^6. The amplification factor referred to the screen grid voltages of the oscillator tubes is 1000-1200. Thus the dc amplifier gain must be about 1000. This gain was obtained by using a two-stage amplifier with a negative feedback coefficient $\beta = 10^{-3}$.

Measurement of the high voltage instability

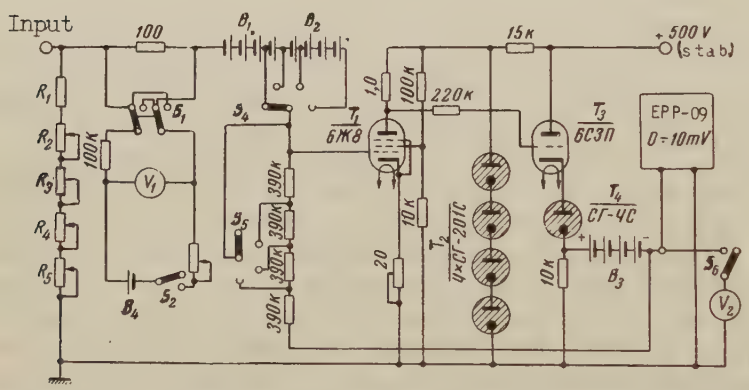

Fig.3. Instrument developed to measure high voltage instability.

A special instrument incorporating an ÉPP-09 recording voltmeter was developed to measure the high voltage instability. This instrument (Fig.3) consists of a single stage dc amplifier with cathode follower output and adjustable negative feedback. Tests showed that this instrument is capable of measuring high voltage instability down to 0.0001%.

Results of our work

On the basis of our analysis of multiple stage voltage multiplying circuits and making use of the above described instrument for measurement for instability, we developed, built and tested a new high-frequency electronically stabilized high voltage supply unit.

Appreciable reduction of high frequency ripple in the new supply unit has been achieved by introducing a bridge type bucking network[3]. Measurements showed that, in addition to the ripple at the main frequency (40 kc), the output voltage comprises a 50 cps ripple component penetrating through the oscillator power sup-

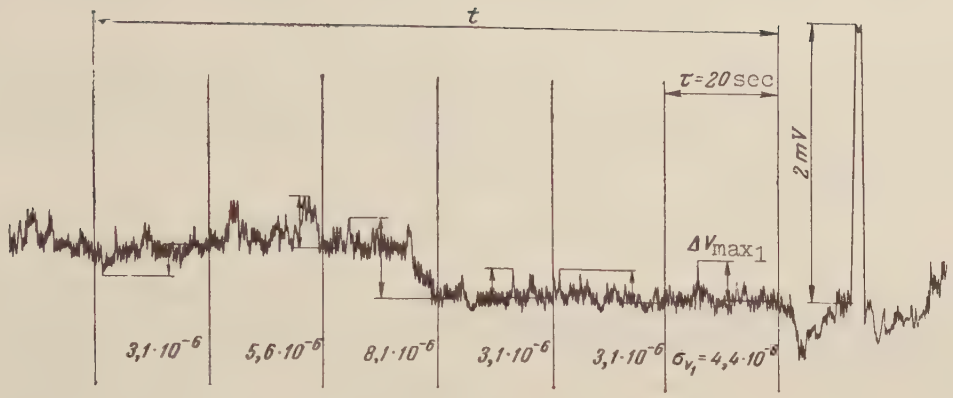

Fig.4. Sample record of high voltage instability

plies and stabilizers. Whereas the 40 kc ripple can be reduced to about 15 mv, i.e., 0.00003% at 50 kv, the 50 cps ripple amounts to about 140 mv (0.0003%), i. e., is one order of magnitude higher. Suppression of this low frequency ripple is extremely difficult.

The high voltage instability was measured by means of the instrument described above. The high voltage arm of the voltage divider has a 500 megohm wire resistor. The instability was evaluated as the average for 30 measurements of 20 sec duration each. With the rectified voltage ranging from 40 to 60 kv, the average instability was $\sigma_{av} = 3.5 \cdot 10^{-6} = 0.00035\%$. A sample voltmeter record is reproduced in Fig.4. Thus the sum instability - fluctuation plus ripple - amounted to $6.5 \cdot 10^{-6}$ or 0.00065%. The high voltage instability of potential supply units furnished with domestic and foreign microscopes is at best 0.001%, not counting ripple. Hence a figure of 0.00065% for the sum of instability and ripple is significant. Unfortunately, this result holds true only for potentials up to 60 kv; above this voltage the instability increases sharply. There is reason to infer that this is due to nonstationary processes (such as leakage, corona, charge migration in the insulating oil, etc.) in the individual components or subassemblies. It is possible that these processes, which are not significant where insulating gaps in other equipment are concerned, cannot be tolerated in high-voltage power supplies where the frequency instability must be minimal. Hence in further development attention must be concentrated on reduction of the field gradients in individual components such as kenotrons, capacitors, etc.

References

1. S.Leisegang, Optik, 11, 2, 51 (1954).
2. E.Everhart & P.Lorrain, Rev.Scient.Instrum., 24, 221 (1953).
3. A.Delong & V.Drahos, Praktika elektronova mikroskopie, Praha, 1958.

POWER SUPPLY FOR A MICROSCOPE WITH A RESOLUTION OF 5 Å

- V.V.Polivanov, R.V.Pogudina & V.V.Il'in

A number of difficulties are encountered in developing power supplies for electromagnetic lenses of high resolution electron microscopes: one must simultaneously reconcile the requirements of high stabilization, smooth and accurate control and a wide range of operating currents.

Reduction of lens current instability

In present power supplies the lens current is stable to within only 0.001%.[1] Through detailed analysis of stabilizer circuits (Fig.1) we were able to effect a further improvement in stability.

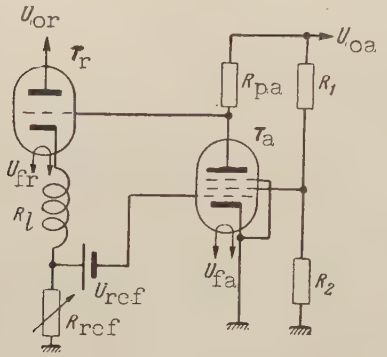

Fig.1. Lens current regulator.

The operation of a stabilizer is highly sensitive to spontaneous fluctuations of the tube plate, screen grid and filament voltages, particularly where the first amplifier stage is concerned. The main cause of these fluctuations is variation in the line voltage.

Let us investigate the possibility of reducing the effect of line voltage variation on the operation of a stabilizer. The change in the lens current dI_l or what is essentially the same thing the current in the regulating tube circuit, can be represented as

$$dI_l = \frac{\partial I_l}{\partial U_{cr}} dU_{cr} + \frac{\partial I_l}{\partial U_{pr}} dU_{pr} + \frac{\partial I_l}{\partial U_{fr}} dU_{fr}^{*}. \qquad (1)$$

Recalling that

$$\frac{\partial I_l}{\partial U_{cr}} = S_{cr}; \quad \frac{\partial I_l}{\partial U_{pr}} = \frac{\partial I_{pr}}{\partial U_{pr}} = \frac{1}{R_{ip}}; \quad \frac{\partial I_l}{\partial U_{fr}} = \frac{\partial I_{pr}}{\partial U_{fr}} = S_{fr},$$

we obtain from (1)

$$dI_l = S_{cr} dU_{cr} + \frac{1}{R_{ip}} dU_{pr} + S_{fr} dU_{fr}; \qquad (2)$$

here S_{cr} and S_{fr} are, respectively, the control grid-to-plate and the filament-to-plate transconductances of the regulating tube.

We determine dU_{cr}, dU_{pr} and dU_{fr}, on the basis of the condition $dR_l = dR_{rcf} = 0$, i.e., for the case of a constant load. For the control grid of the regulating tube, we can write

$$dU_{cr} = dU_{pa} - dU_{kr} \qquad (3)$$

where U_{kr} is the cathode potential of the regulating tube.

The change dU_{pa} in the potential on the plate of the amplifier tube is made up of the partial changes due to fluctuation of the voltages of the amplifier plate supply (dU_{poa}), the control grid (dU_{pca}), the screen grid (dU_{psa}) and the filament (dU_{pfa}):

---

*The subscripts used herein have the following meanings: l - lens, c - control grid, s - screen grid, p - plate, f -filament, r - regulating tube, a - amplifier tube.

$$dU_{pa} = dU_{poa} + dU_{pca} + dU_{psa} + dU_{pfa}, \tag{4}$$

Let us determine each of these terms:

$$dU_{poa} = \frac{R_{ia}}{R_{ia} + R_{pa}} dU_{oa} = m_{pa} dU_{oa}, \tag{5}$$

where

$$m_{pa} = \frac{R_{ia}}{R_{ia} + R_{pa}}. \tag{6}$$

Changes in the control grid voltage give rise to changes in the plate current, which in turn cause changes in the plate voltage:

$$dI_{pca} = S_{ca} dU_{ca} + \frac{1}{R_{ia}} dU_{pca}.$$

Making use of the fact that $dU_{pca} = -dI_{pca} R_{pa}$ we readily obtain

$$dU_{pca} = -m_{ca} dU_{ca} = -m_{ca} R_{ref} dI_l, \tag{7}$$

where

$$m_{ca} = m_{pa} R_{pa} S_{ca}. \tag{8}$$

Similar reasoning leads to

$$dU_{psa} = -m_{sa} dU_{sa}, \tag{9}$$

$$dU_{pfa} = -m_{fa} dU_{fa}, \tag{10}$$

where

$$m_{sa} = m_{pa} R_{pa} S_{sa}. \tag{11}$$

$$m_{fa} = m_{pa} R_{pa} S_{fa}. \tag{12}$$

The change in the regulating tube cathode potential is

$$dU_{kr} = (R_l + R_{ref})\, dI_l. \tag{13}$$

Inserting (5), (7), (9), (10) and (13) into (3) and taking (4) into account, we obtain

$$dU_{cr} = m_{pa} dU_{oa} - m_{ca} dU_{ca} - m_{sa} dU_{sa} - m_{fa} dU_{fa} - (R_l + R_{ref})\, dI_l. \tag{14}$$

Proceeding on analogous assumptions we determine the change in the regulating tube plate voltage:

$$dU_{pr} = m_{pr} dU_{or} - (R_l + R_{ref})\, dI_l, \tag{15}$$

where

$$m_{pr} = \frac{R_{ir}}{R_{ir} + R_l + R_{ref}}. \tag{16}$$

Inserting (14) and (15) into (2) and simplifying, we obtain

$$dI_l = \frac{S_{cr} m_{pa} dU_{0a} - S_{cr} m_{sa} dU_{sa} - S_{cr} m_{fa} dU_{fa} + \frac{1}{R_{ir}} m_{pr} dU_{pr} + S_{fr} dU_{fr}}{1 + S_{cr}(R_l + R_{ref}) + \frac{R_l + R_{ref}}{R_{ir}} + S_{cr} m_{ca} R_{ref}}. \quad (17)$$

Evaluation of the individual terms for real circuits showed that all the terms except the first one in the numerator and the last one in the denominator can be neglected without exceeding the usual scatter in tube parameters. Dropping the negligible term, Eq.(17) simplifies to

$$dI_l = \frac{m_{pa} dU_{0a} - m_{sa} dU_{sa} - m_{fa} dU_{fa}}{m_{ca} R_{ref}}. \quad (18)$$

The terms left out of (17) represent the effect of power supply instability and the regulating tube, while the terms retained reflect the results of instability in the supply to the amplifying tube. The fact that the terms in the numerator of (18) are of opposite sign enables us in principle to minimize lens current fluctuations dI_l due to fluctuations in the line voltage. To accomplish this there must be fulfilled the condition

$$m_{pa} dU_{0a} = m_{sa} dU_{sa} + m_{fa} dU_{fa}. \quad (19)$$

Determination of dU_{0a} and dU_{fa} presents no difficulties:

$$dU_{0a} = U_{0a}\sigma_{0a} \text{ и } dU_{fa} = U_{fa}\sigma_{fa},$$

where σ_{0a} and σ_{fa} are the instabilities in the plate and filament supply voltages, respectively.

In determining dU_{sa} one should take into account the type of circuit used for supplying the screen grid. Thus if the screen grid is fed from a voltage divider (Fig.1) $dU_{0a} = dU_{R_1} + dU_{sa}$, but $dU_{R_1} = R_1 dI_{R_1} = R_1 (dI_{R_2} + dI_{sa})$, $dI_{R_2} = \frac{dU_{sa}}{R_2}$ and $dI_{sa} = S_{sa} dU_{sa}$.

Substituting and transforming, we obtain

$$dU_{sa} = dU_{0a} \frac{1}{\frac{1}{R_2} + S_{sa} + 1}. \quad (20)$$

Obviously, if some other type of supply circuit is used for the screen grid, the expression for dU_{sa} will be different.

If the filament current of the amplifier tube is stabilized, the second term in the right hand part of (19) can also be disregarded, and Eq.(19) is further simplified:

$$m_{pa} dU_{0a} = m_{sa} dU_{sa}. \quad (21)$$

If the screen grid is supplied by a voltage divider this condition can readily be satisfied by proper choice of the divider arms R_1 and R_2.

Improvement of lens current control

In present power supply units the lens current is controlled by varying the reference resistance R_{ref} of the current regulator (Fig.1). The principal shortcoming of this method of control is that there is included in the reference re-

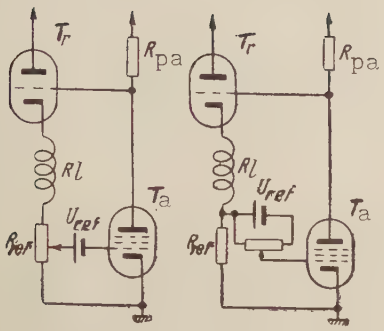

Fig.2. "Potential" lens current control.

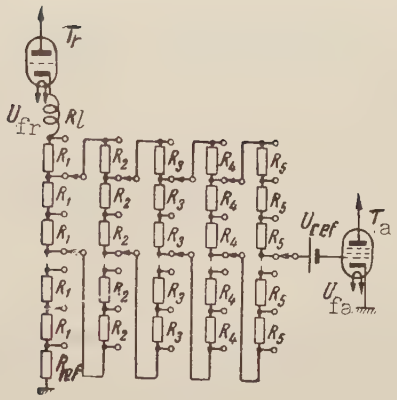

Fig.3. "Potential" lens current control by means of switches.

sistance circuit a number of contact resistances R_k of the control rheostats or switches. Tests have shown that such contact resistances do not remain constant in time. Consequently, each contact introduces an additional fluctuation $dU_{ca} = I_l dR_k$ into the amplifier input voltage, thus aggravating the instability of the lens current.

In addition to varying in time, the contact resistance changes from one switching to another; for example, in the case of wiper or brush type switches the scatter in resistance may attain 3 milliohm. Such deviations are of the same order of magnitude as the changes in the reference resistance necessary to insure smooth current control. As a result, exact continuous control cannot be maintained with an accuracy better than 0.002-0.003%, which in some cases may be inadequate.

In contrast to this "current" control system, for the new power supply for the 5 Å resolution microscope we propose an entirely different "potential" system. Fig.2 shows two possible versions of this method of control. The idea is to transfer the switch or rheostat contacts to circuits that carry low current or no current at all, i.e., to eliminate from the amplifier input circuit all additional fluctuations due to variation in the contact resistance.

In practice, to insure smooth variation of the lens current over a wide range it is essential to employ a system of ganged multiple contact switches arranged as shown in Fig.3. The voltage applied to each subsequent switch is taken off the two preceding stages. This is necessary to insure adequate overlap of the control ranges. While it is impossible with this arrangement to eliminate all flow of current through the switch contacts, the magnitude of the current through the contacts with this arrangement is reduced several orders of magnitude.

Extension of the current control ranges

Methods of extending the range of lens current control were discussed in an earlier article[2]. Developing the new power supply for the objective lens we made use of the calculations carried out for the power unit for the UÉMV-100 microscope. The maximum voltage on the lens coil was reduced to 200 v. By way of regulating tube we employ a 6S18S power triode. Moreover, at certain points in the control range the rectifier supply voltage is changed automatically to insure normal operation of the tube over the entire range.

Results

On the basis of the results of the above described studies of current regulators and controls there was constructed a new power supply source for the objective lens of an experimental electron microscope with a resolution of 5 Å. The new unit reduces the current instability to $\leq 0.0004\%$ and provides exceptionally precise (to within 0.0008%) and smooth current control. Extensive operational tests have shown that the power supply unit is entirely adequate for a microscope of such high resolution.

References

1. P.A.Stoyanov, V.V.Polivanov & G.A.Mikhailovskii, PTE, No.4, 51 (1958). (Trans.Instruments & Experimental Techniques.)

2. V.V.Polivanov, V.V.Il'in, A.V.Iz"yurov, R.V.Pogudina & N.I.Pyatakov, Ibid., No.5, 147 (1960). (Trans.Ibid.)

VACUUM SYSTEM SELECTOR VALVE WITH ONE CONTROL KNOB

- D.V.Fetisov, B.I.Pochtarev & A.N.Kabanov

Among the many types of vacuum equipment employed in modern laboratories an important place is occupied by demountable metal instruments operating at pressures of 10^{-4}-10^{-5} mm Hg. Such instruments include electron microscopes, diffraction cameras, vacuum evaporation units, etc.

Most such instruments require a systematic alternation of vacuum and atmospheric pressure in the working space, which leads to the necessity of using special commutation devices for interconnecting the tubes and pumps in a certain sequence. Such devices should be simple as regards operation and reliable in service.

A fundamental requirement for demountable instruments is a high pumping rate, inasmuch as this determines the limit vacuum in the instrument. This requirement pertains particularly to vacuum evaporation and similar units, inasmuch as the operations carried out in them are short term ones and are generally accompanied by appreciable evolution of gas or vapor.

Experience in the design and operation of different metal vacuum instruments with a volume of 10 to 20 liters and with the seals provided by rubber gaskets provides the basis for approximate evaluation of the dependence of the limit vacuum and time to attainment thereof as a function of the pumping speed.

Data for systems without freezing traps are listed in the accompanying table. The pumping times are given without taking into account the time necessary for establishing the fore vacuum.

Pumping speed $S = S_H/\left(1 + \frac{S_H}{Q}\right)$, liter/sec*	Pumping time to		
	$1 \cdot 10^{-4}$ mm Hg	$5 \cdot 10^{-5}$ mm Hg	$1 \cdot 10^{-5}$ mm Hg
5-10	30-60 min	not attained	
30-50	6-10 min	1-2 hrs	not attained
150-200	1-2 min	4-6 min	10-20 min

---

*S_H is the rated capacity or speed of the high vacuum pump in liter/sec; $Q = 12.1(d^3/l)$ liter/sec is the capacity or conductance of the tube from the pump to the instrument, where d is the inner diameter of the tube in cm and l is the length of the tube in cm.[1]

These figures are approximate, but can be used as the initial data in designing evacuated systems, choosing the pumps and estimating the conductance of tubes.

The design may be regarded as satisfactory if the pumping system provides at the entry to the working volume a pumping rate equal to 25-35% the rated capacity of the high vacuum pump: $S = (0.25\text{-}0.3)S_H$. If this requirement is not fulfilled, the use of a powerful pump may be inexpedient.

For example, assume that the tubing from the evacuated chamber to the high vacuum pump has an inner diameter d = 4 cm and a length l = 60 cm. In this case the pumping speed will be 13.5 liter/sec in using a 500 liter/sec capacity pump, and 10.4 liter/sec with a 40 liter/sec capacity pump. Thus, it will be seen that

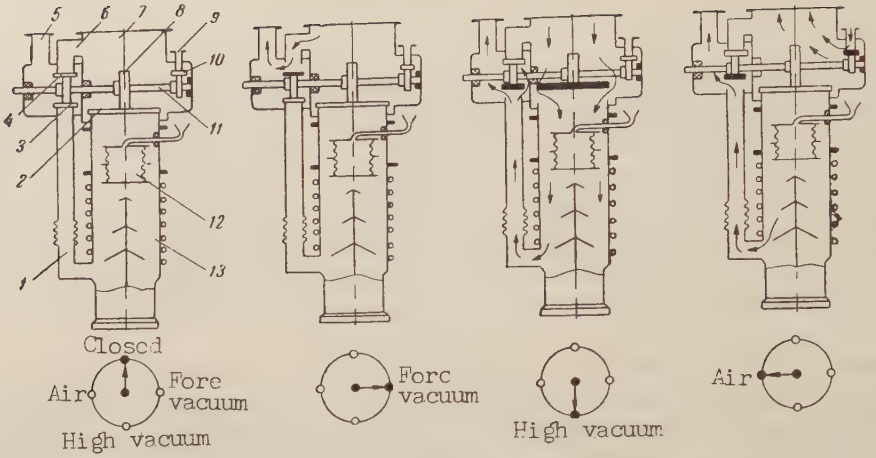

Fig.1. Operation of the vacuum selector valve.

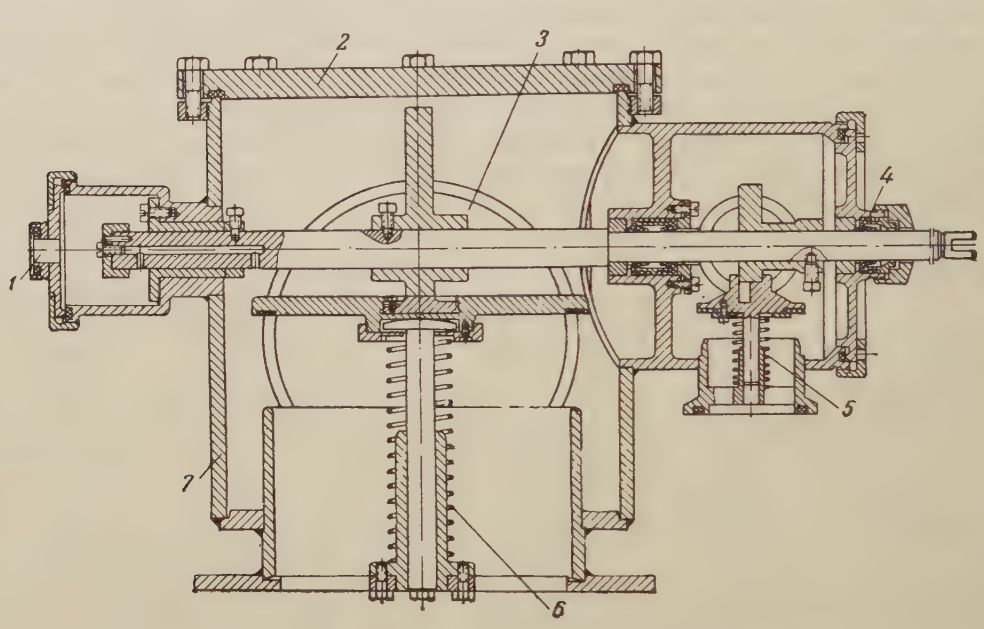

Fig.2. Sectional view of the valve chamber.

despite the great difference between the speeds of the two pumps, in both cases there is obtained almost the same pumping rate and almost the same lower limit of pressure (10^{-4} mm Hg).

As noted above, another essential requirement for pumping systems is simplicity, convenience and reliability of the valve system connecting the various lines. The requirement of simplicity makes it desirable to use a control with a single knob, which simplifies the task of the operator and makes it easier to realize remote control of the system and to introduce the requisite safety interlocks.

Taking these considerations into account, we developed a vacuum selector valve with one control knob, a distinctive feature of which is location of the distributor cam mechanism in the vacuum.[2]

The working cycle of the selector valve unit is diagramed in Fig.1. The valve chamber is divided into two sections by a partition; the cam shaft 11 passes

through this partition and is brought out through the chamber wall. The following components are connected to the chamber sections: the diffusion pump 13, the manifold 7 connecting the chamber with the evacuated volume, the fore-vacuum pump 5, the flanged connecting fitting 9 for admission of air and the exit tube 1 of the diffusion pump. The two sections are connected by the elbow tube 6. Commutation of the ducts is realized by the four valves 2, 3, 4 and 10, controlled by three cams 8, mounted on the cam shaft 11.

The selector settings and corresponding valve positions are the following (the directions of flow are indicated by the arrows in Fig.1):

1. "Closed": all valves closed; both pumps isolated.
2. "Fore vacuum": valve 4 open; instrument connected to fore-vacuum pump.
3. "High vacuum": valves 2 and 3 open; instrument connected to diffusion pump, the discharge of which is connected to the fore-vacuum pump.
4. "Air": valves 3 and 10 open; instrument connected with the atmosphere; at the same time the diffusion pump is still evacuated by the fore-vacuum pump.

All four selector settings are realized by consecutive clock-wise rotation of the cam shaft; the setting detents are 90° apart.

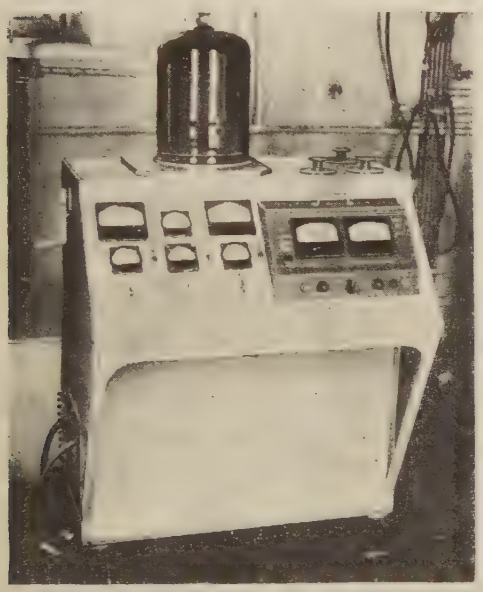

Fig 3. Vacuum unit equipped with selector.

Fig.2 shows a cross sectional view of the valve chamber. The chamber itself 7 is welded of steel tubing. The evacuated instrument can be connected to the selector either through the side branch 3 or by means of a fitting replacing the chamber cover 2. The cam shaft is sealed by conical rubber bushings 4.

The valves are raised by relatively weak springs 5 and 6, so that they can open only if the pressure in the chamber is appreciably below atmospheric. This precludes accidental admission of air to the operating diffusion pump. The selector housing has a special flanged fitting 1 for connecting a vacuum relay intended for automatically breaking the electric circuit of the pump motors in case of admission of air to the instrument. The vacuum relay is included in the selector assembly and is used when the associated equipment operates at a dangerous voltage.

The described selector is intended for use with a type N-5 or N-5S diffusion pump with a rated capacity of 500 liter/sec and a VN-2 fore-vacuum pump with a geometric capacity of 7 liter/sec. In distinction to earlier designs[3], the present selector has a liquid nitrogen trap (12 in Fig.1), installed ahead of the N-5S pump.

Prototypes of the selector valve have been tested in prolonged operation in an electrostatic electron velocity analyzer[4], in a scanning electron microscope, and other equipment.

Fig.3 shows a vacuum preparation unit with such a selector. The glass bell rests on a metal plate attached to the selector chamber. The rate of evacuation of the bell after admission of air and interchange of specimens is 3 min to $1 \cdot 10^{-4}$ mm Hg, 8 min to $1 \cdot 10^{-5}$ mm Hg and 15-20 min to $5 \cdot 10^{-6}$ mm Hg (these times include the fore-vacuum pumping). Despite the evolution of gases the thermal processes under the bell proceed at a pressure of the order of $(1\text{-}2) \cdot 10^{-4}$ mm Hg.

We desire to thank A.I.Maiorov for valuable advice in connection with improvement of some of the components of the selector valve.

References

1. B.I.Korolev, Osnovy vacuumnoi tekhniki (Fundamentals of vacuum technique), M., 1957.

2. D.V.Fetisov & V.I.Pochtarev, Inventor's Certificate No.94394, 1952.

3. A.N.Kabanov, B.I.Pochtarev, V.I.Pochtarev & D.V.Fetisov, Vopr.radioelektroniki, I Elektronika (Questions of radioelectronics, I.Electronics.) 6, 129 (1960).

4. A.N.Kabanov, V.I.Milyutin & D.V.Fetisov, Izv.AN SSSR, Ser.fiz., 23, 459 (1959). (Trans.Bulletin, 23, 443.)

Bulletin of the Academy of Sciences of the USSR - Physical Series
Vol. 25, No. 6 - June 1961

Transactions of the Third All-Union Conference on Electron Microscopy

TABLE OF CONTENTS

	Page Orig.	Trans.
Calculation of electron lens fields - A.G.Vlasov & D.M.Krupp	662	677
Concerning aberration of electron-optical systems - P.P.Kas'yankov & K.P.Dutova	665	680
Electron optics of probe systems - G.G.Dutov	668	683
Achromatization of lenses in multiple-lens magnetic electron microscopes - P.A.Stoyanov	672	687
Design of magnets for the lenses of magnetostatic electron microscopes - G.V.Der-Shvarts & V.P.Rachkov	676	691
Optics of the ÉM-5 and ÉM-7 electron microscopes - V.N.Vertsner, Yu.M.Vorona, Yu.V.Vorob'ev, G.A.Bogdanovskii, Yu.V.Chentsov	680	695
Mirror electron microscope for studying the structure of surfaces - G.V.Spivak, I.A.Pryamkova, D.V.Fetisov, A.N.Kabanov, L.V.Lazareva & A.I.Shilina	683	698
Some questions arising in the development of an x-ray microanalyzer - A.M.Solov'ev & V.N.Vertsner	691	706
Scanning electron microscope and x-ray microanalyzer - Yu.M.Kushnir, D.V.Fetisov, K.K.Raspletin, B.I.Pochtarev, F.U.Spektor, A.N. Kabanov & V.F.Anisimov	695	709
Use of gas microcells in electron microscopy - I.G.Stoyanova	701	715
The UIT-3 unit for etching metals, semiconductors and dielectrics by ion bombardment - G.V.Spivak, F.F.Kushnir & V.E.Yurasova	707	722
Magnetic objective lens for an emission electron microscope - A.M.Rozenfel'd & P.V.Zaitsev	713	726
Investigation of the magnetic circuits of electron microscope lenses - P.A.Stoyanov & L.Yu.Vol'fson	717	730
Modernization of the UÉM-100 electron microscope - G.V.Der-Shvarts, Yu.M.Kushnir, L.B.Rozenfel'd, P.V.Zaitsev & S.V.Bezlepkin	721	733
Electron-optical measurements of electric and magnetic microfields on surfaces - N.N.Sedov, G.V.Spivak & N.F.Isaeva	725	737
Procedure for determining the work function of microsections on the surface of thermionic cathodes - A.V.Druzhinin	730	742

Electron microscopic investigation of semiconductor whiskers - I.G.Sirotenko, G.V.Spivak, I.G.Stoyanova & Z.M.Osad'ko	735	748
Structure and emf of photovoltaic PbS layers prepared by vacuum sublimation - R.Ya.Berlaga & M.I.Rudenok	739	751
Electron microscopic observation of magnetic microfields by means of replicas - L.V.Lazareva & G.V.Spivak	742	753
Objective method of recording electron energy spectra with an electrostatic analyzer - A.N.Kabanov, Yu.M.Kushnir & D.V.Fetisov	748	759
Use of an analyzer for investigating the energy distribution of electrons reflected from metals - Yu.M.Kushnir & A.N.Kabanov	752	762
Ion-optical technique for preparing small diameter apertures - L.B.Rozenfel'd & A.I.Makarov	754	764
Investigation of some types of photographic plates suitable for use in electron microscopy - I.S.Renskii & P.A.Stoyanov	757	766
Some characteristics of carbon and silica replicas made from polished surfaces - L.V.Lazareva & T.F.Filippova	760	769
Evaluation of the performance of the UMT-2 ultramicrotome - Ya.Yu.Komissarchik & V.F.Mashanskii	764	772
Armored high-voltage lead-in - D.V.Fetisov & A.N.Kabanov	766	775
High-voltage source with a high degree of regulation - A.V.Iz"yurov	768	777
Power supply for a microscope with a resolution of 5 Å - V.V.Polivanov, R.V.Pogudina & V.V.Il'in	772	780
Vacuum system selector valve with one control knob - D.V.Fetisov, B.I.Pochtarev & A.N.Kabanov	776	785

Translated in 1962 by
Columbia Technical Translations
5 Vermont Ave., White Plains, N.Y.